Continuum Mechanics and Plasticity

CRC Series: Modern Mechanics and Mathematics

Series Editors: David Gao and Ray W. Ogden

PUBLISHED TITLES

Beyond Perturbation: Introduction to The Homotopy Analysis Method
by Shijun Liao

Mechanics of Elastic Composites
by Nicolaie Dan Cristescu, Eduard-Marius Craciun, and Eugen Soós

Continuum Mechanics and Plasticity
by Han-Chin Wu

FORTHCOMING TITLES

Hybrid Incompatible Finite Element Methods
by Theodore H.H. Pian, Chang-Chun Wu

Microstructural Randomness in Mechanics of Materials
by Martin Ostroja Starzewski

Continuum Mechanics and Plasticity

Han-Chin Wu

CHAPMAN & HALL/CRC

A CRC Press Company

Boca Raton London New York Washington, D.C.

Library of Congress Cataloging-in-Publication Data

Wu, Han-Chin.
Continuum mechanics and plasticity / Han-Chin Wu.
p. cm. — (Modern mechanics and mathematics series ; no. 3)
Includes index.
ISBN 1-58488-363-4 (alk. paper)
1. Continuum mechanics. 2. Plasticity. I. Title. II. CRC series—modern mechanics and mathematics ; 3.

QA808.2.W8 2004
531—dc22 2004055118

International Standard Book Number 1-58488-363-4
Library of Congress Card Number 2004055118
Printed in the United States of America 1 2 3 4 5 6 7 8 9 0
Printed on acid-free paper

Contents

Preface

One of the aims of this book is to bring the subjects of continuum mechanics and plasticity together so that students will learn about the principles of continuum mechanics and how they are applied to the formulation of plasticity theory. Continuum Mechanics and Plasticity were traditionally two separate courses, and students had to make extra efforts to relate the two subjects in order to read the modern literature on plasticity. Another aim of this book is to include sufficient background material about the experimental aspect of plasticity. Experiments are presented and discussed with reference to the verification of theories. With knowledge of the experiments, the reader can make better judgments when realistic constitutive equations of plasticity are used. A third aim is to include anisotropic plasticity in this book. This important topic has not been fully discussed in most plasticity books on engineering mechanics. The final aim of the book is to incorporate research results obtained by me and my coworkers related to the endochronic theory of plasticity, so that these results can be systematically presented and better understood by readers.

Although physically based polycrystal plasticity is emerging as a feasible method, the phenomenological (continuum) approach is still the practical approach for use in the simulation of engineering problems. Most current computations use a theory of plasticity for isotropic material and work with the Cauchy stress. However, material anisotropy has long existed in real structural components and machine parts. Its effect has mostly been neglected for the sake of computational simplicity, but material anisotropy does play a significant role in the manufacturing process. A realistic description of material anisotropy may help reduce scraps in the manufacturing processes and reduce the amount of energy wasted. Also, components may be designed to possess certain predesigned anisotropy to enhance their performance.

This book addresses the issue of material anisotropy by using the contravariant true stress that is defined based on convected coordinates. A material element should be followed during anisotropic plastic deformation, where a square material element will no longer be square, and convected (curvilinear) coordinates should be used together with general tensors. The popular Cauchy stress is not useful in defining the yield criterion, because it is defined with respect to a rectangular Cartesian element. Even though recent works in computational mechanics have mostly been based on the Cartesian coordinate system, an understanding of the curvilinear coordinate system by computational mechanists and engineers will help develop computational algorithms suitable to addressing the issue of material anisotropy. Most books

that cover general tensors in curvilinear coordinates were published in the early 1960s and treat mainly elastic deformations. In this book, I devote a significant number of pages to discussing a modern theory of plasticity using curvilinear coordinates.

Recently published books address mainly computational methods and algorithms, neglecting the significance of experimental study and material anisotropy. Their purpose is to discuss efficient and stable methods and algorithms for analysis and design. In doing so, simple constitutive models are used for computational simplicity. Sometimes, unrealistic conditions, such as a nonsmooth yield function, have been discussed at length. A nonsmooth yield function has never been experimentally observed.

Owing to tremendous advances in computer technologies and methods, computational power doubles and redoubles in a short time. Consequently, there will shortly be a demand for refinements of constitutive models of plasticity. What is acceptable today will no longer be acceptable in the near future. At that time, an acceptable model will, among other things, be able to account for material anisotropy and produce results that compare well with experimental data. This book will help readers in meeting this challenge.

I taught the subjects of continuum mechanics, elasticity, and plasticity in four separate semester-long courses at the University of Iowa from 1970 to 1986. During this period, the contents of these courses were constantly updated. Since 1987, I have been teaching a two-course series to replace these four courses. This new series essentially narrows down the coverage of continuum mechanics to solids (in the sense that no special treatment of fluids and gases is included). However, it provides a more systematic and comprehensive coverage of the subject of the mechanics of solids. This book grew out of my lecture notes for the two-course series.

There were three reasons for this change at the time, and these are still valid today. (1) A modern trend: Owing to recent advances in plasticity, the methods of continuum mechanics have been used to develop new theories of plasticity or to reformulate the existing theories. Therefore, in modern literature, continuum mechanics is essential to the understanding of plasticity. (2) Reduction of the number of courses offered: The original four courses have been reduced to two. Owing to budget constraints, it has been necessary for many engineering colleges, including the College of Engineering at the University of Iowa, to reduce the number of courses offered to students. (3) Suitability for students of computational solid mechanics: Owing to advances in computing technologies and methods, students of computational solid mechanics must use modern continuum mechanics and plasticity to obtain realistic numerical solutions to their engineering problems. These students need not only courses in continuum mechanics and plasticity but also courses that are oriented toward computation and data handling. The students are limited in terms of the number of courses that they can take but still need to learn the subjects well. The two-course series based on this book fits the needs of this student group to integrate subject matter by the most efficient means possible.

The book is divided into two parts: Part I — Fundamentals of Continuum Mechanics and Part II — Continuum Theory of Plasticity. Part I (Chapters 1 to 4) is suitable for use as a textbook at the first-year graduate level for aerospace engineering, civil engineering, engineering mechanics, materials engineering, and mechanical engineering students. It is also suitable for use by advanced undergraduate students of applied mathematics. A second course may be taught to advanced graduate students from selected topics from Part II (Chapters 5 to 12). Since the book contains up-to-date materials, it may also be used by researchers and engineers as a reference book. The chapters are divided into sections and subsections. Technical terms are written in *italic* font when they first appear. Examples are given within the text when further clarification is called for, and exercise problems are given at the end of each chapter.

Mathematical fundamentals and Cartesian tensors are covered in Chapter 1; the concepts of the stress vector, the stress tensor, and stress invariants are discussed in Chapter 2; Chapter 3 discusses the kinematics of deformation; and Chapter 4 discusses the conservation laws, the constitutive equations, and elasticity. In this chapter, examples related to different stress measures are given. I have written Chapter 5 — Fundamentals of Continuum Plasticity from the viewpoint of an experimentalist with constitutive modeling in mind. The reader will acquire a general knowledge about different types of mechanical tests and the resulting material behavior in the small and large strain ranges. Potential sources of data uncertainty have been pointed out and discussed. In particular, I have discussed the hydrostatic pressure effect of yield stress and the assumption of plastic incompressibility. The reader will learn the classical flow theory of plasticity in Chapter 6. I discuss recent advances in plasticity in Chapter 7, both experimentally and theoretically. In particular, I include finite plastic deformations with various objective rates and a discussion of yield surfaces determined using different stress measures. The fundamentals of endochronic theory are given in Chapter 8 and, in Chapter 9, I present topics of endochronic theory, which include anisotropic plasticity, finite strain, porous and granular materials, and a plastically deformed damaged continuum. Anisotropic plasticity is discussed further in Chapters 10 to 12. In Chapter 10, the discussion is of sheet metals. In Chapter 11, first the fundamentals of the curvilinear coordinate system and general tensors and then the stress and strain with reference to the convected material element are discussed. Next different stress tensors and the stress rates are discussed. At the end of the chapter, a general theory of anisotropic plasticity is presented. Finally, in Chapter 12, the theory of Chapter 11 is applied to investigate the path-dependent evolution of the yield surface in the case of the combined axial-torsion of thin-walled tubes.

I learned plasticity from the late Professor Aris Phillips of Yale University, who is well known for his life-time effort to determine yield surfaces. I then had the honor and privilege of working with Professor Kirk C. Valanis, who was a senior professor and departmental chair at Iowa during the 1970s. Professor Valanis is well known for his endochronic theory of plasticity, which

at the time advocated a theory of plasticity without a yield surface. The years of working and having discussions with Kirk were most stimulating and inspiring, and he turned me into a disciple of his theory. As a result, I have spent most of my academic life in experimentally verifying and further developing the endochronic theory. During the same time, I have continued Professor Phillips's efforts in the experimental determination of yield surface, and extended them into the large strain range. There is no doubt that yield surfaces can be experimentally determined, with some data scatter. It may be more appropriate to talk about a yield band with certain amounts of uncertainty than of a yield locus. The direction of plastic strain increment is, therefore, also associated with certain amounts of uncertainty. Kirk has since shown that yield surface can be derived from the endochronic theory in a limit case. I now view yield surface as a means of getting to an approximate solution of the problem at hand. Indeed, in many cases, a theory without a yield surface can have advantages in computation since all equations are continuous.

I am indebted to the late Dr. Owen Richmond and to Dr. Paul T. Wang of Alcoa Laboratories for their continuing support of my research. The research support from the NSF, NASA, and the U.S. Army is also appreciated. I wish to express my sincere gratitude to the University of Iowa for the Career Development Award for the fall semester of the academic year 2001–2002. The award enabled me to plan for the book and start the initial part of my writing. My appreciation also extends to Professor David Y. Gao for his invitation to write this book and to Mr. Robert B. Stern, acquisitions editor and executive editor of CRC Press, for his assistance in publishing this book. Finally, I am thankful to my wife Yumi, whose love, encouragement, and patience enabled me to complete the writing of this book.

Han-Chin Wu
Iowa City, April 2004

Author

Professor Han-Chin Wu received his B.S. degree in civil engineering from National Taiwan University, his M.S. degree in structural engineering from the University of Rhode Island, and his M.S. and Ph.D. degrees in the mechanics of solids from Yale University. He has been teaching at the University of Iowa since 1970 and has supervised 19 Ph.D. students to completion. Dr. Wu is a professor in the Department of Civil and Environmental Engineering. He is also a professor of Mechanical Engineering and a fellow of American Society of Mechanical Engineers. His research interest is in the mechanical behavior (plastic flow, damage, creep, fracture, and fatigue) of metals and porous and granular materials such as porous aluminum, concretes, ice, and soils. His methods are both experimental and theoretical in an effort at constitutive modeling. He is the author of 70 journal publications and more than 100 conference papers and research reports, and he has a patent on an axial–torsional extensometer for large strain testing.

Part I

Fundamentals of Continuum Mechanics

Continuum mechanics is a branch of mechanics concerned with stresses in solids, fluids, and gas and the deformation or motion of these materials. A major assumption is that mass is continuous in a continuous medium and that the density can be defined.

1

Cartesian Tensors

1.1 Introduction

In this chapter, we discuss the basics of Cartesian tensors with the purpose of preparing the reader for subsequent chapters on continuum mechanics and plasticity. Curvilinear coordinates and general tensors as well as more advanced topics are discussed in Chapters 11 and 12.

First, we discuss the notations in detail: both *symbolic* and *index* notations are used in this book. The symbolic notations simplify the equations and will help the reader in understanding the structure of the equations as the subscripts may be confusing. However, when a set of coordinate systems has been assigned, we utilize the index notation.

We first discuss the tensor algebra, and then the differentiation and integration of tensors, which are standard materials. Some references [1–5] are given at the end of the chapter for additional reading.

1.1.1 Notations

In the symbolic notation, a *vector* is expressed by a bold-faced lowercase letter, say **a**, or by notations such as $\vec{a}$, $\breve{a}$, $\underset{\sim}{a}$, etc.; a tensor is expressed by a bold-faced capital letter, say **A**, or by notations such as $\vec{A}$, $\breve{A}$, $\underset{\sim}{A}$, etc. In the index notation, the components of a vector (the meaning of components will be discussed in Section 1.2.1) are denoted by a_i, and the components of a second-rank tensor (discussed in Section 1.3.1) are denoted by A_{ij}, or T_{ijk} for a third-rank tensor. We note that a second-rank tensor has two subscripts, a third-rank tensor has three subscripts, and an nth-rank tensor has n subscripts.

Summation and *range conventions* are used in the index notation. In the summation convention, a repeated index means summation of the term over the range of the index. For example, $A_{kk} = A_{11} + A_{22} + A_{33}$, if the range of the index is from 1 to 3. On the other hand, if the range of the index is from 1 to n, then $A_{kk} = A_{11} + A_{22} + \cdots + A_{\underline{nn}}$, a sum of n terms. We note that the underscored $\underline{n}$ does not imply summation, and the index should not repeat more than once. The notation A_{kkk}, for instance, is not defined. The repeated index

k is called a dummy index because it can be replaced by another index with no difference in its outcome. For example, $A_{kk} = A_{ii} = A_{jj} = A_{11} + A_{22} + A_{33}$.

The range convention applies when there is a free (not repeated) index in a term. The free index takes a value of 1, 2, or 3 for a three-dimensional space. Equation $y_i = C_{ij}x_j$ is actually a set of three equations, and i is the free index. You may apply the range convention as follows:

$$\begin{aligned} &\text{For } i = 1, \quad y_1 = C_{1j}x_j = C_{11}x_1 + C_{12}x_2 + C_{13}x_3 \\ &\text{For } i = 2, \quad y_2 = C_{2j}x_j = C_{21}x_1 + C_{22}x_2 + C_{23}x_3 \\ &\text{For } i = 3, \quad y_3 = C_{3j}x_j = C_{31}x_1 + C_{32}x_2 + C_{33}x_3 \end{aligned} \tag{1.1}$$

Note that the summation convention has been applied in the last equality of each of the above equations.

1.1.2 Cartesian Coordinate System

We use (x_1, x_2, x_3) instead of (x, y, z) to denote the axes of the Cartesian coordinate system. Sometimes, the coordinate axes may simply be denoted by 1, 2, and 3 in a figure. Using the index notation, the axes are x_i. Throughout this book, the right-handed coordinate system will be used.

1.1.3 Special Tensors

There are two special tensors, δ_{ij} and e_{ijk}, which are often used to simplify mathematical expressions. *Kronecker's delta* δ_{ij} is defined as

$$\begin{aligned} \delta_{ij} &= 1 \quad \text{when } i = j \\ &= 0 \quad \text{when } i \neq j \end{aligned} \tag{1.2}$$

Examples are $\delta_{11} = \delta_{22} = \delta_{33} = 1$ and $\delta_{12} = \delta_{21} = \delta_{13} = \delta_{23} = 0$, etc. Using the summation convention, we find $\delta_{ii} = \delta_{11} + \delta_{22} + \delta_{33} = 3$. In the symbolic notation, Kronecker's delta is a *unit tensor* $\mathbf{1}$, or it may be written as $\boldsymbol{\delta}$. A useful feature of Kronecker's delta is its substitution property. We can then write $\delta_{ij}\, a_{ikp} = a_{jkp}$, replacing i by j in the expression a_{ikp}.

The *permutation symbol* e_{ijk} is also known as the alternating tensor, and it is defined by

$$e_{ijk} = \begin{cases} +1 & \text{even permutation of } 1, 2, 3 \\ 0 & \text{two or more subscripts are the same} \\ -1 & \text{odd permutation of } 1, 2, 3 \end{cases} \tag{1.3}$$

Examples are $e_{123} = e_{231} = e_{312} = 1$, $e_{321} = e_{132} = e_{213} = -1$, and $e_{112} = e_{133} = e_{111} = 0$, etc.

1.2 Vectors

1.2.1 Base Vectors and Components

In three-dimensional Euclidean space, the *base vectors* are $\mathbf{e}_1$, $\mathbf{e}_2$, and $\mathbf{e}_3$. The base vectors are unit vectors in the Cartesian coordinate system and are not necessarily unit vectors in the curvilinear coordinate system (curvilinear coordinates are discussed in Chapter 11). In the Cartesian system, the base vectors are mutually perpendicular to each other. A vector $\mathbf{a}$ may be expressed as

$$\mathbf{a} = a_p \mathbf{e}_p = a_1 \mathbf{e}_1 + a_2 \mathbf{e}_2 + a_3 \mathbf{e}_3 \tag{1.4}$$

where a_p are the components of $\mathbf{a}$ relative to the basis $\mathbf{e}_p$.

1.2.2 Vector Addition and Multiplication

Vectors $\mathbf{a}$ and $\mathbf{b}$ may be added as follows:

$$\mathbf{a} + \mathbf{b} = a_p \mathbf{e}_p + b_p \mathbf{e}_p = (a_p + b_p)\mathbf{e}_p \tag{1.5}$$

There are two kinds of multiplication, the *scalar product* and the *vector product*. The scalar product, also known as the *dot product*, of two base vectors $\mathbf{e}_i$ and $\mathbf{e}_j$ is

$$\mathbf{e}_i \cdot \mathbf{e}_j = \delta_{ij} \tag{1.6}$$

Examples are, when $i = 1$ and $j = 2$, $\mathbf{e}_1 \cdot \mathbf{e}_2 = 0$, that is, $\mathbf{e}_1$ is perpendicular to $\mathbf{e}_2$; when $i = 1$ and $j = 3$, $\mathbf{e}_1 \cdot \mathbf{e}_3 = 0$, which means that $\mathbf{e}_1$ is perpendicular to $\mathbf{e}_3$. Generally, $\mathbf{e}_i$ is perpendicular to $\mathbf{e}_j$ for any permutation of i and j. The scalar product of vectors $\mathbf{a}$ and $\mathbf{b}$ is expressed by

$$\mathbf{a} \cdot \mathbf{b} = (a_p \mathbf{e}_p) \cdot (b_q \mathbf{e}_q) = a_p b_q \mathbf{e}_p \cdot \mathbf{e}_q = a_p b_q \delta_{pq} = a_p b_p \tag{1.7}$$

The outcome of the scalar multiplication is also a scalar. Using this expression, the *norm* or the magnitude of vector $\mathbf{a}$ is given by

$$|\mathbf{a}| = [\mathbf{a} \cdot \mathbf{a}]^{1/2} = [a_p a_p]^{1/2} \tag{1.8}$$

Thus, by use of (1.8), the norm of $\mathbf{e}_i$ is one.

The vector product is also known as the *cross product*. The outcome of a cross product is a vector. The cross products between Cartesian base vectors are $\mathbf{e}_2 \times \mathbf{e}_3 = \mathbf{e}_1$, $\mathbf{e}_3 \times \mathbf{e}_1 = \mathbf{e}_2$, $\mathbf{e}_1 \times \mathbf{e}_2 = \mathbf{e}_3$, which may be summarized by the following expression:

$$\mathbf{e}_i \times \mathbf{e}_j = \pm e_{ijp} \mathbf{e}_p \tag{1.9}$$

where the "+" sign applies for the right-handed coordinate system and the "−" sign applies for the left-handed coordinate system. Since the right-handed coordinate system will be used throughout this book, we will disregard the "−" sign from now on. By use of this notation, the cross product between vectors **a** and **b** becomes

$$\mathbf{a} \times \mathbf{b} = (a_p \mathbf{e}_p) \times (b_q \mathbf{e}_q) = a_p b_q \mathbf{e}_p \times \mathbf{e}_q = e_{pqr} a_p b_q \mathbf{e}_r \tag{1.10}$$

Using the dot product, the components of a vector may be found as

$$\mathbf{a} \cdot \mathbf{e}_i = a_p \mathbf{e}_p \cdot \mathbf{e}_i = a_p \delta_{pi} = a_i \tag{1.11}$$

Therefore, vector **a** may be expressed as

$$\mathbf{a} = (\mathbf{a} \cdot \mathbf{e}_p)\mathbf{e}_p \tag{1.12}$$

The scalar triple product of vectors **a**, **b**, and **c** is

$$\mathbf{a} \cdot (\mathbf{b} \times \mathbf{c}) = a_i \mathbf{e}_i \cdot e_{pqr} b_p c_q \mathbf{e}_r = e_{pqr} a_i b_p c_q \delta_{ir} = e_{pqr} a_r b_p c_q = e_{pqr} a_p b_q c_r \tag{1.13}$$

The last expression of (1.13) was obtained by permutation of indices. The scalar triple product represents the volume of an element formed by vectors **a**, **b**, and **c** as its sides.

1.2.3 The *e–δ* Identity

The following identity is known as the *e–δ identity*. This identity has been frequently applied to provide simplified expressions in vector calculus. The identity is

$$e_{ijk} e_{iqr} = \delta_{jq}\delta_{kr} - \delta_{jr}\delta_{kq} = \begin{vmatrix} \delta_{jq} & \delta_{jr} \\ \delta_{kq} & \delta_{kr} \end{vmatrix} \tag{1.14}$$

Note that i is summed.

EXAMPLE 1.1 Prove the *e–δ* identity.

Proof

We first establish the identity

$$e_{pqs} e_{mnr} = \begin{vmatrix} \delta_{mp} & \delta_{mq} & \delta_{ms} \\ \delta_{np} & \delta_{nq} & \delta_{ns} \\ \delta_{rp} & \delta_{rq} & \delta_{rs} \end{vmatrix} \tag{a}$$

To this end, we let

$$\det\ \mathbf{T} = \begin{vmatrix} T_{11} & T_{12} & T_{13} \\ T_{21} & T_{22} & T_{23} \\ T_{31} & T_{32} & T_{33} \end{vmatrix} \tag{b}$$

Since an interchange of two rows in the determinant causes a sign change, we have

$$e_{mnr} \det\ \mathbf{T} = \begin{vmatrix} T_{m1} & T_{m2} & T_{m3} \\ T_{n1} & T_{n2} & T_{n3} \\ T_{r1} & T_{r2} & T_{r3} \end{vmatrix} \tag{c}$$

An interchange of columns causes a sign change too, and we also write

$$e_{pqs} \det\ \mathbf{T} = \begin{vmatrix} T_{1p} & T_{1q} & T_{1s} \\ T_{2p} & T_{2q} & T_{2s} \\ T_{3p} & T_{3q} & T_{3s} \end{vmatrix} \tag{d}$$

For an arbitrary row and column interchange sequence, we can, therefore, write

$$e_{mnr}e_{pqs} \det \mathbf{T} = \begin{vmatrix} T_{mp} & T_{mq} & T_{ms} \\ T_{np} & T_{nq} & T_{ns} \\ T_{rp} & T_{rq} & T_{rs} \end{vmatrix} \tag{e}$$

When $T_{ij} = \delta_{ij}$ and $\det \mathbf{T} = 1$, the above equation is reduced to

$$e_{mnr}e_{pqs} = \begin{vmatrix} \delta_{mp} & \delta_{mq} & \delta_{ms} \\ \delta_{np} & \delta_{nq} & \delta_{ns} \\ \delta_{rp} & \delta_{rq} & \delta_{rs} \end{vmatrix} \tag{f}$$

which is the same as (a). The e–δ identity may then be obtained by setting $m = p$ in (f). Expanding the resulting determinant on the right-hand side of the equation, this leads to

$$\begin{aligned} e_{mnr}e_{mqs} &= \delta_{mm}(\delta_{nq}\delta_{rs} - \delta_{rq}\delta_{ns}) - \delta_{mq}(\delta_{nm}\delta_{rs} - \delta_{rm}\delta_{ns}) + \delta_{ms}(\delta_{nm}\delta_{rq} - \delta_{rm}\delta_{nq}) \\ &= \delta_{mm}(\delta_{nq}\delta_{rs} - \delta_{rq}\delta_{ns}) - 2(\delta_{nq}\delta_{rs} - \delta_{rq}\delta_{ns}) \\ &= \delta_{nq}\delta_{rs} - \delta_{rq}\delta_{ns} = \begin{vmatrix} \delta_{nq} & \delta_{ns} \\ \delta_{rq} & \delta_{rs} \end{vmatrix} \end{aligned} \tag{g}$$

which is the e–δ identity given by (1.14).

EXAMPLE 1.2 The e–δ identity may be applied to prove other identities. An example is to prove the following identity:

$$\mathbf{a} \times (\mathbf{b} \times \mathbf{c}) = \mathbf{b}(\mathbf{a} \cdot \mathbf{c}) - \mathbf{c}(\mathbf{a} \cdot \mathbf{b})$$

Proof

$$\begin{aligned}
\text{LHS} &= a_i \mathbf{e}_i \times (b_j \mathbf{e}_j \times c_k \mathbf{e}_k) = a_i \mathbf{e}_i \times (e_{rjk} b_j c_k \mathbf{e}_r) = e_{rjk} a_i b_j c_k (\mathbf{e}_i \times \mathbf{e}_r) \\
&= e_{rjk} e_{sir} a_i b_j c_k \mathbf{e}_s = e_{rjk} e_{rsi} a_i b_j c_k \mathbf{e}_s = (\delta_{js}\delta_{ki} - \delta_{ji}\delta_{ks}) a_i b_j c_k \mathbf{e}_s \\
&= \delta_{js}\delta_{ki} a_i b_j c_k \mathbf{e}_s - \delta_{ji}\delta_{ks} a_i b_j c_k \mathbf{e}_s = a_i b_j c_i \mathbf{e}_j - a_i b_i c_k \mathbf{e}_k \\
&= (a_i c_i) b_j \mathbf{e}_j - c_k \mathbf{e}_k (a_i b_i) = \text{RHS}
\end{aligned}$$

Similarly, the following identities may be proven:

$$\mathbf{a} \cdot (\mathbf{b} \times \mathbf{c}) = (\mathbf{a} \times \mathbf{b}) \cdot \mathbf{c}$$

$$(\mathbf{a} \times \mathbf{b}) \cdot (\mathbf{c} \times \mathbf{d}) = (\mathbf{a} \cdot \mathbf{c})(\mathbf{b} \cdot \mathbf{d}) - (\mathbf{a} \cdot \mathbf{d})(\mathbf{b} \cdot \mathbf{c})$$

$$(\mathbf{a} \times \mathbf{b}) \times (\mathbf{c} \times \mathbf{d}) = \mathbf{b}[\mathbf{a} \cdot (\mathbf{c} \times \mathbf{d})] - \mathbf{a}[\mathbf{b} \cdot (\mathbf{c} \times \mathbf{d})]$$

1.3 The Transformation of Axes

Consider the rectangular Cartesian coordinate system x_1, x_2, and x_3 shown in Figure 1.1. If we rotate the coordinate system through some angle about its origin O, the new coordinate axes become x_1', x_2', and x_3'. The direction cosines between x_i and x_j' are

$$Q_{ij} = \cos(x_i, x_j') \tag{1.15}$$

where the first subscript denotes the unprimed axes and the second subscript the primed axes. In general,

$$Q_{ij} \neq Q_{ji}, \quad \text{e.g.,} \quad Q_{23} \neq Q_{32}, \quad \text{or} \quad \cos(x_2, x_3') \neq \cos(x_3, x_2').$$

In the matrix form, we write Q_{ij} as

$$[Q] = \begin{bmatrix} Q_{11} & Q_{12} & Q_{13} \\ Q_{21} & Q_{22} & Q_{23} \\ Q_{31} & Q_{32} & Q_{33} \end{bmatrix} \tag{1.16}$$

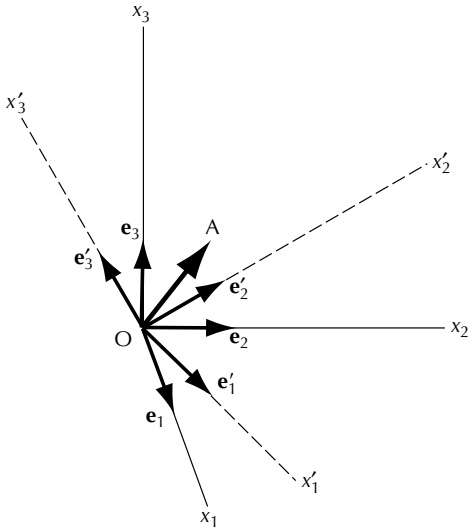

FIGURE 1.1
Transformation of coordinate systems.

We now discuss the properties of the transformation matrix $[Q]$. From vector analysis and referring to Figure 1.1, the unit vector $\overrightarrow{\mathrm{OA}}$ is expressed as

$$\overrightarrow{\mathrm{OA}} = \cos(x_1, \overrightarrow{\mathrm{OA}})\mathbf{e}_1 + \cos(x_2, \overrightarrow{\mathrm{OA}})\mathbf{e}_2 + \cos(x_3, \overrightarrow{\mathrm{OA}})\mathbf{e}_3 \tag{1.17}$$

If we take $\overrightarrow{\mathrm{OA}}$ along the x_1' direction, and denote the vector by $\mathbf{e}_1'$, then (1.17) becomes

$$\begin{aligned}\mathbf{e}_1' &= \cos(x_1, x_1')\mathbf{e}_1 + \cos(x_2, x_1')\mathbf{e}_2 + \cos(x_3, x_1')\mathbf{e}_3 \\ &= Q_{11}\mathbf{e}_1 + Q_{21}\mathbf{e}_2 + Q_{31}\mathbf{e}_3 = Q_{j1}\mathbf{e}_j\end{aligned} \tag{1.18}$$

Equation (1.18) shows that Q_{j1} are direction cosines for the unit vector $\mathbf{e}_1'$. Since the magnitude of $\overrightarrow{\mathrm{OA}}$ is one, we write

$$Q_{11}^2 + Q_{21}^2 + Q_{31}^2 = 1 \quad \text{or} \quad Q_{i1}Q_{i1} = 1 \tag{1.19}$$

Similarly, if we take $\overrightarrow{\mathrm{OA}}$ along the x_2' direction and denote the vector by $\mathbf{e}_2'$, we obtain

$$Q_{12}^2 + Q_{22}^2 + Q_{32}^2 = 1 \quad \text{or} \quad Q_{i2}Q_{i2} = 1 \tag{1.20}$$

Again, if we take $\overrightarrow{OA}$ along the x_3' direction and denote the vector by $\mathbf{e}_3'$, we get

$$Q_{13}^2 + Q_{23}^2 + Q_{33}^2 = 1 \quad \text{or} \quad Q_{i3}Q_{i3} = 1 \tag{1.21}$$

A general form of equation (1.18) is

$$\mathbf{e}_i' = Q_{ji}\mathbf{e}_j \tag{1.22}$$

Since $\mathbf{e}_i'$ and $\mathbf{e}_j'$ $(i \neq j)$ are perpendicular to each other, their dot products are zero. Therefore, from (1.22),

$$\begin{aligned}\mathbf{e}_i' \cdot \mathbf{e}_j' &= (Q_{1i}\mathbf{e}_1 + Q_{2i}\mathbf{e}_2 + Q_{3i}\mathbf{e}_3) \cdot (Q_{1j}\mathbf{e}_1 + Q_{2j}\mathbf{e}_2 + Q_{3j}\mathbf{e}_3) \\ &= Q_{1i}Q_{1j} + Q_{2i}Q_{2j} + Q_{3i}Q_{3j} = 0\end{aligned} \tag{1.23}$$

and we obtain

$$Q_{ki}Q_{kj} = 0 \quad \text{for} \quad i \neq j \tag{1.24}$$

Summarizing (1.19)–(1.21) and (1.24), we write

$$Q_{ki}Q_{kj} = \delta_{ij} \tag{1.25}$$

When $i = j$, (1.25) reduces to (1.19)–(1.21); and when $i \neq j$, (1.25) reduces to (1.24). In the matrix notation, we then have

$$[Q_{ik}]^{\mathrm{T}}[Q_{kj}] = [\delta_{ij}] \quad \text{or simply} \quad [Q]^{\mathrm{T}}[Q] = [1] \tag{1.26}$$

Note that $[Q_{ik}]^T = [Q_{ki}]$ is the *transpose* of matrix $[Q_{ik}]$. When performing matrix multiplication, the summation convention is used *adjacently*, that is, a dummy index is used for two adjacent subscripts in matrix multiplication. Equation (1.26) is an important relationship. The matrix $[Q]$ is *orthogonal*, which will be discussed further in Section 1.6.1.

In a similar manner, we can show that

$$Q_{ik}Q_{jk} = \delta_{ij} \quad \text{or} \quad [Q][Q]^{\mathrm{T}} = [1] \tag{1.27}$$

This is accomplished by taking unit vector $\overrightarrow{OA}$ along x_1, x_2, and x_3, respectively, and finding projections of $\mathbf{e}_i$ on the x_i' axes. Thus,

$$\mathbf{e}_i = Q_{i1}\mathbf{e}_1' + Q_{i2}\mathbf{e}_2' + Q_{i3}\mathbf{e}_3' = Q_{ij}\mathbf{e}_j' \tag{1.28}$$

and the magnitude of the vector is

$$Q_{\underline{i}k}Q_{\underline{i}k} = 1 \quad \text{for} \quad \underline{i} = 1, 2, 3 \tag{1.29}$$

If we consider the dot products between $\mathbf{e}_i$ and $\mathbf{e}_j$, we obtain

$$Q_{ik}Q_{jk} = 0 \quad \text{for} \quad i \neq j \tag{1.30}$$

The above two equations lead to (1.27).

We rewrite (1.22) and (1.28) here to emphasize their importance in the transformation of axes:

$$\mathbf{e}'_i = Q_{ji}\mathbf{e}_j \tag{1.22}$$

and

$$\mathbf{e}_i = Q_{ij}\mathbf{e}'_j \tag{1.28}$$

These are equations relating the base vectors of the primed and unprimed coordinate systems. In (1.22), Q_{ij}^{T} transforms a unit vector $\mathbf{e}_i$ into the unit vector $\mathbf{e}'_i$ and, in (1.28), Q_{ij} transforms the unit vector $\mathbf{e}'_i$ back into $\mathbf{e}_i$. The direction cosines Q_{ki} may also be obtained from

$$\mathbf{e}_k \cdot \mathbf{e}'_i = \mathbf{e}_k \cdot Q_{ji}\mathbf{e}_j = \delta_{kj}Q_{ji} = Q_{ki} \tag{1.29}$$

The transformation formula for vector $\mathbf{a}$ is

$$\mathbf{a} = a'_i\mathbf{e}'_i = a_j\mathbf{e}_j = a_j\, Q_{ji}\mathbf{e}'_i \quad \text{or} \quad a'_i = Q_{ji}\, a_j \tag{1.30}$$

or, in the matrix form,

$$[a'] = [Q]^{\mathrm{T}}[a] \tag{1.31}$$

The inverse relation of (1.31) is obtained by writing

$$\mathbf{a} = a_j\mathbf{e}_j = a'_i\mathbf{e}'_i = a'_iQ_{ji}\mathbf{e}_j \quad \text{or} \quad a_i = Q_{ij}a'_j \tag{1.32}$$

or, in the matrix form,

$$[a] = [Q][a'] \tag{1.33}$$

Note that the same Q_{ij} is used in both relations (1.31) and (1.33).

Finally, we note that the scalar product of vectors $\mathbf{a}$ and $\mathbf{b}$ is

$$\mathbf{a} \cdot \mathbf{b} = a'_ib'_i = Q_{ji}a_jQ_{ki}b_k = \delta_{jk}a_jb_k = a_jb_j = a_ib_i \tag{1.34}$$

We see from (1.34) that the value of $\mathbf{a} \cdot \mathbf{b}$ is independent of the coordinate system to which the components are referred. A quantity with such a property is called an *invariant*.

1.4 The Dyadic Product (The Tensor Product)

Some physical quantities require the specification of two vectors for their description. Quantities of this kind can be described by a *dyadic product*. The dyadic product of two vectors $\mathbf{u}$ and $\mathbf{v}$ is written as $\mathbf{u} \otimes \mathbf{v}$. It has the *associative* and *distributive properties* given by

$$\begin{aligned} &(\alpha\mathbf{u}) \otimes \mathbf{v} = \mathbf{u} \otimes (\alpha\mathbf{v}) = \alpha(\mathbf{u} \otimes \mathbf{v}) \\ &\mathbf{u} \otimes (\mathbf{v} + \mathbf{w}) = \mathbf{u} \otimes \mathbf{v} + \mathbf{u} \otimes \mathbf{w}, \qquad (\mathbf{v} + \mathbf{w}) \otimes \mathbf{u} = \mathbf{v} \otimes \mathbf{u} + \mathbf{w} \otimes \mathbf{u} \end{aligned} \tag{1.35}$$

where α is a scalar. In terms of the components of $\mathbf{u}$ and $\mathbf{v}$, $\mathbf{u} \otimes \mathbf{v}$ may be written as

$$\begin{aligned} \mathbf{u} \otimes \mathbf{v} &= (u_i\mathbf{e}_i) \otimes (v_j\mathbf{e}_j) = u_iv_j\mathbf{e}_i \otimes \mathbf{e}_j \\ &= u_1v_1\mathbf{e}_1 \otimes \mathbf{e}_1 + u_1v_2\mathbf{e}_1 \otimes \mathbf{e}_2 + u_1v_3\mathbf{e}_1 \otimes \mathbf{e}_3 \\ &\quad + u_2v_1\mathbf{e}_2 \otimes \mathbf{e}_1 + u_2v_2\mathbf{e}_2 \otimes \mathbf{e}_2 + u_2v_3\mathbf{e}_2 \otimes \mathbf{e}_3 \\ &\quad + u_3v_1\mathbf{e}_3 \otimes \mathbf{e}_1 + u_3v_2\mathbf{e}_3 \otimes \mathbf{e}_2 + u_3v_3\mathbf{e}_3 \otimes \mathbf{e}_3 \end{aligned} \tag{1.36}$$

The components of $\mathbf{u} \otimes \mathbf{v}$ are u_iv_j, which can be displayed in a matrix:

$$[\mathbf{u} \otimes \mathbf{v}] = \begin{bmatrix} u_1v_1 & u_1v_2 & u_1v_3 \\ u_2v_1 & u_2v_2 & u_2v_3 \\ u_3v_1 & u_3v_2 & u_3v_3 \end{bmatrix} \tag{1.37}$$

The dyadic products $\mathbf{e}_i \otimes \mathbf{e}_j$ of the base vectors $\mathbf{e}_i$ are called *unit dyads*. Thus, the dyadic product $\mathbf{u} \otimes \mathbf{v}$ is expressed in (1.36) in terms of its components u_iv_j and its bases $\mathbf{e}_i \otimes \mathbf{e}_j$.

The form of (1.36) is independent of the choice of the coordinate system. Using (1.22, 1.27, 1.30), we obtain

$$\begin{aligned} u'_iv'_j\mathbf{e}'_i \otimes \mathbf{e}'_j &= Q_{pi}u_pQ_{qj}v_qQ_{ri}\mathbf{e}_r \otimes (Q_{sj}\mathbf{e}_s) = Q_{pi}Q_{ri}Q_{qj}Q_{sj}u_pv_q\mathbf{e}_r \otimes \mathbf{e}_s \\ &= \delta_{pr}\delta_{qs}u_pv_q\mathbf{e}_r \otimes \mathbf{e}_s = u_rv_s\mathbf{e}_r \otimes \mathbf{e}_s = u_iv_j\mathbf{e}_i \otimes \mathbf{e}_j \end{aligned} \tag{1.38}$$

In general, the commutative law is not valid, that is, $\mathbf{u} \otimes \mathbf{v} \neq \mathbf{v} \otimes \mathbf{u}$. An additional property of a dyadic product is that it forms an inner product with a vector. We may take the following relations as definitions:

$$(\mathbf{u} \otimes \mathbf{v}) \cdot \mathbf{w} = \mathbf{u}(\mathbf{v} \cdot \mathbf{w}), \qquad \mathbf{u} \cdot (\mathbf{v} \otimes \mathbf{w}) = (\mathbf{u} \cdot \mathbf{v})\mathbf{w} \tag{1.39}$$

These relations may also be written as

$$\mathbf{u} \otimes \mathbf{v} \cdot \mathbf{w} = \mathbf{u}(\mathbf{v} \cdot \mathbf{w}), \qquad \mathbf{u} \cdot \mathbf{v} \otimes \mathbf{w} = (\mathbf{u} \cdot \mathbf{v})\mathbf{w} \tag{1.40}$$

since there is no possibility of ambiguity. We see in (1.39) and (1.40) that an inner product of a dyadic product with a vector yields another vector.

The concept of a dyadic product can be extended to products of three or more vectors. Thus, the product of three vectors $\mathbf{u}$, $\mathbf{v}$, and $\mathbf{w}$ is a *triad* and is written $\mathbf{u} \otimes \mathbf{v} \otimes \mathbf{w}$. Similarly, we can define *tetrads* or higher-order *polyads*. The triad $\mathbf{u} \otimes \mathbf{v} \otimes \mathbf{w}$ in its component form is written as $u_i v_j w_k \mathbf{e}_i \otimes \mathbf{e}_j \otimes \mathbf{e}_k$.

1.5 Cartesian Tensors

1.5.1 General Properties

We define a *second-rank (order) Cartesian tensor* as a linear combination of dyadic products. Since, from (1.36), a dyadic product is itself a linear combination of unit dyads, a second-rank Cartesian tensor $\mathbf{T}$ can be expressed as a linear combination of unit dyads. This definition of a Cartesian tensor is equivalent to defining the tensor as a linear transformation that transforms a vector into another vector. We see from (1.39) that $\mathbf{u} \otimes \mathbf{v}$ transforms a vector into another vector and, from (1.35), that it obeys the associative and distributive properties of a linear transformation. Therefore, $\mathbf{u} \otimes \mathbf{v}$ is a tensor. In the component form, tensor $\mathbf{T}$ is written as

$$\mathbf{T} = T_{ij}\mathbf{e}_i \otimes \mathbf{e}_j = T_{11}\mathbf{e}_1 \otimes \mathbf{e}_2 + T_{12}\mathbf{e}_1 \otimes \mathbf{e}_2 + T_{13}\mathbf{e}_1 \otimes \mathbf{e}_3 + T_{21}\mathbf{e}_2 \otimes \mathbf{e}_1 + \cdots \tag{1.41}$$

The coefficients T_{ij} are called the *components* of $\mathbf{T}$. We will denote tensor components by the same letter that we use to denote the tensor itself and remark that a tensor exists independently of any coordinate system. Its components can only be specified after a coordinate system has been chosen, and the values of the components depend on the choice of the coordinate system. If, in a new coordinate system with base vectors $\mathbf{e}'_i$, tensor $\mathbf{T}$ has components T'_{ij}, then from (1.41)

$$\mathbf{T} = T_{ij}\mathbf{e}_i \otimes \mathbf{e}_j = T'_{pq}\mathbf{e}'_p \otimes \mathbf{e}'_q \tag{1.42}$$

But, by use of (1.28),

$$T_{ij}\mathbf{e}_i \otimes \mathbf{e}_j = T_{ij}Q_{ip}Q_{jq}\mathbf{e}'_p \otimes \mathbf{e}'_q \tag{1.43}$$

Therefore, by equating the above two equations, their coefficients are related by

$$T'_{pq} = Q_{ip}Q_{jq}T_{ij} \quad \text{or} \quad T'_{pq} = Q^{\mathrm{T}}_{pi}T_{ij}Q_{jq} \tag{1.44}$$

This is the *transformation formula* for components of second-rank tensors. Equation (1.44) may also be considered as an alternative definition of a second-rank tensor. In order to identify a second-rank tensor as such, we may show that its components transform according to (1.44) from one coordinate system, x_i, to another, x_i'. The nine components of T_{ij} may be displayed in a 3×3 square matrix $[T]$, so that the above equation may be written in a matrix equation as

$$[T'] = [Q]^{\mathrm{T}}[T][Q]. \tag{1.45}$$

The matrix form is often convenient for algebraic manipulation.

We now extend the relation (1.41) to express a Cartesian tensor of rank (order) n in terms of components as

$$\mathbf{T} = T_{ij\cdots m}\mathbf{e}_i \otimes \mathbf{e}_j \otimes \cdots \otimes \mathbf{e}_m \tag{1.46}$$

Note that the components $T_{ij\ldots m}$ have n indices and the tensor product has n factors. The components of this nth-rank tensor transform according to the rule

$$T'_{pq\ldots t} = Q_{ip}Q_{jq}\cdots Q_{mt}T_{ij\ldots m} \tag{1.47}$$

From this more general viewpoint, a scalar can be interpreted as a tensor of rank zero, since it has a single component which is unchanged in a coordinate transformation; a vector is considered as a tensor of rank one. Most of the tensors we encounter in this book will be of rank zero (scalars), one (vectors), or two. We will also discuss some fourth-rank tensors due to their importance in continuum mechanics.

The inverse relation to (1.44) is

$$T_{ij} = Q_{ip}Q_{jq}T'_{pq} \quad \text{or} \quad T_{ij} = Q_{ip}T'_{pq}Q^T_{qj} \tag{1.48}$$

Or, in the matrix form, it is written as

$$[T] = [Q][T'][Q]^{\mathrm{T}} \tag{1.49}$$

We also note that the inverse of (1.47) is

$$T_{ij\ldots m} = Q_{ip}Q_{jq}\cdots Q_{mt}T'_{pq\ldots t} \tag{1.50}$$

For a second-rank tensor $\mathbf{T}$, the transpose of $\mathbf{T}$ is defined as

$$\mathbf{T}^{\mathrm{T}} = T_{ij}\mathbf{e}_j \otimes \mathbf{e}_i = T_{ji}\mathbf{e}_i \otimes \mathbf{e}_j \tag{1.51}$$

Tensor $\mathbf{T}$ is symmetric if $\mathbf{T} = \mathbf{T}^{\mathrm{T}}$. Thus, from (1.41) and (1.51), we find $T_{ij} = T_{ji}$ for a symmetric $\mathbf{T}$. With reference to the x_i' system, we have, from (1.44),

$$T'_{qp} = Q_{iq}Q_{jp}T_{ij} = Q_{jp}Q_{iq}T_{ji} = T'_{pq} \tag{1.52}$$

which proves the symmetry with respect to the primed coordinate system. We may conclude that if a tensor is symmetric with reference to one Cartesian system, then it has symmetric components with reference to all Cartesian coordinate systems. Similarly, if $\mathbf{T} = -\mathbf{T}^{\mathrm{T}}$, then $T_{ij} = -T_{ji}$, and $\mathbf{T}$ is an antisymmetric second-rank tensor. An antisymmetric tensor has components

$$\begin{bmatrix} 0 & T_{12} & T_{13} \\ -T_{12} & 0 & T_{23} \\ -T_{13} & -T_{23} & 0 \end{bmatrix} \tag{1.53}$$

Finally, we remark that any second-rank tensor can be decomposed into the sum of a symmetric and an antisymmetric tensor, and that this decomposition is unique. We write

$$\mathbf{T} = \tfrac{1}{2}(\mathbf{T} + \mathbf{T}^{\mathrm{T}}) + \tfrac{1}{2}(\mathbf{T} - \mathbf{T}^{\mathrm{T}}) \tag{1.54}$$

The tensor $(\mathbf{T} + \mathbf{T}^{\mathrm{T}})$ is symmetric and the tensor $(\mathbf{T} - \mathbf{T}^{\mathrm{T}})$ is antisymmetric. We also mention that an identity tensor $\mathbf{I}$ is a special case, where $T_{ij} = \delta_{ij}$. Thus, the identity tensor is written as

$$\mathbf{I} = \mathbf{e}_1 \otimes \mathbf{e}_1 + \mathbf{e}_2 \otimes \mathbf{e}_2 + \mathbf{e}_3 \otimes \mathbf{e}_3 \tag{1.55}$$

with

$$\mathbf{T} \cdot \mathbf{I} = \mathbf{T} \tag{1.56}$$

EXAMPLE 1.3 Show that an arbitrary tensor $\mathbf{A}$ can be expressed as the sum of a *spherical tensor* (i.e., a scalar times the identity tensor) and a tensor with zero trace (trace $\mathbf{A} = A_{ii}$). Prove that this decomposition is unique, and that $\mathbf{A}'$, the traceless part of $\mathbf{A}$, is given by $\mathbf{A}' = \mathbf{A} - \frac{1}{3}(\mathrm{tr}\,\mathbf{A})\mathbf{I}$, where $\mathbf{A}'$ is the *deviator* of $\mathbf{A}$.

Solution

Define

$$\mathbf{B} = \mathbf{A} - \tfrac{1}{3}(\mathrm{tr}\,\mathbf{A})\mathbf{I} \quad \text{and} \quad \mathbf{C} = \tfrac{1}{3}(\mathrm{tr}\,\mathbf{A})\mathbf{I} \tag{a}$$

then

$$\mathbf{A} = \mathbf{B} + \mathbf{C} \tag{b}$$

and $\mathbf{C}$ is a spherical tensor. We now take the trace of the first equation of (a) and get

$$\operatorname{tr}\mathbf{B} = \operatorname{tr}\{\mathbf{A} - \tfrac{1}{3}(\operatorname{tr}\mathbf{A})\mathbf{I}\} = \operatorname{tr}\mathbf{A} - \operatorname{tr}\tfrac{1}{3}(\operatorname{tr}\mathbf{A})\mathbf{I} = \operatorname{tr}\mathbf{A} - \tfrac{1}{3}(\operatorname{tr}\mathbf{A})(3) = 0 \quad \text{(c)}$$

Therefore, $\mathbf{B}$ is traceless, and from (b) $\mathbf{A}$ is the sum of a spherical tensor and a traceless tensor.

To prove the uniqueness, we first assume that this decomposition is not unique. Then, there exists a spherical tensor $\mathbf{D}$ and a traceless tensor $\mathbf{E}$ such that

$$\mathbf{A} = \mathbf{D} + \mathbf{E} \quad \text{(d)}$$

We take the trace of (d) and (b) to find

$$\operatorname{tr}\mathbf{A} = \operatorname{tr}\mathbf{D} + \operatorname{tr}\mathbf{E} = \operatorname{tr}\mathbf{D} = \operatorname{tr}\mathbf{C} \quad \text{(e)}$$

because $\mathbf{E}$ and $\mathbf{B}$ are traceless. Since both $\mathbf{D}$ and $\mathbf{C}$ are spherical tensors, we write

$$\mathbf{D} = D\mathbf{I} \quad \text{and} \quad \mathbf{C} = C\mathbf{I} \quad \text{(f)}$$

where both D and C are scalars. Using (e) and taking the trace of (f), we find $D = C$, that is, $\mathbf{D} = \mathbf{C}$. This leads to $\mathbf{E} = \mathbf{B}$, which proves that the decomposition is unique.

1.5.2 Multiplication of Tensors

Consider a vector $\mathbf{s} = s_i\mathbf{e}_i$ and a second-rank tensor $\mathbf{T} = T_{ij}\mathbf{e}_i \otimes \mathbf{e}_j$ in a coordinate system with base vectors $\mathbf{e}_i$. In a new system with base vectors $\mathbf{e}'_i = Q_{ji}\mathbf{e}_j$, vector $\mathbf{s}$ and tensor $\mathbf{T}$ have components s'_i and T'_{ij}, respectively, so that

$$s'_i = Q_{mi}s_m, \quad T'_{ij} = Q_{ri}Q_{sj}T_{rs} \quad (1.57)$$

The *outer product* of the vector $\mathbf{s}$ and the tensor $\mathbf{T}$ is defined by

$$\mathbf{W} = \mathbf{s} \otimes \mathbf{T} = s_i\mathbf{e}_i \otimes T_{jk}\mathbf{e}_j \otimes \mathbf{e}_k = s_iT_{jk}\mathbf{e}_i \otimes \mathbf{e}_j \otimes \mathbf{e}_k = W_{ijk}\mathbf{e}_i \otimes \mathbf{e}_j \otimes \mathbf{e}_k \quad (1.58)$$

Therefore, the outer product is a third-rank tensor with components given by $W_{ijk} = s_iT_{jk}$. Referring to the new coordinate system, we write

$$\mathbf{W} = \mathbf{s} \otimes \mathbf{T} = s'_iT'_{jk}\mathbf{e}'_i \otimes \mathbf{e}'_j \otimes \mathbf{e}'_k = W'_{ijk}\mathbf{e}'_i \otimes \mathbf{e}'_j \otimes \mathbf{e}'_k \quad (1.59)$$

Hence, $W'_{ijk} = s'_i T'_{jk}$. If we substitute $\mathbf{e}'_i = Q_{ji}\mathbf{e}_j$ into the above equation, we can establish the following transformation formula for the components W_{ijk}:

$$W'_{ijk} = Q_{pi}Q_{rj}Q_{sk}W_{prs} \tag{1.60}$$

We note that the order of multiplication is important and that $\mathbf{s} \otimes \mathbf{T} \neq \mathbf{T} \otimes \mathbf{s}$.

Similarly, the outer product of second-rank tensors $\mathbf{P}$ and $\mathbf{S}$ is

$$\begin{aligned}\mathbf{R} = \mathbf{P} \otimes \mathbf{S} &= P_{ij}\mathbf{e}_i \otimes \mathbf{e}_j \otimes S_{km}\mathbf{e}_k \otimes \mathbf{e}_m = P_{ij}S_{km}\mathbf{e}_i \otimes \mathbf{e}_j \otimes \mathbf{e}_k \otimes \mathbf{e}_m \\ &= R_{ijkm}\mathbf{e}_i \otimes \mathbf{e}_j \otimes \mathbf{e}_k \otimes \mathbf{e}_m\end{aligned} \tag{1.61}$$

and the components are $R_{ijkm} = P_{ij}S_{km}$. $\mathbf{R}$ is a fourth-rank tensor. In a similar manner, we may form the outer products of three or more tensors or vectors. The outer product of a tensor of rank p with a tensor of rank q is a tensor of rank $p + q$. We note that the dyadic product of two vectors is a special case, because vectors are tensors of rank one.

If we equate the last two indices of third-rank tensor W_{ijk}, we obtain

$$W'_{ijj} = W'_{i11} + W'_{i22} + W'_{i33} \tag{1.62}$$

in which i is a free index and can take values of $i = 1, 2, 3$. Using the components transformation formula, we have

$$W'_{ijj} = Q_{pi}Q_{rj}Q_{sj}W_{prs} = Q_{pi}\delta_{rs}W_{prs} = Q_{pi}W_{prr} \tag{1.63}$$

Thus, the components W_{prr} transform as the components of a vector. This operation of reducing the rank of tensor by two by summing on two indices is called *contraction* of the tensor. In (1.63), a third-rank tensor is reduced to a vector by contraction. In the case of a tensor of rank n with components $W_{ijkm\ldots rs}$, if we sum on any pair of its indices such as $k = r$, then the resulting quantities $W_{ijrm\ldots rs}$, are the components of a tensor of rank $n-2$. In particular, contraction of a second-rank tensor T_{ij} leads to T_{ii}, a scalar.

The outer product followed by a contraction leads to an *inner product*. The inner product of vector $\mathbf{s}$ and tensor $\mathbf{T}$ is

$$\mathbf{s} \cdot \mathbf{T} = s_i T_{ik}\mathbf{e}_m \otimes \mathbf{e}_m \otimes \mathbf{e}_k = s_i T_{ik}\mathbf{e}_k \tag{1.64}$$

where the relation $\mathbf{e}_m \otimes \mathbf{e}_m = I$ is applied, in which $\mathbf{I}$ is the identity tensor. The inner product formed by a different order is

$$\mathbf{T} \cdot \mathbf{s} = T_{ij}s_j\mathbf{e}_i \otimes \mathbf{e}_m \otimes \mathbf{e}_m = T_{ij}s_j\mathbf{e}_i = s_i T_{ki}\mathbf{e}_k \tag{1.65}$$

Comparing the two equations given above, we see that $\mathbf{s} \cdot \mathbf{T} = \mathbf{T} \cdot \mathbf{s}$ only if $\mathbf{T}$ is a symmetric tensor. A similar procedure may be applied to form inner

products of second- and higher-rank tensors. From second-rank tensors $\mathbf{U}$ and $\mathbf{V}$, various inner products can be formed, such as

$$\mathbf{U} \cdot \mathbf{V} = U_{ij}V_{jk}\mathbf{e}_i \otimes \mathbf{e}_k, \qquad \mathbf{U}^{\mathrm{T}} \cdot \mathbf{V} = U_{ji}V_{jk}\mathbf{e}_i \otimes \mathbf{e}_k \tag{1.66}$$

These inner products are second-rank tensors. A useful relation involving the inner product is

$$(\mathbf{U} \cdot \mathbf{V})^{\mathrm{T}} = \mathbf{V}^{\mathrm{T}} \cdot \mathbf{U}^{\mathrm{T}} \tag{1.67}$$

Using the concept of inner product, we may derive an expression for the components T_{ij} of a second-rank tensor $\mathbf{T}$. Based on (1.41), we may form the following inner product

$$\begin{aligned} \mathbf{e}_i \cdot \mathrm{T} \cdot \mathbf{e}_j &= \mathbf{e}_i \cdot T_{pq}\mathbf{e}_p \otimes \mathbf{e}_q \cdot \mathbf{e}_j = T_{pq}\mathbf{e}_i \cdot \mathbf{e}_p \otimes \mathbf{e}_q \cdot \mathbf{e}_j \\ &= T_{pq}\mathbf{e}_i \cdot \mathbf{e}_p(\mathbf{e}_q \cdot \mathbf{e}_j) = T_{pq}\mathbf{e}_i \cdot \mathbf{e}_p\delta_{qj} = T_{pq}\delta_{ip}\delta_{qj} = T_{ij} \end{aligned} \tag{1.68}$$

Therefore, the component T_{ij} of tensor $\mathbf{T}$ is given by

$$T_{ij} = \mathbf{e}_i \cdot \mathbf{T} \cdot \mathbf{e}_j \tag{1.69}$$

It can be further shown that, from (1.69), we can obtain the following expression

$$\mathbf{T} \cdot \mathbf{e}_j = T_{pj}\mathbf{e}_p \tag{1.70}$$

1.5.3 The Component Form and Matrices

Matrix operation can be conveniently used to perform transformation of tensor components from one coordinate system to another. For this purpose, we express a tensor equation in terms of a matrix equation in this section. Consider

$$\mathbf{w} = \mathbf{T} \cdot \mathbf{v} \tag{1.71}$$

where $\mathbf{T}$ transforms vector $\mathbf{v}$ into vector $\mathbf{w}$. This equation may be written as

$$w_i\mathbf{e}_i = \mathbf{T} \cdot v_j\mathbf{e}_j = v_jT_{ij}\mathbf{e}_i \tag{1.72}$$

Thus, the components of (1.72) may be arranged in a matrix equation as

$$[w_i] = [T_{ij}][v_j] \tag{1.73}$$

where w_i and v_i may be arranged as the elements of two 3×1 column matrices $[w_i] = [w_1, w_2, w_3]^{\mathrm{T}}$, $[v_i] = [v_1, v_2, v_3]^{\mathrm{T}}$, whereas $[T_{ij}]$ is a 3×3 square matrix. In the case of equation

$$\mathbf{R} = \mathbf{S} \cdot \mathbf{T} \tag{1.74}$$

where **R**, **S**, and **T** are second-rank tensors, we write

$$\mathbf{R} \cdot \mathbf{e}_i = \mathbf{S} \cdot \mathbf{T} \cdot \mathbf{e}_i \tag{1.75}$$

By use of (1.70), we have

$$R_{ji}\mathbf{e}_j = \mathbf{S} \cdot (T_{ji}\mathbf{e}_j) = T_{ji}(\mathbf{S} \cdot \mathbf{e}_j) = T_{ji}S_{kj}\mathbf{e}_k \quad \text{or} \quad R_{ki}\mathbf{e}_k = T_{ji}S_{kj}\mathbf{e}_k \tag{1.76}$$

The component form is now

$$R_{ki} = S_{kj}T_{ji} \tag{1.77}$$

and the matrix form is

$$[R_{ik}] = [S_{ij}][T_{jk}] \tag{1.78}$$

1.5.4 Quotient Law

The *quotient law* may be used to test whether the elements of a set of quantities $A(i, j, k)$ are components of a tensor. If the inner product (summation over i) between $A(i, j, k)$ and an arbitrary tensor, say b_i, is known to yield a tensor C_{jk}, that is,

$$A(i, j, k)b_i = C_{jk} \tag{1.79}$$

then $A(i, j, k)$ is a tensor of type A_{ijk}. Referring to the x'_i coordinate system, the above equation is written as

$$A'(i, j, k)b'_i = C'_{jk} \tag{1.80}$$

Since b'_i and C'_{jk} are both tensors, they obey tensor transformation rules given by (1.30) and (1.44), respectively. By substitution, we obtain

$$A'(i, j, k)b'_i = Q_{pj}Q_{qk}C_{pq} = Q_{pj}Q_{qk}A(r, p, q)b_r = Q_{pj}Q_{qk}A(r, p, q)Q_{ri}b'_i \tag{1.81}$$

or

$$[A'(i, j, k) - Q_{ri}Q_{pj}Q_{qk}A(r, p, q)]b'_i = 0 \tag{1.82}$$

Since b_i^l is an arbitrary tensor and is generally not zero, we conclude that the quantity within the brackets must vanish. Therefore,

$$A'(i,j,k) = Q_{ri}Q_{pj}Q_{qk}A(r,p,q) \tag{1.83}$$

which is the transformation rule for a tensor of type A_{ijk}. This method may be used to test higher rank tensors.

1.6 Rotation of a Tensor

1.6.1 Orthogonal Tensor

The inverse to tensor $\mathbf{T}$ is denoted by $\mathbf{T}^{-1}$, so that

$$\mathbf{T}\cdot\mathbf{T}^{-1} = \mathbf{I} \quad \text{and} \quad \mathbf{T}^{-1}\cdot\mathbf{T} = \mathbf{I} \tag{1.84}$$

In the case that the transpose of $\mathbf{T}$ is equal to the inverse of $\mathbf{T}$, that is,

$$\mathbf{T}^{\mathrm{T}} = \mathbf{T}^{-1} \tag{1.85}$$

then $\mathbf{T}$ is said to be an *orthogonal tensor*. Therefore, for an orthogonal tensor, we have

$$\mathbf{T}\cdot\mathbf{T}^{\mathrm{T}} = \mathbf{I} \quad \text{and} \quad \mathbf{T}^{\mathrm{T}}\cdot\mathbf{T} = \mathbf{I} \qquad \text{with} \quad \det\mathbf{T} = \pm 1 \tag{1.86}$$

where the "+" sign denotes a proper orthogonal transformation (right-handed coordinate system) and the "−" sign denotes an improper orthogonal transformation (left-handed coordinate system).

We now consider the transformation tensor $\mathbf{Q}$ discussed in Section 1.3. Since $\mathbf{Q}$ satisfies (1.86), it is an orthogonal tensor. For the purpose of investigating physical properties of $\mathbf{Q}$, consider two vectors $\mathbf{u}$ and $\mathbf{v}$ transformed by $\mathbf{Q}$:

$$\bar{\mathbf{u}} = \mathbf{Q}\cdot\mathbf{u}, \qquad \bar{\mathbf{v}} = \mathbf{Q}\cdot\mathbf{v} \tag{1.87}$$

The inner products $\mathbf{Q}\cdot\mathbf{u}$ and $\mathbf{Q}\cdot\mathbf{v}$ may be viewed as linear transformations of vectors $\mathbf{u}$ and $\mathbf{v}$ by tensor $\mathbf{Q}$. The scalar product of $\mathbf{u}$ and $\mathbf{v}$ is

$$\bar{\mathbf{u}}\cdot\bar{\mathbf{v}} = (\mathbf{Q}\cdot\mathbf{u})\cdot(\mathbf{Q}\cdot\mathbf{v}) = \mathbf{v}\cdot\mathbf{Q}^{\mathrm{T}}\cdot(\mathbf{Q}\cdot\mathbf{u}) = \mathbf{u}\cdot\mathbf{v} \tag{1.88}$$

which is unchanged under an orthogonal transformation $\mathbf{Q}$. The second equality in (1.88) was a result obtained from the definition of the transpose of a tensor given by $\mathbf{a}\cdot(\mathbf{A}^{\mathrm{T}}\cdot\mathbf{b}) = \mathbf{b}\cdot(\mathbf{A}\cdot\mathbf{a})$.

A special case of the above discussion is $\mathbf{u} = \mathbf{v}$ and $\bar{\mathbf{u}} = \bar{\mathbf{v}}$. Here, (1.88) reduces to

$$\bar{\mathbf{v}} \cdot \bar{\mathbf{v}} = (\mathbf{Q} \cdot \mathbf{v}) \cdot (\mathbf{Q} \cdot \mathbf{v}) = \mathbf{v} \cdot \mathbf{v} \tag{1.89}$$

or

$$|\bar{\mathbf{v}}| = |\mathbf{v}| \tag{1.90}$$

Therefore, the magnitude of a vector is unchanged by an orthogonal transformation. Furthermore, the angle ϕ between the two vectors is expressed by

$$\cos\phi = \frac{\mathbf{u} \cdot \mathbf{v}}{|\mathbf{u}||\mathbf{v}|} = \frac{\bar{\mathbf{u}} \cdot \bar{\mathbf{v}}}{|\bar{\mathbf{u}}||\bar{\mathbf{v}}|} \tag{1.91}$$

which means that the angle between the vectors is also unchanged. Thus, an orthogonal transformation rotates a vector and the components Q_{ij} are the direction cosines.

EXAMPLE 1.4 Show that $(\mathbf{Q} \cdot \mathbf{u}) \cdot (\mathbf{Q} \cdot \mathbf{v}) = \mathbf{u} \cdot \mathbf{v}$.

$$\begin{aligned} \text{LHS} &= (Q_{ij}\mathbf{e}_i \otimes \mathbf{e}_j \cdot u_k\mathbf{e}_k) \cdot (Q_{mn}\mathbf{e}_m \otimes \mathbf{e}_n \cdot v_p\mathbf{e}_p) = Q_{ij}Q_{mn}u_kv_p\mathbf{e}_i\delta_{jk}\mathbf{e}_m\delta_{np} \\ &= Q_{ij}u_jQ_{mn}v_n\delta_{im} = Q_{ij}Q_{in}u_jv_n = \delta_{jn}u_jv_n = u_jv_j = \mathbf{u} \cdot \mathbf{v} = \text{RHS} \end{aligned}$$

EXAMPLE 1.5 Define the transpose of tensor $\mathbf{A}$ by $\mathbf{a} \cdot (\mathbf{A}^{\mathrm{T}} \cdot \mathbf{b}) = \mathbf{b} \cdot (\mathbf{A} \cdot \mathbf{a})$ and shows that it leads to

$$(\mathbf{A}^{\mathrm{T}})^{\mathrm{T}} = \mathbf{A}.$$

By use of (1.65), we have

$$\begin{aligned} \text{LHS} &= \mathbf{a} \cdot (A^{\mathrm{T}}_{ij}b_j\mathbf{e}_i) = a_k\mathbf{e}_k \cdot A^{\mathrm{T}}_{ij}b_j\mathbf{e}_i = a_kA^{\mathrm{T}}_{ij}b_j\delta_{ki} = a_iA^{\mathrm{T}}_{ij}b_j \\ \text{RHS} &= \mathbf{b} \cdot (A_{ij}a_j\mathbf{e}_i) = b_k\mathbf{e}_k \cdot A_{ij}a_j\mathbf{e}_i = b_kA_{ij}a_j\delta_{ki} = b_iA_{ij}a_j \\ &= a_jA_{ij}b_i = a_iA_{ji}b_j \end{aligned}$$

Since the two sides are equal, we obtain $A^{\mathrm{T}}_{ij} = A_{ji}$, that is, the transpose of a matrix is the same as the interchange of the two indices. We then have $(A^{\mathrm{T}}_{ij})^{\mathrm{T}} = A_{ij}$ and we can write

$$\mathbf{A}^{\mathrm{T}} = A^{\mathrm{T}}_{ij}\mathbf{e}_i \otimes \mathbf{e}_j = A_{ji}\mathbf{e}_i \otimes \mathbf{e}_j \quad \text{and} \quad (\mathbf{A}^{\mathrm{T}})^{\mathrm{T}} = A_{ij}\mathbf{e}_i \otimes \mathbf{e}_j = \mathbf{A}$$

1.6.2 Component Form of Rotation of a Tensor

In this section, we derive the component form that describes the rotation of a tensor, and we point out that this transformation equation is different from the one which describes the change of bases. In the case of transformation of bases, it has been shown in Sections 1.2.3 and 1.2.5 that the components transform by

$$[v_i'] = [Q_{ij}]^{\mathrm{T}}[v_j] \quad \text{and} \quad [v_i] = [Q_{ij}][v_j'] \tag{1.92}$$

for a vector v_i, and by

$$[T_{ij}'] = [Q_{ip}]^{\mathrm{T}}[T_{pq}][Q_{qj}] \quad \text{and} \quad [T_{ij}] = [Q_{ip}][T_{pq}'][Q_{qj}]^{\mathrm{T}} \tag{1.93}$$

for a tensor T_{ij}.

By applying rotation $\mathbf{Q}$ to vector $\mathbf{v}$, we write

$$\bar{\mathbf{v}} = \mathbf{Q} \cdot \mathbf{v} \tag{1.94}$$

Thus, vector $\mathbf{v}$ is rotated by $\mathbf{Q}$ into $\bar{\mathbf{v}}$. If the same $\mathbf{Q}$ has rotated the bases $\mathbf{e}_i$ into $\mathbf{e}_i'$, we can write

$$\bar{\mathbf{v}} = \bar{\mathrm{v}}_i'\mathbf{e}_i' = \mathbf{Q} \cdot \mathbf{v} = \mathbf{Q} \cdot v_i\mathbf{e}_i = v_i(\mathbf{Q} \cdot \mathbf{e}_i) = v_i\mathbf{e}_i' \tag{1.95}$$

Therefore,

$$\bar{\mathrm{v}}_i' = v_i \tag{1.96}$$

Equation (1.96) shows that the components of $\bar{\mathbf{v}}$ in $\mathbf{e}_i'$ are the same as those of $\mathbf{v}$ in $\mathbf{e}_i$. This result is obvious, because both the vector and the coordinate system have been rotated by the same amount and their relative positions remain the same. Consider next the components of $\bar{\mathbf{v}}$ in $\mathbf{e}_i$:

$$\bar{\mathbf{v}} = \bar{v}_i\mathbf{e}_i = \mathbf{Q} \cdot \mathbf{v} = \mathbf{Q} \cdot v_i\mathbf{e}_i = v_iQ_{ji}\mathbf{e}_j = v_jQ_{ij}\mathbf{e}_i \tag{1.97}$$

Thus,

$$[\bar{\mathrm{v}}_i] = [Q_{ij}][v_j] \tag{1.98}$$

Note that this equation is different from (1.92). Equation (1.92) describes the components of $\mathbf{v}$ in the $\mathbf{e}_i'$ system, while (1.98) describes the components of the rotated vector $\bar{\mathbf{v}}$ in the $\mathbf{e}_i$ system. The inverse relation of (1.98) is

$$[v_i] = [Q_{ij}]^{\mathrm{T}}[\bar{\mathrm{v}}_j] \tag{1.99}$$

We now apply $\mathbf{Q}$ to tensor $\mathbf{T}$ and write

$$\bar{\mathbf{T}} = \mathbf{Q} \cdot \mathbf{T} \cdot \mathbf{Q}^{\mathrm{T}} \tag{1.100}$$

that is, $\bar{\mathbf{T}}$ is the tensor after rotation. Then,

$$\bar{\mathbf{T}} \cdot \mathbf{e}'_i = \bar{\mathrm{T}}'_{ji}\mathbf{e}'_j = \mathbf{Q} \cdot \mathbf{T} \cdot \mathbf{Q}^{\mathrm{T}} \cdot \mathbf{e}'_i = \mathbf{Q} \cdot \mathbf{T} \cdot \mathbf{e}_i = \mathbf{Q} \cdot T_{ji}\mathbf{e}_j = T_{ji}\mathbf{e}'_j \tag{1.101}$$

Thus,

$$\bar{\mathrm{T}}'_{ji} = T_{ji} \tag{1.102}$$

that is, the components of $\bar{\mathbf{T}}$ in $\mathbf{e}'_i$ are the same as those of $\mathbf{T}$ in $\mathbf{e}_i$, when $\mathbf{e}'_i$ and $\mathbf{e}_i$ are related by $\mathbf{Q}$. To find the component of $\bar{\mathbf{T}}$ with respect to $\mathbf{e}_i$, we write

$$\bar{\mathbf{T}} \cdot \mathbf{e}'_i = \mathbf{Q} \cdot \mathbf{T} \cdot \mathbf{Q}^{\mathrm{T}} \cdot \mathbf{e}'_i = \mathbf{Q} \cdot \mathbf{T} \cdot \mathbf{e}_i = \mathbf{Q} \cdot T_{ji}\mathbf{e}_j = T_{ji}Q_{kj}\mathbf{e}_k \tag{1.103}$$

On the other hand, we have

$$\bar{\mathbf{T}} \cdot \mathbf{e}'_i\, \bar{\mathrm{T}} \cdot \mathbf{Q} \cdot \mathbf{e}_i = \bar{\mathrm{T}} \cdot Q_{ji} \cdot \mathbf{e}_j = Q_{ji}\bar{\mathbf{T}} \cdot \mathbf{e}_j = Q_{ji}\bar{\mathrm{T}}_{kj}\mathbf{e}_k \tag{1.104}$$

Equating (1.103) to (1.104), we find

$$Q_{ji}\bar{\mathrm{T}}_{kj} = T_{ji}Q_{kj} \tag{1.105}$$

Multiplying both sides of the equation by Q_{mi}, the resulting equation reduces to

$$\bar{\mathrm{T}}_{ij} = Q_{im}Q_{jn}T_{mn} \tag{1.106}$$

which, in the matrix form, may be written as

$$[\bar{\mathrm{T}}] = [Q][T][Q]^{\mathrm{T}} \tag{1.107}$$

Note that this equation (1.107) is different from (1.93) in that the latter describes the components of $\mathbf{T}$ in the $\mathbf{e}'_i$ system, while the former describes the components of the rotated tensor $\bar{\mathbf{T}}$ in the $\mathbf{e}_i$ system.

1.6.3 Some Remarks

1.6.3.1 Remark 1 — definition of Q_{ij}

In this book, we define the components of the transformation matrix by $Q_{ij} = \cos(x_i, x'_j)$, in which the first subscript refers to the unprimed axis and

the second subscript to the primed axis. The transformation rule for a second-rank tensor **T** is

$$T'_{ij} = Q_{ki}Q_{mj}T_{km} \tag{1.108}$$

In some books, the following equations are used,

$$T'_{ij} = Q_{ik}Q_{jm}T_{km} \tag{1.109}$$

where the transformation matrix is defined by $Q_{ij} = \cos(x'_i, x_j)$. In this case, the first subscript refers to the primed axis and the second subscript to the unprimed axis. Make a note of this difference.

1.6.3.2 Remark 2 — transformation of bases versus rotation of a tensor

Note the difference in the transformation equations between a tensor **T** subjected to the transformation of bases and the tensor **T** itself undergoing rotation. In the transformation of bases

$$T'_{ij} = Q_{ki}Q_{lj}T_{kl} \quad \text{or} \quad [T'] = [Q]^{\mathrm{T}}[T][Q] \tag{1.110}$$

and in the rotation of a tensor

$$[\bar{\mathrm{T}}] = [Q][T][Q]^{\mathrm{T}} \tag{1.111}$$

For rotation of tensor **T** in the reversed direction, we substitute $[Q]$ by $[Q]^{\mathrm{T}}$ and (1.111) reduces to $[\bar{\mathrm{T}}] = [Q]^{\mathrm{T}}[T][Q]$ which is the same as the result obtained from the rotation of bases. Therefore, rotation of the tensor itself in the opposite direction has the same effect as the rotation of bases. This point is illustrated by Example 1.6.

EXAMPLE 1.6 Consider the rotation of a vector **v** through an angle α into $\bar{\mathbf{v}}$. Observing that the magnitude of the vector remains the same in the rotation, that is, $|\bar{\mathbf{v}}| = |\mathbf{v}|$ and, from Figure 1.2, referring to $\mathbf{e}_i$, we can write

$$\begin{aligned}\bar{\mathrm{v}}_1 &= |\mathbf{v}|\cos(\alpha+\beta) = |\mathbf{v}|(\cos\alpha\cos\beta - \sin\alpha\sin\beta)\\ &= |\mathbf{v}|\left(\cos\alpha\frac{\mathrm{v}_1}{|\mathbf{v}|} - \sin\alpha\frac{\mathrm{v}_2}{|\mathbf{v}|}\right) = \mathbf{v}_1\cos\alpha - \mathbf{v}_2\sin\alpha\end{aligned} \tag{a}$$

$$\begin{aligned}\bar{\mathrm{v}}_2 &= |\mathbf{v}|\sin(\alpha+\beta) = |\mathbf{v}|(\sin\alpha\cos\beta + \cos\alpha\sin\beta)\\ &= |\mathbf{v}|\left(\sin\alpha\frac{\mathrm{v}_1}{|\mathbf{v}|} + \cos\alpha\frac{\mathrm{v}_2}{|\mathbf{v}|}\right) = v_1\sin\alpha + v_2\cos\alpha\end{aligned} \tag{b}$$

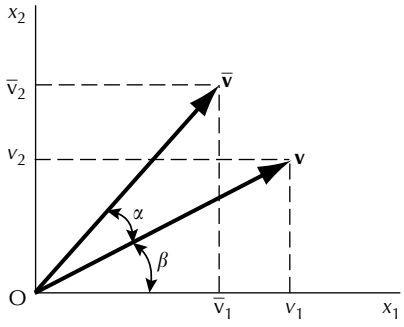

FIGURE 1.2
Components of a vector.

We may then use equations (a) and (b) in a matrix equation as

$$\begin{bmatrix} \bar{v}_1 \\ \bar{v}_2 \end{bmatrix} = \begin{bmatrix} \cos\alpha & -\sin\alpha \\ \sin\alpha & \cos\alpha \end{bmatrix} \begin{bmatrix} v_1 \\ v_2 \end{bmatrix} \tag{c}$$

The component form of this rotation is from (1.98)

$$\bar{v}_i = Q_{ij} v_j \tag{1.98}$$

Comparing (c) and (1.98), we find

$$Q_{ij} = \begin{bmatrix} \cos\alpha & -\sin\alpha \\ \sin\alpha & \cos\alpha \end{bmatrix} \tag{d}$$

However, a rotation of coordinate axes through an angle α in the opposite direction leads to

$$Q^*_{ij} = \begin{bmatrix} \cos\alpha & \sin\alpha \\ -\sin\alpha & \cos\alpha \end{bmatrix} \tag{e}$$

Therefore, from equations (d) and (e), we obtain

$$[Q^*]^{\mathrm{T}} = [Q] \tag{f}$$

The transformation formula in this case is, from (1.92),

$$v'_i = Q^*_{ji} v_j = Q^{*\mathrm{T}}_{ij} v_j \tag{g}$$

Hence,

$$\begin{bmatrix} v'_1 \\ v'_2 \end{bmatrix} = \begin{bmatrix} \cos\alpha & -\sin\alpha \\ \sin\alpha & \cos\alpha \end{bmatrix} \begin{bmatrix} v_1 \\ v_2 \end{bmatrix} \tag{h}$$

Comparing (c) and (h), we conclude that rotation of a vector through an angle α has the same effect as rotation of axes through the same angle α in the opposite direction. Note that in using (1.98) to obtain $\bar{v}_i$, the rotation matrix $[Q]$ is obtained by rotating the coordinate axes through angle α in the same direction as the rotation of vector $\mathbf{v}$.

1.6.3.3 Remark 3 — rotation of a vector about an arbitrary direction

We now consider the rotation of a vector $\mathbf{v}$ about an arbitrary direction with unit vector $\mathbf{n}$ and denoted by $\overline{\mathrm{OA}}$ (Figure 1.3(a)). The angle of rotation is α in the sense of the rotation of a right-handed screw advancing in the direction of $\mathbf{n}$. In the rotation, vector $\mathbf{v}$ is rotated into $\bar{\mathbf{v}}$ and particle P is rotated into $\bar{\mathrm{P}}$. Hence, P and $\bar{\mathrm{P}}$ lie in a plane normal to line $\overline{\mathrm{OA}}$, and the plane intersects $\overline{\mathrm{OA}}$ at B. The vector of $\overline{\mathrm{OB}}$ is $b\mathbf{n}$ and the length $\mathrm{BP} = \overline{\mathrm{BP}} = s$. From the figure, we obtain

$$b = \mathbf{n} \cdot \mathbf{v} = \mathbf{n} \cdot \bar{\mathbf{v}} \tag{1.112}$$

We denote vectors BP and $\overline{\mathrm{BP}}$ by $\mathbf{s}$ and $\bar{\mathrm{s}}$, respectively. Thus,

$$\mathbf{v} = b\mathbf{n} + \mathbf{s} \quad \text{and} \quad \bar{\mathbf{v}} = b\mathbf{n} + \bar{\mathbf{s}} \tag{1.113}$$

In the plane of $\mathrm{BP}\bar{\mathrm{P}}$, the unit vectors $\mathbf{u} = \mathbf{s}/s$ and $\bar{\mathbf{u}} = \bar{\mathbf{s}}/s$ are related by

$$\bar{\mathbf{u}} = \mathbf{u}\cos\alpha + \mathbf{n} \times \mathbf{u}\sin\alpha \tag{1.114}$$

which can be easily justified from Figure 1.3(b). Equation (1.114), when multiplied by s, is

$$\bar{\mathbf{s}} = \mathbf{s}\cos\alpha + \mathbf{n} \times \mathbf{s}\sin\alpha \tag{1.115}$$

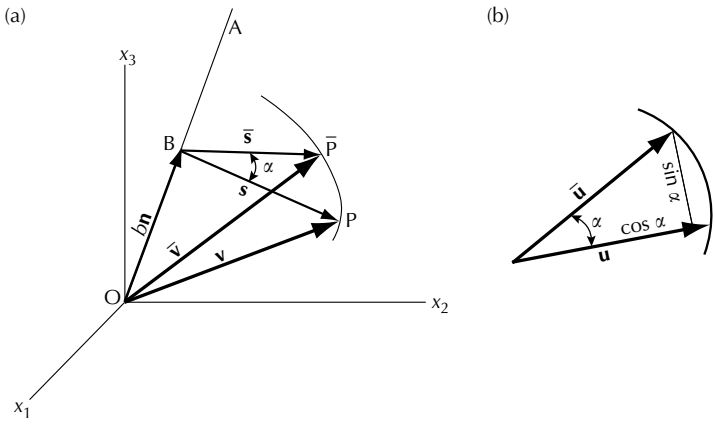

FIGURE 1.3
Rotation of (a) a vector about a direction; (b) a unit vector.

Substituting (1.115) into (1.113), we obtain

$$\begin{aligned}\bar{\mathbf{v}} &= b\mathbf{n} + \mathbf{s}\cos\alpha + \mathbf{n}\times\mathbf{s}\sin\alpha \\ &= b\mathbf{n} + (\mathbf{v} - b\mathbf{n})\cos\alpha + \mathbf{n}\times(\mathbf{v} - \mathrm{b}\mathbf{n})\sin\alpha \\ &= \mathbf{v}\cos\alpha + \mathbf{n}\times\mathbf{v}\sin\alpha + b(1-\cos\alpha)\mathbf{n} \\ &= \mathbf{v}\cos\alpha + \mathbf{n}\times\mathbf{v}\sin\alpha + (\mathbf{n}\cdot\mathbf{v})(1-\cos\alpha)\mathbf{n} \end{aligned} \tag{1.116}$$

This equation may be written as follows in the component form:

$$\bar{\mathbf{v}}_i = v_i\cos\alpha + e_{ikj}n_k v_j\sin\alpha + (1-\cos\alpha)v_j n_j n_i \tag{1.117}$$

By comparing with (1.98), we find that

$$Q_{ij} = \delta_{ij}\cos\alpha + e_{ikj}n_k\sin\alpha + (1-\cos\alpha)n_i n_j \tag{1.118}$$

which is the rotation matrix describing the rotation of α about the line $\overline{\mathrm{OA}}$. In a special case, a rotation about the x_3-axis is obtained by setting $n_3 = 1$ and $n_1 = n_2 = 0$ in (1.118) and we obtain

$$Q_{ij} = \begin{bmatrix} \cos\alpha & -\sin\alpha & 0 \\ \sin\alpha & \cos\alpha & 0 \\ 0 & 0 & 1 \end{bmatrix} \tag{1.119}$$

A rotation in a reverse sense is denoted by a rotation of $-\alpha$. In this case, (1.118) gives

$$\begin{aligned} Q^*_{ij} &= \delta_{ij}\cos(-\alpha) + e_{ikj}n_k\sin(-\alpha) + (1-\cos(-\alpha))n_i n_j \\ &= \delta_{ij}\cos\alpha - e_{ikj}n_k\sin\alpha + (1-\cos\alpha)n_i n_j = Q_{ji} = Q^{\mathrm{T}}_{ij} \end{aligned} \tag{1.120}$$

Thus, we have shown that a rotation in the reverse sense $(-\alpha)$ can be represented by the transpose of the orthogonal tensor $\mathbf{Q}$, which describes the original rotation $(+\alpha)$.

Finally, we note that if the angle α is small, $\cos\alpha \approx 1$ and $\sin\alpha \approx \alpha$. Then, equation (1.118) reduces to

$$Q_{ij} = \delta_{ij} + \alpha n_k e_{kji} \tag{1.121}$$

1.6.3.4 Remark 4 — symbolic versus component form

Relations between tensor quantities may be expressed either in symbolic or in component form. The former are relations between scalars $\alpha, \beta, \ldots$, vectors $\mathbf{u}$, $\mathbf{v}, \ldots$, and tensors $\mathbf{R}, \mathbf{S}, \ldots$, and the latter are relations between scalars $\alpha, \beta, \ldots$, vector components $u_i, v_i, \ldots$, and tensor components $R_{ij}, S_{ij}, \ldots$. The symbolic notation has the advantage that it emphasizes that the relations are physical

statements and that they are independent of the choice of the coordinate system. On the other hand, the component form is often convenient for carrying out algebraic manipulations. In solving problems, it is always necessary at some stage to introduce a coordinate system and components.

1.7 The Isotropic Tensors

A tensor is *isotropic* if it has the same components with respect to a Cartesian coordinate system of any orientation. Isotropic tensors of various ranks are given below:

Scalar: Every scalar is an isotropic tensor, because the scalar does not have a direction.

Vector: There is no nontrivial isotropic vector.

Second-rank tensor: The general expression for an isotropic second-rank tensor is

$$T_{ij} = \lambda \delta_{ij} \tag{1.122}$$

where λ is a constant.

Third-rank tensor: The isotropic third-rank tensor is

$$T_{ijk} = \lambda e_{ijk} \tag{1.123}$$

Fourth-rank tensor: The most general expression for an isotropic fourth-rank tensor is

$$T_{ijkm} = \alpha \delta_{ij}\delta_{km} + \beta \delta_{ik}\delta_{jm} + \gamma \delta_{im}\delta_{jk} \tag{1.124}$$

where α, β, and γ are constants. If T_{ijkm} has the symmetry properties that $T_{ijkm} = T_{jikm}$ and $T_{ijkm} = T_{ijmk}$, then from (1.124)

$$\begin{aligned} T_{ijkm} = T_{jikm} &= \alpha \delta_{ij}\delta_{km} + \beta \delta_{jk}\delta_{im} + \gamma \delta_{jm}\delta_{ik} \\ &= \alpha \delta_{ij}\delta_{km} + \beta \delta_{ik}\delta_{jm} + \gamma \delta_{im}\delta_{jk} \end{aligned} \tag{1.125}$$

By subtracting the two expressions in (1.125), and multiplying the resulting equation by $\delta_{im}\delta_{jk}$, we obtain

$$\delta_{im}\delta_{jk}\gamma(\delta_{jm}\delta_{ik} - \delta_{im}\delta_{jk}) = \beta(\delta_{ik}\delta_{jm} - \delta_{jk}\delta_{im})\delta_{im}\delta_{jk} \tag{1.126}$$

which may be further simplified to yield

$$\gamma(\delta_{ii} - \delta_{ii}\delta_{jj}) = \beta(\delta_{ii} - \delta_{jj}\delta_{ii}) \tag{1.127}$$

or

$$\gamma = \beta \tag{1.128}$$

Hence, (1.124) may be further reduced to

$$T_{ijkm} = \alpha\delta_{ij}\delta_{km} + \beta(\delta_{ik}\delta_{jm} + \delta_{im}\delta_{jk}) \tag{1.129}$$

and we see that the independent constants are now reduced to α and β.

EXAMPLE 1.7 Show that there are no nontrivial isotropic vectors.

Proof

Introduce a 180° rotation of the coordinate system about the x_1-axis as shown in Figure 1.4(a). The transformation matrix for this rotation of axes is

$$[Q] = \begin{bmatrix} 1 & 0 & 0 \\ 0 & -1 & 0 \\ 0 & 0 & -1 \end{bmatrix} \tag{a}$$

The transformation equation for a vector **a** is $a'_i = Q_{ji}a_j$. By applying (a), this equation becomes

$$\begin{bmatrix} a'_1 \\ a'_2 \\ a'_3 \end{bmatrix} = \begin{bmatrix} 1 & 0 & 0 \\ 0 & -1 & 0 \\ 0 & 0 & -1 \end{bmatrix}^{\mathrm{T}} \begin{bmatrix} a_1 \\ a_2 \\ a_3 \end{bmatrix} = \begin{bmatrix} a_1 \\ -a_2 \\ -a_3 \end{bmatrix} \tag{b}$$

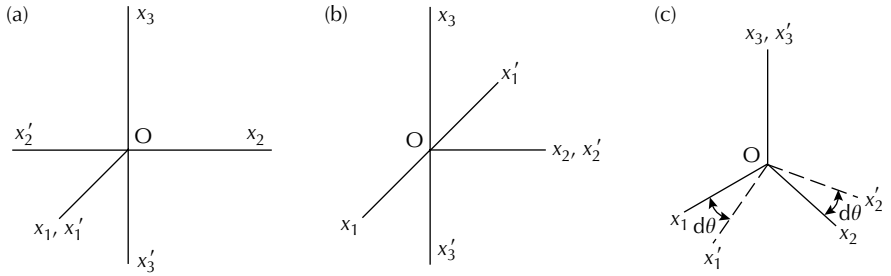

FIGURE 1.4
An 180° rotation of coordinate system about (a) the x_1-axis, (b) the x_2-axis, and (c) rotation of a small angle $d\theta$ about the x_3-axis.

But, if a vector is isotropic, then $a_i' = a_i$ by definition. To satisfy this requirement and equation (b), we must have $a_2 = a_3 = 0$. However, coordinate axes may be labeled in an arbitrary order. Therefore, $a_1 = 0$ as well. We conclude that there are no nontrivial isotropic vectors.

EXAMPLE 1.8 Show that the isotropic second-rank tensor is given by $T_{ij} = \lambda\delta_{ij}$.

Proof

Consider a 180° rotation of the coordinate system about the x_1-axis (see Figure 1.4(a)). The transformation equation for a second-rank tensor $\mathbf{T}$ is $T'_{pq} = Q_{ip}Q_{jq}T_{ij}$. By applying (a) of Example 1.7, this equation becomes

$$[T'] = \begin{bmatrix} T_{11} & -T_{12} & -T_{13} \\ -T_{21} & T_{22} & T_{23} \\ -T_{31} & T_{32} & T_{33} \end{bmatrix} = [T] = \begin{bmatrix} T_{11} & T_{12} & T_{13} \\ T_{21} & T_{22} & T_{23} \\ T_{31} & T_{32} & T_{33} \end{bmatrix} \tag{a}$$

The last equality of the above equation is written based on the definition of an isotropic tensor so that $T'_{ij} = T_{ij}$. Therefore, we conclude that $T_{12} = T_{21} = 0$ and $T_{13} = T_{31} = 0$.

We next introduce a 180° rotation of the coordinate system about the x_2-axis as shown in Figure 1.4(b). The transformation matrix is

$$[Q] = \begin{bmatrix} -1 & 0 & 0 \\ 0 & 1 & 0 \\ 0 & 0 & -1 \end{bmatrix} \tag{b}$$

Substituting (b) into the transformation equation for T_{ij} and considering the definition of an isotropic tensor, we write

$$[T'] = \begin{bmatrix} T_{11} & -T_{12} & T_{13} \\ -T_{21} & T_{22} & -T_{23} \\ T_{31} & -T_{32} & T_{33} \end{bmatrix} \overset{\text{isotropic}}{\equiv} [T] \tag{c}$$

From (c), we conclude that $T_{12} = T_{21} = 0$ and $T_{23} = T_{32} = 0$. Thus, only T_{11}, T_{22}, T_{33} are nonzero. But, since coordinate axis may be labeled in any arbitrary order, we have $T_{11} = T_{22} = T_{33} = \lambda$. Therefore, the second-rank isotropic tensor is written as

$$T_{ij} = \lambda\delta_{ij}$$

EXAMPLE 1.9 Show that the most general fourth-order isotropic tensor has the form

$$T_{ijkm} = \alpha\delta_{ij}\delta_{km} + \beta\delta_{ik}\delta_{jm} + \gamma\delta_{im}\delta_{jk}$$

where α, β, γ are constants.

Proof

A fourth-order tensor transforms as

$$T'_{ijkm} = Q_{ri}Q_{sj}Q_{tk}Q_{nm}T_{rstn} \tag{a}$$

There are $3^4 = 81$ components altogether. First, consider any component which contains the index 1 only *once*. For the coordinate transformation associated with a 180° rotation about the x_1-axis and illustrated by Figure 1.4(a), the transformation matrix is given by (a) of Example 1.7.

Let $i = 1$ and use the Q_{ij} of Figure 1.4(a), equation (a) becomes

$$T'_{1jkm} = Q_{r1}Q_{sj}Q_{tk}Q_{nm}T_{rstn} = Q_{11}Q_{sj}Q_{tk}Q_{nm}T_{1stn} \tag{b}$$

But $j \neq 1$, so the only nonzero terms of Q_{sj} are $Q_{22} = Q_{33} = -1$, in which $j = s$; $k \neq 1$, so the only nonzero terms of Q_{tk} are $Q_{22} = Q_{33} = -1$, in which $k = t$; and $m \neq 1$, so the only nonzero terms of Q_{nm} are $Q_{22} = Q_{33} = -1$, in which $m = n$. Thus, (b) becomes

$$T'_{1jkm} = Q_{11}(-1)(-1)(-1)T_{1stn} = -T_{1stn} = -T_{1jkm} \tag{c}$$

If the tensor is isotropic, then $T'_{1jkm} = T_{1jkm}$, which contradicts the expression in (c). Therefore, all the components which contain the index 1 only once are zero, in order to satisfy this requirement. Similarly, all the components that contain the index 2 only once are zero and all the components that contain the index 3 only once are zero. Thus, from the above special transformation, we see that the components of T_{ijkm} are reduced to the following four groups: $T_{1122}, T_{2211}, T_{1133}, \ldots; T_{1212}, T_{2323}, \ldots; T_{1221}, T_{2112}, T_{2332}, \ldots$; and $T_{1111}, T_{2222}, T_{3333}$.

Furthermore, we remark that the coordinate axes may be labeled in an arbitrary order. Thus, a permutation of the indices 1, 2, 3 cannot affect the values of the components of an isotropic tensor. Therefore,

$$\begin{aligned}
&T_{1122} = T_{2211} = T_{1133} = T_{3311} = T_{2233} = T_{3322} = \alpha, \text{ say}\\
&T_{1212} = T_{2121} = T_{1313} = T_{3131} = T_{2323} = T_{3232} = \beta, \text{ say}\\
&T_{1221} = T_{2112} = T_{1331} = T_{3113} = T_{2332} = T_{3223} = \gamma, \text{ say}\\
&T_{1111} = T_{2222} = T_{3333} = \delta, \text{ say}
\end{aligned} \tag{d}$$

Consider now a rotation shown in Figure 1.4(c) about the x_3-axis with a very small angle of rotation $\mathrm{d}\theta$. The transformation matrix for this case is

$$Q_{ij} = \begin{bmatrix} \cos \mathrm{d}\theta & -\sin \mathrm{d}\theta & 0 \\ \sin \mathrm{d}\theta & \cos \mathrm{d}\theta & 0 \\ 0 & 0 & 1 \end{bmatrix} \approx \begin{bmatrix} 1 & -\mathrm{d}\theta & 0 \\ \mathrm{d}\theta & 1 & 0 \\ 0 & 0 & 1 \end{bmatrix} \tag{e}$$

Equation (e) can be rewritten as

$$Q_{ij} = \begin{bmatrix} 1 & 0 & 0 \\ 0 & 1 & 0 \\ 0 & 0 & 1 \end{bmatrix} + \begin{bmatrix} 0 & -\mathrm{d}\theta & 0 \\ \mathrm{d}\theta & 0 & 0 \\ 0 & 0 & 0 \end{bmatrix}$$

or

$$Q_{ij} = \delta_{ij} + \mathrm{d}\theta e_{3ji} \tag{f}$$

Only e_{321} and e_{312} are not zero in the expressions of e_{3ji}. Note that (f) can also be obtained from (1.121) by letting $n_i = (0, 0, 1)$ and $\alpha = \mathrm{d}\theta$.

Substituting (f) into (a), we have

$$\begin{aligned} T'_{ijkm} &= (\delta_{ri} + \mathrm{d}\theta e_{3ir})(\delta_{sj} + \mathrm{d}\theta e_{3js})(\delta_{tk} + \mathrm{d}\theta e_{3kt})(\delta_{nm} + \mathrm{d}\theta e_{3mn}) T_{rstn} \\ &= (\delta_{ri}\delta_{sj} + \delta_{ri}\,\mathrm{d}\theta e_{3js} + \mathrm{d}\theta e_{3ir}\delta_{sj})(\delta_{tk}\delta_{nm} + \delta_{tk}\,\mathrm{d}\theta e_{3nm} + \mathrm{d}\theta e_{3kt}\delta_{nm}) T_{rstn} \\ &= (\delta_{ri}\delta_{sj}\delta_{tk}\delta_{nm} + \delta_{ri}\delta_{sj}\delta_{tk}\,\mathrm{d}\theta\varepsilon_{3mn} + \delta_{ri}\delta_{sj}\,\mathrm{d}\theta e_{3kt}\delta_{nm} + \delta_{ri}\,\mathrm{d}\theta e_{3js}\delta_{tk}\delta_{nm} \\ &\quad + \mathrm{d}\theta e_{3ir}\delta_{sj}\delta_{tk}\delta_{nm}) T_{rstn} \\ &= T_{ijkm} + \mathrm{d}\theta e_{3mn} T_{ijkn} + \mathrm{d}\theta e_{3kt} T_{ijtm} + \mathrm{d}\theta e_{3js} T_{iskm} + \mathrm{d}\theta e_{3ir} T_{rjkm} \\ &= T_{ijkm} + \mathrm{d}\theta \{e_{3mn} T_{ijkn} + e_{3kt} T_{ijtm} + e_{3js} T_{iskm} + e_{3ir} T_{rjkm}\} \end{aligned} \tag{g}$$

In the above derivation higher order terms in $\mathrm{d}\theta$ have been neglected since $\mathrm{d}\theta$ is infinitesimal. If the tensor T_{ijkm} is isotropic, then $T'_{ijkm} = T_{ijkm}$. Using this information in the last expression of (g), the quantity within the brackets has to be zero. Therefore,

$$e_{3mn} T_{ijkn} + e_{3kt} T_{ijtm} + e_{3js} T_{iskm} + e_{3ir} T_{rjkm} = 0 \tag{h}$$

We now investigate the implication of (h). By choosing $i = 1, j = k = m = 2$, (h) becomes

$$e_{321} T_{1221} + e_{321} T_{1212} + e_{321} T_{1122} + e_{312} T_{2222} = 0$$

or

$$T_{2222} = T_{1221} + T_{1212} + T_{1122} \tag{i}$$

Substituting (d) into (i), we get

$$\delta = \alpha + \beta + \gamma \tag{j}$$

Other choices of indices i, j, k, m in (h) gives either the same relation (j) or relations that are identically satisfied, if we use the isotropy conditions previously obtained. Thus, we have shown that there are only three distinct components of an isotropic fourth-rank tensor, namely α, β and γ; and T_{ijkm} can be written as

$$T_{ijkm} = \alpha\delta_{ij}\delta_{km} + \beta\delta_{ik}\delta_{jm} + \gamma\delta_{im}\delta_{jk} \tag{k}$$

All components of isotropic T_{ijkm} can be found from (k). Examples are

$$\begin{aligned} T_{1122} &= \alpha\delta_{11}\delta_{22} + \beta\delta_{12}\delta_{12} + \gamma\delta_{12}\delta_{12} = \alpha \\ T_{2233} &= \alpha\delta_{22}\delta_{33} + \beta\delta_{23}\delta_{23} + \gamma\delta_{23}\delta_{23} = \alpha \\ T_{1221} &= \alpha\delta_{12}\delta_{21} + \beta\delta_{12}\delta_{21} + \gamma\delta_{11}\delta_{22} = \gamma \end{aligned}$$

and so on.

EXAMPLE 1.10 Using the expression of an isotropic fourth-rank tensor, reduce the generalized Hooke's law to an isotropic relation.

Linearly elastic materials are governed by the generalized Hooke's law as

$$\sigma_{ij} = C_{ijkm}\varepsilon_{km} \tag{a}$$

where σ_{ij} and ε_{ij} are second-rank tensors and C_{ijkm} is a fourth-rank tensor. Due to the symmetric property of σ_{ij} and ε_{ij}, we find $C_{ijkm} = C_{jikm}$ and $C_{ijkm} = C_{ijmk}$. If the material is isotropic, tensor C_{ijkm} should be an isotropic tensor. Thus, from (1.130),

$$C_{ijkm} = \lambda\delta_{ij}\delta_{km} + \mu(\delta_{ik}\delta_{jm} + \delta_{im}\delta_{jk}) \tag{b}$$

Substituting (b) into (a), we obtain

$$\begin{aligned} \sigma_{ij} &= \lambda\delta_{ij}\delta_{km}\varepsilon_{km} + \mu\delta_{ik}\delta_{jm}\varepsilon_{km} + \mu\delta_{im}\delta_{jk}\varepsilon_{km} \\ &= \lambda\varepsilon_{kk}\delta_{ij} + \mu\varepsilon_{ij} + \mu\varepsilon_{ji} \\ &= \lambda\delta_{ij}\varepsilon_{kk} + 2\mu\varepsilon_{ij} \end{aligned} \tag{c}$$

In the derivation, the symmetric property of $\varepsilon_{ij} = \varepsilon_{ji}$ was used. λ and μ are known as Lamé constants.

1.8 Vector and Tensor Calculus

1.8.1 Tensor Field

If to every point x_i of region R there corresponds a scalar ϕ, then we have a *scalar field* $\phi(x_i)$ defined over R. An example of the scalar field is the temperature field, where the temperature in the region R of a continuum is known and may vary from point to point. Similarly, we can define a *vector field*. If to every point x_i of region R corresponds a vector v_i, then we have a vector field $v_i(x_j)$ defined over R. Force field, displacement field, and velocity field are examples of vector field. A *tensor field* can be similarly defined. Stress field and strain field are tensor fields of rank two.

1.8.2 Gradient, Divergence, Curl

We consider differentiation and integration in the study of vector calculus. Differentiation is discussed in this section and integration in a later section. There are three kinds of differentiation: the gradient, the divergence, and the curl. *The gradient* of a scalar field ϕ, denoted by Grad ϕ, is a vector whose components are

$$\text{Grad } \phi = \left[\frac{\partial \phi}{\partial x_1}, \frac{\partial \phi}{\partial x_2}, \frac{\partial \phi}{\partial x_3}\right]^{\mathrm{T}} = \text{a vector} \tag{1.130}$$

In other notations, Grad ϕ may be denoted by

$$\overrightarrow{\text{Grad } \phi} = \frac{\partial \phi}{\partial x_k}\vec{\mathbf{e}}_k = \phi_{,i}\vec{\mathbf{e}}_k = \vec{\nabla}\phi \tag{1.131}$$

The differential operator $\vec{\nabla}$ "del" is used in the last expression of (1.131). In our notation $\vec{\nabla}$ is

$$\vec{\nabla} = \mathbf{e}_k \frac{\partial}{\partial x_k} \tag{1.132}$$

The operator $\vec{\nabla}$ is not commutative with respect to the quantity which it operated in the sense that

$$\vec{\nabla}\phi \neq \phi\vec{\nabla} \tag{1.133}$$

1.8.2.1 Geometric significance of the gradient

The value of the scalar field $\phi(x_k)$ defined over the region R varies in general with x_i. The expression, $\phi(x_k) =$ constant, defines a set of surfaces on which ϕ

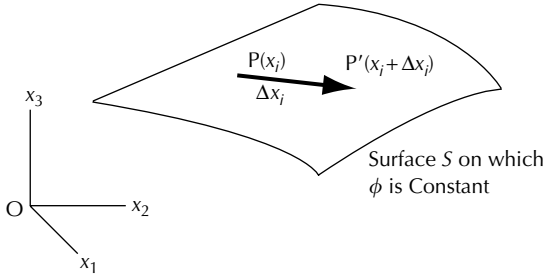

FIGURE 1.5
A constant ϕ surface.

is constant. Consider a point P(x_i) and a neighboring point P′($x_i + \Delta x_i$) on the surface S, and denote the vector from P to P′ by Δx_i as shown in Figure 1.5. Since both points are on the same surface, ϕ evaluated at the two points are the same, and we write

$$\phi(\mathrm{P}') - \phi(\mathrm{P}) = 0 \quad \text{or} \quad \phi(x_i + \Delta x_i) - \phi(x_i) = 0 \tag{1.134}$$

Expanding the function $\phi(x_i + \Delta x_i)$ in Taylor's series, we have

$$\phi(x_i + \Delta x_i) = \phi(x_i) + \phi_{,i}\,\Delta x_i + 0(\Delta x_i)^2 \tag{1.135}$$

But, Δx_i has a small value and we may take it as small as possible in the sense of calculus. In this way, we may neglect the higher order terms in Δx_i and keep only the first-order term in (1.135). Therefore, (1.134) becomes

$$\phi(\mathrm{P}') - \phi(\mathrm{P}) = \phi_{,i}\Delta x_i = 0 \tag{1.136}$$

and this is true for any vector Δx_i through P lying on the surface S. Hence, the gradient $\phi_{,i}$ is normal to the surface S.

1.8.2.2 Differential operators on vectors

There are two differential operators on vector v_i which are well known. They are the divergence and the curl. The divergence of vector $\mathbf{v}$ is written as

$$\mathrm{Div}\,\mathbf{v} \equiv v_{i,i} = \frac{\partial v_i}{\partial x_i} = \left(\frac{\partial v_1}{\partial x_1} + \frac{\partial v_2}{\partial x_2} + \frac{\partial v_3}{\partial x_3}\right) \tag{1.137}$$

In terms of $\vec{\nabla}$, the divergence is

$$\mathrm{Div}\ \mathbf{v} = \vec{\nabla}\cdot\mathbf{v} = \mathbf{e}_k\frac{\partial}{\partial x_k}\cdot(v_m\mathbf{e}_m) = \mathbf{e}_k\cdot\mathbf{e}_m\frac{\partial v_m}{\partial x_k} = \delta_{km}v_{m,k} = v_{k,k} \tag{1.138}$$

The curl of vector $\mathbf{v}$, denoted by vector $\mathbf{w}$, is

$$\mathbf{w} = \text{Curl } \mathbf{v} = \vec{\nabla} \times \mathbf{v} = \mathbf{e}_k \frac{\partial}{\partial x_k} \times (v_m \mathbf{e}_m) = \mathbf{e}_k \times \mathbf{e}_j v_{j,k} = e_{kjm} \mathbf{e}_m v_{j,k} \tag{1.139}$$

and its components are

$$W_m = (\text{Curl } \mathbf{v})_m = e_{kjm} v_{j,k} = e_{mkj} v_{j,k} \tag{1.140}$$

in which $v_{j,k}$ is the velocity gradient if v_i is the velocity. The velocity gradient is an important kinematic quantity and is discussed in Chapter 3. From (1.140), we have $w_1 = v_{3,2} - v_{2,3}$. Vector w_m is the dual vector of tensor $v_{j,k}$ except for a constant multiple factor. Dual vectors are discussed in Chapter 3.

Some operations using the operator $\vec{\nabla}$ are given below:

$$\text{(a)} \quad \vec{\nabla} \cdot (\vec{\nabla}\phi) = \mathbf{e}_j \frac{\partial}{\partial x_j} \cdot (\mathbf{e}_k \phi_{,k}) = \mathbf{e}_j \cdot \mathbf{e}_k \phi_{,kj} = \delta_{jk} \phi_{,kj} = \phi_{,kk} = \nabla^2 \phi \tag{1.141}$$

$$\begin{aligned} \text{(b)} \quad \vec{\nabla} \times (\vec{\nabla}\phi) &= \text{Curl Grad } \phi = \mathbf{e}_j \frac{\partial}{\partial x_j} \times (\mathbf{e}_k \phi_{,k}) = \mathbf{e}_j \times \mathbf{e}_k \phi_{,kj} \\ &= e_{jkm} \mathbf{e}_m \phi_{,kj} = e_{jk1} \mathbf{e}_1 \phi_{,kj} + e_{jk2} \mathbf{e}_2 \phi_{,kj} + e_{jk3} \mathbf{e}_3 \phi_{,kj} \\ &= e_{231} \mathbf{e}_1 \phi_{,32} + e_{321} \mathbf{e}_1 \phi_{,23} + \cdots = 0 \end{aligned} \tag{1.142}$$

We note that e_{jk1} is antisymmetric and $\phi_{,kj}$ is symmetric such that their inner product is zero. For the same reason the other two terms involving $m = 2$ and $m = 3$ are also zero. The above result can also be seen easily by expanding out each term as in the last equality. Since $e_{231} = 1$ and $e_{321} = -1$, the terms of the last equality cancel out in pairs.

$$\begin{aligned} \text{(c)} \quad \vec{\nabla} \cdot (\vec{\nabla} \times \mathbf{v}) &= \mathbf{e}_j \frac{\partial}{\partial x_j} \cdot \left[\mathbf{e}_k \frac{\partial}{\partial x_k} \times (\mathbf{e}_r v_r) \right] \\ &= \mathbf{e}_j \frac{\partial}{\partial x_j} \cdot [\mathbf{e}_k \times \mathbf{e}_r v_{r,k}] = \mathbf{e}_j \frac{\partial}{\partial x_j} \cdot [e_{krs} v_{r,k} \mathbf{e}_s] \\ &= \mathbf{e}_j \cdot \lfloor e_{krs} \mathbf{e}_s v_{r,kj} \rfloor = \delta_{js} e_{krs} v_{r,kj} = e_{krj} v_{r,kj} = 0 \end{aligned} \tag{1.143}$$

The last equality is again obtained by observing that the inner product of an antisymmetric tensor with a symmetric tensor is zero.

$$\begin{aligned} \text{(d)} \quad \vec{\nabla} \times (\vec{\nabla} \times \mathbf{v}) &= \mathbf{e}_s \frac{\partial}{\partial x_s} \times [e_{kjm} v_{m,j} \mathbf{e}_k] = \mathbf{e}_s \times \mathbf{e}_k e_{kjm} v_{m,js} \\ &= -e_{ksr} \mathbf{e}_r e_{kjm} v_{m,js} = -\{\delta_{sj}\delta_{rm} - \delta_{sm}\delta_{rj}\} v_{m,js} \mathbf{e}_r \\ &= -v_{m,ss} \mathbf{e}_m + v_{s,js} \mathbf{e}_j = -v_{m,ss} \mathbf{e}_m + (v_{s,s})_{,j} \mathbf{e}_j \\ &= -\nabla^2 \mathbf{v} + \vec{\nabla}(\vec{\nabla} \cdot v) \end{aligned} \tag{1.144}$$

Note that $\nabla^2\,\mathbf{v}$ is written as:

$$(\vec{\nabla}\cdot\vec{\nabla})\mathbf{v} = \left(\mathbf{e}_i\frac{\partial}{\partial x_i}\cdot\mathbf{e}_j\frac{\partial}{\partial x_j}\right)(v_k\mathbf{e}_k) = \frac{\partial^2 v_k}{\partial x_i\partial x_j}(\mathbf{e}_i\cdot\mathbf{e}_j)\mathbf{e}_k$$

$$= \frac{\partial^2 v_k}{\partial x_j\partial x_j}\mathbf{e}_k = v_{k,jj}\mathbf{e}_k \tag{1.145}$$

By use of (1.39), we have

$$(\vec{\nabla}\cdot\vec{\nabla})\mathbf{v} = \left(\mathbf{v}\otimes\vec{\nabla}\right)\cdot\vec{\nabla} \tag{1.146}$$

Therefore, $\nabla^2\mathbf{v}$ can be written in either of the following two forms

$$\nabla^2\mathbf{v} = \left(\mathbf{v}\otimes\vec{\nabla}\right)\cdot\vec{\nabla} = (\vec{\nabla}\cdot\vec{\nabla})\mathbf{v} \tag{1.147}$$

(e) There are two forms of the divergence of tensor $\mathbf{T}$. They are:

$$\vec{\nabla}\cdot\mathbf{T} = \frac{\partial}{\partial x_k}\mathbf{e}_k\cdot(T_{pq}\mathbf{e}_p\otimes\mathbf{e}_q) = \frac{\partial T_{pq}}{\partial x_k}(\mathbf{e}_k\cdot\mathbf{e}_p)\mathbf{e}_q = \frac{\partial\mathbf{T}_{pq}}{\partial\mathbf{x}_p}\mathbf{e}_q \tag{1.148}$$

$$\mathbf{T}\cdot\vec{\nabla} = \frac{\partial\mathbf{T}_{qp}}{\partial\mathbf{x}_p}\mathbf{e}_q \tag{1.149}$$

The two divergences are in general different, but they are the same if the tensor $\mathbf{T}$ is symmetric. We can further write $\mathbf{T}^T\cdot\vec{\nabla} = \vec{\nabla}\cdot\mathbf{T}$, and this relationship is similar to that of the inner product between a vector and a second-rank tensor presented in (1.64) and (1.65).

1.8.3 The Theorem of Gauss

In continuum mechanics, an important application of the theorem of Gauss is to change an area integral into a volume integral and vice versa. Consider a body of surface S and volume V, with surface element $\mathrm{d}S$ and volume element $\mathrm{d}V$ shown in Figure 1.6, the Gauss theorem is written as

$$\int_S \phi n_i\,\mathrm{d}S = \int_V \phi_{,i}\,\mathrm{d}V \quad \text{for scalar } \phi \tag{1.150}$$

$$\int_S v_j n_i\,\mathrm{d}S = \int_V v_{j,i}\,\mathrm{d}V \quad \text{for vector } v_j \tag{1.151}$$

$$\int_S a_{i_1 i_2\ldots i_N} n_j\,\mathrm{d}S = \int_V a_{i_1 i_2\,\ldots\,i_N,j}\,\mathrm{d}V \quad \text{for tensor } a_{i_1\ldots i_N} \tag{1.152}$$

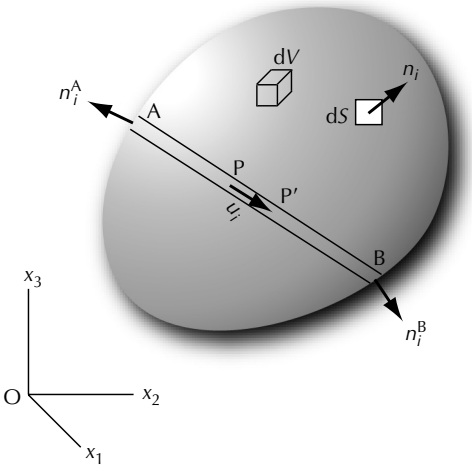

FIGURE 1.6
Surface and volume elements in a deformable body.

Proof

We prove (1.150) here. The proofs of (1.151) and (1.152) can be similarly obtained. A scalar field ϕ is defined in V and we divide the body into an infinite number of parallel infinitesimal cylinders. A generic infinitesimal cylinder is shown in the Figure 1.6 with ends A and B. Ends A and B are parts of the surface area S of the body and has unit outward normal n_i^{A} or n_i^{B}, respectively. We now consider two neighboring points $\mathrm{P}(x_i)$ and $\mathrm{P}'(x_i+\mathrm{d}x_i)$ in the infinitesimal cylinder. The unit vector along the generator of the cylinder is denoted by u_i as shown in the Figure 1.6 and is a constant. The differential $\mathrm{d}\phi$ is given by

$$\mathrm{d}\phi = \frac{\partial \phi}{\partial x_1}\,\mathrm{d}x_1 + \frac{\partial \phi}{\partial x_2}\,\mathrm{d}x_2 + \frac{\partial \phi}{\partial x_3}\,\mathrm{d}x_3 = \phi_{,i}\,\mathrm{d}x_i = u_i \phi_{,i}\,\mathrm{d}s \tag{1.153}$$

where $\mathrm{d}s$ is the length of $\mathrm{d}x_i$. If this expression is integrated over the infinitesimal cylinder, we find

$$\phi_{\mathrm{B}} - \phi_{\mathrm{A}} = u_i \int_{\mathrm{A}}^{\mathrm{B}} \phi_{,i}\,\mathrm{d}s \tag{1.154}$$

The cross-section of the cylinder is

$$\mathrm{d}T = (-n_i u_i\,\mathrm{d}S)_{\mathrm{A}} = (n_i u_i\,\mathrm{d}S)_{\mathrm{B}} \tag{1.155}$$

Note that $n_i u_i$ is negative at A and positive at B. Multiplying both sides of (1.154) by (1.155), we obtain

$$\phi_{\mathrm{B}}(n_i u_i \,\mathrm{d}S)_{\mathrm{B}} - \phi_{\mathrm{A}}(-n_i u_i \,\mathrm{d}S)_{\mathrm{A}} = u_i \int_{\mathrm{A}}^{\mathrm{B}} \phi_{,i} \;\mathrm{d}s\,\mathrm{d}T \tag{1.156}$$

which may be rewritten as

$$(\phi n_i u_i \,\mathrm{d}S)_{\mathrm{B}} + (\phi n_i u_i \,\mathrm{d}S)_{\mathrm{A}} = u_i \int_{\mathrm{A}}^{\mathrm{B}} \phi_{,i} \,\mathrm{d}V \tag{1.157}$$

or

$$u_i \int_{\mathrm{d}S_{\mathrm{A}}+\mathrm{d}S_{\mathrm{B}}} \phi n_i \,\mathrm{d}S = u_i \int_{V_{\text{cylinder}}} \phi_{,i} \,\mathrm{d}V \tag{1.158}$$

In deriving (1.158), we observe that because $\mathrm{d}S_{\mathrm{A}}$ and $\mathrm{d}S_{\mathrm{B}}$ are small surface areas, we assume that ϕ and n_i are constants in $\mathrm{d}S$, then

$$\begin{aligned} u_i \int_{\mathrm{d}S_{\mathrm{A}}+\mathrm{d}S_{\mathrm{B}}} \phi n_i \,\mathrm{d}S &= u_i \int_{\mathrm{d}S_{\mathrm{A}}} \phi n_i \,\mathrm{d}S + u_i \int_{\mathrm{d}S_{\mathrm{B}}} \phi n_i \,\mathrm{d}S \\ &\cong u_i(\phi n_i)_{\mathrm{A}} \int_{\mathrm{d}S_{\mathrm{A}}} \mathrm{d}S + u_i(\phi n_i)_{\mathrm{B}} \int_{\mathrm{d}S_{\mathrm{B}}} \mathrm{d}S \\ &= (\phi n_i u_i \,\mathrm{d}S)_{\mathrm{A}} + (\phi n_i u_i \,\mathrm{d}S)_{\mathrm{B}} = \text{LHS of (1.157)} \end{aligned} \tag{1.159}$$

Equation (1.158) is valid for the infinitesimal cylinder considered. For the whole body, we sum over all infinitesimal cylinders and obtain

$$\int_{S_{\text{all}}} \phi n_i \,\mathrm{d}S = \int_{V_{\text{all}}} \phi_{,i} \,\mathrm{d}V \tag{1.160}$$

which proves equation (1.150). We remark that the theorem of Gauss is still valid for multiply connected region. In that case, we have to make branch cuts to prove the theorem.

Some special cases of the theorem are listed below:

1. Expressions in 3-D:

$$\int_V \mathrm{Div}\;\; \mathbf{v}\;\, \mathrm{d}V = \int_S \mathbf{n}\cdot\mathbf{v}\,\mathrm{d}S \quad \text{(divergence theorem)} \tag{1.161}$$

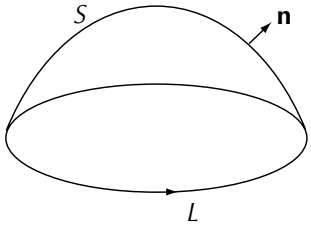

FIGURE 1.7
Contour and surface.

This equation can be obtained by putting $i = j$ in (1.151).

$$\int_V \text{Curl } \mathbf{v}\, \mathrm{d}V = \int_S \mathbf{n} \times \mathbf{v}\, \mathrm{d}S \tag{1.162}$$

This equation can be obtained by multiplying both sides of (1.152) by e_{kij}.

2. Expressions in 2-D:

$$\int_S \text{Div } \mathbf{v}\ \mathrm{d}S = \int_L \mathbf{n} \cdot \mathbf{v}\, \mathrm{d}L \tag{1.163}$$

$$\int_S \text{Curl } \mathbf{v}\ \mathrm{d}S = \int_L \mathbf{n} \times \mathbf{v}\, \mathrm{d}L \tag{1.164}$$

$$\int_L \mathbf{v} \cdot \mathrm{d}\mathbf{L} = \int_S \mathbf{n} \cdot \text{Curl } \mathbf{v}\ \mathrm{d}S \quad \text{(Stoke's theorem)} \tag{1.165}$$

In the two-dimensional case, the theorem changes the surface integral into the line integral and vice versa. Figure 1.7 shows the contour L and the surface S. In (1.165), the left integral is the circulation of $\mathbf{v}$ along the contour L and $\mathbf{n}$ is the unit outward normal on the surface S.

References

1. Malvern, L.E., *Introduction to the Mechanics of a Continuous Medium*, Prentice-Hall, Englewood Cliffs, NJ, 1969.
2. Spencer, A.J.M., *Continuum Mechanics*, Longman, London and New York, 1980.
3. Lai, W.M., Rubin, D., and Krempl, E., *Introduction to Continuum Mechanics*, Pergamon Press, New York, 1974.
4. Fung, Y.C., *First Course in Continuum Mechanics*, Prentice-Hall, Englewood Cliffs, NJ, 1994.
5. Chadwick, P., *Continuum Mechanics*, George Allen & Unwin, London, 1976.

Problems

(1) The equations of motion are

$$\frac{\partial T_{sr}}{\partial x_s} + \rho b_r = \rho a_r$$

Write out the equations in conventional notations, that is, use $x = x_1, y = x_2$ and $z = x_3$.

(2) Prove that

$$\delta_{ij}\delta_{ij} = 3$$
$$e_{ijk}A_jA_k = 0$$
$$\delta_{ij}e_{ijk} = 0$$

(3) If T_{ij} is symmetric, evaluate the expressions (a) $e_{ijk}T_{jk}$ and (b) $e_{ijk}e_{ist}T_{kt}$.

(4) Given that

$$[S_{ij}] = \begin{bmatrix} 1 & 0 & 0 \\ -1 & 2 & 3 \\ 2 & 1 & -1 \end{bmatrix}$$

evaluate (a) S_{ii}, (b) S_{jj}, (c) $S_{ij}S_{ij}$, (d) $S_{jk}S_{kj}$, (e) $S_{mn}S_{nm}$

(5) Using the e–δ identity, show that

$$e_{ikm}e_{jkm} = 2\delta_{ij} \quad \text{and} \quad e_{ijk}e_{ijk} = 6$$

(6) Given vectors $\mathbf{u} = u_i\mathbf{e}_i$ and $\mathbf{v} = v_i\mathbf{e}$, show that the components of $\mathbf{w} = \mathbf{u}\times\mathbf{v}$ are

$$w_1 = u_2v_3 - u_3v_2, \qquad w_2 = u_3v_1 - u_1v_3, \qquad w_3 = u_1v_2 - u_2v_1$$

(7) If $u_i = e_{ijk}v_jw_k$ and $v_i = e_{ijk}s_jt_k$, show that $u_i = s_kw_kt_i - t_kw_ks_i$.

(8) Find the transformation matrix $[Q]$ if the coordinate system is rotated through a positive 90° about the positive x_3-axis.

(9) Can the matrices

$$\begin{bmatrix} 1 & 0 & 0 \\ 0 & 2 & 0 \\ 0 & 0 & 3 \end{bmatrix} \quad \text{and} \quad \begin{bmatrix} 1 & 0 & 0 \\ 0 & 1 & 0 \\ 0 & 0 & 3 \end{bmatrix}$$

be matrices of the same tensor? Why?

(10) The components of a second-rank tensor with respect to the x_i coordinate system are

$$[A] = \begin{bmatrix} 4 & 3 & 0 \\ 3 & -1 & 0 \\ 0 & 0 & 1 \end{bmatrix}$$

Find the components of the same tensor with respect to the x'_i, coordinate system, if $x'_3 = x_3$ and x'_1 is making a 30° counterclockwise angle with the x_1-axis.

(11) Prove that the decomposition of a tensor into a symmetric and an antisymmetric part is unique.

(12) Show that the value of $A_{ij}x_ix_j$ is unchanged if A_{ij} is replaced by its symmetric part.

(13) If A_{ij} is a tensor and B_{ij} is a symmetric tensor, show that the product $A_{ij}B_{ij}$ is independent of antisymmetric part of A_{ij}.

(14) In the coordinate transformation from x_i to x'_i, the transformation rule for the components of a second-rank tensor is $T'_{pq} = Q_{ip}Q_{jq}T_{ij}$, where Q_{ij} is the transformation matrix. Derive the reversed expression of this equation, that is, express T_{ij} in terms of T'_{ij} and Q_{ij}.

(15) Investigate the influence of the coordinate transformation $x'_1 = -x_1$, $x'_2 = x_2$, $x'_3 = x_3$ on the components of a tensor $\mathbf{T}$.

(16) Prove that $\mathbf{e}_i \otimes \mathbf{e}_i = \mathbf{I}$ where $\mathbf{I}$ is the identity tensor.

(17) Show that $\det(\mathbf{e}_i \otimes \mathbf{e}_i) = 1$ and $\det(\mathbf{e}_1 \otimes \mathbf{e}_1) = 0$.

(18) Show that $(\mathbf{a} \otimes \mathbf{b}) \cdot (\mathbf{c} \otimes \mathbf{d}) = (\mathbf{b} \cdot \mathbf{c})(\mathbf{a} \otimes \mathbf{d})$.

(19) Show that if the components of tensor $\mathbf{T}$ are $T_{ij} = \delta_{ij}$ in the x_i coordinate system, then the components are $T'_{ij} = \delta_{ij}$ in the x'_i coordinate system.

(20) A rigid body is rotated through positive 90° about x_2-axis by the right-handed screw rule. Find a matrix representing this rotation.

(21) Suppose that the body of the previous problem is subsequently given a 90° rotation about the x_1-axis by the right-hand screw rule, find the matrix representation of the resultant rotation. If the position of a particle P on the rigid body was (0, 1, 1), what is its position after two rotations?

(22) Reverse the order of above two rotations and find the final position of P.

(23) A rigid body undergoes two rotations. The first is a rotation through a positive 30° angle about a direction specified by the unit vector $\mathbf{n} = 0.286\mathbf{e}_1 + 0.857\mathbf{e}_2 + 0.429\mathbf{e}_3$ with respect to a fixed Cartesian coordinate system with origin at O. This rotation is followed by a second rotation which rotates a positive 90° angle about a direction specified by the unit vector $\mathbf{m} = -0.667\mathbf{e}_1 - 0.667\mathbf{e}_2 + 0.333\mathbf{e}_3$. Both axes of rotation pass through the origin O. If the position of a point P on the rigid body is (1, 1, 0), what is its position after the two rotations?

(24) The velocity field $v_i(x)$ of a rigid body can be written as $v_i = b_i + e_{ijk}c_j x_k$, where the vectors b_i and c_j do not depend on the position of the considered particle. Show that the curl of this velocity field is $2c_i$ while the divergence of the velocity field vanishes.

(25) In the vector field $\mathbf{v}(\mathbf{x})$, let there exist a surface on which $\mathbf{v} = 0$. Show that, at an arbitrary point of this surface, Curl $\mathbf{v}$ is tangential to the surface or vanishes, while Div $\mathbf{v}$ is given by the rate of change of the normal component of $\mathbf{v}$ in the direction of the normal of the surface.

(26) A tensor $\mathbf{M}$ transforms every vector into its mirror image with respect to the plane whose normal is

$$\mathbf{n} = \frac{\sqrt{2}}{2}(\mathbf{e}_1 + \mathbf{e}_2)$$

(a) Find the matrix of $\mathbf{M}$.

(b) Use this linear transformation to find the mirror image of a vector $\mathbf{a} = \mathbf{e}_1 + 2\mathbf{e}_2$.

(Note that this is not a case of rotation. This case is known as reflection.)

(27) Let $\phi(x, y, z)$ and $\psi(x, y, z)$ be scalar functions of positions, and let $\mathbf{v}(x, y, z)$ and $\mathbf{w}(x, y, z)$ be vector functions of position. By writing in the component form, verify the following identities:

(a) $\vec{\nabla}(\phi + \psi) = \vec{\nabla}\phi + \vec{\nabla}\psi$

(b) $\text{Div}(\mathbf{v} + \mathbf{w}) = \text{Div}\ \mathbf{v} + \text{Div}\ \mathbf{w}$

(c) $\text{Div}(\phi\mathbf{w}) = (\vec{\nabla}\phi) \cdot \mathbf{v} + \phi(\text{Div}\ \mathbf{v})$

(28) Consider the integral $\int_L e_{3ij} n_i v_j \, \mathrm{d}L$, where L is the closed boundary of a plane surface S with normal $(0, 0, 1)$; v_i is a vector; n_i is the outward normal of the contour L. Show that this integral is the circulation of vector v_i along L denoted by $\int_L \mathbf{v} \cdot \mathrm{d}\mathbf{L}$.

2

Stress

2.1 Introduction

When forces are applied to a body, they cause the body to deform. In this chapter, we study about the forces and the intensity of forces, and in the next chapter, we study the deformation of the body. The intensity of forces is known as stress, and it is the stress, not the force, that plays an important role in the quantification of effect due to forces. A force may be applied to a small area, and a distributed load of the same resulting magnitude may be applied to a larger area. The effects of the two cases are different locally because the stresses are not the same. The concept of stress needs to be defined, and it can be represented by a second-rank tensor. We investigate the properties of stress in this chapter and we also list some references [1–6] for additional reading.

2.2 Forces

Consider a *body* of volume V and surface S as shown in Figure 2.1. A generic material element of the body has a volume $\mathrm{d}V$, and a generic surface element has area $\mathrm{d}S$ and an *outward normal* $\mathbf{n}$. There are four types of "forces" that act on a body. The "forces" include, in a broad sense, the forces and moments. The four types of "forces" are:

1. *Body forces*: These are forces whose magnitudes are proportional to the mass contained in the material element of the body. The body forces may either be defined per unit mass or per unit volume. An important example of body force is the gravity force, which is expressed as $\rho g \, \mathrm{d}V$, where ρ is the density; and g is the gravitational acceleration.
2. *Surface forces*: These forces act on the surface element $\mathrm{d}S$ of the body. Externally applied loads, contact forces between bodies, and reactions are examples of surface forces, out of which *surface tractions* or *stress vectors* may be defined. The stress vector is the stress force per unit area.

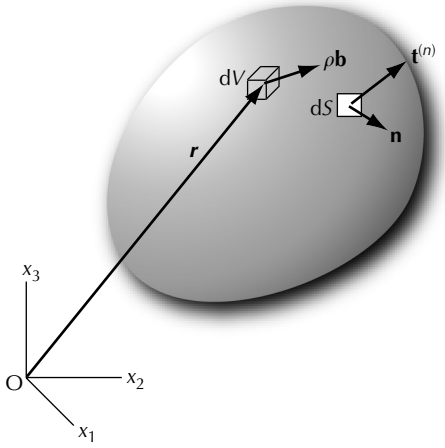

FIGURE 2.1
Body force and surface traction.

3. *Body moments*: These are moments applied to the volumetric element dV. It is usually expressed in terms of moment per unit volume, or moment per unit mass.
4. *Couple stress*: The couple stress is the moment per unit area applied on a surface.

In this chapter, we consider only the first two types of forces — body and surface forces. These are the most common forces that appear in the study of thermo-mechanical behavior of engineering materials. The remaining two types of "forces" are not important in the case of mechanical behavior of materials, but they play an important role in the case of a polarized dielectric solid under the action of an electric field. They also could be significant in the study of bones or materials with microstructures, and/or from the action of an external magnetic field. Even without external couples, couple stress can arise from interactions between adjacent parts of the material other than central-force interaction. In this chapter, we study the basic principles and methods of continuum mechanics.

2.3 Stress Vector

The stress vector is also known as the surface traction. Consider the surface element dS shown in Figure 2.1, where the surface force applied to the element is $\mathbf{p}$. We write

$$\mathbf{p} = \mathbf{t}^{(n)}\, dS \tag{2.1}$$

where

$$\mathbf{t}^{(n)}(x_k) = \lim_{\mathrm{d}S \to 0} \frac{\mathbf{p}}{\mathrm{d}S} \tag{2.2}$$

where $\mathbf{t}^{(n)}$ is the stress vector, which is the intensity of surface force and has a unit of force per unit area. The stress vector is a function of position, a function of x_i, and in general it is different from one point on the surface of the body to another point. The outward normal of $\mathrm{d}S$ is denoted by $\mathbf{n}$, and $\mathbf{t}^{(n)}$ and $\mathbf{n}$ are not in the same direction.

2.4 The Stress Tensor

We now consider the stress inside the body, let us cut out a tetrahedron of infinitesimal size from a body, as shown in Figure 2.2. The triangular surface $\mathrm{d}S^{(n)}$, with outward normal $\mathbf{n}$, is inclined to the coordinate axes. The remaining three sides of the tetrahedron, $\mathrm{d}S_1$, $\mathrm{d}S_2$, and $\mathrm{d}S_3$, lie on the coordinate surfaces, and their outward normals are $-\mathbf{e}_1$, $-\mathbf{e}_2$, and $-\mathbf{e}_3$, respectively. The stress vectors acting on these surfaces are $-\mathbf{t}_1$, $-\mathbf{t}_2$, and $-\mathbf{t}_3$, respectively. The negative sign indicates that these forces act on the surfaces with negative normals. Let us now consider the force equilibrium of the tetrahedron. For this we need to sum the surface forces acting on all faces of the tetrahedron and the body force $\rho\mathbf{b}\,\mathrm{d}V$ acting on the mass of the tetrahedron and then set the result to zero. We obtain

$$-\mathbf{t}_1\,\mathrm{d}S_1 - \mathbf{t}_2\,\mathrm{d}S_2 - \mathbf{t}_3\,\mathrm{d}S_3 + \rho\mathbf{b}\,\mathrm{d}V + \mathrm{d}S^{(n)}\mathbf{t}^{(n)} = 0 \tag{2.3}$$

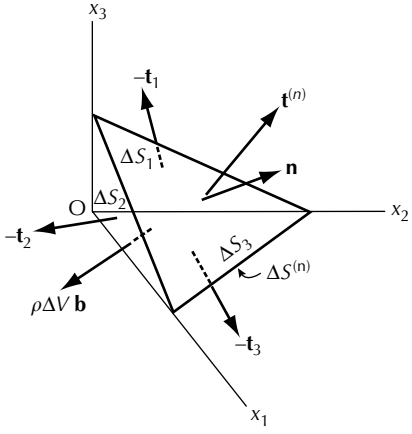

FIGURE 2.2
Stress vectors.

On applying a limiting process, the volume $\mathrm{d}V$ tends to zero, but successive smaller elements retain their surfaces parallel. Since the volume and the area are of the third order and the second order of smallness in length, respectively, in the limit, the term $\rho\mathbf{b}\,\mathrm{d}V$ becomes a higher order of smallness relative to the other terms and can be ignored. Thus, (2.3) becomes

$$\mathbf{t}_1\,\mathrm{d}S_1 + \mathbf{t}_2\,\mathrm{d}S_2 + \mathbf{t}_3\,\mathrm{d}S_3 = \mathrm{d}S^{(n)}\mathbf{t}^{(n)} \tag{2.4}$$

Since $\mathrm{d}S_i$ are projections of the inclined surface $\mathrm{d}S^{(n)}$ onto the coordinate surfaces, we have

$$\frac{\mathrm{d}S_i}{\mathrm{d}S^{(n)}} = n_i = \cos(x_i, n) \tag{2.5}$$

By use of (2.5), (2.4) reduces to

$$\mathbf{t}^{(n)} = \mathbf{t}_i n_i \tag{2.6}$$

Referring to (2.6), we emphasize that $\mathbf{t}^{(n)}$ is a vector acting on the inclined surface $\mathrm{d}S^{(n)}$, and $\mathbf{t}_i$ are vectors acting on the surfaces $\mathrm{d}S_i$. Each of these vectors can be expressed by its components referred to the coordinate axes x_i. To do this, we write

$$\mathbf{t}^{(n)} = t_k^{(n)}\mathbf{e}_k \quad \text{and} \quad \mathbf{t}_i = \sigma_{ik}\mathbf{e}_k \tag{2.7}$$

where $t_k^{(n)}$ are the components of $\mathbf{t}^{(n)}$; and σ_{ik} are the components of $\mathbf{t}_i$ in the coordinate directions. Substituting (2.7) in (2.6), we obtain

$$t_k^{(n)}\mathbf{e}_k = \sigma_{ik}\mathbf{e}_k\, n_i \quad \text{or} \quad t_k^{(n)} = \sigma_{ik}\, n_i \tag{2.8}$$

which, in the matrix form, is written as

$$[t^{(n)}] = [\sigma]^{\mathrm{T}}[n] \tag{2.9}$$

The quantities σ_{ik} are also components of a second-rank tensor from the quotient law discussed in Section 1.5.4. Comparing (2.8) with (1.80), we infer that n_i is an arbitrary tensor (It is arbitrary, since we may choose the direction of the inclined surface.) and $t_k^{(n)}$ is a tensor. Therefore, we conclude that σ_{ik} is a tensor.

The importance of (2.8) is that it relates the stress vector $\mathbf{t}^{(n)}$ acting on a plane with unit normal $\mathbf{n}$ to the stress tensor $\boldsymbol{\sigma}$ in the material element. Knowing $\mathbf{n}$ and $\mathbf{t}^{(n)}$, $\boldsymbol{\sigma}$ may be found from the equation. The stress tensor is expressed using the tensor bases as

$$\boldsymbol{\sigma} = \sigma_{ij}\mathbf{e}_i \otimes \mathbf{e}_j \tag{2.10}$$

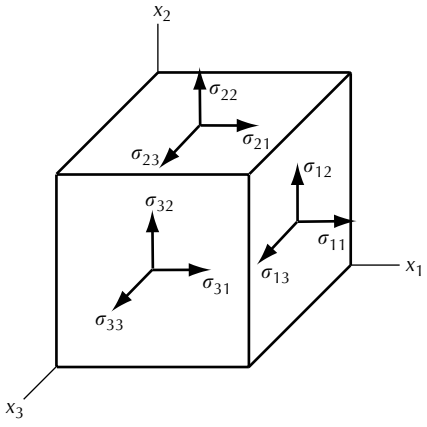

FIGURE 2.3
Stress tensor components.

and in the symbolic notation, (2.8) is written as

$$\mathbf{t}^{(n)} = \boldsymbol{\sigma}^{\mathrm{T}} \cdot \mathbf{n} \tag{2.11}$$

We now discuss the meaning of the stress components σ_{ij}. These are intensity of forces (force per unit area) along the coordinate directions. They vary with the location in the body and their magnitudes and specific characteristics depend on the geometrical shape of the body and the loading condition (surface traction). To determine the distribution of stress in the body, we need to solve a boundary-value problem, by specifying the boundary conditions. However, this problem will not be discussed in this chapter. Instead, we concentrate on understanding the nature of stress at a given point, and consider *the stress at a point*. To visualize the stress at a point, we consider a parallelepiped cut out from the body. The size of the parallelepiped is not important as long as it is infinitesimal. This is so, because, in the sense of calculus, we consider the stress at a point by taking the limit with the size of the parallelepiped of approaching zero. Figure 2.3 shows the components σ_{ij} applied on the faces of the parallelepiped. The first subscript denotes the direction of the normal to the considered plane and the second subscript denotes the direction in which the stress component acts. $\sigma_{11}, \sigma_{22}, \sigma_{33}$ are the normal stresses and $\sigma_{12}, \sigma_{21}, \sigma_{23}, \sigma_{32}, \sigma_{13}, \sigma_{31}$ are the shear stresses.

EXAMPLE 2.1 For given $\mathbf{n}$ and $\mathbf{t}^{(n)}$ on an inclined plane, show by coordinate transformation that σ_{ij} are components of a tensor.

With the orientation of the inclined surface fixed, let us vary the choice of the coordinate system, so that we have x_i and x_i' coordinate systems. In this exercise, $\mathbf{n}$ and $\mathbf{t}^{(n)}$ remain fixed. Using (2.6) and referring to the two coordinate

systems, we have

$$\mathbf{t}_i n_i = \mathbf{t}^{(n)} = t'_i n'_i \tag{a}$$

Referring $\mathbf{t}_i$ to the x_i axes and $\mathbf{t}'_i$ to the x'_i axes, we write

$$\sigma_{ij}\mathbf{e}_j n_i = \sigma'_{ik}\mathbf{e}'_k n'_i \tag{b}$$

But, from (1.28) and (1.32),

$$\mathbf{e}_j = Q_{jk}\mathbf{e}'_k \quad \text{and} \quad n_i = Q_{ip}n'_p \tag{c}$$

So, by substitution

$$\sigma_{ij}Q_{jk}\mathbf{e}'_k Q_{ip}n'_p = \sigma'_{ik}\mathbf{e}'_k n'_i \quad \text{or} \quad \sigma_{ij}Q_{jk}Q_{ip}n'_p = \sigma'_{ik}n'_i \tag{d}$$

Since this relation is true for all $\mathbf{n}$, the above equation reduces to

$$\sigma'_{ij} = Q_{ki}Q_{mj}\sigma_{km} \quad \text{or} \quad [\sigma'] = [Q]^{\mathrm{T}}[\sigma][Q] \tag{e}$$

Therefore, we can conclude that σ_{ij} are components of a second-rank tensor because they obey the transformation rule of a second-rank tensor.

EXAMPLE 2.2 Show that the components of tensor equation (2.11) is (2.8).

$$\text{LHS of (2.11)} = t_i^{(n)}\mathbf{e}_i \tag{a}$$

$$\text{RHS of (2.11)} = \sigma_{ji}\mathbf{e}_i \otimes \mathbf{e}_j \cdot n_k\mathbf{e}_k = \sigma_{ji}n_k\mathbf{e}_i\delta_{lk} = \sigma_{ji}n_j\mathbf{e}_i \tag{b}$$

Equating (a) with (b), we obtain (2.8).

2.5 Equations of Equilibrium

We derive the equations of equilibrium by summing all the forces applied to a body and reducing it to the local form. Refer to the body of Figure 2.1, and note that every portion of this body is in equilibrium. Consider that only surface tractions and body force apply to this body. The "global form" of the equations of equilibrium is then

$$\int_V \rho b_i \, \mathrm{d}V + \int_S t_i^{(n)} \, \mathrm{d}S = 0 \tag{2.12}$$

By use of (2.8), (2.12) becomes

$$\int_V \rho b_i \, \mathrm{d}V + \int_S \sigma_{ji} n_j \, \mathrm{d}S = 0 \tag{2.13}$$

We now use the Gauss theorem to change the second integral of (2.13) into a volume integral. Then, we obtain

$$\int_V (\rho b_i + \sigma_{ji,j}) \, \mathrm{d}V = 0 \tag{2.14}$$

Since the region of integration V is arbitrary and every part of the medium is in equilibrium, we conclude that the integrand must be zero to make the integral zero. Thus,

$$\rho b_i + \sigma_{ji,j} = 0 \quad \text{or} \quad \frac{\partial \sigma_{ji}}{\partial x_j} + \rho b_i = 0 \tag{2.15}$$

Equations (2.15) are the *equations of equilibrium* in the local form, and they may be expanded into a familiar form as

$$\begin{aligned}
\frac{\partial \sigma_{11}}{\partial x_1} + \frac{\partial \sigma_{21}}{\partial x_2} + \frac{\partial \sigma_{31}}{\partial x_3} + \rho b_1 = 0 \\
\frac{\partial \sigma_{12}}{\partial x_1} + \frac{\partial \sigma_{22}}{\partial x_2} + \frac{\partial \sigma_{32}}{\partial x_3} + \rho b_2 = 0 \\
\frac{\partial \sigma_{13}}{\partial x_1} + \frac{\partial \sigma_{23}}{\partial x_2} + \frac{\partial \sigma_{33}}{\partial x_3} + \rho b_3 = 0
\end{aligned} \tag{2.16}$$

EXAMPLE 2.3 Show that the mean value theorem may be used to reduce the "global form" of the equations of equilibrium to the "local form."

The mean value theorem is

$$\int_a^b f(x) \, \mathrm{d}x = (b - a) f(\xi), \quad \text{with } a \leq \xi \leq b \tag{a}$$

On the right-hand side of (a), the function $f(\xi)$ is evaluated at some point in the range of a and b. In the case of equation (2.14), the function f is $\rho b_i + \sigma_{ji,j}$, which is evaluated at some interior point in ΔV. Thus, (2.14) becomes

$$\int_V (\rho b_i + \sigma_{ji,j}) \, \mathrm{d}V = \Delta V (\rho b_i + \sigma_{ji,j}) = 0 \tag{b}$$

Since $\Delta V \neq 0$, we obtain

$$\rho b_i + \sigma_{ji,j} = 0 \tag{c}$$

2.6 Symmetry of the Stress Tensor

The stress tensor is symmetric, that is, $\sigma_{12} = \sigma_{21}$, $\sigma_{23} = \sigma_{32}$, and $\sigma_{31} = \sigma_{13}$, so that the nine components of σ_{ij} reduce to six independent components. This is not an assumption, but is the result of conservation of angular momentum. A simple way to show this is to project the stresses on the parallelepiped of Figure 2.3 onto a coordinate plane, say the $(x_1 - x_2)$ plane, as shown in Figure 2.4. By summing moment about O, we get

$$\sigma_{12} = \sigma_{21} \tag{2.17a}$$

Similarly, by projecting the stresses and the parallelepiped onto the other two coordinate planes and summing moments about O, we find

$$\sigma_{23} = \sigma_{32} \quad \text{and} \quad \sigma_{31} = \sigma_{13} \tag{2.17b}$$

A rigorous proof of the symmetry of the stress tensor may be obtained by considering the conservation of angular momentum. We consider the general case that the body moment per unit volume M_i is included in the derivation. The effect of M_i will then be discussed. Referring to Figure 2.1, we have

$$\rho(\mathbf{r} \times \mathbf{b})_i = \rho e_{ijk} x_j b_k = \text{moment of } \rho b_k \text{ about the origin} \tag{2.18}$$

$$(\mathbf{r} \times \mathbf{t}^{(n)})_i = e_{ijk} x_j t_k^{(n)} = \text{moment of } t_k^{(n)} \text{ about the origin} \tag{2.19}$$

Summing moment about the origin O, we write

$$\int_V \rho e_{ijk} x_j b_k \, dV + \int_S e_{ijk} x_j t_k^{(n)} \, dS + \int_V M_i \, dV = 0 \tag{2.20}$$

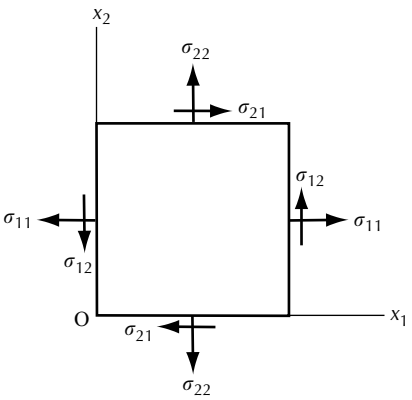

FIGURE 2.4
2 D stress components.

The second integral in (2.20) may be transformed into a volume integral by use of the Gauss theorem. Thus, (2.20) becomes

$$\int_V \left[\rho e_{ijk} x_j b_k + \frac{\partial}{\partial x_r}(e_{ijk} x_j \sigma_{rk}) + M_i \right] \mathrm{d}V = 0 \tag{2.21}$$

The second term in (2.21) is

$$e_{ijk}\left[\frac{\partial x_j}{\partial x_r}\sigma_{rk} + x_j \frac{\partial \sigma_{rk}}{\partial x_r}\right] = e_{ijk}(\sigma_{jk} + x_j \sigma_{rk,r}) = e_{ijk}\sigma_{jk} + e_{ijk} x_j(-\rho b_k) \tag{2.22}$$

where the last expression was obtained from the equations of equilibrium. Hence, (2.21) becomes

$$\int_V [\rho e_{ijk} x_j b_k + e_{ijk}\sigma_{jk} - \rho e_{ijk} x_j b_k + M_i] \, \mathrm{d}V = 0 \tag{2.23}$$

which leads to

$$\int_V (e_{ijk}\sigma_{jk} + M_i) \, \mathrm{d}V = 0 \tag{2.24}$$

Since the integrand is continuous and the volume V is arbitrary, we obtain

$$e_{ijk}\sigma_{jk} + M_i = 0 \tag{2.25}$$

We now discuss the meaning of (2.25) in two different cases as follows:

1. If the body moment is absent, that is, $M_i = 0$, then (2.25) reduces to

$$e_{ijk}\sigma_{jk} = 0 \tag{2.26}$$

For $i = 1$, (2.26) gives $e_{123}\sigma_{23} + e_{132}\sigma_{32} = 0$. Since $e_{123} = 1$ and $e_{132} = -1$, we obtain $\sigma_{23} = \sigma_{32}$. For $i = 2$, (2.26) leads to $\sigma_{13} = \sigma_{31}$; and for $i = 3$, (2.26) leads to $\sigma_{21} = \sigma_{12}$. Therefore, we write

$$\sigma_{ij} = \sigma_{ji} \tag{2.27}$$

2. If $M_i \neq 0$, then $\sigma_{ij} \neq \sigma_{ji}$, and the stress tensor is not symmetric.

2.7 Principal Stresses

If we pass a plane through the parallelepiped of Figure 2.3 and cut the element into two parts, then one of the two parts may be viewed as a tetrahedron

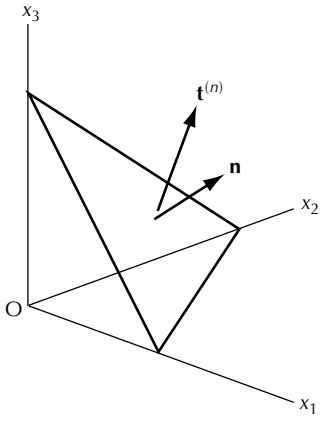

FIGURE 2.5
Stress vector on an inclined plane.

shown in Figure 2.5. Within the tetrahedron the stress is σ_{ij} as defined in Figure 2.3. The unit normal to the plane is $\mathbf{n}$, and the associated stress vector $\mathbf{t}^{(n)}$may be found from (2.8) or (2.11). Generally, the two vectors $\mathbf{n}$ and $\mathbf{t}^{(n)}$ have different directions as shown in Figure 2.5. We now inquire whether we can cut the parallelepiped in a specific direction (find an $\mathbf{n}$), such that $\mathbf{n}$ and $\mathbf{t}^{(n)}$ have the same direction. If such an $\mathbf{n}$ exists, then $\mathbf{t}^{(n)} = \lambda\mathbf{n}$, where λ is the magnitude of vector $\mathbf{t}^{(n)}$. In this event, using (2.6), we obtain

$$\mathbf{t}_i n_i = \lambda \mathbf{n} \tag{2.28}$$

Substituting (2.7) into (2.28), we have

$$\sigma_{ij}\mathbf{e}_j n_i = \lambda n_j \mathbf{e}_j \quad \text{and} \quad \sigma_{ij} n_i = \lambda n_j \tag{2.29}$$

which may be written as

$$(\sigma_{ij} - \lambda\delta_{ij}) n_i = 0 \tag{2.30}$$

The solution of this set of equations would make $\mathbf{t}^{(n)}$ lie in the direction of $\mathbf{n}$. The solution includes finding the direction $\mathbf{n}$ and the magnitude λ. Mathematically speaking, (2.30) is a statement of the *eigenvalue problem*.

The trivial solution $n_i = 0$ of the homogeneous equations (2.30) does not satisfy the unit vector condition $n_1^2 + n_2^2 + n_3^2 = 1$, so it cannot be our answer.

The condition that a nontrivial solution exists for n_i is that

$$|\sigma_{ij} - \lambda\delta_{ij}| = \begin{vmatrix} \sigma_{11} - \lambda & \sigma_{12} & \sigma_{13} \\ \sigma_{21} & \sigma_{22} - \lambda & \sigma_{23} \\ \sigma_{31} & \sigma_{32} & \sigma_{33} - \lambda \end{vmatrix} = 0 \tag{2.31}$$

Expanding the determinant in (2.31), we obtain

$$\lambda^3 - J_1\lambda^2 + J_2\lambda - J_3 = 0 \tag{2.32}$$

where

$$\begin{aligned} J_1 &= \text{tr}(\sigma_{ij}) = \sigma_{ii} \\ J_2 &= \text{tr cofactor}(\sigma_{ij}) = \begin{vmatrix} \sigma_{22} & \sigma_{23} \\ \sigma_{32} & \sigma_{33} \end{vmatrix} + \begin{vmatrix} \sigma_{11} & \sigma_{13} \\ \sigma_{31} & \sigma_{33} \end{vmatrix} + \begin{vmatrix} \sigma_{11} & \sigma_{12} \\ \sigma_{21} & \sigma_{22} \end{vmatrix} \\ J_3 &= \det\ \sigma_{ij} \end{aligned} \tag{2.33}$$

The quantities J_1, J_2, and J_3 are called the principal *invariants* of σ_{ij}, because they remain invariant with a rotation of the coordinate system. Referring to two coordinate systems x_i and x_i', the invariants transform as

$$\sigma_{ii} = \sigma_{ii}', \quad \text{tr cofactor}(\sigma_{ij}) = \text{tr cofactor}(\sigma_{ij}'), \quad \det\sigma_{ij} = \det\sigma_{ij}' \tag{2.34}$$

Therefore, $J_1 = J_1'$, $J_2 = J_2'$ and $J_3 = J_3'$. The stress invariants are further discussed in Section 2.11. Note that stresses $(\lambda_1, \lambda_2, \lambda_3)$ found by solving the characteristic equation (2.32) are called principal stresses and are often denoted by $(\sigma_1, \sigma_2, \sigma_3)$. In the mathematical language, λ_r $(r = 1, 2, 3)$ are eigenvalues and the three corresponding $n_i^{(r)}$ are eigenvectors. The eigenvalue problem is discussed in Section 2.8.

2.8 Properties of Eigenvalues and Eigenvectors

The eigenvalue problem is governed by equation (2.30). It is the governing equation of many engineering problems. The properties of the eigenvalues and eigenvectors for a symmetric tensor σ_{ij} are summarized below:

1. Eigenvalues are real.
2. Eigenvectors are real.
3. Eigenvectors are orthogonal.
4. If eigenvalues are distinct, eigenvectors can be determined uniquely.

5. If two eigenvalues are identical, one eigenvector corresponding to the distinct eigenvalue is unique, other two eigenvectors lie in a plane normal to the unique eigenvector.
6. If all three eigenvalues are identical, then all directions in the space x_i are eigen directions. In this case $\sigma_{ij} = \lambda\delta_{ij}$.
7. The principal stress components $\bar{\sigma}_{ij}$ and the stress components σ_{ij} are related by $[\bar{\sigma}] = [Q]^{\mathrm{T}}[\sigma][Q]$, where the transformation matrix $[Q]$ is defined by the eigenvectors (direction cosines between the eigenvectors and coordinate axes) and this subject is discussed in Section 2.12.

EXAMPLE 2.4 Show that if σ_{ij} is symmetric, then three real roots λ_1, λ_2, λ_3 exist in (2.30).

This is proven by contradiction. First, we let λ be complex, that is, $\lambda = \alpha + i\beta$. For the sake of generality, let n_i be complex too, that is, $n_i = \mu_i + i\xi_i$. Then, α, β, μ_i, and ξ_i are real. By substitution, (2.30) becomes

$$\sigma_{ij}(\mu_i + i\xi_i) - (\alpha + i\beta)(\mu_j + i\xi_j) = 0 \tag{a}$$

By equating real and imaginary parts in (a), we obtain

$$\begin{aligned} \sigma_{ij}\mu_i &= \alpha\mu_j - \beta\xi_j \\ \sigma_{ij}\xi_i &= \beta\mu_j + \alpha\xi_j \end{aligned} \tag{b}$$

Multiplying the first equation of (b) by ξ_j and the second equation of (b) by μ_j and subtracting the two resulting equations, we get

$$\beta(\xi_j\xi_j + \mu_j\mu_j) = 0 \tag{c}$$

Since the quantity within the parenthesis is nonnegative, we have

$$\beta = 0 \tag{d}$$

Hence, all eigenvalues are real.

EXAMPLE 2.5 Show that if σ_{ij} is symmetric, then all eigenvectors of (2.30) are real.

Proof

Equation (2.30) may be written as

$$\begin{aligned} (\sigma_{11} - \lambda)n_1 + \sigma_{21}n_2 + \sigma_{31}n_3 &= 0 \\ \sigma_{12}n_1 + (\sigma_{22} - \lambda)n_2 + \sigma_{32}n_3 &= 0 \\ \sigma_{13}n_1 + \sigma_{23}n_2 + (\sigma_{33} - \lambda)n_3 &= 0 \end{aligned} \tag{a}$$

Because the determinant of (a) is zero, the rank is at most two (the rank of a matrix is the dimension of the largest square submatrix with a nonvanishing determinant that is contained in the matrix); therefore, the three equations are linearly dependent and the third equation can be expressed in terms of the former two. If we delete the last equation, then the number of equation is less than the number of unknown. Hence, a real solution for n_1, n_2, and n_3 always exists. If the 3×2 matrix has rank two, then we can solve for n_1 and n_2 (say) in terms of n_3, that is,

$$n_1 = N_1 n_3 \quad \text{and} \quad n_2 = N_2 n_3 \tag{b}$$

where N_1 and N_2 are proportional factors determined by the two equations. But $\mathbf{n}$ is a unit vector and it must satisfy

$$n_1^2 + n_2^2 + n_3^2 = 1 \tag{c}$$

Substituting (b) into (c), we obtain

$$(N_1^2 + N_2^2 + 1) n_3^2 = 1 \tag{d}$$

which may be solved to yield

$$n_3 = (1 + N_1^2 + N_2^2)^{-1/2} \tag{d}$$

Expressions in (b) and (e) form the solution of (a). In this case, $\mathbf{n}$ can be found uniquely. If the rank is less than two, then $\mathbf{n}$ cannot be determined uniquely, the physical significance being that there may exist more than one $\mathbf{n}$ such that

$$\mathbf{t}^{(n)} = \lambda \mathbf{n} \tag{f}$$

An example is, when $\sigma_{11} = \sigma_{22}$, then $\mathbf{n}$ cannot be determined uniquely.

EXAMPLE 2.6 Show that eigenvectors are mutually orthogonal.

Case 1: All λ's are distinct

In this case $\lambda_1 \neq \lambda_2 \neq \lambda_3$. Choose two such directions $n_i^{(r)}$ and $n_i^{(s)}, r \neq s$, then (2.30) becomes

$$\sigma_{ij} n_i^{(r)} - \lambda_r n_j^{(r)} = 0 \tag{a}$$

$$\sigma_{ij} n_i^{(s)} - \lambda_s n_j^{(s)} = 0 \tag{b}$$

Multiplying (a) by $n_j^{(s)}$ and (b) by $n_j^{(r)}$, and subtracting the two resulting equations, we find

$$(\lambda_r - \lambda_s) n_i^{(r)} n_i^{(s)} = 0 \tag{c}$$

But since $\lambda_r \neq \lambda_s$, it follows that $n_i^{(r)}\, n_i^{(s)} = 0$, or $\mathbf{n}^{(r)} \cdot \mathbf{n}^{(s)} = 0$, for $r \neq s$. Therefore, $\mathbf{n}^{(r)}$ and $\mathbf{n}^{(s)}$ are mutually orthogonal. In general, we may write

$$n_i^{(r)} n_i^{(s)} = \delta_{rs} \tag{d}$$

Case 2: Two λ's are not distinct

Assume that $\lambda_1 \neq \lambda_2$ and $\lambda_2 = \lambda_3$. Choose one characteristic direction $\mathbf{n}^{(1)}$ and let x_1' coincide with $\mathbf{n}^{(1)}$ then σ_{ij}' will have the form

$$\begin{bmatrix} \sigma_{11}' & 0 & 0 \\ 0 & \sigma_{22}' & \sigma_{23}' \\ 0 & \sigma_{32}' & \sigma_{33}' \end{bmatrix} \tag{e}$$

We then examine the characteristic direction in the x_i' system. The characteristic equation is (for $\lambda = \lambda_2$)

$$\begin{bmatrix} \sigma_{11}' - \lambda_2 & 0 & 0 \\ 0 & \sigma_{22}' - \lambda_2 & \sigma_{23}' \\ 0 & \sigma_{32}' & \sigma_{33}' - \lambda_2 \end{bmatrix}^{\mathrm{T}} \begin{bmatrix} n_1^{(2)} \\ n_2^{(2)} \\ n_3^{(2)} \end{bmatrix} = 0 \tag{f}$$

Evidently, $n_1^{(2)} = 0$, since the first equation of (f) is $\left(\sigma_{11}' - \lambda_2\right) n_1^{(2)} = 0$ and $\sigma_{11}' = \lambda_1 \neq \lambda_2$. This implies that $x_1' \perp \mathbf{n}^{(2)}$ or $\mathbf{n}^{(1)} \perp n^{(2)}$. The remaining two equations are

$$\begin{aligned} (\sigma_{22}' - \lambda_2) n_2^{(2)} + \sigma_{23}' n_3^{(2)} &= 0 \\ \sigma_{32} n_2^{(2)} + (\sigma_{33}' - \lambda_2) n_3^{(2)} &= 0 \end{aligned} \tag{g}$$

The determinant of (g) vanishes for nontrivial solution of $n_2^{(2)}$ and $n_3^{(2)}$. Thus,

$$\begin{vmatrix} (\sigma_{22}' - \lambda_2) & \sigma_{23}' \\ \sigma_{32}' & (\sigma_{33}' - \lambda_2) \end{vmatrix} = 0 \tag{h}$$

or

$$\lambda_2^2 - \lambda_2(\sigma_{22}' + \sigma_{33}') - \sigma_{23}'\sigma_{32}' + \sigma_{22}'\sigma_{33}' = 0 \tag{i}$$

The two roots are

$$\lambda_{2,3} = \frac{\sigma'_{22} + \sigma'_{33}}{2} \pm \frac{1}{2}\sqrt{(\sigma'_{22} + \sigma'_{33})^2 - 4(\sigma'_{22}\sigma'_{33} - \sigma'_{32}\sigma'_{23})}$$
$$= \frac{\sigma'_{22} + \sigma'_{33}}{2} \pm \frac{1}{2}\sqrt{(\sigma'_{22} - \sigma'_{33})^2 + 4(\sigma'_{32}\sigma'_{23})} \tag{j}$$

The only condition which makes λ_2 and λ_3 not be distinct is for the discriminant to vanish, that is,

$$\sigma'_{23} = \sigma'_{32} = 0 \quad \text{and} \quad \sigma'_{22} = \sigma'_{33} = \lambda_2 \tag{k}$$

Substituting these results in (g), we see that any values of $n_2^{(2)}$ and $n_3^{(2)}$ and, similarly $n_2^{(3)}$ and $n_3^{(3)}$, will satisfy the characteristic equation.

2.9 Normal and Shear Components

We observed in Section 2.7 that on an inclined plane with unit normal $\mathbf{n}$, the stress vector $\mathbf{t}^{(n)}$ and $\mathbf{n}$ generally have different directions. The two vectors have the same direction only when $\mathbf{n}$ is the principal direction of σ_{ij}. In the general case, $\mathbf{t}^{(n)}$ may be decomposed into two components: one in the normal direction denoted by σ^{N} and the other in the tangential direction denoted by σ^{S} as shown in Figure 2.6. σ^{N} is called the *normal component* and σ^{S} the *shear component* of the stress vector. The normal component is expressed by

$$\sigma^{\mathrm{N}} = \mathbf{t}^{(n)} \cdot \mathbf{n} = \sigma_{ji} n_j n_i \tag{2.35}$$

and the shear component is obtained from

$$|\mathbf{t}^{(n)}|^2 = (\sigma^{\mathrm{N}})^2 + (\sigma^{\mathrm{S}})^2 \tag{2.36}$$

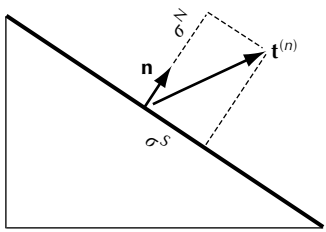

FIGURE 2.6
Normal and shear stress components.

2.9.1 Directions Along which Normal Components of σ_{ij} are Maximized or Minimized

We like to find an $\mathbf{n}$ such that σ^{N} is maximized or minimized. It is noted that $\mathbf{n}$ is subject to the condition $n_i n_i = 1$. The method of Lagrangian multiplier denoted by λ is used, so that we maximize or minimize the expression

$$F = \sigma_{ji} n_i n_j - \lambda n_i n_i \tag{2.37}$$

The differentiation of (2.37) yields

$$\frac{\partial F}{\partial n_i} = 0 \quad \text{or} \quad \sigma_{ji} n_j - \lambda n_i = 0 \tag{2.38}$$

But, (2.38) is the condition that n_i be a principal direction. Hence, the principal directions make σ^{N} either maximum or minimum, and the max. (or min.) normal component is equal to the max. (or min.) principal value of σ_{ij}.

2.9.2 The Maximum Shear Stress

We use (2.36) to obtain the expression of the shear component σ^{S}. We find first from (2.8) and (2.35) the following expressions:

$$|\mathbf{t}^{(n)}|^2 = \sigma_{ji} n_j \sigma_{ki} n_k \tag{2.39}$$

$$(\sigma^{\mathrm{N}})^2 = \sigma_{ji} n_i n_j \sigma_{mk} n_k n_m \tag{2.40}$$

For simplicity, we let x_i coincide with principal axes, then we have only the principal stresses $\sigma_1, \sigma_2, \sigma_3$ and the shear stresses are zero. In this case, (2.35) reduces to

$$\sigma^{\mathrm{N}} = \sigma_1 n_1^2 + \sigma_2 n_2^2 + \sigma_3 n_3^2 \tag{2.41}$$

and (2.39) becomes

$$|\mathbf{t}^{(n)}|^2 = \sigma_1^2 n_1^2 + \sigma_2^2 n_2^2 + \sigma_3^2 n_3^2 \tag{2.42}$$

Substituting (2.41) and (2.42) into (2.36), we obtain

$$(\sigma^{\mathrm{S}})^2 = \sigma_1^2 n_1^2 + \sigma_2^2 n_2^2 + \sigma_3^2 n_3^2 - \left(\sigma_1 n_1^2 + \sigma_2 n_2^2 + \sigma_3 n_3^2\right)^2 \tag{2.43}$$

or

$$(\sigma^{\mathrm{S}})^2 + [(\sigma_1 n_1^2) + (\sigma_2 n_2^2) + \sigma_3(1 - n_1^2 - n_2^2)]^2 = \sigma_1^2 n_1^2 + \sigma_2^2 n_2^2 + \sigma_3^2 (1 - n_1^2 - n_2^2) \tag{2.44}$$

To find the maximum σ^{S}, we set the derivatives to zero:

$$\frac{\partial(\sigma^{\mathrm{S}})^2}{\partial n_1} = 0, \qquad \frac{\partial(\sigma^{\mathrm{S}})^2}{\partial n_2} = 0 \tag{2.45}$$

and we find

$$2[\sigma_1 n_1^2 + \sigma_2 n_2^2 + \sigma_3(1 - n_1^2 - n_2^2)]n_1(\sigma_1 - \sigma_3) = n_1(\sigma_1^2 - \sigma_3^2) \tag{2.46}$$

$$2[\sigma_1 n_1^2 + \sigma_2 n_2^2 + \sigma_3(1 - n_1^2 - n_2^2)]n_2(\sigma_2 - \sigma_3) = n_2(\sigma_2^2 - \sigma_3^2) \tag{2.47}$$

We now discuss three cases depending on whether the principal stresses are distinct or not.

Case 1: The three principal stresses are distinct, that is, $\sigma_1 \neq \sigma_2 \neq \sigma_3$

Common factors of $(\sigma_1 - \sigma_3)$ and $(\sigma_2 - \sigma_3)$ can be cancelled out from (2.46) and (2.47), respectively, so that the two equations become

$$2[\sigma_1 n_1^2 + \sigma_2 n_2^2 + \sigma_3(1 - n_1^2 - n_2^2)]n_1 = n_1(\sigma_1 + \sigma_3) \tag{2.48}$$

$$2[\sigma_1 n_1^2 + \sigma_2 n_2^2 + \sigma_3(1 - n_1^2 - n_2^2)]n_2 = n_2(\sigma_2 + \sigma_3) \tag{2.49}$$

It follows that n_1 and n_2 cannot both be different from zero, because otherwise n_1 can be cancelled out from (2.48) and n_2 cancelled out from (2.49) to obtain the following two equations:

$$\sigma_1 n_1^2 + \sigma_2 n_2^2 + \sigma_3(1 - n_1^2 - n_2^2) - \frac{\sigma_1 + \sigma_3}{2} = 0 \tag{2.50}$$

$$\sigma_1 n_1^2 + \sigma_2 n_2^2 + \sigma_3(1 - n_1^2 - n_2^2) - \frac{\sigma_2 + \sigma_3}{2} = 0 \tag{2.51}$$

If these two equations are to be satisfied, we must have $\sigma_1 = \sigma_2$, in contradiction with the hypothesis that $\sigma_1 \neq \sigma_2$. Either n_1 or n_2, therefore, must be zero. Let $n_1 = 0$, then from (2.49) we obtain

$$2[\sigma_2 n_2^2 + \sigma_3(1 - n_2^2)]n_2 = n_2(\sigma_2 + \sigma_3) \tag{2.52}$$

which may be simplified to

$$n_2^2(\sigma_2 - \sigma_3) = \frac{\sigma_2 - \sigma_3}{2} \quad \text{or} \quad n_2 = \pm\sqrt{\frac{1}{2}} = \pm\cos 45^\circ \tag{2.53}$$

Therefore, the solution is

$$n_1 = 0, \qquad n_2 = \pm\sqrt{\frac{1}{2}}, \qquad n_3 = \pm\sqrt{\frac{1}{2}} \tag{2.54a}$$

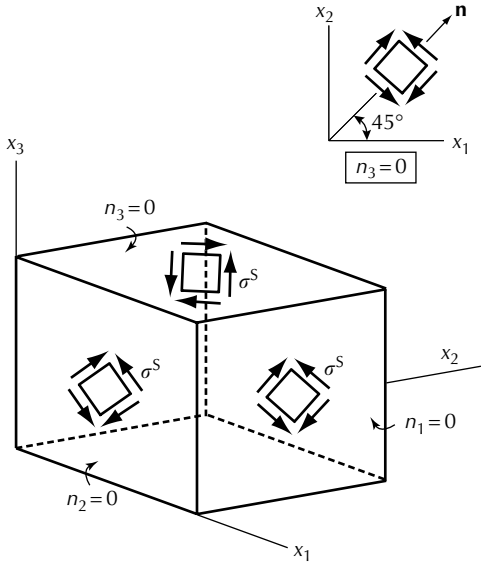

FIGURE 2.7
Maximum shear stresses.

The other two cases are

$$n_1 = \pm\sqrt{\frac{1}{2}}, \qquad n_2 = 0, \qquad n_3 = \pm\sqrt{\frac{1}{2}} \tag{2.54b}$$

$$n_1 = \pm\sqrt{\frac{1}{2}}, \qquad n_2 = \pm\sqrt{\frac{1}{2}}, \qquad n_3 = 0 \tag{2.54c}$$

The shear stresses σ^S active in the planes of $n_1 = 0$, $n_2 = 0$, or $n_3 = 0$ are shown in Figure 2.7. In the insert, we show the plane of $n_3 = 0$. It is seen that the maximum shear stresses are making $\pm 45°$ angles with the coordinate axes.

Finally, we note that in all cases of (2.54)

$$\sigma^S = \frac{\sigma_2 - \sigma_3}{2} \quad \text{or} \quad \frac{\sigma_1 - \sigma_3}{2} \quad \text{or} \quad \frac{\sigma_1 - \sigma_2}{2} \tag{2.55}$$

which may be obtained by substituting, respectively, the planes of (2.54a,b,c) into equation (2.44) for σ^S.

Case 2: Two principal stresses are not distinct and we consider the case of $\sigma_2 = \sigma_3 \neq \sigma_1$

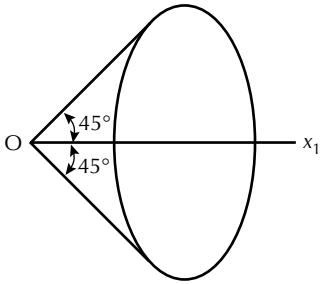

FIGURE 2.8
Maximum shear stress in the case of $\sigma_2 = \sigma_3 \neq \sigma_1$.

This is a case of rotational symmetry about the x_1-axis. In this case, n_2 is arbitrary; since $\sigma_3 \neq \sigma_1$, we may use (2.48) to obtain

$$n_1^2(\sigma_1 - \sigma_3) = \frac{\sigma_1 - \sigma_3}{2} \tag{2.56}$$

We note that $n_1 \neq 0$, because, if $n_1 = 0$, then upon choosing $n_2 = 0$, we obtain $n_3 = 1$. Using (2.44), the case of $n_1 = 0$ leads to $\sigma^S = 0$, which is the minimum shear stress, in contradiction with the goal of finding the maximum shear stress. Simplifying (2.56), we find

$$n_1 = \pm\sqrt{\frac{1}{2}}, \qquad n_2 = \text{arbitrary}, \qquad n_3 = \text{arbitrary} \tag{2.57}$$

In this discussion, special attention is given to the relation $n_1^2 + n_2^2 + n_3^2 = 1$. Figure 2.8 shows a cone with generator in the x_1 direction. The maximum shear stress σ^S lies on the surface of the cone and its magnitude is given by $\sigma^S = \frac{1}{2}(\sigma_1 - \sigma_2)$ found on substitution of (2.57) into (2.44).

Case 3: All principal stresses are equal, that is, $\sigma_1 = \sigma_2 = \sigma_3 = \sigma$

This is a case of hydrostatic pressure.
In this case, we found from (2.43) that

$$(\sigma^S)^2 = \sigma^2(n_1^2 + n_2^2 + n_3^2) - \sigma^2(n_1^2 + n_2^2 + n_3^2)^2 = 0 \tag{2.58}$$

with arbitrary n_1, n_2, n_3, that is, the shear stress is zero in all directions.

Finally, the following conclusion may be stated: the maximum shear stress is equal to one-half the difference between the greatest and least normal stresses and acts on the plane that bisects the angle between the directions of the largest and smallest principal stresses.

2.10 Mean and Deviatoric Stresses

Any tensor of rank two can be written as

$$C_{ij} = \alpha\delta_{ij} + B_{ij} = \frac{(C_{11} + C_{22} + C_{33})}{3}\delta_{ij} + \begin{bmatrix} \{C_{11} - \frac{1}{3}(C_{11} + C_{22} + C_{33})\} & C_{12} & C_{13} \\ C_{21} & \{C_{22} - \frac{1}{3}(C_{11} + C_{22} + C_{33})\} & C_{23} \\ C_{31} & C_{32} & \{C_{33} - \frac{1}{3}(C_{11} + C_{22} + C_{33})\} \end{bmatrix} \tag{2.59}$$

In a similar manner, the stress tensor σ_{ij} can be written as

$$\sigma_{ij} = \frac{(\sigma_{11} + \sigma_{22} + \sigma_{33})}{3}\delta_{ij} + \begin{bmatrix} \{\sigma_{11} - \frac{1}{3}(\sigma_{11} + \sigma_{22} + \sigma_{33})\} & \sigma_{12} & \sigma_{13} \\ \sigma_{21} & \{\sigma_{22} - \frac{1}{3}(\sigma_{11} + \sigma_{22} + \sigma_{33})\} & \sigma_{23} \\ \sigma_{31} & \sigma_{32} & \{\sigma_{33} - \frac{1}{3}(\sigma_{11} + \sigma_{22} + \sigma_{33})\} \end{bmatrix} \tag{2.60}$$

or

$$\sigma_{ij} = \tfrac{1}{3}\sigma_{kk}\delta_{ij} + \sigma'_{ij} \tag{2.61}$$

where $\frac{1}{3}\sigma_{kk}$ is the *mean stress*; and

$$\sigma'_{ij} = \begin{bmatrix} \{\sigma_{11} - \frac{1}{3}(\sigma_{11} + \sigma_{22} + \sigma_{33})\} & \sigma_{12} & \sigma_{13} \\ \sigma_{21} & \{\sigma_{22} - \frac{1}{3}(\sigma_{11} + \sigma_{22} + \sigma_{33})\} & \sigma_{23} \\ \sigma_{31} & \sigma_{32} & \{\sigma_{33} - \frac{1}{3}(\sigma_{11} + \sigma_{22} + \sigma_{33})\} \end{bmatrix} \tag{2.62}$$

is the *deviatoric stress* tensor. Thus, the stress may be decomposed into the hydrostatic (mean stress) and deviatoric parts. This property of stress is particularly useful in the study of plasticity which is discussed further in the later chapters of this book. Plastic yielding and plastic deformation of metals are known to be independent of the hydrostatic stress but are dependent on the deviatoric stress.

2.11 Octahedral Shearing Stress

The concept of octahedral shearing stress is useful in plasticity as well. Consider principal stress axes. If the normal n_i of a plane in this stress space makes equal angles with the three axes, there are eight directions which satisfy $n_1^2 = n_2^2 = n_3^2 = \frac{1}{3}$. The eight planes associated with these eight directions are called the *octahedral planes*. The planes form equal angles with the principal directions and form a diamond shaped region around the zero stress point.

The shearing stress σ_o^S that acts on the octahedral planes is called the *octahedral shearing stress*. From (2.43), in the principal stress space, we can show that the align reduces to

$$(\sigma^S)^2 = (\sigma_1 - \sigma_2)^2 n_1^2 n_2^2 + (\sigma_2 - \sigma_3)^2 n_2^2 n_3^2 + (\sigma_3 - \sigma_1)^2 n_3^2 n_1^2 \tag{2.63}$$

If $n_1^2 = n_2^2 = n_3^2 = \frac{1}{3}$, then (2.63) reduces to

$$9(\sigma_o^S)^2 = (\sigma_1 - \sigma_2)^2 + (\sigma_2 - \sigma_3)^2 + (\sigma_3 - \sigma_1)^2 \tag{2.64}$$

This is the expression for octahedral shearing stress. On the other hand, the normal component acting on the octahedral plane is given from (2.41) by

$$\sigma_o^N = \tfrac{1}{3}(\sigma_1 + \sigma_2 + \sigma_3) = \text{mean stress} \tag{2.65}$$

We now show that the octahedral shearing stress may be expressed in terms of the stress invariants. To this end, we observe that align (2.64) can be rewritten as:

$$\begin{aligned} 9(\sigma_o^S)^2 &= 2(\sigma_1^2 + \sigma_2^2 + \sigma_3^2) - 2(\sigma_1\sigma_2 + \sigma_2\sigma_3 + \sigma_3\sigma_1) \\ &= 2[(\sigma_1 + \sigma_2 + \sigma_3)^2 - 2(\sigma_1\sigma_2 + \sigma_1\sigma_3 + \sigma_2\sigma_3)] - 2(\sigma_1\sigma_2 + \sigma_2\sigma_3 + \sigma_3\sigma_1) \\ &= 2[J_1^2 - 2J_2] - 2J_2 = 2J_1^2 - 6J_2 \end{aligned} \tag{2.66}$$

where (2.33) was used in the principal coordinate system. It is seen that the octahedral shearing stress σ_o^S is invariant with rotation of coordinate axes. If J_1 and J_2 are expressed in terms of stress components taken relative to arbitrary (x_1, x_2, x_3) axes — not principal axes as above —, equation (2.66), on the substitution of (2.33), becomes

$$9(\sigma_o^S)^2 = (\sigma_{11} - \sigma_{22})^2 + (\sigma_{22} - \sigma_{33})^2 + (\sigma_{33} - \sigma_{11})^2 + 6\sigma_{12}^2 + 6\sigma_{13}^2 + 6\sigma_{23}^2 \tag{2.67}$$

This expression forms the basis for von Mises yield criterion discussed in Chapter 6 .

2.12 The Stress Invariants

We would like to see now that the stress invariants defined in (2.33) remain unchanged under rotation of the coordinate system. Let us assume that coordinates x_i rotate into x_i'. The first stress invariant is

$$J_1 = \sigma_{ii} \tag{2.68}$$

In the coordinate system x_i', we denote the components of σ_{ij} by σ_{ij}', then the first invariant in the x_i' system is $J_1' = \sigma_{ii}'$. Using the transformation align of the second-rank tensor (1.46), we have

$$\sigma_{ii}' = Q_{ri}Q_{si}\sigma_{rs} = \delta_{rs}\sigma_{rs} = \sigma_{ss} = \sigma_{ii} \tag{2.69}$$

Comparing (2.68) and (2.69), we find

$$J_1 = J_1' \tag{2.70}$$

which shows that J_1 indeed remains unchanged with rotation of the coordinate system.

The third invariant is

$$J_3 = \det \sigma = \tfrac{1}{6} e_{ijk}e_{rst}\sigma_{ir}\sigma_{js}\sigma_{kt} \tag{2.71}$$

In the primed coordinate system,

$$\begin{aligned} J_3' &= \tfrac{1}{6} e_{ijk}e_{rst}\sigma_{ir}'\sigma_{js}'\sigma_{kt}' \\ &= \tfrac{1}{6} e_{ijk}e_{rst}Q_{ai}Q_{br}\sigma_{ab}Q_{cj}Q_{ds}\sigma_{cd}Q_{ek}Q_{ft}\sigma_{ef} \\ &= \tfrac{1}{6} (e_{ijk}Q_{ai}Q_{cj}Q_{ek})(e_{rst}Q_{br}Q_{ds}Q_{ft})\sigma_{ab}\sigma_{cd}\sigma_{ef} \\ &= \tfrac{1}{6} e_{ace}e_{bdf}\sigma_{ab}\sigma_{cd}\sigma_{ef} = J_3 \end{aligned} \tag{2.72}$$

It is seen from (2.72) that J_3 is an invariant. In the derivation of (2.72), we used the relation $e_{ijk}' = e_{ijk}$, which indicates that the permutation symbol is a third-rank isotropic tensor.

The second invariant is

$$J_2 = \text{tr cofactor}\, \sigma = M_{ii} \tag{2.73}$$

Note that we use M_{ij} to denote the matrix of the cofactors and not the minors. We now find the expressions for the minors. To do this, we first expand the

determinant of the stress matrix as

$$\begin{vmatrix} \sigma_{11} & \sigma_{12} & \sigma_{13} \\ \sigma_{21} & \sigma_{22} & \sigma_{23} \\ \sigma_{31} & \sigma_{32} & \sigma_{33} \end{vmatrix} = \sigma_{11} \begin{vmatrix} \sigma_{22} & \sigma_{23} \\ \sigma_{32} & \sigma_{33} \end{vmatrix} - \sigma_{12} \begin{vmatrix} \sigma_{21} & \sigma_{23} \\ \sigma_{31} & \sigma_{33} \end{vmatrix} + \sigma_{13} \begin{vmatrix} \sigma_{21} & \sigma_{22} \\ \sigma_{31} & \sigma_{32} \end{vmatrix} \tag{2.74}$$

We then differentiate (2.74) to obtain the minors as

$$M_{11} = \frac{\partial |\boldsymbol{\sigma}|}{\partial \sigma_{11}}, \text{ etc.} \tag{2.75}$$

Generally, we write

$$M_{ij} = \frac{\partial |\boldsymbol{\sigma}|}{\partial \sigma_{ij}} \tag{2.76}$$

Using (2.76) and (2.71), and observing the notations

$$\frac{\partial \sigma_{ir}}{\partial \sigma_{pq}} = \delta_{ip}\delta_{rq} \tag{2.77}$$

We find

$$M_{pq} = \tfrac{1}{6}\{e_{pjk}e_{qst}\sigma_{js}\sigma_{kt} + e_{ipk}e_{rqt}\sigma_{ir}\sigma_{kt} + e_{ijp}e_{rsq}\sigma_{ir}\sigma_{js}\} \tag{2.78}$$

The second and third terms on the right-hand side are equal to the first term, and (2.78) may be simplified to obtain

$$M_{pq} = \tfrac{1}{2}e_{pjk}e_{qst}\sigma_{js}\sigma_{kt} \tag{2.79}$$

Hence, we find

$$\begin{aligned} J_2 = M_{ii} &= \tfrac{1}{2}e_{ijk}e_{ist}\sigma_{js}\sigma_{kt} = \tfrac{1}{2}(\delta_{js}\delta_{kt} - \delta_{jt}\delta_{ks})\sigma_{js}\sigma_{kt} = \tfrac{1}{2}\{\sigma_{jj}\sigma_{kk} - \sigma_{jk}\sigma_{kj}\} \\ &= \tfrac{1}{2}\{[\operatorname{tr}\boldsymbol{\sigma}]^2 - \operatorname{tr}(\boldsymbol{\sigma})^2\} = \tfrac{1}{2}\{J_1^2 - \operatorname{tr}(\boldsymbol{\sigma}^2)\} \end{aligned} \tag{2.80}$$

Since J_1 and $\operatorname{tr}(\boldsymbol{\sigma}^2)$ are invariant, we may conclude that J_2 remains invariant with rotation of the coordinate system.

Another representation of J_2 may be obtained as follows. Using (2.79), we write

$$M_{pq}\sigma_{rq} = \tfrac{1}{2}e_{pjk}e_{qst}\sigma_{js}\sigma_{kt}\sigma_{rq} \tag{2.81}$$

By use of the identity proven in Example 2.7, (2.81) reduces to

$$\sigma_{rq}M_{pq} = \tfrac{1}{2}e_{pjk}e_{rjk}|\boldsymbol{\sigma}| = \delta_{pr}|\boldsymbol{\sigma}| \tag{2.82}$$

Note that the identity $e_{irs}e_{jrs} = 2\delta_{ij}$ has been used in the derivation of (2.82). In the symbolic notation, (2.82) may be written as

$$\boldsymbol{\sigma} \cdot \mathbf{M}^{\mathrm{T}} = \mathbf{1} \cdot |\boldsymbol{\sigma}| \tag{2.83}$$

If we multiply (2.83) from the left by $\boldsymbol{\sigma}^{-1}$, we obtain

$$\mathbf{M}^{\mathrm{T}} = \boldsymbol{\sigma}^{-1}|\boldsymbol{\sigma}| \quad \text{or} \quad \boldsymbol{\sigma}^{-1} = \frac{\mathbf{M}^{\mathrm{T}}}{|\boldsymbol{\sigma}|} \tag{2.84}$$

This indicates that the inverse of the matrix $\boldsymbol{\sigma}$ is the transpose of its cofactors divided by the determinant of the matrix. Using (2.84), we find the following expression for the second invariant

$$J_2 = \mathrm{tr}(\mathbf{M}) = \mathrm{tr}\,\mathbf{M}^{\mathrm{T}} = \mathrm{tr}(\boldsymbol{\sigma}^{-1})|\boldsymbol{\sigma}| \tag{2.85}$$

EXAMPLE 2.7 Prove the identity $e_{mpq}\det\mathbf{A} = e_{ijk}A_{im}A_{jp}A_{kq}$.

Proof

The determinant of matrix $[A]$ is

$$\det\mathbf{A} = \begin{vmatrix} A_{11} & A_{12} & A_{13} \\ A_{21} & A_{22} & A_{23} \\ A_{31} & A_{32} & A_{33} \end{vmatrix} = \begin{vmatrix} A_{11} & A_{21} & A_{31} \\ A_{12} & A_{22} & A_{32} \\ A_{13} & A_{23} & A_{33} \end{vmatrix} \tag{a}$$

An interchange of column or row of the determinant causes a sign change, and this may be expressed by

$$e_{mpq}\det\mathbf{A} = \begin{vmatrix} A_{1m} & A_{1p} & A_{1q} \\ A_{2m} & A_{2p} & A_{2q} \\ A_{3m} & A_{3p} & A_{3q} \end{vmatrix} = \begin{vmatrix} A_{1\mathrm{m}} & A_{2\mathrm{m}} & A_{3\mathrm{m}} \\ A_{1\mathrm{p}} & A_{2\mathrm{p}} & A_{3\mathrm{p}} \\ A_{1\mathrm{q}} & A_{2\mathrm{q}} & A_{3\mathrm{q}} \end{vmatrix} \tag{b}$$

A triple product of three vectors is

$$\mathbf{a} \cdot (\mathbf{b} \times \mathbf{c}) = e_{ijk}a_ib_jc_k = \begin{vmatrix} a_1 & a_2 & a_3 \\ b_1 & b_2 & b_3 \\ c_1 & c_2 & c_3 \end{vmatrix} \tag{c}$$

When we let $a_i = A_{im}$, $b_i = A_{ip}$, and $c_i = A_{iq}$, (b) and (c) combine to give

$$e_{mpq}\det\mathbf{A} = e_{ijk}A_{im}A_{jp}A_{kq} \tag{d}$$

which proves the identity. Finally, we note that

$$\mathbf{a} \times \mathbf{b} = \begin{vmatrix} \mathbf{i} & \mathbf{j} & \mathbf{k} \\ a_x & a_y & a_z \\ b_x & b_y & b_z \end{vmatrix} = \begin{vmatrix} \mathbf{i} & a_x & b_x \\ \mathbf{j} & a_y & b_y \\ \mathbf{k} & a_z & b_z \end{vmatrix} \tag{e}$$

2.13 Spectral Decomposition of a Symmetric Tensor of Rank Two

In this section, we discuss a representation of a symmetric second rank tensor by its eigenvalues and eigenvectors. To this end, we derive the following relation first

$$n_i^{(r)} n_j^{(r)} = \delta_{ij} \qquad (r \text{ summed}) \tag{2.86}$$

If we denote the directions of the normalized eigenvectors $n_i^{(1)}$, $n_i^{(2)}$, $n_i^{(3)}$ by x_1', x_2', x_3', respectively, we can then make use of (1.22), which relates the base vectors of the two coordinate systems. Thus, unit vectors $\mathbf{n}^{(r)}$ may be represented by

$$\mathbf{n}^{(r)} = n_k^{(r)} \mathbf{e}_k = Q_{kr} \mathbf{e}_k \tag{2.87}$$

where $n_k^{(r)}$are direction cosines of $\mathbf{n}^{(r)}$ with respect to the $\mathbf{e}_k$ system and

$$n_k^{(r)} = Q_{kr} \tag{2.88}$$

The inverse of (2.87) is

$$\mathbf{e}_k = n_k^{(r)} \mathbf{n}^{(r)} \tag{2.89}$$

On the other hand, following the same procedure and using a different normalized eigenvector, we obtain

$$\mathbf{e}_m = n_m^{(s)} \mathbf{n}^{(s)} \tag{2.90}$$

We then form the dot product from (2.89) and (2.90) as,

$$\mathbf{e}_k \cdot \mathbf{e}_m = n_k^{(r)} \mathbf{n}^{(r)} \cdot n_m^{(s)} \mathbf{n}^{(s)} = n_k^{(r)} n_m^{(s)} \delta_{rs} = n_k^{(r)} n_m^{(r)} \tag{2.91}$$

In the derivation, we note that eigenvectors are orthogonal expressed by

$$n_i^{(r)} n_i^{(s)} = \delta_{rs} \tag{2.92}$$

Hence (2.91) reduces to

$$n_k^{(r)} n_m^{(r)} = \delta_{km} \tag{2.86}$$

We now use this result to derive a representation of a symmetric tensor by its eigenvalues and eigenvectors. To this end, we start with

$$\sigma_{ij} n_i^{(r)} = \lambda_r n_j^{(r)} \quad (r \text{ not summed}) \tag{2.93}$$

Then, by multiplying both sides of (2.93) by $n_k^{(r)}$ and summing over r, we have

$$\sigma_{ij}\, n_i^{(r)} n_k^{(r)} = \sum_r \lambda_r n_j^{(r)} n_k^{(r)} \tag{2.94}$$

Using (2.86), (2.94) reduces to

$$\sigma_{ij} = \sum_r \lambda_r n_i^{(r)} n_j^{(r)} \tag{2.95}$$

Equation (2.95) is the spectral decomposition of σ_{ij}.

A remark is in order. In the study of coordinate transformation in Chapter 1, we have

$$Q_{ki} Q_{kj} = \delta_{ij} \tag{1.25}$$

$$Q_{ik} Q_{jk} = \delta_{ij} \tag{1.27}$$

where Q_{ij} is the transformation matrix between coordinate systems x_i and x_i'. In this section, we obtain the relations

$$n_i^{(r)} n_i^{(s)} = \delta_{rs} \tag{2.92}$$

$$n_i^{(r)} n_j^{(r)} = \delta_{ij} \tag{2.86}$$

where $n_i^{(r)}$ are normalized eigenvectors. Since from (2.88) $n_k^{(r)} = Q_{kr}$, then upon substitution, (2.92) and (2.86) reduce to (1.25) and (1.27), respectively. Also, the $[Q]$ matrix may be written as

$$[Q] = [n^{(1)} \quad n^{(2)} \quad n^{(3)}] = \begin{bmatrix} n_1^{(1)} & n_1^{(2)} & n_1^{(3)} \\ n_2^{(1)} & n_2^{(2)} & n_2^{(3)} \\ n_3^{(1)} & n_3^{(2)} & n_3^{(3)} \end{bmatrix} \tag{2.96}$$

2.14 Powers of a Tensor

Powers of a tensor σ_{ij} is usually written as

$$\text{Square of } \sigma_{ij} = \sigma_{ip}\sigma_{pj} = \boldsymbol{\sigma}^2 \tag{2.97}$$

$$\text{Cube of } \sigma_{ij} = \sigma_{ip}\sigma_{pq}\sigma_{qj} = \boldsymbol{\sigma}^3, \text{etc.} \tag{2.98}$$

For a second-rank symmetric tensor, we have the representation

$$\sigma_{ij} = \sum_r \lambda_r n_i^{(r)} n_j^{(r)} \tag{2.99}$$

If n is a positive integer, the nth power of a tensor $\boldsymbol{\sigma}$ defined to be the positive tensor $\boldsymbol{\sigma}^n$ whose components are

$$\sigma_{ij}^n = \sum_r \lambda_r^n n_i^{(r)} n_j^{(r)} \tag{2.100}$$

This expression may be proven as follows: from (2.30), we have $\sigma_{ij}n_i = \lambda n_j$, so that

$$(\sigma_{ij}\sigma_{jp})n_i = \lambda\sigma_{jp}n_j = \lambda^2 n_p \tag{2.101}$$

which shows that the square of σ_{ij} has the eigenvalue of λ^2 and the eigenvector of n_i. The same method may continue for the third power of σ_{ij} and for the general case of nth power.

If n is a fraction number, then all eigenvalues need be positive. A tensor $\boldsymbol{\sigma}$ is said to be *positive*, if it has positive principal values and three linearly independent principal vectors (eigenvectors). A tensor $\boldsymbol{\sigma}$ is said to be *positive definite* if it is coefficients of a positive definite quadratic form. It may be easily shown that a positive symmetric tensor is also positive definite. Knowing a positive $\boldsymbol{\sigma}$, we can find the square root of this tensor $\boldsymbol{\sigma}^{1/2} = \sqrt{\boldsymbol{\sigma}}$ by first finding the principal directions and the principal values σ_1, σ_2, and σ_3 of $\boldsymbol{\sigma}$; and then, in the principal space, we take the square root of the principal values so that the matrix is

$$\bar{\boldsymbol{\sigma}}^{1/2} = \begin{bmatrix} \sigma_1^{1/2} & 0 & 0 \\ 0 & \sigma_2^{1/2} & 0 \\ 0 & 0 & \sigma_3^{1/2} \end{bmatrix} \tag{2.102}$$

Finally, we apply the transformation equation to obtain $\boldsymbol{\sigma}^{1/2}$ referred to the x_i axes. The equation used in the axes transformation is

$$[\sigma]^{1/2} = [Q][\bar{\sigma}]^{1/2}[Q]^{\mathrm{T}} \tag{2.103}$$

EXAMPLE 2.8 Show that a positive symmetric tensor is also positive definite.

If a tensor is positive, its eigenvalues are all positive, that is, $\lambda_1 > 0$, $\lambda_2 > 0$, $\lambda_3 > 0$. In the principal coordinate system, the expression of quadratic form $\sigma_{ij}n_in_j$ is $\lambda_1 n_1^2 + \lambda_2 n_2^2 + \lambda_3 n_3^2$. If $\lambda_1 > 0$, $\lambda_2 > 0$, and $\lambda_3 > 0$, then $\lambda_1 n_1^2 + \lambda_2 n_2^2 + \lambda_3 n_3^2 > 0$, which shows that the quadratic form is positive definite. On the other hand, it may be shown that a positive definite (symmetric) tensor is positive. To this end, we consider $\sigma_{ij}n_in_j > 0$. In the principal coordinate system, the quadratic form is reduced to

$$\lambda_1 n_1^2 + \lambda_2 n_2^2 + \lambda_3 n_3^2 > 0 \tag{a}$$

We note that n_i is one of the eigenvectors, so that if $n_1 \neq 0$ and $n_2 = n_3 = 0$, (a) reduces to $\lambda_1 n_1^2 > 0$, which leads to $\lambda_1 > 0$. Similarly, $\lambda_2 > 0$, $\lambda_3 > 0$ and, therefore, $\boldsymbol{\sigma}$ is a positive tensor.

2.15 Cayley–Hamilton Theorem

The aim of this section is to indicate that, by use of the Cayley–Hamilton theorem, a high-order matrix polynomial may be reduced to a lower order one. In this manner, a nonlinear expression can be reduced to an expression with second-order term as its highest power term, and thus simplifying the mathematics involved. According to this theorem, a square matrix satisfies its own characteristic align, that is,

$$\boldsymbol{\sigma}^3 - J_1\boldsymbol{\sigma}^2 + J_2\boldsymbol{\sigma} - J_3\boldsymbol{\delta} = \mathbf{0} \tag{2.104}$$

In the principal space, (2.104) is written as

$$\lambda_r^3 - J_1\lambda_r^2 + J_2\lambda_r - J_3 = 0 \quad \text{where } r = 1, 2, 3 \tag{2.105}$$

and, in the matrix form, (2.105) is

$$\begin{bmatrix} \sigma_1^3 & 0 & 0 \\ 0 & \sigma_2^3 & 0 \\ 0 & 0 & \sigma_3^3 \end{bmatrix} - J_1 \begin{bmatrix} \sigma_1^2 & 0 & 0 \\ 0 & \sigma_2^2 & 0 \\ 0 & 0 & \sigma_3^2 \end{bmatrix} + J_2 \begin{bmatrix} \sigma_1 & 0 & 0 \\ 0 & \sigma_2 & 0 \\ 0 & 0 & \sigma_3 \end{bmatrix} - J_3 \begin{bmatrix} 1 & 0 & 0 \\ 0 & 1 & 0 \\ 0 & 0 & 1 \end{bmatrix} = 0 \tag{2.106}$$

where $\sigma_1, \sigma_2, \sigma_3$ are the three principal values. In the index notation, (2.104) is written as

$$\sigma_{im}\sigma_{mn}\sigma_{nj} - J_1\sigma_{im}\sigma_{mj} + J_2\sigma_{ij} - J_3\sigma_{ij} = 0 \tag{2.107}$$

This equation is valid in the general case and not necessarily in the principal directions. But the formal proof is lengthy and is to be found in a textbook on linear algebra. The proof will not be discussed here.

We show next that the expression of J_2 may be found by using this theorem. Multiplying (2.104) by $\boldsymbol{\sigma}^{-1}$, we find

$$\boldsymbol{\sigma}^2 - J_1\boldsymbol{\sigma} + J_2\boldsymbol{\delta}J_3\boldsymbol{\sigma}^{-1} = 0 \tag{2.108}$$

Taking the trace of all terms in the above equation, we obtain

$$\operatorname{tr}\boldsymbol{\sigma}^2 - J_1^2 + 3J_2 - J_3\operatorname{tr}(\boldsymbol{\sigma}^{-1}) = 0 \tag{2.109}$$

Since the last term is, from (2.85), $-J_2$, (2.109) may be solved to yield

$$J_2 = \tfrac{1}{2}(J_1^2 - \operatorname{tr}\boldsymbol{\sigma}^2) \tag{2.110}$$

This expression is similar to that derived earlier in (2.80).

By use of the Cayley–Hamilton theorem, we can reduce the nth (positive integer) power of a matrix to a linear combination of the second, first, and zeroth powers. For example, if we multiply (2.104) by $\boldsymbol{\sigma}$, we obtain

$$\boldsymbol{\sigma}^4 - J_1\boldsymbol{\sigma}^3 + J_2\boldsymbol{\sigma}^2 - J_3\boldsymbol{\sigma} = 0 \tag{2.111}$$

By applying (2.104) again, (2.111) becomes

$$\boldsymbol{\sigma}^4 - J_1\{J_1\boldsymbol{\sigma}^2 - J_2\boldsymbol{\sigma} + J_3\boldsymbol{\delta}\} + J_2\boldsymbol{\sigma}^2 - J_3\boldsymbol{\sigma} = 0 \tag{2.112}$$

which leads to

$$\boldsymbol{\sigma}^4 = \boldsymbol{\sigma}^2\{J_1^2 - J_2\} - \boldsymbol{\sigma}\{J_1J_2 - J_3\} + J_1J_3\boldsymbol{\delta} \tag{2.113}$$

It is seen that $\boldsymbol{\sigma}^4$ may be expressed in terms of $\boldsymbol{\sigma}^2$, $\boldsymbol{\sigma}$, and $\boldsymbol{\delta}$. It is important to note that the coefficients of the second, first, and zeroth-power terms are functions of the invariants of $\boldsymbol{\sigma}$. In a similar manner, a matrix of any power higher than two may be expressed in terms of $\boldsymbol{\sigma}^2$, $\boldsymbol{\sigma}$, and $\boldsymbol{\delta}$.

References

1. Malvern, L.E., *Introduction to the Mechanics of a Continuous Medium*, Prentice-Hall, Englewood Cliffs, NJ, 1969.
2. Prager, W., *Introduction to Mechanics of Continua*, Ginn, Boston, MA, 1961.
3. Eringen, A.C., *Mechanics of Continua*, Wiley, New York, 1967.

4. Fung, Y.C., *Foundations of Solid Mechanics*, Prentice-Hall, Englewood Cliffs, NJ, 1965.
5. Truesdell, C. and Toupin, R., The Classical Field Theories, in *Handbuch der Physik*, Vol. III/1, S. Flugge, Ed., Springer-Verlag, Berlin, 1960.
6. Sokolnikoff, I.S., *Mathematical Theory of Elasticity*, McGraw-Hill, New York, 1956.

Problems

(1) A specimen used for uniaxial tensile testing of material has a middle section (the gauge section) of reduced cross-section. The stress is uniformly distributed within this section. You may consider this section as a circular cylinder. When the specimen is pulled, what stress boundary conditions (stress vectors) apply in the middle section of the specimen?

(2) An infinitesimal material element is subjected to hydrostatic pressure p as shown in Figure 2.9. Determine the stress vector acting on surface a–a′ of the element.

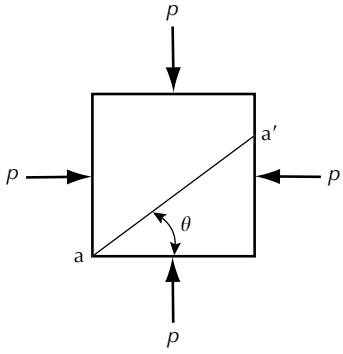

FIGURE 2.9

(3) The bar shown in Figure 2.10 has a cross-sectional area A and is subjected to the axial load P. Determine the stress vector acting on the inclined surface a–a′.

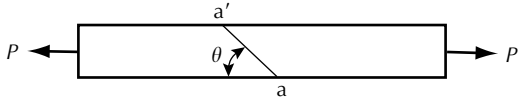

FIGURE 2.10

(4) The state of stress for the infinitesimal tetrahedron OABC shown in Figure 2.11 is

$$[\sigma] = \begin{bmatrix} 20 & -60 & 40 \\ -60 & 0 & 80 \\ 40 & 80 & -20 \end{bmatrix} \text{ MPa}$$

Determine the stress vector acting on the inclined plane ABC.

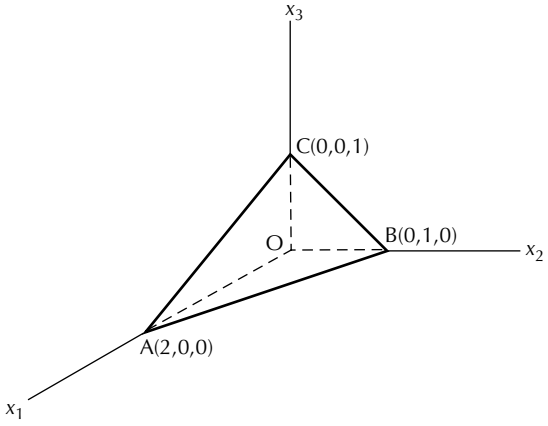

FIGURE 2.11

(5) Let the components of the stress tensor at point P be given in matrix form by

$$[\sigma] = \begin{bmatrix} 21 & -63 & 42 \\ -63 & 0 & 84 \\ 42 & 84 & -21 \end{bmatrix} \text{ MPa}$$

Determine the stress vector on a plane passing through P, parallel to the x_3-axis and making a 30° counterclockwise angle from the x_1-axis.

(6) If the components of the stress tensor is given by

$$\sigma_{ij} = \begin{bmatrix} 1 & 0.5 & 0 \\ 0.5 & -1 & -0.2 \\ 0 & -0.2 & 0 \end{bmatrix} \text{ MPa}$$

determine the stress vector acting on a surface whose normal is $\mathbf{n} = 0.2\mathbf{e}_1 + 0.3\mathbf{e}_2 + \sqrt{0.87}\mathbf{e}_3$. What are the normal and shear components acting on the surface?

(7) In the principal stress space, determine the expression of stress vector (in terms of stress components) acting on the octahedral plane in the first quadrant of the stress space.

(8) Stress is a second-rank tensor. If the stress components referring to the x_i coordinate system are

$$[\sigma_{ij}] = \begin{bmatrix} 6 & 2 & 0 \\ 2 & -1 & 0 \\ 0 & 0 & 1 \end{bmatrix} \text{ MPa}$$

find the stress components of the same tensor with respect to the x'_i system if $x'_3 = x_3$ and x'_1 is making a 30° angle counterclockwise with the x_1-axis.

(9) The stress tensor at point P has the following components with respect to the x_i coordinate system

$$[\sigma] = \begin{bmatrix} 20 & 0 & -10 \\ 0 & 8 & 0 \\ -10 & 0 & 24 \end{bmatrix} \text{ MPa}$$

Referring to Figure 2.12, if the x'_1-axis makes equal angles θ with the three x_i axes and the x'_2-axis lies in the x_1x_2 plane, determine the components of the stress tensor referred to the right-handed x'_i coordinate system.

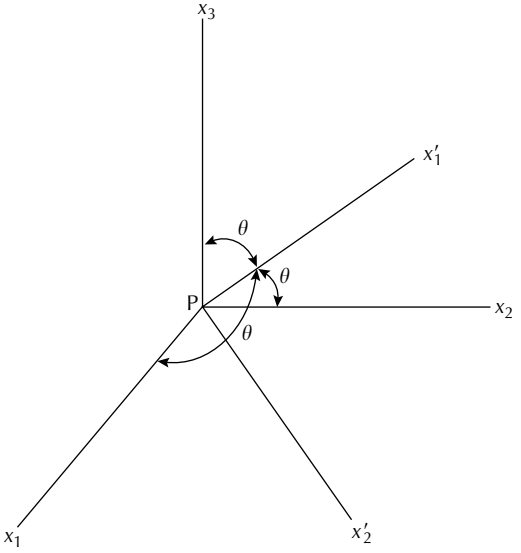

FIGURE 2.12

(10) The stress tensor is $\sigma_{ij} = \alpha(\nu_i\nu'_j + \nu_j\nu'_i)$, where α is a scalar and $\boldsymbol{\nu}$ and $\boldsymbol{\nu}'$ are unit vectors. Determine the principal stresses and axes. (Hint: to simplify the computation, choose the x_1-axis parallel to ν and the x_3-axis normal to $\boldsymbol{\nu}$ and $\boldsymbol{\nu}'$).

(11) Let $\mathbf{t}_1$, $\mathbf{t}_2$, and $\mathbf{t}_3$ be the stress vectors acting on surface elements that are normal to the coordinate axes. Show that the sum of the squares of the magnitudes of these vectors is independent of the orientation of the coordinate axes.

(12) Consider the following stress distribution

$$\boldsymbol{\sigma} = \begin{bmatrix} ax_2 & b & 0 \\ b & 0 & 0 \\ 0 & 0 & 0 \end{bmatrix}$$

where a and b are constants. Determine and sketch the distribution of the stress vector acting on the square in the $x_1 = 0$ plane, with vertices located at (0, 1, 1), (0, −1, 1), (0, 1, −1), (0, −1, −1).

(13) A block of unit thickness is subjected to forces shown in Figure 2.13. The area of face (1) is A_1 and the area of face (2) is A_2. (a) Determine the stress vectors acting on these two surfaces; (b) find the conditions which must be satisfied by the forces and areas for the block to be in equilibrium; (c) if the stress is uniformly distributed in the block, determine the components of the stress tensor; (d) if principal stresses apply on the material element shown with orientation specified by ϕ, find the second stress invariant J_2 at this configuration.

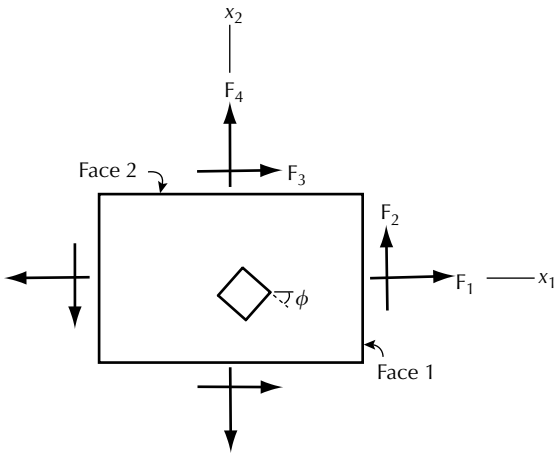

FIGURE 2.13

(14) For the state of stress given by

$$[\sigma] = \begin{bmatrix} 10 & 30 & -50 \\ 30 & 0 & 0 \\ -50 & 0 & 0 \end{bmatrix} \text{MPa}$$

find the components of the deviatoric stress σ'_{ij} and determine the principal invariants of the deviatoric stress.

(15) Cut out a tetrahedron of infinitesimal size from a body. The normal of the inclined face makes equal angles with the three coordinate axes. Find the force that must be applied on the inclined face so that it will produce a state of stress given by the following matrix

$$[\sigma] = \begin{bmatrix} 30 & -10 & 20 \\ -10 & 0 & 10 \\ 20 & 10 & 10 \end{bmatrix} \text{MPa}$$

For equilibrium, what forces must be applied to the faces normal to the coordinate axes?

(16) The second invariant of the deviatoric part of $\boldsymbol{\sigma}$ is denoted by J_2'. Show that $\partial J_2'/\partial \sigma_{pq} = -\sigma_{qp}'$. Note that the differentiation is taken with respect to σ_{pq} and not σ_{pq}'.

(17) If $[Q] = [\mathbf{n}^{(1)} \quad \mathbf{n}^{(2)} \quad \mathbf{n}^{(3)}]$ and $[Q]^{\mathrm{T}}[Q] = [\delta]$, show that by use of $(\sigma_{ij} - \lambda\delta_{ij})n_i = 0$, it may be shown that

$$[Q]^{\mathrm{T}}[\sigma][Q] = \begin{bmatrix} \lambda_1 & 0 & 0 \\ 0 & \lambda_2 & 0 \\ 0 & 0 & \lambda_3 \end{bmatrix}$$

that is, $[\sigma]$ may be diagonalized by use of $[Q]$. Show also that $\operatorname{tr}\mathbf{Q}^{\mathrm{T}}\boldsymbol{\sigma}\mathbf{Q} = \lambda_1 + \lambda_2 + \lambda_3$.

(18) A stress field is given by the matrix

$$[\sigma] = \begin{bmatrix} (1 + x_1^2)x_2 + \frac{1}{2}x_2^2 & (1 - x_2^2)x_1 & 0 \\ (1 - x_2^2)x_1 & -\frac{1}{2}(x_2^2 - 4x_2) & 0 \\ 0 & 0 & (4 - x_1^2)x_2 \end{bmatrix}$$

Find the expression for the second invariant of the deviatoric stress.

(19) If J_1, J_2, and J_3 denote the principal invariants of the stress tensor σ_{ij} and J_1', J_2', and J_3' denote the principal invariants of the deviatoric stress σ_{ij}', show that

$$J_1 = J_1' + 3\sigma_m = 3\sigma_m$$
$$J_2 = J_2' + \frac{1}{3}J_1^2$$
$$J_3 = J_3' + \frac{2}{9}J_1 J_2' + \frac{1}{27}J_1^3$$

3

Motion and Deformation

3.1 Introduction

In this chapter, we consider the *motion* of a body and, in particular, we concentrate on the study of *deformation* and the *rate of change* of a material element on or within the body. We assume the reader has familiarized himself with the concepts of strain and strain-rate in the study of elementary mechanics of deformable bodies. Strain describes the change in the geometry of an element in a body. But strain and strain-rate need to be defined. There are several measures of strain that people use. Deformation is a more general terminology to use than strain in describing the geometrical change of a material element (see [1–4] for further reading).

The particles of the body may occupy various positions in a three-dimensional space. The complete specification of the positions of the particles of a body is called the *configuration* of a body. The configuration of the body at the reference time (or initial or undeformed state) and at the current time (or deformed state) is the *reference configuration* denoted by R_0, and the *current configuration* denoted by R_t, respectively. To fix the concept of deformation, let us consider a material point P within a neighborhood N_0 at the reference configuration. Referred to in Figure 3.1, point P moves to point p within a neighborhood N_t at the current configuration due to load applied to the body. The concept of deformation may be understood by taking two photographs of the material element, one at the reference configuration and the other at the current configuration. We then compare and characterize the size and shape of the material element in the two photographs. The change in the size and shape of the material element is called the deformation of the material element and it indicates its need to be quantified. We also observe that time is not a factor in the study of deformation.

To describe the two configurations, a *material* (Lagrangian) *coordinate system*, denoted by X_R, and a *spatial* (Eulerian) *coordinate system*, denoted by x_i, is introduced. The position of the material point P at the reference configuration is specified by the material coordinates X_R and that of p at the current configuration is specified by the spatial coordinates x_i. For convenience, the undeformed configuration of a material element is often chosen as the

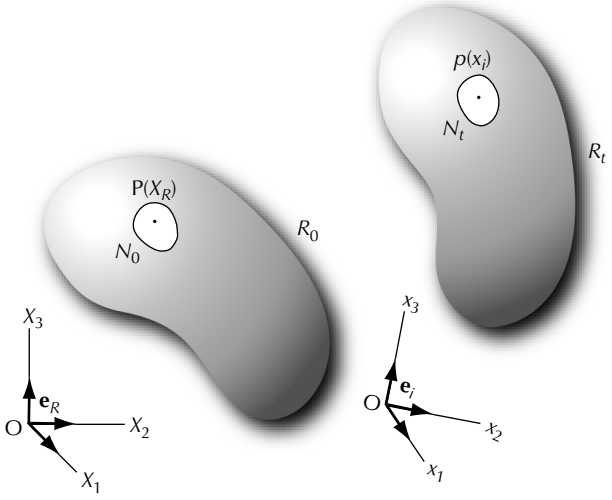

FIGURE 3.1
Reference and current configurations.

reference configuration. But, any other configuration may also be chosen as the reference configuration, if needed. Once a reference configuration has been chosen, all the material points of a body can be described by the material coordinates X_R. In the general case, the axes of X_R and x_i do not have the same origin and orientation as shown in Figure 3.1. But, in many cases, it is convenient to select the two coordinate systems such that they have the same origin and orientation. This selection leads to simplicity and is used in most of the topics discussed in this book.

Motion may be viewed as a family of deformations continuously varying in time, and the deformations between two configurations have been discussed in the previous paragraph. When a continuum is in motion, physical quantities associated with a material element of the body (such as density ρ, velocity $\mathbf{v}$, etc.) change with location and time. The motion of a continuous body may be described in two ways: *material* and *spatial descriptions*. The material description has been used mostly in solid mechanics and the spatial description in fluid mechanics. Some recent works have used a mixed description. We now discuss the two descriptions in the light of time-dependent motions.

3.2 Material and Spatial Descriptions

3.2.1 Material Description

The material description is also known as the *Lagrangian description*. In this description, a material element is followed. The observer sits on top of the body and moves with the body. He observes changes in the physical

quantities of the body as functions of the material element identified by the material coordinates X_R and time t. Therefore, we write

$$\rho = \rho(X_R, t), \qquad \mathbf{v} = \mathbf{v}(X_R, t), \text{ etc.} \tag{3.1}$$

3.2.2 Spatial Description

The spatial description is also known as the *Eulerian description*. Here, the observer observes the changes in physical quantities at a fixed location in the laboratory. Hence, the quantities are described in terms of the location in space denoted by the spatial coordinates x_i and time t. In effect, we describe and measure the quantities at a fixed location and they are functions of time. Spatial positions are occupied by different particles at different times. Therefore, the spatial description does not provide direct information related to changes in the properties of the material element as the body moves. In this description, we write

$$\rho = \rho(x_i, t), \qquad \mathbf{v} = \mathbf{v}(x_i, t), \text{ etc.} \tag{3.2}$$

If we know the motion of the body, then the two descriptions are related and are equivalent. One description can be obtained from the other.

The correlation between the two descriptions is now discussed. During the motion of the body, particle P with position vector $\mathbf{X}$ moves to point p with position vector $\mathbf{x}$ and the *displacement* is

$$\mathbf{u} = \mathbf{x} - \mathbf{X} \tag{3.3}$$

In the material description, the above equation is written as

$$\mathbf{u}(\mathbf{X}, t) = \mathbf{x}(\mathbf{X}, t) - \mathbf{X} \tag{3.4}$$

and, in the spatial description, it is written as

$$\mathbf{u}(\mathbf{x}, t) = \mathbf{x} - \mathbf{X}(\mathbf{x}, t) \tag{3.5}$$

The *velocity* $\mathbf{v}$ of a particle is the rate of change of its displacement, and, in the material description, it is written as

$$\mathbf{v}(\mathbf{X}, t) = \frac{\partial \mathbf{u}(\mathbf{X}, t)}{\partial t} = \frac{\partial [\mathbf{x}(\mathbf{X}, t) - \mathbf{X}]}{\partial t} = \frac{\partial \mathbf{x}(\mathbf{X}, t)}{\partial t} \equiv \frac{\mathrm{D}\mathbf{x}}{\mathrm{D}t} \tag{3.6}$$

where $\mathrm{D}/\mathrm{D}t$ is called the *material derivative*. The motion of the particle is followed and material coordinate $\mathbf{X}$ is fixed during this motion. In the index

notation, (3.6) is written as

$$v_i(X_R, t) = \frac{\partial x_i(X_R, t)}{\partial t} \tag{3.7}$$

Note that the expression in (3.7) is different from the spatial description, which is $v_i(x_j, t)$ for the particle velocity. The relationship between the two descriptions is illustrated in Example 3.1.

EXAMPLE 3.1 A body undergoes the motion defined by

$$x_1 = X_1(1 + a_1 t + a_2 t^2), \qquad x_2 = X_2, \qquad x_3 = X_3 \tag{a}$$

where a_1 and a_2 are constants. Find the displacement and velocity in both the material and spatial descriptions.

Solution

In the material description, we have from (3.4),

$$u_i(X_R, t) = x_i(X_R, t) - X_i \tag{b}$$

When equation (a) is substituted into (b), we obtain

$$\begin{aligned} u_1 &= x_1 - X_1 = X_1(a_1 t + a_2 t^2) \\ u_2 &= x_2 - X_2 = 0 \\ u_3 &= x_3 - X_3 = 0 \end{aligned} \tag{c}$$

Equations (c) represent the components of the displacement vector at time t in the material description. To obtain the displacement in the spatial description, we substitute for X_1 by use of (a) and obtain

$$u_1 = \frac{x_1(a_1 t + a_2 t^2)}{1 + a_1 t + a_2 t^2}, \qquad u_2 = 0, \qquad u_3 = 0 \tag{d}$$

Equations (d) are the displacement components in the spatial description. For the velocity, we differentiate (a) with respect to t, keeping X_R fixed, to obtain

$$v_1 = X_1(a_1 + 2a_2 t), \qquad v_2 = 0, \qquad v_3 = 0 \tag{e}$$

Equation (e) is in the material description and, for the spatial description, we eliminate X_1 from (e) to obtain

$$v_1 = \frac{x_1(a_1 + 2a_2 t)}{1 + a_1 t + a_2 t^2}, \qquad v_2 = 0, \qquad v_3 = 0 \tag{f}$$

We see that (f) is in the spatial description.

3.3 Description of Deformation

We refer to the motion of a continuum when a body is undergoing change in geometry due to applied forces. The motion is generally described by the set of equations

$$x_i = x_i(X_R, t) \qquad i = 1, 2, 3 \tag{3.8}$$

These equations describe the change in position of a generic particle P with coordinates X_R into p with coordinates x_i. The functional relationship in (3.8) is generally nonlinear and its dependence on time t is discussed later in this chapter associated with material rate of change and rate of deformation. In this section, we study the deformation, that is, we set t to a constant time in (3.8). It is assumed that the mapping between X_R and x_i is one-to-one and onto; that is, for every *particle* in R_0 there corresponds one *point* only in R_t and to every point in R_t there corresponds one particle only in R_0. Thus, the relation can be inverted to yield

$$X_R = X_R(x_i, t) \tag{3.9}$$

This assumption automatically satisfies the physical principle of conservation of mass and is a property of continuity. Motion described by (3.8) is the material description, where the variables are the material coordinates X_R and time t; motion described by (3.9) is a spatial description, where the variables are x_i and t. In this section, we study the deformation that has taken place at a specified time t.

A special case of (3.8) is that x_i is a linear function of X_R such that

$$x_i = Q_{iR}(t) X_R \tag{3.10}$$

If Q_{iR} is an orthogonal tensor, then Q_{iR} rotates vector X_R into vector x_i, which has been discussed in Section 1.6.2.

3.4 Deformation of a Neighborhood

Consider the deformation of a small material vector $\mathrm{d}\mathbf{X}$, which maps into vector $\mathrm{d}\mathbf{x}$ in the deformed configuration. Vector $\mathrm{d}\mathbf{X}$ connects two neighboring points in neighborhood N_0 and it may be considered as a *line element* between the two points. Due to deformation, the initial line element $\mathrm{d}\mathbf{X}$ deforms into the current (deformed) line element $\mathrm{d}\mathbf{x}$ and they are related by

$$\mathrm{d}\mathbf{x} = \frac{\partial \mathbf{x}}{\partial \mathbf{X}} \cdot \mathrm{d}\mathbf{X} = \mathbf{F} \cdot \mathrm{d}\mathbf{X} \tag{3.11}$$

where $\mathbf{F} = \partial \mathbf{x}/\partial \mathbf{X}$ is called the *deformation gradient*, which plays an important role in modern continuum mechanics. In the component form, the deformation gradient $\mathbf{F}$ is written as

$$\mathbf{F} = \frac{\partial x_i}{\partial X_R}\mathbf{e}_i \otimes \mathbf{e}_R = F_{iR}\mathbf{e}_i \otimes \mathbf{e}_R \tag{3.12}$$

where $\mathbf{e}_R$ and $\mathbf{e}_i$ are base vectors of the material and special coordinate systems, respectively. Substituting (3.12) into (3.11), we have

$$\mathrm{d}x_i\mathbf{e}_i = \frac{\partial x_i}{\partial X_R}\mathbf{e}_i \otimes \mathbf{e}_R \cdot \mathrm{d}X_S\mathbf{e}_S = \frac{\partial x_i}{\partial X_R}\mathrm{d}X_S\mathbf{e}_i\delta_{RS} = \frac{\partial x_i}{\partial X_R}\mathrm{d}X_R\mathbf{e}_i \tag{3.13}$$

Thus, the component form is obtained as

$$\mathrm{d}x_i = \frac{\partial x_i}{\partial X_R}\mathrm{d}X_R = F_{iR}\mathrm{d}X_R \tag{3.14}$$

Note that the derivative $\partial x_i/\partial X_R$ is evaluated at point P and is common to all vectors $\mathrm{d}X_R$ emanated from P within the neighborhood N_0. (In the mathematical expression $f(x) = f_0 + f'(0)x + \mathrm{O}(x^2)$, the first derivative $f'(0)$ is independent of x.) In the matrix form, (3.14) is written as

$$\begin{bmatrix} \mathrm{d}x_1 \\ \mathrm{d}x_2 \\ \mathrm{d}x_3 \end{bmatrix} = \begin{bmatrix} x_{1,1} & x_{1,2} & x_{1,3} \\ x_{2,1} & x_{2,2} & x_{2,3} \\ x_{3,1} & x_{3,2} & x_{3,3} \end{bmatrix} \begin{bmatrix} \mathrm{d}X_1 \\ \mathrm{d}X_2 \\ \mathrm{d}X_3 \end{bmatrix} \tag{3.15}$$

and the Jacobian of the transformation is

$$\mathrm{J} = \left| \frac{\partial x_i}{\partial X_R} \right| = \det[F] \neq 0 \tag{3.16}$$

If both x_i and X_R systems are right (or left) handed for all t, then $\det[F] > 0$. This means that an infinitesimal volume element (with finite value) cannot be deformed into a point. The volume change is discussed further later in this chapter.

Some simple examples of finite deformation is considered in the concluding part of this section. We use *finite* versus *infinitesimal* to distinguish large deformation from small deformation. In this chapter, most of our discussions are aimed at finite deformations. But, at the end of the chapter, we consider infinitesimal deformation as a special case.

3.4.1 Homogeneous Deformations

Deformations of the form

$$x_i = c_i + A_{iR} X_R \tag{3.17}$$

are *homogeneous deformations*. In (3.17), c_i and A_{iR} are constants or functions of time, but not functions of position X_R. In this case, the deformation is the same for all points throughout the body being studied. We note that (3.17) is a linear form of the deformation equation (3.8).

3.4.1.1 Uniform extensions

We consider a cube undergoing extensions in all three directions, so that

$$x_1 = \lambda_1 X_1, \qquad x_2 = \lambda_2 X_2, \qquad x_3 = \lambda_3 X_3 \tag{3.18}$$

where λ_i specify the deformation and are constants or functions of time t. Note that (3.18) is a special case of (3.17). The deformation gradient of (3.18) may be found from (3.12) as

$$[F] = \begin{bmatrix} \lambda_1 & 0 & 0 \\ 0 & \lambda_2 & 0 \\ 0 & 0 & \lambda_3 \end{bmatrix} \tag{3.19}$$

If $\lambda_1 = \lambda_2 = \lambda_3$, the cube undergoes a uniform expansion or contraction in all directions and is referred to as a uniform dilatation. The volume of a material element in the cube was initially $\mathrm{d}V = \mathrm{d}X_1 \mathrm{d}X_2 \mathrm{d}X_3$ and is now $\mathrm{d}v = \mathrm{d}x_1 \mathrm{d}x_2 \mathrm{d}x_3 = \lambda_1 \lambda_2 \lambda_3 \mathrm{d}X_1 \mathrm{d}X_2 \mathrm{d}X_3$. Therefore, when there is no volume change, we write $\lambda_1 \lambda_2 \lambda_3 = 1$. The volume change of an element is discussed further in a later section.

In the case of an extension in the x_1 direction of a long bar of uniform cross-section, $\lambda_2 = \lambda_3$. When $\lambda_1 > 1$, that is, stretching, it is usually observed that $\lambda_2 < 1$. Note that $\lambda_i > 0$, because the length of a line element cannot become negative.

3.4.1.2 Simple shear

In this deformation, parallel planes are displaced relative to each other with the distance between the planes unchanged. A square element is deformed into a parallelepiped. Thus, particle P with position vector **X** moves to p with position vector **x** as shown in Figure 3.2. The following set of equations describes a simple shear deformation:

$$x_1 = X_1 + X_2 \tan\gamma, \qquad x_2 = X_2, \qquad x_3 = X_3 \tag{3.20}$$

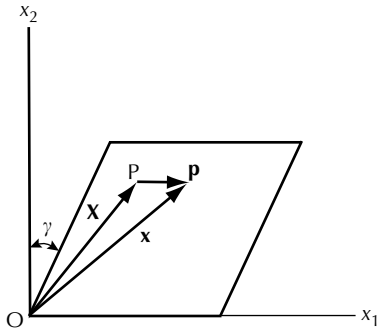

FIGURE 3.2
Simple shear deformation.

where angle γ measures the amount of shear; the $X_2 =$ constant planes are the shear planes; and X_1 is the shear direction. The deformation gradient of simple shear is found from (3.20) as

$$[F] = \begin{bmatrix} 1 & \tan\gamma & 0 \\ 0 & 1 & 0 \\ 0 & 0 & 1 \end{bmatrix} \tag{3.21}$$

3.4.2 Nonhomogeneous Deformations

Equation (3.17) of homogeneous deformation leads to a deformation gradient **F**, which is not a function of position X_R. Examples are (3.19) and (3.21). In the case of *nonhomogeneous deformations*, **F** is a function of position, that is, the deformation will be different from point to point. We consider torsion of a circular cylinder as an example of nonhomogeneous deformation. Referring to Figure 3.3, we choose the X_3 axis to coincide with the axis of the cylinder. If the cylinder is twisted about the X_3 axis, then plane cross-sections remain plane but are rotated rigidly through an angle τX_3 about the X_3 axis. It is seen that this angle is proportional to the coordinate X_3, that is, the angle is zero at the base of the cylinder where $X_3 = 0$ and increases its value as X_3 increases. The quantity τ denotes the *angle of twist per unit length* and is a constant if the torque is applied at the two ends of the cylinder. In order to find the equations of transformation that govern the deformation due to torsion, let us consider a typical cross-section shown in the insert of Figure 3.3. In the action of torsion, particle P(X_1, X_2, X_3) with a radial distance R from the center of the circular section is rotated into p(x_1, x_2, x_3), also with a radial distance R. At the initial position P, we have

$$X_1 = R\cos\alpha, \quad X_2 = R\sin\alpha, \qquad \text{with } R = \left(X_1^2 + X_2^2\right)^{1/2} \tag{3.22}$$

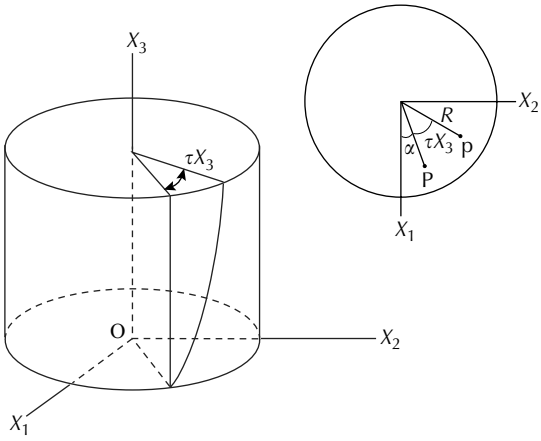

FIGURE 3.3
Torsion of a circular cylinder.

After deformation at p, we write

$$x_1 = R\cos(\tau X_3 + \alpha), \qquad x_2 = R\sin(\tau X_3 + \alpha) \tag{3.23}$$

We then expand the cosine and sine functions in (3.23) and, by use of (3.22), obtain

$$x_1 = X_1\cos\tau X_3 - X_2\sin\tau X_3, \qquad x_2 = X_1\sin\tau X_3 + X_2\cos\tau X_3, \qquad x_2 = X_3 \tag{3.24}$$

Note that the equation in the 3-direction has been added due to the fact that the cross-section at a distance X_3 from the base of the cylinder has merely undergone a rigid-body rotation. We conclude that (3.24) are the transformation equations that describe the deformation of a circular cylinder subjected to torsion. Differentiating (3.24), the deformation gradient **F** is found as

$$[F] = \begin{bmatrix} \cos\tau X_3 & -\sin\tau X_3 & -\tau(X_1\sin\tau X_3 + X_2\cos\tau X_3) \\ \sin\tau X_3 & \cos\tau X_3 & \tau(X_1\cos\tau X_3 - X_2\sin\tau X_3) \\ 0 & 0 & 1 \end{bmatrix} \tag{3.25}$$

It is seen that the deformation gradient depends on position for this nonhomogeneous problem. We have assumed in this discussion that the cylinder is undergoing a fixed-end torsion. In this case, there is no length change in the cylinder and the radius R of the cylinder does not change. The free-end torsion is discussed in a later chapter related to plastic deformation.

3.5 The Deformation Gradient

The deformation gradient plays an important role in modern continuum mechanics and is discussed in detail here. The deformation gradient **F** is a second-rank tensor; according to the *polar decomposition theorem*, a second-rank tensor can be expressed as a product of a positive symmetric tensor with an orthogonal tensor. There are two decompositions: the right and the left decompositions. They are expressed as

$$\mathbf{F} = \mathbf{R} \cdot \mathbf{U} \qquad \text{right decomposition} \tag{3.26}$$

$$\mathbf{F} = \mathbf{V} \cdot \mathbf{R} \qquad \text{left decomposition} \tag{3.27}$$

where **U** and **V** are positive symmetric tensors, and **R** is an orthogonal tensor.

3.5.1 The Polar Decomposition Theorem

This theorem applies to any second-rank tensor, and there are the right and left decompositions as shown in (3.26) and (3.27). In this subsection, we consider a second-rank tensor F_{ij}. This tensor acquires the physical meaning of deformation gradient in later sections. We now derive the right decomposition and consider tensor F_{ij} transforms vector v_i into vector v_i'; the relation is

$$v_i' = F_{ij} v_j \tag{3.28}$$

If the transformation (or mapping) is one-to-one, then the magnitude of vector v_i' is

$$|\mathbf{v}'|^2 = v_i' v_i' = F_{ij} F_{ik} v_j v_k = F_{ki}^{\mathrm{T}} F_{ij} v_j v_k > 0 \tag{3.29}$$

This is a positive definite quadratic form. The coefficient $C_{kj} = F_{ki}^{\mathrm{T}} F_{ij}$ is a positive definite tensor. It is obvious that $C_{kj} = C_{jk}$. Since **C** is positive, a tensor $\mathbf{U} \equiv \sqrt{\mathbf{C}}$ is well defined and it has the same eigenvectors as **C**. Thus,

$$\mathbf{U}^2 = \mathbf{F}^{\mathrm{T}} \cdot \mathbf{F} \equiv \mathbf{C} \tag{3.30}$$

Since **C** is symmetric, **U** is symmetric too. Now let $\mathbf{R} \equiv \mathbf{F} \cdot \mathbf{U}^{-1}$ and it is seen that if we define **R** in this manner, then **R** is an orthogonal tensor. Using this expression for **R**, we have

$$\begin{aligned} \mathbf{R}^{\mathrm{T}} \cdot \mathbf{R} &= (\mathbf{F} \cdot \mathbf{U}^{-1})^{\mathrm{T}} \cdot (\mathbf{F} \cdot \mathbf{U}^{-1}) = (\mathbf{U}^{-1})^{\mathrm{T}} \cdot \mathbf{F}^{\mathrm{T}} \cdot \mathbf{F} \cdot \mathbf{U}^{-1} \\ &= \mathbf{U}^{-1} \cdot \mathbf{F}^{\mathrm{T}} \cdot \mathbf{F} \cdot \mathbf{U}^{-1} = \mathbf{U}^{-1} \cdot \mathbf{C} \cdot \mathbf{U}^{-1} = \mathbf{1} \end{aligned} \tag{3.31}$$

Equation (3.30) is used in the last identity of (3.31). We see from (3.31) that $\mathbf{R}$ is an orthogonal tensor. In the above derivation, we also used the symmetric property of $\mathbf{U}$ and the relation $(\mathbf{U}^{-1})^{\mathrm{T}} = \mathbf{U}^{-1}$. We have thus shown that $\mathbf{F} = \mathbf{R} \cdot \mathbf{U}$ in which $\mathbf{R}$ is orthogonal and $\mathbf{U}$ is positive and symmetric.

Following an analogous procedure, we derive the left decomposition. The resulting equations are

$$\mathbf{F} = \mathbf{V} \cdot \mathbf{R}^* \quad \text{and} \quad \mathbf{V}^2 = \mathbf{F} \cdot \mathbf{F}^{\mathrm{T}} \equiv \mathbf{B} \tag{3.32}$$

We now show that the orthogonal tensor $\mathbf{R}^*$ of the left decomposition in the first equation of (3.32) is indeed equal to the orthogonal tensor $\mathbf{R}$ of the right decomposition. From (3.32), we write

$$\mathbf{F} = \mathbf{V} \cdot \mathbf{R}^* = \mathbf{R}^* \cdot (\mathbf{R}^{*\mathrm{T}} \cdot \mathbf{V} \cdot \mathbf{R}^*) \tag{3.33}$$

and view the last expression in (3.33) as the right decomposition. Since the right decomposition is unique (see Example 3.2), we compare (3.33) with (3.26) to obtain

$$\mathbf{R}^* = \mathbf{R} \quad \text{and} \quad \mathbf{U} = \mathbf{R}^{\mathrm{T}} \cdot \mathbf{V} \cdot \mathbf{R} \tag{3.34}$$

We see that $\mathbf{U}$ and $\mathbf{V}$ are related through equation (3.34). This relation can also be written as

$$\mathbf{V} = \mathbf{R} \cdot \mathbf{U} \cdot \mathbf{R}^{\mathrm{T}} \tag{3.35}$$

Tensor $\mathbf{B}$ defined in (3.32) can be shown to be related to tensor $\mathbf{C}$ defined in (3.30). From the definition of $\mathbf{B}$, we have

$$\mathbf{B} = \mathbf{F} \cdot \mathbf{F}^{\mathrm{T}} = \mathbf{R} \cdot \mathbf{U} \cdot \mathbf{U}^{\mathrm{T}} \cdot \mathbf{R}^{\mathrm{T}} = \mathbf{R} \cdot \mathbf{U}^2 \cdot \mathbf{R}^{\mathrm{T}} = \mathbf{R} \cdot \mathbf{C} \cdot \mathbf{R}^{\mathrm{T}} \tag{3.36}$$

Hence,

$$\mathbf{B} = \mathbf{R} \cdot \mathbf{C} \cdot \mathbf{R}^{\mathrm{T}} \quad \text{or} \quad \mathbf{C} = \mathbf{R}^{\mathrm{T}} \cdot \mathbf{B} \cdot \mathbf{R} \tag{3.37}$$

EXAMPLE 3.2 Show that the right decomposition (3.26) is unique.

Proof

Assume two decompositions exist:

$$\mathbf{F} = \mathbf{R} \cdot \mathbf{U} = \bar{\mathbf{R}} \cdot \bar{\mathbf{U}} \tag{a}$$

Then, the transpose of (a) is

$$\mathbf{F}^{\mathrm{T}} = \mathbf{U}^{\mathrm{T}} \cdot \mathbf{R}^{\mathrm{T}} = \bar{\mathbf{U}}^{\mathrm{T}} \cdot \bar{\mathbf{R}}^{\mathrm{T}} \tag{b}$$

Multiplying (a) and (b), we get

$$\begin{aligned}\mathbf{F}^{\mathrm{T}} \cdot \mathbf{F} &= \mathbf{U}^{\mathrm{T}} \cdot \mathbf{R}^{\mathrm{T}} \cdot \mathbf{R} \cdot \mathbf{U} = \bar{\mathbf{U}}^{\mathrm{T}} \cdot \bar{\mathbf{R}}^{\mathrm{T}} \cdot \bar{\mathbf{R}} \cdot \bar{\mathbf{U}} \\ &= \mathbf{U}^{\mathrm{T}} \cdot \mathbf{U} = \bar{\mathbf{U}}^{\mathrm{T}} \cdot \bar{\mathbf{U}}^{\mathrm{T}} \\ &= \mathbf{U}^2 = \bar{\mathbf{U}}^2 \end{aligned} \tag{c}$$

From (c), we conclude that $\mathbf{U} = \bar{\mathbf{U}}$ and is positive. The uniqueness of $\mathbf{R}$ follows from (a). Since $\mathbf{U} = \bar{\mathbf{U}}$, we conclude that $\mathbf{R} = \bar{\mathbf{R}}$.

3.5.2 Polar Decompositions of the Deformation Gradient

If the tensor $\mathbf{F}$ in the previous subsection is assigned a physical meaning, then all the derived quantities have physical significance. The polar decompositions of the deformation gradient $\mathbf{F}$ are

$$\mathbf{F} = \mathbf{R} \cdot \mathbf{U} = \mathbf{V} \cdot \mathbf{R} \qquad F_{iR} = R_{iS} U_{SR} = V_{ij} R_{jR} \tag{3.38}$$

where

$$\mathbf{F} = \text{deformation gradient} = F_{iR} \mathbf{e}_i \otimes \mathbf{e}_R \tag{3.39a}$$

$$\mathbf{U} = \text{right stretch tensor} = U_{RS} \mathbf{e}_R \otimes \mathbf{e}_S \tag{3.39b}$$

$$\mathbf{V} = \text{left stretch tensor} = V_{ij} \mathbf{e}_i \otimes \mathbf{e}_j \tag{3.39c}$$

$$\mathbf{R} = \text{rotation tensor (orthogonal tensor)} = R_{iR} \mathbf{e}_i \otimes \mathbf{e}_R \tag{3.39d}$$

$$\mathbf{C} = \mathbf{F}^{\mathrm{T}} \cdot \mathbf{F} = \mathbf{U}^2 = \text{right Cauchy–Green deformation tensor,}$$

$$C_{RS} = (\partial x_i / \partial X_R)(\partial x_i / \partial X_S) \tag{3.40}$$

$$\mathbf{B} = \mathbf{F} \cdot \mathbf{F}^{\mathrm{T}} = \mathbf{V}^2 = \text{left Cauchy–Green deformation tensor,}$$

$$B_{ij} = (\partial x_i / \partial X_R)(\partial x_j / \partial X_R) \tag{3.41}$$

where $\mathbf{e}_R$ and $\mathbf{e}_i$ are base vectors for the material and spatial system, respectively.

We now discuss the physical meaning of the polar decompositions. The deformation gradient $\mathbf{F}$ deforms an element in two parts. In the right decomposition, the element is first purely deformed to a quantity $\mathbf{U}$. A rotation $\mathbf{R}$ then follows the deformation. This rotation represents the rotation of the principal axis of the stretch tensor $\mathbf{U}$, which will be illustrated by Example 3.3. The above statement may be understood by applying $\mathbf{F}$ to a line element $\mathrm{d}\mathbf{X}$. Thus,

$$\mathrm{d}\mathbf{x} = \mathbf{F} \cdot \mathrm{d}\mathbf{X} = \mathbf{R} \cdot (\mathbf{U} \cdot \mathrm{d}\mathbf{X}) \tag{3.42}$$

In the left decomposition, the element is first rotated through **R** and then deformed by **V**. This statement may be verified by

$$d\mathbf{x} = \mathbf{F} \cdot d\mathbf{X} = \mathbf{V} \cdot (\mathbf{R} \cdot d\mathbf{X}) \tag{3.43}$$

The two modes of decomposition are fully equivalent. We obtain the same final result.

EXAMPLE 3.3 Consider a simple shear problem defined by

$$x_1 = X_1 + kX_2, \quad x_2 = X_2, \quad x_3 = X_3 \qquad \text{where } k = \frac{2}{\sqrt{3}} \tag{a}$$

(a) Find **F**, **U**, **V**, and **R**.
(b) Use the right decomposition to draw figures showing the deformed state of the initially rectangular element at each stage of deformation.
(c) Use the left decomposition to draw figures showing the deformed state of the initially rectangular element at each stage of deformation.
(d) Study the deformation of a diagonal of the initially rectangular element.
(e) Study the deformation of a circle in the initially rectangular element.

Solution

(a) Using (a), (3.39), and (3.40), we obtain

$$[F] = \begin{bmatrix} 1 & k & 0 \\ 0 & 1 & 0 \\ 0 & 0 & 1 \end{bmatrix}, \quad [F]^{\mathrm{T}} = \begin{bmatrix} 1 & 0 & 0 \\ k & 1 & 0 \\ 0 & 0 & 1 \end{bmatrix}, \tag{b}$$

$$[C] = [F]^{\mathrm{T}}[F] = \begin{bmatrix} 1 & k & 0 \\ k & (k^2+1) & 0 \\ 0 & 0 & 1 \end{bmatrix} = \begin{bmatrix} 1 & \frac{2}{\sqrt{3}} & 0 \\ \frac{2}{\sqrt{3}} & \frac{7}{3} & 0 \\ 0 & 0 & 1 \end{bmatrix} \tag{c}$$

To determine the principal values and directions of $[C]$, we consider the characteristic equation

$$\begin{bmatrix} 1-\lambda & \frac{2}{\sqrt{3}} & 0 \\ \frac{2}{\sqrt{3}} & \frac{7}{3}-\lambda & 0 \\ 0 & 0 & 1-\lambda \end{bmatrix} \begin{bmatrix} n_1 \\ n_2 \\ n_3 \end{bmatrix} = 0 \tag{d}$$

By setting the determinant of the coefficient matrix to 0, we obtain $\lambda_{(i)} = 3, \frac{1}{3}, 1$. The corresponding eigenvectors are found to be

$$\mathbf{n}_u^{(1)^{\mathrm{T}}} = \left[\frac{1}{2}, \frac{\sqrt{3}}{2}, 0\right], \qquad \mathbf{n}_u^{(2)^{\mathrm{T}}} = \left[-\frac{\sqrt{3}}{2}, \frac{1}{2}, 0\right], \qquad \mathbf{n}_u^{(3)^{\mathrm{T}}} = [0, 0, 1] \tag{e}$$

with the following transformation matrix between x_i and x_i' (see (2.96)):

$$[Q_u] = \left[\mathbf{n}_u^{(1)} \quad \mathbf{n}_u^{(2)} \quad \mathbf{n}_u^{(3)}\right] = \begin{bmatrix} \frac{1}{2} & \frac{-\sqrt{3}}{2} & 0 \\ \frac{\sqrt{3}}{2} & \frac{1}{2} & 0 \\ 0 & 0 & 1 \end{bmatrix} \tag{f}$$

These eigenvectors are shown in Figure 3.4 with $\phi = 60°$. Referring to the principal axes x_i', tensors **C** and **U** have components

$$[C'] = \begin{bmatrix} 3 & 0 & 0 \\ 0 & \frac{1}{3} & 0 \\ 0 & 0 & 1 \end{bmatrix} \quad \text{and} \quad [U'] = \left[\sqrt{C'}\right] = \begin{bmatrix} \sqrt{3} & 0 & 0 \\ 0 & \frac{1}{\sqrt{3}} & 0 \\ 0 & 0 & 1 \end{bmatrix} \tag{g}$$

It may also be verified that $\mathbf{C}'$ is obtainable from the following transformation:

$$\begin{aligned}[C'] = [Q_u^{\mathrm{T}}][C][Q_u] &= \begin{bmatrix} \frac{1}{2} & \frac{\sqrt{3}}{2} & 0 \\ \frac{-\sqrt{3}}{2} & \frac{1}{2} & 0 \\ 0 & 0 & 1 \end{bmatrix} \begin{bmatrix} 1 & \frac{2}{\sqrt{3}} & 0 \\ \frac{2}{\sqrt{3}} & \frac{7}{3} & 0 \\ 0 & 0 & 1 \end{bmatrix} \begin{bmatrix} \frac{1}{2} & \frac{-\sqrt{3}}{2} & 0 \\ \frac{\sqrt{3}}{2} & \frac{1}{2} & 0 \\ 0 & 0 & 1 \end{bmatrix} \\ &= \begin{bmatrix} 3 & 0 & 0 \\ 0 & \frac{1}{3} & 0 \\ 0 & 0 & 1 \end{bmatrix}\end{aligned} \tag{h}$$

In addition, **U** can be determined by the following transformation:

$$[U] = [Q_u][U'][Q_u^{\mathrm{T}}] = \begin{bmatrix} \frac{\sqrt{3}}{2} & \frac{1}{2} & 0 \\ \frac{1}{2} & \frac{5}{2\sqrt{3}} & 0 \\ 0 & 0 & 1 \end{bmatrix} \tag{i}$$

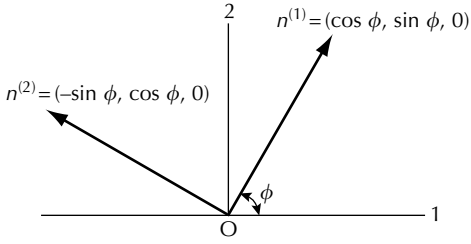

FIGURE 3.4
Eigenvectors of **C** in simple shear deformation.

Since $\det[U] = 1$, we find

$$[U^{-1}] = \frac{(\text{cof}[U])^{\text{T}}}{\det[U]} = \begin{bmatrix} \dfrac{5}{2\sqrt{3}} & \dfrac{-1}{2} & 0 \\ \dfrac{-1}{2} & \dfrac{\sqrt{3}}{2} & 0 \\ 0 & 0 & 1 \end{bmatrix} \tag{j}$$

and $[R]$ to be

$$[R] = [F][U^{-1}] = \begin{bmatrix} \dfrac{\sqrt{3}}{2} & \dfrac{1}{2} & 0 \\ \dfrac{-1}{2} & \dfrac{\sqrt{3}}{2} & 0 \\ 0 & 0 & 1 \end{bmatrix} \tag{k}$$

The matrix in (k) describes a clockwise rotation of 30° of the continuum about the x_3 axis. Note that

$$[R][R]^{\text{T}} = \begin{bmatrix} \dfrac{\sqrt{3}}{2} & \dfrac{1}{2} & 0 \\ \dfrac{-1}{2} & \dfrac{\sqrt{3}}{2} & 0 \\ 0 & 0 & 1 \end{bmatrix} \begin{bmatrix} \dfrac{\sqrt{3}}{2} & \dfrac{-1}{2} & 0 \\ \dfrac{1}{2} & \dfrac{\sqrt{3}}{2} & 0 \\ 0 & 0 & 1 \end{bmatrix} = \begin{bmatrix} 1 & 0 & 0 \\ 0 & 1 & 0 \\ 0 & 0 & 1 \end{bmatrix} \tag{m}$$

which shows that $\mathbf{R}^{\text{T}} = \mathbf{R}^{-1}$ and **R** is therefore an orthogonal tensor.

On the other hand, we may find from the left decomposition

$$[V] = [F][R^{-1}] = \begin{bmatrix} \dfrac{5}{2\sqrt{3}} & \dfrac{1}{2} & 0 \\ \dfrac{1}{2} & \dfrac{\sqrt{3}}{2} & 0 \\ 0 & 0 & 1 \end{bmatrix} \tag{n}$$

It may be easily shown that

$$[V'] = [U'] = \begin{bmatrix} \sqrt{3} & 0 & 0 \\ 0 & \dfrac{1}{\sqrt{3}} & 0 \\ 0 & 0 & 1 \end{bmatrix} \tag{o}$$

and the principal directions of $\mathbf{V}$ are

$$\mathbf{n}_v^{(1)^{\mathrm{T}}} = \left[\frac{\sqrt{3}}{2},\ \frac{1}{2},\ 0\right], \quad \mathbf{n}_v^{(2)^{\mathrm{T}}} = \left[-\frac{1}{2},\ \frac{\sqrt{3}}{2},\ 0\right], \quad \mathbf{n}_v^{(3)^{\mathrm{T}}} = [0,\ 0,\ 1] \tag{p}$$

with the transformation matrix given by

$$[Q_v] = \left[\mathbf{n}_v^{(1)} \quad \mathbf{n}_v^{(2)} \quad \mathbf{n}_v^{(3)}\right] \tag{q}$$

By use of (3.35), $\mathbf{R}$ rotates $\mathbf{U}$ into $\mathbf{V}$. It also rotates vectors $\mathbf{n}_u$ into $\mathbf{n}_v$. Putting all eigenvectors together in a matrix form, we may write

$$[Q_v] = [R][Q_u] = \begin{bmatrix} \dfrac{\sqrt{3}}{2} & \dfrac{1}{2} & 0 \\ \dfrac{-1}{2} & \dfrac{\sqrt{3}}{2} & 0 \\ 0 & 0 & 1 \end{bmatrix} \begin{bmatrix} \dfrac{1}{2} & \dfrac{-\sqrt{3}}{2} & 0 \\ \dfrac{\sqrt{3}}{2} & \dfrac{1}{2} & 0 \\ 0 & 0 & 1 \end{bmatrix} = \begin{bmatrix} \dfrac{\sqrt{3}}{2} & -\dfrac{1}{2} & 0 \\ \dfrac{1}{2} & \dfrac{\sqrt{3}}{2} & 0 \\ 0 & 0 & 1 \end{bmatrix} \tag{r}$$

All $\mathbf{n}_u$ vectors that form Q_u are rotated clockwise at a 30° angle into the $\mathbf{n}_v$ vectors. This rotation is shown in Figure 3.5.

(b) Consider a square element ABCD with unit side length, as shown in Figure 3.6. Using (3.42), the square ABCD is first deformed by $\mathbf{U}$ into A′B′C′D′, which is subsequently rotated by $\mathbf{R}$ into A″B″C″D″. Thus, in the application

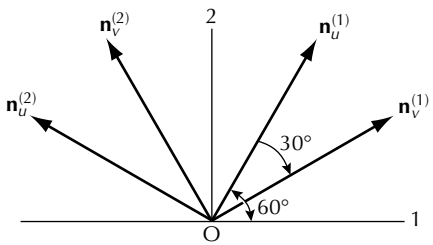

FIGURE 3.5
Rotation of $\mathbf{n}_u$ into $\mathbf{n}_v$.

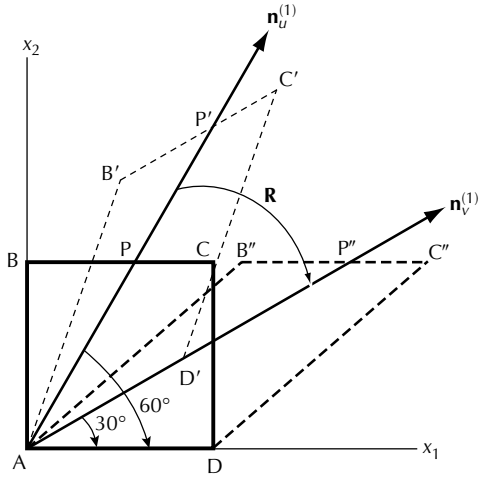

FIGURE 3.6
Right polar decomposition.

of **U**, line element AB is deformed into A′B′, AC into A′C′, etc. The deformed line elements are

$$\mathrm{A'B'} = \begin{bmatrix} \frac{\sqrt{3}}{2} & \frac{1}{2} & 0 \\ \frac{1}{2} & \frac{5}{2\sqrt{3}} & 0 \\ 0 & 0 & 1 \end{bmatrix} \begin{bmatrix} 0 \\ 1 \\ 0 \end{bmatrix} = \begin{bmatrix} \frac{1}{2} \\ \frac{5\sqrt{3}}{6} \\ 0 \end{bmatrix} \tag{s1}$$

$$\mathrm{A'P'} = \begin{bmatrix} \frac{\sqrt{3}}{2} & \frac{1}{2} & 0 \\ \frac{1}{2} & \frac{5}{2\sqrt{3}} & 0 \\ 0 & 0 & 1 \end{bmatrix} \begin{bmatrix} \frac{1}{\sqrt{3}} \\ 1 \\ 0 \end{bmatrix} = \begin{bmatrix} 1 \\ \sqrt{3} \\ 0 \end{bmatrix} \tag{s2}$$

$$\mathrm{A'C'} = \begin{bmatrix} \frac{\sqrt{3}}{2} & \frac{1}{2} & 0 \\ \frac{1}{2} & \frac{5}{2\sqrt{3}} & 0 \\ 0 & 0 & 1 \end{bmatrix} \begin{bmatrix} 1 \\ 1 \\ 0 \end{bmatrix} = \begin{bmatrix} \frac{1+\sqrt{3}}{2} \\ \frac{3+5\sqrt{3}}{6} \\ 0 \end{bmatrix} \tag{s3}$$

$$\mathrm{A'D'} = \begin{bmatrix} \frac{\sqrt{3}}{2} & \frac{1}{2} & 0 \\ \frac{1}{2} & \frac{5}{2\sqrt{3}} & 0 \\ 0 & 0 & 1 \end{bmatrix} \begin{bmatrix} 1 \\ 0 \\ 0 \end{bmatrix} = \begin{bmatrix} \frac{\sqrt{3}}{2} \\ \frac{1}{2} \\ 0 \end{bmatrix} \tag{s4}$$

in which AP is a principal direction of **U**. Note that this method of finding the deformed shape of an element is valid only when **F** is not a function of position. If **F** is a function of position, then the line elements must be divided into small increments, and this method is applied to each increment. Alternatively, the set of transformation equations (3.8) may be used to find the deformed shape of the element point by point.

The rotation of A′B′C′D′ into A″B″C″D″ is obtained by applying **R** to the deformed line element A′B′, A′P′, etc. given by (s1 to s4). The resulting line elements are

$$\mathrm{A''B''} = \begin{bmatrix} \frac{\sqrt{3}}{2} & \frac{1}{2} & 0 \\ -\frac{1}{2} & \frac{\sqrt{3}}{2} & 0 \\ 0 & 0 & 1 \end{bmatrix} \begin{bmatrix} \frac{1}{2} \\ \frac{5\sqrt{3}}{6} \\ 0 \end{bmatrix} = \begin{bmatrix} \frac{2\sqrt{3}}{3} \\ 1 \\ 0 \end{bmatrix} \tag{s5}$$

$$\mathrm{A''P''} = \begin{bmatrix} \frac{\sqrt{3}}{2} & \frac{1}{2} & 0 \\ -\frac{1}{2} & \frac{\sqrt{3}}{2} & 0 \\ 0 & 0 & 1 \end{bmatrix} \begin{bmatrix} 1 \\ \sqrt{3} \\ 0 \end{bmatrix} = \begin{bmatrix} \sqrt{3} \\ 1 \\ 0 \end{bmatrix} \tag{s6}$$

$$\mathrm{A''C''} = \begin{bmatrix} \frac{\sqrt{3}}{2} & \frac{1}{2} & 0 \\ -\frac{1}{2} & \frac{\sqrt{3}}{2} & 0 \\ 0 & 0 & 1 \end{bmatrix} \begin{bmatrix} \frac{1+\sqrt{3}}{2} \\ \frac{3+5\sqrt{3}}{6} \\ 0 \end{bmatrix} = \begin{bmatrix} \frac{3+2\sqrt{3}}{3} \\ 1 \\ 0 \end{bmatrix} \tag{s7}$$

$$\mathrm{A''D''} = \begin{bmatrix} \frac{\sqrt{3}}{2} & \frac{1}{2} & 0 \\ -\frac{1}{2} & \frac{\sqrt{3}}{2} & 0 \\ 0 & 0 & 1 \end{bmatrix} \begin{bmatrix} \frac{\sqrt{3}}{2} \\ \frac{1}{2} \\ 0 \end{bmatrix} = \begin{bmatrix} 1 \\ 0 \\ 0 \end{bmatrix} \tag{s8}$$

The two stages of deformation and rotation are shown in Figure 3.6.

(c) Using (4.43), the square ABCD is first rotated into A′B′C′D′ by **R**.

$$\begin{bmatrix} \frac{\sqrt{3}}{2} & \frac{1}{2} & 0 \\ -\frac{1}{2} & \frac{\sqrt{3}}{2} & 0 \\ 0 & 0 & 1 \end{bmatrix} \begin{bmatrix} 0 & \frac{1}{\sqrt{3}} & 1 & 1 \\ 1 & 1 & 1 & 0 \\ 0 & 0 & 0 & 0 \end{bmatrix} = \begin{bmatrix} \frac{1}{2} & 1 & \frac{1+\sqrt{3}}{2} & \frac{\sqrt{3}}{2} \\ \frac{\sqrt{3}}{2} & \frac{1}{\sqrt{3}} & \frac{-1+\sqrt{3}}{2} & -\frac{1}{2} \\ 0 & 0 & 0 & 0 \end{bmatrix} \tag{t1}$$

Note that the first matrix is **R**, the second matrix is formed by the column vectors AB, AP, AC, and AD, and the third matrix is a collection of column vectors A′B′, A′P′, A′C′, and A′D′. In the second step, the square A′B′C′D′ is deformed into A″B″C″D″ by **V**, given by the following equation

$$\begin{bmatrix} \frac{5}{2\sqrt{3}} & \frac{1}{2} & 0 \\ \frac{1}{2} & \frac{\sqrt{3}}{2} & 0 \\ 0 & 0 & 1 \end{bmatrix} \begin{bmatrix} \frac{1}{2} & 1 & \frac{1+\sqrt{3}}{2} & \frac{\sqrt{3}}{2} \\ \frac{\sqrt{3}}{2} & \frac{1}{\sqrt{3}} & \frac{-1+\sqrt{3}}{2} & -\frac{1}{2} \\ 0 & 0 & 0 & 0 \end{bmatrix}$$

$$= \begin{bmatrix} \frac{2\sqrt{3}}{3} & \sqrt{3} & \frac{3+2\sqrt{3}}{3} & 1 \\ 1 & 1 & 1 & 0 \\ 0 & 0 & 0 & 0 \end{bmatrix} \qquad \text{(t2)}$$

In equation (t2), the first matrix is **V**, the second matrix consists of column vectors A′B′, A′P′, A′C′, and A′D′, and the third matrix is a collection of column vectors A″B″, A″P″, A″C″, and A″D″. The two stages of rotation and deformation are shown in Figure 3.7. Comparing (s5 to s8) with (t2), we see that the results obtained from the left decomposition is the same as those from the right decomposition.

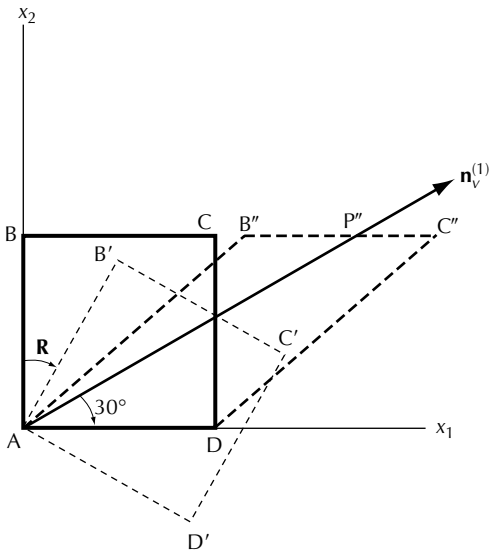

FIGURE 3.7
Left polar decomposition.

(d) A straight line passing through the origin is given by

$$X_2 = X_1 \tan\theta \tag{u}$$

where θ is the angle between the line and the X_1 axis. Substituting (a) into (u), this line is deformed into

$$x_1 = \left(\frac{1}{\tan\theta} + k\right) x_2 \tag{v}$$

The diagonal of the initial square element has $\theta = 45°$. This angle is deformed into α where

$$\tan\alpha = \frac{x_2}{x_1} = \frac{1}{1+k} \tag{w}$$

(e) A circle in the initial element is given by

$$X_1^2 + X_2^2 = a^2 \tag{x}$$

where a is the radius. Substituting (a) into (x), this circle is deformed into

$$x_1^2 - 2kx_1x_2 + (1+k^2)x_2^2 = a^2 \tag{y}$$

It is observed that a circle is deformed into an ellipse with the semimajor axis making an angle of β with the positive x_1 axis. It can be shown that $\tan 2\beta = 2/k$. Thus, when $k = 2/\sqrt{3}$, $\beta = 30°$.

3.6 The Right Cauchy–Green Deformation Tensor

We now discuss some popular strain measures. Any strain measure is as good as the other as long as its definition is clear and correctly used. It is a matter of convenience to choose one measure over another for the description of the problem at hand. We discuss in this section a popular strain measure called the *right Cauchy–Green tensor*. Other popular measures are discussed in sections 3.9 and 3.10.

3.6.1 The Physical Meaning

Consider a line element dX_R with length dS deforming into dx_i with length ds. We have

$$dx_i = \frac{\partial x_i}{\partial X_R} dX_R \tag{3.44}$$

Dividing both sides of (3.44) by (ds dS), we obtain

$$\lambda n_i = \frac{\partial x_i}{\partial X_R} N_R \tag{3.45}$$

where

$$N_R = \frac{\mathrm{d}X_R}{\mathrm{d}S} \quad \text{and} \quad n_i = \frac{\mathrm{d}x_i}{\mathrm{d}s} \tag{3.46}$$

specify the directions (unit vectors) of the line element before and after deformation, respectively. The extension ratio (or stretch ratio) λ is defined by

$$\lambda = \frac{\mathrm{d}s}{\mathrm{d}S} \tag{3.47}$$

The notation λ is a popular notation for stretch ratio and should not be confused with the eigenvalues used in Chapter 2. Because of many notations, symbols, and quantities, the same notation may be used to mean different quantities. You should pay special attention to the definition of each notation used.

Using (3.45), we form

$$\lambda^2 = (\lambda n_i)(\lambda n_i) = \frac{\partial x_i}{\partial X_R}\frac{\partial x_i}{\partial X_S} N_R N_S = C_{RS} N_R N_S \tag{3.48}$$

or

$$\lambda^2 = C_{RS} N_R N_S \tag{3.49}$$

Note that C_{RS} is a symmetric tensor and is positive definite. Given a deformation (3.8), $\mathbf{F}$ and $\mathbf{C}$ may be found. If we specify the initial direction N_R of a line element, then the direction and magnitude of the deformed line element may be found using (3.45) and (3.49), respectively.

In order to visualize the meaning of the diagonal terms C_{11}, C_{22}, C_{33} and the off diagonal terms C_{12}, C_{23}, etc., of C_{RS}, let us consider two line elements $\mathrm{d}X_R^{(1)}$ and $\mathrm{d}X_R^{(2)}$, which deform into $\mathrm{d}x_i^{(1)}$ and $\mathrm{d}x_i^{(2)}$, respectively. The angle between the two line elements is Φ in the initial configuration and ϕ in the current configuration as shown in Figure 3.8. The initial and deformed line elements are related by

$$\mathrm{d}x_i^{(1)} = \frac{\partial x_i}{\partial X_R}\mathrm{d}X_R^{(1)} \tag{3.50}$$

$$\mathrm{d}x_i^{(2)} = \frac{\partial x_i}{\partial X_R}\mathrm{d}X_R^{(2)} \tag{3.51}$$

Then, we form the inner product of the two line elements

$$dx_i^{(1)} dx_i^{(2)} = \frac{\partial x_i}{\partial X_R} \frac{\partial x_i}{\partial X_S} dX_R^{(1)} dX_S^{(2)} = C_{RS} dX_R^{(1)} dX_S^{(2)} \tag{3.52}$$

On the other hand, the inner product may be expressed in terms of the lengths of the line elements and the angle ϕ as

$$dx_i^{(1)} dx_i^{(2)} = ds_1 ds_2 \cos\phi_{12} \tag{3.53}$$

where ds_1 and ds_2 are the lengths of the two line elements after deformation and ϕ_{12} is the inclusion angle. Let dS_1 and dS_2 be the lengths of the two line elements before deformation, then

$$\frac{dX_R^{(1)}}{dS_1} = N_R^{(1)} \qquad \frac{dX_R^{(2)}}{dS_2} = N_R^{(2)} \tag{3.54}$$

Using (3.54) and equating (3.52) to (3.53), we obtain

$$\frac{ds_1}{dS_1} \frac{ds_2}{dS_2} \cos\phi_{12} = C_{RS} N_R^{(1)} N_S^{(2)} \tag{3.55}$$

From (3.55), we obtain information for C_{11}, C_{22}, C_{33}. Let us consider a line element oriented initially along X_1, then $N_1^{(1)} = 1$, $N_2^{(1)} = 0$, $N_3^{(1)} = 0$. In this case, (3.55) reduces to

$$\left(\frac{ds_1}{dS_1}\right)^2 = C_{11} = \lambda_1^{(2)} \tag{3.56a}$$

We note that C_{11} is related to the extension ratio λ_1 along X_1. Similarly, if we consider line elements oriented initially along X_2 and X_3, respectively, we obtain

$$C_{22} = \left(\frac{ds_2}{dS_2}\right)^2 \quad \text{and} \quad C_{33} = \left(\frac{ds_3}{dS_3}\right)^2 \tag{3.56b,c}$$

We now consider the angle changes between the two line elements as shown in Figure 3.8. In a special case, the two line elements are initially 90° to each other. Let $dX_i^{(1)}$ be along the X_1 direction and $dX_i^{(2)}$ be along the X_2 direction, then the unit normals are $N_R^{(1)} \sim [1,0,0]$ and $N_S^{(2)} \sim [0,1,0]$. Equation (3.55) now reduces to

$$\frac{ds_1}{dS_1} \frac{ds_2}{dS_2} \cos\phi_{12} = C_{12} \tag{3.57}$$

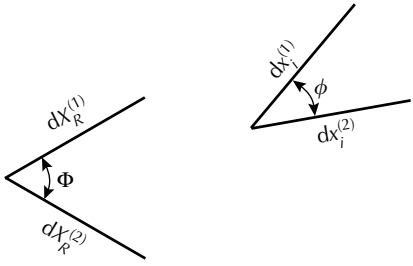

FIGURE 3.8
Deformation of two line elements.

Making use of (3.56), (3.57) becomes

$$\cos\phi_{12} = \frac{C_{12}}{\sqrt{C_{11}}\sqrt{C_{22}}} \tag{3.58}$$

Note that (3.58) relates C_{12} to ϕ_{12}, which is the angle after deformation. The angle ϕ_{12} may no longer be 90° and the two line elements are in general not oriented along the coordinate axes after deformation. Using a similar procedure, we relate C_{23} to ϕ_{23} and C_{31} to ϕ_{31}. These equations are summarized and we write

$$\cos\phi_{RS} = \frac{C_{RS}}{\sqrt{C_{RR}}\sqrt{C_{SS}}} \qquad (R, S \text{ not summed}) \tag{3.59}$$

It may be concluded that the diagonal terms C_{11}, C_{22}, C_{33} are related to the extension ratios λ_1, λ_2, λ_3, respectively; they represent the stretching along the coordinate directions; the off-diagonal terms C_{12}, C_{23}, C_{31} are related to the current angles ϕ_{RS}, respectively; they are different from the initial angles Φ_{RS} and, therefore, represent shearing deformation. Finally, we remark that, if the triad formed by the three initial line elements are along the principal directions of C_{RS}, then $C_{12} = C_{23} = C_{31} = 0$. From (3.59), we find $\phi_{12} = \phi_{23} = \phi_{31} = 90°$, that is, the triad remains mutually perpendicular to each other after deformation. Furthermore, in the undeformed state, C_{RS} does not vanish, that is, $C_{11} = 1$, $C_{22} = 1$, $C_{33} = 1$, and $C_{12} = \cos\phi_{12} = 0$, etc., or we may write $C_{RS} = \delta_{RS}$ in the undeformed configuration.

3.6.2 Transformation Properties of C_{RS}

In this subsection, we consider the transformation properties of C_{RS} with respect to the rotation and translation of either the material coordinate system or the spatial coordinate system. Let $\bar{X}_R$ be an alternative material system,

which is related to X_R by

$$\bar{X}_R = M_{SR}X_S + a_R \tag{3.60}$$

where M_{RS} is a rotation matrix, that is,

$$M_{TR}M_{TS} = \delta_{RS} = M_{RT}M_{ST} \qquad \text{with } |M_{RS}| = 1 \tag{3.61}$$

Both **M** and **a** are independent of X_R. Also, let $\bar{x}_i$ be an alternative spatial system such that

$$\bar{x}_i = Q_{ji}(t)x_j + b_i(t) \tag{3.62}$$

where

$$Q_{ij}Q_{ik} = \delta_{jk} = Q_{ji}Q_{ki} \qquad \text{with } |Q_{ij}| = 1 \tag{3.63}$$

Note that each of $\bar{X}_R$ and $\bar{x}_i$ differs from the original system by a rigid-body rotation plus a translation.

3.6.2.1 Rotation and translation of material system

Referring to X_R and $\bar{X}_R$, the expressions of C_{RS} are, respectively,

$$C_{RS} = \frac{\partial x_i}{\partial X_R}\frac{\partial x_i}{\partial X_S} \quad \text{and} \quad \bar{C}_{RS} = \frac{\partial x_i}{\partial \bar{X}_R}\frac{\partial x_i}{\partial \bar{X}_R} \tag{3.64}$$

By the chain rule of differentiation, we have

$$C_{RS} = \frac{\partial x_i}{\partial \bar{X}_T}\frac{\partial \bar{X}_\mathrm{T}}{\partial X_R}\frac{\partial x_i}{\partial \bar{X}_V}\frac{\partial \bar{X}_V}{\partial X_S} = \frac{\partial x_i}{\partial \bar{X}_T}M_{RT}\frac{\partial x_i}{\partial \bar{X}_V}M_{SV} = M_{RT}M_{SV}\bar{C}_{TV} \tag{3.65}$$

or

$$\bar{C}_{RS} = M_{TR}M_{VS}C_{TV} \tag{3.66}$$

Therefore, C_{RS} transforms as a second-order tensor with rotation of the material system but it remains invariant with translation of the material system. This result is expected because both subscripts of C_{RS} refer to the material system. We note that $\bar{C}_{RS}$ in this subsection should not be confused with the $\bar{C}_{RS}$ matrix referring to the principal coordinate system and used in most other sections.

3.6.2.2 Rotation and translation of the spatial system

Referring to x_i and $\bar{x}_i$, the expressions of C_{RS} are, respectively,

$$C_{RS} = \frac{\partial x_i}{\partial X_R}\frac{\partial x_i}{\partial X_S} \quad \text{and} \quad \underline{C}_{RS} = \frac{\partial \bar{x}_i}{\partial X_R}\frac{\partial \bar{x}_i}{\partial X_R} \tag{3.67}$$

The second equation in (3.67), by use of (3.62), is further written as

$$\begin{aligned}\underline{C}_{RS} &= \frac{\partial \bar{x}_i}{\partial x_j}\frac{\partial x_j}{\partial X_R}\frac{\partial \bar{x}_i}{\partial x_k}\frac{\partial x_k}{\partial X_S} = Q_{ji}\frac{\partial x_j}{\partial X_R}Q_{ki}\frac{\partial x_k}{\partial X_S} \\ &= \delta_{jk}\frac{\partial x_j}{\partial X_R}\frac{\partial x_k}{\partial X_S} = \frac{\partial x_k}{\partial X_R}\frac{\partial x_k}{\partial X_S} = C_{RS}\end{aligned} \tag{3.68}$$

We conclude that C_{RS} remains invariant with rotation and translation of the spatial system. This is also expected, because both subscripts of C_{RS} refer to the material system and it does not matter which spatial coordinate system we use.

3.6.3 Eigenvalues and Eigenvectors of C_{RS}

C_{RS} is a symmetric matrix and it has three real eigenvalues and three real eigenvectors. The properties of eigenvalues and eigenvectors are discussed in Section 2.7. We use $\bar{X}_R$ to denote the principal coordinate system of C_{RS}. The principal values (eigenvalues) $\bar{C}_{RS}$ are related to C_{RS} by

$$\bar{C}_{RS} = Q_{PR}Q_{QS}C_{PQ} = \begin{bmatrix} \left(\dfrac{\mathrm{d}s_1}{\mathrm{d}S_1}\right)^2 & 0 & 0 \\ 0 & \left(\dfrac{\mathrm{d}s_2}{\mathrm{d}S_2}\right)^2 & 0 \\ 0 & 0 & \left(\dfrac{\mathrm{d}s_3}{\mathrm{d}S_3}\right)^2 \end{bmatrix} = \begin{bmatrix} \lambda_1^2 & 0 & 0 \\ 0 & \lambda_2^2 & 0 \\ 0 & 0 & \lambda_3^2 \end{bmatrix} \tag{3.69}$$

We see that, when C_{RS} are expressed in the principal frame, it becomes a diagonal matrix. The eigenvectors, or the principal directions, are $\mathbf{n}_C^{(R)}$ with $R = 1, 2$, and 3. Figure 3.9 shows the eigenvectors in the neighborhood N_0 of an undeformed body. Whatever the deformation of N_0, there exists one set of three line elements, which are mutually orthogonal. The three line elements may extend during deformation and the triad may rotate, but the angles between them will always be right angles.

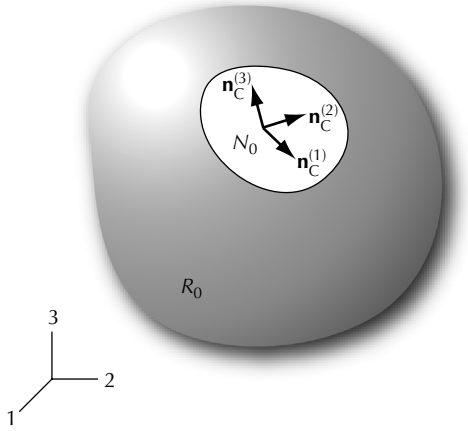

FIGURE 3.9
Eigenvectors in the neighborhood N_0.

3.6.4 Principal Invariants of C_{RS}

Similar to the stress invariants discussed in Section 2.12, we define the invariants for C_{RS} as

$$I_1 = C_{RR} = C_{11} + C_{22} + C_{33} \tag{3.70}$$

$$I_2 = \text{tr}(\text{cof.}\,\mathbf{C}) = I_3\text{tr}(\mathbf{C}^{-1}) \tag{3.71}$$

$$I_3 = \det \mathbf{C} \tag{3.72}$$

We now discuss the geometric significance of I_1, I_2, and I_3.

In principal axes, the invariants I_1, I_2, and I_3 may be associated with the geometric properties of a material element. The matrix of $\mathbf{C}$ is a diagonal matrix as shown in (3.69). In this system, the expressions for the invariants are

$$I_1 = \lambda_1^2 + \lambda_2^2 + \lambda_3^2 \tag{3.73}$$

$$\begin{aligned} I_2 &= \lambda_2^2\lambda_3^2 + \lambda_1^2\lambda_3^2 + \lambda_1^2\lambda_2^2 \\ &= \lambda_1^2\lambda_2^2\lambda_3^2\left(\frac{1}{\lambda_1^2} + \frac{1}{\lambda_2^2} + \frac{1}{\lambda_3^2}\right) = I_3\left(\frac{1}{\lambda_1^2} + \frac{1}{\lambda_2^2} + \frac{1}{\lambda_3^2}\right) = I_3\,\text{tr}(\mathbf{C}^{-1}) \end{aligned} \tag{3.74}$$

$$I_3 = \lambda_1^2\lambda_2^2\lambda_3^2 \tag{3.75}$$

In the case that the initial lengths are $dS_1 = 1$, $dS_2 = 1$, and $dS_3 = 1$, (3.69) reduces to

$$\mathbf{C} = \begin{bmatrix} ds_1^2 & 0 & 0 \\ 0 & ds_2^2 & 0 \\ 0 & 0 & ds_2^2 \end{bmatrix} \tag{3.76}$$

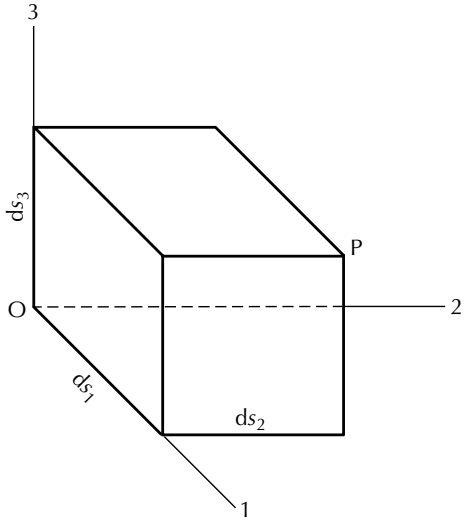

FIGURE 3.10
Deformed cuboid for geometric interpretations of strain invariants.

and

$$I_1 = |\overline{\mathrm{OP}}|^2 = \mathrm{d}s_1^2 + \mathrm{d}s_2^2 + \mathrm{d}s_3^2 \tag{3.77}$$

$I_2 =$ sum of squares of areas of three mutually perpendicular faces of deformed cuboid

$$= \begin{vmatrix} \mathrm{d}s_2^2 & 0 \\ 0 & \mathrm{d}s_3^2 \end{vmatrix} + \begin{vmatrix} \mathrm{d}s_1^2 & 0 \\ 0 & \mathrm{d}s_3^2 \end{vmatrix} + \begin{vmatrix} \mathrm{d}s_1^2 & 0 \\ 0 & \mathrm{d}s_2^2 \end{vmatrix} = \mathrm{d}s_2^2\,\mathrm{d}s_3^2 + \mathrm{d}s_1^2\,\mathrm{d}s_3^2 + \mathrm{d}s_1^2\,\mathrm{d}s_2^2 \tag{3.78}$$

$$I_3 = \text{square of volumes of deformed unit cuboid} = (\mathrm{d}s_1\,\mathrm{d}s_2\,\mathrm{d}s_3)^2 \tag{3.79}$$

The above geometric interpretations are clear when we refer to Figure 3.10.

3.7 Deformation of Volume and Area of a Material Element

We investigate first the deformation of a volumetric element within the neighborhood N_0 and then investigate how an area element deforms during deformation. The initial volume of an infinitesimal parallelepiped within N_0 is $\mathrm{d}V_0$, which is the scalar triple product of the three vectors

forming the sides of the parallelepiped. The deformed volume is denoted by dV. We have

$$dV_0 = d\mathbf{X}^{(1)} \cdot \left(d\mathbf{X}^{(2)} \times d\mathbf{X}^{(3)}\right) = \mathbf{e}_{PQR} dX_P^{(1)} dX_Q^{(2)} dX_R^{(3)} \tag{3.80}$$

$$\begin{aligned} dV &= e_{ijk}\, dx_i^{(1)} dx_j^{(2)} dx_k^{(3)} = e_{ijk} \frac{\partial x_i}{\partial X_P} dX_P^{(1)} \frac{\partial x_j}{\partial X_Q} dX_Q^{(2)} \frac{\partial x_k}{\partial X_R} dX_R^{(3)} \\ &= e_{ijk} \frac{\partial x_i}{\partial X_P} \frac{\partial x_j}{\partial X_Q} \frac{\partial x_k}{\partial X_R} dX_P^{(1)} dX_Q^{(2)} dX_R^{(3)} = e_{PQR} \left| \frac{\partial x_i}{\partial X_P} \right| dX_P^{(1)} dX_Q^{(2)} dX_R^{(3)} \end{aligned} \tag{3.81}$$

From (3.80) and (3.81), we obtain

$$dV = \left| \frac{\partial x_i}{\partial X_P} \right| dV_0 \quad \text{or} \quad \frac{dV}{dV_0} = \left| \frac{\partial x_i}{\partial X_P} \right| = \det \mathbf{F} \tag{3.82}$$

Let dm be the mass of the volumes dV and dV_0 and ρ and ρ_0 be the densities of dV and dV_0, respectively. Equation (3.82) may be rewritten as

$$\frac{\rho_0}{\rho} = \left| \frac{\partial x_i}{\partial X_P} \right| = \det \mathbf{F} = J \tag{3.83}$$

Now that

$$I_3 = |C_{RS}| = \left| \frac{\partial x_i}{\partial X_R} \frac{\partial x_i}{\partial X_S} \right| = |\mathbf{F}^{\mathrm{T}} \cdot \mathbf{F}| = |\mathbf{F}^{\mathrm{T}}|\,|\mathbf{F}| = |\mathbf{F}|^2 \tag{3.84}$$

we find from (3.83) and (3.84) that

$$I_3 = \left(\frac{dV}{dV_0} \right)^2 = \left(\frac{\rho_0}{\rho} \right)^2 \tag{3.85}$$

We consider next the deformation of an area element. Referring to Figure 3.11, line elements $dX_R^{(1)}$ and $dX_R^{(2)}$ form the initial area dA, which has a unit normal of N_R. The two line elements deform into $dx_i^{(1)}$ and $dx_i^{(2)}$, and area dA deforms into da with unit normal n_i. The two areas can be expressed as vectors given by

$$dA_R = N_R dA \quad \text{and} \quad da_i = n_i da \tag{3.86}$$

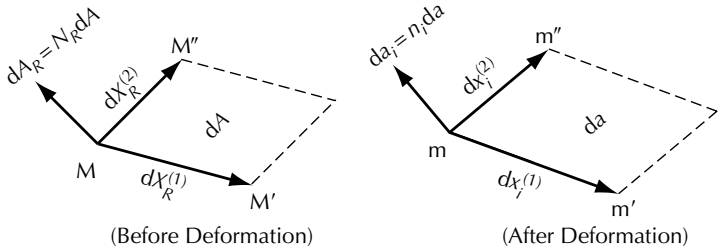

FIGURE 3.11
Deformation of area element.

In addition, the undeformed area is

$$\mathrm{d}A_R = e_{RST}\mathrm{d}X_S^{(1)}\mathrm{d}X_T^{(2)} \qquad \text{with } (\mathrm{d}A)^2 = \mathrm{d}A_R\mathrm{d}A_R \tag{3.87}$$

and the deformed area is

$$\mathrm{d}a_i = e_{ijk}\mathrm{d}x_j^{(1)}\mathrm{d}x_k^{(2)} \qquad \text{with } (\mathrm{d}a)^2 = \mathrm{d}a_i\mathrm{d}a_i \tag{3.88}$$

We now proceed to find the relation between the two areas. By way of the chain rule of differentiation, (3.87) can be written as

$$\mathrm{d}A_R = e_{RST}\frac{\partial X_S}{\partial x_m}\frac{\partial X_T}{\partial x_n}\mathrm{d}x_m^{(1)}\mathrm{d}x_n^{(2)} \tag{3.89}$$

Multiplying (3.89) by $\partial X_R/\partial x_k$, we obtain

$$\begin{aligned}\frac{\partial X_R}{\partial x_k}\mathrm{d}A_R &= e_{RST}\frac{\partial X_S}{\partial x_m}\frac{\partial X_T}{\partial x_n}\frac{\partial X_R}{\partial x_k}\mathrm{d}x_m^{(1)}\mathrm{d}x_n^{(2)} = \left|\frac{\partial X_M}{\partial x_r}\right| e_{kmn}\mathrm{d}x_m^{(1)}\mathrm{d}x_n^{(2)} \\ &= \left|\frac{\partial X_M}{\partial x_r}\right|\mathrm{d}a_k\end{aligned} \tag{3.90}$$

Equation (3.88) and the identity discussed in Example 2.7 have been used in the above derivation. Thus, we may conclude that

$$\frac{\partial X_R}{\partial x_k}\mathrm{d}A_R = \left|\frac{\partial X_M}{\partial x_r}\right|\mathrm{d}a_k \tag{3.91}$$

or using (3.83),

$$\mathrm{d}a_i = J\frac{\partial X_R}{\partial x_i}\mathrm{d}A_R \quad \text{or} \quad \mathrm{d}\mathbf{a} = J(\mathbf{F}^{-1})^{\mathrm{T}}\cdot\mathrm{d}\mathbf{A} \tag{3.92}$$

Equation (3.92) relating $\mathrm{d}A_R$ to $\mathrm{d}a_i$ is called Nanson's formula.

3.8 The Left Cauchy–Green Deformation Tensor

The left Cauchy–Green tensor **B** is defined in (3.41). It is seen that both subscripts of B_{ij} refer to the spatial coordinate system. **B** is invariant with rotation of the material system and transforms as a second-rank tensor with rotation of the spatial system. We now show that the invariants of **B**, denoted by I_B, II_B, and III_B, coincide with those of **C**, denoted by $I_C = I_1$, $II_C = I_2$, and $III_C = I_3$. From (3.70), we have

$$I_C = C_{RR} = \frac{\partial x_i}{\partial X_R}\frac{\partial x_i}{\partial X_R} = B_{ii} = I_B \tag{3.93}$$

and from (2.79), the second invariant is

$$II_B = \tfrac{1}{2}\left(I_B^2 - \operatorname{tr}\mathbf{B}^2\right) \tag{3.94}$$

where $\mathbf{B}^2 = B_{ip}B_{pj}$ and the trace of this expression is

$$\begin{aligned}\operatorname{tr}\mathbf{B}^2 = B_{ip}B_{pi} &= \frac{\partial x_i}{\partial X_R}\frac{\partial x_p}{\partial X_R}\frac{\partial x_p}{\partial X_S}\frac{\partial x_i}{\partial X_S} = \left(\frac{\partial x_i}{\partial X_R}\frac{\partial x_i}{\partial X_S}\right)\left(\frac{\partial x_p}{\partial X_R}\frac{\partial x_p}{\partial X_S}\right)\\ &= C_{RS}C_{RS} = \operatorname{tr}\mathbf{C}^2\end{aligned} \tag{3.95}$$

Substituting (3.93) and (3.95) into (3.94), we obtain

$$II_B = II_C \tag{3.96}$$

For the third invariant, we have from (3.72) and (3.84)

$$III_C = |\mathbf{C}| = |\mathbf{F}^{\mathrm{T}} \cdot \mathbf{F}| = |\mathbf{F}^{\mathrm{T}}||\mathbf{F}| = |\mathbf{F}|^2 \tag{3.97}$$

On the other hand,

$$III_B = |\mathbf{F} \cdot \mathbf{F}^{\mathrm{T}}| = |\mathbf{F}||\mathbf{F}^{\mathrm{T}}| = |\mathbf{F}|^2 \tag{3.98}$$

Comparing (3.97) and (3.98), we find

$$III_B = III_C \tag{3.99}$$

3.9 The Lagrangian and Eulerian Strain Tensors

3.9.1 Definitions

The two classical strain measures discussed in this section are widely used in mechanics literature. Usually, they are derived from a different approach

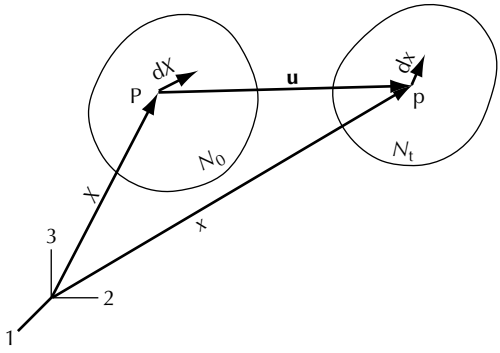

FIGURE 3.12
The displacement vector.

than the one given here. Having discussed the right and left Cauchy–Green deformation tensors, we may define the Lagrangian and Eulerian strains as

$$2\mathbf{E} = \mathbf{C} - \mathbf{1} \tag{3.100}$$

$$2\mathbf{e} = \mathbf{1} - \mathbf{B}^{-1} \tag{3.101}$$

where **E** is the *Lagrangian strain* tensor (also known as Green's tensor) and **e** is the *Eulerian strain* tensor. We point out, from (3.100), that **C** is positive for $\mathbf{E} > -\frac{1}{2}$. In this discussion, we observe that deformation of a continuum may be described by different strain measures. In fact, there are several alternative measures of deformation that are being used in the literature. The displacement vector **u** introduced in (3.3) is now considered. Refer to Figure 3.12 and let the material and spatial coordinate systems coincide for simplicity. If a material point P moves to p during deformation, the vector from P to p is the displacement vector **u**. We may write

$$\mathbf{x} = \mathbf{X} + \mathbf{u} \quad \text{or} \quad x_i = \delta_{iR} X_R + u_i \tag{3.102}$$

Using (3.102), (3.100) becomes

$$\begin{aligned} 2E_{RS} = C_{RS} - \delta_{RS} &= \frac{\partial x_m}{\partial X_R}\frac{\partial x_m}{\partial X_S} - \delta_{RS} \\ &= \frac{\partial\left(\delta_{mM}X_M + u_m\right)}{\partial X_R}\frac{\partial\left(\delta_{mN}X_N + u_m\right)}{\partial X_S} - \delta_{RS} \\ &= \left(\delta_{mR} + \frac{\partial u_m}{\partial X_R}\right)\left(\delta_{mS} + \frac{\partial u_m}{\partial X_S}\right) - \delta_{RS} \\ &= \delta_{mR}\delta_{mS} + \delta_{mR}\frac{\partial u_m}{\partial X_S} + \delta_{mS}\frac{\partial u_m}{\partial X_R} + \frac{\partial u_m}{\partial X_R}\frac{\partial u_m}{\partial X_S} - \delta_{RS} \end{aligned} \tag{3.103}$$

Note that we choose to have the origin of the material and spatial coordinate systems coincide. In general, they may not coincide, but since the vector connecting the two origins is a constant, it drops out in the differentiation. Thus, (3.103) may be simplified to yield

$$E_{RS} = \frac{1}{2}\left(\frac{\partial u_R}{\partial X_S} + \frac{\partial u_S}{\partial X_R} + \frac{\partial u_k}{\partial X_R}\frac{\partial u_k}{\partial X_S}\right) \tag{3.104}$$

Equation (3.104) is known as the *strain–displacement relation*.

Similarly, from (3.101), we obtain

$$e_{ij} = \frac{1}{2}\left(\frac{\partial u_i}{\partial x_j} + \frac{\partial u_j}{\partial x_i} - \frac{\partial u_R}{\partial x_i}\frac{\partial u_R}{\partial x_j}\right) \tag{3.105}$$

where u_R and u_i are respectively components of the displacement vector $\mathbf{u}$ in the material and spatial coordinate systems. Since both coordinate systems are Cartesian and coincide in this consideration, u_R is the same as u_i. Also, X_R is the same as X_i.

Some remarks are in order.

1. Both E_{RS} and e_{ij} are symmetric tensors.
2. A line element $\mathrm{d}X_R$ with length $\mathrm{d}S$ in the neighborhood of N_0 deforms into $\mathrm{d}x_i$ with length $\mathrm{d}s$ in the neighborhood of N_t. It is possible to show that

$$\mathrm{d}s^2 - \mathrm{d}S^2 = 2E_{RS}\mathrm{d}X_R\mathrm{d}X_S = 2e_{ij}\mathrm{d}x_i\mathrm{d}x_j \tag{3.106}$$

3. For small deformation, that is, $\partial u_i/\partial X_R \ll 1$, and $\partial u_R/\partial x_j \ll 1$, but u_i may not be small, we can approximately write

$$E_{ij} \cong \frac{1}{2}\left(\frac{\partial u_i}{\partial X_j} + \frac{\partial u_j}{\partial X_i}\right) \cong e_{ij} \cong \frac{1}{2}\left(\frac{\partial u_i}{\partial x_j} + \frac{\partial u_j}{\partial x_i}\right) = \varepsilon_{ij} \tag{3.107}$$

   It is not necessary to distinguish the material coordinates X_R from the spatial coordinates x_i (see Example 3.4). The tensor ε_{ij} is called the *infinitesimal strain tensor* or the *engineering strain*. Both $\mathbf{E}$ and $\mathbf{e}$ reduce to $\boldsymbol{\varepsilon}$ when an approximation is made such that the second and the higher powers of the displacement gradients are neglected.
4. On the other hand, the infinitesimal strain tensor may be mathematically defined by

$$\varepsilon_{ij} = \frac{1}{2}\left(\frac{\partial u_i}{\partial x_j} + \frac{\partial u_j}{\partial x_i}\right) \tag{3.108}$$

Physically, $\boldsymbol{\varepsilon}$ cannot be an exact measure of deformation, because it does not remain constant in a rigid-body rotation. In a counterclockwise rigid-body rotation through an angle α about the positive X_3 axis, the transformation of the position vector of a material point is given by (see Example 1.6)

$$x_1 = X_1 \cos\alpha - X_2 \sin\alpha, \qquad x_2 = X_1 \sin\alpha + X_2 \cos\alpha, \qquad x_3 = X_3 \tag{3.109}$$

and the displacement components are

$$\begin{aligned} u_1 &= -X_1(1 - \cos\alpha) - X_2 \sin\alpha, \\ u_2 &= X_1 \sin\alpha - X_2(1 - \cos\alpha), \qquad u_3 = 0 \end{aligned} \tag{3.110}$$

Using (3.108), the infinitesimal strain $\boldsymbol{\varepsilon}$ is determined to be

$$\varepsilon_{ij} = \begin{bmatrix} -(1 - \cos\alpha) & 0 & 0 \\ 0 & -(1 - \cos\alpha) & 0 \\ 0 & 0 & 0 \end{bmatrix} \tag{3.111}$$

It is seen that ε_{11} and ε_{22} are not 0. However, if α is small, then these quantities are small and may be neglected. Although the infinitesimal strain tensor is not an exact measure of deformation, it is convenient for use in the applications involving small strains. An advantage of this strain tensor is its linear relation with respect to the displacement gradient. This allows for the application of the techniques of linear analysis in solving boundary-value problems in the linear theory of elasticity, and also helps keep the equations of the theory of plasticity simple. Nevertheless, in using (3.108), we must keep in mind that the rigid-body rotation has to be small.

EXAMPLE 3.4 Show that, in the case of small displacement gradient, we may write $\partial u_i/\partial x_j \cong \partial u_i/\partial X_j$ and it is not necessary to distinguish the material coordinates X_R from the spatial coordinates x_i.

Solution

From (3.102), we have

$$x_i = X_i + u_i \tag{a}$$

By differentiating (a), we obtain

$$\frac{\partial u_i}{\partial x_j} = \delta_{ij} - \frac{\partial X_i}{\partial x_j} \tag{b}$$

In the symbolic notation, (b) can be written as

$$\begin{aligned}\frac{\partial \mathbf{u}}{\partial \mathbf{x}} &= \mathbf{1} - \mathbf{F}^{-1} = \mathbf{1} - \{\mathbf{1} + (\mathbf{F} - \mathbf{1})\}^{-1} \\ &= \mathbf{1} - \{\mathbf{1} - (\mathbf{F} - \mathbf{1}) + (\mathbf{F} - \mathbf{1})^2 - (\mathbf{F} - \mathbf{1})^3 + \cdots\} \\ &= (\mathbf{F} - \mathbf{1}) - (\mathbf{F} - \mathbf{1})^2 + (\mathbf{F} - \mathbf{1})^3 - \cdots \end{aligned} \tag{c}$$

in which the binomial expansion was used. In the index notation, the factor $(\mathbf{F} - \mathbf{1})$ is

$$\frac{\partial x_i}{\partial X_j} - \delta_{ij} = \frac{\partial u_i}{\partial X_j} \tag{d}$$

By substitution, (c) becomes

$$\frac{\partial u_i}{\partial x_j} = \frac{\partial u_i}{\partial X_j} - \frac{\partial u_i}{\partial X_R}\frac{\partial u_R}{\partial X_j} + \frac{\partial u_i}{\partial X_R}\frac{\partial u_R}{\partial X_S}\frac{\partial u_S}{\partial X_j} - \cdots \tag{e}$$

Hence, by neglecting the higher-order terms in the displacement gradient, we may write

$$\frac{\partial u_i}{\partial x_j} \cong \frac{\partial u_i}{\partial X_j} \tag{f}$$

and it is not necessary to distinguish the material coordinates X_R from the spatial coordinates x_i.

3.9.2 Geometric Interpretation of the Strain Components

We consider here as in Section 3.6.1 a line element $\mathrm{d}X_R$ with length $\mathrm{d}S$ deforming into $\mathrm{d}x_i$ with length $\mathrm{d}s$. We relate the stretching of this line element to the components of $\mathbf{E}$ rather than to the components of $\mathbf{C}$. From the usual definition of strain, we define the *relative elongation* of the line element as

$$\varepsilon = \frac{\mathrm{d}s - \mathrm{d}S}{\mathrm{d}S} = \frac{\mathrm{d}s}{\mathrm{d}S} - 1 = \lambda - 1 \tag{3.112}$$

This definition of relative elongation is valid for large deformation as well. From (3.106), we have

$$\mathrm{d}s^2 = \mathrm{d}S^2 + 2E_{RS}\mathrm{d}X_R\mathrm{d}X_S \tag{3.113}$$

Dividing (3.113) by $\mathrm{d}S^2$, we obtain

$$\lambda^2 = \frac{\mathrm{d}s^2}{\mathrm{d}S^2} = 1 + 2E_{RS}\frac{\mathrm{d}X_R}{\mathrm{d}S}\frac{\mathrm{d}X_S}{\mathrm{d}S} = 1 + 2E_{RS}N_RN_S \tag{3.114}$$

or

$$\lambda = [1 + 2E_{RS}N_R N_S]^{1/2} \tag{3.115}$$

where N_R denotes the initial direction of the line element. We have discarded the "$-$" solution in (3.115), since $\lambda = \mathrm{d}s/\mathrm{d}S \geq 0$ always. Therefore, the relative elongation is from (3.112) given by

$$\varepsilon = \lambda - 1 = [1 + 2E_{RS}N_R N_S]^{1/2} - 1 \tag{3.116}$$

If we know E_{RS} and specify a direction N_R, then from (3.116) we obtain the elongation of this line element. Equation (3.115) may be compared with (3.49), in which the components of $\mathbf{C}$ are used. These expressions show that the extension ratio can be obtained by the use of two different strain measures. The two equations are related by

$$\begin{aligned} \lambda^2 &= 1 + 2E_{RS}N_R N_S = N_R N_R + 2E_{RS}N_R N_S \\ &= (\delta_{RS} + 2E_{RS})N_R N_S = C_{RS}N_R N_S \end{aligned} \tag{3.117}$$

We now consider the meaning of the diagonal and off-diagonal components of the E_{RS} matrix. To discuss the diagonal component E_{11}, let us consider a line element in the X_1 direction before deformation. We then have $N_1 = 1$, $N_2 = 0$, and $N_3 = 0$; and, from (3.114), we obtain

$$\lambda_{11}^2 = 1 + 2E_{11} \quad \text{and} \quad \varepsilon_{11} = \lambda_{11} - 1 = \sqrt{1 + 2E_{11}} - 1 \tag{3.118}$$

Equation (3.118) shows that E_{11} is related to the stretching of the line element, which is initially in the X_1 direction. Similarly, if we consider line elements initially along X_2 and X_3 directions, respectively, we get

$$\varepsilon_{22} = \sqrt{1 + 2E_{22}} - 1 \quad \text{and} \quad \varepsilon_{33} = \sqrt{1 + 2E_{33}} - 1 \tag{3.119}$$

Starting with the Eulerian strain components e_{ij}, we can also obtain expressions for the relative elongations for fibers, which after deformation are in the directions of the x_1, x_2, and x_3 axes. However, the interpretation of e_{11}, e_{22}, and e_{33} as the relative elongations of fibers can only be justified for small strain. If we choose a line element, which is in the x_1 direction after deformation, then (3.106) leads to

$$(\mathrm{d}s - \mathrm{d}S)(\mathrm{d}s + \mathrm{d}S) = 2e_{ij}\mathrm{d}x_i\mathrm{d}x_j = 2e_{11}n_1 n_1 \mathrm{d}s^2 = 2e_{11}\mathrm{d}s^2 \tag{3.120}$$

By use of the definition of relative elongation, (3.120) may be written as

$$\frac{\mathrm{d}s - \mathrm{d}S}{\mathrm{d}S} = e_{11}\left[\frac{\mathrm{d}s}{\mathrm{d}S}\frac{2\mathrm{d}s}{\mathrm{d}s + \mathrm{d}S}\right] \approx e_{11} \tag{3.121}$$

The last expression of (3.121) is true only for small deformation that $ds \approx dS$. In this case, e_{11} may be interpreted as the relative elongation for fibers in the x_1 direction, and we note that for small deformation $x_1 \approx X_1$. However, in large deformation, no simple correlation between e_{11} and relative elongation can be found from (3.121).

To investigate the off-diagonal terms of E_{RS}, let us consider two line elements $dX_R^{(1)}$ and $dX_R^{(2)}$, which deform into $dx_i^{(1)}$ and $dx_i^{(2)}$, respectively. The angle between the two line elements is Φ in the initial configuration and ϕ in the current configuration as shown in Figure 3.8. The dot product of $dX_R^{(1)}$ and $dX_R^{(2)}$ is

$$dS_1 dS_2 \cos\Phi = dX_R^{(1)} dX_R^{(2)} \tag{3.122}$$

and the dot product of $dx_i^{(1)}$ and $dx_i^{(2)}$ is

$$ds_1 ds_2 \cos\phi = dx_i^{(1)} dx_i^{(2)} \tag{3.123}$$

Subtracting (3.122) from (3.123), we obtain

$$\begin{aligned} ds_1 ds_2 \cos\phi - dS_1 dS_2 \cos\Phi &= dx_i^{(1)} dx_i^{(2)} - dX_R^{(1)} dX_R^{(2)} \\ &= \left[\frac{\partial x_i}{\partial X_R} \frac{\partial x_i}{\partial X_S} - \delta_{RS} \right] dX_R^{(1)} dX_S^{(2)} \\ &= \left[\left(\frac{\partial u_i}{\partial X_R} + \delta_{iR} \right) \left(\frac{\partial u_i}{\partial X_S} + \delta_{iS} \right) - \delta_{RS} \right] dX_R^{(1)} dX_S^{(2)} \\ &= 2E_{RS} dX_R^{(1)} dX_S^{(2)} \end{aligned} \tag{3.124}$$

The relations in (3.103) are used in the derivation of (3.124). Dividing the above expression by $dS_1 dS_2$, we obtain

$$\frac{ds_1}{dS_1} \frac{ds_2}{dS_2} \cos\phi - \cos\Phi = 2E_{RS} \frac{dX_R^{(1)}}{dS_1} \frac{dX_S^{(2)}}{dS_2} = 2E_{RS} N_R^{(1)} N_S^{(2)} \tag{3.125}$$

This relation may be further simplified by use of (3.112), which, for the two line elements, are

$$\frac{ds_1}{dS_1} = \lambda_1 \quad \text{and} \quad \frac{ds_2}{dS_2} = \lambda_2 \tag{3.126}$$

Using (3.126), (3.125) may be solved to yield

$$\cos\phi = \frac{2E_{RS} N_R^{(1)} N_S^{(2)} + \cos\Phi}{\lambda_1 \lambda_2} \tag{3.127}$$

where Φ is the angle between the two line elements before deformation and ϕ is the angle after deformation. Given Φ, E_{RS}, $N_R^{(1)}$, and $N_S^{(2)}$, the deformed angle ϕ may be determined. Note that the stretch ratios λ_1 and λ_2 are determined from (3.115).

To investigate the meaning of E_{12}, E_{23}, E_{31}, let us consider some special cases. If $\Phi = 90°$, that is, the two line elements are perpendicular to each other before deformation, then $\cos\Phi = 0$. In addition, let $\cos\phi = \cos(90° - \theta) = \sin\theta$, where θ is the angle change due to deformation, then (3.127) reduces to

$$\sin\theta = \frac{2E_{RS}N_R^{(1)}N_S^{(2)}}{\lambda_1\lambda_2} \tag{3.128}$$

Since θ is generally not 0 from (3.128), we may conclude that two initially perpendicular line elements (not along the coordinate axes) do not remain perpendicular after deformation. If the two line elements are respectively lying along the X_1 and X_2 axes initially, then $N_1^{(1)} = 1$, $N_2^{(1)} = N_3^{(1)} = 0$ and $N_2^{(2)} = 1$, $N_1^{(2)} = N_3^{(2)} = 0$, and from (3.128) E_{12} is related to θ_{12}. Similarly, we find the expressions for other off-diagonal terms of E_{RS} ($R \neq S$). The relations are summarized as

$$\sin\theta_{12} = \frac{2E_{12}}{\lambda_1\lambda_2}, \qquad \sin\theta_{23} = \frac{2E_{23}}{\lambda_2\lambda_3}, \qquad \sin\theta_{13} = \frac{2E_{13}}{\lambda_1\lambda_3} \tag{3.129}$$

We observe from (3.129) that the off-diagonal terms of E_{RS} are related to the shearing deformations and that an initially orthogonal triad with elements along the X_R directions will no longer be orthogonal after deformation.

We consider a special case, where X_1, X_2, and X_3 are principal directions. Then, $E_{12} = E_{23} = E_{31} = 0$ and $E_{11} = E_1, E_{22} = E_2, E_{33} = E_3$. If the two line elements are respectively lying along X_1 and X_2 initially, then from (3.129) we obtain $\theta_{12} = 0$, which means that there is no angle change, that is, $\phi = \Phi = 90°$. Similarly, we show that $\theta_{23} = \theta_{31} = 0$. This finding has the implication that a rectangular triad having elements in the three principal directions before deformation remains rectangular (does not have angle changes) after deformation. The volume element formed by the triad is rotated and may be stretched. However, if, before deformation, the triad is in directions other than the principal directions, then there are angle changes after deformation even if E_{RS} refers to the principal directions. The angle changes for this case are calculated from (3.128).

3.9.3 The Volumetric Strain

Using (3.82) and (3.100), we have

$$\left(\frac{dV}{dV_0}\right)^2 = |\mathbf{F}^T \cdot \mathbf{F}| = |\mathbf{C}| = |\delta_{RS} + 2E_{RS}| \tag{3.130}$$

Since the above expression is the third invariant of **C**, a simplified expression is obtained by using the principal coordinate system. Thus,

$$\left(\frac{dV}{dV_0}\right)^2 = (1+2E_1)+(1+2E_2)(1+2E_3)$$
$$= 1+2(E_1+E_2+E_3)+4(E_1E_2+E_1E_3+E_2E_3)+8E_1E_2E_3 \tag{3.131}$$

or

$$\left(\frac{dV}{dV_0}\right)^2 = 1+2I_E+4II_E+8III_E \tag{3.132}$$

where I_E, II_E, and III_E are the principal invariants of **E**. But, from (3.116), we note that

$$1+\varepsilon_1 = \sqrt{1+2E_1} \tag{3.133}$$

in which ε_1 is the relative elongation along principal direction 1. Using (3.133), (3.131) becomes

$$\frac{dV}{dV_0} = (1+\varepsilon_1)(1+\varepsilon_2)(1+\varepsilon_3) = \lambda_1\lambda_2\lambda_3 \tag{3.134}$$

We note that the volumetric strain for small deformation is

$$\frac{dV-dV_0}{dV_0} = \frac{dV}{dV_0} - 1 = (1+\varepsilon_1)(1+\varepsilon_2)(1+\varepsilon_3) - 1 \approx \varepsilon_1+\varepsilon_2+\varepsilon_3 \tag{3.135}$$

by neglecting the high-power terms in $\varepsilon_1, \varepsilon_2$, or ε_3. In the finite deformation, the volumetric strain can be defined by $(dV - dV_0)/dV$, which leads to the logarithmic volumetric strain of $\ln(dV)$.

EXAMPLE 3.5 Consider the deformation governed by

$$x_1 = \alpha_1 X_1, \qquad x_2 = \alpha_2 X_2, \qquad x_3 = \alpha_3 X_3 \tag{a}$$

where α_i are constants. In a one-dimensional stretching along the 1 direction, determine the values of E_{11}, e_{11}, the relative elongation ε, and the true strain $\varepsilon^{\log}$, if α_1 takes the values of 1.01, 1.02, 1.05, 1.10, and 1.20. Compare these values with the engineering strain ε^{eng}.

Solution

Using (a), we find

$$[C] = [F]^{\mathrm{T}}[F] = \begin{bmatrix} \alpha_1^2 & 0 & 0 \\ 0 & \alpha_2^2 & 0 \\ 0 & 0 & \alpha_3^2 \end{bmatrix} \quad \text{and} \quad [B]^{-1} = \begin{bmatrix} \dfrac{1}{\alpha_1^2} & 0 & 0 \\ 0 & \dfrac{1}{\alpha_2^2} & 0 \\ 0 & 0 & \dfrac{1}{\alpha_3^2} \end{bmatrix} \tag{b}$$

Substituting (b) into (3.100) and (3.101), we obtain

$$E_{11} = \tfrac{1}{2}\,(C_{11} - 1) = \tfrac{1}{2}(\alpha_1^2 - 1) \tag{c}$$

$$e_{11} = \frac{1}{2}(1 - B_{11}^{-1}) = \frac{1}{2}\left(1 - \frac{1}{\alpha_1^2}\right) \tag{d}$$

Since $N_1 = 1, N_2 = N_3 = 0$, the relative elongation ε may be found from (3.116) and (c) as

$$\varepsilon = \alpha_1 - 1 \tag{e}$$

Note that this result is the same as that obtained from the definition of engineering strain, where

$$\varepsilon^{\mathrm{eng}} = \frac{x - X}{X} = \alpha_1 - 1 \tag{f}$$

The true strain is defined by $\mathrm{d}\varepsilon^{\log} = \mathrm{d}x/x$. If the initial strain is 0 and the initial length of the specimen is X, this expression may be integrated to find

$$\varepsilon^{\log} = \ln\left(\frac{x}{X}\right) = \ln \alpha_1 \tag{g}$$

Expressions (c) to (g) are plotted in Figure 3.13 against α_1. The curve for the engineering strain $\varepsilon^{\mathrm{eng}}$ is a straight line. The curve for E_{11} lies above the straight line and the curves for $\varepsilon^{\log}$ and e_{11} lie below the straight line. We note that, at a strain of $\varepsilon^{\mathrm{eng}} = 0.05$, the corresponding logarithmic strain is $\varepsilon^{\log} = 0.0488$, which is 2.4% smaller than $\varepsilon^{\mathrm{eng}}$; at $\varepsilon^{\mathrm{eng}} = 0.1, \varepsilon^{\log} = 0.0953$, which is 4.9% smaller than $\varepsilon^{\mathrm{eng}}$; and at $\varepsilon^{\mathrm{eng}} = 0.2, \varepsilon^{\log} = 0.1823$, which is 9.7% smaller than $\varepsilon^{\mathrm{eng}}$.

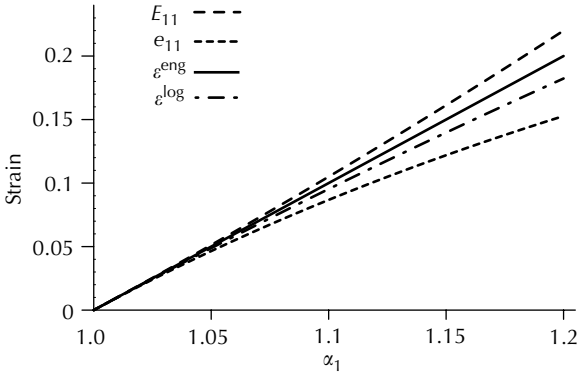

FIGURE 3.13
Comparison of strain measures in one-dimensional stretching.

3.10 Other Strain Measures

Several other strain measures have been used in the literature. We mention in this section two families of strains, which are defined based on the stretch tensors **U** and **V** discussed in Section 3.5. Both **U** and **V** are positive, symmetric tensors, they share the same eigenvalues λ_i and their eigenvectors are related by the transformation given by equation (r) of Example 3.3. In the proposed strain measures, the eigenvalues are a function of λ_i such that

$$\varepsilon_i = f(\lambda_i) \tag{3.136}$$

A useful form for function f is given by

$$\begin{aligned} f(\lambda_i) &= \frac{\lambda_i^\kappa - 1}{\kappa}, \quad \kappa \neq 0 \\ &= \ln \lambda_i, \qquad \kappa = 0 \end{aligned} \tag{3.137}$$

The two families of strains are written using either $\mathbf{n}_u^{(i)}$ or $\mathbf{n}_v^{(i)}$ as their eigenvectors. Thus,

$$\mathbf{E} = \mathbf{f}(\mathbf{U}) = \sum_i f(\lambda_i)\mathbf{n}_u^{(i)} \otimes \mathbf{n}_u^{(i)} \quad \text{or} \quad \mathbf{e} = \mathbf{f}(\mathbf{V}) = \sum_i f(\lambda_i)\mathbf{n}_v^{(i)} \otimes \mathbf{n}_v^{(i)} \tag{3.138}$$

where **E** may be called the generalized Lagrangian strain and **e** the generalized Eulerian strain. Some commonly used strain measures may be

obtained from (3.138). They are

$$\begin{aligned}
&\text{Engineering strain } (\kappa = 1): && \varepsilon^{\text{eng}} = \lambda - 1 \\
&\text{Logarithmic strain } (\kappa = 0): && \varepsilon^{\log} = \ln \lambda \\
&\text{Lagrangian strain } (\kappa = 2): && E = \tfrac{1}{2}(\lambda^2 - 1) \\
&\text{Eulerian strain } (\kappa = -2): && e = \frac{1}{2}\left(1 - \frac{1}{\lambda^2}\right)
\end{aligned} \tag{3.139}$$

The last two strain measures are written in the spectral form as

$$\mathbf{E} = \sum_i \frac{1}{2}(\lambda^2 - 1)\mathbf{n}_u^{(i)} \otimes \mathbf{n}_u^{(i)} \quad \text{and} \quad \mathbf{e} = \sum_i \frac{1}{2}\left(1 - \frac{1}{\lambda^2}\right)\mathbf{n}_v^{(i)} \otimes \mathbf{n}_v^{(i)} \tag{3.140}$$

A disadvantage of strain measures defined by (3.138) is the necessity of calculating the principal components first and then performing axes transformation to the actual axes. A popular method to avoid axes transformation is to use strain measures with $\kappa = 2$ or -2 so that the strain tensors may be directly calculated from either the stretch tensors **U** and **V** or the right and left Cauchy–Green tensors **C** and **B**.

3.11 Material Rate of Change

We discussed the concept of deformation and its measures in the earlier sections. As mentioned earlier, the deformation describes the geometrical change of a material element between the current and the reference configurations corresponding to two different fixed times. The study now extends to the motion of the body, which is a family of deformations continuously varying in time. The *material rate of change* (or *material derivative*) is an important concept used in the description of the motion and we discuss it in this section. The material rate of change of a physical quantity ϕ is the rate of change of ϕ with respect to a particle. This rate is also known as the *substantial derivative* in fluid mechanics. There are material and spatial descriptions for the material rate of change and we discuss them in this section.

3.11.1 Material Description of the Material Derivative

In the material description, **X** is held constant, and the material derivative is the same as the partial derivative with respect to time t. Therefore, we write

$$\frac{\mathrm{D}}{\mathrm{D}t}\phi(X, t) = \frac{\partial \phi(\mathbf{X}, t)}{\partial t} \tag{3.141}$$

or in the index notation

$$\frac{\mathrm{D}}{\mathrm{D}t}\phi(X_R,t) = \frac{\partial \phi(X_R,t)}{\partial t} \tag{3.142}$$

3.11.2 Spatial Description of the Material Derivative

In the spatial description, ϕ is a function of $\mathbf{x}$ and t. The material derivative of ϕ is the total derivative of ϕ, differentiating with respect to both variables. Thus,

$$\frac{\mathrm{D}}{\mathrm{D}t}\phi(\mathbf{x},t) = \frac{\partial \phi(\mathbf{x},t)}{\partial t} + \left.\frac{\partial \phi}{\partial \mathbf{x}}\right|_t \cdot \left.\frac{\partial \mathbf{x}}{\partial t}\right|_{\mathbf{X}} \tag{3.143}$$

Note that the last differentiation is carried out by keeping $\mathbf{X}$ constant. This is so because we are considering the material derivative. The particle velocity has been discussed in (3.6), and using the expression, (3.143) becomes

$$\frac{\mathrm{D}}{\mathrm{D}t}\phi(\mathbf{x},t) = \frac{\partial \phi(\mathbf{x},t)}{\partial t} + \overrightarrow{\mathrm{Grad}\,\phi} \cdot \mathbf{v}(\mathbf{x},t) \tag{3.144}$$

In the last expression of (3.144), notation $\mathbf{v}$ represents $\mathbf{v}(\mathbf{x},t)$. The same notation $\mathbf{v}$ may be used to represent $\mathbf{v}(\mathbf{X},t)$ in the material description. These are actually two different functions denoting the same velocity. But for the sake of simplicity in notations, we use the same notation $\mathbf{v}$. The independent variables of the function should be specified in case confusion arises.

In a similar manner, we discuss the material differentiation of a vector. Acceleration, which is the material derivative of the velocity vector, is a good example and is given by

$$\mathbf{f} = \frac{\mathrm{D}\mathbf{v}}{\mathrm{D}t} = \frac{\partial \mathbf{v}}{\partial t} + (\mathrm{Grad}\ \mathbf{v}) \cdot \mathbf{v} \tag{3.145}$$

The last expression of (3.145) may be derived by writing

$$\mathbf{Grad}\ \mathbf{v} \equiv \left(\frac{\partial \mathrm{v}_i}{\partial \mathrm{x}_j}\mathbf{e}_i \otimes \mathbf{e}_j\right) = \nabla \otimes \mathbf{v} \tag{3.146}$$

Thus,

$$\begin{aligned}(\mathrm{Grad}\ \mathbf{v}) \cdot \mathbf{v} &= \left(\frac{\partial v_i}{\partial x_j}\mathbf{e}_i \otimes \mathbf{e}_j\right) \cdot v_k \mathbf{e}_k = \frac{\partial v_i}{\partial x_j} v_k \mathbf{e}_i (\mathbf{e}_j \cdot \mathbf{e}_k) \\ &= \frac{\partial v_i}{\partial x_j} v_k \mathbf{e}_i \delta_{jk} = \frac{\partial v_i}{\partial x_k} v_k \mathbf{e}_i \end{aligned} \tag{3.147}$$

Using (3.147), the index form of (3.145) is

$$f_i = \frac{\mathrm{D}v_i}{\mathrm{D}t} = \frac{\partial v_i}{\partial t} + \frac{\partial v_i}{\partial x_k} v_k \tag{3.148}$$

Generally, the material derivative in the spatial description is represented by the following operator

$$\frac{\mathrm{D}}{\mathrm{D}t} = \frac{\partial}{\partial t} + v_k \frac{\partial}{\partial x_k} \tag{3.149}$$

If this operator is applied to a function $\phi(\mathbf{x}, t)$, then the first term indicates the local rate of change, which is the contribution of the time dependence of ϕ. This term may also be called the transient term. The second term is the convective term, which is the contribution by the motion of the particle. To illustrate this point, let us consider fluid flowing in a tube and we assume that the flow is steady and is one-dimensional along the x direction (see Figure 3.14). In a steady flow, the velocity at any location x does not change with time. The observer sitting at a location x does not see any change of v, so that $\partial v/\partial t = 0$. However, the velocity may differ from one location to the other. The acceleration of the particle is then given by

$$\text{Acceleration} = \frac{\text{change of velocity}}{\text{time increment}} = \frac{(\partial v/\partial x)\Delta x}{\Delta t} = \frac{(\partial v/\partial x)v\Delta t}{\Delta t} = v\frac{\partial v}{\partial x} \tag{3.150}$$

This acceleration is known as the convective acceleration and is due to the motion of the fluid.

In a nonsteady flow, the velocity changes with time at a fixed station x. It changes from v to $v + (\partial v/\partial t)\Delta t$ in time interval Δt and the acceleration at this station x is given by

$$\text{Acceleration} = \frac{\text{change of velocity}}{\text{time increment}} = \frac{(\partial v/\partial t)\Delta t}{\Delta t} = \frac{\partial v}{\partial t} \tag{3.151}$$

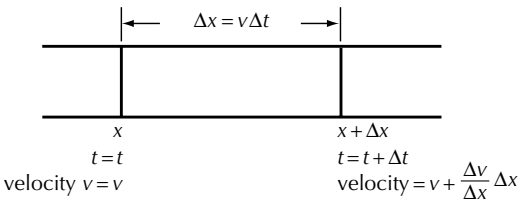

FIGURE 3.14
Fluid flowing in a tube.

This is the transient term of acceleration and there is no convective acceleration because we consider the acceleration at a fixed station. In the general case, that is, the station is not fixed at x and the flow is nonsteady, the total acceleration is therefore

$$f = \frac{\partial v}{\partial t} + v\frac{\partial v}{\partial x} \tag{3.152}$$

In summary, the material rate of change, which is the rate of change of a physical quantity with respect to a specified particle, can be specified either by using a material description or a spatial description. In the material description, X_R is specified and the particle is colored red. The material rate for a physical quantity is seen by an observer sitting on top of the particle and moving with the particle. Thus, the material rate changes with respect to t only. In the spatial description, the spatial coordinate changes (convects) with the particle, and the material rate of change has two parts, the convective and the transient. Thus, the acceleration of a specified (red) particle is what an observer who stands still in the laboratory sees.

3.12 Dual Vectors and Dual Tensors

The concept of dual vector and dual tensor is useful in the subsequent sections of this chapter. Given a tensor of the second-rank T_{ij}, let us form the following vector

$$t_i = -\tfrac{1}{2}e_{ijk}T_{jk} \tag{3.153}$$

Vector t_i is called the *dual vector* (or *axial vector*) of tensor T_{ij}. We can show that the dual vector depends only on the antisymmetric part of tensor T_{ij}. Thus,

$$t_i = -\tfrac{1}{2}e_{ijk}T_{jk} = -\tfrac{1}{2}e_{ijk}\left(T^S_{jk} + T^A_{jk}\right) = -\tfrac{1}{2}e_{ijk}T^A_{jk} \tag{3.154}$$

in which the superscripts S and A denote the symmetric and the antisymmetric parts, respectively. We note that the dual vector of a symmetric tensor vanishes and it has the components given below

$$\mathbf{t} = -\frac{1}{2}\begin{bmatrix} T_{23} - T_{32} \\ T_{31} - T_{13} \\ T_{12} - T_{21} \end{bmatrix} \tag{3.155}$$

which forms a column vector. If we multiply both sides of (3.153) by e_{ijk}, we obtain

$$e_{ijk}t_i = -\tfrac{1}{2}e_{ijk}e_{irs}T_{rs} = -\tfrac{1}{2}(\delta_{jr}\delta_{ks} - \delta_{js}\delta_{kr})T_{rs} = -\tfrac{1}{2}(T_{jk} - T_{kj}) \tag{3.156}$$

Therefore, if T_{ij} is symmetric, then from (3.156), $t_i = 0$; and if T_{ij} is antisymmetric, $e_{ijk}t_i = -T_{jk}$, that is,

$$T_{jk} = -e_{ijk}t_i \tag{3.157}$$

T_{jk} is called the *dual tensor* of a given vector t_i and the dual tensor is antisymmetric with components given by

$$\mathbf{T} = \begin{bmatrix} 0 & -t_3 & t_2 \\ t_3 & 0 & -t_1 \\ -t_2 & t_1 & 0 \end{bmatrix} \tag{3.158}$$

EXAMPLE 3.6 Use the dual vector–dual tensor concept to describe the angular velocity of rigid-body rotation of a continuum.

Solution

Let us consider a rigid body that instantaneously rotates about an axis passing through point P in the body, and P has position vector $\mathbf{r}_0$ (see Figure 3.15). Note that for an infinitesimal rotation, we consider the increments of angular and linear displacements $\mathrm{d}\boldsymbol{\theta}$ and $\mathrm{d}\mathbf{x}$, respectively, instead of angular and linear velocities $\boldsymbol{\omega} = \mathrm{d}\boldsymbol{\theta}/\mathrm{d}t$ and $\mathbf{v} = \mathrm{d}\mathbf{x}/\mathrm{d}t$ and similar results may be obtained. The vector $\boldsymbol{\omega}$ shown specifies the magnitude of angular velocity ω, the direction of the axis of rotation, and the sense of rotation. The velocity of point A specified by position vector $\mathbf{r}$ is then

$$\mathbf{v} = \boldsymbol{\omega} \times (\mathbf{r} - \mathbf{r}_0) \tag{a}$$

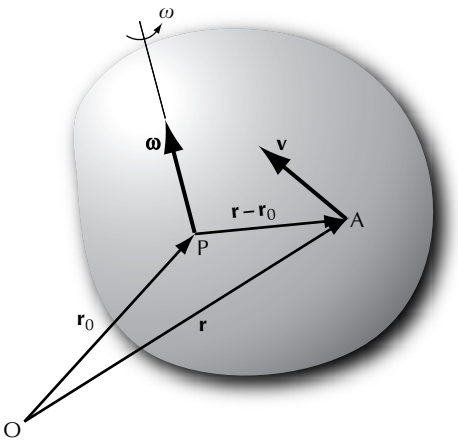

FIGURE 3.15
Angular velocity in rigid-body rotation.

In the index notation, (a) is written as

$$v_i = e_{ijk}\omega_j(x_k - x_k^{(0)}) \tag{b}$$

From vector $\boldsymbol{\omega}$ we define its dual tensor as

$$\Omega_{jk} = -e_{ijk}\omega_i \tag{c}$$

Substituting (c) into (b), we obtain

$$v_i = \Omega_{ik}(x_k - x_k^{(0)}) \quad \text{or} \quad \mathbf{v} = \boldsymbol{\Omega} \cdot (\mathbf{r} - \mathbf{r}_0) \tag{d}$$

We see that the angular velocity can be represented either by vector $\boldsymbol{\omega}$ or tensor $\boldsymbol{\Omega}$.

3.13 Velocity of a Particle Relative to a Neighboring Particle

We consider two particles P and P′ in a continuum in motion. The coordinate of P is X_R initially, and x_i at time t. For the sake of simplicity, the origins and axes of the material and spatial coordinate systems coincide. The coordinate of P′ is $X_R + \Delta X_R$ initially, and $x_i + \Delta x_i$ at time t. The line element between the two particles is $\mathrm{d}X_R$ initially and $\mathrm{d}x_i$ at time t. The initial and deformed line element are related by

$$\mathrm{d}x_i = \frac{\partial x_i}{\partial X_R}\mathrm{d}X_R \tag{3.159}$$

The relative velocity of P′ with respect to P is

$$\begin{aligned} \mathrm{d}v_i &\equiv v_i(\mathrm{P}', t) - v_i(\mathrm{P}, t) = v_i(X_R + \mathrm{d}X_R, t) - v_i(X_R, t) \\ &= \tilde{v}_i(x_j + \mathrm{d}x_j, t) - \tilde{v}_i(x_j, t) \end{aligned} \tag{3.160}$$

in which the particle velocity is either expressed in the material description by the use of function $v_i(X_R, t)$ or in the spatial description by the use of function $\tilde{v}_i(x_i, t)$. From the material description, (3.160) may be further written as

$$\mathrm{d}v_i = \frac{\mathrm{D}}{\mathrm{D}t}[x_i(X_R + \mathrm{d}X_R, t) - x_i(X_R, t)] \tag{3.161}$$

Observing that $\mathrm{d}x_i$ denotes the line element connecting two adjacent material particles, (3.161) reduces to

$$\mathrm{d}v_i = \frac{\mathrm{D}}{\mathrm{D}t}(\mathrm{d}x_i) \tag{3.162}$$

It is seen from (3.162) that the order of differentiation between d and D/Dt is interchangeable.

Using the spatial description, from (3.160), we write

$$\mathrm{d}v_i = \tilde{v}_i(x_j + \mathrm{d}x_j, t) - \tilde{v}_i(x_j, t) \tag{3.163}$$

The first term on the right-hand side may be expanded in Taylor's series and, by retaining only the first-order term, (3.163) becomes

$$\mathrm{d}v_i = \tilde{v}_i(x_j, t) + \frac{\partial \tilde{v}_i}{\partial x_k}\mathrm{d}x_k - \tilde{v}_i(x_j, t) = \frac{\partial \tilde{v}_i}{\partial x_k}\mathrm{d}x_k = v_{i,j}\mathrm{d}x_j \tag{3.164}$$

Combining (3.162) and (3.164), we obtain

$$\mathrm{d}v_i = \frac{\mathrm{D}(\mathrm{d}x_i)}{\mathrm{D}t} = v_{i,j}\mathrm{d}x_j \tag{3.165}$$

where $v_{i,j} = L_{ij}$ is known as the *velocity gradient* tensor. This tensor is generally not symmetric and so it can be split into symmetric and antisymmetric parts. Therefore, we write

$$L_{ij} = v_{i,j} = \tfrac{1}{2}(v_{i,j} + v_{j,i}) + \tfrac{1}{2}(v_{i,j} - v_{j,i}) = D_{ij} + W_{ij} \tag{3.166}$$

where

$$D_{ij} = \tfrac{1}{2}(v_{i,j} + v_{j,i}) \quad \text{or} \quad \mathbf{D} = \tfrac{1}{2}(\mathbf{L} + \mathbf{L}^{\mathrm{T}}) \tag{3.167}$$

and

$$W_{ij} = \tfrac{1}{2}(v_{i,j} - v_{j,i}) \quad \text{or} \quad \mathbf{W} = \tfrac{1}{2}(\mathbf{L} - \mathbf{L}^{\mathrm{T}}) \tag{3.168}$$

in which D_{ij} is *the rate of deformation* tensor and W_{ij} is the *spin tensor*. Therefore, (3.165) may be rewritten as

$$\mathrm{d}v_i = D_{ij}\mathrm{d}x_j + W_{ij}\mathrm{d}x_j \tag{3.169}$$

3.14 Physical Significance of the Rate of Deformation Tensor

In order to see the physical significance of the rate of deformation tensor D_{ij}, let us consider two material line elements, $\mathrm{d}x_i^{(1)}$ and $\mathrm{d}x_i^{(2)}$, at the current configuration in the spatial system. Let ϕ be the angle formed by the two line elements, with unit vectors $n_i^{(1)}$ and $n_i^{(2)}$and lengths $\mathrm{d}s_1$ and $\mathrm{d}s_2$, respectively.

We then differentiate the inner product $\mathrm{d}x_i^{(1)}\mathrm{d}x_i^{(2)}$ of the two line elements to yield

$$\frac{\mathrm{D}}{\mathrm{D}t}\left[\mathrm{d}x_i^{(1)}\mathrm{d}x_i^{(2)}\right] = v_{i,j}\mathrm{d}x_j^{(1)}\mathrm{d}x_i^{(2)} + \mathrm{d}x_i^{(1)}v_{i,j}\mathrm{d}x_j^{(2)} = \mathrm{d}x_i^{(1)}\mathrm{d}x_j^{(2)}[v_{i,j} + v_{j,i}] \tag{3.170}$$

or

$$\frac{\mathrm{D}}{\mathrm{D}t}\left[\mathrm{d}x_i^{(1)}\mathrm{d}x_i^{(2)}\right] = 2\mathrm{D}_{ij}\mathrm{d}x_i^{(1)}\mathrm{d}x_j^{(2)} \tag{3.171}$$

On the other hand, since $\mathrm{d}x_i^{(1)}\mathrm{d}x_i^{(2)} = \mathrm{d}s_1\mathrm{d}s_2\cos\phi$, we obtain the following equation by differentiation,

$$\frac{\mathrm{D}}{\mathrm{D}t}\left[\mathrm{d}x_i^{(1)}\mathrm{d}x_i^{(2)}\right] = \frac{\mathrm{D}}{\mathrm{D}t}(\mathrm{d}s_1)\mathrm{d}s_2\cos\phi + \mathrm{d}s_1\frac{\mathrm{D}}{\mathrm{D}t}(\mathrm{d}s_2)\cos\phi - \mathrm{d}s_1\mathrm{d}s_2\sin\phi\frac{\mathrm{D}\phi}{\mathrm{D}t} \tag{3.172}$$

Equating (3.171) and (3.172), and dividing the resulting equation by $\mathrm{d}s_1\mathrm{d}s_2$, we obtain

$$\frac{1}{\mathrm{d}s_1}\frac{\mathrm{D}}{\mathrm{D}t}(\mathrm{d}s_1)\cos\phi + \frac{1}{\mathrm{d}s_2}\frac{\mathrm{D}}{\mathrm{D}t}(\mathrm{d}s_2)\cos\phi - \sin\phi\frac{\mathrm{D}\phi}{\mathrm{D}t} = 2D_{ij}n_i^{(1)}n_j^{(2)} \tag{3.173}$$

Note that $n_i = \mathrm{d}x_i/\mathrm{d}s$ in the above equation.

Special cases may be deduced from (3.173). If the two line elements coincide, then $\phi = 0$ and $\mathrm{d}s_1 = \mathrm{d}s_2 = \mathrm{d}s$. In this case, (3.173) reduces to

$$\frac{1}{\mathrm{d}s}\frac{\mathrm{D}}{\mathrm{D}t}(\mathrm{d}s) = D_{ij}n_in_j \tag{3.174}$$

The expression on the left-hand side of (3.174) is precisely the definition of *true strain-rate*, which is the rate of length change per unit length at the current configuration. Knowing D_{ij} and specifying a direction n_i, the strain-rate along this direction may be found from (3.174). Using the concept of stretch ratio $\lambda = \mathrm{d}s/\mathrm{d}S$, where $\mathrm{d}S$ does not change with time, (3.174) may be expressed as

$$\frac{\dot{\lambda}}{\lambda} = D_{ij}n_in_j \tag{3.175}$$

In particular, let $n_i = (1,0,0)$, then $(1/\mathrm{d}s_1)((\mathrm{D}/\mathrm{D}t)\mathrm{d}s_1) = \dot{\lambda}_1/\lambda_1 = D_{11}$, where D_{11} is time rate of change (extension or contraction) per unit length of an element, which at time t is oriented along the x_1 axis. A similar interpretation applies to D_{22} and D_{33}.

To see the physical meaning of the off-diagonal terms of the D_{ij} matrix, let $\phi = 90°$ in (3.173). Then, the two line elements are perpendicular to each other at time t. In this case, (3.173) reduces to

$$-\frac{\mathrm{D}\phi}{\mathrm{D}t} = 2D_{ij}n_i^{(1)}n_j^{(2)} \tag{3.176}$$

In particular let $n_i^{(1)}$ be along the x_1 axis and $n_i^{(2)}$ be along x_2, then

$$-\frac{\mathrm{D}\phi}{\mathrm{D}t} = 2D_{12} \tag{3.177}$$

It is seen that D_{12} is the *shear rate*. The quantity $-\mathrm{D}\phi/\mathrm{D}t$ is the rate of change of the right angle between the two elements $\mathrm{d}x_i^{(1)}$ and $\mathrm{d}x_i^{(2)}$. The negative sign means that the angle ϕ is decreasing. If we let $\theta = 90° - \phi$, then $\mathrm{D}\theta/\mathrm{D}t = -\mathrm{D}\phi/\mathrm{D}t$, that is, θ is increasing. A similar interpretation applies to D_{13} and D_{23}.

EXAMPLE 3.7 Show that the necessary and sufficient condition for rigid-body motion of a continuum is $D_{ij} = 0$.

Proof

The length ds of a deformed line element is

$$\mathrm{d}s^2 = \mathrm{d}x_i\mathrm{d}x_i \tag{a}$$

Material differentiation of (a) yields

$$\frac{\mathrm{D}}{\mathrm{D}t}(\mathrm{d}s^2) = \frac{\mathrm{D}}{\mathrm{D}t}(\mathrm{d}x_i\mathrm{d}x_i) = 2\frac{\mathrm{D}}{\mathrm{D}t}(\mathrm{d}x_i)\mathrm{d}x_i = 2v_{i,j}\mathrm{d}x_j\mathrm{d}x_i \tag{b}$$

where we used (3.165). We observe that the last expression of (b) is symmetric in i and j and it may be further written as

$$\frac{\mathrm{D}}{\mathrm{D}t}(\mathrm{d}s^2) = (v_{i,j} + v_{j,i})\mathrm{d}x_i\mathrm{d}x_j = 2D_{ij}\mathrm{d}x_i\mathrm{d}x_j \tag{c}$$

In (c), dx_i is a vector connecting two neighboring points and it is arbitrary and nonzero. The quantity $\mathrm{D}(\mathrm{d}s^2)/\mathrm{D}t$ is 0, if and only if $D_{ij} = 0$. But $\mathrm{D}(\mathrm{d}s^2)/\mathrm{D}t = 0$ implies that the length of an arbitrary line element in a body does not change, which precisely is the definition for a rigid body.

3.15 Physical Significance of the Spin Tensor

Consider a pure rigid-body rotation, which is a special case of motion of a continuum. Let the motion be described by

$$x_i = Q_{iR}(t)X_R \tag{3.178}$$

where Q_{iR} is a function of time t and is orthogonal such that

$$Q_{iR}(t)Q_{jR}(t) = \delta_{ij}, \qquad Q_{iR}(t)Q_{iS}(t) = \delta_{RS}, \quad \text{and} \quad |Q_{iR}| = 1 \tag{3.179}$$

Differentiating (3.178) with respect to time, we obtain

$$v_i = \dot{Q}_{iR}X_R \quad \text{where } \dot{Q}_{iR} = \frac{\mathrm{d}}{\mathrm{d}t}Q_{iR} \tag{3.180}$$

In the above expression, the velocity is expressed in the material system X_R that does not change with time.

On the other hand, the velocity may be expressed in the spatial description. To show this, we invert (3.178) to yield

$$X_R = Q_{jR}x_j \tag{3.181}$$

By substitution, we obtain from (3.180) and (3.181)

$$v_i = \dot{Q}_{iR}Q_{jR}x_j \tag{3.182}$$

We see that the velocity is in the spatial description in (3.182).

If we differentiate the first equation of (3.179), we find

$$\Omega_{ij} = \dot{Q}_{iR}Q_{jR} = -Q_{iR}\dot{Q}_{jR} \tag{3.183}$$

From (3.183), we see that the quantity Ω_{ij} is antisymmetric. Substituting this result back into (3.182), we find that rigid-body rotation of a continuum is governed by the following velocity field

$$v_i = \Omega_{ij}(t)x_j \tag{3.184}$$

At any instant of time t, the increment of (3.184) can be compared with (3.165) and (3.169). This can be seen in the case of rigid-body rotation $L_{ij} = W_{ij} = \Omega_{ij}$ and $D_{ij} = 0$, where the spin tensor can be identified with the angular velocity of the rigid-body motion. The angular velocity tensor Ω_{ij} is further related to the velocity gradient through (3.168). Since Ω_{ij} is antisymmetric, it has only

three nonzero independent components in the off-diagonal terms. In terms of the dual vector ω_k as in (3.158), the matrix of Ω_{ij} is

$$\Omega_{ij} = \begin{bmatrix} 0 & -\omega_3 & \omega_2 \\ \omega_3 & 0 & -\omega_1 \\ -\omega_2 & \omega_1 & 0 \end{bmatrix} \tag{3.185}$$

Also, using (3.157), we form

$$e_{ijm}\Omega_{ij} = -e_{ijm}e_{ijk}\omega_k = -2\delta_{mk}\omega_k \tag{3.186}$$

or

$$\omega_k = -\tfrac{1}{2}e_{ijk}\Omega_{ij} \tag{3.187}$$

Substituting (3.157) into (3.184), the particle velocity is now given by

$$v_i = -e_{ijk}\omega_k x_j = e_{kji}\omega_k x_j \quad \text{or} \quad \mathbf{v} = \boldsymbol{\omega} \times \mathbf{x} \tag{3.188}$$

where $\boldsymbol{\omega}$ is the angular velocity vector of the rigid-body rotation.

We note that in a general motion of a continuum, $\mathbf{W}$ is not equal to $\boldsymbol{\Omega}$ and is determined by (3.168), expressed in terms of velocity gradients. The dual vector of $\mathbf{W}$ is given by

$$w_k = -\tfrac{1}{2}e_{ijk}\tfrac{1}{2}(v_{i,j} - v_{j,i}) = -\tfrac{1}{2}e_{ijk}v_{i,j} = \tfrac{1}{2}e_{jik}v_{i,j} \tag{3.189}$$

or

$$\mathbf{w} = \tfrac{1}{2}\operatorname{Curl}\mathbf{v} \tag{3.190}$$

This is the *vorticity* vector, which is frequently used in fluid mechanics.

3.16 Expressions for D and W in Terms of F

Although (3.167) and (3.168) may be used to describe a continuum undergoing general motions, we derive here the expressions of $\mathbf{D}$ and $\mathbf{W}$ in terms of the deformation gradient $\mathbf{F}$. We do this because $\mathbf{F}$ has been used extensively in the description of deformation. The velocity gradient $\mathbf{L}$ may be written as

$$\mathbf{L} = \frac{\partial \mathbf{v}}{\partial \mathbf{x}} = \frac{\partial \mathbf{v}}{\partial \mathbf{X}} \cdot \frac{\partial \mathbf{X}}{\partial \mathbf{x}} = \dot{\mathbf{F}} \cdot \mathbf{F}^{-1} = -\mathbf{F} \cdot (\mathbf{F}^{-1})^{\cdot} \tag{3.191}$$

where the last equality has been obtained from the differentiation of $\mathbf{F}\cdot\mathbf{F}^{-1}=\mathbf{1}$. If we use the right polar decomposition of $\mathbf{F}$ given by (3.26), then (3.191) becomes

$$\begin{aligned}\mathbf{L}&=-(\mathbf{R}\cdot\mathbf{U})\cdot((\mathbf{R}\cdot\mathbf{U})^{-1})^{\cdot}=-\mathbf{R}\cdot\mathbf{U}\cdot(\mathbf{U}^{-1}\cdot\mathbf{R}^{-1})^{\cdot}\\&=-\mathbf{R}\cdot\mathbf{U}\cdot[(\mathbf{U}^{-1})^{\cdot}\cdot\mathbf{R}^{-1}+\mathbf{U}^{-1}\cdot(\mathbf{R}^{-1})^{\cdot}]=-\mathbf{R}\cdot\mathbf{U}\cdot(\mathbf{U}^{-1})^{\cdot}\cdot\mathbf{R}^{\mathrm{T}}-\mathbf{R}\cdot\dot{\mathbf{R}}^{\mathrm{T}}\\&=\mathbf{R}\cdot\dot{\mathbf{U}}\cdot\mathbf{U}^{-1}\cdot\mathbf{R}^{\mathrm{T}}+\dot{\mathbf{R}}\cdot\mathbf{R}^{\mathrm{T}}\end{aligned}\tag{3.192}$$

In the derivation of (3.192), we recognized the relation $\mathbf{R}^{-1}=\mathbf{R}^{\mathrm{T}}$ and used the results obtained from the differentiation of relations $\mathbf{U}\cdot\mathbf{U}^{-1}=\mathbf{1}$ and $\mathbf{R}\cdot\mathbf{R}^{\mathrm{T}}=\mathbf{1}$. We now take the transpose of (3.192) to yield

$$\mathbf{L}^{\mathrm{T}}=\mathbf{R}\cdot(\mathbf{R}\cdot\dot{\mathbf{U}}\cdot\mathbf{U}^{-1})^{\mathrm{T}}+(\dot{\mathbf{R}}\cdot\mathbf{R}^{\mathrm{T}})^{\mathrm{T}}\tag{3.193}$$

Therefore, from (3.192) and (3.193), we obtain

$$\mathbf{D}=\tfrac{1}{2}(\mathbf{L}+\mathbf{L}^{\mathrm{T}})=\tfrac{1}{2}\mathbf{R}\cdot(\dot{\mathbf{U}}\cdot\mathbf{U}^{-1}+\mathbf{U}^{-1}\cdot\dot{\mathbf{U}})\cdot\mathbf{R}^{\mathrm{T}}\tag{3.194}$$

and

$$\mathbf{W}=\tfrac{1}{2}(\mathbf{L}-\mathbf{L}^{\mathrm{T}})=\tfrac{1}{2}\mathbf{R}\cdot(\dot{\mathbf{U}}\cdot\mathbf{U}^{-1}-\mathbf{U}^{-1}\cdot\dot{\mathbf{U}})\cdot\mathbf{R}^{\mathrm{T}}+\dot{\mathbf{R}}\cdot\mathbf{R}^{\mathrm{T}}\tag{3.195}$$

Similarly, by use of the left polar decomposition (3.27), we may show that

$$\mathbf{D}=\tfrac{1}{2}(\dot{\mathbf{V}}\cdot\mathbf{V}^{-1}+\mathbf{V}^{-1}\cdot\dot{\mathbf{V}}+\mathbf{V}\cdot\dot{\mathbf{R}}\cdot\mathbf{R}^{\mathrm{T}}\cdot\mathbf{V}^{-1}-\mathbf{V}^{-1}\cdot\dot{\mathbf{R}}\cdot\mathbf{R}^{\mathrm{T}}\cdot\mathbf{V})\tag{3.196}$$

and

$$\mathbf{W}=\tfrac{1}{2}(\dot{\mathbf{V}}\cdot\mathbf{V}^{-1}-\mathbf{V}^{-1}\cdot\dot{\mathbf{V}}+\mathbf{V}\cdot\dot{\mathbf{R}}\cdot\mathbf{R}^{\mathrm{T}}\cdot\mathbf{V}^{-1}+\mathbf{V}^{-1}\cdot\dot{\mathbf{R}}\cdot\mathbf{R}^{\mathrm{T}}\cdot\mathbf{V})\tag{3.197}$$

EXAMPLE 3.8 Show that the spin tensor $\mathbf{W}$ describes the angular velocity of the principal axes of the rate of deformation tensor $\mathbf{D}$.

Proof

Let n_i be a normalized eigenvector of D_{ij} and $n_i=\mathrm{d}x_i/\mathrm{d}s$. We take the material derivative of n_i and write

$$\begin{aligned}\dot{n}_i&=\frac{\mathrm{D}}{\mathrm{D}t}\left(\frac{\mathrm{d}x_i}{\mathrm{d}s}\right)=\frac{1}{\mathrm{d}s}\frac{\mathrm{D}}{\mathrm{D}t}(\mathrm{d}x_i)-\frac{1}{\mathrm{d}s^2}\frac{\mathrm{D}}{\mathrm{D}t}(\mathrm{d}s)\mathrm{d}x_i=\frac{1}{\mathrm{d}s}v_{i,j}\mathrm{d}x_j-\frac{1}{\mathrm{d}s}\frac{\mathrm{D}}{\mathrm{D}t}(\mathrm{d}s)\frac{\mathrm{d}x_i}{\mathrm{d}s}\\&=v_{i,j}n_j-\frac{\dot{\lambda}}{\lambda}n_i=v_{i,j}n_j-D_{jk}n_jn_kn_i=(D_{ij}+W_{ij})n_j-D_{jk}n_jn_kn_i\end{aligned}\tag{a}$$

Note that, in the derivation of (a), we used $\lambda = ds/dS$, $\dot{\lambda} = \dfrac{D}{Dt}(ds)/dS$ and (3.175). Denoting by $n_i^{(p)}$ (for $p = 1, 2, 3$) the eigenvectors of D_{ij}, we write

$$(D_{ij} - D_{(p)}\delta_{ij})n_j^{(p)} = 0 \tag{b}$$

where $D_{(p)}$ is the corresponding principal value of D_{ij}. Using (b), we replace $D_{ij}n_j^{(p)}$ by $D_{(p)}n_i^{(p)}$, and using relation $n_i^{(p)}n_j^{(p)} = \delta_{ij}$ given by (2.86), equation (a) may be written as

$$\begin{aligned}\dot{n}_i^{(p)} &= D_{(p)}n_i^{(p)} + W_{ij}n_j^{(p)} - D_{(p)}n_k^{(p)}n_k^{(p)}n_i^{(p)} = W_{ij}n_j^{(p)} \\ &= -e_{ijm}w_m n_j^{(p)} = e_{ijk}w_j n_k^{(p)}\end{aligned} \tag{c}$$

In the symbolic notation, (c) is written as

$$\dot{\mathbf{n}}^{(\mathbf{p})} = \mathbf{w} \times \mathbf{n}^{(\mathbf{p})} \tag{d}$$

This expression shows that $\mathbf{w}$ is the angular velocity of $\mathbf{n}^{(\mathbf{p})}$, which is a principal direction of the rate of deformation tensor $\mathbf{D}$.

3.17 Material Derivative of Strain Measures

We introduced several strain measures in earlier sections of this chapter. In this section, we explore the relationships between the material derivatives, denoted by a dot, of $\mathbf{C}$ and $\mathbf{E}$ and the rate of deformation $\mathbf{D}$. Let us differentiate (3.40) first to obtain

$$\begin{aligned}\dot{C}_{RS} &= \frac{\partial x_i}{\partial X_R}\frac{\partial v_i}{\partial X_S} + \frac{\partial v_i}{\partial X_R}\frac{\partial x_i}{\partial X_S} = \frac{\partial x_i}{\partial X_R}\frac{\partial v_i}{\partial x_k}\frac{\partial x_k}{\partial X_S} + \frac{\partial v_i}{\partial x_k}\frac{\partial x_k}{\partial X_R}\frac{\partial x_i}{\partial X_S} \\ &= \left(\frac{\partial v_i}{\partial x_k} + \frac{\partial v_k}{\partial x_i}\right)\frac{\partial x_i}{\partial X_R}\frac{\partial x_k}{\partial X_S} = 2D_{ik}\frac{\partial x_i}{\partial X_R}\frac{\partial x_k}{\partial X_S}\end{aligned} \tag{3.198}$$

We then differentiate (3.100) and find

$$2\dot{E}_{RS} = \dot{C}_{RS} \tag{3.199}$$

Summarizing (3.198) and (3.199), we have

$$\dot{E}_{RS} = \frac{1}{2}\dot{C}_{RS} = D_{ik}\frac{\partial x_i}{\partial X_R}\frac{\partial x_k}{\partial X_S} \tag{3.200}$$

Equation (3.200) relates the material derivatives $\dot{E}_{RS}$ and $\dot{C}_{RS}$ to the rate of deformation D_{ij}.

EXAMPLE 3.9 Show that the material derivative of the Jacobian is given by

$$\frac{\mathrm{D}J}{\mathrm{D}t} = J\frac{\partial v_k}{\partial x_k} \tag{a}$$

Proof

$$\frac{\mathrm{D}J}{\mathrm{D}t} = \frac{\mathrm{D}|\partial x_i/\partial X_R|}{\mathrm{D}t} = \frac{\partial J}{\partial(\partial x_k/\partial X_S)}\frac{\mathrm{D}(\partial x_k/\partial X_S)}{\mathrm{D}t} = \frac{\partial J}{\partial(\partial x_k/\partial X_S)}\frac{\partial v_k}{\partial x_m}\frac{\partial x_m}{\partial X_S} \tag{b}$$

Using (2.76), the expression $\partial J/\partial\left(\dfrac{\partial x_k}{\partial X_S}\right)$ in (b) is the cofactor of matrix $\frac{\partial x_k}{\partial X_S}$, and according to (2.84), we write

$$\frac{\partial J}{\partial(\partial x_k/\partial X_S)} = J\frac{\partial X_S}{\partial x_k} \tag{c}$$

Substituting (c) into (b), we obtain (a).

3.18 Material Derivative of Area and Volume Elements

We first find the material derivative of an area element. The deformed and initial areas are related by Nanson's formula (3.92), and the differentiation of (3.92) leads to

$$\frac{\mathrm{D}}{\mathrm{D}t}(\mathrm{d}a_i) = \frac{\mathrm{D}}{\mathrm{D}t}\left(J\frac{\partial X_R}{\partial x_i}\mathrm{d}A_R\right) = \left(\frac{\mathrm{D}J}{\mathrm{D}t}\frac{\partial X_R}{\partial x_i} + J\frac{\mathrm{D}}{\mathrm{D}t}\left(\frac{\partial X_R}{\partial x_i}\right)\right)\mathrm{d}A_R \tag{3.201}$$

Deriving an expression to represent the last term of (3.201), we differentiate the expression

$$\frac{\partial x_i}{\partial X_R}\frac{\partial X_R}{\partial x_j} = \delta_{ij} \tag{3.202}$$

to obtain

$$\frac{\mathrm{D}}{\mathrm{D}t}\left(\frac{\partial x_i}{\partial X_R}\right)\frac{\partial X_R}{\partial x_j} + \frac{\partial x_i}{\partial X_R}\frac{\mathrm{D}}{\mathrm{D}t}\left(\frac{\partial X_R}{\partial x_j}\right) = 0 \tag{3.203}$$

This equation may be further simplified to yield

$$\frac{\partial v_i}{\partial x_j} + \frac{\partial x_i}{\partial X_R}\frac{\mathrm{D}}{\mathrm{D}t}\left(\frac{\partial X_R}{\partial x_j}\right) = 0 \tag{3.204}$$

which reduces to

$$\frac{\mathrm{D}}{\mathrm{D}t}\left(\frac{\partial X_R}{\partial x_j}\right) = -\frac{\partial v_i}{\partial x_j}\frac{\partial X_R}{\partial x_i} \tag{3.205}$$

Substituting (3.205) and the expression of Example 3.9 into (3.201) to obtain

$$\begin{aligned}\frac{\mathrm{D}}{\mathrm{D}t}(\mathrm{d}a_i) &= \left(\frac{\mathrm{D}J}{\mathrm{D}t}\frac{\partial X_R}{\partial x_i} + J\frac{\mathrm{D}}{\mathrm{D}t}\left(\frac{\partial X_R}{\partial x_i}\right)\right)\mathrm{d}A_R \\ &= J\frac{\partial v_k}{\partial x_k}\frac{\partial X_R}{\partial x_i}\mathrm{d}A_R - J\frac{\partial v_k}{\partial x_i}\frac{\partial X_R}{\partial x_k}\mathrm{d}A_R = \frac{\partial v_k}{\partial x_k}\mathrm{d}a_i - \frac{\partial v_k}{\partial x_i}\mathrm{d}a_k\end{aligned} \tag{3.206}$$

we may conclude that the material rate of an area element is

$$\frac{\mathrm{D}}{\mathrm{D}t}(\mathrm{d}a_i) = \frac{\partial v_k}{\partial x_k}\mathrm{d}a_i - \frac{\partial v_k}{\partial x_i}\mathrm{d}a_k \tag{3.207}$$

Finally, let us consider the material derivative of the volume element. Since $\mathrm{d}V = J\,\mathrm{d}V_0$, we can differentiate the equation to obtain

$$\frac{\mathrm{D}(\mathrm{d}V)}{\mathrm{D}t} = \frac{\mathrm{D}}{\mathrm{D}t}(J\mathrm{d}V_0) = \frac{\mathrm{D}J}{\mathrm{D}t}\mathrm{d}V_0 = J\frac{\partial v_k}{\partial x_k}\mathrm{d}V_0 = \frac{\partial v_k}{\partial x_k}\mathrm{d}V = D_{kk}\mathrm{d}V \tag{3.208}$$

The material derivative of the logarithmic volumetric strain is then

$$\frac{\mathrm{D}}{\mathrm{D}t}[\ln(\mathrm{d}V)] = \frac{1}{\mathrm{d}V}\frac{\mathrm{D}(\mathrm{d}V)}{\mathrm{D}t} = v_{k,k} = \mathrm{Div}\,\mathbf{v} = D_{kk} \tag{3.209}$$

All of the last three forms in (3.209) have been used in the continuum mechanics literature. When there is no volume change, we have from (3.208) or (3.209), $v_{k,k} = D_{kk} = \mathrm{Div}\,\mathbf{v} = 0$. This is a necessary and sufficient condition for the material element to undergo no volume change. We note that a material element undergoing no volume change is merely a geometrical condition. It has no implication as to whether the material is compressible or not. But, when a material element does not suffer any volume change in all loading conditions, the material is then incompressible.

References

1. Truesdell, C. and Toupin, R. S. Flugge (ed.) The Classical Field Theories, in *Handbuch der Physik*, Vol. III/1, Springer-Verlag, Berlin, 1960.
2. Spencer, A.J.M., *Continuum Mechanics*, Longman, London and New York, 1980.
3. Chadwick, P., *Continuum Mechanics*, George Allen & Unwin, London, 1976.
4. Eringen, A.C., *Mechanics of Continua*, Wiley, New York, 1967.

Problems

(1) In the deformation defined by

$$x_1 = \lambda_1 X_1, \qquad x_2 = \lambda_2 X_2, \qquad x_3 = \lambda_3 X_3$$

find the expressions for the following tensors: **F**, **C**, **U**, **R**, where λ_i are constants. If $\lambda_1 = 1.2, \lambda_2 = 0.8$, and $\lambda_3 = 1$, sketch the deformed shape of a unit cube.

(2) In the deformation of problem 1 with $\lambda_1 = 1.2, \lambda_2 = 0.8$, and $\lambda_3 = 1$, determine the deformed length of a diagonal connecting point O $(0, 0, 0)$ to point C $(1, 1, 1)$. Determine also the final orientation of this diagonal.

(3) Consider the following deformation and refer to Figure 3.16

$$x_1 = \lambda_1 X_1 + X_2 \tan\gamma, \qquad x_2 = \lambda_2 X_2, \qquad x_3 = \lambda_3 X_3$$

where λ_i and γ are constants. Sketch the deformed shape of square OABC in the $X_1 - X_2$ plane. The sides are initially of unit length.

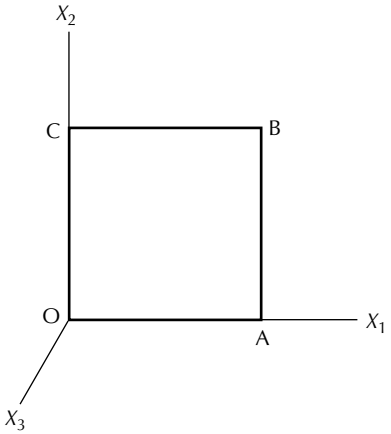

FIGURE 3.16

(4) For the simple shearing deformation given by $x_1 = X_1 + kX_2, x_2 = X_2, x_3 = X_3$, where k is a constant, find the components of **C** in terms of k and determine the eigenvalues and eigenvectors of **C**. Discuss the eigenvalues and eigenvectors of **C** as k varies from negative to positive and from small to large values.

(5) For the simple shearing deformation given by $x_1 = X_1 + kX_2, x_2 = X_2, x_3 = X_3$, where k is a constant, represent by a sketch the deformed area to which the

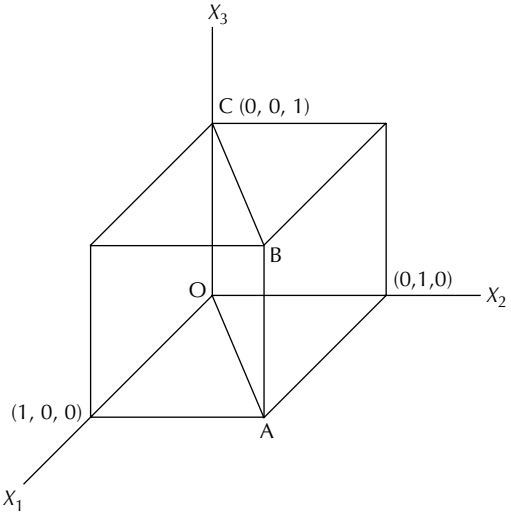

FIGURE 3.17

original area OABC transforms (see Figure 3.17). Obtain an expression to describe the direction of the line element OA after deformation.

(6) Consider the following deformation

$$x_1 = \sqrt{2}X_1 + \tfrac{3}{4}X_2, \qquad x_2 = X_1 - \tfrac{3}{4}X_2 + \tfrac{1}{4}X_3, \qquad x_3 = \sqrt{2}X_3$$

Find (a) the direction after the deformation of a line element, which is initially oriented with a direction ratio 1:1:1; (b) the stretch ratio of this line element.

(7) By use of the imaging-based method, the locations of the four corners of a two-dimensional, initially square, material element have been determined after deformation. The initial and deformed elements are shown in Figure 3.18. Using the property that **F** transforms undeformed line elements into deformed line elements, determine the components of **F** and **C**.

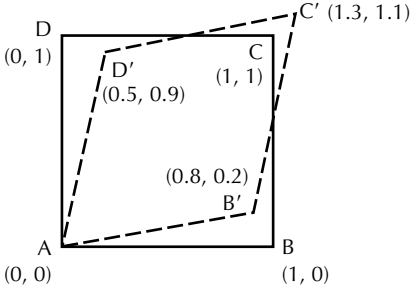

FIGURE 3.18

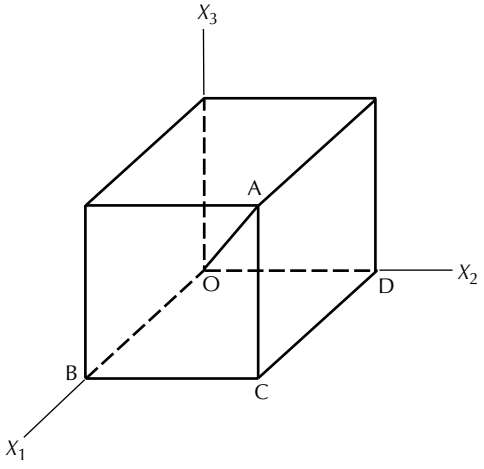

FIGURE 3.19
Figure for Problem 11.

(8) Show that

$$F_{iR} = \begin{bmatrix} \cos\theta & -\sin\theta & 0 \\ \sin\theta & \cos\theta & 0 \\ 0 & 0 & 1 \end{bmatrix}$$

describes a rigid-body rotation.

(9) A square element is subjected to a uniaxial extension in the 1 direction, and is then rotated about the positive 3 direction through an angle of 90°. Determine the deformation gradient **F**.

(10) In the case of plane strain, experimental measurements give stretch ratios λ of 0.8 and 1.2 in the X_1 and X_2 directions, respectively, and 0.6 in the direction making a 45° angle with the X_1 axis. Determine the components of **C** and **E**.

(11) Consider the unit cube shown in Figure 3.19, which undergoes the deformation

$$x_1 = \alpha\left(X_1 - \tfrac{1}{2}X_2\right), \qquad x_2 = \beta X_2, \qquad x_3 = \gamma X_3$$

where α, β, and γ are constants. Determine

(a) the deformed length of diagonal OA

(b) the angle between OB and OD after deformation

(c) the condition that constants α, β, and γ must satisfy if the material is incompressible.

(12) For the deformation of Problem (11), determine the expressions for components of tensors **F**, **C**, **U**, **V**, **R**, **B**, **E**, and **e**. Use $\alpha = 1.2$, $\beta = \gamma = 0.9$.

(13) In the case of simple shear deformation of a square block governed by

$$x_1 = X_1 + kX_2, \qquad x_2 = X_2, \qquad x_3 = X_3$$

where k is constant, determine the extension ratios for the sides and the diagonals. Find the volume of the block before and after deformation.

(14) The most general two-dimensional homogeneous deformation is defined by the following linear transformation

$$x_1 = aX_1 + bX_2, \qquad x_2 = cX_1 + \mathrm{d}X_2, \qquad x_3 = X_3$$

Find components of **C**, **B**, and **E** in terms of constants a, b, c, and d.

(15) Consider the following deformation and refer to Figure 3.16

$$x_1 = X_1 + \tfrac{1}{2}X_2^2, \qquad x_2 = X_2, \qquad x_3 = X_3$$

(a) Sketch the deformed shape of square OABC in the $X_1 - X_2$ plane. The sides are initially of unit length.

(b) Consider at point O two line elements: $\mathrm{d}\mathbf{X}^{(1)} = \mathrm{d}X^{(1)}\mathbf{e}_1$ and $\mathrm{d}\mathbf{X}^{(2)} = \mathrm{d}X^{(2)}\mathbf{e}_2$. Find the deformed line elements $\mathrm{d}\mathbf{x}^{(1)}$ and $\mathrm{d}\mathbf{x}^{(2)}$, and calculate the dot product $\mathrm{d}\mathbf{x}^{(1)} \cdot \mathrm{d}\mathbf{x}^{(2)}$. Determine the change in the original right angle between $\mathrm{d}\mathbf{X}^{(1)}$ and $\mathrm{d}\mathbf{X}^{(2)}$ due to deformation.

(c) Do the same thing as in (b) for two line elements $\mathrm{d}\mathbf{X}^{(1)} = \mathrm{d}X^{(1)}\mathbf{e}_1$ and $\mathrm{d}\mathbf{X}^{(2)} = \mathrm{d}X^{(2)}\mathbf{e}_2$ located at point C.

(16) In the initial configuration, a circular cylinder with radius R has its axis aligned with the X_3 direction. If the cylinder undergoes the deformation

$$\begin{aligned} x_1 &= \alpha\{X_1 \cos(\tau X_3) + X_2 \sin(\tau X_3)\} \\ x_2 &= \alpha\{-X_1 \sin(\tau X_3) + X_2 \cos(\tau X_3)\} \\ x_3 &= \beta X_3 \end{aligned}$$

determine the conditions that need to be satisfied by constants α, β, and τ so that the volume is preserved during deformation. Determine the length of a line element in the deformed configuration, which initially has unit length and lies on the surface of the cylinder along the X_3 direction. Determine also the initial length of a line element on the surface of the cylinder that, in the deformed configuration, has unit length and lies in the X_3 direction.

(17) For an isotropic material, the coefficient of thermal expansion is $\alpha_{ij} = \alpha\delta_{ij}$, where α is a constant. A line element of length L elongates an amount $\mathrm{d}L$ if the temperature is raised by $\mathrm{d}T$, so that $\mathrm{d}L = \alpha \mathrm{d}TL$. For a block of $L_1 \times L_2 \times L_3$ subjected to this change in temperature, write down the set of three transformation equations that describes this deformation. Find the components of **F** and determine the current length of a diagonal of the block, which had an initial length of L.

(18) If the eigenvalues for $\mathbf{U}$ are $\lambda_{(i)} = 3, \frac{1}{3}, 1$ and the corresponding eigenvectors are

$$\mathbf{n}_u^{(1)^{\mathrm{T}}} = \left[\frac{1}{2}, \frac{\sqrt{3}}{2}, 0\right], \qquad \mathbf{n}_u^{(2)^{\mathrm{T}}} = \left[-\frac{\sqrt{3}}{2}, \frac{1}{2}, 0\right], \qquad \mathbf{n}_u^{(3)^{\mathrm{T}}} = (0, 0, 1)$$

use $\mathbf{E} = \mathbf{f}(\mathbf{U}) = \sum_i f(\lambda_i)\mathbf{n}_u^{(i)} \otimes \mathbf{n}_u^{(i)}$ with $f(\lambda_i) = \frac{\lambda_i^\kappa - 1}{\kappa}$ to determine the components of $\mathbf{E}$ with respect to the X_R system when $\kappa = 2$ and -2.

(19) If the eigenvalues for $\mathbf{V}$ are $\lambda_{(i)} = 3, \frac{1}{3}, 1$ and the corresponding eigenvectors are

$$\mathbf{n}_v^{(1)^{\mathrm{T}}} = \left[\frac{\sqrt{3}}{2}, \frac{1}{2}, 0\right], \quad \mathbf{n}_v^{(2)^{\mathrm{T}}} = \left[-\frac{1}{2}, \frac{\sqrt{3}}{2}, 0\right], \quad \mathbf{n}_v^{(3)^{\mathrm{T}}} = [0,\ 0,\ 1]$$

use $\mathbf{e} = \mathbf{f}(\mathbf{V}) = \sum_i f(\lambda_i)\mathbf{n}_v^{(i)} \otimes \mathbf{n}_v^{(i)}$ with $f(\lambda_i) = (\lambda_i^\kappa - 1)/\kappa$ to determine the components of $\mathbf{e}$ with respect to the x_i system when $\kappa = 2$ and -2. Assume that X_R and x_i coincide for simplicity.

(20) Consider a rectangular triad before deformation. Discuss what would happen to this triad after deformation. Would it remain rectangular? Under what condition?

(21) Let the displacement field be given by

$$u_1 = \tfrac{1}{4}(X_3 - X_2), \qquad u_2 = \tfrac{1}{4}(X_1 - X_3), \qquad u_3 = \tfrac{1}{4}(X_2 - X_1)$$

Determine the volume ratio $\mathrm{d}V/\mathrm{d}V_0$.

(22) Show that the velocity field

$$v_1 = 2x_3 - 3x_2, \qquad v_2 = 3x_1 - x_3, \qquad v_3 = x_2 - 2x_1$$

corresponds to a rigid-body rotation. Determine this rotation by a vector so that we know the axis of rotation.

(23) Consider the motion

$$x_1 = X_1 + \tfrac{1}{2}X_2^2 t, \qquad x_2 = X_2, \qquad x_3 = X_3$$

At $t = 0$, the corners of a unit square are at O (0, 0, 0), A (1, 0, 0), B (1, 1, 0), and C (0, 1, 0). Sketch the deformed shape of square OABC in the $X_1 - X_2$ plane when $t = 1$ and when $t = 2$.

(24) For the motion of Problem (23), determine the velocity and acceleration of a particle in both material and spatial descriptions.

(25) For the motion of Problem (23), determine the expressions for $\mathbf{L}$, $\mathbf{D}$, and $\mathbf{W}$.

(26) For the velocity field $v_1 = -\alpha x_2, v_2 = \alpha x_1, v_3 = \beta$, where α and β are constants, find the components of tensors $\mathbf{L}$, $\mathbf{D}$, and $\mathbf{W}$.

(27) Let a velocity field be described by $v_i = \alpha x_j \mu_i v_j$, where the scalar α and the orthogonal unit vectors $\boldsymbol{\mu}$ and $\boldsymbol{\nu}$ are independent of the coordinate x_i. Show that this velocity field represents simple shearing. Find the principal values and directions of the rate of deformation **D** with respect to the directions of $\boldsymbol{\mu}$ and $\boldsymbol{\nu}$.

(28) Prove that, if the D_{ij} components of a velocity field are independent of the coordinates and the principal invariants I_D and III_D are both 0, the velocity field represents simple shearing.

(29) Consider the motion

$$x_1 = X_1 + kX_2^2 t^2, \qquad x_2 = (1 + kt)X_2, \qquad \text{and} \qquad x_3 = X_3$$

where k is a constant and the material coordinate X_R designates the position of a particle at t = 0.

(a) At $t = 0$ the corners of a unit square are at O (0, 0, 0), A (0, 1, 0), B (1, 1, 0), and C (1, 0, 0). Sketch the shape of the square at $t = 1.5$.

(b) Obtain the spatial description of the velocity and acceleration fields.

(c) Obtain the expressions for the rate of deformation **D** and the spin tensor **W**.

(d) What happens to the volume of an infinitesimal element located initially at (0.6, 0.5, 1)?

(30) In the motion of a continuum, the velocity of a particle is given by

$$v_1 = (x_1^2 + x_1 x_2)\mathrm{e}^{-kt}, \qquad v_2 = (x_2^2 - x_1 x_2)\mathrm{e}^{-kt}, \qquad v_3 = 0$$

where k is a constant and t is time. Determine the following properties at point (1, 1, 1) when $t = 0$:

(a) the principal values of the rate of deformation **D**,

(b) the maximum shear rate.

(31) For the motion of Problem (30), determine the volumetric strain-rate defined by $(1/\mathrm{d}V)((\mathrm{D}(\mathrm{d}V))/\mathrm{D}t)$, where $\mathrm{d}V$ is the current volume of an element.

(32) The velocity field of a continuum is prescribed by

$$v_1 = f(x_2) - x_2 g(r), \qquad v_2 = x_1 g(r), \qquad v_3 = 0 \qquad \text{with } r = (x_1^2 + x_2^2)^{1/2}$$

Determine the rate of deformation **D** and the vorticity vector **w**, which is the dual vector of the spin tensor **W**. Discuss the type of motion that the continuum is undergoing.

(33) Let the components of **D** be

$$[D] = \begin{bmatrix} \alpha & \beta & \beta \\ \beta & \alpha & \beta \\ \beta & \beta & \alpha \end{bmatrix}$$

Consider a line element with direction denoted by the unit vector **n**. If the rate of extension of the line element is α, find the condition that the components of **n** must fulfill.

(34) Consider the motion of a deformable element. Do all line elements in Figure 3.20 spin with the same angular velocity? The spin of which line element does the spin tensor **W** describe?

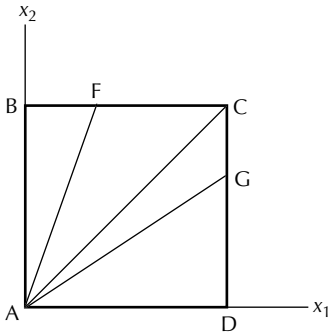

FIGURE 3.20

4

Conservation Laws and Constitutive Equation

4.1 Introduction

This chapter discusses the governing equations of a body undergoing deformation. The equations include the *conservation laws* of physics and the *constitutive equations*. The conservation laws of physics are the conservation of mass, linear momentum, angular momentum, and energy. These laws are first developed in the *global form* and then reduced to the *local form*. The global form considers forces, momentum, or energy acted on the whole deformable body, whereas the local form refers to a generic infinitesimal element of the body.

The conservation laws are applicable to a body of any material. To distinguish between deformation of a body made of different materials, we need *constitute equations*. As an example, let us consider applying a tensile force to a long bar. The conservation laws for the problem are the same no matter what material the bar is made of. However, experiments show that long bars made of wood or steel will undergo different amounts of deformation when subjected to the same tensile force. Therefore, in order to accurately describe the elongation of the bars, we need to introduce constitutive equations, which accurately represent the two different materials of the bars, that is, we need a constitutive equation of for wood and another for steel.

Constitutive equations are a set of equations, which describe the thermomechanical properties of a material. Depending on the simplicity/complexity of the material behavior that we wish to describe, we may need one constitutive equation or a set of constitutive equations. Hooke's law is the most well-known constitutive equation for solids, and it is also the simplest form that a constitutive equation for solid can have. However, there is a limitation to the validity of Hooke's law. It is usually applicable when the deformation is small and linearly elastic at room temperature. The equation needs to be modified or extended to a set of (nonlinear) equations when the deformation is large and nonelastic and not at constant temperature.

Hooke's law is also known as the *stress–strain relation*, because the equation relates the stress to the strain; for isotropic linearly elastic solid, it is

written as

$$\boldsymbol{\sigma} = 2\mu\boldsymbol{\varepsilon} + \lambda \mathbf{I}\varepsilon_{kk} \tag{4.1}$$

where $\boldsymbol{\sigma}$ and $\boldsymbol{\varepsilon}$ are the engineering stress and strain, respectively, and μ and λ are the Lamé constants.'

The effect of temperature on the material behavior is not discussed in this chapter. Even at constant temperature, the material behavior of a real material can be quite complex. Realistic constitutive equations should be used in order to obtain useful solutions of engineering problems. In addition to the elastic behavior, some materials exhibit strong viscous behaviors and some are significantly influenced by plastic deformation. The viscous behaviors are observable in the forms of the strain-rate effect, creep and stress relaxation. These behaviors are usually discussed within the contest of viscoelasticity and viscoplasticity. The viscoplastic behavior is discussed in Chapter 5. The subject of plastic deformation is one of the main topics of this book and is thoroughly discussed in the later part of the book.

In this chapter, we first derive the conservation equations. The bulk material rate of change is discussed. This is useful in the derivation of the conservation laws in the global form. In the local form, we derive the conservation equations for an infinitesimal material element at the deformed configuration. This is a spatial description. We then discuss the material description of the conservation laws, which leads to the discussion of several stress-measures, referring to the deformed or undeformed configurations. In the topics related to constitutive equations, we first discuss the general principles, including the principle of material objectivity. We then derive the constitutive equation for large elastic deformation, which include different types of formulations. Emphasis is placed upon hyperelasticity and some examples are given. Finally, the generalized Hooke's law for infinitesimal elastic deformation is discussed.

4.2 Bulk Material Rate of Change

We discuss the bulk material rate here, because it is useful when we consider the global form of the conservation laws in the next section. The *bulk material rate* is the material rate of change of a physical property defined over a material body. Referring to Figure 4.1, we let the material body occupy the space shown by the solid line at time t and let the body occupy the space shown by the dashed line at time $t + \Delta t$. The volume and surface of the body at t and $t + \Delta t$ are (V, S) and (V', S'), respectively. Let $\phi(x_i, t)$ be a property of the continuum, which is a tensor quantity. Considering the volume integral

$$I = \int_V \phi \, \mathrm{d}V \tag{4.2}$$

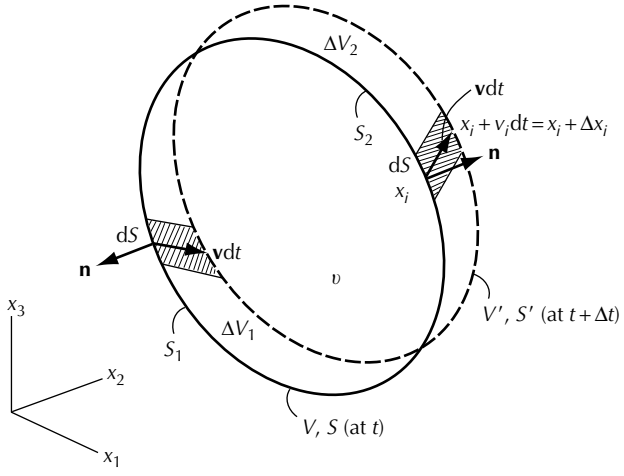

FIGURE 4.1
Bulk material rate of change.

we are then interested in finding the derivative $\mathrm{D}I/\mathrm{D}t$. To fix ideas, let us assume that $\phi = \rho(x_i, t)$ is the density of the continuum, then the integral $I = \int_V \rho \, \mathrm{d}V$ is the total mass of the body. The derivative of (4.2) is

$$\begin{aligned}\frac{\mathrm{D}I}{\mathrm{D}t} &= \lim_{\Delta t \to 0} \frac{[\int_{V'} \phi(x_i + \Delta x_i, t + \Delta t)\mathrm{d}V' - \int_V \phi(x_i, t)\mathrm{d}V]}{\Delta t} \\ &= \lim_{\Delta t \to 0} \frac{[\int_V \phi(x_i, t + \Delta t)\mathrm{d}V - \int_V \phi(x_i, t)\mathrm{d}V]}{\Delta t} \\ &\quad + \lim_{\Delta t \to 0} \frac{[\int_{V'} \phi(x_i + \Delta x_i, t + \Delta t)\mathrm{d}V' - \int_V \phi(x_i, t + \Delta t)\mathrm{d}V]}{\Delta t} \end{aligned} \tag{4.3}$$

In the second equality of (4.3), the term $\int_V \phi(x_i, t + \Delta t)\mathrm{d}V$ has been added and subtracted. We now find physical interpretations for the terms of (4.3). Letting $V = \upsilon + \Delta V_1$, $V' = \upsilon + \Delta V_2$, then υ is the common volume of V and V' and is denoted by the shaded area in Figure 4.1; ΔV_1 is the volume in V and ΔV_2 is the volume in V' both of which are denoted by the moon-shaped area. Equation (4.3) may be interpreted as

$$\begin{aligned}\frac{\mathrm{D}I}{\mathrm{D}t} &= \lim_{\Delta t \to 0} \frac{(\text{Total mass in } V \text{ at } t + \Delta t - \text{ Total mass in } V \text{ at } t)}{\Delta t} \\ &\quad + \lim_{\Delta t \to 0} \frac{(\text{Total mass in } V' \text{ at } t + \Delta t - \text{ Total mass in } V \text{ at } t + \Delta t)}{\Delta t} \\ &= (\text{Rate of increase of mass in fixed region } V) \\ &\quad + \lim_{\Delta t \to 0} \frac{(\text{Total mass in } \Delta V_2 \text{ at } t + \Delta t - \text{ that in } \Delta V_1 \text{ at } t + \Delta t)}{\Delta t} \end{aligned} \tag{4.4}$$

where the last term is the net amount of mass increased in V per unit time. Equation (4.3) may then be written as

$$\begin{aligned}\frac{\mathrm{D}I}{\mathrm{D}t} &= \int_V \frac{\partial \phi}{\partial t}\mathrm{d}V + \lim_{\Delta t\to 0}\frac{(\int_{\Delta V_2}\phi\,\mathrm{d}V - \int_{\Delta V_1}\phi\,\mathrm{d}V)}{\Delta t} \\ &= \int_V \frac{\partial \phi}{\partial t}\mathrm{d}V + \lim_{\Delta t\to 0}\frac{[\int_{S_2}\phi\mathbf{v}\Delta t\cdot\mathbf{n}\,\mathrm{d}S + \int_{S_1}\phi\mathbf{v}\Delta t\cdot(\mathbf{n}\,\mathrm{d}S)]}{\Delta t}\end{aligned} \tag{4.5}$$

Note that the surface S of the body at time t is seen in Figure 4.1 to be divided into S_1 and S_2 so that $S = S_1 + S_2$. A particle on the surface S_2 has coordinates x_i with velocity $\mathbf{v}$, and the particle moves to a new position $x_i + \Delta x_i$ during the time interval Δt, and we write $x_i + v_i\Delta t = x_i + \Delta x_i$. Denoting the area element at this particle by $\mathrm{d}S$ and its unit normal by $\mathbf{n}$, we observe that this area element sweeps through a volume $\Delta V = \mathbf{v}\Delta t\cdot\mathbf{n}\mathrm{d}S$ during the time interval Δt, and area S_2 sweeps through volume ΔV_2. The same thing may be said of particles on surface S_1, except that the scalar product $\Delta V = \mathbf{v}\Delta t\cdot\mathbf{n}\mathrm{d}S$ is negative. This may be seen from Figure 4.1, because vectors $\mathbf{n}$ and $\mathbf{v}$ form an obtuse angle. Thus, during time interval Δt, surface S_1 sweeps through volume ΔV_1. The two integrals within the parenthesis in (4.5) can then be added to form one integral and the equation becomes

$$\begin{aligned}\frac{\mathrm{D}I}{\mathrm{D}t} &= \int_V \frac{\partial\phi}{\partial t}\mathrm{d}V + \int_S \phi v_i n_i\,\mathrm{d}S = \int_V \frac{\partial\phi}{\partial t}\mathrm{d}V + \int_V (\phi v_i)_{,i}\,\mathrm{d}V \\ &= \int_V \left(\frac{\partial\phi}{\partial t} + \phi_{,i}v_i + \phi v_{i,i}\right)\mathrm{d}V\end{aligned} \tag{4.6}$$

The Gauss theorem discussed in Section 1.8.3 was used in the derivation of (4.6), which may be further written as

$$\frac{\mathrm{D}}{\mathrm{D}t}\int_V \phi\,\mathrm{d}V = \int_V \left(\frac{\mathrm{D}\phi}{\mathrm{D}t} + \phi v_{i,i}\right)\mathrm{d}V \tag{4.7}$$

This is the material derivative of the integral of a property ϕ defined over volume V. We used $\phi = \rho$ in the above derivation for easy interpretation, but (4.7) is valid for any scalar property of the material.

We now consider an alternative derivation of (4.7). Let $\mathbf{I} = I(t)$ which, in general, is a function of time and we write

$$I = \int_V \phi\,\mathrm{d}V = \int_{V_0}\phi(X_R, t)\det\mathbf{F}\,\mathrm{d}V_0 \tag{4.8}$$

In arriving at the last equality of (4.8), (3.82) and the coordinate transformation $X_R = X_R(x_i, t)$ was applied. Noting that V_0 is time independent, we

differentiate (4.8) to obtain

$$\frac{\mathrm{D}I}{\mathrm{D}t} = \int_{V_0} \left[\frac{\mathrm{D}\phi}{\mathrm{D}t} \det \mathbf{F} + \phi \frac{\mathrm{D}}{\mathrm{D}t} (\det \mathbf{F}) \right] \mathrm{d}V_0 \tag{4.9}$$

To further reduce equation (4.9) to a simple form, we apply the following expression that was deduced in Example 3.9

$$\frac{\mathrm{D}J}{\mathrm{D}t} = J \frac{\partial v_k}{\partial x_k} \tag{4.10}$$

Note that $J = \det \mathbf{F}$. Using (4.10), (4.9) becomes

$$\frac{\mathrm{D}I}{\mathrm{D}t} = \int_{V_0} \left[\frac{\mathrm{D}\phi}{\mathrm{D}t} \det \mathbf{F} + \phi \ \det \mathbf{F} \, v_{i,i} \right] \mathrm{d}V_0 = \int_{V_0} \left[\frac{\mathrm{D}\phi}{\mathrm{D}t} + \phi v_{i,i} \right] \det \mathbf{F} \, \mathrm{d}V_0 \tag{4.11}$$

Therefore, we may conclude that

$$\frac{\mathrm{D}I}{\mathrm{D}t} = \int_{V} \left[\frac{\mathrm{D}\phi}{\mathrm{D}t} + \phi v_{i,i} \right] \mathrm{d}V \tag{4.12}$$

which is the same as (4.7).

4.3 Conservation Laws

There are three conservation laws from physics, and they are valid for all materials. They are: (i) the conservation of mass, (ii) the conservation of momentum, and (iii) the conservation of energy. These laws are discussed individually and written in mathematical expressions in this section.

4.3.1 The Conservation of Mass

The mass of a body is preserved when only thermo-mechanical behavior is being considered. In this case, the rate of change of mass is zero. Setting $\phi = \rho$ in (4.2), the integral I is the mass of the body. The *global form* of the conservation of mass is written as

$$\frac{\mathrm{D}}{\mathrm{D}t} \int_V \rho \, \mathrm{d}V = 0 \tag{4.13}$$

Using (4.7), (4.13) may be further written as

$$\frac{\mathrm{D}}{\mathrm{D}t} \int_V \rho \, \mathrm{d}V = 0 = \int_V \left(\frac{\mathrm{D}\rho}{\mathrm{D}t} + \rho v_{i,i} \right) \mathrm{d}V \tag{4.14}$$

which must be true for all volume elements. Thus, the *local form* (or differential form) of the conservation of mass is

$$\frac{\mathrm{D}\rho}{\mathrm{D}t} + \rho v_{i,i} = 0 \tag{4.15}$$

But, since

$$\frac{\mathrm{D}\rho}{\mathrm{D}t} = \frac{\partial \rho(x_i, t)}{\partial t} + \frac{\partial \rho}{\partial x_j} v_j \tag{4.16}$$

we obtain from (4.15)

$$\frac{\partial \rho}{\partial t} + \frac{\partial (\rho v_i)}{\partial x_i} = 0 \tag{4.17}$$

Equation (4.17) is known as the *continuity equation* in fluid mechanics.

4.3.2 The Conservation of Momentum

We need to consider both the conservation of linear momentum and angular momentum. The rate of change of linear momentum is equal to the resultant force and the conservation equation is

$$\frac{\mathrm{D}}{\mathrm{D}t} \int_V \rho v_i \, \mathrm{d}V = \int_V b_i \, \mathrm{d}V + \int_S t_i^{(n)} \, \mathrm{d}S \tag{4.18}$$

Equation (4.18) is the *conservation of linear momentum* in the global form. The left-hand side of (4.18) is the rate of change of linear momentum. The first term on the right-hand side is the total body force and the second term is the total surface traction. Using (2.8) and an identity proven in Example 4.1, (4.18) may be written as

$$\int_V b_i \, \mathrm{d}V + \int_S \sigma_{ki} n_k \, \mathrm{d}S = \frac{\mathrm{D}}{\mathrm{D}t} \int_V \rho v_i \, \mathrm{d}V = \int_V \rho \frac{\mathrm{D}v_i}{\mathrm{D}t} \, \mathrm{d}V \tag{4.19}$$

or, by use of the Gauss theorem, we obtain

$$\int_V \left(b_i + \sigma_{ki,k} - \rho \frac{\mathrm{D}v_i}{\mathrm{D}t} \right) \mathrm{d}V = 0 \tag{4.20}$$

In the local form, (4.20) reduces to

$$\sigma_{ki,k} + b_i = \rho \frac{\mathrm{D}v_i}{\mathrm{D}t} \tag{4.21}$$

which is known as the *equation of motion*.

The conservation of angular momentum states that the rate of change of the angular momentum is equal to the sum of moments of forces acting on the body. This law leads to the symmetry of stress tensor and has been discussed in Section 2.6 for the case when material element is in equilibrium. In the case of material element in motion, we have

$$\int_V \rho e_{ijk} x_i b_j \, \mathrm{d}V + \int_S e_{ijk} x_i t_j^{(n)} \, \mathrm{d}S = \frac{\mathrm{D}}{\mathrm{D}t} \int_V \rho e_{ijk} x_i v_j \, \mathrm{d}V \tag{4.22}$$

The first term on the left-hand side of (4.22) denotes the moment due to the body force, the second term denotes the moment due to surface traction, and the term on the right-hand side denotes the rate of change of the angular momentum. Using (2.8) and the Gauss theorem, (4.22) is written as

$$\begin{aligned} \int_V \left[\rho e_{ijk} x_i b_j + \frac{\partial}{\partial x_m} (e_{ijk} x_i \sigma_{mj}) \right] \mathrm{d}V &= \int_V \rho e_{ijk} \frac{\mathrm{D}}{\mathrm{D}t} (x_i v_j) \, \mathrm{d}V \\ &= \int_V \rho e_{ijk} \left(v_i v_j + x_i \frac{\mathrm{D}v_j}{\mathrm{D}t} \right) \mathrm{d}V \end{aligned} \tag{4.23}$$

in which $\rho e_{ijk} v_i v_j = 0$. Hence,

$$\int_V e_{ijk} x_i \left\{ \sigma_{mj,m} + b_j - \rho \frac{\mathrm{D}v_j}{\mathrm{D}t} \right\} \mathrm{d}V + \int_V e_{ijk} \sigma_{ji} \, \mathrm{d}V = 0 \tag{4.24}$$

By use of the equation of motion (4.21), the first integral of (4.24) vanishes, and therefore,

$$e_{ijk} \sigma_{ij} = 0 \tag{4.25}$$

which leads to

$$\sigma_{ij} = \sigma_{ji} \tag{4.26}$$

using an argument similar to that used in Section 2.6. Thus, we have shown that the conservation of angular momentum leads to the symmetry of the stress tensor for a body in motion.

EXAMPLE 4.1 Show that $\mathrm{D}/\mathrm{D}t \int_V \rho\phi \, \mathrm{d}V = \int_V \rho (\mathrm{D}\phi/\mathrm{D}t) \, \mathrm{d}V$, where ϕ is a physical property defined in V.

Proof

From (5.7), we have

$$\frac{\mathrm{D}}{\mathrm{D}t} \int (\rho\phi) \mathrm{d}V = \int \left(\frac{\mathrm{D}}{\mathrm{D}t} (\phi\rho) + \phi\rho v_{i,i} \right) \mathrm{d}V = \int_V \left\{ \phi \left(\frac{\mathrm{D}\rho}{\mathrm{D}t} + \rho v_{i,i} \right) + \rho \frac{\mathrm{D}\phi}{\mathrm{D}t} \right\} \mathrm{d}V \tag{a}$$

In the last equality, $D\rho/Dt + \rho v_{i,i} = 0$ due to conservation of mass. Hence, (a) reduces to

$$\frac{D}{Dt}\int_V \rho\phi \, dV = \int_V \rho \frac{D\phi}{Dt} dV \tag{b}$$

4.3.3 The Conservation of Energy

The law of conservation of energy is the first law of thermodynamics. According to this law, the sum of material derivatives of the internal and kinetic energies is equal to the sum of the rate of work of body and surface forces plus all other energies that enter the body per unit time. Other energies may include thermal, electrical, magnetic, or chemical energies. In this elementary text, we consider only the thermal energies and write

$$\frac{DE}{Dt} + \frac{DK}{Dt} = \frac{DW}{Dt} + \frac{DQ}{Dt} \tag{4.27}$$

The equation is now explained term by term. E denotes the internal energy of the material element and is an *extensive* quantity, that is, an internal energy density ε may be defined either per unit volume or per unit mass. In the case that ε is defined per unit mass, we write

$$E = \int_V \rho\varepsilon \, dV \tag{4.28}$$

An extensive quantity is doubled if the mass or volume is doubled. On the other hand, the density cannot be defined for an *intensive* quantity. Examples of intensive quantities are temperature and pressure. The internal energy includes all forms of energy in a system other than kinetic energy and potential energy. It represents energy modes on the microscopic level such as energy associated with nuclear spin, molecular binding, molecular translation and rotation, and molecular vibration, etc.

The kinetic energy is related to the motion of the macroscopic element and is written as

$$K = \frac{1}{2}\int_V \rho v_i v_i \, dV \tag{4.29}$$

The second term in (4.27) is the rate of change of the kinetic energy and the third term is the rate of work due to external forces and is written as

$$\frac{DW}{Dt} = \int_V b_i v_i \, dV + \int_S t_i^{(n)} v_i \, dS \tag{4.30}$$

and the last term of (4.27) is the rate of heat supply.

There are two categories of heat supply: the heat flowing across the boundary and the heat source. The heat flowing through area element $\mathrm{d}S$ is $-h_i n_i \mathrm{d}S$, where h_i is the heat flux vector and the direction of h_i is the direction of the heat flow. The magnitude of h_i is the amount of heat per unit time per unit area normal to the direction of heat flow. Therefore, the part of $\mathrm{D}Q/\mathrm{D}t$ due to conduction is $-\int_S h_i n_i \,\mathrm{d}S$. We note that heat flowing into the volume element is considered positive. Since the angle between h_i and n_i is obtuse, the negative sign is needed to make the heat flow positive. The part of $\mathrm{D}Q/\mathrm{D}t$ due to distributed heat sources is $\mathrm{D}/\mathrm{D}t \int_V \rho q \,\mathrm{d}V$; where q is the heat supply per unit mass. Hence, the equation of conservation of energy in the global form, (4.27), may be written as

$$\begin{aligned}&\frac{\mathrm{D}}{\mathrm{D}t}\int_V \rho\varepsilon \,\mathrm{d}V + \frac{\mathrm{D}}{\mathrm{D}t}\int_V \frac{1}{2}\rho v_i v_i \,\mathrm{d}V \\ &\quad = \int_V b_i v_i \,\mathrm{d}V + \int_S t_i^{(n)} v_i \,\mathrm{d}S - \int_S h_i n_i \,\mathrm{d}S + \frac{\mathrm{D}}{\mathrm{D}t}\int_V \rho q \,\mathrm{d}V \end{aligned} \tag{4.31}$$

Using the result of Example 4.1, (4.31) becomes

$$\begin{aligned}&\int_V \rho \frac{\mathrm{D}\varepsilon}{\mathrm{D}t}\mathrm{d}V + \int_V \rho v_i \frac{\mathrm{D}v_i}{\mathrm{D}t}\mathrm{d}V \\ &\quad = \int_V (\sigma_{ki} v_i)_{,k} \,\mathrm{d}V + \int_V b_i v_i \,\mathrm{d}V - \int_V h_{i,i} \,\mathrm{d}V + \int_V \rho \frac{\mathrm{D}q}{\mathrm{D}t}\mathrm{d}V \end{aligned} \tag{4.32}$$

The first integral on the right-hand side of (4.32) is

$$\int_V (\sigma_{ki} v_i)_{,k} \,\mathrm{d}V = \int_V (\sigma_{ki,k} v_i + \sigma_{ki} v_{i,k}) \,\mathrm{d}V \tag{4.33}$$

Then, by use of the equation of motion (4.21), the energy balance equation may be simplified. Hence, (4.32) reduces to

$$\rho \frac{\mathrm{D}\varepsilon}{\mathrm{D}t} = \sigma_{ki} v_{i,k} - h_{i,i} + \rho \frac{\mathrm{D}q}{\mathrm{D}t} = \sigma_{ki} D_{ik} - h_{i,i} + \rho \frac{\mathrm{D}q}{\mathrm{D}t} \tag{4.34}$$

This is the local form of the first law of thermodynamics for a continuous medium. Note that no kinetic energy term appears in the local form of the first law, since it gets canceled out by the rate of work done.

Some remarks are in order. The conservation laws derived in this section apply to all materials whether they are fluid or solid, dissipative or elastic (conservative). In particular, the first law as derived applies to all materials as well as processes reversible or irreversible. The validity of these equations

is subject to the constraint of a one-to-one and onto transformation which excludes: (a) diffusion processes; (b) chemical effects such as reactions and phase changes; (c) electromagnetic phenomena; and (d) polar media, that is, materials with distributed surface and body moments whose deformation requires account of local rotation and higher order deformation gradients. To address these sophisticated behaviors, the equations would have to be modified. Nevertheless, the equations in this section provide the foundations for further studies.

4.4 The Constitutive Laws in the Material Description

The local form of conservation laws of Section 4.3 is written based on an infinitesimal material element at the deformed configuration. In particular, the forces are applied to the element at the deformed configuration. In the study of continuum mechanics undergoing large deformation, it is necessary to distinguish between quantities that have been defined with reference to the deformed configuration and those that have been defined with reference to the reference configuration. The former is used in the spatial description of the conservation laws and the latter the material description. It is preferable by some investigators to use one description for solving certain problems and use the other description for other types of problems. The decision is based on the material properties and boundary conditions of the problems. We like to emphasize that, in the material description of conservation laws, the forces are still applied to the element at the deformed configuration, but some quantities as defined are referred to the reference configuration. In this section, we discuss the material description of the constitutive laws.

4.4.1 The Conservation of Mass

The conservation of mass is expressed as

$$\mathrm{d}m = \rho_0 \, \mathrm{d}V_0 = \rho \, \mathrm{d}V \tag{4.35}$$

which, from (3.82), may also be written as

$$\frac{\mathrm{d}V}{\mathrm{d}V_0} = \det(\mathbf{F}) = J = \frac{\rho_0}{\rho} \tag{4.36}$$

or

$$\rho_0 = \rho \det(\mathbf{F}) \tag{4.37}$$

This is a form of the conservation of mass and it may also be written as

$$\frac{\mathrm{D}}{\mathrm{D}t}(\rho \det \mathbf{F}) = 0 \tag{4.38}$$

4.4.2 The Conservation of Momentum

We first discuss different stress measures referred to either deformed or undeformed configurations and then express the conservation of momentum using these stress measures.

4.4.2.1 The Piola–Kirchhoff stress tensors

The stress tensor σ_{ij} that we have been using so far is called the *Cauchy stress* and it is defined based on a deformed element using the spatial description. The components of $\boldsymbol{\sigma}$ refer to a Cartesian coordinate system. Sometimes it is desirable to define stress measures that refer to the undeformed or reference configuration. In this section, we discuss two such stress measures known as *the first and second Piola–Kirchhoff stresses* (or the 1st P–K and 2nd P–K stresses for short).

In the instantaneous state (at time t), the infinitesimal force $\mathrm{d}P_i$ transmitted in the surface element $\mathrm{d}a_i$ is given by

$$\mathrm{d}p_i = t_i^{(n)}\,\mathrm{d}a = \sigma_{ji} n_j\,\mathrm{d}a = \sigma_{ji}\,\mathrm{d}a_j \quad \text{or} \quad \mathrm{d}\mathbf{p} = \boldsymbol{\sigma}^{\mathrm{T}} \cdot \mathbf{n}\,\mathrm{d}a \tag{4.39}$$

For the same infinitesimal force, we may define a stress vector $t_i^{(0)}$ and a stress tensor $T_{Ri}^{(0)}$ as in the following expressions. Both new stress vector and stress tensor refer to the initial state. Thus,

$$\mathrm{d}p_i = t_i^{(0)}\,\mathrm{d}A = T_{Ri}^{(0)} N_R\,\mathrm{d}A = T_{Ri}^{(0)}\,\mathrm{d}A_R \quad \text{or} \quad \mathrm{d}\mathbf{p} = (\mathbf{T}^{(0)})^{\mathrm{T}} \cdot \mathbf{N}\,\mathrm{d}A \tag{4.40}$$

By comparing (4.39) and (4.40), we see that $t_i^{(n)}$ and $t_i^{(0)}$ act in the same direction but are different in magnitude. $T_{Ri}^{(0)}$ is called the *Lagrangian stress*, or the 1st P–K stress, and it is also known as the *nominal stress*. By use of the Nanson's formula (3.92), we may combine (4.39) and (4.40) to obtain

$$\mathrm{d}p_i = \sigma_{ji}\,\mathrm{d}a_j = \sigma_{ji} J \frac{\partial X_R}{\partial x_j}\mathrm{d}A_R = T_{Ri}^{(0)}\,\mathrm{d}A_R \tag{4.41}$$

From the last two expressions of (4.41), we find the relation between $\mathbf{T}^{(0)}$ and $\boldsymbol{\sigma}$ as

$$T_{Ri}^{(0)} = J\sigma_{ji}\frac{\partial X_R}{\partial x_j} \quad \text{or} \quad \mathbf{T}^{(0)} = J\mathbf{F}^{-1} \cdot \boldsymbol{\sigma} \tag{4.42}$$

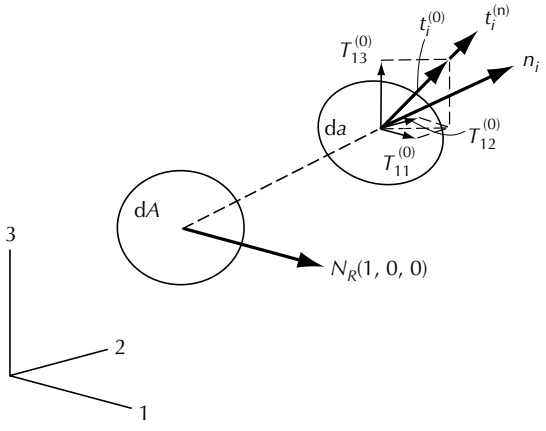

FIGURE 4.2
First P–K stresses.

With the help of tensor bases, (4.42) may be written as

$$\begin{aligned} T_{Ri}^{(0)}\mathbf{e}_R \otimes \mathbf{e}_i &= J\frac{\partial X_R}{\partial x_i}\mathbf{e}_R \otimes \mathbf{e}_i \cdot (\sigma_{mn}\mathbf{e}_m \otimes \mathbf{e}_n) \\ &= J\frac{\partial X_R}{\partial x_i}\sigma_{mn}(\mathbf{e}_R \otimes \mathbf{e}_i) \cdot (\mathbf{e}_m \otimes \mathbf{e}_n) = J\frac{\partial X_R}{\partial x_i}\sigma_{mn}(\mathbf{e}_i \cdot \mathbf{e}_m) \cdot (\mathbf{e}_R \otimes \mathbf{e}_n) \\ &= J\frac{\partial X_R}{\partial x_i}\sigma_{in}\mathbf{e}_R \otimes \mathbf{e}_n = J\sigma_{ji}\frac{\partial X_R}{\partial x_j}\mathbf{e}_R \otimes \mathbf{e}_i \end{aligned} \tag{4.43}$$

The components of (4.43) lead to the first expression of (4.42). It is useful at this point to illustrate the physical significance of the components $T_{Ri}^{(0)}$ of the 1st P–K stress. Consider area element dA with a normal $N_R = [1, 0, 0]$. This area is deformed into da with a normal n_i. The stress vectors $t_i^{(n)}$ and $t_i^{(0)}$ for this case are shown in Figure 4.2. They have the same direction but different magnitudes. The stress vector $t_i^{(0)}$ is then decomposed into components $T_{11}^{(0)}$, $T_{12}^{(0)}$, and $T_{13}^{(0)}$ with respect to the x_i coordinate system. Using a similar procedure, we can consider an area with normal $N_R[0, 1, 0]$ to define $T_{21}^{(0)}$, $T_{22}^{(0)}$, and $T_{23}^{(0)}$; and a similar approach is used to define $T_{31}^{(0)}$, $T_{32}^{(0)}$, and $T_{33}^{(0)}$.

Note that σ_{ij} is symmetric, but, from (4.42), $T_{Ri}^{(0)}$ is not. Since $T_{Ri}^{(0)}$ is not symmetric, this tensor is difficult to use in constitutive equations that are to represent the stress components in terms of the components of the symmetric strain tensor. This difficulty can be avoided by defining a symmetric stress called the *Piola–Kirchhoff stress* (or the 2nd P–K stress), which is now explained. Before the infinitesimal force dp_j transmitted in the deformed configuration is referred to the surface element in the reference configuration, let it be subjected to the same transformation that changes the deformed side dx_i of the surface element da into the corresponding initial side dX_R of dA. That is, we

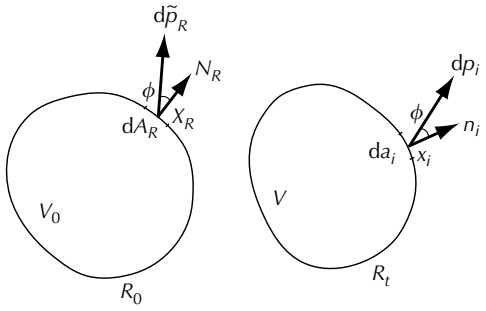

FIGURE 4.3
The fictitious force $d\tilde{p}_R$.

introduce a *fictitious force* (or the pseudo-force) $\mathrm{d}\tilde{p}_R$ such that

$$\mathrm{d}\tilde{p}_R = \frac{\partial X_R}{\partial x_j}\mathrm{d}p_j \tag{4.44}$$

which follows the same transformation as in

$$\mathrm{d}X_R = \frac{\partial X_R}{\partial x_j}\mathrm{d}x_j \tag{4.45}$$

In this operation, the external loading is transformed back to the material description first, and the 2nd P–K stress is then defined per unit undeformed area. The fictitious force $\mathrm{d}\tilde{p}_R$ and the initial area $\mathrm{d}A_R$ have been stretched and rotated the same amount relative to the final position $\mathrm{d}p_i$ and $\mathrm{d}a_i$, respectively. This definition of $\mathrm{d}\tilde{p}_R$ is illustrated in Figure 4.3. Using this fictitious force we now define the 2nd P–K stress tensor Π_{RS} which refers to the initial area $\mathrm{d}A_R$ and the relation is

$$\mathrm{d}\tilde{p}_R = \Pi_{SR}N_S\,\mathrm{d}A = \Pi_{SR}\,\mathrm{d}A_S \quad \text{or} \quad \mathrm{d}\tilde{\mathbf{p}} = \mathbf{\Pi}\cdot\mathbf{N}\,\mathrm{d}A \tag{4.46}$$

Note that the form of (4.46) is similar to that of (4.40). We now proceed to determine the relation between Π_{RS} and σ_{ij}. Substituting (4.39) into (4.44), we have

$$\mathrm{d}\tilde{p}_R = \frac{\partial X_R}{\partial x_j}\sigma_{kj}\,\mathrm{d}a_k = \frac{\partial X_R}{\partial x_j}\sigma_{kj}J\frac{\partial X_S}{\partial x_k}\mathrm{d}A_S \tag{4.47}$$

Comparing (4.46) and (4.47), we obtain

$$\Pi_{RS} = J\sigma_{jk}\frac{\partial X_R}{\partial x_j}\frac{\partial X_S}{\partial x_k} \quad \text{or} \quad \Pi_{RS} = T^{(0)}_{Ri}\frac{\partial X_S}{\partial x_i} \tag{4.48}$$

It is then easy to show that

$$T_{Ri}^{(0)} = \Pi_{RS} \frac{\partial x_i}{\partial X_S} \tag{4.49}$$

which is the relation between $T_{Ri}^{(0)}$ and Π_{RS}. In the symbolic notation, the above relations may be written as

$$\mathbf{\Pi} = J\mathbf{F}^{-1} \cdot \boldsymbol{\sigma} \cdot \mathbf{F}^{-\mathrm{T}} \quad \text{and} \quad \mathbf{\Pi} = \mathbf{T}^{(0)} \cdot \mathbf{F}^{-\mathrm{T}} \qquad \text{where } \mathbf{F}^{-T} = (\mathbf{F}^{-1})^{\mathrm{T}} \tag{4.50}$$

Using the tensor bases, the 2nd P–K stress is written as

$$\mathbf{\Pi} = \Pi_{RS} \mathbf{e}_R \otimes \mathbf{e}_S \tag{4.51}$$

Various stress measures are further discussed in Chapter 11 referring to curvilinear coordinates.

EXAMPLE 4.2 For the problem of simple shearing, if the X_R and the x_i systems coincide, that is, the 1-axis is horizontal and the 2-axis vertical, discuss the directions of $T_{Ri}^{(0)}$ and find the equations relating $T_{Ri}^{(0)}$ to the Cauchy stress σ_{ij} (note that both σ_{ij} and $T_{Ri}^{(0)}$ are Cartesian components).

Solution

Figure 4.4 shows that a square element is deformed into a parallelogram by simple shearing. The initial areas for Face 1 and Face 2 of the square element are $\mathrm{d}A^{(1)}$ and $\mathrm{d}A^{(2)}$ and they are deformed into $\mathrm{d}a^{(1)}$ and $\mathrm{d}a^{(2)}$, respectively. The unit normal to the areas are $N_R^{(1)}$ and $N_R^{(2)}$ and they are deformed into $n_i^{(1)}$ and $n_i^{(2)}$, respectively. We now consider the forces and stress components acting on the two faces of the element.

On face 1: The unit normals are $N_R^{(1)} = [1, 0]$ and $n_i^{(1)} = [\cos\gamma, -\sin\gamma]$, where γ is the shearing angle of the element shown in Figure 4.4. The initial and deformed areas are related by

$$\mathrm{d}a^{(1)} \cos\gamma = \mathrm{d}A^{(1)} \tag{a}$$

Using (4.39), the infinitesimal force acting on this face is

$$\mathrm{d}p_i^{(1)} = t_i^{(n)1}\, \mathrm{d}a^{(1)} = \sigma_{ji} n_j^{(1)}\, \mathrm{d}a^{(1)} = (\sigma_{1i} n_1^{(1)} + \sigma_{2i} n_2^{(1)})\, \mathrm{d}a^{(1)} \tag{b}$$

On the other hand, the same force may be expressed in terms of (4.40) as

$$\mathrm{d}p_i^{(1)} = t_i^{(0)1}\, \mathrm{d}A^{(1)} = T_{Ri}^{(0)} N_R^{(1)}\, \mathrm{d}A^{(1)} = T_{1i}^{(0)}\, \mathrm{d}A^{(1)} \tag{c}$$

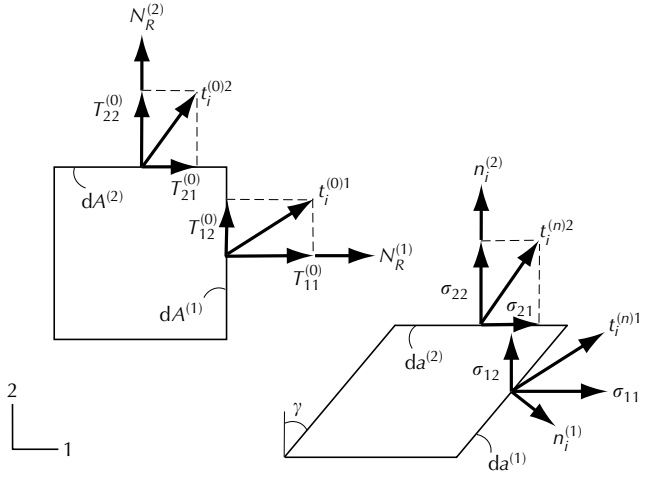

FIGURE 4.4
Stress components in simple shearing.

By comparing (b) and (c), we obtain

$$(\sigma_{1i} n_1^{(1)} + \sigma_{2i} n_2^{(1)})\, da^{(1)} = T_{1i}^{(0)}\, dA^{(1)} \tag{d}$$

which, by use of (a), may be simplified to yield

$$\sigma_{1i} \cos\gamma + \sigma_{2i}(-\sin\gamma) = T_{1i}^{(0)} \cos\gamma \tag{e}$$

From (e), we obtain

$$T_{11}^{(0)} = \sigma_{11} - \sigma_{21} \tan\gamma \quad \text{and} \quad T_{12}^{(0)} = \sigma_{12} - \sigma_{22} \tan\gamma \tag{f}$$

On face 2: The unit normals are $N_R^{(2)} = [0, 1]$ and $n_R^{(2)} = [0, 1]$, and the area does not change, so that $da^{(2)} = dA^{(2)}$. Following the same procedure as in Face 1, we find

$$dp_i^{(2)} = t_i^{(n)2}\, da^{(2)} = \sigma_{ji} n_j^{(2)}\, da^{(2)} = \sigma_{2i} n_2^{(2)}\, da^{(2)} = \sigma_{2i}\, da^{(2)} \tag{g}$$

$$dp_i^{(2)} = t_i^{(0)2}\, dA^{(2)} = T_{Ri}^{(0)} N_R^{(2)}\, dA^{(2)} = T_{2i}^{(0)} N_2^{(2)}\, dA^{(2)} = T_{2i}^{(0)}\, dA^{(2)} \tag{h}$$

From (g) and (h), we obtain

$$\sigma_{2i}\, da^{(2)} = T_{2i}^{(0)}\, dA^{(2)} = T_{2i}^{(0)}\, da^{(2)} \qquad \text{with } dA^{(2)} = da^{(2)} \tag{i}$$

Therefore, we find

$$\sigma_{2i} = T_{2i}^{(0)}, \qquad \sigma_{21} = T_{21}^{(0)}, \qquad \sigma_{22} = T_{22}^{(0)} \tag{j}$$

We now summarize the stress components found from (f) and (j) as

$$T_{11}^{(0)} = \sigma_{11} - \sigma_{21}\tan\gamma, \qquad T_{22}^{(0)} = \sigma_{22}, \qquad T_{12}^{(0)} = \sigma_{12} - \sigma_{22}\tan\gamma$$

$$T_{21}^{(0)} = \sigma_{21} = \sigma_{12} \quad \text{and} \quad T_{12}^{(0)} \neq T_{21}^{(0)} \tag{k}$$

We remark that on Face 1, the normal $\mathbf{n}^{(1)}$ is not in the direction of any x_i axis. The stress vector $\mathbf{t}^{(n)1}$ is further related to vectors $\mathbf{t}_i$, by use of (2.6), acting on cross-sections of the material element that are parallel to the coordinate planes of the x_i system, and the vectors $\mathbf{t}_i$ further define the components of the Cauchy stress. On the other hand, since $\mathbf{N}^{(1)}$ is in the direction of X_1, $\mathbf{t}^{(0)1}$ is already acting on a plane parallel to a coordinate plane, and, therefore, its components with respect to the x_i system define the $T_{Ri}^{(0)}$ stress.

EXAMPLE 4.3 Find the stress components of Example 4.2 using (4.42).

Solution

From (3.20), the simple shear may be described by

$$x_1 = X_1 + X_2\tan\gamma, \quad x_2 = X_2 \tag{a}$$

The deformation gradient is

$$[F] = \begin{bmatrix} 1 & \tan\gamma \\ 0 & 1 \end{bmatrix} \qquad \text{with } J = |\mathbf{F}| = 1 \tag{b}$$

From (4.42), we write

$$\sigma_{ij} = J^{-1}\frac{\partial x_i}{\partial X_R}T_{Rj}^{(0)} = F_{iR}T_{Rj}^{(0)} \tag{c}$$

The components are

$$\sigma_{11} = F_{1R}T_{R1}^{(0)} = F_{11}T_{11}^{(0)} + F_{12}T_{21}^{(0)} = T_{11}^{(0)} + T_{21}^{(0)}\tan\gamma \tag{d}$$

$$\sigma_{12} = F_{1R}T_{R2}^{(0)} = F_{11}T_{12}^{(0)} + F_{12}T_{22}^{(0)} = T_{12}^{(0)} + T_{22}^{(0)}\tan\gamma \tag{e}$$

$$\sigma_{21} = F_{2R}T_{R1}^{(0)} = F_{21}T_{11}^{(0)} + F_{22}T_{21}^{(0)} = T_{21}^{(0)} \tag{f}$$

$$\sigma_{22} = F_{2R}T_{R2}^{(0)} = F_{21}T_{12}^{(0)} + F_{22}T_{22}^{(0)} = T_{22}^{(0)} \tag{g}$$

These results are the same as those obtained in Example 4.2.

EXAMPLE 4.4 For the problem of simple shearing discussed in Example 4.2, find the components of the 2nd P–K stress Π_{RS}.

Solution

Using the expression for $\mathbf{F}$ found in Example 4.3 and noting that $J = |\mathbf{F}| = 1$, we find

$$[F]^{-1} = \frac{\partial X_S}{\partial x_k} = \begin{bmatrix} 1 & -\tan\gamma \\ 0 & 1 \end{bmatrix} \tag{a}$$

From (4.50) we have

$$\Pi_{RS} = T^{(0)}_{Ri} \frac{\partial X_S}{\partial x_i} \tag{b}$$

Using (a), (b) reduces to

$$[\Pi] = \begin{bmatrix} T^{(0)}_{11} - T^{(0)}_{12}\tan\gamma & T^{(0)}_{12} \\ T^{(0)}_{21} - T^{(0)}_{22}\tan\gamma & T^{(0)}_{22} \end{bmatrix} \tag{c}$$

Using (k) of Example 4.2, we obtain from (c)

$$\begin{aligned} \Pi_{11} &= T^{(0)}_{11} - T^{(0)}_{12}\tan\gamma = \sigma_{11} - 2\sigma_{12}\tan\gamma + \sigma_{22}\tan^2\gamma \\ \Pi_{12} &= T^{(0)}_{12} = \sigma_{12} - \sigma_{22}\tan\gamma \\ \Pi_{21} &= T^{(0)}_{21} - T^{(0)}_{22}\tan\gamma = \sigma_{12} - \sigma_{22}\tan\gamma = \Pi_{12} \\ \Pi_{22} &= T^{(0)}_{22} = \sigma_{22} \end{aligned} \tag{d}$$

EXAMPLE 4.5 In the case of uniform extension along the 1-direction, the applied tensile force is P, shown in Figure 4.5(a); the initial dimensions of the rectangular bar are $X_1 \times X_2 \times X_3$ with cross-sectional area A; and the current dimensions are $x_1 \times x_2 \times x_3$ with cross-sectional area a. Find the components of $\boldsymbol{\sigma}$, $\mathbf{T}^{(0)}$, and $\boldsymbol{\Pi}$.

Solution

Consider the deformation

$$x_1 = \lambda_1 X_1, \qquad x_2 = \lambda_2 X_2, \qquad x_3 = \lambda_3 X_3 \tag{a}$$

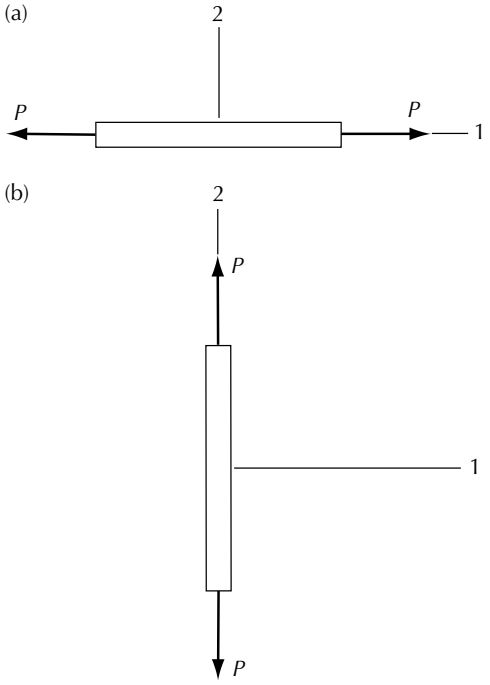

FIGURE 4.5
Effect of rotation on stress components.

The deformation gradient is

$$[F] = \begin{bmatrix} \lambda_1 & 0 & 0 \\ 0 & \lambda_2 & 0 \\ 0 & 0 & \lambda_3 \end{bmatrix} \qquad [F^{-1}] = \begin{bmatrix} \dfrac{1}{\lambda_1} & 0 & 0 \\ 0 & \dfrac{1}{\lambda_2} & 0 \\ 0 & 0 & \dfrac{1}{\lambda_3} \end{bmatrix} \tag{b}$$

and $J = \det \mathbf{F} = \lambda_1\lambda_2\lambda_3$. The components of the Cauchy stress are

$$\sigma_{11} = \frac{P}{a}, \qquad \text{other components} = 0 \tag{c}$$

The components of the 1st P–K stress may be found from (4.42) in the matrix form as

$$[T^{(0)}] = J[F^{-1}][\sigma] \tag{d}$$

and the components of the 2nd P–K stress may be found from (4.50) in the matrix form as

$$[\Pi] = J[F^{-1}][\sigma][F^{-T}] \tag{e}$$

Substituting the above information into (d) and (e) and performing the matrix multiplications, we obtain

$$T^{(0)}_{Ri} = (\lambda_1\lambda_2\lambda_3)\begin{bmatrix} \dfrac{\sigma_{11}}{\lambda_1} & 0 & 0 \\ 0 & 0 & 0 \\ 0 & 0 & 0 \end{bmatrix}, \qquad \Pi_{RS} = (\lambda_1\lambda_2\lambda_3)\begin{bmatrix} \dfrac{\sigma_{11}}{\lambda_1^2} & 0 & 0 \\ 0 & 0 & 0 \\ 0 & 0 & 0 \end{bmatrix} \tag{f}$$

The nonzero term of $T^{(0)}$ is

$$T^{(0)}_{11} = \lambda_2\lambda_3\sigma_{11} = \frac{x_2}{X_2}\frac{x_3}{X_3}\sigma_{11} = \frac{a}{A}\sigma_{11} = \frac{a}{A}\left(\frac{P}{a}\right) = \frac{P}{A}$$

It is seen that $T^{(0)}_{11}$ is the nominal stress, that is, force over initial area, but σ_{11} is the true stress. This physical interpretation of $\mathbf{T}^{(0)}$ is good only for deformation that does not involve rotation. In the case of simple shear, as discussed in Example 4.2, no such assertion can be made about the 1st P–K stress.

The nonzero component of Π_{RS} is

$$\Pi_{11} = (\lambda_1\lambda_2\lambda_3)\frac{\sigma_{11}}{\lambda_1^2} = \frac{\lambda_2\lambda_3}{\lambda_1}\sigma_{11} = \frac{a}{A}\frac{\sigma_{11}}{\lambda_1} = \frac{a}{A}\frac{P}{a}\frac{1}{\lambda_1} = \frac{1}{\lambda_1}\left(\frac{P}{A}\right) \tag{g}$$

We see from (g) that no clear physical meaning can be associated with Π_{11}. However, from (4.44), the fictitious force is

$$[\mathrm{d}\tilde{p}] = [F^{-1}][\mathrm{d}p] = \begin{bmatrix} \dfrac{1}{\lambda_1} & 0 & 0 \\ 0 & \dfrac{1}{\lambda_2} & 0 \\ 0 & 0 & \dfrac{1}{\lambda_3} \end{bmatrix}\begin{bmatrix} P \\ 0 \\ 0 \end{bmatrix} = \begin{bmatrix} \dfrac{P}{\lambda_1} \\ 0 \\ 0 \end{bmatrix} \tag{h}$$

Thus, (g) may be written as

$$\Pi_{11} = \frac{\mathrm{d}\tilde{p}_{11}}{A} \tag{i}$$

It is the component of the fictitious force $[\mathrm{d}\tilde{p}]$ in the X_1 direction divided by the initial cross-sectional area A.

EXAMPLE 4.6 Referring to Example 4.5 and Figure 4.5(b), if, after the stretch, the specimen is rotated 90° counterclockwise and the traction P also rotates with it, determine the expressions for the Cauchy stress, the 1st P–K stress, and the 2nd P–K stress components after rotation and thereafter discuss the physical meaning of the three stress tensors.

Solution

Let us call the initial stretching of the specimen discussed in Example 4.5 stage 1, and the quantities of this stage are denoted by

$$[F^{(1)}] = \begin{bmatrix} \lambda_1 & 0 & 0 \\ 0 & \lambda_2 & 0 \\ 0 & 0 & \lambda_3 \end{bmatrix} \qquad [\sigma^{(1)}] = \begin{bmatrix} \dfrac{P}{a} & 0 & 0 \\ 0 & 0 & 0 \\ 0 & 0 & 0 \end{bmatrix}$$

$$[T^{0(1)}] = (\lambda_1\lambda_2\lambda_3) \begin{bmatrix} \dfrac{\sigma_{11}}{\lambda_1} & 0 & 0 \\ 0 & 0 & 0 \\ 0 & 0 & 0 \end{bmatrix} = \begin{bmatrix} \dfrac{P}{A} & 0 & 0 \\ 0 & 0 & 0 \\ 0 & 0 & 0 \end{bmatrix} \tag{a}$$

$$[\Pi^{(1)}] = (\lambda_1\lambda_2\lambda_3) \begin{bmatrix} \dfrac{\sigma_{11}}{\lambda_1^2} & 0 & 0 \\ 0 & 0 & 0 \\ 0 & 0 & 0 \end{bmatrix} = \begin{bmatrix} \dfrac{P}{A\lambda_1} & 0 & 0 \\ 0 & 0 & 0 \\ 0 & 0 & 0 \end{bmatrix}$$

We now apply a rotation $\mathbf{Q}$ to various tensors to obtain the quantities of the second stage denoted by

$$\mathbf{F}^{(2)} = \mathbf{Q} \cdot \mathbf{F}^{(1)}, \qquad \boldsymbol{\sigma}^{(2)} = \mathbf{Q} \cdot \boldsymbol{\sigma}^{(1)} \cdot \mathbf{Q}^{\mathrm{T}}$$

$$\begin{aligned} \mathbf{T}^{0(2)} &= \mathbf{J}[\mathbf{F}^{(2)}]^{-1} \cdot \boldsymbol{\sigma}^{(2)} = \mathbf{J}[\mathbf{F}^{(1)}]^{-1} \cdot \mathbf{Q}^{-1} \cdot \mathbf{Q} \cdot \boldsymbol{\sigma}^{(1)} \cdot \mathbf{Q}^{\mathrm{T}} \\ &= \mathbf{J}[\mathbf{F}^{(1)}]^{-1} \cdot \boldsymbol{\sigma}^{(1)} = \mathbf{T}^{0(1)} \cdot \mathbf{Q}^{\mathrm{T}} \\ \boldsymbol{\Pi}^{(2)} &= \mathbf{T}^{0(2)} \cdot [\mathbf{F}^{(2)}]^{-\mathrm{T}} = \mathbf{T}^{0(1)} \cdot \mathbf{Q}^{\mathrm{T}} \cdot [[\mathbf{F}^{(1)}]^{-1} \cdot \mathbf{Q}^{-1}]^{\mathrm{T}} \\ &= \mathbf{T}^{0(1)} \cdot \mathbf{Q}^{\mathrm{T}} \cdot [\mathbf{Q}^{-1}]^{\mathrm{T}} \cdot [\mathbf{F}^{(1)}]^{-\mathrm{T}} \\ &= \mathbf{T}^{0(1)} \cdot [\mathbf{Q}^{-1} \cdot \mathbf{Q}]^{\mathrm{T}} \cdot [\mathbf{F}^{(1)}]^{-\mathrm{T}} = \mathbf{T}^{0(1)} \cdot [\mathbf{F}^{(1)}]^{-\mathrm{T}} = \boldsymbol{\Pi}^{(1)} \end{aligned} \tag{b}$$

It is seen from (b) that under a rotation $\mathbf{Q}$, the Cauchy stress $\boldsymbol{\sigma}$ transforms like a second-rank tensor; the 1st P–K stress transforms like a first-rank tensor; and the 2nd P–K stress transforms like a tensor of rank zero.

For this example, the rotation is

$$[Q] = \begin{bmatrix} 0 & -1 & 0 \\ 1 & 0 & 0 \\ 0 & 0 & 1 \end{bmatrix} \tag{c}$$

Using (c) in (b), the stresses in stage 2 are

$$[\sigma^{(2)}] = [Q][\sigma^{(1)}][Q]^{\mathrm{T}}$$

$$= \begin{bmatrix} 0 & -1 & 0 \\ 1 & 0 & 0 \\ 0 & 0 & 1 \end{bmatrix} \begin{bmatrix} \frac{P}{a} & 0 & 0 \\ 0 & 0 & 0 \\ 0 & 0 & 0 \end{bmatrix} \begin{bmatrix} 0 & 1 & 0 \\ -1 & 0 & 0 \\ 0 & 0 & 1 \end{bmatrix} = \begin{bmatrix} 0 & 0 & 0 \\ 0 & \frac{P}{a} & 0 \\ 0 & 0 & 0 \end{bmatrix} \tag{d}$$

$$[T^{0(2)}] = [T^{0(1)}][Q]^{\mathrm{T}} = \begin{bmatrix} \frac{P}{A} & 0 & 0 \\ 0 & 0 & 0 \\ 0 & 0 & 0 \end{bmatrix} \begin{bmatrix} 0 & 1 & 0 \\ -1 & 0 & 0 \\ 0 & 0 & 1 \end{bmatrix} = \begin{bmatrix} 0 & \frac{P}{A} & 0 \\ 0 & 0 & 0 \\ 0 & 0 & 0 \end{bmatrix} \tag{e}$$

$$[\Pi^{(2)}] = [\Pi^{(1)}] = \begin{bmatrix} \frac{P}{A\lambda_1} & 0 & 0 \\ 0 & 0 & 0 \\ 0 & 0 & 0 \end{bmatrix} \tag{f}$$

We see from (d) that the Cauchy stress has a nonzero component in

$$\sigma_{22}^{(2)} = \frac{P}{a} \tag{g}$$

which still lives up to the interpretation of true stress even after the rotation. From (e), we see that the 1st P–K stress has only one nonzero component in

$$T_{12}^{0(2)} = \frac{P}{A}, \qquad \text{other } T_{Ri}^{0(2)} = 0 \tag{h}$$

The second subscript $i = 2$ indicates that the force P is in the 2-direction, while the first subscript $R = 1$ indicates that this 1st P–K stress component lies on an undeformed area with normal $\mathbf{N} = [1, 0, 0]$. This nonzero component is, therefore, a shear stress and it indicates that the interpretation of nominal stress is no longer appropriate, since a normal stress turns into a shear stress due to rotation.

We see from (f) that the 2nd P–K stress does not change due to the imposed rotation. A normal stress before rotation remains a normal stress and a shear stress before rotation remains a shear stress. It is useful from computational viewpoint to define the 2nd P–K stress, because it is symmetric, it does not change due to imposed rotation, and it is the energy conjugate of Lagrangian

strain **E** (the concept of work conjugate will be discussed in Section 4.4.3). We note, however, that the physical meaning of the 2nd P–K stress is not clear. In equation (i) of Example 4.5, the 11 component of this stress is the fictitious force divided by initial area A. The fictitious force $\mathrm{d}\tilde{p}_R$ involves stretching and rotation of $\mathrm{d}p_i$ and, therefore, the 2nd P–K stress does not have the physical meaning of a pure stress. For this reason the 2nd P–K stress should not be used to define the yield criterion, the fracture criterion, or to set up material instability conditions.

4.4.2.2 Conservation of momentum

From (4.39) and (4.40) we have

$$t_i^{(\mathrm{n})}\,\mathrm{d}a = \sigma_{ji} n_j\,\mathrm{d}a = T_{Ri}^{(0)} N_R\,\mathrm{d}A \tag{4.52}$$

Integrating (4.52) over the surface of the body, we write

$$\int_S \sigma_{ij} n_i\,\mathrm{d}a = \int_{S_0} T_{Ri}^{(0)} N_R\,\mathrm{d}A = \int_{V_0} \frac{\partial T_{Ri}^{(0)}}{\partial X_R}\,\mathrm{d}V_0 \tag{4.53}$$

Let B_i be the body force per unit volume of the undeformed body, we then write

$$B_i\,\mathrm{d}V_0 = b_i\,\mathrm{d}V \quad \text{or} \quad B_i = b_i \frac{\mathrm{d}V}{\mathrm{d}V_0} = b_i J \tag{4.54}$$

Integrating (4.54) over the undeformed volume of the body, the resulting total body force is

$$\int_{V_0} B_i\,\mathrm{d}V_0 \tag{4.55}$$

We note that in the above equations, the forces are applied to the deformed body, although the integrals are over the undeformed body V_0. The momentum is also referred to the deformed body V at time t, and the rate of change of linear momentum is

$$\frac{\mathrm{D}}{\mathrm{D}t}\int_V \rho v_i\,\mathrm{d}V = \frac{\mathrm{D}}{\mathrm{D}t}\int_{V_0} \rho_0 v_i\,\mathrm{d}V_0 = \int_{V_0} \rho_0 \frac{\mathrm{D}v_i}{\mathrm{D}t}\mathrm{d}V_0 \tag{4.56}$$

Using (4.53), (4.55) and (4.56), the conservation of linear momentum is now

$$\int_{V_0} \rho_0 \frac{\mathrm{D}v_i}{\mathrm{D}t}\mathrm{d}V_0 = \int_{V_0} \frac{\partial T_{Ri}^{(0)}}{\partial X_R}\mathrm{d}V_0 + \int_{V_0} B_i\,\mathrm{d}V_0 \tag{4.57}$$

which leads to the following equation of motion in the material description

$$\frac{\partial T_{Ri}^{(0)}}{\partial X_R} + B_i = \rho_0 \frac{\mathrm{D}v_i}{\mathrm{D}t} \tag{4.58}$$

In terms of the 2nd P–K stress, the equation of motion becomes

$$\frac{\partial}{\partial X_R}\left(\Pi_{RS}\frac{\partial x_i}{\partial X_S}\right) + B_i = \rho_0 \frac{\mathrm{D}v_i}{\mathrm{D}t} \tag{4.59}$$

4.4.3 The Conservation of Energy

The spatial description for the conservation of energy is given in (4.31). Referring to the undeformed state, this equation can be written as

$$\begin{aligned}&\frac{\mathrm{D}}{\mathrm{D}t}\int_{V_0}\rho_0\varepsilon\,\mathrm{d}V_0 + \frac{\mathrm{D}}{\mathrm{D}t}\int_{V_0}\frac{1}{2}\rho_0 v_i v_i\,\mathrm{d}V_0\\ &\quad= \int_{V_0} B_i v_i\,\mathrm{d}V_0 + \int_{S_0} T_{Ri}^{(0)} N_R v_i\,\mathrm{d}S_0 - \int_{S_0} h_R N_R\,\mathrm{d}S_0 + \frac{\mathrm{D}}{\mathrm{D}t}\int_{V_0}\rho_0 q\,\mathrm{d}V_0\end{aligned} \tag{4.60}$$

where h_R is the component of the heat flux vector referring to the material coordinates, so that $h_R = (\partial X_R/\partial x_i)\mathbf{h}_i$. The energy balance equation (4.60) further becomes

$$\begin{aligned}&\int_{V_0}\rho_0\frac{\mathrm{D}\varepsilon}{\mathrm{D}t}\mathrm{d}V_0 + \int_{V_0}\rho_0 v_i\frac{\mathrm{D}v_i}{\mathrm{D}t}\mathrm{d}V_0\\ &\quad= \int_{V_0} B_i v_i\,\mathrm{d}V_0 + \int_{V_0}\left(v_i\frac{\partial T_{Ri}^{(0)}}{\partial X_R} + T_{Ri}^{(0)}\frac{\partial v_i}{\partial X_R}\right)\mathrm{d}V_0\\ &\qquad- \int_{V_0}\frac{\partial h_R}{\partial X_R}\mathrm{d}V_0 + \int_{V_0}\rho_0\frac{\mathrm{D}q}{\mathrm{D}t}\mathrm{d}V_0\end{aligned} \tag{4.61}$$

Three terms in the above equation cancel out due to the equation of motion (4.58). We then obtain

$$\int_{V_0}\left(\rho_0\frac{\mathrm{D}\varepsilon}{\mathrm{D}t} - T_{Ri}^{(0)}\frac{\partial v_i}{\partial X_R} + \frac{\partial h_R}{\partial X_R} - \rho_0\frac{\mathrm{D}q}{\mathrm{D}t}\right)\mathrm{d}V_0 = 0 \tag{4.62}$$

which leads to the conservation of energy in the local form as

$$\rho_0\frac{\mathrm{D}\varepsilon}{\mathrm{D}t} = T_{Ri}^{(0)}\frac{\partial v_i}{\partial X_R} - \frac{\partial h_R}{\partial X_R} + \rho_0\frac{\mathrm{D}q}{\mathrm{D}t} \tag{4.63}$$

The rate of work term on the right-hand side of (4.63) should be discussed further. This term represents part of work rate that affects the strain energy of a material element (the idea of strain energy is discussed in the later sections of this chapter). This term is sometimes called the specific rate of work per unit mass or the stress power. In this term, the rate of work $\dot{w}$ is obtained using the 1st P–K stress, which may be expressed in terms of the 2nd P–K stress using (4.49). Thus,

$$T^{(0)}_{Ri}\frac{\partial v_i}{\partial X_R} = T^{(0)}_{Ri}\frac{\partial}{\partial X_R}\left(\frac{\mathrm{D}x_i}{\mathrm{D}t}\right) = T^{(0)}_{Ri}\frac{\mathrm{D}}{\mathrm{D}t}\left(\frac{\partial x_i}{\partial X_R}\right) = T^{(0)}_{Ri}\frac{\mathrm{D}F_{iR}}{\mathrm{D}t} \tag{4.64}$$

$$\begin{aligned} T^{(0)}_{Ri}\frac{\partial v_i}{\partial X_R} &= \Pi_{RS}\frac{\partial x_i}{\partial X_S}\frac{\partial v_i}{\partial X_R} = \Pi_{RS}\frac{\partial x_i}{\partial X_S}\frac{\partial v_i}{\partial x_r}\frac{\partial x_r}{\partial X_R} \\ &= \frac{1}{2}\left(\frac{\partial v_i}{\partial x_r} + \frac{\partial v_r}{\partial x_i}\right)\Pi_{RS}\frac{\partial x_i}{\partial X_S}\frac{\partial x_r}{\partial X_R} = \Pi_{RS}\left(D_{ir}\frac{\partial x_i}{\partial X_S}\frac{\partial x_r}{\partial X_R}\right) = \Pi_{RS}\frac{DE_{RS}}{\mathrm{D}t} \end{aligned} \tag{4.65}$$

Equation (3.200) was used in the last expression of (4.65). In addition, $\dot{w}$ may also be expressed in terms of the Cauchy stress. Using (4.42), we write

$$T^{(0)}_{Ri}\frac{\partial v_i}{\partial X_R} = \frac{\rho_0}{\rho}\sigma_{ji}\frac{\partial X_R}{\partial x_j}\frac{\partial v_i}{\partial X_R} = \frac{\rho_0}{\rho}\sigma_{ji}\frac{\partial v_i}{\partial x_j} = \frac{\rho_0}{\rho}\sigma_{ji}D_{ij} \tag{4.66}$$

We conclude from (4.64 to 4.66) that the specific rate of work per unit mass may be written as

$$\dot{w} = \frac{1}{\rho}\sigma_{ij}\mathrm{D}_{ij} = \frac{1}{\rho_0}T^{(0)}_{Ri}\frac{\mathrm{D}F_{iR}}{\mathrm{D}t} = \frac{1}{\rho_0}\Pi_{RS}\frac{\mathrm{D}E_{RS}}{\mathrm{D}t} \tag{4.67}$$

We have thus found three pairs of *work (or energy) conjugates*. They are $\boldsymbol{\sigma}$ and $\mathbf{D}$, $\mathbf{T}^{(0)}$ and $\mathbf{F}$, and $\boldsymbol{\Pi}$ and $\mathbf{E}$. The conjugate stress and strain should be used in any formulation of continuum mechanics problems.

Using (4.67), the energy balance equation can also be written as

$$\rho_0\frac{\mathrm{D}\varepsilon}{\mathrm{D}t} = \Pi_{RS}\frac{\mathrm{D}E_{RS}}{\mathrm{D}t} - \frac{\partial h_R}{\partial X_R} + \rho_0\frac{\mathrm{D}q}{\mathrm{D}t} \tag{4.68}$$

4.5 Objective Tensors

Only objective tensors are used to formulate the constitutive equations. *Objectivity* is also known as *reference frame indifference*. Tensor quantities that depend only on the orientation of the spatial reference frame, which is given by $\mathbf{Q}$, and not on the other aspects of the motion of the reference frame

(e.g., translation, velocity and acceleration, angular velocity and angular acceleration) are said to be indifferent, or objective. Consider two observers each having his/her own reference frame. Components of a tensor observed by two different observers are different. This difference is due to the different orientations of the observers but not to relative motions between the observers. In this contest, we are not talking about the change of coordinate system (each observer is free to choose a coordinate system), but are concerned with the change of observer positions and orientations, or the change of reference frame. Therefore, in the discussion of objectivity, transformation of coordinate system does not play any part.

The reference frame of an observer may be conveniently denoted by $(\mathrm{o}, \mathbf{x})$, where $\mathbf{x}$ is a spatial coordinate system with origin O. We may imagine that one observer is attached to the continuous body and moves with the body and the other observer is stationary. Then, the two reference frames attached to the two observers are differed by a translation of the origin and a rotation of orientation. In the general case, both observers may not be stationary. Let us introduce two reference frames $(\mathrm{o}, \mathbf{x})$ and $(\bar{\mathrm{o}}, \bar{\mathbf{x}})$ as shown in Figure 4.6. Consider a particle P in the body. The position vector of the particle in $(\bar{\mathrm{o}}, \bar{\mathbf{x}})$ at time t is $\bar{\mathbf{x}}$ and that of the same particle in $(\mathrm{o}, \mathbf{x})$ at time t is $\mathbf{x}$. The latter vector is seen by an observer sitting in $(\bar{\mathrm{o}}, \bar{\mathbf{x}})$ as $\mathbf{Q}^{\mathrm{T}} \cdot \mathbf{x}$. These position vectors are thus related by

$$\bar{\mathbf{x}} = \mathbf{c}(t) + \mathbf{Q}^{\mathrm{T}} \cdot \mathbf{x} \quad \text{or} \quad \bar{x}_i = c_i + Q_{ji} x_j \tag{4.69}$$

where $\mathbf{c}$ is the position vector of o in $(\bar{\mathrm{o}}, \bar{\mathbf{x}})$ and $\mathbf{Q}$ is an orthogonal tensor that gives the orientation of $(\mathrm{o}, \mathbf{x})$ relative to $(\bar{\mathrm{o}}, \bar{\mathbf{x}})$. Thus, $(\mathrm{o}, \mathbf{x})$ is different from $(\bar{\mathrm{o}}, \bar{\mathbf{x}})$ by a rigid-body translation $\mathbf{c}$ and **a** rotation $\mathbf{Q}$.

Definiton of objective tensors

A scalar f, a vector $\mathbf{v}$, and a second-rank tensor $\mathbf{T}$ are objective, if for reference frames $(\bar{\mathrm{o}}, \bar{\mathbf{x}})$ and $(\mathrm{o}, \mathbf{x})$, related by (4.69), the corresponding scalar $\bar{f}$, vector $\bar{\mathbf{v}}$,

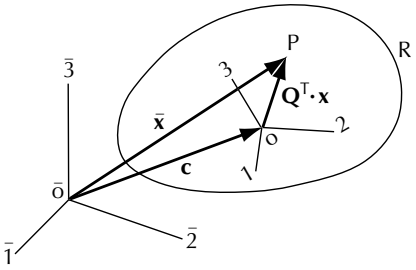

FIGURE 4.6
Rotation of reference frames.

and tensor $\bar{\mathbf{T}}$ are related by

$$\bar{f} = f \qquad \text{(scalar)} \tag{4.70}$$

$$\bar{\mathbf{v}} = \mathbf{Q}^{\mathrm{T}} \cdot \mathbf{v} \quad \text{or} \quad \bar{v}_i = Q_{ji} v_j \qquad \text{(vector)} \tag{4.71}$$

$$\bar{\mathbf{T}} = \mathbf{Q}^{\mathrm{T}} \cdot \mathbf{T} \cdot \mathbf{Q} \quad \text{or} \quad \bar{T}_{ij} = Q_{ri} Q_{sj} T_{rs} \qquad \text{(tensor)} \tag{4.72}$$

We note that a rotation of the body is equivalent to the rotation of the reference frame of the same magnitude but in opposite direction (see Section 1.6). Therefore, if we consider a rigid rotation of the body with fixed reference frame, then (4.69) to (4.72) become

$$\bar{\mathbf{x}} = \mathbf{c}(t) + \mathbf{Q} \cdot \mathbf{x} \tag{4.73}$$

$$\bar{f} = f \qquad \text{(scalar)} \tag{4.74}$$

$$\bar{\mathbf{v}} = \mathbf{Q} \cdot \mathbf{v} \qquad \text{(vector)} \tag{4.75}$$

$$\bar{T} = \mathbf{Q} \cdot \mathbf{T} \cdot \mathbf{Q}^{\mathrm{T}} \qquad \text{(tensor)} \tag{4.76}$$

Either (4.69)–(4.72) or (4.73)–(4.76) may be used to define objectivity. Since the objectivity should be valid for *any* rotation $\mathbf{Q}$, we shall make no effort to specify the sense of rotation, when the objectivity of a quantity is being investigated.

4.6 Property of Deformation and Motion Tensors Under Reference Frame Transformation

We investigate the transformation property of tensors $\mathbf{F}$, $\mathbf{C}$, $\mathbf{B}$, $\mathbf{v}$, $\mathbf{L}$, $\mathbf{D}$, and $\mathbf{W}$. Using (4.69), the transformation equation for F_{iR} is

$$\bar{F}_{iR} = \frac{\partial \bar{x}_i}{\partial X_R} = \frac{\partial \bar{x}_i}{\partial x_k} \frac{\partial x_k}{\partial X_R} = Q_{ki}(t) \frac{\partial x_k}{\partial X_R} = Q_{ki} F_{kR} \tag{4.77}$$

which may be written in the matrix form as

$$[\bar{F}] = [Q]^{\mathrm{T}} [F] \tag{4.78}$$

that is, $\mathbf{F}$ behaves like a vector in a rotation $\mathbf{Q}^{\mathrm{T}}$ of the body or a rotation $\mathbf{Q}$ of the spatial reference frame. Note that since $\mathbf{Q}$ is arbitrary, we can use either $\mathbf{Q}$ or $\mathbf{Q}^{\mathrm{T}}$ in the discussion of objectivity. Even though $\mathbf{F}$ is a second-rank tensor, it transforms as a vector in the reference frame transformation (also referred to as the *observer transformation*). This rule of transformation should be expected, because only subscript i in F_{iR} refers to the spatial reference frame.

In the case of **C**, the expression is

$$\bar{C}_{RS} = \frac{\partial \bar{x}_m}{\partial X_R}\frac{\partial \bar{x}_m}{\partial X_S} = Q_{km}\frac{\partial x_k}{\partial X_R}Q_{nm}\frac{\partial x_n}{\partial X_S} = Q_{km}Q_{nm}\frac{\partial x_k}{\partial X_R}\frac{\partial x_n}{\partial X_S}$$
$$= \delta_{kn}\frac{\partial x_k}{\partial X_R}\frac{\partial x_n}{\partial X_S} = \frac{\partial x_k}{\partial X_R}\frac{\partial x_k}{\partial X_S} = C_{RS} \tag{4.79}$$

Thus, **C** transforms like a scalar in the observer transformation. The left Cauchy–Green deformation tensor **B** transforms like

$$\bar{B}_{ij} = \frac{\partial \bar{x}_i}{\partial X_R}\frac{\partial \bar{x}_j}{\partial X_R} = Q_{ki}\frac{\partial x_k}{\partial X_R}Q_{mj}\frac{\partial x_m}{\partial X_R} = Q_{ki}Q_{mj}B_{km} \tag{4.80}$$

which may be written in the matrix form as

$$[\bar{B}] = [Q]^{\mathrm{T}}[B][Q] \tag{4.81}$$

Thus, **B** transforms like a second-order tensor in the observer transformation.

Consider now the observer transformation of velocity v_i. Differentiating (4.69), we have

$$\frac{\mathrm{D}\bar{x}_i}{\mathrm{D}t} = \bar{v}_i = Q_{ji}v_j + \dot{Q}_{ji}x_j \tag{4.82}$$

Inverting the relation (4.69) and letting $c_i = 0$, (4.82) becomes

$$\bar{v}_i = Q_{ji}v_j + \dot{Q}_{ji}Q_{jk}\bar{x}_k \tag{4.83}$$

We see from (4.83) that v_i is a first-rank tensor, but under the observer transformation, it is not objective. If it were objective, we would have $\bar{v}_i = Q_{ji}\, v_j$ for any Q_{ij}. Note that in the rigid rotation of the spatial reference frame, the spin of the frame is related to Q_{ij} through (3.184), (3.187), and (3.188), and given by $\dot{Q}_{ij}Q_{kj} = \Omega_{ik} = e_{kij}\omega_j$. Therefore,

$$\bar{\mathbf{v}} = \mathbf{Q}^{\mathrm{T}} \cdot \mathbf{v} + \boldsymbol{\omega} \times \mathbf{r} \tag{4.84}$$

The velocity gradient is now investigated by differentiating (4.83). We obtain

$$\bar{v}_{i,r} = \frac{\partial \bar{v}_i}{\partial \bar{x}_r} = Q_{ji}\frac{\partial v_j}{\partial x_s}\frac{\partial x_s}{\partial \bar{x}_r} + \dot{Q}_{ji}Q_{jr} = Q_{ji}Q_{sr}v_{j,s} + \dot{Q}_{ji}Q_{jr} \tag{4.85}$$

This shows that the velocity gradient tensor is not an objective tensor either because of the presence of the second term on the right-hand side of (4.85).

We show that the symmetric part of $v_{i,j}$ is objective, whereas the antisymmetric part of $v_{i,j}$ is not. To this end, we interchange i and r to obtain

$$\frac{\partial \bar{v}_r}{\partial \bar{x}_i} = Q_{jr}Q_{si}v_{j,s} + \dot{Q}_{jr}Q_{ji} \tag{4.86}$$

Adding (4.85) and (4.86), we find

$$\bar{D}_{ir} = \frac{1}{2}\left(\frac{\partial \bar{v}_i}{\partial \bar{x}_r} + \frac{\partial \bar{v}_r}{\partial \bar{x}_i}\right) = \frac{1}{2}\{Q_{ji}Q_{sr}v_{j,s} + Q_{jr}Q_{si}v_{j,s}\} + \frac{1}{2}\{\dot{Q}_{ji}Q_{jr} + \dot{Q}_{jr}Q_{ji}\} \tag{4.87}$$

We note that since

$$\frac{\mathrm{D}}{\mathrm{D}t}(Q_{ji}Q_{jr}) = \dot{Q}_{ji}Q_{jr} + \dot{Q}_{jr}Q_{ji} = \frac{\mathrm{D}}{\mathrm{D}t}(\delta_{ir}) = 0 \tag{4.88}$$

Equation (4.87) becomes

$$\bar{D}_{ir} = Q_{ji}Q_{sr}D_{js} \tag{4.89}$$

Therefore, D_{ij} is an objective tensor. It is not surprising that D_{ij} is objective, because D_{ij} represents the rate of deformation that describes the rate of stretching of line elements, and this stretching may be measured by a ruler and is independent of the orientation of the observer. Now, let us consider the antisymmetric part of $v_{i,j}$. From (4.85) and (4.86), we obtain

$$\begin{aligned}\bar{W}_{ir} &= \frac{1}{2}\left(\frac{\partial \bar{v}_i}{\partial \bar{x}_r} - \frac{\partial \bar{v}_r}{\partial \bar{x}_i}\right) = Q_{ji}Q_{sr}W_{js} + \frac{1}{2}(\dot{Q}_{ji}Q_{jr} - \dot{Q}_{jr}Q_{ji}) \\ &= Q_{ji}Q_{sr}W_{js} + \dot{Q}_{ji}Q_{jr}\end{aligned} \tag{4.90}$$

Because of the presence of the second term, the spin tensor is not objective. The last expression has been obtained by observing that $\dot{Q}_{jr}Q_{ji} = -\dot{Q}_{ji}Q_{jr}$. In the case of rigid-body motion, $L_{ij} = W_{ij} = \Omega_{ij}$, and (4.90) is reduced to

$$\bar{\Omega}_{ir} = Q_{ji}Q_{sr}\Omega_{js} + \Omega_{ir} \tag{4.91}$$

In the symbolic notation, equations (4.85), (4.89), and (4.90) are written as

$$\bar{\mathbf{L}} = \mathbf{Q}^{\mathrm{T}} \cdot \mathbf{L} \cdot \mathbf{Q} + \dot{\mathbf{Q}}^{\mathrm{T}} \cdot \mathbf{Q}, \tag{4.92a}$$

$$\bar{\mathbf{D}} = \mathbf{Q}^{\mathrm{T}} \cdot \mathbf{D} \cdot \mathbf{Q}, \tag{4.92b}$$

$$\bar{\mathbf{W}} = \mathbf{Q}^{\mathrm{T}} \cdot \mathbf{W} \cdot \mathbf{Q} + \dot{Q}^{\mathrm{T}} \cdot \mathbf{Q} \tag{4.92c}$$

It is seen that $\mathbf{L}$ and $\mathbf{W}$ depend on the spin of the rotating system, but $\mathbf{D}$ depends only on the orientation of the reference (spatial) frame. Note that

for two chosen coordinate systems, $\mathbf{L}$ transforms like a second-rank tensor if $\dot{\mathbf{Q}} = \mathbf{0}$.

4.7 Objective Rates

In the small strain mechanics, constitutive equations of the *rate form* have been widely used. Investigators have used the stress, stress rate, and higher-order stress rates on the one hand and the strain, strain-rate, and higher-order strain-rates on the other to propose constitutive equations of the following form

$$f(\sigma, \dot{\sigma}, \ddot{\sigma}, \ldots) = g(\varepsilon, \dot{\varepsilon}, \ddot{\varepsilon}, \ldots) \tag{4.93}$$

where f and g are nonlinear functions generally. When the mechanics of finite strain is of interest, we ask the question regarding the appropriate rates to use in the constitutive equations. We emphasize here that only objective tensors and objective rates can be used.

4.7.1 Some Objective Rates

Supposing that a symmetric tensor $\mathbf{T}$ is an objective tensor, such that

$$\bar{\mathbf{T}} = \mathbf{Q}^{\mathrm{T}} \cdot \mathbf{T} \cdot \mathbf{Q} \tag{4.94}$$

then, we inquire whether the rate $\mathrm{D}\mathbf{T}/\mathrm{D}t$ is objective. If this rate is not objective, then we cannot interpret the physical significance using it. To answer the above question, we differentiate (4.94) to obtain

$$\frac{\mathrm{D}\bar{\mathbf{T}}}{\mathrm{D}t} = \frac{\mathrm{D}}{\mathrm{D}t}(\mathbf{Q}^{\mathbf{T}} \cdot \mathbf{T} \cdot \mathbf{Q}) = \dot{\mathbf{Q}}^{\mathrm{T}} \cdot \mathbf{T} \cdot \mathbf{Q} + \mathbf{Q}^{\mathrm{T}} \cdot \dot{\mathbf{T}} \cdot \mathbf{Q} + \mathbf{Q}^{\mathrm{T}} \cdot \mathbf{T} \cdot \dot{\mathbf{Q}} \tag{4.95}$$

The superposed "dot" denotes the material derivative. The presence of $\dot{\mathbf{Q}}^{\mathrm{T}} \cdot \mathbf{T} \cdot \mathbf{Q}$ and $\mathbf{Q}^{\mathrm{T}} \cdot \mathbf{T} \cdot \dot{\mathbf{Q}}$ in (4.95) shows that $\dot{\mathbf{T}}$ is *not* objective.

To determine an objective derivative, we eliminate $\dot{\mathbf{Q}}$ and $\dot{\mathbf{Q}}^{\mathrm{T}}$ from (4.95), since these terms cannot appear in a reference frame transformation. From equation (4.92a), we obtain

$$\bar{\mathbf{L}} \cdot \mathbf{Q}^{\mathrm{T}} = \mathbf{Q}^{\mathrm{T}} \cdot \mathbf{L} \cdot \mathbf{Q} \cdot \mathbf{Q}^{\mathrm{T}} + \dot{\mathbf{Q}}^{\mathrm{T}} \quad \text{or} \quad \dot{\mathbf{Q}}^{\mathrm{T}} = \bar{\mathbf{L}} \cdot \mathbf{Q}^{\mathrm{T}} - \mathbf{Q}^{\mathrm{T}} \cdot \mathbf{L} \tag{4.96}$$

By taking the transpose of (4.96), we obtain

$$\dot{\mathbf{Q}} = \mathbf{Q} \cdot \bar{\mathbf{L}}^{\mathrm{T}} - \mathbf{L}^{\mathrm{T}} \cdot \mathbf{Q} \tag{4.97}$$

By substitution, we then have from (4.95)

$$\begin{aligned}\frac{\mathrm{D}\bar{\mathbf{T}}}{\mathrm{D}t} &= (\bar{\mathbf{L}}\cdot\mathbf{Q}^{\mathrm{T}} - \mathbf{Q}^{\mathrm{T}}\cdot\mathbf{L})\cdot\mathbf{T}\cdot\mathbf{Q} + \mathbf{Q}^{\mathrm{T}}\cdot\dot{\mathbf{T}}\cdot\mathbf{Q} + \mathbf{Q}^{\mathrm{T}}\cdot\mathbf{T}\cdot(\mathbf{Q}\cdot\bar{\mathbf{L}}^{\mathrm{T}} - \mathbf{L}^{\mathrm{T}}\cdot\mathbf{Q}) \\ &= \bar{\mathbf{L}}\cdot\mathbf{Q}^{\mathrm{T}}\cdot\mathbf{T}\cdot\mathbf{Q} - \mathbf{Q}^{\mathrm{T}}\cdot\mathbf{L}\cdot\mathbf{T}\cdot\mathbf{Q} + \mathbf{Q}^{\mathrm{T}}\cdot\dot{\mathbf{T}}\cdot\mathbf{Q} + \mathbf{Q}^{\mathrm{T}}\cdot\mathbf{T}\cdot\mathbf{Q}\cdot\bar{\mathbf{L}}^{\mathrm{T}} \\ &\quad - \mathbf{Q}^{\mathrm{T}}\cdot\mathbf{T}\cdot\mathbf{L}^{\mathrm{T}}\cdot\mathbf{Q} \\ &= \bar{\mathbf{L}}\cdot\bar{\mathbf{T}} - \mathbf{Q}^{\mathrm{T}}\cdot\mathbf{L}\cdot\mathbf{T}\cdot\mathbf{Q} + \mathbf{Q}^{\mathrm{T}}\cdot\dot{\mathbf{T}}\cdot\mathbf{Q} + \bar{\mathbf{T}}\cdot\bar{\mathbf{L}}^{\mathrm{T}} - \mathbf{Q}^{\mathrm{T}}\cdot\mathbf{T}\cdot\mathbf{L}^{\mathrm{T}}\cdot\mathbf{Q} \qquad (4.98)\end{aligned}$$

Equation (4.98) can be rearranged into the following form

$$\frac{\mathrm{D}\bar{\mathbf{T}}}{\mathrm{D}t} - \bar{\mathbf{L}}\cdot\bar{\mathbf{T}} - \bar{\mathbf{T}}\cdot\bar{\mathbf{L}}^{\mathrm{T}} = \mathbf{Q}^{\mathrm{T}}\cdot\left(\frac{\mathrm{D}T}{\mathrm{D}t} - \mathbf{L}\cdot\mathbf{T} - \mathbf{T}\cdot\mathbf{L}^{\mathrm{T}}\right)\cdot\mathbf{Q} \qquad (4.99)$$

It follows that the derivative $((\mathrm{D}\mathbf{T}/\mathrm{D}t) - \mathbf{L}\cdot\mathbf{T} - \mathbf{T}\cdot\mathbf{L}^{\mathrm{T}})$ is an objective derivative. This derivative may also be expressed in the index notation as

$$\frac{\mathrm{D}T_{ij}}{\mathrm{D}t} - v_{i,k}\,T_{kj} - T_{ik}v_{j,k} \qquad (4.100)$$

Similarly, we can show that the following rates are objective rates. The *Jaumann rate* is given by

$$\mathbf{T}^{\nabla} = \frac{\mathrm{D}\mathbf{T}}{\mathrm{D}t} - \mathbf{W}\cdot\mathbf{T} + \mathbf{T}\cdot\mathbf{W} \quad \text{and} \quad \bar{\mathbf{T}}^{\nabla} = \mathbf{Q}^{\mathrm{T}}\cdot\mathbf{T}^{\nabla}\cdot\mathbf{Q} \qquad (4.101)$$

and the *convected rate* is given by

$$\mathbf{T}^{*} = \frac{\mathrm{D}\mathbf{T}}{\mathrm{D}t} + \mathbf{L}^{\mathrm{T}}\cdot\mathbf{T} + \mathbf{T}\cdot\mathbf{L} \quad \text{and} \quad \bar{\mathbf{T}}^{*} = \mathbf{Q}^{\mathrm{T}}\cdot\mathbf{T}^{*}\cdot\mathbf{Q} \qquad (4.102)$$

The Jaumann rate defined in (4.101) is based on the spin tensor $\mathbf{W}$. We may use another tensor $\boldsymbol{\omega}$, which represents the rate of rotation of some physical quantity to define the same objective rate. In this case, $(\mathrm{D}\mathbf{T}/\mathrm{D}t) - \boldsymbol{\omega}\cdot\mathbf{T} + \mathbf{T}\cdot\boldsymbol{\omega}$ is called the co-rotational rate. The physical significance and application of these rates will be discussed later in connection with some constitutive models. Finally, we note that, if $\mathbf{T}$ is stress, then these are objective stress rates.

EXAMPLE 4.7 Derive the convected rate.

Solution

We have from (4.92a)

$$\bar{\mathbf{L}} = \mathbf{Q}^{\mathrm{T}}\cdot\mathbf{L}\cdot\mathbf{Q} + \dot{\mathbf{Q}}^{\mathrm{T}}\cdot\mathbf{Q} = \mathbf{Q}^{\mathrm{T}}\cdot\mathbf{L}\cdot\mathbf{Q} - \mathbf{Q}^{\mathrm{T}}\cdot\dot{\mathbf{Q}} \qquad (a)$$

Multiplying (a) from the left by $\mathbf{Q}$, we obtain

$$\mathbf{Q}\cdot\bar{\mathbf{L}} = \mathbf{L}\cdot\mathbf{Q} - \dot{\mathbf{Q}} \quad \text{or} \quad \dot{\mathbf{Q}} = \mathbf{L}\cdot\mathbf{Q} - \mathbf{Q}\cdot\bar{\mathbf{L}} \tag{b}$$

Taking the transpose of (b), we have

$$\dot{\mathbf{Q}}^{\mathrm{T}} = \mathbf{Q}^{\mathrm{T}}\cdot\mathbf{L}^{\mathrm{T}} - \bar{\mathbf{L}}^{\mathrm{T}}\cdot\mathbf{Q}^{\mathrm{T}} \tag{c}$$

Hence, after substitution of (b) and (c), (4.95) becomes

$$\begin{aligned}\frac{\mathrm{D}\bar{\mathbf{T}}}{\mathrm{D}t} &= (\mathbf{Q}^{\mathrm{T}}\cdot\mathbf{L}^{\mathrm{T}} - \bar{\mathbf{L}}^{\mathrm{T}}\cdot\mathbf{Q}^{\mathrm{T}})\cdot\mathbf{T}\cdot\mathbf{Q} + \mathbf{Q}^{\mathrm{T}}\cdot\dot{\mathbf{T}}\cdot\mathbf{Q} + \mathbf{Q}^{\mathrm{T}}\cdot\mathbf{T}\cdot(\mathbf{L}\cdot\mathbf{Q} - \mathbf{Q}\cdot\bar{\mathbf{L}}) \\ &= \mathbf{Q}^{\mathrm{T}}\cdot\mathbf{L}^{\mathrm{T}}\cdot\mathbf{T}\cdot\mathbf{Q} - \bar{\mathbf{L}}^{\mathrm{T}}\cdot\bar{\mathbf{T}} + \mathbf{Q}^{\mathrm{T}}\cdot\dot{\mathbf{T}}\cdot\mathbf{Q} + \mathbf{Q}^{\mathrm{T}}\cdot\mathbf{T}\cdot\mathbf{L}\cdot\mathbf{Q} - \bar{\mathbf{T}}\cdot\bar{\mathbf{L}} \\ &= \mathbf{Q}^{\mathrm{T}}\cdot(\dot{\mathbf{T}} + \mathbf{L}^{\mathrm{T}}\cdot\mathbf{T} + \mathbf{T}\cdot\mathbf{L})\cdot\mathbf{Q} - \bar{\mathbf{L}}^{\mathrm{T}}\cdot\bar{\mathbf{T}} - \bar{\mathbf{T}}\cdot\bar{\mathbf{L}}\end{aligned} \tag{d}$$

From (d), we write

$$\frac{\mathrm{D}\bar{\mathbf{T}}}{\mathrm{D}t} + \bar{\mathbf{L}}^{\mathrm{T}}\cdot\bar{\mathbf{T}} + \bar{\mathbf{T}}\cdot\bar{\mathbf{L}} = \mathbf{Q}^{\mathrm{T}}\cdot\left(\frac{\mathrm{D}\mathbf{T}}{\mathrm{D}t} + \mathbf{L}^{\mathrm{T}}\cdot\mathbf{T} + \mathbf{T}\cdot\mathbf{L}\right)\cdot\mathbf{Q} \tag{e}$$

which shows that $(\mathrm{D}\mathbf{T}/\mathrm{D}t + \mathbf{L}^{\mathrm{T}}\cdot\mathbf{T} + \mathbf{T}\cdot\mathbf{L})$ is an objective rate. In the index notation, the convected rate is written as

$$\frac{\mathrm{D}T_{ij}}{\mathrm{D}t} + T_{im}v_{m,j} + T_{mj}v_{m,i} \tag{f}$$

EXAMPLE 4.8 Derive the Jaumann rate.

Solution

From (4.92), we have

$$\bar{\mathbf{W}} = \mathbf{Q}^{\mathrm{T}}\cdot\mathbf{W}\cdot\mathbf{Q} + \dot{\mathbf{Q}}^{\mathrm{T}}\cdot\mathbf{Q} = \mathbf{Q}^{\mathrm{T}}\cdot\mathbf{W}\cdot\mathbf{Q} - \mathbf{Q}^{\mathrm{T}}\cdot\dot{\mathbf{Q}} \tag{a}$$

Multiplying (a) by $\mathbf{Q}$ from the left, we have

$$\mathbf{Q}\cdot\bar{\mathbf{W}} = \mathbf{W}\cdot\mathbf{Q} - \dot{\mathbf{Q}} \quad \text{or} \quad \dot{\mathbf{Q}} = \mathbf{W}\cdot\mathbf{Q} - \mathbf{Q}\cdot\bar{\mathbf{W}} \tag{b}$$

Taking the transpose of (b), we obtain

$$\dot{\mathbf{Q}}^{\mathrm{T}} = \mathbf{Q}^{\mathrm{T}}\cdot\mathbf{W}^{\mathrm{T}} - \bar{\mathbf{W}}^{\mathrm{T}}\cdot\mathbf{Q}^{\mathrm{T}} \tag{c}$$

Substituting (b) and (c) into (4.95), we find

$$\begin{aligned}\frac{\mathrm{D}\bar{\mathbf{T}}}{\mathrm{D}t} &= (\mathbf{Q}^{\mathrm{T}}\cdot\mathbf{W}^{\mathrm{T}}-\bar{\mathbf{W}}^{\mathrm{T}}\cdot\mathbf{Q}^{\mathrm{T}})\cdot\mathbf{T}\cdot\mathbf{Q}+\mathbf{Q}^{\mathrm{T}}\cdot\dot{\mathbf{T}}\cdot\mathbf{Q}+\mathbf{Q}^{\mathrm{T}}\cdot\mathbf{T}\cdot(\mathbf{W}\cdot\mathbf{Q}-\mathbf{Q}\cdot\bar{\mathbf{W}})\\ &= \mathbf{Q}^{\mathrm{T}}\cdot\mathbf{W}^{\mathrm{T}}\cdot\mathbf{T}\cdot\mathbf{Q}-\bar{\mathbf{W}}^{\mathrm{T}}\cdot\bar{\mathbf{T}}+\mathbf{Q}^{\mathrm{T}}\cdot\dot{\mathbf{T}}\cdot\mathbf{Q}+\mathbf{Q}^{\mathrm{T}}\cdot\mathbf{T}\cdot\mathbf{W}\cdot\mathbf{Q}-\bar{\mathbf{T}}\cdot\bar{\mathbf{W}}\\ &= \mathbf{Q}^{\mathrm{T}}\cdot(\dot{\mathbf{T}}+\mathbf{W}^{\mathrm{T}}\cdot\mathbf{T}+\mathbf{T}\cdot\mathbf{W})\cdot\mathbf{Q}-\bar{\mathbf{W}}^{\mathrm{T}}\cdot\bar{\mathbf{T}}-\bar{\mathbf{T}}\cdot\bar{\mathbf{W}}\end{aligned}\tag{d}$$

From (d) we conclude that

$$\frac{\mathrm{D}\bar{\mathbf{T}}}{\mathrm{D}t}+\bar{\mathbf{W}}^{\mathrm{T}}\cdot\bar{\mathbf{T}}+\bar{\mathbf{T}}\cdot\bar{\mathbf{W}}=\mathbf{Q}^{\mathrm{T}}\cdot\left(\frac{\mathrm{D}\mathbf{T}}{\mathrm{D}t}+\mathbf{W}^{\mathrm{T}}\cdot\mathbf{T}+\mathbf{T}\cdot\mathbf{W}\right)\cdot\mathbf{Q}\tag{e}$$

But $\mathbf{W}^{\mathrm{T}}=-\mathbf{W}$, (e) then becomes

$$\frac{\mathrm{D}\bar{\mathbf{T}}}{\mathrm{D}t}-\bar{\mathbf{W}}\cdot\bar{\mathbf{T}}+\bar{\mathbf{T}}\cdot\bar{\mathbf{W}}=\mathbf{Q}^{\mathrm{T}}\cdot\left(\frac{\mathrm{D}\mathbf{T}}{\mathrm{D}t}-\mathbf{W}\cdot\mathbf{T}+\mathbf{T}\cdot\mathbf{W}\right)\cdot\mathbf{Q}\tag{f}$$

Therefore,

$$\mathbf{T}^{\nabla}=\frac{\mathrm{D}\mathbf{T}}{\mathrm{D}t}-\mathbf{W}\cdot\mathbf{T}+\mathbf{T}\cdot\mathbf{W}\tag{g}$$

is an objective rate.

4.7.2 Physical Meaning of the Jaumann Stress Rate

Let a body spin with an angular velocity $\mathbf{w}$ with reference frame at time t denoted by x_i. Let $\bar{x}_i$ be another reference frame which is attached to the body and spins with it. Let $\bar{x}_i$ coincide with x_i at time t, when the stress at a generic point P in the body is $\bar{\sigma}_{ij}(t)=\sigma_{ij}(t)$. At time $t+\mathrm{d}t$, the stress at particle P is $\bar{\sigma}_{ij}(t+\mathrm{d}t)$ referred to the rotating axes $\bar{x}_i$. Then, according to Jaumann, the stress rate may be defined as

$$\sigma_{ij}^{\nabla}=\lim_{\Delta t\to 0}\frac{1}{\Delta t}[\bar{\sigma}_{ij}(t+\Delta t)-\bar{\sigma}_{ij}(t)]\tag{4.103}$$

The relation Q_{ij} between the two reference frames may be found by considering the spin of the reference frame (see Figure 4.7) which rotates base vectors $\mathbf{e}_i$ into $\bar{\mathbf{e}}_i$. From (1.22), the relation is

$$\bar{\mathbf{e}}_i=Q_{ji}\mathbf{e}_j\tag{4.104}$$

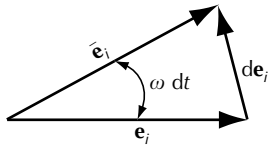

FIGURE 4.7
Spin of the reference frame.

The angle of rotation is $\omega\,\mathrm{d}t$, where ω is the angular velocity. Using $\mathbf{n}$ to denote the unit normal to the plane formed by $\mathbf{e}_i$ and $\bar{\mathbf{e}}_i$, the angular velocity vector is

$$\mathbf{w} = \omega\mathbf{n} = \omega n_i \mathbf{e}_i = w_i \mathbf{e}_i \tag{4.105}$$

Therefore, $w_i = \omega n_i$. Referring to Figure 4.7, we write

$$\bar{\mathbf{e}}_i = \mathbf{e}_i + \mathrm{d}\mathbf{e}_i = \mathbf{e}_i + \mathbf{w}\,\mathrm{d}t \times \mathbf{e}_i \tag{4.106}$$

Using (4.104), (4.106) becomes

$$Q_{ji}\mathbf{e}_j = \mathbf{e}_i + \omega n_j\,\mathrm{d}t\mathbf{e}_j \times \mathbf{e}_i = \mathbf{e}_i + \omega n_k\,\mathrm{d}t\,e_{ijk}\mathbf{e}_j \tag{4.107}$$

The components of (4.107) are

$$Q_{ji} = \delta_{ij} + \omega n_k\,\mathrm{d}te_{ijk} \tag{4.108}$$

which may be rewritten as

$$Q_{ij} = \delta_{ij} - \omega n_k\,\mathrm{d}te_{ijk} \tag{4.109}$$

Equation (4.109) describes the rotation of the reference frame. This equation may be compared with (1.118) and the same result can be obtained from (1.118) by setting $\cos\alpha = 1$, $\sin\alpha = \alpha$, $\alpha = \omega\,\mathrm{d}t$, and $w_k = \omega n_k$.

The stress tensor at P at time $t + \mathrm{d}t$ referred to the reference frame x_i is

$$\sigma_{ij}(t + \mathrm{d}t) = \sigma_{ij}(t) + \frac{\mathrm{D}\sigma_{ij}}{\mathrm{Dt}}\mathrm{d}t \tag{4.110}$$

The stresses $\bar{\sigma}_{ij}(t+\mathrm{d}t)$ and $\sigma_{ij}(t+\mathrm{d}t)$, referring to $\bar{x}_i$ and x_i systems, respectively, are related by $\bar{\sigma}_{ij} = Q_{pi}Q_{qj}\sigma_{pq}$, so that by use of (4.109), we write

$$\begin{aligned}\bar{\sigma}_{ij}(t+\mathrm{d}t) &= Q_{pi}Q_{qj}\sigma_{pq}(t+\mathrm{d}t)\\ &= (\delta_{pi} - e_{pim}w_m\mathrm{d}t)(\delta_{qj} - e_{qjn}w_n\,\mathrm{d}t)\left\{\sigma_{pq}(t) + \frac{\mathrm{D}\sigma_{pq}}{\mathrm{D}t}\,\mathrm{d}t\right\}\\ &= \sigma_{ij}(t) + \left\{\frac{\mathrm{D}\sigma_{ij}}{\mathrm{D}t} - e_{pim}w_m\sigma_{pj} - e_{qjn}w_n\sigma_{iq}\right\}\mathrm{d}t + O(\mathrm{d}t^2)\end{aligned} \tag{4.111}$$

Hence, by neglecting the higher order terms in $\mathrm{d}t$ and using (4.103), we obtain

$$\sigma_{ij}^{\nabla} = \frac{\mathrm{D}\sigma_{ij}}{\mathrm{D}t} - e_{pim}w_m\sigma_{pj} - e_{qjn}w_n\sigma_{iq} \tag{4.112}$$

Noting that

$$W_{jk} = -e_{ijk}w_i \quad \text{and} \quad -W_{jq} = W_{qj} \tag{4.113}$$

we then have

$$\sigma_{ij}^{\nabla} = \frac{\mathrm{D}}{\mathrm{D}_t}\sigma_{ij} - W_{ip}\sigma_{pj} + \sigma_{iq}W_{qj} \tag{4.114}$$

This is the Jaumann stress rate and is the same as the expression in (4.101).

4.8 Finite Elasticity

We study the topic of elasticity in the remaining part of this chapter. *Elasticity* investigates the specific material behavior which is reversible, that is, if a material is elastic, then upon the removal of loading, the material will recover its original state. Elastic material is an ideal material and it is a good approximation for most materials in the small strain range. In the finite strain range, rubber is known to exhibit an elastic behavior to a good approximation. There are several approaches to formulating the constitutive equation for an elastic material. The Cauchy elasticity is discussed first and then the hyperelasticity. Emphasis is given to hyperelasticity and provide several examples in the application. Finally, in the last section of this chapter, hypo-elasticity is discussed, which, strictly speaking, is not elasticity.

4.8.1 The Cauchy Elasticity

In the investigation of a constitutive equation, we consider the stress and deformation of an infinitesimal material element. If the material is elastic, then the stress $\boldsymbol{\sigma}$ is, by definition, a function of the current deformation written as

$$\boldsymbol{\sigma} = \mathbf{g}(\mathbf{F}) \tag{4.115}$$

where $\mathbf{g}$ is a tensor-valued function of $\mathbf{F}$ and is in general a nonlinear function. We use the deformation gradient $\mathbf{F}$ to denote deformation for the purpose of generality, and we show next by use of objectivity that the deformation cannot be represented by $\mathbf{F}$. Under observer transformation of (4.69), an arbitrary $\mathbf{Q}^{\mathrm{T}}$, (4.115) is written in the barred frame as

$$\bar{\boldsymbol{\sigma}} = \mathbf{g}(\bar{\mathbf{F}}) \tag{4.116}$$

which by use of (4.71) and (4.72) is

$$\mathbf{Q}^{\mathrm{T}} \cdot \boldsymbol{\sigma} \cdot \mathbf{Q} = \mathbf{g}(\mathbf{Q}^{\mathrm{T}} \cdot \mathbf{F}) \tag{4.117}$$

or

$$\mathbf{Q}^{\mathrm{T}} \cdot \mathbf{g}(\mathbf{F}) \cdot \mathbf{Q} = \mathbf{g}(\mathbf{Q}^{\mathrm{T}} \cdot \mathbf{F}) \tag{4.118}$$

for an arbitrary orthogonal $\mathbf{Q}$. Equation (4.118) gives the restriction on the form of $\mathbf{g}$ in (4.115). In particular, if we choose $\mathbf{Q} = \mathbf{R}$ and, by applying $\mathbf{F} = \mathbf{R} \cdot \mathbf{U}$ from the polar decomposition theorem, we obtain

$$\mathbf{Q}^{\mathrm{T}} \cdot \mathbf{F} = \mathbf{R}^{\mathrm{T}} \cdot \mathbf{F} = \mathbf{R}^{\mathrm{T}} \cdot \mathbf{R} \cdot \mathbf{U} = \mathbf{U} \tag{4.119}$$

Note that the observer transformation is valid for any $\mathbf{Q}$, but if we make a special choice of it, we can observe useful information from this orientation of the observer. The information is still there, but it cannot be visualized from another orientation $\mathbf{Q}$. Making use of (4.119), (4.118) becomes

$$\mathbf{R}^{\mathrm{T}} \cdot \mathbf{g}(\mathbf{F}) \cdot \mathbf{R} = \mathbf{g}(\mathbf{U}) \tag{4.120}$$

Combining (4.115) and (4.120), we obtain

$$\boldsymbol{\sigma} = \mathbf{R} \cdot \mathbf{g}(\mathbf{U}) \cdot \mathbf{R}^{\mathrm{T}} \tag{4.121}$$

We see from (4.121) that $\boldsymbol{\sigma}$ depends on a nonlinear function of $\mathbf{U}$ and depends on $\mathbf{R}$ explicitly. But, since $\mathbf{U}$ is related to $\mathbf{C}$ from (3.40) and $\mathbf{C}$ is related to $\mathbf{E}$ from (3.100), equivalent forms of (4.121) are

$$\boldsymbol{\sigma} = \mathbf{R} \cdot \mathbf{f}(\mathbf{C}) \cdot \mathbf{R}^{\mathrm{T}} \tag{4.122}$$

and

$$\boldsymbol{\sigma} = \mathbf{R} \cdot \mathbf{h}(\mathbf{E}) \cdot \mathbf{R}^{\mathrm{T}} \tag{4.123}$$

where $\mathbf{f}$ is a tensor-valued function of $\mathbf{C}$ and $\mathbf{h}$ is a tensor-valued function of $\mathbf{E}$. One of (4.121), (4.122), or (4.123) may be used as the constitutive equation for anisotropic elastic materials. For a given deformation, $\mathbf{R}$, $\mathbf{U}$, $\mathbf{C}$, and $\mathbf{E}$ can be determined. If explicit functions $\mathbf{g}$, $\mathbf{f}$, or $\mathbf{h}$ are known, then by use of one of the above constitutive equations the stress $\boldsymbol{\sigma}$ may be determined.

In the case that the material is isotropic, (4.122) may be rewritten as

$$\hat{\boldsymbol{\sigma}} \equiv \mathbf{R}^{\mathrm{T}} \cdot \boldsymbol{\sigma} \cdot \mathbf{R} = \mathbf{f}(\mathbf{C}) \tag{4.124}$$

Following a representation theorem of Rivlin and Ericksen [1] for an isotropic tensor function of a tensor, (4.124) is written as

$$\hat{\boldsymbol{\sigma}} = \varphi_0 \mathbf{1} + \varphi_1 \mathbf{C} + \varphi_2 \mathbf{C}^2 \tag{4.125}$$

where φ_0, φ_1, and φ_2 are scalar invariant functions of the three principal invariants of $\mathbf{C}$. Equation (4.125) can also be derived by expressing the function $\mathbf{f}$ in (4.124) as a polynomial of $\mathbf{C}$ and applying the Cayley–Hamilton theorem (Section 2.15) successively. From (2.104), we write

$$\mathbf{C}^3 = I_1 \mathbf{C}^2 - I_2 \mathbf{C} + I_3 \mathbf{I} \tag{4.126}$$

where I_1, I_2, and I_3 are principal invariants of $\mathbf{C}$. By successive applications of (4.126), (4.124) reduces to (4.125). From (4.125), we have

$$\begin{aligned} \boldsymbol{\sigma} &= \mathbf{R} \cdot \hat{\boldsymbol{\sigma}} \cdot \mathbf{R}^{\mathrm{T}} = \mathbf{R} \cdot (\varphi_0 \mathbf{1} + \varphi_1 \mathbf{C} + \varphi_2 \mathbf{C}^2) \cdot \mathbf{R}^{\mathrm{T}} \\ &= \varphi_0 \mathbf{R} \cdot \mathbf{R}^{\mathrm{T}} + \varphi_1 \mathbf{R} \cdot \mathbf{C} \cdot \mathbf{R}^{\mathrm{T}} + \varphi_2 \mathbf{R} \cdot \mathbf{C} \cdot \mathbf{C}^{\mathrm{T}} \cdot \mathbf{R}^{\mathrm{T}} \end{aligned} \tag{4.127}$$

The last term of (4.127), using (3.37), is

$$\mathbf{R} \cdot \mathbf{C} \cdot \mathbf{C}^{\mathrm{T}} \cdot \mathbf{R}^{\mathrm{T}} = \mathbf{R} \cdot \mathbf{C} \cdot (\mathbf{R}^{\mathrm{T}} \cdot \mathbf{R}) \cdot \mathbf{C}^{\mathrm{T}} \cdot \mathbf{R}^{\mathrm{T}} = (\mathbf{R} \cdot \mathbf{C} \cdot \mathbf{R}^{\mathrm{T}}) \cdot (\mathbf{R} \cdot \mathbf{C} \cdot \mathbf{R}^{\mathrm{T}})^{\mathrm{T}} = \mathbf{B} \cdot \mathbf{B}^{\mathrm{T}} \tag{4.128}$$

Substituting (3.37) and (4.128) into (4.127), we obtain

$$\boldsymbol{\sigma} = \varphi_0 \mathbf{1} + \varphi_1 \mathbf{B} + \varphi_2 \mathbf{B}^2 \tag{4.129}$$

where $\varphi_k = \varphi_k(I_1, I_2, I_3)$ and we note that the principal invariants of $\mathbf{C}$ and $\mathbf{B}$ are the same. By use of the Cayley–Hamilton theorem, (4.129) may be written in a slightly different form. From (2.104), we write

$$\mathbf{B}^3 - I_1 \mathbf{B}^2 + I_2 \mathbf{B} - I_3 \mathbf{1} = \mathbf{0} \tag{4.130}$$

Multiplying (4.130) by $\mathbf{B}^{-1}$, we get

$$\mathbf{B}^2 = I_1\mathbf{B} - I_2\mathbf{1} + I_3\mathbf{B}^{-1} \tag{4.131}$$

Finally, we substitute (4.131) into (4.129) to obtain

$$\boldsymbol{\sigma} = \alpha_0\mathbf{1} + \alpha_1\mathbf{B} + \alpha_{-\mathbf{1}}\mathbf{B}^{-1} \tag{4.132}$$

where

$$\alpha_0 = \varphi_0 - \varphi_2 I_2, \qquad \alpha_1 = \varphi_1 + \varphi_2 I_1, \qquad \alpha_{-1} = \varphi_2 I_3 \tag{4.133}$$

Either (4.129) or (4.132) can be used as the constitutive equation for an isotropic elastic material.

4.8.2 Hyperelasticity

A material is called *hyperelastic* or Green-elastic if there exists an elastic potential function, widely known as the strain-energy density function W, which is a scalar function of one of the strain or deformation tensors. Hyperelasticity uses the conservation of energy principle, leaving out the thermal effect. We postulate that the elastic material is capable of storing strain-energy and write

$$\boxed{\text{Rate of work done on body } R} = \boxed{\text{Rate of change of strain-energy in } R} \tag{4.134}$$

It may be shown that the strain-energy density is equal to the Helmholz free energy for isothermal process and is equal to the internal energy for isentropic process. This is further discussed in a later chapter. But, we mention for now that the free energy is the portion of internal energy available for doing work at constant temperature.

If the strain-energy density W is defined per unit undeformed volume, then

$$\text{Total strain-energy} = \int W\,\mathrm{d}V_0 = \int W\frac{\mathrm{d}V_0}{\mathrm{d}V}\mathrm{d}V = \int \frac{\rho}{\rho_0}W\,\mathrm{d}V \tag{4.135}$$

The rate of change of the strain-energy is then

$$\frac{\mathrm{D}}{\mathrm{D}t}\int \frac{\rho}{\rho_0}W\,\mathrm{d}V = \int \frac{\rho}{\rho_0}\frac{\mathrm{D}W}{\mathrm{D}t}\mathrm{d}V \tag{4.136}$$

and the rate of work done is

$$\int_S t_i^{(n)} v_i\,\mathrm{d}S = \int_S \sigma_{ki}n_k v_i\,\mathrm{d}S = \int_V (\sigma_{ki}v_i)_{,k}\,\mathrm{d}V = \int_V (\sigma_{ki,k}v_i + \sigma_{ki}v_{i,k})\,\mathrm{d}V \tag{4.137}$$

But the term $\int_V (\sigma_{ki,k} v_i) \mathrm{d}V$ in (4.137) cancels out with the kinetic energy term and the body force term by use of the equation of motion as discussed in Section 4.3.3. Therefore, the rate of work done that affects the rate of change of strain-energy is

$$\int_V \sigma_{ki} v_{i,k} \, \mathrm{d}V \tag{4.138}$$

Substituting (4.136) and (4.138) into (4.134), this balance of energy in the local form, is given by

$$\frac{\rho}{\rho_0} \frac{\mathrm{D}W}{\mathrm{D}t} = \sigma_{ji} v_{i,j} = \sigma_{ji} \frac{\partial v_i}{\partial X_R} \frac{\partial X_R}{\partial x_j} \tag{4.139}$$

or by use of (4.42)

$$\begin{aligned} \frac{\mathrm{D}W}{\mathrm{D}t} &= \frac{\rho_0}{\rho} \sigma_{ji} \frac{\partial X_R}{\partial x_j} \frac{\partial v_i}{\partial X_R} = T^{(0)}_{Ri} \frac{\partial v_i}{\partial X_R} = T^{(0)}_{Ri} \frac{\partial}{\partial X_R} \left(\frac{\mathrm{D}x_i}{\mathrm{D}t} \right) \\ &= T^{(0)}_{Ri} \frac{\mathrm{D}}{\mathrm{D}t} \left(\frac{\partial x_i}{\partial X_R} \right) = T^{(0)}_{Ri} \frac{\mathrm{D}F_{iR}}{\mathrm{D}t} \end{aligned} \tag{4.140}$$

where $T^{(0)}_{Ri}$ is the 1st P–K stress.

In the case of elastic material, the stress is a function of current deformation. If the deformation is expressed by the deformation gradient F_{iR}, the strain-energy density W is a function of F_{iR}. Thus,

$$\frac{\mathrm{D}W(F_{iR})}{\mathrm{D}t} = \frac{\partial W}{\partial F_{iR}} \frac{\mathrm{D}F_{iR}}{\mathrm{D}t} \tag{4.141}$$

By the substitution of (4.141) into (4.140), we then obtain

$$\left(\frac{\partial W}{\partial F_{iR}} - T^{(0)}_{Ri} \right) \frac{\mathrm{D}F_{iR}}{\mathrm{D}t} = 0 \tag{4.142}$$

Since this equation should hold for all $\mathrm{D}F_{iR}/\mathrm{D}t$ and since W and $T^{(0)}_{Ri}$ are functions of F_{iR}, but independent of $\mathrm{D}F_{iR}/\mathrm{D}t$, the left-hand side of the above equation must vanish for all arbitrary value of $\mathrm{D}F_{iR}/\mathrm{D}t$. It follows that

$$T^{(0)}_{Ri} = \frac{\partial W}{\partial F_{iR}} \tag{4.143}$$

or, by use of (4.42),

$$\sigma_{ij} = \frac{\rho}{\rho_0} \frac{\partial x_i}{\partial X_R} \frac{\partial W(\mathbf{F})}{\partial F_{jR}} = \frac{\rho}{\rho_0} F_{iR} \frac{\partial W}{\partial F_{jR}} \tag{4.144}$$

This is the most general constitutive equation of an elastic material undergoing finite deformation if we make use of the strain-energy density function. In the last step, the symmetric property of σ_{ij} is invoked.

We now consider the effect of objectivity on the form of strain-energy function W. By applying objectivity, we have in the barred reference frame

$$\sigma_{ij} = \frac{\rho}{\rho_0}\bar{F}_{iR}\frac{\partial \bar{W}}{\partial \bar{F}_{jR}} = \frac{\rho}{\rho_0}\bar{F}_{iR}\frac{\partial \bar{W}}{\partial F_{rS}}\frac{\partial F_{rS}}{\partial \bar{F}_{jR}} \tag{4.145}$$

But, from (4.78),

$$\bar{F}_{iR} = Q_{ki}F_{kR}, \qquad F_{rS} = Q_{rm}\bar{F}_{mS}, \qquad \frac{\partial F_{rS}}{\partial \bar{F}_{jR}} = Q_{rm}\delta_{mj}\delta_{SR} = Q_{rj}\delta_{SR} \tag{4.146}$$

Hence, after substitution, (4.145) becomes

$$\bar{\boldsymbol{\sigma}}_{ij} = \frac{\rho}{\rho_0}Q_{ki}F_{kR}\frac{\partial \bar{W}}{\partial F_{rS}}Q_{rj}\delta_{SR} = Q_{ki}Q_{rj}\frac{\rho}{\rho_0}F_{kR}\frac{\partial \bar{W}}{\partial F_{rR}} \tag{4.147}$$

Therefore, by comparing (4.147) with (4.144), we conclude that

$$\bar{\sigma}_{ij} = Q_{ki}Q_{rj}\sigma_{kr} \quad \text{or} \quad \bar{\boldsymbol{\sigma}} = \mathbf{Q}^{\mathrm{T}} \cdot \boldsymbol{\sigma} \cdot \mathbf{Q} \qquad \text{if } W(\mathbf{F}) = \bar{W}(\bar{\mathbf{F}}) \tag{4.148}$$

which states that objectivity of the stress tensor is satisfied if the strain-energy density W is form-invariant with rotation of the spatial reference frame. Hence,

$$\bar{W}(\bar{\mathbf{F}}) = W(\bar{\mathbf{F}}) = W(\mathbf{F}) \tag{4.149}$$

The last equality is equivalent to the condition that

$$W(\mathbf{Q}^{\mathrm{T}} \cdot \mathbf{F}) = W(\mathbf{F}) \qquad \text{for } \textit{any} \text{ orthogonal } \mathbf{Q} \tag{4.150}$$

In particular, if we choose $\mathbf{Q} = \mathbf{R}$ and, by applying $\mathbf{F} = \mathbf{R} \cdot \mathbf{U}$ from the polar decomposition theorem, we obtain

$$\mathbf{Q}^{\mathrm{T}} \cdot \mathbf{F} = \mathbf{R}^{\mathrm{T}} \cdot \mathbf{F} = \mathbf{R}^{\mathrm{T}} \cdot \mathbf{R} \cdot \mathbf{U} = \mathbf{U} \tag{4.119}$$

as in the discussion of the Cauchy elasticity. Therefore, by substituting (4.119) into (4.150), we obtain

$$W(\mathbf{F}) = W(\mathbf{U}) \tag{4.151}$$

which means that W depends on $\mathbf{F}$ only through its dependence on $\mathbf{U}$. But, since $\mathbf{U}$ is related to $\mathbf{C}$ by (3.40), the strain-energy density may also be expressed in terms of $\mathbf{C}$ as

$$W(\mathbf{U}) = W(\sqrt{\mathbf{C}}) = \tilde{W}(\mathbf{C}) = W(\mathbf{C}) \tag{4.152}$$

The tilde in the last expression has been dropped for simplicity. We may do this, since the function is as yet unspecified. We have thus shown from the application of objectivity that the strain-energy density function is a function of the right Cauchy–Green deformation tensor $\mathbf{C}$. Using this property, we now have

$$\begin{aligned}\frac{\partial W}{\partial F_{jR}} &= \frac{\partial W}{\partial C_{ST}}\frac{\partial C_{ST}}{\partial F_{jR}} = \frac{\partial W}{\partial C_{ST}}\frac{\partial((\partial x_i/\partial X_S)(\partial x_i/\partial X_T))}{\partial(\partial x_j/\partial X_R)} \\ &= \frac{\partial W}{\partial C_{ST}}\left\{\delta_{ij}\delta_{SR}\frac{\partial x_i}{\partial X_T} + \delta_{ij}\delta_{TR}\frac{\partial x_i}{\partial X_S}\right\} \\ &= \frac{\partial W}{\partial C_{RT}}\frac{\partial x_j}{\partial X_T} + \frac{\partial W}{\partial C_{SR}}\frac{\partial x_j}{\partial X_S} = 2\frac{\partial W}{\partial C_{SR}}\frac{\partial x_j}{\partial X_S}\end{aligned} \tag{4.153}$$

Note that the last equality is obtained by observing the symmetric property of C_{RS}. Therefore, the stress of equation (4.144) can be written as

$$\sigma_{ij} = 2\frac{\rho}{\rho_0}\frac{\partial x_i}{\partial X_R}\frac{\partial x_j}{\partial X_S}\frac{\partial W}{\partial C_{RS}} \tag{4.154}$$

In terms of the 2nd P–K stress tensor, the constitutive equation for hyperelastic material is given from (4.48) and (4.154) by

$$\begin{aligned}\Pi_{RS} &= J\sigma_{jk}\frac{\partial X_R}{\partial x_j}\frac{\partial X_S}{\partial x_k} = 2\frac{\partial x_j}{\partial X_P}\frac{\partial x_k}{\partial X_Q}\frac{\partial W}{\partial C_{PQ}}\frac{\partial X_R}{\partial x_j}\frac{\partial X_S}{\partial x_k} \\ &= 2\frac{\partial W}{\partial C_{PQ}}\delta_{PR}\delta_{QS} = 2\frac{\partial W}{\partial C_{RS}}\end{aligned} \tag{4.155}$$

Hence,

$$\Pi_{RS} = 2\frac{\partial W(\mathbf{C})}{\partial C_{RS}} = \frac{\partial W(\mathbf{E})}{\partial E_{RS}} \tag{4.156}$$

where E_{RS} is the Lagrangian strain tensor defined by (3.100). It is seen that by use of the 2nd P–K stress, the stress is the partial derivative of the strain-energy density function with respect to a deformation tensor. The constitutive equation is thus greatly simplified. We note that this equation applies to fully anisotropic elastic materials.

4.8.3 Isotropic Hyperelastic Materials

A material is said to be isotropic, if its constitutive equation remains form-invariant with rotation of the material coordinate system X_R. This statement is similar to that of material objectivity. The difference is that we rotate the material coordinate system here. The isotropic statement imposes a constraint on the constitutive equations (4.154) and (4.156), and, since in hyperelasticity the stress is expressed in terms of the strain-energy density function, the constraint of isotropy is imposed on the strain-energy density W(**C**). Therefore, we state that an elastic material is isotropic if its strain-energy density function is form-invariant with rotation of the material coordinate system.

THEOREM A necessary and sufficient condition that $W(\mathbf{C})$ be form-invariant with rotation of the material coordinate system is that W is a function only of the invariants of C_{RS}, and not a function of the components of C_{RS}.

Proof

From the spectral representation (2.95) of a symmetric second-rank tensor by its eigenvalues and eigenvectors, we write

$$C_{RS} = \sum_{Q} C_Q N_R^{(Q)} N_S^{(Q)} = C_1 N_R^{(1)} N_S^{(1)} + C_2 N_R^{(2)} N_S^{(2)} + C_3 N_R^{(3)} N_S^{(3)} \tag{4.157}$$

Then, the strain-energy density function is given by

$$W = W(C_1, C_2, C_3; N_R^{(1)}, N_R^{(2)}, N_R^{(3)} \tag{4.158}$$

where the eigenvalues C_Q remain invariant on the rotation of X_R; and $N_R^{(Q)}$ are the eigenvectors. We now make use of a theorem on invariants (see Green and Adkins [2]) which states that: a scalar-valued function $\phi(\boldsymbol{\alpha}^{(1)}, \boldsymbol{\alpha}^{(2)}, \ldots, \boldsymbol{\alpha}^{(m)})$ of m vectors $\boldsymbol{\alpha}^{(1)}, \boldsymbol{\alpha}^{(2)}, \ldots, \boldsymbol{\alpha}^{(m)}$ is invariant under all proper orthogonal transformations if and only if it can be expressed as a function of all possible inner products $\boldsymbol{\alpha}^{(r)} \cdot \boldsymbol{\alpha}^{(s)} (r, s = 1, 2, \ldots, m)$ and the determinant $|\boldsymbol{\alpha}^{(r)}|$, that is,

$$\phi = \phi(\boldsymbol{\alpha}^{(r)} \cdot \boldsymbol{\alpha}^{(s)}, |\boldsymbol{\alpha}^{(r)}|) \tag{4.159}$$

In the case of (4.158), the eigenvectors are orthogonal so that

$$N_R^{(P)} N_R^{(Q)} = \delta_{PQ} \quad \text{and} \quad |N_R^{(P)}| = 1 \tag{4.160}$$

Therefore, the strain-energy function is

$$W = W(C_1, C_2, C_3) \tag{4.161}$$

In the above expression, the indices 1, 2, and 3 are arbitrarily chosen depending on the designation of the coordinate axes. Since W must be a symmetric function of C_1, C_2, and C_3, it must be form-invariant with permutation of the indices, that is,

$$W(C_1, C_2, C_3) = W(C_1 + C_2 + C_3, C_1C_2 + C_2C_3 + C_3C_1, C_1C_2C_3) \tag{4.162}$$

or

$$W = W(I_1, I_2, I_3) \tag{4.163}$$

where I_1, I_2, and I_3 are the three principal invariants of C_{RS} defined in Section 3.6.4 and this concludes the proof of the theorem.

To obtain the constitutive equation for isotropic hyperelastic material, we consider

$$\frac{\partial W}{\partial C_{RS}} = \frac{\partial W}{\partial I_1}\frac{\partial I_1}{\partial C_{RS}} + \frac{\partial W}{\partial I_2}\frac{\partial I_2}{\partial C_{RS}} + \frac{\partial W}{\partial I_3}\frac{\partial I_3}{\partial C_{RS}} \tag{4.164}$$

where

$$\frac{\partial I_1}{\partial C_{RS}} = \delta_{RS}, \qquad \frac{\partial I_2}{\partial C_{RS}} = I_1\delta_{RS} - C_{RS}, \qquad \frac{\partial I_3}{\partial C_{RS}} = \text{cofactor}(C_{RS}) = I_3 C^{-1}_{RS} \tag{4.165}$$

The expressions for the three invariants are given in Sections 2.12 and 3.6.4. In particular, we mention here that

$$I_2 = \tfrac{1}{2}(I_1^2 - C_{RS}C_{RS}) \tag{4.166}$$

By substitution, we then obtain from (4.156)

$$\Pi_{RS} = 2\frac{\partial W}{\partial C_{RS}} = 2\left\{\frac{\partial W}{\partial I_1}\frac{\partial I_1}{\partial C_{RS}} + \frac{\partial W}{\partial I_2}\frac{\partial I_2}{\partial C_{RS}} + \frac{\partial W}{\partial I_3}\frac{\partial I_3}{\partial C_{RS}}\right\} \tag{4.167}$$

or

$$\Pi_{RS} = 2\left\{\frac{\partial W}{\partial I_1}\delta_{RS} + \frac{\partial W}{\partial I_2}(I_1\delta_{RS} - C_{RS}) + I_3\frac{\partial W}{\partial I_3}C^{-1}_{RS}\right\} \tag{4.168}$$

To express the above equation in terms of the Cauchy stress, we obtain from (4.50)

$$\sigma_{ij} = \frac{\rho}{\rho_0}\frac{\partial x_i}{\partial X_R}\frac{\partial x_j}{\partial X_S}\Pi_{RS} \tag{4.169}$$

Using (4.168), each term in (4.169) needs to be multiplied by a factor and these terms are

$$\frac{\partial x_i}{\partial X_R}\frac{\partial x_j}{\partial X_S}\delta_{RS} = \frac{\partial x_i}{\partial X_R}\frac{\partial x_j}{\partial X_R} = B_{ij} = \text{left Cauchy–Green tensor} \tag{4.170}$$

$$\frac{\partial x_i}{\partial X_R}\frac{\partial x_j}{\partial X_S}C_{RS} = \frac{\partial x_i}{\partial X_R}\frac{\partial x_j}{\partial X_S}\left(\frac{\partial x_k}{\partial X_R}\frac{\partial x_k}{\partial X_S}\right) = \left(\frac{\partial x_i}{\partial X_R}\frac{\partial x_k}{\partial X_R}\right)\left(\frac{\partial x_k}{\partial X_S}\frac{\partial x_j}{\partial X_S}\right) = B_{ik}B_{kj} \tag{4.171}$$

$$\begin{aligned}\frac{\partial x_i}{\partial X_R}\frac{\partial x_j}{\partial X_S}C^{-1}_{RS} &= \frac{\partial x_i}{\partial X_R}\frac{\partial x_j}{\partial X_S}\left(\frac{\partial X_R}{\partial x_k}\frac{\partial X_S}{\partial x_k}\right)\\ &= \left(\frac{\partial x_i}{\partial X_R}\frac{\partial X_R}{\partial x_k}\right)\left(\frac{\partial x_j}{\partial X_S}\frac{\partial X_S}{\partial x_k}\right) = \delta_{ik}\delta_{jk} = \delta_{ij}\end{aligned} \tag{4.172}$$

By substituting these expressions into (4.168) and (4.169), we obtain

$$\sigma_{ij} = \frac{2}{\sqrt{I_3}}\left\{\frac{\partial W}{\partial I_1}B_{ij} + \frac{\partial W}{\partial I_2}(I_1 B_{ij} - B_{ik}B_{kj}) + I_3\frac{\partial W}{\partial I_3}\delta_{ij}\right\} \tag{4.173}$$

or

$$\sigma_{ij} = \frac{2}{\sqrt{I_3}}\left\{\left(\frac{\partial W}{\partial I_1} + I_1\frac{\partial W}{\partial I_2}\right)B_{ij} - \frac{\partial W}{\partial I_2}B_{ik}B_{kj} + I_3\frac{\partial W}{\partial I_3}\delta_{ij}\right\} \qquad \text{with } I_3 = \left(\frac{\rho_0}{\rho}\right)^2 \tag{4.174}$$

Equation (4.174) is the constitutive equation for isotropic hyperelasticity and we observe that the scalar coefficients of (4.174) are derived from a single scalar function $W(I_1, I_2, I_3)$. Equation (4.174) has the same form as the constitutive equation (4.129) of Cauchy elasticity. But, in the case of Cauchy elasticity, there are three scalar functions $\varphi_k(I_1, I_2, I_3)$ which need to be determined from experiments.

We now discuss the constraints due to incompressibility. Under moderate stress 10,000 psi (68.9 MPa), the assumption of incompressibility is valid for rubber. When the material is incompressible, we can write

$$I_3 = \left(\frac{\rho_0}{\rho}\right)^2 = 1 \tag{4.175}$$

In this case $\partial W/\partial I_3|_{I_3=1}$ is indeterminate and is no longer a material property. Incompressibility is a kinematic constraint expressed by $v_{i,i} = D_{ii} = 0$. The mechanical effect of such a constraint is to give rise to an arbitrary hydrostatic pressure $-p\mathbf{1}$ which does no work. From the energy equation (4.34),

the term $\sigma_{ki}v_{i,k} = \sigma_{ki}D_{ik}$ is not affected by superimposed hydrostatic pressure, that is,

$$(\sigma_{ki} - p\delta_{ki})D_{ik} = \sigma_{ki}D_{ik} - p\delta_{ki}D_{ik} = \sigma_{ki}D_{ik} - pD_{ii} = \sigma_{ki}D_{ik} \tag{4.176}$$

Incompressible materials are capable only of isochoric deformations. The arbitrary hydrostatic pressure is not given by a constitutive equation but is determined by the equations of motion (or equilibrium) and boundary conditions. In this case, the strain-energy density function is written as $W(I_1, I_2)$ and from (4.173) the hyperelastic constitutive equation for incompressible material is written as

$$\sigma_{ij} = 2\{W_1 B_{ij} + W_2(I_1 B_{ij} - B_{ik}B_{kj}) - p\delta_{ij}\} \tag{4.177}$$

where $W_i = \partial W/\partial I_i$. By use of the Cayley–Hamilton theorem (4.177) may also be written as

$$\sigma_{ij} = -p\delta_{ij} + 2W_1 B_{ij} - 2W_2 B_{ij}^{-1} \tag{4.178}$$

EXAMPLE 4.9 The hydrostatic pressure is expressed in the form of Cauchy stress by $\sigma_{ij} = -p\delta_{ij}$. Find corresponding expressions using the 1st and 2nd P–K stresses and discuss the physical meanings of these expressions, if any. Consider cases where the deformation gradient **F** has or does not have a diagonal form.

Solution

From (4.42) and (4.48), we have

$$T_{Ri}^{(0)} = -Jp\delta_{ji}\frac{\partial X_R}{\partial x_j} = -Jp\frac{\partial X_R}{\partial x_i} \tag{a}$$

$$\Pi_{RS} = -Jp\delta_{jk}\frac{\partial X_R}{\partial x_j}\frac{\partial X_S}{\partial x_k} = -Jp\frac{\partial X_R}{\partial x_k}\frac{\partial X_S}{\partial x_k} = -JpC_{RS}^{-1} \tag{b}$$

If **F** has a diagonal form such as

$$[F] = \begin{bmatrix} \lambda_1 & 0 & 0 \\ 0 & \lambda_2 & 0 \\ 0 & 0 & \lambda_3 \end{bmatrix} \qquad [F^{-1}] = \begin{bmatrix} \dfrac{1}{\lambda_1} & 0 & 0 \\ 0 & \dfrac{1}{\lambda_2} & 0 \\ 0 & 0 & \dfrac{1}{\lambda_3} \end{bmatrix} \tag{c}$$

then (a) and (b) become

$$T_{Ri}^{(0)} = -Jp\begin{bmatrix} \dfrac{1}{\lambda_1} & 0 & 0 \\ 0 & \dfrac{1}{\lambda_2} & 0 \\ 0 & 0 & \dfrac{1}{\lambda_3} \end{bmatrix} \qquad \Pi_{RS} = -Jp\begin{bmatrix} \dfrac{1}{\lambda_1^2} & 0 & 0 \\ 0 & \dfrac{1}{\lambda_2^2} & 0 \\ 0 & 0 & \dfrac{1}{\lambda_3^2} \end{bmatrix} \tag{d}$$

There are only normal components in both stress tensors and the sum of the diagonal terms for both cases are

$$\operatorname{tr}\mathbf{T}^{(0)} = -Jp\left(\frac{1}{\lambda_1} + \frac{1}{\lambda_2} + \frac{1}{\lambda_3}\right) \qquad \operatorname{tr}\boldsymbol{\Pi} = -Jp\left(\frac{1}{\lambda_1^2} + \frac{1}{\lambda_2^2} + \frac{1}{\lambda_3^2}\right) \tag{e}$$

We see from (e) that both $\operatorname{tr}\mathbf{T}^{(0)}$ and $\operatorname{tr}\boldsymbol{\Pi}$ are multiples of the hydrostatic stress p, but affected by the stretching or contraction of the material element through λ_i.

If $\mathbf{F}$ does not have the diagonal form, then both $T_{Ri}^{(0)}$ and Π_{RS} do not have the diagonal form. In other words, even though we can still find $\operatorname{tr}\mathbf{T}^{(0)}$ and $\operatorname{tr}\boldsymbol{\Pi}$ and both are multiples of the hydrostatic stress p, shear stresses arise in both $T_{Ri}^{(0)}$ and Π_{RS} so that it is fair to say that the 1st and 2nd P–K stresses are hydrostatic pressure sensitive, while the Cauchy stress is not. The shear components of the Cauchy stress are not affected by the superimposed hydrostatic pressure.

4.8.4 Applications of Isotropic Hyperelasticity

This section discusses some simple applications of the constitutive equation for isotropic hyperelasticity. If the strain-energy function W is known for an incompressible material, then the stress is determined by (4.177) or (4.178) up to a hydrostatic pressure, which is in turn determined from the boundary condition. The complexity of the governing equations usually calls for numerical means to solve them. However, some simple problems may be solved by the inverse method. In this method, we first assume a suitable form for the deformation and then use the constitutive equations to find the associated stresses and consider the restrictions imposed by the equations of equilibrium. Finally, we determine the surface tractions necessary to maintain the deformation.

These simple problems serve to illustrate the method of solution in finite elasticity, and some of these problems have added importance in that they may be experimentally investigated. They are then used to determine the form of the strain-energy function of a given elastic material. The following

two forms of the strain-energy function are well known. They are

$$W = C(I_1 - 3) \tag{4.179}$$

and

$$W = C_1(I_1 - 3) + C_2(I_2 - 3) \tag{4.180}$$

in which C, C_1, and C_2 are constants. Form (4.179) is known as the Neo-Hookean form which was derived from kinetic theory of rubber by Treloar. Form (4.180) is known as the Mooney form or the Mooney–Rivlin form. Following Rivlin [3], the strain-energy function $W = W(I_1, I_2, I_3)$ of an isotropic material, which is normally expressed in a polynomial of I_1, I_2, and I_3, may be equally expressed as a polynomial function of $(I_1 - 3)$, $(I_2 - 3)$, and $(I_3 - 1)$. Thus,

$$W = \sum_{\alpha,\beta,\gamma} A_{\alpha\beta\gamma}(I_1 - 3)^\alpha (I_2 - 3)^\beta (I_3 - 1)^\gamma \tag{4.181}$$

where $A_{\alpha\beta\gamma}$ are constants. When the material is undeformed, $C_{11} = C_{22} = C_{33} = 1$, and $I_1 - 3 = 0$, $I_2 - 3 = 0$, $I_3 - 1 = 0$. Following this approach, the strain-energy function for incompressible material is given by

$$W = \sum_{\alpha,\beta} A_{\alpha\beta}(I_1 - 3)^\alpha (I_2 - 3)^\beta \tag{4.182}$$

4.8.4.1 *Uniaxial extension*

In the case of uniform extensions, the deformation is given by (3.18). Using (3.18), we find

$$[B] = \begin{bmatrix} \lambda_1^2 & 0 & 0 \\ 0 & \lambda_2^2 & 0 \\ 0 & 0 & \lambda_3^2 \end{bmatrix}, \qquad [B^2] = \begin{bmatrix} \lambda_1^4 & 0 & 0 \\ 0 & \lambda_2^4 & 0 \\ 0 & 0 & \lambda_3^4 \end{bmatrix} \tag{4.183}$$

Substituting (4.183) into (4.177), we obtain

$$\sigma_{11} = 2\{W_1\lambda_1^2 + W_2(I_1\lambda_1^2 - \lambda_1^4) - p\} \tag{4.184a}$$

$$\sigma_{22} = 2\{W_1\lambda_2^2 + W_2(I_1\lambda_2^2 - \lambda_2^4) - p\} \tag{4.184b}$$

$$\sigma_{33} = 2\{W_1\lambda_3^2 + W_2(I_1\lambda_3^2 - \lambda_3^4) - p\} \tag{4.184c}$$

For uniaxial test, $\sigma_{22} = \sigma_{33} = 0$. Using these conditions and subtracting (4.184b) from (4.184a), we obtain

$$\sigma_{11} = 2\{W_1(\lambda_1^2 - \lambda_2^2) + W_2[I_1(\lambda_1^2 - \lambda_2^2) - (\lambda_1^4 - \lambda_2^4)]\} \tag{4.185}$$

which reduces to

$$\sigma_{11} = 2(\lambda_1^2 - \lambda_2^2)\{W_1 + W_2(I_1 - \lambda_1^2 - \lambda_2^2)\} \tag{4.186}$$

or

$$\sigma_{11} = 2(\lambda_1^2 - \lambda_2^2)\{W_1 + \lambda_3^2 W_2\} \tag{4.187}$$

The expression $I_1 = \lambda_1^2 + \lambda_2^2 + \lambda_3^2$ was used to arrive at this equation. In addition, by subtracting (4.184c) from (4.184b), we obtain

$$0 = 2(\lambda_2^2 - \lambda_3^2)\{W_1 - \lambda_1^2 W_2\} \tag{4.188}$$

This quantity must vanish for all λ_1 and, therefore, $\lambda_2 = \lambda_3$. If the material is incompressible, then $\det \mathbf{F} = 1$, so that

$$\lambda_1 \lambda_2^2 = 1 \qquad \text{with } \lambda_2 = \lambda_3 \tag{4.189}$$

Hence, by substituting (4.189) into (4.187), we obtain

$$\frac{\sigma_{11}}{\lambda_1^2 - (1/\lambda_1)} = 2\left\{W_1 + \frac{1}{\lambda_1} W_2\right\} \tag{4.190}$$

In the experiments of uniaxial tension and compression, σ_{11} and λ_1 may be measured and the left-hand side of (4.190) may be calculated. The details of the experiments are reported in Rivlin and Saunders [4] from vulcanized rubber test-pieces. The experimental results show that when $\sigma_{11}/(\lambda_1^2 - \lambda_1^{-1})$ is plotted against $1/\lambda_1$, the material response for the case of $1/\lambda_1 < 1$ (tension) is quite different from that for the case of $1/\lambda_1 > 1$ (compression). The experimental data in the tension zone and in the compression zone can be best fitted by the Mooney form (4.180) and the Neo-Hookean form (4.179), respectively. Figure 4.8 shows a schematic plot of the two models each applied in the recommended zone.

4.8.4.2 Simple shear

The simple shear deformation has been previously discussed in Section 3.4.1.2 and Example 3.3. The transformation equations for this deformation are

$$x_1 = X_1 + kX_2, \qquad x_2 = X_2, \qquad x_3 = X_3 \tag{4.191}$$

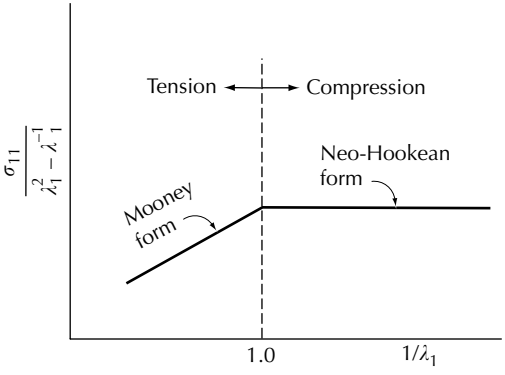

FIGURE 4.8
Uniaxial tension and compression.

where k is a nonzero constant, and, based on (4.191), we find

$$[B] = \begin{bmatrix} 1+k^2 & k & 0 \\ k & 1 & 0 \\ 0 & 0 & 1 \end{bmatrix} \qquad [B^{-1}] = \begin{bmatrix} 1 & -k & 0 \\ -k & 1+k^2 & 0 \\ 0 & 0 & 1 \end{bmatrix} \tag{4.192}$$

with

$$I_1 = 3 + k^2, \qquad I_2 = 3 + k^2 \quad \text{and} \quad I_3 = 1 \tag{4.193}$$

Thus, there is no change in volume during simple shearing. Using the hyperelastic constitutive equation (4.178), we find

$$\sigma_{11} = -p + 2(1+k^2)W_1 - 2W_2 \tag{4.194a}$$

$$\sigma_{22} = -p + 2W_1 - 2(1+k^2)W_2 \tag{4.194b}$$

$$\sigma_{33} = -p + 2W_1 - 2W_2 \tag{4.194c}$$

$$\sigma_{12} = k\mu(k^2) \qquad \sigma_{23} = \sigma_{31} = 0 \tag{4.194d}$$

in which the hydrostatic pressure p is to be determined by the prescribed boundary conditions and

$$\mu(k^2) = 2(W_1 + W_2) \tag{4.194e}$$

where $\mu(k^2)$ is usually referred to as the generalized shear modulus. We note that k is the shear strain, and when we reverse the direction of shear, we change the sign of the shear stress. This is satisfied only when $\mu(k^2) > 0$.

In the case of small deformations, it is known that the simple shear deformation can be maintained by applying only shear stresses without normal

stresses on the faces of the specimen. In a finite deformation, we inquire whether this is still true, for shear strain $k \neq 0$. By setting $\sigma_{11} = \sigma_{22} = \sigma_{33} = 0$, we obtain from (4.194) that

$$\begin{aligned} -p + 2(1+k^2)W_1 - 2W_2 &= 0 \\ -p + 2W_1 - 2(1+k^2)W_2 &= 0 \\ -p + 2W_1 - 2W_2 &= 0 \end{aligned} \tag{4.195}$$

Solving the set of equations in (4.195) for a nontrivial solution for $-p, 2W_1$, and $-2W_2$, the determinant of the coefficient matrix has to be zero. Thus,

$$\begin{vmatrix} 1 & 1+k^2 & 1 \\ 1 & 1 & 1+k^2 \\ 1 & 1 & 1 \end{vmatrix} = k^4 = 0 \tag{4.196}$$

We obtain from (4.196) that $k = 0$, which corresponds to no shear deformation and is in contradiction with the assumption that $k \neq 0$. On the other hand, the trivial solution of $p = W_1 = W_2 = 0$, from (4.194a–e), leads to $\mu(k^2) = 0$ and $\sigma_{12} = \sigma_{11} = \sigma_{22} = \sigma_{33} = 0$, that is, the shear strain $k \neq 0$ gives rise to no stresses, in contradiction with experimental observations. We therefore conclude that the simple shear deformation cannot be maintained by applying only shear stresses on the faces of the specimen. Generally, normal stresses must also be applied. From (4.194), the mean stress is

$$\tfrac{1}{3}\sigma_{kk} = (-p + 2W_1 - 2W_2) + \tfrac{2}{3}k^2(W_1 - W_2) \tag{4.197}$$

When k, $-p$, W_1, and W_2 are all nonzero, then (4.197) gives rise to a nonzero mean stress. If normal stresses are not applied, then the material element will either expand or contract in volume according to the sign of the mean stress. However, this deformation is not a simple shear deformation.

From (4.194a–e), we may also obtain

$$\sigma_{11} - \sigma_{22} = k\sigma_{12} \tag{4.198}$$

This relation does not depend on the form of the strain-energy function. An implication of this equation is that during shearing, the normal stresses σ_{11} and σ_{22} cannot be equal. The existence of these unequal normal stresses is called the Poynting effect. This effect was first investigated by Poynting [5] who performed a series of torsion experiments on metal wires and observed the lengthening of wires when no axial force was applied. This effect is also known as the axial effect and is discussed later related to plastic deformation.

In order to maintain the simple shear deformation, normal stress σ^N and shear stress σ^S must be applied on the inclined faces of the deformed

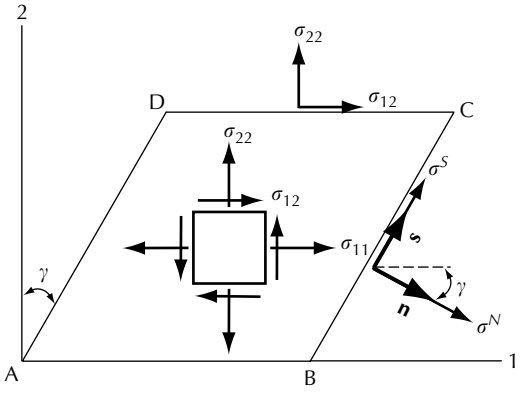

FIGURE 4.9
Simple shear.

specimen. These stresses are now calculated. Referring to Figure 4.9, the outward normal **n** to the inclined surface BC has components

$$[n] = [\cos\ \gamma, -\sin\ \gamma, 0] \tag{4.199}$$

where the angle γ is defined by $k = \tan\gamma$, with $\sin\gamma = k/\sqrt{1+k^2}$ and $\cos\gamma = 1/\sqrt{1+k^2}$. The unit tangential vector **s** has components

$$[s] = [\sin\gamma, \cos\gamma, 0] \tag{4.200}$$

The normal and shear components are then

$$\sigma^N = \sigma_{ij} n_j n_i = [\cos\gamma \quad -\sin\gamma \quad 0] \begin{bmatrix} \sigma_{11} & \sigma_{12} & 0 \\ \sigma_{12} & \sigma_{22} & 0 \\ 0 & 0 & \sigma_{33} \end{bmatrix} \begin{bmatrix} \cos\gamma \\ -\sin\gamma \\ 0 \end{bmatrix}$$

$$= \sigma_{11}\cos^2\gamma + \sigma_{22}\sin^2\gamma - \sigma_{12}\sin 2\gamma \tag{4.201}$$

$$\sigma^S = \sigma_{ij} n_j s_i = \frac{(\sigma_{11} - \sigma_{22})}{2}\sin 2\gamma + \sigma_{12}\cos 2\gamma \tag{4.202}$$

Since $\sin 2\gamma = 2k/(1+k^2)$, $\cos 2\gamma = (1-k^2)/(1+k^2)$, and $\sigma_{11} - \sigma_{22} = k\sigma_{12}$, it is easily shown that

$$\sigma^{\mathrm{N}} = \sigma_{22} - k\sigma^S \quad \text{and} \quad \sigma^S = \frac{\sigma_{12}}{1+k^2} \tag{4.203}$$

We now see that $\sigma^S < \sigma_{12}$ and $\sigma^N < \sigma_{22}$. This assures that if σ_{22} is in compression and is negative, so is σ^N in compression.

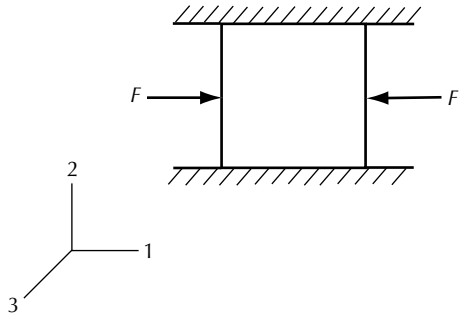

FIGURE 4.10
Biaxial compression of a cubic block.

EXAMPLE 4.10 Find the state of stress in the biaxial compression of a cubic block.

Solution

This test is sometimes referred to as the confined compression test. Referring to Figure 4.10, the block is confined in the 2-direction, while a compressive force F is applied in the 1-direction. The 3-direction is free. The deformation is governed by

$$x_1 = \lambda_1 X_1, \qquad x_2 = \lambda_2 X_2, \qquad x_3 = \lambda_3 X_3 \tag{a}$$

and we find from (a)

$$[F] = \begin{bmatrix} \lambda_1 & 0 & 0 \\ 0 & \lambda_2 & 0 \\ 0 & 0 & \lambda_3 \end{bmatrix}, \qquad [B] = \begin{bmatrix} \lambda_1^2 & 0 & 0 \\ 0 & \lambda_2^2 & 0 \\ 0 & 0 & \lambda_3^2 \end{bmatrix}, \qquad [B^2] = \begin{bmatrix} \lambda_1^4 & 0 & 0 \\ 0 & \lambda_2^4 & 0 \\ 0 & 0 & \lambda_3^4 \end{bmatrix} \tag{b}$$

with $|F| = \lambda_1\lambda_2\lambda_3 = \lambda_1\lambda_3 = 1$. We used $\lambda_2 = 1$, since the block cannot deform along the 2-direction. The stresses are found by putting (b) into (4.177), which leads to (4.184a–c). Because the 3-direction is free, we write $\sigma_{33} = 0$. Using this constraint, (4.184c) becomes

$$p = W_1\lambda_3^2 + W_2(I_1\lambda_1^3 - \lambda_3^4) \tag{c}$$

Substituting (c) into (4.184a), we then obtain

$$\sigma_{11} = 2\{W_1\lambda_1^2 + W_2(I_1\lambda_1^2 - \lambda_1^4) - W_1\lambda_3^2 - W_2(I_1\lambda_3^2 - \lambda_3^4)\} \tag{d}$$

The first invariant of **B** is

$$I_1 = \lambda_1^2 + \lambda_2^2 + \lambda_3^2 = \lambda_1^2 + 1 + \frac{1}{\lambda_1^2} \tag{e}$$

Applying (e), (d) may be further reduced to

$$\sigma_{11} = 2\left(\lambda_1^2 - \frac{1}{\lambda_1^2}\right)\{W_1 + W_2\} \tag{f}$$

Similarly, we obtain the following equation from (4.184b)

$$\sigma_{22} = 2\left(1 - \frac{1}{\lambda_1^2}\right)\{W_1 + W_2\lambda_1^2\} \tag{g}$$

For the Neo-Hookean form given by (4.179), $W_1 = C$ and $W_2 = 0$. The stresses are found from (f) and (g) as

$$\sigma_{11} = 2\left(\lambda_1^2 - \frac{1}{\lambda_1^2}\right)C, \quad \sigma_{22} = 2\left(1 - \frac{1}{\lambda_1^2}\right)C, \qquad C = \text{constant} \tag{h}$$

From (h), we find the following stress ratio which indicates a confined stress in the 2-direction

$$\xi = \frac{\sigma_{22}}{\sigma_{11}} = \frac{1}{1 + \lambda_1^2} \tag{i}$$

Equation (i) is plotted against λ_1 in Figure 4.11. We note that $\xi = 1.0$ when $\lambda_1 = 0$; $\xi = 0.5$ when $\lambda_1 = 1$; and $\xi = 0$ when $\lambda_1 \to \infty$.

For the Mooney form given by (4.180), $W_1 = C_1$ and $W_2 = C_2$. The stresses are found from (f) and (g) as

$$\sigma_{11} = 2\left(\lambda_1^2 - \frac{1}{\lambda_1^2}\right)\{C_1 + C_2\}, \quad \sigma_{22} = 2\left(1 - \frac{1}{\lambda_1^2}\right)\left\{C_1 + C_2\lambda_1^2\right\},$$
$$C_1,\ C_2 = \text{constants} \tag{j}$$

From (j), we find the following stress ratio

$$\xi = \frac{\sigma_{22}}{\sigma_{11}} = \frac{C_1 + C_2\lambda_1^2}{(1 + \lambda_1^2)(C_1 + C_2)} \tag{k}$$

We see from (k) that $\xi = C_1/(C_1 + C_2)$ when $\lambda_1 = 0$; $\xi = 0.5$ when $\lambda_1 = 1$; and $\xi = C_2/(C_1 + C_2)$ when $\lambda_1 \to \infty$. The exact shape of the curve depends on the values of C_1 and C_2. In a special case when $C_1 = C_2$, we obtain $\xi = 0.5$ for

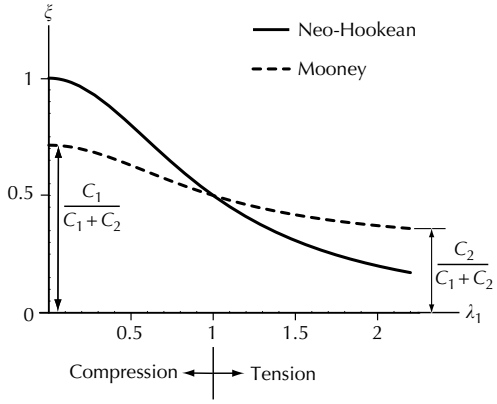

FIGURE 4.11
The ξ ratio plotted against λ_1.

all λ_1. According to Rivlin and Saunders [4], $W_1 > W_2$ for vulcanized natural rubber, and, therefore, $C_1 > C_2$. Equation (k) is plotted in Figure 4.11 for the case of $C_1 = 2.5C_2$ ($C_1 > C_2$). We note that the confining stress σ_{22} is always smaller than σ_{11} for both models. They are equal only in the Neo-Hookean model when $\lambda_1 = 0$, which is a limiting case and cannot realistically happen.

4.9 Infinitesimal Theory of Elasticity

4.9.1 Constitutive Equation

We showed in Section 3.9.1 that, in the case of small displacement gradient, it is not necessary to distinguish the material coordinates X_R from the spatial coordinates x_i. Thus, the infinitesimal strain tensor

$$\varepsilon_{ij} = \tfrac{1}{2}(u_{i,j} + u_{j,i}) \tag{4.204}$$

can and will be used. In this case, both Lagrangian strain **E** and Enlerian strain **e** reduce to **ε**. There are no distinctions among different stress measures and σ_{ij} is used to denote the stress which is also known as the engineering stress. To show that this is indeed the case, we denote the magnitude of the displacement gradient by

$$\varepsilon = (u_{i,R} \cdot u_{i,R})^{1/2} \tag{4.205}$$

We use the notation ε to indicate that this is a small quantity, and it should not be confused with the strain ε used in Chapter 3.

The deformation gradient is

$$F_{iR} = \delta_{iR} + u_{i,R} = \delta_{iR} + \mathrm{O}(\varepsilon) \tag{4.206}$$

where $O(\varepsilon)$ indicates that the magnitude of this term has the order of ε. The determinant is

$$|F_{iR}| = \det(\delta_{iR} + u_{i,R}) = 1 + O(\varepsilon) + O(\varepsilon^2) + O(\varepsilon^3) \tag{4.207}$$

Thus,

$$\rho_0 = \rho|F_{iR}| = \rho(1 + O(\varepsilon) + O(\varepsilon^2) + O(\varepsilon^3)) \tag{4.208}$$

On the other hand the inverse deformation gradient $\mathbf{F}^{-1}$ is

$$X_{R,i} = \delta_{Ri} - u_{R,i} = \delta_{Ri} - O(\varepsilon) \tag{4.209}$$

so that from (4.42) and (4.48) the Piola–Kirchhoff stresses are related to σ_{ij} by

$$T^{(0)}_{Ri} = \frac{\rho_0}{\rho}\sigma_{ji}\frac{\partial X_R}{\partial x_j} = (1 + O(\varepsilon) + \cdots)(\delta_{Rj} - O(\varepsilon))\sigma_{ji} \tag{4.210}$$

and

$$\Pi_{RS} = \frac{\rho_0}{\rho}\sigma_{jk}\frac{\partial X_R}{\partial x_j}\frac{\partial X_S}{\partial x_k} = (1 + O(\varepsilon) + \cdots)(\delta_{Rj} - O(\varepsilon))(\delta_{Sk} - O(\varepsilon))\sigma_{jk} \tag{4.211}$$

In the limit, when $\varepsilon \to 0$, we have

$$T^{(0)}_{Ri} \approx (\delta_{Rj} - O(\varepsilon))\sigma_{ji} \approx \sigma_{Ri} \tag{4.212}$$

$$\Pi_{RS} \approx (\delta_{Rj}\delta_{Sk} + O(\varepsilon))\sigma_{jk} \approx \sigma_{RS} \tag{4.213}$$

which show that the 1st and 2nd P–K stresses are indistinguishable from σ_{ij}.

The constitutive equation for infinitesimal theory of elasticity at room temperature may be obtained by taking the strain-energy function $W(\varepsilon_{ij})$ in a quadratic form, that is,

$$W = \tfrac{1}{2}C_{ijkl}\varepsilon_{ij}\varepsilon_{kl} \tag{4.214}$$

By differentiation of (4.214) with respect to ε_{ij}, we obtain

$$\sigma_{ij} = \frac{\partial W}{\partial \varepsilon_{ij}} = C_{ijkl}\varepsilon_{kl} \tag{4.215}$$

Equation (4.215) is known as the generalized Hooke's law, where C_{ijkl} is a fourth-rank tensor. If the material is isotropic, then C_{ijkl} should be an isotropic tensor, that is, from (1.129)

$$C_{ijkl} = \lambda\delta_{ij}\delta_{kl} + \mu(\delta_{ik}\delta_{jl} + \delta_{il}\delta_{jk}) \tag{4.216}$$

By combining (4.215) and (4.216), we then obtain

$$\sigma_{ij} = \lambda\delta_{ij}\varepsilon_{kk} + 2\mu\varepsilon_{ij} \tag{4.217}$$

where λ and μ are Lamé constants. Note that the number of material constants has been reduced from 81 to 2.

Equation (4.217) may be inverted to express strain in terms of stress. To this end, we make a contraction of (4.217) to get

$$\sigma_{ii} = 3\lambda\varepsilon_{ii} + 2\mu\varepsilon_{ii} = (2\mu + 3\lambda)\varepsilon_{ii} \tag{4.218}$$

so that (4.218) may be solved for ε_{ii} and substituted into (4.217) to obtain

$$\sigma_{ij} = \frac{\lambda\sigma_{kk}}{2\mu + 2\lambda}\delta_{ij} + 2\mu\varepsilon_{ij} \tag{4.219}$$

Finally, we rewrite (4.219) as

$$2\mu\varepsilon_{ij} = \sigma_{ij} - \frac{\lambda}{3\lambda + 2\mu}\sigma_{kk}\delta_{ij} \tag{4.220}$$

This is the equation that we wanted to derive.

4.9.2 Homogeneous Deformations

4.9.2.1 Hydrostatic stress

Consider the strain

$$\varepsilon_{ij} = \begin{bmatrix} \varepsilon_{11} & 0 & 0 \\ 0 & \varepsilon_{22} & 0 \\ 0 & 0 & \varepsilon_{33} \end{bmatrix} \tag{4.221}$$

In the case of hydrostatic stress, $\varepsilon_{11} = \varepsilon_{22} = \varepsilon_{33} = \alpha$. Substituting into (4.217), the stress is

$$\sigma_{ij} = (2\mu + 3\lambda)\alpha\delta_{ij} = -p\delta_{ij} \tag{4.222}$$

Therefore,

$$P = -(2\mu + 3\lambda)\alpha \tag{4.223}$$

and the volumetric strain is

$$\varepsilon_{kk} = 3\alpha = \frac{\sigma_{kk}}{3K} = \frac{-3p}{3K} = \frac{-p}{K} \tag{4.224}$$

where K is the bulk modulus and $\sigma_{kk}/3$ is the mean stress. Thus, by use of (4.223),

$$K = \frac{-p}{3\alpha} = \frac{-p}{(-3p)/(2\mu + 3\lambda)} = \lambda + \frac{2}{3}\mu \tag{4.225}$$

Note that since a hydrostatic pressure always causes the volume to decrease ($\alpha < 0$), we have $K > 0$. In the case that $p < 0$, the volume expands and it is known as dilation.

4.9.2.2 Uniaxial tension

When $\sigma_{11} = \sigma_{22} = 0$ and $\sigma_{33} \neq 0$, Hooke's law reduces to

$$\begin{aligned} \sigma_{11} &= 2\mu\varepsilon_{11} + \lambda(\varepsilon_{11} + \varepsilon_{22} + \varepsilon_{33}) = 0 \\ \sigma_{22} &= 2\mu\varepsilon_{22} + \lambda(\varepsilon_{11} + \varepsilon_{22} + \varepsilon_{33}) = 0 \\ \sigma_{33} &= 2\mu\varepsilon_{33} + \lambda(\varepsilon_{11} + \varepsilon_{22} + \varepsilon_{33}) \end{aligned} \tag{4.226}$$

Comparing the first two equations of (4.226), we find

$$\varepsilon_{11} = \varepsilon_{22} = -\frac{\lambda}{2\mu}(\varepsilon_{33} + 2\varepsilon_{22}) \tag{4.227}$$

which may be solved to obtain

$$\varepsilon_{11} = \varepsilon_{22} = -\frac{\lambda}{2(\lambda + \mu)}\varepsilon_{33} = -\nu\varepsilon_{33} \tag{4.228}$$

where

$$\nu = \frac{1}{2}\frac{\lambda}{\lambda + \mu} \tag{4.229}$$

is Poisson's ratio. By substituting these expressions into the third equation of (4.226), we obtain

$$\begin{aligned} \sigma_{33} &= 2\mu\varepsilon_{33} + \lambda(1 - 2\nu)\varepsilon_{33} = (2\mu + \lambda - 2\nu\lambda)\varepsilon_{33} \\ &= \left(2\mu + \lambda - \frac{\lambda^2}{\lambda + \mu}\right)\varepsilon_{33} = \frac{\mu(3\lambda + 2\mu)}{\lambda + \mu}\varepsilon_{33} = E\,\varepsilon_{33} \end{aligned} \tag{4.230}$$

where $E = \mu(3\lambda + 2\mu)/(\lambda + \mu)$ is known as Young's modulus. In an elastic material, $E > 0$ and $\nu > 0$.

4.9.2.3 Simple shear

In the infinitesimal deformation, simple shear does not give rise to normal stresses. The nonzero strain components are $\varepsilon_{12} = \varepsilon_{21}$ only. From (4.217), the shear stress is

$$\sigma_{12} = 2\mu\varepsilon_{12} \tag{4.231}$$

where $\mu > 0$ is the shear modulus. The engineering shear strain is $2\varepsilon_{12}$.

4.9.3 Boundary-Value Problems

In solving boundary-value problems of isothermal infinitesimal elasticity, the fundamental equations are the equations of motion,

$$\sigma_{ki,k} + b_i = \rho \frac{D^2 u_i}{Dt^2} \tag{4.232}$$

the constitutive equations,

$$\sigma_{ij} = \lambda\delta_{ij}\varepsilon_{kk} + 2\mu\varepsilon_{ij} \tag{4.233}$$

and the strain–displacement relation,

$$\varepsilon_{ij} = \tfrac{1}{2}(u_{i,j} = +u_{j,i}) \tag{4.234}$$

There are three equations in (4.232), six equations in (4.233) and six equations in (4.234), and the unknowns are $\sigma_{ij}, \varepsilon_{ij}, u_i$. We have 15 equations to solve for 15 unknowns. In finding the solution, the boundary conditions should be used. There are three types of boundary-value problems: the displacement boundary-value problems have u_i specified on the boundary S; the traction boundary-value problems have the stress vector $t_i^{(n)}$ specified on S; and the mixed boundary-value problems have u_i specified on part of S and $t_i^{(n)}$ specified on the remaining part of S. The surface traction is given, from (2.8), by

$$t_i^{(n)} = \sigma_{ji} n_j \tag{2.8}$$

4.10 Hypoelasticity

Hypoelasticity is not elasticity, because the stress in hypoelasticity depends on the strain-path. This type of constitutive equation is popular in computational mechanics as it is of the rate-type. The rate-type equations have

advantages over other types of equations due to the ease in numerical computation. We first write the generalized Hooke's law (4.217) of the infinitesimal elasticity in the rate form as

$$\dot{\sigma}_{ij} = 2\mu\dot{\varepsilon}_j + \lambda\delta_{ij}\dot{\varepsilon}_{kk} \tag{4.235}$$

and then inquire what the corresponding constitutive equation should be for finite deformation. We learned at the beginning of this chapter that objective rates need to be used in a constitutive equation. The Jaumann stress-rate is a popular objective stress rate and is used together with the rate of deformation tensor, so that an appropriate hypoelastic constitutive equation is written as

$$\sigma_{ij}^{\nabla} = 2\mu D_{ij} + \lambda\delta_{ij}D_{kk} \tag{4.236}$$

A discussion using other objective stress-rates is given in Chapter 7 in connection with the study of plastic deformation. We discuss now a simple example using (4.236). Let us consider simple shear having the following equations

$$x_1 = X_1 + 2\omega t\, X_2, \qquad x_2 = X_2, \qquad x_3 = X_3 \tag{4.237}$$

$$u_1 = 2\omega t\, X_2, \quad u_2 = u_3 = 0, \qquad \omega = \text{constant} \tag{4.238}$$

$$[L] = \begin{bmatrix} 0 & 2\omega & 0 \\ 0 & 0 & 0 \\ 0 & 0 & 0 \end{bmatrix}, \qquad [D] = \begin{bmatrix} 0 & \omega & 0 \\ \omega & 0 & 0 \\ 0 & 0 & 0 \end{bmatrix}, \qquad [W] = \begin{bmatrix} 0 & \omega & 0 \\ -\omega & 0 & 0 \\ 0 & 0 & 0 \end{bmatrix} \tag{4.239}$$

Substituting (4.239) into (4.236), we find

$$\sigma_{ij}^{\nabla} = 2\mu D_{ij} \quad \text{and} \quad D_{kk} = 0 \tag{4.240}$$

But the Jaumann rate is

$$\sigma^{\nabla} = \frac{\mathrm{D}\sigma}{\mathrm{D}t} - \mathbf{W}\cdot\boldsymbol{\sigma} + \boldsymbol{\sigma}\cdot\mathbf{W} = 2\mu\mathbf{D} \tag{4.241}$$

For the stress given by

$$[\sigma] = \begin{bmatrix} \sigma_{11} & \sigma_{12} & 0 \\ \sigma_{12} & \sigma_{22} & 0 \\ 0 & 0 & 0 \end{bmatrix} \tag{4.242}$$

we can compute the following matrices

$$[\sigma][W] = \begin{bmatrix} -\omega\sigma_{12} & \omega\sigma_{11} & 0 \\ -\omega\sigma_{22} & \omega\sigma_{12} & 0 \\ 0 & 0 & 0 \end{bmatrix},$$
$$-[W][\sigma] = ([\sigma][W])^{\mathrm{T}} = \begin{bmatrix} -\omega\sigma_{12} & -\omega\sigma_{22} & 0 \\ \omega\sigma_{11} & \omega\sigma_{12} & 0 \\ 0 & 0 & 0 \end{bmatrix} \tag{4.243}$$

Substituting (4.242) and (4.243) into (4.241), the component equations are

$$\frac{\mathrm{d}\sigma_{11}}{\mathrm{d}t} = 2\omega\sigma_{12}, \qquad \frac{\mathrm{d}\sigma_{22}}{\mathrm{d}t} = -2\omega\sigma_{12}, \qquad \frac{\mathrm{d}\sigma_{12}}{\mathrm{d}t} = 2\mu\omega - \omega(\sigma_{11} - \sigma_{22}) \tag{4.244}$$

Note that $\mathrm{D}/\mathrm{D}t = \mathrm{d}/\mathrm{d}t$ in this homogeneous deformation. By differentiating (4.244c) with respect to t and making use of (4.244a,b), we obtain the ordinary differential equation

$$\frac{\mathrm{d}^2\sigma_{12}}{\mathrm{d}t^2} = -4\omega^2\sigma_{12} \tag{4.245}$$

The general solution of (4.245) is

$$\sigma_{12} = A\,\sin(2\omega t) + B\,\cos(2\omega t) \tag{4.246}$$

where A and B are constants. We define the shear strain by $\gamma = \int_0^t D_{12}\,\mathrm{d}t$, and, during loading, the shear strain is

$$\gamma = 2\omega t \tag{4.247}$$

Note that γ is not a component of a strain tensor. By taking the initial shear stress to be $\sigma_{12}(t = 0) = 0$, we find from (4.246) that $B = 0$. Therefore, we obtain the following stress components

$$\sigma_{12} = \mu \sin\gamma, \quad \sigma_{11} = -\sigma_{22} = \mu(1 - \cos\gamma), \qquad \text{other } \sigma_{ij} = 0 \tag{4.248}$$

It can be seen from (4.248) that the shear and axial stresses oscillate with the increasing shear strain, and these are physically unacceptable with any real material. Nagtegall and de Jong [6] discussed this oscillatory behavior of the shear stress in his application of a plasticity model. The work triggered a long-lasting investigation of objective stress rates by various investigators, and the subject is discussed further in Chapter 7 in connection with finite plasticity. Equations of (4.248) are plotted in Figure 4.12 with $\mu = 26.2$ GPa, which is a typical value for cast high-purity aluminum.

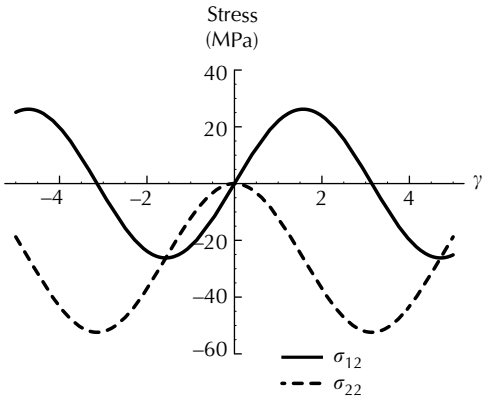

FIGURE 4.12
Hypoelastic stress–strain curves by use of Jaumann stress rate.

References

1. Rivlin, R.S. and Ericksen, J.L., Stress–deformation relations for isotropic materials, *J. Ration. Mech. Anal.*, 4, 323, 1955.
2. Green, A.E. and Adkins, T.E., *Large Elastic Deformations*, Oxford University Press, Oxford, 1960, 7.
3. Rivlin, R.S., Some topics in finite elasticity, in *Proc. 1st Symp. Naval Structural Mech.*, Goodier, J.N. and Hoff, N.J., Eds., 1958, 169.
4. Rivlin, R.S. and Saunders, D.W., Large elastic deformations of isotropic materials VII. Experiments on the deformation of rubber, *Phil. Trans. R. Soc. Lond.*, A243, 251, 1951.
5. Poynting, J.H., On pressure perpendicular to the shear planes in finite pure shears, and on the lengthening of loaded wires when twisted, *Proc. R. Soc.*, A82, 546, 1909.
6. Nagtegall, J.C. and de Jon, J.E., Some aspects of non-isotropic workhardening in finite strain plasticity, in *Proc. Workshop on Plasticity of Metals at Finite Strain: Theory, Experiment and Computation*, Lee, E.H. and Mallet, R.L., Eds., Stanford University, 1981, 65.

Problems

(1) Consider uniform extension of a material element followed by simple shearing. In the uniform extension along the X_2 direction, a particle at $\mathbf{X}$ is displaced to $\mathbf{X}'$ by

$$X_1' = \beta(t)X_1, X_2' = \alpha(t)X_2, X_3' = \beta(t)X_3$$

The subsequent simple shearing is expressed as

$$x_1 = X_1' + 2\eta(t)X_2', \qquad x_2 = X_2', \qquad x_3 = X_3'$$

where $2\eta(t)$ is the shear strain after the uniform extension. Find the components of the 1st and 2nd P–K stresses expressed in terms of the Cauchy stress components.

(2) For isotropic hyperelastic materials, show that the principal axes of the Cauchy stress and the left Cauchy–Green tensor coincide.

(3) Consider a compressible isotropic hyperelastic material. For the deformation given by

$$x_1 = \alpha(t)X_1, \qquad x_2 = \alpha(t)X_2, \qquad x_3 = \alpha(t)X_3$$

discuss the corresponding state of stress. Obtain an expression for the stress vector and discuss the volume change of the material element.

(4) Discuss the simple shear problem by means of Cauchy elasticity, that is,

$$\sigma_{ij} = \chi_0\delta_{ij} + \chi_1 B_{ij} + \chi_{-1}B_{ij}^{-1}$$

where χ_0, χ_1, and χ_{-1} are functions of I_1, I_2, and I_3.

(5) Find the state of stress in the biaxial compression of a cubic block discussed in Example 4.10, if the strain-energy function is given by

$$W = \sum_i C_1(\lambda_i^2 - 1) + C_2\left(\frac{1}{\lambda_i^2} - 1\right)$$

where C_1 and C_2 are constants and λ_i are the stretch ratios.

(6) Find the state of stress in the simple torsion of a circular cylinder of incompressible hyperelastic material with length l and radius a. The deformation of this problem is expressed by

$$\begin{aligned} x_1 &= (\cos\,\tau X_3)X_1 - (\sin\,\tau X_3)X_2, \\ x_2 &= (\sin\,\tau X_3)X_1 + (\cos\,\tau X_3)X_2, \\ x_3 &= X_3 \end{aligned}$$

where τ is the angle of twist per unit length and is a constant.

Part II

Continuum Theory of Plasticity

Although physically based polycrystal plasticity is emerging as a feasible method, the phenomenological (continuum) approach is still the practical approach for use in the simulation of engineering problems.

5

Fundamentals of Continuum Plasticity

5.1 Introduction

A general description of plasticity is given in this chapter. Plastic deformation can be easily observed by stretching a thin copper wire. If we stretch a piece of copper wire beyond its elastic limit, then we observe a permanent change in length of the copper wire after the release of the load. This is because the wire is permanently elongated and has undergone a *plastic deformation*. The copper wire is very soft and easily stretched by a small force. The elastic limit of the material (copper) can be easily exceeded. In this one-dimensional case, the experimental stress–strain curve for copper is sketched in Figure 5.1. We use this figure to illustrate properties and terminologies of plastic deformation. When the stress increases from O to A, the strain also has a proportional increase. The process of increasing the stress is known as *loading*. The initial yielding of the material occurs at A and the stress at this point is known as the *yield stress* and is denoted by σ_y. The yield stress is generally regarded as equal to the elastic limit, but the *elastic limit* and the *proportional limit* are experimentally indistinguishable for metals. Several definitions of yield stress have been proposed and they are discussed in Chapter 6. Should the stress be reduced from A back to O, we have an *unloading process*. OA is the elastic region and the Hooke's law applies in this region. All strains within the elastic region are recovered upon unloading and are elastic strains. Point A is the first point beyond which nonrecoverable strain occurs. This strain is permanent and is known as the plastic strain, which is either time-independent or time-dependent. In plasticity, we are interested in the time-independent nonrecoverable strain. The time-dependent nonrecoverable strain is related to creep.

The curve OABE is the *stress–strain curve* for monotonic loading. The initial yielding of material occurs at A and yielding continues as the curve ABE is traversed. The strain at B is ε, which can be divided into the elastic ε^e and plastic ε^p parts, where

$$\varepsilon = \varepsilon^e + \varepsilon^p \tag{5.1}$$

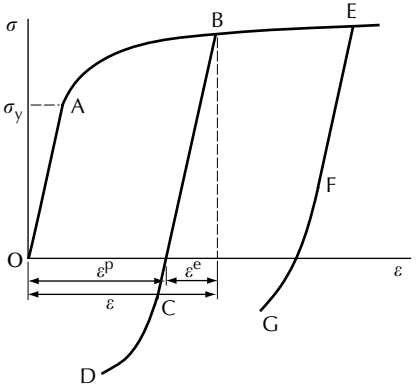

FIGURE 5.1
Schematic stress–strain curve for Cu and Al.

The elastic and plastic strains for point B are shown in Figure 5.1. Curves BCD and EFG are unloading stress–strain curves. The initial part of the unloading curves is straight and the curves gradually bend over. In the figure, sections BC and EF are straight with slopes similar to that of section OA. Generally, for a good approximation, these slopes are assumed to be equal. But, experimental data show that the unloading slope depends on the strain level where the unloading begins to take place. Thus, $E_{OA} > E_{CB} > E_{FE}$, that is, the slope is smaller if unloading occurs at a higher strain level. C and F are points of reverse yielding. Usually, the reverse yielding can occur on the compressive stress side as in point C, but as the strain at which unloading takes place gets higher, the reverse yielding occur on the tension side as in point F. The effect of the decrease in the yield stress in the reverse loading, that is, $|\sigma_{yC}| < |\sigma_{yB}|$, is known as the *Bauschinger effect* and it is an anisotropic hardening.

The description of the stress–strain curve presented above is based on experimental observations and data. An enormous challenge in plasticity is to formulate a realistic mathematical model for describing the observed material behavior. The task is known as *constitutive modeling* and the end product is a constitutive model or a set of constitutive equations. Various theories using different approaches and points of views have been proposed to formulate constitutive equations for metallic materials. Theories have also been formulated based on dislocations and slips. Although physically based *polycrystal plasticity* is emerging as a feasible method, the phenomenological (or continuum) approach is still the practical approach for use in the computational mechanics. Presently, there are great research efforts aiming to bridge the gap between mechanics at microscopic and continuum level. Some exciting results have already been reported and they provide input to the continuum theory of plasticity. Some of these inputs are discussed in Chapter 7 in connection with finite plasticity. In spite of the interest in plasticity at the microscopic level, the continuum theory is still the backbone for the study of plasticity.

In this book, we discuss the continuum approach of plasticity. Most of our discussions are related to the plastic deformation of metals, although some may be applicable to other materials as well. In the study of plasticity, theories and experiments have gone hand-in-hand. Experimental results have led to the development of theories and theoretical studies have suggested new experiments. The ultimate goal is to develop a theory of plasticity that can be experimentally verified.

Experimental results have been greatly influenced by the loading equipment and measuring technology. Problems associated with the loading equipment are the stiffness of the loading machine and the kind of the loading machine. Is it a *dead-weight machine* or is it a *servo-controlled hydraulic testing system*? Older data were gathered by use of dead-weight machine. Dead-weight machines have an advantage in providing steady, well-controlled load increments and it can be used to obtain creep strains, but it cannot be used to execute a strain-controlled test program. Some dead-weight machines have *cross-talks*, that is, the axial load is influenced by the torsion load and vice versa in an axial–torsion test machine, resulting in inaccurate experimental results. Most commercially available servo-hydraulic machines have acceptable cross-talk level. An important advantage of the servo-hydraulic machines is that it is fully automated and it can execute either a strain-controlled or a stress-controlled test program. Due to the nature of the closed-loop servo-controlled machine, the data scatter to an extent which depends on the time interval of data acquisition. This data scatter may affect the accuracy of the data collected. Some examples that are sensitive to this data scatter are Young's modulus of the stress–strain curve and yield stresses. These effects are further discussed in a later section.

The strain can be measured by measuring the motion (displacement and rotation) of the *cross-heads* of the test machine. This method of measurement is, however, influenced by the stiffness of the machine and the shape of the specimens. Let ΔL and $\Delta\phi$, respectively, be the displacement and rotation of the cross-heads, r be the radius of a cylindrical specimen and L be the length of the specimen between the grips, then the axial strain ε and shear strain γ, respectively, are written as $\varepsilon = \Delta L/L$ and $\gamma = r\Delta\phi L$. Since L includes the lengths of the enlarged gripping sections and the uniform gauge section of the specimen, the strains determined by use of the above expressions represent the average strains of the specimen and do not accurately represent the strains of the gauge section. It is the strains of the gauge section that are meaningful.

The stiffness of the machine is not a factor, if we directly measure the strains in the gauge section of the specimen. *Extensometers* or *strain gauges* may be used to accomplish the job. Extensometers may be self-designed and is also available commercially. The resolution of extensometers is around 10^{-3} strain, but it can measure strains of up to about 15%. Extensometer for larger strains needs to be self-designed. Wu and Xu [1] built an axial–torsion extensometer that may be installed and clipped on the uniform gauge section of the specimen. Shear strains of up to 200% have been measured by Wu et al. [2]

using this extensometer. Electrical-resistance strain gauges and strain rosettes are commercially available and they are easy to use. The resolution for this type of strain gauges is around 10^{-6} and it therefore provides much more accurate strain measurements than the extensometers. But, these gauges are limited to a strain of around 2% and either peel off or broken beyond 2% strain. A *post-yield type strain gauge* is available and it can measure axial strains of up to around 15%. No post-yield strain-rosettes are as yet commercially available.

To design an experiment and collect valid data is a challenge and must be carefully pursued. The extension of one-dimensional plasticity into a multi-dimensional plasticity provides an even greater challenge both experimentally and theoretically. In the early development, two major schools of thought were developed; the *flow theory* and the *deformation theory*. The deformation theory was proposed by Hencky in 1924 and the approach was used thereafter by Russian researchers. The Hencky equation is

$$\varepsilon_{ij} = \frac{k\sigma_{kk}}{3}\delta_{ij} + \psi s_{ij} \tag{5.2}$$

where k and ψ are scalars. We note that the total strain ε_{ij} rather than the strain increment $d\varepsilon_{ij}$ is found from (5.2) and, therefore, the deformation theory is also known as the total strain theory. On the other hand, the flow theory emphasizing the strain increment is also known as the incremental theory. The deformation theory is convenient for use, due to mathematical simplicity, in solving problems with proportional loading. The final state of strain is determined by the final state of stress. However, it is known that the equations of deformation theory are not suitable for nonproportional loading condition and the deformation theory will not be further pursued in this book.

In this chapter we describe the fundamentals of plasticity from an experimentalist's view point. The concepts of flow theory is discussed in Chapter 6. The major concepts of flow plasticity are: the *yield surface*, the *flow rule*, the *strain-hardening rule*, and the *loading–unloading conditions*. Experimental evidence is presented together with the mathematical representations and assumptions of the theory are discussed. One of the major assumptions is the *plastic incompressibility* of metallic materials.

Recent developments in plasticity are given in Chapter 7. It includes experimental and theoretical developments both for infinitesimal and finite plasticity. Other developments, such as the *endochronic theory*, are discussed in Chapters 8 and 9. The author has been involved in the development and verification of this theory, and a detailed account of the theory is given. The thermo-mechanical theory of internal state variables is first presented in Chapter 8 and the presentation of the endochronic theory follows. The endochronic theory is an internal variables theory.

Material anisotropy is an important topic of plasticity. The anisotropic properties of metal sheets are discussed in Chapter 10 and, in Chapters 11 and 12, we present a general theory of anisotropic plasticity. Since a square material element in the reference configuration gets distorted by deformation,

curvilinear coordinates must be used and the stress and strain refer to this distorted element. In this way, we investigate the change in properties of the same material mass.

5.2 Some Basic Mechanical Tests

In this section, we discuss some basic experiments used to characterize the mechanical behavior of a material. They include the uniaxial tension test, uniaxial compression test, torsion test, and the creep test. These are one-dimensional tests and aimed to produce axial and shear stress–strain curves and creep curves. They are very simple theoretically, but it is not so simple experimentally to obtain valid data. We refer to Bell [3] for a detailed account of experiments carried out during the first half of the 20th century.

5.2.1 The Uniaxial Tension Test

Uniaxial tensile testing can be carried out quickly and easily and is used to measure the strength and ductility of materials. The specimens for tension test can be round or flat specimens and they consist of enlarged end sections and a reduced gauge section. The round specimens can have threaded ends for gripping and the flat specimens can either be with or without a pin-hole for connection to the load-train. The longer the gauge section is the more accurate the test results will be.

The general shape of the loading stress–strain curve shown in Figure 5.1 is typical of those for aluminum, copper, brass, 304 stainless steel, and high-strength steels such as AISI 4142 steel in the small strain range, that is, when the strain is $<5\%$. The curve does not show a definite yield point. However, the stress–strain curve for low-carbon steel shows a definite upper and lower yield point. After the initial yielding, the stress–strain curve remains flat, during which *Lüder's band* propagates and plastic strain accumulates. Strain-hardening begins when the strain is about 1.5 to 2.0%.

Uniaxial tension test is limited to relatively small strains due to *necking* (a plastic instability) of the specimen. Few metals can stretch $>50\%$ before necking. Thinning of a sheet specimen can occur at a strain $<10\%$. Diametral extensometers have been used at the neck of cylindrical specimens to control tensile test with diametral strain. However, this is not a direct test, because assumptions have to be made to perform the area and triaxiality corrections in order to reconstruct a tensile stress–strain curve. Indirect tests have been used to construct the tensile stress–strain curve at large strain. For instance, sheet rolling, which is relatively insensitive to plastic instability, may be performed to various amounts of thickness reduction and tension specimens cut from the prestrained specimens. These specimens are then tested in uniaxial tension to determine the flow stress.

Even in the small strain range, one important aspect of the tension testing is the large range of data scatter. It is important to know how much confidence we can put in the experimental stress–strain curve. Data scatter associated with tensile testing has been traditionally attributed to the material inhomogeneities. Only recently have researchers suspected that a significant percentage of the data scatter is caused by *test system misalignment*. In a tensile testing system, schematically shown in Figure 5.2, the *load-train* is an assembly of universal joints, pull rods each of length L, grips, and specimen of length l. Some systems have a universal joint at the upper end of the upper pull rod and another at the lower end of the lower pull rod, but some systems have a universal joint only at the upper end of the upper pull rod. Several types of grips have been used: wedge grips, grips with threaded ends, and grips with pinned connections. The former two types are considered to be fixed grips and the latter allows the specimen to rotate about the pins. The fixed grips are one extreme and can sustain moments; while the pin-grips are the other extreme and cannot sustain any significant moment at the pins.

Penny and Leckie [4], using a bi-linear stress–strain curve, investigated the effect of test system misalignment on the stress–strain curve. The numerical results show that for a moderately low value of *eccentricity* ($e/d = 10\%$, where e is eccentricity and d is half-width of specimen) the yield stress shows a 10% drop. More importantly, the results indicate a reduction in the ultimate load that the specimen can sustain. Wu and Rummler [5] pointed out that

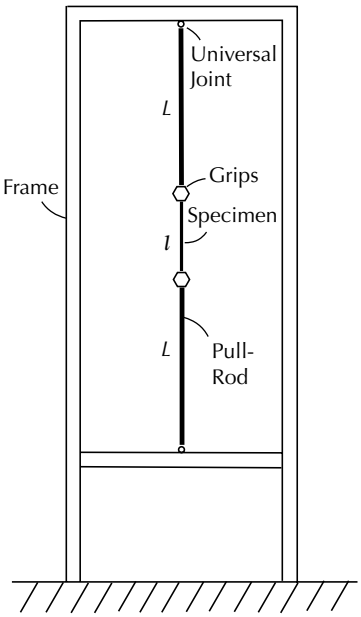

FIGURE 5.2
A tensile testing machine.

the analysis of Penny and Leckie [4] did not correctly predict the effect of test system misalignment, because these authors did not include the effect of pull rods in their analysis even though they mention it as a factor contributing to bending of the specimen. Furthermore, they assumed that the neutral axis (N.A.) of the rectangular cross-sectioned bar remained at the geometrical centerline of the specimen during testing. Due to this assumption, the force P and end moment M acting on the specimen were linearly related. The analysis of Wu and Rummler [5] considered the effect of the pull rods and showed that the neutral axis would move as loading was applied and did not remain at the geometrical centerline of the specimen during testing. Due to the motion of N.A., the relation between P and M was nonlinear.

Three cases of misalignment were considered by Wu and Rummler [5] to be critical and were analyzed separately and their results compared: the symmetric case, the cantilever case, and the case of the pinned specimen with eccentricity. The symmetric case was found to be the most critical one among the three cases and its formulation is given here. The formulation of the other two cases is identical to the one described except for the expressions of the end moment M. The load-train of the symmetric case is shown in Figure 5.3. The offsets and displacements, although exaggerated in the figure, are assumed to be small compared to the width of the specimen. BC represents the misalignment at the upper grip and is denoted by δ^*. This is an overall misalignment

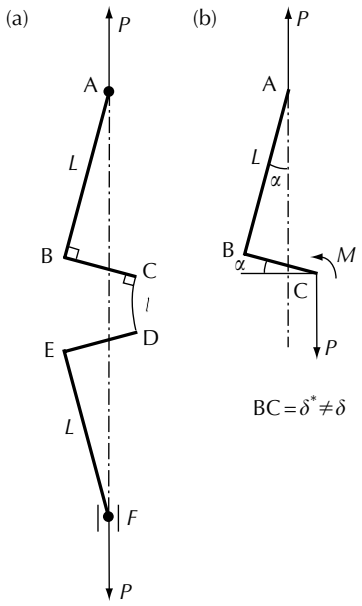

FIGURE 5.3
(a) The load-train, (b) effect of pull-rod (From Wu, H.C. and Rummler, D.R., *J. Eng. Mater. Technol.*, 101, 68, 1979. With permission from ASME).

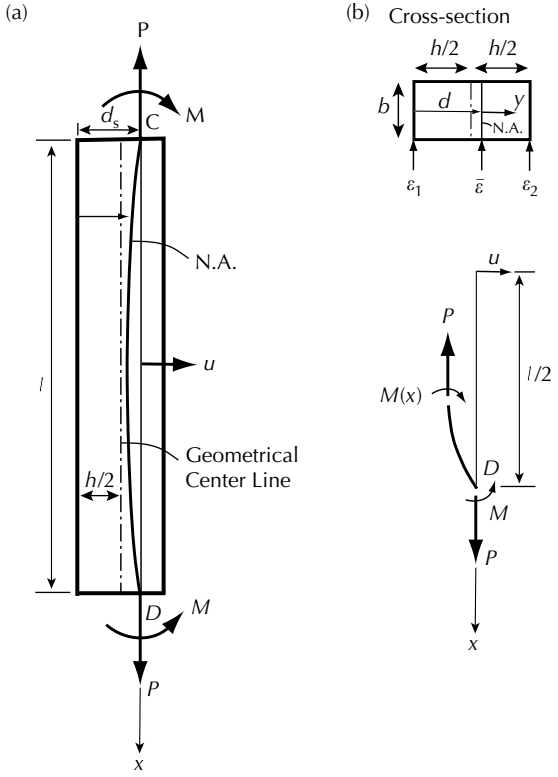

FIGURE 5.4
(a) Deflection, (b) moment and force on a specimen (From Wu, H.C. and Rummler, D.R., *J. Eng. Mater. Technol.*, 101, 68, 1979. With permission from ASME).

effect including the misalignments between the pull rod and the grip and between the grip and the specimen. It is to be noted that δ^* changes as the load increases and its value at zero load is δ. Let point C denote the N.A. at the upper end of the specimen. At zero load, the N.A. coincides with the geometrical centerline of the specimen at end C, but, as the load increases, the N.A. moves away from the geometrical centerline and δ changes to δ^*. Force P and moment M acting at C are shown in Figure 5.3(b). The coordinate system is chosen as follows: the x-axis is fixed to the N.A. of the specimen at the ends (grips), see Figure 5.4(a). Since the N.A. for the whole specimen moves when load is applied, the x-axis also moves (rigid body motion) with it. The deflection u is measured from the x-axis and the y-axis is measured from the N.A. A cross-section of the specimen is also shown, in which $\mathrm{d}(x)$ specifies the location of the N.A. $\varepsilon_1(x), \varepsilon_2(x)$, and $\bar{\varepsilon}$ are, respectively, the longitudinal strain at the right fiber, left fiber, and the N.A. of the specimen. That $\bar{\varepsilon}$ is constant for all x is to be noted. Figure 5.4(b) shows the moment $M(x)$ at an arbitrary point of the specimen.

Under the assumption of plane cross-sections remaining plane during deformation, the strain at a point in the specimen is given by

$$\varepsilon(x, y) = \bar{\varepsilon} - \frac{y}{\rho(x)} \tag{5.3}$$

where $\rho(x)$ is the radius of curvature of the N.A. It is then easy to show that

$$\frac{1}{\rho} = \frac{1}{h}(\varepsilon_2 - \varepsilon_1) \tag{5.4}$$

and

$$d = \rho(\varepsilon_2 - \bar{\varepsilon}) \tag{5.5}$$

Note that $\bar{\varepsilon}$ and ρ remain constant with varying y.

Force acting on the specimen must be balanced to satisfy equilibrium. Thus,

$$P = \int_A \sigma \, \mathrm{d}A = b \int_{-d}^{h-d} \sigma \, \mathrm{d}y \tag{5.6}$$

in which b is the thickness and A is the cross-sectional area of the specimen. Any nonlinear stress–strain relation can be used to express P in terms of the strain by use of (5.6). We will use an equation that is fully discussed in Chapter 8 and has been shown to closely describe the stress–strain curves of metallic materials. The equation is

$$\sigma = A_1(1 + \beta_1\varepsilon)[1 - (1 + \beta_1\varepsilon)^{-n}] \tag{5.7}$$

where A_1, β_1, and n are material constants and the stress on the N.A. is

$$\frac{P}{A} = \sigma(\bar{\varepsilon}) = A_1(1 + \beta_1\bar{\varepsilon})[1 - (1 + \beta_1\bar{\varepsilon})^{-n}] \tag{5.8}$$

Upon the application of constitutive equations (5.7) and (5.6) reduces to

$$P = \frac{bA_1}{\beta_1}\rho\left\{\frac{1}{2}(m_2^2 - m_1^2) - \frac{1}{2-n}(m_2^{2-n} - m_1^{2-n})\right\} \tag{5.9}$$

where

$$m_1 = 1 + \beta_1\varepsilon_1 \quad \text{and} \quad m_2 = 1 + \beta_1\varepsilon_2 \tag{5.10}$$

The balance of moment in the specimen is given by

$$M(x) = -\int_A \sigma y \, \mathrm{d}A \tag{5.11}$$

Using (5.3), which relates y to $\varepsilon(x)$, (5.11) is written as

$$M(x) = -P\bar{\varepsilon}\rho(x) + b\rho^2 \int_{\varepsilon_1}^{\varepsilon_2} \sigma\varepsilon \, \mathrm{d}\varepsilon = M + Pu \tag{5.12}$$

The last equality of (5.12) is found from the equilibrium of a segment of the specimen shown in Figure 5.4(b). Referring to Figure 5.3(b), we can establish the following relation

$$M = P(\delta^* \cos\alpha - L \sin\alpha) \tag{5.13}$$

which reduces in the case of small α to

$$M = P(\delta^* - L\alpha) \tag{5.14}$$

Combining (5.12) and (5.14), and using (5.7), we obtain

$$\begin{aligned} &P(\delta^* + u - L\alpha) \\ &\quad = -P\bar{\varepsilon}\rho + \frac{b\rho^2 A_1}{\beta_1^2}\left\{\frac{1}{3}(m_2^3 - m_1^3) - \frac{1}{3-n}(m_2^{3-n} - m_1^{3-n})\right\} \\ &\quad - \frac{b\rho^2 A_1}{\beta_1^2}\left\{\frac{1}{2}(m_2^2 - m_1^2) - \frac{1}{2-n}(m_2^{2-n} - m_1^{2-n})\right\} \end{aligned} \tag{5.15}$$

The curvature relation is

$$\frac{1}{\rho} = \frac{\mathrm{d}^2 u}{\mathrm{d}x^2} \tag{5.16}$$

Substituting (5.4), (5.10) into (5.16), we obtain

$$\frac{\mathrm{d}^2 u}{\mathrm{d}x^2} = \frac{1}{h\beta_1}(m_2 - m_1) \tag{5.17}$$

Equations (5.9), (5.15), and (5.17) form a system of equations with three variable functions $m_1(x)$, $m_2(x)$, and $u(x)$ subjected to the following boundary conditions

$$\frac{\mathrm{d}u}{\mathrm{d}x} = 0 \quad \text{at } x = 0 \qquad \text{and} \qquad u = 0 \quad \text{at } x = \frac{l}{2} \tag{5.18}$$

Because of symmetry only half of the specimen is considered. To solve the equation set, it is necessary to specify $\bar{\varepsilon}$ and δ in addition to the constants associated with the load-train, specimen geometry, and the constitutive equation. The eccentricity δ is related to δ^* by $\delta^* = \delta + (d_s - (h/2))$, where d_s specifies the location of the N.A. of the specimen at the grip end. This relation may be

visualized from Figure 5.4(a). At zero load, $d_s = h/2$ and $\delta^* = \delta$. The tensile force P is calculated using (5.8). After the solutions for $m_1(x)$, $m_2(x)$, and $u(x)$ have been found, it is easy then to calculate $\varepsilon_1(x)$, $\varepsilon_2(x)$, $\rho(x)$, and $d(x)$.

A numerical example was presented in Wu and Rummler [5] for annealed aluminum. The symmetrical case is presented here. The constants for the constitutive model (5.7) are $A_1 = 37.9$ MPa, $n = 33.33$, and $\beta_1 = 54.55$. ASTM standard sheet-type rectangular specimen is used in this calculation. The dimensions are 63.5 mm (length), 12.7 mm (width), and 3.2 mm (thickness). For the analysis the specimens are assumed to have constant cross-section between grips. In the calculation, the eccentricity is normalized with respect to the width δ/h and is taken as 0.05. The eccentricity of 10% is considered by Penny and Leckie [4] to be moderate. Three different lengths L (127, 254, and 381 mm) of the pull rod were considered in the symmetric case. These are within the range of the commercial testing machines. The effect of pull rod length with respect to specimen length L/l has been found to be significant. The larger the ratio L/l the smaller the percentage of misalignment error. Figure 5.5 shows the four calculated stress–strain curves. The solid curve is the σ versus $\bar{\varepsilon}$ curve, which is obtained from (5.8). This curve is the ideal

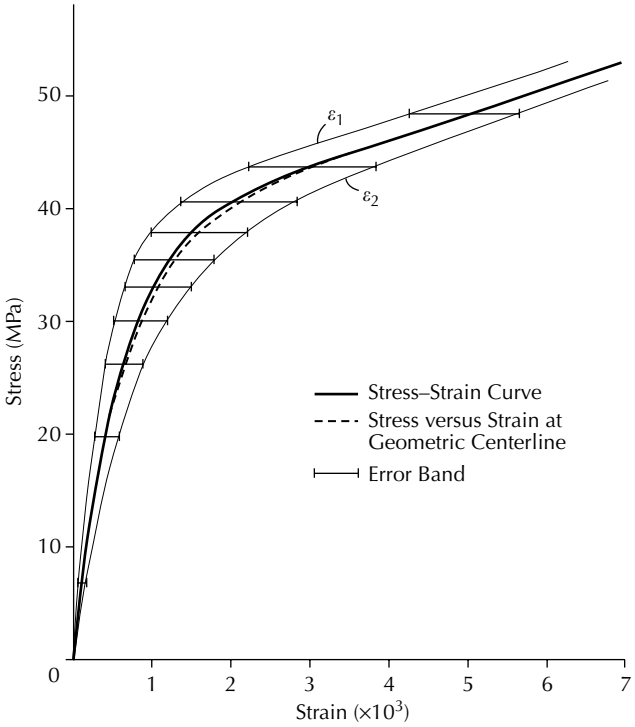

FIGURE 5.5
Effect of misalignment on stress–strain curve (From Wu, H.C. and Rummler, D.R., *J. Eng. Mater. Technol.*, 101, 68, 1979. With permission from ASME).

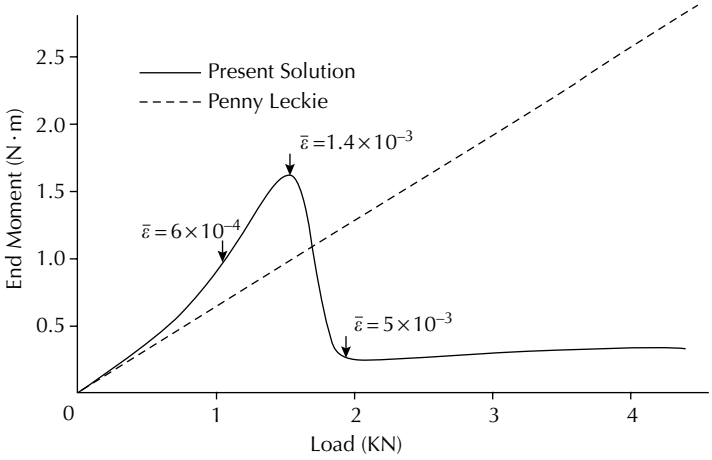

FIGURE 5.6
End-moment versus load (From Wu, H.C. and Rummler, D.R., *J. Eng. Mater. Technol.*, 101, 68, 1979. With permission from ASME).

stress–strain curve and should be the same as that obtained in the case of a perfect test system alignment. The dashed curve is the σ versus $\varepsilon_{\text{cent}}$ curve, which would be obtained by use of an average-type extensometer, where $\varepsilon_{\text{cent}}$ is the strain at the geometric centerline. It is seen that the two curves almost coincide except for the knee portion of the curve. The remaining two curves are obtained from the left and right fibers of the cross-section (see Figure 5.4(b)). The results indicate that the error band for these two curves is quite large for the moderate eccentricity considered. We therefore recommend that, if electrical-resistance strain gauges are used to measure the strain, two gauges are required, one at each side of the flat specimen. The average reading of the two gauges will then provide the strain on the geometrical centerline $\varepsilon_{\text{cent}}$, which is very close to the real strain on the N.A. as shown in Figure 5.5.

The end moment M is plotted (solid curve) against the load P in Figure 5.6. Several strain levels are identified in the figure. The comparison of these strain levels with the stress–strain curve of Figure 5.5 shows that the sudden change of the M–P curve is indeed related to the development of plastic strain in the specimen. The effect of plastic deformation is such that the N.A. of the specimen moves according to the amount of plastic strain. The N.A. moves drastically when the strain levels are within the knee portion of the σ–ε curve. In the figure, the linear relationship assumed by Penny and Leckie [4] is shown in dashed line.

5.2.2 The Uniaxial Compression Test

This test is sometimes called the *unconfined compression test*. The specimen is usually a cylinder. The stress–strain curve obtained from the compression

test is very close to that obtained from the uniaxial tension test in the small strain range. Lüder's band has also been observed after initial yielding for mild steel. However, the strength differential (or S–D) effect has also been a topic of intense investigation. According to Nadai [6], the compression curve lies above the tension curve for wrought iron, carbon steel, and nickel steel, but differs little from the tension curve for copper and aluminum. Spitzig et al. [7] tested 4310 and 4330 steels to a strain of about 4% and found that the S–D effect for both steels was $5.5 \pm 1\%$. The *S–D effect* was defined by

$$\text{S–D} = 2\frac{|\sigma_c| - |\sigma_t|}{|\sigma_c| + |\sigma_t|} \tag{5.19}$$

where the subscripts c and t refer to compression and tension, respectively. For both materials tested the S–D effect occurred in the lower yield region as well as throughout the remainder of the curves.

In a conventional compression test, the specimen is placed between the platens of the cross-heads. Due to the frictional restraint on the ends of the specimen by the platens, the specimen would show a "barreling" effect, which shows a bulged lateral surface as in Figure 5.7(a). As the compressive load increases, two "end cones" form. The two end cones remain elastic, while plastic deformation occurs in the remaining part of the specimen. According to Nadai [6, p. 341], the angle ϕ, which specifies the conical surface, depends on the diameter to height ratio of the cylindrical specimen. It is apparent that the state of stress is not uniform in the specimen and the stress–strain curve obtained from this test is questionable to some extent. Investigators have lubricated specimen ends and platens with various materials, for example, Taylor and Quinney [8], Bridgman [9], and more recently

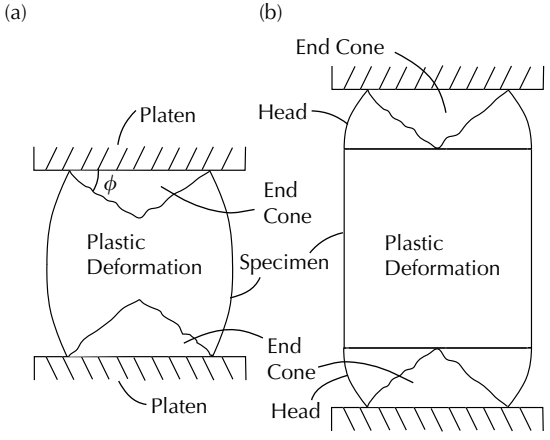

FIGURE 5.7
(a) Barreling effect in compression test, (b) method of Wu [14] to eliminate barreling (From Wu, H.C. et al., *Eng. Fracture Mech.*, 8, 365, 1976. With permission from Elsevier).

Armstrong et al. [10]. The barreling effect has been reduced by the lubrication, but some degrees of barreling still persist. Lubrication was achieved in the testing of Gunasekera et al. [11] by using a thin PTFE (Hostaflon) sheet on either side of the specimen. These authors found that the ratio of PTFE thickness to specimen diameter affects test results. Khan and Liang [12] tested three BCC metals, using rectangular block specimens, under uniaxial compression and then, after finite deformation, under biaxial compression. A layer of thin Teflon sheet (0.0762 mm or 0.003 in.) was used as the lubricant. A small amount of graphite powder lubricant was also put between the Teflon sheets and the surfaces of the apparatus and the specimen. These authors found that the specimen underwent fairly large compressive strain without appreciable barreling. In the testing of brittle materials such as concrete, brush bearing platens have been used to reduce the frictional effect [13].

In [14], the author proposed a method to further reduce the frictional restraint by introducing two heads, one on top and one underneath the specimen, during compression tests (see Figure 5.7(b)). The two heads should be of the same material, width, and thickness as the specimen. It was shown by Coker and Filon [15], using the technique of photoelasticity, that if the height of each head was greater than 0.4 times the height of the specimen, the stress distribution was almost uniform throughout the cross-section of specimen. This method has been proven to be very satisfactory in the testing of ice and cast iron by the author and his coworkers. The advantage of using this method of testing is that, when under compression, the material just above and below the contact surfaces between the heads and the specimen will expand the same amount, since they are of the same composition. The friction at the contact surfaces will thus be a minimum if not equal to zero. Moreover, the contact surfaces may be polished and lubricated to allow horizontal sliding motion of material elements that are adjacent to these contact surfaces, if the elements have a tendency to move. As a result of this arrangement, a uniform lateral expansion of the specimen can be achieved (Figure 5.7(b)) in contrast to the bulged lateral surface under conventional method of testing (Figure 5.7(a)). The strain state as well as the stress state will then be uniform throughout the specimen.

The author tested columnar grained ice in compression [16] using this testing arrangement. The specimens were rectangular in shape with dimensions: 8 cm wide, 12 cm high, and 4 cm thick. In the columnar grained ice, ice grows in the form of columns (along the thickness direction) with the axis of crystallographic symmetry (c-axis) randomly oriented but parallel to the face of the specimen. The ice is thus transversely isotropic. The long direction of the columnar ice crystals was perpendicular to the load direction and underwent very little deformation when the specimen was tested. The top and bottom ice blocks were also prepared from the same ice. These ice blocks (or heads) were of the same crystal orientation, width, thickness as the specimen, but the height was only 6 cm (half that of the specimen). With this experimental arrangement, a uniform strain (stress) state was

achieved within the specimen. This was checked with strain gauges that were embedded at three different locations of a cross-section inside the specimen. No barreling of specimens was observed and the end cones occurred in the two heads. The specimen and the heads were initially transparent before load was applied. As the compressive load increased at a small strain rate, slips within the crystals and micro-cracks, which were largely intercrystalline, formed two families of parallel lines, each making an angle of approximately 45° with the loading direction. The specimen became nontransparent due to these microcracks. The two end cones in the heads remained transparent, however, since no microcracks formed within those regions. The specimens remain whole, without macrocracks. When the specimens were tested at higher strain rates, macroscopic cracks developed parallel to the direction of loading. Finally, we mention that ice can also be viewed as a model material. It is polycrystalline and at low strain rate it is ductile under compression. The author also tested cast iron using the method with two heads (blocks). Specimens of 2.54 cm cube were tested to a compressive strain of 20% without barreling.

Large changes in specimen geometry occur when test is carried out to the large strain range using conventional method of testing. Remachining has been practiced due to barreling. Starting with a very large cylindrical specimen, the diameter is machined down after the test so that we again have a cylindrical specimen for the second compression. After the second compression, the specimen is again remachined to reduce the diameter and to have a favorable length/diameter ratio for the next compression test. According to Hecker et al. [17], a recommended length/diameter ratio is 1.6. The compression test may continue with additional rounds of remachining. Some stress–strain curves for tension and compression in the large strain range may be found in [10] and [17].

5.2.3 The Torsion Test

The shear stress–strain curve of a material is traditionally determined by a torsion test. The shape of the shear stress–strain curve is about the same as that for a tension stress–strain curve, but the magnitudes of the two curves are not the same. In a torsion test, the specimens can be either solid cylinders or thin-walled tubes, and the experimental data is recorded in the form of a torque versus angle of twist curve. We discuss in this section how the shear stress–strain curve can be determined from the experimental data. Since the stress distribution is nonlinear along the radius of a specimen, when plastic strain develops, a theory is needed to determine the shear stress–strain curve from the experimental data. Some solutions are first presented that are useful for obtaining a shear stress–strain curve under loading condition. The determination of cyclic shear stress–strain curve is then discussed. We consider only torsion test in the small strain range. The discussion of torsion in the large strain range is deferred to Section 5.5.

5.2.3.1 The shear stress–strain curve

Several methods are used by various investigators to determine the shear stress–strain curve from the torque–twist data [6, Ch. 21], [18,19]. One of the methods is the quasielastic (QE) approximation [18] which is equivalent to assuming a linear shear stress distribution with respect to the radius in the specimen and finding the shear stress–strain relation at the surface of the specimen. It is clear that this method overestimates the shear stress for a given strain and it gives upper bound of the shear stress–strain curves. The thin-walled tube approximation is the simplest and most well-known method. It gives the lower bound of the shear stress–strain curves. Nadai's surface stress method [6, Ch. 21] requires some sophisticated data analysis since the shear stress is nonlinearly distributed along the radius of a solid circular cylinder. This solution is usually considered as an exact solution for finding the shear stress–strain curve from a specimen of solid circular cylinder [19]. Brown [19] and Batdorf and Robert [18] extended Nadai's solution to the case of tubular specimens. But these methods require the stresses to be determined by an iterative procedure. An approximation proposed by Brown [19] can give an approximated surface stress for a tubular specimen by use of a single equation.

5.2.3.1.1 The quasielastic solution

Consider a solid circular cylinder in pure torsion, in which the twist is θ radian per unit length. The shear strain is then given by $\gamma = r\theta$, where r is the radius of the field point under consideration. The torque applied to a solid circular cylinder is then given by the integral

$$M = \int_0^{r_0} 2\pi r^2 \tau \, \mathrm{d}r \tag{5.20}$$

where τ is the shear stress at radius r, and r_0 is the external radius. When the material is linearly elastic, the stress is proportional to strain, and the shear strain is proportional to radius r. The surface stress is found to be

$$\tau_0 = \mu\theta r_0 = \frac{2M}{\pi r_0^3} \tag{5.21}$$

where

$$M = \int_0^{r_0} 2\pi r^2 \mu r\theta \, \mathrm{d}r = \frac{\pi}{2} r_0^4 \mu\theta \tag{5.22}$$

and μ is shear modulus. In the case of tubular specimen, (5.20) can be written as

$$M = \int_{r_1}^{r_0} 2\pi r^2 \tau \, \mathrm{d}r \tag{5.23}$$

where r_1 is the internal radius of the specimen. Then, the surface stress is given by

$$\tau_0 = \frac{2r_0 M}{\pi(r_0^4 - r_1^4)} \tag{5.24}$$

5.2.3.1.2 The thin-walled tube approximation

By assuming the shear stress, denoted by τ_0, to be uniformly distributed across the wall-thickness, (5.23) may be integrated to yield

$$\tau_0 = \frac{3M}{2\pi(r_0^3 - r_1^3)} \tag{5.25}$$

Equation (5.25) was called the full plastic solution by Brown [19]. On the other hand, the following expression is usually used for thin-walled tube

$$\tau_0 = \frac{M}{2\pi r_{\mathrm{m}}^2 t} \tag{5.26}$$

where r_{m} is the mean radius of the tubular specimen and $t = r_0 - r_1$ is the wall-thickness of the specimen. When t is small, (5.25) and (5.26) give very close results. As an example, the shear stresses calculated from the above two equations are compared below for $t = 3.17$ mm (1/8 in.) and 6.35 mm (1/4 in.):

$$\frac{(\tau_0)_{25}}{(\tau_0)_{26}} = 0.997 \qquad \text{for 3.17 mm tube with } r_{\mathrm{m}} = 17.46 \text{ mm}$$

$$\frac{(\tau_0)_{25}}{(\tau_0)_{26}} = 0.991 \qquad \text{for 6.35 mm tube with } r_{\mathrm{m}} = 19.05 \text{ mm}$$

where $(\tau_0)_{25}$ and $(\tau_0)_{26}$ are the shear stresses calculated from (5.25) and (5.26), respectively. Since the difference is small, (5.26) will be used for comparison later in this section.

5.2.3.1.3 Nadai's exact solution

By writing (5.20) as

$$M = \frac{2\pi}{\theta^3} \int_0^{\gamma_0} \tau(\gamma)\gamma^2 \, \mathrm{d}\gamma \tag{5.27}$$

where $\gamma_0 = r_0\theta$, Nadai [6, Ch. 21] multiplied both sides of (5.27) by θ^3 and differentiated the equation with respect to θ to obtain

$$\frac{\mathrm{d}}{\mathrm{d}\theta}(M\theta^3) = \frac{\mathrm{d}}{\mathrm{d}\theta}\left(2\pi \int_0^{\gamma_0} \tau(\gamma)\gamma^2 \, \mathrm{d}\gamma\right) = 2\pi \frac{\partial \gamma_0}{\partial \theta}[\tau(\gamma_0)\gamma_0^2] \tag{5.28}$$

where the shear stress $\tau(\gamma)$ is a nonlinear function of γ. In performing the differentiation in (5.28), we note that in the integral of (5.27), γ may be viewed as a parameter of integration so that the integrand is not a function of θ, but the upper limit of integration γ_0 is. Equation (5.28) may then be written as

$$\tau_0 = \frac{1}{2\pi r_0^3}\left(3M + \theta\frac{\mathrm{d}M}{\mathrm{d}\theta}\right) \tag{5.29}$$

Using this expression the shear stress on the outer surface of a solid circular cylinder can be determined from the torque–twist curve. Nadai's solution is considered as exact solution [19] by most investigators. Brown [19] and Batdorf [18] extended the above equation to the following for the case of tubular specimens

$$\tau_0 = \frac{1}{r_0^3}\left[\tau_1 r_1^3 + \frac{1}{2\pi}\left(3M + \theta\frac{\mathrm{d}M}{\mathrm{d}\theta}\right)\right] \tag{5.30}$$

where τ_1 is the shear stress at the inner surface of the tube. This equation may be used to determine the surface shear stress–strain curve from a torque–twist curve of a tube using an iterative procedure explained in [18,19].

5.2.3.1.4 Brown's approximation

Brown [19] suggested the following form for the shear stress–strain curve

$$\tau_0 = AM(\theta) + B\theta\frac{\mathrm{d}M}{\mathrm{d}\theta} \tag{5.31}$$

where A and B are constants. Equation (5.31) reduces to (5.24) in the special case of $\theta(\mathrm{d}M/\mathrm{d}\theta) = M$, and reduces to (5.25) when $\theta(\mathrm{d}M/\mathrm{d}\theta) = 0$. Thus, A and B may be determined by comparing the two special cases with (5.24) and (5.25), respectively. Therefore, (5.31) may be written as

$$\tau_0 = \frac{1}{2\pi}\left[\frac{3M}{r_0^3 - r_1^3} + \left(\frac{4r_0}{r_0^4 - r_1^4} - \frac{3}{r_0^3 - r_1^3}\right)\theta\frac{\mathrm{d}M}{\mathrm{d}\theta}\right] \tag{5.32}$$

Equation (5.32) was proposed to provide an approximation for tubular specimens. But it is exact for the special case of solid cylinder, since it reduces to (5.29) when r_1 is zero. This approximation can lead to good result for small deformation [19]. The text of this section is extracted with permission from [20] Copyright ASTM International, 100 Barr Harbor Dr., W. Conshohocken, PA.

5.2.3.2 Cyclic shear stress–strain curve

Nadai's solution (5.29) gives the shear stress–strain curve on the outer surface of a solid shaft. The strength of this solution is that it is independent of constitutive equation, and the loading history is accounted for only through the input of the M versus θ curve. The latter point has not been generally recognized by researchers due to the existence of residual stress during unloading. The shear stress distribution in a solid shaft subjected to cyclic torsion was shown to be quite complicated by Wu et al. [21]. In spite of this, Wu et al. [22] have shown that Nadai's solution can be used to determine the unloading–reloading–cyclic loading shear stress–strain curve using a solid shaft. This method greatly simplifies the study of cyclic plasticity and multi-axial plasticity in the infinitesimal strain range, since costly tubular specimens are no longer needed.

When unloading occurs, each material element along the radius of the specimen follows a different unloading stress path, resulting in a different state of stress. Thus, the stress distribution along the radius during unloading is complicated. However, Nadai's solution shows that the shear stress on the surface of a solid shaft depends only on the information on the outer surface of the shaft and not directly on the deformation history in the interior part of the shaft.

The shear strain is $\gamma = r\theta$, where γ varies with r for a given θ. On the outer surface of the shaft, the shear strain is γ_0. The shear strain during unloading is $\gamma = r\theta = \gamma^* + \bar{\gamma}$, where $\gamma^* = r\theta^*$, and θ^* is the angle of twist corresponding to the state when unloading begins; and $\bar{\gamma} = r(\theta - \theta^*)$ is the additional shear strain incurred during unloading. The shear stress during unloading is $\tau(\gamma) = \tau(\gamma^*) + f(\bar{\gamma})$, where $\tau(\gamma^*)$ denotes the local shear stress when unloading begins. The function $f(\bar{\gamma})$ represents the change in shear stress caused by the unloading. Both $\tau(\gamma^*)$ and $f(\bar{\gamma})$ vary along the radius and their explicit functional forms are not needed in the derivation. Using (5.20), the torque is

$$\begin{aligned} M &= \int_0^{r_0} 2\pi\tau(\gamma^*)r^2 \mathrm{d}r + \int_0^{r_0} 2\pi f(\bar{\gamma})r^2 \,\mathrm{d}r \\ &= M^* + \frac{2\pi}{(\theta-\theta^*)^3}\int_0^{\bar{\gamma}_0} \bar{\gamma}^2 f(\bar{\gamma})\,\mathrm{d}\bar{\gamma} \end{aligned} \tag{5.33}$$

where

$$M^* = \int_0^{r_0} 2\pi\tau(\gamma^*)r^2\,\mathrm{d}r \tag{5.34}$$

We note that at the onset of unloading, the torque is M^*, the corresponding angle of twist is θ^*, and the shear strain is γ^*. In addition, we have $\bar{\gamma}_0 = r_0(\theta - \theta^*)$ and $\mathrm{d}\bar{\gamma} = (\theta - \theta^*)\mathrm{d}r$. In the last integral of (5.33), $\bar{\gamma}$ may be viewed as the parameter of integration so that only the upper limit of

the integral is a function of θ. The function $f(\bar{\gamma})$ evaluated at the outer surface of the solid shaft, denoted by $f(\bar{\gamma}_0)$, is now determined. This quantity is needed in the unloading stress–strain curve. The lower limit of the integral is zero because r is zero at the center of the shaft; the upper limit $\bar{\gamma}_0$ is evaluated on the outer surface. For unloading after plastic deformation has occurred, it is not easy to find an analytical expression for $f(\bar{\gamma})$. However, it is certain that $f(\bar{\gamma})$ varies continuously from $r = 0$ to $r = r_0$.

Multiplying both side of (5.33) by $(\theta - \theta^*)^3$ and differentiating the resulting equation partially with respect to θ, we obtain

$$3(M - M^*) + (\theta - \theta^*)\frac{\mathrm{d}M}{\mathrm{d}\theta} = 2\pi r_0^3 f(\bar{\gamma}_0) \tag{5.35}$$

Note that M^* is a function of θ^*, but not a function of θ. The function $f(\bar{\gamma}_0)$ is determined from (5.35) and the shear stress on the outer surface of the shaft is found from $\tau(\gamma) = \tau(\gamma^*) + f(\bar{\gamma})$ by setting $r = r_0$ as

$$\tau_0(\gamma) - \tau_0(\gamma^*) = \frac{1}{2\pi r_0^3}\left\{3(M - M^*) + (\theta - \theta^*)\frac{\mathrm{d}M}{\mathrm{d}\theta}\right\} \tag{5.36}$$

This equation has the same form as (5.29). But, the differences between the current values and those at first unloading, that is, $\tau_0(\gamma) - \tau_0(\gamma^*)$, $(M - M^*)$, and $(\theta - \theta^*)$, should be used in the equation. Thus, it has been shown that Nadai's solution is also applicable to the unloading case. In fact, this equation can be shown by a similar procedure to be valid for each segment of a cyclic loading program. Torque $M(\theta)$ varies continuously with θ during cyclic loading, but its derivative $\mathrm{d}M/\mathrm{d}\theta$ is piecewise continuous with a jump at each loading reversal.

Equation (5.36) is now used to determine the loading–unloading–reloading shear stress–strain curve in the infinitesimal strain range. A set of experimental data from Wu et al. [21] for 4140 steel is used in the calculation. In the experiments of [21], a solid shaft of 16.1 mm (0.634 in.) diameter and a tubular specimen of 12.7 mm (0.5 in.) inner diameter and 16.1 mm (0.634 in.) outer diameter were tested in torsion. By use of the experimentally determined M versus θ curve of the solid shaft, the shear stress–strain curve for each segment of the loading–unloading–reloading program is calculated from (5.36). In the computation, the geometrical change is neglected due to small strain consideration. The resulting curve is plotted in Figure 5.8 and shown by the dashed curve. The experimental M curve for the tubular specimen is then used, together with the thin-walled approximation of (5.26), to determine another shear stress–strain curve (the solid curve), which is also shown in the figure. It is seen that the two stress–strain loops agree closely. The curve determined from the solid shaft is an exact solution, while the other curve is an approximation.

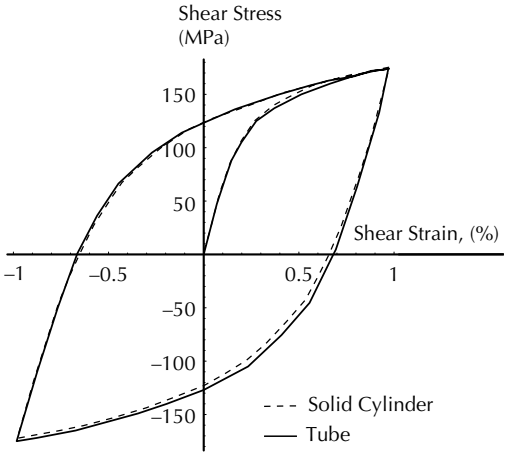

FIGURE 5.8
Cyclic shear stress–strain curve determined from torsion of solid shaft.

5.2.4 Strain Rate, Temperature, and Creep

Metallic materials are generally strain-rate sensitive at high temperature, but not equally sensitive at room temperature. There are exceptions such as AISI Type 304 stainless steel and others. The 304 stainless steel is strain-rate sensitive at room temperature even at the low strain-rate range of 10^{-6} to 10^{-3} s^{-1}; on the other hand, materials such as aluminum alloys are not strain-rate sensitive in this range. Metals are generally strain-rate sensitive under dynamic loading. A set of constant strain-rate stress–strain curves may be experimentally determined. The curves for materials such as aluminum alloys or brass are shown schematically in Figure 5.9(a). Figure 5.9(b) shows similar curves for mild steel. The stress–strain curve for a higher strain-rate lies above that for a lower strain-rate. The temperature effect is shown schematically in Figure 5.9(c), in which a stress–strain curve at a higher temperature lies below that at a lower temperature, that is, the material becomes softer at higher temperature. It is known that the strain-rate effect and the temperature effect are related.

Due to low strain-rate sensitivity of most metals at room temperature in the strain-rate range of 10^{-6} to 10^{-3} s^{-1} (or quasi-static), the permanent deformation of metals has been classified as plastic deformation or rate-independent plastic deformation. This is an approximation, because in reality the metals are more or less strain-rate dependent. However, it is a reasonable approximation and it enables the development of theories of plasticity. The strain-rate sensitive plasticity is also known as *viscoplasticity*. Most theories of viscoplasticity are formulated by adding the strain-rate sensitivity to a theory of plasticity. The strain-rate effect is especially significant under dynamic loading. Even within the quasi-static strain-rate range, the present of strain rate leads to creep and stress relaxation.

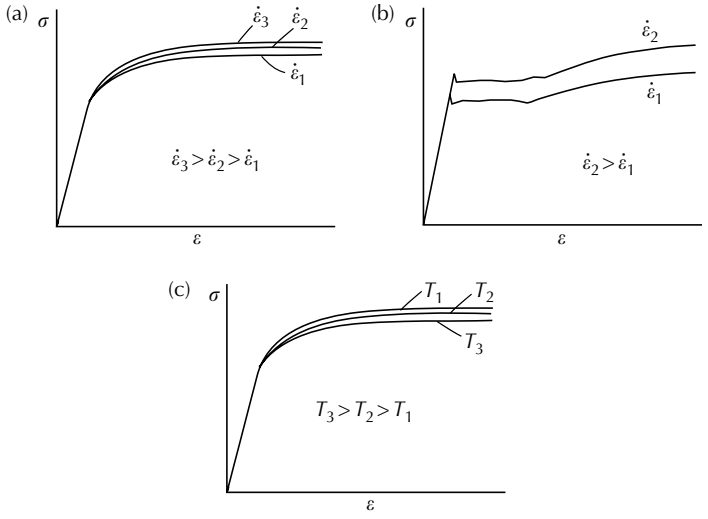

FIGURE 5.9
(a) Schematic constant strain-rate stress–strain curves, (b) constant strain-rate stress–strain curves for mild steel, (c) the effect of temperature.

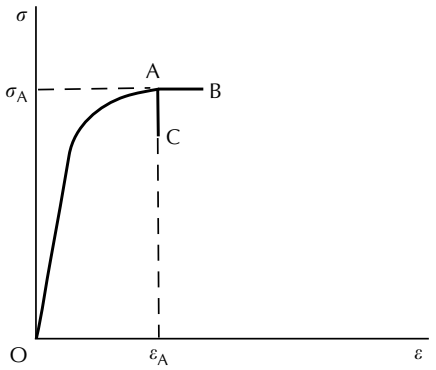

FIGURE 5.10
Loading stress–strain curve, creep, and stress relaxation.

Some fundamental concepts of strain-rate effect are constant strain-rate stress–strain curves as previously discussed, creep, and stress relaxation. Creep is the deformation developed as time elapses when the applied stress is kept constant. On the other hand, when the strain is kept constant, the stress relaxes with time. In Figure 5.10, OA shows the loading stress–strain curve; AB shows that the strain creeps from A to B while the stress is kept constant at σ_A; and AC shows that the stress relaxes from A to C while the strain is kept constant at ε_A. A typical creep curve is a plot of strain against time and it is divided into three stages: the primary creep, the secondary creep,

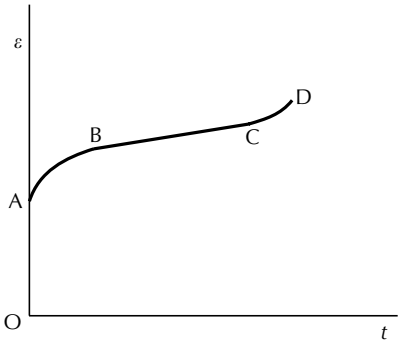

FIGURE 5.11
A schematic creep curve with three stages.

and the tertiary creep, as shown in Figure 5.11. The *primary creep* (also known as the transient creep) (AB) occurs at the beginning of the creep process. During this stage, the creep rate decreases continually. The creep rate remains nearly constant in the *secondary* (or steady state) *creep* stage (BC), and the creep rate increases continually until rupture during the *tertiary creep* stage (CD). It is convenient to separate the creep into three stages. However, no observations are available that show creep to be completely separated into three independent stages. It takes a long time to reach the tertiary stage; tertiary stage begins after 1940 h of creep, for instance, for an austenitic stainless steel tested at 704°C under a stress of 90.9 MPa (13,200 psi) [23]. The creep curves are dependent on the hold stresses. The higher the hold stress, the larger is the creep strain. Creep tests conducted at constant load or constant stress also give different creep curves.

In the past (before about 1980), plastic deformation and creep were investigated separately. Experiment to determine plastic behavior was performed by use of screw-driven universal testing machines and creep experiment was conducted by dead load machines. An accurate control of rate of loading or rate of straining was difficult in both cases. This method of experimental investigation gave rise to separate theories for plastic deformation and creep behavior. In this manner, the inelastic strain consists of a time-independent plastic strain term and a time-dependent creep strain term; these terms are calculated using plasticity and creep theories, respectively.

Recently (after about 1980), new type servo-controlled testing equipment permits an accurate control of rate of loading or straining under quasi-static condition. It provides the means of recording the nonlinear, inelastic behavior of materials in detail and with great accuracy. The machine is so powerful that interactions between plasticity and creep can also be investigated. In this connection, we are interested in the primary and secondary creep stages. It is difficult to draw a line between the two stages as previously mentioned and we will show continuous creep curves. Some interaction phenomena that have been reported are: the cyclic hardening or softening with hold time;

the effect of creep prestrain on the subsequent plastic behavior; and the effect of plastic strain on the subsequent creep behavior. Corum et al. [24] showed that the stress amplitude in the cyclic tension–compression tests with a constant strain amplitude was enhanced by the preceding creep for AISI Type 304 stainless steel. Ikegami and Niitsu [25] found that SUS 304 stainless steel hardens in the direction of the preloading not only by plastic strain but also by creep strain. The hardening by creep is nearly equal to that by plastic strain. Wu and Ho [26] investigated strain hardening of 304 stainless steel by creep and found that the material hardened by creep is the same as that hardened by plastic deformation. Kujawski et al. [27], Wu and Yao [28], Wu and Ho [29], and Xia and Ellyin [30] observed that the creep curves are different even at the same holding stress but for different strain- or stress-rate loading histories prior to creep. In order to describe the aforementioned plasticity–creep interaction, recent efforts in material constitutive relation lean towards a unified theory for plasticity and creep.

A fundamental issue of the creep test is the large range of data scatter. Some of the scatter may be attributed to the material inhomogeneities, but there are two other important factors contributing to the scatter. One factor is the test system misalignment and the other is the negligence of the pre-loading stage in a creep test by the investigators. These two factors are further explained. The misalignment in creep was investigated by Penny and Leckie [4] and Hayhurst [31]. These research workers generally agreed that data scatter in creep testing could be partially attributed to specimen alignment. Poor specimen alignment could result in bending stress (or strain) superimposed on the required mean axial stress (or strain). This bending stress (or strain) could be high enough to cause premature failure in brittle materials; in ductile materials, plastic deformation could occur and reduce the bending stress (or strain). Analyses of misalignment were presented by these investigators. The results show that the creep curves scatter due to eccentric loading. More significantly, these analyses predicted that the scatter would increase with the creep time.

The result of Wu and Wang [32] does not support all of the above assertions. Wu and Wang [32] considered the effect of pull-rods and the symmetric case of misalignment shown in Figure 5.3. The symmetric case is the most severe case of misalignment as discussed in [5]. It was pointed out in [32] that the following assumptions and/or conditions used by [4] and [31] are not realistic: (1) the applied load P is linearly related to the end moment M; (2) $\mathrm{d}P/\mathrm{d}t = \mathrm{d}M/\mathrm{d}t = 0$; (3) the neutral axis of the specimen is fixed; and (4) the absence of pull-rod effect. The analysis of Wu and Wang [32] relaxed all of the aforementioned assumptions and led to different results as compared with [4] and [31]. While the numerical results of [32] show that the errors induced by the test system misalignment are significant in the creep test, these errors will diminish with time. Thus, the most severe effect of misalignment occurs at the beginning of the creep test. Creep tests conducted with long pull-rods and large initial strain level (high creep stress) will tend to minimize the effect of misalignment.

Another factor that is contributing to the scatter of creep data is the negligence of the preloading stage in a creep test. Due to the nature of dead load creep machines, the strain rate of the preloading stage in a traditional creep test is neither observable nor recordable. The way that the load (weight) is applied greatly affects the creep strain. Wu and Ho [29] conducted creep tests by use of a servo-controlled materials test system, and investigated the effect of the preloading stage on the subsequent creep. Two sets of test histories were used. One had a constant strain-rate preloading and the other had a constant stress-rate preloading. In the case with constant strain-rate preloading, the specimen was pulled in the strain-control mode while the computer monitored the strain and stress magnitude. The strain-rates were set at 2×10^{-6}, 10^{-5}, 10^{-4}, and 10^{-3} s^{-1}. As soon as the stress magnitude reached the preset creep holding stress, the loading process stopped. The test system was programmed to switch to the load-control mode instantaneously and then kept the stress at this constant magnitude, while the creep strain was being recorded. In the case with constant stress-rate preloading, the test was straightforward without control mode switching. The tests were performed under stress control at constant stress-rates of 2.07 and 20.7 MPa/s. As the stress reached the preset value, the creep process began.

Each test result to be discussed was the average of two specimens. Most results were very consistent except for the case of constant strain-rate loading at 10^{-5} s^{-1}, where data scatter was apparent. A third test was conducted for this case and the result shown is the average of three tests. Two remarks can be made from the strain–time profiles of the whole creep process (the loading stage and the creep stage) shown in Figure 5.12, in which the starting point of the creep stage is marked by *. First, the profiles confirm the constant strain-rate control of each curve prior to reaching the hold stress. Second, the profiles show that the initial creep strain rates are indeed a continuation of the preloading strain rates. Therefore, the initial creep strain rate of creep tests with strain-controlled preloading is known. Figure 5.13 shows the creep curves of various constant strain-rate preloading at the same holding stress of 206.7 MPa (30 ksi).

For constant stress-rate preloading, the initial creep strain rate is also determined at the end of the loading stage. Thus, in the discussion of the creep stage, the initial creep rate is regarded as a known value. Figure 5.14 shows the strain–time profiles of the creep tests with constant stress-rate preloading. The starting points of the creep stage are marked by * in the figure. It is seen that, during the preloading stage, the strain rate is constant in the elastic range and increases rapidly during elastic–plastic transition. The figure also shows that the initial creep strain rate is a continuation of the preloading strain rate. Figure 5.15 shows the creep curves for two creep tests with preloadings of two different constant stress rates. The hold stress for both tests was 206.7 MPa (30 ksi), same as the hold stress for the creep tests shown in Figure 5.13. In the elastic region, stress-rates of 2.07 and 20.7 MPa/s correspond to strain-rates of 1×10^{-5} and 1×10^{-4} s^{-1}, respectively. Because the initial creep rate of the creep test with faster stress-rate preloading is large, the corresponding creep

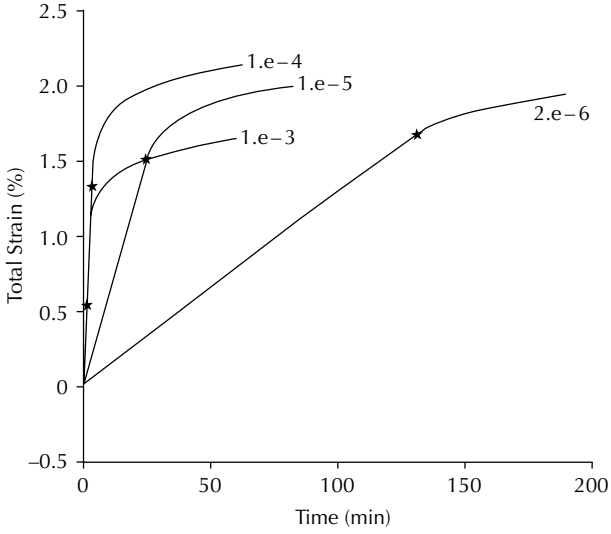

FIGURE 5.12
Strain–time profiles of creep tests with various constant strain-rate preloading (From Wu, H.C. and Ho, C.C., *J. Eng. Mater. Technol.*, 117, 260, 1995. With permission from ASME).

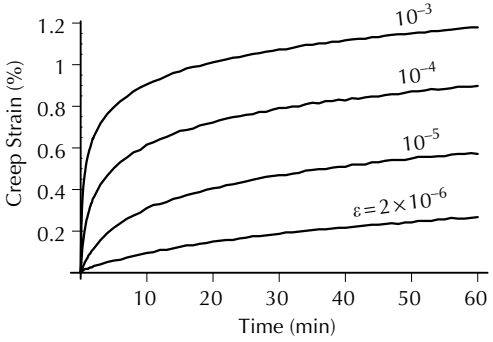

FIGURE 5.13
Creep curves of various constant strain-rate preloading at the same hold stress (From Wu, H.C. and Ho, C.C., *J. Eng. Mater. Technol.*, 117, 260, 1995. With permission from ASME).

strain is larger than that of the creep test with a slower stress-rate preloading. Comparing creep curves of Figure 5.13 and Figure 5.15 with the same preloading strain-rate in the elastic region and having the same hold stress, the creep strains of constant stress-rate preloading approximately double those of constant strain-rate preloading. We may conclude that the preloading stage greatly affects the subsequent creep strain and that the traditional creep test using a dead load machine is vulnerable to data scatter, because neither the strain- nor the stress-rate of the loading stage can be controlled.

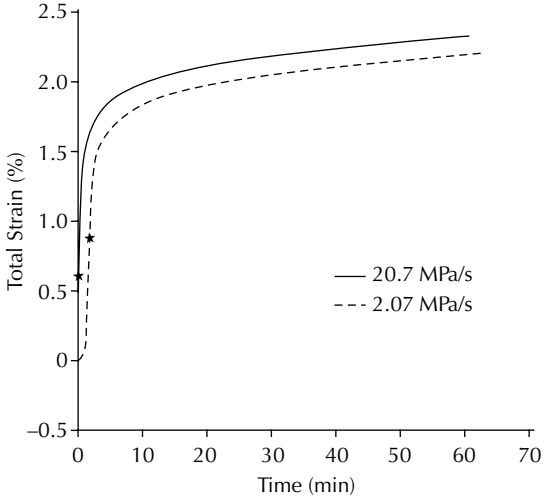

FIGURE 5.14
Strain–time profiles of creep tests with constant stress-rate preloading (From Wu, H.C. and Ho, C.C., *J. Eng. Mater. Technol.*, 117, 260, 1995. With permission from ASME).

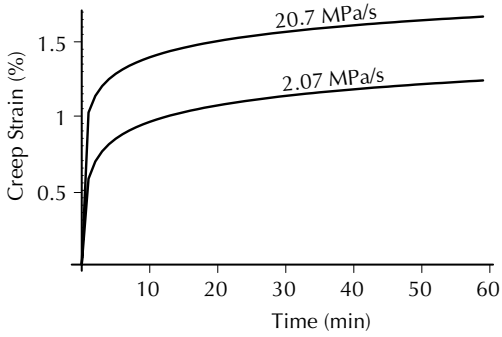

FIGURE 5.15
Creep curves of two constant stress-rate preloading at the same hold stress (From Wu, H.C. and Ho, C.C., *J. Eng. Mater. Technol.*, 117, 260, 1995. With permission from ASME).

5.3 Modeling the Stress–Strain Curve

For the purpose of applications and further theoretical studies, it is useful to develop a mathematical model for the one-dimensional stress–strain curve OABE shown in Figure 5.1. This is a generic stress–strain curve, it can be the curve for tension, compression, or shear. In 1909, Ludwik [33] proposed a stress–strain relationship to be used when the deformation was sufficiently

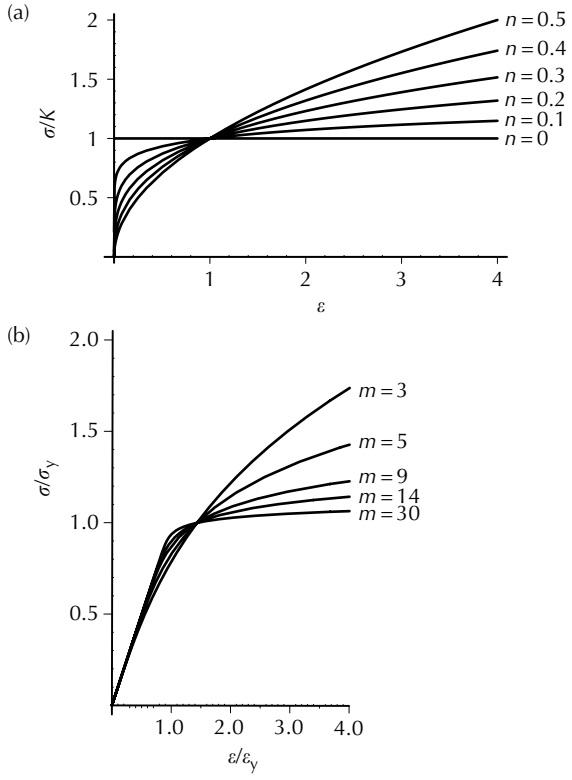

FIGURE 5.16
(a) The Ludwik equation, (b) the Ramberg–Osgood equation.

large so that the elastic strain could be neglected. The Ludwik equation is

$$\sigma = K\varepsilon^n \tag{5.37}$$

where K is a strength coefficient and n is a strain-hardening exponent usually lying between 0 and 0.5. The equation predicts a zero initial stress and an infinite initial slope, except for $n = 0$ which represents a rigid perfectly plastic material without strain-hardening. The higher the value of n, the more pronounced is the strain-hardening characteristic of the material. The Ludwik equation is plotted in Figure 5.16(a) for $n = 0$, 0.1, 0.2, 0.3, 0.4, and 0.5. If this equation is used to describe the plastic behavior and we combine the equation with Hooke's law, which is used to describe the elastic behavior, the resulting equation can be used to describe the total material behavior. Writing the total strain as the sum of elastic and plastic parts, we obtain

$$\varepsilon = \varepsilon^{\mathrm{e}} + \varepsilon^{\mathrm{p}} = \frac{\sigma}{E} + \left(\frac{\sigma}{K}\right)^{1/n} \tag{5.38}$$

This equation, known as the Ramberg–Osgood Equation [34], is used by many investigators to express the monotonic loading curve of strain-hardening materials, especially ones without a sharply defined yield stress. For a large number of metals, if the true stress is plotted versus the true plastic strain, a straight line results on a log–log plot and equation (5.38) proves useful. We rewrite (5.38) as

$$\frac{\varepsilon}{\varepsilon_y} = \frac{\sigma}{\sigma_y} + \alpha \left(\frac{\sigma}{\sigma_y}\right)^m \tag{5.39}$$

where

$$\alpha = \frac{E(\sigma_y)^{m-1}}{K^m} \quad \text{and} \quad m = \frac{1}{n} \tag{5.40}$$

and σ_y and ε_y are the yield stress and yield strain, respectively, and related by $\sigma_y = E\varepsilon_y$; m is a hardening exponent; and α is a constant. Equation (5.38) is plotted in Figure 5.16(b) for $\alpha = 3/7$ and $m = 3, 5, 9, 14$, and ∞. Note that (5.39) has three parameters.

Other models have been proposed in the literature, but they will not be discussed here. Generally, the models describe similar curves using different mathematical expressions. Instead, we give some remarks related to the stress–strain curves in the large strain range. Many investigators specify that their equations relate the true stress to the true strain. The true strain is well defined and the definition of true strain or logarithmic strain $\varepsilon^{\log}$ has been discussed in Section 3.10. It may be shown from (3.139) that true strain is related to the engineering strain ε^{eng} by

$$\varepsilon^{\log} = \ln(1 + \varepsilon^{\text{eng}}) \tag{5.41}$$

The true stress (or the Cauchy stress) is also well defined and it is related to the nominal stress (or the 1st P–K stress) by (4.42). In the case of uniaxial stress for isotropic materials, the deformation gradient and stress components are

$$[F] = \begin{bmatrix} \lambda & 0 & 0 \\ 0 & \lambda_2 & 0 \\ 0 & 0 & \lambda_2 \end{bmatrix}, \qquad [\sigma] = \begin{bmatrix} \sigma & 0 & 0 \\ 0 & 0 & 0 \\ 0 & 0 & 0 \end{bmatrix}, \qquad [T^{(0)}] = \begin{bmatrix} s & 0 & 0 \\ 0 & 0 & 0 \\ 0 & 0 & 0 \end{bmatrix} \tag{5.42}$$

Assuming that the material is incompressible at large strain, the Jacobian of the transformation is

$$J = \det \mathbf{F} = \lambda\lambda_2^2 = 1 \tag{5.43}$$

Substituting (5.42) and (5.43) into (4.42), we obtain

$$s = \frac{\sigma}{\lambda} = \sigma \exp(-\varepsilon^{\log}) \tag{5.44}$$

where

$$\lambda = \exp(\varepsilon^{\log}) \tag{5.45}$$

Equation (5.44) has been used to convert the stress–strain curve expressed in terms of the true stress σ into that expressed in terms of the nominal stress and vice versa.

In the tension test, the nominal stress is easily determined, because the initial cross-sectional area of the specimen is known. In this case, (5.44) is used to convert the nominal stress into the true stress. Both stress–strain curves are shown in Figure 5.17(a). Recently, some investigators have used diametral extensometers to measure the diametral strains in the cylindrical tension specimens. These diametral strains are then converted to the longitudinal strains based on a constant volume assumption. Let the volume be $V = A_0 l_0 = Al$, where A denotes the cross-sectional area and l the length of the specimen. The subscript 0 denotes the undeformed condition. If the volume remains constant, the differentiation of the above equation leads to

$$\mathrm{d}\varepsilon^{\log} = \frac{\mathrm{d}l}{l} = -\frac{\mathrm{d}A}{A} \quad \text{or} \quad \varepsilon^{\log} = \ln\left(\frac{A_0}{A}\right) \tag{5.46}$$

The diametral strain is related to the change of area. The reduction of area defined by $(A_0 - A)/A_0$ is often used. However, we need to remember that this approach is based on the constant volume assumption and it is a good approximation when the strain is large.

In the compression test, the specimen is repeatedly remachined. The stress thus obtained is close to the true stress. We then use (5.44) to convert the true stress into the nominal stress. In doing so, we remark that the strain $\varepsilon^{\log}$ is negative in compression. The stress–strain curves for compression are shown in Figure 5.17(b) plotting against the absolute value of the true strain.

5.4 The Effects of Hydrostatic Pressure

The hydrostatic pressure plays a significant role in the formulation of a modern theory of plasticity. It has been assumed by many researchers that plastic yielding of metals is independent of superimposed hydrostatic pressure and that metals are plastically incompressible. In this section, we examine the experimental findings that have been reported in the literature so that the validity of the aforementioned assumptions can be assessed. We would like

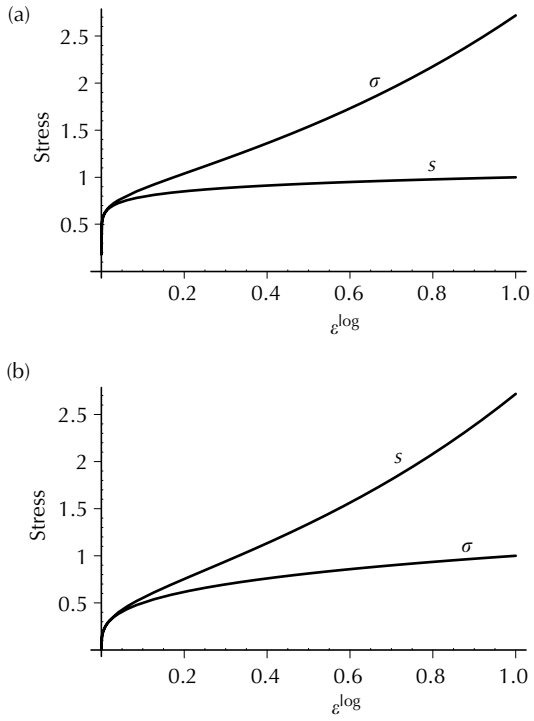

FIGURE 5.17
Stress–strain curve expressed in two stress measures, (a) tensile and (b) compression.

to mention that the dependence of the yield stress and the compressibility of material on the hydrostatic pressure are well recognized for such porous materials as geotechnical materials and is not be discussed in this section (see Chapter 9 for discussion).

Bridgman published a large volume of papers related to high hydrostatic pressure. The experiments related to the studies of large plastic flow under the effect of hydrostatic pressure are well summarized in Bridgman [9]. From the many solids studied, the "absolute compressibility" of the material is given from [3, p. 493] by

$$-\frac{\Delta V}{V_0} = a\,p - b\,p^2 \tag{5.47}$$

where p is the hydrostatic pressure measured in kgf/cm^2(1 kgf/cm^2 = 98.1 kPa), ΔV the volume change, V_0 the initial volume at atmospheric pressure, and a and b are constants determined from experiments, for example, $a = 5.826 \times 10^{-7}$ and $b = 0.8 \times 10^{-12}$ for iron. We note that the absolute compressibility expressed by (5.47) is a volumetric strain and would like to mention a special note by Bell [3, p. 494] that Bridgman measured the change

in length in a single direction from which, assuming isotropy, he computed the change of volume.

In the tension of steel under hydrostatic pressure, Bridgman [9, p. 49] measured the change in length of the specimen and by the assumption of volume constancy he determined the area reduction of the neck in the tension specimen. He found that the flow stress and the stress at maximum load increase almost linearly with pressure for pressure up to 2,800 MPa (400,000 psi) for various heat treatment of a steel, Bridgman [9, p. 69–70].

Bridgman [9, p. 195] conducted uniaxial compression test using specimens of various metals to determine plastic volume change. No hydrostatic pressure was applied in this series of tests. He used a dilatometer apparatus for determining the change of volume of the specimen during the test. He argued for the superiority of a direct measurement (by use of dilatometer) of the volume change as compared with its indirect determination from measurements of the change of longitudinal and lateral dimensions. Bridgman considered a cylinder of mild steel plastically shortened to 0.85 its initial length by an axial load of 689 MPa (100 ksi), and he compared the radius of the cylinder under two conditions: assuming no change of volume and assuming the full elastic change of volume corresponding to this stress. He found that the radius in the two cases differs only by 0.07%, which is a difficult task for measurement. Bridgman did not compare the circumferential strain, however. If he did, he would have found that the difference is 0.94%, and the circumferential strains are 0.08465 and 0.08545, respectively, which is not a difficult task for today's measurement technology.

Bridgman immersed the specimen undergoing plastic deformation in a dilatometer, which was filled with a liquid and provided with a capillary open to the atmosphere in which the liquid meniscus moved in response to changes in volume of the contents of the dilatometer. Of the materials examined under compression, negative plastic volumetric strains were shown by annealed high-carbon steel, 303 stainless steel, copper, and hard-drawn brass, and the opposite effect, a positive plastic volumetric strain, was shown by mild steel and iron. With these differences, the plastic volumetric strains were small, however, and most volume changes were recoverable on release of stress. Examples were: the plastic volumetric strain for 1035 steel was 0.0001 for an axial strain of 0.02; it was 0.00012 for 303 stainless steel for an axial strain of 0.135; and it was 0.00015 for high-carbon steel for an axial strain of 0.14.

Crossland [35] and Hu [36] found that the yield stress in torsion was sensitive to the presence of hydrostatic pressure up to 280 MPa (40 ksi). Crossland found that the upper yield stress of mild steel decreased by 10% and Hu found that it decreased by 6.5% over the same range of hydrostatic pressure. Permanent volume expansion was observed for 4310 and 4330 steels by Spitzig et al. [7]. These authors determined the density at the uniform gauge section of the specimen. Measurements were made both before and after straining specimens up to 4% plastic strain, and, therefore, these were permanent volume changes. Additional volume-change measurements were made during deformation on several tension specimens with rosette strain

gauges. It was found that tensile and compressive testing under hydrostatic pressure up to 1100 MPa (160 ksi) raises the stress–strain curve by about 6.5%, but does not significantly affect the work-hardening characteristics. The plastic volumetric strain increased proportionally with the axial strain, and it was about 2×10^{-4} when the axial strain was 0.04. Volume-change measurements made from the strain gauges were similar in magnitude to those obtained from the density measurements. For the hydrostatic pressure of 1400 MPa (200 ksi) the elastic volumetric strain is 8.78×10^{-3} and the plastic volumetric strain is only 2% of this amount.

It may be concluded that the yield stress of metallic materials depends on superimposed hydrostatic pressure. The yield stress in tension, compression, or torsion may increase or decrease with pressure depending on material tested. Further investigation to experimentally quantify this effect is warranted. However, for a first approximation, the assumption that plastic yielding of metals is independent of superimposed hydrostatic pressure is reasonable. We are convinced that the plastic volumetric strain is small compared to the elastic volumetric strain. Therefore, the assumption of plastic incompressibility is well established. The assumption of plastic incompressibility is expressed in terms of the increments of the plastic strain as

$$\mathrm{d}\varepsilon^{\mathrm{p}}_{kk} = \mathrm{d}\varepsilon^{\mathrm{p}}_{11} + \mathrm{d}\varepsilon^{\mathrm{p}}_{22} + \mathrm{d}\varepsilon^{\mathrm{p}}_{33} = 0 \tag{5.48}$$

5.5 Torsion Test in the Large Strain Range

5.5.1 Introduction

Torsion tests in the large strain range provide results that are useful in the development and verification of microstructure-based and phenomenological constitutive models of crystalline solid. The test is quite complex since, in addition to shear stress and shear strain, the axial and hoop strains and the axial stress are also important, making torsion test a multi-axial test. There are two end-conditions in the torsion test: the fixed-end and the free-end torsion. In the *fixed-end torsion*, the length change of the specimen is prevented, and, because of this, axial stress is developed during torsion. On the other hand, the length change is permitted in the *free-end torsion*, but the axial stress is zero during torsion. The existence of axial stress or axial strain in the torsion test is generally known as the *axial effect*. Some torsion tests are cited as: Poynting [37], Swift [38], Hughes [39], Hodierne [40], Ronay [41,42], Baily et al. [43], Billington [44], Lindholm et al. [45], Van Arsdale et al. [46], Montheillet et al. [47], Wu et al. [2,48], Lipkin and Lowe [49], White et al. [50], Weerasooriya and Swanson [51], Toth et al. [52], and Miller and McDowell [53].

Several problems related to such torsion tests need to be addressed. If these problems are not carefully considered, then the validity of test results may be questioned. The problems are associated with the homogeneity of the

material, the strain measurement, the specimen geometry, and the determination of the shear stress–strain curve from the experimental torque versus angle of twist curve. These problems have been discussed in [2] and the following discussions are based on [2].

(1) The material homogeneity:

If the material is not homogeneous, nonuniform deformation will occur, leading to regions that remain almost undeformed while plastic deformation occurs in the remaining part of the specimen. The strain concentration will lead to an early development of shear band localization in the specimen. This is a very serious problem, especially when long gauge-length specimens are used. In the research of [2], well controlled, homogeneous material was supplied by a material manufacturer and macroscopically uniform plastic deformation (no apparent regions of strain concentration were observed by eye inspection after the test) was obtained in all specimens tested.

(2) The strain measurement:

An important problem associated with the torsion test and the combined axial–torsion test is the strain measurement. A transducer that measures and controls normal and shear strains in the large strain range is not generally available. Almost all experimental results reported in the literature use the relative motion between the grips to compute the axial and shear strains. This method does not lead to accurate strain measurements due to the geometry of the specimen, which has enlarged ends.

An axial–torsional extensometer has been designed and built by Wu and Xu [1], see Figure 5.18. This extensometer measures strains in the gauge section of the solid shaft or tubular specimens. Specifications of the extensometer have been determined in terms of the linearity, cross-talk, and hysteresis, and have been reported in Wu and Xu [1]. In particular, the cross-talk between axial and shear channels is $<0.1\%$. The extensometer is capable of providing signals for feedback control so that both strain- and stress-controlled experiments may be performed.

This extensometer has been redesigned with the purpose of providing strain measurements for free- and fixed-end torsion tests and combined axial–torsion test for test temperature up to 150°C (300°F). Heat resistant transducers (LVDT's and RVDT's) are used. This is necessary, because the extensometer is attached to the specimen and enclosed in the furnace during the test. In addition, most parts of the extensometer use the same material that has been carefully selected, minimal thermal expansion being the requirement.

The calibration for elevated temperature testing is difficult. First, there are no axial and torsional calibrators available for elevated temperature. Second, the calibration at room temperature cannot be directly used for elevated temperature, since the sensitivity of the transducers (LVDT's and RVDT's) used in the extensometer changes with temperature. Thus, the calibration has to be

FIGURE 5.18
Axial–torsion extensometer (From Wu, H.C. et al., *Int. J. Plasticity*, 13, 873, 1998. With permission from Elsevier).

carried out at the test condition and it will be discussed in detail in the next subsection.

(3) The specimen geometry:

Torsion tests have been conducted by use of tubular specimen, solid shaft, and specimen of *Lindholm configuration*. Tubular specimens are used throughout this research. The advantages for this type of specimen are: (a) accurate shear strain measurement may be obtained because of the long gauge section that this type of specimen has; (b) accurate strain measurements may be obtained in axial and hoop strains; (c) the specimen may be used for combined axial–torsional testing; (d) the specimen is suitable for test involving unloading–reloading–cyclic loading; and (e) the specimen may be used for investigation of shear band localization. The axial strain mentioned in (b) is greatly influenced by the specimen geometry, which is discussed at length in the next section. Since relatively thick-walled tubes are used in this investigation, the integrated effect for axial strain would cause the measured axial strain to be less than the actual strain. In the following paragraphs, a discussion is given to solid shaft specimens and Lindholm configuration specimens.

Solid shafts can achieve very large strain without buckling. They can be used to determine the loading–unloading–cyclic shear stress–strain curve by means of the fixed-end torsion test, see Wu et al. [22]. However, the test requires a specially designed axial–torsion materials test system, which has the capability of achieving a very large twist angle in one test run while keeping the two ends fixed. This option is very expensive and is not generally

available. In the free-end torsion test, the solid shaft leads to low-length change compared with a tubular specimen. The axial elongation is a function of shear strain that varies linearly along the radius of the solid shaft. The inner core of the shaft has less axial strain than the outer layer and acts to restrict the axial elongation of the whole shaft, resulting in residual axial stresses in the specimen. Therefore, solid shafts are not useful for the determination of the axial effect.

Specimens of Lindholm configuration have been used by many investigators to conduct torsion tests (see [45,50]). This is a thin-walled tubular specimen with two ends, two shoulder sections and a very short gauge section. A very special feature is that the gauge length is only a small fraction of the radius of the tube. Due to the short gauge length, a very large shear strain (say 10.0) may be applied. It is common to insert a plug and sleeve into the annulus to prevent buckling at large strain level. The plug and sleeve, together with the relatively rigid ends of the specimen, restrict the development of the hoop strain at large shear strains. This is an important drawback since, with the assumption of plastic incompressibility, the radial strain is incorrectly inferred. It is known (Taylor and Quinney [54] and also experimental data of [2]) that during torsion the hoop strain is not equal to the radial strain. In fact, the wall-thickness changes only very slightly during torsion while the magnitude of hoop strain can be 0.8 to 0.9 times that of the axial strain when the shear strain is 150%. Another shortcoming of this specimen is the underdevelopment of the axial strain during free-end torsion, which is related to the axial stress developed during fixed-end torsion. An additional drawback of the specimen is the inaccurate strain measurement. Due to the short gauge length, it is almost necessary to measure the shear and axial strains by the relative rotation and displacement of the two ends. The readings thus obtained are not representative of the actual strains in the gauge section because of the effect of the shoulder section of the specimen. Thus, this specimen configuration is not recommended for the fixed-end torsion (Lipkin and Lowe [49]) due to the ambiguity of the constraint of the gauge section characteristic of fixed-end tests. Furthermore, this specimen cannot be used for combined axial–torsional testing, nor can it be used for the experimental investigation of shear band localization.

(4) The determination of shear stress–strain curve:

It takes a theory to convert the torque versus angle of twist curve into the shear stress–strain curve. Most theories such as Nadai [6] or Canova et al. [55] do not account for length change of the specimen subjected to torsion and, therefore, do not lead to accurate results for free-end torsion. Although the method may be used to obtain accurate shear stress–strain curve for the fixed-end torsion test (see [22]), the required test system is generally not available as previously discussed. Therefore, the free-end torsion of tubular specimens is still a practical test for the determination of true shear stress–strain curve. For this purpose, experimental data for axial and hoop strains are also needed. Based on the Nadai method, Wu et al. [20,22]

developed a method which, by accounting for the axial and hoop strains, provides a true shear stress–strain curve from the free-end torsion test. This true shear stress–strain curve is consistent with that determined from the fixed-end torsion test. It should be emphasized that, in this method, the reduction of shear stress–strain curve from the torque-angle of twist curve is strictly a consideration of the applied torque and specimen geometry and no material properties are directly involved. The task is to determine an experimental shear stress–strain curve so that it may be used for the verification of any constitutive equation. The method of Wu et al. is presented in Section 5.5.4.

5.5.2 Experimental Program and Procedures

The experimental program of Wu et al. [2] includes free- and fixed-end torsional testing of extruded and cast high-purity aluminum. (Text of this section follows [2] with permission from Elsevier.) Tubular specimens were supplied by Alcoa Technical Center (ATC) and the material had the following chemical compositions by weight: 99.74% Al, 0.15% Fe, 0.08% Si, and 0.03% Ti. The annealed cast aluminum was initially isotropic and had equiaxed grains with grain size of 160 microns. The annealed extruded aluminum had an initial fiber type extrusion texture and the grains were slightly elongated with the grain size of 250 microns along the extruded direction and 220 microns along the transverse direction. The experiments were conducted at room and elevated temperatures. The purposes of the experimental program were to determine the true shear stress–strain curves, the axial effect, and the hoop strain at several temperature levels, and to investigate the influence of specimen gauge length on the axial and hoop strains.

5.5.2.1 Specimen geometry and test conditions

Tubular specimens with three different gauge lengths were used. The specimen with a long ($L = 82.6$ mm, 3.25 in.) uniform gauge section is called the long specimen; the specimen with a medium ($L = 38.1$ mm, 1.5 in.) uniform gauge section is called the medium specimen; and the specimen with a short ($L = 19.05$ mm, 0.75 in.) uniform gauge section is called the short specimen in this study. Figure 5.19 shows the dimensions of a long specimen with L marked on the drawing. For shorter specimens, the total length of the specimens remains at 177.8 mm or 7.0 in., but the enlarged ends are longer. Most specimens have the same outer diameter (OD = 38.1 mm, 1.5 in.) and inner diameter (ID = 25.4 mm, 1.0 in.) and a wall-thickness of 6.4 mm (0.25 in.). The L/r_0 ratio is 4.34 for long specimen, 2.0 for medium specimen, and 1.0 for short specimen. The t_0/r_0 ratio is 0.33 for most specimens. Note that the short specimen here has a much longer gauge section than the Lindholm-type specimen, which has $L/r_0 = 0.25$ and $t_0/r_0 = 0.5$, see Miller and McDowell [53].

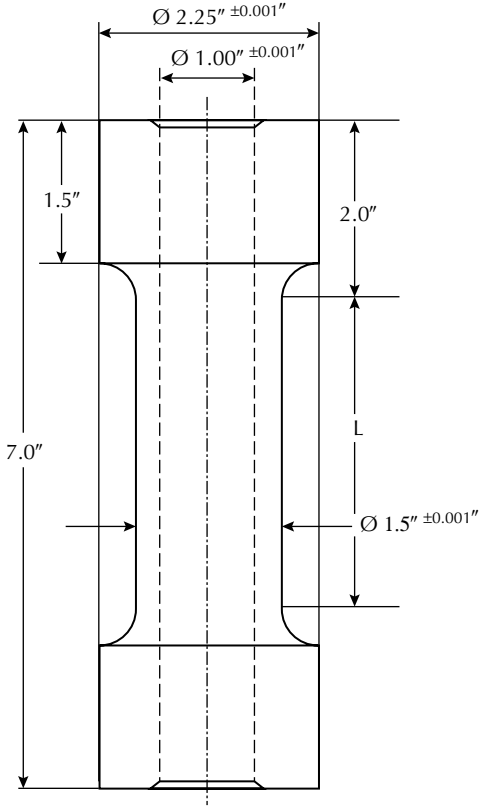

FIGURE 5.19
Specimen for finite torsion (1 in. = 25.4 mm) (From Wu, H.C. et al., *Int. J. Plasticity*, 13, 873, 1998. With permission from Elsevier).

The experiments were conducted by use of an axial–torsion material test system. An axial–torsion extensometer designed and built by Wu and Xu [1] was used to control and measure the strains within the gauge section of the specimen. In order to have maximum relative rotation applied to the specimen, the piston of the test system was prerotated to the maximum negative position (−50°) by the rotation control. Therefore, a maximum rotation angle of up to 100° could be applied to the specimen at each test run. At room temperature, several test runs were required for long specimens in free-end torsion in order to reach a large shear strain of over 100%. However, only one test run was practical for free-end torsion at elevated temperature and for fixed-end torsion at all temperatures including the room temperature. For each test run, the shear strain magnitude that could be attained depended on the gauge length of the specimen. One run of a long specimen produced about 40% of shear strain and about 110% of shear strain for a short specimen. The strain rate was $1.732 \times 10^{-3}\ s^{-1}$ for all tests.

The torque versus relative rotation curve and the axial extension or axial load versus relative rotation were recorded. Specimens of three different gauge lengths were used to study the influence of gauge length on the axial effect during torsion.

5.5.2.2 Torsion test at room and elevated temperature

To test the specimens at elevated temperature, the extensometer was redesigned and rebuilt according to Wu and Xu [1]. Most parts of the new extensometer used the same material. The material (304 stainless steel) was carefully selected with minimal thermal expansion being the requirement. Heat resistant transducers (LVDT's and RVDT's) were used, so that strain measurement or controlled biaxial straining at a temperature up to 150°C (300°F) was possible by use of the new extensometer.

The calibration procedure for room temperature testing is the same as the one described by Wu and Xu [1]. For elevated temperature, the calibration is much more difficult. First, there are no axial and torsional calibrators available for elevated temperature. Second, the calibration at room temperature cannot be directly used for elevated temperature, since the sensitivities of the transducers (LVDT's and RVDT's) used in the extensometer change with temperature. Thus, the calibration of the extensometer has to be carried out at the test condition, that is, at elevated temperatures.

The calibration was accomplished by means of transducers (stroke and rotation) of the test machine. The procedures of calibration are described as follows: first, the extensometer was calibrated for both axial and torsion at room temperature by use of an MTS displacement calibrator and a Klinger rotation stage. The accuracy is 0.0025 mm (0.0001 in.) and 0.01°, respectively. Then the extensometer was attached to the test machine by use of a set of fixtures inside the environmental chamber. The fixtures have been designed so that the extensometer measures the relative motion of the grips (no specimens are used for this part of calibration). Known displacements were applied to the stroke and rotation control of the test machine. The strokes and rotations were then recorded and plotted against the output of the extensometer as in Figure 5.20(a) and (b). It is seen that these are straight lines for both axial and rotational outputs. The curves of Figure 5.20(a) are independent of units (SI unit or inches) used in the displacement measurement. Next, the environmental chamber was heated up to the test conditions at 95°C (200°F) and 150°C (300°F), respectively. During the heating a water cooling system was used to cut the heat transfer to the piston and transducers of the test machine. The same displacement and rotation as before was then applied at the test system control and the extensometer outputs were recorded. The sensitivity of the extensometer was reduced due to the high temperature, but the output curves remained straight lines, so that the linearity of the extensometer held. It should be mentioned that the ratio of the outputs of the extensometer at room and elevated temperatures are the calibration factors. At each temperature, two calibration factors were obtained, one for the axial and the other for

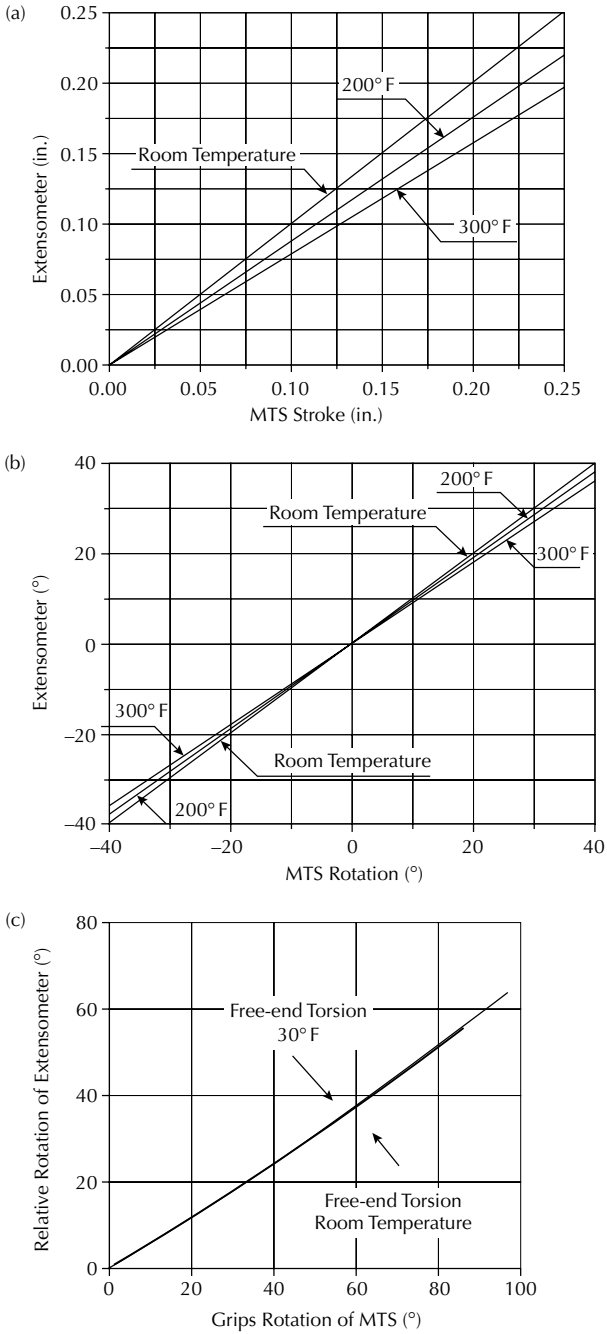

FIGURE 5.20
(a) Extensometer axial displacement calibration, (b) extensometer relative rotation calibration, (c) calibration of relative rotation at elevated temperature (From Wu, H.C. et al., *Int. J. Plasticity*, 13, 873, 1998. With permission from Elsevier).

rotation. Those factors were used to correct the actual readings of an elevated temperature test. The heating process was gradual to insure that the temperature in the specimen was uniformly distributed. About 2 h of heating time was needed for the environmental chamber used.

This procedure of calibration could not be used for temperature >150°C (300°F), which is the upper temperature limit for the LVDTs and RVDTs of the extensometer. For higher temperature tests, a different method of calibration must be used and specimens were required in this procedure. Calibration curves were determined at room and 150°C temperatures. It was then assumed that these curves were still valid at higher temperatures. A total of four short specimens of cast aluminum were used for the calibration tests in free- and fixed-end torsion conditions.

Figure 5.20(c) shows the calibration curves plotting the grips rotation of the test machine against the relative rotation within the gauge length, measured by the extensometer, of a short specimen tested in free-end torsion at two different temperatures. It is seen that no noticeable differences can be found between the two curves. This curve describes the geometrical characteristic of the specimen and shows that the relation has not been affected by temperature. Similar calibration curves for short specimen subjected to fixed-end torsion have also been obtained. Again, temperature does not have a noticeable influence on the calibration curve. The calibration curves plotting the stroke of the test system versus the axial extension within the gauge length of a specimen have also been determined and it has been found that the curve is not affected by test temperature either. An assumption is then made that these curves remain unchanged at higher temperatures at 205°C (400°F) and 315°C (600°F), so that they may be used to convert the stroke and rotation readings recorded during tests at 205°C and 315°C into axial and shear strains, respectively. At these temperatures, due to an added heating element, about 3 to 4 h of heating time were needed for the environmental chamber to reach a steady uniform temperature.

5.5.2.3 The hoop strain measurement

There are rarely any experimental data reported concerning the hoop strain. Baily et al. [43], recorded the hoop strain by taking readings of final diameter for nine specimens, which were tested at different levels of shear strain. However, a plug was used during the torsion tests, which might have restricted the diametral change. Although the diameter reduction was observed by many investigators (Swift [38], Freudenthal and Ronay [56], Ronay [41]) no reliably recorded data were taken either during the tests or after the tests. Data of diameter can provide important information as much as the axial extension does.

In [2], the hoop strain was determined by accurately measuring the diameter change during torsion. A ring was attached to the middle of the gauge section of the specimen by use of four, equally spaced (90° apart), spring-loaded pins. Two pins located at the opposite side of the diameter of the specimen

formed a pair. The displacement of each pin was measured by a LVDT and the readings for each pair of pins were averaged. This data and that obtained from the second pair of pins were then averaged to provide the data for diametral change during torsion.

In order to confirm the measured diametral change, a micrometer with 0.0025 mm (0.0001 in.) accuracy was used to measure the diameter. The measurement was taken at upper, middle, and lower cross-sections within the gauge section after each test run at room temperature. Several test runs were conducted, one after the other, so that a shear strain of 200% was obtained. After the tests, the specimens were cut in the middle section and the diameters were again measured. The data were consistent with the LVDT readings. The hoop strain was then computed by dividing the diametral change by the initial diameter.

In the tests for measuring the diametral change, the axial and shear strains were determined by the stroke and rotation, respectively, of the test machine. These readings were then converted into axial and shear strains by use of a set of calibration curves, one of which is shown in Figure 5.20(c).

5.5.3 Experimental Results and Discussions

Experimental results of [2] were analyzed and presented in terms of true shear stress–strain curve, axial strain, hoop strain, and axial stress. The difference between the cast and the extruded aluminum and the effect of test temperature are discussed in each item. Finally, the effect of specimen geometry is also discussed.

5.5.3.1 The true shear stress–strain curve

Raw experimental data in terms of torque versus angle of twist curves were analyzed by the modified Nadai method presented by Wu et al. [20]. The method accounts for length change in free-end torsion, and it is a method to determine the true shear stress–strain curve without measurement of radial and hoop strains. The true shear stress is defined in Wu et al. [20,22] based on the current cross-section of the specimen. The method of Wu et al. [20,22] is discussed in Section 5.5.4. The axial strain was computed simply by dividing the axial extension by the initial gauge length. It was a good approximation, since the axial extension was a small deformation. In the case of fixed-end torsion, Nadai's method [6] was used, since there was no axial length change.

Figure 5.21 shows the shear stress–strain curves for extruded aluminum at room and 150°C (300°F) temperatures. It is seen that the stress is lower at 150°C and that the shear stress–strain curve of fixed-end torsion is slightly higher than that for free-end torsion. This difference is due to the analysis (Wu et al. [20]) which assumes that the hoop strain and axial strain ratio is 0.5. According to the experimental results to be presented later in this section, this ratio is much greater than 0.5. An analysis by use of [22] with

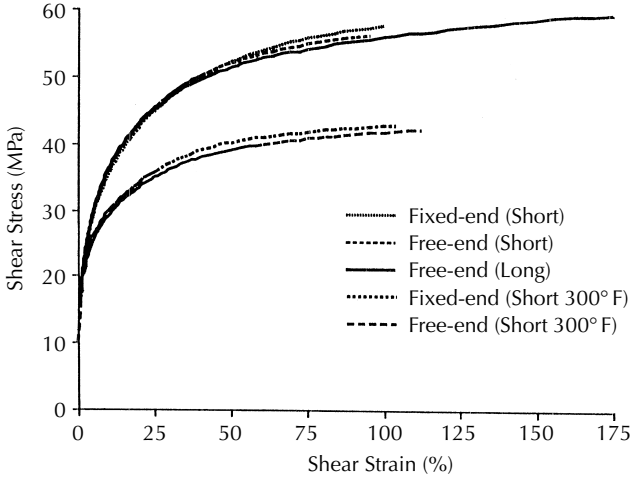

FIGURE 5.21
Shear stress–strain curves for extruded aluminum (From Wu, H.C. et al., *Int. J. Plasticity*, 13, 873, 1998. With permission from Elsevier).

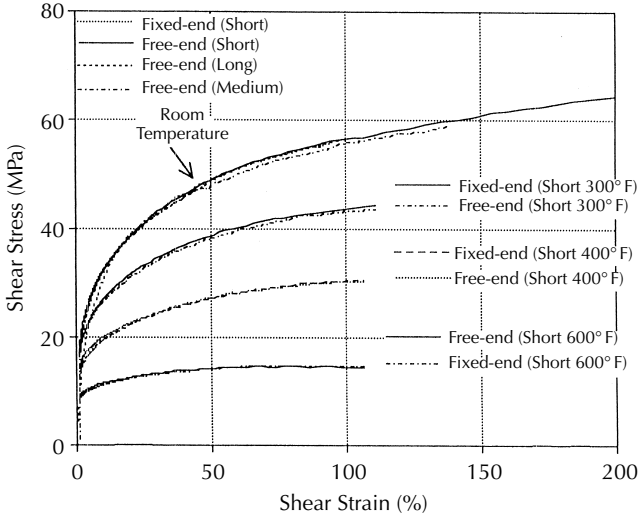

FIGURE 5.22
Shear stress–strain curves for cast aluminum (From Wu, H.C. et al., *Int. J. Plasticity*, 13, 873, 1998. With permission from Elsevier).

the hoop strain and axial strain ratio equal to 0.9 would make the two curves coincide. This correction has been made for curves in Figure 5.22 which are for cast aluminum. It suffices to mention that the curves for fixed-end torsion in Figure 5.21 are the true stress–strain curves.

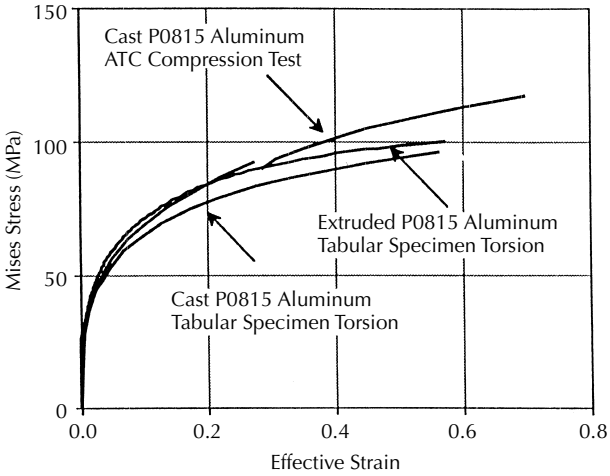

FIGURE 5.23
Comparison of mises stress obtained from torsion and compression (From Wu, H.C. et al., *Int. J. Plasticity*, 13, 873, 1998. With permission from Elsevier).

The curves of Figure 5.22 were obtained from free- and fixed-end torsion tests at room, 150°C (300°F), 205°C (400°F), and 315°C (600°F) temperatures using long, medium, or short specimens. It is seen that these curves are strongly affected by temperature. The higher the temperature is, the lower is the shear stress–strain curve. Short specimens were tested at all four temperatures. The curves of those specimens under fixed- and free-end condition are indistinguishable at all temperature levels. Long and medium gauge length specimens were also used in the room temperature testing under free-end condition. It is seen that the curves at room temperature for specimens of all gauge lengths are very close to each other. Figure 5.23 shows the experimental data of cast and extruded aluminum from the present torsion tests compared to the compression tests obtained by Wang et al. [57]. Note that there is an interruption in the compression curve due to unloading and specimen remachining. The curves are plotted in the form of Mises stress versus effective strain. (The Mises stress is defined based on the Mises yield criterion, which is discussed in Chapter 6 in connection with the flow theory of plasticity; and the effective strain is defined based on the second invariant of the strain tensor.) It is seen that the torsion curve for extruded aluminum, which has prestrain texture, lies higher than that for cast aluminum. Furthermore, the figure shows that the mises stress cannot be used to obtain a unified stress–strain curve for cast aluminum, because the stress for compression test is higher than that for torsion test. This is so because the two tests lead to different textures.

5.5.3.2 The axial strain

The axial effect takes the form of length change during free-end torsion. Figure 5.24 summarizes test data for axial extension versus shear strain for

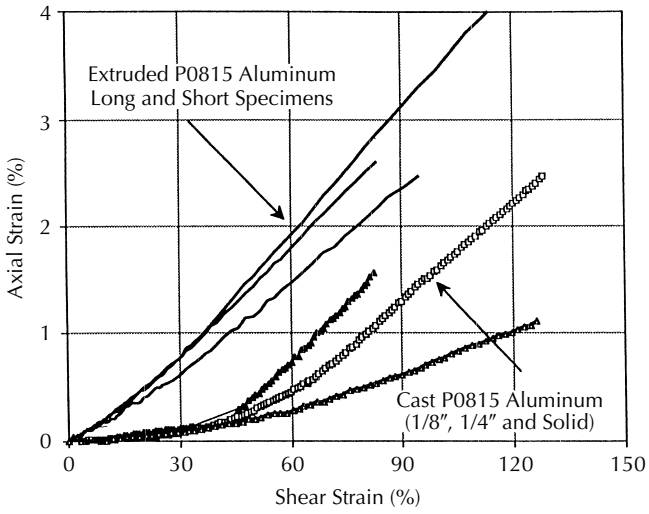

FIGURE 5.24
Axial strain in free-end torsion for cast and extruded aluminum (From Wu, H.C. et al., *Int. J. Plasticity*, 13, 873, 1998. With permission from Elsevier).

cast and extruded aluminum. The effect of specimen geometry is significant and is discussed in a subsequent section. For extruded aluminum, the axial extension starts to increase at the early stage of torsion test and continues to increase thereafter. The notation EAL denotes extruded aluminum with long specimen and EAS denotes extruded aluminum with short specimen. The wall-thickness was 6.4 mm for both curves. The slopes of axial strain curves decrease slightly at large shear strain level. For cast aluminum, the rate of axial extension is very small when the shear strain is <50%, but it is larger at larger shear strain and is almost the same as that of the extruded aluminum when the shear strain is >50%. In the figure, CA1/8 denotes cast aluminum tubular specimen with 3.2 mm (1/8 in.) wall-thickness and medium gauge length; CA1/4 denotes cast aluminum tubular specimen with 6.4 mm (1/4 in.) wall-thickness and long gauge length; and CASOL denotes cast aluminum solid shaft specimen. This figure shows that the development of axial effect in the cast aluminum was delayed by a shear strain of approximately 50% when compared with the extruded aluminum.

Figure 5.25 shows that the test temperature does not have a significant influence on the axial extension for cast aluminum. In the case of extruded aluminum (not shown in the figure), the axial extension curve at room temperature is slightly higher than that at 150°C (300°F), but they almost coincide. This finding does not agree with the assertion [41] that a higher temperature would give rise to a larger axial extension, and it is not consistent with the temperature effect observed in the axial stress developed during fixed-end torsion test discussed in the next subsection. Different textures are developed at different test temperatures and they can cause different amounts of length

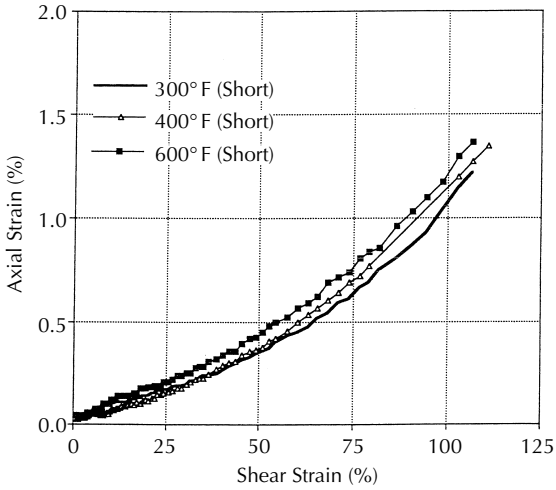

FIGURE 5.25
Axial strain in free-end torsion at elevated temperature (From Wu, H.C. et al., *Int. J. Plasticity*, 13, 873, 1998. With permission from Elsevier).

change. It is believed that the specimen geometry effect is responsible for this inconsistency. The geometry effect is important in the free-end torsion test and not as important in the fixed-end torsion test. Therefore, it is believed that the observed dependence of the axial stress on temperature is a true effect. From this viewpoint, one can then infer that a temperature effect should also exist in the length change, but it should be further investigated.

5.5.3.3 The hoop strain

For a few specimens where the outer diameter change was measured during free-end torsion, the hoop strain was computed from the diametral change. Figure 5.26 shows the axial and hoop strains plotted against the shear strain for cast and extruded aluminum at room temperature. Two long specimens of extruded aluminum (marked "textured" in the figure) were tested and the results are very consistent. The axial strain was about 5.5–6% and the hoop strain was about 4.0–4.5% when the shear strain was 150%. In the case of cast aluminum (marked "nontextured"), two medium and one short specimen were tested. It is seen that the development of the axial and hoop strains was delayed as compared to the curves of extruded aluminum. In all curves, no noticeable differences can be observed between specimens for shear strain of $<100\%$. Some differences can be seen for larger shear strains. However, it is interesting to note that a specimen of smaller axial strain tends to develop smaller hoop strain as well. Therefore, the hoop strain is closely related to the axial strain.

In Figure 5.27, the ratio of the hoop strain increment normalized with respect to the axial strain increment is plotted against the shear strain for

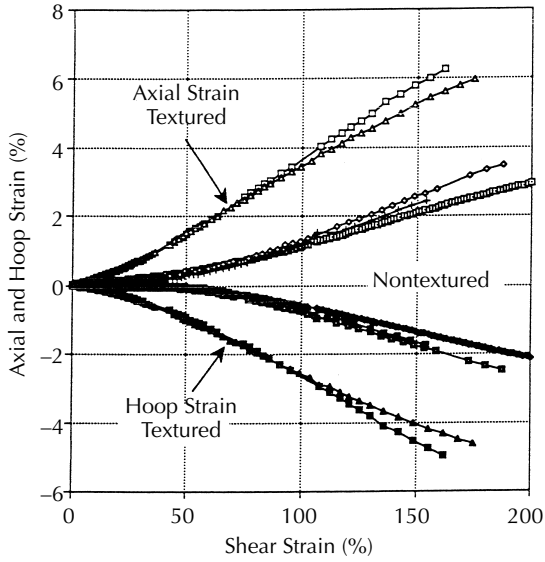

FIGURE 5.26
Hoop strains in free-end torsion (From Wu, H.C. et al., *Int. J. Plasticity*, 13, 873, 1998. With permission from Elsevier).

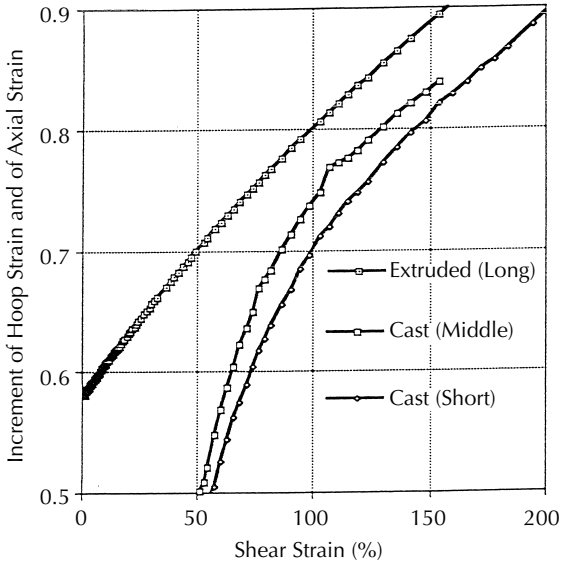

FIGURE 5.27
Ratio of increments of hoop and axial strains in free-end torsion (From Wu, H.C. et al., *Int. J. Plasticity*, 13, 873, 1998. With permission from Elsevier).

an extruded long specimen, a cast medium length specimen and a cast short specimen. For the extruded specimen, the ratio is over 0.5 at the beginning and increases almost linearly with the shear strain. When the shear strain is >150%, the ratio is over 0.9. For the cast specimens, the ratio is hard to determine at shear strain of <50% due to the smallness of both hoop and axial strains. The ratio is over 0.5 when the shear strain is 50% and it increases with the shear strain thereafter. The ratio is about 0.9 at a shear strain of 200%. The hoop strain or the aforementioned ratio is rarely reported in the literature. At large shear strain, the hoop strain increment is about 90% of the axial strain increment, and if the volume of the material keeps constant during plastic deformation, the radial strain increment is then only about 10% of the axial strain increment.

Bailey et al. [43] reported experimental data of 1100 aluminum where the hoop and axial strain ratio was <0.33 when calculated from the plot of Bailey's experiment. This ratio is very low compared with that found in this investigation. However, Bailey used a very short gauge length, Lindholm-type specimen and a plug inside the specimen which might have restricted the development of hoop strain.

5.5.3.4 The axial stress

The axial stress can be observed in a fixed-end torsion test. It is calculated by dividing the axial load by the initial cross-sectional area of the specimen. The axial stress is in compression and is monotonically increasing with the increasing shear strain for the material tested. The slope of the curves decreases at large shear strain level.

Figure 5.28 shows the axial stress developed during the fixed-end torsion test. It is seen that temperature has only a small effect on the axial stress development when shear strain is <50% but it significantly reduces the axial compressive stress when shear strain is >50%. It is interesting to note that at 315°C (600°F), the axial stress development is greatly reduced. Even so, the normal stress was still in compression and it reached the maximum compressive stress at a shear strain of approximately 100%.

The axial stress starts to develop right away even at small shear strain level for extruded aluminum (marked "textured" in the figure). On the other hand, the axial stress does not develop much at small shear strain level for the cast aluminum (marked "nontextured"). However, a significant increase in the axial stress occurs starting at a shear strain of about 50%. As the shear strain increases, the axial stress increases too and it will eventually reach a saturated value.

5.5.3.5 The geometry effect

The geometry of the specimen has a very significant effect on the results of free-end torsion. Figure 5.24 shows that the smallest amount of axial strain is observed if the solid shaft is used. For tubular specimen, the axial

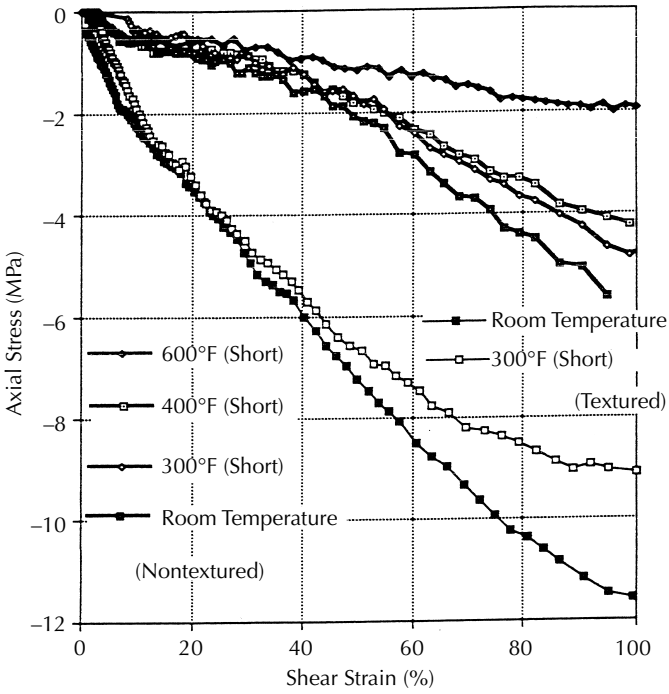

FIGURE 5.28
Axial stress in fixed-end torsion for cast and extruded aluminum (From Wu, H.C. et al., *Int. J. Plasticity*, 13, 873, 1998. With permission from Elsevier).

strain increases when the wall-thickness is reduced. The axial strain actually varies through the wall-thickness. It is higher at the outside radius and lower at the interior. The measured values reflect the integrated effect for axial strain. This effect is less for thin-walled tube but its usefulness is limited by buckling. Thus, relatively thick-walled tubes may be used as a compromise. The influence of wall-thickness is so great that the curve for 3.2 mm (0.125 in.) wall-thickness has larger axial strain than that for the curve for 6.4 mm (0.25 in.) wall-thickness, even though the former has a medium gauge length and the latter has a long gauge length. The effect of gauge length on the axial strain is depicted in Figure 5.29. All tubular specimens in this figure have the same wall-thickness of 6.4 mm but have different gauge lengths. It is seen that the specimen with long gauge length has the largest axial strain.

For short gauge length specimens, the shoulder restricted the hoop strain development which in turn reduced the axial extension. This reasoning leads to the conclusion that the Lindholm type specimen, which has a very short gauge section (very short compared with the short specimens in this study), is not suitable for use in the study of axial effect. The long and thick-walled specimen may be used, and this has been shown by Wu et al. [20,22] not to reduce the accuracy of the shear stress–stain curve. The long and thick-walled

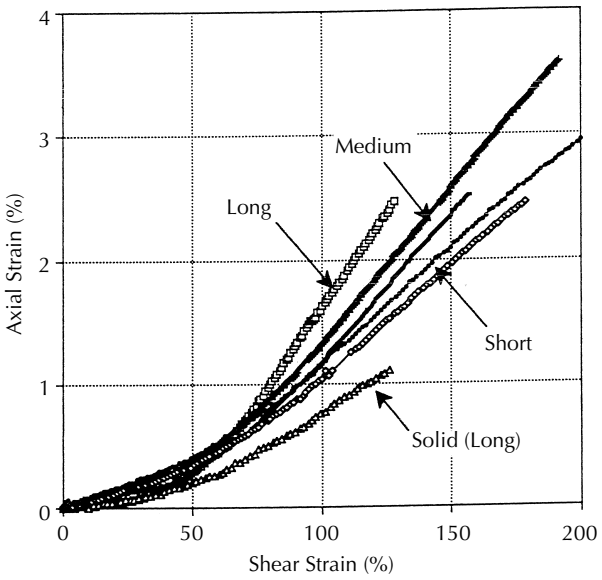

FIGURE 5.29
Effect of specimen gauge length on axial strain in free-end torsion (From Wu, H.C. et al., *Int. J. Plasticity*, 13, 873, 1998. With permission from Elsevier).

specimen will reduce experimental scatter caused by the inhomogeneity of the material, the machining tolerance and errors of deformation measurement, since a larger volume of material is involved.

Figure 5.30 shows the axial strain plotted against gauge length for cast aluminum specimens at different shear strain levels. These data are taken directly from Figure 5.29. At the 100% shear strain level, the axial strain is linearly related to the gauge length of the specimen. The longer the specimen is, the more axial strain is produced. At the 125% and 150% shear strain levels, the figure shows a gradual trend towards approaching a steady axial strain as the gauge length increases. It is believed that the axial strain will reach a steady magnitude as the gauge length is increased further. More experimental data are needed using even longer gauge length specimens. However, this may not be easily accomplished due to inhomogeneity in the material when the gauge length is even longer.

The gauge length and wall-thickness may have a significant influence on the axial stress in fixed-end torsion. This effect has not yet been studied by the author and his coworkers.

5.5.3.6 Conclusions drawn from the torsion test

An axial–torsional extensometer for high temperature testing and its calibration procedures at room and elevated temperatures have been developed. The extensometer enables an accurate control and determination of strains in

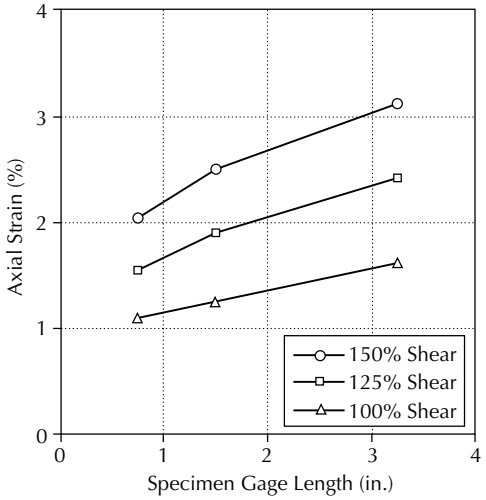

FIGURE 5.30
Axial strain versus gauge length at constant shear strain (1 in. = 25.4 mm) (From Wu, H.C. et al., *Int. J. Plasticity*, 13, 873, 1998. With permission from Elsevier).

a combined axial–torsional condition in the large strain range. A procedure for determining the hoop strain during large strain torsion tests has also been developed.

Based on torsion experiments on long, medium, and short tubular specimens of extruded and cast high purity aluminum, the following conclusions may be drawn:

1. Shear stress–strain curves obtained from free- and fixed-end torsion tests of long, medium, and short specimens are consistent. Only a few experimental scatter of <1.5% in stress can be observed. This result is shown systematically for both room and elevated temperatures.
2. Axial extension increases with shear strain in free-end torsion of extruded and cast aluminum. The axial extension is almost not affected by temperature in the range of temperature tested. This, however, is not consistent with the axial stress developed in the fixed-end torsion tests. The temperature effect should be further investigated.
3. Hoop strain in free-end torsion is of a significant magnitude compared with axial strain at large shear strain level. It is about 80 to 90% of axial strain. If the volume of the material remains constant during plastic deformation, then the radial strain is only about 10 to 20% of the axial strain. This experimental result is different from the usual assumption (see [58]) made in theoretical studies in which the hoop and radial strains are assumed to be of equal magnitude in an initially isotropic material.

4. Axial stress is always in compression for the fixed-end torsion and it is significantly influenced by temperature. Temperature reduces the magnitude of axial stress. The axial stress of extruded aluminum tested at 150°C (300°F) reached a minimum at a shear strain of about 100%. The axial stress of cast aluminum at 315°C (600°F) reached a minimum at a shear strain of about 100%.
5. The specimen gauge length affects axial extension as well as hoop strain. A short gauge length will limit the development of hoop strain at large shear strain level and, therefore, reduces the axial strain.
6. Extrusion of material increases the shear flow stress and causes significant axial effect to occur right at the beginning of the torsion test.
7. Long and thick-walled tubular specimen is suitable for large strain torsion test. Important factors associated with this test are: an accurate determination of shear stress–strain curve from the torque–twist curve, an accurate strain measurement, and the understanding of the effect of specimen geometry.

5.5.4 Determination of Shear Stress–Strain Curve

It takes a theory to convert the torque versus angle of twist curve into the shear stress–strain curve. Most theories such as those discussed in Section 5.2.3.1 or Canova et al. [55] do not account for length change of the specimen subjected to torsion and, therefore, do not lead to accurate results for free-end torsion. Although these methods may be used to obtain accurate shear stress–strain curve for the fixed-end torsion test (see [22]), the required test system is generally not available as previously discussed. Therefore, the free-end torsion of tubular specimens is still a practical test for the determination of true shear stress–strain curve. For this purpose, experimental data for axial and hoop strains are also needed. Wu et al. [20,22] developed a method which, by accounting for the axial and hoop strains, provides a true shear stress–strain curve from the free-end torsion test. This true shear stress–strain curve is consistent with that determined from the fixed-end torsion test. It should be emphasized that, in this method, the reduction of shear stress–strain curve from the torque-angle of twist curve is strictly a consideration of specimen geometry and no material properties are directly involved. The task is to determine an experimental shear stress–strain curve so that it may be used for the verification of any constitutive equation.

The following derivation is based on [22]. The analysis in [20] by the same authors assumed that hoop and radial strains are equal during torsion and it can be considered as a special case of [22]. However, Taylor and Quinney [54] showed that hoop and radial strains are not equal during torsion of tubes. This result has also been confirmed experimentally by Wu et al. [2] which has been discussed in Section 5.5.3. By use of this new solution, the shear stress–strain curves obtained from free- and fixed-end torsion tests coincide.

In the present analysis, the hoop and radial strains are not equal, and the following assumptions are made: (a) plane sections remain plane; (b) all radii remain straight; and (c) plastic deformation is incompressible. The axial, hoop, and radial strains are generally in the small strain range, so that the small strain relations for the normal strain components are used in this analysis. Furthermore, the normal strains are plastic strains because no elastic normal strains exist when the specimen is subjected to torsion.

The condition of plastic incompressibility gives

$$\varepsilon_V = \varepsilon_{11} + \varepsilon_{22} + \varepsilon_{33} = 0 \tag{5.49}$$

where ε_{11} is the axial strain, and ε_{22} and ε_{33} are the radial strain and the hoop strain of a specimen, respectively. Since, in torsion, all normal strains are functions of the twist angle, they may be written as

$$\varepsilon_{11} = A(\theta), \qquad \varepsilon_{22} = -R(\theta), \quad \text{and} \quad \varepsilon_{33} = -H(\theta) \tag{5.50}$$

Therefore, (5.49) becomes

$$A(\theta) - H(\theta) - R(\theta) = 0 \tag{5.51}$$

In these expressions, the normal strains are assumed to be uniform over the wall of the tube.

Consider now the current outer diameter (r_{oc}), the current inner diameter (r_{ic}) and the current wall-thickness (t_{c}) of a tubular specimen under free-end torsion. The hoop strain is defined by considering the change in length of the circumference of the tube, and it gives

$$r_{\text{oc}} = r_0(1 - H) \tag{5.52}$$

The current wall-thickness is

$$t_{\text{c}} = t_0(1 - R) = cr_i(1 - A + H) \tag{5.53}$$

where t_0 is the initial wall-thickness and $t_0 = cr_i$. Parameter c specifies the initial wall-thickness. Thus,

$$\begin{aligned} r_{\text{ic}} &= r_{\text{oc}} - t_{\text{c}} = r_{\text{oc}} - t_0(1 - A + H) = r_0(1 - H) - t_0(1 - A + H) \\ &= r_i(1 - H) + t_0(A - 2H) = r_i[1 - (1 + 2c)H + cA] \end{aligned} \tag{5.54}$$

From (5.52) and (5.54), the current shear strains at outer (γ_{oc}) and inner (γ_{ic}) diameters are given as

$$\gamma_{\text{oc}} = \theta r_0(1 - H) \tag{5.55}$$

$$\gamma_{ic} = \theta r_i[1 - (1 + 2c)H + cA] \tag{5.56}$$

The applied torque is

$$M = \int_{r_{ic}}^{r_{oc}} 2\pi r^2 \tau \, dr \tag{5.57}$$

or

$$M\theta^3 = \int_{\gamma_{ic}}^{r_{oc}} 2\pi \gamma^2 f(\gamma) \, d\gamma \tag{5.58}$$

where the shear stress is $\tau = f(\gamma)$. Differentiating (5.58) with respect to θ, it is found that

$$\frac{d(M\theta^3)}{d\theta} = 2\pi \tau_{oc} \gamma_{oc}^2 \frac{d\gamma_{oc}}{d\theta} - 2\pi \tau_{ic} \gamma_{ic}^2 \frac{d\gamma_{ic}}{d\theta} \tag{5.59}$$

Considering the right-hand side of (5.59) term by term and using (5.55) and (5.56), it is found that

$$\gamma_{oc}^2 \frac{d\gamma_{oc}}{d\theta} \approx \theta^2 r_0^3 \left[1 - 3H - \theta \frac{dH}{d\theta}\right] \tag{5.60}$$

$$\gamma_{ic}^2 \frac{d\gamma_{ic}}{d\theta} \approx \theta^2 r_i^3 \left[1 - \frac{3}{2}(1 + 2c)H + 3c\,A - \left(\frac{1 + 2c}{2}\right)\theta \frac{dH}{d\theta} + c\,\theta \frac{dA(\theta)}{d\theta}\right] \times \left[1 - \frac{3}{2}(1 + 2c)H - \left(\frac{1 + 2c}{2}\right)\theta \frac{dH}{d\theta}\right] \tag{5.61}$$

In the derivation of (5.60) and (5.61), H, dH/dq, A, and dA/dq are considered to have the same order of magnitude of smallness; this is experimentally justified in [20]. When higher order terms of these quantities are neglected, by use of (5.60) and (5.61), (5.59) becomes

$$\tau_{oc} = \frac{1}{r_0^3[1 - D(H)]} \left\{\tau_{ic} r_i^3 [1 - (1 + 2c)D(H) + c\,D(A)] + \frac{1}{2\pi} D(M)\right\} \tag{5.62}$$

where the operator is $D(\,) = 3(\,) + \theta \, d(\,)/d\theta$. This equation may be used to determine the shear stress–strain curve from the experimentally determined $M(\theta)$, $A(\theta)$, and $H(\theta)$ curves using an iterative procedure like that used in [20] and explained below. The approximation of $H(\theta) = 0.9A(\theta)$, justified by experimental results of Wu et al. [2], may be made. An iterative procedure is used due to the fact that, for a given θ in (6.62), two unknown stresses τ_{oc} and τ_{1c} need to be evaluated. Let us observe that $\gamma = r_1\theta_2 = r_0\theta_1$ and, for a given angle of twist, say θ_1, another twist angle is defined by $\theta_2 = (r_0/r_1)\theta_1$.

This constitutes the mechanism of iteration, and we start the iteration procedure at the elastic region. When the shear deformation is small in the elastic region, the stress at the outer surface is known and given by (5.24). Note that $\tau = f(\gamma)$, and τ_{oc} for θ_1 is equivalent to τ_{1c} for θ_2. We then increase the twist angle, θ, by a factor of (r_0/r_1) for each step, so that τ_{1c} in the (i)th step takes the value of τ_{oc} in the $(i-1)$th step. Suitable choices of the starting value, θ_1, will enable any required point on the stress–strain curve to be obtained. The parameter c, which shows the effect of wall-thickness, is present in the equation. However, numerical results show that this effect is very minor and does not show an apparent effect on the curves obtained. This is expected, since the experimental results of Wu et al. [2] show that the wall-thickness does not change much during torsion and, therefore, it may be inferred that the wall-thickness is not an important factor. In the case of $H(\theta) = 1/2A(\theta)$, which is assumed by many investigators, (5.62) reduces to

$$\tau_{oc} = \frac{1}{r_0^3}\left[\tau_{ic} r_i^3 + \frac{D(M)}{2\pi(1-(1/2)D(A))}\right] \tag{5.63}$$

which is the same as (34) of [20]. Note that c drops out of this equation. In the special case, when $r_i = 0$, (5.63) reduces to

$$\tau_{oc} = \frac{D(M)}{2\pi r_0^3(1-(1/2)D(A))} \tag{5.64}$$

which is (26) of [20] for solid shaft. Also, when $r_i = 0$ and $A = H = R = 0$, (5.62) reduces to Nadai's solution (5.29).

To evaluate (5.62), a set of experiments was conducted using tubular specimens of extruded, high purity aluminum. Details of these experiments were reported in [2]. All specimens had the same inner and outer diameters and the same wall-thickness, but different uniform gauge sections. Two long specimens were tested in free-end torsion; one short specimen was tested in free-end torsion; and one short specimen was tested in fixed-end torsion. Torque versus shear strain curves were recorded in all cases. In the free-end torsion test, the axial strain was also recorded. In addition, a measuring device was built to measure the changes in diameter during the free-end torsion test of long specimens. The hoop strain was thus determined. The axial and hoop strains are plotted against the shear strain in Figure 5.26. It is seen that the hoop strain has a magnitude of approximately 0.9 times the axial strain, and that the gauge length has a significant effect on the magnitude of the axial strain. The hoop strain of the short specimen was not measured.

Data for the axial and hoop strain were used to compute the shear stress–strain curve for the free-end torsion by use of (5.62). Since the hoop strain of the short specimen was not measured, a relation similar to the long specimens,

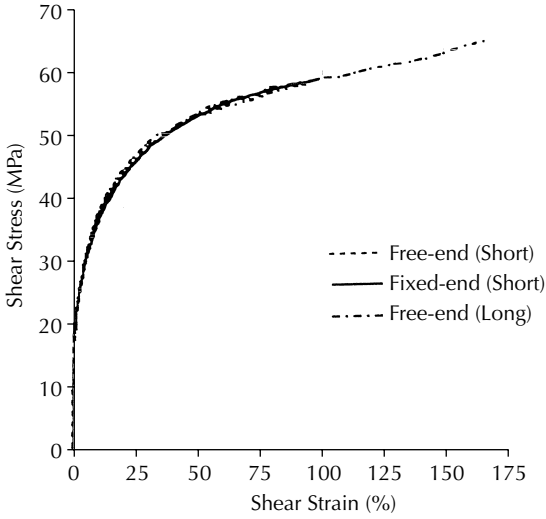

FIGURE 5.31
Shear stress–strain curve determined (From method of Wu, H.C. et al., *J. Eng. Mater. Technol.*, 119, 113, 1997. With permission).

$H(\theta) = 0.9\, A(\theta)$, was assumed. We used (5.30) to analyze the data for fixed-end torsion using the same iteration procedure. Figure 5.31 shows the shear stress–strain curves thus obtained. It is seen that no noticeable differences in the shear stress–strain curves of free- and fixed-end torsions can be found. In the figure, data of the two long specimens tested in the free-end condition were averaged to give one curve.

References

1. Wu, H.C. and Xu, Z., An axial–torsional extensometer for finite deformation, *J. Eng. Mater. Technol.*, 112, 330, 1990.
2. Wu, H.C., Xu, Z., and Wang, P.T., Torsion test of aluminum in the large strain range, *Int. J. Plasticity*, 13, 873, 1998.
3. Bell, J.F., The experimental foundations of solid mechanics, in *Handbuch der Physik*, Via/1, Flügge, Ed., Springer, Berlin, 1973.
4. Penny, R.K. and Leckie, F.A., The mechanics of tensile testing, *Int. J. Mech. Sci.*, 10, 262, 1968.
5. Wu, H.C. and Rummler, D.R., Analysis of misalignment in the tension test, *J. Eng. Mater. Technol.*, 101, 68, 1979.
6. Nadai, A., *Theory of Flow and Fracture of Solids*, Vol. I, McGraw-Hill, New York, 1950, 343.

7. Spitzig, W.A., Sober, R.J., and Richmond, O., Pressure dependence of yielding and associated volume expansion in tempered martensite, *Acta Metall.*, 23, 885, 1975.
8. Taylor, G.I. and Quinney, H., The latent energy remaining in a metal after cold working, *Proc. Roy. Soc. (London)*, Ser. A, 143, 307, 1934.
9. Bridgman, P.W., *Studies in Large Plastic Flow and Fracture*, McGraw-Hill, New York, 1952, 118.
10. Armstrong, P.E., Hockett, J.E., and Sherby, O.D., Large strain multidirectional deformation of 1100 aluminum at 300 K, *J. Mech. Phys. Solids*, 30, 37, 1982.
11. Gunasekera, J.S., Havranek, J., and Littlejohn, M.H., The effect of specimen size on stress–strain behavior in compression, *J. Eng. Mater. Technol.*, 104, 274, 1982.
12. Khan, A.S. and Liang, R., Behaviors of three BCC metals during non-proportional multi-axial loadings: experiments and modeling, *Int. J. Plasticity*, 16, 1443, 2000.
13. Kupher, H., Hilsdorf, H.K., and Rusch, H., Behavior of concrete under biaxial stresses, *Am. Concrete Inst. J. Proc.*, 60, 209, 1963.
14. Wu, H.C., Dual failure criterion for plain concrete, *J. Eng. Mech. Div., ASCE*, 100, 1167, 1974.
15. Coker, E.G. and Filon, L.N.G., *Photoelasticity*, 2nd Edn., Cambridge Press, London, 1957, 587.
16. Wu, H.C., Chang, K.J., and Schwarz, J., Fracture in the compression of columnar grained ice, *Eng. Fracture Mech.*, 8, 365, 1976.
17. Hecker, S.S., Stout, M.G., and Eash, D.T., Experiments on plastic deformation at finite strains, in *Proc. Research Workshop: Plasticity of Metals at Finite Strain-Theory, Experiment and Computation*, Lee, E.H. and Mallett, R.L., Eds., Stanford University and RPI, Palo Alto, CA, 1982, 162.
18. Batdorf, S.B. and Robert, W.C.K., Shear plastic stress–strain relation obtained from torque–twist data, *J. Eng. Mater. Technol.*, 108, 354, 1986.
19. Brown, M.W., Torsional stresses in tubular specimens, *J. Strain Anal.*, 13, 23, 1978.
20. Wu, H.C., Xu, Z.Y., and Wang, P.T., The shear stress–strain curve determination from torsion test in the large strain range, *ASTM J. Testing Eval.*, 20, 396, 1992.
21. Wu, H.C., Aboutorabi, M.R., and Chen, P.C.T., Cyclic torsion of a circular cylinder and its residual stress distribution, *J. Eng. Mater. Technol.*, 107, 48, 1985.
22. Wu, H.C., Xu, Z.Y., and Wang, P.T., Determination of shear stress–strain curve from torsion test for loading–unloading and cyclic loading, *J. Eng. Mater. Technol.*, 119, 113, 1997.
23. Garofalo, F., *Fundamentals of Creep and Creep-Rupture in Metals*, Macmillan, New York, 1965, 6.
24. Corum, J.M., Greenstreet, W.L., Liu, K.C., Pugh, C.E., and Swindeman, R.W., Interim Guidelines for Detailed Inelastic Analysis of High-Temperature Reactor System Components, ORNL-5014, 1974.
25. Ikegami, K. and Niitsu, Y., Experimental evaluation of the interaction effect between plastic and creep deformation, *Eng. Fract. Mech.*, 21, 897, 1985.
26. Wu, H.C. and Ho, C.C., Strain hardening of annealed 304 stainless steel by creep, *J. Eng. Mater. Technol.*, 115, 345, 1993.

27. Kujawski, D., Kallianpur, V., and Krempl, E., An experimental study of uniaxial creep, cyclic creep and relaxation of AISI type 304 stainless steel at room temperature, *J. Mech. Phys. Solids*, 28, 129, 1980.
28. Wu, H.C. and Yao, J. C., Investigation of Creep by Using of Closed Loop Servo-Hydraulic Test System, Report G302-81-001, Division of Materials Engineering, The University of Iowa, Iowa City, IA, 1981.
29. Wu, H.C. and Ho, C.C., An investigation of transient creep by means of endochronic viscoplasticity and experiment, *J. Eng. Mater. Technol.*, 117, 260, 1995.
30. Xia, Z. and Ellyin, F., An experimental study on the effect of prior plastic straining on creep behavior of 304 stainless steel, *J. Eng. Mater. Technol.*, 115, 200, 1993.
31. Hayhurst, D.R., The effects of test variables on scatter in high-temperature tensile creep-rupture data, *Int. J. Mech. Sci.*, 16, 829, 1974.
32. Wu, H.C. and Wang, T.P., Analysis of test system misalignment in the creep test, *J. Eng. Mater. Technol.*, 104, 280, 1982.
33. Ludwik, P., *Elemente derTechnologischen Mechanik*, Springer-Verlag, Berlin, 1909.
34. Ramberg, W. and Osgood, W., Description of stress–strain curves by three parameters, NACA Tech. Note No. 902, 1943.
35. Crossland, B., The effect of fluid pressure on the shear properties of metals, *Proc. Inst. Mech. Engrs.*, 168, 935, 1954.
36. Hu, L.W., Plastic stress–strain relations and hydrostatic stress, in *Proc. 2nd Symposium on Naval Struc. Mech.*, Lee, E.H. and Symonds, P.S., Eds., Brown University, Pergamon Press, 1960, 194.
37. Poynting, J.H., On pressure perpendicular to the shear-planes in finite pure shears, and on lengthening of loaded wires when twisted, *Proc. Roy. Soc. London* A, 82, 546, 1909.
38. Swift, H.W., Length changes in metals under torsional overstrain, *Engineering*, 163, 253, 1947.
39. Hughes, D.E.R., The hot-torsion test for assessing hot-working properties of steels, *J. Iron Steel Inst.* 170, 214, 1952.
40. Hodierne, F.A., A torsion test for use in metal working studies. *J. Inst. Metals* 91, 267, 1962.
41. Ronay, M., On second-order strain accumulation in aluminum in reversed cyclic torsion at elevated temperatures, *Int. J. Solids Struct.*, 3, 167, 1967.
42. Ronay, M., Second-order elongation of metal tubes in cyclic torsion, *Int. J. Solids Struct.* 4, 509, 1968.
43. Bailey, J.A., Naos, S.L., and Nawab, K.C., Anisotropy in plastic torsion, *J. Basic Eng.*, 94, 231, 1972.
44. Billington, E.W., Non-linear mechanical response of various metals: 3, Swift effect considered in relations to the stress–strain behavior in simple compression, tension and torsion, *J. Phys. D: Appl. Phys.*, 10, 553, 1977.
45. Lindholm, U.S., Nagy, A., Johnson, G.R., and Hoegfeldt, J.M., Large strain, high strain rate testing of copper, *J. Eng. Mater. Technol.*, 102, 376, 1980.
46. Van Arsdale, W.E., Hart, E.W., and Jenkins, J.J., Elongation upon torsion in a theory for the inelastic behavior of metals, *J. Appl. Phys.*, 51, 953, 1980.
47. Montheillet, F., Cohen, M., and Jonas, J.J., Axial stresses and texture development during the torsion testing on Al, Cu and a-Fe, *Acta Metall.* 32, 2077, 1984.

48. Wu, H.C. and Xu, Z., An experimental investigation of the axial effect during torsion, in *Advances in Constitutive Laws for Engineering Materials*, Fan, J. and Murakami, S., Eds., International Academic Publishers, 1989, 232.
49. Lipkin, J. and Lowe, T.C., Axial effects during reversed torsional deformation. *Advances in Plasticity 1989*, Kahn, A.S. and Tokuda, M., Eds., Pergamon Press, Oxford, 1989, 625.
50. White, C.S., Bronkhorst, C.A., and Anand, L., An improved isotropic-kinematics hardening model for moderate deformation metal plasticity, *Mech. Mater.*, 10, 127, 1990.
51. Weerasooriya, T. and Swanson, R.A., Experimental evaluation of the Taylor-type polycrystal model for the finite deformation of an fcc metal (OFHC copper), U.S. Army Materials Technology Laboratory, Watertown, MA, 1991.
52. Toth, L.S., Jonas, J.J., Daniel, D., and Bailey, A., Texture development and length changes in copper bars subjected to free end torsion, *Textures Microstruct.*, 19, 245, 1992.
53. Miller, M.P. and McDowell, D.L., The effect of stress-state on the large strain inelastic deformation behavior of 304L stainless steel, *ASME J. Eng. Mat. Tech.* 118, 28, 1996.
54. Taylor, G.I. and Quinney, H., The plastic distortion of metal, *Phil. Trans. Roy. Soc.* A, 230, 323, 1931.
55. Canova, G.R., Shrivastava, S., Jonas, J.J., and Sell, C.G., The use of torsion testing to assess material formability, *ASTM STP 753*, Newby, J.R. and Niemeier, B.A., Eds., 189, 1982.
56. Freudenthal, A. M. and Ronay, M., Second-order effects in dissipative media. *Proc., Royal. Soc. London* A, 292, 14, 1966.
57. Wang, P.T., Panchanandeeswaran, S., and Wu, H.C., Comparison of flow stress and texture for P0818 cast aluminum deformed in compression and in torsion. Alcoa Technical Center Research Report, 1995.
58. Canova, G.R., Kocks, U.F., and Jonas, J.J., Theory of torsion texture development, *Acta Metall.*, 32, 211, 1984.

Problems

(1) Derive equation (5.30).

(2) Derive equation (5.32).

(3) The experimental M (kN m) versus θ (rad/m) relation in the small deformation range is defined by the following set of data: $\{M, \theta\} = \{(0, 0), (0.025, 0.0047), (0.0509, 0.0174), (0.07, 0.06), (0.097, 0.174), (0.116, 0.348), (0.149, 0.693), (0.181, 1.35)\}$. The cylindrical specimen has a radius of 0.008052 m. Determine the shear stress–strain curve by use of the Nadai method.

(4) The shear stress–strain curve is influenced by the axial pretension of the specimen. Assuming that a cylindrical specimen has been prestrained axially to a plastic strain of ε^{P} in the small strain range, use the Nadai method to derive equations which can be used to determine the shear stress–strain curve, if the torque M versus angle of twist θ relation has been experimentally recorded.

(5) For the experimental data of $(\sigma \text{ MPa}, \varepsilon) = \{(0,0), (11, 0.000156), (22.6, 0.0058), (31.1, 0.02), (43, 0.058), (51.7, 0.116), (66.2, 0.231), (80.3, 0.45)\}$, determine the parameters of (a) the Ludwik equation and (b) the Ramberg–Osgood equation. Show the curves in a graph.

(6) In a simple compression test, if the true stress–strain curve is expressed by the Ludwik equation, determine the expression relating the load and the logarithmic strain. The curve plotting the load against the logarithmic strain shows an inflection point. At what strain does the inflection point occur?

(7) Use the Ramberg–Osgood equation to investigate the error band in the stress–strain curve, due to test system misalignment similar to Figure 5.5. Use the same dimensions and constants as in Wu and Rummler [5] for the symmetrical case.

(8) A 25 mm diameter cylindrical rod is tested in tension to a load of 45 kN. An identical rod is also tested in tension to the same load but submerged in pressurized fluid of 35 MPa during the test. Which rod experiences the larger shear stress, assuming that the deformation is small?

(9) For an isotropic iron rod, the volume change under hydrostatic pressure is given by (5.47). Denoting the axial strain by ε and the transverse strain by ε_t, plot the ε_t versus ε curves for various constant pressure p. Find the relation between ε_t and ε, when the material is assumed to be incompressible.

(10) In the determination of the shear stress–strain curve, at what shear strain-rate must the specimen be tested, if the corresponding axial stress–strain curve is obtained at a constant strain rate of 10^{-4} s^{-1}?

6

The Flow Theory of Plasticity

6.1 Introduction

Based on the experimental findings mentioned in Chapter 5 and some additional experiments discussed in this chapter, various theories of plasticity have been proposed in the literature. We present the major concepts and the formulation of the flow theory of plasticity in this chapter. The flow theory is the oldest and most widely known theory of plasticity and can serve as a basis for discussing improvements of any theory of plasticity or a new theory. The flow theory is formulated here in the three-dimensional stress space, but only the original form of the theory is discussed. Discussion of improvements to the flow theory, the extension of the theory to finite plastic deformation, and modern theories is deferred to Chapter 7.

According to the flow theory, the constitutive equations of plasticity consist of (1) a yield criterion, (2) a flow rule, (3) a strain-hardening rule, and (4) the loading–unloading conditions. The yield criterion determines the stress state when yielding occurs; the flow rule describes the increment of plastic strain when yielding occurs; the hardening rule describes how the material is strain-hardened as the plastic strain increases; and the loading–unloading conditions specify the next move in the loading program. These are the major concepts of the flow theory and are explained in the following sections.

6.2 The Concept of Yield Criterion

The yield stress σ_y is shown in the one-dimensional stress–strain curve of Figure 5.1. If we look at Figure 5.1 from the point of view of the stress axis, we see that if the applied stress is less than σ_y, the material behaves elastically, but, as soon as the stress σ reaches σ_y plastic yielding occurs, which is the *initial yielding*. Therefore, the condition $\sigma = \sigma_y$ is the yield criterion. The yield criterion defines the *elastic region* in the stress space (the stress axis in this one-dimensional case). When $\sigma > \sigma_y$, which corresponds to curve ABE in

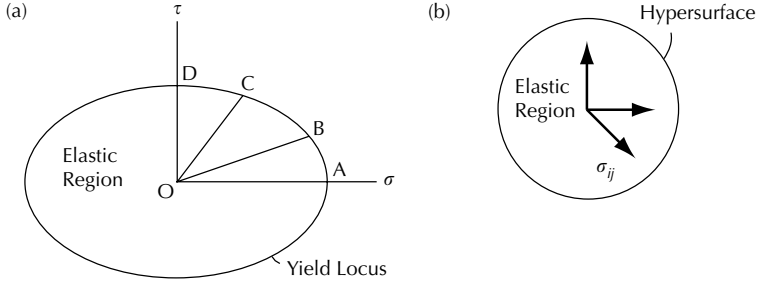

FIGURE 6.1
(a) Yield locus in a two-dimensional stress space and (b) yield surface in the nine-dimensional stress space.

Figure 5.1, the material is undergoing *strain-hardening*, and the material is subjected to subsequent yielding.

In the two-dimensional stress space (τ, σ), which is one of the simplest possible multidimensional stress spaces, we consider the case of combined axial–torsion of a thin-walled tube. σ is the axial stress and τ is the shear stress acting on an infinitesimal material element on the wall of the tubular specimen. Figure 6.1(a) shows the (τ, σ) space. If we conduct an experiment starting with zero loading at O, we can take different proportional stress-paths OA, OB, etc. Following the stress-path OA, the material is initially in the elastic state and yielding occurs when the stress point reaches A. A similar situation applies to other paths. Thus, A, B, C, and D are points where yielding occurs. Other yield points can be obtained when other paths are followed, including paths in other quadrants of the two-dimensional stress space. We can then connect all yield points A, B, C, D, etc. with a smooth closed curve and this curve is known as the *yield locus* (or *yield surface* if multidimensional). It is the two-dimensional version of the yield criterion of the material in this stress space. All experimentally determined yield loci are convex. The yield locus defines the elastic region in the stress space. Hooke's law is applicable within the elastic region, and the flow rule is used when the stress point is on the yield locus.

Similarly, yield surfaces may be experimentally determined under other loading conditions. Examples are those in the principal stress space (σ_1, σ_2) and in the three-dimensional stress space $(\sigma_{12}, \sigma_{11}, \sigma_{22})$. The former may be determined by testing a tubular specimen subjected to axial loading and internal pressure and the latter by testing a tubular specimen in combined axial–torsion with internal pressure. Generally, the yield criterion in the nine-dimensional stress space σ_{ij} is represented by a *hypersurface* shown in Figure 6.1(b). The yield surface is a function f of stress so that the following conditions apply:

$$\begin{array}{lll} f(\sigma_{ij}) = 0 \quad \text{or} \quad f(\sigma_{ij}) = k^2 & & \text{plastic state} \\ f(\sigma_{ij}) < 0 & & \text{elastic state} \\ f(\sigma_{ij}) > 0 & & \text{impossible} \end{array} \tag{6.1}$$

where k is the shear yield stress, that is, the yield stress at point D in Figure 6.1(a). In the case of combined axial–torsion, the yield loci for several initially isotropic metals have been experimentally determined and reported in the literature. In all cases, the loci are very close to ellipses. These loci are close to circles if plotted in the $(\sqrt{3}\tau, \sigma)$ space. The experimental yield loci include those for copper, aluminum, and mild steel at room temperature determined by Taylor and Quinney [1], 6061-T6 aluminum at room temperature by Bertsch and Findley [2], copper at room temperature by Mair and Pugh [3], pure aluminum at constant temperatures from 21 to 152°C (70 to 305°F) by Phillips and Tang [4], AISI 304 stainless steel at room temperature by Wu and Yeh [5] and Wu and Ho [6], SUS304 stainless steel at room temperature by Ishikawa [7], and many more data that have been reported in the literature. It is fair to conclude that the experimental results for isotropic metals lead to initial yield surfaces which can be well represented by a circle in the $(\sqrt{3}\tau, \sigma)$ space.

There are two points of interest related to the yield surface: (1) the definition of yield and (2) the initial versus subsequent yield surfaces. The yield stress is easily identifiable for mild steel, because it has an upper yield point. But, it is not so easily identified for other metals when the stress–strain curve bends gradually in the elastic–plastic transition zone. The definition of yield is very important in that the characteristics of the subsequent yield surface depend on the definition of yield. Three definitions of yield have been used by investigators, and it is important to know the definition of yield used in an experiment so that proper interpretation of the experimental yield surface may be made. The three definitions of yield are proportional limit, proof strain, and backward extrapolation. Figure 6.2 shows the three definitions of yield, in which the yield stress determined by the proportional limit is denoted by σ_{pr}, that determined by a proof strain is denoted by σ_{pf}, and that determined by backward extrapolation is denoted by σ_{ex}. The three yield stresses are generally different. The *proportional limit* is the point that marks

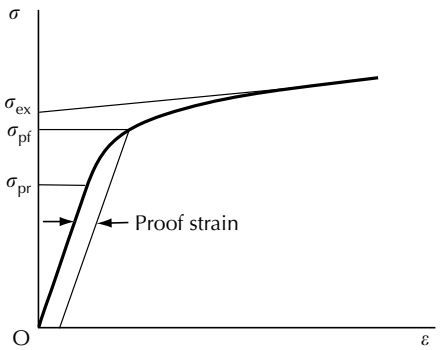

FIGURE 6.2
Three definitions of yield.

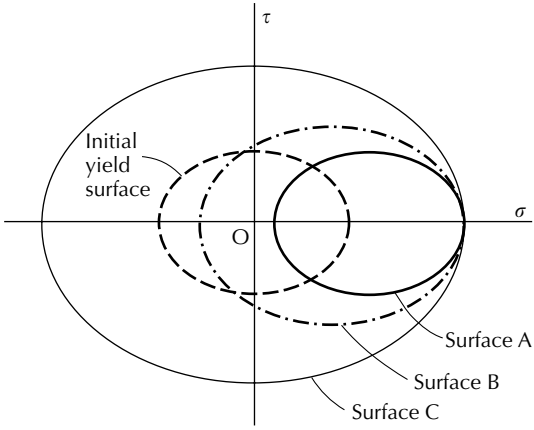

FIGURE 6.3
Subsequent yield surfaces determined by three proof strains.

the end of the proportional elastic straight line. It is an ideal case and is not practical. The *proof strain* (also called the offset plastic strain) is the definition of yield most often used in a modern experiment and it is shown in the figure. Different magnitudes of offset plastic strains may be used by investigators. A small proof strain such as 5μ (or 5×10^{-6}) would result in *subsequent yield surfaces* not containing the origin of the stress space and showing no or insignificant *cross effect* (no increase in size of the subsequent yield surface normal to the loading direction), see [4] and [5]. The use of 5μ is an attempt to approximate the proportional limit, which is theoretically the correct one to use. A proof strain of 0.001 would result in subsequent yield surfaces that contain the origin and show significant cross effect, see for instance [3]. Figure 6.3 shows schematic subsequent yield surfaces determined by small (Surface A), medium (Surface B), and large (Surface C) proof strains. The *backward extrapolation* method was used in [1], which extrapolates the stress–strain curve back to the load axis in order to define the yield stress. The subsequent yield surface determined by this method is an expansion in size of the initial yield surface with the origin remaining as the center of the yield surface. We note that this method (and also one that uses a large proof strain) requires an excessive amount of overstrain to define a yield point and one specimen can be used for the determination of only one point on a yield surface. Clearly, in order to determine a yield surface, the method requires a large number of identical specimens, and it is technically difficult to have two identical specimens. On the other hand, a small proof strain such as 5μ allows barely enough plastic strain to define the inception of the yield point. In this manner, material is only very slightly hardened due to the probing effect necessarily piercing the yield surface for the determination of the yield point. Thus, one specimen can be used to determine the whole initial yield surface and the subsequent yield surfaces. The effect of various definitions of yield on the size and shape of subsequent yield surfaces was not clear until discussions by Mair and Pugh [3]

and Szczepinski [8]. We discuss the evolution of yield surface (expansion, motion, distortion, and rotation) in greater detail in Chapter 7.

The question whether the path of loading carries a pointed vertex (or corner) with it was a topic of debate in 1950–1960s. The question was triggered by the theories of plasticity of Batdorf and Budiansky [9] and of Lin [10,11], which are based on polycrystalline models. Modern experiments have shown that the corners do not exist on the yield surfaces [12]. Rounded corners have been observed due to distortion of yield surfaces. But they are all smooth, convex surfaces.

6.2.1 Mathematical Expressions of Yield Surface

In the modeling of the yield criterion, we refer to Section 5.4 concerning the effect of hydrostatic pressure on yielding. We concluded that, for a first approximation, the assumption that plastic yielding of metals is independent of superimposed hydrostatic pressure is reasonable. Based on this assumption, the yield function f is a function of the deviatoric stress, that is, (6.1) may be written as

$$f(\sigma'_{ij}) = k^2 \tag{6.2}$$

where σ'_{ij} is the deviatoric stress defined by (2.60). For an isotropic metal, the yield function f is a function of the principal stress invariants of σ'_{ij} so that (6.2) becomes

$$f(J'_2, J'_3) = k^2 \tag{6.3}$$

where the invariants are defined in (2.79) and (2.71) as

$$\begin{aligned} J'_1 &= \sigma'_{11} + \sigma'_{22} + \sigma'_{33} = 0 \\ J'_2 &= -\tfrac{1}{2}\sigma'_{ij}\sigma'_{ij} \\ J'_3 &= \tfrac{1}{6}\, e_{ace}\, e_{bdf}\, \sigma'_{ab}\, \sigma'_{cd}\sigma'_{ef} \end{aligned} \tag{6.4}$$

The use of only the second invariant J'_2 in the yield function leads to satisfactory results for most metals. In this case, the yield function is

$$f(J'_2) = k^2 \tag{6.5}$$

Mises [13] used a simple form of (6.5) which is

$$-J'_2 = k^2 \quad \text{or} \quad \tfrac{1}{2}\sigma'_{ij}\,\sigma'_{ij} = k^2 \tag{6.6}$$

Equation (6.6) is known as the *Mises yield criterion* and is widely used. A physical interpretation of the Mises yield criterion is that yielding begins when the elastic distortion energy reaches a critical value. This interpretation is reasonable for isotropic materials.

Using (6.6), an explicit yield function may be obtained for each specified loading condition. In the case of plane stress condition subjected to principal stresses, the stress and deviatoric stress components are

$$[\sigma] = \begin{bmatrix} \sigma_1 & 0 & 0 \\ 0 & \sigma_2 & 0 \\ 0 & 0 & 0 \end{bmatrix}, \qquad [\sigma'] = \begin{bmatrix} \dfrac{2\sigma_1 - \sigma_2}{3} & 0 & 0 \\ 0 & \dfrac{2\sigma_2 - \sigma_1}{3} & 0 \\ 0 & 0 & \dfrac{-(\sigma_1 + \sigma_2)}{3} \end{bmatrix} \tag{6.7}$$

Then, (6.6) is reduced to

$$\frac{1}{2}\left\{\left(\frac{2\sigma_1 - \sigma_2}{3}\right)^2 + \left(\frac{2\sigma_2 - \sigma_1}{3}\right)^2 + \left(\frac{\sigma_1 + \sigma_2}{3}\right)^2\right\} = k^2 \tag{6.8}$$

or

$$\sigma_1^2 + \sigma_2^2 - \sigma_1\sigma_2 = 3k^2 \tag{6.9}$$

In the case of combined axial–torsion of a thin-walled tube, the stresses are

$$[\sigma] = \begin{bmatrix} \sigma & \tau & 0 \\ \tau & 0 & 0 \\ 0 & 0 & 0 \end{bmatrix}, \qquad [\sigma'] = \begin{bmatrix} \dfrac{2\sigma}{3} & \tau & 0 \\ \tau & \dfrac{-\sigma}{3} & 0 \\ 0 & 0 & \dfrac{-\sigma}{3} \end{bmatrix} \tag{6.10}$$

and (6.6) reduces to

$$\sigma^2 + 3\tau^2 = 3k^2 \tag{6.11}$$

From (6.11) we see that the Mises yield criterion leads to an ellipse, and it is a circle when plotted in the $(\sqrt{3}\tau, \sigma)$ space. This result agrees with experimental findings as previously mentioned. Using (6.11), the relationship between the yield stress in tension and that in shear may be determined. Setting $\sigma = 0$, (6.11) gives $\tau = k$, which is the shear yield stress. On the other hand, by setting $\tau = 0$, (6.11) gives $\sigma_y = Y = \sqrt{3}k$. Thus, according to the Mises yield criterion, Y and k are related by $Y = \sqrt{3}k$.

Some alternative forms of (6.6) are

$$(\sigma_1 - \sigma_2)^2 + (\sigma_2 - \sigma_3)^2 + (\sigma_3 - \sigma_1)^2 = 6k^2 \tag{6.12}$$

or

$$(\sigma_{11}-\sigma_{22})^2+(\sigma_{22}-\sigma_{33})^2+(\sigma_{33}-\sigma_{11})^2+6(\sigma_{12}^2+\sigma_{23}^2+\sigma_{31}^2)=6k^2 \quad (6.13)$$

Another well-known yield criterion is the *Tresca yield criterion*. Tresca [14] assumed that yielding occurred when the maximum shear stress reached a certain value, that is,

$$\tau_{\max}=\tau \quad \text{or} \quad \tfrac{1}{2}(\sigma_1-\sigma_2)=k \quad (6.14)$$

In this expression, σ_3 is the intermediate principal stress. A similar equation may be written, when another stress is the intermediate stress. In the case of combined axial–torsion of a thin-walled tube, we have

$$\sigma_1=\frac{\sigma}{2}+\sqrt{\left(\frac{\sigma}{2}\right)^2+\tau^2} \quad \text{and} \quad \sigma_2=\frac{\sigma}{2}-\sqrt{\left(\frac{\sigma}{2}\right)^2+\tau^2} \quad (6.15)$$

Substituting (6.15) into (6.14), we obtain

$$\sigma^2+4\tau^2=4k^2 \quad (6.16)$$

Setting $\sigma=0$, (6.16) gives $\tau=k$, which is the shear yield stress. On the other hand, by setting $\tau=0$, (6.16) yields $\sigma=Y=2k$. Thus, according to Tresca's yield criterion, Y and k are related by $Y=2k$.

The Mises and Tresca yield criteria may be compared in the axial–torsion case. Expressing the equations in terms of the tensile yield stress Y, (6.11) and (6.16) reduce, respectively, to

$$\sigma^2+3\tau^2=Y^2 \qquad \text{Mises} \quad (6.17)$$

$$\sigma^2+4\tau^2=Y^2 \qquad \text{Tresca} \quad (6.18)$$

We have already mentioned that the Mises yield criterion has been shown to agree with experimental data. Since there is a difference between (6.17) and (6.18), Tresca's yield criterion is not realistic. In addition, Tresca's yield criterion contains corners on the yield surface that have not been experimentally observed.

6.2.2 Geometrical Representation of Yield Surface in the Principal Stress Space

If yielding is assumed to be independent of hydrostatic pressure, the yield surface is represented by a right cylinder whose axis is equally inclined to the three principal stress axes, Figure 6.4. In the figure, OH is the hydrostatic axis along which the pressure increases. For the Mises yield criterion, it is a circular cylinder and any plane cutting through the cylinder, perpendicular

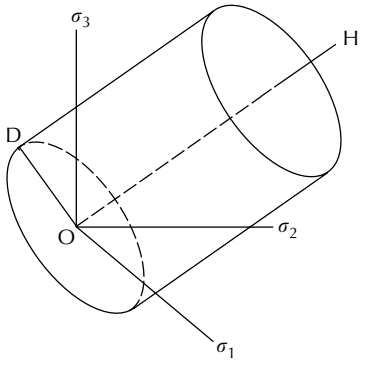

FIGURE 6.4
Yield surface is represented by a right cylinder in the principal stress space.

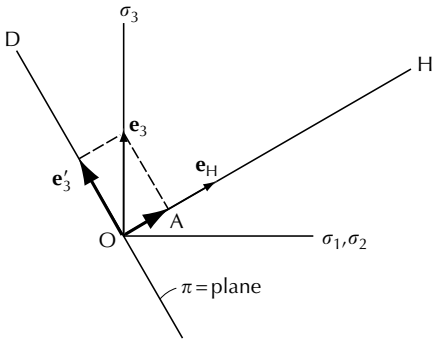

FIGURE 6.5
Decomposition of $\mathbf{e}_3$ into hydrostatic and deviatoric parts.

to the hydrostatic axis, will result in a circular yield locus. A plane passing through the origin O and is normal to the OH axis is known as the *π-plane*. OD is a radius of the circular locus and is perpendicular to OH. The yield function can be discussed based on the yield locus on the π-plane, which represents the deviatoric stress. Any stress vector in this stress space may be projected onto this plane.

Consider now the transformation of unit vectors. Figure 6.5 shows the DOH plane. Let $\mathbf{e}_H$ be the unit vector along OH and $\mathbf{e}_i$ be the unit vectors along the stress axes. Then, we have

$$\mathbf{e}_H = \frac{1}{\sqrt{3}}(\mathbf{e}_1 + \mathbf{e}_2 + \mathbf{e}_3) \tag{6.19}$$

The length of OA is

$$\mathbf{e}_3 \cdot \mathbf{e}_H = \frac{1}{\sqrt{3}} \tag{6.20}$$

Thus, the vector $\overrightarrow{OA}$ is

$$\overrightarrow{OA} = \frac{1}{\sqrt{3}}\mathbf{e}_H = \frac{1}{3}(\mathbf{e}_1 + \mathbf{e}_2 + \mathbf{e}_3) \tag{6.21}$$

Denoting the deviator of $\mathbf{e}_3$ by $\mathbf{e}'_3$, we have

$$\mathbf{e}'_3 = \mathbf{e}_3 - \tfrac{1}{3}(\mathbf{e}_1 + \mathbf{e}_2 + \mathbf{e}_3) = \tfrac{1}{3}(2\mathbf{e}_3 - \mathbf{e}_1 - \mathbf{e}_2) \tag{6.22a}$$

Note that $\mathbf{e}'_3$ is not a unit vector. Similarly, we obtain

$$\mathbf{e}'_1 = \tfrac{1}{3}(2\mathbf{e}_1 - \mathbf{e}_2 - \mathbf{e}_3) \tag{6.22b}$$

and

$$\mathbf{e}'_2 = \tfrac{1}{3}(2\mathbf{e}_2 - \mathbf{e}_3 - \mathbf{e}_1) \tag{6.22c}$$

The equation of the π-plane is now obtained by requiring a vector $\boldsymbol{\sigma} = (\sigma_1, \sigma_2, \sigma_3)$ lying in the plane normal to the OH axis, that is,

$$\boldsymbol{\sigma} \cdot \mathbf{e}_H = \mathbf{0} \quad \text{or} \quad \sigma_1 + \sigma_2 + \sigma_3 = 0 \tag{6.23}$$

Figure 6.6 shows the π-plane, where the axes σ'_i are the projections of the σ_i axes onto this plane. The circle represents the Mises yield criterion and the hexagon represents Tresca's yield criterion. Due to the six-fold symmetry,

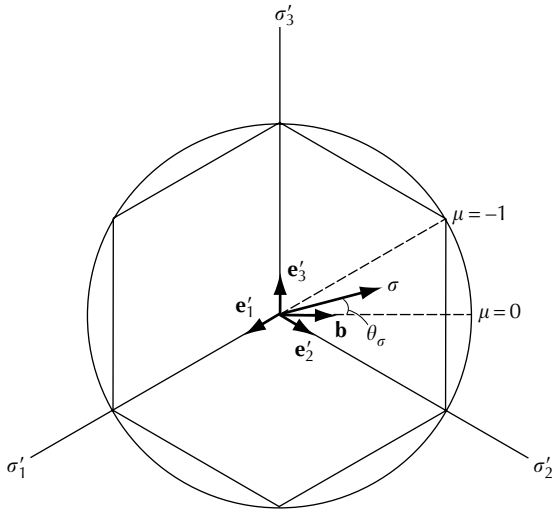

FIGURE 6.6
The π-plane.

only a 30° segment of yield locus needs to be investigated regarding to the shape of the yield locus. Let $\boldsymbol{\sigma}$ be a vector with its orientation specified by the angle θ_σ, where θ_σ varies from 0 to 30°. Let $\mathbf{b}$ be a vector defined by

$$\mathbf{b} = \tfrac{1}{2}(-\mathbf{e}_1' + \mathbf{e}_2') = \tfrac{1}{2}(-\mathbf{e}_1 + \mathbf{e}_2) \tag{6.24}$$

Then,

$$\cos\theta_\sigma = \frac{(1/2)(-\sigma_1 + \sigma_2)}{(1/\sqrt{2})\sqrt{\sigma_1^2 + \sigma_2^2 + \sigma_3^2}} \tag{6.25}$$

or

$$\tan\theta_\sigma = \frac{3\sigma_3}{\sqrt{3}(\sigma_2 - \sigma_1)} = \frac{2\sigma_3 - \sigma_1 - \sigma_2}{\sqrt{3}(\sigma_2 - \sigma_1)} \tag{6.26}$$

The last step was obtained by use of (6.23). A *Lode parameter* ν_σ [15] is defined by

$$\nu_\sigma = \frac{2\sigma_3 - \sigma_1 - \sigma_2}{(\sigma_1 - \sigma_2)} \tag{6.27}$$

so that

$$\tan\theta_\sigma = -\frac{\nu_\sigma}{\sqrt{3}} \tag{6.28}$$

By use of this parameter, the state of stress may be specified along a 30° segment of the yield locus. When $\theta_\sigma = 0$ and $\nu_\sigma = 0$, this is a case of pure shear; when $\theta_\sigma = 30°$ and $\nu_\sigma = -1$, this is the case of uniaxial tension or compression depending on the location of the stress point in the π-plane.

6.3 The Flow Rule

The *flow rule* specifies the increment of plastic strain once the material has yielded. According to Hill [16], the early work was known as the *Lévy–Mises equation*, which specifies the increment of total strain

$$\mathrm{d}\varepsilon_{ij} = \mathrm{d}\lambda\sigma_{ij}' \tag{6.29}$$

where $\mathrm{d}\lambda$ is a scalar factor of proportionality. This equation was later extended to allow for the elastic strain and takes the form

$$\mathrm{d}\varepsilon_{ij} = \mathrm{d}\varepsilon_{ij}^{\mathrm{e}} + \mathrm{d}\varepsilon_{ij}^{\mathrm{p}} \qquad \text{with } \mathrm{d}\varepsilon_{ij}^{\mathrm{p}} = \mathrm{d}\lambda\sigma_{ij}' \tag{6.30}$$

which is known as the *Prandtl–Reuss equation*. The total strain increment $d\varepsilon$ is the sum of the elastic $d\varepsilon_{ij}^{e}$ and the plastic $d\varepsilon_{ij}^{p}$ increments. An important assumption has been made in (6.30) that the principal axes of plastic strain increment and deviatoric stress are coincident. Experimental efforts to validate this assumption are: Taylor and Quinney [1], Lode [15], Hundy and Green [17], and Lianis and Ford [18]. It is fair to conclude that this assumption holds true at the initial yield surface. If in the principal plastic strain space, a Lode parameter ν_ε is defined, similar to (6.27) in the stress space, we write

$$\nu_\varepsilon = \frac{2\,d\varepsilon_3^p - d\varepsilon_1^p - d\varepsilon_2^p}{(d\varepsilon_1^p - d\varepsilon_2^p)} = -\sqrt{3}\tan\theta_\varepsilon \tag{6.31}$$

where θ_ε specifies the orientation of the plastic-strain-increment vector. Plotting $-\nu_\varepsilon$ versus $-\nu_\sigma$, the experimental results show a straight-line relationship, which is schematically shown in Figure 6.7. Therefore, we may conclude that $\nu_\varepsilon = \nu_\sigma$ and $\theta_\sigma = \theta_\varepsilon$. Experimental efforts to validate the assumption related to subsequent yield surface can be found in Phillips and Moon [19] and Ohashi et al. [20]. These authors show that the plastic strain increment is normal to the subsequent yield surfaces. Other efforts concerning the direction of plastic strain increment are not direct experimental observations. Theoretical interpretations are involved and they are discussed in Chapter 7.

If the yield function is the Mises yield function given by (6.6), then the plastic strain increment may be written as

$$d\varepsilon_{ij}^p = d\lambda \frac{\partial f}{\partial \sigma_{ij}} = d\lambda \sigma'_{ij} \tag{6.32}$$

From (6.23), the plastic strain increment is proportional to the gradient of the yield surface and is, therefore, normal to the yield surface. This is usually referred to as the *normality condition*. A flow rule obeying the normality condition is referred to as an *associated flow rule*. On the other hand, a flow rule in

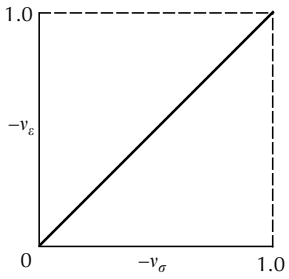

FIGURE 6.7
Linear relation between Lode parameters for stress and strain.

which the plastic strain increment is not normal to the yield surface is known as a *nonassociated flow rule*. Nonassociated flow rule has been used for geotechnical materials. A plastic potential $\bar{g}(\sigma_{ij})$ has also been proposed in the literature so that the plastic strain increment is

$$d\varepsilon_{ij}^{p} = d\lambda \frac{\partial \bar{g}}{\partial \sigma_{ij}} \tag{6.33}$$

The equation $\bar{g}(\sigma_{ij}) = \text{constant}$ forms the surface of plastic potential in the stress space. When the plastic potential is the same as the yield function, that is, $\bar{g} = f$, then (6.33) reduces to (6.32). In this case, $d\varepsilon_{ij}^{p}$ is normal to the yield surface. However, when $\bar{g} \neq f$, $d\varepsilon_{ij}^{p}$ is normal to the surface of constant plastic potential but is not normal to the yield surface and we have a nonassociated flow rule.

6.4 The Elastic-Perfectly Plastic Material

The *elastic-perfectly plastic material* is an idealized material. It is a bilinear stress–strain curve as shown in Figure 6.8. This idealized material is a good approximation for mild steel, which has a definite yield stress. It can also be used to describe materials with weak strain-hardening. For this material, the stress can never be greater than the yield stress σ_y, and, in the multiaxial case, the stress point can never go outside of the yield surface, while the yield surface is fixed in the stress space. Explicit equations for the elastic-perfectly plastic material are:

Yield surface: If we use the Mises yield criterion, then from (6.6)

$$f = \tfrac{1}{2}\sigma'_{ij}\,\sigma'_{ij} - k^2 = 0 \tag{6.34}$$

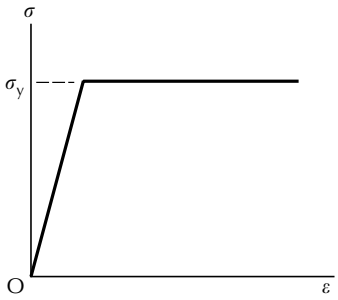

FIGURE 6.8
An elastic-perfectly plastic material.

Flow rule:

$$\mathrm{d}\varepsilon_{ij} = \mathrm{d}\varepsilon_{ij}^{\mathrm{e}} + \mathrm{d}\varepsilon_{ij}^{\mathrm{p}}$$

$$\text{with} \quad \mathrm{d}\varepsilon_{ij}^{\mathrm{e}} = \frac{1}{9K}\mathrm{d}\sigma_{kk}\delta_{ij} + \frac{1}{2\mu}\mathrm{d}\sigma'_{ij} \qquad \text{(The Hooke's law)}$$

$$\text{and} \quad \mathrm{d}\varepsilon_{ij}^{\mathrm{p}} = \mathrm{d}\lambda\,\sigma'_{ij} \qquad \text{(The flow rule)}$$

$$\text{Thus,} \quad \mathrm{d}\varepsilon_{ij} = \frac{1}{9K}\mathrm{d}\sigma_{kk}\delta_{ij} + \frac{1}{2\mu}\mathrm{d}\sigma'_{ij} + \mathrm{d}\lambda\sigma'_{ij}$$

(The Prandtl–Reuss equation) (6.35)

in which K is the bulk modulus; μ is the shear modulus; and $\mathrm{d}\lambda$ is an as yet undetermined factor with the value

$$\begin{aligned}
\mathrm{d}\lambda = 0 \quad & \text{when } f < k^2 \text{ or } f = k^2, \text{but } \mathrm{d}f < 0 \text{ (elastic state or unloading)} \\
= 0 \quad & \text{when } f = k^2 \text{ and } \mathrm{d}f = 0 \text{ (neutral loading)} \\
> 0 \quad & \text{when } f = k^2 \text{ and } \mathrm{d}f = 0 \text{ (plastic state)}
\end{aligned} \tag{6.36}$$

Expression (6.36a) describes the condition when the stress point is either inside the yield surface or is on the yield surface but is about to move inward; (6.36b) describes the condition when the stress point is moving on the yield surface; and (6.36c) describes the condition when the stress point is stationary on the yield surface. We make the following remarks for this model:

1. The increments of plastic strain depend on the current values of deviatoric stress and not on the stress increment.
2. The principal axes of stress and of plastic-strain-increment tensor coincide. The flow rule satisfies the experimental finding that the plastic-strain-increment vector is normal to the yield surface if the Mises yield criterion is used.
3. No plastic volume change during plastic deformation is assumed, that is, $\mathrm{d}\varepsilon_{ii}^{\mathrm{p}} = \mathrm{d}\lambda\sigma'_{ii} = 0$.
4. The magnitude of plastic strain increment is determined by $\mathrm{d}\lambda$, which in turn is determined by the actual increment of plastic work given by

$$\begin{aligned}
\mathrm{d}W^{\mathrm{p}} &= \sigma_{ij}\mathrm{d}\varepsilon_{ij}^{\mathrm{p}} = \mathrm{d}\lambda\sigma_{ij}\sigma'_{ij} = \mathrm{d}\lambda(\tfrac{1}{3}\sigma_{kk}\delta_{ij} + \sigma'_{ij})\sigma'_{ij} \\
&= \mathrm{d}\lambda(\tfrac{1}{3}\sigma_{kk}\sigma'_{ii} + \sigma'_{ij}\sigma'_{ij}) = -2\,\mathrm{d}\lambda\,J'_2 = 2\,\mathrm{d}\lambda\,k^2
\end{aligned} \tag{6.37}$$

From (6.37), we obtain

$$\mathrm{d}\lambda = \frac{\sigma_{ij}\mathrm{d}\varepsilon_{ij}^{\mathrm{p}}}{2k^2} = \frac{((1/3)\sigma_{kk}\delta_{ij} + \sigma'_{ij})\mathrm{d}\varepsilon_{ij}^{\mathrm{p}}}{2k^2} = \frac{\sigma'_{ij}\mathrm{d}\varepsilon_{ij}^{\mathrm{p}}}{2k^2} = \frac{\sigma'_{ij}\mathrm{d}e_{ij}^{\mathrm{p}}}{2k^2} \tag{6.38}$$

where $d\varepsilon_{ij}^{p} = \frac{1}{3}\delta_{ij}d\varepsilon_{kk}^{p} + de_{ij}^{p} = de_{ij}^{p}$. A slightly different form of (6.38) can be found if we consider the following expressions:

$$\begin{aligned} &\sigma'_{ij}de_{ij} = \sigma'_{ij}(de_{ij}^{e} + de_{ij}^{p}), \quad de_{ij}^{e} = \frac{d\sigma'_{ij}}{2\mu}, \\ &dJ'_2 = -\sigma'_{ij}d\sigma'_{ij} = 0 \ (-J'_2 = k^2 = \text{const}) \\ &\text{and} \quad \sigma'_{ij}de_{ij} = \frac{\sigma'_{ij}d\sigma'_{ij}}{2\mu} + \sigma'_{ij}de_{ij}^{p} = \sigma'_{ij}de_{ij}^{p} \end{aligned} \tag{6.39}$$

Using the last expression of (6.39), (6.38) becomes

$$d\lambda = \frac{\sigma'_{ij}de_{ij}}{2k^2} = \frac{\sigma'_{ij}(d\varepsilon_{ij} - \frac{1}{3}\delta_{ij}d\varepsilon_{kk})}{2k^2} = \frac{\sigma'_{ij}d\varepsilon_{ij}}{2k^2} \tag{6.40}$$

The Prandtl–Reuss equation may then be written as

$$d\varepsilon_{ij} = \frac{1}{9K}d\sigma_{kk}\delta_{ij} + \frac{1}{2\mu}d\sigma'_{ij} + \frac{\sigma'_{ij}\sigma'_{km}d\varepsilon_{km}}{2k^2} \tag{6.41}$$

This equation relates $d\varepsilon_{ij}$ to $d\sigma_{ij}$ and σ_{ij}, and it can be written in the form

$$[d\varepsilon_{ij}] = [A_{ijkm}][d\sigma_{km}] \tag{6.42}$$

where A_{ijkm} is a function of σ_{ij}. Note that this method of determination of $d\lambda$ works when f is a function of stress only and is in the form of the Mises yield criterion. In the more general expressions for f, $d\lambda$ may be determined by use of the consistency condition to be discussed later.

The class of perfectly plastic material is an idealization with the purpose of keeping the constitutive equation simple. This idealization is reasonable for materials that do not show significant strain-hardening. The adequacy of this idealization depends on the purpose and requirement of the specific application. If only monotonic loading is of interest and it does not call for a refined solution, then this idealization may very well lead to a satisfactory solution with a minimum amount of mathematics. However, due to the progress in industries, which give rise to problems that are subjected to complex loading conditions and impose stricter requirements, this idealization is no longer adequate in many applications. In those cases, refinement of the theory is called for and strain-hardening should be considered. The refinement of the flow theory is discussed in Chapter 7.

An example to demonstrate the differences between an elastic material and an elastic-perfectly plastic material is given by a strain-controlled test with proportional strain path as shown in Figure 6.9. Assuming that the experiment begins at point O′ (Figure 6.9(a)), moves to B′, and continues

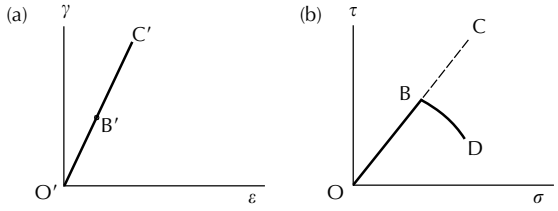

FIGURE 6.9
(a) A proportional strain path and (b) corresponding stress trajectories for elastic (OBC) and elastic-perfectly plastic material (OBD).

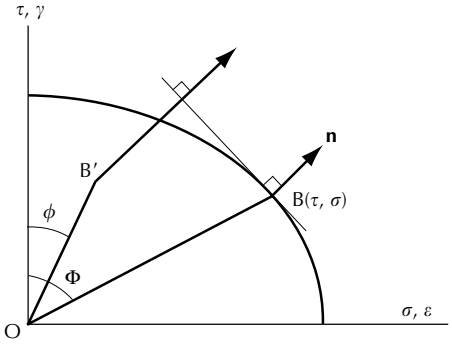

FIGURE 6.10
A controlled linear stress path and its corresponding strain path.

on to point C′ in the strain space. The corresponding trajectories in the stress space shown in Figure 6.9(b) are OBC for elastic material and OBD for elastic-perfectly plastic material. It is seen that the two stress paths show drastic differences for the same strain path. It is a nonlinear path for the latter case. Details related to stress- and strain-controlled tests for an elastic-perfectly plastic material are discussed in Examples 6.1 to 6.3.

EXAMPLE 6.1 In a stress-controlled combined tension–torsion test of a tubular specimen of an elastic-perfectly plastic material, if the stress-path OB (Figure 6.10) is linear, find the corresponding strain path.

Solution

The states of stress and strain are

$$\sigma_{ij} = \begin{bmatrix} \sigma & \tau & 0 \\ \tau & 0 & 0 \\ 0 & 0 & 0 \end{bmatrix}, \qquad \sigma'_{ij} = \begin{bmatrix} \frac{2}{3}\sigma & \tau & 0 \\ \tau & -\frac{\sigma}{3} & 0 \\ 0 & 0 & -\frac{\sigma}{3} \end{bmatrix}, \qquad \varepsilon_{ij} = \begin{bmatrix} \varepsilon & \frac{\gamma}{2} & 0 \\ \frac{\gamma}{2} & 0 & 0 \\ 0 & 0 & 0 \end{bmatrix} \tag{a}$$

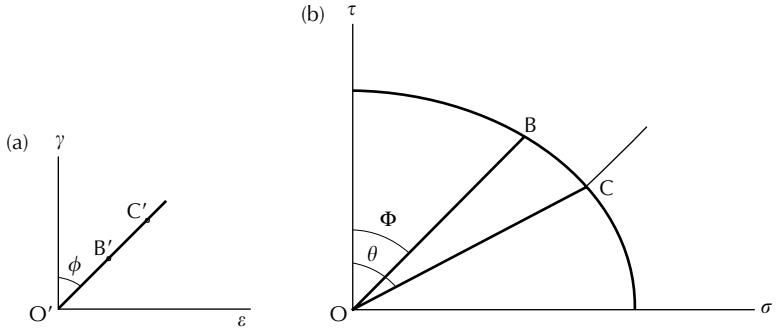

FIGURE 6.11
(a) A controlled proportional strain path and (b) the corresponding stress path.

Lateral strains have been neglected due to the smallness of their magnitudes, but they may be considered for better accuracy. In the elastic state from O to B (and also O′B′ in the strain space), the relations are

$$\varepsilon^{\mathrm{e}} = \frac{\sigma}{E}, \qquad \gamma^{\mathrm{e}} = \frac{\tau}{\mu} \tag{b}$$

and the slope of the strain path (Figure 6.11(a)) is defined by

$$\tan\phi = \frac{\varepsilon^{\mathrm{e}}}{\gamma^{\mathrm{e}}} = \frac{\mu}{E}\frac{\sigma}{\tau} = \frac{\mu}{E}\tan\Phi \tag{c}$$

where Φ is known. The strain path during the elastic state is denoted by OB′. In the elastic–plastic state, $\mathrm{d}\lambda \neq 0$, and the Prandtl–Reuss equation is from (6.41)

$$\mathrm{d}\varepsilon_{ij} = \frac{1}{9K}\mathrm{d}\sigma_{kk}\delta_{ij} + \frac{1}{2\mu}\mathrm{d}\sigma'_{ij} + \frac{\sigma'_{ij}\sigma'_{km}\mathrm{d}\varepsilon_{km}}{2k^2} \tag{d}$$

Since the test is stress-controlled and follows a straight path, the stress point will remain at B after yielding has occurred. Thus, $\mathrm{d}\sigma_{ij} = 0$. Hence, we have

$$\mathrm{d}\varepsilon_{ij} = \frac{\sigma'_{ij}\sigma'_{km}\mathrm{d}\varepsilon_{km}}{2k^2} \tag{e}$$

The nonzero components of (e) are

$$\mathrm{d}\varepsilon = \frac{\sigma}{3k^2}\left(\frac{2}{3}\sigma\,\mathrm{d}\varepsilon + \tau\,\mathrm{d}\gamma\right), \qquad \mathrm{d}\varepsilon_{12} = \frac{\tau}{3k^2}\left(\frac{2}{3}\sigma\,\mathrm{d}\varepsilon + \tau\,\mathrm{d}\gamma\right) \tag{f}$$

and the strain increment has the following slope after yielding has occurred

$$\frac{\mathrm{d}\varepsilon_{12}}{\mathrm{d}\varepsilon} = \frac{3\tau}{2\sigma} \quad \text{or} \quad \frac{\mathrm{d}\gamma}{\mathrm{d}\varepsilon} = \frac{3\tau}{\sigma} \tag{g}$$

We now show that this direction is parallel to the normal to the yield surface at B. This is the direction of the strain path after yielding has occurred at B′. The yield surface is

$$f = \tfrac{1}{2}\sigma'_{ij}\sigma'_{ij} - k^2 = 0 \tag{h}$$

For the stress state of (a), (h) reduces to

$$f = \sigma^2 + 3\tau^2 - 3k^2 = 0 \tag{i}$$

The gradient of the yield surface is

$$\frac{\partial f}{\partial \sigma_{ij}} = \frac{\partial f}{\partial \sigma'_{rs}}\frac{\partial \sigma'_{rs}}{\partial \sigma_{ij}} = \frac{\partial f}{\partial \sigma'_{rs}}\left(\delta_{ri}\delta_{sj} - \frac{1}{3}\delta_{rs}\delta_{ij}\right) = \sigma'_{rs}\left(\delta_{ri}\delta_{sj} - \frac{1}{3}\delta_{rs}\delta_{ij}\right) = \sigma'_{ij} \tag{j}$$

So, the components of the normal **n** are proportional to

$$n_\sigma \propto \sigma'_{11} = \tfrac{2}{3}\sigma, \qquad n_\tau \propto \sigma'_{12} = \tau \tag{k}$$

with a slope

$$\frac{n_\tau}{n_\sigma} = \frac{3\tau}{2\sigma} \tag{l}$$

Note that this slope is the same as that of $\mathrm{d}\varepsilon_{12}/\mathrm{d}\varepsilon$ in (g).

It is wrong to differentiate the yield function (i) in the τ–σ subspace to obtain the normal as

$$n_\sigma \propto \frac{\partial f}{\partial \sigma} = 2\sigma, \qquad n_\tau \propto \frac{\partial f}{\partial \tau} = 6\tau, \qquad \frac{n_\tau}{n_\sigma} = \frac{3\tau}{\sigma} \tag{m}$$

This slope is different from that in (l). The correct way is to make distinction between σ_{12} and σ_{21} and differentiate the yield function with respect to σ_{12}. But, the τ–σ stress space is convenient for engineering application and, in this case, we must work with the engineering shear strain γ instead of the tensorial shear strain ε_{12}. Therefore, we use the γ–ε strain space, and observe that the slope in this strain space given by the second equation of (g) is the same as the slope in (m).

EXAMPLE 6.2 In a strain-controlled, combined tension–torsion test of a tubular specimen of an elastic-perfectly plastic material, if the strain-path OB′C′ is linear (Figure 6.11(a)), find the corresponding stress path.

Solution

The states of stress and strain are given in (a) of Example 6.1 and the elastic phase of the problem is the same as in Example 6.1. In this range, the slope of the strain path is known and is given by

$$m = \tan\phi = \frac{\varepsilon}{\gamma} = \frac{\mathrm{d}\varepsilon}{\mathrm{d}\gamma} = \frac{\mu}{E}\frac{\sigma}{\tau} \tag{a}$$

Yielding can occur when the stress reaches B and the strain reaches B′. The last relation of (a) is

$$\sigma - \frac{mE}{\mu}\tau = 0 \tag{b}$$

The stresses at B may be determined from the intersection of (b) with the yield locus (6.11). They are

$$\sigma_{\mathrm{B}} = \frac{\sqrt{3}\,mkE}{\sqrt{3\mu^2 + m^2E^2}} \quad \text{and} \quad \tau_{\mathrm{B}} = \frac{\sqrt{3}\,k\mu}{\sqrt{3\mu^2 + m^2E^2}} \tag{c}$$

If yielding would occur at B with a stationary stress point (Figure 6.11(b)), that is, $\mathrm{d}\sigma_{ij} = 0$, then using (6.41), the Prandtl–Reuss equation would have components

$$\mathrm{d}\varepsilon = \mathrm{d}\varepsilon^{\mathrm{p}} = \frac{\sigma}{3k^2}\left(\frac{2}{3}\sigma\,\mathrm{d}\varepsilon + \tau\,\mathrm{d}\gamma\right), \qquad \mathrm{d}\gamma = \mathrm{d}\gamma^{\mathrm{p}} = \frac{\tau}{k^2}\left(\frac{2}{3}\sigma\,\mathrm{d}\varepsilon + \tau\,\mathrm{d}\gamma\right) \tag{d}$$

and the direction of the plastic strain increment evaluated at B would be

$$\frac{\mathrm{d}\gamma}{\mathrm{d}\varepsilon} = \frac{3\tau_{\mathrm{B}}}{\sigma_{\mathrm{B}}} = \frac{3\mu}{mE} \neq \frac{1}{m} \tag{e}$$

We see that the slope of the strain increment in (e) is not the same as the controlled slope $1/m$, and, therefore, the stress point cannot be stationary at B, and $\mathrm{d}\lambda = 0$ at B. The stress point must move away from B in a neutral loading along the yield locus until it reaches point C, where the normal of the yield locus is parallel to the controlled strain slope O′B′C′ of Figure 6.11(a). The Prandtl–Reuss equation applies and we set the slope in (e) to $1/m$, that is,

$$\sigma - 3m\tau = 0 \tag{f}$$

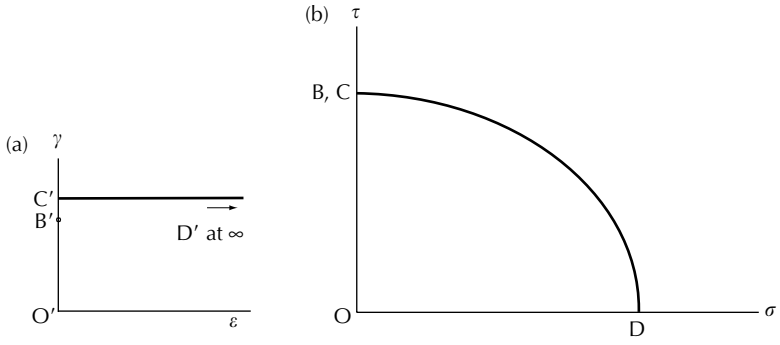

FIGURE 6.12
(a) A controlled strain path and (b) the corresponding stress path.

The intersection between this line and the yield locus (6.11) is found at

$$\sigma_C = \frac{3mk}{\sqrt{1+3m^2}}, \qquad \tau_C = \frac{k}{\sqrt{1+3m^2}}, \qquad \text{with } \frac{\sigma_C}{\tau_C} = 3m = 3\tan\phi \tag{g}$$

Thus, the slope of OC is defined by angle θ as

$$\theta = \tan^{-1}(3\tan\phi) \tag{h}$$

The stress point stays at C upon further increase of the strain point beyond C′.

EXAMPLE 6.3 In a strain-controlled, combined tension–torsion test of a tubular specimen of an elastic-perfectly plastic material, determine the stress-path that corresponds to the strain-path OB′C′D′ shown in Figure 6.12(a). Yielding occurs at B′.

Solution

The elastic state is governed by Hooke's law. Plastic deformation occurs from B′ to C′, while the stress stays at B. The states of stress and strain during this stage are

$$\sigma_{ij} = \begin{bmatrix} 0 & \tau & 0 \\ \tau & 0 & 0 \\ 0 & 0 & 0 \end{bmatrix}, \qquad \sigma'_{ij} = \begin{bmatrix} 0 & \tau & 0 \\ \tau & 0 & 0 \\ 0 & 0 & 0 \end{bmatrix}, \qquad \varepsilon_{ij} = \begin{bmatrix} 0 & \frac{\gamma}{2} & 0 \\ \frac{\gamma}{2} & 0 & 0 \\ 0 & 0 & 0 \end{bmatrix} \tag{a}$$

The nonzero component of the Prandtl–Reuss equation is

$$\mathrm{d}\gamma = \frac{\mathrm{d}\tau}{\mu} + \frac{\tau^2 \mathrm{d}\gamma}{k^2} \tag{b}$$

or

$$\mathrm{d}\tau = \mu\left(1 - \frac{\tau^2}{k^2}\right)\mathrm{d}\gamma \tag{c}$$

But, on the yield locus, using (6.11) and (a), $\tau^2 = k^2$. Thus, $\mathrm{d}\tau = 0$ and C stays at B on the yield locus.

Next, we consider the stage from C′ to D′. The strain-path C′D′ has increment in the axial strain only, while the shear strain is kept constant, that is, $\mathrm{d}\gamma = 0$. Due to the effect of elastic strain, $\mathrm{d}\gamma^{\mathrm{p}} \neq 0$. Therefore, plastic deformation occurs. The states of stress and strain are the same as that of (a) of Example 6.1. Putting $\mathrm{d}\gamma = 0$, the shear component of the Prandtl–Reuss equation (6.41) is

$$\mathrm{d}\tau = -\frac{2\sigma\tau\mu}{\sigma^2 + 3\tau^2}\mathrm{d}\varepsilon \tag{d}$$

Substituting (d) into the differential form of yield function (6.11), we obtain

$$\mathrm{d}\sigma = \frac{6\tau^2\mu}{\sigma^2 + 3\tau^2}\mathrm{d}\varepsilon \tag{e}$$

It is easy to show that the stress increment $(\mathrm{d}\tau, \mathrm{d}\sigma)$ is tangential to the yield locus. This is not a neutral loading, however, because the plastic strain is taking place. The plastic strain increments are found from (6.41) as

$$\mathrm{d}\varepsilon^{\mathrm{p}} = \frac{2}{9}\frac{\sigma^2\mathrm{d}\varepsilon}{k^2} \quad \text{and} \quad \mathrm{d}\gamma^{\mathrm{p}} = \frac{2}{3}\frac{\sigma\tau\mathrm{d}\varepsilon}{k^2} \qquad \text{with } \mathrm{d}\gamma = 0 \tag{f}$$

By use of (d) and (e), both $\mathrm{d}\tau$ and $\mathrm{d}\sigma$ may be calculated for a given $\mathrm{d}\varepsilon$. These equations may be integrated to obtain a closed form solution. From (d) and (6.11), we have

$$\mathrm{d}\tau = -\frac{2\mu\tau\sqrt{k^2 - \tau^2}}{\sqrt{3}\,k^2}\mathrm{d}\varepsilon \quad \text{or} \quad \frac{\mathrm{d}\tau}{\tau\sqrt{k^2 - \tau^2}} = -\frac{2\mu\mathrm{d}\varepsilon}{\sqrt{3}\,k^2} \tag{g}$$

This equation may be integrated to obtain

$$\varepsilon = \frac{\sqrt{3}}{2}\frac{k}{\mu}\ln\left[\frac{1 - \sqrt{1 - (\tau/k)^2}}{\tau/k}\right] \tag{h}$$

where, by use of the boundary condition that $\tau = k$ when $\varepsilon = 0$, the integration constant is zero. Introducing now nondimensional variables $X = \mu\varepsilon/k$

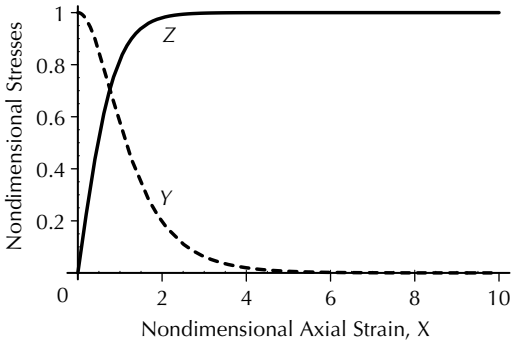

FIGURE 6.13
Nondimensional shear (Y) and axial (Z) stresses as axial strain increases.

for strain and $Y = \tau/k$ for stress, (h) may be solved for Y to yield

$$Y = \frac{2e^{(2X)/\sqrt{3}}}{1 + e^{(4X)/\sqrt{3}}} \tag{i}$$

Figure 6.13 shows the plot of Y versus X. It is seen that the shear stress gradually reduces as the axial strain increases.

Similarly, (e) may be integrated to yield

$$Z = \frac{\sigma}{\sqrt{3}k} = \frac{-1 + e^{(4X)/\sqrt{3}}}{1 + e^{(4X)/\sqrt{3}}} \tag{j}$$

Z may be plotted against X and the relationship is also shown in Figure 6.13. Using (i) and (j), X may be eliminated to obtain

$$Y^2 + Z^2 = 1 \tag{k}$$

which is the yield locus (6.11). Thus, the stress point moves, generating plastic deformation, along the yield locus and end up in D as shown in Figure 6.12(b).

EXAMPLE 6.4 Define an equivalent (effective) stress as $\bar{\sigma} = \sqrt{3/2}\{\sigma'_{ij}\sigma'_{ij}\}^{1/2}$ and an equivalent (effective) plastic strain increment as $d\bar{\varepsilon}^p = \sqrt{2/3} \times \{d\varepsilon^p_{ij} d\varepsilon^p_{ij}\}^{1/2}$, show that the plastic work increment is $dW^p = \sigma_{ij} d\varepsilon^p_{ij} = \bar{\sigma} d\bar{\varepsilon}^p$.

Solution

From (6.37), we have

$$dW^p = \sigma_{ij} d\varepsilon^p_{ij} = 2d\lambda\, k^2 \tag{a}$$

Using (6.32), (6.34), and (a), the equivalent plastic strain increment is

$$\begin{aligned} \mathrm{d}\bar{\varepsilon}^{\mathrm{p}} &= \sqrt{\frac{2}{3}}\left\{\mathrm{d}\varepsilon_{ij}^{\mathrm{p}}\mathrm{d}\varepsilon_{ij}^{\mathrm{p}}\right\}^{1/2} = \sqrt{\frac{2}{3}}\mathrm{d}\lambda\left\{\sigma'_{ij}\sigma'_{ij}\right\}^{1/2} = \sqrt{\frac{2}{3}}\mathrm{d}\lambda(\sqrt{2}k) \\ &= \frac{2}{\sqrt{3}}\frac{\mathrm{d}\lambda}{k}k^2 = \frac{\mathrm{d}W^{\mathrm{p}}}{\sqrt{3}\,k} \end{aligned} \tag{b}$$

Thus,

$$\mathrm{d}W^{\mathrm{p}} = \sqrt{3}k\,\mathrm{d}\bar{\varepsilon}^{\mathrm{p}} \tag{c}$$

On the other hand, the equivalent stress is

$$\bar{\sigma} = \sqrt{\frac{3}{2}}\left\{\sigma'_{ij}\sigma'_{ij}\right\}^{1/2} = \sqrt{\frac{3}{2}}(\sqrt{2}k) = \sqrt{3}k \tag{d}$$

Combining (c) and (d), we obtain

$$\mathrm{d}W^{\mathrm{p}} = \sigma_{ij}\mathrm{d}\varepsilon_{ij}^{\mathrm{p}} = \bar{\sigma}\,\mathrm{d}\bar{\varepsilon}^{\mathrm{p}} \tag{e}$$

Note that equivalent (or effective) quantities such as the equivalent (or effective) stress, the equivalent (or effective) strain, or the equivalent (or effective) strain rate are often used in dealing with the multidimensional behavior of isotropic materials. This equivalent quantity often represents the magnitude of that quantity.

6.5 Strain-Hardening

There are three classes of materials: the *strain-hardening material*, the perfectly-plastic material, and the *strain-softening material*. Generally, metals are strain-hardening (or work-hardening) materials and geotechnical materials may exhibit strain-softening under certain conditions. Several criteria have been proposed to classify the materials. Generally, the strain-hardening material is regarded as a stable material. Drucker [21] proposed to classify materials by the now well-known *Drucker's postulate*, which is not a law of thermodynamics, but a means of classification. Materials obeying Drucker's postulate can then be studied by a theory of plasticity that can be built up based on that postulate.

In the multiaxial stress state, strain-hardening is considered in the form of hardening rules for subsequent yield surfaces. Experimental determination of subsequent yield surfaces is discussed in Chapter 7. It has been observed that the yield surface, upon application of a deformation history, will undergo expansion, distortion, translation, and rotation. A precise description of these

characteristics is deferred to Chapter 12. In this section, we discuss a simplified version of the hardening rules and consider only the expansion (isotropic hardening) and translation (kinematic hardening) of the yield surface. This simplified version has been widely used in the mechanics literature.

6.5.1 Drucker's Postulate

Drucker's postulate consists of two parts: the *stability in the small* and the *stability in the large*. These are described by the following statements:

1. The stability in the small: The work done by an *external agency*, which slowly applies an additional set of forces to the already stressed material, over the displacement it produces, is positive.
2. The stability in the large: The net work performed by the *external agency* over the *cycle* of application and removal is positive, if plastic deformation has occurred in the cycle.

The aforementioned external agency is entirely separate and distinct from the agency that causes the existing state of stress and that has produced the existing state of strain. The cycle of application is the stress cycle and is different from Ilyushin's strain cycle, which is not as restrictive as the stress cycle.

The meaning of the above statements are now explained. In the one-dimensional case, let us consider Figure 6.14(a). The stress at A is already the existed state. The stability in the small says that an external agency increases the stress from A to C and the work done represented by area ACE is positive; the stability in the large says that the work done by the external agency over the stress cycle of σ^* to σ_A and then to σ_C and then back down to σ^* and represented by area BACDB is positive. σ^* is an arbitrary stress state in the elastic region.

In the multidimensional case, we consider a stress cycle described in Figure 6.14(b). At time $t = 0$, the stress point is at B and denoted by σ_{ij}^*, which is an arbitrary point within or on the current yield surface, so that

$$f(\sigma_{ij}^*, \varepsilon_{ij}^{\mathrm{p}}, \kappa) \leq 0 \tag{6.43}$$

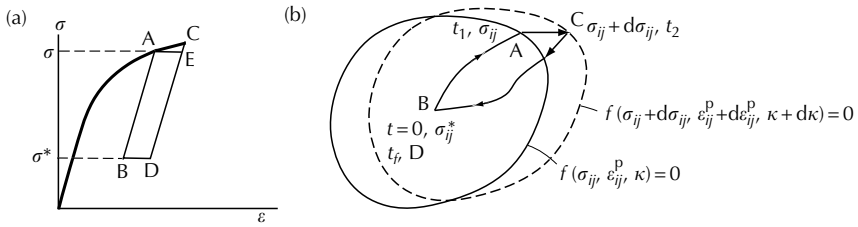

FIGURE 6.14
Stress cycles: (a) one-dimensional and (b) multiaxial.

where κ is a strain-hardening parameter. The yield function is expressed in terms of stress σ_{ij}, which is possible as in (6.12) or (6.13). Furthermore, for strain-hardening materials, the yield function f depends on the prestraining history and we include the plastic strain $\varepsilon_{ij}^{\mathrm{p}}$ and a parameter κ in the yield function for generality. At point A ($t = t_1$), the stress point σ_{ij} is on the yield surface so that

$$f(\sigma_{ij}^*, \varepsilon_{ij}^{\mathrm{p}}, \kappa) = 0 \tag{6.44}$$

The stress point then pierces the yield surface and carries the yield surface with it, until at point C, where $t_2 = t_1 + \mathrm{d}t$, it reaches the dashed curve which is governed by

$$f(\sigma_{ij} + \mathrm{d}\sigma_{ij}, \varepsilon_{ij}^{\mathrm{p}} + \mathrm{d}\varepsilon_{ij}^{\mathrm{p}}, \kappa + \mathrm{d}\kappa) = 0 \tag{6.45}$$

Additional plastic deformation has occurred during this step. Unloading then follows, which brings the stress point back to σ_{ij}^* at B. The corresponding time is $t = t_f$. At this point,

$$f(\sigma_{ij}^*, \varepsilon_{ij}^{\mathrm{p}} + \mathrm{d}\varepsilon_{ij}^{\mathrm{p}}, \kappa + \mathrm{d}\kappa) \le 0 \tag{6.46}$$

The work done during this stress cycle is

$$W = \int_0^{t_f} (\sigma_{ij} - \sigma_{ij}^*)\dot{\varepsilon}_{ij}\mathrm{d}t = \int_{t_1}^{t_2} (\sigma_{ij} - \sigma_{ij}^*)\dot{\varepsilon}_{ij}^{\mathrm{p}}\mathrm{d}t \ge 0 \tag{6.47}$$

The last expression has accounted for the fact that the work done by the elastic strain $\mathrm{d}\varepsilon_{ij}^{\mathrm{e}}$ for a closed path is zero. In this stress cycle, the plastic deformation only occurs in the step AC. We now take Taylor series expansion of the above integral about $t = t_1$ as

$$W(t_2) = \left[(\sigma_{ij} - \sigma_{ij}^*)\dot{\varepsilon}_{ij}^{\mathrm{p}}\right]_{t=t_1}\mathrm{d}t + \tfrac{1}{2}[\dot{\sigma}_{ij}\dot{\varepsilon}_{ij}^{\mathrm{p}} + (\sigma_{ij} - \sigma_{ij}^*)\ddot{\varepsilon}_{ij}^{\mathrm{p}}]_{t_1}(\mathrm{d}t)^2 + \cdots \ge 0 \tag{6.48}$$

with $W(t_1) = 0$. For the stability in the small, σ_{ij}^* and σ_{ij} coincide at t_1, and the above expression is reduced to

$$W = \tfrac{1}{2}\dot{\sigma}_{ij}\dot{\varepsilon}_{ij}^{\mathrm{p}}(\mathrm{d}t)^2 + \cdots \ge 0 \tag{6.49}$$

Take the time increment $\mathrm{d}t$ small enough that the higher order terms in $\mathrm{d}t$ are negligible, we obtain

$$\dot{\sigma}_{ij}\dot{\varepsilon}_{ij}^{\mathrm{p}} \ge 0 \quad \text{or} \quad \mathrm{d}\sigma_{ij}\mathrm{d}\varepsilon_{ij}^{\mathrm{p}} \ge 0 \tag{6.50}$$

which is the expression for the stability in the small.

In the case of $\sigma_{ij}^* \neq \sigma_{ij}$ at t_1, by neglecting the second and higher order terms, we have from (6.48)

$$W = (\sigma_{ij} - \sigma_{ij}^*)\, \dot{\varepsilon}_{ij}^{\mathrm{p}} \mathrm{d}t \geq 0 \quad \text{or} \quad (\sigma_{ij} - \sigma_{ij}^*)\, \mathrm{d}\varepsilon_{ij}^{\mathrm{p}} \geq 0 \tag{6.51}$$

This is the expression for the stability in the large.

By the use of Drucker's postulate, it is possible to show that the yield surface is convex and that the plastic strain increment is normal to the yield surface. Without the use of this postulate, these two effects would have been two separate assumptions. We discuss the case that the yield surface is smooth without corners. Let σ_{ij} be any regular point on the yield surface and σ_{ij}^* be an *arbitrary* point inside or on the yield surface. Let $\mathrm{d}\varepsilon_{ij}^{\mathrm{p}}$ be the plastic strain increment at σ_{ij}. Then, (6.51) shows that the vectors $(\sigma_{ij} - \sigma_{ij}^*)$ and $\mathrm{d}\varepsilon_{ij}^{\mathrm{p}}$ are making an acute angle and that the arbitrary σ_{ij}^* must lie on the side of the hyperplane opposite to that from which $\mathrm{d}\varepsilon_{ij}^{\mathrm{p}}$ is directed. $\mathrm{d}\varepsilon_{ij}^{\mathrm{p}}$ is normal to the hyperplane as shown in Figure 6.15(a). Since σ_{ij} is a regular point of the yield surface, the hyperplane must be tangent to the yield surface, and, therefore, $\mathrm{d}\varepsilon_{ij}^{\mathrm{p}}$ is normal to the yield surface at the point of tangency σ_{ij}. This also establishes the convexity of the yield surface at point σ_{ij}.

Next, we show that the direction of $\mathrm{d}\varepsilon_{ij}^{\mathrm{p}}$ is independent of the direction of $(\sigma_{ij} - \sigma_{ij}^*)$ if the yield surface is regular. Assuming that two different $(\sigma_{ij} - \sigma_{ij}^*)$ give rise to two different $\mathrm{d}\varepsilon_{ij}^{\mathrm{p}}$. Then, the yield surface $f_1 = 0$, which is perpendicular to $\mathrm{d}\varepsilon_{ij}^{\mathrm{p}(1)}$ must intersect with the yield surface $f_2 = 0$, which is perpendicular to $\mathrm{d}\varepsilon_{ij}^{\mathrm{p}(2)}$ at an angle (see Figure 6.15(b)). Thus, the yield surface is nonregular at σ_{ij}, which contradicts with the assumption that it be regular at σ_{ij}. Therefore, the two $\mathrm{d}\varepsilon_{ij}^{\mathrm{p}}$'s must not be different and the direction of $\mathrm{d}\varepsilon_{ij}^{\mathrm{p}}$ is independent of the direction of $(\sigma_{ij} - \sigma_{ij}^*)$.

In the case when $f = 0$ is nonregular at σ_{ij}, the normality condition cannot be established. Drucker's postulate only requires that $\mathrm{d}\varepsilon_{ij}^{\mathrm{p}}$ lie within a bounded angle at a pointed vertex of the yield surface. However, nonregular yield

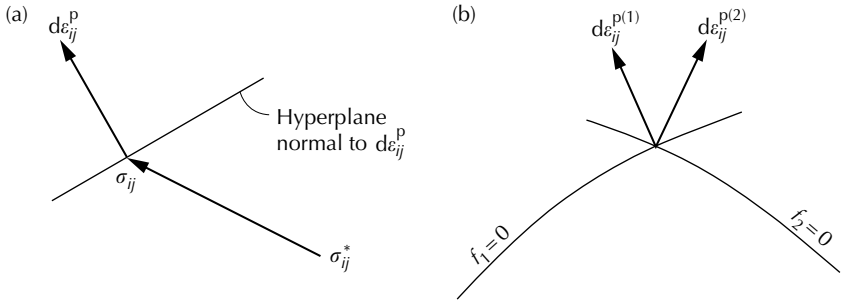

FIGURE 6.15
Normality of plastic strain increment.

surfaces have not been experimentally observed as mentioned in Section 6.2. Therefore, this case will not be pursued.

6.5.2 The Isotropic-Hardening Rule

We call a strain-hardening an *isotropic hardening*, if the subsequent yield surface is an isotropic expansion of the initial yield surface as shown in Figure 6.16(a). The Bauschinger effect is not considered in the isotropic hardening. The yield function is expressed by

$$f(\sigma_{ij}) = Y^2 \tag{6.52}$$

where Y is the yield stress under uniaxial tension. Y represents the radius of the yield surface and, when it increases, the yield surface expands in size. Y can be a function of either one of the two quantities that are used to measure the degree of hardening: the plastic work per unit volume defined by

$$W^{\mathrm{p}} = \int \sigma_{ij}\, \mathrm{d}\varepsilon_{ij}^{\mathrm{p}} \tag{6.53}$$

or the equivalent plastic strain with increment defined by

$$\mathrm{d}\bar{\varepsilon}^{\mathrm{p}} = \sqrt{\frac{2}{3}} \left\{ \mathrm{d}\varepsilon_{ij}^{\mathrm{p}} \mathrm{d}\varepsilon_{ij}^{\mathrm{p}} \right\}^{1/2} \tag{6.54}$$

An equivalent stress defined by

$$\bar{\sigma} = \sqrt{\frac{3}{2}} \left\{ \sigma'_{ij} \sigma'_{ij} \right\}^{1/2} \tag{6.55}$$

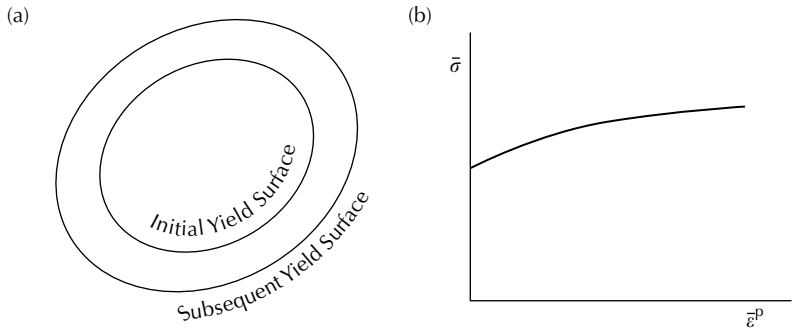

FIGURE 6.16
(a) Isotropic hardening and (b) schematic equivalent stress–plastic strain curve.

is usually introduced to describe the isotropic hardening. The equivalent stress can also take the following forms

$$\bar{\sigma} = \sqrt{\frac{1}{2}}\left\{(\sigma_{11}-\sigma_{22})^2+(\sigma_{22}-\sigma_{33})^2+(\sigma_{33}-\sigma_{11})^2+6\sigma_{12}^2+6\sigma_{23}^2+6\sigma_{31}^2\right\}^{1/2}$$
$$= \sqrt{\frac{1}{2}}\left\{(\sigma_1-\sigma_2)^2+(\sigma_2-\sigma_3)^2+(\sigma_3-\sigma_1)^2\right\}^{1/2} \tag{6.56}$$

The equivalent stress is defined based on the Mises yield criterion (6.6), observing $Y = \sqrt{3}\,k$. Equation (6.6) reduces to $Y = \sqrt{(3/2)}\{\sigma'_{ij}\sigma'_{ij}\}^{1/2}$, which is of the same form as (6.55). Thus, $\bar{\sigma} = Y$ and we write either

$$Y = \bar{\sigma} = F(W^{\mathrm{p}}) \tag{6.57}$$

or

$$Y = \bar{\sigma} = H\left(\int \mathrm{d}\bar{\varepsilon}^{\mathrm{p}}\right) \tag{6.58}$$

where F and H are functions and these functions are to be determined by plotting experimental stress–strain curves in the form of $\bar{\sigma}$ versus $\bar{\varepsilon}^{\mathrm{p}}$ as shown in Figure 6.16(b).

There are efforts to obtain a universal stress–strain curve, such as (6.57) or (6.58), which encompasses all states of stress [22]. Using this concept, a shear stress–strain curve can be deduced from a tensile stress–strain curve. We invert the function of (6.58) to obtain

$$\int \mathrm{d}\bar{\varepsilon}^{\mathrm{p}} = H^{-1}(\bar{\sigma}) \quad \text{or} \quad \mathrm{d}\bar{\varepsilon}^{\mathrm{p}} = \hat{F}(\bar{\sigma})\mathrm{d}\bar{\sigma} \tag{6.59}$$

where the function H is known from experiment. Using the flow rule (6.35), the equivalent plastic strain increment is from (6.54)

$$\mathrm{d}\bar{\varepsilon}^{\mathrm{p}} = \sqrt{\frac{2}{3}}\left\{\mathrm{d}\lambda^2\sigma'_{ij}\sigma'_{ij}\right\}^{1/2} = \sqrt{\frac{2}{3}}\,\mathrm{d}\lambda\sqrt{\frac{2}{3}}\bar{\sigma} = \frac{2}{3}\mathrm{d}\lambda\bar{\sigma} \tag{6.60}$$

Equating (6.59) and (6.60), we find

$$\mathrm{d}\lambda = \frac{3}{2}F(\bar{\sigma})\mathrm{d}\bar{\sigma} \qquad \text{where } F(\bar{\sigma}) = \frac{\hat{F}(\bar{\sigma})}{\bar{\sigma}} \tag{6.61}$$

Therefore, the flow rule is written as

$$\mathrm{d}\varepsilon^{\mathrm{p}}_{ij} = \tfrac{3}{2}F(\bar{\sigma})\mathrm{d}\bar{\sigma}\sigma'_{ij} \tag{6.62}$$

In the case of uniaxial tension, (6.62) reduces to

$$\mathrm{d}\varepsilon^{\mathrm{p}} = \mathrm{d}\varepsilon^{\mathrm{p}}_{11} = \tfrac{3}{2}F(\bar{\sigma})\mathrm{d}\bar{\sigma}\,(\tfrac{2}{3}\sigma) = F(\bar{\sigma})\mathrm{d}\bar{\sigma}\,\sigma \tag{6.63}$$

and, in the case of pure torsion in a thin tube, (6.62) is

$$\tfrac{1}{2}\mathrm{d}\gamma^{\mathrm{p}} = \mathrm{d}\varepsilon^{\mathrm{p}}_{12} = \tfrac{3}{2}F(\bar{\sigma})\mathrm{d}\bar{\sigma}\,\tau \tag{6.64}$$

The expression of equivalent stress for uniaxial tension is

$$\bar{\sigma} = \sqrt{\frac{3}{2}}\{\sigma'_{ij}\sigma'_{ij}\}^{1/2} = \sqrt{\frac{3}{2}}\left\{\left(\frac{2}{3}\sigma\right)^2 + 2\left(-\frac{\sigma}{3}\right)^2\right\}^{1/2} = \sigma \tag{6.65}$$

and for pure torsion is

$$\bar{\sigma} = \sqrt{\frac{3}{2}}\{\sigma'_{ij}\sigma'_{ij}\}^{1/2} = \sqrt{\frac{3}{2}}\{2\tau^2\}^{1/2} = \sqrt{3}\,\tau \tag{6.66}$$

Thus, we find

$$\tau = \frac{\sigma}{\sqrt{3}} \tag{6.67}$$

Substituting (6.67) into (6.63) and (6.64), we obtain

$$\mathrm{d}\gamma^{\mathrm{p}} = \sqrt{3}\,\mathrm{d}\varepsilon^{\mathrm{p}} \tag{6.68}$$

We now use (6.67) and (6.68) to deduce a shear stress–strain curve (τ, γ) from a known tensile stress–strain curve (σ, ε). In a monotonic loading condition, (6.68) is integrated to yield

$$\gamma^{\mathrm{p}} = \sqrt{3}\varepsilon^{\mathrm{p}} \quad \text{or} \quad (\gamma - \gamma^{\mathrm{e}}) = \sqrt{3}(\varepsilon - \varepsilon^{\mathrm{e}}) \quad \text{or} \quad \gamma - \frac{\tau}{\mu} = \sqrt{3}\left(\varepsilon - \frac{\sigma}{E}\right) \tag{6.69}$$

Using (6.67) and the relations of elastic constants, (6.69) reduces to

$$\frac{\gamma}{\sqrt{3}} = \varepsilon - \left(\frac{1-2\nu}{3E}\right)\sigma \tag{6.70}$$

where ν is Poisson's ratio. Knowing (σ, ε) for any point on the tensile curve, we can use (6.67) and (6.70) to determine the corresponding point (τ, γ) on the shear curve. We can also use a graphical method to accomplish the task. Referring to Figure 6.17, we need to establish first, the two elastic lines with slopes E and μ. At point A on the tensile line, the stress is σ_{A}. Segment $\overline{\mathrm{AB}}$ is the

corresponding plastic strain ε^p, which is known. Next, locate point C on the elastic shear line with stress equals to $\sigma_A/\sqrt{3}$. The length of line segment $\overline{CD}$ is $\sqrt{3}\,\varepsilon^p$ and, therefore, point D can be located. The process may be repeated for all points to determine the shear stress–strain curve.

EXAMPLE 6.5 In the case of combined axial–torsion of a thin-walled tube, if we use the Mises yield function and isotropic hardening, the flow rule is given by (6.62). (a) Determine the function $F(\bar{\sigma})$ from a uniaxial tension test. (b) For the general case of combined tension and torsion, find the expressions for the axial and shear strain increments. (c) For a stress-controlled proportional stress-path OBC shown in Figure 6.18, find the corresponding strain path. (d) For a stress-controlled torsion from O to A followed by tension ABCD while

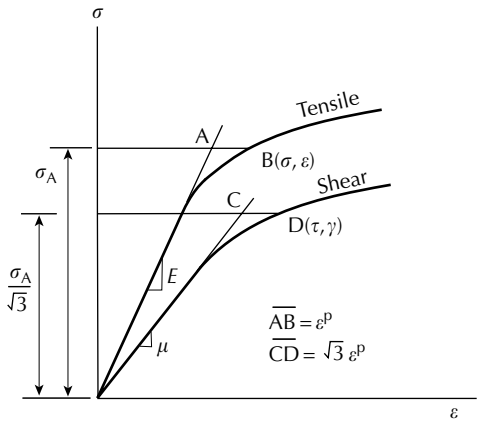

FIGURE 6.17
Determination of shear stress–strain curve from the tension stress–strain curve.

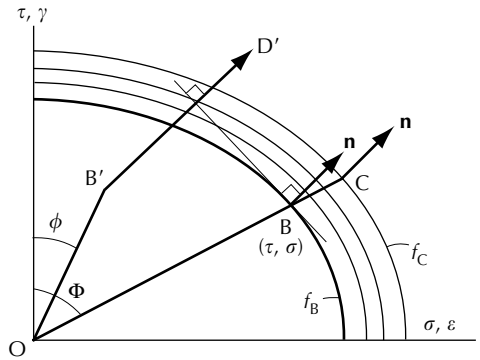

FIGURE 6.18
Stress-controlled proportional stress path assuming isotropic hardening.

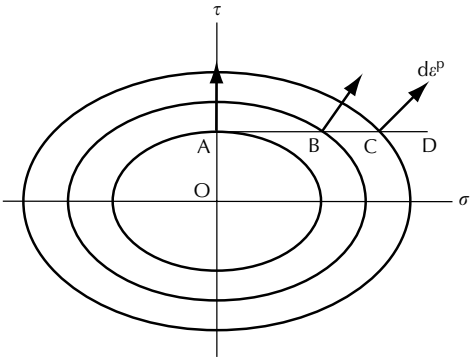

FIGURE 6.19
A torsion–tension stress path assuming isotropic hardening.

keeping the shear stress constant at τ_A (Figure 6.19), discuss the corresponding strain path.

Solution

For a combined axial–torsion test, the states of stress and strain are

$$\sigma_{ij} = \begin{bmatrix} \sigma & \tau & 0 \\ \tau & 0 & 0 \\ 0 & 0 & 0 \end{bmatrix}, \qquad \sigma'_{ij} = \begin{bmatrix} \frac{2}{3}\sigma & \tau & 0 \\ \tau & -\frac{\sigma}{3} & 0 \\ 0 & 0 & -\frac{\sigma}{3} \end{bmatrix}, \qquad \varepsilon_{ij} = \begin{bmatrix} \varepsilon & \frac{\gamma}{2} & 0 \\ \frac{\gamma}{2} & 0 & 0 \\ 0 & 0 & 0 \end{bmatrix} \tag{a}$$

The equivalent stress and its increment are from (6.55) and (a)

$$\bar{\sigma} = \{\sigma^2 + 3\tau^2\}^{1/2}, \qquad \mathrm{d}\bar{\sigma} = \frac{\sigma\,\mathrm{d}\sigma + 3\tau\,\mathrm{d}\tau}{\bar{\sigma}} \tag{b}$$

In the case of uniaxial tension, the Prandtl–Reuss equation is

$$\mathrm{d}\varepsilon = \mathrm{d}\varepsilon_{11} = \frac{\mathrm{d}\sigma}{E} + \frac{3}{2}F(\bar{\sigma})\mathrm{d}\bar{\sigma}\left(\frac{2}{3}\sigma\right) \tag{c}$$

and the equivalent stress and its increment are

$$\bar{\sigma} = \sigma, \qquad \mathrm{d}\bar{\sigma} = \frac{\sigma\,\mathrm{d}\sigma}{\bar{\sigma}} \tag{d}$$

Using (d), (c) may be written as

$$\frac{\mathrm{d}\varepsilon}{\mathrm{d}\sigma} = \frac{1}{E_t} = \frac{1}{E} + \frac{F(\bar{\sigma})\sigma^2}{\bar{\sigma}} \tag{e}$$

where E_t is the slope of the tensile stress–strain curve. Solving (e), we find

$$F(\bar{\sigma}) = \frac{1}{\bar{\sigma}}\left[\frac{1}{E_t} - \frac{1}{E}\right] \tag{f}$$

For the general case of combined tension and torsion, by use of the flow rule (6.62) and the elastic strains, the two components of the Prandtl–Reuss equation are

$$\begin{aligned} \mathrm{d}\varepsilon &= \frac{\mathrm{d}\sigma}{E} + \frac{\sigma}{(\bar{\sigma})^2}\left[\frac{1}{E_t} - \frac{1}{E}\right](\sigma\,\mathrm{d}\sigma + 3\tau\,\mathrm{d}\tau) \\ \mathrm{d}\gamma &= \frac{\mathrm{d}\tau}{\mu} + \frac{3\tau}{(\bar{\sigma})^2}\left[\frac{1}{E_t} - \frac{1}{E}\right](\sigma\,\mathrm{d}\sigma + 3\tau\,\mathrm{d}\tau) \end{aligned} \tag{g}$$

For the stress-controlled proportional stress-path OBC shown in Figure 6.18, the elastic state OB′ is the same as that of Example 6.1 and shown previously in Figure 6.10 with angle ϕ. At point B of Figure 6.18, yielding first occurs with corresponding yield locus f_{B}. The normal to the yield locus is denoted by **n**. As the stress path proceeds from B to C, the stress point carries the yield locus with it and the yield locus makes an isotropic expansion. The normal to the yield locus f_{C} at C is still **n**. Taking the plastic strain part of (g), we obtain the following ratio for the plastic strain increments

$$\frac{\mathrm{d}\gamma^{\mathrm{p}}}{\mathrm{d}\varepsilon^{\mathrm{p}}} = \frac{3\tau}{\sigma} \tag{h}$$

It is easily shown that this slope is normal to the yield locus. However, the strain-path B′D′ is not in the same direction as the normal **n** because of the elastic strain. Path B′D′ has to be determined by integrating (g).

We now discuss a stress-controlled torsion from O to A followed by tension ABCD while keeping the shear stress constant at τ_{A} (Figure 6.19). During the stage of tensile loading ABCD, the strain increments are given by (g) with $\mathrm{d}\tau = 0$. Thus,

$$\begin{aligned} \mathrm{d}\varepsilon &= \frac{\mathrm{d}\sigma}{E} + \frac{\sigma^2}{(\bar{\sigma})^2}\left[\frac{1}{E_t} - \frac{1}{E}\right](\mathrm{d}\sigma) \\ \mathrm{d}\gamma &= \frac{3\tau_{\mathrm{A}}\sigma}{(\bar{\sigma})^2}\left[\frac{1}{E_t} - \frac{1}{E}\right](\mathrm{d}\sigma) \end{aligned} \tag{i}$$

We see from (i) that the plastic strain ratio is

$$\frac{\mathrm{d}\gamma^{\mathrm{p}}}{\mathrm{d}\varepsilon^{\mathrm{p}}} = \frac{3\tau_{\mathrm{A}}}{\sigma} = \tan\varphi \tag{j}$$

The angle φ of the plastic strain vector changes from 90° at A to smaller angles as the axial stress σ increases. As σ becomes large, the angle φ tends

to zero. We note that this result is merely a prediction of the model with isotropic hardening. Related experimental results are discussed in Chapter 7. The plastic-strain-increment vectors are shown in Figure 6.19. Finally, we mention that the strain path is found by integrating the expression (k) which is obtained by eliminating $d\sigma$ from (i)

$$\frac{d\gamma}{d\varepsilon} = \frac{[3\tau_A \sigma/(\bar{\sigma})^2][(1/E_t) - (1/E)]}{1/E + (\sigma^2/(\bar{\sigma})^2)[(1/E_t) - (1/E)]} \tag{k}$$

6.5.3 The Kinematic-Hardening Rule

The *kinematic-hardening rule* assumes that the yield surface translates without rotation in the stress space. The shape and size of yield surface remain unchanged during motion of yield surface. This hardening rule has been introduced by Prager [23] to account for Bauschinger effect. Hodge [24] pointed out that the concept of kinematic hardening must be applied in the nine-dimensional stress space. In the nine-dimensional space, the initial yield surface is given by

$$f(\sigma_{ij}) = 0 \tag{6.71}$$

and the subsequent yield surface by

$$f(\sigma_{ij} - \alpha_{ij}) = 0 \tag{6.72}$$

where α_{ij} is the total translation of center of initial yield surface and is termed *back stress* by some investigators. Note that for Mises criterion, we write

$$(\sigma'_{ij} - \alpha^D_{ij})(\sigma'_{ij} - \alpha^D_{ij}) = 2k^2 \tag{6.73}$$

where α^D_{ij} is the deviatoric part of α_{ij}. Hodge [24] further suggested the concept of combined isotropic–kinematic hardening. In this case, the yield surface translates, defined by α_{ij}, and expands as well, which is defined by the change in k.

The evolution rule of α_{ij} in the stress space is of interest. Prager [23] proposed a linear-hardening rule as

$$d\alpha_{ij} = c\, d\varepsilon^p_{ij} \tag{6.74}$$

where c is a constant. Ziegler [25] proposed a modified kinematic-hardening rule as

$$d\alpha_{ij} = d\mu(\sigma_{ij} - \alpha_{ij}) \qquad \text{where } d\mu > 0 \tag{6.75}$$

The directions of $d\alpha_{ij}$ are different between (6.74) and (6.75) and they are shown in Figure 6.20. In (6.75), $d\mu$ is a parameter and should not be mixed with the shear modulus. In the figure, O is the origin of the nine-dimensional stress space and O′ is the center of the current yield surface. The current stress point is at P. According to (6.74), the center of yield surface would translate in a direction normal to the yield surface at P and this increment of translation is denoted by $d\alpha_{ij}^{(P)}$ in the figure. On the other hand, according to (6.75), the increment of translation of the yield surface, denoted by $d\alpha_{ij}^{(Z)}$, is along the direction of O′P. We note that the two rules are the same if the current yield surface is a hypersphere, which is true when the Mises yield surface is considered and a combined isotropic–kinematic hardening is applied.

The linear kinematic hardening can only be applied to a material with a bilinear stress–strain curve when unloading and reverse loading is considered. For a nonlinear stress–strain curve, the linear kinematic-hardening rule would result in an unloading curve, which bends in an unnatural way and such an unloading curve has never been observed. Figure 6.21(a) shows such

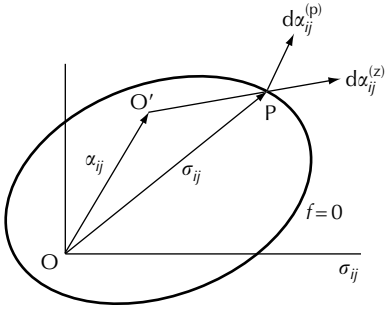

FIGURE 6.20
Kinematic-hardening rules by Prager and Ziegler.

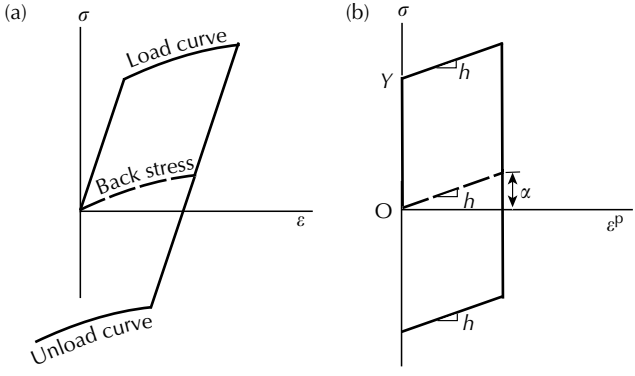

FIGURE 6.21
Linear kinematic-hardening: (a) nonlinear stress–strain curve and (b) bilinear stress–strain curve.

a behavior in the one-dimensional loading–unloading stress–strain curve. The linear kinematic hardening rule, applied to a bilinear stress–strain curve (a special case of (6.58)), is shown in Figure 6.21(b), where the stress σ is plotted against the plastic strain ε^{p}. In the figure, Y is the initial yield stress and the slope of the linear kinematic hardening is h, that is,

$$\mathrm{d}\alpha = h\,\mathrm{d}\varepsilon^{\mathrm{p}} \tag{6.76}$$

In the case of uniaxial loading, the increment of the back stress is

$$\mathrm{d}\alpha_{ij} = \begin{bmatrix} \mathrm{d}\alpha & 0 & 0 \\ 0 & 0 & 0 \\ 0 & 0 & 0 \end{bmatrix} \quad \text{and} \quad \mathrm{d}\alpha_{ij}^{\mathrm{D}} = \begin{bmatrix} \frac{2}{3}\mathrm{d}\alpha & 0 & 0 \\ 0 & -\frac{\mathrm{d}\alpha}{3} & 0 \\ 0 & 0 & -\frac{\mathrm{d}\alpha}{3} \end{bmatrix} \tag{6.77}$$

Thus, from (6.74), the first element of the linear kinematic hardening rule is

$$\tfrac{2}{3}\mathrm{d}\alpha = c\,\mathrm{d}\varepsilon^{\mathrm{p}} \tag{6.78}$$

Comparing (6.76) with (6.78), we obtain

$$h = \tfrac{3}{2}c \tag{6.79}$$

and the stress–stress curve during loading is given by

$$\sigma = Y + h\,\varepsilon^{\mathrm{p}} \tag{6.80}$$

Thus, h is also the slope of the stress–strain curve.

In case of nonlinear loading curve, the yield function is

$$f(\sigma_{ij} - \alpha_{ij}) = Y^2 \tag{6.81}$$

in which both Y and α_{ij} are not constant for combined isotropic–kinematic hardening. The increment of stress in the uniaxial stress σ versus plastic strain ε^{p} plot consists of two parts, that is,

$$\mathrm{d}\sigma = \mathrm{d}Y + \mathrm{d}\alpha \tag{6.82}$$

Introduce an isotropic–kinematic-hardening parameter β, which is a number $0 \le \beta \le 1$. Then, we may write

$$\mathrm{d}Y = \beta h\,\mathrm{d}\varepsilon^{\mathrm{p}} \quad \text{and} \quad \mathrm{d}\alpha = (1-\beta)h\,\mathrm{d}\varepsilon^{\mathrm{p}} \tag{6.83}$$

and (6.82) becomes

$$\mathrm{d}\sigma = h\,\mathrm{d}\varepsilon^{\mathrm{p}} \tag{6.84}$$

The extreme value $\beta = 1$ characterizes isotropic hardening and $\beta = 1$ characterizes kinematic hardening. When β has a value between 0 and 1, then we have a case of combined isotropic–kinematic hardening.

The combined isotropic-linear kinematic-hardening rule cannot lead to a reasonable unloading curve. Nonlinear kinematic-hardening rules will have to be used to describe the unloading curve. A nonlinear kinematic-hardening rule was first used by Armstrong and Frederick [26] and written as

$$\mathrm{d}\alpha_{ij} = \tfrac{2}{3}c\,\mathrm{d}\varepsilon^{\mathrm{p}}_{ij} - \kappa\alpha_{ij}\,\mathrm{d}\bar{\varepsilon}^{\mathrm{p}} \tag{6.85}$$

where c and κ are material constants. This rule has gained popularity in recent literatures. We will see in Chapter 8 that this hardening rule is also a part of the endochronic theory of plasticity proposed by Valanis [27] and was applied by Wu and Yang [28] and Wu et al. [29]. Denoting the increment of equivalent plastic strain by the increment of a monotonically increasing positive parameter z, so that

$$\mathrm{d}z = |\mathrm{d}\bar{\varepsilon}^{\mathrm{p}}| \tag{6.86}$$

then (6.85) may be written as

$$\frac{\mathrm{d}\alpha_{ij}}{\mathrm{d}z} + \kappa\alpha_{ij} = \frac{2c}{3}\frac{\mathrm{d}\varepsilon^{\mathrm{p}}_{ij}}{\mathrm{d}z} \tag{6.87}$$

If c and κ are constants, then (6.87) is a linear ordinary differential equation with constant coefficients and the solution is

$$\alpha_{ij}(z) = \frac{2c}{3}\int_{z_0}^{z} \mathrm{e}^{-\kappa(z-z')}\frac{\mathrm{d}\varepsilon^{\mathrm{p}}_{ij}(z')}{\mathrm{d}z'}\mathrm{d}z' + \alpha_{ij}(0)\,\mathrm{e}^{-\kappa(z-z_0)} \tag{6.88}$$

In (6.88), z is the current value of the parameter; z_0 is the initial value of z; and $\alpha_{ij}(0)$ is the initial value of $\alpha_{ij}(z)$. In the case of uniaxial loading–unloading, (6.90) reduces to

$$\alpha(z) = \frac{2c}{3}\int_{z_0}^{z} \mathrm{e}^{-\kappa(z-z')}\frac{\mathrm{d}\varepsilon^{\mathrm{p}}(z')}{\mathrm{d}z'}\mathrm{d}z' + \alpha(0)\,\mathrm{e}^{-\kappa(z-z_0)} \tag{6.89}$$

Referring to Figure 6.22, let us consider loading along OA and then unloading to B. The initial conditions are $z_0 = 0$ and $\alpha(0) = 0$. We note that

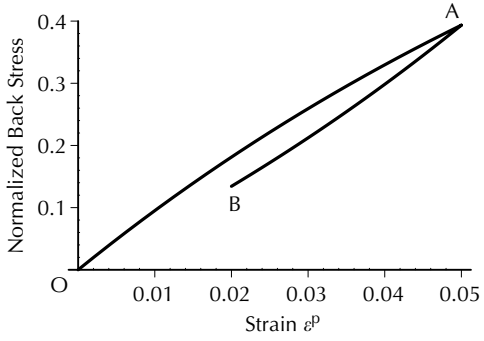

FIGURE 6.22
Loading–unloading curves for nonlinear kinematic-hardening.

$[d\varepsilon^p(z')/dz'] = +1$ during loading, and $[d\varepsilon^p(z')/dz'] = -1$ during unloading. Using these conditions, (6.89) may be integrated during loading to yield

$$y = 1 - e^{-\kappa z} = 1 - e^{-\kappa\varepsilon^p} \qquad \text{with } y = \frac{3\kappa}{2c}\alpha \tag{6.90}$$

where y is a normalized back stress. Unloading occurs at point A and (6.89) is integrated to obtain the unloading curve as

$$\begin{aligned}\alpha(z) &= \frac{2c}{3}\int_0^{z_A} e^{-\kappa(z_A - z')}(+1)\,dz' + \frac{2c}{3}\int_{z_A}^{z} e^{-\kappa(z-z')}(-1)\,dz' + \alpha(0)e^{-\kappa(z-z_0)} \\ &= \alpha(z_A) + \frac{2c}{3}\int_{z_A}^{z} e^{-\kappa(z-z')}(-1)\,dz' = \frac{2c}{3\kappa}[1 - e^{-\kappa z_A}] - \frac{2c}{3\kappa}[1 - e^{-\kappa(z-z_A)}] \\ &= \frac{2c}{3\kappa}e^{-\kappa z_A}[e^{-\kappa(z-2z_A)} - 1]\end{aligned} \tag{6.91}$$

The value of z at A is denoted by z_A. Referring to (6.86), during loading, we have $dz = d\bar{\varepsilon}^p = d\varepsilon^p$; but during unloading, when $z > z_A$, we have $dz = -d\varepsilon^p$. This relation may be integrated starting from point A to obtain

$$\varepsilon = \varepsilon_A + z_A - z = 2z_A - z \tag{6.92}$$

Substituting (6.92) into (6.91), we obtain

$$y = e^{-\kappa\varepsilon_A^p}[e^{\kappa\varepsilon^p} - 1] \tag{6.93}$$

Equations (6.90) and (6.93) are plotted in Figure 6.22. We see that the curves for loading and unloading do not coincide and they are curved. The slopes for loading and unloading curves starting at any point such as A are different.

The differential form (6.85) for the uniaxial loading–unloading is

$$\begin{aligned} \mathrm{d}\alpha = c\,\mathrm{d}\varepsilon^{\mathrm{p}} - \kappa\alpha\,\mathrm{d}\bar{\varepsilon}^{\mathrm{p}} &= (c-\kappa\alpha)\mathrm{d}\varepsilon^{\mathrm{p}} \qquad \text{for loading} \\ &= (c+\kappa\alpha)\mathrm{d}\varepsilon^{\mathrm{p}} \qquad \text{for unloading} \end{aligned} \tag{6.94}$$

where (6.94) defines the slopes for the two cases. Finally, we mention that the linear kinematic-hardening rule leads to a straight line applicable to both loading and unloading.

6.5.4 General Form of Subsequent Yield Function and its Flow Rule

In order to have a more general description of yield surface, let us consider that the yield function is a function of stress σ_{ij}, plastic strain $\varepsilon^{\mathrm{p}}_{ij}$, and a parameter κ, and write

$$f(\sigma_{ij}\cdot\varepsilon^{\mathrm{p}}_{ij},\kappa)=0 \quad \text{or} \quad f(\sigma_{ij}\cdot\varepsilon^{\mathrm{p}}_{ij},\kappa_1)=\kappa_0=\text{const} \tag{6.95}$$

where κ_0 represents the size of the yield surface. Referring to Figure 6.23, points A and B have the same $\varepsilon^{\mathrm{p}}_{ij}$ and κ_0, and, without κ_1, we are not able to distinguish A from B. We have to know $\mathrm{d}\varepsilon^{\mathrm{p}}_{ij}$ and $\mathrm{d}\kappa_1$ to determine the subsequent yield surface. The flow rule is from (6.32)

$$\mathrm{d}\varepsilon^{\mathrm{p}}_{ij} = \mathrm{d}\lambda\frac{\partial f}{\partial\sigma_{ij}} \tag{6.32}$$

On the other hand, Drucker's postulate gives

$$\mathrm{d}\sigma_{ij}\mathrm{d}\varepsilon^{\mathrm{p}}_{ij} = \mathrm{d}\lambda\,\mathrm{d}\sigma_{ij}\frac{\partial f}{\partial\sigma_{ij}} > 0 \tag{6.96}$$

where $(\partial f/\partial\sigma_{ij})\mathrm{d}\sigma_{ij} > 0$ represents the loading condition. Comparing the above two expressions we found $\mathrm{d}\lambda > 0$.

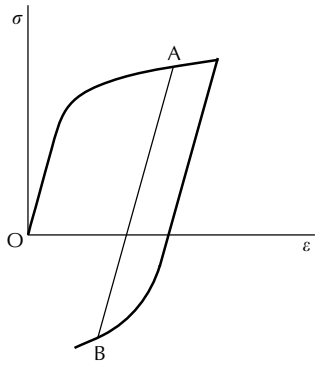

FIGURE 6.23
Parameters for yield surface.

The parameter $d\lambda$ is determined by use of the *consistency condition*, Prager [30]. Since loading from a plastic state must again lead to a plastic state, the stress and plastic strain that exist after the infinitesimal changes $d\sigma_{ij}$, $d\varepsilon_{ij}^{p}$, and $d\kappa$ have taken place must still satisfy (6.97), which is

$$f(\sigma_{ij}, \varepsilon_{ij}^{p}, \kappa) = 0 \tag{6.97}$$

By use of the consistency condition, the increment of the yield function is zero, that is,

$$df = \frac{\partial f}{\partial \sigma_{ij}} d\sigma_{ij} + \frac{\partial f}{\partial \varepsilon_{ij}^{p}} d\varepsilon_{ij}^{p} + \frac{\partial f}{\partial \kappa} + d\kappa = 0 \tag{6.98}$$

In Figure 6.24, the stress at point A is $\sigma_{ij}^{(A)}$ and it is on the yield surface

$$f\left(\sigma_{ij}^{(A)}, \varepsilon_{ij}^{p(A)}, \kappa^{(A)}\right) = 0 \tag{6.99}$$

An infinitesimal loading has moved the stress point from A to B and it carries the yield surface with it, so that the stress at B is $\sigma_{ij}^{(B)}$ and the yield surface that B is on is

$$f\left(\sigma_{ij}^{(B)}, \varepsilon_{ij}^{p(B)}, \kappa^{(B)}\right) = 0 \tag{6.100}$$

while

$$f\left(\sigma_{ij}^{(B)}, \varepsilon_{ij}^{p(A)}, \kappa^{(A)}\right) > 0 \tag{6.101}$$

Substituting (6.32) into (6.98), we have

$$df = \frac{\partial f}{\partial \sigma_{ij}} d\sigma_{ij} + d\lambda \frac{\partial f}{\partial \varepsilon_{ij}^{p}} \frac{\partial f}{\partial \sigma_{ij}} + \frac{\partial f}{\partial \kappa} d\kappa = 0 \tag{6.102}$$

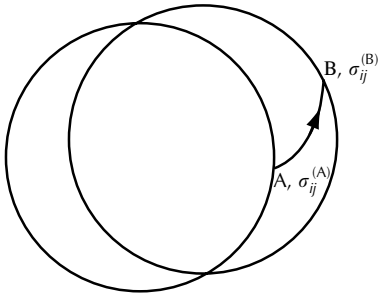

FIGURE 6.24
The consistency condition.

which may be solved to obtain $d\lambda$ as

$$d\lambda = -\frac{(\partial f/\partial \kappa)d\kappa + (\partial f/\partial \sigma_{ij})d\sigma_{ij}}{(\partial f/\partial \sigma_{rs})(\partial f/\partial \varepsilon^{p}_{rs})} \tag{6.103}$$

Therefore, by use of (6.32), the flow rule is

$$d\varepsilon^{p}_{ij} = \frac{(\partial f/\partial \kappa)(\partial f/\partial \sigma_{ij})d\kappa + (\partial f/\partial \sigma_{km})(\partial f/\partial \sigma_{ij})d\sigma_{km}}{-[(\partial f/\partial \sigma_{rs})(\partial f/\partial \varepsilon^{p}_{rs}]} \tag{6.104}$$

Note that this equation consists of two parts. One part is due to $d\kappa$ and the other part is due to $d\sigma_{ij}$; but the stress increments appear in the scalar form involving summation.

The increment $d\kappa$ may be assumed to be a linear function of $d\varepsilon^{p}_{ij}$, such that

$$d\kappa = h_{rs}(\sigma_{mn}, \varepsilon^{p}_{mn})d\varepsilon^{p}_{rs} = h_{11}d\varepsilon^{p}_{11} + h_{12}d\varepsilon^{p}_{12} + \cdots \tag{6.105}$$

Then,

$$d\kappa = h_{km}d\lambda\frac{\partial f}{\partial \sigma_{km}} \tag{6.106}$$

By use of (6.106), (6.102) reduces to

$$df = \frac{\partial f}{\partial \sigma_{ij}}d\sigma_{ij} + d\lambda\left[\frac{\partial f}{\partial \varepsilon^{p}_{ij}}\frac{\partial f}{\partial \sigma_{ij}} + \frac{\partial f}{\partial \kappa}h_{km}\frac{\partial f}{\partial \sigma_{km}}\right] = 0 \tag{6.107}$$

We then solve (6.107) for $d\lambda$ to obtain

$$d\lambda = \frac{-(\partial f/\partial \sigma_{ij})d\sigma_{ij}}{(\partial f/\partial \sigma_{rs})(\partial f/\partial \varepsilon^{p}_{rs}) + (\partial f/\partial \kappa)(\partial f/\partial \sigma_{rs})h_{rs}} \tag{6.108}$$

Therefore,

$$d\varepsilon^{p}_{ij} = \frac{(\partial f/\partial \sigma_{km})(\partial f/\partial \sigma_{ij})d\sigma_{km}}{-[(\partial f/\partial \sigma_{rs})(\partial f/\partial \varepsilon^{p}_{rs}) + (\partial f/\partial \kappa)(\partial f/\partial \sigma_{rs})h_{rs}]} \tag{6.109}$$

This equation shows that $d\varepsilon^{p}_{ij}$ is linearly related to $d\sigma_{km}$ and (6.109) is in the following form

$$d\varepsilon^{p}_{ij} = A_{ijkm}(\sigma_{rs}, \varepsilon^{p}_{rs}, \kappa)d\sigma_{km} \tag{6.110}$$

We have thus shown that the linear relation of (6.110) between the plastic strain and stress increments follows from the normality condition of plastic strain-rate by assuming a linear relationship for $d\kappa$ given by (6.105). A special case of (6.110) is, Hill [16, p. 33],

$$d\varepsilon_{ij}^{p} = G_{ij}\frac{\partial f}{\partial \sigma_{km}}d\sigma_{km} \tag{6.111}$$

where G_{ij} is a symmetric function of stress and strain history, but is not a function of $d\sigma_{km}$. In addition, $G_{ii} = 0$. Equation (6.111) has been applied in [16] to the case of isotropic hardening. If we choose

$$G_{ij} = h\frac{\partial g}{\partial \sigma_{ij}} \tag{6.112}$$

then, (6.111) becomes

$$d\varepsilon_{ij}^{p} = h\frac{\partial g}{\partial \sigma_{ij}}\frac{\partial f}{\partial \sigma_{km}}d\sigma_{km} \tag{6.113}$$

in which $h = h(J_2, J_3)$ and $g = g(J_2, J_3)$ is the plastic potential. We see that (6.113) is in the form of (6.109).

Another special case of (6.112) is

$$d\varepsilon_{ij}^{p} = G\frac{\partial f}{\partial \sigma_{ij}}\frac{\partial f}{\partial \sigma_{km}}d\sigma_{km} \tag{6.114}$$

This form was used by Drucker [31]. In the equation, G is any positive scalar function of stress, strain, and history κ, but is independent of $d\sigma_{km}$.

An important special case is the kinematic hardening. Consider the yield function

$$f(\sigma_{ij} - \alpha_{ij}) = 0 \tag{6.115}$$

in the stress space. Let $p_{ij} = \sigma_{ij} - \alpha_{ij}$, then

$$\begin{aligned}\frac{\partial f}{\partial \sigma_{km}} &= \frac{\partial f}{\partial p_{ij}}\frac{\partial p_{ij}}{\partial \sigma_{km}} = \frac{\partial f}{\partial p_{ij}}\delta_{ik}\delta_{jm} = \frac{\partial f}{\partial p_{km}}\\ \frac{\partial f}{\partial \alpha_{km}} &= \frac{\partial f}{\partial p_{ij}}\frac{\partial p_{ij}}{\partial \alpha_{km}} = -\frac{\partial f}{\partial p_{km}}\end{aligned} \tag{6.116}$$

Thus,

$$\frac{\partial f}{\partial \sigma_{ij}} = -\frac{\partial f}{\partial \alpha_{ij}} \tag{6.117}$$

Using the yield function (6.115), the consistency condition is

$$\mathrm{d}f = \frac{\partial f}{\partial \sigma_{ij}}\mathrm{d}\sigma_{ij} + \frac{\partial f}{\partial \alpha_{ij}}\mathrm{d}\alpha_{ij} = 0 \tag{6.118}$$

Using (6.117), we then have

$$\frac{\partial f}{\partial \sigma_{ij}}\mathrm{d}\sigma_{ij} - \frac{\partial f}{\partial \sigma_{ij}}\mathrm{d}\alpha_{ij} = 0 \tag{6.119}$$

If we apply Prager's linear-hardening rule, we obtain

$$\frac{\partial f}{\partial \sigma_{ij}}\mathrm{d}\sigma_{ij} - \frac{\partial f}{\partial \sigma_{ij}}c\,\mathrm{d}\varepsilon_{ij}^{\mathrm{p}} = 0 \tag{6.120}$$

or

$$\frac{\partial f}{\partial \sigma_{ij}}\mathrm{d}\sigma_{ij} - c\frac{\partial f}{\partial \sigma_{ij}}\mathrm{d}\lambda\,\frac{\partial f}{\partial \sigma_{ij}} = 0 \tag{6.121}$$

Hence,

$$\mathrm{d}\lambda = \frac{(\partial f/\partial \sigma_{km})\mathrm{d}\sigma_{km}}{c[(\partial f/\partial \sigma_{ij})(\partial f/\partial \sigma_{ij})]} \tag{6.122}$$

and the flow rule is

$$\mathrm{d}\varepsilon_{ij}^{\mathrm{p}} = \frac{(\partial f/\partial \sigma_{ij})(\partial f/\partial \sigma_{km})\mathrm{d}\sigma_{km}}{c[(\partial f/\partial \sigma_{ij})(\partial f/\partial \sigma_{ij})]} \tag{6.123}$$

This equation may also be derived from (6.106) by setting $\mathrm{d}\kappa = 0$. Equation (6.104) becomes

$$\mathrm{d}\varepsilon_{ij}^{\mathrm{p}} = \frac{(\partial f/\partial \sigma_{ij})(\partial f/\partial \sigma_{km})\mathrm{d}\sigma_{km}}{-[(\partial f/\partial \sigma_{rs})(\partial f/\partial \varepsilon_{rs}^{\mathrm{p}})]} \tag{6.124}$$

In this case, the yield function is given by $f(\sigma_{ij}, \varepsilon_{ij}^{\mathrm{p}}) = 0$, where σ_{ij} and $\varepsilon_{ij}^{\mathrm{p}}$ are treated as independent variables. By use of Prager's linear-hardening rule, we write

$$\frac{\partial f}{\partial \varepsilon_{rs}^{\mathrm{p}}} = \frac{\partial f}{\partial \alpha_{rs}}c = -\frac{\partial f}{\partial \sigma_{rs}}c \tag{6.125}$$

Combining (6.124) and (6.125), we obtain (6.123). If we use Ziegler's kinematic-hardening rule, then

$$\mathrm{d}\alpha_{ij} = \mathrm{d}\mu(\sigma_{ij} - \alpha_{ij}) \qquad \text{with } \mathrm{d}\mu > 0 \tag{6.126}$$

The consistency condition is

$$df = \frac{\partial f}{\partial \sigma_{ij}} d\sigma_{ij} - \frac{\partial f}{\partial \sigma_{ij}} d\mu \, (\sigma_{ij} - \alpha_{ij}) = 0 \tag{6.127}$$

Therefore, we obtain

$$d\mu = \frac{(\partial f / \partial \sigma_{ij}) d\sigma_{ij}}{(\sigma_{km} - \alpha_{km})(\partial f / \partial \sigma_{km})} \tag{6.128}$$

and

$$d\alpha_{ij} = \frac{(\partial f / \partial \sigma_{rs}) d\sigma_{rs} (\sigma_{ij} - \alpha_{ij})}{(\sigma_{km} - \alpha_{km})(\partial f / \partial \sigma_{km})} \tag{6.129}$$

We see that the evolution of α_{ij} is not directly related to $d\varepsilon_{ij}^{p}$. But, the flow rule for this case is still given by (6.32), in which $d\lambda$ cannot be determined from the consistency condition. Instead, $d\lambda$ is determined from the normality condition as follows: we define a plastic modulus K along the direction of the outward normal $\mathbf{n}$ at the stress point on the yield surface. The stress increment projected along $\mathbf{n}$ is $d\sigma = \mathbf{n} \cdot d\boldsymbol{\sigma}$ and the following relation holds:

$$(\mathbf{n} \cdot d\boldsymbol{\sigma})\mathbf{n} = K \, d\varepsilon^{p} \qquad \text{with } K > 0 \tag{6.130}$$

Therefore, the flow rule is

$$d\boldsymbol{\varepsilon}^{p} = \frac{1}{K}(\mathbf{n} \cdot d\boldsymbol{\sigma})\mathbf{n} = \frac{d\sigma}{K}\mathbf{n} \tag{6.131}$$

6.6 The Return-Mapping Algorithm

We discussed in Section 6.5.4 how the plasticity factor $d\lambda$ can be determined by means of the consistency condition of Prager [30]. This method has been applied extensively in the literature to solve boundary-valued problems of plastic deformation involving simple states of stress. For multidimensional engineering problems of plasticity, a numerical algorithm has been developed, which is known as the *return-mapping algorithm* (or the backward Euler integration algorithm). For constitutive equations in the rate form, the numerical procedure calls for the determination of quantities at step $(n+1)$ using information at step (n). The return-mapping algorithm assures that the incremental step from (n) to $(n+1)$ is consistent with the flow rule and hardening rule, and the stress point at step $(n+1)$ is lying on the subsequent yield surface.

Referring to Figure 6.25, the current stress $\sigma^{(n)}$ is at A and the stress at the next step $\sigma^{(n+1)}$ is at B. The task is to determine the stress at point B

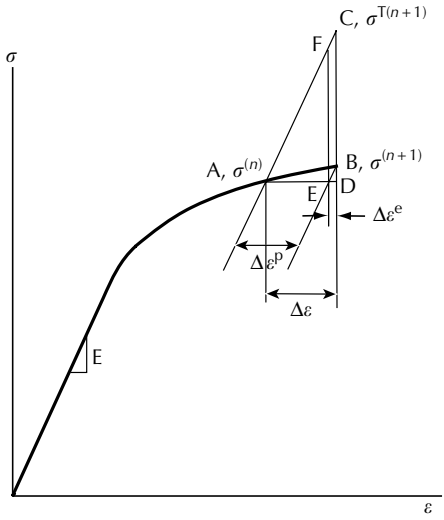

FIGURE 6.25
The return-mapping algorithm in one-dimensional stress.

for a strain increment $\Delta\varepsilon$. Starting from A, point C is the trial step known as the *elastic predictor*, its stress denoted by $\sigma^{T(n+1)}$. DC is obtained by multiplying the total strain increment $\Delta\varepsilon$ by the elastic modulus E. From the figure, we see that AE is the plastic strain increment $\Delta\varepsilon^p$ and ED is the elastic strain increment $\Delta\varepsilon^e$. BC is equal to EF, which is obtained by multiplying $\Delta\varepsilon^p$ by the elastic modulus E. BC is known as the *plastic corrector*. The stress increment DB = elastic predictor − plastic corrector = DC − BC.

In the multidimensional case, the algorithm is formulated below:
The elastic predictor is

$$\sigma_{ij}^{T(n+1)} = \sigma_{ij}^{(n)} + C_{ijkm}\Delta\varepsilon_{km}^{(n+1)} \tag{6.132}$$

and the plastic corrector is $C_{ijkm}\Delta\varepsilon_{km}^{p(n+1)}$, so that the stress at step $(n+1)$ is

$$\sigma_{ij}^{(n+1)} = \sigma_{ij}^{T(n+1)} - C_{ijkm}\Delta\varepsilon_{km}^{p(n+1)} = \sigma_{ij}^{(n)} + C_{ijkm}\Delta\varepsilon_{km}^{(n+1)} - C_{ijkm}\Delta\varepsilon_{km}^{p(n+1)} \tag{6.133}$$

Similar procedure should be applied to other variables of the model, such as the back stress to account for the evolution of that variable. Figure 6.26 illustrates this algorithm in the multidimensional stress space.

Let the yield surface at step (n) be

$$f\left(\sigma_{ij}^{(n)}, \kappa^{(n)}\right) = 0 \tag{6.134}$$

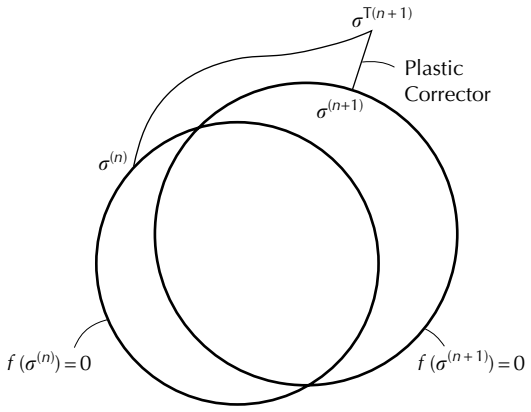

FIGURE 6.26
The return-mapping algorithm in the multidimensional stress space.

so that $\sigma_{ij}^{(n)}$ is on the yield surface. If $\sigma_{ij}^{(n+1)}$ is inside the surface, such that

$$f\left(\sigma_{ij}^{(n+1)}, \kappa^{(n)}\right) < 0 \tag{6.135}$$

then $\sigma_{ij}^{(n+1)}$ is in an elastic state where Hooke's law applies and $d\lambda = 0$. On the other hand, if $\sigma_{ij}^{(n+1)}$ is outside of the yield surface at step (n), such that

$$f\left(\sigma_{ij}^{(n+1)}, \kappa^{(n)}\right) > 0 \tag{6.136}$$

then, the return-mapping algorithm ensures that it is lying on the yield surface corresponding to step $(n+1)$, that is,

$$f\left(\sigma_{ij}^{(n+1)}, \kappa^{(n+1)}\right) = 0 \tag{6.137}$$

In this case, $d\lambda > 0$, which can be determined by substituting (6.133) and the flow rule into (6.137) and solving the resulting equation for $d\lambda$.

Additional information about the return-mapping algorithm may be found in Simo and Hughes [32]. It suffices to mention that, for associative plasticity with convex yield surfaces, the plastic corrector phase of the algorithm has the unique property that it yields the so-called closest point projection.

6.7 Combined Axial–Torsion of Strain-Hardening Materials

We consider a thin-walled tube made of strain-hardening metal. The coordinate system is chosen so that the radial direction is denoted by 1, the hoop

direction is 2, and the axial direction is 3. The Mises yield criterion will be used together with three cases of strain-hardening rule: the isotropic hardening, the kinematic hardening, and the combined isotropic–kinematic hardening. We will first derive the equations for axial tension and pure torsion, and then present, in Example 6.6, the case in which the tube is first subjected to torsion into the plastic range and then subjected to tension while holding the shear stress constant. This problem will be referred to as the *tor–ten stress path* in this book. We would like to find and compare the plastic strains developed due to this loading history using different strain-hardening rules.

The yield function is

$$f = \xi_{ij}^{\mathrm{D}} \xi_{ij}^{\mathrm{D}} - 2k^2 = 0 \qquad \text{with } \xi_{ij}^{\mathrm{D}} = \sigma'_{ij} - \alpha_{ij}^{\mathrm{D}} \tag{6.138}$$

where k is the shear yield stress which is related to the tensile yield stress by $Y = \sqrt{3}k$. α_{ij}^{D} is the deviatoric part of back stress α_{ij} and ξ_{ij}^{D} is the deviatoric part of ξ_{ij}. Using the isotropic–kinematic-hardening parameter β introduced in (6.83), the isotropic-hardening rule is

$$\mathrm{d}Y = \beta h \, \mathrm{d}\bar{\varepsilon}^{\mathrm{p}} \tag{6.139}$$

where $\mathrm{d}\bar{\varepsilon}^{\mathrm{p}}$ is the equivalent plastic strain increment defined by (6.60). The linear kinematic-hardening rule is

$$\mathrm{d}\alpha_{ij}^{\mathrm{D}} = \tfrac{2}{3}(1-\beta) h \, \mathrm{d}\varepsilon_{ij}^{\mathrm{p}} \tag{6.140}$$

and the flow rule is

$$\mathrm{d}\varepsilon_{ij}^{\mathrm{p}} = \mathrm{d}\lambda \, \xi_{ij}^{\mathrm{D}} \tag{6.141}$$

In the uniaxial tension, the deviatoric stress, plastic strain increment, and the deviator of the back stress are

$$[\sigma'] = \begin{bmatrix} \dfrac{-\sigma}{3} & 0 & 0 \\ 0 & \dfrac{-\sigma}{3} & 0 \\ 0 & 0 & \dfrac{2\sigma}{3} \end{bmatrix}, \qquad [\mathrm{d}\varepsilon^{\mathrm{p}}] = \begin{bmatrix} \dfrac{-\mathrm{d}\varepsilon^{\mathrm{p}}}{2} & 0 & 0 \\ 0 & \dfrac{-\mathrm{d}\varepsilon^{\mathrm{p}}}{2} & 0 \\ 0 & 0 & \mathrm{d}\varepsilon^{\mathrm{p}} \end{bmatrix},$$

$$[\alpha^{\mathrm{D}}] = \begin{bmatrix} \dfrac{-\alpha}{3} & 0 & 0 \\ 0 & \dfrac{-\alpha}{3} & 0 \\ 0 & 0 & \dfrac{2\alpha}{3} \end{bmatrix} \tag{6.142}$$

Substituting (6.142) into (6.138), we obtain

$$\sigma = Y + \alpha \tag{6.143}$$

In the case of uniaxial tension, we have from (6.60) and (6.142)

$$\mathrm{d}\bar{\varepsilon}^{\mathrm{p}} = \sqrt{\frac{2}{3}} \left\{ (\mathrm{d}\varepsilon^{\mathrm{p}})^2 + 2 \left(\frac{-\mathrm{d}\varepsilon^{\mathrm{p}}}{2} \right)^2 \right\}^{1/2} = \mathrm{d}\varepsilon^{\mathrm{p}} \tag{6.144}$$

Thus,

$$\mathrm{d}Y = \beta h \, \mathrm{d}\varepsilon^{\mathrm{p}} \tag{6.145}$$

Using (6.140) and (6.142), the 33 component equation is

$$\tfrac{2}{3}\mathrm{d}\alpha = \tfrac{2}{3}(1-\beta)h \, \mathrm{d}\varepsilon^{\mathrm{p}} \tag{6.146}$$

Therefore,

$$\mathrm{d}\alpha = (1-\beta)h \, \mathrm{d}\varepsilon^{\mathrm{p}} \tag{6.147}$$

Substituting (6.145) and (6.147) into the differential of (6.143), we obtain

$$\mathrm{d}\sigma = h \, \mathrm{d}\varepsilon^{\mathrm{p}} \tag{6.148}$$

This equation describes the tensile stress–strain curve for a linear-hardening material independent of the hardening rule.

In the torsion of the tube, the deviatoric stress, plastic strain increment, and the deviator of the back stress are

$$[\sigma'] = \begin{bmatrix} 0 & 0 & 0 \\ 0 & 0 & \tau \\ 0 & \tau & 0 \end{bmatrix}, \qquad [\mathrm{d}\varepsilon^{\mathrm{p}}] = \begin{bmatrix} 0 & 0 & 0 \\ 0 & 0 & \dfrac{\mathrm{d}\gamma^{\mathrm{p}}}{2} \\ 0 & \dfrac{\mathrm{d}\gamma^{\mathrm{p}}}{2} & 0 \end{bmatrix}, \qquad [\alpha^{\mathrm{D}}] = \begin{bmatrix} 0 & 0 & 0 \\ 0 & 0 & \alpha \\ 0 & \alpha & 0 \end{bmatrix} \tag{6.149}$$

Using (6.149), the yield function reduces to

$$\tau = k + \alpha \tag{6.150}$$

From (6.60) we have

$$\mathrm{d}\bar{\varepsilon}^{\mathrm{p}} = \frac{\mathrm{d}\gamma^{\mathrm{p}}}{\sqrt{3}} \tag{6.151}$$

and the isotropic-hardening rule is from (6.139)

$$dY = \beta h \frac{d\gamma^p}{\sqrt{3}} \quad \text{or} \quad dk = \frac{\beta h}{3} d\gamma^p \tag{6.152}$$

The 23 component equation of (6.140) is now

$$d\alpha = \tfrac{1}{3}(1-\beta)h\, d\gamma^p \tag{6.153}$$

The differential form of (6.150) is then obtained as

$$d\tau = \tfrac{1}{3} h\, d\gamma^p \tag{6.154}$$

This equation describes the shear stress–strain curve. We note that if the shear stress is $\sqrt{3}\tau$ and the shear strain is $d\gamma^p/\sqrt{3}$, then (6.154) and (6.148) have the same slope h.

EXAMPLE 6.6 Study the tor–ten stress path using the Mises yield criterion with hardening rules given by $\beta = 1$, 0, and 0.5.

Solution

We use the return-mapping algorithm in this calculation and consider a hypothetical material with shear modulus $\mu = 26.2$ GPa and the initial shear yield stress $k = 6.35$ MPa. In all three cases, that is, $\beta = 1$, 0, and 0.5, we obtain the same shear stress–strain curve shown in Figure 6.27. The slope of the tensile stress–strain curve is assumed to be $h = \mu/40$. The first phase of the tor–ten path is in pure torsion and the phase ends when the shear strain $\gamma = 0.01$ and the corresponding shear stress τ is 8.47 MPa. At this point, denoted by A in Figure 6.28(a) to (c), the current shear yield stress k is 8.46 MPa for $\beta = 1$, 6.35 MPa for $\beta = 0$, and 7.41 MPa for $\beta = 0.5$; the

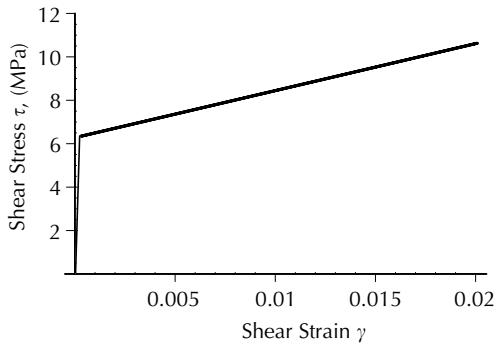

FIGURE 6.27
The shear stress–strain curve for Example 6.5.

equivalent plastic strain $\bar{\varepsilon}^p$ is 0.0056 for all three cases; and the shear back stress α_{23} is 0 for $\beta = 1$, 2.13 MPa for $\beta = 0$, and 1.47 MPa for $\beta = 0.5$.

During the second face of the stress path, AB, the shear stress is kept constant at $\sigma_{23} = 8.47$ MPa, while the axial strain ε increases. The corresponding axial stress σ_{33} will increase as ε increases. Point B in Figure 6.28(a) to (c) corresponds to $\varepsilon = 0.012$. The quantities $\sigma_{33}, \alpha_{33}, \alpha_{22}, \alpha_{23}, k, \bar{\varepsilon}^p$, and γ need to be updated, and $d\gamma^p$ and $d\varepsilon^p$ need to be calculated at each step. Several points along stress-path AB have been chosen for study. The corresponding

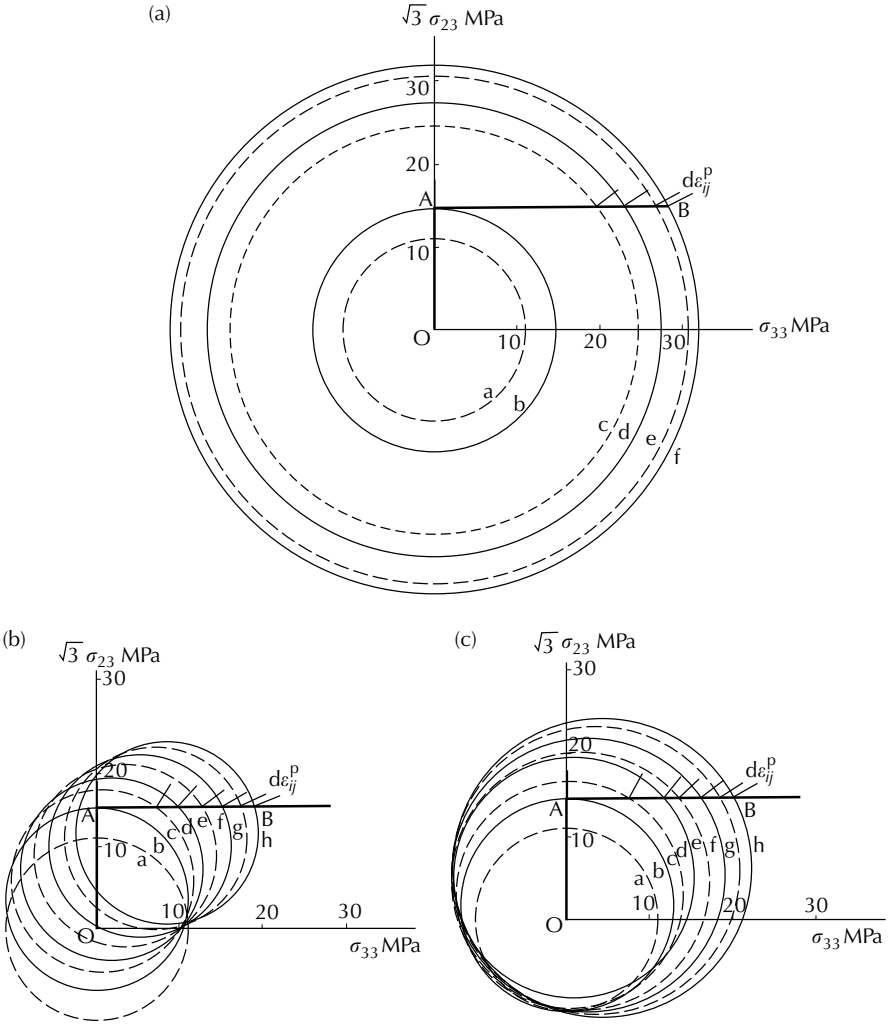

FIGURE 6.28
Tor–ten path showing evolutions of yield locus and direction of plastic strain increment for three hardening rules: (a) $\beta = 1$, (b) $\beta = 0$, and (c) $\beta = 0.5$.

TABLE 6.1

Yield Loci and Direction Angles of Plastic Strain Increments

	$\beta = 1$		$\beta = 0$		$\beta = 0.5$	
Yield locus	ε	θ (°)	ε	θ (°)	ε	θ (°)
f_b	0	90	0	90	0	90
f_c	0.001	37.5	0.001	58.3	0.001	61.4
f_d	0.005	32.9	0.0025	47.7	0.0025	51.1
f_e	0.01	28.5	0.005	36.9	0.005	43.3
f_f	0.012	26.9	0.0075	30.0	0.0075	37.2
f_g			0.01	24.8	0.01	32.7
f_h			0.012	22.0	0.012	29.5

yield loci f_a, f_b, f_c, etc. passing through these points are shown in the figures and are denoted by a, b, c, etc. The yield loci denoted by letter a are the initial yield loci in all three cases. Yield loci with corresponding ε values are listed in Table 6.1. It is clear from Figure 6.28(a) that the yield locus expands centering at the origin O for isotropic hardening. In the case of kinematic hardening, shown in Figure 6.28(b), the yield locus keeps the original size but moves while the tor–ten stress path is pursued. Figure 6.28(c) shows a case of combined isotropic–kinematic hardening with $\beta = 0.5$. In this case, the yield locus both expands and moves. The short inclined lines in the figures show the directions of $d\varepsilon_{ij}^{p}$ with components $((d\gamma^{p}/\sqrt{3}), d\varepsilon^{p})$. An angle

$$\theta = \frac{180}{\pi} \tan^{-1}\left[\frac{d\gamma^{p}/\sqrt{3}}{d\varepsilon^{p}}\right] \tag{a}$$

which is the inclined angle of $d\varepsilon_{ij}^{p}$ is defined. At the beginning of the stress path at A, $\theta = 90°$ for all three cases. In the case of $\beta = 1$, θ decreases to 37.5° at $\varepsilon = 0.001$ and continues to decrease as ε increases and $\theta = 26.9°$ at point B. In the case of $\beta = 0$, θ decreases to 58.3° at $\varepsilon = 0.001$ and continues to decrease as ε increases and $\theta = 22.0°$ at point B. In the case of $\beta = 0.5$, θ decreases to 61.4° at $\varepsilon = 0.001$ and continues to decrease as ε increases and $\theta = 29.5°$ at point B. These angles are listed in Table 6.1. In all cases the directions are normal to the corresponding yield loci. It is evident that different hardening rules lead to different plastic strains.

Figure 6.29 plots σ_{33} versus ε during the stress-path AB. It is seen that the three cases of strain-hardening lead to very different stresses. Isotropic hardening ($\beta = 1$) leads to the highest stress of the three cases. This effect can also been seen directly from Figure 6.28(a). The strain paths corresponding to stress-path AB are shown in Figure 6.30. The case of $\beta = 0.5$ leads to the highest shear strain. We know that the shear strain has started from the prestrain value of 0.01 during this tension phase. But, the increase in the shear

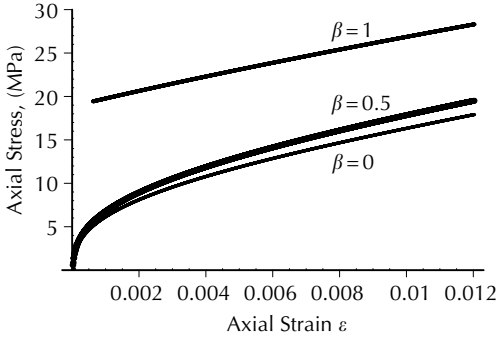

FIGURE 6.29
Axial stresses for tor–ten path.

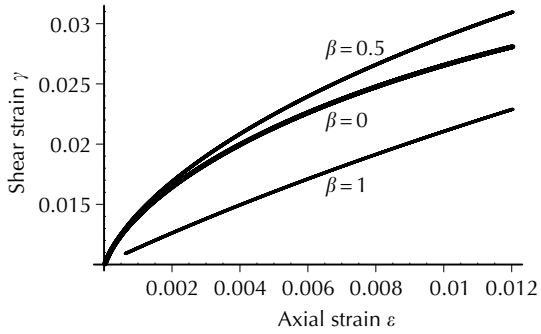

FIGURE 6.30
Strain paths for tor–ten path.

strain is still larger than the increase in the tensile strain for cases involving kinematic hardening and the increase is about the same as the increase in the axial strain for the isotropic-hardening case.

6.8 Flow Theory in the Strain Space

The flow theory of plasticity previously presented has been formulated in the stress space. The state of stress is represented by a point in this space and is sometimes referred to as the stress point. If this stress point is located within the yield surface, the material is in the elastic state; and if the stress point is on the yield surface, the material is in the plastic state. The yield surface is defined by a function of stress and other parameters, and the yield surface can expand, distort, or move in the stress space. When the material is in its plastic state, plastic flow occurs according to a flow rule, which defines the direction and magnitude of the plastic strain increment. Therefore, in this formulation, the stress is the independent variable and the plastic strain

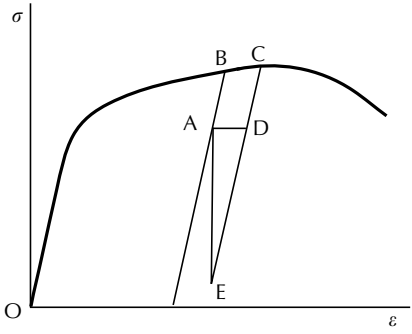

FIGURE 6.31
Stress–strain curve of a strain-softening material.

rate (or increment) is the dependent variable. This formulation of plasticity works well for metals and generally works well for strain-hardening materials defined in Drucker's sense, see Section 6.5.

Some materials, such as geotechnical materials (soils, concretes, rocks, ice, etc.) are strain-softening materials. The axial stress–strain curve for this type of materials has a positive slope initially. But, after it reaches a peak, the slope turns into negative. In the region of negative slope, plastic deformation continues with decreasing stress. Figure 6.31 shows a schematic stress–strain curve of a strain-softening material. The stability of strain-softening materials is defined by an *Ilyushin postulate* [33], which states that the work done by external forces on a material over a closed cycle of strain is positive. In this postulate, work is done over a *cycle of strain* rather than a cycle of stress as is in Drucker's postulate. Drucker's postulate is more restrictive than Ilyushin's postulate. Referring to Figure 6.31, Drucker's postulate says that area ABCDA is positive, but Ilyushin's postulate says that area ABCEA is positive.

Ilyushin used strain as an independent variable and stress was a response. He proposed a yield function in the strain space [34] but much of his effort was related to characterizing the stress response to a predetermined strain path. Ilyushin's work is further discussed in Chapter 7. A flow theory of plasticity expressed in the strain space was proposed by Naghdi and Trapp [35]. Casey and Naghdi [36] further showed that the stress space formulation is a special case of the strain space formulation. In the strain space formulation, the stress response is given by the constitutive equation

$$\sigma_{ij} = \sigma_{ij}(\varepsilon_{rs}, \varepsilon^{\mathrm{p}}_{rs}, \kappa) \tag{6.155}$$

where κ is the work-hardening parameter. At fixed values of $\varepsilon^{\mathrm{p}}_{ij}$ and κ, (6.155) may be inverted to obtain ε_{ij} as a function of σ_{ij}, $\varepsilon^{\mathrm{p}}_{ij}$, and κ. The yield function (or loading function) in the strain space is

$$g(\varepsilon_{ij}, \varepsilon^{\mathrm{p}}_{ij}, \kappa) = 0 \tag{6.156}$$

which corresponds to yield function

$$f(\sigma_{ij}, \varepsilon_{ij}^{\mathrm{p}}, \kappa) = 0 \tag{6.157}$$

in the stress space. The flow rule is

$$\dot{\varepsilon}_{ij}^{\mathrm{p}} = \lambda \rho_{ij} \frac{\partial g}{\partial \varepsilon_{rs}} \dot{\varepsilon}_{rs}, \qquad \text{if } g = 0 \quad \text{and} \quad \frac{\partial g}{\partial \varepsilon_{rs}} \dot{\varepsilon}_{rs} > 0 \tag{6.158}$$

where λ and ρ_{ij} are, respectively, a positive scalar-valued function and a nonzero symmetric tensor-valued function of ε_{ij}, $\varepsilon_{ij}^{\mathrm{p}}$, and κ. If the evolution of κ is

$$\dot{\kappa} = \beta_{ij} \dot{\varepsilon}_{ij}^{\mathrm{p}} \tag{6.159}$$

then, by use of the consistency condition, it may be shown that

$$\frac{(\partial f / \partial \sigma_{ij}) \dot{\sigma}_{ij}}{(\partial g / \partial \varepsilon_{rs}) \dot{\varepsilon}_{rs}} = 1 - \lambda \xi \frac{\partial f}{\partial \sigma_{ij}} \frac{\partial g}{\partial \varepsilon_{ij}} \tag{6.160}$$

where ξ is a nonnegative function of ε_{ij}, $\varepsilon_{ij}^{\mathrm{p}}$, and κ. It is seen from (6.160) that the loading conditions in the two spaces are not equal during loading. However, they are equal during unloading and neutral loading. Extensive experimental work has been carried out to determine yield surfaces in the stress space, which is discussed in Chapter 7. Little has been reported concerning experimental determination of yield surfaces in the strain space. But, according to Naghdi and his coworkers [35,36], the yield surface in the stress space can be transformed into the strain space.

6.9 Remarks

We have presented in this chapter the fundamental concept of the flow theory of plasticity. All main elements of the theory have been presented in their simplest forms. We have considered no distortion of the yield surface and the associated flow rule (with normality condition) is used in its simplest form. The isotropic hardening, the kinematic hardening, and the combined isotropic–kinematic hardening have been discussed together with a nonlinear rule of kinematic hardening. In a simplest multiaxial case, the case of combined axial–torsion presented in Section 6.7, we compare results of this simple flow theory using three hardening rules. We have shown that, using this simple model, all three hardening rules lead to the same results for uniaxial tension and pure torsion, but the results for combined axial–torsion vary greatly with the hardening rule assumed. The ultimate question is how

valid these results are. They show a wide range of differences, and apparently only one of them, or maybe none of them, are correct. In order to establish the validity of a model, the results need to be verified by experimental findings.

It is the purpose of Chapter 7 to discuss experiments aiming at providing experimental facts that can be used to verify, improve, and refine the theory of plasticity. We will discuss some recently formulated theories and also discuss ideas that extend the theory of plasticity into the finite strain range.

References

1. Taylor, G.I. and Quinney, H., The plastic distortion of metal, *Phil. Trans. Roy. Soc*. A. 230, 323, 1931.
2. Bertsch, P.K. and Findley, W.N., An experimental study of subsequent yield surfaces-corners, normality, Bauschinger effect and allied effects, *Proc. 4th U.S. Natl. Cong. Appl. Mech*., 893, 1962.
3. Mair, W.M. and Pugh, H.L.D., Effect of prestrain on yield surfaces in copper, *J. Mech. Eng. Sci*., 6, 150, 1964.
4. Phillips, A. and Tang, J.L., The effect of loading path on the yield surface at elevated temperatures, *Int. J. Solids Struct*., 8, 463, 1972.
5. Wu, H.C. and Yeh, W.C., On the experimental determination of yield surfaces and some results of annealed 304 stainless steel, *Int. J. Plasticity*, 7, 803, 1991.
6. Wu, H.C. and Ho, C.C., Strain-hardening of annealed 304 stainless steel by creep, *J. Eng. Mat. Tech*., 115, 345, 1993.
7. Ishikawa, H., Subsequent yield surface probed from its current center, *Int. J. Plasticity*, 13, 533, 1997.
8. Szczepinski, W., On the effect of plastic deformation on yield criterion, *Arch. Mech*., 15, 276, 1963.
9. Batdorf, S.B. and Budiansky, B.A., A mathematical theory of plasticity based on the concept of slip, *NACA*, TN 1871, 1949.
10. Lin, T.H., A proposed theory of plasticity based on slips, *Proc. Second U.S. Natl. Congress Appl. Mech*., 461, 1954.
11. Lin, T.H., On stress–strain relations based on slips, *Proc. Third U.S. Natl. Congress Appl. Mech*., 581, 1958.
12. Phillips, A., A review of quasistatic experimental plasticity and viscoplasticity, *Int. J. Plasticity*, 2, 315, 1986.
13. Mises, R. von, Mechanik der Fasten Korper im plastisch defomablen Zustand, *Göttingen Nachrichten, Math. Phys. Kl*., 581, 1913.
14. Tresca, H., On the flow of solid bodies subjected to high pressure, *C.R. Acad. Sci. Paris*, 59, 754, 1864.
15. Lode, W., Versuche über den Einfluss der mittleren Hauptspannung auf das Fliessen der Metalle, Eisen, Kupfer und Nickel, *Z. Phys*., 36, 913, 1926.
16. Hill, R., *The Mathematical Theory of Plasticity*, Clarendon Press, Oxford, 1950, 38.
17. Hundy, B.B. and Green, A.P., A determination of plastic stress–strain relations, *J. Mech. Phys. Solids*, 3, 16, 1954.
18. Lianis, G. and Ford, H., An experimental investigation of the yield criterion and the stress–strain law, *J. Mech. Phys. Solids*, 5, 215, 1957.

19. Phillips, A. and Moon, H., An experimental investigation concerning yield surfaces and loading surfaces, *Acta Mech.*, 27, 91, 1977.
20. Ohashi, Y., Kawashima, K., and Yokochi, T., Anisotropy due to plastic deformation of initially isotropic mild steel and its analytical formulation, *J. Mech. Phys. Solids*, 23, 277, 1975.
21. Drucker, D.C., A more fundamental approach to plastic stress–strain relations, in *Proc. 1st U.S. Natl. Congress Appl. Mech.*, ASME 487, 1951.
22. Bell, J.F., The experimental foundations of solid mechanics, *Handbuch der Physik*, Via/1, Flügge, Ed., Springer, Berlin, 1973.
23. Prager, W., The theory of plasticity: a survey of recent achievements (James Clayton Lecture), *Proc. Inst. Mech. Eng.*, 169, 41, 1955.
24. Hodge, Jr., P.G., Piecewise linear plasticity, *Proc. 9th Int. Congress. Appl. Mech.*, 8, 65, 1957.
25. Ziegler, H., A modification of Prager's hardening rule, *Quart. Appl. Math.*, 17, 55, 1959.
26. Armstrong, P.J. and Frederick, C.O., A mathematical representation of the multiaxial Bauschinger effect, G.E.G.B. Report RD/B/N 731, Berceley Nuclear Laboratories, 1966.
27. Valanis, K.C., A theory of viscoplasticity without a yield surface, *Arch. Mech.* 23, 517, 1971.
28. Wu, H.C. and Yang, R.J., Application of the improved endochronic theory of plasticity to loading with multi-axial strain-path, *Int. J. Non-Linear Mech.*, 18, 395, 1983.
29. Wu, H.C., Yang, C.C., and Chu, S.C., Further application of endochronic constitutive equation to loading with non-proportional axial–torsional strain-path, *Int. J. Non-Linear Mech.*, 20, 41, 1985.
30. Prager, W., Recent developments in the mathematical theory of plasticity, *J. Appl. Phys.*, 20, 235, 1949.
31. Drucker, D.C., A definition of stable inelastic material, *J. Appl. Mech.*, 26, 101, 1959.
32. Simo, J.C. and Hughes, T.J.R., *Computational Inelasticity*, Springer-Verlag, New York, 1998.
33. Ilyushin, A.A., On the postulate of plasticity, *PMM*, 25, 503, 1961.
34. Ilyushin, A.A., *Plasticity*, Izdat. Akad. Nauk. SSSR, Moscow, 196, 1963.
35. Naghdi, P.M. and Trapp, J.A., The significance of formulating plasticity theory with reference to loading surfaces in strain space, *Int. J. Eng. Sci.*, 13, 785, 1975.
36. Casey, J. and Naghdi, P.M., On the nonequivalence of the stress space and strain space formulations of plasticity theory, *J. Appl. Mech.*, 50, 350, 1983.

Problems

(1) A cylindrical specimen is loaded in tension from 0 to a stress of 500 MPa and has undergone a strain of 0.2 at this point. This point is denoted by A in Figure 6.32. Unloading then occurs following a curve as shown in the figure. Determine the yield point during unloading, if yield is defined by a proof strain of (a) 0.1%, (b) 0.5%, or (c) 1.0%. Assuming that the yield surface remains circular after prestrain in the two-dimensional principal stress space, sketch the yield

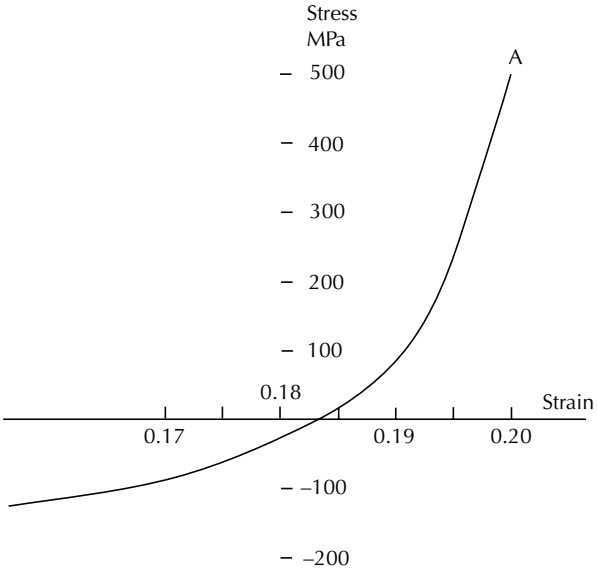

FIGURE 6.32
Figure for Problem 1.

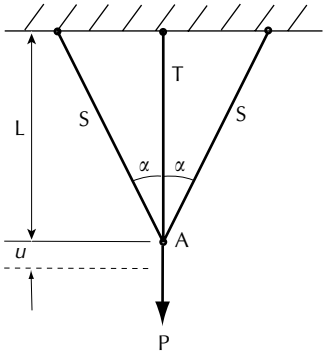

FIGURE 6.33
Figure for Problem 2.

surfaces corresponding this state of stress using the yield stresses previously determined based on different amounts of proof strain.

(2) Consider the three-bar truss shown in Figure 6.33. All bars have the same cross-sectional area A_0 and are made of an elastic-perfectly plastic material. Due to the application of force P, the displacement at A is u downward. Assume that the deformation is small so that $u/L \ll 1$. Determine displacement u, the stresses σ_T and σ_S in bars T and S, respectively, and the corresponding strains ε_T and ε_S, expressed in terms of $p = P/A_0$. Plot the p versus u/L diagram. (Hint: Consider the elastic phase, the end of the elastic phase when the first bar yields, the elastic–plastic phase, and the end of this second phase.)

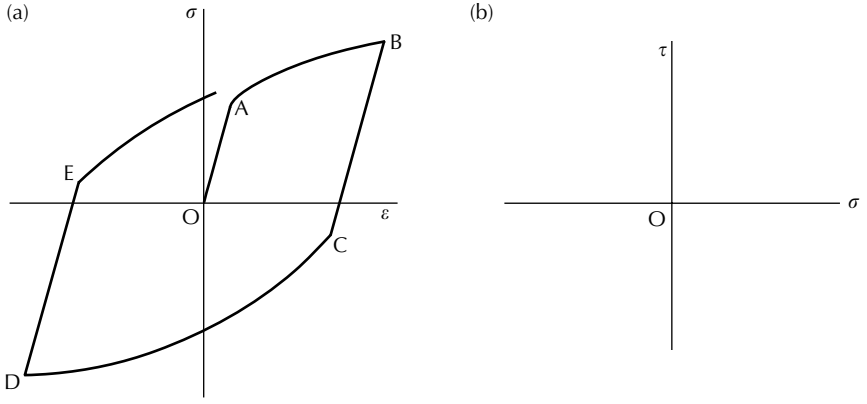

FIGURE 6.34
Figure for Problem 3.

(3) Figure 6.34(a) shows a sketch of uniaxial loading–unloading–reloading curve. Assume that the material obeys Mises yield criterion with kinematic hardening. Sketch in Figure 6.34(b) the yield surfaces that correspond to the stress states of A, B, C, D, and E. Figure 6.34(b) describes the shear versus axial stress space in the combined axial–torsion of a thin-walled tube.

(4) A long cylindrical pressure vessel is made of a metal with shear yield stress of $k = 560$ MPa and the maximum internal pressure during use is limited to 35 MPa. Considering the middle section of the vessel away from the ends, if no section of the vessel is to yield according to the Mises yield criterion, determine the required wall thickness if the outer radius is 600 mm.

(5) A closed-ended thin-walled tube is subjected to an axial tensile force F, which is less than F_0 necessary to cause yielding. Apply a gradually increasing internal pressure p and determine p expressed in terms of F when yielding occurs. Use Mises yield criterion and denote the wall thickness by t and the mean radius of the tube by r.

(6) A metal of yield stress $Y = 300$ MPa is subjected to a principal stress state of $(\sigma_1, \sigma_2 = -0.2\sigma_1, \sigma_3 = 0.5\sigma_1)$. If the stress ratios remain constant as the stresses increase, determine σ_1 at yielding using the Mises yield criterion.

(7) Derive (6.12).

(8) Derive (6.13).

(9) In a biaxial tension–compression test of perfectly-plastic material, (a) sketch the Mises yield locus, if $Y = 250$ MPa; find the components of the plastic strain increment at the loading point specified by (b) $\sigma_x = 250$ MPa and $\sigma_y = 250$ MPa; and (c) $\sigma_x = -100$ MPa and $\sigma_y = 184.52$ MPa.

(10) Find the expression of equivalent stress $\bar{\sigma} = \sqrt{3/2}\{\sigma'_{ij}\sigma'_{ij}\}^{1/2}$ in the case of uniaxial stress.

(11) Find the expression of equivalent plastic strain increment $\mathrm{d}\bar{\varepsilon}^{\mathrm{p}} = \sqrt{\frac{2}{3}}\{\mathrm{d}\varepsilon^{\mathrm{p}}_{ij}\mathrm{d}\varepsilon^{\mathrm{p}}_{ij}\}^{1/2}$ in the case of uniaxial tension.

(12) What is the definition of a convex function?

(13) If the yield function is $f = f(\sigma_{ij} - c(\kappa_1)\varepsilon^{\mathrm{p}}_{ij}) = \kappa_0$, where $\kappa_0 =$ constant and $\dot{\kappa}_1 = (\dot{\varepsilon}^{\mathrm{p}}_{km}\dot{\varepsilon}^{\mathrm{p}}_{km})^{1/2}$, assume that the normality condition holds, show that the flow rule is

$$\mathrm{d}\varepsilon^{\mathrm{p}}_{ij} = \frac{-(\partial f/\partial\sigma_{km})(\partial f/\partial\sigma_{ij})\mathrm{d}\sigma_{km}}{(\partial f/\partial\sigma_{rs})(\partial f/\partial\varepsilon^{\mathrm{p}}_{rs}) + [(\partial f/\partial\sigma_{\mathrm{rs}})(\partial f/\partial\sigma_{\mathrm{rs}})]^{1/2}(\partial f/\partial\kappa_1)}$$

(14) Using the equations of Problem (13), show that for Mises's yield criterion, the flow rule is

$$\mathrm{d}\varepsilon^{\mathrm{p}}_{ij} = \frac{(\partial f/\partial\sigma_{km})(\partial f/\partial\sigma_{ij})\mathrm{d}\sigma_{km}}{2c\kappa_0 + \sqrt{2\kappa_0}(\partial c/\partial\kappa_1)\varepsilon^{\mathrm{p}}_{\mathrm{rs}}(\partial f/\partial\sigma_{\mathrm{rs}})}$$

(15) In the case of uniaxial stress, show that the flow rule of Problem (14) reduces to $\mathrm{d}\sigma = E_t\mathrm{d}\varepsilon^{\mathrm{p}}$. Determine the expression of E_t.

7

Advances in Plasticity

7.1 Introduction

We discussed the basic concepts and formulation of plasticity in Chapter 6. With this knowledge we are ready to explore what other possibilities are there to improve the theory of plasticity. In fact, a great deal of work has been done since 1950 aiming to observe and understand plastic deformation and the mechanics of it. More realistic constitutive models have been proposed. While significant progress has been made, still more research work is desirable if the constitutive modeling of plastic deformation is to keep pace with the ever advancing technologies, methods, and equipment of computation. We are currently in a situation where high-powered computational mechanics is using concepts of plasticity that are basic and unsophisticated. The requirement for accuracy of the simulated results will go hand-in-hand with the requirements for safety, efficiency, and cost reduction such as reducing the wastes of manufacturing, as various related industries advance. The sophistication of constitutive modeling holds the key to this accuracy requirement. We would like to emphasize that the task of improving the constitutive modeling depends significantly on experimental findings. The experiments will guide the development of theories and theoretical investigation will in turn suggest new experimental conditions. In this chapter, we attempt to describe the state of the art in terms of the experiments which are carried out to improve constitutive modeling.

In the theoretical developments, two approaches have been taken by researchers: the traditional plasticity approach with its improvements and a *plastic strain trajectory approach*, in which the stress depends on the plastic strain trajectory. The traditional plasticity approach is stress-controlled. The stress is the input and the strain is the response. In this approach, we propose a yield function in the stress-space, a flow rule which is usually related to the stress and/or stress increment, and a strain-hardening rule with the back stress moving in the stress space. We discuss in this chapter some modern works belonging to this group. In the plastic strain trajectory approach, the plastic strain path is the input and the stress is found as a response. The relationship between the plastic strain trajectory and the stress is established

through a functional or a modulus, depending on whether the constitutive equation is in an integral form or in a differential form. The two forms are equivalent if the boundary conditions are specified. This approach, including the *endochronic theory* of plasticity by Valanis [1,2], is briefly described in this chapter. The endochronic theory, which has been derived from the thermomechanical theory of internal state variables, is fully discussed in Chapter 8.

We discuss in this chapter how a constitutive equation may be extended to the finite deformation range. The concept of material objectivity discussed in Chapter 4 must be applied. Appropriate stress and strain measures and their rates should be used. Finally, material texture will develop as plastic deformation proceeds, resulting in *material anisotropy*. How can the change of material texture be described at the phenomenological level? We attempt to provide research results which address the aforementioned questions.

7.2 Experimenal Determination of Yield Surfaces

The flow theory of plasticity is built upon the concept of yield surface, and therefore yield surface is by far the most important element of all the elements of the theory. We have already discounted Tresca's yield criterion in the Chapter 6 and concentrated on the Mises yield criterion. But how valid is the Mises yield criterion? Generally speaking, it is a good approximation for initial yield surface (see Section 6.2), although some deviations, such as those shown by Ohashi and Tokuda [3], have been reported. The evolution of the yield surface is of interest to many researchers. As was mentioned in Section 6.2, the size and shape of subsequent yield surfaces depend greatly on the definition of yield. The yield Surface C of Figure 6.3 determined by the method of backward extrapolation encloses a large elastic region which lies outside of Surfaces B and A. If we insist that the region inside the yield surface is elastic, then the strain is elastic at any point in this region if Surface C is considered as the yield surface. But the same point is outside Surfaces B and A, and therefore, referring to Surfaces B and A, plastic deformation would occur. Apparently, plastic strain is being neglected if Surface C is considered as the yield surface.

The quest for more accurate descriptions of the plastic behavior calls for a proportional limit (or small proof strain) definition of yield, and the challenge is to determine how the yield surface evolves when the material is subjected to various loading histories. These experiments determine the yield function and the back stress which is the center of the yield surface. These are two pieces of information that are central to the flow theory of plasticity. The study of *evolution of yield surface* has led to the improvements of the theory of plasticity. The effect of various definitions of yield on the size and shape of subsequent yield surfaces has been previously mentioned. Other factors that affect the determination of yield surface have been discussed by Wu and Yeh [4] and these factors are discussed next (following [4], with permission from Elsevier).

7.2.1 Factors Affecting the Determination of Yield Surface

Due to the availability of closed-loop, servo-controlled hydraulic testing machines with sophisticated computer-controlled circuits, it is even more appropriate than ever to discuss some of the factors affecting the determination of yield surface. In earlier test machines, either deadweight or mechanical, "experience" of the investigator was often an important factor in obtaining "reasonable" yield surfaces. With the use of a closed-loop test machine, the "experience" of an investigator can apply only before the beginning of a test or after a test has been completed and no in-between adjustment can be made during the test to smooth out the data. Therefore, it is likely that more data scatter is observed when a closed-loop machine is used, see Phillips and Lu [5]. These data represent more closely the experimental results in their raw form.

The definition of yield by means of a 5μ equivalent plastic strain has gained popularity in the recent literature. One of the reasons for the popularity is that the definition of yield of 5μ is close to that based on the proportional limit and, therefore, one specimen may be used to determine the initial and all of the subsequent yield surfaces. A strain of 5μ is, however, a very small strain measured by resistance strain gauges, and there are factors that affect the experiment and may cause a variation of several microstrains. Thus, 5μ is a very sensitive definition of yield and the resulting data scatter is to be expected. Even though the yield point is based on a proof strain of 5μ, it must be mentioned that the actual plastic strain incurred before a yield point can be confirmed is approximately 10μ. This amount depends on the technical details used by the investigator. The factors presented in the following subsections should be considered in connection with the determination of yield surfaces.

7.2.1.1 The elastic modulus and the zero offset strain

For an accurate determination of plastic strain, the "zero offset strain" as shown in Figure 7.1(a) and denoted by ε^{R} should be accounted for. In the figure, the circular dots represent acquired data for a one-dimensional stress–strain curve and the straight line is an approximation determined by the least mean-square method, using some selected data in the elastic region. Accordingly, the axial plastic strain, $\Delta\varepsilon^{\mathrm{P}}$, can be determined by

$$\Delta\varepsilon^{\mathrm{P}} = \varepsilon - \varepsilon^{\mathrm{R}} - \frac{\sigma}{E} \tag{7.1}$$

where ε is the axial strain; σ is the axial stress; E is Young's modulus, which is the slope of the straight line, and ε^{R} the zero offset strain. The quantity ε^{R} is measured by intersecting the straight line with the ε-axis and is therefore related to the value of E. Ideally, ε^{R} should be zero. However, due to the nature of the servo-controlled machine and the time interval of data acquisition, the data will scatter somewhat (exaggerated to show the effect) as shown in Figure 7.1(a). Therefore, some amount of ε^{R} is bound to be present.

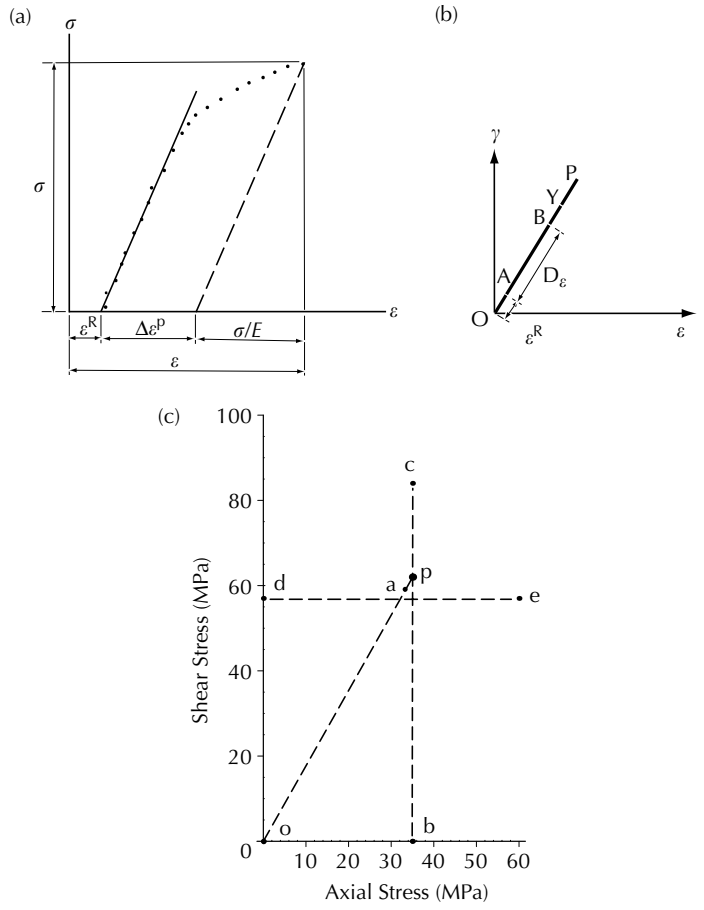

FIGURE 7.1
(a) Zero offset strain, (b) strain domain D_ε, (c) effect of probing path (From Wu, H.C. and Yeh, W.C., *Int. J. Plasticity*, 7, 803, 1991. With permission from Elsevier).

The accuracy and the numerical value of the elastic modulus are highly dependent upon the number of data points used in the least square analysis. A different number of data points leads to different values for the elastic modulus, and also leads to different initial zero offset strains. The zero offset strain is shown in (7.1) to affect the amount of proof strain. This effect is quite significant, especially when the proof strain is as small as 5μ.

In an effort to estimate the range of variation in the elastic modulus and the zero offset strain with respect to the number of data points used in the least square analysis, a *strain domain*, D_ε, is defined in the strain space and shown as $\overline{AB}$ in Figure 7.1(b). Data points lying between A and B are used in the least square analysis. All data points of this domain are within the elastic region. $\overline{OP}$ represents a probing path of proportional straining on which a

yield point Y is to be determined. Point O indicates the point from which the probe emanates, and it may differ from the strain-free origin in the case when subsequent yield surfaces are to be determined. Considering a pure torsion test, Wu and Yeh [4] found that ε^R varies up to 5μ when D_ε is $< 0.01\%$, but the variation is still 2 to 3μ even with $D_\varepsilon > 0.01\%$. This amount of variation is large indeed when the definition of yield is set at 5μ.

Adding to the complication is the fact that the slope of elastic loading associated with probes of different paths may be slightly different from one another. This was experimentally verified by Ivey [6] and Wu and Yang [7]. Ivey reported that when a specimen of 2024-T4 aluminum was subjected to prestrain in tension followed by a pure torsion while keeping the tensile strain constant, the shear modulus varies by an amount depending upon the magnitude of the prestrain in tension. Wu and Yang found that, for a one-dimensional tension–compression test, the slope of the unloading curve at various strain was not quite the same levels for both 6061-T6 aluminum and 4142 steel. Thus, the elastic modulus and the zero offset strain ε^R vary from one probe to the other, and their magnitudes should be determined for each path. However, this is usually not practical and not accounted for in the experiments. Therefore, this effect contributes to the data scatter of yield surfaces.

7.2.1.2 The effect of strain domain on the yield stress

As the elastic modulus and the zero offset strain are affected by D_ε, the equivalent plastic strain is affected through an equation similar to (7.1). Consequently, the yield stress thus determined is also affected. The yield stress determined in the previously mentioned pure torsion test with varied D_ε but a constant R_ε of 0.01% shows severe fluctuations when the strain domain D_ε is very small, and it becomes steady when D_ε is greater than approximately 0.01%.

7.2.1.3 The effect of probing path

In order to minimize the effect of probes, consecutive probes are chosen not to be on the same side of the yield surface. Yet, the effect of probes is still significant in that radial and nonradial probing paths do not lead to consistent yield points. This assertion is substantiated by the results of an experiment involving strain paths oa, obc, and ode illustrated by Figure 7.1(c). In the radial probe oa, the yield point was determined at "a" and any point beyond this point is in the postyielding state. Consequently, the point "p" of the line "bc" is considered to be in a yielded state. However, as judged by the probe of nonradial path obc, this particular point "p" was still in the elastic region. Point "c" was the yield point for this path. The yield point of path ode was determined to be at e. Figure 7.1(c) has thus demonstrated the probing path dependence of the yield point when it is determined by a small proof strain of 5μ.

7.2.1.4 The effect of strain rate in probing

It is known that some metallic materials exhibit significant strain-rate effect even at room temperature, as mentioned in Section 5.2.4. The experimental constant strain-rate stress–strain curves show that stresses at different strain rates are significantly unequal only in the postyielded range and thus a large offset strain definition of yield would lead to a yield stress which is quite strain-rate dependent. However, a rather weak rate sensitivity is evident when a small proof strain is used. It is thus reasonable to assume that for a proof strain as small as 5μ, the strain-rate effect in the probing is negligible. A similar conclusion was drawn by Ellis et al. [8] in connection with their testing of 316 stainless steel. For the range of probing rate (100 to 500 $\mu\varepsilon$/min) used, the writers concluded that the probing rate had little effect on yield behavior and that the difference in size and position of the yield surfaces they determined was more related to the sequence in which the yield surfaces were determined rather than the probing rate.

7.2.2 A Summary of Experiments Related to the Determination of Yield Surfaces

Extensive literature is available on the issue of experimental determination of yield surfaces, with prestrains (i.e., specimen subjected to strain before a yield surface is determined) within the strain range (2% or less) of an electrical-resistance strain gauge. The experimental works described here were carried out at room temperature. Most experiments were conducted using thin-walled tubes subjected to combined tension and torsion. This group includes Taylor and Quinney [9], Naghdi et al. [10], and Ivey [6] with prestrain in torsion; McComb [11] with prestrain in tension; Mair and Pugh [12] with prestrain in tension, partially unloaded and then strained in torsion; Bertsch and Findley [13] with zigzag paths in small steps; Phillips and Moon [14], Phillips and Lu [5], Shiratori et al. [15], and Ishikawa [16] with various prestrain histories; Wu and Yeh [4] with proportional paths of loading-unloading-reloading-cyclic steady state. Experiments were conducted by Lode [17] and Hu and Bratt [18] using thin-walled tubes subjected to tension and internal pressure. Plate specimens were used by Szczepinski [19], Szczepinski and Miastkowski [20], and Shiratori and Ikegami [21].

The experimental results generally confirmed that the initial yield surface is closed to the Mises ellipse and the subsequent yield surfaces are obtained from the expansion in size, the motion, and distortion of the Mises ellipse. If the yielding is defined using a small (5 to 10μ) proof strain, then the size of the ellipse does not change, that is, no cross effect has been observed. The discussion in this section is devoted to the effect of loading path on the yield surface, which includes the stress-controlled path and the strain-controlled path. The path may be linear or nonlinear, and a proportional strain path may not lead to a proportional stress path depending on material tested.

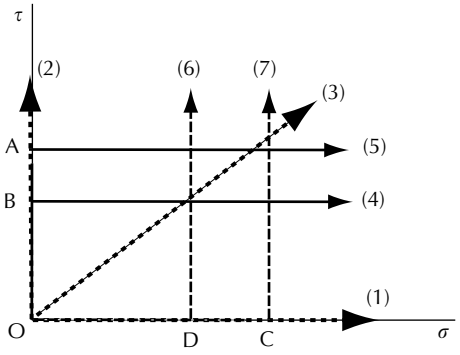

FIGURE 7.2
Loading paths for combined axial–torsion.

7.2.2.1 Proportional path

The proportional path includes monotonic axial loading, path (1) of Figure 7.2, monotonic torsion loading, path (2), and proportional combined tension and torsion, path (3). Most early works reported in the literature were conducted using load-control machines and were therefore controlling the stress path. Servo-controlled hydraulic test machines have been used in more recent works and stress- or strain-controlled tests are possible. Both cases (i.e., stress- or strain-control) lead to the same result for monotonic axial loading and monotonic torsion in the small strain range. Phillips and Tang [22], Ishikawa [16], and most experiments reported in the literature used a prestress path. Wu and Yeh [4] used prestrain paths for monotonic axial and monotonic torsion prestrains, but a prestress path for a combined tension and torsion proportional loading. A conclusion arrived at from all available experimental data is that the yield surface undergoes kinematic hardening along the direction of loading and gets distorted with the "flattened rear part" of the yield surface facing the origin of the stress space. The extent of kinematic hardening and the amount of isotropic hardening depend upon the material tested and upon the definition yield. Thus, if plotted in the $\sqrt{3}\tau$ versus σ space, where τ is the shear stress and σ the axial stress, the initial yield surface for an initially isotropic material is a circle and the subsequent yield surfaces can be approximately described by flattened ellipses. In a combined tension–torsion proportional loading, the initial yield surface, which is a circle, will gradually become distorted as the prestrain increases, with the flattened ellipse facing the origin of the stress space. Note that this flattened ellipse is a result of distortion and not a rotation of the yield surface. In fact, it is fair to say that no rotation of yield surface occurs during proportional loading. Subsequent yield surfaces with proportional prestrains are shown schematically in Figure 7.3. We note that some subsequent yield surfaces in the literature show a "rounded nose" in the direction of prestressing but a flat rear on the side opposite to the prestress (see the solid curves), but some reported experimental yield surfaces do not

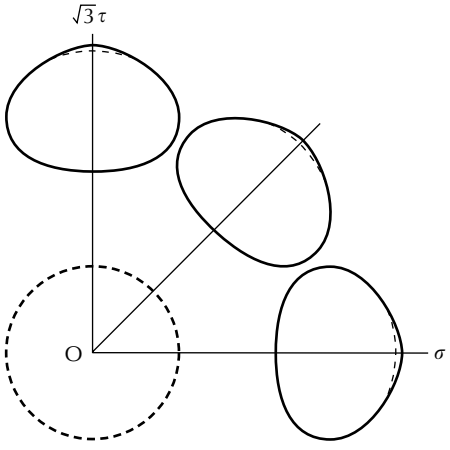

FIGURE 7.3
Subsequent yield surfaces with proportional prestrain.

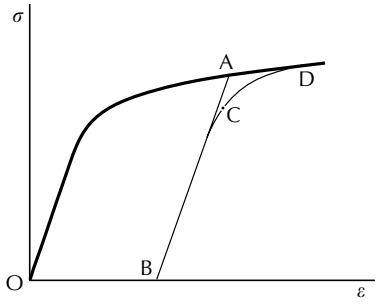

FIGURE 7.4
Loading point and yield point.

show these characteristics (see the dashed curves). The reason for differences is related to the point picked as the yield point when reloading takes place in the yield surface probing. Referring to Figure 7.4, the material is first loaded from O to A, which moves the yield surface to its current state. Partial unloading from A to B would put the stress point at the center of the current yield surface. BCD represents the probing of the current yield surface and C is the yield point. If point A, which is known as the loading point is considered a point on the yield surface, then the yield surface will show a rounded nose. On the other hand, if C is considered a point on the yield surface, then the yield surface does not show a rounded nose. Some authors [14] distinguish between these two points and consider the ideas of loading surface and yield surface. But most experimental results found in the literature do not make this distinction.

In the case of combined axial–torsion, only three papers have reported test results on proportional loading into the large strain range and they are discussed here. Helling et al. [23] conducted stress-controlled tests on several

materials and obtained data showing the evolution of yield surface up to a shear prestrain of $\gamma/\sqrt{3} = 0.32$ under torsion, path (2) of Figure 7.2. The paper did not specify whether they were free- or fixed-end torsion tests. But since the authors did not report the axial stress during the torsion test, one can assume that the tests were conducted under the free-end torsion condition. The results are similar to those obtained in the small strain range, except that isotropic hardening is significant for some materials. The paper did not discuss path (1) — monotonic axial preloading — but it did report a case of proportional loading, path (3), with a result similar to those observed in small strain. The flattened ellipse was facing the origin of the stress space. However, this case was conducted with an effective prestrain of only 5%, which is small.

Wu et al. [24] tested annealed 304 stainless steel and determined the initial and subsequent yield surfaces for two loading paths. Path (1) in axial loading had an axial prestrain of 20% and path (2) in free-end torsion had a shear prestrain of 20%. Experimental results showed that both the forward and rear parts deflated as the loading proceeded. These results contradict what is known at the small strain level, where the forward part inflates. In addition, for a prestrain of only 20%, the cross effect is very significant for the material tested. This cross effect was not apparent in the work of Wu and Yeh [4] for the same material at small strain level.

The experiments reported in Wu [25] provide another set of test data related to the evolution of yield surface with large prestrains. In the experimental determination of subsequent yield surfaces, a major difficulty is that strain gauges used to probe the previous yield surface are no longer functional when subsequent prestrain for the next yield surface exceeds 2%. Since the same specimen is used to determine several subsequent yield surfaces, the sum of all preloading (or prestrains) is the prestrain before next yield surface probing. The method used to overcome this difficulty was to unload the specimen after the specimen had been subjected to a predetermined amount of prestrain. The specimen was then removed from the test machine and new strain gauges were installed and cured. The specimen was then mounted again on the test machine and gradually loaded to merge with the stress–strain curve of prestraining, monitored by an axial–torsional extensometer designed and built by Wu and Xu [26]. At this point, a subsequent yield surface was probed using the newly installed strain gauges. The same method was used to determine other subsequent yield surfaces.

Experiments were conducted for path (1) up to an axial prestrain of $\varepsilon = 0.45$ and for path (2) up to a shear prestrain of $\gamma = 0.4$. The test for path (2) was conducted under the free-end torsion condition. Note remarked that the test data for both paths (1) and (2) enable the determination of a complete set of parameters that can be used to calculate the combined axial–torsion response of the tube.

Owing to prestrains into the finite deformation range, the expansion (or contraction) of yield surfaces is significant for the materials tested by Helling et al. [23], Wu et al. [24], and Wu [25], even though yield was determined by a proof strain of 5μ.

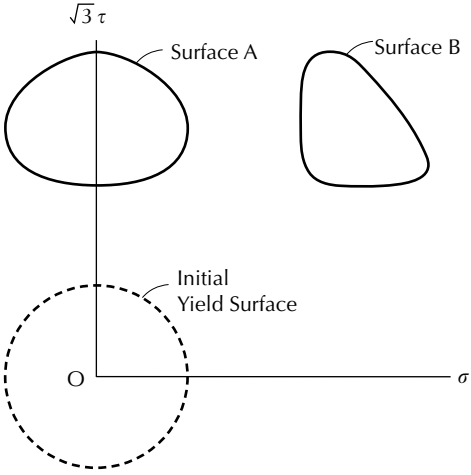

FIGURE 7.5
Evolution of yield surface for tor–ten path (4).

7.2.2.2 Stress-controlled torsion–tension path

Two stress-controlled torsion–tension paths (tor–ten for short) are meaningful. These paths are illustrated in Figure 7.2. Path (4) denotes a path with pretorsion from O to A, followed by an elastic unloading to an approximated center of the current yield surface at B. Axial loading is then applied, keeping the shear stress constant at the value of τ_B. Path (5) denotes a path with pretorsion from O to A, followed by an axial loading while keeping the shear stress constant at the value of τ_A.

The tor–ten path (4) has been investigated by several investigators, including Phillips and Tang [22], Shiratori et al. [15], Ishikawa [16], and Helling et al. [23]. Figure 7.5 shows schematically the evolution of the yield surface for tor–ten path (4). Test results show that the yield surface (Surface A) at the end of the pretorsion stage serves as the basis for the subsequent yield surfaces (Surface B) generated by tension. The surface flattens without rotation as the axial stress increases. All results have been obtained in the small strain range, including the tests of Helling et al. [23] for this case. No experimental data for the large strain range has been found in the literature for this test.

Tor–ten path (5) has been investigated by Helling et al. [23]. The data have been obtained for tests up to a total prestrain (torsion and tension) of only 5%. Test results shows a rotation of yield surface as the axial stress increases. The yield surfaces of path (5) are shown schematically in Figure 7.6. Surface A denotes the yield surface at the end of the pretorsion stage and Surface B the yield surface after tensile stressing has been applied.

7.2.2.3 Stress-controlled tension–torsion path

The stress-controlled tension–torsion paths are the counter part of the stress-controlled tor–ten paths. Results should be similar in nature to those discussed

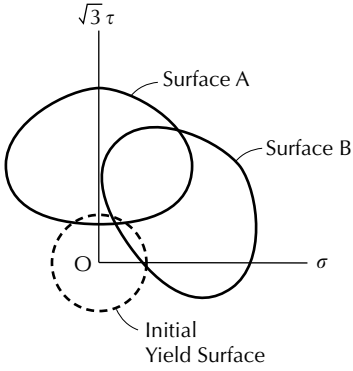

FIGURE 7.6
Evolution of yield surface for tor–ten path (5) (From Helling, D.E. et al., *J. Eng. Mater. Technol.*, 108, 313, 1986. With permission from ASME).

in Section 7.2.2.2. There are two cases: path (6) denotes a path with pretension from O to C (see Figure 7.2), followed by an elastic unloading to an approximated center of the current yield surface at D. Torsion loading is then applied while keeping the axial stress constant at the value of σ_D. Path (7) denotes a path with pretension from O to C, followed by a torsion loading while keeping the axial stress constant at the value of σ_C. Path (6) has been investigated by several investigators, including Phillips and Tang [22], Shiratori et al. [15], and Ishikawa [16], and path (7) has been investigated by Helling et al. [23]. These investigations have all been conducted with prestrains in the small strain range.

7.2.2.4 Other paths

Experiments have been conducted following other stress-controlled paths and some with unloading and cyclic loading. However, the investigators were interested in other aspects of plastic behaviors and no information about the corresponding yield surfaces was reported. The investigations associated with the variation of plastic strain increment along a stress path will be discussed in the next section, related to the experimental investigation of the flow rule.

Strain-controlled loading paths have been used by several investigators to investigate the stresses arisen from the strain-path. The purpose of these experiments was to determine the relationship between stress components and the given plastic strain increment and was not related to the determination of yield surface. These experiments will be discussed in Section 7.5.

7.2.3 Yield Surface Versus Loading Surface

Based on experimental observations, Phillips and his coworkers proposed the idea of loading surface. A description of two-surface theory may be found in

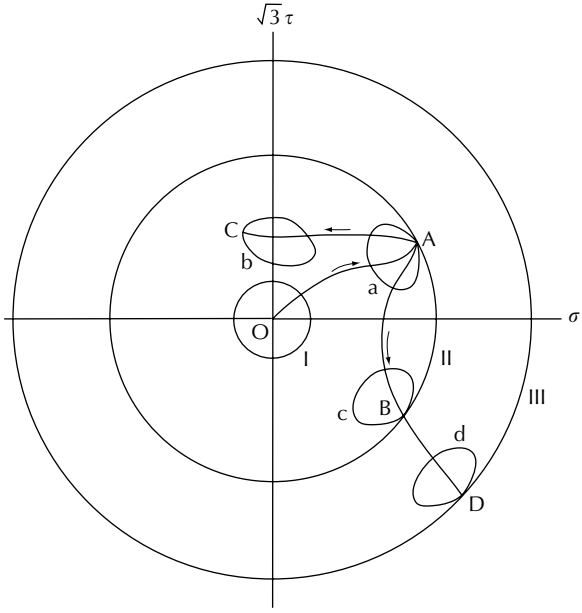

FIGURE 7.7
Motion of yield surface and the loading surface (From Phillips, A., *Int. J. Plasticity*, 2, 315, 1986. With permission from Elsevier).

Phillips [27]. The main concept that is different from the traditional concept of plasticity is to consider plastic flow as rate dependent. Plastic strain takes time to develop and the existence of an equilibrium stress is postulated at which plastic strain is fully developed, see Wu [28], Phillips and Wu [29], Phillips [30], and Krempl [31].

A loading surface represents the largest state of stress achieved in the loading history, and it expands isotropically upon loading. Figure 7.7 shows the motion of the yield surface and the loading surface in the stress space. The yield surface tends to become tangential to the loading surface when it moves towards the loading surface. But, when the stressing point penetrates the loading surface, it will drag the loading surface with it and the loading surface expands. Referring to Figure 7.7, the initial yield surface which is also the initial loading surface is denoted by I. A stress path from O to A will cause the loading surface to expand to the surface labeled as II, and a stress path AD will cause the loading surface to expand further to Surface III. On the other hand, stress path AC does not cause the loading surface to expand because path AC does not penetrate the corresponding loading surface, Surface II.

Surfaces labeled as a, b, c, and d are yield surfaces. Since plastic strain takes time to develop, the experimentally determined yield surface after path OA is Surface a only after the stressing point has stayed at A for a sufficient length of time. If the prestress point does not stay at A for a sufficient length of time before the yield surface is probed, then the obtained yield surface will

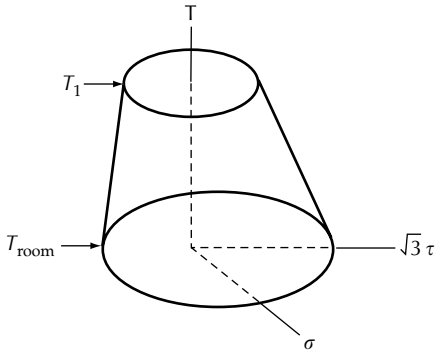

FIGURE 7.8
Yield Surface in the stress–temperature space (From Phillips, A., *Int. J. Plasticity*, 2, 315, 1986. With permission from Elsevier).

be a distance away from the loading surface and does not touch the loading surface.

7.2.4 Yield Surface at Elevated Temperature

Phillips and his coworkers [32–35] conducted a series of experiments and determined yield surfaces at elevated temperatures which were lower than $0.3T_m$, where T_m is the absolute melting temperature of the material. Thin-walled tubes of 1100-0 aluminum were tested. The yield surface in the stress–temperature space is shown schematically in Figure 7.8, where the surface is depicted between two constant temperatures T_1 and T_{room} with $T_1 > T_{room}$. An isothermal yield surface may be obtained by passing a plane normal to the temperature axis. The yield surface (the isotherm) shrinks as the temperature increases. The yield surface is actually a conoid with a ridge at the top. The length of the ridge depends on the prestrain history, measured by equivalent plastic strain. The initial yield surface is a cone with an elliptical base. The length of the ridge is zero because the equivalent plastic strain is zero. As the equivalent plastic strain increases with the prestraining history, the length of the ridge also increases with a narrower width for the corresponding isothermal yield surfaces. A ridge is formed when the width of the isothermal yield surface at the top is zero. The ridge is perpendicular to the direction of preloading. For each value of equivalent plastic strain, there corresponds a temperature T_{max} which defines the height of the conoid with a ridge at the top. The temperature T_{max} decreases with the increasing equivalent plastic strain. Finally, we mention that the distortion and motion of the yield surface can occur either by an increment of loading history or by a temperature increment or by a combination of the two. Figure 7.9 shows a case of initial and subsequent isothermal yield surfaces determined by Phillips and Tang [22] at 21, 66, 108, and 152°C (70, 151, 227, and 305°F) due to prestress in tension.

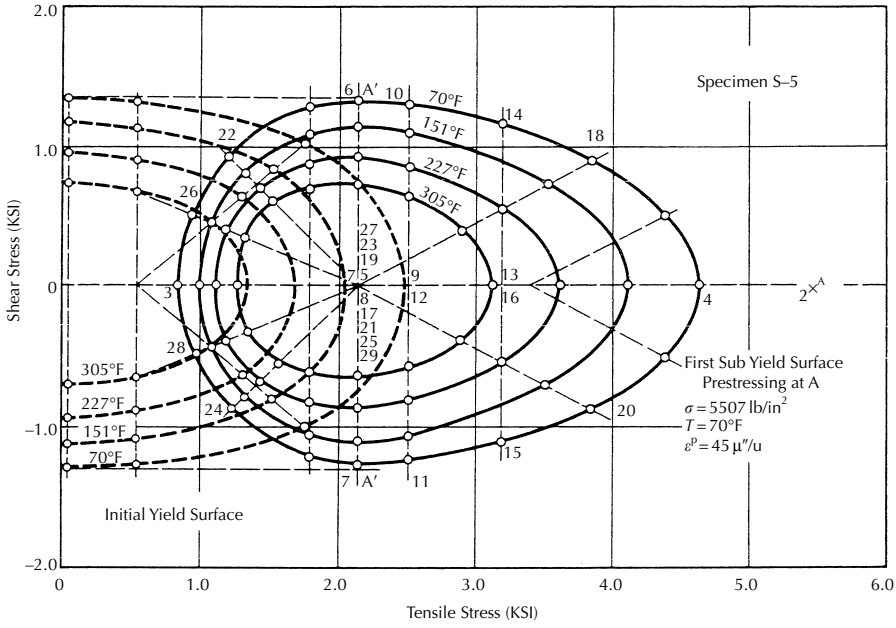

FIGURE 7.9
A case of initial and subsequent isothermal yield surfaces (From Phillips, A. and Tang, J.L., *Int. J. Solids Struct.*, 8, 463, 1972. With permission from Elsevier).

7.3 The Direction of the Plastic Strain Increment

It was mentioned in Section 6.3 that an important assumption concerning the plastic strain increment $d\varepsilon_{ij}^{p}$ is that the principal axes of plastic strain increment and deviatoric stress are coincident, which is known as the normality rule and which says that $d\varepsilon_{ij}^{p}$ is normal to the yield surface. It was also mentioned that this assumption has been experimentally verified. But, it is to be emphasized here that those verifications were valid for initial yield surface only. The following question remains: Is $d\varepsilon_{ij}^{p}$ normal to the subsequent yield surface? A direct answer can be found from the works of Phillips and Moon [14] and Ohashi et al. [36] who showed that the plastic strain increment is indeed normal to the subsequent yield surfaces.

Figure 4 of Phillips and Moon [14] is reproduced as Figure 7.10. In the figure, the initial yield surface is labeled as 0 and the first prestressing path is OA. The yield surface corresponding to A is labeled as I. In this discussion, we do not emphasize the difference between a loading surface and a yield surface as the writers did. The next stage of stressing went from B to C in tension. Path BC is nearly tangential to the first subsequent yield Surface I. The second subsequent yield surface labeled as II was then determined. This surface

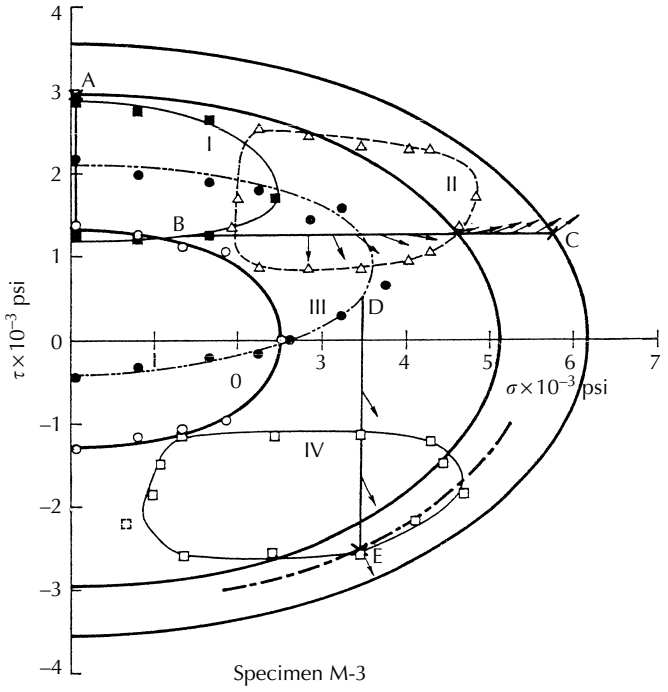

FIGURE 7.10
Plastic strain increment vector (From Phillips, A. and Moon, H., *Acta Mech.*, 27, 91, 1977. With permission from Springer).

shows further distortion from the previous surface and it translated not only in the direction of prestressing but also by a small amount in the direction perpendicular to the prestressing direction. Owing to the distortion, it is difficult to judge whether rotation had taken place in yield Surface II. The directions of $d\varepsilon_{ij}^{p}$ along path BC are also shown in the figure. These directions rotated from the direction normal to the yield surface from which the prestressing was initiated to the direction normal to the final yield surface. We note that this stress path is similar to tor–ten path (5) discussed in Section 7.2.2.2. The second stage of both paths is tangential to the yield surface. The only difference is that the path of Phillips and Moon started from the opposite side of the first subsequent yield surface, while path (5) starts from the prestress point A. Another stress, similar in nature, is shown in Figure 7.10. Starting from the yield surface labeled as III, stress path DE was applied. This stress path was again nearly tangential to the yield surface. At the end of the stressing, a yield surface was determined and labeled as IV. A distortion of yield surface had taken place and the surface had moved not only in the direction of prestressing but also in the lateral direction. Owing to the distortion, it is difficult to judge whether the yield surface had rotated. Small vectors in the figure show the variations in the direction of $d\varepsilon_{ij}^{p}$.

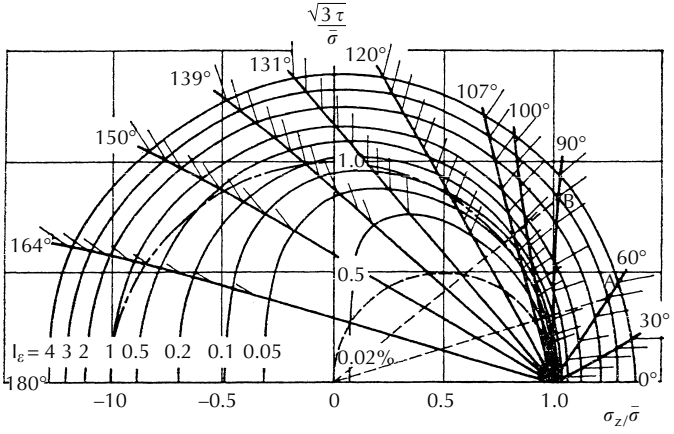

FIGURE 7.11
Plastic strain increment vector (From Ohasi, Y. et al., *J. Mech. Phys. Solids*, 23, 277, 1975. With permission from Elsevier).

Ohashi et al. [36] prestressed a tubular specimen in tension (first stress path) to a tensile stress of $\sigma_z/\bar{\sigma} = 1.0$, where $\bar{\sigma} = 235$ MPa. The corresponding prestrain at this point was 2%. A second stress path was then applied in combined axial–torsion, emanating from the prestress point making an angle θ with the first stress path. Figure 3 of Ohashi et al. [36] is shown as Figure 7.11, in which $\theta = 0$, 30, 60, 90, 100, 107, 120, 131, 139, 150, 164, and 180°. The strain data along each stress path were recorded and the equi-strain curves based on $I_\varepsilon = \{(\varepsilon^p)^2 + (\gamma^p/\sqrt{3})^2\}^{1/2}$ and corresponding to $I_\varepsilon = 0.02\%$, 0.05%, 0.1%, 0.2%, 0.5%, and 1%, 2%, 3%, and 4% are found and shown in the figure. These curves are similar to subsequent yield surfaces determined by the use of different amounts of proof strains, and these are yield surfaces corresponding to the prestress point at $\sigma_z/\bar{\sigma} = 1.0$. The short segments on the second stress path for each θ show the directions of the plastic strain increment vector $(\gamma^p/\sqrt{3}, \varepsilon^p)$. Ohashi et al. [36] found that the plastic strain increment vector is almost normal to the equi-strain curves, except for the range of $I_\varepsilon \leq 0.05\%$ and $139° < \theta < 164°$.

Other investigations of the plastic strain increment did not report the yield surfaces along the stress paths and therefore the information provided is not complete enough to directly benefit the constitutive modeling. Nevertheless, these works are useful in that they can provide qualitative results for certain observed behaviors of materials. Phillips and Kaechele [37] conducted stress-controlled tests on thin-walled tubes of aluminum 2S-O following tor–ten path (5) and ten–tor path (7). The tests were conducted in a strain range up to 1.5%. The stress paths are shown schematically in Figure 7.12 in the $(\sqrt{3}\tau, \sigma)$ space. The short segments on the stress paths show the directions of the plastic strain increment vector $(\gamma^p/\sqrt{3}, \varepsilon^p)$. For tor–ten path (5), the plastic strain increment was along the shear direction before a sudden change of direction

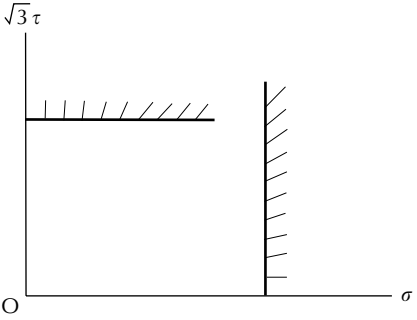

FIGURE 7.12
Plastic strain increment vector (From Phillips, A. and Kaechele, L., *J. Appl. Mech.*, 23, 43, 1956).

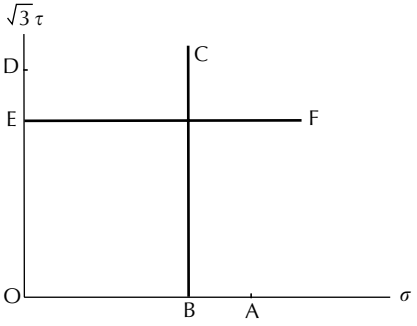

FIGURE 7.13
Stress paths of Khan and Wang (From Khan, A.S. and Wang, X., *J. Mech. Phys. Solids*, 36, 519, 1988. With permission).

took place in the stress path. The direction of the plastic strain increment gradually changes afterward. In the case of ten–tor path (7), the plastic strain increment was initially along the tension direction and the direction gradually changes after the change in direction of the stress path.

Khan and Wang [38] conducted combined axial–torsion tests on OHFC copper, following two stress paths shown in Figure 7.13. In path OABC, the specimen was first stressed in tension to A into the plastic region. Partial unloading and reverse loading then took place from A to B while keeping the shear stress zero. Finally, torsion was increased from B to C while keeping the axial stress constant. In path ODEF, the specimen was subjected to shear stress from O to D, unloading from D to E, and then loading from E to F. The two paths are similar in nature. The corresponding strain paths are shown schematically in Figure 7.14. From the figure we see that during segment BC of path OABC, the increment of axial strain ε changes from negative to positive as the shear stress increases while keeping the axial stress σ constant. Similarly, during segment EF of path ODEF, the increment of shear strain γ changes from negative to positive as the axial stress increases while keeping

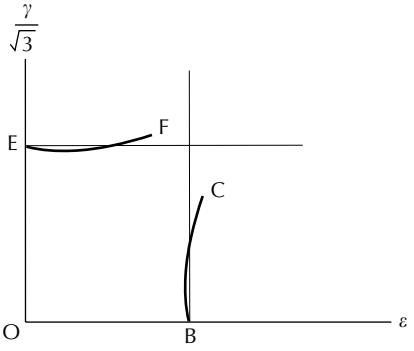

FIGURE 7.14
The corresponding strain paths of Khan and Wang (From Khan, A.S. and Wang, X., *J. Mech. Phys. Solids*, 36, 519, 1988. With permission).

the shear stress τ constant. The curves have been exaggerated to show the sign change in $d\varepsilon$ and $d\gamma$.

7.4 Multisurface Models of Flow Plasticity

It was mentioned in Section 7.2.3 that Phillips [27] proposed a multisurface model in which the yield surfaces are bounded by the loading surface. However, in most of the investigations by Phillips, emphasis was placed on how to describe the change of the yield surface and the direction of the plastic strain increment. Little was done to propose and verify the flow rule in terms of plastic modulus, particularly for complex loading paths including unloading and reloading. With a correctly determined plastic modulus, the flow rule should describe the nonlinear stress–strain curves. Multisurface models that attempt to accomplish just that are discussed in this section. These models emphasize the description of cyclic loading behavior.

7.4.1 The Mroz Kinematic-Hardening Model

The work of Mroz [39] has a large following, particularly in computational mechanics. Mroz approximated the one-dimensional stress–strain curve OABCDE by n linear segments of constant tangent moduli $E_1, E_2, \ldots, E_n$, as in Figure 7.15. The tangent modulus decreases as the strain increases. This is the idea of a "field of work-hardening moduli." If the stress–strain curve of Figure 7.15 is projected onto the stress space, then we have a one-dimensional stress space in the σ-axis. In the multidimensional stress space, this field is defined by a configuration of surfaces of constant work-hardening modulus. Each nodal stress (stress at A, B, C, etc.) is represented by a surface

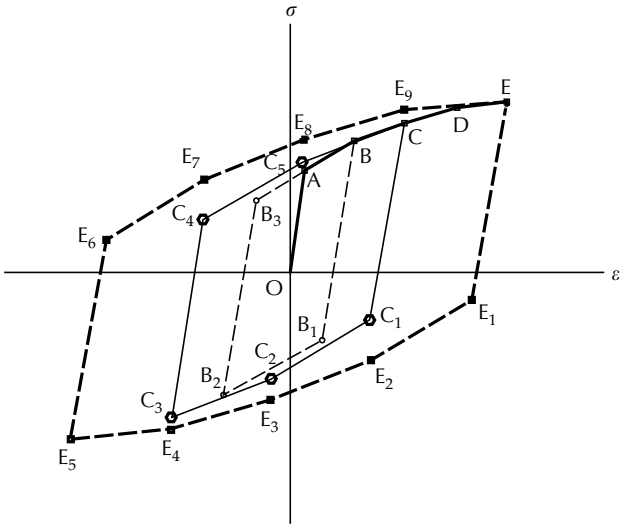

FIGURE 7.15
Mroz's Field of work-hardening moduli concept.

geometrically similar to the initial yield surface but of different size. These surfaces are expressed by

$$f_m\left(\sigma_{ij} - \alpha_{ij}^{(m)}\right) = Y_m^2 \tag{7.2}$$

where $m = 0, 1, 2, \ldots$. Using the Mises yield criterion, the surfaces are concentric circles in the two-dimensional stress space, as shown in Figure 7.16(a). Thus, surface f_A is the initial yield surface passing through point A of Figure 7.15 and f_B is the surface passing through point B, etc.

In Mroz's hardening rule, the surfaces cannot intersect but consecutively contact at similar points and push each other. Similar points are stress points on different surfaces with the same outward normal. During loading sequence OABCDE, surface f_A translates so as to touch surface f_B at the point of loading; next, surfaces f_A and f_B move together until they contact surface f_C, and so on. The surfaces at stress state C are shown in Figure 7.16(b). Since all surfaces can contact only at the similar points, the active surface translates in the direction parallel to the vector connecting the current stress point $\boldsymbol{\sigma}_m$ to the corresponding similar point $\boldsymbol{\sigma}_{m+1}$ of the next surface. This hardening rule is expressed by

$$\mathrm{d}\boldsymbol{\alpha}_m = \mathrm{d}\mu\,(\boldsymbol{\sigma}_{m+1} - \boldsymbol{\sigma}_m) \tag{7.3}$$

where $\mathrm{d}\mu$ is a scalar to be determined by the consistency condition; $\mathrm{d}\boldsymbol{\alpha}_m$ describes the translation of the active surface f_m. Figure 7.17 is a sketch of Mroz's hardening rule.

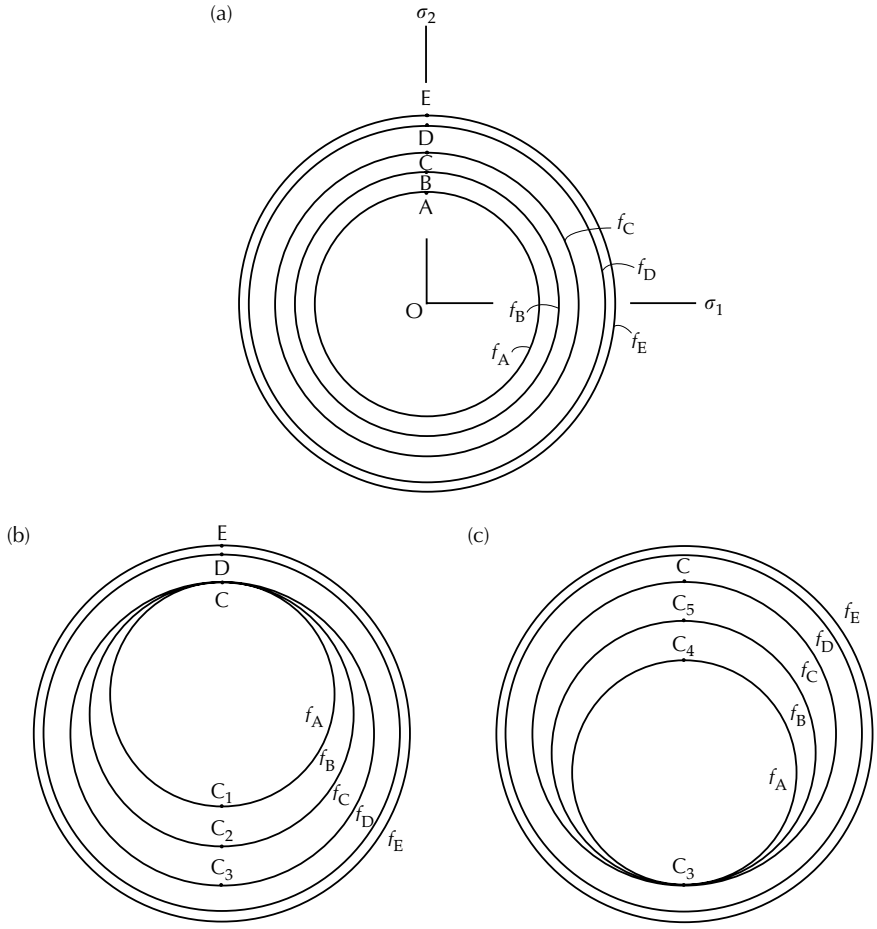

FIGURE 7.16
(a) A family of concentric circles, (b) surfaces at stress state C of Figure 7.15, (c) surfaces at stress state C_3 of Figure 7.15.

The discussion of the one-dimensional loading shown in Figure 7.15 is continued here. After reaching stress state C shown in Figure 7.16(b), if unloading takes place, then the stress point will move from C to C_1 elastically. Reverse plastic flow occurs at C_1 and surface f_A translates downwards until it contacts surface f_B at C_2. We see from the figure that the stress difference between C_1 and C_2 is twice that between A and B. Further unloading from C_2 to C_3 will induce additional plastic deformation and the stress point carries surfaces f_A and f_B with it until it contacts surface f_C at C_3. This state of stress is shown in Figure 7.16(c). We mention again that the stress difference between C_2 and C_3 is twice that between B and C. The reloading from C_3 to C_4 is again elastic, but plastic deformation occurs from C_4 to C_5. The stress point carries surface f_A with it until it contacts surface f_B. Further loading from C_5 to C translates both

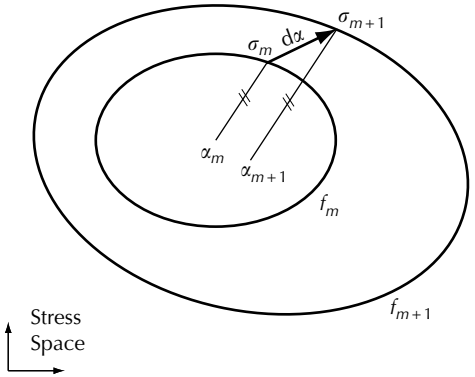

FIGURE 7.17
Mroz's hardening rule.

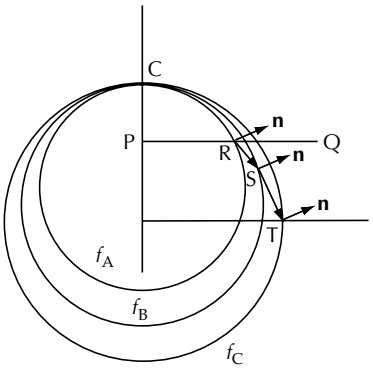

FIGURE 7.18
A case of nonproportional loading (Mroz's model).

f_A and f_B and returns the stress state back to C, as shown in Figure 7.16(b). We have thus completed one cycle of loading–unloading–reloading. Additional loading cycles follow the same path C–C_1–C_2–C_3–C_4–C_5–C and this is the steady loop and no cyclic hardening is possible by use of Mroz's model. We also show in Figure 7.15 a steady loop with unloading starting at B and a loop with unloading starting at E.

Looking at a loop of cyclic loading, we find that the difference in stress for each piecewise-linear step during unloading or reloading is twice that of the corresponding step during loading. The difference in the strain for each step also has the same characteristic. We may conclude that the slopes of E_1E_2 and E_6E_7 are the same as that of AB, and the slopes of E_2E_3 and E_7E_8 are the same as that of BC, etc. In fact, the loading, unloading, and reloading curves are similar and they satisfy Masing's formula [40].

A case of nonproportional loading is now considered. Upon loading to C as in Figure 7.16(b), the specimen is partially unloaded to a point P, Figure 7.18.

The stress point then moves along PQ, and when it reaches point R, it will move along the direction of RS. The normal to surface f_B at S is the same as the normal to surface f_A at point R. S is the point at which f_A will be tangential to and not intersecting f_B. In the next step the stress point will move from S to T. Again, the normal to f_C at T is parallel to the normal previously mentioned at R and S. The work-hardening modulus on this loading path decreases and becomes equal to that at C when the stress path intersects f_C at T. Mroz [39] used this example to illustrate a case of nonproportional loading. We remark that the stress path after the partial unloading is PRST and not PRQ. In a stress-controlled tor–ten test, with stress point moving along PQ as in paths (4) and (5) of Figure 7.2, the contact between f_A and f_B takes place at a location other than S.

7.4.2 The Two-Surface Model of Dafalias and Popov

Dafalias and Popov [41,42] proposed a two-surface model and defined a continuous variation of the plastic modulus $d\sigma/d\varepsilon^p = E^p$ between these two surfaces. This is in contrast to Mroz's model presented in Section 7.4.1, which proposes a piecewise constant plastic moduli field and a number n of associated surfaces. In the two-surface model a *bounding surface* is proposed in the stress space in addition to the yield surface (sometimes also called the loading surface). The loading surface is used interchangeably with the yield surface in this discussion and does not have the same meaning as that defined by Phillips, mentioned in Section 7.2.3. The bounding surface always encloses the yield surface and is a generalization of the bounds observed in the experimental results for uniaxial random cyclic loading on a grade 60 steel specimen. The details of the experimental random cyclic loading curve were presented in [41].

Figure 7.19 shows a simplified schematic cyclic curve with some parameters of the model indicated. Lines XX′ and YY′ are the bounds for the material tested. They can be curves for other materials. Curve 0–1–2 is a loading stress–plastic strain curve and it merges with the bounding line XX′ when the loading continues. If unloading occurs at point 2, then the unloading curve would follow 2–3–4 and merge with the bound line YY′. On the other hand, if reloading starts at A, then AB is elastic and plastic deformation begins to occur at B. Experimental results indicated that the curve after B is steeper than curve Section 3–A, that is, the plastic moduli are not of the same magnitude between the two curve sections. Dafalias and Popov [41,42] suggested that E_p be a function of two parameters, the distance δ of the stress state under consideration, such as point A, from the corresponding bound $\bar{A}$, and the value of δ at the initiation of yielding for each loading process, denoted by δ_{in}. The δ_{in} changes at each reversal and is associated with the most recent event of unloading–reloading. In fact, this is an assumption of fading memory, where the material remembers only the most recent loading history. Thus, we write

$$E^p = E^p(\delta, \delta_{in}) \tag{7.4}$$

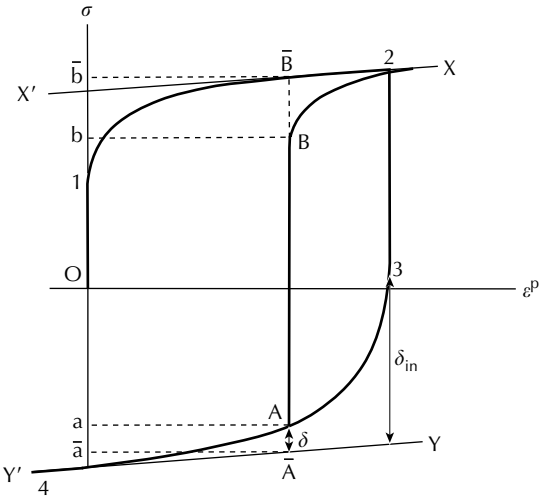

FIGURE 7.19
Bounds and parameters of two-surface model.

with the property that

$$E^{\mathrm{p}} \to \infty \qquad \text{when } \delta \to \delta_{\mathrm{in}} \tag{7.5}$$

for a smooth transition from the elastic into elasto-plastic range and

$$\bar{E}^{\mathrm{p}} = E^{\mathrm{p}}\,(0, \delta_{\mathrm{in}}) \qquad \text{when } \delta \to 0 \tag{7.6}$$

where $\bar{E}^{\mathrm{p}}$ is the slope of the bound line and E^{p} monotonically increases as δ decreases. Dafalias and Popov [42] recommended the following expression for E^{p}:

$$E^{\mathrm{p}} = \bar{E}^{\mathrm{p}} + h\left(\frac{\delta}{\delta_{\mathrm{in}} - \delta}\right) \tag{7.7}$$

where h is a function of δ_{in} and a nonlinear form for h has been chosen to model the complex random cyclic loading curve presented in Dafalias and Popov [41].

Referring to Figure 7.19 again, points A, B, $\bar{\mathrm{A}}$, and $\bar{\mathrm{B}}$ are projected onto the stress axis and the corresponding points are denoted by a, b, $\bar{\mathrm{a}}$, and $\bar{\mathrm{b}}$. a and b are points on the yield surface, whereas $\bar{\mathrm{a}}$ and $\bar{\mathrm{b}}$ are points on the bounding surface. The rates of change of centers of yield and bounding surfaces are related to the plastic strain rate by

$$\dot{\alpha} = E^{\alpha}\dot{\varepsilon}^{\mathrm{p}} \tag{7.8}$$

and

$$\dot{\beta} = E^{\beta}\dot{\varepsilon}^{\mathrm{P}} = \dot{\alpha} - (E^{\alpha} - E^{\beta})\dot{\varepsilon}^{\mathrm{P}} \tag{7.9}$$

respectively. When there is no isotropic hardening of the yield surface, $E^{\alpha} = E^{\mathrm{P}}$; and when there is no isotropic hardening of the bounding surface, $E^{\beta} = E^{\mathrm{P}}$. In this case, the two bounds are parallel straight lines in the one-dimensional case.

In the multiaxial stress space, the yield surface f and the bounding surface $\bar{f}$ are

$$f(\sigma_{ij} - \alpha_{ij}, q_n) = 0 \quad \text{and} \quad \bar{f}(\bar{\sigma}_{ij} - \beta_{ij}, q_n) = 0 \tag{7.10}$$

where α_{ij} and β_{ij} denote the centers of f and $\bar{f}$, respectively, and q_n are internal variables (which will be further discussed in Chapter 8). The two surfaces may deform and translate in stress space in a coupled way. The evolution of q_n is given by

$$\begin{aligned} \dot{q}_n &= \dot{q}_n(\sigma_{ij}, \dot{\sigma}_{ij}, q_m, \xi_m)H(L) \qquad && \text{when } f = 0 \\ \dot{q}_n &= 0 && \text{when } f < 0 \end{aligned} \tag{7.11}$$

where $H(L)$ is the Heaviside step function and L is the loading function, which under the isothermal condition is

$$L = \dot{\sigma} = \dot{\sigma}_{ij} n_{ij} \tag{7.12}$$

in which $\mathbf{n}$ is the unit normal to the yield surface. Internal variables q_n represent the dependence of the yield surface on the history of deformation. One of the q_n may describe isotropic hardening. ξ_m in (7.11) are internal variables associated with abrupt changes of the loading processes. In the present case, they are the δ_{in}'s. These parameters remain constant during the loading process.

The continuously changing δ and the initial value δ_{in} define the generalized plastic modulus K with the properties

$$K = K(\delta, \delta_{\mathrm{in}}), \qquad \bar{K} = K(0, \delta_{\mathrm{in}}), \qquad K(\delta_{\mathrm{in}}, \delta_{\mathrm{in}}) = \infty \tag{7.13}$$

where $\bar{K}$ is the generalized plastic modulus on the bounding surface and is an increasing function of δ for a given δ_{in}. The distance δ is from point a on the yield surface $f = 0$ to a similar point ā on the bounding surface $\bar{f} = 0$ (see Figure 7.20). At similar points, the normals to the respective surfaces are equal. Let the stress at point a be σ_{ij} and the stress at point ā be $\bar{\sigma}_{ij}$, then δ is defined by

$$\delta = [(\bar{\sigma}_{ij} - \sigma_{ij})(\bar{\sigma}_{ij} - \sigma_{ij})]^{1/2} \tag{7.14}$$

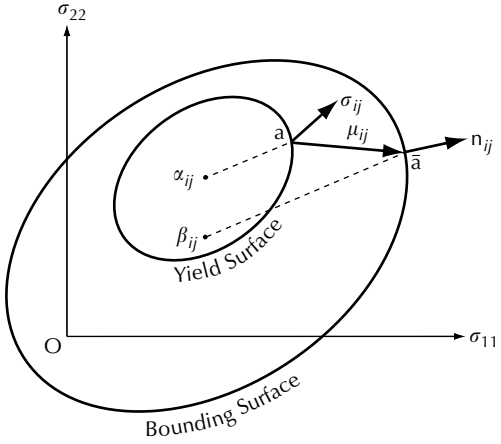

FIGURE 7.20
Two-surface model in two-dimensional stress space (From Dafalias, Y.F. and Popov, E.P., *J. Appl. Mech.*, 98, 645, 1976. With permission from ASME).

For simplicity, we assume that the bounding surface is an isotropic expansion of $f = 0$, but both surfaces are allowed to move. The centers for the two surfaces are α_{ij} and β_{ij}, respectively, as shown in Figure 7.20. Since the two surfaces are similar, the radii connecting the two centers and the corresponding stress points are parallel. Thus, it is written as

$$\bar{\sigma}_{ij} - \beta_{ij} = m(\sigma_{ij} - \alpha_{ij}) \tag{7.15}$$

where m is a proportional factor which can be a function of q_n. This relation may be further written as

$$\bar{\sigma}_{ij} - \sigma_{ij} = m(\sigma_{ij} - \alpha_{ij}) + \beta_{ij} - \sigma_{ij} \tag{7.16}$$

and be substituted into (7.14) to obtain an expression for δ.

Several rules of evolution of α_{ij} and β_{ij} have been used in the literature in conjunction with the two-surface model. The following discussion follows Dafalias and Popov [42]. Assuming linear dependence of $\dot{\varepsilon}^{\mathrm{p}}_{ij}$ on the stress rate, the flow rule, assuming normality, is

$$\dot{\varepsilon}^{\mathrm{p}}_{ij} = \frac{1}{K}\langle L\rangle n_{ij} \tag{7.17}$$

where $\langle\ \rangle$ is the Macauley bracket defining the operation $\langle L\rangle = LH(L)$. From (7.17), we found

$$\langle L\rangle = \langle\dot{\sigma}\rangle = K\left(\dot{\varepsilon}^{\mathrm{p}}_{ij}\dot{\varepsilon}^{\mathrm{p}}_{ij}\right)^{1/2} \tag{7.18}$$

Working with the magnitudes and projection of the stress rate onto the normal direction, this relation is a generalized relation of $\dot{\sigma} = E^{\mathrm{p}}\dot{\varepsilon}^{\mathrm{p}}$ in the one-dimensional case, that is, E^{p} has been generalized into K. We now use the same procedure to generalize (7.8) by writing

$$\dot{\alpha} = \dot{\alpha}_{ij} n_{ij} = K^{\alpha} \left(\dot{\varepsilon}^{\mathrm{p}}_{ij} \dot{\varepsilon}^{\mathrm{p}}_{ij} \right)^{1/2} = \frac{K^{\alpha}}{K} \langle L \rangle \tag{7.19}$$

Denoting the unit vector along $\dot{\alpha}_{ij}$ by v_{ij}, which is, in general, not in the same direction as n_{ij}, we may write

$$\dot{\alpha}_{ij} = \dot{\alpha}^{v} v_{ij} \tag{7.20}$$

where $\dot{\alpha}^{v}$ is the magnitude. Substituting (7.20) into (7.19), we have

$$\dot{\alpha} = \dot{\alpha}_{ij} n_{ij} = \dot{\alpha}^{v} v_{ij} n_{ij} \tag{7.21}$$

Therefore,

$$\dot{\alpha}_{ij} = \frac{\dot{\alpha}}{v_{rs} n_{rs}} v_{ij} = \frac{1}{v_{rs} n_{rs}} \frac{K^{\alpha}}{K} \langle L \rangle v_{ij} \tag{7.22}$$

The modulus K^{α}/K can be determined by substituting (7.22) into the consistency condition. Referring to the yield surface given in (7.10), the consistency condition is

$$\dot{f} = \frac{\partial f}{\partial \sigma_{ij}} \dot{\sigma}_{ij} + \frac{\partial f}{\partial \alpha_{ij}} \dot{\alpha}_{ij} + \frac{\partial f}{\partial q_n} \dot{q}_n = 0 \tag{7.23}$$

Denoting the magnitude of $\partial f / \partial \sigma_{ij}$ by

$$g = \left(\frac{\partial f}{\partial \sigma_{ij}} \frac{\partial f}{\partial \sigma_{ij}} \right)^{1/2} \tag{7.24}$$

we write

$$\frac{\partial f}{\partial \sigma_{ij}} = g n_{ij} \tag{7.25}$$

In addition, we assume that $\dot{q}_n$ is linear in $\dot{\sigma}_{ij}$, that is,

$$\dot{q}_n = r_n \langle L \rangle \tag{7.26}$$

where r_n is a scalar. Using (7.24) to (7.26), (7.23) reduces to

$$\frac{K^{\alpha}}{K} = 1 + \frac{1}{g} \frac{\partial f}{\partial q_n} r_n \tag{7.27}$$

We then substitute (7.27) into (7.22) to obtain $\dot{\alpha}_{ij}$. This relation applies to any kinematic-hardening rule for which ν_{ij} is specified. A special case is obtained when $\partial f/\partial q_n = 0$. In this case, $K^\alpha = K$, which corresponds to $E^\alpha = E^\mathrm{p}$ in the one-dimensional case.

The same procedure may be used again to generalize (7.9). By differentiating (7.10), the consistency condition for the bounding surface is

$$\dot{\bar{f}} = \frac{\partial \bar{f}}{\partial \bar{\sigma}_{ij}}\dot{\bar{\sigma}}_{ij} + \frac{\partial \bar{f}}{\partial \beta_{ij}}\dot{\beta}_{ij} + \frac{\partial f}{\partial q_n}\dot{q}_n = 0 \tag{7.28}$$

Writing

$$\bar{g} = \left(\frac{\partial \bar{f}}{\partial \bar{\sigma}_{ij}}\frac{\partial \bar{f}}{\partial \bar{\sigma}_{ij}}\right)^{1/2}, \qquad \frac{\partial \bar{f}}{\partial \bar{\sigma}_{ij}} = \bar{g}n_{ij} \tag{7.29}$$

and

$$\bar{L} = \dot{\bar{\sigma}} = \dot{\bar{\sigma}}_{ij}n_{ij} = \bar{K}\left(\dot{\varepsilon}^\mathrm{p}_{ij}\dot{\varepsilon}^\mathrm{p}_{ij}\right)^{1/2} = \frac{\bar{K}}{K}\langle L\rangle \tag{7.30}$$

and using them in (7.28), the consistency condition is

$$n_{ij}\dot{\beta}_{ij} = \bar{L} + \frac{1}{\bar{g}}\frac{\partial \bar{f}}{\partial q_n}r_n L \tag{7.31}$$

We now generalize (7.9) to obtain

$$\dot{\beta} = \dot{\beta}_{ij}n_{ij} = K^\beta\left(\dot{\varepsilon}^\mathrm{p}_{ij}\dot{\varepsilon}^\mathrm{p}_{ij}\right)^{1/2} = \frac{K^\beta}{K}\langle L\rangle \tag{7.32}$$

and denote the unit vector along $\dot{\beta}_{ij}$ by ξ_{ij}, then

$$\dot{\beta}_{ij} = \dot{\beta}^\xi \xi_{ij} \tag{7.33}$$

where $\dot{\beta}^\xi$ is the magnitude. But, $\dot{\beta}$ is the projection of $\dot{\beta}_{ij}$ along n_{ij}, and, therefore, we have

$$\dot{\beta} = \dot{\beta}_{ij}n_{ij} = \dot{\beta}^\xi \xi_{ij}n_{ij} \quad \text{and} \quad \dot{\beta}^\xi = \frac{\dot{\beta}}{\xi_{ij}n_{ij}} \tag{7.34}$$

Hence,

$$\dot{\beta}_{ij} = \frac{\dot{\beta}}{\xi_{rs}n_{rs}}\xi_{ij} = \frac{1}{\xi_{rs}n_{rs}}\frac{K^\beta}{K}\langle L\rangle \xi_{ij} \tag{7.35}$$

For simplicity, consider a case $\nu_{ij} = \xi_{ij} = \mu_{ij}$. This assumption is similar to Mroz's hardening rule, where μ_{ij} is a unit vector going from point a to point ā (see Figure 7.20). For this case, (7.22) reduces to

$$\dot{\alpha}_{ij} = \frac{1}{\mu_{rs} n_{rs}} \frac{K^{\alpha}}{K} \langle L \rangle \mu_{ij} \tag{7.36}$$

and (7.35) reduces to

$$\dot{\beta}_{ij} = \frac{1}{\mu_{rs} n_{rs}} \frac{K^{\beta}}{K} \langle L \rangle \mu_{ij} \tag{7.37}$$

Analogous to the second expression of (7.9), we write

$$\dot{\beta}_{ij} = \dot{\alpha}_{ij} - M \mu_{ij} \tag{7.38}$$

From (7.36) to (7.38), the following is obtained

$$M = \frac{1}{\mu_{rs} n_{rs}} \frac{K^{\alpha} - K^{\beta}}{K} \langle L \rangle \tag{7.39}$$

Substituting (7.30), (7.38), and (7.39) into (7.31) obtains

$$\frac{K^{\beta}}{K} = \frac{\bar{K}}{K} + \frac{1}{\bar{g}} \frac{\partial \bar{f}}{\partial q_n} r_n \tag{7.40}$$

Using (7.27) and (7.40), (7.39) may be further written as

$$M = \frac{1}{\mu_{rs} n_{rs}} \left[\left(1 - \frac{\bar{K}}{K} \right) + \left(\frac{1}{g} \frac{\partial f}{\partial q_n} r_n - \frac{1}{\bar{g}} \frac{\partial \bar{f}}{\partial q_n} r_n \right) \right] \langle L \rangle \tag{7.41}$$

In the case that both f and $\bar{f}$ are not functions of q_n, (7.41) becomes

$$M = \frac{1}{\mu_{rs} n_{rs}} \left(1 - \frac{\bar{K}}{K} \right) \langle L \rangle \tag{7.42}$$

and (7.40) yields $K^{\beta} = \bar{K}$. In the limit, when the yield surface contacts the bounding surface, $\delta = 0$, and $K = \bar{K}$, the two surfaces will then move together upon further loading. From (7.36) and (7.37), we have

$$\dot{\beta}_{ij} = \dot{\alpha}_{ij} \tag{7.43}$$

7.5 The Plastic Strain Trajectory Approach

The strain (total strain, not plastic strain) trajectory approach was initiated by Ilyushin [43,44], who represented the stress and deviatoric strain tensors in a five-dimensional vector space. He then investigated the characteristics of the stress response to a predetermined strain trajectory. Further investigations using this approach are reported by Lensky [45] and Ohashi and his coworkers [3,36,46,47]. A theory by Pipkin and Rivlin [48] is similar to Ilyushin's theory but using strain tensors, and Zhou et al. [49] consider the plastic strain trajectory. In an independent effort, Valanis [1,2] developed an endochronic theory of plasticity using irreversible thermodynamics of internal variables. The resulting constitutive equation, if expressed in an integral form, resembles that presented by Ilyushin [50]. In this constitutive equation, stress is a functional of the plastic strain history. The differences between the two developments will be addressed in Section 7.5.2. Wu and his coworkers [51–55] have contributed to the experimental verifications and applications of the endochronic theory. The endochronic theory of plasticity will be further discussed in Chapters 8 and 9.

7.5.1 The Theory of Ilyushin

Ilyushin worked with the deviator of the strain tensor (not plastic strain). When the strain is large, the plastic strain may be approximated by the total strain. The theory is, however, not suitable for describing the elastic–plastic transition behavior. The deviatoric strain e_{ij} has only five independent components. Thus, e_{ij} may be represented by a vector in a five-dimensional space as

$$\mathbf{e} = \sum_{i=1}^{5} \varepsilon_i \mathbf{u}_i \tag{7.44}$$

in which $\mathbf{u}_i$ are unit vectors along axes of the five-dimensional space. The magnitude of this vector must be equal to the magnitude of tensor e_{ij}, so that

$$\sum_{i,j=1,2,3} e_{ij} e_{ij} \equiv \sum_{i=1}^{5} (\varepsilon_i)^2 \tag{7.45}$$

If we define

$$\varepsilon_3 = \sqrt{2} e_{12}, \qquad \varepsilon_4 = \sqrt{2} e_{23}, \qquad \varepsilon_5 = \sqrt{2} e_{31} \tag{7.46}$$

then (7.45) and (7.46) are reduced to

$$(e_{11})^2 + (e_{22})^2 + (e_{33})^2 = (\varepsilon_1)^2 + (\varepsilon_2)^2 \tag{7.47}$$

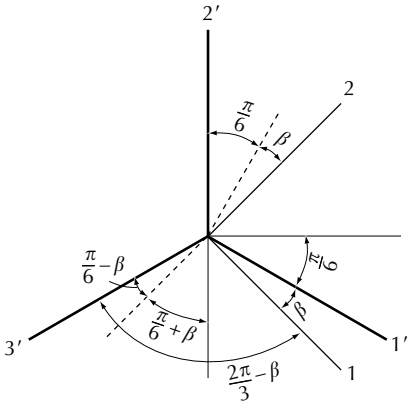

FIGURE 7.21
Coordinate transformation in the deviatoric strain plane.

The relationships between components of $(\varepsilon_1, \varepsilon_2)$ and (e_{11}, e_{22}) are found from the coordinate transformation given in Figure 7.21. Note that $e_{33} = -(e_{11} + e_{22})$. In the figure, axes 1′, 2′, and 3′ denote the coordinate axes for e_{11}, e_{22}, and e_{33}, respectively, in the π-plane; whereas 1 and 2 denote the axes of ε_1 and ε_2. The 1-axis is making angle β with the 1′-axis. Projecting ε_1 and ε_2 onto the 1′ and 2′ directions, respectively gives

$$e_{11} = m(\varepsilon_1 \cos\beta + \varepsilon_2 \sin\beta) \tag{7.48a}$$

$$e_{22} = m\left(-\varepsilon_1 \sin\left(\beta + \frac{\pi}{6}\right) + \varepsilon_2 \cos\left(\beta + \frac{\pi}{6}\right)\right) \tag{7.48b}$$

where the factor m is introduced so that (7.47) is satisfied. Substituting (7.48) into (7.47), we obtain $m = \sqrt{2/3}$. Using this value of m, we found from (7.48) that

$$\begin{aligned} e_{11}\sqrt{\frac{3}{2}} &= \varepsilon_1 \cos\beta + \varepsilon_2 \sin\beta \\ e_{22}\sqrt{\frac{3}{2}} &= -\varepsilon_1 \sin\left(\beta + \frac{\pi}{6}\right) + \varepsilon_2 \cos\left(\beta + \frac{\pi}{6}\right) \\ e_{33}\sqrt{\frac{3}{2}} &= \varepsilon_1 \sin\left(\beta - \frac{\pi}{6}\right) - \varepsilon_2 \cos\left(\beta - \frac{\pi}{6}\right) \end{aligned} \tag{7.49}$$

The third equation of (7.49) was found from $e_{33} = -(e_{11} + e_{22})$. The first two equations of (7.49) may then be solved to obtain

$$\begin{aligned} \varepsilon_1 &= \sqrt{2}\left(e_{11} \cos\left(\beta + \frac{\pi}{6}\right) - e_{22} \sin\beta\right) \\ \varepsilon_2 &= \sqrt{2}\left(e_{11} \sin\left(\beta + \frac{\pi}{6}\right) + e_{22} \cos\beta\right) \end{aligned} \tag{7.50}$$

Finally, if the angle is set to $\beta = 0$, then we have

$$\varepsilon_1 = \sqrt{\frac{3}{2}}e_{11}, \qquad \varepsilon_2 = \sqrt{2}\left(e_{22} + \frac{1}{2}e_{11}\right), \qquad \varepsilon_3 = \sqrt{2}e_{12}, \qquad \varepsilon_4 = \sqrt{2}e_{23}, \quad \varepsilon_5 = \sqrt{2}e_{31} \tag{7.51}$$

These are the five components in the plastic strain space.

Similarly, the deviatoric stress σ'_{ij} with $\sigma'_{11}+\sigma'_{22}+\sigma'_{33} = 0$ may be represented in a five-dimensional stress space by the following components:

$$\sigma_1 = \sqrt{\frac{3}{2}}\sigma'_{11}, \qquad \sigma_2 = \sqrt{2}\left(\sigma'_{22} + \frac{1}{2}\sigma'_{11}\right), \qquad \sigma_3 = \sqrt{2}\sigma'_{12}, \qquad \sigma_4 = \sqrt{2}\sigma'_{23}, \qquad \sigma_5 = \sqrt{2}\sigma'_{31} \tag{7.52}$$

The next step is to establish a relationship between the stress and the strain increment, and this relationship is expressed in terms of the arc length s measured along the strain path. In the case of combined axial–torsion, the stress is (σ_1, σ_3) and the strain increment is $(\mathrm{d}\varepsilon_1, \mathrm{d}\varepsilon_3)$. A plane strain trajectory is shown in Figure 7.22, and the arc length is

$$\mathrm{d}s = \sqrt{(\varepsilon_1)^2 + (\varepsilon_3)^2} \tag{7.53}$$

If the current strain state is represented by point A, unit vector $\mathbf{p}_1$ is tangential to the trajectory at A, and unit vector $\mathbf{p}_3$ is the principal normal. A similar figure is presented in [49] but in the plastic strain space. According to the Frenet formulas for curves in space, we have the following relations:

$$\frac{\mathrm{d}\mathbf{p}_1}{\mathrm{d}s} = \kappa\mathbf{p}_3, \qquad \frac{\mathrm{d}\mathbf{p}_3}{\mathrm{d}s} = -\kappa\mathbf{p}_1 \tag{7.54}$$

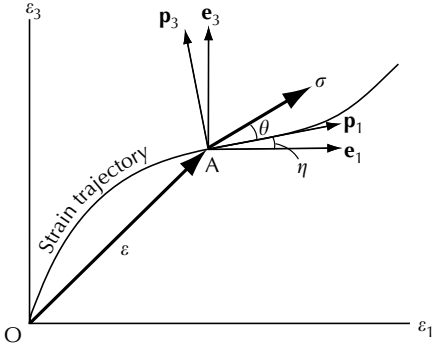

FIGURE 7.22
A plane strain trajectory and stress (From Zhou, Z.-D. et al., *Int. J. Plasticity*, 19, 1377, 2003. With permission from Elsevier).

where κ is the curvature. Writing the stress vector as

$$\boldsymbol{\sigma} = P\mathbf{p}_1 + N\mathbf{p}_3 \tag{7.55}$$

Lensky [45] and Ohashi and his coworkers [3,36,46,47] conducted combined axial–torsion experiments to determine the variations of P, N, the magnitude of $\boldsymbol{\sigma}$, denoted by σ, and the angle of delay θ between vectors $\boldsymbol{\sigma}$ and $\mathrm{d}\boldsymbol{\varepsilon}$ as functions of s. The angle of delay is found from

$$\cos\theta = \frac{\boldsymbol{\sigma}\cdot \mathrm{d}\boldsymbol{\varepsilon}}{\sigma\, \mathrm{d}s} \tag{7.56}$$

These authors believe that these relationships are the constitutive equations of the material under investigation. Trajectories investigated include proportional strain trajectories, strain trajectories with two straight branches, orthogonal bilinear trajectories with a rounded corner, and more general curvilinear strain trajectories. The results show that the arc length s and the curvature κ are two important parameters defining the constitutive behavior of the material.

Ilyushin proposed a postulate of isotropy, see [45], which states that, for a strain trajectory starting from the origin of the strain space, the stress response is defined by the intrinsic geometry of the strain trajectory and is invariant with respect to transformation of strain trajectory by means of rotation or reflection. Ilyushin further proposed the principle of delay, which states that the stress response to a strain trajectory is not defined by the whole strain trajectory, but by the recent past of the trajectory with length λ known as the trace of delay. This is in fact a statement of fading memory. In the case of a curved trajectory followed by a straight trajectory, at a distance λ after the beginning of the straight trajectory, the stress vector becomes tangent to the trajectory. This is a very intuitive statement, because experimental results show that the stress path and the strain path do not coincide even for a proportional straining.

Ilyushin [50] further proposed the following integral constitutive equation

$$\boldsymbol{\sigma}(s) = \int_0^s \mathbf{K}[s, s'; \kappa_i(s), \kappa_i(s')]\mathrm{d}\boldsymbol{\varepsilon}(s'), \quad i = 1,2,3,4 \tag{7.57}$$

where s' is the running parameter of integration; the kernel function multiplied by $\mathrm{d}\boldsymbol{\varepsilon}(s')$ represents the contribution of $\mathrm{d}\boldsymbol{\varepsilon}(s')$ to the stress vector at s'; and κ_i represents the geometry of the strain trajectory. A recent derivation of (7.57) by Zhou et al. [49] in the plastic strain space is now discussed with permission from Elsevier.

Referring to Figure 7.22, in which the axes should be renamed $\varepsilon_1^{\mathrm{p}}$ and $\varepsilon_3^{\mathrm{p}}$, the plastic strain increment is

$$\mathrm{d}\boldsymbol{\varepsilon}^{\mathrm{p}} = \mathrm{d}\varepsilon_1^{\mathrm{p}}\mathbf{e}_1 + \mathrm{d}\varepsilon_3^{\mathrm{p}}\mathbf{e}_3 = \mathrm{d}s\mathbf{p}_1 \tag{7.58}$$

and the stress is

$$\boldsymbol{\sigma} = \sigma_1 \mathbf{e}_1 + \sigma_3 \mathbf{e}_3 = \sigma(\cos\theta \mathbf{p}_1 + \sin\theta \mathbf{p}_3) \tag{7.59}$$

where $\mathbf{e}_i$ are base vectors of the Cartesian coordinate system; and θ is the angle of delay between vectors $\boldsymbol{\sigma}$ and $\mathrm{d}\boldsymbol{\varepsilon}^{\mathrm{p}}$. We now define the length of the plastic strain path by

$$\mathrm{d}s = \sqrt{\left(\varepsilon_1^{\mathrm{p}}\right)^2 + \left(\varepsilon_3^{\mathrm{p}}\right)^2} \tag{7.60}$$

Differentiating (7.59) with respect to s and using (7.54), we obtain

$$\dot{\boldsymbol{\sigma}} = g_1 \mathbf{p}_1 + g_3 \mathbf{p}_3 \tag{7.61}$$

where

$$g_1 = \dot{\sigma}\cos\theta - \sigma(\kappa + \dot{\theta})\sin\theta, \qquad g_3 = \dot{\sigma}\sin\theta + \sigma(\kappa + \dot{\theta})\cos\theta \tag{7.62}$$

We now make use of the transformation equations

$$\mathbf{p}_1 = \cos\eta \mathbf{e}_1 + \sin\eta \mathbf{e}_3, \qquad \mathbf{p}_3 = -\sin\eta \mathbf{e}_1 + \cos\eta \mathbf{e}_3 \tag{7.63}$$

and the relations

$$\cos\eta = \frac{\mathrm{d}\varepsilon_1^{\mathrm{p}}}{\mathrm{d}s}, \qquad \sin\eta = \frac{\mathrm{d}\varepsilon_3^{\mathrm{p}}}{\mathrm{d}s} \tag{7.64}$$

and substituting (7.63) and (7.64) into (7.61) to obtain

$$\dot{\boldsymbol{\sigma}} = \dot{\sigma}_1 \mathbf{e}_1 + \dot{\sigma}_3 \mathbf{e}_3 = \left(g_1 \frac{\mathrm{d}\varepsilon_1^{\mathrm{p}}}{\mathrm{d}s} - g_3 \frac{\mathrm{d}\varepsilon_3^{\mathrm{p}}}{\mathrm{d}s}\right)\mathbf{e}_1 + \left(g_1 \frac{\mathrm{d}\varepsilon_3^{\mathrm{p}}}{\mathrm{d}s} + g_3 \frac{\mathrm{d}\varepsilon_1^{\mathrm{p}}}{\mathrm{d}s}\right)\mathbf{e}_3 \tag{7.65}$$

We have thus found from (7.65) that

$$\begin{bmatrix} \mathrm{d}\sigma_1 \\ \mathrm{d}\sigma_3 \end{bmatrix} = \begin{bmatrix} g_1 & -g_3 \\ g_3 & g_1 \end{bmatrix} \begin{bmatrix} \mathrm{d}\varepsilon_1^{\mathrm{p}} \\ \mathrm{d}\varepsilon_3^{\mathrm{p}} \end{bmatrix} \tag{7.66}$$

Experimental results show that σ can be expressed by

$$\sigma(s - s', \kappa) = \sum_{\rho=1}^{n} \frac{R_\rho}{A_\rho} \mathrm{e}^{-A_\rho(s-s')}, \qquad A_\rho = A_\rho(s, \kappa) \tag{7.67}$$

where R_ρ and A_ρ are material constants. Substituting (7.67) into (7.62) and neglecting terms of higher order of smallness, we obtain

$$\begin{aligned} g_1 &= \sum_{\rho=1}^{3} R_\rho N_\rho \, \mathrm{e}^{-A_\rho(s-s')}, \qquad N_\rho = \cos\theta - \sin\theta \frac{(\kappa + (\mathrm{d}\theta/\mathrm{d}s))}{A_\rho} \\ g_3 &= \sum_{\rho=1}^{3} R_\rho M_\rho \, \mathrm{e}^{-A_\rho(s-s')}, \qquad M_\rho = \sin\theta + \cos\theta \frac{(\kappa + (\mathrm{d}\theta/\mathrm{d}s))}{A_\rho} \end{aligned} \tag{7.68}$$

Substituting (7.68) into (7.66) and integrating the equation, yields

$$\begin{bmatrix} \sigma_1 \\ \sigma_2 \end{bmatrix} = \sum_{\rho=1}^{3} \int_0^s R_\rho \, \mathrm{e}^{-A_\rho(s-s')} \begin{bmatrix} N_\rho & -M_\rho \\ M_\rho & N_\rho \end{bmatrix} \begin{bmatrix} \mathrm{d}\varepsilon_1^{\mathrm{p}} \\ \mathrm{d}\varepsilon_3^{\mathrm{p}} \end{bmatrix} \tag{7.69}$$

This is the constitutive equation for a plastic strain trajectory.

7.5.2 The Endochronic Theory of Plasticity

The endochronic theory of plasticity was developed by Valanis [1] from the thermo-mechanical theory of internal variables. The theory will be discussed in detail in Chapter 8. The word *endochronic* is a Greek word for *intrinsic time* or *internal time*. Valanis introduced an intrinsic time ζ, which is monotonically increasing and is defined by

$$\mathrm{d}\zeta^2 = P_{ijkm} \, \mathrm{d}\varepsilon_{ij} \, \mathrm{d}\varepsilon_{km} \tag{7.70}$$

where P_{ijkm} is a positive definite material tensor. In a special case, $\mathrm{d}\zeta$ may be defined by the length of the strain path, that is,

$$\mathrm{d}\zeta^2 = \mathrm{d}\varepsilon_{ij} \, \mathrm{d}\varepsilon_{ij} \tag{7.71}$$

The constitutive equation has two parts, the deviatoric and volumetric part. They are

$$\begin{aligned} \sigma'_{ij} &= 2 \int_{\zeta_0}^{\zeta} \mu(\zeta - \zeta') \frac{\mathrm{d}e_{ij}}{\mathrm{d}\zeta'} \mathrm{d}\zeta' \\ \sigma_{kk} &= 3 \int_{\zeta_0}^{\zeta} K(\zeta - \zeta') \frac{\mathrm{d}\varepsilon_{kk}}{\mathrm{d}\zeta'} \mathrm{d}\zeta \end{aligned} \tag{7.72}$$

where $\mu(\zeta)$ and $K(\zeta)$ are kernels of the integrals. In the one-dimensional stressing, (7.72) reduces to

$$\sigma = \int_0^{\zeta} E(\zeta - \zeta') \frac{\mathrm{d}\varepsilon}{\mathrm{d}\zeta'} \, \mathrm{d}\zeta' \tag{7.73}$$

where $E(\zeta)$ is a kernel function. Equations (7.72) and (7.73) are in the same form as (7.57), except that only the length of the strain path and not the curvature nor the torsion of the strain trajectory is included in the formulation. These geometrical parameters of the strain path may be accounted for by use of internal variables, and they have not been included for the sake of simplicity. It has been shown that using only the length of the strain path, the endochronic theory is capable of describing stress responses to complex strain paths.

This version of endochronic theory is similar to but not quite the same as Ilyushin's theory. One of the differences is in the definition of intrinsic time. The endochronic theory defines the intrinsic time by (7.70) using a material tensor P_{ijkm}, whereas Ilyushin's theory uses the arc length as the intrinsic time. Another difference, more significantly, is that the endochronic theory is capable of accounting for volume change during deformation by use of the second equation of (7.72), while the theory of Ilyushin is formulated based on the deviatoric strain and no discussions have been given over to the volume change. It has been found that this version of endochronic theory does not correctly describe the unloading slope for metals and that it incorrectly predicts the same entropy production for further loading or unloading starting at a point already in the plastic state.

Owing to the aforementioned deficiencies, an improved endochronic theory was developed by Valanis [2]. The new theory is free from the aforementioned deficiencies. In the new version, the intrinsic time is defined by the plastic strain as

$$\mathrm{d}\zeta^2 = P_{ijkm}\mathrm{d}\varepsilon^{\mathrm{p}}_{ij}\,\mathrm{d}\varepsilon^{\mathrm{p}}_{km} \tag{7.74}$$

The deviatoric part of the constitutive equation is

$$\sigma'_{ij} = 2G_0\int_0^{\zeta}\rho(\zeta-\zeta')\frac{\mathrm{d}\varepsilon^{\mathrm{p}}_{ij}}{\mathrm{d}\zeta'}\mathrm{d}\zeta' \tag{7.75}$$

where G_0 is a material constant and $\rho(\zeta)$ is a kernel function. The volumetric change can be accounted for using the volumetric constitutive equation and the details of derivations are given in Chapter 8. It is shown in Chapter 8 that the flow theory of plasticity may be derived from the new version of the endochronic theory. In addition, this theory is shown in Chapter 9 to apply to geotechnical materials which undergo plastic volume change during deformation.

7.6 Finite Plastic Deformation

Plastic deformations are large in cases such as metal forming, strain localization, ductile fracture, soil mechanics, and pavement analysis, etc. A plasticity

theory of finite deformation must be used for these cases. The theories presented in previous sections of this chapter may be extended to the finite deformation range. The extension is not straightforward, however, and it has led to different opinions and heated debates. To extend an infinitesimal theory into a finite theory, we encounter concepts such as the stress measure, the strain measure, the decomposition of strain into elastic and plastic parts, the objective rate (of stress, back stress, etc.), the observer independent yield function, and the rotation of material texture. The stress and strain measures and the decomposition of strain are discussed first. The objective rate is then discussed in connection with hypoelasticity and discussion of its effects in plasticity is deferred until after a finite plasticity theory has been presented. Then the finite plastic simple shear deformation using different objective rates, and, finally, the yield function are discussed.

7.6.1 The Stress and Strain Measures

Either the Eulerian or the Lagrangian description may be used. The stress measures have already been discussed in Section 4.4.2.1 and strain measures in Sections 3.6, 3.9, and 3.10. In the Eulerian description, the stress and strains are referred to the current (deformed) configuration. The Cauchy stress $\boldsymbol{\sigma}$ is usually used in this configuration. This is the true stress, which is the force per unit deformed area. The Kirchhoff stress, which is defined by $S_{ij} = J\sigma_{ij}$ where J is the Jacobian of the deformation equations, has also been used by some investigators. The Kirchhoff stress is also discussed in Chapter 11 in connection with the curvilinear coordinate system. Although we can use the Eulerian strain $\mathbf{e}$ or the left Cauchy–Green tensor $\mathbf{B}$, it is more convenient to use the rate of deformation tensor $\mathbf{D}$, which has the meaning of strain rate. The rate of deformation can be decomposed into the elastic and plastic parts and will be further discussed. In the Lagrangian description, the stress and strain refer to the undeformed (reference) configuration. The nonsymmetric 1st P–K stress $\mathbf{T}^{(0)}$ and the symmetric 2nd P–K stress $\boldsymbol{\Pi}$ have been used. Popular strain measures are the right Cauchy–Green tensor $\mathbf{C}$ and the Lagrangian strain (Green's strain or Almansi strain) $\mathbf{E}$. There is no unified approach available. The selection of the stress and strain measures greatly depends on the preference and convenience of the investigator and the problem at hand.

7.6.2 The Decomposition of Strain and Strain Rate

In the small deformation theory, it is customary to write

$$\varepsilon_{ij} = \varepsilon_{ij}^{\mathrm{e}} + \varepsilon_{ij}^{\mathrm{p}} \quad \text{and} \quad \mathrm{d}\varepsilon_{ij} = \mathrm{d}\varepsilon_{ij}^{\mathrm{e}} + \mathrm{d}\varepsilon_{ij}^{\mathrm{p}} \tag{7.76}$$

However, in finite deformation, the decomposition

$$E_{RS} = E_{RS}^{\mathrm{e}} + E_{RS}^{\mathrm{p}} \tag{7.77}$$

cannot be justified. This may be easily seen by considering the strain–displacement relation

$$E_{RS} = \frac{1}{2}\left(\frac{\partial u_R}{\partial X_S} + \frac{\partial u_S}{\partial X_R} + \frac{\partial u_k}{\partial X_R}\frac{\partial u_k}{\partial X_S}\right) \tag{7.78}$$

which cannot be separated into the sum of two parts because of the nonlinear terms in the displacement gradient. An additive decomposition was proposed by Green and Naghdi [56], who defined $\mathbf{E}^{\mathrm{e}} = \mathbf{E} - \mathbf{E}^{\mathrm{p}}$ but explained that $\mathbf{E}^{\mathrm{e}}$ was not an ordinary elastic strain tensor. It was defined merely to represent the difference between the total strain $\mathbf{E}$ and the plastic strain $\mathbf{E}^{\mathrm{p}}$. The introduction of $\mathbf{E}^{\mathrm{e}}$ was not necessary, because the use of $\mathbf{E}$ and $\mathbf{E}^{\mathrm{p}}$ was sufficient in their theory.

On the other hand, the rate of deformation tensor can be separated into two parts because of the linear expression in the velocity gradient, that is,

$$D_{ij} = \tfrac{1}{2}(v_{i,j} + v_{j,i}) \tag{7.79}$$

It is possible to define two velocities v_i^{e} and v_i^{p}, such that

$$D_{ij}^{\mathrm{e}} = \tfrac{1}{2}\big(v_{i,j}^{\mathrm{e}} + v_{j,i}^{\mathrm{e}}\big) \quad \text{and} \quad D_{ij}^{\mathrm{p}} = \tfrac{1}{2}\big(v_{i,j}^{\mathrm{p}} + v_{j,i}^{\mathrm{p}}\big) \tag{7.80}$$

Thus,

$$D_{ij} = D_{ij}^{\mathrm{e}} + D_{ij}^{\mathrm{p}} \tag{7.81}$$

We note that, in this connection, no attempt is made to separate the deformation gradient $\mathbf{F}$ into the elastic and plastic parts. In fact, $\mathbf{F}$ does not play a part in the formulation of (7.81).

Another effort has been undertaken by researchers to derive the expressions of $\mathbf{D}^{\mathrm{e}}$ and $\mathbf{D}^{\mathrm{p}}$ starting from $\mathbf{F}$. This effort involves some assumptions and physical justifications. Lee [57] introduced the concept of multiplicative decomposition of $\mathbf{F}$. The deformation gradient has been previously discussed in Section 3.4. Let $\mathbf{X}$ express the initial configuration of the body, $\mathbf{x}$ the elastic–plastic deformed state (the current configuration), and $\mathbf{p}$ the state after de-stressing to zero stress. The deformation gradient $\mathbf{F} = \partial\mathbf{x}/\partial\mathbf{X}$ with components $F_{iR} = \partial x_i/\partial X_R$ expresses the total deformation. The deformation gradient $\mathbf{F}^{\mathrm{p}}$ from the initial state $\mathbf{X}$ to the plastically deformed state $\mathbf{p}$ expresses the plastic deformation

$$\mathbf{F}^{\mathrm{p}} = \frac{\partial \mathbf{p}}{\partial \mathbf{X}} \tag{7.82}$$

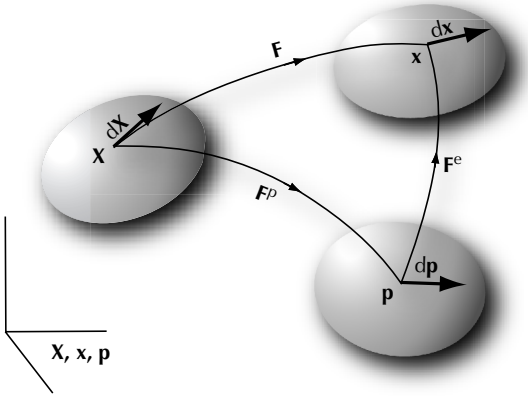

FIGURE 7.23
Decomposition of **F**.

and $\mathbf{F}^e$, from the plastically deformed configuration **p** to **x**, expresses the elastic component of the deformation in the configuration **x**, that is,

$$\mathbf{F}^e = \frac{\partial \mathbf{x}}{\partial \mathbf{p}} \tag{7.83}$$

Thus,

$$\mathbf{F} = \mathbf{F}^e \cdot \mathbf{F}^p \tag{7.84}$$

by the chain rule of differentiation. This decomposition of F into $\mathbf{F}^e$ and $\mathbf{F}^p$ is depicted by Figure 7.23. The intermediate configuration **p** is obtained by an elastic de-stressing to zero stress from the current configuration **x** and it represents a pure plastic deformation from **X** to **p**. If the plastic deformation is homogeneous, no residual stresses exist upon de-stressing and in this case $\mathbf{F}^e$ and $\mathbf{F}^p$ are continuous functions. However, if the plastic deformation is non-homogeneous, residual stresses will result upon destressing. In order for all infinitesimal material elements to reach a zero stress state, individual material elements will have to undergo a different amount of de-stressing. Therefore, in this case, $\mathbf{F}^e$ and $\mathbf{F}^p$ can be defined as point-functions that relate the deformations in the infinitesimal material elements. In addition, we mention that the intermediate state **p** is not uniquely defined, because the elastic de-stressing can involve an arbitrary rigid-body rotation, which does not affect the stress. In order to have a unique **p**, we assume that the elastic de-stressing involves only pure deformation so that, by use of the polar decomposition of Section 3.5.2, the elastic part of the deformation gradient is

$$\mathbf{F}^e = \mathbf{V}^e \tag{7.85}$$

which is a symmetric tensor.

Using (7.84) and (3.100), the Lagrangian strain is

$$\begin{aligned}\mathbf{E} &= \tfrac{1}{2}(\mathbf{F}^{\mathrm{T}} \cdot \mathbf{F} - \mathbf{1}) = \tfrac{1}{2}(\mathbf{F}^{\mathrm{pT}} \cdot \mathbf{F}^{\mathrm{eT}} \cdot \mathbf{F}^{\mathrm{e}} \cdot \mathbf{F}^{\mathrm{p}} - \mathbf{1}) \\ &= \tfrac{1}{2}[\mathbf{F}^{\mathrm{pT}} \cdot (\mathbf{F}^{\mathrm{eT}} \cdot \mathbf{F}^{\mathrm{e}} - \mathbf{1}) \cdot \mathbf{F}^{\mathrm{p}}] + \tfrac{1}{2}[\mathbf{F}^{\mathrm{pT}} \cdot \mathbf{F}^{\mathrm{p}} - \mathbf{1}] = \mathbf{F}^{\mathrm{pT}} \cdot \mathbf{E}^{\mathrm{e}} \cdot \mathbf{F}^{\mathrm{p}} + \mathbf{E}^{\mathrm{p}} \end{aligned} \tag{7.86}$$

where

$$\mathbf{E}^{\mathrm{e}} = \tfrac{1}{2}(\mathbf{F}^{\mathrm{eT}} \cdot \mathbf{F}^{\mathrm{e}} - \mathbf{1}), \qquad \mathbf{E}^{\mathrm{p}} = \tfrac{1}{2}(\mathbf{F}^{\mathrm{pT}} \cdot \mathbf{F}^{\mathrm{p}} - \mathbf{1}) \tag{7.87}$$

It is seen from (7.86) that the additive decomposition of $\mathbf{E}^{\mathrm{e}}$ and $\mathbf{E}^{\mathrm{p}}$, as defined here, does not hold, that is,

$$\mathbf{E} \neq \mathbf{E}^{\mathrm{e}} + \mathbf{E}^{\mathrm{p}} \tag{7.88}$$

The velocity gradient in the current configuration $\mathbf{x}$ is

$$\mathbf{L} = \frac{\partial \mathbf{v}}{\partial \mathbf{x}} = \frac{\partial \mathbf{v}}{\partial X} \cdot \frac{\partial \mathbf{X}}{\partial \mathbf{x}} = \dot{\mathbf{F}} \cdot \mathbf{F}^{-1} \tag{7.89}$$

where $\dot{\mathbf{F}}$ is the material derivative of $\mathbf{F}$. Substituting (7.84) into (7.89), we obtain

$$\mathbf{L} = (\mathbf{F}^{\mathrm{e}} \cdot \mathbf{F}^{\mathrm{p}}) \cdot (\mathbf{F}^{\mathrm{e}} \cdot \mathbf{F}^{\mathrm{p}})^{-1} = \dot{\mathbf{F}}^{\mathrm{e}} \cdot \mathbf{F}^{\mathrm{e}^{-1}} + \mathbf{F}^{\mathrm{e}} \cdot \dot{\mathbf{F}}^{\mathrm{p}} \cdot \mathbf{F}^{\mathrm{p}^{-1}} \cdot \mathbf{F}^{\mathrm{e}^{-1}} \tag{7.90}$$

If we now choose the elastic de-stressing without rotation and the expression for $\mathbf{F}^{\mathrm{e}}$ given by (7.85), and let

$$\mathbf{L}^{\mathrm{p}} = \dot{\mathbf{F}}^{\mathrm{p}} \cdot \mathbf{F}^{\mathrm{p}^{-1}} = \mathbf{D}^{\mathrm{p}} + \mathbf{W}^{\mathrm{p}} \tag{7.91}$$

then

$$\mathbf{L} = \dot{\mathbf{V}}^{\mathrm{e}} \cdot \mathbf{V}^{\mathrm{e}^{-1}} + \mathbf{V}^{\mathrm{e}} \cdot \mathbf{D}^{\mathrm{p}} \cdot \mathbf{V}^{\mathrm{e}^{-1}} + \mathbf{V}^{\mathrm{e}} \cdot \mathbf{W}^{\mathrm{p}} \cdot \mathbf{V}^{\mathrm{e}^{-1}} \tag{7.92}$$

From (7.92), the rate of deformation $\mathbf{D}$ and the spin tensor $\mathbf{W}$ take the form

$$\begin{aligned}\mathbf{D} &= \mathbf{D}^{\mathrm{e}} + \mathbf{V}^{\mathrm{e}} \cdot \mathbf{D}^{\mathrm{p}} \cdot \mathbf{V}^{\mathrm{e}^{-1}}\big|_{\mathrm{S}} + \mathbf{V}^{\mathrm{e}} \cdot \mathbf{W}^{\mathrm{p}} \cdot \mathbf{V}^{\mathrm{e}^{-1}}\big|_{\mathrm{S}} \\ \mathbf{W} &= \mathbf{W}^{\mathrm{e}} + \mathbf{V}^{\mathrm{e}} \cdot \mathbf{D}^{\mathrm{p}} \cdot \mathbf{V}^{\mathrm{e}^{-1}}\big|_{\mathrm{A}} + \mathbf{V}^{\mathrm{e}} \cdot \mathbf{W}^{\mathrm{p}} \cdot \mathbf{V}^{\mathrm{e}^{-1}}\big|_{\mathrm{A}}\end{aligned} \tag{7.93}$$

where $\mathbf{D}^{\mathrm{e}}$, $\mathbf{W}^{\mathrm{e}} (= 0$, if $\mathbf{V}^{\mathrm{e}} = \mathbf{V}^{\mathrm{eT}})$, $\mathbf{D}^{\mathrm{p}}$, and $\mathbf{W}^{\mathrm{p}}$ are the symmetric and antisymmetric parts of $\dot{\mathbf{V}}^{\mathrm{e}} \cdot \mathbf{V}^{\mathrm{e}^{-1}}$ and $\mathbf{L}^{\mathrm{p}}$, respectively, and the subscripts S and A denote the symmetric and antisymmetric parts of a tensor. Looking at the expression for rate of deformation in (7.93), all three terms on the right-hand side of the equation are nonzero, in general. This indicates a very involved coupling of

$\mathbf{V}^e, \mathbf{D}^p$, and $\mathbf{W}^p$ in combining to produce the total rate of deformation $\mathbf{D}$. In this formulation, (7.92) cannot be reduced to the additive decomposition of $\mathbf{D}$, expressed by (7.81), in the general case. However, elastic strain is small and negligible for most metals undergoing large plastic deformation, and we may use the approximation that $\mathbf{V}^e \approx \mathbf{1}$ to reduce (7.93) to

$$\mathbf{D} = \mathbf{D}^e + \mathbf{D}^p, \qquad \mathbf{W} = \mathbf{W}^e + \mathbf{W}^p \tag{7.94}$$

On the other hand, Dafalias [58] introduced the concept of plastic spin based on Mandel's concept of director vectors [59]. The *plastic spin* is a macroscopic representation of the rotation of material texture caused by plastic deformation. One way of observing the texture experimentally is to plot the pole figures. The rotation (or tilting) of texture has been observed experimentally by Montheillet et al. [60], Stout and O'Rourke [61], Toth et al. [62], and Wang et al. [63] in the torsion of thin-walled tubes or solid bars. Dafalias [64] further used the difference between the total spin $\mathbf{W}$ and the plastic spin $\mathbf{W}^p$, termed *constitutive spin* $\boldsymbol{\omega}$ to form the corotational rate. According to Dafalias, using $\mathbf{F}^e = \mathbf{V}^e$, (7.90) may be rewritten as

$$\begin{aligned}\mathbf{L} = \mathbf{D} + \mathbf{W} &= \dot{\mathbf{V}}^e \cdot \mathbf{V}^{e^{-1}} + \mathbf{V}^e \cdot \dot{\mathbf{F}}^p \cdot \mathbf{F}^{p^{-1}} \cdot \mathbf{V}^{e^{-1}} \\ &= \boldsymbol{\omega} + \mathbf{V}^{e\nabla} \cdot \mathbf{V}^{e^{-1}} + \mathbf{V}^e \cdot \mathbf{F}^{p\nabla} \cdot \mathbf{F}^{p^{-1}} \cdot \mathbf{V}^{e^{-1}}\end{aligned} \tag{7.95}$$

where the superscript ∇ denote the corotational rate, which has been discussed in Section 4.7.1. Since $\mathbf{V}^e$ transforms as a second-order tensor and $\mathbf{F}^p$ transforms as a vector upon the rotation of $\mathbf{x}$ (observer transformation), their corotational derivatives are

$$\mathbf{V}^{e\nabla} = \dot{\mathbf{V}}^e + \mathbf{V}^e \cdot \boldsymbol{\omega} - \boldsymbol{\omega} \cdot \mathbf{V}^e, \qquad \mathbf{F}^{p\nabla} = \dot{\mathbf{F}}^p - \boldsymbol{\omega} \cdot \mathbf{F}^p \tag{7.96}$$

respectively. Restricting further to small elastic deformation for which $\mathbf{V}^e \approx \mathbf{1}$, the following are obtained from (7.95)

$$\begin{aligned}\mathbf{D} &= \mathbf{V}^{e\nabla} + (\mathbf{F}^{p\nabla} \cdot \mathbf{F}^{p^{-1}})_S = \mathbf{D}^e + \mathbf{D}^p \\ \mathbf{W} &= \boldsymbol{\omega} + (\mathbf{F}^{p\nabla} \cdot \mathbf{F}^{p^{-1}})_A = \boldsymbol{\omega} + \mathbf{W}^p\end{aligned} \tag{7.97}$$

with $\mathbf{D}^e = \mathbf{V}^{e\nabla}$, rate of a symmetric elastic deformation; $\mathbf{D}^p$ and $\mathbf{W}^p$ the rates of plastic deformation and plastic spin, respectively. Thus, a portion of the total spin $\mathbf{W}$ is "absorbed" by the plastic spin and the rest accommodated by the constitutive spin $\boldsymbol{\omega}$.

Dafalias [64] discussed the two definitions of "plastic spin" used in the literature and cautioned against defining the plastic spin as the antisymmetric part of the velocity gradient at the plastically deforming intermediate configuration. He suggested that the rotation of texture must be governed by a separate rule and not by the general kinematics of deformation. In the

continuum approach, constitutive equations must be provided not only for $\mathbf{D}^{\mathrm{p}}$ but also for $\mathbf{W}^{\mathrm{p}}$, Mandel [59] and Kratochvil [65]. Dafalias writes

$$\mathbf{W}^{\mathrm{p}} = \langle\lambda\rangle\boldsymbol{\Omega}^{\mathrm{p}}(\boldsymbol{\sigma}, \mathbf{s}) \tag{7.98}$$

where λ is a parameter. An internal state variable $\mathbf{s}$ macroscopically describes the state of the microstructures. Using the representation theorem of Wang [66], $\boldsymbol{\Omega}^{\mathrm{p}}$ can be represented by

$$\boldsymbol{\Omega}^{\mathrm{p}} = \eta_1(\mathbf{s}\cdot\boldsymbol{\sigma} - \boldsymbol{\sigma}\cdot\mathbf{s}) + \eta_2(\mathbf{s}\cdot\boldsymbol{\sigma}^2 - \boldsymbol{\sigma}^2\cdot\mathbf{s}) + \eta_3(\boldsymbol{\sigma}\cdot\mathbf{s}\cdot\boldsymbol{\sigma}^2 - \boldsymbol{\sigma}^2\cdot\mathbf{s}\cdot\boldsymbol{\sigma}) \tag{7.99}$$

where η_1, η_2, and η_3 are scalar valued functions of the invariants $\mathrm{tr}\,\boldsymbol{\sigma}$, $\mathrm{tr}\,\boldsymbol{\sigma}^2$, $\mathrm{tr}\,\boldsymbol{\sigma}^3$, $\mathrm{tr}(\mathbf{s}\cdot\boldsymbol{\sigma})$, and $\mathrm{tr}(\mathbf{s}\cdot\boldsymbol{\sigma}^2)$. Dafalias [64] and Loret [67] used the following simplified form to investigate the simple shear problem:

$$\mathbf{W}^{\mathrm{p}} = \eta(\boldsymbol{\alpha}\cdot\boldsymbol{\sigma} - \boldsymbol{\sigma}\cdot\boldsymbol{\alpha}) \tag{7.100}$$

where η is a parameter and $\mathbf{s}$ is taken to be the back stress $\boldsymbol{\alpha}$. In addition, Dafalias [68] proposed the following form when he investigated plastic materials with kinematic hardening

$$\mathbf{W}^{\mathrm{p}} = c(\boldsymbol{\alpha}\cdot\mathbf{D}^{\mathrm{p}} - \mathbf{D}^{\mathrm{p}}\cdot\boldsymbol{\alpha}) \tag{7.101}$$

where c is a parameter.

EXAMPLE 7.1 Derive the corotational rate of vector $\mathbf{g}$.

Solution

Let $\mathbf{g}$ be subjected to an orthogonal transformation such that

$$\bar{\mathbf{g}} = \mathbf{Q}^{\mathrm{T}}\cdot\mathbf{g} \tag{a}$$

Then,

$$\frac{\mathrm{D}\bar{\mathbf{g}}}{\mathrm{D}t} = \dot{\mathbf{Q}}^{\mathrm{T}}\cdot\mathbf{g} + \mathbf{Q}^{\mathrm{T}}\cdot\dot{\mathbf{g}} \tag{b}$$

From the third equation of (4.92), we have

$$\bar{\mathbf{W}} = \mathbf{Q}^{\mathrm{T}}\cdot\mathbf{W}\cdot\mathbf{Q} + \dot{\mathbf{Q}}^{\mathrm{T}}\cdot\mathbf{Q} = \mathbf{Q}^{\mathrm{T}}\cdot\mathbf{W}\cdot\mathbf{Q} - \mathbf{Q}^{\mathrm{T}}\cdot\dot{\mathbf{Q}} \tag{c}$$

or

$$\dot{\mathbf{Q}} = \mathbf{W}\cdot\mathbf{Q} - \mathbf{Q}\cdot\bar{\mathbf{W}} \tag{d}$$

and

$$\dot{\mathbf{Q}}^{\mathrm{T}} = \mathbf{Q}^{\mathrm{T}} \cdot \mathbf{W}^{\mathrm{T}} - \bar{\mathbf{W}}^{\mathrm{T}} \cdot \mathbf{Q}^{\mathrm{T}} \tag{e}$$

Substituting (e) into (b), we obtain

$$\frac{\mathrm{D}\bar{\mathbf{g}}}{\mathrm{D}t} = (\mathbf{Q}^{\mathrm{T}} \cdot \mathbf{W}^{\mathrm{T}} - \bar{\mathbf{W}}^{\mathrm{T}} \cdot \mathbf{Q}^{\mathrm{T}}) \cdot \mathbf{g} + \mathbf{Q}^{\mathrm{T}} \cdot \dot{\mathbf{g}} \tag{f}$$

which leads to

$$\dot{\bar{\mathbf{g}}} - \bar{\mathbf{W}} \cdot \bar{\mathbf{g}} = \mathbf{Q}^{\mathrm{T}} \cdot (\dot{\mathbf{g}} - \mathbf{W} \cdot \mathbf{g}) \tag{g}$$

It is to be noted that $\mathbf{W}$ is antisymmetric. The corotational rate of $\mathbf{g}$ can thus be defined as

$$\overset{\nabla}{\mathbf{g}} = \dot{\mathbf{g}} - \mathbf{W} \cdot \mathbf{g} \tag{h}$$

7.6.3 The Objective Rates

In Section 4.7 it was mentioned that only objective rates can be used to formulate a constitutive equation. There are many objective rates, however, and a reasonable objective rate should lead to results that can be verified by experiments. Different objective rates lead to different results and some are physically unacceptable results. For instance, it is known in hypoelasticity [69] that Jaumann rate gives rise to oscillatory shear and axial stresses with the increasing shear strain (see Section 4.10). In spite of this finding, some investigators continued to use the Jaumann rate in the finite deformation analysis. In the study of plasticity, Nagtegal and de Jong [70] analyzed the simple shear problem (shearing with constraint in axial direction) by use of the Jaumann rate for back stress using Prager's linear kinematic-hardening rule. They showed an oscillatory shear stress response to monotonically increasing shear strain. This work triggered a series of investigations to look for objective stress rate appropriate for the description of metallic behavior in the finite strain range. Investigators have compared several objective stress rates with the purpose of eliminating the oscillatory stress–strain response. Yet, certain unreasonable behaviors, such as axial stress being zero or compressive with unacceptably large value, still exist in the available models. Furthermore, the majority of these models are for specimens subjected to loading only. When unloading or cyclic simple shearing are considered, the aforementioned unusual stress–strain behaviors can manifest itself in the unloading curve or the stress–strain loops. Discussions have been centered around two possibilities of eliminating the oscillatory behavior. One is to find an objective rate that does not give rise to oscillatory stress responses even using a linear

constitutive equation. The other is to add a nonlinear term to the constitutive equation and, in this case, Jaumann rate does not lead to oscillatory stresses.

In this subsection, the objective rate is discussed in connection with hypoelasticity. The effect of objective rate in plasticity is deferred to a later section. In the case of simple shear deformation, the hypoelastic constitutive equation is from (4.240)

$$\sigma_{ij}^{*} = 2\mu D_{ij} \quad \text{and} \quad D_{kk} = 0 \tag{7.102}$$

where $\boldsymbol{\sigma}^{*}$ an objective rate and μ is the shear modulus. The simple shear deformation is governed by the following equations

$$x_1 = X_1 + 2\omega t X_2, \qquad x_2 = X_2, \qquad x_3 = X_3 \tag{7.103}$$

$$u_1 = 2\omega t X_2, \qquad u_2 = u_3 = 0, \qquad \omega = \text{const} \tag{7.104}$$

$$[L] = \begin{bmatrix} 0 & 2\omega & 0 \\ 0 & 0 & 0 \\ 0 & 0 & 0 \end{bmatrix}, \qquad [D] = \begin{bmatrix} 0 & \omega & 0 \\ s\omega & 0 & 0 \\ 0 & 0 & 0 \end{bmatrix}, \qquad [W] = \begin{bmatrix} 0 & \omega & 0 \\ -\omega & 0 & 0 \\ 0 & 0 & 0 \end{bmatrix} \tag{7.105}$$

The case of $\boldsymbol{\sigma}^{*}$ equaling to the Jaumann rate $\boldsymbol{\sigma}^{\nabla} = (\mathrm{D}\boldsymbol{\sigma}/\mathrm{D}t) - \mathbf{W}\cdot\boldsymbol{\sigma} + \boldsymbol{\sigma}\cdot\mathbf{W}$ has been discussed in Section 4.10. Following the procedures of Section 4.10, This section discusses the solutions of (7.102) and (7.105) using the Cotter–Rivlin stress rate [71], Oldroyd's convected stress rate [72], the Green–McInnis rate [69], and the mixed objective stress rates. In the case of the Cotter–Rivlin stress rate, the stress rate is

$$\boldsymbol{\sigma}^{*} = \frac{\mathrm{D}\boldsymbol{\sigma}}{\mathrm{D}t} + \mathbf{L}^{\mathrm{T}}\cdot\boldsymbol{\sigma} + \boldsymbol{\sigma}\cdot\mathbf{L} \tag{7.106}$$

and the solution is

$$\sigma_{11} = 0, \qquad \sigma_{22} = -4\mu\gamma^2, \qquad \sigma_{12} = 2\mu\gamma \tag{7.107}$$

where $\gamma = 2\omega t$. Note that σ_{12} increases linearly and σ_{22} nonlinearly with γ. Even though the shear stress–strain curve does not oscillate, which satisfies the requirement, the magnitude of the axial stress is greater than that of the shear stress. According to the experimental findings of Montheillet et al. [60], White and Anand (reported in [73]), and Wu et al. [74], the magnitude of axial stress is about 10% of shear stress. The predicted high σ_{22} of this model makes the model unacceptable.

In the case of Oldroyd's rate, the stress rate is

$$\boldsymbol{\sigma}^{*} = \frac{\mathrm{D}\boldsymbol{\sigma}}{\mathrm{D}t} - \mathbf{L}\cdot\boldsymbol{\sigma} - \boldsymbol{\sigma}\cdot\mathbf{L}^{\mathrm{T}} \tag{7.108}$$

On the other hand, Truesdell's rate [75] is

$$\boldsymbol{\sigma}^* = \frac{\mathrm{D}\boldsymbol{\sigma}}{\mathrm{D}t} + \boldsymbol{\sigma}\,\mathrm{tr}\,\mathbf{D} - \mathbf{L}\cdot\boldsymbol{\sigma} - \boldsymbol{\sigma}\cdot\mathbf{L}^{\mathrm{T}} \tag{7.109}$$

Since $\mathrm{tr}\,\mathbf{D} = 0$, (7.109) reduces to (7.108). The solution of this case is

$$\sigma_{11} = 4\mu\gamma^2, \qquad \sigma_{22} = 0, \qquad \sigma_{12} = 2\mu\gamma \tag{7.110}$$

This model predicts a zero σ_{22} and a high magnitude of σ_{11} which are unacceptable for real materials.

Using the Green–McInnis rate

$$\boldsymbol{\sigma}^* = \frac{\mathrm{D}\boldsymbol{\sigma}}{\mathrm{D}t} - \mathbf{W}^*\cdot\boldsymbol{\sigma} + \boldsymbol{\sigma}\cdot\mathbf{W}^* \qquad \text{where } \mathbf{W}^* = \dot{\mathbf{R}}\cdot\mathbf{R}^{\mathrm{T}} \tag{7.111}$$

in which tensor $\mathbf{R}$ is the orthogonal rotation tensor of the polar decomposition of the deformation gradient $\mathbf{F}$, Dienes [69] obtained the following solution

$$\begin{aligned}\sigma_{11} &= -\sigma_{22} = 4\mu[\cos 2\beta \ln(\cos\beta) + \beta\sin(2\beta) - \sin^2\beta]\\ \sigma_{12} &= 2\mu\cos 2\beta[2\beta - 2\tan 2\beta\ln(\cos\beta) - \tan\beta]\end{aligned} \tag{7.112}$$

where

$$\tan\beta = \omega t = \tfrac{1}{2}\gamma \tag{7.113}$$

The shear stress–strain curve of this model does not oscillate but the magnitude of axial stress is in the order of shear stress and does not agree with the experimental finding of approximately one-tenth of the magnitude of the shear stress.

All the aforementioned solutions of hypoelasticity are plotted in Figure 7.24.

EXAMPLE 7.2 Use the Green–McInnis rate to find the stresses for simple shearing.

Solution

The motion for simple shearing is from (3.20)

$$x_1 = X_1 + 2X_2\tan\beta, \qquad x_2 = X_2, \qquad x_3 = X_3 \tag{a}$$

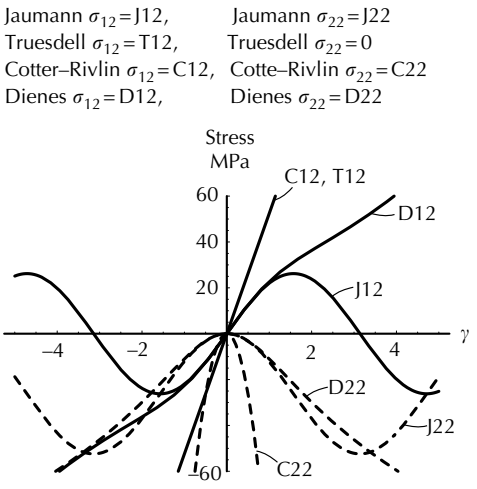

FIGURE 7.24
Simple shear of hypoelastic material.

From (a), we find

$$[F] = \begin{bmatrix} 1 & 2\tan\beta & 0 \\ 0 & 1 & 0 \\ 0 & 0 & 1 \end{bmatrix}, \qquad [D] = \begin{bmatrix} 0 & \sec^2\beta\dot{\beta} & 0 \\ \sec^2\beta\dot{\beta} & 0 & 0 \\ 0 & 0 & 0 \end{bmatrix},$$
$$[U^2] = [F]^{\mathrm{T}}[F] = \begin{bmatrix} 1 & 2\tan\beta & 0 \\ 2\tan\beta & 4\tan^2\beta + 1 & 0 \\ 0 & 0 & 1 \end{bmatrix} \tag{b}$$

The eigenvalues and eigenvectors of $[U^2]$ are

$$\begin{aligned} &\lambda_1 = 1, \qquad \lambda_2 = 1 + 2\tan^2\beta + 2\tan\beta\sec\beta, \\ &\lambda_3 = 1 + 2\tan^2\beta - 2\tan\beta\sec\beta \\ &\mathbf{n}_1^{\mathrm{T}} = \begin{bmatrix} 0 & 0 & 1 \end{bmatrix}, \qquad \mathbf{n}_2^{\mathrm{T}} = \frac{[(2\tan\beta - \sec\beta) \quad -2 \quad 1]}{\sqrt{(2\tan\beta - \sec\beta)^2 + 5}}, \\ &\mathbf{n}_3^{\mathrm{T}} = \frac{[(2\tan\beta + \sec\beta) \quad -2 \quad 1]}{\sqrt{(2\tan\beta + \sec\beta)^2 + 5}} \end{aligned} \tag{c}$$

Therefore, $[U]$ is

$$[U] = [\mathbf{n}_1 \quad \mathbf{n}_2 \quad \mathbf{n}_3] \begin{bmatrix} 1 & 0 & 0 \\ 0 & \lambda_2^{1/2} & 0 \\ 0 & 0 & \lambda_3^{1/2} \end{bmatrix} \begin{bmatrix} \mathbf{n}_1^{\mathrm{T}} \\ \mathbf{n}_2^{\mathrm{T}} \\ \mathbf{n}_3^{\mathrm{T}} \end{bmatrix} \tag{d}$$

We find

$$[R] = [F][U]^{-1} = \begin{bmatrix} \cos\beta & \sin\beta & 0 \\ -\sin\beta & \cos\beta & 0 \\ 0 & 0 & 1 \end{bmatrix}, \qquad [\dot{R}] = \begin{bmatrix} \sin\beta\dot{\beta} & \cos\beta\dot{\beta} & 0 \\ -\cos\beta\dot{\beta} & -\sin\beta\dot{\beta} & 0 \\ 0 & 0 & 0 \end{bmatrix} \tag{e}$$

and

$$[w^*] = [\dot{R}][R]^{\mathrm{T}} = \begin{bmatrix} 0 & \dot{\beta} & 0 \\ \dot{\beta} & 0 & 0 \\ 0 & 0 & 0 \end{bmatrix} \tag{f}$$

Using the Green–McInnis rate (7.111), the nonzero components of (7.102) are

$$\frac{\mathrm{d}\sigma_{11}}{\mathrm{d}t} - 2\dot{\beta}\sigma_{12} = 0 \tag{g}$$

$$\frac{\mathrm{d}\sigma_{12}}{\mathrm{d}t} + \dot{\beta}(\sigma_{11} - \sigma_{22}) = 2\mu \sec^2\beta\dot{\beta} \tag{h}$$

$$\frac{\mathrm{d}\sigma_{22}}{\mathrm{d}t} + 2\dot{\beta}\sigma_{12} = 0 \tag{i}$$

Equations (g) to (i) are combined to yield

$$\frac{\mathrm{d}^2\sigma_{11}}{\mathrm{d}\beta^2} + 4\sigma_{11} = \frac{4\mu}{\cos^2\beta} \qquad \text{with } \sigma_{22} = -\sigma_{11} \tag{j}$$

The general solution for (j) is

$$\sigma_{11} = 4\mu(\cos 2\beta \ln\cos\beta + \beta\sin 2\beta - \sin^2\beta) + c_1\cos 2\beta + c_2\sin 2\beta \tag{k}$$

where c_1 and c_2 are constants and they vanish when all initial (at $\beta = 0$) stress components are zero. Substituting (k) into (g), gives (7.112).

7.6.4 A Theory of Finite Elastic–Plastic Deformation

The rate of deformation **D** is used in this section. According to the concept of work conjugate discussed in Section 4.4.3, the Cauchy stress $\boldsymbol{\sigma}$ is the work conjugate of **D**. An objective stress rate should be used and we use the Jaumann rate in this discussion. Other objective stress rates will be discussed in the next section. The Jaumann stress rate is

$$\sigma_{ij}^{\nabla} = \dot{\sigma}_{ij} - W_{ip}\sigma_{pj} + \sigma_{ip}W_{pj} \tag{7.114}$$

where $\dot{\sigma}_{ij} = \mathrm{D}\sigma_{ij}/\mathrm{D}t$. Denoting the deviatoric part of D_{ij} by d_{ij}, we have $d_{ij} = d^{\mathrm{e}}_{ij} + d^{\mathrm{p}}_{ij}$. The Mises yield criterion is

$$f = \xi^{\mathrm{D}}_{ij}\,\xi^{\mathrm{D}}_{ij} - \frac{2Y^2}{3} = 0 \tag{7.115}$$

where $\xi^{\mathrm{D}}_{ij} = \sigma'_{ij} - \alpha^{\mathrm{D}}_{ij}$; the superscript D denotes the deviatoric part of the quantity and Y is the current yield stress in tension. The plastic region is characterized by $f = 0$ and $d^{\mathrm{p}}_{ij}\,\mathrm{d}\sigma'_{ij} > 0$, while the elastic region is characterized by either $f < 0$ or $f = 0$ and $d^{\mathrm{p}}_{ij}\,\mathrm{d}\sigma'_{ij} \le 0$. The tensor α_{ij} is the back stress.

The elastic behavior is governed by

$$\sigma'^{\nabla}_{ij} = 2\mu d^{\mathrm{e}}_{ij} \tag{7.116}$$

where μ is the shear modulus. The flow rule is

$$d^{\mathrm{p}}_{ij} = \dot{\lambda}\frac{\partial f}{\partial \sigma_{ij}} \tag{7.117}$$

where $\dot{\lambda}$ is a scalar factor of proportionality. Using (7.115), (7.117) reduces to

$$d^{\mathrm{p}}_{ij} = \dot{\lambda}\xi^{\mathrm{D}}_{ij} \tag{7.118}$$

For simplicity, the linear isotropic-hardening rule is used and is written as

$$\dot{Y} = \beta h \bar{d}^{\mathrm{p}} \tag{7.119}$$

where $\bar{d}^{\mathrm{p}}$ is the equivalent plastic strain rate defined by

$$\bar{d}^{\mathrm{p}} = \left(\tfrac{2}{3}d^{\mathrm{p}}_{ij}d^{\mathrm{p}}_{ij}\right)^{1/2} \tag{7.120}$$

and h is the slope of isotropic-hardening curve. The parameter β was previously discussed in (6.85) and $\beta = 1$ for isotropic hardening. Prager's linear kinematic-hardening rule is used, that is,

$$\alpha^{\mathrm{D}\nabla}_{ij} = \tfrac{2}{3}(1-\beta)h d^{\mathrm{p}}_{ij} \tag{7.121}$$

where $\beta = 0$ or kinematic hardening. The parameter β lies within $0 \le \beta \le 1$. When β has a value between 0 and 1, then we have a combined isotropic–kinematic hardening.

The factor $\dot{\lambda}$ is determined from the consistency condition. Differentiating (7.115), gives

$$\dot{f} = 2\xi_{ij}^{\mathrm{D}}\xi_{ij}^{\mathrm{D}\nabla} - \frac{4Y}{3}\dot{Y} = 0 \tag{7.122}$$

The expressions in (7.122) can be shown as

$$\begin{aligned}
\xi_{ij}^{\mathrm{D}}\xi_{ij}^{\mathrm{D}\nabla} &= \xi_{ij}^{\mathrm{D}}\big(\sigma_{ij}^{\prime\nabla} - \alpha_{ij}^{\mathrm{D}\nabla}\big) = \xi_{ij}^{\mathrm{D}}\big[2\mu d_{ij}^{\mathrm{e}} - \tfrac{2}{3}(1-\beta)h d_{ij}^{\mathrm{p}}\big] \\
&= 2\mu d_{ij}\xi_{ij}^{\mathrm{D}} - \big[2\mu + \tfrac{2}{3}(1-\beta)h\big]\dot{\lambda}\big(\tfrac{2}{3}Y^2\big) \\
\tfrac{2}{3}Y\dot{Y} &= \tfrac{2}{3}Y\beta h\bar{d}^{\mathrm{p}} = \tfrac{2}{3}Y\beta h\big(\tfrac{2}{3}\dot{\lambda}^2\xi_{ij}^{\mathrm{D}}\xi_{ij}^{\mathrm{D}}\big)^{1/2} = \tfrac{4}{9}\beta h Y^2\dot{\lambda}
\end{aligned} \tag{7.123}$$

By substituting the two expressions of (7.123) into (7.122), we obtain

$$2\mu d_{ij}\xi_{ij}^{\mathrm{D}} = \tfrac{2}{3}\dot{\lambda}\,Y^2\big[2\mu + \tfrac{2}{3}(1-\beta)h + \tfrac{2}{3}\beta h\big] \tag{7.124}$$

which may be solved for $\dot{\lambda}$ to obtain

$$\dot{\lambda} = \frac{3}{2}\frac{d_{ij}\xi_{ij}^{\mathrm{D}}}{Y^2(1 + (h/3\mu))} \tag{7.125}$$

Having found the expression for $\dot{\lambda}$, the rate of deformation may now be written as

$$d_{ij} = d_{ij}^{\mathrm{e}} + d_{ij}^{\mathrm{p}} = \frac{\sigma_{ij}^{\prime\nabla}}{2\mu} + \frac{3}{2}\frac{d_{km}\xi_{km}^{\mathrm{D}}\xi_{ij}^{\mathrm{D}}}{Y^2(1 + h/3\mu)} \tag{7.126}$$

This equation may be inverted to obtain

$$\sigma_{ij}^{\prime\nabla} = 2\mu\left[\delta_{ik}\delta_{jm} - \frac{\xi_{km}^{\mathrm{D}}\xi_{ij}^{\mathrm{D}}}{(2/3)Y^2(1 + h/3\mu)}\right]d_{km} \tag{7.127}$$

that is, the stress rate is expressed in terms of the rate of deformation d_{ij}. This equation is often written as

$$\sigma_{ij}^{\prime\nabla} = L_{ijkm}d_{km} \tag{7.128}$$

to facilitate computation. We note that the volumetric behavior is assumed to be elastic which is described by

$$\tfrac{1}{3}\dot{\sigma}_{kk} = KD_{kk} \tag{7.129}$$

where K is the bulk modulus.

EXAMPLE 7.3 Using the theory of this section to derive the stress–strain relation for uniaxial stress.

Solution

In the case of uniaxial stress

$$[\sigma'] = \begin{bmatrix} \frac{2}{3}\sigma & 0 & 0 \\ 0 & -\frac{\sigma}{3} & 0 \\ 0 & 0 & -\frac{\sigma}{3} \end{bmatrix}, \qquad [D^{\mathrm{p}}] = [d^{\mathrm{p}}] = \begin{bmatrix} \dot{\varepsilon}^{\mathrm{p}} & 0 & 0 \\ 0 & -\frac{1}{2}\dot{\varepsilon}^{\mathrm{p}} & 0 \\ 0 & 0 & -\frac{1}{2}\dot{\varepsilon}^{\mathrm{p}} \end{bmatrix} \tag{a}$$

$$[\alpha^{\mathrm{D}}] = \begin{bmatrix} \frac{2\alpha}{3} & 0 & 0 \\ 0 & -\frac{\alpha}{3} & 0 \\ 0 & 0 & \frac{\alpha}{3} \end{bmatrix}$$

Using (a), the yield function (7.115) is reduced to

$$\sigma = Y + \alpha \tag{b}$$

and, using (7.125), the equivalent plastic strain rate is

$$\bar{d}^{\mathrm{p}} = \{\tfrac{2}{3}[(\dot{\varepsilon}^{\mathrm{p}})^2 + 2(-\tfrac{1}{2}\dot{\varepsilon}^{\mathrm{p}})^2]\}^{1/2} = \dot{\varepsilon}^{\mathrm{p}} \tag{c}$$

The linear isotropic-hardening rule is then given by

$$\dot{Y} = \beta h \dot{\varepsilon}^{\mathrm{p}} \tag{d}$$

and the linear kinematic-hardening rule is from (7.121) and (7.130) reduces to

$$\dot{\alpha} = (1 - \beta) h \dot{\varepsilon}^{\mathrm{p}} \tag{e}$$

We note that due to $\mathbf{W}=\mathbf{0}$, $\boldsymbol{\sigma}^{\nabla} = \dot{\boldsymbol{\sigma}}$, and $\boldsymbol{\alpha}^{\mathrm{D}\nabla} = \dot{\boldsymbol{\alpha}}^{\mathrm{D}}$. The expression for (d) is the same as (6.147) and the expression for (e) is the same as (6.149). The roles of isotropic and kinematic hardening are similar to those shown in Figure 6.21(b). Using (d) and (e), the stress–plastic strain curve is given by

$$\dot{\sigma} = \dot{Y} + \dot{\alpha} = \beta h \dot{\varepsilon}^{\mathrm{p}} + (1 - \beta) h \dot{\varepsilon}^{\mathrm{p}} = h \dot{\varepsilon}^{\mathrm{p}} \tag{f}$$

The slope of the stress–plastic strain curve may be identified as

$$h = \frac{\dot{\sigma}}{\dot{\varepsilon}^{\mathrm{p}}} = \frac{\mathrm{d}\sigma}{\mathrm{d}\varepsilon^{\mathrm{p}}} \tag{g}$$

where the slope is a function of ε^{p}. The total strain is

$$\dot{\varepsilon} = \dot{\varepsilon}^{\mathrm{e}} + \dot{\varepsilon}^{\mathrm{p}} = \frac{\dot{\sigma}}{E} + \frac{\dot{\sigma}}{h} = \left(\frac{1}{E} + \frac{1}{h}\right)\dot{\sigma} \tag{h}$$

where E is the elastic modulus. In the stress–strain curve, the slope is

$$\frac{\mathrm{d}\sigma}{\mathrm{d}\varepsilon} = \frac{1}{(1/E) + (1/h)} = \mathrm{E_t} \tag{i}$$

where E_{t} is the tangent modulus. Therefore,

$$E_{\mathrm{t}} = \frac{hE}{h + E} \tag{j}$$

This equation relates E_{t} to E and h. Using (i), the axial stress–strain curve may be plotted. It is noted that the flow rule is not explicitly used in this one-dimensional case.

EXAMPLE 7.4 A rectangular metal block with edges parallel to the x, y, z-axes is compressed in the x-direction between overlapping rigid plates. Expansion is allowed only in the y-direction, and is prevented in the z-direction by rigid dies. All contact surfaces are perfectly lubricated so that the deformation is plane and uniform. The compressive strain in the x-direction is controlled and it increases monotonically from zero. Determine the stresses. Use the theory of this section and assume that the material hardens only by isotropic hardening.

Solution

Assume that in the elastic region, the behavior is hypoelastic so that

$$\dot{\sigma}_{ij} = \lambda\delta_{ij}D_{kk} + 2\mu\left(D_{ij} - D^{\mathrm{p}}_{ij}\right) \qquad \text{with } D_{kk} = D^{\mathrm{e}}_{kk} \tag{a}$$

We note that since $\mathbf{W} = \mathbf{0}$ for this problem, $\sigma^{\nabla}_{ij} = \dot{\sigma}_{ij}$. The flow rule is

$$D^{\mathrm{p}}_{ij} = \dot{\phi}\sigma'_{ij} \tag{b}$$

where $D^{\mathrm{p}}_{ij} = d^{\mathrm{p}}_{ij}$ due to plastic incompressibility. Parameter ϕ is used here so that a distinction can be made between this parameter and the Lamé constant λ used in (a). The equivalent plastic strain rate is

$$\bar{D}^{\mathrm{p}} = \left(\tfrac{2}{3}D^{\mathrm{p}}_{ij}D^{\mathrm{p}}_{ij}\right)^{1/2} \tag{c}$$

and the yield function is

$$f = \sigma'_{ij}\sigma'_{ij} - \frac{2Y^2}{3} = 0 \tag{d}$$

with the consistency condition

$$\dot{f} = 2\sigma'_{ij}\dot{\sigma}'_{ij} - \frac{4Y}{3}\dot{Y} = 0 \tag{e}$$

The isotropic hardening is

$$\dot{Y} = h\bar{D}^{\mathrm{p}}, \qquad \beta = 1 \tag{f}$$

Using (7.125), we obtain

$$\dot{\phi} = \frac{3}{2}\frac{D_{ij}\sigma'_{ij}}{Y^2(1 + h/3\mu)} \tag{g}$$

Substituting (g) and (b) into (a), we find

$$\dot{\sigma}_{ij} = \lambda\delta_{ij}D_{kk} + 2\mu D_{ij} - BD_{km}\sigma'_{km}\sigma'_{ij} \tag{h}$$

where

$$B = \frac{3\mu}{Y^2(1 + h/3\mu)} \tag{i}$$

The boundary conditions are

$$\sigma_x \neq 0, \qquad \sigma_{\mathrm{y}} = 0, \qquad \sigma_z \neq 0, \qquad D_x \neq 0 \text{ (known)}, \qquad D_y \neq 0, D_z = 0 \tag{j}$$

Apply the conditions $\dot{\sigma}_y = 0$ and $D_z = 0$ in (h) gives

$$D_y = -\frac{C_1}{C_2}D_x \tag{k1}$$

where

$$C_1 = 3\lambda + B(\sigma_x + \sigma_z)(2\sigma_x - \sigma_z) \tag{k2}$$

$$C_2 = 3\lambda + 6\mu - B(\sigma_x + \sigma_z)^2 \tag{k3}$$

The other two components of (h) are

$$\dot{\sigma}_x = \lambda(D_x + D_y) + 2\mu D_x - A(2\sigma_x - \sigma_z) \tag{l1}$$

$$\dot{\sigma}_z = \lambda(D_x + D_y) - A(2\sigma_z - \sigma_x) \tag{l2}$$

where

$$A = \left(\frac{-1}{\sigma_x + \sigma_z}\right)[\lambda(D_x + D_y) + 2\mu D_y] \tag{l3}$$

and (k1) was used in the derivation of (l3). Equations (l1) to (l3) can be further reduced to

$$\dot{\sigma}_x = C_3 D_x + C_4 D_y \tag{m1}$$

$$\dot{\sigma}_z = C_5 D_x + C_6 D_y \tag{m2}$$

where

$$\begin{aligned} C_3 &= 2\mu + \lambda\left(\frac{3\sigma_x}{\sigma_x + \sigma_z}\right), \qquad C_4 = C_3 + 2\mu\left(\frac{\sigma_x - 2\sigma_z}{\sigma_x + \sigma_z}\right) \\ C_5 &= \lambda\left(\frac{3\sigma_z}{\sigma_x + \sigma_z}\right), \qquad C_6 = C_5 - 2\mu\left(\frac{\sigma_x - 2\sigma_z}{\sigma_x + \sigma_z}\right) \end{aligned} \tag{m3}$$

Finally, we substitute (k1) into (m1) and (m2) to obtain

$$\dot{\sigma}_x = \left(C_3 - \frac{C_1 C_4}{C_2}\right) D_x \quad \text{and} \quad \dot{\sigma}_z = \left(C_5 - \frac{C_1 C_6}{C_2}\right) D_x \tag{n}$$

It is to be noted that C_i are functions of σ_x, σ_z and material constants. If we know D_x, then σ_x and σ_z may be calculated by the integration of (n), and D_y may be found from (k1). Additional exercises may be performed by plotting the σ_x versus $\int D_x \, dt$ and σ_z versus $\int D_x \, dt$ curves. In addition, D_y may be plotted as a function of D_x and the effect of h on the results discussed. An experimental study of the biaxial compression problem was conducted by Khan and Wang [76].

7.6.5 A Study of Simple Shear Using Rigid-Plastic Equations with Linear Kinematic Hardening

The subject of study in this section is the problem of simple shear using rigid-plastic equations with linear kinematic hardening, that is, $\beta = 0$. Three objective rates are considered. They are the Jaumann rate, the Dafalias rate, and Lee's rate [77].

7.6.5.1 The Jaumann rate

The Mises yield criterion is

$$\tfrac{3}{2}(\boldsymbol{\sigma}' - \boldsymbol{\alpha}^{\mathrm{D}}) \cdot (\boldsymbol{\sigma}' - \boldsymbol{\alpha}^{\mathrm{D}}) = Y^2 \tag{7.130}$$

The kinematic-hardening rule is from (7.121)

$$\alpha_{ij}^{\mathrm{D}\nabla} = \tfrac{2}{3} h D_{ij} \tag{7.131}$$

where $d_{ij}^{\mathrm{p}} = d_{ij} = D_{ij}$ and $D_{kk} = 0$. The Jaumann rate is given by (7.114) and the flow rule is from (7.118)

$$D_{ij} = \dot{\lambda}\left(\sigma_{ij}' - \alpha_{ij}^{\mathrm{D}}\right) \tag{7.132}$$

Using the finite simple shear straining described by (7.105), we obtain from (7.132)

$$\sigma_{11}' = \alpha_{11}^{\mathrm{D}}, \qquad \sigma_{22}' = \alpha_{22}^{\mathrm{D}}, \qquad \sigma_{12}' = \alpha_{12}^{\mathrm{D}} + \frac{\omega}{\dot{\lambda}} = \alpha_{12}^{\mathrm{D}} + \frac{Y}{\sqrt{3}} \tag{7.133}$$

The last expression was obtained using (7.132) and (7.130). The expression of (7.131) is in the form of (7.102), whose solution in the case of Jaumann rate is given by (4.248). Therefore, the solution for (7.131) is

$$\alpha_{12}^{\mathrm{D}} = \frac{h}{3}\sin\gamma, \qquad \alpha_{11}^{\mathrm{D}} = -\alpha_{22}^{\mathrm{D}} = \frac{h}{3}(1 - \cos\gamma) \tag{7.134}$$

From (7.134) we infer that $\alpha_{11}^{\mathrm{D}} + \alpha_{22}^{\mathrm{D}} = 0$ and, therefore, from the first two equations of (7.133) we obtain $\sigma_{22}' = -\sigma_{11}'$ or $(2\sigma_{22} - \sigma_{11})/3 = -(2\sigma_{11} - \sigma_{22})/3$. Thus, $\sigma_{11} + \sigma_{22} = 0$ or $\sigma_{kk} = 0$, since $\sigma_{33} = 0$. Using this result, we conclude that $\sigma_{11} = \sigma_{11}'$ and $\sigma_{22} = \sigma_{22}'$. Equations (7.133) and (7.134) combine to yield

$$\sigma_{12} = \frac{Y}{\sqrt{3}} + \frac{h}{3}\sin\gamma, \qquad \sigma_{11} = -\sigma_{22} = \frac{h}{3}(1 - \cos\gamma), \qquad \text{other } \sigma_{ij} = 0 \tag{7.135}$$

This is the solution for the simple shear problem by use of the Jaumann rate for the back stress. It is seen that all nonzero stress components are oscillatory. Finally, it is easy to show that by eliminating γ from the equations of (7.134), we find

$$\left(\alpha_{12}^{\mathrm{D}}\right)^2 + \left(\frac{h}{3} - \alpha_{11}^{\mathrm{D}}\right)^2 = \left(\frac{h}{3}\right)^2 \tag{7.136}$$

that is, the back stress is making a circular motion when the Jaumann rate is used.

7.6.5.2 The Dafalias rate

The yield function is given by (7.130) and the flow rule is given by (7.132). Upon the substitution of (7.105) into (7.132), we obtain (7.133). The kinematic-hardening rule is

$$\alpha_{ij}^{\mathrm{D}^*} = \tfrac{2}{3} h D_{ij} \tag{7.137}$$

in which

$$\alpha_{ij}^{\mathrm{D}^*} = \frac{\mathrm{D}\alpha_{ij}^{\mathrm{D}}}{\mathrm{D}t} - \omega_{ij}\alpha_{ji}^{\mathrm{D}} + \alpha_{ij}^{\mathrm{D}}\omega_{ji} \tag{7.138}$$

is the Dafalias rate; ω_{ij} is the constitutive spin defined by (7.97) and is written as

$$\omega_{ij} = W_{ij} - W_{ij}^{\mathrm{p}} = W_{ij} - \eta\left(\alpha_{ij}^{\mathrm{D}} D_{ji} - D_{ij}\alpha_{ji}^{\mathrm{D}}\right) \tag{7.139}$$

where η is a parameter which describes the strength of plastic spin. By use of (7.105), it is easily shown that

$$[\omega] = \xi \begin{bmatrix} 0 & \omega & 0 \\ -\omega & 0 & 0 \\ 0 & 0 & 0 \end{bmatrix} \qquad \text{with } \xi = 1 - \eta\left(\alpha_{11}^{\mathrm{D}} - \alpha_{22}^{\mathrm{D}}\right) \tag{7.140}$$

Thus, (7.137) is reduced to

$$\frac{\mathrm{D}}{\mathrm{D}t}\begin{bmatrix} \alpha_{11}^{\mathrm{D}} & \alpha_{12}^{\mathrm{D}} & 0 \\ \alpha_{12}^{\mathrm{D}} & \alpha_{22}^{\mathrm{D}} & 0 \\ 0 & 0 & 0 \end{bmatrix} - \xi\omega \begin{bmatrix} 2\alpha_{12}^{\mathrm{D}} & \left(\alpha_{22}^{\mathrm{D}} - \alpha_{11}^{\mathrm{D}}\right) & 0 \\ \left(\alpha_{22}^{\mathrm{D}} - \alpha_{11}^{\mathrm{D}}\right) & -2\alpha_{12}^{\mathrm{D}} & 0 \\ 0 & 0 & 0 \end{bmatrix} = \frac{2}{3} h \begin{bmatrix} 0 & \omega & 0 \\ \omega & 0 & 0 \\ 0 & 0 & 0 \end{bmatrix} \tag{7.141}$$

The nonzero components of the equation are

$$\begin{aligned} \frac{\mathrm{D}\alpha_{11}^{\mathrm{D}}}{\mathrm{D}t} &= 2\alpha_{12}^{\mathrm{D}}\left(1 - \eta\alpha_{11}^{\mathrm{D}} + \eta\alpha_{22}^{\mathrm{D}}\right)\omega \\ \frac{\mathrm{D}\alpha_{22}^{\mathrm{D}}}{\mathrm{D}t} &= -2\alpha_{12}^{\mathrm{D}}\left(1 - \eta\alpha_{11}^{\mathrm{D}} + \eta\alpha_{22}^{\mathrm{D}}\right)\omega \\ \frac{\mathrm{D}\alpha_{12}^{\mathrm{D}}}{\mathrm{D}t} &= \frac{2}{3} h\omega + \left(\alpha_{22}^{\mathrm{D}} - \alpha_{11}^{\mathrm{D}}\right)\left(1 - \eta\alpha_{11}^{\mathrm{D}} + \eta\alpha_{22}^{\mathrm{D}}\right)\omega \end{aligned} \tag{7.142}$$

Since $\alpha_{11}^{\mathrm{D}} = \alpha_{22}^{\mathrm{D}} = 0$ initially, $\alpha_{11}^{\mathrm{D}} = -\alpha_{22}^{\mathrm{D}}$ for all t. Using this result, (7.142) is simplified to yield

$$\frac{\mathrm{d}\alpha_{11}^{\mathrm{D}}}{\mathrm{d}\gamma} = \left(1 - 2\eta\alpha_{11}^{\mathrm{D}}\right)\alpha_{12}^{\mathrm{D}}, \qquad \frac{\mathrm{d}\alpha_{12}^{\mathrm{D}}}{\mathrm{d}\gamma} = \frac{h}{3} - \left(1 - 2\eta\alpha_{11}^{\mathrm{D}}\right)\alpha_{11}^{\mathrm{D}} \tag{7.143}$$

where $\gamma = 2\omega t$. We now introduce dimensionless variables $\hat{\alpha}_{11} = \alpha_{11}^{\mathrm{D}}/Y$ and $\hat{\alpha}_{12} = \alpha_{12}^{\mathrm{D}}/Y$, and a parameter $\hat{h} = h/(3Y)$, so that (7.143) may be written as

$$\frac{\mathrm{d}\hat{\alpha}_{11}}{\mathrm{d}\gamma} = (1 - \hat{h}\rho\hat{\alpha}_{11})\hat{\alpha}_{12}, \qquad \frac{\mathrm{d}\hat{\alpha}_{12}}{\mathrm{d}\gamma} = \hat{h} - (1 - \hat{h}\rho\hat{\alpha}_{11})\hat{\alpha}_{11} \tag{7.144}$$

where

$$\hat{h}\rho = 2\eta Y \tag{7.145}$$

The equations in (7.143) are solved numerically by Dafalias [58]. The boundary condition is $\alpha_{ij}^{\mathrm{D}} = 0$ at initial yielding. Similar to (7.133), we may establish that

$$\sigma_{11} = \alpha_{11}^{\mathrm{D}}, \qquad \sigma_{22} = \alpha_{22}^{\mathrm{D}} = -\alpha_{11}^{\mathrm{D}}, \qquad \sigma_{12} = \alpha_{12}^{\mathrm{D}} + \frac{Y}{\sqrt{3}} \tag{7.146}$$

In Figure 7.25(a), we plot the shear stress–strain curves with values of $\hat{h} = 1.0, 1.5, 1.6, 1.7, 1.75$, and 2.0, while keeping $\rho = 0.08$. The corresponding axial stress versus shear strain curves are plotted in Figure 7.25(b), and the corresponding back stress paths as the shear strain γ increases are plotted in Figure 7.25(c). It clearly shows that the solution is very sensitive to the relative value between $\hat{h}$ and ρ. A large ρ indicates a strong plastic spin and the corresponding constitutive spin is small. When $\hat{h}$ is relatively small such as 1.0, the constitutive spin is significant and it causes the back stress to spin as indicated in Figure 7.25(c). As a result, both the axial and shear stresses are oscillatory. The stresses are not oscillatory for larger $\hat{h}$, but they are very sensitive to this parameter as seen from Figure 7.25(b) and (c). We would also like to mention that generally the magnitude of axial stress of this model is larger than the shear stress, which is not reasonable.

7.6.5.3 The rate of Lee

Lee et al. [77] proposed a spin $\mathbf{W}^*$ to replace the spin tensor $\mathbf{W}$ in the Jaumann rate, achieving nonoscillatory stresses in simple shearing. The tensor $\mathbf{W}^*$ is determined by the angular velocity of the material line element which is instantaneously coincident with the eigenvector associated with the maximum eigenvalue of back stress $\boldsymbol{\alpha}$. The spin $\mathbf{W}^*$ is expressed by

$$W_{ij}^* = W_{ij} + D_{ik}n_k n_j - n_i n_k D_{kj} \tag{7.147}$$

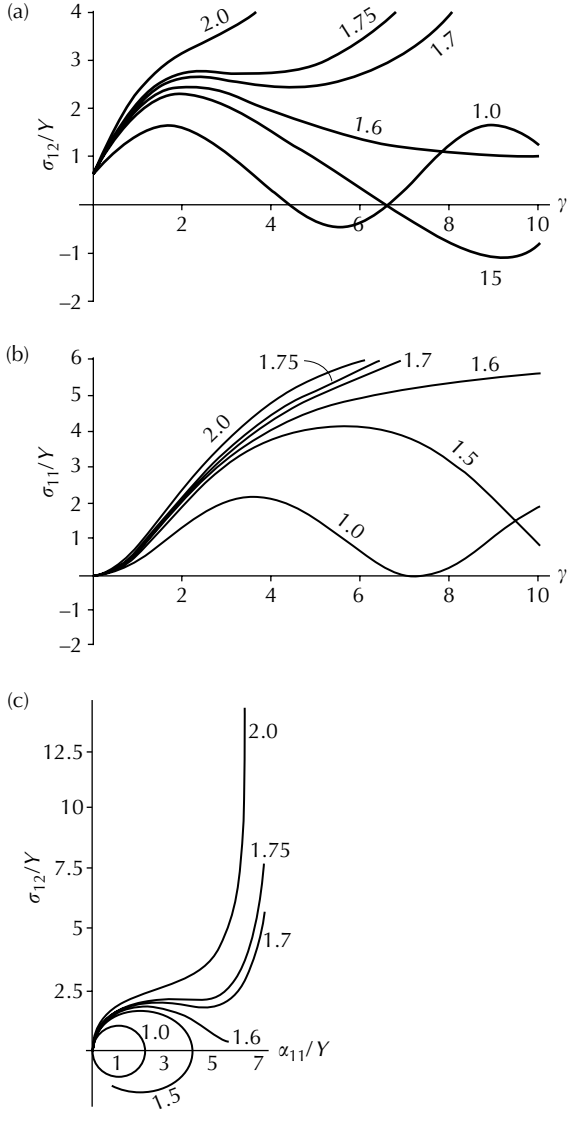

FIGURE 7.25
Simple shear using Dafalias's rate: (a) shear stress–strain curves, (b) axial stress, (c) back stress.

where $\mathbf{n}$ is that eigenvector of $\boldsymbol{\alpha}$. Lee et al. [77] pointed out that kinematic hardening is an anisotropic phenomenon for which specific directions embedded in the material and the rotation of these particular directions play a significant role. It is noted, however, that the rotation of the eigenvector used to define $\mathbf{W}^*$ is a part of the kinematics of deformation and is not directly related to the rotation of the material texture. Dafalias rate is different

in that it contains a parameter that is related to the spin of the material texture.

Following [77], we now use $\mathbf{W}^*$ in connection with the corotational rate to investigate the simple shear deformation. The rate of Lee et al. may be written as

$$\boldsymbol{\alpha}^{\mathrm{D}^*} = \frac{\mathrm{D}\boldsymbol{\alpha}^{\mathrm{D}}}{\mathrm{D}t} - \mathbf{W}^* \cdot \boldsymbol{\alpha}^{\mathrm{D}} + \boldsymbol{\alpha}^{\mathrm{D}} \cdot \mathbf{W}^* \tag{7.148}$$

Since a corotational rate is objective, Lee's rate is objective. For the simple shear deformation defined by (7.105), the line element associated with $\mathbf{W}^*$ is on the (x_1, x_2) plane. Thus, $[n]^{\mathrm{T}} = [n_1 \quad n_2 \quad 0]$. Substituting this expression of $[n]$ into (7.147), we find

$$[W^*] = 2n_2^2\omega \begin{bmatrix} 0 & 1 & 0 \\ -1 & 0 & 0 \\ 0 & 0 & 0 \end{bmatrix} \qquad \text{with } n_1^2 + n_2^2 = 1 \tag{7.149}$$

Using (7.149) and (7.148), the nonzero components of the linear kinematic-hardening rule (7.137) are

$$\begin{aligned} &\dot{\alpha}_{11}^{\mathrm{D}} - 4n_2^2\omega\alpha_{12}^{\mathrm{D}} = 0 \\ &\dot{\alpha}_{22}^{\mathrm{D}} + 4n_2^2\omega\alpha_{12}^{\mathrm{D}} = 0 \\ &\dot{\alpha}_{12}^{\mathrm{D}} - 2n_2^2\omega\left(\alpha_{22}^{\mathrm{D}} - \alpha_{11}^{\mathrm{D}}\right) = \frac{2h}{3}\omega \end{aligned} \tag{7.150}$$

Equations in (7.150) are further reduced to

$$\dot{\alpha}_{12}^{\mathrm{D}} = \frac{2h}{3}\omega - 4n_2^2\omega\alpha_{11}^{\mathrm{D}}, \qquad \dot{\alpha}_{11}^{\mathrm{D}} - 4n_2^2\omega\alpha_{12}^{\mathrm{D}} = 0, \quad \text{and} \quad \alpha_{22}^{\mathrm{D}} = -\alpha_{11}^{\mathrm{D}} \tag{7.151}$$

We now determine the eigenvector $\mathbf{n}$. We have

$$\begin{bmatrix} \alpha_{11}^{\mathrm{D}} - \lambda & \alpha_{12}^{\mathrm{D}} & 0 \\ \alpha_{12}^{\mathrm{D}} & \alpha_{22}^{\mathrm{D}} - \lambda & 0 \\ 0 & 0 & 0 - \lambda \end{bmatrix} \begin{bmatrix} n_1 \\ n_2 \\ 0 \end{bmatrix} = \begin{bmatrix} 0 \\ 0 \\ 0 \end{bmatrix} \tag{7.152}$$

From (7.152), we obtain

$$n_1 = \sqrt{1 - n_2^2}, \qquad n_2 = \frac{1}{\sqrt{R^2 + 1}}, \qquad R = \frac{-\alpha_{22}^{\mathrm{D}} + \sqrt{\left(\alpha_{22}^{\mathrm{D}}\right)^2 + \left(\alpha_{12}^{\mathrm{D}}\right)^2}}{\alpha_{12}^{\mathrm{D}}} \tag{7.153}$$

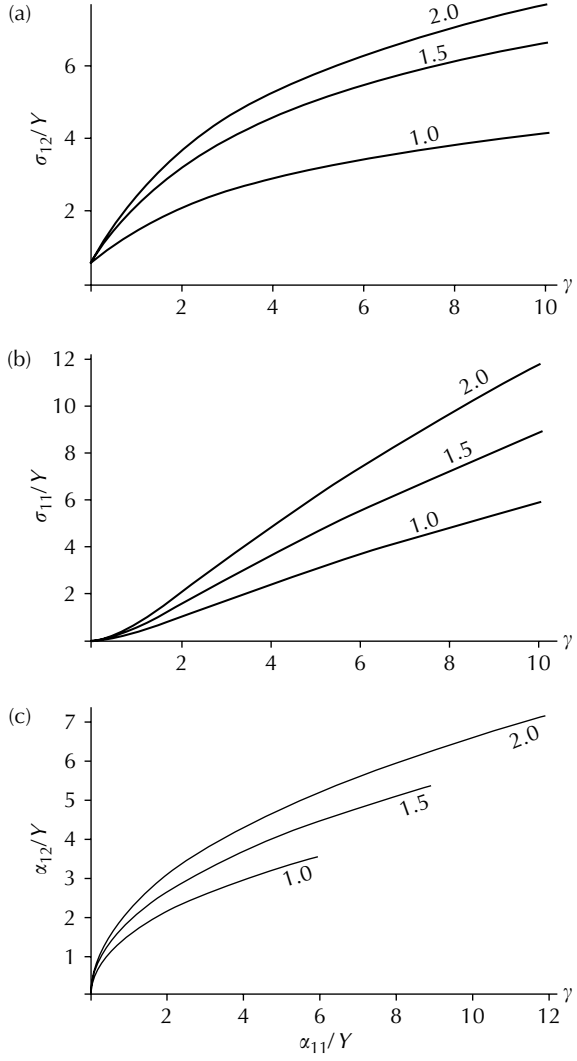

FIGURE 7.26
Simple shear using Lee's rate: (a) shear stress–strain curves, (b) axial stress, (c) back stress.

The positive n_2 is chosen which corresponds to the maximum eigenvalue. In this way, n_2 is expressed in terms of components α_{22}^{D} and α_{12}^{D}. Knowing α_{ij}^{D}, we determine $[n]$, which may then be substituted into (7.151). Finally, we mention that (7.146) still applies in this case.

Numerical results for simple shear using Lee's rate are plotted in Figure 7.26(a) to (c). The curves are plotted for $\hat{h} = 1.0$, 1.5, and 2.0. We see that all curves are not oscillatory, but the predicted axial stress is too large.

EXAMPLE 7.5 Show that $\mathbf{W}^*$ of Lee's rate represents the spin of a material line element.

Solution

Let the line element be $\mathrm{d}x_i$ and be denoted by

$$\mathrm{d}x_i = n_i \,\mathrm{d}s \tag{a}$$

where n_i is the unit vector along the line element and $\mathrm{d}s$ is the length of the line element. The relative velocity between the ends of the line element is

$$\mathrm{d}v_i = \frac{\partial v_i}{\partial x_j}\,\mathrm{d}x_j = L_{ij} n_j \,\mathrm{d}s \tag{b}$$

The component of $\mathrm{d}\mathbf{v}$ normal to $\mathbf{n}$ determines the spin $\mathbf{W}^*$ of that line element to within an arbitrary spin. The component of $\mathrm{d}\mathbf{v}$ normal to $\mathbf{n}$ is denoted by

$$\mathrm{d}\mathbf{v}^* = \mathrm{d}\mathbf{v} - (\mathrm{d}\mathbf{v}\cdot\mathbf{n})\mathbf{n} \tag{c}$$

Then, (c) in the subscript notation is

$$\begin{aligned}\mathrm{d}v_i^* &= \mathrm{d}v_i - \mathrm{d}v_k n_k n_i = L_{ij} n_j \,\mathrm{d}s - L_{kj} n_j \,\mathrm{d}s n_k n_i \\ &= (D_{ij} + W_{ij}) n_j \,\mathrm{d}s - (D_{kj} + W_{kj}) n_j n_k n_i \,\mathrm{d}s \\ &= D_{ij} n_j \,\mathrm{d}s + W_{ij} n_j \,\mathrm{d}s - D_{kj} n_j n_k n_i \,\mathrm{d}s \end{aligned} \tag{d}$$

But,

$$\mathrm{d}\mathbf{v}^* = \mathbf{w}^* \times \mathbf{n}\,\mathrm{d}s \tag{e}$$

where $\mathbf{w}^*$ is the dual vector of $\mathbf{W}^*$. In the index notation, (e) is

$$\mathrm{d}v_i^* = e_{ijk} w_j^* n_k \,\mathrm{d}s = e_{kij} w_j^* n_k \,\mathrm{d}s = -W_{ki}^* n_k \,\mathrm{d}s = W_{ik}^* n_k \,\mathrm{d}s \tag{f}$$

Equating (d) and (f), we obtain

$$W_{ik}^* n_k = D_{ij} n_j (n_k n_k) + W_{ij} n_j - D_{kj} n_j n_k n_i \tag{g}$$

which reduces to

$$W_{ij}^* = W_{ij} + D_{ik} n_k n_j - n_i n_k D_{kj} \tag{h}$$

EXAMPLE 7.6 Let the simple shear motion be

$$[D] = \begin{bmatrix} 0 & \omega & 0 \\ \omega & 0 & 0 \\ 0 & 0 & 0 \end{bmatrix}, \qquad [W] = \begin{bmatrix} 0 & \omega & 0 \\ -\omega & 0 & 0 \\ 0 & 0 & 0 \end{bmatrix} \tag{a}$$

Find the expression of [W*].

Solution

Let $[n] = (\cos\theta, \sin\theta, 0)$, then from (7.147)

$$[W^*] = \begin{bmatrix} 0 & 2\omega\sin^2\theta & 0 \\ -2\omega\sin^2\theta & 0 & 0 \\ 0 & 0 & 0 \end{bmatrix} \tag{b}$$

Since

$$w_k^* = -\tfrac{1}{2} e_{ijk} W_{ij}^* \tag{c}$$

We find

$$[w^*]^{\mathrm{T}} = \begin{bmatrix} 0 & 0 & -2\omega\sin^2\theta \end{bmatrix} \tag{d}$$

Thus, the angular velocity $w_3^* = \dot{\theta}$ of the line element varies with the direction of the line element defined by angle θ. The line along the x_1-axis does not rotate and the spin is maximum along the x_2-axis.

7.6.5.4 Remarks about objective rates of plasticity

The spin **W** is overemphasized by the Jaumann rate. In simple shear, **W** is the angular velocity $\dot{\theta}$ of the line element, along the principal direction of **D**, making a $\theta = \pi/4$ angle with the x_1-axis. Referring to Figure 7.27, a square material element initially at $OA_0\,B_0\,C$ assumes the shape OABC during simple shearing. As the shear strain becomes large, all lines emanating from O and lying within the angle $\angle$AOC have small angles θ, which are less than $\pi/4$. According to Lee et al. [77], these lines do not have the same $\dot{\theta}$ and do not rotate much. The line along OC does not spin at all and the line along OA does not spin as much as **W**. This effect may be seen from Example 7.5 by using a small θ in equation (d). It is noted that both D_{ij} and W_{ij} refer to a square element, with sides parallel to the x_1 and x_2 axes, defined at the current configuration. Therefore, **W** represents the spin of this new element which does not contain the same material mass as the original element. The Jaumann rate overemphasizes **W** because it does not represent the spin of the original material element.

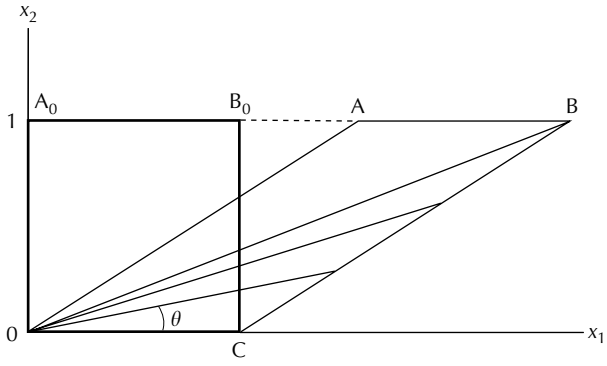

FIGURE 7.27
Rotation of line element during simple shearing.

From the discussions of previous subsections, we see that some objective rates lead to oscillatory stress components in simple shearing when the shear strain is monotonically increasing. This effect is of course in violation of experimental observations. Of the several objective rates discussed none can lead to acceptable stress responses using a linear kinematic-hardening equation. Several rates lead to an axial stress which is about the same or larger in magnitude than the shear stress, while experimental results show that the axial stress is about one-tenth of the magnitude of the shear stress. A conclusion may be drawn that these rates will have to be applied to a nonlinear kinematic-hardening equation.

The concept of constitutive spin proposed by Dafalias [64] is promising. It introduces a constitutive equation for the plastic spin which is a macroscopic description of the spin of material texture. From the experimental investigation of material textures [60–63], it is known that the spin (or tilting) of the material texture is not directly expressed by the general kinematics of deformation. In the case of torsion, for instance, a monotonic increasing shear deformation can cause the texture to rotate in a direction of decreasing shear strain and then reverse its direction as the shear strain becomes larger. This is the evidence that plastic spin should not be defined by the general kinematics of deformation.

The plastic deformation induced anisotropy is described to a large extent by the kinematic hardening. Since plastic deformation changes the material texture, it is reasonable to use the back stress to describe the texture rotation. As previously mentioned, the plastic spin is independent of the kinematics of deformation, while the stress rate and the strain rate are dependent of the same. Therefore, different objective rates should be used for back stress, stress, and strain. In Wu [78,79], we use Dafalias rate for the back stress, and the convected rate for the stress and strain. This approach will be further discussed in Chapter 11 in connection with a curvilinear coordinate system.

7.6.6 The Yield Criterion for Finite Plasticity

Most works of finite plasticity have focused on the decomposition of deformation into elastic and plastic parts and the objective stress rates or back stress rates. Little attention has been given to the yield criterion applicable in the finite deformation range. Most theoretical works have assumed that the Mises yield criterion can be used. Some apply the Mises criterion expressed in terms of the Cauchy stress and some the 2nd P–K stress. The main concern is that yield criterion should be observer independent. For an isotropic material, this statement is equivalent to the requirement that the yield criterion be independent of rigid-body rotation of the material element. However, this is only an approximation because the material does not remain isotropic during plastic deformation. A yield criterion is observer independent, if it is defined by stress invariants. It is noted, however, that a square material element used to define the Cauchy stress does not remain square during plastic deformation. If referring to the orientation of another observer, a square element is chosen to describe the state of stress, the aforementioned two square elements do not contain the same material mass. The two elements can be compared only when material isotropy is assumed and the concept of stress invariants is based on this assumption. In Chapter 11, an observer independent yield criterion will be defined in terms of the contravariant true stress, which remains unchanged either during an observer transformation or when the material element undergoes a superimposed rigid-body rotation.

In the remainder of this section, we investigate the effect of stress measure on the shape, size, and translation of the yield surface when the specimen has been prestrained into the finite deformation range. Specifically, we compare the yield surfaces in the combined axial–torsion problem when the yield function is defined by the Cauchy stress, the 1st P–K stress, and the 2nd P–K stress, following the study of Wu et al. [24]. Usually, the stresses in the experimental data are the physical components in the cylindrical-coordinates system, so that all stress components have the same unit. The physical components will be discussed in Chapter 11 in connection with the curvilinear coordinates. The physical components in the present case are components of a tensor referred to unit vectors $\mathbf{e}_r$, $\mathbf{e}_\theta$, $\mathbf{e}_z$ in the radial, tangential, and axial direction, respectively.

EXAMPLE 7.7 Determine the physical components of the deformation gradient $\mathbf{F}$ in the cylindrical coordinate system.

Solution

Let (r, θ, z) be the cylindrical coordinates of a point having Cartesian coordinates (x, y, z). The following equations hold

$$x = r\cos\theta, \qquad y = r\sin\theta, \qquad z = z \tag{a}$$

An inversion of (a) yields

$$r^2 = x^2 + y^2, \qquad \theta = \tan^{-1}\left(\frac{y}{x}\right), \qquad z = z \tag{b}$$

The unit base vectors of the cylindrical system are $(\mathbf{e}_r, \mathbf{e}_\theta, \mathbf{e}_z)$, and the unit vectors of the Cartesian system are $(\mathbf{e}_x, \mathbf{e}_y, \mathbf{e}_z)$. These unit vectors are related by

$$\mathbf{e}_r = \cos\theta \mathbf{e}_x + \sin\theta \mathbf{e}_y, \qquad \mathbf{e}_\theta = -\sin\theta \mathbf{e}_x + \cos\theta \mathbf{e}_y \tag{c}$$

Taking the partial derivatives of (b) and using (a), we obtain

$$\begin{aligned} &\frac{\partial r}{\partial x} = \frac{x}{r} = \cos\theta, \qquad \frac{\partial r}{\partial y} = \frac{y}{r} = \sin\theta, \\ &\frac{\partial \theta}{\partial x} = \frac{-y}{x^2 + y^2} = \frac{-y}{r^2} = \frac{-\sin\theta}{r}, \qquad \frac{\partial \theta}{\partial y} = \frac{\cos\theta}{r} \end{aligned} \tag{d}$$

Differentiation of (c) gives

$$\begin{aligned} &\frac{\partial \mathbf{e}_r}{\partial r} = \frac{\partial \mathbf{e}_\theta}{\partial r} = \frac{\partial \mathbf{e}_z}{\partial r} = \frac{\partial \mathbf{e}_z}{\partial \theta} = \frac{\partial \mathbf{e}_r}{\partial z} = \frac{\partial \mathbf{e}_\theta}{\partial z} = \frac{\partial \mathbf{e}_z}{\partial z} = 0 \\ &\frac{\partial \mathbf{e}_r}{\partial \theta} = \mathbf{e}_\theta, \qquad \frac{\partial \mathbf{e}_\theta}{\partial \theta} = -\mathbf{e}_r \end{aligned} \tag{e}$$

Consider now the undeformed position vector $\mathbf{P}$ and the current position vector $\mathbf{p}$ of a point expressed in the cylindrical system as

$$\mathbf{P} = R\mathbf{e}_R + Z\mathbf{e}_Z, \qquad \mathbf{p} = r\mathbf{e}_r + z\mathbf{e}_z \tag{f}$$

where (R, Z) and (r, z) are components of the undeformed and deformed position vectors, respectively; $(\mathbf{e}_R, \mathbf{e}_Z)$ and $(\mathbf{e}_r, \mathbf{e}_z)$ are the unit vectors of the two systems. Using (e), the differential forms for (f) are

$$\mathrm{d}\mathbf{P} = \mathrm{d}R\mathbf{e}_R + R\,\mathrm{d}\Theta\mathbf{e}_\Theta + \mathrm{d}Z\mathbf{e}_Z, \qquad \mathrm{d}\mathbf{p} = \mathrm{d}r\mathbf{e}_r + r\mathrm{d}\theta\mathbf{e}_\theta + \mathrm{d}z\mathbf{e}_z \tag{g}$$

We now proceed to find a relation between the components of $\mathrm{d}\mathbf{p}$ and those of $\mathrm{d}\mathbf{P}$. To this end, we note that r, θ, z are functions of R, Θ, Z. Thus, by chain rule of differentiation, we obtain

$$\begin{aligned} \mathrm{d}r &= \frac{\partial r}{\partial R}\mathrm{d}R + \frac{\partial r}{R\partial\Theta}R\,\mathrm{d}\Theta + \frac{\partial r}{\partial Z}\mathrm{d}Z \\ r\,\mathrm{d}\theta &= \frac{r\partial\theta}{\partial R}\mathrm{d}R + \frac{r\partial\theta}{R\partial\Theta}R\mathrm{d}\Theta + \frac{r\partial\theta}{\partial Z}\mathrm{d}Z \\ \mathrm{d}z &= \frac{\partial z}{\partial R}\mathrm{d}R + \frac{\partial z}{R\partial\Theta}R\mathrm{d}\Theta + \frac{\partial z}{\partial Z}\mathrm{d}Z \end{aligned} \tag{h}$$

Using (h), the components of (g) may be written in matrices as

$$[\mathrm{d}p] = \begin{bmatrix} \mathrm{d}r \\ r\,\mathrm{d}\theta \\ \mathrm{d}z \end{bmatrix} = \begin{bmatrix} \dfrac{\partial r}{\partial R} & \dfrac{\partial r}{R\partial\Theta} & \dfrac{\partial r}{\partial Z} \\ \dfrac{r\partial\theta}{\partial R} & \dfrac{r\partial\theta}{R\partial\Theta} & \dfrac{r\partial\theta}{\partial Z} \\ \dfrac{\partial z}{\partial R} & \dfrac{\partial z}{R\partial\Theta} & \dfrac{\partial z}{\partial Z} \end{bmatrix} \begin{bmatrix} \mathrm{d}R \\ R\,\mathrm{d}\Theta \\ \mathrm{d}Z \end{bmatrix} = [F][\mathrm{d}P] \tag{i}$$

where the components of the deformation gradient are

$$[F] = \begin{bmatrix} \dfrac{\partial r}{\partial R} & \dfrac{\partial r}{R\partial\Theta} & \dfrac{\partial r}{\partial Z} \\ \dfrac{r\partial\theta}{\partial R} & \dfrac{r\partial\theta}{R\partial\Theta} & \dfrac{r\partial\theta}{\partial Z} \\ \dfrac{\partial z}{\partial R} & \dfrac{\partial z}{R\partial\Theta} & \dfrac{\partial z}{\partial Z} \end{bmatrix} \tag{j}$$

7.6.6.1 Relations among stress measures for thin-walled tubes

The text of this section was originally presented in [24]. Considering the axial–torsion of a thin-walled tube, two sets of cylindrical coordinates $(X^1, X^2, X^3) = (R, \Theta, Z)$ and $(x^1, x^2, x^3) = (r, \theta, z)$ are used to describe the undeformed and deformed status, respectively. The two sets of coordinates are related by

$$\begin{aligned} r &= \lambda_m R_m - \lambda_2(R_m - R) = (\lambda_m - \lambda_2)R_m + \lambda_2 R \\ \theta &= \Theta + \varphi\lambda_3 Z \\ z &= \lambda_3 Z \end{aligned} \tag{7.154}$$

in the range of $R_1 \geq R \geq R_0$, where R_1 and R_0 are the undeformed outer and inner radii, respectively; and $r_1 \geq r \geq r_0$, where r_1 and r_0 are the deformed outer and inner radius, respectively; $\lambda_m = r_m/R_m$ describes the stretch ratio of the mean radii which are denoted by R_m and r_m in the undeformed and deformed status, respectively; $\lambda_2 = h/H$ describes the stretch ratio of the wall-thicknesses, which are denoted by H and h in the undeformed and deformed status, respectively; $\lambda_3 = z/Z$ describes the deformation in the axial direction, which is denoted by Z and z in the undeformed and deformed status, respectively; and φ is the angle of twist per unit deformed length and is related to the shear strain γ by

$$\gamma = r\varphi \tag{7.155}$$

We note that if the value of λ_i $(i = m, 2, 3)$ is greater than one, then it implies stretching; if it is equal to one, then there is no length change; and there is contraction when this value is less than one. Taylor and Quinney [9] found

that the hoop and radial strains are not equal for a thin-walled tube under combined tension–torsion loading condition. According to Taylor and Quinney, the values of λ_m and λ_2 are the same for the tension only condition but are different and depend on the constitutive equations used for the combined tension–torsion loading condition.

It has been shown in Example 7.6 that the physical components of deformation gradient **F** are

$$[F] = \begin{bmatrix} \dfrac{\partial r}{\partial R} & \dfrac{\partial r}{R\partial\Theta} & \dfrac{\partial r}{\partial Z} \\ \dfrac{r\partial\theta}{\partial R} & \dfrac{r\partial\theta}{R\partial\Theta} & \dfrac{r\partial\theta}{\partial Z} \\ \dfrac{\partial z}{\partial R} & \dfrac{\partial z}{R\partial\Theta} & \dfrac{\partial z}{\partial Z} \end{bmatrix} \tag{7.156}$$

Using (7.154), (7.156) reduces to

$$[F] = \begin{bmatrix} \lambda_2 & 0 & 0 \\ 0 & \dfrac{r}{R} & \varphi\lambda_3 r \\ 0 & 0 & \lambda_3 \end{bmatrix} = \begin{bmatrix} \lambda_2 & 0 & 0 \\ 0 & \lambda_m & \gamma\lambda_3 \\ 0 & 0 & \lambda_3 \end{bmatrix} \tag{7.157}$$

The last expression of (7.157) is found by considering the mean radius of the tube, where $R = R_m$, $r = r_m = \lambda_m R_m$ and $\gamma = r_m\varphi$. The inverse of the above matrix is

$$[F]^{-1} = \begin{bmatrix} \lambda_2^{-1} & 0 & 0 \\ 0 & \lambda_m^{-1} & -R_m\varphi \\ 0 & 0 & \lambda_3^{-1} \end{bmatrix} \tag{7.158}$$

When the material is incompressible, which is a reasonable assumption for metallic materials undergoing large plastic deformation, the Jacobian is

$$J = \beta_2\beta_3\beta_m = 1 \tag{7.159}$$

We now proceed to find the relations among the components of Cauchy stress $\boldsymbol{\sigma}$, 1st P–K stress $\mathbf{T}^{(0)}$, and 2nd P–K stress $\boldsymbol{\Pi}$. These relations have been previously discussed in Section 4.4.2.1, and the equations are from (4.42) and (4.50)

$$\boldsymbol{\sigma} = J^{-1}\mathbf{F}\cdot\mathbf{T}^{(0)} \quad \text{and} \quad \boldsymbol{\Pi} = \mathbf{T}^{(0)}\cdot\mathbf{F}^{-\mathrm{T}} \tag{7.160}$$

For the case of thin-walled tube under axial–torsional loading condition, the stress states of $\boldsymbol{\sigma}$, $\mathbf{T}^{(0)}$, and $\boldsymbol{\Pi}$ are given by their respective physical

components as

$$[\sigma]=\begin{bmatrix}0&0&0\\0&0&\tau\\0&\tau&\sigma\end{bmatrix},\qquad [T^{(0)}]=\begin{bmatrix}0&0&0\\0&T^{\theta\theta}&T^{\theta z}\\0&T^{z\theta}&T^{zz}\end{bmatrix},\qquad [\Pi]=\begin{bmatrix}0&0&0\\0&\Pi^{\theta\theta}&\Pi^{\theta z}\\0&\Pi^{z\theta}&\Pi^{zz}\end{bmatrix} \tag{7.161}$$

in which $\sigma^{zz}=\sigma$ is the axial stress which is equal to the axial force divided by $2\pi r_m h$; $\sigma^{\theta z}=\sigma^{z\theta}=\tau$ is the shear stress, which is equal to the torque divided by $2\pi r_m^2 h$; $\sigma^{\theta\theta}=0$ due to symmetry and $\sigma^{rr}=0$ due to no surface tractions on both the inner and outer lateral surfaces of the tube. The last condition is an approximation, but it is justifiable when the wall is thin. Substituting (7.157) to (7.159) and (7.161) into (7.160), we obtain

$$[\sigma]=\begin{bmatrix}0&0&0\\0&\lambda_m T^{\theta\theta}+\varphi R_m\lambda_m\lambda_3 T^{z\theta}&\lambda_m T^{\theta z}+\varphi R_m\lambda_m\lambda_3 T^{zz}\\0&\lambda_3 T^{z\theta}&\lambda_3 T^{zz}\end{bmatrix} \tag{7.162}$$

$$[T^{(0)}]=\begin{bmatrix}0&0&0\\0&-\tau R_m\varphi&\dfrac{1}{\lambda_m}(\tau-\varphi R_m\lambda_m\sigma)\\0&\dfrac{\tau}{\lambda_3}&\dfrac{\sigma}{\lambda_3}\end{bmatrix} \tag{7.163}$$

$$[\Pi]=\begin{bmatrix}0&0&0\\0&\dfrac{1}{\lambda_m}\left(T^{\theta\theta}-\varphi R_m\lambda_m T^{\theta z}\right)&\dfrac{T^{\theta z}}{\lambda_3}\\0&\dfrac{1}{\lambda_m}\left(T^{z\theta}-\varphi R_m\lambda_m T^{zz}\right)&\dfrac{T^{zz}}{\lambda_3}\end{bmatrix} \tag{7.164}$$

The component $T^{z\theta}$, which equals the torque divided by $2\pi R_m H r_m$, and the component T^{zz}, which equals the axial force divided by $2\pi R_m H$, are known quantities from experiment, where R_m is the mean radius of the tube in the undeformed configuration and an approximated r_m may be obtained by measuring the deformed outer radius r_1 and then subtracting $H/2$ from it. For convenience, most experimental results in the literatures are presented in terms of the 1st P–K stress components T^{zz} and $T^{z\theta}$. However, this is only an approximation since r_m is not measured in most experiments. The current wall-thickness h is very difficult to measure.

The other components of $\mathbf{T}^{(0)}$ cannot be readily determined experimentally in the case considered. However, they may be expressed in terms of T^{zz} and $T^{z\theta}$. To this end, we obtain, from (7.161) and (7.162), the following relations

$$\sigma^{\theta\theta}=0=\lambda_m T^{\theta\theta}+\varphi R_m\lambda_m\lambda_3 T^{z\theta} \tag{7.165}$$

$$\sigma^{\theta z}=\tau=\lambda_m T^{\theta z}+\varphi R_m\lambda_m\lambda_3 T^{zz} \tag{7.166}$$

$$\sigma^{z\theta} = \tau = \lambda_3 T^{z\theta} \tag{7.167}$$

$$\sigma^{zz} = \sigma = \lambda_3 T^{zz} \tag{7.168}$$

From (7.165), we obtain

$$T^{\theta\theta} = -\varphi R_m \lambda_3 T^{z\theta} \tag{7.169}$$

and, by substituting (7.167) into (7.166), we have

$$T^{\theta z} = \frac{1}{\lambda_m}\left(\lambda_3 T^{z\theta} - \varphi R_m \lambda_m \lambda_3 T^{zz}\right) \tag{7.170}$$

Thus, all components of the 1st P–K stress may be determined.

By using (7.167) and (7.168), Cauchy stress components may be calculated. In view of (7.161), the state of Cauchy stress can be completely determined. It is seen that when the axial strain is equal to zero, that is, $\lambda_3 = 1$, we have $\sigma^{z\theta} = T^{z\theta}$ and $\sigma^{zz} = T^{zz}$. But if the axial strain is large, then the difference between the two measures can be large. These transformation equations are used in the next section where theoretical predictions of yield surfaces are compared with experimental data.

For the axial prestrain only condition, we have λ_m equaling λ_2 [9]. From (7.159), we then obtain the relations among λ_i as

$$\lambda_m = \lambda_2 = \sqrt{\frac{1}{\lambda_3}} \tag{7.171}$$

For the torsional prestrain only condition, all values of λ_i's may be approximated by one. This may be estimated by use of experimental results of Wu and Xu [80] for pure torsion of 304 stainless steel. It has been found that for an angle of relative grip rotation of 32.5°, φ is 12.76 rad/m and the corresponding engineering shear strain is 10.3%, which gives rise to an axial strain ε of 0.23%. Using (7.154), we found that $\lambda_3 = 1.0023$ which may be approximated by 1 in this case. Since the diameter of the thin-walled tube undergoes a small amount of change during pure torsion, we obtain the following approximated relations among λ_i, that is, $\lambda_m \cong \lambda_2 \cong \lambda_3 \cong 1$. These relations are used in the next section and are further discussed.

7.6.6.2 Experimental determination of yield surfaces

Experiments were conducted, by use of a computer-controlled, axial–torsional, closed-looped, electrohydraulic materials test system. The same batch of annealed 304 stainless steel specimens as in Wu and Yeh [4] was used in this investigation. Detailed information about the material, specimens, strain measurement, and experimental procedures may be found in Wu and Yeh [4] and Wu et al. [24]. We only mention here that initial and

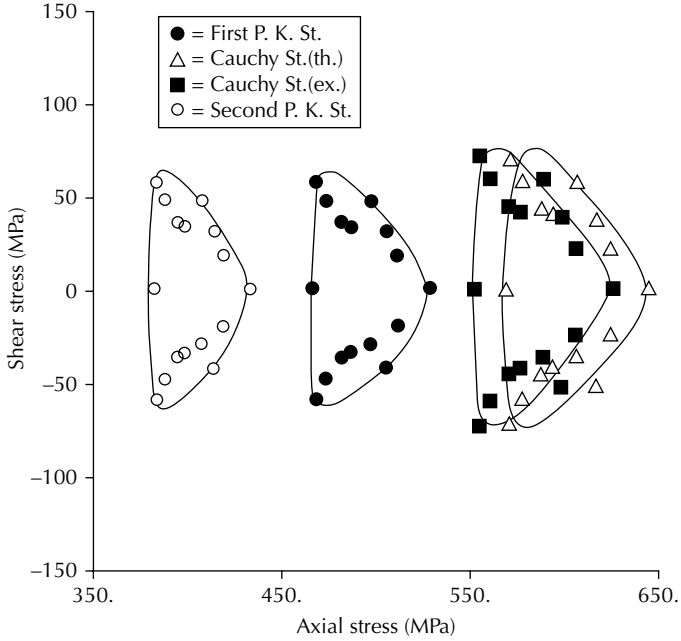

FIGURE 7.28
Subsequent yield surfaces due to tension prestrain determined by various stress measures (From Wu, H.C. et al., *J. Appl. Mech.*, 62, 626, 1995. With permission from ASME).

subsequent yield surfaces were determined for two loading paths. Path (1) in axial loading had an axial prestrain of 20% and path (2) in free-end torsion had a shear prestrain of 20%. After the subsequent yield surface was determined for each loading path, the specimen was removed from the test machine and cut through the cross-section in the middle of the gauge section. By measuring the change of the cross-sectional area, it was found that the reduction of the cross-sectional area was 17% for path (1) and no observable area change was found for path (2).

Now the effect of stress measure on the shape, size, and translation of the yield surface is investigated. Figure 7.28 shows the subsequent yield surfaces for path (1). The experimental yield surface (using the 1st P–K stress components) is shown in the middle of the figure. Also shown in the figure are the theoretical yield surfaces of the Cauchy stress components determined from (7.161), (7.167), and (7.168) and the 2nd P–K stress components obtained by (7.164). As an independent verification, the experimental Cauchy yield surface is also shown in the figure. The experimental Cauchy stress components were determined based on the measured deformed area. The agreement between the two Cauchy yield surfaces is generally good. However, it may be observed from the figure that the amount of axial strain affects the size of the Cauchy yield surface. In fact, from (7.167) and (7.168), $\sigma = \lambda_3 T^{zz}$ and $\tau = \lambda_3 T^{z\theta}$ and the Cauchy yield surface is an isotropic expansion of

the 1st P–K yield surface with λ_3 being the factor of expansion. For an axial prestrain of 20%, the size of the Cauchy yield surface is about 20% larger than that of the corresponding 1st P–K yield surface. We also note that the translation (the back stress) of the former yield surface is 20% more than that of the latter. In the case of the 2nd P–K stress, we have $\Pi^{z\theta} \cong (T^{z\theta}/\lambda_m)$ and $\Pi^{zz} \cong (T^{zz}/\lambda_3)$ from (7.164) for φ approximately equal to zero (φ is zero during axial prestrain and is very small and negligible during the probing of yield surface). The 2nd P–K yield surface is about 9.5% larger than that of the 1st P–K yield surface in the shear direction but is about 17% smaller in the axial direction. The back stress of the former is 17% less than that of the latter. These results have suggested that the evolution rules for both isotropic and kinematic hardening are stress measure dependent.

Figure 7.29 shows the subsequent yield surfaces determined by each stress measure for path (2). Due to no observable change in the cross-sectional area, the Cauchy stress components σ and τ are almost identical to the 1st P–K stress components T^{zz} and $T^{z\theta}$ from (7.167) and (7.168). Therefore, the Cauchy and the 1st P–K yield surfaces are indistinguishable in the figure. However, the components of the 2nd P–K stress are different from those of the Cauchy stress. Using the approximation that all λ's are equal to 1, (7.164) reduces to $\Pi^{z\theta} \cong T^{z\theta} - \varphi R_m T^{zz}$ and $\Pi^{zz} \cong T^{zz}$, that is, the component $\Pi^{z\theta}$ depends

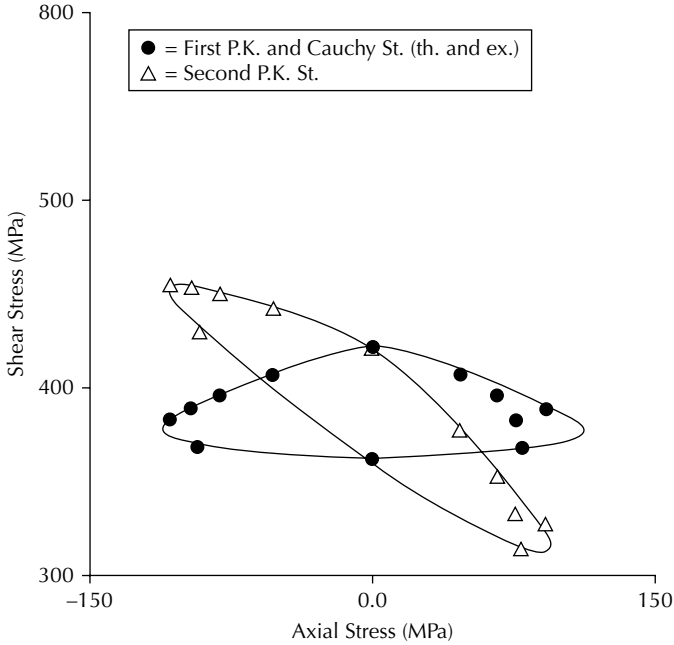

FIGURE 7.29
Subsequent yield surfaces due to torsion prestrain determined by various stress measures (From Wu, H.C. et al., *J. Appl. Mech.*, 62, 626, 1995. With permission from ASME).

on the twist angle per unit length φ. This leads to a rotation of the 2nd P–K surface, with the angle of rotation increasing with the shear strain. It also leads to a further distortion of the 2nd P–K surface in that the yield surface is not symmetric with respect to the shear stress axis. These results complicate the hardening rule associated with the 2nd P–K yield surface.

In the aforementioned example, the theoretical results in the case of pretorsion are calculated based on the approximation that all λ's are equal to 1. Without this approximation, the axial strain exists but is very small. It is less than 0.3% for a prestrain in torsion of 20%. In this case, $1.003 > \lambda_3 > 1$ and, from Wu et al. [74] where the circumferential strain was investigated, we obtain $0.9973 < \lambda_m < 1$. Thus, the effect of this approximation is very small. Also, we emphasize that the rotation and distortion of the 2nd P–K surface is independent of this approximation.

EXAMPLE 7.8 Transform the Mises yield criterion in the Cauchy stress space into the stress spaces of the 1st and 2nd P–K stresses.

Solution

The Mises yield surface in the Cauchy stress space is

$$(\sigma - \alpha_\sigma)^2 + 3(\tau - \alpha_\tau)^2 = k^2 \tag{a}$$

where α_σ and α_τ are, respectively, the axial and shear components of the back stress. k is the shear yield stress and is assumed to be constant in this discussion. Using (7.167) and (7.168), (a) is transformed into

$$\left(T^{zz} - \frac{\alpha_\sigma}{\lambda_3}\right)^2 + 3\left(T^{z\theta} - \frac{\alpha_\tau}{\lambda_3}\right)^2 = \left(\frac{k}{\lambda_3}\right)^2 \tag{b}$$

Using (7.164), (b) is further transformed into an equation in the $\Pi^{z\theta}$ versus Π^{zz} stress space.

In the case of axial prestrain only, $\varphi \cong 0$ and $\alpha_\tau = 0$; and using (7.171), the yield function in the $\Pi^{z\theta}$ versus Π^{zz} stress space may be written as

$$\frac{(\Pi^{zz} - (\alpha_\sigma/\lambda_3^2))^2}{(k/\lambda_3^2)} + \frac{(\Pi^{z\theta})^2}{(k/\sqrt{3\lambda_3})^2} = 1 \tag{c}$$

By comparing equations (a), (b), and (c), we see that the semimajor axes (in the axial stress direction) of the ellipses are k for the Cauchy yield surface, k/λ_3 for the 1st P–K surface, and k/λ_3^2 for the 2nd P–K surface. The semiminor axes (in the shear stress direction) are, respectively, $k/\sqrt{3}$, $k/\sqrt{3}\lambda_3$, and $k/\sqrt{3\lambda_3}$. The back stress for the three yield surfaces are respectively α_σ, α_σ/λ_3, and $\alpha_\sigma/\lambda_3^2$. It is seen that the size, shape, and the back stress of the yield surfaces are all influenced by the deformation of the material element when different stress measures are used.

In the case of torsion only prestrain, $\alpha_\sigma = 0$. If we use the approximation that all λ's are one, then the yield surface in the 2nd P–K stress space is governed by the equation

$$(\Pi^{zz})^2 + 3[(\Pi^{z\theta} + \varphi R_m \Pi^{zz}) - \alpha_\tau]^2 = k^2 \qquad \text{(d)}$$

This equation contains a $6\varphi R_m \Pi^{z\theta} \Pi^{zz}$ term, and a rotation in the ellipse will occur.

7.6.6.3 Discussions

We have seen from the previous section that the size, shape, and position of the subsequent yield surfaces depend greatly on the stress measure used to define the yield surface. The different positions of the yield surfaces in the stress space correspond to different degrees of kinematic hardening. We have seen that the hardening rules (isotropic and kinematic hardening) depend greatly on the definition of stress. The 2nd P–K stress which is often used in the computational mechanics can lead to a yield surface which rotates due to a shear prestrain, while no rotations have been found for this proportional path using the Cauchy stress or the 1st P–K stress. Therefore, the yield surface and the hardening rule should be paired. They vary with the definition of stress.

The yield surface defined by the 2nd P–K stress is independent of imposed rigid-body rotation. In order for the Cauchy yield surface (yield surface defined by the Cauchy stress) to be independent of rigid-body rotation, the yield function has to be a function of stress invariants. The yield surface will be discussed further in Chapter 11 using the true stress in the convected coordinate system. The contravariant components of the true stress do not change with imposed rigid-body rotation.

References

1. Valanis, K.C., A theory of viscoplasticity without a yield surface, *Arch. Mech.*, 23, 517, 1971.
2. Valanis, K.C., Fundamental consequences of a new intrinsic time measure-plasticity as a limit of the endochronic theory, *Arch. Mech.*, 32, 171, 1980.
3. Ohashi, Y. and Tokuda, M., Precise measurement of plastic behavior of mild steel tubular specimens subjected to combined torsion and axial force, *J. Mech. Phys. Solids*, 21, 214, 1973.
4. Wu, H.C. and Yeh, W.C., On the experimental determination of yield surfaces and some results of annealed 304 stainless steel, *Int. J. Plasticity*, 7, 803, 1991.
5. Phillips, A. and Lu, W.Y., An experimental investigation of yield surfaces and loading surfaces of pure aluminum with stress-controlled and strain-controlled paths of loading, *J. Eng. Mater. Technol.*, 106, 349, 1984.

6. Ivey, H.J., Plastic stress–strain relations and yield surfaces for aluminum alloys, *J. Mech. Eng. Sci.*, 3, 15, 1961.
7. Wu, H.C. and Yang, C.C., Investigation of the one-dimensional endochronic constitutive equation for metals by the Rivlin test, *J. Eng. Mater. Technol.*, 106, 264, 1984.
8. Ellis, J.R., Robinson, D.N., and Pugh, C.E., Time dependence in biaxial yield of type 316 stainless steel at room temperature, *J. Eng. Mater. Technol.*, 105, 250, 1983.
9. Taylor, G. I. and Quinney, H., The plastic distortion of metal, *Phil. Trans. Roy. Soc.* A, 230, 323, 1931.
10. Naghdi, P.M., Essenburg, F., and Koff, W., Experimental study of initial and subsequent yield surface in plasticity, *J. Appl. Mech.*, 201, 1958.
11. McComb, H.G. Jr., Some experiments concerning subsequent yield surface in plasticity, NASA TN D-396, 1960.
12. Mair, W.M. and Pugh, H.L.D., Effect of prestrain on yield surfaces in copper, *J. Mech. Eng. Sci.*, 6, 150, 1964.
13. Bertsch, P.K. and Findley, W.N., An experimental study of subsequent yield surfaces-corners, normality, Bauschinger effect and allied effects, *Proc. 4th U.S. Nat. Cong. Appl. Mech.*, 893, 1962.
14. Phillips, A. and Moon, H., An experimental investigation concerning yield surfaces and loading surfaces, *Acta Mech.*, 27, 91, 1977.
15. Shiratori, E., Ikegami, K., Yoshida, F., Kaneko, K., and Koike, S., The subsequent yield surface after preloading under combined axial load and torsion, *Bull. JSME*, 19, 877, 1976.
16. Ishikawa, H., Subsequent yield surface probed from its current center, *Int. J. Plasticity*, 13, 533, 1997.
17. Lode, W., Versuche über den Einfluss der mittleren Hauptspannung auf das Fliessen der Metalle, Eisen, Kupfer und Nickel, *Z. Phys.*, 36, 913, 1926.
18. Hu, L.W. and Bratt, J.F., Effect of tensile plastic deformation on yield criterion, *J. Appl. Mech.*, 25, 411, 1958.
19. Szczepinski, W., On the effect of plastic deformation on yield criterion, *Arch. Mech.*, 15, 276, 1963.
20. Szczepinski, W. and Miastkowski, J., An experimental study of the effect of the prestraining history on the yield surfaces of an aluminum alloy, *J. Mech. Phys. Solids*, 16, 153, 1968.
21. Shiratori, E. and Ikegami, K., Experimental study of the subsequent yield surface by using cross-shaped specimens, *J. Mech. Phys. Solids*, 16, 373, 1968.
22. Phillips, A. and Tang, J.L., The effect of loading path on the yield surface at elevated temperatures, *Int. J. Solids Structures*, 8, 463, 1972.
23. Helling, D.E., Miller, A.K., and Stout, M.G., An experimental investigation of the yield loci of 1100-0 aluminum, 70:30 brass, and an overaged 2024 aluminum alloy after various prestrains. *J. Eng. Mater. Technol.*, 108, 313, 1986.
24. Wu, H.C., Lu, J.K., and Pan, W.F., Some observations on yield surfaces for 304 stainless steel at large strain, *J. Appl. Mech.*, 62, 626, 1995.
25. Wu, H.C., Effect of loading-path on the evolution of yield surface for anisotropic metals subjected to large pre-strain, *Int. J. Plasticity*, 19, 1773, 2003.
26. Wu, H.C. and Xu, Z., An axial–torsional extensometer for finite deformation, *J. Eng. Mater. Technol.*, 112, 330, 1990.
27. Phillips, A., A review of quasistatic experimental plasticity and viscoplasticity, *Int. J. Plasticity*, 2, 315, 1986.

28. Wu, H.C., *Viscoplasticity Under Complex States of Stress*, Ph.D. thesis submitted to Yale University, New Haven, CT, 1970.
29. Phillips, A. and Wu, H.C., A theory of viscoplasticity, *Int. J. Solids Struct.*, 9, 15, 1973.
30. Phillips, A., Experimental plasticity. Some thoughts on its present status and possible future trends, in *Problems of Plasticity*, Sawczuk, A. Ed., Nordhoff International Publishing Leyden, 1974, 193.
31. Krempl, E., Models of viscoplasticity. Some comments on equilibrium (back) stress and drag stress, *Acta Mech.*, 69, 25, 1987.
32. Phillips, A., Liu, K., and Justusson, W.J., An experimental investigation of yield surfaces at elevated temperatures, *Acta Mech.*, 14, 119, 1972.
33. Phillips, A. and Kasper, R., On the foundations of thermoplasticity — an experimental investigation, *J. Appl. Mech.*, 40, 891, 1973.
34. Phillips, A., Tang, J.-L., and Ricciuti, M., Some new observations on yield surfaces, *Acta Mech.*, 20, 23, 1974.
35. Phillips, A. and Kawahara, W.A., The effect of thermal loading on the yield surface of aluminum, An experimental investigation, *Acta Mech.*, 50, 249, 1984.
36. Ohashi, Y., Kawashima, K., and Yokochi, T., Anisotropy due to plastic deformation of initially isotropic mild steel and its analytical formulation, *J. Mech. Phys. Solids*, 23, 277, 1975.
37. Phillips, A. and Kaechele, L., Combined stress tests in plasticity, *J. Appl. Mech.*, 23, 43, 1956.
38. Khan, A.S. and Wang, X., On non-proportional infinitesimal plastic deformation after finite plastic prestressing and partial unloading, *J. Mech. Phys. Solids*, 36, 519, 1988.
39. Mroz, Z., On the description of anisotropic workhardening, *J. Mech. Phys. Solids*, 15, 163, 1967.
40. Masing, G., *Wiss. Veröff. Siemens-Konzern*, III Band, 1927.
41. Dafalias, Y.F. and Popov, E.P., A model of nonlinear hardening materials for complex loading, *Acta Mech.*, 21, 173, 1975.
42. Dafalias, Y.F. and Popov, E.P., Plastic internal variables formalism of cyclic plasticity, *J. Appl. Mech.*, 98, 645, 1976.
43. Ilyushin, A.A., On the relation between stresses and small strains in continuum mechanics, *Prikl. Mat. Mekh.*, 18, 641, 1954 (in Russian).
44. Ilyushin, A.A., *Plasticity*, Izdat. Akad. Nauk. SSSR, Moscow, 1963 (in Russian).
45. Lensky, V.S., Analysis of plastic behavior of metals under complex loading, in *Proc. 2nd Symposium on Naval Struc. Mech.*, Lee, E.H. and Symonds, P.S., Eds., Brown University, Pergamon Press, 1960, 259.
46. Ohashi, Y., Tokuda, M., and Tanaka, Y., Precise experimental results on plastic behavior of brass under complex loading, *Bull. De L'Acad. Polon. Des Sci.*, Ser. Sciences Tech., 26, 261, 1978.
47. Ohashi, Y., Kurita, Y., Suzuki, T., and Tokuda, M., Effect of curvature of the strain trajectory on the plastic behavior of brass, *J. Mech. Phys. Solids*, 29, 69, 1981.
48. Pipkin, A.C. and Rivlin, R.S., Mechanics of rate-independent materials, *J. Appl. Math. Phys. (ZAMP)*, 16, 313, 1965.
49. Zhou, Z.-D., Zhao, S.-X., and Kuang, Z.-B., An integral elasto-plastic constitutive theory, *Int. J. Plasticity*, 19, 1377, 2003.
50. Ilyushin, A.A., in *Problems in the Theory of Plasticity*, Izdat. Akad. Nauk. SSSR, Moscow, 1961, 3 (in Russian).

51. Wu, H.C. and Yang, R.J., Application of the improved endochronic theory of plasticity to loading with multi-axial strain-path, *Int. J. Non-Linear Mech.*, 18, 395, 1983.
52. Wu, H.C., Yang, C.C., and Chu, S.C., Further application of endochronic constitutive equation to loading with non-proportional axial–torsional strain-path, *Int. J. Non-Linear Mech.*, 20, 41, 1985.
53. Wu, H.C., Aboutorabi, M.R., and Chen, P.C.T., Cyclic torsion of a circular cylinder and its residual stress distribution, *J. Eng. Mater. Technol.*, 107, 48, 1985.
54. Wu, H.C. and Yeh, W.C., Some considerations in the endochronic description of anisotropic hardening, *Acta Mech.*, 69, 59, 1987.
55. Wu, H.C. and Ho, C.C., An investigation of transient creep by means of endochronic viscoplasticity and experiment, *J. Eng. Mater. Technol.*, 117, 260, 1995.
56. Green, A.E. and Naghdi, P.M., A general theory of an elastic–plastic continuum, *Arch. Rat. Mech. Anal.*, 18, 251, 1965.
57. Lee, E.H., Elastic–plastic deformations at finite strains, *J. Appl. Mech.*, 36, 1, 1969.
58. Dafalias, Y.F., A missing link in the macroscopic constitutive formulation of large plastic deformations, in *Plasticity Today*, Sawczuk, A. and Bianchi, G., Eds., Elsevier Applied Science, London, 1983, 135.
59. Mandel, J., Plasticité classique et viscoplasticité, CISM Courses and Lectures 97, Springer, New York, 1971.
60. Montheillet, F., Cohen, M., and Jonas, J.J., Axial stresses and texture development during the torsion testing of Al, Cu and A-Fe, *Acta Metall.*, 32, 2077, 1984.
61. Stout, M.G. and O'Rourke, J.A., Experimental deformation textures of OFE copper and 70 : 30 brass from wire drawing, compression and torsion, *Metall. Trans.* 20A, 125, 1989.
62. Toth, L.S., Jonas, J.J., Daniel, D., and Bailey, J.A., Texture development and length changes in copper bars subjected to free-end torsion, *Text. Microstruct.* 19, 245, 1992.
63. Wang, P.T., Panchanadeeswaran, S., and Wu, H.C., Comparison of flow stress and texture for P0815 cast aluminum deformed in compression and in torsion. Alcoa Technical Center Research Report, Alcoa Center, Pa., U.S.A., 1995.
64. Dafalias, Y.F., Plastic spin: necessity or redundancy?, *Int. J. Plasticity*, 14, 909, 1998.
65. Kratochvil, J., Finite strain theory of crystalline elastic–inelastic materials, *J. Appl. Phys.*, 42, 1104, 1971.
66. Wang, C.C., A new representation theorem for isotropic functions: an answer to Professor G.F. Smith's criticism of my paper on representations for isotropic functions, *Arch. Rat. Mech. Anal.*, 36, 166, 1970.
67. Loret, B., On the effects of plastic rotation in the finite deformation of anisotropic elastoplastic materials, *Mech. Mater.*, 2, 287, 1983.
68. Dafalias, Y.F., The plastic spin, *J. Appl. Mech.*, 52, 865, 1985.
69. Dienes, J.K., On the analysis of rotation and stress rate in deforming bodies, *Acta Mech.*, 32, 217, 1979.
70. Nagtegall, J.C. and de Jong, J.E., Some aspects of non-isotropic workhardening in finite strain plasticity, in *Proc. Workshop on Plasticity of Metals at Finite Strain:*

Theory, Experiment and Computation, Lee, E.H. and Mallet, R.L., Eds., Stanford University, 1981, 65.
71. Cotter, B.A. and Rivlin, R.S., Tensors associated with time-dependent stress, *Quart. Appl. Math.*, 18, 177, 1955.
72. Oldroyd, J.G., On the formulation of rheological equations of state, *Proc. Roy. Soc.*, A, 200, 523, 1950.
73. Aifantis, E.C., The physics of plastic deformation, *Int. J. Plasticity*, 3, 221, 1987.
74. Wu, H.C., Xu, Z., and Wang, P.T., Torsion test of aluminum in the large strain range, *Int. J. Plasticity*, 13, 873, 1998.
75. Truesdell, C., The simplest rate theory of pure elasticity, *Comm. Pure Appl. Math.*, 8, 123, 1955.
76. Khan, A.S. and Wang, X., An experimental study of large finite plastic deformation in annealed 1100 aluminum during proportional and nonproportional biaxial compression, *Int. J. Plasticity*, 6, 485, 1990.
77. Lee, E.H., Mallet, R.L., and Wertheimer, T.B., Stress analysis of anisotropic hardening in finite-deformation plasticity, *J. Appl. Mech.*, 50, 554, 1983.
78. Wu, H.C., On finite plastic deformation of anisotropic metallic materials, *Int. J. Plasticity*, 19, 91, 2003.
79. Wu, H.C., Effect of loading-path on the evolution of yield surface for anisotropic metals subjected to large pre-strain, *Int. J. Plasticity*, 19, 1773, 2003.
80. Wu, H.C. and Xu, Z., An experimental investigation of the axial effect during torsion, in *Advances in Constitutive Laws for Engineering Materials*, Fan, J. and Murakami, S., Eds., Int. Academic Publishers, Pergamon Press, Beijing, 1989, 232.

Problems

(1) Write a report about additional experimental evidence showing the normality of the plastic strain increment to the subsequent yield surface.

(2) Write a report about Ilyushin's isotropy postulate.

(3) Referring to Figure 7.18 in a stress-controlled loading problem, how do surfaces f_A, f_B, and f_C move when the stress point follows path PQ?

(4) Derive (7.97) from (7.95).

(5) In simple shear problem using Cotter–Rivlin stress rate, show that the solution is given by (7.107) for hypoelastic materials.

(6) In simple shear problem using Truesdell's stress rate, show that the solution is given by (7.110) for hypoelastic materials.

(7) In the problem of rectangular metal block discussed in Example 7.3, if $\mu = 26$ GPa and $\lambda = 33$ GPa, plot the σ_x versus $\int D_x \, dt$ and σ_z versus $\int D_x \, dt$ curves. In addition, plot D_y as a function of D_x and discuss the effect of h on the results.

(8) Use the Jaumann rate to investigate and plot the loading–unloading curve of simple shearing. The material is rigid-plastic with linear kinematic hardening.

During loading, the simple shear deformation is governed by

$$x_1 = X_1 + 2\omega t X_2, \qquad x_2 = X_2, \qquad x_3 = X_3$$

and its displacement field is

$$u_1 = 2\omega t X_2, \qquad u_2 = u_3 = 0, \qquad \omega = \text{const}$$

The unloading starts at t^* and the displacement field during unloading is

$$u_1 = [2\omega t* - 2\omega(t - t*)]x_2 = 2\omega(2t* - t)x_2, \quad u_2 = u_3 = 0, \qquad \text{for } t > t*.$$

(9) Show that (7.101) may be derived from (7.100).

(10) Solve Problem (8) using the Dafalias rate.

(11) Solve Problem (8) using Lee's rate.

(12) Find the physical components of deformation gradient **F** in the spherical coordinate system.

(13) In an uniaxial stress test, the following data have been recorded for the axial stress–strain curve: (plastic strain, stress (MPa))={(0, 100), (0.005, 289.59), (0.01, 336.82), (0.02, 369.03), (0.04, 397.35), (0.06, 420.78), (0.1, 458.86), (0.14, 489.12), (0.2, 526.71)}. The stress has been calculated based on the undeformed cross-sectional area. Plot the equivalent stress versus equivalent plastic strain curves using the Cauchy stress, the 1st P–K stress and the 2nd P–K stress as stress measure, respectively.

(14) In a torsion test of thin-walled tubular specimen, the following data have been recorded for the shear stress–strain curve: (plastic shear strain, shear stress (MPa))={(0, 100), (0.005, 273.36), (0.01, 309.48), (0.02, 334.87), (0.04, 362.20), (0.06, 387.10), (0.1, 428.59), (0.14, 469.60), (0.2, 521.34)}. The stress has been calculated based on the undeformed cross-sectional area. Plot the equivalent stress versus equivalent plastic strain curves using the Cauchy stress, the 1st P–K stress and the 2nd P–K stress as stress measure, respectively. Compare these curves with those obtained in Problem (13).

8

Internal Variable Theory of Thermo-Mechanical Behaviors and Endochronic Theory of Plasticity

8.1 Introduction

There are several approaches to irreversible thermodynamics. One of them, the internal variable theory, is widely used in recent literature of mechanics of solids. In this chapter, the concept and equations of the *internal variable theory of irreversible thermodynamics*, which are used to describe the thermo-mechanical behavior of materials are first discussed. Based on this thermodynamic foundation, it is shown how a theory of plasticity, known as the endochronic theory, can be developed. Applications of the endochronic theory to metals, geotechnical materials, and damage mechanics are then discussed in this chapter and Chapter 9.

The theory of thermodynamics that is presented owes much to the work of Valanis [1–4]. A summary of Valanis' works on the internal variable theory of thermodynamics is nicely presented in [5], although it does not contain recent works on the gradient theory. The gradient theory is outside scope of this book, but readers are referred to [4] for further reading. The endochronic theory of plasticity was developed by Valanis [6,7] and this author had the privilege of learning the theory directly from Professor Valanis and has been heavily involved in the further development and verification of the theory. Other researchers have also made significant contributions to the theory.

8.2 Concepts and Terminologies of Thermodynamics

8.2.1 The First Law of Thermodynamics

Irreversible thermodynamics is also known as the nonequilibrium thermodynamics. It is needed because we are dealing with an *irreversible system*, which is a material region R. A reversible system exists only in an ideal gas or an ideal elastic material. It is assumed that the system possesses an internal

energy E with density ε (read also Section 4.3.3). Readers are referred to Callen [8] for measurability of internal energy.

The mechanical variables are stress, deformation, and mass. In addition, temperature is a variable. A *mechanical process* is a process during which energy (in the absence of heat supply, e.g., heat sources) is transmitted to the system through an adiabatic boundary by motion of the boundary and/or application of long-range forces. The *adiabatic boundary* is a boundary through which no heat can flow. This type of energy is called *work*, denoted by W. A *thermal process* is a process during which energy flows through the boundary of the system and/or is supplied to its interior while its boundary remains stationary and there are no long range (gravitational, say) forces acting. This type of energy is called *heat*, denoted by Q. *Conduction* is a process during which energy is supplied to the system by heat flow through its boundary. A boundary and/or a process which is not adiabatic will be called *diathermal*. Conduction is a diathermal process.

The first law of thermodynamics is a statement of the conservation of energy discussed in Section 4.3.3. In the local form, which applies to an infinitesimal neighborhood of a material region, the energy balance equation is from (4.34)

$$\rho\dot{\varepsilon} = \sigma_{ki}v_{i,k} - h_{i,i} + \rho\dot{q} \tag{8.1}$$

where ρ is the current mass density; h_i is the *heat flux vector*, in which the direction of the vector is the direction of the heat flow; q is the internal energy supply per unit mass by radiation or "other sources" such as electric conductors; and the dot denotes the material differentiation. We note that $|h_i|$ is the amount of energy flow per unit area normal to the direction of heat flow per unit time.

Referring to the undeformed configuration, the energy balance equation is from (4.68)

$$\dot{\varepsilon} = \frac{1}{\rho_0}\Pi_{RS}\dot{E}_{RS} - \frac{1}{\rho_0}\frac{\partial h_R}{\partial X_R} + \dot{q} = \frac{1}{\rho_0}\Pi_{RS}\dot{E}_{RS} + \dot{Q} \qquad \text{with } \dot{Q} = -\frac{1}{\rho_0}\frac{\partial h_R}{\partial X_R} + \dot{q} \tag{8.2}$$

where $\dot{Q}$ is the *rate of heat supply* per unit volume (conduction and radiation).

8.2.2 State Variables, State Functions, and the Second Law of Thermodynamics

The change of internal energy may be accomplished through (1) a purely thermal process (radiation, heat conduction, etc.), which changes the temperature of the system, or (2) an adiabatic process, that is, work, which changes the position of the boundary and causes the system to deform. Thus, strain and temperature are measures of the internal energy of the system. They are called *state variables*, since they serve to define the *state of the system*. Internal

energy is a *state function*, which is a function of state variables. The thermodynamic state of the system is represented by the state functions. One of the main tasks of thermodynamics is to establish those quantities that are state functions and those that are not and to establish useful relationships between state functions. In a reversible system, the internal energy and stress are state functions written as

$$\varepsilon = \varepsilon(E_{RS}, T) \quad \text{and} \quad \Pi_{RS} = \Pi_{RS}(E_{PQ}, T) \tag{8.3}$$

where E_{RS} is the strain and T the temperature.

The fundamental issue is that the increment of heat supply $\mathrm{d}Q$ is *not* an exact differential. The meaning of this statement is not obvious without further clarifications and definitions. A reversible system is said to undergo a reversible process if its thermodynamic state is being changed under adiabatic conditions. It is an irreversible process when the process is diathermal. In this case, $\mathrm{d}Q$ is not an exact differential, where $\oint \mathrm{d}Q \neq 0$ following a closed contour in the (E_{RS}, T) space. From (8.2), we have

$$\oint \mathrm{d}\varepsilon = \oint \frac{1}{\rho_0} \Pi_{RS}\, \mathrm{d}E_{RS} + \oint \mathrm{d}Q \tag{8.4}$$

The integral on the left-hand side is zero because ε is a state function given by (8.3). The first integral on the right-hand side represents the amount of work done on the system, which in general is *not* zero when the path of integration involves thermal processes. The statement may be better understood by examining the Carnot cycle, which is a reversible cycle for ideal gas carried out with the piston–cylinder arrangement. The Carnot cycle goes through two reversible isothermal processes connected by two reversible adiabatic processes and the work done is not zero. Thus, from (8.4)

$$\oint \mathrm{d}Q \neq 0 \tag{8.5}$$

Hence, $\mathrm{d}Q$ is not an exact differential and we cannot write $Q = Q(E_{RS}, T)$. However, in the case of an ideal gas, $\mathrm{d}Q/T$ is an exact differential in the sense that $\oint \mathrm{d}Q/T = 0$. Therefore, deriving $\mathrm{d}S = \mathrm{d}Q/T$, we find that $\mathrm{d}S$ is an exact differential. Thus, in the case of a gas $\mathrm{d}Q = T\, \mathrm{d}S(E_{RS}, T)$, where $S = S(E_{RS}, T)$, which is a state function known as *entropy*.

An important contribution by Valanis [2] is the proof of the existence of entropy in irreversible systems, establishing the entropy as a state function. We now consider the reversible system and leave the irreversible system for later discussion. In the case of the reversible system, the energy equation (8.2) is written as

$$\mathrm{d}\varepsilon - \frac{1}{\rho_0} \Pi_{RS}\, \mathrm{d}E_{RS} = \mathrm{d}Q = \theta(E_{RS}, T)\, \mathrm{d}\eta(E_{RS}, T) \tag{8.6}$$

where θ is the *integrating factor*; η is the specific entropy, and (8.6) is integrable so that η is a state function, that is, $\eta = \eta(E_{RS}, T)$. The equation $\mathrm{d}\eta = \mathrm{g}Q/\theta$ is also known as the second law of thermodynamics. The factor $\theta(E_{RS}, T)$ has the significance of empirical temperature. We note that entropy is dimensionless, and temperature has the dimensions of energy [8]. The units of temperature depend on the nature of the thermometric substance used. Temperature measured by a mercury thermometer is not exactly the same as that given by an electrical resistance thermometer except at their common points. Degree Kelvin is the absolute temperature.

Using (8.3), (8.6) is

$$\frac{\partial \varepsilon}{\partial E_{RS}}\mathrm{d}E_{RS} + \frac{\partial \varepsilon}{\partial T}\mathrm{d}T - \frac{1}{\rho_0}\Pi_{RS}\mathrm{d}E_{RS} = \theta\left(\frac{\partial \eta}{\partial E_{RS}}\,\mathrm{d}E_{RS} + \frac{\partial \eta}{\partial T}\mathrm{d}T\right) \tag{8.7}$$

Since E_{RS} and T can be independently varied and $\mathrm{d}E_{RS}$ and $\mathrm{d}T$ are arbitrary, the following are obtained

$$\frac{1}{\rho_0}\Pi_{RS} = \left.\frac{\partial \varepsilon}{\partial E_{RS}}\right|_T - \theta\left.\frac{\partial \eta}{\partial E_{RS}}\right|_T \quad \text{and} \quad \frac{\partial \varepsilon}{\partial T} = \theta\frac{\partial \eta}{\partial T} \tag{8.8}$$

Since $\theta = \theta(E_{RS}, T)$, we can express the state functions as $\varepsilon = \varepsilon(\theta, E_{RS})$ and $\eta = \eta(\theta, E_{RS})$. Using the chain rule of differentiation, we have

$$\begin{aligned}
\frac{\partial \varepsilon}{\partial T} &= \left.\frac{\partial \varepsilon}{\partial \theta}\right|_{E_{RS}}\left.\frac{\partial \theta}{\partial T}\right|_{E_{RS}}, \qquad \frac{\partial \eta}{\partial T} = \left.\frac{\partial \eta}{\partial \theta}\right|_{E_{RS}}\left.\frac{\partial \theta}{\partial T}\right|_{E_{RS}} \\
\left.\frac{\partial \varepsilon}{\partial E_{RS}}\right|_T &= \left.\frac{\partial \varepsilon}{\partial \theta}\right|_{E_{RS}}\left.\frac{\partial \theta}{\partial E_{RS}}\right|_T + \left.\frac{\partial \varepsilon}{\partial E_{RS}}\right|_\theta \\
\left.\frac{\partial \eta}{\partial E_{RS}}\right|_T &= \left.\frac{\partial \eta}{\partial \theta}\right|_{E_{RS}}\left.\frac{\partial \theta}{\partial E_{RS}}\right|_T + \left.\frac{\partial \eta}{\partial E_{RS}}\right|_\theta
\end{aligned} \tag{8.9}$$

By substituting (8.9) into (8.8), we obtain

$$\frac{1}{\rho_0}\Pi_{RS} = \left.\frac{\partial \varepsilon}{\partial E_{RS}}\right|_\theta - \theta\left.\frac{\partial \eta}{\partial E_{RS}}\right|_\theta \quad \text{and} \quad \frac{\partial \varepsilon}{\partial \theta} = \theta\frac{\partial \eta}{\partial \theta} \tag{8.10}$$

This equation has the same form as (8.8). It shows that the form of the equation is independent of the temperature scale used, and the state functions can be expressed as $\varepsilon = \varepsilon(E_{RS}, \theta)$ and $\Pi_{RS} = \Pi_{RS}(E_{PQ}, \theta)$.

We now introduce a new state function, defined by $\Psi(E_{RS}, \theta) = \varepsilon - \theta\eta$, which is known as the *Helmholtz free energy*. Differentiating Ψ, we have

$$\left.\frac{\partial \Psi}{\partial E_{RS}}\right|_\theta = \left.\frac{\partial \varepsilon}{\partial E_{RS}}\right|_\theta - \theta\left.\frac{\partial \eta}{\partial E_{RS}}\right|_\theta \quad \text{and} \quad \frac{\partial \Psi}{\partial \theta} = \frac{\partial \varepsilon}{\partial \theta} - \theta\frac{\partial \eta}{\partial \theta} - \eta.$$

We then substitute these expressions into (8.10) to obtain

$$\frac{1}{\rho_0}\Pi_{RS} = \frac{\partial \Psi}{\partial E_{RS}} \quad \text{and} \quad \eta = -\frac{\partial \Psi}{\partial \theta} \tag{8.11}$$

These are the constitutive equations for reversible systems.

8.3 Thermodynamics of Internal State Variables

8.3.1 Irreversible Systems

In some systems, the state functions are not uniquely determined by the state variables E_{RS} and T of the system. For instance, in materials undergoing plastic deformation, the current state of stress will depend on the whole history of the deformation. In the case of uniaxial loading–unloading at constant temperature, the stress, which is a state function, is not uniquely determined by the strain E_{11}, as shown in Figure 8.1. Both points A and B have the same strain, but the states of the internal structure of the material are different at the two points. It is therefore necessary to introduce other macroscopic parameters, additional to strain and temperature, which are representative of the internal structure of the material.

Another example that shows the inadequacy of the state of strain in predicting the state of stress is given in Figure 8.2. We represent the unknown material to be tested at constant temperature by a black box. Within the black box there are the spring and dashpot elements with elastic moduli E_1 and E_2 for the springs. If we do not know the internal structure of the black box and test it macroscopically, the state of stress σ cannot be described uniquely in terms of the state of strain of the black box. Other parameters (internal variables) will have to be used in order to determine the stress. However, if we

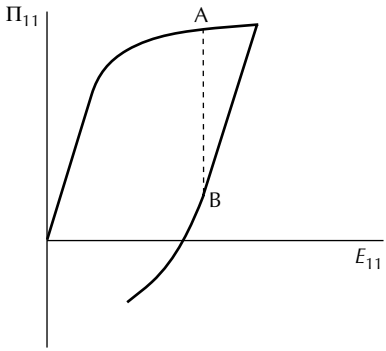

FIGURE 8.1
Stress not uniquely determined by strain.

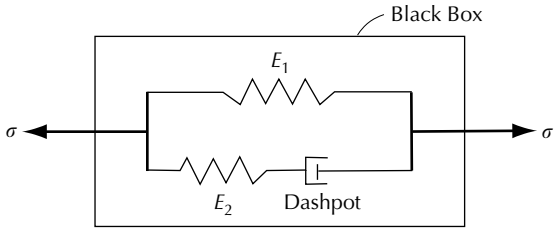

FIGURE 8.2
Test of black box.

open the black box and know the internal structure and constitution of the black box, that is, we know the properties and arrangement of the springs and the dashpot, then we know that the overall strain of the black box is the same as the strain of spring 1, and, if we also know the strain of the dashpot as a function of time, we are able to describe the stress uniquely. The strain of the dashpot is the internal variable needed to uniquely describe the stress. For this example, the stress is a function of the overall strain and the strain of the dashpot.

In the materials modeling, n parameters may be needed to uniquely define the stress state. These parameters are called *internal (state) variables* and are denoted by $\mathbf{q}^r$, where $r = 1, \ldots, n$. Internal state variables are called internal coordinates by some authors. They can be scalars, but, generally, they are tensors.

It is assumed that sufficient additional state variables (not all observable) can always be found to describe the thermodynamic state of an irreversible system. As previously mentioned, the internal state variables are the macroscopic representations of microscopic effects that have physical meanings. They may represent observed effects due to slips at the crystallographic level or represent dislocations, etc. Owing to the difference in scale, these effects may not be directly observable at the macroscopic scale and are represented by the internal variables. In the mechanics literature, some investigators have been able to identify the physical meanings of their internal variables at the microscopic level. In that case, they are able to use the evolution rules for those physical quantities obtained from experiments at the microscopic level. Mathematically speaking, the internal variables are state variables and the state functions are defined in terms of the state variables. As long as the evolution equations are provided for the state variables, the problem can be solved without assigning physical meanings to the internal variables.

For an irreversible system, the state functions are functions of strain, temperature, and n numbers of internal variables, and they are represented by

$$\varepsilon = \varepsilon(E_{RS}, \theta, q^r_{RS}), \quad \eta = \eta(E_{RS}, \theta, q^r_{RS}), \quad \Pi_{RS} = \Pi_{RS}(E_{PQ}, \theta, q^r_{RS}), \quad r = 1, \ldots, n \tag{8.12}$$

Valanis [2] proved the existence of an entropy function η and that the Pfaffian form (8.6) of the first law of thermodynamics is integrable even for irreversible systems, and thus the entropy is a state function. In an earlier effort, Valanis showed that the constitutive equations for irreversible systems are

$$\frac{1}{\rho_0}\Pi_{RS} = \left.\frac{\partial \varepsilon}{\partial E_{RS}}\right|_{\theta, q^r_{PQ}} - \theta \left.\frac{\partial \eta}{\partial E_{RS}}\right|_{\theta, q^r_{PQ}} \quad \text{and} \quad \left.\frac{\partial \varepsilon}{\partial \theta}\right|_{E_{PQ}, q^r_{PQ}} = \theta \left.\frac{\partial \eta}{\partial \theta}\right|_{E_{PQ}, q^r_{PQ}} \tag{8.13}$$

Valanis [2] assumed that the system behaves reversibly when q^r_{RS} are constants and $\mathrm{d}q^r_{RS} = 0$ for all r. The derivation from (8.6) to (8.10) can then be used to establish (8.13) for irreversible systems. By using the Helmholtz free energy $\Psi = \varepsilon - \eta\theta$, where $\Psi = \psi(E_{RS}, \theta, q^r_{RS})$, (8.13) is further written as

$$\frac{1}{\rho_0}\Pi_{RS} = \frac{\partial \Psi}{\partial E_{RS}} \quad \text{and} \quad \eta = -\frac{\partial \Psi}{\partial \theta} \tag{8.14}$$

These are powerful results and were independently obtained by Valanis [1] and Coleman and Gurtin [9].

8.3.2 The Clausius–Duhem Inequality

By putting $\varepsilon = \Psi + \eta\theta$ into the first law of thermodynamics (8.6), we have

$$\mathrm{d}\Psi + \eta\,\mathrm{d}\theta + \theta\,\mathrm{d}\eta - \frac{1}{\rho_0}\Pi_{RS}\,\mathrm{d}E_{RS} = \mathrm{d}Q \tag{8.15}$$

or

$$\frac{\partial \Psi}{\partial E_{RS}}\mathrm{d}E_{RS} + \frac{\partial \Psi}{\partial \theta}\mathrm{d}\theta + \frac{\partial \Psi}{\partial q^r_{RS}}\mathrm{d}q^r_{RS} + \eta\,\mathrm{d}\theta + \theta\,\mathrm{d}\eta - \frac{1}{\rho_0}\Pi_{RS}\,\mathrm{d}E_{RS} = \mathrm{d}Q \tag{8.16}$$

Using (8.14), (8.16) is reduced to

$$\theta\,\mathrm{d}\eta + \frac{\partial \Psi}{\partial q^r_{RS}}\mathrm{d}q^r_{RS} = \mathrm{d}Q \tag{8.17}$$

The second term on the left-hand side of (8.17) is absent in a reversible system. In the rate form, (8.17) may be rewritten as

$$\theta\dot{\eta} + \left.\frac{\partial \Psi}{\partial q^r_{RS}}\right|_{E_{PQ}, \theta} \dot{q}^r_{RS} = \theta\dot{\eta} + \dot{\Psi}\big|_{E_{PQ}, \theta} = \dot{Q} \tag{8.18}$$

The term $\dot{\Psi}|_{E_{PQ},\theta} = (\partial\Psi/\partial q^r_{RS})|_{E_{PQ},\theta}\dot{q}^r_{RS}$ is the rate of change of the Helmholtz free energy under constant strain and temperature. We now invoke the *Kelvin postulate* which states that the free energy cannot increase if the strain and the temperature are kept constant, [5]. The postulate is thus written in the mathematical form as

$$\dot{\Psi}|_{E_{PQ},\theta} \leq 0 \tag{8.19}$$

If we define

$$\theta\dot{\gamma} \equiv -\dot{\Psi}|_{E_{PQ},\theta} \tag{8.20}$$

then, from (8.19) and (8.20), we obtain

$$\dot{\gamma} \geq 0 \tag{8.21}$$

where $\dot{\gamma}$ is known as the *entropy production*. Substituting (8.20) into (8.18), we have

$$\dot{\eta} = \frac{\dot{Q}}{\theta} + \dot{\gamma} \tag{8.22}$$

which results in

$$\dot{\eta} \geq \frac{\dot{Q}}{\theta} \tag{8.23}$$

This inequality is known as the *Clausius–Duhem inequality*, and the equality holds only for reversible systems. Using (8.22), (8.18) may be written as

$$(\dot{Q} + \theta\dot{\gamma}) + \frac{\partial\Psi}{\partial q^r_{RS}}\dot{q}^r_{RS} = \dot{Q} \tag{8.24}$$

which reduces to

$$\theta\dot{\gamma} = -\frac{\partial\Psi}{\partial q^r_{RS}}\dot{q}^r_{RS} \geq 0 \tag{8.25}$$

This is an alternate form for the Clausius–Duhem inequality.

8.3.3 The Helmholtz Formulation of Thermo-Mechanical Behavior

Most of the discussions in the previous section belong to the Helmholtz formulation. We summarize the equations of this formulation here for later reference.

First law of thermodynamics:

$$\dot{\varepsilon} = \frac{1}{\rho_0}\Pi_{RS}\dot{E}_{RS} - \frac{1}{\rho_0}\frac{\partial h_R}{\partial X_R} + \dot{q} \tag{8.26}$$

Clausius–Duhem (rate of dissipation) inequality:

$$-\frac{\partial \Psi}{\partial q^r_{RS}}\dot{q}^r_{RS} \geq 0 \tag{8.27}$$

Heat conduction equation:

$$h_R = h_R(E_{PQ}, \theta, \theta_{,P}, q^r_{PQ}) \tag{8.28}$$

where $\theta_{,R}$ is the temperature gradient. Equation (8.28) is a generalized form of Fourier's law of heat conduction, which states that the heat flux vector is proportional to the temperature gradient $\theta_{,R}$.

The state functions are

$$\begin{aligned} &\Psi = \Psi(E_{RS}, \theta, q^r_{RS}), \qquad &&\varepsilon = \varepsilon(E_{RS}, \theta, q^r_{RS}) \\ &\eta = \eta(E_{RS}, \theta, q^r_{RS}), \qquad &&\Pi_{RS} = \Pi_{RS}(E_{PQ}, \theta, q^r_{PQ}) \end{aligned} \tag{8.29}$$

The relations between state functions are

$$\Pi_{RS} = \rho_0 \frac{\partial \Psi}{\partial E_{RS}}, \qquad \eta = -\frac{\partial \Psi}{\partial \theta} \tag{8.30}$$

These relations apply to all materials irrespective of their constitution. The internal state variables q^r_{RS} represent the constitutive nature of the material. These internal variables distinguish one material from the other. In an elastic material, $q^r_{RS} = 0$; whereas in a viscoelastic material, $q^r_{RS} \neq 0$, and the change of q^r_{RS} is governed by a set of *evolution equations* for q^r_{RS}. From (8.27), the rate of change $\dot{q}^r_{RS}$ should be related to $\partial\Psi/\partial q^r_{RS}$ so that the inequality is not violated. The simplest relation between the two quantities is expressed in terms of a functional relationship so that

$$\dot{q}^r_{RS} = f^r_{RS}\left(\frac{\partial \Psi}{\partial q^r_{PQ}}\right) = f^r_{RS}(E_{PQ}, \theta, q^r_{PQ}) \qquad \text{where } r = 1, \ldots, n \tag{8.31}$$

The last expression in (8.31) is obtained due to $\Psi = \Psi(E_{PQ}, \theta, q^r_{PQ})$. The evolution equations for q^r_{RS} of a material undergoing plastic deformation will be discussed later in conjunction with the endochronic theory of plasticity.

Knowing $\Psi, h_{,R}$, and f^r_{RS}, the expressions for Π_{RS} and η can be obtained from (8.30). The forms of h_R and f^r_{RS} are subject to the constraints

$$-\frac{\partial \Psi}{\partial q^r_{RS}}\dot{q}^r_{RS} \geq 0 \quad \text{and} \quad h_R\theta_{,R} \leq 0 \tag{8.32}$$

The second inequality of (8.32) describes the nature of heat conduction. Heat flows from high to low temperature.

In the Helmholtz formulation, there are $22 + n$ equations. They are listed below with the number of equations shown at the end of the equations:

$$\begin{array}{ll}
\text{Conservation of mass} & 1 \\
\text{Equation of motion} & 3 \\
\text{Conservation of energy} & 1 \\
\text{Strain–displacement equations} & 6 \\
\Pi_{RS} = \rho_0 \dfrac{\partial \Psi(E_{PQ}, \theta, q^r_{PQ})}{\partial E_{RS}} & 6 \\
\eta = -\dfrac{\partial \Psi(E_{PQ}, \theta, q^r_{PQ})}{\partial \theta} & 1 \\
\varepsilon = \varepsilon(E_{PQ}, \theta, q^r_{PQ}) \quad \text{or} \quad \Psi = \Psi(E_{PQ}, \theta, q^r_{PQ}) & 1 \\
h_R = h_R(E_{PQ}, \theta, \theta_{,P}, q^r_{PQ}) & 3 \\
\dot{q}^r_{RS} = f^r_{RS}(E_{PQ}, \theta, q^r_{PQ}) & n
\end{array} \tag{8.33}$$

The $22 + n$ unknowns are $\rho(1), \Pi_{RS}(6), \eta(1), \varepsilon(1), h_R(3)$, the displacements $u_i(3), E_{RS}(6), \theta(1)$, and $q^r_{RS}(n)$, with the number of unknowns shown inside the parenthesis. Thus, the solution for the set of equations can be determined.

8.3.4 The Gibbs Formulation of Thermo-Mechanical Behavior

The *Gibbs formulation* is complementary to the Helmholtz formulation. In the Helmholtz formulation, strain is the independent variable and stress is the dependent variable; in the Gibbs formulation, stress is the independent variable and strain is the dependent variable. Thus, the state functions are functions of Π_{RS}, θ, and q^r_{RS}. The energy equation is from (8.26)

$$\dot{\varepsilon} = \frac{1}{\rho_0}\Pi_{RS}\dot{E}_{RS} - \frac{1}{\rho_0}\frac{\partial h_R}{\partial X_R} + \dot{q} \tag{8.34}$$

For an irreversible system at constant q^r_{RS}, following Valanis [2], we may write

$$\dot{\varepsilon}|_{q^r_{PQ}} - \frac{1}{\rho_0}\Pi_{RS}\dot{E}_{RS} = \theta\dot{\eta}|_{q^r_{PQ}} \tag{8.35}$$

Let $\Psi = \varepsilon - \eta\theta$, we have

$$\dot{\Psi}|_{q^r_{PQ}} = \dot{\varepsilon}|_{q^r_{PQ}} - \eta\dot{\theta} - \dot{\eta}|_{q^r_{PQ}}\theta \tag{8.36}$$

Substituting (8.36) into (8.35), we obtain

$$\dot{\Psi}|_{q^r_{PQ}} - \frac{1}{\rho_0}\Pi_{RS}\dot{E}_{RS} + \eta\dot{\theta} = 0 \tag{8.37}$$

The *Gibbs free energy* is now defined as

$$\Phi = \Psi - \frac{1}{\rho_0}\Pi_{RS}E_{RS} \tag{8.38}$$

By differentiation, we then have

$$\dot{\Psi}|_{q^r_{PQ}} = \dot{\Phi}|_{q^r_{PQ}} + \frac{1}{\rho_0}\Pi_{RS}\dot{E}_{RS}|_{q^r_{PQ}} + \frac{1}{\rho_0}\dot{\Pi}_{RS}E_{RS} \tag{8.39}$$

Substituting (8.39) into (8.37), we obtain

$$\left.\frac{\partial\Phi}{\partial\Pi_{RS}}\right|_{\theta,q^r_{PQ}}\dot{\Pi}_{RS} + \left.\frac{\partial\Phi}{\partial\theta}\right|_{\Pi_{PQ},q^r_{PQ}}\dot{\theta} + \frac{1}{\rho_0}\dot{\Pi}_{RS}E_{RS} + \eta\dot{\theta} = 0 \tag{8.40}$$

Since the stress and the temperature can be arbitrarily varied, it is concluded that

$$E_{RS} = -\rho_0\left.\frac{\partial\Phi}{\partial\Pi_{RS}}\right|_{\theta,q^r_{PQ}} \quad \text{and} \quad \eta = -\left.\frac{\partial\Phi}{\partial\theta}\right|_{\Pi_{PQ},q^r_{PQ}} \tag{8.41}$$

These are the constitutive equations in the Gibbs formulation. In the following functions, we note the differences in the independent variables: $\mathbf{E} = \mathbf{E}(\mathbf{\Pi}, \theta, \mathbf{q}^r)$, $\Phi = \Phi(\mathbf{\Pi}, \theta, \mathbf{q}^r)$, but $\Psi = \Psi(\mathbf{E}, \theta, \mathbf{q}^r)$.

Differentiating (8.38), we have

$$\dot{\Phi} = \dot{\Psi} - \frac{1}{\rho_0}\dot{\Pi}_{RS}E_{RS} - \frac{1}{\rho_0}\Pi_{RS}\dot{E}_{RS} \tag{8.42}$$

or

$$\begin{aligned}\frac{\partial\Phi}{\partial\Pi_{RS}}\dot{\Pi}_{RS} + \frac{\partial\Phi}{\partial\theta}\dot{\theta} + \frac{\partial\Phi}{\partial q^r_{RS}}\dot{q}^r_{RS} \\ = \frac{\partial\Psi}{\partial E_{RS}}\dot{E}_{RS} + \frac{\partial\Psi}{\partial\theta}\dot{\theta} + \frac{\partial\Psi}{\partial q^r_{RS}}\dot{q}^r_{RS} - \frac{1}{\rho_0}\dot{\Pi}_{RS}E_{RS} - \frac{1}{\rho_0}\Pi_{RS}\dot{E}_{RS}\end{aligned} \tag{8.43}$$

Using (8.14) and (8.41), (8.43) reduces to

$$\frac{\partial \Phi}{\partial q^r_{RS}} \dot{q}^r_{RS} = \frac{\partial \Psi}{\partial q^r_{RS}} \dot{q}^r_{RS} \tag{8.44}$$

The Clausius–Duhem inequality (8.32) becomes

$$\frac{\partial \Psi}{\partial q^r_{RS}} \dot{q}^r_{RS} = \frac{\partial \Phi}{\partial q^r_{RS}} \dot{q}^r_{RS} \leq 0 \tag{8.45}$$

The evolution equations for q^r_{RS} are

$$\dot{q}^r_{RS} = g^r_{RS}(\Pi_{PQ}, \theta, q^r_{PQ}) \tag{8.46}$$

Note that the functions g^r_{RS} must satisfy the constraint of Clausius–Duhem inequality. In addition, from (8.31) and (8.46), g^r_{RS} is related to f^r_{RS} by the equation

$$g^r_{RS} = f^r_{RS}[E_{PQ}(\Pi_{TU}, \theta, q^s_{TU}), \theta, q^s_{TU}] \qquad \text{with } r, s = 1, \ldots, n \tag{8.47}$$

The functions g^r_{RS} can be nonlinear. However, linear functions work extremely well for applications to be discussed in connection with the endochronic theory. In the case of linear functions, the evolution equations are

$$\frac{\partial \Phi}{\partial q^r_{RS}} + b^r_{RSPQ} \dot{q}^r_{PQ} = 0 \qquad (r \text{ not summed}) \tag{8.48}$$

where b^r_{RSPQ} is a positive definite fourth-rank tensor. Knowing Φ, an explicit form of constitutive equations can be obtained.

8.4 The Endochronic Theory of Plasticity

8.4.1 The Concepts of the Endochronic Theory

Valanis developed the endochronic theory of plasticity in two major papers [6,7]. The Greek word endochronic means intrinsic (or internal) time. The deformation history is represented by a monotonically increasing time-like parameter ζ known as the endochronic (or intrinsic) time. The endochronic time accounts for the intrinsic material properties and is defined as

$$\mathrm{d}\zeta^2 = P_{RSPQ}\, \mathrm{d}E_{RS}\, \mathrm{d}E_{PQ} \tag{8.49}$$

where P_{RSPQ} is a fourth-rank tensor, which could depend on E_{RS}. This concept of intrinsic time is different from that of Ilyushin [10] and Pipkin and Rivlin [11], using the arc length of the strain path as a parameter. In that case,

$$\mathrm{d}\zeta^2 = \mathrm{d}E_{RS}\,\mathrm{d}E_{RS} \tag{8.50}$$

We note that (8.50) is a special case of (8.49).

Another original idea of Valanis' is to develop a theory that describes the stress–strain curve without a yield surface. The stress–strain curves of metals such as aluminum, brass, and high-strength steel do not show an apparent yield point. As we have discussed in Section 6.2, several definitions of yield surfaces are available and there are factors affecting the experimental determination of yield surfaces. Valanis tried to avoid the use of yield surface and showed in [6] that, using the thermodynamics of the internal variable and the concept of intrinsic time, it was indeed possible to develop a theory which not only does not have a yield point but can also successfully describe metal behaviors such as the Baushinger effect in unloading behavior, hardening due to shear prestrain, cyclic stress–strain loops, and cyclic hardening. At the time when [6] was published, the flow theory of plasticity was not yet successful in theoretically describing these complex behaviors of metals.

This theory of Valanis [6] is simple in form and will be referred to as the *simple endochronic theory*. This theory has many advantages because of its simplicity in calculation. Take the cyclic loading as an example, the flow theory of plasticity would need to determine whether the current state is in the plastic state and, if so, apply the flow rule, which is incremental. An intense numerical integration is needed. The equations of the endochronic theory, on the other hand, may be integrated to obtain a closed form solution without having to determine the yield point. However, there are drawbacks of the simple endochronic theory. The unloading curve has a slope slightly larger than the initial slope of the stress–strain curve. If, in a plastic state, a small amount of stress unloading occurs and is immediately followed by a reloading back to the original stress level, then a stress–strain loop does not form. If this unloading–reloading cycle continues, then cyclic creep or ratcheting would occur without reaching a steady state, that is, the strain would continue to increase as the stress cycling continues, but not in agreement with experimental findings. Another drawback is related to the rate of entropy production. In a plastic state, increments in loading and unloading will result in the same rate of entropy production, which is not acceptable.

Despite the drawbacks, the simple endochronic theory continues to be used by some investigators because of its simplicity and because the concept of yield surface is not needed. It provides a good approximation to metals when only loading is of interest, or under certain loading histories such as cyclic loading.

An *improved endochronic theory*, or simply the "endochronic theory" in the remainder of this chapter, was proposed by Valanis [7] to remove the aforementioned drawbacks. The improved theory uses plastic strain to define the

intrinsic time, while the simple endochronic theory uses the total strain. Valanis [7] showed that a limiting case of this new formulation leads to the definition of yield surface. In fact, the flow theory of plasticity can be derived from the endochronic theory, including the flow rule and the strain-hardening rules. However, the forms of the flow rule and strain-hardening rules are derived; whereas these forms and rules are separately assumed in the traditional flow theory of plasticity.

This author has been heavily involved in the development and verification of the endochronic theory. Specially designed experiments have been conducted by the author and his coworkers which are then used to verify the theory. These investigations will be discussed in later sections of this chapter and in Chapter 9.

8.4.2 The Simple Endochronic Theory of Plasticity

The simple endochronic theory has been derived for small isothermal deformation in [6], using the Helmholtz formulation discussed in Section 8.3.3. In the small deformation, the stress is $\boldsymbol{\sigma}$ and the strain is $\boldsymbol{\varepsilon}$. Equation (8.30) reduces to

$$\boldsymbol{\sigma} = \frac{\partial \Psi}{\partial \boldsymbol{\varepsilon}}, \quad \eta = -\frac{\partial \Psi}{\partial \theta}, \quad -\frac{\partial \Psi}{\partial \mathbf{q}^r} \cdot \dot{\mathbf{q}}^r \geq 0 \qquad (r \text{ not summed}) \tag{8.51}$$

From the last expression of (8.51), we see that $\dot{\mathbf{q}}^r$ cannot be independent of $-\partial\Psi/\partial\mathbf{q}^r$. Otherwise, an arbitrary choice of $\dot{\mathbf{q}}^r$ may violate the inequality. Therefore, $\dot{\mathbf{q}}^r$ and $-\partial\Psi/\partial\mathbf{q}^r$ must be related. The relation can be in the form of a function or of a functional, or something else. For the sake of simplicity, a function is assumed in the ensuing discussion. Furthermore, a linear form is assumed such that

$$\frac{\partial \Psi}{\partial q^r_{ij}} + b^r_{ijkm}\dot{q}^r_{km} = 0 \qquad (r \text{ not summed}) \tag{8.52}$$

where b^r_{ijkm} is a symmetric positive definite tensor. Note that this linear form has been proven to be adequate in most applications. Other forms may be considered if called for. However, we like the linear form because of its mathematical simplicity. Substituting (8.52) into the last expression of (8.51), we obtain

$$b^r_{ijkm}\dot{q}^r_{ij}\dot{q}^r_{km} \geq 0 \qquad (r \text{ not summed}) \tag{8.53}$$

The intrinsic time is from (8.49)

$$\mathrm{d}\zeta^2 = P_{ijkm}\,\mathrm{d}\varepsilon_{ij}\,\mathrm{d}\varepsilon_{km} \tag{8.54}$$

In the endochronic theory, all developments are with respect to the increment of intrinsic time. The evolution equation for the internal variables can then be expressed with respect to the intrinsic time as

$$\frac{\partial \Psi}{\partial q^r_{ij}} + b^r_{ijkm}(\zeta)\frac{\mathrm{d}q^r_{km}}{\mathrm{d}\zeta} = 0 \qquad (r \text{ not summed}) \tag{8.55}$$

where $b^r_{ijkm}(\zeta)$ is a function of intrinsic time ζ and $b^r_{ijkm} = (b^r_0)_{ijkm} f(\zeta)$; (8.55) may then be written as

$$\frac{\partial \Psi}{\partial q^r_{ij}} + (b^r_0)_{ijkm} f(\zeta)\frac{\mathrm{d}q^r_{km}}{\mathrm{d}\zeta} = 0 \qquad (r \text{ not summed}) \tag{8.56}$$

or

$$\frac{\partial \Psi}{\partial q^r_{ij}} + (b^r_0)_{ijkm}\frac{\mathrm{d}q^r_{km}}{\mathrm{d}z} = 0 \qquad (r \text{ not summed}) \tag{8.57}$$

where $(b^r_0)_{ijkm}$ is a fourth-rank constant tensor; the intrinsic time has been scaled by a factor f and z is the intrinsic timescale. The relation is

$$\mathrm{d}z = \frac{\mathrm{d}\zeta}{f(\zeta)} \tag{8.58}$$

The scaling factor $f(\zeta)$ will be identified later as the isotropic hardening function. The case of $f = 1$ corresponds to no isotropic hardening. Generally, (8.58) may be integrated from the initial intrinsic time ζ_0 to the current intrinsic time ζ as

$$z = \int_{\zeta_0}^{\zeta} \frac{\mathrm{d}\zeta}{f(\zeta)} \tag{8.59}$$

As a first approximation, we use the linear form

$$f(\zeta) = 1 + \beta\zeta \tag{8.60}$$

and, in this case, (8.59) becomes

$$z = \frac{1}{\beta}\ln(1 + \beta\zeta) \tag{8.61}$$

with initial values $\zeta_0 = z_0 = 0$; β is a constant.

In summary, the endochronic equations of the Helmholtz formulation for small isothermal deformation are

$$\begin{aligned} &\Psi = \Psi(\boldsymbol{\varepsilon}, \mathbf{q}^r), \qquad \boldsymbol{\sigma} = \frac{\partial \Psi}{\partial \boldsymbol{\varepsilon}}, \qquad \frac{\partial \Psi}{\partial \mathbf{q}^r} + \underline{\mathbf{b}}_0^r \cdot \frac{\mathrm{d}\mathbf{q}^r}{\mathrm{d}z} = 0, \\ &\mathrm{d}z = \frac{\mathrm{d}\zeta}{f(\zeta)}, \qquad \mathrm{d}\zeta^2 = \mathrm{d}\boldsymbol{\varepsilon} \cdot \underline{\mathbf{P}} \cdot \mathrm{d}\boldsymbol{\varepsilon} \end{aligned} \tag{8.62}$$

where a boldfaced letter with an underscore, such as $\underline{\mathbf{P}}$, denotes a fourth-rank tensor. To obtain an explicit constitutive equation, the free energy is expressed in a quadratic form as

$$\Psi = \tfrac{1}{2}\boldsymbol{\varepsilon} \cdot \underline{\mathbf{A}} \cdot \boldsymbol{\varepsilon} + \boldsymbol{\varepsilon} \cdot \underline{\mathbf{B}}^r \cdot \mathbf{q}^r + \tfrac{1}{2}\mathbf{q}^r \cdot \underline{\mathbf{C}}^r \cdot \mathbf{q}^r \tag{8.63}$$

where $\underline{\mathbf{A}}$, $\underline{\mathbf{B}}^r$, $\underline{\mathbf{C}}^r$ are fourth-rank constant tensors. Note that linear terms in $\boldsymbol{\varepsilon}$ are absent to accommodate the requirement that the reference state is unstressed. In addition, linear terms in $\mathbf{q}^r$ are absent if the reversal of the sign of strain history leaves the form of the stress response invariant. Substituting (8.63) into (8.62), we obtain

$$\boldsymbol{\sigma} = \underline{\mathbf{A}} \cdot \boldsymbol{\varepsilon} + \sum_r \underline{\mathbf{B}}^r \cdot \mathbf{q}^r \quad \text{and} \quad \underline{\mathbf{B}}^r \cdot \boldsymbol{\varepsilon} + \underline{\mathbf{C}}^r \cdot \mathbf{q}^r + \underline{\mathbf{b}}_0^r \cdot \frac{\mathrm{d}\mathbf{q}^r}{\mathrm{d}z} = 0 \tag{8.64}$$

If $\underline{\mathbf{A}}, \underline{\mathbf{B}}^r, \underline{\mathbf{C}}^r$ and $\underline{\mathbf{b}}_0^r$ are isotropic functions and, since $\boldsymbol{\sigma}, \boldsymbol{\varepsilon}$, and $\mathbf{q}^r$ are symmetric tensors, the isotropic expressions for these tensors are from (1.129)

$$\begin{aligned} &A_{ijkm} = A_1\delta_{ij}\delta_{km} + A_2\delta_{ik}\delta_{jm}, \qquad B^r_{ijkm} = B^r_1\delta_{ij}\delta_{km} + B^r_2\delta_{ik}\delta_{jm}, \\ &C^r_{ijkm} = C^r_1\delta_{ij}\delta_{km} + C^r_2\delta_{ik}\delta_{jm}, \qquad (b^r_0)_{ijkm} = b^r_1\delta_{ij}\delta_{km} + b^r_2\delta_{ik}\delta_{jm} \end{aligned} \tag{8.65}$$

Substituting (8.65) into (8.64) and separating the resulting equations into the hydrostatic and deviatoric parts, we find

$$\begin{aligned} \sigma_{kk} &= (3A_1 + A_2)\varepsilon_{kk} + \sum_r (3B^r_1 + B^r_2)q^r_{kk} \\ \sigma'_{ij} &= A_2 e_{ij} + \sum_r B^r_2 p^r_{ij} \end{aligned} \tag{8.66}$$

$$\begin{aligned} &B^r_0\varepsilon_{kk} + C^r_0 q^r_{kk} + b^r_0 \frac{\mathrm{d}q^r_{kk}}{\mathrm{d}z} = 0 \\ &B^r_2 e_{ij} + C^r_2 p^r_{ij} + b^r_2 \frac{\mathrm{d}p^r_{ij}}{\mathrm{d}z} = 0 \end{aligned} \qquad (r \text{ not summed}) \tag{8.67}$$

where the deviatoric parts are

$$e_{ij} = \varepsilon_{ij} - \tfrac{1}{3}\delta_{ij}\varepsilon_{kk}, \qquad \sigma'_{ij} = \sigma_{ij} - \tfrac{1}{3}\delta_{ij}\sigma_{kk}, \qquad p^r_{ij} = q^r_{ij} - \tfrac{1}{3}\delta_{ij}q^r_{kk} \tag{8.68}$$

and

$$\begin{aligned} A_0 &= \tfrac{1}{3}(3A_1 + A_2), \qquad B_0^r = \tfrac{1}{3}(3B_1^r + B_2^r), \\ C_0^r &= \tfrac{1}{3}(3C_1^r + C_2^r), \qquad b_0^r = \tfrac{1}{3}(3b_1^r + b_2^r) \end{aligned} \tag{8.69}$$

Equations in (8.67) are constant coefficient linear ordinary differential equations and the solutions are

$$\begin{aligned} q_{kk}^r &= -\frac{B_0^r}{b_0^r}\int_{z_0}^{z} \exp\left(-\frac{C_0^r}{b_0^r}(z-z')\right)\varepsilon_{kk}(z')\,\mathrm{d}z' \qquad \text{with } q_{kk}^r(0) = 0 \\ p_{ij}^r &= -\frac{B_2^r}{b_2^r}\int_{z_0}^{z} \exp\left(-\frac{C_2^r}{b_2^r}(z-z')\right)e_{ij}(z')\,\mathrm{d}z' \qquad \text{with } p_{ij}^r(0) = 0 \end{aligned} \tag{8.70}$$

Combining (8.66) and (8.70) yields

$$\sigma = \frac{1}{3}\sigma_{kk} = \int_{z_0}^{z} K(z-z')\frac{\mathrm{d}\varepsilon_{kk}}{\mathrm{d}z'}\mathrm{d}z' \quad \text{and} \quad \sigma_{ij}' = 2\int_{z_0}^{z}\mu(z-z')\frac{\mathrm{d}e_{ij}}{\mathrm{d}z'}\mathrm{d}z' \tag{8.71}$$

where the kernel functions are given by

$$\begin{aligned} K(z) &= \left(A_0 - \sum_r \frac{(B_0^r)^2}{C_0^r}\right)H(z) + \sum_r \frac{(B_0^r)^2}{C_0^r}\mathrm{e}^{-\lambda_r z} \qquad \text{with } \lambda_r = \frac{C_0^r}{b_0^r} \\ 2\mu(z) &= \left(A_2 - \sum_r \frac{(B_2^r)^2}{C_2^r}\right)H(z) + \sum_r \frac{(B_2^r)^2}{C_2^r}\mathrm{e}^{-\rho_r z} \qquad \text{with } \rho_r = \frac{C_2^r}{b_2^r} \end{aligned} \tag{8.72}$$

where $H(z)$ is the *Heaviside step function*. These kernel functions are also known as the *heredity functions*. If $2\mu(z)$ is plotted against z, the curve has a value of A_2 at $z = 0$ and relaxes gradually to $[A_2 - \sum_r((B_2^r)^2/C_2^r)]$ as z increases and becomes large. Similarly, $K(z)$ has an initial value of A_0 and relaxes to $(A_0 - \sum_r((B_0^r)^2/C_0^r))$. The functions $\mu(z)$ and $K(z)$ are sums of positive decaying exponential terms, where one or more of the exponents may be zero. This describes the effect of fading memory. In the event that the hydrostatic response is elastic as most metals are, $B_0^r = C_0^r = 0$ and q_{kk}^r is constant. The first equation of (8.72) reduces to

$$K(z) = A_0 H(z) \tag{8.73}$$

and the hydrostatic stress–strain curve is from (8.71)

$$\sigma = \tfrac{1}{3}\sigma_{kk} = A_0\varepsilon_{kk} \tag{8.74}$$

Valanis and Wu [12] investigated the representation of heredity functions and showed that the theory was able to describe observed behavior of metals under conditions of cyclic deformation. In addition, Wu and his coworkers [13–16] applied the theory to investigate the problem of viscoplastic wave propagation in thin rods and thin-walled tubes.

By differentiation, the deviatoric part of the constitutive equation in (8.71) can be written in a differential form. In the simple case of $\mu(z) = \mu_0 \, e^{-\alpha z}$, where μ_0 and α are constants, we have

$$\boldsymbol{\sigma}' = 2\mu_0 \int_0^z e^{-\alpha(z-z')} \frac{d\mathbf{e}}{dz'} dz' \tag{8.75}$$

and

$$\frac{d\boldsymbol{\sigma}'}{dz} = (-\alpha)2\mu_0 \int_0^z e^{-\alpha(z-z')} \frac{d\mathbf{e}}{dz'} dz' + 2\mu_0 \frac{d\mathbf{e}}{dz} \tag{8.76}$$

or

$$\frac{d\boldsymbol{\sigma}'}{dz} + \alpha\boldsymbol{\sigma}' = 2\mu_0 \frac{d\mathbf{e}}{dz} \tag{8.77}$$

This is the constitutive equation in the differential form. From (8.77), we see that the plastic strain increment is

$$d\mathbf{e}^p = d\mathbf{e} - \frac{d\boldsymbol{\sigma}'}{2\mu_0} = \frac{\alpha}{2\mu_0} dz \boldsymbol{\sigma}' \tag{8.78}$$

This is in the form of the Prandtl–Reuss relation, when the elastic strain is considered. On the other hand, the function $\mu(z)$ may contain more terms. For example, $\mu(z) = \mu_0 + \mu_1 \, e^{-\alpha z}$, where μ_0, μ_1, and α are constants. We then obtain

$$d\mathbf{e}^p = \frac{\alpha}{2\bar{\mu}} \boldsymbol{\sigma}' \, dz - \frac{\mu_0}{\bar{\mu}} \alpha \mathbf{e} \, dz \qquad \text{with } \bar{\mu} = \mu_0 + \mu_1 \tag{8.79}$$

Equation (8.79) is not in the form of the Prandtl–Reuss relation.

EXAMPLE 8.1 Determine the endochronic constitutive equation for uniaxial tension.

Solution

In uniaxial tension, (8.71) reduces to

$$\sigma = \int_0^z E(z - z') \frac{d\varepsilon}{dz'} dz' \tag{a}$$

The stress is σ, the strain is ε, and $E(z)$ is the heredity function. We assume that the specimen is initially in an annealed state so that $z_0 = 0$. We consider the simplest case possible, when $E(z)$ has only one exponential term, that is,

$$E(z) = E_0 \, \mathrm{e}^{-\alpha z} \tag{b}$$

where E_0 and α are constants. The intrinsic time increment is from (8.54)

$$\mathrm{d}\zeta = \pm k \, \mathrm{d}\varepsilon \tag{c}$$

in which k is assumed to be a constant for simplicity. The positive and negative sign in (c) are for loading and unloading. We use the linear form for intrinsic timescale given by (8.60), which is integrated to yield (8.61). We then obtain from (8.61) the expression $1 + \beta\zeta = \mathrm{e}^{\beta z}$, which leads to

$$\frac{\mathrm{d}\zeta}{\mathrm{d}z} = \mathrm{e}^{\beta z} \tag{d}$$

where β is a constant. Substituting (b) into (a) and using (c) and (d), we obtain

$$\begin{aligned}
\sigma &= E_0 \int_0^z \mathrm{e}^{-\alpha(z-z')} \frac{\mathrm{d}\varepsilon}{\mathrm{d}\zeta'} \frac{\mathrm{d}\zeta'}{\mathrm{d}z'} \mathrm{d}z' = E_0 \int_0^z \mathrm{e}^{-\alpha(z-z')} \left(\frac{1}{k}\right) (\mathrm{e}^{\beta z'}) \mathrm{d}z' \\
&= \frac{E_0 \, \mathrm{e}^{\beta z}}{k(\alpha+\beta)} [1 - \mathrm{e}^{-(\alpha+\beta)z}] = \frac{E_0(1+\beta\zeta)}{k\beta(1+\alpha/\beta)} [1 - (1+\beta\zeta)^{-(1+\alpha/\beta)}] \\
&= \frac{E_0}{k\beta n}(1+\beta\zeta) \left\{ 1 - \frac{1}{(1+\beta\zeta)^n} \right\} \qquad \text{with } n = 1 + \frac{\alpha}{\beta}
\end{aligned} \tag{e}$$

In loading starting from zero load and zero strain, (c) can be integrated to yield

$$\zeta = k\varepsilon \tag{f}$$

Using (f), (e) becomes

$$\sigma = \frac{E_0}{\beta_1 n}(1+\beta_1\varepsilon) \left\{ 1 - \frac{1}{(1+\beta_1\varepsilon)^n} \right\} \qquad \text{with } \beta_1 = k\beta \tag{g}$$

This is the endochronic stress–strain relation with three parameters E_0, β_1, and n. This equation is able to describe the stress–strain curve for most metallic materials. The three parameters may be determined by a method described in Example 8.2. A method by use of the optimization technique is given by Jao et al. [17].

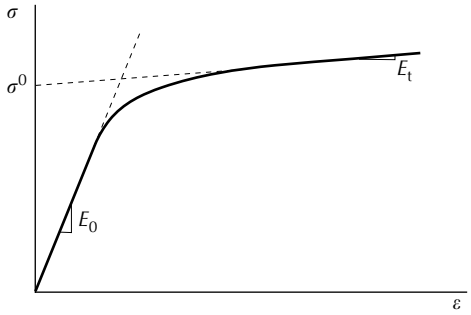

FIGURE 8.3
A stress–strain curve.

EXAMPLE 8.2 Determine the three parameters of the endochronic stress–strain relation

$$\sigma = \frac{E_0}{\beta_1 n}(1+\beta_1\varepsilon)\left\{1-\frac{1}{(1+\beta_1\varepsilon)^n}\right\} \tag{a}$$

Solution

A hypothetical experimental stress–strain curve is shown in Figure 8.3, and we like to determine E_0, β_1, and n so that (a) describes this experimental curve. We first determine E_0, E_t, and σ^0 from the experimental curve. E_0 is the slope at $\varepsilon = 0$; E_t is the tangent modulus at large ε; and σ^0 is the intercept of the asymptote of the stress–strain curve with the stress axis. We note that $E_0 = (\mathrm{d}\sigma/\mathrm{d}\varepsilon)|_{\varepsilon\to 0}$, and this is about the same as Young's modulus for materials that has a very straight initial curve. E_0 should be slightly larger than the conventional value for Young's modulus, if the material starts to bend right from the beginning of the stress–strain curve. The asymptote at large ε is found from (a) as

$$\sigma = \frac{E_0}{\beta_1 n}(1+\beta_1\varepsilon) \tag{b}$$

with slope

$$E_t = \left.\frac{\mathrm{d}\sigma}{\mathrm{d}\varepsilon}\right|_{\varepsilon\to\text{large}} = \frac{E_0}{n} \tag{c}$$

Therefore,

$$n = \frac{E_0}{E_t} \tag{d}$$

The intercept of the asymptote with the stress axis is found by setting $\varepsilon = 0$ in (b). Thus,

$$\sigma^0 = \frac{E_0}{\beta_1 n} \tag{e}$$

From (e), we obtain

$$\beta_1 = \frac{E_0}{n\sigma^0} \tag{f}$$

Therefore, knowing E_0, E_t, and σ^0, we find n from (d) and β_1 from (f).

EXAMPLE 8.3 If the free energy Ψ is positive definite, that is,

$$\Psi = \tfrac{1}{2}\boldsymbol{\varepsilon} \cdot \underline{\mathbf{A}} \cdot \boldsymbol{\varepsilon} + \boldsymbol{\varepsilon} \cdot \underline{\mathbf{B}}^r \cdot \mathbf{q}^r + \tfrac{1}{2}\mathbf{q}^r \cdot \underline{\mathbf{C}}^r \cdot \mathbf{q}^r > 0 \tag{a}$$

and if

$$A_{ijkm} = A_1\delta_{ij}\delta_{km} + A_2\delta_{ik}\delta_{jm}, \qquad C^r_{ijkm} = C^r_1\delta_{ij}\delta_{km} + C^r_2\delta_{ik}\delta_{jm} \tag{b}$$

show that

$$A_1 + \tfrac{1}{3}A_2 > 0, \qquad A_2 > 0 \quad \text{and} \quad C^r_1 + \tfrac{1}{3}C^r_2 > 0, \qquad C^r_2 > 0 \tag{c}$$

Solution

The free energy is positive definite, $\Psi > 0$, for any $\boldsymbol{\varepsilon}$ and $\mathbf{q}^r$ subjected to the thermodynamic constraints discussed in Section 8.3.3. In a special case, $\Psi > 0$ for $\boldsymbol{\varepsilon} = 0$ and arbitrary nonzero $\mathbf{q}^r$, so that

$$\Psi = \tfrac{1}{2}\mathbf{q}^r \cdot \underline{\mathbf{C}}^r \cdot \mathbf{q}^r > 0 \tag{d}$$

Therefore, $\underline{\mathbf{C}}^r$ must be positive definite. Another special case is when $\mathbf{q}^r = 0$ subjected to nonzero arbitrary $\boldsymbol{\varepsilon}$. Then,

$$\Psi = \tfrac{1}{2}\boldsymbol{\varepsilon} \cdot \underline{\mathbf{A}} \cdot \boldsymbol{\varepsilon} > 0 \tag{e}$$

that is, $\underline{\mathbf{A}}$ must be positive definite.

Using (b) and (e), we have

$$\Psi = \tfrac{1}{2}(A_1\varepsilon_{ii}\varepsilon_{kk} + A_2\varepsilon_{ik}\varepsilon_{ik}) \tag{f}$$

which may be written in the matrix form as

$$\Psi = [\varepsilon]^{\mathrm{T}}[A][\varepsilon] = \frac{1}{2}\begin{bmatrix}\varepsilon_{11}\\ \varepsilon_{22}\\ \varepsilon_{33}\\ \varepsilon_{12}\\ \varepsilon_{13}\\ \varepsilon_{21}\\ \varepsilon_{21}\\ \varepsilon_{31}\\ \varepsilon_{32}\end{bmatrix}^{\mathrm{T}} \times \begin{bmatrix} A_1+A_2 & A_1 & A_1 & 0 & 0 & 0 & 0 & 0 & 0\\ A_1 & A_1+A_2 & A_1 & 0 & 0 & 0 & 0 & 0 & 0\\ A_1 & A_1 & A_1+A_2 & 0 & 0 & 0 & 0 & 0 & 0\\ 0 & 0 & 0 & 2A_2 & 0 & 0 & 0 & 0 & 0\\ 0 & 0 & 0 & 0 & 2A_2 & 0 & 0 & 0 & 0\\ 0 & 0 & 0 & 0 & 0 & 2A_2 & 0 & 0 & 0\\ 0 & 0 & 0 & 0 & 0 & 0 & 2A_2 & 0 & 0\\ 0 & 0 & 0 & 0 & 0 & 0 & 0 & 2A_2 & 0\\ 0 & 0 & 0 & 0 & 0 & 0 & 0 & 0 & 2A_2 \end{bmatrix} \begin{bmatrix}\varepsilon_{11}\\ \varepsilon_{22}\\ \varepsilon_{33}\\ \varepsilon_{12}\\ \varepsilon_{13}\\ \varepsilon_{21}\\ \varepsilon_{21}\\ \varepsilon_{31}\\ \varepsilon_{32}\end{bmatrix} \tag{g}$$

Since Ψ is positive definite, $[A]$ is a positive definite matrix, that is, the determinant of every principal minor should be nonnegative. Therefore,

(a) $A_1 + A_2 > 0$ (h)

(b) $$\begin{vmatrix} A_1+A_2 & A_1 \\ A_1 & A_1+A_2 \end{vmatrix} = A_2(2A_1 + A_2) > 0 \tag{i}$$

(c) $$\begin{vmatrix} A_1+A_2 & A_1 & A_1 \\ A_1 & A_1+A_2 & A_1 \\ A_1 & A_1 & A_1+A_2 \end{vmatrix} = A_2^2(3A_1 + A_2) > 0 \tag{j}$$

(d) $$\begin{bmatrix} A_1+A_2 & A_1 & A_1 & 0 \\ A_1 & A_1+A_2 & A_1 & 0 \\ A_1 & A_1 & A_1+A_2 & 0 \\ 0 & 0 & 0 & 2A_2 \end{bmatrix} = (2A_2)A_2^2(3A_1 + A_2) > 0 \tag{k}$$

From (h) to (k), it is concluded that

$$A_2 > 0, \qquad A_1 + A_2 > 0, \qquad 2A_1 + A_2 > 0, \qquad 3A_1 + A_2 > 0 \tag{m}$$

Plotting the above inequalities in the A_2 versus A_1 space, it is found that the solution is bounded by

$$A_2 > 0 \quad \text{and} \quad 3A_1 + A_2 > 0 \tag{n}$$

Using a similar procedure, the following inequalities can be established

$$C_1^r + \tfrac{1}{3}C_2^r > 0 \quad \text{and} \quad C_2^r > 0 \tag{o}$$

An alternate proof is obtained by considering simple loading conditions. We rewrite (f) as

$$\Psi = \frac{1}{2}\left(A_1 + \frac{A_2}{3}\right)(\varepsilon_{kk})^2 + \frac{1}{2}A_2 e_{ik}e_{ik} \tag{p}$$

In the case of hydrostatic strain, the strain components are $\varepsilon_{11} = \varepsilon_{22} = \varepsilon_{33} = \varepsilon$ and $e_{ij} = 0$, (p) reduces to

$$\Psi = \frac{1}{2}\left(A_1 + \frac{A_2}{3}\right)(3\varepsilon)^2 > 0 \quad \text{or} \quad A_1 + \frac{A_2}{3} > 0 \tag{q}$$

In the case of shear with $\varepsilon_{12} \neq 0$ and other $\varepsilon_{ij} = 0$, we have from (p)

$$\Psi = A_2(e_{12})^2 > 0 \quad \text{or} \quad A_2 > 0 \tag{r}$$

The physical meanings are not clear if the same procedure is applied to $\Psi = \frac{1}{2}\mathbf{q}^r \cdot \underline{\mathbf{C}}^r \cdot \mathbf{q}^r > 0$.

8.4.3 The Improved Endochronic Theory of Plasticity

Valanis [7] used a strain-like tensor Q_{ij} to define the intrinsic time as

$$\mathrm{d}\zeta^2 = \mathrm{d}Q_{ij}\mathrm{d}Q_{ij} \qquad \text{where } Q_{ij} = \varepsilon_{ij} - K_{ijkm}\sigma_{km} \tag{8.80}$$

This definition of intrinsic time is a generalization of (8.54). In one-dimensional straining, (8.80) reduces to

$$\mathrm{d}\zeta = |Q| = \left|\mathrm{d}\varepsilon - k_1\frac{\mathrm{d}\sigma}{E_0}\right| \qquad \text{with } 0 \le k_1 \le 1 \tag{8.81}$$

When $k_1 = 0, \mathrm{d}\zeta = |\mathrm{d}\varepsilon|$, which is the simple endochronic theory; but when $k_1 = 1$, Q has the meaning of plastic strain. This new definition of intrinsic time removes the drawbacks mentioned for the simple endochronic theory, and, in addition, the case of $k_1 = 1$ leads to the existence of yield surface. We shall demonstrate the latter assertion in the discussions to follow.

We first show that the deviatoric constitutive equation of (8.71)

$$\boldsymbol{\sigma}' = 2\int_{z_0}^{z} \mu(z-z')\frac{\mathrm{d}\mathbf{e}}{\mathrm{d}z'}\mathrm{d}z' = 2\mu_0 \int_{z_0}^{z} \xi(z-z')\frac{\mathrm{d}\mathbf{e}}{\mathrm{d}z'}\mathrm{d}z' \tag{8.82}$$

may be written in the following form

$$\boldsymbol{\sigma}' = 2\mu_0 \int_{0}^{z} \rho(z-z')\frac{\mathrm{d}\mathbf{Q}}{\mathrm{d}z'}\mathrm{d}z' \tag{8.83}$$

where

$$\mathbf{Q} = \mathbf{e} - k_1\frac{\boldsymbol{\sigma}'}{2\mu_0}, \qquad \mu(z) = \mu_0\xi(z), \qquad \xi(0) = 1 \tag{8.84}$$

The relation between $\xi(z)$ and $\rho(z)$ may be found by the method of Laplace transformation. From (8.82), we have

$$\bar{\boldsymbol{\sigma}}' = 2\mu_0\bar{\xi}p\bar{\mathbf{e}} \qquad \text{with } \mathbf{e}(0) = 0 \tag{8.85}$$

where $\bar{f}(p)$ is the transform of the function $f(z)$ and p is the parameter of Laplace transformation. We note that $L(\mathrm{d}f(z)/\mathrm{d}z) = p\bar{f}(p) - f(0)$. On the other hand, (8.83) is transformed into

$$\bar{\boldsymbol{\sigma}}' = 2\mu_0\bar{\rho}p\bar{\mathbf{Q}} \qquad \text{with } \mathbf{Q}(0) = 0 \tag{8.86}$$

Using the Laplace transform of (8.84), (8.86) is further written as

$$\bar{\boldsymbol{\sigma}}' = 2\mu_0\bar{\rho}p\left(\bar{e} - k_1\frac{\bar{\sigma}'}{2\mu_0}\right) \tag{8.87}$$

Substituting (8.85) into (8.87), the resulting equation is

$$\bar{\rho} - k_1\bar{\rho}p\bar{\xi} = \bar{\xi} \tag{8.88}$$

which may be written as

$$\bar{\rho} - k_1\bar{\rho}(p\bar{\xi} - \xi(0)) - k_1\bar{\rho}\xi(0) = \bar{\xi} \tag{8.89}$$

An inverse transform of (8.89) gives us

$$(1-k_1)\rho(z) - k_1\int_{0}^{z} \rho(z-z')\frac{\mathrm{d}\xi}{\mathrm{d}z'}\mathrm{d}z' = \xi(z) \qquad \text{with } \xi(0) = 1 \tag{8.90}$$

It can be shown that, for $k_1 = 1$, the solution of (8.90) is

$$\rho(z) = \rho_0 \delta(z) + \rho_1(z) \tag{8.91}$$

where

$$\rho_1(z) = \sum_{r=1}^{n-1} R_r \mathrm{e}^{-\beta_r z}, \qquad \xi(z) = \sum_{r=1}^{n} \xi_r \mathrm{e}^{-\alpha_r z}, \qquad \sum_{r=1}^{n} \xi_r = 1 \tag{8.92}$$

and $\delta(z)$ is the Dirac delta function; R_r, ξ_r, β_r, α_r, and ρ_0 are constants.

Using (8.91) and (8.92), (8.83) becomes

$$\boldsymbol{\sigma}' = 2\mu_0\rho_0 \frac{\mathrm{d}\mathbf{Q}(z)}{\mathrm{d}z} + 2\mu_0 \int_0^z \rho_1(z - z') \frac{\mathrm{d}\mathbf{Q}(z')}{\mathrm{d}z'} \mathrm{d}z' \tag{8.93}$$

Equation (8.93) is the constitutive equation of the endochronic theory. This equation may be used directly to calculate the stress–strain response curves. On the other hand, based on this equation, the flow rule, the yield surface, and its hardening rules can be derived, thereby establishing a connection between the present theory and the flow theory of plasticity. By doing so, the physical meanings of some functions and parameters of this theory become clear. The differences between this theory and the flow theory are that the forms of the flow rule, yield surface, and hardening rule are related in this theory and they evolve with respect to the intrinsic time, while they are quite open to differently proposed forms in the classical flow theory. In the following subsection, we derive the flow rule, the yield surface, and the hardening rule.

EXAMPLE 8.4 In the simple case of

$$\xi(z) = \xi_1 \, \mathrm{e}^{-\alpha_1 z} + \xi_2 \, \mathrm{e}^{-\alpha_2 z} \tag{a}$$

determine the expression for $\rho(z)$.

Solution

The Laplace transform of (a) is

$$\bar{\xi}(p) = \frac{\xi_1}{p + \alpha_1} + \frac{\xi_2}{p + \alpha_2} \tag{b}$$

Substituting (b) into (8.88), we have

$$\bar{\rho} = \frac{\bar{\xi}(p)}{1 - k_1 p \bar{\xi}(p)} = \frac{p + \lambda}{(1 - k_1)p^2 + (\alpha_1 + \alpha_2 - k_1\lambda)p + \alpha_1\alpha_2} \tag{c}$$

where $\lambda = \xi_1\alpha_2 + \xi_2\alpha_1$. In the case of $k_1 \to 1$, (c) becomes

$$\bar{\rho} \approx \frac{p+\lambda}{(1-k_1)p^2 + (\alpha_1+\alpha_2-\lambda)p + \alpha_1\alpha_2} = \frac{p+\lambda}{(1-k_1)(p+\beta_1)(p+\beta_2)} \qquad \text{(d)}$$

where

$$\beta_1 = \frac{\bar{\lambda}}{1-k_1}, \qquad \beta_2 = \frac{\alpha_1\alpha_2}{\bar{\lambda}}, \qquad \bar{\lambda} = \alpha_1\xi_1 + \alpha_2\xi_2 \qquad \text{(e)}$$

Equation (d) may be further written as

$$\bar{\rho} = \frac{1}{1-k_1}\left[\frac{((\lambda-\beta_1)/(\beta_2-\beta_2))}{p+\beta_1} + \frac{((\lambda-\beta_2)/(\beta_1-\beta_2))}{p+\beta_2}\right] \qquad \text{(f)}$$

which may then be inverse transformed into

$$\rho(z) = \frac{1}{1-k_1}\left\{\frac{\lambda-\beta_1}{\beta_2-\beta_1}e^{-\beta_1 z} + \frac{\lambda-\beta_2}{\beta_1-\beta_2}e^{-\beta_2 z}\right\} \qquad \text{(g)}$$

Using (e), we find that

$$\frac{\lambda-\beta_1}{\beta_2-\beta_1} \approx 1 \quad \text{and} \quad \frac{1}{1-k_1}\frac{\lambda-\beta_2}{\beta_1-\beta_2} \approx \frac{\lambda\bar{\lambda}-\alpha_1\alpha_2}{\bar{\lambda}^2} \qquad \text{(h)}$$

Therefore, (g) becomes

$$\rho(z) = \frac{1}{1-k_1}\exp\left(-\frac{\bar{\lambda}}{1-k_1}z\right) + \left(\frac{\lambda\bar{\lambda}-\alpha_1\alpha_2}{\bar{\lambda}^2}\right)\exp\left(-\frac{\alpha_1\alpha_2}{\bar{\lambda}}z\right) \qquad \text{(i)}$$

When $k_1 \to 1$, (i) reduces to

$$\rho(z) = \rho_0\delta(z) + \left(\frac{\lambda\bar{\lambda}-\alpha_1\alpha_2}{\bar{\lambda}^2}\right)\exp\left(-\frac{\alpha_1\alpha_2}{\bar{\lambda}}z\right) = \rho_0\delta(z) + \rho_1(z) \qquad \text{(j)}$$

Thus,

$$\rho_1(z) = \left(\frac{\lambda\bar{\lambda}-\alpha_1\alpha_2}{\bar{\lambda}^2}\right)\exp\left(-\frac{\alpha_1\alpha_2}{\bar{\lambda}}z\right) \qquad \text{(k)}$$

8.4.4 Derivation of the Flow Theory of Plasticity from Endochronic Theory

In the case of $k_1 = 1$, the deviatoric part of the endochronic constitutive equation is from (8.93)

$$\boldsymbol{\sigma}' = 2\mu_0\rho_0\frac{\mathrm{d}\mathbf{Q}(z)}{\mathrm{d}z} + 2\mu_0\int_0^z \rho_1(z-z')\frac{\mathrm{d}\mathbf{Q}(z')}{\mathrm{d}z'}\mathrm{d}z' \tag{8.93}$$

with the intrinsic time defined from (8.80) by

$$\mathrm{d}\zeta^2 = \mathrm{d}Q_{ij}\,\mathrm{d}Q_{ij} \qquad \text{where } \mathrm{d}Q_{ij} = \mathrm{d}\varepsilon^{\mathrm{p}}_{ij} = \mathrm{d}e_{ij} - \frac{\mathrm{d}\sigma'_{ij}}{2\mu_0} \tag{8.94}$$

If we let

$$\boldsymbol{\alpha} = 2\mu_0\int_0^z \rho_1(z-z')\frac{\mathrm{d}\mathbf{Q}(z')}{\mathrm{d}z'}\mathrm{d}z' \quad \text{and} \quad \sigma'_{\mathrm{y}} = 2\mu_0\rho_0 \tag{8.95}$$

then, (8.93) can be written as

$$\boldsymbol{\sigma}' = \sigma'_{\mathrm{y}}\frac{\mathrm{d}\mathbf{Q}}{\mathrm{d}\zeta}f(z) + \boldsymbol{\alpha} \tag{8.96}$$

which may be further written as

$$\mathrm{d}\mathbf{Q} = \frac{\mathrm{d}\zeta}{\sigma'_{\mathrm{y}}f(z)}(\boldsymbol{\sigma}' - \boldsymbol{\alpha}) \tag{8.97}$$

This equation may be considered as the flow rule using the concept of the flow theory of plasticity. By substituting (8.97) into (8.94), we obtain

$$\mathrm{d}\zeta^2 = \mathrm{d}\mathbf{Q}\cdot\mathrm{d}\mathbf{Q} = \left(\frac{\mathrm{d}\zeta}{\sigma'_{\mathrm{y}}f(z)}\right)^2(\boldsymbol{\sigma}' - \boldsymbol{\alpha})\cdot(\boldsymbol{\sigma}' - \boldsymbol{\alpha}) \tag{8.98}$$

or

$$[(\boldsymbol{\sigma}' - \boldsymbol{\alpha})\cdot(\boldsymbol{\sigma}' - \boldsymbol{\alpha}) - (\sigma'_{\mathrm{y}}f(z))^2]\mathrm{d}\zeta^2 = 0 \tag{8.99}$$

Therefore, we obtain from (8.99) either

$$(\boldsymbol{\sigma}' - \boldsymbol{\alpha})\cdot(\boldsymbol{\sigma}' - \boldsymbol{\alpha}) = (\sigma'_{\mathrm{y}}f(z))^2 \quad \text{with } \mathrm{d}\zeta^2 \neq 0 \tag{8.100}$$

or

$$\mathrm{d}\zeta^2 = 0 \tag{8.101}$$

Equation (8.100) is the yield criterion with combined isotropic–kinematic hardening. $\boldsymbol{\alpha}$ represents the back stress and $f(z)$ represents the isotropic hardening. We will call $f(z)$ the *isotropic-hardening function*. The yield criterion applies when

$$\begin{aligned} \mathrm{d}\zeta^2 &= \mathrm{d}Q_{ij}\,\mathrm{d}Q_{ij} = \mathrm{d}\varepsilon^{\mathrm{p}}_{ij}\,\mathrm{d}\varepsilon^{\mathrm{p}}_{ij} \\ &= (\mathrm{d}\varepsilon^{\mathrm{p}}_{11})^2 + (\mathrm{d}\varepsilon^{\mathrm{p}}_{22})^2 + (\mathrm{d}\varepsilon^{\mathrm{p}}_{33})^2 + 2(\mathrm{d}\varepsilon^{\mathrm{p}}_{12})^2 + 2(\mathrm{d}\varepsilon^{\mathrm{p}}_{23})^2 + 2(\mathrm{d}\varepsilon^{\mathrm{p}}_{31})^2 \neq 0 \end{aligned} \tag{8.102}$$

Since all terms in (8.102) are positive, $\mathrm{d}\varepsilon^{\mathrm{p}}_{ij} \neq 0$ when $\mathrm{d}\zeta^2 \neq 0$. $\mathrm{d}\zeta^2 = 0$ only when all components of the plastic strain increments are zero. The case of $\mathrm{d}\zeta^2 = 0$ is given by (8.101) and further written as

$$\begin{aligned} \mathrm{d}\zeta^2 &= \mathrm{d}\varepsilon^{\mathrm{p}}_{ij}\,\mathrm{d}\varepsilon^{\mathrm{p}}_{ij} = \left(\mathrm{d}e_{ij} - \frac{\mathrm{d}\sigma'_{ij}}{2\mu_0}\right)\left(\mathrm{d}e_{ij} - \frac{\mathrm{d}\sigma'_{ij}}{2\mu_0}\right) \\ &= \left(\mathrm{d}e_{11} - \frac{\mathrm{d}\sigma'_{11}}{2\mu_0}\right)^2 + \left(\mathrm{d}e_{22} - \frac{\mathrm{d}\sigma'_{22}}{2\mu_0}\right)^2 + \left(\mathrm{d}e_{33} - \frac{\mathrm{d}\sigma'_{33}}{2\mu_0}\right)^2 \\ &\quad + 2\left(\mathrm{d}e_{12} - \frac{\mathrm{d}\sigma'_{12}}{2\mu_0}\right)^2 + 2\left(\mathrm{d}e_{23} - \frac{\mathrm{d}\sigma'_{23}}{2\mu_0}\right)^2 + 2\left(\mathrm{d}e_{31} - \frac{\mathrm{d}\sigma'_{31}}{2\mu_0}\right)^2 = 0 \end{aligned} \tag{8.103}$$

Since all terms in (8.103) are positive, $\mathrm{d}\zeta^2 = 0$ only when all terms are zero, that is,

$$\mathrm{d}e_{ij} - \frac{\mathrm{d}\sigma'_{ij}}{2\mu_0} = 0 \quad \text{or} \quad \mathrm{d}\sigma'_{ij} = 2\mu_0\,\mathrm{d}e_{ij} \quad \text{and} \quad \sigma'_{ij} = 2\mu_0 e_{ij} \tag{8.104}$$

When all components of the plastic strain increments are zero, the material behavior is described by (8.104), which is the elastic constitutive equation.

We have thus shown that the flow theory of plasticity may be derived from the endochronic theory when $k_1 = 1$. The yield function is given by (8.100); the flow rule is given by (8.97); the back stress is given by (8.95); and the isotropic hardening is given by the function $f(z)$. We see from (8.97) that the normality condition between the plastic strain increment and the yield surface (8.100) is satisfied. The evolution of back stress may be written in a differential form by differentiating (8.95). If, for simplicity, only one exponential term is used in $\rho_1(z)$, that is, $\rho_1(z) = \hat{\rho}\,\mathrm{e}^{-\alpha z}$, where $\hat{\rho}$ and α are constants, then

$$\boldsymbol{\alpha} = 2\mu_0\hat{\rho}\int_0^z \mathrm{e}^{-\alpha(z-z')}\frac{\mathrm{d}\boldsymbol{\varepsilon}^{\mathrm{p}}(z')}{\mathrm{d}z'}\mathrm{d}z' \tag{8.105}$$

and

$$\frac{\mathrm{d}\boldsymbol{\alpha}}{\mathrm{d}z} = 2\mu_0\hat{\rho}\frac{\mathrm{d}\boldsymbol{\varepsilon}^{\mathrm{p}}}{\mathrm{d}z} - \alpha\boldsymbol{\alpha} \tag{8.106}$$

This is a nonlinear evolution equation for $\boldsymbol{\alpha}$ and was used by Wu and Yang [18] and Wu et al. [19] as mentioned in Section 6.5.3. This equation is also known as the Armstrong–Frederick evolution equation. Another special case of (8.95) is when $\rho_1(z) = \hat{\rho} =$ constant. In this case, (8.95) becomes

$$\boldsymbol{\alpha} = 2\mu_0\hat{\rho}\boldsymbol{\varepsilon}^{\mathrm{p}} \quad \text{or} \quad \mathrm{d}\boldsymbol{\alpha} = c\,\mathrm{d}\boldsymbol{\varepsilon}^{\mathrm{p}} \qquad \text{with } c = 2\mu_0\hat{\rho} \tag{8.107}$$

which is the linear kinematic hardening of Prager [20] and Ziegler [21]. In the general case, when $\rho_1(z)$ is given by (8.92), the evolution equation for $\boldsymbol{\alpha}$ is

$$\frac{\mathrm{d}\boldsymbol{\alpha}}{\mathrm{d}z} = \sum_{r=1}^{n-1} 2G_0R_r\frac{\mathrm{d}\boldsymbol{\varepsilon}^{p}}{\mathrm{d}z} - \sum_{r=1}^{n-1}\beta_r\boldsymbol{\alpha}_r \qquad \text{with } \boldsymbol{\alpha} = \sum_{r=1}^{n-1}\boldsymbol{\alpha}_r \tag{8.108}$$

8.4.5 Applications of the Endochronic Theory to Metals

The endochronic theory is applied to describe several aspects of metallic deformation. They include loading–unloading, cyclic loading, loading with multi-axial strain paths, and the viscoplastic effect. Additional applications will be discussed in Chapter 9.

8.4.5.1 The loading–unloading stress–strain curves

In the case of uniaxial stress, the endochronic constitutive equation is

$$\sigma = E_0\int_0^z \rho(z-z')\frac{\mathrm{d}\varepsilon^{\mathrm{p}}}{\mathrm{d}z'}\mathrm{d}z' \tag{8.109}$$

We investigate three functional forms of the isotropic-hardening function $f(z)$. They are:

$$\begin{aligned}&\text{Form (a): } f(z) = \mathrm{e}^{\beta z}, \qquad \text{Form (b): } f(z) = C - (C-1)\mathrm{e}^{-\beta_{\mathrm{c}}z},\\ &\text{and} \quad \text{Form (c): } f(z) = \mathrm{e}^{-\beta_{\mathrm{s}}z}\end{aligned} \tag{8.110}$$

The equation $\mathrm{d}\zeta/\mathrm{d}z = f(z)$ is plotted in the ζ versus z space in Figure 8.4(a) for the three forms. The slope of the asymptote for form (a) is ∞, that for form (b) is C, and for form (c) is 0. The curve of form (c) approaches a value of $1/\beta_{\mathrm{s}}$ when z is large. The straight line at 45° angle is the case of $f(z) = 1$, which represents the nonhardening behavior. This line separates the ζ–z space into hardening zone and softening zone. When form (b) is used, the value of C dictates the material behavior. The case of $C > 1$ corresponds to strain

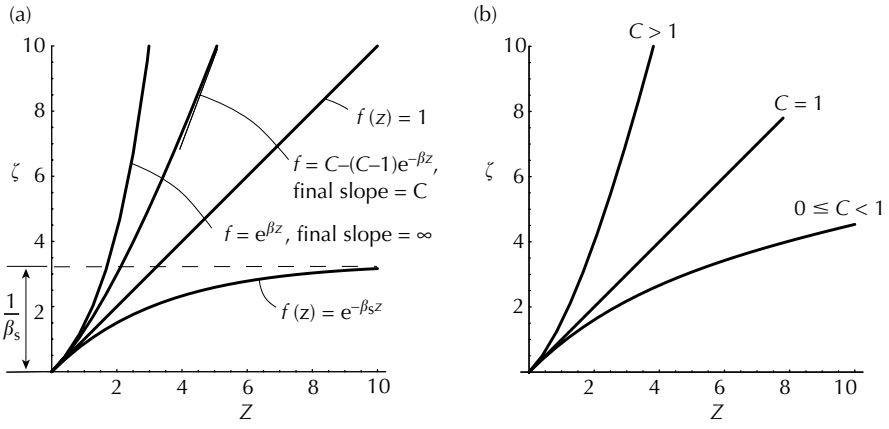

FIGURE 8.4
(a) Three forms of isotropic-hardening function $f(z)$, (b) effect of C on form (b).

hardening; $C = 1$ corresponds to nonhardening; and $0 \leq C < 1$ corresponds to strain softening. This relation is depicted in Figure 8.4(b). The ζ–z graph is monotonically increasing as long as $C \geq 0$. Parameter β_c controls how fast the curve bends.

We consider the kernel function expressed by

$$E_0\rho(z) = E_0\delta(z) + E_1\,\mathrm{e}^{-\mu z} + E_2 \tag{8.111}$$

where E_0, E_1, E_2, and μ are constants. Experience shows that (8.111) is adequate under most loading conditions for metals. In the case of loading, we assume $k_1 = 1$, and from (8.81), we have $\mathrm{d}\zeta = \mathrm{d}\varepsilon^{\mathrm{p}}$, which becomes $\zeta = \varepsilon^{\mathrm{p}}$ when the loading starts from the virgin state. Either form (a) or form (b) of $f(z)$, given by (8.110), can be used to represent the loading–unloading curves of strain-hardening materials. Even though form (a) is simple, according to Wu and Yip [22], it does not lead to the steady stress–strain loop in strain-controlled cyclic loading. In the interest of cyclic loading to be discussed in the next subsection, following [22] form (b) is used in the following derivation. Using (8.111), (8.109) is

$$\begin{aligned}\sigma = {} & E_0\int_0^z \delta(z-z')(+1)[C-(C-1)\mathrm{e}^{-\beta_c z'}]\mathrm{d}z' \\ & + E_1\int_0^z \mathrm{e}^{-\alpha(z-z')}(+1)[C-(C-1)\mathrm{e}^{-\beta_c z'}]\mathrm{d}z' + E_2\int_0^z [C-(C-1)\mathrm{e}^{-\beta_c z'}]\mathrm{d}z'\end{aligned} \tag{8.112}$$

which may be integrated to yield

$$\sigma = E_0[C - (C-1)e^{-\beta_c z}] + E_1\left\{\frac{C}{\mu}(1 - e^{-\mu z}) + \frac{C-1}{\beta_c - \mu}(e^{-\beta_c z} - e^{-\mu z})\right\} + E_2\zeta \tag{8.113}$$

We now determine the material constants. When $z = \zeta = 0$, we find from (9.113) that $E_0 = \sigma_y$, which is the initial yield stress. The asymptote of the stress–strain curve may be found by putting $z \to \infty$, and is given by

$$\sigma = \sigma_y C + E_1\left(\frac{C}{\alpha}\right) + E_2\zeta \tag{8.114}$$

in which E_2 is the slope of the asymptote and is the tangent modulus E_t at large strain. The intercept σ^0 of the asymptote with the stress axis is obtained by putting $\zeta = 0$ into (8.114), which leads to $E_1 = (\sigma^0/C - \sigma_y)\alpha$. Thus, (9.113) is rewritten as

$$\begin{aligned}\sigma =& \sigma_y[C - (C-1)e^{-\beta_c z}] + \left(\frac{\sigma^0}{C} - \sigma_y\right) \\ &\times \left\{C(1 - e^{-\alpha z}) + \frac{\alpha(C-1)}{\beta_c - \alpha}(e^{-\beta_c z} - e^{-\alpha z})\right\} + E_2\zeta\end{aligned} \tag{8.115}$$

where σ_y is the yield stress and E_2 is the slope of the asymptote. These two material constants are shown in Figure 8.5 and may be determined from an experimental stress–strain curve. Parameter α describes the form of the kernel function and is related to the rate of fading memory; C and β_c are parameters of the hardening function.

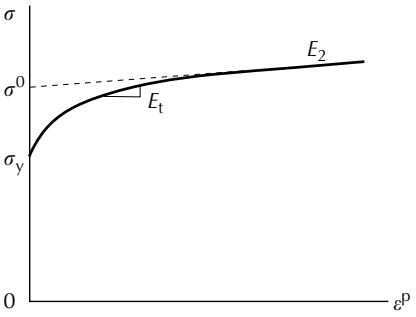

FIGURE 8.5
Material constants of the endochronic model.

We now consider unloading starting from $z = z^*$. During unloading $z > z^*$ and the integral in (8.109) is divided into two integrals

$$\sigma = E_0 \int_0^{z^*} \rho(z - z') \frac{\mathrm{d}\varepsilon^{\mathrm{p}}}{\mathrm{d}z'} \mathrm{d}z' + E_0 \int_{z^*}^{z} \rho(z - z') \frac{\mathrm{d}\varepsilon^{\mathrm{p}}}{\mathrm{d}z'} \mathrm{d}z' \tag{8.116}$$

Using (8.111) as the kernel function, the first integral of (8.116) consists of three terms. They are

$$\begin{aligned}
&E_0 \int_0^{z^*} \delta(z - z')[C - (C-1)\mathrm{e}^{-\beta_{\mathrm{c}} z'}] \mathrm{d}z' = 0, \\
&E_1 \int_0^{z^*} \mathrm{e}^{-\alpha(z - z')}[C - (C-1)\mathrm{e}^{-\beta_{\mathrm{c}} z'}] \mathrm{d}z' \\
&\qquad = E_1 \, \mathrm{e}^{-\alpha z} \left\{ \frac{C}{\alpha}(\mathrm{e}^{-\alpha z^*} - 1) + \frac{C-1}{\beta_{\mathrm{c}} - \alpha}(\mathrm{e}^{-(\beta_{\mathrm{c}} - \alpha) z^*} - 1) \right\}, \\
&E_2 \int_0^{z^*} \frac{\mathrm{d}\zeta'}{\mathrm{d}z'} \mathrm{d}z' = E_2 \zeta^*
\end{aligned} \tag{8.117}$$

The second integral also has three terms, given by

$$\begin{aligned}
&E_0 \int_{z^*}^{z} \delta(z - z')(-1)[C - (C-1)\mathrm{e}^{-\beta_{\mathrm{c}} z'}] \mathrm{d}z' = -\sigma_{\mathrm{y}}[C - (C-1)\mathrm{e}^{-\beta_{\mathrm{c}} z}], \\
&E_1 \int_{z^*}^{z} \mathrm{e}^{-\alpha(z - z')}(-1)[C - (C-1)\mathrm{e}^{-\beta_{\mathrm{c}} z'}] \mathrm{d}z' \\
&\qquad = -E_1 \left\{ \frac{C}{\alpha}(1 - \mathrm{e}^{-\alpha(z - z^*)}) + \frac{C-1}{\alpha - \beta_{\mathrm{c}}}(\mathrm{e}^{-\beta_{\mathrm{c}} z} - \mathrm{e}^{-\alpha(z - z^*) - \beta_{\mathrm{c}} z^*}) \right\} \\
&E_2 \int_0^{z} (-1) \frac{\mathrm{d}\zeta'}{\mathrm{d}z'} \mathrm{d}z' = -E_2(\zeta - \zeta^*)
\end{aligned} \tag{8.118}$$

Using (8.117) and (8.118), (8.116) is reduced to

$$\begin{aligned}
\sigma = &- \sigma_{\mathrm{y}}[C - (C-1)\mathrm{e}^{-\beta_{\mathrm{c}} z}] + \left(\frac{\sigma^0}{C} - \sigma_{\mathrm{y}} \right) C[2\,\mathrm{e}^{-\alpha(z - z^*)} - \mathrm{e}^{-\alpha z} - 1] \\
&- \left(\frac{\sigma^0}{C} - \sigma_{\mathrm{y}} \right) \alpha \left(\frac{C-1}{\alpha - \beta_{\mathrm{c}}} \right) [2\,\mathrm{e}^{-\alpha(z - z^*) - \beta_{\mathrm{c}} z^*} - \mathrm{e}^{-\alpha z} - \mathrm{e}^{-\beta_{\mathrm{c}} z}] + E_2(2\zeta^* - \zeta)
\end{aligned} \tag{8.119}$$

During the unloading stage, the following relation holds

$$\mathrm{d}\zeta = -\mathrm{d}\varepsilon^{\mathrm{p}} \qquad \text{with initial condition } \zeta^* = \varepsilon^{\mathrm{p}^*} \tag{8.120}$$

Integration of (8.120) results in

$$\varepsilon^{\mathrm{p}} = 2\zeta^* - \zeta \tag{8.121}$$

The loading–unloading curves have been calculated and compared with experimental results for 304 stainless steel by Wu and Yip [22].

8.4.5.2 A strain-controlled cyclic loading

Since most experiments have been conducted by controlling the total strain amplitude $\Delta\varepsilon$, a small amount of approximation is involved in this theoretical representation by considering a constant plastic strain amplitude cycling. Figure 8.6(a) shows a schematic drawing for strain cycles plotted against time t and the notation used to denote intrinsic time z at each half cycle. Figure 8.6(b) shows the corresponding cyclic stress–strain curve. The loading in the previous subsection can be viewed as the first $\frac{1}{4}$ cycle which is valid

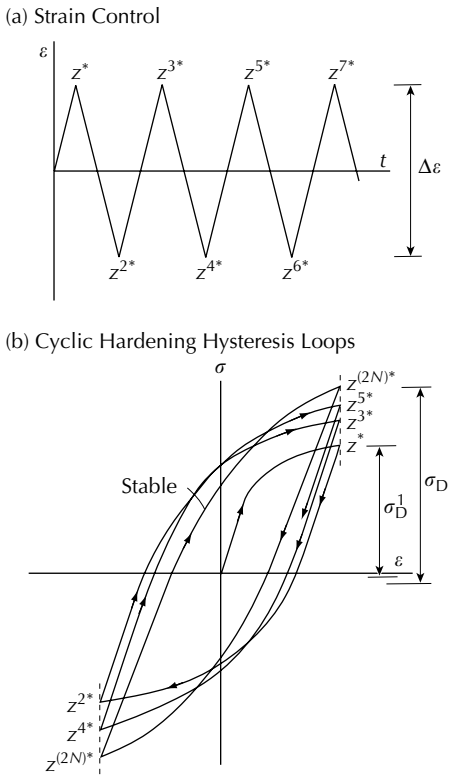

FIGURE 8.6
(a) Strain cycles against time, (b) cyclic hardening hysteresis loops (From Wu, H.C. and Yip, M.C., *J. Eng. Mater. Technol.*, 103, 212, 1981. With permission from ASME).

for $0 < z < z^*$ and the unloading in the previous subsection can be viewed as the first unloading of the cyclic loading valid for $z^* < z < z^{**}$. We continue to derive the equations for the first reloading and the subsequent loading.

Using the same procedure, the first reloading is valid for $z^{**} < z < z^{3^*}$ and the equation has been found to be

$$\begin{aligned}\sigma &= \sigma_y[C - (C-1)e^{-\beta_c z}] + \left(\frac{\sigma^0}{C} - \sigma_y\right) C[-2\,e^{-\alpha(z-z^{**})} \\ &\quad + 2\,e^{-\alpha(z-z^*)} - e^{-\alpha} z + 1] - \left(\frac{\sigma^0}{C} - \sigma_y\right) \alpha \left(\frac{C-1}{\alpha - \beta_c}\right) \\ &\quad \times [-2e^{-\alpha(z-z^{**})-\beta_c z^{**}} + 2e^{-\alpha(z-z^*)-\beta_c z^*} - e^{-\alpha z} + e^{-\beta_c z}] \\ &\quad + E_2(\zeta + 2\zeta^* - 2\zeta^{**}) \qquad \text{with } \varepsilon^p = 2\zeta^* - 2\zeta^{**} + \zeta \end{aligned} \tag{8.122}$$

This procedure may be continued. A general expression of the response function for the constant total strain amplitude cyclic loading test may be found to be

$$\begin{aligned}\sigma &= (-1)^{2N}\sigma_y[C - (C-1)e^{-\beta_c z}] \\ &\quad + \left(\frac{\sigma^0}{C} - \sigma_y\right) C\{1 - e^{-\alpha z} + 2[e^{-\alpha(z-z^*)} - 1] - 2[e^{-\alpha(z-z^{**})} - 1] \\ &\quad + \cdots - [(-1)^{2N}2][e^{-\alpha(z-z^{2N^*})} - 1]\} \\ &\quad - \left(\frac{\sigma^0}{C} - \sigma_y\right) \frac{\alpha(C-1)}{\alpha - \beta_c}\{e^{-\beta_c z} - e^{-\alpha z} + 2[e^{-\alpha(z-z^*)-\beta_c z^*} - e^{-\beta_c z}] \\ &\quad - \cdots - (-1)^{2N}2[e^{-\alpha(z-z^{2N^*})-\beta_c z^{2N^*}} - e^{-\beta_c z}]\} \\ &\quad + E_2\varepsilon^p \qquad \text{for } z > z^{2N^*} \end{aligned} \tag{8.123}$$

where

$$\varepsilon^p = \zeta + 2(\zeta^* - \zeta) - 2(\zeta^{**} - \zeta) + \cdots - (-1)^{2N} \cdot 2(\zeta^{2N^*} - \zeta) \tag{8.124}$$

and $N = \frac{1}{2}, 1, 1\frac{1}{2}, 2, \ldots$. If the above equation is examined at $z = z^{2N^*}$ and $z = z^{2N^*+}$, a drop or jump in stress of magnitude $2\sigma_y f(z) = 2\sigma_y[C - (C-1)e^{-\beta_c z^{2N^*}}]$ results, which corresponds to the elastic response upon reversal of loading direction. The magnitude of the jump in stress is determined by the isotropic expansion of the yield surface. For a sufficiently large z, the hysteresis loop becomes steady. In this case the jump or drop in stress becomes a constant value of $2C\sigma_y$.

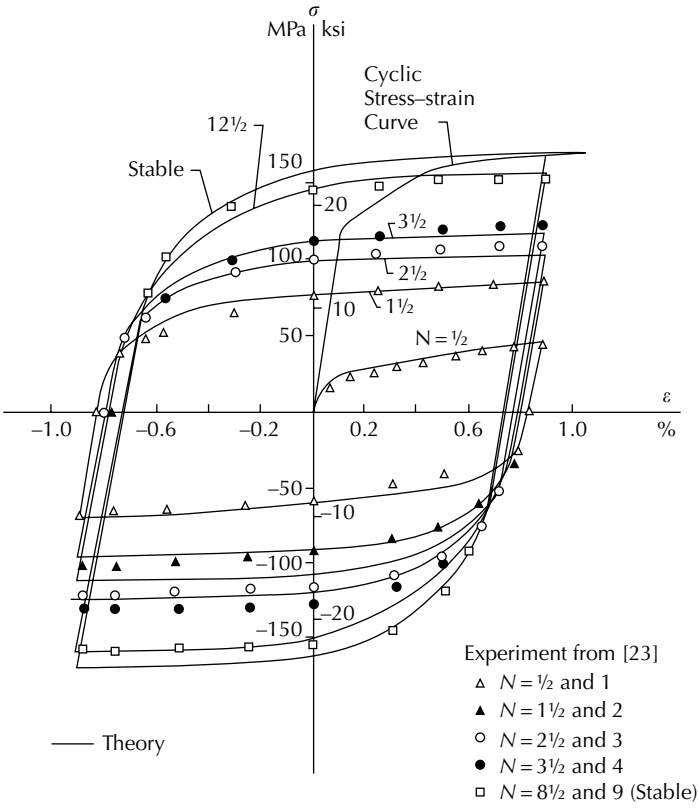

FIGURE 8.7
Theory and experimental data (From Wu, H.C. and Yip, M.C., *J. Eng. Mater. Technol.*, 103, 212, 1981. With permission from ASME).

We now use (8.123) to predict the cyclic stress–strain loops experimentally obtained by Lamba and Sidebottom [23]. These authors obtained cyclic stress–strain curves of oxygen-free high-conductivity copper covering curves from the first cycle to the stable loop. The hardening effect was extremely rapid in the first few cycles of the test. After further reversals, hardening ceased and a steady stress range was achieved. Figure 8.7 illustrates the experimental data and the theoretical prediction from (8.123). The material parameters used in the calculation are: $\sigma^0 = 25$ ksi (1.73×10^2 MPa), $\sigma_y = 2$ ksi (13.78 MPa), $E_2 = 0$, $C = 8.75$, $\beta_c = 40$, $\alpha = 3000$, and $\Delta\varepsilon = 1.75\%$.

Finally, we mention that the same theory was applied by Wu et al. [24] to investigate the problem of cyclic full-reversed torsional loading of a solid bar with circular cross-section. Numerical techniques were employed to obtain the solution. The parameters of the constitutive model were determined from the test data of thin-walled specimens. These parameters were then used without alteration to compute stress distributions within the solid specimen.

Special attention was given to the residual stress distribution. Reasonable results were obtained. The relation of torque versus strain at the outermost fiber of the solid specimen provided an ultimate check of the theory as applied to this case.

8.4.5.3 Loading with multiaxial strain path

From (8.93), the constitutive equation for metals is

$$\boldsymbol{\sigma}' = \sigma'_{\mathrm{y}} \frac{\mathrm{d}\varepsilon^{\mathrm{p}}(z)}{\mathrm{d}z} + 2\mu_2 \int_0^z \mathrm{e}^{-\alpha(z-z')} \frac{\mathrm{d}\varepsilon^{\mathrm{p}}(z')}{\mathrm{d}z'} \mathrm{d}z' + 2\mu_1 \varepsilon^{\mathrm{p}} \tag{8.125}$$

where σ'_{y} is the deviatoric yield stress; μ_1 and μ_2 are constants. The volumetric behavior is elastic, given by (8.74). Only one exponential term in the kernel function is used for simplicity. We applied (8.125) to describe two strain-controlled combined axial–torsion tests (paths 01A and 02B) shown in Figure 8.8. Form (b) of (8.110) is the isotropic-hardening function used in this derivation. The state of stress and its deviator and the plastic strain are

$$[\sigma] = \begin{bmatrix} \sigma & \tau & 0 \\ \tau & 0 & 0 \\ 0 & 0 & 0 \end{bmatrix}, \qquad [\sigma'] = \begin{bmatrix} \dfrac{2\sigma}{3} & \tau & 0 \\ \tau & -\dfrac{\sigma}{3} & 0 \\ 0 & 0 & -\dfrac{\sigma}{3} \end{bmatrix}, \qquad [\varepsilon^{\mathrm{p}}] = \begin{bmatrix} \varepsilon^{\mathrm{p}} & \eta^{\mathrm{p}} & 0 \\ \eta^{\mathrm{p}} & -\dfrac{\varepsilon^{\mathrm{p}}}{2} & 0 \\ 0 & 0 & -\dfrac{\varepsilon^{\mathrm{p}}}{2} \end{bmatrix} \tag{8.126}$$

where η^{p} is the tensorial shear strain. The intrinsic time is obtained from

$$\mathrm{d}\zeta^2 = \mathrm{d}\varepsilon^{\mathrm{p}} \cdot \underline{\mathbf{K}} \cdot \mathrm{d}\varepsilon^{\mathrm{p}} \tag{8.127}$$

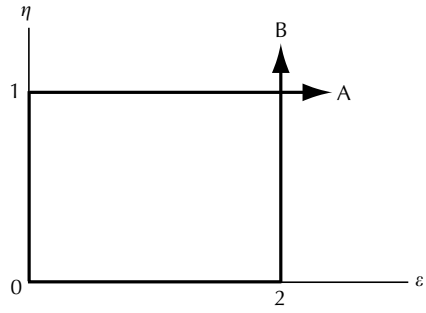

FIGURE 8.8
Two strain paths of combined axial–torsion.

as

$$\mathrm{d}\zeta = [k_1^2(\mathrm{d}\varepsilon^{\mathrm{p}})^2 + k_2^2(\mathrm{d}\eta^{\mathrm{p}})^2]^{1/2} \tag{8.128}$$

where k_1 and k_2 are constants. We follow the work of Wu and Yang [25] in the following discussion with permission from Elsevier.

(A) Path 01A

The specimen is first strained in pure torsion from 0 to 1 (Figure 8.8) and then strained in tension from 1 to A while keeping the total shear strain constant. The plastic shear strain at 1 is denoted by η_*^{p}, the corresponding shear stress by τ^*, and the intrinsic time by z^*. There are two stages in this path. The first stage is straining from 0 to 1 and the second stage from 1 to A. We have a pure torsion in the first stage and the equations are from (8.125)

$$\tau = \sigma_{\mathrm{y}}' \frac{\mathrm{d}\eta^{\mathrm{p}}}{\mathrm{d}z} + 2\mu_2 \int_0^z \mathrm{e}^{-\alpha(z-z')} \frac{\mathrm{d}\eta^{\mathrm{p}}}{\mathrm{d}z'} \mathrm{d}z' + 2\mu_1 \eta^{\mathrm{p}} \quad \text{and} \quad \sigma = 0 \tag{8.129}$$

Since during this stage, $\mathrm{d}\zeta = k_2\, \mathrm{d}\eta^{\mathrm{p}}$, (8.129) may be integrated. In the second stage, (8.125) gives

$$\sigma = 1.5 \left(\sigma_{\mathrm{y}}' \frac{\mathrm{d}\varepsilon^{\mathrm{p}}}{\mathrm{d}z} + 2\mu_2 \int_{z^*}^z \mathrm{e}^{-\alpha(z-z')} \frac{\mathrm{d}\varepsilon^{\mathrm{p}}}{\mathrm{d}z'} \mathrm{d}z' + 2\mu_1 \varepsilon^{\mathrm{p}} \right) \tag{8.130}$$

and

$$\tau = \sigma_{\mathrm{y}}' \frac{\mathrm{d}\eta^{\mathrm{p}}}{\mathrm{d}z} + 2\mu_2 X\, \mathrm{e}^{-\alpha z} + 2\mu_2 \int_{z^*}^z \mathrm{e}^{-\alpha(z-z')} \frac{\mathrm{d}\eta^{\mathrm{p}}}{\mathrm{d}z'} \mathrm{d}z' + 2\mu_1 \eta^{\mathrm{p}} \tag{8.131}$$

where

$$X = \int_0^{z^*} \mathrm{e}^{\alpha z'} \frac{\mathrm{d}\eta^{\mathrm{p}}}{\mathrm{d}z'} \mathrm{d}z' = \frac{1}{k_2} \left\{ \frac{C}{\alpha} [\mathrm{e}^{\alpha z^*} - 1] - \frac{C-1}{\alpha - \beta} [\mathrm{e}^{(\alpha-\beta)z^*} - 1] \right\} \tag{8.132}$$

Equation (8.131) may be reduced to a closed-form expression for τ in terms of z, which is accomplished by use of the following procedure.

We note that η remains constant during this stage and we have

$$\mathrm{d}\eta^{\mathrm{p}} = -\frac{\mathrm{d}\tau}{2\mu_0} \tag{8.133}$$

in which μ_0 is the shear modulus. (8.133) is then integrated to yield

$$\eta^{\mathrm{p}} = \eta_*^{\mathrm{p}} - \frac{1}{2\mu_0}(\tau - \tau^*) \tag{8.134}$$

Letting $z - z^* = t$ and $z' - z^* = t'$ and making use of (8.133) and (8.134), (8.131) may be written as

$$\tau = \frac{-\sigma_y'}{2\mu_0}\frac{d\tau}{dt} + 2\mu_2 e^{-\alpha(t+z^*)}X - \frac{\mu_2}{\mu_0}\int_0^t e^{-\alpha(t-t')}\frac{d\tau}{dt'}dt' + 2\mu_1\left[\eta_*^p - \frac{1}{2\mu_0}(t - t^*)\right] \tag{8.135}$$

Laplace transform of (8.135) gives

$$\bar{\tau} = \frac{\bar{Q}}{\bar{R}} = \frac{p\{(p+\alpha)\sigma_y'\tau^* + 4\mu_0\mu_2 e^{-\alpha z^*}X + 2\mu_2\tau^*\} + 4\mu_0\mu_1(\eta_*^p + (\tau^*/2\mu_0))(p+\alpha)}{p\{\sigma_y' p^2 + [\alpha\sigma_y' + 2(\mu_0+\mu_1+\mu_2)]p + 2(\mu_0+\mu_1)\alpha\}} \tag{8.136}$$

which, by partial fraction, can be reduced to

$$\bar{\tau} = \frac{2}{p}\frac{\mu_0\mu_1}{\mu_0+\mu_1}\left(\eta_*^p + \frac{\tau^*}{2\mu_0}\right) + \frac{A}{p-\alpha'} + \frac{B}{p-\beta'} \tag{8.137}$$

where $\bar{\tau}$ is the Laplace transform of $\tau(z)$ and A, B, α', β' are constants. Constants α' and β' are the zeros of $\bar{R}(p) = 0$; $A = \bar{Q}(\alpha')/\bar{R}'(\alpha')$, $B = \bar{Q}(\beta')/\bar{R}'(\beta')$, and $\bar{R}'(p) = d\bar{R}/dp$. The functions $\bar{Q}(p)$ and $\bar{R}(p)$ are defined in (8.136). Finally, (8.137) may be inverted to yield

$$\tau = \frac{2\mu_0\mu_1}{\mu_0+\mu_1}\left(\eta_*^p + \frac{\tau^*}{2\mu_0}\right) + A e^{\alpha'(z-z^*)} + B e^{\beta'(z-z^*)} \tag{8.138}$$

which is the expression relating τ to z.

The equation for axial stress (8.130) may be written in a form convenient for numerical computation. Let $S = \int_{z^*}^{z} e^{-\alpha(z-z')}(d\varepsilon^p/dz')dz'$; then by differentiating this integral with respect to z, we obtain

$$\frac{dS}{dz} = \frac{d\varepsilon^p}{dz} - \alpha S \tag{8.139}$$

in which, when $d\varepsilon^p/dz$ is known, S may be computed step by step. Thus, σ may be found from

$$\sigma = 1.5\left(\sigma_y'\frac{d\varepsilon^p}{dz} + 2\mu_2 S + 3\mu_1\varepsilon^p\right) \tag{8.140}$$

The quantity $d\varepsilon^p/dz$ is computed from the equation below which is found from (8.128) and (8.133)

$$\left(\frac{d\varepsilon^p}{dz}\right)^2 = \frac{1}{k_1^2}\left[\left(\frac{d\zeta}{dz}\right)^2 - \left(\frac{k_2}{2G_0}\right)^2\left(\frac{d\tau}{dz}\right)^2\right] \tag{8.141}$$

The quantity $d\zeta/dz$ is given by form (b) of (8.110) and $d\tau/dz$ is found by differentiation of (8.138). Therefore, by assuming a value for z, τ, and $d\tau/dz$ may be computed from (8.138), and $d\varepsilon^p/dz$ may be found from (8.141). Using the latter value, S can be found step by step from (8.139) and σ can be obtained from (8.140). Furthermore, knowing the value of $d\varepsilon^p/dz$ and using (8.133), ε^p and η^p can be computed.

(B) Path 02B

The specimen is first strained in pure tension from 0 to 2 (Figure 8.8) and then strained in torsion from 2 to B while keeping the total axial strain constant. The plastic tensile strain at 2 is denoted by ε_*^p, the corresponding tensile stress by σ^*, and the intrinsic time by $\hat{z}^*$. There are two stages in this path. The first stage is straining in pure tension from 0 to 2, and the second stage from 2 to B. The equations for stage 1 are

$$\sigma = 1.5\left(\sigma_y'\frac{d\varepsilon^p}{dz} + 2\mu_2\int_0^z e^{-\alpha(z-z')}\frac{d\varepsilon^p}{dz'}dz' + 2\mu_1\varepsilon^p\right) \quad \text{and} \quad \tau = 0 \tag{8.142}$$

and the equations for stage 2 are

$$\sigma = 1.5\left(\sigma_y'\frac{d\varepsilon^p}{dz} + 2\mu_2 Y e^{-\alpha z} + 2\mu_2\int_{\hat{z}^*}^z e^{-\alpha(z-z')}\frac{d\varepsilon^p}{dz'}dz' + 2\mu_1\varepsilon^p\right) \tag{8.143}$$

and

$$\tau = \sigma_y'\frac{d\eta^p}{dz} + 2\mu_2\int_{\hat{z}^*}^z e^{-\alpha(z-z')}\frac{d\eta^p}{dz'}dz' + 2\mu_1\eta^p \tag{8.144}$$

where

$$Y = \int_0^{\hat{z}^*} e^{\alpha z'}\frac{d\varepsilon^p}{dz'}dz' = \frac{1}{k_1}\left\{\frac{C}{\alpha}[e^{\alpha\hat{z}^*} - 1] - \frac{C-1}{\alpha-\beta}[e^{(\alpha-\beta)\hat{z}^*} - 1]\right\} \tag{8.145}$$

Following a similar procedure as in Path 01A, we find

$$\sigma = \frac{E_0E_t}{E_0+E_t}\left(\varepsilon_*^p + \frac{\sigma^*}{E_0}\right) + \hat{A}\,e^{\hat{\alpha}'(z-\hat{z}^*)} + \hat{B}\,e^{\hat{\beta}'(z-\hat{z}^*)} \tag{8.146}$$

$$d\varepsilon^p = -\frac{d\sigma}{E_0} \tag{8.147}$$

$$\hat{S} = \int_{\hat{z}*}^{z} e^{-\alpha(z-z')} \frac{d\eta^p}{dz'} dz' \tag{8.148}$$

$$\frac{d\hat{S}}{dz} = \frac{d\eta^p}{dz} - \alpha \hat{S} \tag{8.149}$$

$$\tau = \sigma_y' \frac{d\eta^p}{dz} + 2\mu_2 \hat{S} + 2\mu_1 \eta^p \tag{8.150}$$

and

$$\left(\frac{d\eta^p}{dz}\right)^2 = \frac{1}{k_2^2}\left[\left(\frac{d\zeta}{dz}\right)^2 - \left(\frac{k_1}{E_0}\right)^2 \left(\frac{d\sigma}{dz}\right)^2\right] \tag{8.151}$$

in which $\hat{\alpha}', \hat{\beta}', \hat{A}, \hat{B}$ are constants; E_0 is Young's modulus and $E_t = 3\mu_1$. Assuming a value for z, σ, and $d\sigma/dz$ may be computed from (8.146), and $d\eta^p/dz$ may be found from (8.151). Using the latter value, $\hat{S}$ can be found step by step from (8.149) and τ can be obtained from (8.150). Furthermore, knowing the value of $d\eta^p/dz$ and using (8.147), ε^p and η^p can be computed.

For the purpose of assessing the validity of the derived equations, the theoretical results are compared with the experimental data obtained by Ohashi et al. [26] for thin-walled tubular brass (60% Cu, 40% Zn) specimens. The constants of the theory have been determined in [25] to be $\sigma_y' = 95.02$ MPa, $\beta = 4.3996$, $C = 4.5799$, $\mu_0 = 12.74$ GPa, $\mu_2 = 6.37$ GPa, $\mu_1 = 49.0$ MPa, $k_1 = 1$, and $\alpha = 500$. The material response for Path 01A is shown in Figure 8.9 after torsion prestrain of $\eta^p = 4.33 \times 10^{-3}$, 8.66×10^{-3}, 17.32×10^{-3}, and 25.98×10^{-3}. It is seen that the theory agrees well qualitatively with the experiment. There are quantitative discrepancies between the theory and experiment at the knee portion of the axial stress curve, however. In addition, the theory predicted a faster relaxation of shear stress than the experimental data indicated.

Ohashi and his coworkers [27,28] have described the same experimental data using the simple endochronic theory with very good agreement. Ohashi et al. made the kernel function a tensor quantity. Thus, different stress components are associated with different components of the kernel function and the parameters are different for each component of the kernel function. In addition, the intrinsic time was made a function of the arc length as well as the radius of curvature of the strain path. More parameters have been introduced into the theory by this generalization.

Using the method of solution of Wu and Yang [25], the endochronic constitutive equation (8.125) was applied by Wu et al. [29] to investigate the stress response to two cyclic, nonproportional strain paths in the axial–torsion strain space. The first path involved a cyclic axial straining and unstraining following a shear prestrain, and the second path was cyclic in shear after a

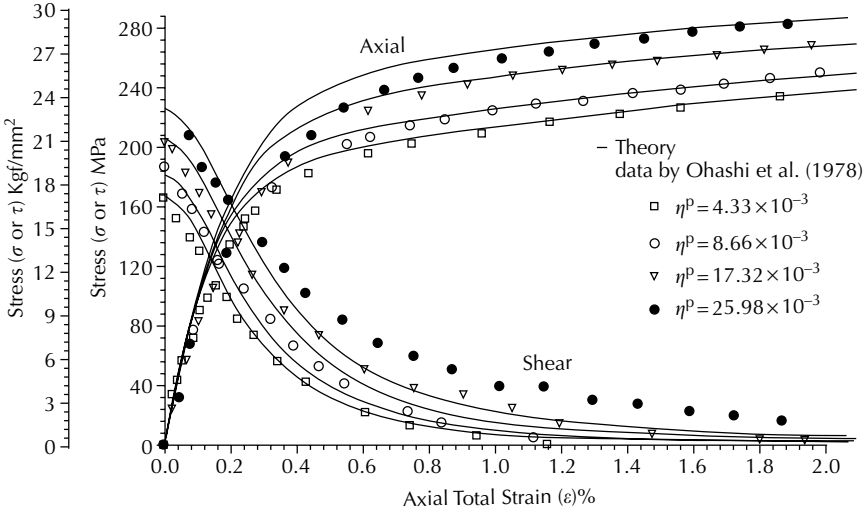

FIGURE 8.9
Stress response to strain path of torsion followed by tension (From Wu, H.C. and Yang, R.J., *Int. J. Non-Linear Mech.*, 18, 395, 1983. With permission from Elsevier).

prestrain in tension. Type 304 stainless steel tubular specimens were tested at constant strain-rate of 5×10^{-4} per second. The theory was capable of predicting the stress response to the two cyclic strain paths considered.

Further investigation of multiaxial straining was conducted by Wu et al. [30]. Plastic strain-controlled experiments were conducted on 304 stainless steel tubular specimens. The plastic strain-control was feasible by means of a computer-aided material test system. Three in-phase plastic strain paths (a pure axial path, a pure torsional path, and an axial–torsion in-phase path) and two out-of-phase plastic-strain paths (small and large perturbations from the axial–torsion in-phase path) were studied, and the endochronic constitutive equation (8.125) was used to obtain theoretical results for the five strain paths considered. It was shown that the theory and experiment have good agreement. Furthermore, both experimental and theoretical results show that strain hardening is enhanced by out-of-phase loading. Figure 8.10(a) shows the theoretical and experimental plastic strain path of path 5, the out-of-phase path with large perturbation from the axial–torsion in-phase path. The corresponding axial stress versus plastic axial strain plot is shown in Figure 8.10(b), and the corresponding shear stress versus plastic shear strain plot is shown in Figure 8.10(c).

Finally, we mention that Wu and Yeh [31] applied (8.125) to investigate the combined axial-internal pressure loading of tubular specimens and compared their results with their own experimental data. Additional work on endochronic theory and its application have been conducted by Valanis and his coworkers [32,33] and by Atluri and coworkers in numerical computation [34,35].

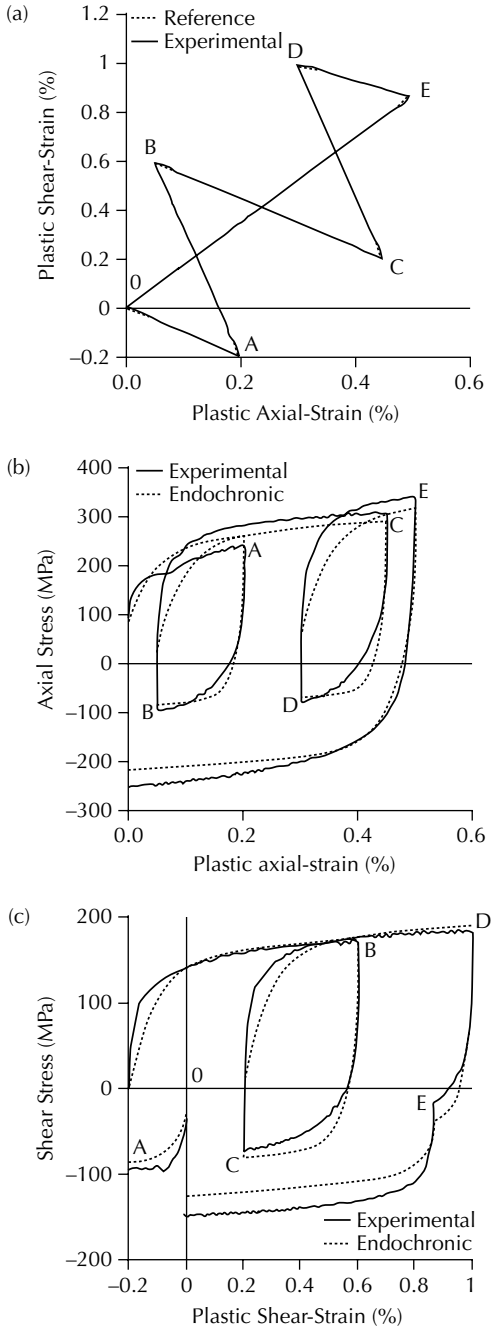

FIGURE 8.10
Response to zigzag plastic strain path: (a) plastic strain path, (b) axial stress, (c) shear stress (From Wu, H.C. et al., *J. Eng. Mater. Technol.*, 108, 262, 1986. With permission from ASME).

8.4.6 The Endochronic Theory of Viscoplasticity

A general introduction of the strain-rate effect is given in Section 5.2.4. The strain-rate sensitive plasticity is also known as the viscoplasticity. Based on the flow theory of plasticity, the viscoplastic effect was investigated by Perzyna [36], Phillips and Wu [37], Krempl [38], and others. The endochronic viscoplasticity provides a framework for a unified theory to discuss the constant strain-rate stress–strain curves, the creep curves, and the stress relaxation all together. In describing the viscoplastic behavior, Valanis [6] defines the intrinsic time as

$$\mathrm{d}\zeta^2 = P_{ijkm}\,\mathrm{d}\varepsilon_{ij}\,\mathrm{d}\varepsilon_{km} + g^2\,\mathrm{d}t^2 \tag{8.152}$$

where g is a material parameter. The intrinsic time given by (8.49) is a reduced version for strain-rate independent plasticity. The simple endochronic viscoplasticity was applied by Wu and his coworkers [39–41] to study the stress wave propagation for strain-rate sensitive materials. In Wu and Yip [42], the strain-rate and strain-rate history effects on the dynamic behavior of metals were investigated using the improved endochronic theory. Lin and Wu [43] further applied the theory to viscoplastic wave propagation. Furthermore, the theory was applied by Wu and Ho [44] to discuss the phenomenon of transient creep. In this subsection, we discuss the strain-rate effect for uniaxial loading following the work of [42] and creep following [44].

To obtain a more general form of the intrinsic time measure, which accounts for strain-rate, it is assumed that a spectrum of r intrinsic times exists and each intrinsic time corresponds to an internal state variable. Thus, for each intrinsic time, we write

$$\mathrm{d}\zeta_i^2 = h_i(\varepsilon^{\mathrm{p}})(\mathrm{d}\varepsilon^{\mathrm{p}})^2 + g_i(\varepsilon^{\mathrm{p}})(\mathrm{d}t)^2, \qquad i = 1, 2, \ldots, r \tag{8.153}$$

where h_i and g_i are functions of $\mathrm{d}\varepsilon^{\mathrm{p}}$, and t is the real time. (8.153) can be written as

$$\mathrm{d}\zeta_{\mathrm{i}} = \pm\left[h_i(\varepsilon^{\mathrm{p}}) + \frac{g_i(\varepsilon^{\mathrm{p}})}{(\dot{\varepsilon}^{\mathrm{p}})^2}\right]^{1/2}\mathrm{d}\varepsilon^{\mathrm{p}}, \qquad i = 1, 2, \ldots, r \tag{8.154}$$

Introducing an average intrinsic time measure such that

$$\mathrm{d}\zeta = \Lambda(\mathrm{d}\zeta_1, \mathrm{d}\zeta_2, \ldots, \mathrm{d}\zeta_r) \tag{8.155}$$

then, using (8.154), we obtain

$$\mathrm{d}\zeta = \pm k(\varepsilon^{\mathrm{p}}, \dot{\varepsilon}^{\mathrm{p}})\mathrm{d}\varepsilon^{\mathrm{p}} \tag{8.156}$$

The function k is known as the strain-rate sensitivity function and it is a function of ε^{p} and $\dot{\varepsilon}^{\mathrm{p}}$. For simplicity, we assume that k is a function of $\dot{\varepsilon}^{\mathrm{p}}$

only, that is,

$$d\zeta = k(\dot{\varepsilon}^p)|d\varepsilon^p| \tag{8.157}$$

This relation is the same as that proposed earlier in [39], except that we now use the plastic strain instead of the total strain. In the three-dimensional version, (8.157) is

$$(d\zeta)^2 = k^2(|\dot{\varepsilon}^p|)d\boldsymbol{\varepsilon}^p \cdot d\boldsymbol{\varepsilon}^p \tag{8.158}$$

Let us now consider the constant strain-rate stress–strain curves. Using (8.111), form (a) of (8.110), and (8.157), (8.109) may be integrated while holding $\dot{\varepsilon}^p$ constant to yield

$$\sigma = \sigma_y^D(1 + \beta_1\varepsilon^p) + (\sigma^0 - \sigma_y^D)(1 + \beta_1\varepsilon^p)\{1 - (1 + \beta_1\varepsilon^p)^{-n}\} + E_2\varepsilon^p \tag{8.159}$$

where

$$\sigma_y^D = \frac{\sigma_y}{k(\dot{\varepsilon}^p)} \tag{8.160}$$

and

$$n = \frac{\alpha}{\beta} + 1 \quad \text{and} \quad \beta_1 = \beta k = \frac{E_t - E_2}{\sigma^0} \tag{8.161}$$

Note that σ_y is the static yield stress. The dynamic yield stress σ_y^D, the tangent modulus E_t at large ε^p, and the intercept of the asymptote to the stress–strain curve with the stress axis σ^0 can be measured directly from each constant strain-rate stress–strain curve (see Figure 8.5). For the sake of simplicity, we have not introduced new notations for E_t and σ^0. But these are dynamic quantities and they vary with each constant strain-rate stress–strain curve. For most materials, the constant strain-rate stress–strain curves for various strain-rates are parallel to each other at large ε^p and, in this case, E_t does not vary with the strain-rate. Using the method of Example 8.2, the relations in (8.161) have been obtained. The parameters β_1, n, and E_2 are determined by the trial and error method so that the theoretical curve agrees with the experimental reference curve. The experimental reference curve is usually taken as the constant strain-rate stress–strain curve that has the lowest strain-rate $\dot{\varepsilon}_0^p$ of all the curves. The following function has been used by Lin and Wu [39] and Wu and Yip [42] to define the strain-rate sensitivity function k

$$k(\dot{\varepsilon}^p) = 1 - k_s \log\left(\frac{\dot{\varepsilon}^p}{\dot{\varepsilon}_0^p}\right) \tag{8.162}$$

where k_s is a material parameter. Figure 8.11 shows that (1.162) can fit nicely to the experimental data of Karnes and Ripperger [45] for annealed high-purity aluminum for the strain-rate range from 10^{-4} to 10^{3} s^{-1}. The strain-rate is shown as $\dot{\theta}$ in the figure. From each experimental constant strain-rate stress–strain curve, we determine the dynamic yield stress σ_y^D, and, since we know σ_y , $k(\dot{\varepsilon}^p)$ can be found from (8.160).

Equation (8.159) describes a set of stress–strain curves at various constant strain-rates. By use of (8.162), the theoretical constant strain-rate stress–strain curves thus obtained are compared with the experimental curves of [45] and shown in Figure 8.12. The parameters for theoretical curves are $E_0 = 10 \times 10^6$ psi (6.89×10^4 MPa), $\sigma_0^0 = 1 \times 10^3$ psi (6.89 MPa), $\sigma_y = 0.75 \times 10^3$ psi

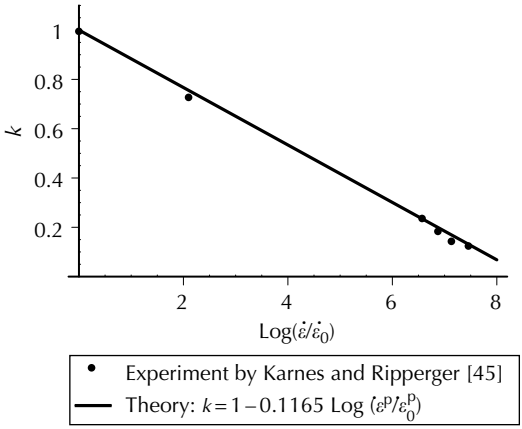

FIGURE 8.11
Strain-rate sensitivity function k (From Wu, H.C. and Yip, M.C., *Int. J. Solids Struct.*, 16, 515, 1980. With permission from Elsevier).

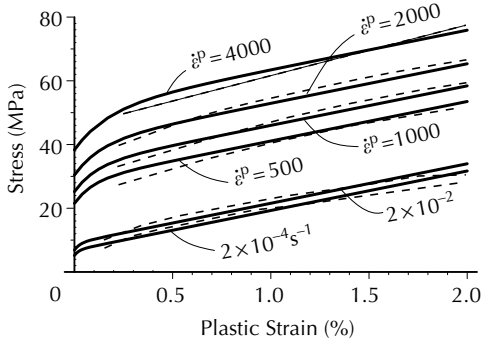

FIGURE 8.12
Constant strain-rate stress–strain curves for aluminum (From Wu, H.C. and Yip, M.C., *Int. J. Solids Struct.*, 16, 515, 1980. With permission from Elsevier).

(5.17 MPa), $\beta = 180$, $n = 25$, and $E_2 = 0$. We note that σ_0^0 is the intercept of the asymptotic line with the stress axis for the reference stress–strain curve.

The foregoing work is relevant to strain-hardening metallic materials such as f.c.c. metals. For materials such as mild steel, strain-softening occurs after initial yielding. However, the material switches from strain softening to strain-hardening at a strain of approximately 2%, and we shall call this type of materials strain softening–hardening materials. The ζ–z relation for this type of materials requires special attention. We use (8.110) form (c) for the strain-softening portion and form (a) for the strain-hardening portion of the material behavior, and introduce a critical intrinsic time ζ_{cr} (with the corresponding z_{cr}) to indicate the point of changeover from softening to hardening in a stress–strain curve. Thus, the following relations apply:

$$\frac{\mathrm{d}\zeta}{\mathrm{d}z} = f(z) = \mathrm{e}^{-\beta_{\text{s}} z} \quad \text{and} \quad \zeta = \frac{1}{\beta_{\text{s}}}(1 - \mathrm{e}^{-\beta_{\text{s}} z}) \qquad \text{with } \beta_{\text{s}} > 0, \quad \text{for } z \le z_{\text{cr}} \tag{8.163}$$

$$\frac{\mathrm{d}\zeta}{\mathrm{d}z} = b_h \, \mathrm{e}^{\beta_h (z - z_{\text{cr}})} \quad \text{and} \quad \zeta = \zeta_{\text{cr}} - \frac{b_h}{\beta_h}[1 - \mathrm{e}^{\beta_h (z - z_{\text{cr}})}] \qquad \text{for } z \le z_{\text{cr}} \tag{8.164}$$

where β_{s}, β_h, b_h are material parameters. Assuming that the ζ–z relation is smooth and differentiable at the critical point, we have

$$b_h = \mathrm{e}^{-\beta_{\text{s}} z_{\text{cr}}} \tag{8.165}$$

Thus, b_h can be calculated if β_{s} and z_{cr} are known. The ζ–z relation for strain softening–hardening materials is shown schematically in Figure 8.13.

Using the isotropic-hardening function defined by (8.163) to (8.165) and the strain-rate sensitivity function defined by (8.162), (8.109) leads to the constant strain-rate stress–strain curves for mild steel shown in Figure 8.14. The plastic strain-rate is denoted by $\dot{\theta}$ in the figure. Theoretical results compare favorably with the experimental data of Cambell and Marsh [46] in the

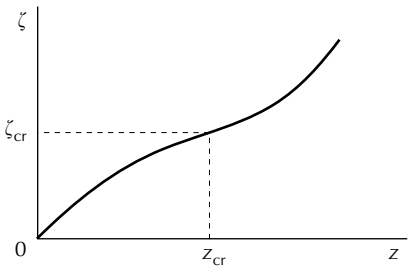

FIGURE 8.13
Isotropic-hardening function f for strain softening–hardening materials.

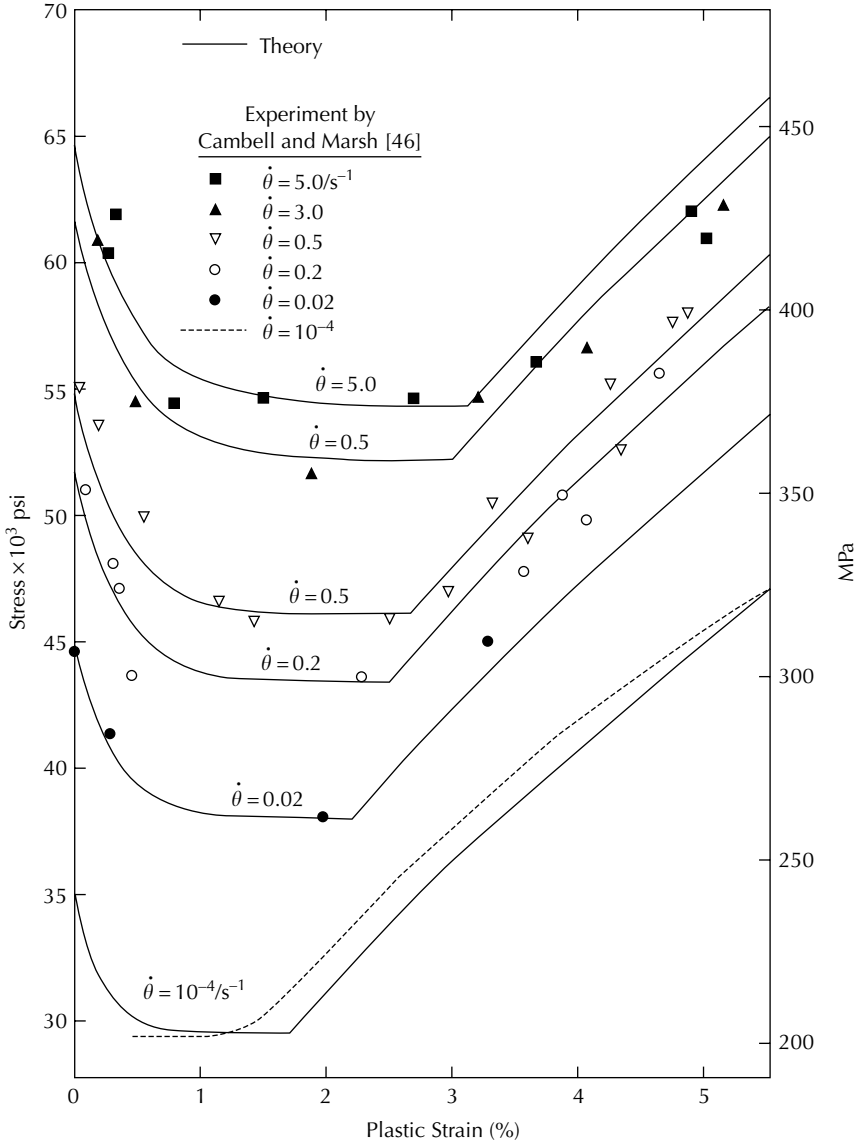

FIGURE 8.14
Constant strain-rate stress–strain curves for mild steel (From Wu, H.C. and Yip, M.C., *Int. J. Solids Struct.*, 16, 515, 1980. With permission from Elsevier).

range of strain-rate from 10^{-4} to 5 s^{-1}. The details of the theoretical work are reported in [42].

Wu and Yip [42] also considered the strain-rate history effect in two loading sequences: the low–high strain-rate change test sequence and the high–low strain-rate change test sequence. In the first test sequence, the specimens

were tested initially at a low prescribed constant strain-rate and tested at a higher strain-rate in the subsequent loading. In the second test sequence, the specimens were first tested at a high strain-rate and subsequently tested at a lower strain-rate. Both strain-hardening materials and strain softening–hardening materials were investigated. Different test sequences resulted in different subsequent stress–strain behaviors. Lin and Wu [43] used a nonlinear form of (8.162) to describe the strain-rate sensitive behavior of α-titanium.

The intrinsic time defined by (8.158) is applicable to describing constant strain-rate stress–strain curves as previously shown. In the unified theory, (8.158) is combined with (8.152) to yield

$$(\mathrm{d}z)^2 = \left(\frac{\mathrm{d}\zeta}{f(\zeta)}\right)^2 + g^2\,\mathrm{d}t^2 \tag{8.166}$$

where

$$(\mathrm{d}\zeta)^2 = k^2(|\dot{\varepsilon}^{\mathrm{p}}|)\mathrm{d}\varepsilon^{\mathrm{p}} \cdot \mathrm{d}\varepsilon^{\mathrm{p}} \quad \text{and} \quad k(|\dot{\varepsilon}^{\mathrm{p}}|) = 1 - k_{\mathrm{s}} \log\left(\frac{|\dot{\varepsilon}^{\mathrm{p}}|}{|\dot{\varepsilon}^{\mathrm{p}}|_0}\right) \tag{8.167}$$

The intrinsic time expressed by (8.166) and (8.167) provides a versatile definition of intrinsic time. In this way, the strain-rate sensitive plasticity (the rate dependence) can be accounted for by the function $k(|\dot{\varepsilon}^{\mathrm{p}}|)$, and (8.167) shows that the accumulation of ζ is strain-rate dependent. Creep or stress relaxation behavior (the time dependence) is accounted for by the function g. Although both rate dependence and time dependence are time-dependent behaviors, it is convenient to use these terminologies.

A flow theory of viscoplasticity can be derived from the endochronic viscoplasticity equations. The method of derivation and the resulting equations are the same as those presented in Section 8.4.4, except that the yield stress is replaced by the dynamic yield stress. The *dynamic yield stress* is defined by (8.160) through the strain-rate sensitivity function k. The flow rule remains the same as in (8.97), which is

$$\mathrm{d}\boldsymbol{\varepsilon}^{\mathrm{p}} = \frac{(\boldsymbol{\sigma}' - \boldsymbol{\alpha})}{\sigma'_{\mathrm{y}}}\mathrm{d}z \tag{8.168}$$

but the yield criterion is now

$$(\boldsymbol{\sigma}' - \boldsymbol{\alpha}) \cdot (\boldsymbol{\sigma}' - \boldsymbol{\alpha}) = \left(\frac{\sigma'_{\mathrm{y}} f(z)}{k}\right)^2 \qquad \text{with } \mathrm{d}\zeta^2 \neq 0 \tag{8.169}$$

or

$$\mathrm{d}\zeta^2 = 0 \tag{8.170}$$

The function k describes the strain-rate sensitivity of the dynamic loading surface so that σ'_y/k is the size of the constant strain-rate dynamic loading surface, which is also known as the SCISR (surface of constant inelastic strain-rate) — an acronym introduced by Robinson [47]. The function f denotes the size of the SCISR due to isotropic hardening and $\boldsymbol{\alpha}$ denotes the location of the center of the SCISR. The distortion of the yield and loading surfaces is not described by (8.169). That subject has been discussed by Wu et al. [48] and Wu and Lu [49].

In the case of time-dependent deformation process (creep or stress relaxation), $g \neq 0$; (8.167) and (8.168) may be substituted into (8.166) to obtain

$$\mathrm{d}z^2 = k^2(|\dot{\varepsilon}^{\mathrm{p}}|)\frac{|\boldsymbol{\sigma}' - \boldsymbol{\alpha}|^2}{(\sigma'_{\mathrm{y}}f)^2}\mathrm{d}z^2 + g^2\,\mathrm{d}t^2 \tag{8.171}$$

or

$$\mathrm{d}z = \frac{g}{\sqrt{1 - k^2(|\boldsymbol{\sigma} - \boldsymbol{\alpha}|^2/(\sigma'_{\mathrm{y}}f)^2)}}\mathrm{d}t \tag{8.172}$$

Note that since $\mathrm{d}z > 0$ and $\mathrm{d}t > 0$, it must be that $g > 0$. A creep test is preceded by a constant strain-rate test. During this stage of plastic deformation, the stress point is on the yield surface which from (8.169) is

$$\left|\boldsymbol{\sigma}' - \boldsymbol{\alpha}\right| = \frac{\sigma'_{\mathrm{y}}f(z)}{k} \quad \text{or} \quad 1 - k^2\frac{|\boldsymbol{\sigma}' - \boldsymbol{\alpha}|^2}{(\sigma'_{\mathrm{y}}f)^2} = 0 \tag{8.173}$$

However, since the stress point in the stress space stays at the same point but the back stress increases during creep as experimentally observed by Wu and Ho [50] for annealed 304 stainless steel (there may also be isotropic hardening for other materials), the stress point, which is on the SCISR when creep begins, falls back into the "elastic region" of that SCISR as the SCISR moves during creep. In the case of stress relaxation, the stress point also falls back into the "elastic region" of the SCISR as the stress level reduces. Therefore, during time-dependent inelastic behavior

$$1 - k^2\frac{|\boldsymbol{\sigma}' - \boldsymbol{\alpha}|^2}{(\sigma'_{\mathrm{y}}f)^2} \neq 0 \tag{8.174}$$

In an effort to unify the definition of intrinsic time for both plastic deformation and time-dependent inelastic behavior, the function g must reduce to zero in the case of plastic deformation. To this end, the following form of g has been

found to be satisfactory

$$g = B\sqrt{1 - k^2\frac{|\boldsymbol{\sigma}' - \boldsymbol{\alpha}|^2}{(\sigma_y' f)^2}} \tag{8.175}$$

where B is a scaling function. Substituting (8.175) into (8.172), the intrinsic time for time-dependent inelastic behavior is now given by

$$\mathrm{d}z = B\,\mathrm{d}t \tag{8.176}$$

and the time-dependent inelastic strain (creep) may be found from (8.168) as

$$\mathrm{d}\boldsymbol{\varepsilon}^{\mathrm{p}} = \mathrm{d}\mathbf{e} - \frac{\mathrm{d}\boldsymbol{\sigma}'}{2\mu_0} = \frac{(\boldsymbol{\sigma}' - \boldsymbol{\alpha})}{\sigma_y'}\,B\,\mathrm{d}t \tag{8.177}$$

which is rewritten as

$$\mathrm{d}\boldsymbol{\sigma}' = 2\mu_0\left[\mathrm{d}\mathbf{e} - \frac{(\boldsymbol{\sigma}' - \boldsymbol{\alpha})}{\sigma_y'}\,B\,\mathrm{d}t\right] \tag{8.178}$$

In the rate form, (8.178) is

$$\dot{\boldsymbol{\sigma}}' = 2\mu_0\left[\dot{\mathbf{e}} - \frac{(\boldsymbol{\sigma}' - \boldsymbol{\alpha})}{\sigma_y'}\,B\right] \tag{8.179}$$

Creep and stress relaxation are now discussed separately. In the case of creep, the stress holds constant, that is, $\dot{\boldsymbol{\sigma}}' = 0$, and the creep strain-rate $(\dot{\boldsymbol{\varepsilon}}^{\mathrm{p}})_{\mathrm{c}}$ equals the total strain-rate. Therefore, from (8.179)

$$(\dot{\boldsymbol{\varepsilon}}^{\mathrm{p}})_{\mathrm{c}} = \dot{\mathbf{e}} = \frac{(\boldsymbol{\sigma}' - \boldsymbol{\alpha})}{\sigma_y'}\,B \tag{8.180}$$

The form of the scaling function B is now investigated. Miller [51] suggested that the creep rate is a function of kinematic and isotropic hardenings and proposed the expression

$$(\dot{\boldsymbol{\varepsilon}}^{\mathrm{p}})_{\mathrm{c}} = \varphi\left(\frac{\boldsymbol{\sigma}' - \boldsymbol{\alpha}}{R}\right) \tag{8.181}$$

where R denotes isotropic hardening; $\boldsymbol{\sigma}'$ is the hold stress; and φ is a non-linear function to be further discussed. Thus, during the creep process, both kinematic and isotropic hardenings are active. The form of (8.181) encompasses the experimental observations that both isotropic and kinematic hardenings can be important factors in creep [50]. This equation is, therefore,

used in this chapter. In classical creep theories and unified viscoplasticity theories, the power, the exponential, and the hyperbolic sine functions are usually used to provide a description of creep strain. Of these functional forms, the power form has been broadly used because of its numerical simplicity. This function is now used in this writing, so that

$$B = \frac{b\sigma'_y}{|\boldsymbol{\sigma}' - \boldsymbol{\alpha}|}\left(\frac{k|\boldsymbol{\sigma}' - \boldsymbol{\alpha}|}{\sigma'_y f}\right)^m \tag{8.182}$$

where b and m are material parameters. Finally by substituting (8.182) into (8.180), the creep strain-rate is obtained as

$$(\dot{\boldsymbol{\varepsilon}}^p)_c = b\left(\frac{k|\boldsymbol{\sigma}' - \boldsymbol{\alpha}|}{\sigma'_y f}\right)^m \frac{(\boldsymbol{\sigma}' - \boldsymbol{\alpha})}{|\boldsymbol{\sigma}' - \boldsymbol{\alpha}|} \tag{8.183}$$

which is a specials case of (8.181). At the very beginning when creep is about to occur, the stress is still on the loading surface (SCISR) so that, from (8.169), $|\boldsymbol{\sigma}' - \boldsymbol{\alpha}| = (\sigma'_y f)/k$, $g = 0$, and (8.183) does not apply yet. However, only a small perturbation so that $|\boldsymbol{\sigma}' - \boldsymbol{\alpha}| < (\sigma'_y f)/k$ would start the creep process and make (8.183) applicable. Since the perturbation is small, $|\boldsymbol{\sigma}' - \boldsymbol{\alpha}| \approx (\sigma'_y f)/k$, so that $(\dot{\boldsymbol{\varepsilon}}^p)_c = b$. Therefore, b may be identified as the initial creep strain-rate. During the process of stress relaxation, the total strain increment $d\mathbf{e} = 0$ so that, by use of (8.179), the rate of stress relaxation is

$$\dot{\boldsymbol{\sigma}}' = -2\mu_0 B\frac{\boldsymbol{\sigma}' - \boldsymbol{\alpha}}{\sigma'_y} \tag{8.184}$$

Wu and Ho [44] applied the foregoing theory to describe their own experimental results for AISI type 304 stainless steel. Isotropic hardening is insignificant for this material [52]. It has been shown in [44] that the viscoplastic endochronic constitutive equation is capable of describing the inelastic behavior of this rate-sensitive metal for a variety of loading histories. The features include combined isotropic–kinematic hardening, rate sensitivity of plastic deformation, creep, and stress relaxation. In particular, the creep curves with a constant strain-rate preloading stage previously shown in Figure 5.13 are well predicted. In addition, they found that (1) meaningful results of transient creep can be obtained only from creep tests with a carefully controlled constant strain-rate preloading stage; (2) a correlation between constant strain-rate and constant stress-rate stress–strain curves can be achieved by means of the viscoplastic endochronic constitutive equations; (3) with the same strain-rate in the elastic region, the stress–strain curve of constant stress-rate is stiffer than that of constant strain-rate; (4) a correlation between creep with constant strain-rate and constant stress-rate preloadings can be achieved by means of the viscoplastic endochronic constitutive equations;

and (5) the initial creep rate is a continuation of the strain-rate of preloading and the creep curves are noticeably influenced by the initial creep rate.

References

1. Valanis, K.C., The viscoelastic potential and its thermodynamic foundation, Iowa State Univ., ERI Report 52, 1967, *J. Math. Phys*., 48, 262, 1968.
2. Valanis, K.C., Irreversibility and existence of entropy, *Int. J. Nonlinear Mech*., 6, 337, 1971.
3. Valanis, K.C., Proper tensorial formulation of the internal variable theory, The endochronic time spectrum, *Arch. Mech*., 29, 173, 1977.
4. Valanis, K.C., A gradient theory of internal variables, *Acta Mech*., 116, 1, 1996.
5. Valanis, K.C., *Irreversible Thermodynamics of Continuous Media*, Springer-Verlag, Udine, 1971.
6. Valanis, K.C., A theory of viscoplasticity without a yield surface, *Arch. Mech.* 23, 517, 1971.
7. Valanis, K.C., Fundamental consequences of a new intrinsic time measure-plasticity as a limit of the endochronic theory, *Arch. Mech.* 32, 171, 1980.
8. Callen, H.B., *Thermodynamics*, John Wiley & Sons, New York, 1960, 15.
9. Coleman, B. and Gurtin, M., Thermodynamics of internal state variables, *J. Chem. Phys*., 47, 599, 1967.
10. Ilyushin, A.A., On the relation between stresses and small strains in continuum mechanics, *Prikl. Mat. Mekh*., 18, 641, 1954 (in Russian).
11. Pipkin, A.C. and Rivlin, R.S., Mechanics of rate-independent materials, *J. Appl. Math. Phys. (ZAMP)*, 16, 313, 1965.
12. Valanis, K.C. and Wu, H.C., Endochronic representation of cyclic creep and relaxation of metals, *J. Appl. Mech*., 42, 67, 1975.
13. Wu, H.C. and Lin, H.C., Combined plastic waves in a thin-walled tube, *Int. J. Solids Struct*., 10, 903, 1974.
14. Lin, H.C. and Wu, H.C., Strain-rate effect in the endochronic theory of viscoplasticity, *J. Appl. Mech*., 43, 92, 1976.
15. Kosinski, W. and Wu, H.C., On steady viscoplastic waves. Endochronic theory, *Bull. L'Acad. Polon. Sci., Ser. Sci. Tech*., 26, 109, 1978.
16. Wu, H.C. and Yip, M.C., Finite difference solution for the uniaxial endochronic viscoplastic wave problem, *J. Appl. Mech*., 45, 221, 1978.
17. Jao, S.Y., Arora, J.S., and Wu, H.C., An optimization approach for material-constant determination for the endochronic constitutive model, *Comput. Mech*., 8, 25, 1991.
18. Wu, H.C. and Yang, R.J., Application of the improved endochronic theory of plasticity to loading with multi-axial strain-path, *Int. J. Non-Linear Mech*., 18, 395, 1983.
19. Wu, H.C., Yang, C.C., and Chu, S.C., Further application of endochronic constitutive equation to loading with non-proportional axial–torsional strain-path, *Int. J. Non-Linear Mech*., 20, 41, 1985.
20. Prager, W., The theory of plasticity: a survey of recent achievements (James Clayton Lecture), *Proc. Inst. Mech. Eng*., 169, 41, 1955.

21. Ziegler, H., A modification of Prager's hardening rule, *Quart. Appl. Math.*, 17, 55, 1959.
22. Wu, H.C. and Yip, M.C., Endochronic description of cyclic hardening behavior for metallic materials, *J. Eng. Mater. Technol.*, 103, 212, 1981.
23. Lamba, H.S. and Sidebottom, O.M., Proportional biaxial cyclic hardening of annealed oxygen-free high-conductivity copper, *J. Test. Evaluation*, 6, 260, 1978.
24. Wu, H.C., Aboutorabi, M.R., and Chen, P.C.T., Cyclic torsion of a circular cylinder and its residual stress distribution, *J. Eng. Mater. Technol.*, 107, 48, 1985.
25. Wu, H.C. and Yang, R.J., Application of the improved endochronic theory of plasticity to loading with multi-axial strain-path, *Int. J. Non-Linear Mech.*, 18, 395, 1983.
26. Ohashi, Y., Tokuda, M., and Tanaka, Y., Precise experimental results on plastic behavior of brass under complex loading, *Bull. De L'Acad. Polon. Des Sci., Ser. Sci. Tech.*, 26, 261, 1978.
27. Ohashi, Y., Tokuda, M., Mitake, T., Kurita, Y., and Suzuki, T., Stress–strain relation of integral type for deformation of brass along strain trajectories consisting of three normal straight branches, *Archs. Mech.*, 32, 125, 1980.
28. Ohashi, Y., Tokuda, M., Suzuki, T., and Kurita, Y., Stress–strain relation of brass for the plastic deformation along bi-linear strain trajectories with various corner angles, *Bull. Japan. Soc. Mech. Eng.*, 24, 1909, 1981.
29. Wu, H.C., Yang, C.C., and Chu, S.C., Further application of endochronic constitutive equation to loading with non-proportional axial–torsional strain-path, *Int. J. Non-Linear Mech.*, 20, 41, 1985.
30. Wu, H.C., Yao, J.C., and Chu, S.C., Investigation of endochronic constitutive equation subjected to plastic strain-controlled axial-torsional deformation, *J. Eng. Mater. Technol.*, 108, 262, 1986.
31. Wu, H.C. and Yeh, W.C., Further verification of endochronic theory under biaxial load, *J. Eng. Mater. Technol.*, 111, 115, 1989.
32. Valanis, K.C. and Fan, J., Endochronic analysis of cyclic elastoplastic strain fields in a notched plate, *J. Appl. Mech.*, 50, 789, 1983.
33. Valanis, K.C. and Lee, C.F., Endochronic theory of cyclic plasticity with application, *J. Appl. Mech.*, 51, 367, 1984.
34. Watanabe, O. and Atluri, S.N., A new endochronic approach to computational elastoplasticity: example of a cyclically loaded cracked plate, *J. Appl. Mech.*, 52, 857, 1985.
35. Watanabe, O. and Atluri, S.N., Internal time, general internal variable, and multi-yield-surface theories of plasticity and creep: a unification of concepts, *Int. J. Plasticity*, 2, 37, 1986.
36. Perzyna, P., The constitutive equations for rate sensitive plastic materials, *Quart. Appl. Math.*, 20, 321, 1963.
37. Phillips, A. and Wu, H.C., A theory of viscoplasticity, *Int. J. Solids Struct.*, 9, 15, 1973.
38. Krempl, E., Models of viscoplasticity. Some comments on equilibrium (back) stress and drag stress, *Acta Mech.*, 69, 25, 1987.
39. Lin, H.C. and Wu, H.C., Strain-rate effect in the endochronic theory of viscoplasticity, *J. Appl. Mech.*, 43, 92, 1976.
40. Wu, H.C. and Yip, M.C., Finite difference solution for the uniaxial endochronic viscoplastic wave problem, *J. Appl. Mech.*, 45, 221, 1978.

41. Kosinski, W. and Wu, H.C., On steady viscoplastic waves. Endochronic theory, *Bull. L'Acad. Polon. Scien., Ser. Sci. Tech.*, 26, 109, 1978.
42. Wu, H.C. and Yip, M.C., Strain rate and strain rate history effects on the dynamic behavior of metallic materials, *Int. J. Solids Struct.*, 16, 515, 1980.
43. Lin, H.C. and Wu, H.C., On the rate-dependent endochronic theory of viscoplasticity and its application to plastic-wave propagation, *Int. J. Solids Struct.*, 19, 587, 1983.
44. Wu, H.C. and Ho, C.C., An investigation of transient creep by means of endochronic viscoplasticity and experiment, *J. Eng. Mater. Technol.*, 117, 260, 1995.
45. Karnes, C.H. and Ripperger, E.A., Strain-rate effect in cold worked high-purity aluminum, *J. Mech. Phys. Solids*, 14, 75, 1966.
46. Cambell, J.D. and Marsh, K.J., The effect of strain-rate on the post-yield flow of mild steel, *J. Mech. Phys. Solids*, 11, 49, 1963.
47. Robinson, D.N., On thermomechanical testing in support of constitutive equation development for high temperature alloys, NASA CR 174879, 1985.
48. Wu, H.C., Hong, H.K., and Lu, J.K., An endochronic theory accounted for deformation induced anisotropy, *Int. J. Plasticity*, 11, 145, 1995.
49. Wu, H.C. and Lu, J.K., Further development and application of an endochronic theory accounted for deformation induced anisotrophy, *Acta Mech.*, 109, 11, 1995.
50. Wu, H.C. and Ho, C.C., Strain hardening of annealed 304 stainless steel by creep, *J. Eng. Mater. Technol.*, 115, 345, 1993.
51. Miller, A.K., An inelastic constitutive model for monotonic, cyclic, and creep deformation, *J. Eng. Mater. Technol.*, 98, 97, 1976.
52. Wu, H.C. and Yeh, W.C., On the experimental determination of yield surfaces and some results of annealed 304 stainless steel, *Int. J. Plasticity*, 7, 803, 1991.

Problems

(1) Derive (8.66) and (8.67).

(2) Derive (8.71) and (8.72).

(3) In the simple endochronic theory, if in the one-dimensional straining the intrinsic time is defined by $d\zeta = \pm k\, d\varepsilon$, where k is a constant, plot the ε versus ζ relation for straining followed by unstraining.

(4) For a thin-walled tube made of an initially isotropic material subjected to combined axial–torsion, determine k_1 and k_2 in the expression $d\zeta^2 = k_1^2(d\varepsilon^p)^2 + k_2^2(d\eta^p)^2$, where ζ is intrinsic time and η^p is the plastic part of the tensorial shear strain.

(5) Show that the solution of (8.90) is given by (8.91) and (8.92), if $k_1 = 1$.

(6) We consider here the kernel function $\xi(z)$ of the deviatoric constitutive equation (8.82). In Example 8.2, the kernel function is given by two exponential terms. Consider now the case that the kernel function consists of n number of

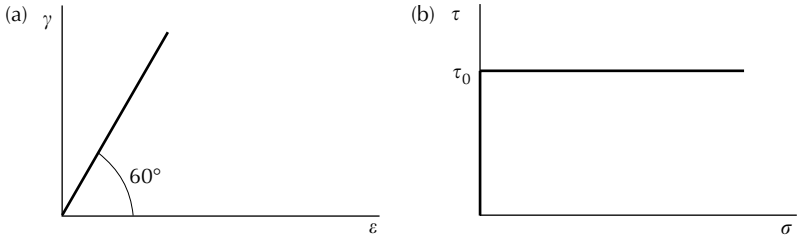

FIGURE 8.15
(a) Figure of Problem (8), (b) Figure of Problem (9).

exponential terms, show that in the case of $k_1 \approx 1$, the deviatoric stress is

$$\boldsymbol{\sigma}' = 2\mu_0 \int_0^z \xi(z - z') \frac{\mathrm{d}\mathbf{e}}{\mathrm{d}z'} \mathrm{d}z' = 2\mu_0 \int_0^z \rho(z - z') \frac{\mathrm{d}\mathbf{Q}}{\mathrm{d}z'} \mathrm{d}z'$$

where $\rho(z) = \delta(z) + \sum_{\mathrm{s}}^{n-1} R_{\mathrm{s}} \mathrm{e}^{-\alpha_{\mathrm{s}} z} + R_0$.

(7) In the strain controlled cyclic loading discussed in Section 8.4.5.2, the amplitude of the total strain is kept constant throughout the test. The amplitude of the plastic strain $\Delta\tilde{\varepsilon}^{\mathrm{p}}$ becomes constant at stable condition. Let $\Delta\tilde{\zeta}$ denote the change in ζ in $\frac{1}{4}$-cycle at the stable condition and the corresponding change in z is $\Delta\tilde{z}$. Show that, if Form (b) of (8.110) is used for the f function, then when z is large $\Delta\tilde{\zeta}/C = \Delta\tilde{z} =$ constant. Show that the cyclic stress–strain curve is

$$\sigma = \sigma^0 - (\sigma^0 - C\sigma_{\mathrm{y}}) \left\{ \frac{2\mathrm{e}^{-2\alpha\Delta\tilde{z}}}{1 + \mathrm{e}^{-2\alpha\Delta\tilde{z}}} \right\} + E_2 \varepsilon^{\mathrm{p}}$$

(8) In a strain-controlled combined tension–torsion test of a tubular specimen, if the strain-path is linear shown in Figure 8.15(a), use the endochronic constitutive equation to determine the corresponding stress-path.

(9) In a stress-controlled combined tension–torsion test of a tubular specimen, consider the tor-ten path shown in Figure 8.15(b). Use the endochronic constitutive equation to determine the corresponding strain-path. Plot the strain-path.

(10) In the constant strain-rate uniaxial stress test, if the test is conducted at a low strain-rate into the plastic strain range and then changed to a higher constant strain-rate, what happens to the stress–strain curve?

9

Topics in Endochronic Plasticity

9.1 Introduction

The endochronic theory of plasticity presented in Chapter 8 is further developed in this chapter and applied to investigate topics such as anisotropic plasticity, finite plastic deformation, engineering materials with plastic volumetric deformation, and damage mechanics. It is seen that the endochronic theory is versatile and is applicable to a wide range of engineering materials.

9.2 An Endochronic Theory of Anisotropic Plasticity

Material anisotropy is a significant factor affecting metal forming, and it is of special importance in the case of sheet metals. The anisotropic properties of sheet metals are discussed in Chapter 10 from the viewpoint of the flow theory of plasticity. A general theory of anisotropic plasticity is developed in Chapter 11 using a convected coordinate system. In this section, we discuss the anisotropic plastic behaviors of metals using a endochronic plasticity. We discuss the topic of deformation induced anisotropy and develop an endochronic theory for anisotropic sheet metals.

9.2.1 An Endochronic Theory Accounting for Deformation Induced Anisotropy

In the endochronic theory, the free energy function is from (8.63) given by

$$\Psi = \tfrac{1}{2}\boldsymbol{\varepsilon}\cdot\underline{\mathbf{A}}\cdot\boldsymbol{\varepsilon} + \boldsymbol{\varepsilon}\cdot\underline{\mathbf{B}}^{r}\cdot\mathbf{q}^{r} + \tfrac{1}{2}\mathbf{q}^{r}\cdot\underline{\mathbf{C}}^{r}\cdot\mathbf{q}^{r} \tag{9.1}$$

The constitutive equation and the evolution equations are from (8.51) and (8.57)

$$\boldsymbol{\sigma} = \frac{\partial\Psi}{\partial\boldsymbol{\varepsilon}} \quad \text{and} \quad \frac{\partial\Psi}{\partial\mathbf{q}^{r}} + \underline{\mathbf{b}}^{r}\cdot\frac{\mathrm{d}\mathbf{q}^{r}}{\mathrm{d}z} = 0, \qquad r = 1,2,\ldots,n \tag{9.2}$$

where $\underline{\mathbf{A}}, \underline{\mathbf{B}}^r, \underline{\mathbf{C}}^r$, and $\underline{\mathbf{b}}^r$ are isotropic fourth-rank constant tensors; $\boldsymbol{\sigma}$, $\boldsymbol{\varepsilon}$, and $\mathbf{q}^r$ are symmetric tensors. By use of (9.1) and (9.2), the constitutive equation becomes

$$\begin{aligned} \sigma_{kk} &= 3A_0\varepsilon_{kk} + \sum_r 3\,B_0^r q_{kk}^r \\ \sigma'_{ij} &= A_2 e_{ij} + \sum_r B_2^r p_{ij}^r \end{aligned} \tag{9.3}$$

To consider deformation induced anisotropy, the evolution of $\mathbf{q}^r$ must depend on the strain path. This may be achieved by having an anisotropic $\underline{\mathbf{b}}^r$. Following Wu and Yeh [1], we define a strain path with reference to a coordinate system. Thus, we may talk about the normal strain and the shear strain. The internal structure of a material changes differently when it is under normal strain and under shear strain. Hence, q_{11}^r evolves differently than q_{12}^r. We assume that q_{ij}^r is symmetric and write its components in a matrix form as

$$[q^r] = [q_{11}^r, q_{22}^r, q_{33}^r, q_{23}^r, q_{13}^r, q_{12}^r]^{\mathrm{T}} \tag{9.4}$$

We assume further that, in the internal structure, no coupled effect exists either between shear and normal components or among shear components. Then, tensor b_{ijkm}^r is of the following form:

$$[b^r] = \begin{bmatrix} b_1^r & b_2^r & b_2^r & 0 & 0 & 0 \\ b_2^r & b_1^r & b_2^r & 0 & 0 & 0 \\ b_2^r & b_2^r & b_1^r & 0 & 0 & 0 \\ 0 & 0 & 0 & b_3^r & 0 & 0 \\ 0 & 0 & 0 & 0 & b_3^r & 0 \\ 0 & 0 & 0 & 0 & 0 & b_3^r \end{bmatrix} \tag{9.5}$$

The matrix in (9.5) is obtained by considering symmetry during permutation of 1, 2, and 3. We further have

$$\begin{aligned} &b_{1111}^r = b_{2222}^r = b_{3333}^r = b_1^r, \qquad b_{2323}^r = b_{1313}^r = b_{1212}^r = b_3^r, \\ &b_{1122}^r = b_{1133}^r = b_{2233}^r = b_{3311}^r = \cdots = b_2^r, \qquad \text{other } b_{ijkm}^r = 0 \end{aligned} \tag{9.6}$$

We now consider the evolution of $\mathbf{q}^r$. Using (9.1), we obtain the following expression

$$\frac{\partial \Psi}{\partial q_{ij}^r} = B_1^r \varepsilon_{kk}\delta_{ij} + B_2^r \varepsilon_{ij} + C_1^r q_{kk}^r \delta_{ij} + C_2^r q_{ij}^r \tag{9.7}$$

On the other hand, we have

$$\underline{\mathbf{b}}^r \cdot \dot{\mathbf{q}}^r = \begin{bmatrix} b_1^r \dot{q}_{11}^r + b_2^r \dot{q}_{22}^r + b_2^r \dot{q}_{33}^r \\ b_2^r \dot{q}_{11}^r + b_1^r \dot{q}_{22}^r + b_2^r \dot{q}_{33}^r \\ b_2^r \dot{q}_{11}^r + b_2^r \dot{q}_{22}^r + b_1^r \dot{q}_{33}^r \\ b_3^r \dot{q}_{23}^r \\ b_3^r \dot{q}_{13}^r \\ b_3^r \dot{q}_{12}^r \end{bmatrix} = \begin{bmatrix} (b_1^r - b_2^r)\dot{q}_{11}^r + b_2^r \dot{q}_{kk}^r \\ (b_1^r - b_2^r)\dot{q}_{22}^r + b_2^r \dot{q}_{kk}^r \\ (b_1^r - b_2^r)\dot{q}_{33}^r + b_2^r \dot{q}_{kk}^r \\ b_3^r \dot{q}_{23}^r \\ b_3^r \dot{q}_{13}^r \\ b_3^r \dot{q}_{12}^r \end{bmatrix} \tag{9.8}$$

Substituting (9.7) and (9.8) into the second equation of (9.2), we obtain the evolution equations for the cases of $i = j$ and $i \neq j$. Thus, the governing equations are summarized below. The hydrostatic equations are

$$\begin{aligned} \sigma_{kk} &= 3A_0 \varepsilon_{kk} + 3 \sum_r B_0^r q_{kk}^r \\ B_0^r \varepsilon_{kk} &+ C_0^r q_{kk}^r + b_0^r \frac{\mathrm{d}q_{kk}^r}{\mathrm{d}z} = 0 \end{aligned} \tag{9.9}$$

and the deviatoric equations are

$$\begin{aligned} \sigma'_{ij} &= A_2 e_{ij} + \sum_r B_2^r \, p_{ij}^r \\ B_2^r e_{ij} + C_2^r p_{ij}^r &+ (b_1^r - b_2^r)\frac{\mathrm{d}p_{ij}^r}{\mathrm{d}z} = 0, \qquad i = j \\ B_2^r e_{ij} + C_2^r p_{ij}^r &+ b_3^r \frac{\mathrm{d}p_{ij}^r}{\mathrm{d}z} = 0, \qquad i \neq j \end{aligned} \tag{9.10}$$

It is assumed that the material is plastically incompressible so that only the deviatoric part of the constitutive equation is of further interest. The evolution equations in (9.10) for $i = j$ and $i \neq j$ can be solved separately to yield expressions for $p_{\underline{i}\underline{i}}^r$ ($\underline{i}$ not summed) and p_{ij}^r, which are then substituted into the first equation of (9.10) to yield

$$\begin{aligned} \sigma'_{\underline{i}\underline{i}} &= A_2 e_{\underline{i}\underline{i}} - \sum_r \frac{B_2^r B_2^r}{C_2^r} \int_0^z \mathrm{e}^{-\rho_r (z - z')} e_{\underline{i}\underline{i}}(z') \mathrm{d}z', \qquad \underline{i} \text{ not summed} \\ \sigma'_{ij} &= A_2 e_{ij} - \sum_r \frac{B_2^r B_2^r}{C_2^r} \int_0^z \mathrm{e}^{-\beta_r (z - z')} e_{ij}(z') \mathrm{d}z', \qquad i \neq j \end{aligned} \tag{9.11}$$

where

$$\rho_r = \frac{C_2^r}{b_1^r - b_2^r}, \qquad \beta_r = \frac{C_2^r}{b_3^r} \tag{9.12}$$

By use of Laplace transformation as in Section 8.4.3, (9.11) may be rewritten in terms of plastic strain as

$$\sigma'_{ij} = \sigma'_{\mathrm{y}} \frac{\mathrm{d}e^{\mathrm{p}}_{ij}}{\mathrm{d}z} + \int_0^z \lambda_{ijkm}(z - z') \frac{\mathrm{d}e^{\mathrm{p}}_{km}}{\mathrm{d}z'} \mathrm{d}z' \tag{9.13}$$

where

$$[\lambda] = \begin{bmatrix} \mu & & & & & 0 \\ & \mu & & & & \\ & & \mu & & & \\ & & & \nu & & \\ & & & & \nu & \\ 0 & & & & & \nu \end{bmatrix} \quad \text{with} \quad \begin{aligned} \mu(z) &= \sum_r \mu_r \, \mathrm{e}^{-m_r z} + \mu_1 \\ \nu(z) &= \sum_r \nu_r \, \mathrm{e}^{-n_r z} + \nu_1 \end{aligned} \tag{9.14}$$

in which μ_r, m_r, ν_r, and n_r are material constants of the kernel functions $\mu(z)$ and $\nu(z)$. Note that in the case of $b_1^r = b_2^r + b_3^r$, we find $\rho_r = \beta_r$, which leads to $\mu(z) = \nu(z)$. Thus, the following endochronic equation for the isotropic rate of kinematic hardening is recovered:

$$\sigma'_{ij} = \sigma'_{\mathrm{y}} \frac{\mathrm{d}e^{\mathrm{p}}_{ij}}{\mathrm{d}z} + \int_0^z \mu(z - z') \frac{\mathrm{d}e^{\mathrm{p}}_{ij}}{\mathrm{d}z'} \mathrm{d}z' \tag{9.15}$$

We note that the anisotropic form (9.13) is the same as that used by Ohashi and his coworkers [2,3].

Let us further consider the anisotropic endochronic equation (9.13) and, following Wu et al. [4], establish a relation between the definition of the intrinsic time and the form of the yield function. In (9.13), the back stress is

$$\alpha_{ij} = \int_0^z \lambda_{ijkm}(z - z') \frac{\mathrm{d}e^{\mathrm{p}}_{km}}{\mathrm{d}z'} \mathrm{d}z' \tag{9.16}$$

Thus, (9.13) is written as

$$\sigma'_{ij} - \alpha_{ij} = \sigma'_{\mathrm{y}} \frac{\mathrm{d}e^{\mathrm{p}}_{ij}}{\mathrm{d}z} = \sigma'_{\mathrm{y}} f(z) \frac{\mathrm{d}e^{\mathrm{p}}_{ij}}{\mathrm{d}\zeta} \tag{9.17}$$

resulting in the following flow rule

$$\mathrm{d}e^{\mathrm{p}}_{ij} = \frac{1}{\sigma'_{\mathrm{y}}} (\sigma'_{ij} - \alpha_{ij}) \, \mathrm{d}z \tag{9.18}$$

Define the intrinsic time as

$$\mathrm{d}\zeta^2 = \mathrm{d}\mathbf{e}^{\mathrm{p}} \cdot \underline{\mathbf{K}} \cdot \mathrm{d}\mathbf{e}^{\mathrm{p}} \tag{9.19}$$

in which $\underline{\mathbf{K}}$ is a fourth-rank tensor. Then, by using (9.18), (9.19) becomes

$$\mathrm{d}\zeta^2 = (\boldsymbol{\sigma}' - \boldsymbol{\alpha}) \frac{\mathrm{d}\zeta}{\sigma'_{\mathrm{y}} f} \cdot \underline{\mathbf{K}} \cdot (\boldsymbol{\sigma}' - \boldsymbol{\alpha}) \frac{\mathrm{d}\zeta}{\sigma'_{\mathrm{y}} f} \tag{9.20}$$

or

$$[(\boldsymbol{\sigma}' - \boldsymbol{\alpha}) \cdot \underline{\mathbf{K}} \cdot (\boldsymbol{\sigma}' - \boldsymbol{\alpha}) - (\sigma'_{\mathrm{y}} f)^2] \mathrm{d}\zeta^2 = 0 \tag{9.21}$$

Therefore,

$$\begin{aligned} &\text{Either } (\boldsymbol{\sigma}' - \boldsymbol{\alpha}) \cdot \underline{\mathbf{K}} \cdot (\boldsymbol{\sigma}' - \boldsymbol{\alpha}) = (\sigma'_{\mathrm{y}} f)^2 \qquad \text{with } \mathrm{d}\zeta^2 \neq 0 \\ &\quad \text{or} \quad \mathrm{d}\zeta = 0 \quad \text{elastic behavior} \end{aligned} \tag{9.22}$$

The first equation of (9.22) is the yield criterion of this anisotropic version of the endochronic plasticity and the second equation of (9.22) describes the elastic behavior, which may be seen from (9.19) due to the positive definiteness of $\underline{\mathbf{K}}$. The condition $\mathrm{d}\zeta = 0$ leads to the elastic constitutive equation as in (8.104).

From (9.19), due to the symmetry of $\mathrm{d}e^{\mathrm{p}}_{ij}$, K_{ijkm} enjoys the following symmetry:

$$\begin{aligned} &\mathrm{d}e^{\mathrm{p}}_{ij} K_{ijkm}\, \mathrm{d}e^{\mathrm{p}}_{km} = \mathrm{d}e^{\mathrm{p}}_{km} K_{kmij}\, \mathrm{d}e^{\mathrm{p}}_{ij}, \qquad \mathrm{d}e^{\mathrm{p}}_{ij} K_{ijkm}\, \mathrm{d}e^{\mathrm{p}}_{km} = \mathrm{d}e^{\mathrm{p}}_{ij} K_{ijmk}\, \mathrm{d}e^{\mathrm{p}}_{mk}, \\ &K_{ijkm} = K_{kmij} = K_{ijmk} \end{aligned} \tag{9.23}$$

The number of independent components of $\underline{\mathbf{K}}$ is reduced from 81 to 21. In most previous investigations, $\underline{\mathbf{K}}$ was assumed to be isotropic throughout the course of deformation for mathematical simplicity. This assumption is now relaxed so that $\underline{\mathbf{K}}$ depends on the direction of loading. Equation (9.19) simply asserts that the rate of accumulation of the intrinsic time ζ is not the same when the material is subjected to shear or subjected to tension. However, $\underline{\mathbf{K}}$ is initially isotropic for initially isotropic materials. In which case, the first equation of (9.22) reduces to the Mises yield criterion.

Equation (9.22) represents a distortion from the Mises yield criterion due to the presence of $\underline{\mathbf{K}}$. This criterion may be used for the initial as well as the subsequent yielding. In particular, (9.22) can accommodate the idea that the initial yield surface is of the type of Mises, but the subsequent yield surfaces are obtained by the compression and stretching of the Mises yield surface. It should also be pointed out that while the plastic strain increment is still given by (9.18) in this modified theory, this tensor is no longer normal to the yield surface when $\underline{\mathbf{K}}$ is not isotropic.

An important point to make here is that a formal link between the definition of intrinsic time and the form of the yield function has been established. The definition of intrinsic time directly affects the form of the yield function, so that

the intrinsic time defined by (9.19) leads to a yield function defined by (9.22). On the other hand, a slightly different definition of intrinsic time, such as

$$\mathrm{d}\zeta^2 = \mathrm{d}\boldsymbol{\varepsilon}^{\mathrm{p}} \cdot \underline{\mathbf{K}} \cdot \mathrm{d}\boldsymbol{\varepsilon}^{\mathrm{p}} + \mathrm{tr}(\mathbf{L} \cdot \mathrm{d}\boldsymbol{\varepsilon}^{\mathrm{p}})\, \mathrm{d}\zeta \tag{9.24}$$

would lead to a yield function given by

$$(\boldsymbol{\sigma}' - \boldsymbol{\alpha}) \cdot \underline{\mathbf{K}} \cdot (\boldsymbol{\sigma}' - \boldsymbol{\alpha}) + \sigma_{\mathrm{y}}' f(z)\ \mathrm{tr}[\mathbf{L} \cdot (\boldsymbol{\sigma}' - \boldsymbol{\alpha})] = (\sigma_{\mathrm{y}}' f(z))^2 \tag{9.25}$$

where $\mathbf{L}$ is a material tensor.

Explicit equations can be obtained from the theory of this subsection in the case of axial–torsion loading of a thin-walled tubular specimen. Since the material is assumed to be plastically incompressible and the cylindrical coordinates (r, θ, z) are used in this discussion, the conditions $\mathrm{d}\varepsilon_{zz}^{\mathrm{p}} + \mathrm{d}\varepsilon_{rr}^{\mathrm{p}} + \mathrm{d}\varepsilon_{\theta\theta}^{\mathrm{p}} = 0$ and $\mathrm{d}\varepsilon_{rr}^{\mathrm{p}} = \mathrm{d}\varepsilon_{\theta\theta}^{\mathrm{p}}$ apply. The latter condition is a good approximation in the case of small plastic deformation, but it is not so when plastic deformation is large; see Wu et al. [5] for further discussion. The matrices of the deviatoric stress $\boldsymbol{\sigma}'$, the back stress $\boldsymbol{\alpha}$, and the plastic strain increment $\mathrm{d}\boldsymbol{\varepsilon}^{\mathrm{p}}$ are

$$[\sigma'] = \begin{bmatrix} \dfrac{-\sigma}{3} & 0 & 0 \\ 0 & \dfrac{-\sigma}{3} & \tau \\ 0 & \tau & \dfrac{2\sigma}{3} \end{bmatrix}, \qquad [\alpha] = \begin{bmatrix} \dfrac{-\alpha_{zz}}{3} & 0 & 0 \\ 0 & \dfrac{-\alpha_{zz}}{3} & \alpha_{\theta z} \\ 0 & \alpha_{\theta z} & \dfrac{2\alpha_{zz}}{3} \end{bmatrix},$$
$$[\mathrm{d}\varepsilon^{\mathrm{p}}] = \begin{bmatrix} \dfrac{-\mathrm{d}\varepsilon^{\mathrm{p}}}{2} & 0 & 0 \\ 0 & \dfrac{-\mathrm{d}\varepsilon^{\mathrm{p}}}{2} & \mathrm{d}\eta^{\mathrm{p}} \\ 0 & \mathrm{d}\eta^{\mathrm{p}} & \mathrm{d}\varepsilon^{\mathrm{p}} \end{bmatrix} \tag{9.26}$$

which may also be written as column vectors as

$$[\sigma'] = \begin{bmatrix} \dfrac{-\sigma}{3} \\ \dfrac{2\sigma}{3} \\ \tau \end{bmatrix}, \qquad [\alpha] = \begin{bmatrix} \dfrac{-\alpha_{zz}}{3} \\ \dfrac{2\alpha_{zz}}{3} \\ \alpha_{\theta z} \end{bmatrix}, \qquad [\mathrm{d}\varepsilon^{\mathrm{p}}] = \begin{bmatrix} \dfrac{-\mathrm{d}\varepsilon^{\mathrm{p}}}{2} \\ \mathrm{d}\varepsilon^{\mathrm{p}} \\ \mathrm{d}\eta^{\mathrm{p}} \end{bmatrix} \tag{9.27}$$

Then, the fourth-rank tensor $\underline{\mathbf{K}}$ is given by the square matrix

$$[K] = \begin{bmatrix} K_{11} & K_{12} & K_{13} \\ K_{12} & K_{22} & K_{23} \\ K_{13} & K_{23} & K_{33} \end{bmatrix} \tag{9.28}$$

Substituting (9.27) and (9.28) into (9.19), we obtain

$$d\zeta^2 = d\boldsymbol{\varepsilon}^p \cdot \underline{\mathbf{K}} \cdot d\boldsymbol{\varepsilon}^p = K_1(d\varepsilon^p)^2 + 2K_3(d\varepsilon^p)(d\eta^p) + K_2(d\eta^p)^2 \tag{9.29}$$

where

$$K_1 = \frac{K_{11}}{4} - K_{12} + K_{22}, \qquad K_2 = K_{33}, \qquad K_3 = \frac{1}{2}(2K_{23} - K_{13}) \tag{9.30}$$

and, by using (9.18), the yield function (9.22) becomes

$$\tfrac{4}{9}K_1(\sigma - \alpha_{zz})^2 + \tfrac{4}{3}K_3(\sigma - \alpha_{zz})(\tau - \alpha_{\theta z}) + K_2(\tau - \alpha_{\theta z})^2 = (\sigma_y' f(z))^2 \tag{9.31}$$

It can be seen from (9.31) that the yield function is an ellipse in the σ versus τ space. As plastic deformation occurs, the ellipse will change its shape, depending on the values of K_1 and K_2, when the semimajor and semiminor axes change their lengths. At the same time, isotropic hardening takes place according to function $f(z)$ and the ellipse translates according to the magnitude of the back stress $\boldsymbol{\alpha}$. In addition, rotation of the yield surface occurs according to the value of $2K_3$. Therefore, the major features of subsequent yield surfaces as observed experimentally by Phillips and Tang [6] and Wu and Yeh [7] can all be described. From the experimental results of Phillips and his coworkers, the initial value of K_3 is zero. Then by comparing equation (9.31) with the Mises yield criterion, the initial values of K_1 and K_2 are determined to be 3/2 and 2, respectively. Wu and Lu [8] have established a procedure to determine the metric of the anisotropic intrinsic time using information related to the yield surface of 304 stainless steel.

9.2.2 An Endochronic Theory for Anisotropic Sheet Metals

The contents of this section were initially presented by Wu and Hong [9] and are reproduced here with permission from Elsevier. In the Helmholtz formulation, the free energy is

$$\Psi = \frac{1}{2}\sum_r A^r_{ijkm}(\varepsilon_{ij} - q^r_{ij})(\varepsilon_{km} - q^r_{km}) \tag{9.32}$$

where A^r_{ijkm} are constants. For a rolled metal sheet, let x denote the rolling direction (RD), y the transverse direction (TD), and z the normal direction (ND). The nonzero strain components are ε_x, ε_y, ε_{xy}, and ε_z. No energy is stored due to ε_z. Thus, (9.32) reduces to

$$\begin{aligned}\Psi = \frac{1}{2}\sum_r [&A^r(\varepsilon_x - q^r_x)^2 + B^r(\varepsilon_y - q^r_y)^2 + 2D^r(\varepsilon_{xy} - q^r_{xy})^2 \\ &+ 2C^r(\varepsilon_x - q^r_x)(\varepsilon_y - q^r_y)]\end{aligned} \tag{9.33}$$

where A^r, B^r, C^r, and D^r are constants. The stress components are

$$\sigma_x = \frac{\partial \Psi}{\partial \varepsilon_x} = \sum_r [A^r(\varepsilon_x - q_x^r) + C^r(\varepsilon_y - q_y^r)] \tag{9.34a}$$

$$\sigma_y = \frac{\partial \Psi}{\partial \varepsilon_y} = \sum_r [B^r(\varepsilon_y - q_y^r) + C^r(\varepsilon_x - q_x^r)] \tag{9.34b}$$

$$\sigma_{xy} = \frac{\partial \Psi}{\partial \varepsilon_{xy}} = \sum_r [D^r(\varepsilon_{xy} - q_{xy}^r)] \tag{9.34c}$$

and the evolution equations for the internal variables are from (8.57):

$$\frac{\partial \Psi}{\partial q_{ij}^r} + b_{ijkm}^r \frac{\mathrm{d}q_{km}^r}{\mathrm{d}z} = 0 \qquad (r \text{ not summed}) \tag{9.35}$$

In the rolled sheet metal, the components of internal variables are (q_x^r, q_y^r, q_{xy}^r) and it is assumed that there are no coupling effects among these components, so that the dissipation tensor has the following form

$$[b^r] = \begin{bmatrix} b_x^r & 0 & 0 \\ 0 & b_y^r & 0 \\ 0 & 0 & b_{xy}^r \end{bmatrix} \tag{9.36}$$

Using (9.33) and (9.36), (9.35) reduces to

$$\frac{\mathrm{d}q_x^r}{\mathrm{d}z} + P^r q_x^r + U^r q_y^r = P^r \varepsilon_x + U^r \varepsilon_y \tag{9.37a}$$

$$\frac{\mathrm{d}q_y^r}{\mathrm{d}z} + Q^r q_y^r + V^r q_x^r = Q^r \varepsilon_y + V^r \varepsilon_x \tag{9.37b}$$

$$\frac{\mathrm{d}q_{xy}^r}{\mathrm{d}z} + R^r q_{xy}^r = R^r \varepsilon_{xy} \tag{9.37c}$$

where

$$P^r = \frac{A^r}{b_x^r}, \qquad U^r = \frac{C^r}{b_x^r}, \qquad Q^r = \frac{B^r}{b_y^r}, \qquad V^r = \frac{C^r}{b_y^r}, \qquad R^r = \frac{D^r}{b_{xy}^r} \tag{9.38}$$

Note that (9.37a,b) are coupled in q_x^r and q_y^r. A standard procedure may be used to decouple the equations. The resulting equations are

$$\frac{\mathrm{d}\bar{q}_x^r}{\mathrm{d}z} + \lambda_1^r \bar{q}_x^r = \tilde{C}^r \varepsilon_x + \tilde{D}^r \varepsilon_y \tag{9.39a}$$

$$\frac{\mathrm{d}\bar{q}_y^r}{\mathrm{d}z} + \lambda_2^r \bar{q}_y^r = \tilde{E}^r \varepsilon_x + \tilde{F}^r \varepsilon_y \tag{9.39b}$$

where λ_1^r and λ_2^r are eigenvalues of the matrix $\begin{bmatrix} P^r & U^r \\ V^r & Q^r \end{bmatrix}$. Note that since $U^r \neq 0$ and $V^r \neq 0$, there are always two real eigenvalues. $\bar{q}_x^r$ and $\bar{q}_y^r$ are related to q_x^r and q_y^r through the eigenvectors of the matrix by the following relations

$$q_x^r = U^r(\bar{q}_x^r + \bar{q}_y^r), \qquad q_y^r = (-P^r + \lambda_1^r)\bar{q}_x^r + (-P^r + \lambda_2^r)\bar{q}_y^r \tag{9.40}$$

and

$$\begin{aligned} \tilde{C}^r &= \frac{[-(P^r)^2 + \lambda_2^r P^r - P^r V^r + \lambda_1^r V^r]}{U^r(\lambda_2^r - \lambda_1^r)} \\ \tilde{D}^r &= \frac{[-P^r U^r + \lambda_2^r U^r - P^r Q^r + \lambda_1^r Q^r]}{U^r(\lambda_2^r - \lambda_1^r)} \\ \tilde{E}^r &= \frac{(U^r P^r + U^r V^r)}{U^r(\lambda_2^r - \lambda_1^r)} \\ \tilde{F}^r &= \frac{[(U^r)^2 + U^r Q^r]}{U^r(\lambda_2^r - \lambda_1^r)} \end{aligned} \tag{9.41}$$

Note that (9.39a,b) are now decoupled in $\bar{q}_x^r$ and $\bar{q}_y^r$. These equations may be integrated with results substituted into (9.40) to obtain

$$\begin{aligned} q_x^r = {} & U^r \int_0^z \mathrm{e}^{-\lambda_1^r(z-z')}[\tilde{C}^r \varepsilon_x(z') + \tilde{D}^r \varepsilon_y(z')]\mathrm{d}z' \\ & + U^r \int_0^z \mathrm{e}^{-\lambda_2^r(z-z')}[\tilde{E}^r \varepsilon_x(z') + \tilde{F}^r \varepsilon_y(z')]\mathrm{d}z' \end{aligned} \tag{9.42a}$$

$$\begin{aligned} q_y^r = {} & (-P^r + \lambda_1^r) \int_0^z \mathrm{e}^{-\lambda_1^r(z-z')}[\tilde{C}^r \varepsilon_x(z') + \tilde{D}^r \varepsilon_y(z')]\mathrm{d}z' \\ & + (-P^r + \lambda_2^r) \int_0^z \mathrm{e}^{-\lambda_2^r(z-z')}[\tilde{E}^r \varepsilon_x(z') + \tilde{F}^r \varepsilon_y(z')]\mathrm{d}z' \end{aligned} \tag{9.42b}$$

Also, (9.37c) may be integrated to yield

$$q_{xy}^r = R^r \int_0^z \mathrm{e}^{-R^r(z-z')} \varepsilon_{xy}(z')\mathrm{d}z' \tag{9.42c}$$

with $q_x^r(0) = q_y^r(0) = q_{xy}^r(0) = 0$. By substitution of (9.42) into (9.34) and by use of integration by parts, the following expressions are found

$$\sigma_x = Y_1\varepsilon_x(z) + Y_2\varepsilon_y(z) + \sum_r \left\{ M^r \int_0^z \mathrm{e}^{-\lambda_1^r(z-z')} \left[\tilde{C}^r \frac{\mathrm{d}\varepsilon_x}{\mathrm{d}z'} + \tilde{D}^r \frac{\mathrm{d}\varepsilon_y}{\mathrm{d}z'} \right] \mathrm{d}z' \right\} + \sum_r \left\{ N^r \int_0^z \mathrm{e}^{-\lambda_2^r(z-z')} \left[\tilde{E}^r \frac{\mathrm{d}\varepsilon_x}{\mathrm{d}z'} + \tilde{F}^r \frac{\mathrm{d}\varepsilon_y}{\mathrm{d}z'} \right] \mathrm{d}z' \right\} \tag{9.43a}$$

$$\sigma_y = Y_3\varepsilon_y(z) + Y_4\varepsilon_x(z) + \sum_r \left\{ K^r \int_0^z \mathrm{e}^{-\lambda_1^r(z-z')} \left[\tilde{C}^r \frac{\mathrm{d}\varepsilon_x}{\mathrm{d}z'} + \tilde{D}^r \frac{\mathrm{d}\varepsilon_y}{\mathrm{d}z'} \right] \mathrm{d}z' \right\} + \sum_r \left\{ L^r \int_0^z \mathrm{e}^{-\lambda_2^r(z-z')} \left[\tilde{E}^r \frac{\mathrm{d}\varepsilon_x}{\mathrm{d}z'} + \tilde{F}^r \frac{\mathrm{d}\varepsilon_y}{\mathrm{d}z'} \right] \mathrm{d}z' \right\} \tag{9.43b}$$

$$\sigma_{xy} = \sum_r \left\{ D^r \int_0^z \mathrm{e}^{-R^r(z-z')} \frac{\mathrm{d}\varepsilon_{xy}}{\mathrm{d}z'} \mathrm{d}z' \right\} \tag{9.43c}$$

where

$$\begin{gathered} Y_1 = A - \sum_r M^r \tilde{C}^r - \sum_r N^r \tilde{E}^r, \qquad Y_2 = C - \sum_r M^r \tilde{D}^r - \sum_r N^r \tilde{F}^r \\ Y_3 = B - \sum_r K^r \tilde{D}^r - \sum_r L^r \tilde{F}^r, \qquad Y_4 = C - \sum_r K^r \tilde{C}^r - \sum_r L^r \tilde{E}^r \\ A = \sum_r A^r, \quad B = \sum_r B^r, \quad C = \sum_r C^r, \\ M^r = \frac{1}{\lambda_1^r}\left[A^r U^r + C^r(-P^r + \lambda_1^r)\right], \qquad N^r = \frac{1}{\lambda_2^r}\left[A^r U^r + C^r(-P^r + \lambda_2^r)\right] \\ K^r = \frac{1}{\lambda_1^r}\left[C^r U^r + B^r(-P^r + \lambda_1^r)\right], \qquad L^r = \frac{1}{\lambda_2^r}\left[C^r U^r + B^r(-P^r + \lambda_2^r)\right] \end{gathered} \tag{9.44}$$

Note that all quantities given in (9.44) are constants. A special case of (9.43) is used to derive the following equations

$$\begin{aligned} \sigma_x &= K^{-3/2} \int_0^z G(z-z') \left[(H+F) \frac{\mathrm{d}\varepsilon_x}{\mathrm{d}z'} + H \frac{\mathrm{d}\varepsilon_y}{\mathrm{d}z'} \right] \mathrm{d}z' \\ \sigma_y &= K^{-3/2} \int_0^z G(z-z') \left[(G+H) \frac{\mathrm{d}\varepsilon_y}{\mathrm{d}z'} + H \frac{\mathrm{d}\varepsilon_x}{\mathrm{d}z'} \right] \mathrm{d}z' \\ \sigma_{xy} &= K^{-3/2} \int_0^z G_{xy}(z-z') \left[\frac{M}{N} \frac{\mathrm{d}\varepsilon_{xy}}{\mathrm{d}z'} \right] \mathrm{d}z' \end{aligned} \tag{9.45}$$

where

$$\begin{aligned} G(z) &= \sum_r G^r \mathrm{e}^{-\lambda^r z} \qquad \text{with } G(0) = \sum_r G^r = 1 \\ G_{xy}(z) &= \sum_r G^r_{xy} \mathrm{e}^{-\lambda^r_{xy} z} \qquad \text{with } G_{xy}(0) = \sum_r G^r_{xy} = 1 \\ K &= \tfrac{2}{3}(F+G+H) \quad \text{and} \quad M = (H+F)(G+H) - H^2 \end{aligned} \tag{9.46}$$

Constitutive equations (9.45) are suitable for use in sheet metals. These are expressions for the stress components in terms of the histories of the total strain components ε_x, ε_y, and ε_{xy}. In the equations, $E, F, G, H, G^r, G^r_{xy}, \lambda^r$, and λ^r_{xy} are constants with $r = 1, \ldots, n$. The derivation of (9.45) is given in [9].

It is now desirable to express the stress in terms of the histories of plastic strain components $\varepsilon^{\mathrm{p}}_x$, $\varepsilon^{\mathrm{p}}_y$, and $\varepsilon^{\mathrm{p}}_{xy}$ so that

$$\begin{aligned} \sigma_x &= K^{-3/2} \int_0^z \rho(z-z') \left[(H+F) \frac{\mathrm{d}\varepsilon^{\mathrm{p}}_x}{\mathrm{d}z'} + H \frac{\mathrm{d}\varepsilon^{\mathrm{p}}_y}{\mathrm{d}z'} \right] \mathrm{d}z' \\ \sigma_y &= K^{-3/2} \int_0^z \rho(z-z') \left[(G+H) \frac{\mathrm{d}\varepsilon^{\mathrm{p}}_y}{\mathrm{d}z'} + H \frac{\mathrm{d}\varepsilon^{\mathrm{p}}_x}{\mathrm{d}z'} \right] \mathrm{d}z' \\ \sigma_{xy} &= K^{-3/2} \int_0^z \rho_{xy}(z-z') \left[\frac{M}{N} \frac{\mathrm{d}\varepsilon^{\mathrm{p}}_x}{\mathrm{d}z'} \right] \mathrm{d}z' \end{aligned} \tag{9.47}$$

The forms of expressions in the square brackets on the right-hand side of (9.45) and (9.47) are assumed to be the same. These forms are established based on plastic deformation for sheet metals, which is further discussed in Chapter 10. The coefficients F, G, H, M, and N are those of the yield function initially proposed by Hill [10]. The kernel functions $\rho(z)$ and $\rho_{xy}(z)$ can be determined from knowledge of $G(z)$ and $G_{xy}(z)$ using the method of Laplace transformation discussed in Section 8.4.3. Omitting the details of derivation, which may be found in [9], the kernel functions are

$$\begin{aligned} \rho(z) &= \delta(z) + \rho_1(z) \qquad \text{with } \rho_1(z) = \sum_{r=1}^{n-1} R^r \mathrm{e}^{-\mu_r z} \\ \rho_{xy}(z) &= \delta(z) + \rho_{xy1}(z) \qquad \text{with } \rho_{xy1}(z) = \sum_{r=1}^{n-1} R^r_{xy}\, \mathrm{e}^{-\mu_{xyr} z} \end{aligned} \tag{9.48}$$

where R^r, R^r_{xy}, μ_r, and μ_{xyr} are positive constants. Substituting (9.48) into (9.47), the constitutive equations for sheet metals may be obtained:

$$\begin{aligned} \sigma_x = {} & K^{-3/2} \left[(H+F) \frac{\mathrm{d}\varepsilon^{\mathrm{p}}_x}{\mathrm{d}z} + H \frac{\mathrm{d}\varepsilon^{\mathrm{p}}_y}{\mathrm{d}z} \right] \\ & + K^{-3/2} \int_0^z \rho_1(z-z') \left[(H+F) \frac{\mathrm{d}\varepsilon^{\mathrm{p}}_x}{\mathrm{d}z'} + H \frac{\mathrm{d}\varepsilon^{\mathrm{p}}_y}{\mathrm{d}z'} \right] \mathrm{d}z' \end{aligned} \tag{9.49a}$$

$$\sigma_y = K^{-3/2}\left[(G+H)\frac{d\varepsilon_y^p}{dz} + H\frac{d\varepsilon_x^p}{dz}\right] + K^{-3/2}\int_0^z \rho_1(z-z')\left[(G+H)\frac{d\varepsilon_y^p}{dz'} + H\frac{d\varepsilon_x^p}{dz'}\right]dz' \tag{9.49b}$$

$$\sigma_{xy} = K^{-3/2} + K^{-3/2}\int_0^z \rho_{xy1}(z-z')\left[\frac{M}{N}\frac{d\varepsilon_x^p}{dz'}\right]dz' \tag{9.49c}$$

Denoting

$$\begin{aligned}
\alpha_x &= K^{-3/2}\int_0^z \rho_1(z-z')\left[(H+F)\frac{d\varepsilon_x^p}{dz'} + H\frac{d\varepsilon_y^p}{dz'}\right]dz' \\
\alpha_y &= K^{-3/2}\int_0^z \rho_1(z-z')\left[(G+H)\frac{d\varepsilon_y^p}{dz'} + H\frac{d\varepsilon_x^p}{dz'}\right]dz' \\
\alpha_{xy} &= K^{-3/2}\int_0^z \rho_{xy1}(z-z')\left[\frac{M}{N}\frac{d\varepsilon_x^p}{dz'}\right]dz'
\end{aligned} \tag{9.50}$$

(9.49a,b) may be further written as

$$\begin{aligned}
\left[(H+F)\frac{d\varepsilon_x^p}{d\zeta} + H\frac{d\varepsilon_y^p}{d\zeta}\right] &= \frac{\sigma_x - \alpha_x}{K^{-3/2}f} \\
\left[(G+H)\frac{d\varepsilon_y^p}{d\zeta} + H\frac{d\varepsilon_x^p}{d\zeta}\right] &= \frac{\sigma_y - \alpha_y}{K^{-3/2}f}
\end{aligned} \tag{9.51}$$

which may then be solved for

$$M\frac{d\varepsilon_x^p}{d\zeta} = \frac{(G+H)(\sigma_x - \alpha_x)}{K^{-3/2}f} - \frac{H(\sigma_y - \alpha_y)}{K^{-3/2}f} \tag{9.52a}$$

$$M\frac{d\varepsilon_y^p}{d\zeta} = \frac{(H+F)(\sigma_y - \alpha_y)}{K^{-3/2}f} - \frac{H(\sigma_x - \alpha_x)}{K^{-3/2}f} \tag{9.52b}$$

Also, (9.49c) is rewritten as

$$\frac{M}{N}\frac{d\varepsilon_{xy}^p}{d\zeta} = \frac{\sigma_{xy} - \alpha_{xy}}{K^{-3/2}f} \tag{9.52c}$$

Therefore, in an anisotropic sheet, it takes a multiaxial stress state to produce a single plastic strain component. Equations (9.52) may be viewed as the flow rule using the concept of the flow theory of plasticity. It may be easily

shown that the plastic strain increment as given by (9.52) is normal to the yield surface to be discussed in the next paragraph. We note that, in the theory of Section 9.2.1, the plastic strain increment is necessarily pointing along the radial direction, emanating from the center of the yield surface, and it is not normal to the yield surface after the yield surface has suffered a distortion. Finally, plastic incompressibility is assumed so that

$$\mathrm{d}\varepsilon_x^{\mathrm{p}} + \mathrm{d}\varepsilon_y^{\mathrm{p}} + \mathrm{d}\varepsilon_z^{\mathrm{p}} = 0 \tag{9.53}$$

It was established in [4] that the definition of the intrinsic time determines the form of the yield function. For sheet metals, we now show that the proposed definition of intrinsic time leads to Hill's 1948 quadratic yield criterion. The intrinsic time is defined using the concept of equivalent plastic strain increment discussed in the appendix of [9], that is,

$$\begin{aligned}\mathrm{d}\zeta = \mathrm{d}\bar{\varepsilon} = \Bigg\{ & \frac{(G+H)}{K^3}[(H+F)\mathrm{d}\varepsilon_x^{\mathrm{p}} + H\mathrm{d}\varepsilon_y^{\mathrm{p}}]^2 \\ & - \frac{2H}{K^3}[(H+F)\mathrm{d}\varepsilon_x^{\mathrm{p}} + H\mathrm{d}\varepsilon_y^{\mathrm{p}}][(G+H)\mathrm{d}\varepsilon_y^{\mathrm{p}} + H\mathrm{d}\varepsilon_x^{\mathrm{p}}] \\ & + \frac{(H+F)}{K^3}[(G+H)\mathrm{d}\varepsilon_y^{\mathrm{p}} + H\mathrm{d}\varepsilon_x^{\mathrm{p}}]^2 + \frac{2N}{K^3}\left(\frac{M}{N}\mathrm{d}\varepsilon_{xy}^{\mathrm{p}}\right)^2 \Bigg\}^{1/2}\end{aligned} \tag{9.54}$$

Upon substitution of flow rule (9.51) or (9.52), we obtain from (9.54)

$$\begin{aligned}\Bigg\{ & \frac{(G+H)}{K^3}\left(\frac{\sigma_x - \alpha_x}{K^{-3/2}f}\right)^2 - \frac{2H}{K^3}\left(\frac{\sigma_x - \alpha_x}{K^{-3/2}f}\right)\left(\frac{\sigma_y - \alpha_y}{K^{-3/2}f}\right) \\ & + \frac{(H+F)}{K^3}\left(\frac{\sigma_y - \alpha_y}{K^{-3/2}f}\right)^2 + \frac{2H}{K^3}\left(\frac{\sigma_{xy} - \alpha_{xy}}{K^{-3/2}f}\right)^2 - 1 \Bigg\} \mathrm{d}\zeta^2 = 0\end{aligned} \tag{9.55}$$

Thus, either $\mathrm{d}\zeta = 0$ and the quantity in the bracket $\{\ \} \neq 0$, or $\mathrm{d}\zeta \neq 0$ and the bracket $\{\ \} = 0$. The cases of $\mathrm{d}\zeta = 0$ and $\mathrm{d}\zeta \neq 0$ correspond to the elastic and plastic behavior, respectively. In the latter case, after simplification, we obtain

$$\begin{aligned}& (G+H)(\sigma_x - \alpha_x)^2 - 2H(\sigma_x - \alpha_x)(\sigma_y - \alpha_y) + (H+F)(\sigma_y - \alpha_y)^2 \\ & \quad + 2N(\sigma_{xy} - \alpha_{xy})^2 = f^2\end{aligned} \tag{9.56}$$

This is an extended version of Hill's yield criterion [10]. The isotropic hardening is expressed by f and the kinematic hardening is expressed by α_x, α_y, and α_{xy}. Coefficients F, G, H, and N are determined from experiments that together with the plastic strain ratio $R_\alpha = \mathrm{d}\varepsilon_{y'}^{\mathrm{p}}/\mathrm{d}\varepsilon_{z'}^{\mathrm{p}}$ are discussed further in Chapter 10. The plastic strain ratio is related to the test of a sheet type tension

specimen, where x' is along the longitudinal direction of the specimen, y' is the transverse direction, and $z' = z$.

EXAMPLE 9.1 Show that the flow rule given by (9.52) obeys the normality rule and is normal to the yield surface given by (9.56).

Solution

The yield function from (9.56) is

$$\begin{aligned} 2\phi = {} & (G+H)(\sigma_x - \alpha_x)^2 - 2H(\sigma_x - \alpha_x)(\sigma_y - \alpha_y) \\ & + (H+F)(\sigma_y - \alpha_y)^2 + N(\sigma_{xy} - \alpha_{xy})^2 + N(\sigma_{yx} - \alpha_{yx})^2 - f^2 \end{aligned} \tag{a}$$

Let us perform the following partial differentiation

$$\begin{aligned} \frac{\partial \phi}{\partial \sigma_x} &= (G+H)(\sigma_x - \alpha_x) - H(\sigma_y - \alpha_y) \\ \frac{\partial \phi}{\partial \sigma_y} &= -H(\sigma_x - \alpha_x) + (H+F)(\sigma_y - \alpha_y) \\ \frac{\partial \phi}{\partial \sigma_{xy}} &= N(\sigma_{xy} - \alpha_{xy}) \end{aligned} \tag{b}$$

Comparing (b) with (9.52), we see that the two sets of equations differ only by a scalar multiple factor. Therefore, we may conclude that (9.52) satisfies the normality condition.

9.3 Endochronic Plasticity in the Finite Strain Range

In [11], Valanis considered internal variables $\mathbf{q}^r$ $(r = 1, 2, \ldots, n)$ as quantities which transform as tensors with rotation of the material coordinate system, but remain invariant with rotation of the spatial system. In [12], these variables were regarded as quantities that transform as tensors with rotation of the spatial coordinate system, giving rise to a spatial formulation of the thermodynamics of internal variables. For tensors in the material coordinate system, care was taken to distinguish between the covariant, contravariant, and mixed components. This distinction gave rise to different constitutive equations depending on which components were chosen as independent variables. Valanis [13] further investigated the stress rate and the rate of evolution for the back stress, and recommended that the convected rates be used. He distinguished the convected rate for covariant stress from that for contravariant stress, and applied them to show that, by use of the convected rates, Prager's linear kinematic-hardening rule did not lead to an oscillatory shear stress–strain curve under simple shearing. It is well known

that the shear stress–strain curve oscillates when the Jaumann rate is used (Section 7.6.3). Valanis [13] further mentioned that while the two convected rates have clear and distinct physical meanings, the Jaumann rate is the average of the aforementioned two rates and the physical meaning is obscure. The convected rates are further discussed in Chapter 11 in conjunction with the curvilinear coordinate system.

While the use of a convected rate is most appropriate for stress and kinematic variables, the use of a convected rate for the back stress is questionable. The back stress is a way to represent anisotropy resulting from the change of material texture due to plastic deformation. While Dafalias [14] uses the concept of plastic spin to account for the change of material texture (see Section 7.6.2), he cautions against associating the plastic spin with the general kinematics of deformation. The concept of plastic spin has been introduced into the endochronic theory by Im and Atluri [15] and Wu et al. [5]. We follow [5] in the remaining part of this section. We first discuss the concept of a corotational integral, which is useful in the ensuing discussion of endochronic theory for large strain.

9.3.1 Corotational Integrals

Suppose that a flexible body moves in space. The triad of unit vectors of frame $\bar{x}_i$ that rotates with the body coincides with that of the reference frame x_i at time zero. The two sets of coordinates are related by

$$[\bar{x}] = [M]^{\mathrm{T}}[x] \tag{9.57}$$

where $[M]$ is the matrix of an orthogonal tensor, such that $[M][M]^{\mathrm{T}} = [I]$. Then, the following transformation laws apply

$$\begin{aligned} &[\bar{g}] = [M]^{\mathrm{T}}[g] \qquad [g] = [M][\bar{g}] \\ &[\bar{T}] = [M]^{\mathrm{T}}[T][M] \qquad [T] = [M][\bar{T}][M]^{\mathrm{T}} \end{aligned} \tag{9.58}$$

where $[g]$ is the matrix of a first-rank tensor and $[T]$ is the matrix of a second-rank tensor; $[\bar{g}]$ and $[\bar{T}]$ refer to the $\bar{x}_i$ frame and we may write their corotational derivatives as

$$\left[\overset{\nabla}{g}\right] = [\dot{g}] - [\Omega][g], \qquad \left[\overset{\nabla}{T}\right] = [\dot{T}] - [\Omega][T] + [T][\Omega] \tag{9.59}$$

where

$$[\Omega] = [\dot{M}][M]^{\mathrm{T}} \tag{9.60}$$

and a dot over a tensor denotes its material derivative. It is easy to show that

$$\left[\overset{\nabla}{T}\right] = [M][\dot{\bar{T}}][M]^{\mathrm{T}} = [M]\dot{\overline{[M]^{\mathrm{T}}[T][M]}}[M]^{\mathrm{T}} \tag{9.61}$$

The expressions of (9.61) show that the corotational rate of $\mathbf{T}$ with respect to the reference frame x_i is obtained by finding the material rate of $\bar{\mathbf{T}}$ with respect to frame $\bar{x}_i$ and then transporting the result back to the reference frame x_i. It may be shown that the corotational rate is objective by considering a superposed rigid body rotation $\mathbf{Q}$, such that $[M'] = [Q][M]$. Thus,

$$[\bar{T}] = [QM]^{\mathrm{T}}[T'][QM] = [M]^{\mathrm{T}}[Q]^{\mathrm{T}}[T'][Q][M] = [M]^{\mathrm{T}}[T][M] \tag{9.62}$$

The last expression of (9.62) is obtained from (9.58) and we conclude from (9.62) that

$$[T'] = [Q][T][Q]^{\mathrm{T}} \tag{9.63}$$

Therefore, by using the first expression of (9.61), we obtain

$$\left[\overset{\nabla}{T'}\right] = [M'][\dot{\bar{T}}][M']^{\mathrm{T}} = [Q][M]\left([M]^{\mathrm{T}}\left[\overset{\nabla}{T}\right][M]\right)[M]^{\mathrm{T}}[Q]^{\mathrm{T}} = [Q]\left[\overset{\nabla}{T}\right][Q]^{\mathrm{T}} \tag{9.64}$$

which shows that the corotational rate is objective.

Let us now consider the integral $\Phi\{T\}$ of the second-order objective tensor $\mathbf{T}$ [16,17], which is a function of t and t', that is, $\mathbf{T} = \mathbf{T}(t, t')$. Here, t is the current time and t' is a dummy parameter of integration. Referring to the corotational frame $\bar{x}_i$, the integral is defined as:

$$\Phi\{\bar{T}\} = \int_0^t [\bar{T}(t,t')]\mathrm{d}t' = \int_0^t [M(t')]^{\mathrm{T}}[T(t,t')][M(t')]\mathrm{d}t' = [M(t)]^{\mathrm{T}}\Phi\{T\}[M(t)] \tag{9.65}$$

with

$$\Phi\{T\} = [M(t)]\left[\int_0^t [M(t')]^{\mathrm{T}}[T(t,t')][M(t')]\mathrm{d}t'\right][M(t)]^{\mathrm{T}} \tag{9.66}$$

The integral $\Phi\{T\}$ is known as the corotational integral. Physically, the corotational integral first transfers the tensor $\mathbf{T}$ to the $\bar{x}_i$ frame to obtain $\bar{\mathbf{T}}$ and, after integration in the $\bar{x}_i$ frame, it transports the result back to the x_i frame. Note that $\mathbf{T}(t')$ is a special case of $\mathbf{T}(t, t')$.

Let us consider the expression of the back stress $\boldsymbol{\alpha}$, which will be used later. Let the expression of back stress $\boldsymbol{\alpha}$ for small deformation be

$$\boldsymbol{\alpha} = \int_0^z \mu(z - z') \frac{\mathrm{d}\boldsymbol{\varepsilon}^{\mathrm{p}}}{\mathrm{d}z'} \mathrm{d}z' \tag{9.67}$$

where z is the intrinsic time. We now extend expression (9.67) to large deformation by use of (9.66). The integrand of (9.67) is a second-order tensor, which becomes tensor $\mu(z - z')\mathbf{D}/\dot{z}$ in the case of large deformation. Then $\boldsymbol{\alpha}$ is the corotational integral $\Phi\{\mu(z - z')\mathbf{D}/\dot{z}\}$. It follows from (9.66) that

$$[\alpha] = [M(z)] \left[\int_0^z \mu(z - z') \frac{[M(z')]^{\mathrm{T}}[D][M(z')]}{\dot{z}'} \mathrm{d}z' \right] [M(z)]^{\mathrm{T}} \tag{9.68}$$

On the other hand, by use of (9.61), we obtain the corotational rate of $\boldsymbol{\alpha}$ as

$$\left[\overset{\nabla}{\alpha} \right] = [M][\dot{\bar{\alpha}}][M]^{\mathrm{T}} \tag{9.69}$$

We further determine $\dot{\bar{\boldsymbol{\alpha}}}$ as follows

$$[\dot{\bar{\alpha}}] = \frac{\mathrm{d}[\bar{\alpha}]}{\mathrm{d}t} = \frac{\mathrm{d}[\bar{\alpha}]}{\mathrm{d}z} \frac{\mathrm{d}z}{\mathrm{d}t} = \frac{\mathrm{d}[\bar{\alpha}]}{\mathrm{d}z} \dot{z} \tag{9.70}$$

Note that the dot represents material differentiation. In the study of constitutive equations, $\boldsymbol{\alpha}$ is not a function of x_i and, therefore, the material differentiation is the same as the ordinary differentiation. From (9.58) and (9.68), we obtain

$$[\bar{\alpha}] = [M]^{\mathrm{T}}[\alpha][M] = \int_0^z \mu(z - z') \frac{[M(z')]^{\mathrm{T}}[D][M(z')]}{\dot{z}'} \mathrm{d}z' \tag{9.71}$$

The derivative of (9.71) with respect to z is

$$\frac{[\mathrm{d}\bar{\alpha}]}{\mathrm{d}z} = \mu(0) \frac{[M(z)]^{\mathrm{T}}[D][M(z)]}{\dot{z}} + \int_0^z \frac{\mathrm{d}\mu(z - z')}{\mathrm{d}z} \frac{[M(z')]^{\mathrm{T}}[D][M(z')]}{\dot{z}'} \mathrm{d}z' \tag{9.72}$$

By substituting (9.72) and (9.70) in (9.69), we obtain the corotational rate of $\boldsymbol{\alpha}$ as

$$\left[\overset{\nabla}{\dot{\alpha}} \right] = \dot{z} \left\{ \mu(0) \frac{[D]}{\dot{z}} + [M] \int_0^z \frac{\mathrm{d}\mu(z - z')}{\mathrm{d}z} \frac{[M(z')]^{\mathrm{T}}[D][M(z')]}{\dot{z}'} \mathrm{d}z' [M]^{\mathrm{T}} \right\} \tag{9.73}$$

EXAMPLE 9.2 Show that the corotational integral $\Phi\{T\}$ is objective.

Solution

We consider a superposed rigid-body rotation $\mathbf{Q}$, such that $[M'] = [Q][M]$. With reference to the primed system, (9.65) is written as

$$\Phi\{\bar{T}\} = \int_0^t [\bar{T}(t,t')]\mathrm{d}t' = \int_0^t [M'(t')]^{\mathrm{T}}[T'(t,t')][M'(t')]\mathrm{d}t' = [M'(t)]^{\mathrm{T}}\Phi'\{T'\}[M'(t)] \tag{a}$$

which can be rewritten as

$$\begin{aligned}
\Phi'\{T'\} &= [M'(t)]\left[\int_0^t [M'(t')]^{\mathrm{T}}[T'(t,t')][M'(t')]\mathrm{d}t'\right][M'(t)]^{\mathrm{T}} \\
&= [Q(t)][M(t)]\Bigg[\int_0^t [M(t')]^{\mathrm{T}}[Q(t')]^{\mathrm{T}}[Q(t')][T(t,t')][Q(t')]^{\mathrm{T}} \\
&\quad \times [Q(t')][M(t')]\mathrm{d}t'\Bigg][M(t)]^{\mathrm{T}}[Q(t)]^{\mathrm{T}} \\
&= [Q(t)][M(t)]\left[\int_0^t [M(t')]^{\mathrm{T}}[T(t,t')][M(t')]\mathrm{d}t'\right][M(t)]^{\mathrm{T}}[Q(t)]^{\mathrm{T}} \\
&= [Q(t)]\Phi\{T\}[Q(t)]^{\mathrm{T}}
\end{aligned} \tag{b}$$

Equation (b) shows that the corotational integral $\Phi\{T\}$ is objective.

EXAMPLE 9.3 Show that the corotational integration of the corotational derivative $\overset{\nabla}{\mathbf{T}}$ recovers the original tensor $\mathbf{T}$, if $\mathbf{T} = \mathbf{T}(t')$, that is, $\mathbf{T}$ is not a function of t.

Solution

From (9.66) and using the first equation of (9.61), the corotational integral of $\overset{\nabla}{\mathbf{T}}$ is

$$\begin{aligned}
\Phi\left\{\overset{\nabla}{T}\right\} &= [M(t)]\left[\int_0^t [M(t')]^{\mathrm{T}}\left[\overset{\nabla}{T}(t')\right][M(t')]\mathrm{d}t'\right][M(t)]^{\mathrm{T}} \\
&= [M(t)]\int_0^t [\dot{\bar{T}}(t')]\mathrm{d}t'[M(t)]^{\mathrm{T}} = [M(t)][\bar{T}][M(t)]^{\mathrm{T}} = [T]
\end{aligned} \tag{a}$$

Equation (a) demonstrates that the corotational integral of a corotational rate of a tensor is the tensor itself. Therefore, the corotational integral is the inverse operation of the corotational derivative.

EXAMPLE 9.4 Consider the integral for small deformation given by

$$\boldsymbol{\alpha} = \int_0^z \mu(z - z') \frac{\mathrm{d}\boldsymbol{\varepsilon}^{\mathrm{p}}}{\mathrm{d}z'} \mathrm{d}z' \tag{a}$$

In the case of $\mu(z) = \mu_0 \mathrm{e}^{-\lambda z}$, where μ_0 and λ are constant parameters, the differentiation of (a) gives rise to

$$\dot{\boldsymbol{\alpha}} = \mu_0 \dot{\boldsymbol{\varepsilon}}^{\mathrm{p}} - \lambda \boldsymbol{\alpha} \dot{z} \tag{b}$$

In the case of $\mu(z) = \mu_1 \mathrm{e}^{-\lambda z} + \mu_2$, where $\mu(0) = \mu_1 + \mu_2$, μ_1, μ_2, and λ are constant parameters, the differentiation of (a) gives rise to

$$\dot{\boldsymbol{\alpha}} = \mu(0) \dot{\boldsymbol{\varepsilon}}^{\mathrm{p}} - \lambda \boldsymbol{\alpha} \dot{z} + \lambda \mu_2 \dot{z} \boldsymbol{\varepsilon}^{\mathrm{p}} \tag{c}$$

Extend (a) to large deformation and determine the corotational rates.

Solution

For the case of $\mu(z) = \mu_0 \mathrm{e}^{-\lambda z}$, $\mathrm{d}\mu(z - z')/\mathrm{d}z = -\lambda \mu_0 \mathrm{e}^{-\lambda(z - z')}$, (9.73) becomes

$$\begin{aligned} \left[\overset{\nabla}{\alpha} \right] &= \mu(0)[D] + \dot{z} \left\{ [M] \int_0^z (-\lambda) \mu_0 \mathrm{e}^{-\lambda(z - z')} \frac{[M(z')]^{\mathrm{T}} [D] [M(z')]}{\dot{z}'} \mathrm{d}z' [M]^{\mathrm{T}} \right\} \\ &= \mu_0 [D] - \lambda \dot{z} [\alpha] \end{aligned} \tag{d}$$

Note that (d) is in the same form as (b). When $\mu(z) = \mu_1 \mathrm{e}^{-\lambda z} + \mu_2$, then from (9.68)

$$\begin{aligned} [\alpha] &= [M(z)] \left[\int_0^z \mu_1 \mathrm{e}^{-\lambda(z - z')} \frac{[M(z')]^{\mathrm{T}} [D] [M(z')]}{\dot{z}'} \mathrm{d}z' \right] [M(z)]^{\mathrm{T}} \\ &\quad + [M(z)] \left[\int_0^z \mu_2 \frac{[M(z')]^{\mathrm{T}} [D] [M(z')]}{\dot{z}'} \mathrm{d}z' \right] [M(z)]^{\mathrm{T}} \\ &= [\alpha]^{(1)} + [\alpha]^{(2)} \end{aligned} \tag{e}$$

where

$$\begin{aligned} [\alpha]^{(1)} &= [M(z)] \left[\int_0^z \mu_1 \mathrm{e}^{-\lambda(z - z')} \frac{[M(z')]^{\mathrm{T}} [D] [M(z')]}{\dot{z}'} \mathrm{d}z' \right] [M(z)]^{\mathrm{T}} \\ [\alpha]^{(2)} &= [M(z)] \left[\int_0^z \mu_2 \frac{[M(z')]^{\mathrm{T}} [D] [M(z')]}{\dot{z}'} \mathrm{d}z' \right] [M(z)]^{\mathrm{T}} \end{aligned} \tag{f}$$

The integral on the right-hand side of (9.73) is

$$[M]\int_0^z \frac{\mathrm{d}\mu(z-z')}{\mathrm{d}z}\frac{[M(z')]^{\mathrm{T}}[D][M(z')]}{\dot{z}'}\mathrm{d}z'[M]^{\mathrm{T}}$$
$$= -\lambda[M(z)]\left[\int_0^z \mu_1 \mathrm{e}^{-\lambda(z-z')}\frac{[M(z')]^{\mathrm{T}}[D][M(z')]}{\dot{z}'}\mathrm{d}z'\right][M(z)]^{\mathrm{T}} = -\lambda[\alpha]^{(1)} \tag{g}$$

Substituting (g) into (9.73), we obtain

$$\left[\overset{\nabla}{\alpha}\right] = \mu(0)[D] - \lambda[\alpha]^{(1)}\dot{z} = \mu(0)[D] - \lambda[\alpha]\dot{z} + \lambda[\alpha]^{(2)}\dot{z} \tag{h}$$

The corotational derivative (h) is not quite of the same form as (c).

9.3.2 Endochronic Equations for Finite Plastic Deformation

In the small strain range, the endochronic constitutive equation is from (8.93) and (8.125)

$$\boldsymbol{\sigma}' = \sigma_{\mathrm{y}}'\frac{\mathrm{d}\boldsymbol{\varepsilon}^{\mathrm{p}}}{\mathrm{d}z} + \int_0^z \mu(z-z')\frac{\mathrm{d}\boldsymbol{\varepsilon}^{\mathrm{p}}}{\mathrm{d}z'}\mathrm{d}z' \tag{9.74}$$

The intrinsic time is

$$\mathrm{d}\zeta^2 = \mathrm{d}\boldsymbol{\varepsilon}^{\mathrm{p}}\cdot\mathrm{d}\boldsymbol{\varepsilon}^{\mathrm{p}} \qquad \text{with } \frac{\mathrm{d}\zeta}{\mathrm{d}z} = f(z) \tag{9.75}$$

The following yield function may be derived

$$(\boldsymbol{\sigma}'-\boldsymbol{\alpha})\cdot(\boldsymbol{\sigma}'-\boldsymbol{\alpha}) = (\sigma_y' f(z))^2 \tag{9.76}$$

with the flow rule given by

$$\mathrm{d}\boldsymbol{\varepsilon}^{\mathrm{p}} = \frac{\mathrm{d}z}{\sigma_{\mathrm{y}}'}(\boldsymbol{\sigma}'-\boldsymbol{\alpha}) \tag{9.77}$$

where $f(z)$ is the isotropic hardening function and $\boldsymbol{\alpha}$ is the back stress given by

$$\boldsymbol{\alpha} = \int_0^z \mu(z-z')\frac{\mathrm{d}\boldsymbol{\varepsilon}^{\mathrm{p}}}{\mathrm{d}z'}\mathrm{d}z' \tag{9.78}$$

This set of equations will now be extended to the finite strain range by use of stress and strain measures for finite deformation, the concept of corotational derivative and corotational integral, and the concept of constitutive

spin (Section 7.6.2). To this end, (9.75) and (9.77) are written as

$$\dot{\zeta}^2 = \mathbf{D}^{\mathrm{p}} \cdot \mathbf{D}^{\mathrm{p}} \tag{9.79}$$

$$\mathbf{D}^{\mathrm{p}} = \frac{1}{\sigma'_{\mathrm{y}}}(\boldsymbol{\sigma}' - \boldsymbol{\alpha})\dot{z} \tag{9.80}$$

We extend (9.78) to large deformation by use of (9.66) and the resulting equation, (9.68), is

$$\boldsymbol{\alpha} = \mathbf{M}(z) \cdot \left[\int_0^z \mu(z - z') \frac{\mathbf{M}^{\mathrm{T}}(z') \cdot \mathbf{D}^{\mathrm{p}} \cdot \mathbf{M}(z')}{\dot{z}'} \mathrm{d}z' \right] \cdot \mathbf{M}^{\mathrm{T}}(z) \tag{9.81}$$

The integration in (9.81) is with respect to z', which is not t' as in (9.66). The intrinsic time z is a monotonically increasing parameter and it does not change during elastic deformation or rigid-body rotation. In general, $\mathbf{M}(z)$ is not a unique function of z, because rotation may continue even when z is not changing. This multivalued association of $\mathbf{M}(z)$ to z does not invalidate the meaning of integral (9.81), as pointed out by Dafalias [17].

For simplicity in the subsequent calculations, we consider

$$\mu(z) = \mu_1 \exp(-\lambda z) + \mu_2 \tag{9.82}$$

The corresponding corotational rate of $\boldsymbol{\alpha}$ has been found in Example 9.5 to be

$$\overset{\nabla}{\boldsymbol{\alpha}} = (\mu_1 + \mu_2)\mathbf{D}^{\mathrm{p}} - \lambda \boldsymbol{\alpha} \dot{z} + \lambda \boldsymbol{\alpha}^{(2)} \dot{z} \tag{9.83}$$

where

$$\boldsymbol{\alpha}^{(2)} = \mu_2 \, \mathbf{M}(z) \cdot \left[\int_0^z \frac{\mathbf{M}^{\mathrm{T}}(z') \cdot \mathbf{D}^{\mathrm{p}} \cdot \mathbf{M}(z')}{\dot{z}'} \mathrm{d}z' \right] \cdot \mathbf{M}^{\mathrm{T}}(z) \tag{9.84}$$

Equation (9.83) is the evolution equation of the back stress in terms of the plastic strain rate $\mathbf{D}^{\mathrm{p}}$, the back stress $\boldsymbol{\alpha}$, and the intrinsic time z. Note that (9.83) is in the incremental form, except for $\boldsymbol{\alpha}^{(2)}$, which is represented by an integral in (9.84). It is shown in the next section that in solving the problem of a thin-walled tube under torsion, this integral may be integrated so that (9.83) becomes a truly incremental form.

The plastic spin, from (7.100), may be written as

$$\mathbf{W}^{\mathrm{p}} = \frac{C_1 \dot{\zeta}}{(\sigma'_{\mathrm{y}} f(z))^2} (\boldsymbol{\alpha} \cdot \boldsymbol{\sigma}' - \boldsymbol{\sigma}' \cdot \boldsymbol{\alpha}) \tag{9.85}$$

where C_1 is dimensionless and is a scalar function of the isotropic invariants of $\boldsymbol{\sigma}'$ and $\boldsymbol{\alpha}$. Using the second expression of (9.75) and the flow rule (9.80), (9.85) becomes

$$\begin{aligned}\mathbf{W}^{\mathrm{p}} &= \frac{C_1 f(z)\dot{z}}{(\sigma_y' f(z))^2}(\boldsymbol{\alpha}\cdot\boldsymbol{\sigma}' - \boldsymbol{\alpha}^2 + \boldsymbol{\alpha}^2 - \boldsymbol{\sigma}'\cdot\boldsymbol{\alpha}) \\ &= \frac{C_1}{\boldsymbol{\sigma}_y' f(z)}\left[\boldsymbol{\alpha}\cdot\frac{(\boldsymbol{\sigma}'-\boldsymbol{\alpha})\dot{z}}{\sigma_y'} + \frac{(\boldsymbol{\alpha}-\boldsymbol{\sigma}')\dot{z}}{\sigma_y'}\cdot\boldsymbol{\alpha}\right] \\ &= \frac{C_1}{\sigma_y' f(z)}(\boldsymbol{\alpha}\cdot\mathbf{D}^{\mathrm{p}} - \mathbf{D}^{\mathrm{p}}\cdot\boldsymbol{\alpha}) = K(\boldsymbol{\alpha}\cdot\mathbf{D}^{\mathrm{p}} - \mathbf{D}^{\mathrm{p}}\cdot\boldsymbol{\alpha}) \qquad \text{with } K = \frac{C_1}{\sigma_y' f(z)}\end{aligned} \tag{9.86}$$

The above expression is the same as (7.101). Equation (9.86) together with (7.138) is substituted into (9.83) when the corotational rate is used in the calculation.

9.3.3 Application to a Rigid-Plastic Thin-Walled Tube Under Torsion

In the consideration of a thin-walled tube under torsion in the large strain range, the elastic strain is neglected, so that the condition of plastic incompressibility is represented by

$$\dot{\varepsilon}_r + \dot{\varepsilon}_\theta + \dot{\varepsilon}_z = 0 \tag{9.87}$$

where $\dot{\varepsilon}_r$ denotes the plastic strain-rate in the radial direction; $\dot{\varepsilon}_\theta$ denotes the plastic strain-rate in the tangential direction; and $\dot{\varepsilon}_z$ denotes the plastic strain-rate in the axial direction of the tube. The plastic shear strain 2η is related to the angle of twist per unit length φ by

$$2\eta = r\varphi \tag{9.88}$$

in which r is the outer radius of the tube. The rate of deformation and spin tensors are expressed as

$$[D^{\mathrm{p}}] = \begin{bmatrix} \dot{\varepsilon}_r & 0 & 0 \\ 0 & \dot{\varepsilon}_\theta & \dot{\eta} \\ 0 & \dot{\eta} & \dot{\varepsilon}_z \end{bmatrix}, \qquad [W] = \begin{bmatrix} 0 & 0 & 0 \\ 0 & 0 & \dot{\eta} \\ 0 & -\dot{\eta} & 0 \end{bmatrix} \tag{9.89}$$

The equations in (9.89) are now used to derive the explicit expressions for plastic spin and back stress. Let the back stress be symmetric so that

$$[\alpha] = \begin{bmatrix} \alpha_{rr} & 0 & 0 \\ 0 & \alpha_{\theta\theta} & \alpha_{\theta z} \\ 0 & \alpha_{\theta z} & \alpha_{zz} \end{bmatrix} \tag{9.90}$$

Then, since $\mathbf{D}^{\mathrm{p}}$ and $\boldsymbol{\alpha}$ are symmetric, we note that $\mathbf{D}^{\mathrm{p}} \cdot \boldsymbol{\alpha} = (\boldsymbol{\alpha} \cdot \mathbf{D}^{\mathrm{p}})^{\mathrm{T}}$. Therefore,

$$\boldsymbol{\alpha} \cdot \mathbf{D}^{\mathrm{p}} - \mathbf{D}^{\mathrm{p}} \cdot \boldsymbol{\alpha} = \begin{bmatrix} 0 & 0 & 0 \\ 0 & 0 & (\alpha_{\theta\theta} - \alpha_{zz})\dot{\eta} + \alpha_{\theta z}(\dot{\varepsilon}_z - \dot{\varepsilon}_\theta) \\ 0 & -(\alpha_{\theta\theta} - \alpha_{zz})\dot{\eta} - \alpha_{\theta z}(\dot{\varepsilon}_z - \dot{\varepsilon}_\theta) & 0 \end{bmatrix} \tag{9.91}$$

Equation (9.91) is substituted in (9.86) to calculate the plastic spin $\mathbf{W}^{\mathrm{p}}$. On the other hand, the constitutive spin $\boldsymbol{\omega}$ is defined in (7.97) as

$$\boldsymbol{\omega} = \mathbf{W} - \mathbf{W}^{\mathrm{p}} = \begin{bmatrix} 0 & 0 & 0 \\ 0 & 0 & -\omega \\ 0 & \omega & 0 \end{bmatrix} \tag{9.92}$$

where

$$\omega = K[(\alpha_{\theta\theta} - \alpha_{zz})\dot{\eta} + \alpha_{\theta z}(\dot{\varepsilon}_z - \dot{\varepsilon}_\theta)] - \dot{\eta} \tag{9.93}$$

Since the tensor $\boldsymbol{\alpha}$ is symmetric and the tensor $\boldsymbol{\omega}$ is antisymmetric, we have $\boldsymbol{\alpha} \cdot \boldsymbol{\omega} = -(\boldsymbol{\omega} \cdot \boldsymbol{\alpha})^{\mathrm{T}}$. Therefore, in order to find explicit expressions for the corotational rate, we first find

$$\boldsymbol{\omega} \cdot \boldsymbol{\alpha} - \boldsymbol{\alpha} \cdot \boldsymbol{\omega} = \begin{bmatrix} 0 & 0 & 0 \\ 0 & -2\omega\alpha_{\theta z} & -\omega(\alpha_{zz} - \alpha_{\theta\theta}) \\ 0 & -\omega(\alpha_{zz} - \alpha_{\theta\theta}) & 2\omega\alpha_{\theta z} \end{bmatrix} \tag{9.94}$$

Using (9.59), the corotational derivative of $\boldsymbol{\alpha}$ is

$$\overset{\nabla}{\boldsymbol{\alpha}} = \dot{\boldsymbol{\alpha}} - \boldsymbol{\omega} \cdot \boldsymbol{\alpha} + \boldsymbol{\alpha} \cdot \boldsymbol{\omega} \tag{9.95}$$

We then obtain the following expressions by combining (9.95) and (9.83)

$$\dot{\boldsymbol{\alpha}} = \boldsymbol{\omega} \cdot \boldsymbol{\alpha} - \boldsymbol{\alpha} \cdot \boldsymbol{\omega} + \overset{\nabla}{\boldsymbol{\alpha}} = (\boldsymbol{\omega} \cdot \boldsymbol{\alpha} - \boldsymbol{\alpha} \cdot \boldsymbol{\omega}) + (\mu_1 + \mu_2)\mathbf{D}^{\mathrm{p}} - \lambda\boldsymbol{\alpha}\dot{z} + \lambda\boldsymbol{\alpha}^{(2)}\dot{z} \tag{9.96}$$

where, from (9.84),

$$\boldsymbol{\alpha}^{(2)} = \mu_2 \int_0^z \frac{\mathbf{D}^{\mathrm{p}}}{\dot{z}'} \mathrm{d}z' \tag{9.97}$$

In the last expression, it has been assumed that the corotational axes are parallel to the reference axes, so that $\mathbf{M} = \mathbf{1}$. This is indeed the case for the torsion problems under consideration. The deformation is homogeneous

without rigid-body motion of the tube and the angle of twist per unit length is constant along the tube.

In the numerical calculation, we can define a tensor $\boldsymbol{\kappa}$ as

$$\boldsymbol{\kappa} = \boldsymbol{\omega}\,\mathrm{d}t = \begin{bmatrix} 0 & 0 & 0 \\ 0 & 0 & -\kappa \\ 0 & \kappa & 0 \end{bmatrix} \tag{9.98}$$

in which the following expression has been determined by use of (9.93)

$$\kappa = \omega\,\mathrm{d}t = K[(\alpha_{\theta\theta} - \alpha_{zz})\mathrm{d}\eta + \alpha_{\theta z}(\mathrm{d}\varepsilon_z - \mathrm{d}\varepsilon_\theta)] - \mathrm{d}\eta \tag{9.99}$$

Then, (9.96) reduces to

$$\mathrm{d}\boldsymbol{\alpha} = (\boldsymbol{\kappa}\cdot\boldsymbol{\alpha} - \boldsymbol{\alpha}\cdot\boldsymbol{\kappa}) + (\mu_1 + \mu_2)\mathbf{D}^{\mathrm{p}}\,\mathrm{d}t - \lambda\,\boldsymbol{\alpha}\,\mathrm{d}z + \lambda\,\boldsymbol{\alpha}^{(2)}\,\mathrm{d}z \tag{9.100}$$

The equations derived in this section can be used to describe the response of a thin-walled tube subjected to various combined axial–torsion loading conditions. Two special cases are considered in the following paragraphs.

9.3.3.1 Torsion with axial prestress

Denoting the axial prestress by $\sigma_z = \sigma_{\mathrm{c}} = \text{constant}$, the stress tensor and the deviatoric stress tensor are

$$[\sigma] = \begin{bmatrix} 0 & 0 & 0 \\ 0 & 0 & \tau \\ 0 & \tau & \sigma_{\mathrm{c}} \end{bmatrix} \quad \text{and} \quad [\sigma'] = \begin{bmatrix} \dfrac{-\sigma_{\mathrm{c}}}{3} & 0 & 0 \\ 0 & \dfrac{-\sigma_{\mathrm{c}}}{3} & \tau \\ 0 & \tau & \dfrac{2\sigma_{\mathrm{c}}}{3} \end{bmatrix} \tag{9.101}$$

Note that the hoop stress σ_θ is zero due to symmetry. The flow rule is, from (9.80), (9.89), (9.90), and (9.101), written as

$$\begin{aligned} \frac{\mathrm{d}\varepsilon_r}{\mathrm{d}z} &= -\frac{\sigma_{\mathrm{c}}/3 + \alpha_{rr}}{\sigma'_{\mathrm{y}}}, & \frac{\mathrm{d}\varepsilon_\theta}{\mathrm{d}z} &= -\frac{\sigma_{\mathrm{c}}/3 + \alpha_{\theta\theta}}{\sigma'_{\mathrm{y}}} \\ \frac{\mathrm{d}\varepsilon_z}{\mathrm{d}z} &= \frac{2\sigma_{\mathrm{c}}/3 - \alpha_{zz}}{\sigma'_{\mathrm{y}}}, & \frac{\mathrm{d}\eta}{\mathrm{d}z} &= \frac{\tau - \alpha_{\theta z}}{\sigma'_{\mathrm{y}}} \end{aligned} \tag{9.102}$$

The intrinsic time is then given from (9.79) and (9.89) by

$$\dot{\zeta}^2 = \dot{\varepsilon}_r^2 + \dot{\varepsilon}_\theta^2 + \dot{\varepsilon}_z^2 + 2\dot{\eta}^2 = \dot{z}^2 f^2(z) \tag{9.103}$$

Therefore,

$$\dot{\eta}^2 = \tfrac{1}{2}\left[\dot{z}^2 f^2(z) - \left(\dot{\varepsilon}_r^2 + \dot{\varepsilon}_\theta^2 + \dot{\varepsilon}_z^2\right)\right] \tag{9.104}$$

By use of (9.87), (9.104) reduces to

$$\begin{aligned}\dot{\eta}^2 &= \frac{1}{2}\left[\dot{z}^2 f^2(z) - 2\left(\dot{\varepsilon}_z^2 - \dot{\varepsilon}_\theta \dot{\varepsilon}_r\right)\right] \\ &= \frac{1}{2}\dot{z}^2\left\{f^2(z) - 2\left[\left(\frac{\mathrm{d}\varepsilon_z}{\mathrm{d}z}\right)^2 - \left(\frac{\mathrm{d}\varepsilon_\theta}{\mathrm{d}z}\right)\left(\frac{\mathrm{d}\varepsilon_r}{\mathrm{d}z}\right)\right]\right\}\end{aligned} \tag{9.105}$$

Substituting (9.102) in (9.105), we then obtain

$$\pm \mathrm{d}\eta = \mathrm{d}z\sqrt{\frac{1}{2}f^2(z) - \left(\frac{1}{\sigma_y'}\right)^2\left[\left(\frac{2\sigma_c}{3} - \alpha_{zz}\right)^2 - \left(\frac{\sigma_c}{3} + \alpha_{rr}\right)\left(\frac{\sigma_c}{3} + \alpha_{\theta\theta}\right)\right]} \tag{9.106}$$

The "+" sign is for loading and "−" is for unloading.

To perform the numerical calculation of $\mathrm{d}\boldsymbol{\alpha}$ by use of (9.100), $\boldsymbol{\alpha}^{(2)}$ must first be determined. To obtain $\alpha_{\theta z}^{(2)}$ from (9.97), we use (9.89) to get

$$\alpha_{\theta z}^{(2)} = \mu_2 \int_0^z \frac{D_{\theta z}^{\mathrm{p}}}{\dot{z}'}\mathrm{d}z' = \mu_2 \int_{\eta(0)}^{\eta(z)} \mathrm{d}\eta = \mu_2 \eta \tag{9.107}$$

In the last expression, the limits of integration are $\eta(0) = 0$ and $\eta(z) = \eta$. Similarly, we obtain the following components for $\boldsymbol{\alpha}^{(2)}$ during loading

$$\alpha_{rr}^{(2)} = \mu_2 \varepsilon_{\mathrm{r}}, \qquad \alpha_{\theta\theta}^{(2)} = \mu_2 \varepsilon_\theta, \qquad \alpha_{zz}^{(2)} = \mu_2 \varepsilon_z \tag{9.108}$$

Therefore, from (9.98), (9.100), (9.107), and (9.108), we obtain the following equations

$$\begin{aligned}\mathrm{d}\alpha_{rr} &= (\mu_1 + \mu_2)\mathrm{d}\varepsilon_r - \lambda\alpha_{rr}\,\mathrm{d}z + \lambda\mu_2\varepsilon_r\,\mathrm{d}z \\ \mathrm{d}\alpha_{\theta\theta} &= -2\alpha_{\theta z}\kappa + (\mu_1 + \mu_2)\mathrm{d}\varepsilon_\theta - \lambda\alpha_{\theta\theta}\,\mathrm{d}z + \lambda\mu_2\varepsilon_\theta\,\mathrm{d}z \\ \mathrm{d}\alpha_{zz} &= 2\alpha_{\theta z}\kappa + (\mu_1 + \mu_2)\mathrm{d}\varepsilon_z - \lambda\alpha_{zz}\,\mathrm{d}z + \lambda\mu_2\varepsilon_z\,\mathrm{d}z \\ \mathrm{d}\alpha_{\theta z} &= (\alpha_{\theta\theta} - \alpha_{zz})\kappa + (\mu_1 + \mu_2)\mathrm{d}\eta - \lambda\alpha_{\theta z}\,\mathrm{d}z + \lambda\mu_2\eta\,\mathrm{d}z\end{aligned} \tag{9.109}$$

with the initial conditions $\eta(0) = 0$, $\varepsilon_i(0) = 0$, and $\alpha_{ij}(0) = 0$. Thus, in a step-by-step calculation, we can use

$$\begin{aligned}&\boldsymbol{\alpha} = \boldsymbol{\alpha} + \mathrm{d}\boldsymbol{\alpha}, \qquad \varepsilon_r = \varepsilon_r + \mathrm{d}\varepsilon_r, \qquad \varepsilon_\theta = \varepsilon_\theta + \mathrm{d}\varepsilon_\theta, \\ &\varepsilon_z = \varepsilon_z + \mathrm{d}\varepsilon_z, \qquad \eta = \eta + \mathrm{d}\eta\end{aligned} \tag{9.110}$$

Finally, we note that for the case of free-end torsion, the ends of the specimen are totally unconstrained with $\sigma_c = 0$. Thus, the equations for free-end torsion may be obtained by setting $\sigma_c = 0$ in the equations of this subsection.

9.3.3.2 Fixed-end torsion

In the case of fixed-end torsion, $\dot{\varepsilon}_z = 0$. Assuming incompressibility, we find from (9.87) that $\dot{\varepsilon}_\theta = -\dot{\varepsilon}_r \neq 0$. Hence, (9.89) becomes

$$[D^{\mathrm{p}}] = \begin{bmatrix} \dot{\varepsilon}_r & 0 & 0 \\ 0 & -\dot{\varepsilon}_r & \dot{\eta} \\ 0 & \dot{\eta} & 0 \end{bmatrix} \tag{9.111}$$

Note that this is different from the simple shear assumption where $\dot{\varepsilon}_\theta = 0$. The stress tensor and the deviatoric stress tensor are

$$[\sigma] = \begin{bmatrix} 0 & 0 & 0 \\ 0 & 0 & \tau \\ 0 & \tau & \sigma \end{bmatrix} \quad \text{and} \quad [\sigma'] = \begin{bmatrix} \dfrac{-\sigma}{3} & 0 & 0 \\ 0 & \dfrac{-\sigma}{3} & \tau \\ 0 & \tau & \dfrac{2\sigma}{3} \end{bmatrix} \tag{9.112}$$

in which $\boldsymbol{\sigma}$ may vary. Again, we mention that the hoop stress is zero, which is different from the simple shear assumption that $\sigma_\theta \neq 0$. The flow rule, from (9.80), has the following component equations:

$$\begin{aligned} &\frac{\mathrm{d}\varepsilon_r}{\mathrm{d}z} = -\frac{\sigma/3 + \alpha_{rr}}{\sigma'_{\mathrm{y}}}, \qquad \frac{\mathrm{d}\varepsilon_\theta}{\mathrm{d}z} = -\frac{\sigma/3 + \alpha_{\theta\theta}}{\sigma'_{\mathrm{y}}}, \\ &\alpha_{zz} = \frac{2\sigma}{3}, \qquad \frac{\mathrm{d}\eta}{\mathrm{d}z} = \frac{\tau - \alpha_{\theta z}}{\sigma'_{\mathrm{y}}} \end{aligned} \tag{9.113}$$

The first two equations of (9.113) may be combined to yield

$$\frac{\mathrm{d}\varepsilon_r}{\mathrm{d}z} = \frac{\alpha_{\theta\theta} - \alpha_{rr}}{2\sigma'_{\mathrm{y}}} \tag{9.114}$$

The intrinsic time is then, from (9.79) and (9.111), given by

$$\dot{\xi}^2 = 2\dot{\varepsilon}_r^2 + 2\dot{\eta}^2 = \dot{z}^2 f^2(z) \tag{9.115}$$

Therefore,

$$\dot{\eta}^2 = \dot{z}^2 \left\{ \frac{1}{2} f^2(z) - \left(\frac{\mathrm{d}\varepsilon_r}{\mathrm{d}z} \right)^2 \right\} \tag{9.116}$$

Then, by substituting (9.114) in (9.116), we obtain

$$\pm \mathrm{d}\eta = \frac{\mathrm{d}z}{2} \sqrt{2f^2(z) - \left(\frac{\alpha_{\theta\theta} - \alpha_{rr}}{\sigma'_{\mathrm{y}}} \right)^2} \tag{9.117}$$

The "+" sign is for loading and "−" is for unloading.

We may also obtain the following components of $\boldsymbol{\alpha}^{(2)}$ by using the same procedure as that which leads to (9.107) and (9.108)

$$\alpha^{(2)}_{\theta z} = \mu_2 \eta, \qquad \alpha^{(2)}_{rr} = \mu_2 \varepsilon_r, \qquad \alpha^{(2)}_{\theta\theta} = -\mu_2 \varepsilon_r, \qquad \alpha^{(2)}_{zz} = 0 \tag{9.118}$$

Therefore, from (9.98) to (9.100) and (9.118), we obtain the following component equations

$$\begin{aligned}
\mathrm{d}\alpha_{rr} &= (\mu_1 + \mu_2)\mathrm{d}\varepsilon_r - \lambda\alpha_{rr}\,\mathrm{d}z + \lambda\mu_2\varepsilon_r\,\mathrm{d}z \\
\mathrm{d}\alpha_{\theta\theta} &= -2\alpha_{\theta z}\kappa - (\mu_1 + \mu_2)\mathrm{d}\varepsilon_r - \lambda\alpha_{\theta\theta}\,\mathrm{d}z - \lambda\mu_2\varepsilon_r\,\mathrm{d}z \\
\mathrm{d}\alpha_{zz} &= 2\alpha_{\theta z}\kappa - \lambda\alpha_{zz}\,\mathrm{d}z \\
\mathrm{d}\alpha_{\theta z} &= (\alpha_{\theta\theta} - \alpha_{zz})\kappa + (\mu_1 + \mu_2)\mathrm{d}\eta - \lambda\alpha_{\theta z}\mathrm{d}z + \lambda\mu_2\eta\,\mathrm{d}z
\end{aligned} \tag{9.119}$$

with the initial conditions $\eta(0) = 0$, $\varepsilon_r(0) = 0$, and $\alpha_{ij}(0) = 0$. We again use (9.110) for a step-by-step calculation.

9.3.3.3 Comparison of theoretical and experimental results

In this section, we compare the theoretical and experimental results initially presented in [5] and reprinted here with permission from Elsevier. There are seven material constants in this model: c, β, C_1, σ'_{y}, μ_1, μ_2, and λ where c and β are used in the isotropic-hardening function $f(z)$ and describe the rate and saturation value of isotropic hardening; C_1 fixes the magnitude of plastic spin; σ'_{y} is a material constant proportional to the initial yield stress in shear ($\sigma'_{\mathrm{y}} = \sqrt{2}\tau_{\mathrm{y}}$); and μ_1, μ_2, and λ are used in the kernel function $\mu(z)$, which describes the evolution of back stress. These material constants are determined by fitting the theory to the experimental stress–strain curve during loading. After they have been determined, the constitutive equations are applied to predict experimental results of specimens subjected to different loading conditions. Three different materials have been investigated, 70 : 30 brass, Ni-200, and Al-1100. All shear strains reported in the experimental results are for the outer surface of the tubular specimen.

For the 70 : 30 brass material, the material constants have been determined to fit the experimental data of Stout (reported in Im and Atluri [15]) for the case of simple torsion (Figure 9.1). The constants are $c = 3.1$, $\beta = 15.4$, $C_1 = 4.5$, $\sigma'_{\mathrm{y}} = 90$ MPa, $\mu_1 = 200$ MPa, $\mu_2 = 50$ MPa, and $\lambda = 7.2$. These constants are then used in the equations for torsion with axial stress $\sigma_{\mathrm{c}} = 0$ (equations in Section 9.3.3.1) to predict behavior of the same material for two different strain paths, that is, monotonic and cyclic free-end torsion. The strain range of the monotonic torsion is from 0 to 4, whereas the specimen under cyclic loading is strained from 0 to 1.7, unstrained back to 0, and then restrained to 2.0. The results found from this theory are compared with the experimental data of Swift [18]. Figure 9.2 shows the axial strain of both monotonic and cyclic free-end torsion. It is seen that the theory does predict the trend of variation for the axial strain during torsion. We note that experiments of Swift and Stout were conducted in different laboratories and material conditions, and

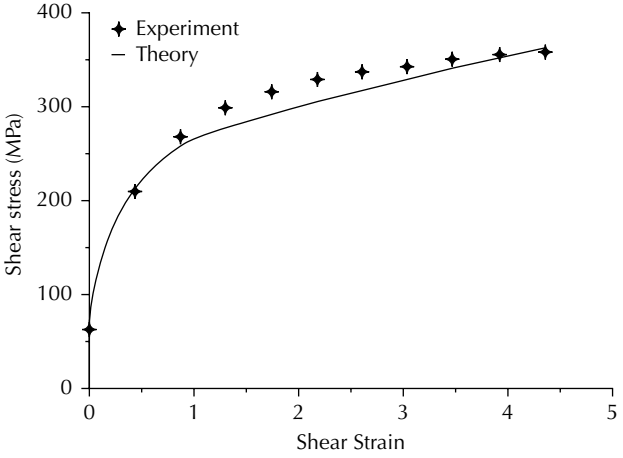

FIGURE 9.1
Shear stress–strain curve of 70 : 30 brass (From Wu, H.C. et al., *Int. J. Solids Struct.*, 32, 1079, 1995. With permission from Elsevier).

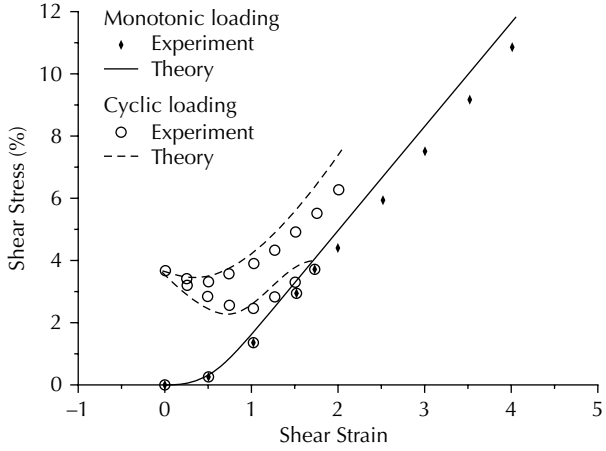

FIGURE 9.2
Axial strain versus shear strain for 70 : 30 brass (From Wu, H.C. et al., *Int. J. Solids Struct.*, 32, 1079, 1995. With permission from Elsevier).

the agreement demonstrated here is therefore considered as very satisfactory. The effect of C_1 is investigated and shown in Figure 9.3 for 70 : 30 brass. This figure shows the dependence of the axial strain on C_1 in the case of monotonic free-end torsion. It is seen that a suitable C_1 can be determined to achieve a good agreement with the experimental results.

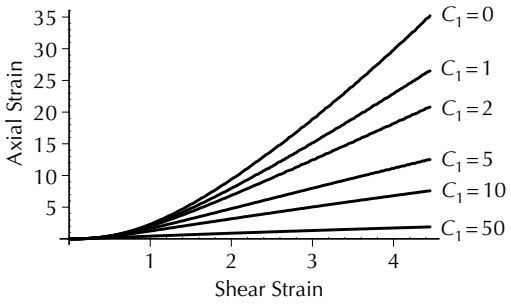

FIGURE 9.3
Effect of parameter C_1 of plastic spin on the axial strain during torsion (From Wu, H.C. et al., *Int. J. Solids Struct.*, 32, 1079, 1995. With permission from Elsevier).

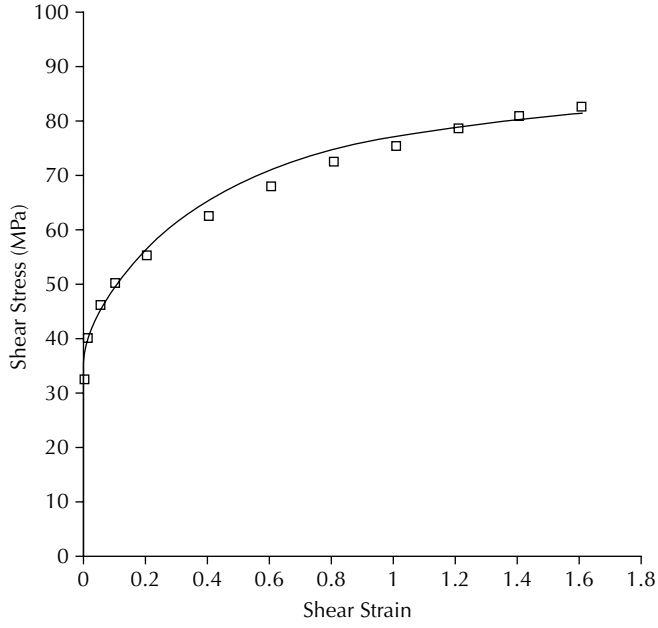

FIGURE 9.4
Shear stress–strain curve of Ni-200 with 0.01 MPa axial prestress (From Wu, H.C. et al., *Int. J. Solids Struct.*, 32, 1079, 1995. With permission from Elsevier).

The experimental data for Ni-200 are taken from Hart and Chang [19]. The material constants have been determined by fitting the shear stress–strain curve (Figure 9.4) which was determined from torsion with a 0.01 MPa prestress. The constants have been determined to be $c = 14.2$, $\beta = 5.5$, $C_1 = 9$, $\sigma'_y = 40$ MPa, $\mu_1 = 45$ MPa, $\mu_2 = 40$ MPa, and $\lambda = 9.5$. Using these constants and the constitutive equations of Section 9.3.3.1, we have predicted the axial

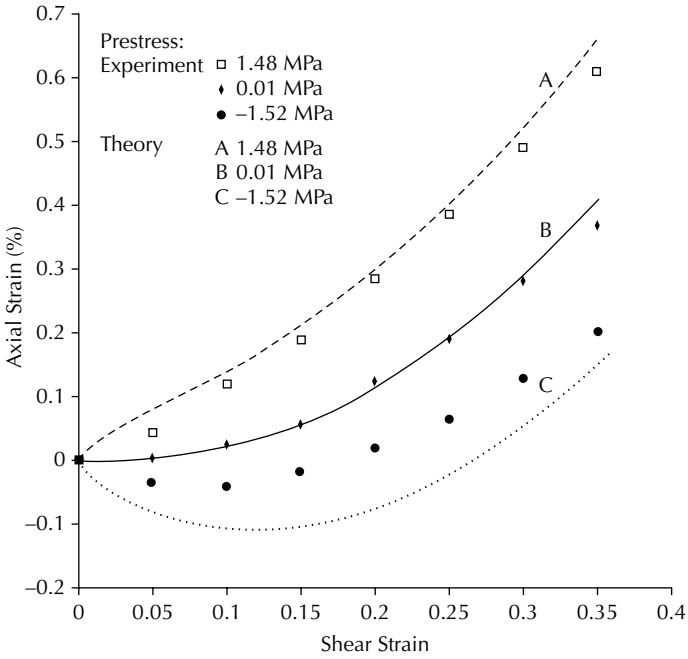

FIGURE 9.5
Axial strain for Ni-200 during torsion with axial prestresses (From Wu, H.C. et al., *Int. J. Solids Struct.*, 32, 1079, 1995. With permission from Elsevier).

strain associated with torsion with prestresses of 1.48, 0.01, and −1.52 MPa. The results, shown in Figure 9.5, are quite satisfactory.

Figure 9.6 shows the experimental shear stress–strain curve under simple shear condition (fixed-end torsion), obtained by White et al. [20] for Al-1100 material. The theoretical result of the present theory is also shown. The material constants are $c = 2.14$, $\beta = 4.5$, $C_1 = 4.5$, $\sigma_y' = 55$ MPa, $\mu_1 = 1.8$ MPa, $\mu_2 = 0.15$ MPa, and $\lambda = 1.64$. Wu and Xu [21] also obtained a shear stress–strain curve for Al-1100, but in a smaller deformation range (12% strain). The curve agrees with the one shown in Figure 9.6. Using these constants and the constitutive equations of Section 9.3.3.1, we predicted the axial strain in the case of torsion with prestresses of −6.9 and −20.7 MPa. The results found from this theory (the solid and dashed curves) are compared with the experimental data of Wu and Xu [21] and shown in Figure 9.7. Figure 9.8 shows the prediction (the solid and dashed curves) of the hoop and axial strains, respectively, for the free-end torsion condition (i.e., with $\sigma_c = 0$). The experimental data of Bailey et al. [22] are also shown in the figure. Even though the theory agrees well with experiment in terms of the axial strain, there are discrepancies in the hoop strain at large shear strain level. These discrepancies may be explained by taking a closer look at the specimens and the procedure used in the experiments of Bailey et al. [22]. The specimens used

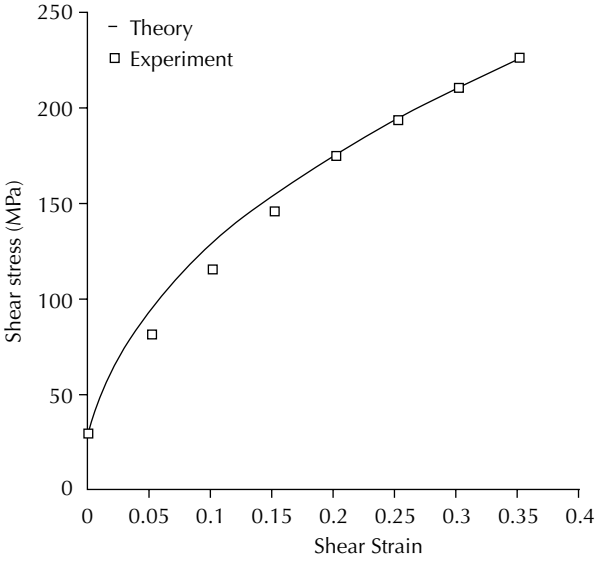

FIGURE 9.6
Shear stress–strain curve of Al-1100 (From Wu, H.C. et al., *Int. J. Solids Struct*., 32, 1079,1995. With permission from Elsevier).

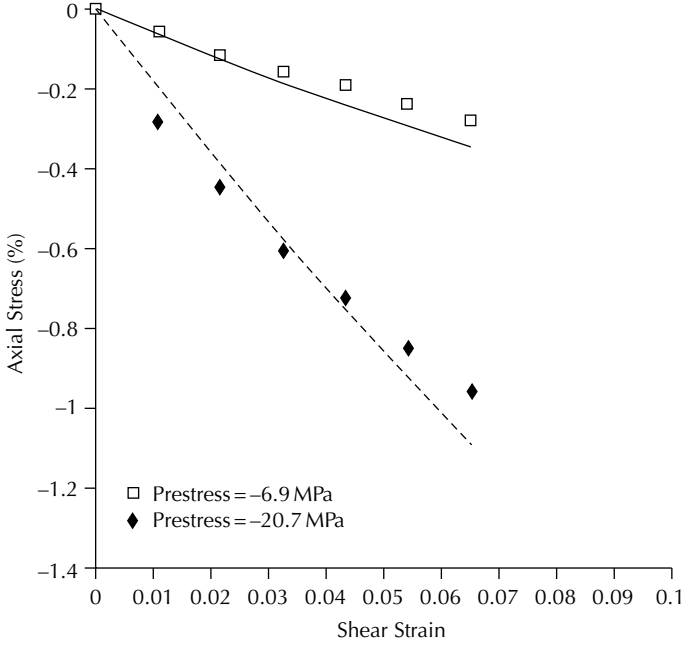

FIGURE 9.7
Axial strain for Al-1100 during torsion with compressive axial prestresses (From Wu, H.C. et al., *Int. J. Solids Struct*., 32, 1079,1995. With permission from Elsevier).

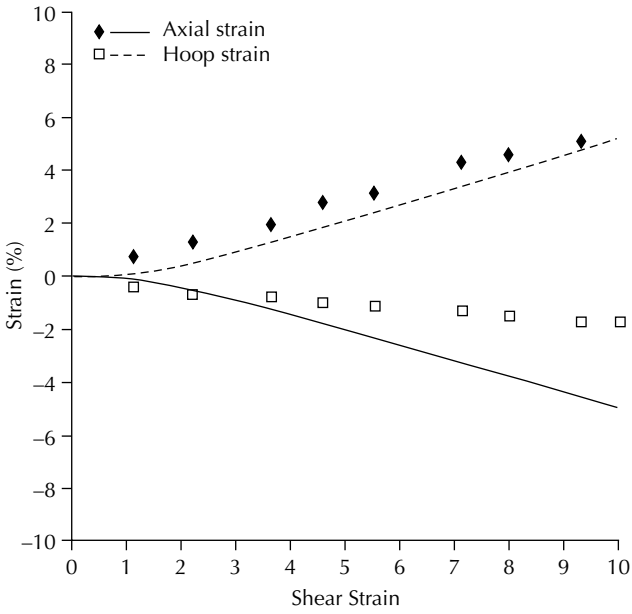

FIGURE 9.8
Hoop and axial strains under free-end torsion (From Wu, H.C. et al., *Int. J. Solids Struct.*, 32, 1079,1995. With permission from Elsevier).

by them had a very short gauge length of 3.2 mm (0.125 in.) compared with a radius of 19 mm (0.75 in.). The radius of the relatively rigid ends of the specimen did not change, which in turn restricted the development of hoop strain at large shear strain level. Another possible restriction on the hoop strain is due to a plug and sleeve inserted into the specimens to prevent buckling at large strain level. The authors thought that there was sufficient clearance to allow for any reduction in diameter during test. However, we believe that there was contact between the specimens and the plug at large shear strain level and, therefore, the reduction in diameter was restricted. If there were no contact, then the plug would not have been needed in the experiment. We believe that these are the reasons causing the experimental hoop strain to be on the low side compared with the theoretical result. Wu et al. [23] conducted the same experiments using extruded high purity aluminum with specimens of a much longer gauge length (82.6 mm or 3.25 in.) and without the plug. The outer radius of the specimens was 19 mm (0.75 in.). The results are shown in Figure 9.9. It is seen that these curves have the same trends as those of the theoretical curves shown in Figure 9.8, that is, the hoop and axial strains at large shear strain level have almost the same magnitude, whereas the results of Bailey et al. [22] show that the hoop strain does not increase much with the axial strain at large shear strain level.

In some published writings such as Canova et al. [24], the rate of hoop strain is assumed to be equal to the rate of radial strain, $\dot{\varepsilon}_\theta = \dot{\varepsilon}_r$, for a thin-walled

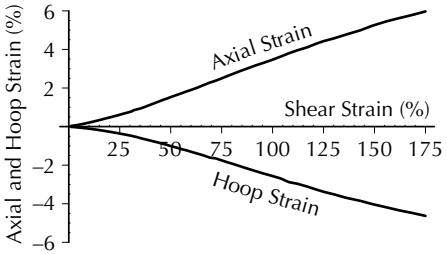

FIGURE 9.9
Experimental hoop and axial strains under free-end torsion (From Wu, H.C. et al, *Int. J. Plasticity*, 13, 873, 1998. With permission from Elsevier).

tube under tension–torsion loading condition. This assumption is good only for the axial loading condition. Taylor and Quinney [25] showed that the hoop strain is not equal to the radial strain under combined tension–torsion loading. In this calculation, we have found that the rate of radial strain is almost zero, that is, the wall thickness changes very little. And, from (9.87), the magnitude of the hoop strain is nearly the same as that of the axial strain, in agreement with the experimental observation. We mention that the analysis of Lowe and Lipkin [26] and Qian and Wu [27], by use of polycrystal plasticity, also leads to the same trends as predicted by our theory for the axial and hoop strains.

9.4 An Endochronic Theory for Porous and Granular Materials

Porous-granular (PG) *material* is a class of material that includes geotechnical materials (concretes, rocks, soils, ice, etc.), porous metals made out of metal powders by sintering, and ceramics. The response of PG materials to loading generally consists of four parts, that is, the hydrostatic response, the deviatoric response, the *shear-enhanced volumetric response*, and the *hydrostatic pressure-enhanced shear response*. A significant characteristic of this class of materials is the existence of voids (or cracks) within the material. The pores collapse and close or grow under loading–unloading conditions, and material is either consolidated or damaged. This process is irreversible (plastic deformation and damage) and upon removal of the load a permanent change in the volume of the specimen is observed. Thus, plastic volumetric strain occurs when PG materials are subjected to hydrostatic pressure. Figure 9.10 shows a schematic volumetric stress–strain curve with both the initial and the final slopes equal to the elastic bulk modulus K_0. The deviatoric stress–strain response for this class of materials is similar to that observed for metallic materials. A phenomenon similar to yielding occurs as the deviatoric stress–strain curve bends toward the strain axis.

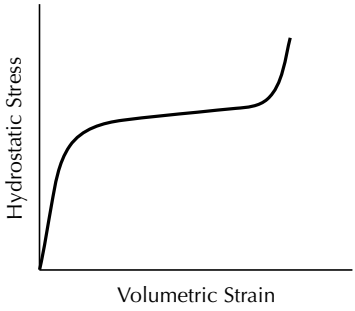

FIGURE 9.10
Schematic volumetric stress–strain curve for porous-granular materials (From Wu, H.C., in *Modern Approaches to Plasticity*, Elsevier, Amsterdam, 1993. With permission from D. Kolymbas).

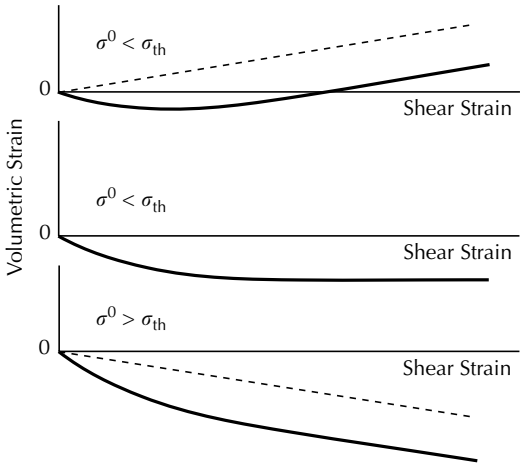

FIGURE 9.11
Shear-enhanced volumetric strain (From Wu, H.C., in *Modern Approaches to Plasticity*, Elsevier, Amsterdam, 1993. With permission from D. Kolymbas).

A special property of PG materials is that during the application of deviatoric stress, a specimen exhibits a volumetric change that can either be a contraction or dilation depending on the state of hydrostatic stress σ^0 as compared with a threshold stress σth within the specimen. This coupled behavior between volumetric and deviatoric responses is generally referred to as the shear-enhanced volumetric strain or *densification* in soil mechanics. Figure 9.11 illustrates this behavior. Another coupled behavior is the hydrostatic pressure-enhanced shear deformation, which is sometimes referred to as the *shear travel*. In the last effect, additional deviatoric deformation occurs as the hydrostatic stress increases, while keeping the deviatoric stress constant. Figure 9.12 shows that along stress-paths BC, DE, and FG, on which the deviatoric stress is kept constant, shear travel occurs as is seen by the increase

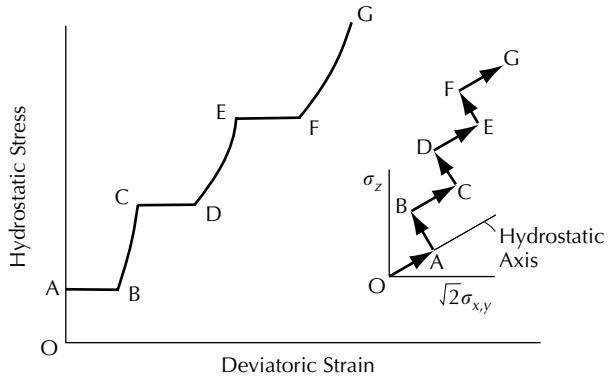

FIGURE 9.12
The shear travel effect (From Wu, H.C. and Aboutorabi, M.R., *Int. J. Plasticity*, 4, 163, 1988. With permission from Elsevier).

in the deviatoric strain for each of the path segment. A threshold deviatoric stress may be defined above which the shear travel strain is positive and below which it is negative.

The hydrostatic and deviatoric responses may be viewed as the *primary behavior* while the coupled responses are *secondary*. In a theoretical treatment, the degree of importance of each response is therefore different. The hydrostatic and deviatoric responses should be the main part of a constitutive equation and they are directly related to both yield surface and flow rule if such concepts are used in the formulation. However, there may indeed be cases in which no such concepts are used. In such cases, the hydrostatic and deviatoric responses should still be the main part of a constitutive equation. The coupled effects are secondary and can be accounted for by the flow rule or by the evolution equation of a parameter. They also influence the shape of yield surfaces.

In the case of soils, the most common test for the study of their mechanical behavior has traditionally been the conventional constant confining pressure triaxial test (simply known as the *conventional triaxial compression*, CTC). In such a test, a cylindrical specimen is prepared in a flexible membrane of a material such as polyurethane, and is placed in a chamber that can be pressurized, usually by filling it with water. An all-around constant confining pressure is applied. Then, a loading ram can be used to apply an axial load along the long axis of the cylinder. In this test, the mean stress increases with the axial load and the observed stress–strain behavior is a combination of hydrostatic–deviatoric behavior. This test is denoted by CTC in Figure 9.13 and the stress path for this test is making an angle with HC (the *hydrostatic compression*). The stresses in this figure are principal stresses. σ_z is the axial stress of the cylindrical specimen. *Unconfined compression tests* (UC) and *confined compression tests* (CC) have been used to test materials such as concretes, rocks, and ice. Cylindrical specimens are tested in the axial

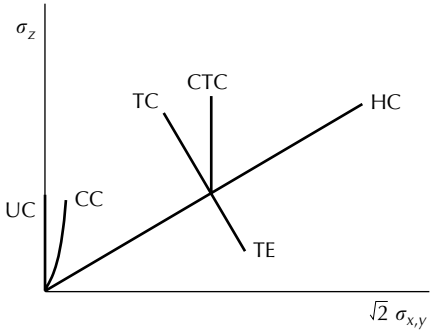

FIGURE 9.13
Illustration of various tests in the stress space.

direction either with free lateral surface (UC) or confinement in a rigid cell (CC). The lateral stress builds up with increasing axial stress in the CC test. Both tests involve the mean stress and the deviatoric stress.

The aforementioned traditional tests are not designed to separate the hydrostatic behavior from the deviatoric behavior. Since both behaviors are of primary importance in the characterization of PG materials, the *true triaxial test* has been developed to test the hydrostatic and deviatoric behaviors separately. The true triaxial device permits application of three independent (principal) stresses on a cubical specimen. The application of the stresses can be such that any path of loading in the three-dimensional stress space can be followed. Some of the paths are shown in Figure 9.13. The HC path corresponds to the application of an all-around hydrostatic pressure in *isotropic consolidation*. TC stands for *triaxial compression* and TE stands for *triaxial extension*. In the latter two tests, the deviatoric stress is applied under the condition of constant hydrostatic pressure, enabling us to concentrate on the deviatoric stress–strain response. Finally, we mention that direct shear testing and torsion of a solid shaft have also been conducted by researchers to characterize material behavior in shear.

In this section, a version of endochronic theory of plasticity is presented that accounts for all the aforementioned responses. This theory has been derived based on the work of Wu and Aboutorabi [28] and Wu [29]. It is presented here with permission from Elsevier. We present the theory first and its applications to concretes, sand, and porous aluminum are discussed.

9.4.1 The Endochronic Equations

The theory as derived in [28] has four elements corresponding to those previously mentioned. It has been modified in [29] so that the strain-rate sensitivity may be accounted for. The stress–strain curve is decomposed into volumetric and deviatoric stress–strain curves. The decomposition gives insight into

material behavior and is of special importance due to the significant role played by the plastic volumetric deformation.

This theory uses the Gibbs formulation described in Section 8.3.4. The Gibbs free energy Φ is a function of stress $\boldsymbol{\sigma}$ and two groups of internal variables, $\boldsymbol{\gamma}$ and $\boldsymbol{\pi}$. There are h number of $\boldsymbol{\gamma}$'s related to the volumetric deformation and s number of $\boldsymbol{\pi}$'s related to the deviatoric deformation. The reason for using the Gibbs formulation is that the hydrostatic and deviatoric stresses may be independently varied, which is a requirement for the derivation of the set of equations to be discussed in this chapter. This requirement is difficult to satisfy in the Helmholtz formulation, since in that case the strain, $\boldsymbol{\varepsilon}$ is used as an independent variable and it is difficult to independently vary the volumetric and the deviatoric strains for the PG materials. A hydrostatic intrinsic time z_{H} is defined to register the history of volumetric deformation, and a deviatoric intrinsic time z_{D} is used to register the history of deviatoric deformation.

In the Gibbs formulation, strain ε_{ij} is given by

$$\varepsilon_{ij} = -\frac{\partial \Phi}{\partial \sigma_{ij}} \tag{9.120}$$

and the evolution equations for γ_{ij}^{h} and π_{ij}^{s} are given by

$$\begin{aligned} &\frac{\partial \Phi}{\partial \gamma_{ij}^{h}} + M_{ijkm}^{h} \frac{\mathrm{d}\gamma_{km}^{h}}{\mathrm{d}z_{\mathrm{H}}} = 0 \quad (h \text{ not summed}) \\ &\frac{\partial \Phi}{\partial \pi_{ij}^{s}} + N_{ijkm}^{s} \frac{\mathrm{d}\pi_{\mathrm{km}}^{s}}{\mathrm{d}z_{\mathrm{D}}} = 0 \quad (s \text{ not summed}) \end{aligned} \tag{9.121}$$

where M_{ijkl}^{h} and M_{ijkl}^{s} are positive semidefinite fourth-order isotropic constant tensors. These linear evolution equations are chosen for mathematical simplicity and they can be nonlinear if. However, they are shown to be adequate for the class of materials under consideration. These evolution equations are related to the rate of entropy production within the material. By expanding the Gibbs free energy Φ in series and using only the quadratic and linear terms, the expression for Φ may be substituted into (9.120) to (9.121). Each resulting equation can then be divided into volumetric and deviatoric parts. By doing so, it may be found that the volumetric strain ε_{kk} is the sum of the hydrostatic strain, $\varepsilon_{kk}^{\mathrm{H}}$, and densification strain, $\varepsilon_{kk}^{\mathrm{S}}$. The deviatoric strain e_{ij} is the sum of strain due to deviatoric loading, e_{ij}^{S}, and strain developed due to the coupling with the hydrostatic loading, e_{ij}^{H}. The internal variables are divided into two parts as

$$\gamma_{ij}^{h} = \tfrac{1}{3}\delta_{ij}\gamma_{kk}^{h} + g_{ij}^{h}, \qquad \pi_{ij}^{s} = \tfrac{1}{3}\delta_{ij}\pi_{kk}^{s} + p_{ij}^{s} \tag{9.122}$$

where g_{ij}^h is the deviatoric part of γ_{ij}^h, p_{ij}^s is the deviatoric part of π_{ij}^s, and δ_{ij} is the Kronecker delta.

The intrinsic times ζ_H and ζ_D are defined by

$$d\zeta_H = k_H\left(\dot{\theta}_{kk}\right)|d\theta_{kk}| \quad \text{and} \quad d\zeta_D^2 = k_D(\dot{Q})^2 dQ_{ij} dQ_{ij} \tag{9.123}$$

where the volumetric strain-like increment $d\theta_{kk}$ is defined as

$$d\theta_{kk} = d\varepsilon_{kk}^H - k_1 \frac{d\sigma_{kk}}{3K_0} \tag{9.124}$$

and the deviatoric strain-like tensor dQ_{ij} is defined as

$$dQ_{ij} = de_{ij}^S - k_2 \frac{d\sigma'_{ij}}{2\mu_0} \tag{9.125}$$

where $\sigma = \sigma_{kk}/3 =$ mean pressure, $\sigma'_{ij} =$ deviatoric stress; k_1 and k_2 are constants between 0 and 1. In the limiting case that $k_1 = k_2 = 1, \theta_{kk}$ reduces to the usual definition of volumetric plastic strain and Q_{ij} reduces to the deviatoric plastic strain. K_0 is the bulk modulus and μ_0 is the shear modulus. The functions $k_H(\dot{\theta}_{kk})$ and $k_D(\dot{Q})$ are the strain-rate sensitivity functions (see Section 8.4.6), which enable the description of the strain-rate sensitive stress–strain behavior in the volumetric and deviatoric responses, respectively. These are functions of the strain-rates $\dot{\theta}_{kk}$ and $\dot{Q}$, where $\dot{Q} = (\frac{1}{2}\dot{Q}_{ij}\dot{Q}_{ij}F)^{1/2}$. The following expressions may be used

$$k_H(\dot{\theta}_{kk}) = 1 - k_h \log\left(\frac{\dot{\theta}_{kk}}{\dot{\theta}_{kk0}}\right), \qquad k_D(\dot{Q}) = 1 - k_d \log\left(\frac{\dot{Q}}{\dot{Q}_0}\right) \tag{9.126}$$

where k_h and k_d are constants; $\dot{\theta}_{kk0}$ and $\dot{Q}_0$ are reference strain rates usually taken as the lowest strain rates of the test series. Then, the following defines the governing equations for each component of strain:

Volumetric:

$$\begin{aligned} &\varepsilon_{kk}^H = 3A_0\sigma_{kk} + 3\sum_h B_0^h \gamma_{kk}^h \\ &M_0^h \frac{d\gamma_{kk}^h}{dz_H} + E_0^h \gamma_{kk}^h - B_0^h \sigma_{kk} = 0 \qquad \text{for all } h \text{ (no sum on } h) \\ &\frac{d\zeta_H}{dz_H} = h(\zeta_H) \end{aligned} \tag{9.127}$$

Deviatoric:

$$
\begin{aligned}
& e_{ij}^{\mathrm{S}} = A_2 \sigma_{ij}' + \sum_s C_2^s p_{ij}^s \\
& N_2^s \frac{\mathrm{d}p_{ij}^s}{\mathrm{d}z_{\mathrm{D}}} + F_2^s p_{ij}^s - C_2^s \sigma_{ij}' = 0 \qquad \text{for all } s \text{ (no sum on } s) \\
& \frac{\mathrm{d}\zeta_{\mathrm{D}}}{\mathrm{d}z_{\mathrm{D}}} = f(\zeta_{\mathrm{D}}, \sigma^0)
\end{aligned}
\tag{9.128}
$$

Shear-enhanced volumetric strain:

$$
\begin{aligned}
& \varepsilon_{kk}^{\mathrm{S}} = \textstyle\sum_{\mathrm{s}} C_0^s \pi_{kk}^s \\
& N_0^s \frac{\mathrm{d}\pi_{kk}^s}{\mathrm{d}z_{\mathrm{D}}} + F_0^s \pi_{kk}^s - C_0^s (\sigma_{kk} - \xi) = 0, \qquad s = 1 \\
& N_0^s \frac{\mathrm{d}\pi_{kk}^s}{\mathrm{d}z_{\mathrm{D}}} + F_0^s \pi_{kk}^s - C_0^s \sigma_{kk} = 0, \qquad s \neq 1
\end{aligned}
\tag{9.129}
$$

Pressure-enhanced shear strain:

$$
\begin{aligned}
& e_{ij}^{\mathrm{H}} = \textstyle\sum_h B_2^h g_{ij}^h \\
& M_2^h \frac{\mathrm{d}g_{ij}^h}{\mathrm{d}z_{\mathrm{H}}} + E_2^h g_{ij}^h - B_2^h (\sigma_{ij}' - D_{ij}) = 0, \qquad h = 1 \\
& M_2^h \frac{\mathrm{d}g_{ij}^h}{\mathrm{d}z_{\mathrm{H}}} + E_2^h g_{ij}^h - B_2^h \sigma_{ij}' = 0, \qquad h \neq 1
\end{aligned}
\tag{9.130}
$$

In the above equations, $f(\zeta_{\mathrm{D}},\ \sigma^0)$ = the deviatoric-hardening function, σ^0 = confining hydrostatic stress at initial shear loading, $A_0, A_2, B_0^h, B_2^h, C_0^s, C_2^s, E_0^h, E_2^h, F_0^s, F_2^s, M_0^h, M_2^h, N_0^s, N_2^s$ = parameters of the theory (for engineering application, they can be combined and the number of material constants reduced), ξ = threshold mean confining pressure, D_{ij} = threshold deviatoric stress.

The equations for hydrostatic and deviatoric responses are now further investigated. These equations can be written in a form such that, in the limiting case of $k_1 = k_2 = 1$, yield conditions can exist with respect to both the hydrostatic and deviatoric stresses. This case also enables a geometric representation of the model in the stress space, so that the physical meaning of the model may be visualized. The geometric representation is further explained. The values of k_1 and k_2 do not have to be one. A value of 0.95 has been found to facilitate numerical computation. In this case, the constitutive equations are continuous and there is the advantage of not having to deal with the yield conditions in the numerical calculation. This aspect is indeed a very important strength of the present approach. In this way, even though yield stress is defined in the theory, it can be circumvented during computation by assuming k_1 not equal to one. In this approach, the results will be closely related to

those obtained from the case of $k_1 = k_2 = 1$, where the yield conditions are used. The equations for hydrostatic and deviatoric responses are considered further in the following subsections.

9.4.1.1 The hydrostatic response

The volumetric strain increment $\mathrm{d}\varepsilon_{kk}^{\mathrm{H}}$ and the linear evolution for internal variable γ_{kk}^{h} are from (9.127) given by

$$\mathrm{d}\varepsilon_{kk}^{\mathrm{H}} = 3A_0\,\mathrm{d}\sigma_{kk} + 3\sum_h B_0^h\,\mathrm{d}\gamma_{kk}^h, \qquad \frac{\mathrm{d}\gamma_{kk}^h}{\mathrm{d}z_{\mathrm{H}}} = \frac{B_0^h}{M_0^h}\sigma_{kk} - \frac{E_0^h}{M_0^h}\gamma_{kk}^h \tag{9.131}$$

In order to account for strain hardening, the intrinsic time z_{H} is scaled by

$$\frac{\mathrm{d}\zeta_{\mathrm{H}}}{\mathrm{d}z_{\mathrm{H}}} = h(\theta_{kk}, \zeta_{\mathrm{H}}) \tag{9.132}$$

where the function h represents isotropic hardening and the increment of volumetric intrinsic time $\mathrm{d}\zeta_{\mathrm{H}} > 0$ is defined in terms of plastic strain as in (9.123). The form of the hardening function is

$$h(\theta_{kk}) = \frac{C - (C - \theta_m)\mathrm{e}^{-\mu\theta_{kk}}}{\theta_m - \theta_{kk}} \tag{9.133}$$

This form accounts for the experimentally observed fact that as material compacts, its ability to undergo plastic volumetric strains diminishes and eventually an elastic response is observed with a modulus equal to the initial bulk modulus. Thus, a maximum plastic volumetric strain of θ_m may be achieved. The material constants C and μ control the extent and rate of isotropic hardening. The values of these constants may be adjusted to fit the volumetric stress–strain curves of various PG materials, including soil.

By the substitution of (9.123), (9.124), (9.132), and the second equation of (9.131) into the first equation of (9.131), the following equations may be found

$$\mathrm{d}\varepsilon_{kk}^{\mathrm{H}}[1 \pm X] = \frac{\mathrm{d}\sigma_{kk}}{3K_0}[1 \pm k_1 X] \tag{9.134}$$

where

$$X = \sum_h X^h \qquad \text{with } X^h = \frac{B_0^h}{hM_0^h} = \left(B_0^h\sigma_{kk} - E_0^h\gamma_{kk}^h\right) \tag{9.135}$$

Note that $k_1 \neq 1$ and initially $\sigma_{kk} = \gamma^h_{kk} = 0$. Hence, the constant A_0 may be identified, that is, $A_0 = 1/9K_0$ and when $h \to \infty$, (9.134) yields

$$\mathrm{d}\varepsilon^{\mathrm{H}}_{kk} = \frac{\mathrm{d}\sigma_{kk}}{3} \cdot \frac{1}{K_0} \tag{9.136}$$

Equation (9.136) indicates a linear stress–strain response with a slope equal to the initial bulk modulus at large volumetric strain. When loading reverts to unloading the only change in the equations takes place in (9.134), where the negative sign in the brackets changes to positive. Note that in this investigation, tensile stress is considered to be positive. Knowing $\mathrm{d}\varepsilon^{\mathrm{H}}_{kk}$ and the current values of $z_{\mathrm{H}}, \sigma_{kk}$ and γ^h_{kk}, (9.134) may be used to calculate $\mathrm{d}\sigma_{kk}$. (9.123), (9.124), and (9.132) can then be used to determine $\mathrm{d}\theta_{kk}$ and $\mathrm{d}z_{\mathrm{H}}$, and (9.131) leads to $\mathrm{d}\gamma^h_{kk}$. Therefore, $z_{\mathrm{H}}, \sigma_{kk}$, and γ^h_{kk} can be updated. This step-by-step procedure is used to calculate the volumetric stress–strain curve.

For the case of $k_1 = 1$, it is shown now that the previous equations can describe a physical situation when the material experiences a combined isotropic–kinematic hardening in the volumetric behavior. Both tensile (further limited by fracture) and compressive hydrostatic stresses are included in this discussion and it is shown that the combined isotropic–kinematic hardening arises naturally in the volumetric response of the endochronic formulation. To this end, the first equation of (9.131) is solved for $\mathrm{d}\sigma_{kk}$ and the result substituted into (9.124) to obtain

$$\begin{aligned}\mathrm{d}\theta_{kk} &= (1-k_1)\mathrm{d}\varepsilon^{\mathrm{H}}_{kk} + 3k_1\left(\sum_h \frac{B^h_0 B^h_0}{M^h_0}\sigma_{kk} - \sum_h \frac{B^h_0 E^h_0}{M^h_0}\gamma^h_{kk}\right)\mathrm{d}z_{\mathrm{H}} \\ &= \varphi^{\mathrm{H}}_{kk} + \psi^{\mathrm{H}}_{kk}\,\mathrm{d}z_{\mathrm{H}}\end{aligned} \tag{9.137}$$

where

$$\begin{aligned}\varphi^{\mathrm{H}}_{kk} &= (1-k_1)\mathrm{d}\varepsilon^{\mathrm{H}}_{kk} \\ \psi^{\mathrm{H}}_{kk} &= 3k_1\left(\sum_h \frac{B^h_0 B^h_0}{M^h_0}\sigma_{kk} - \sum_h \frac{B^h_0 E^h_0}{M^h_0}\gamma^h_{kk}\right)\end{aligned} \tag{9.138}$$

But, from (9.123) and (9.132),

$$h\,\mathrm{d}z_{\mathrm{H}} = \mathrm{d}\zeta_{\mathrm{H}} = \pm k_{\mathrm{H}}\,\mathrm{d}\theta_{kk} = \pm k_{\mathrm{H}}(\varphi^{\mathrm{H}}_{kk} + \psi^{\mathrm{H}}_{kk}\,\mathrm{d}z_{\mathrm{H}}) \tag{9.139}$$

or

$$\left(\beta^{\mathrm{H}}_{kk} \mp \frac{h}{k_{\mathrm{H}}}\right)\mathrm{d}z_{\mathrm{H}} + \varphi^{\mathrm{H}}_{kk} = 0 \tag{9.140}$$

When $k_1 = 1, \varphi_{kk}^{\mathrm{H}} = 0$. Thus,

$$\left(\psi_{kk}^{\mathrm{H}} \mp \frac{h}{k_{\mathrm{H}}}\right) \mathrm{d}z_{\mathrm{H}} = 0 \tag{9.141}$$

Since during plastic deformation, $\mathrm{d}z_{\mathrm{H}} \neq 0$, then,

$$\psi_{kk}^{\mathrm{H}} = \pm \frac{h}{k_{\mathrm{H}}} \tag{9.142}$$

By substituting (9.138) into (9.142), it is found that

$$\sigma_{kk} - \alpha_{kk}^{\mathrm{H}} = \pm \frac{\sigma_{kk}^{y}}{k_{\mathrm{H}}} h \tag{9.143}$$

where

$$\sigma_{kk}^{y} = \left(3 \sum_{h} \frac{B_0^h B_0^h}{M_0^h}\right)^{-1} \quad \text{and} \quad \alpha_{kk}^{\mathrm{H}} = 3\sigma_{kk}^{y} \sum_{h} \frac{B_0^h E_0^h}{M_0^h} \gamma_{kk}^{h} \tag{9.144}$$

This expression may be viewed as a yield criterion for hydrostatic stress with $\sigma_{kk}^{y} h / k_{\mathrm{H}}$ denoting the isotropic hardening and α_{kk}^{H} denoting the kinematic hardening. Note that in the isotropic hardening, σ_{kk}^{y} is the initial quasistatic yield stress, which when divided by k_{H} becomes the dynamic yield stress. h is the isotropic-hardening function. The flow rule is given from (9.137) by

$$\mathrm{d}\theta_{kk} = \psi_{kk}^{\mathrm{H}} \, \mathrm{d}z_{\mathrm{H}} = \frac{\mathrm{d}z_{\mathrm{H}}}{\sigma_{kk}^{y}} (\sigma_{kk} - \alpha_{kk}^{\mathrm{H}}) \tag{9.145}$$

9.4.1.2 The deviatoric response

In the deviatoric response, from (9.128), the equations are

$$\mathrm{d}e_{ij}^{\mathrm{S}} = A_2 \, \mathrm{d}\sigma_{ij}' + \sum_{s} C_2^s \, \mathrm{d}p_{ij}^s, \quad \frac{\mathrm{d}p_{ij}^s}{\mathrm{d}z_{\mathrm{D}}} = \frac{C_2^s}{N_2^s} \sigma_{ij}' - \frac{F_2^s}{N_2^s} p_{ij}^s \tag{9.146}$$

Note that the evolution of p_{ij}^s is defined with respect to the deviatoric intrinsic time z_{D}. For the first increment of loading from the virgin state, since $\sigma_{ij}' = p_{ij}^s = 0$, (9.146) yields

$$\left[\frac{\mathrm{d}e_{ij}^{\mathrm{S}}}{\mathrm{d}\sigma_{ij}'}\right]_0 = A_2 \tag{9.147}$$

Therefore, A_2 is identified as the inverse of the initial slope $2\mu_0$ of the deviatoric stress–strain curve. Thus, $A_2 = \frac{1}{2}\mu_0$. The deviatoric intrinsic time increment $\mathrm{d}\zeta_\mathrm{D}$ is defined as in (9.123) and is related to z_D through the hardening function $f(z_\mathrm{D})$ defined by (9.128). It will be shown subsequently that function f represents isotropic hardening in the deviatoric behavior.

Solving the first equation of (9.146) for $\mathrm{d}\sigma'_{ij}$ and substituting the result together with the second equation of (9.146) into (9.125) yields

$$\mathrm{d}Q_{ij} = \varphi^\mathrm{D}_{ij} + \psi^\mathrm{D}_{ij}\mathrm{d}z_\mathrm{D} \tag{9.148}$$

where

$$\begin{aligned} \varphi^\mathrm{D}_{ij} &= (1-k_2)\mathrm{d}e^\mathrm{S}_{ij} \\ \psi^\mathrm{D}_{ij} &= k_2 \sum_s C^s_2 \left(\frac{C^s_2}{N^s_2}\sigma'_{ij} - \frac{F^s_2}{N^s_2}p^s_{ij} \right) \end{aligned} \tag{9.149}$$

Then, by substituting the third equation of (9.128) and (9.148) into (9.123), the following quadratic equation is obtained

$$P\,\mathrm{d}z^2_\mathrm{D} + W\,\mathrm{d}z_\mathrm{D} + R = 0 \tag{9.150}$$

where

$$P = \psi^\mathrm{D}_{ij}\psi^\mathrm{D}_{ij} - \left(\frac{f}{k_\mathrm{D}}\right)^2, \qquad W = 2\varphi^D_{ij}\psi^D_{ij}, \qquad R = \varphi^\mathrm{D}_{ij}\varphi^\mathrm{D}_{ij} \tag{9.151}$$

Therefore, P, W, and R are functions that are defined in terms of the constants of the model and increments of input variables. When (9.150) is solved for $\mathrm{d}z_\mathrm{D}$, the second equation of (9.146) can be used to obtain $\mathrm{d}p^s_{ij}$. By substitution, the deviatoric stress increment $\mathrm{d}\sigma'_{ij}$ can then be found from the first equation of (9.146).

In the case of $k_2 = 1$, (9.149) and (9.151) give $\varphi^\mathrm{D}_{ij} = R = W = 0$. Thus, (9.150) is reduced to $P\,\mathrm{d}z^2_\mathrm{D} = 0$. Since $\mathrm{d}z_\mathrm{D} \neq 0$ when there is plastic deformation, P must be zero. Hence, the first equation of (9.151) leads to

$$(\sigma'_{ij} - \alpha^\mathrm{D}_{ij})(\sigma'_{ij} - \alpha^\mathrm{D}_{ij}) = \left(\frac{\sigma'_y f}{k_\mathrm{D}}\right)^2 \tag{9.152}$$

where

$$\sigma'_\mathrm{y} = \left(\sum_s \frac{C^s_2 C^s_2}{N^s_2}\right)^{-1}, \qquad \alpha^\mathrm{D}_{ij} = \sigma'_\mathrm{y}\sum_s \frac{C^s_2 F^s_2}{N^s_2}p^s_{ij} \tag{9.153}$$

This is the Mises yield criterion with combined isotropic–kinematic hardening, in which $\sigma'_y f/k_D$ describes the isotropic hardening and α^D_{ij} the kinematic hardening in the deviatoric behavior. Note that in the isotropic hardening, σ'_y is the quasistatic deviatoric yield stress, which when divided by k_D becomes the dynamic yield stress and f is the isotropic-hardening function. From (9.148), the plastic strain increment is now given by

$$de^p_{ij} = \psi^D_{ij}\, dz_D = \frac{dz_D}{\sigma'_y}\left(\sigma'_{ij} - \alpha^D_{ij}\right) \tag{9.154}$$

which is normal to the deviatoric yield surface. It has thus been shown that in the case of $k_1 = k_2 = 1$, the present endochronic theory is equivalent to a flow theory of plasticity, which obeys the Mises yield criterion with combined isotropic–kinematic hardening, both in the hydrostatic and deviatoric responses.

9.4.1.3 Geometric representation of the model

There is a simple geometrical representation of the proposed model for the case of $k_1 = k_2 = 1$, in which two yield criteria are defined, one for volumetric behavior and the other for deviatoric behavior. The material constants of the model depend on the initial density of the material, and these constants are then used to describe subsequent material behavior.

The two yield criteria exist in a space plotting the hydrostatic stress $\sigma_{kk}/3$ against the equivalent stress σ_{eq}, which is defined as the square root of the second invariant of the deviatoric stress tensor (see Figure 9.14). The volumetric yield criterion is represented by two vertical yield lines and the deviatoric yield criterion by two horizontal yield lines. These yield lines are not necessarily straight due to the cross effects between the hydrostatic and deviatoric responses. These are shown by the thin curves in Figure 9.14. The distance

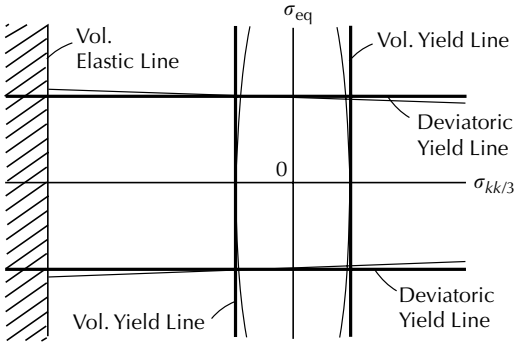

FIGURE 9.14
Geometric representation of the model (From Wu, H.C. et al., *Int. J. Plasticity*, 6, 207, 1990. With permission from Elsevier).

between the yield lines can expand, resulting in isotropic hardening. The two yield lines as a set can also move, resembling the kinematic hardening. According to this model, combined isotropic–kinematic hardening takes place in both the volumetric and deviatoric responses. A volumetric elastic line may be established in the hydrostatic compression region indicating a limit beyond which the volumetric response is elastic again. This phenomenon corresponds with the bending upward of the volumetric stress–strain curve at large strain level, where the modulus is elastic.

According to this model, the volumetric and deviatoric yield limits are individually imposed. The model allows for the situation that yielding has already occurred volumetrically but not yet occurred deviatorically. This is a situation that is frequently observed in sands, which have a very low volumetric yield limit. Thus, the deviatoric response in this case would initially be elastic and then plastic when the deviatoric yield limit is reached. In the case of sand, the volumetric yield lines are collapsed into a line passing through the origin as shown in Figure 9.15. In this figure, compressive stress is considered positive as is the usual practice of soil mechanics. The failure lines (FL) are shown together with lines showing the initial yield lines and the subsequent yield lines obtained by isotropic and kinematic hardening, respectively. The idea of volumetric compaction yield surface and shear yield surface and of representing them as horizontal and vertical straight lines in the J_1 versus $\sqrt{J_2}$ space was briefly mentioned by Johnson and Green [30]. This idea is similar to the present model and is described by the endochronic constitutive equations of this section.

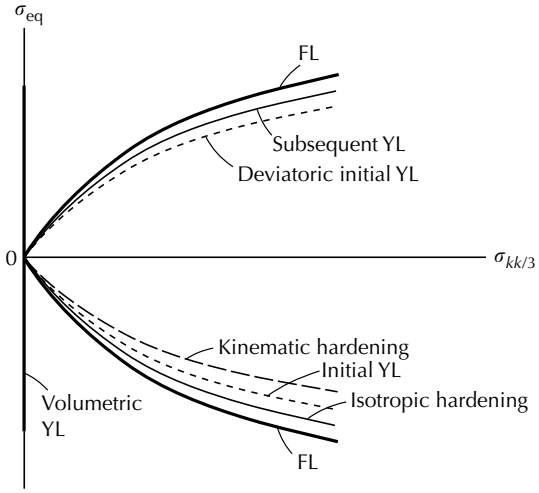

FIGURE 9.15
Yield lines for sand (From Wu, H.C., in *Modern Approaches to Plasticity*, Elsevier, Amsterdam, 1993. With permission from D. Kolymbas).

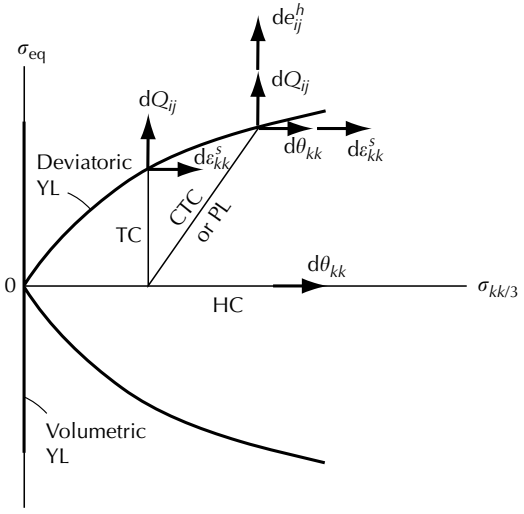

FIGURE 9.16
Plastic strain increments of the model (From Wu, H.C., in *Modern Approaches to Plasticity*, Elsevier, Amsterdam, 1993. With permission from D. Kolymbas).

The volumetric plastic strain increment $d\theta_{kk}$ is given by (9.145) and the deviatoric plastic strain increment dQ_{ij} is given by (9.154), which is normal to the deviatoric yield surface. These equations resemble the flow rule of a flow theory of plasticity. However, additional plastic strain increments $d\varepsilon^S_{kk}$ and de^H_{ij} need to be considered in this model. These increments are due to coupled effects as discussed earlier and the occurrence of the increments depends on the stress path. Figure 9.16 shows the plastic strain increments associated with various stress paths in a true triaxial test. A hydrostatic compression test (HC) will give rise to $d\theta_{kk}$ only; a TC test will give rise to dQ_{ij} and $d\varepsilon^S_{kk}$; and a CTC test or a proportional loading test (PL) will lead to all four increments, that is, $d\theta_{kk}, dQ_{ij}, d\varepsilon^S_{kk}$, and de^H_{ij}. It is difficult to compare the present plastic strain increments with the associative or nonassociative flow rules of the classical theory. In that theory, the direction of the total plastic strain increment is investigated with respect to a plastic potential in the stress space, and combines both the deviatoric and hydrostatic behaviors. Whether the flow rule is associative or nonassociative is still a point of debate. In the present model, no such complication is involved, however.

9.4.2 Application to Concrete

The endochronic theory of the previous section has been applied in [28] to investigate the experimental results of concrete reported by Scavuzzo et al. [31]. Cubical specimens were tested under a true triaxial test. In such a test, σ_x, σ_y, σ_z are principal stresses and ε_x, ε_y, ε_z are principal strains.

The material is not strain-rate sensitive and the strain-rate sensitivity functions are $k_{\mathrm{H}} = k_{\mathrm{D}} = 1$. For the isotropic-hardening functions, (9.133) is used for h and the form for f is chosen as

$$f(z_{\mathrm{D}}) = C_p - (C_p - 1)\mathrm{e}^{-\mu z_{\mathrm{D}}} \tag{9.155}$$

where C_p and μ are constants. Equations of Sections 9.4.1.1 and 9.4.1.2 are used to describe the hydrostatic and deviatoric behaviors. In the consideration of shear-enhanced volumetric strain, we use two internal variables, and (9.129) becomes

$$\begin{aligned} &\varepsilon^{\mathrm{S}}_{kk} = C^1_0 \pi^1_{kk} + C^2_0 \pi^2_{kk} \\ &\frac{\mathrm{d}\pi^1_{kk}}{\mathrm{d}z_{\mathrm{D}}} = \frac{C^1_0}{N}(\sigma_{kk} - \xi), \qquad \frac{\mathrm{d}\pi^2_{kk}}{\mathrm{d}z_{\mathrm{D}}} = \frac{C^2_0}{N}\sigma_{kk} - \frac{F^2_0}{N}\pi^2_{kk} \end{aligned} \tag{9.156}$$

All deviatoric constants associated with the internal variable π^1 are assumed to be zero. The above equations may be combined to yield

$$\frac{\mathrm{d}\varepsilon^{\mathrm{S}}_{kk}}{\mathrm{d}z_{\mathrm{D}}} = I^1(\sigma_{kk} - \xi) - \chi^2 \varepsilon^{\mathrm{S}}_{kk} + I^1 \chi^2 \int_0^{z_{\mathrm{D}}} (\sigma_{kk} - \xi)\, \mathrm{d}z_{\mathrm{D}} + I^2 \sigma_{kk} + \chi^2 \pi_0 \tag{9.157}$$

where

$$I^1 = \frac{C^1_0 C^1_0}{N}, \qquad I^2 = \frac{C^2_0 C^2_0}{N}, \quad \chi^2 = \frac{F^2_0}{N}, \qquad \pi_0 = C^1_0 \pi^1_{kk}(0) = -C^2_0 \pi^2_{kk}(0) \tag{9.158}$$

Following Wu et al. [32], $\xi = \sigma_{th}$. In addition, I^1, I^2, χ^2, and π_0 may be determined to complete the characterization of the shear-enhanced volumetric strain response. Finally, we mention that the shear travel effect is determined by use of (9.130).

In an effort to describe the experimental data for concrete obtained by Scavuzzo et al. [31], the endochronic equations presented for the hydrostatic, deviatoric, shear-enhanced volumetric strain, and pressure-enhanced shear strain were solved by Wu and Aboutorabi [28] in an iterative incremental fashion utilizing a computer. The increment in stress path is input into a program that computes from it an increment for the hydrostatic stress and one for the deviatoric stress. Then, accordingly, the hydrostatic and deviatoric modules are called on to find the corresponding increment of strains and increment of intrinsic time. If any coupling strains are to be evaluated, then the increments of the intrinsic times are passed on to the shear-enhanced volumetric strain and pressure-enhanced shear strain modules to find such strains. Any

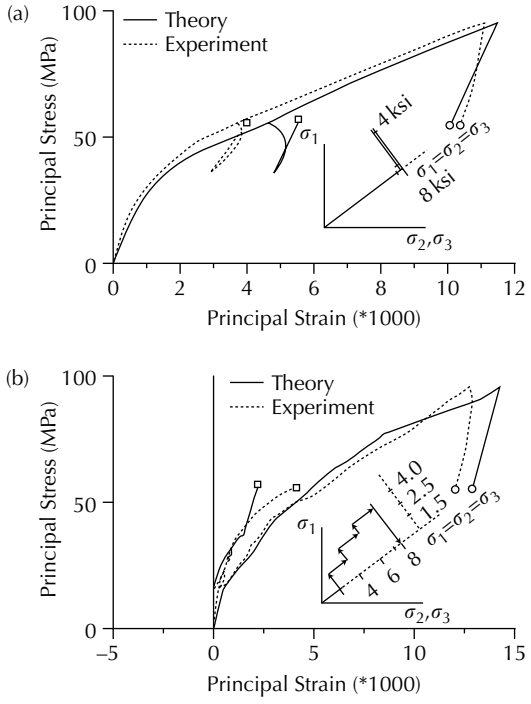

FIGURE 9.17
Behavior of concrete subjected to various stress paths — inserts show stress paths (From Wu, H.C. and Aboutorabi, M.R., *Int. J. Plasticity*, 4, 163, 1988. With permission from Elsevier).

stress path that is neither purely hydrostatic nor deviatoric is approximated by a staircase path (i.e., as a series of consecutive hydrostatic and deviatoric increments). The outputs of the theoretical computations are presented in [28]. They constitute a rather extensive study of various stress paths. It is fair to say that the model has done a good job in describing such a diverse loading program. In Figure 9.17(a) and (b), we show two cases. For each stress path the stress–strain relations in both 1- (vertical) and 2-directions are presented. The 1-direction is marked with ∘ and the 2-direction with □. Since the tests are all performed in the deviatoric plane, the loadings in the 2- and 3-directions are the same and the result for the 3-direction is identical to that for the 2-direction.

9.4.3 Application to Sand

Sand is a cohesionless soil. It has mechanical properties similar to those described in the introductory paragraphs of Section 9.4. They are the hydrostatic response, the deviatoric response, the shear-enhanced volumetric response, and the hydrostatic pressure-enhanced shear response. In the

terminology of soil mechanics, the hydrostatic response is known as isotropic consolidation. The volumetric stress–strain curve bends toward the stress axis. The deviatoric behavior depends on hydrostatic stress (or the normal stress) and the deviatoric (or shear) stress–strain curve bends toward the strain axis. There is no shear strength at zero confining pressure. The shear-enhanced volumetric response is also known as densification or dilation.

The first application of the endochronic theory to the description of mechanical behavior of sand was due to Bazant and Krizek [33], using the simple endochronic theory (see Section 8.4.2). Valanis and his coworkers [34,35] have also contributed extensively to this subject. Our approach is different from aforementioned works in that we use the Gibbs formulation. The equations are similar to those presented in Section 9.4.1. Using this formulation, Wu and Wang [36] obtained theoretical results of isotropic consolidation and deviatoric response, which compare favorably with experimental results of Lade [37] for Sacramento River sand subjected to loading–unloading. In addition, the shear hysteretic loops for loose crystal silica No. 20 sand reported in [38] were theoretically investigated in [36]. We [36] also investigated densification and the results compared favorably with those reported in [39].

The shear hysteresis of sand was further investigated by Wu and Sheu [40] using a method of integration similar to that discussed in Section 8.4.5.2, resulting in closed-form solutions. The theory predicted the test results of Silver and Seed [41] at the 1st, 2nd, 10th, and 300th cycles reasonably well. Nine cases of relative densities and vertical stresses were considered. Additional works in the endochronic modeling of sand are Wu et al. [32] considering a true triaxial test and Wu and Aboutorabi [42] considering sand behavior subjected to a circular stress path. Furthermore, the undrained response of sand was discussed in [29].

9.4.4 Application to Porous Aluminum

Recent developments in the techniques of powder metallurgy (P/M) have made it possible to solidify all kinds of metallic powders into structure components of controlled porosity. Application of endochronic theory to describe the phenomenological behavior of porous aluminum was carried out by Aboutorabi et al. [43], and Wang and Wu [44]. However, these applications were limited to isotropic consolidation and monotonic uniaxial straining, using the experimental results of Schock et al. [45] and some limited experimental data for high-purity aluminum P/M. Using specimens of high-purity aluminum P/M, Wu et al. [46] conducted a series of experiments under various cyclic straining conditions and showed that the endochronic theory presented in Section 9.4.1 can be used to describe the experimental results reasonably well.

The theory of Section 9.4.1 has four elements. They are the hydrostatic response, the deviatoric response, the densification, and the shear travel. Although densification and shear travel are two important coupled behaviors

between hydrostatic and deviatoric elements, their determination cannot be accomplished by uniaxial stress experiments and awaits further investigation by use of other specimen configurations and loading conditions. In [46], these two effects are neglected, and the efforts have been focused on the evaluation of the hydrostatic and deviatoric behaviors subjected to cyclic loading. Due to consistent results obtained even with this approximation, it may be concluded that densification and shear travel are of secondary importance for the material tested under uniaxial stress condition.

The decomposition of the axial stress–strain curve into volumetric and deviatoric stress–strain curves gives further insight into the material behavior. This is of special importance due to the significant role played by the plastic volumetric deformation. The hydrostatic and deviatoric elements of the endochronic theory are now discussed separately and concepts of the present formulation are interpreted in terms of those of the classical plasticity.

In a uniaxial strain-controlled test, the strain and stress states are

$$[\varepsilon] = \begin{bmatrix} \varepsilon_1 & 0 & 0 \\ 0 & \varepsilon_2 & 0 \\ 0 & 0 & \varepsilon_2 \end{bmatrix}, \qquad [\sigma] = \begin{bmatrix} \sigma_1 & 0 & 0 \\ 0 & 0 & 0 \\ 0 & 0 & 0 \end{bmatrix} \tag{9.159}$$

where 1 is in the axial direction of the cylindrical specimen. The volumetric strain is $\varepsilon_v = \varepsilon_1 + 2\varepsilon_2$ and the mean stress is $\sigma_{kk} = \sigma_1/3$. The deviatoric strain and stress are

$$\begin{aligned} [e] &= \begin{bmatrix} \frac{2}{3}(\varepsilon_1 - \varepsilon_2) & 0 & 0 \\ 0 & -\frac{1}{3}(\varepsilon_1 - \varepsilon_2) & 0 \\ 0 & 0 & -\frac{1}{3}(\varepsilon_1 - \varepsilon_2) \end{bmatrix}, \\ [\sigma'] &= \begin{bmatrix} \frac{2}{3}\sigma_1 & 0 & 0 \\ & -\frac{1}{3}\sigma_1 & 0 \\ & 0 & -\frac{1}{3}\sigma_1 \end{bmatrix} \end{aligned} \tag{9.160}$$

The hydrostatic response is described by (9.133) and (9.134). Several cyclic straining paths were tested. One of them is shown in Figure 9.18(a) and another in Figure 9.18(b). Both theoretical and experimental results are shown in the figures. Only one internal variable $\mathbf{p}$ is used for simplicity in the discussion of the deviatoric response. Since we have $\sigma'_{11} = -2\sigma'_{22} = -2\sigma'_{33}$ and $e_{11} = -2e_{22} = -2e_{33}$, only the 11-components of (9.146) and (9.125) are independent equations. Combing these equations and (9.123) with $k_{\mathrm{D}} = 1$, we obtain

$$\mathrm{d}e_{11}[1 \pm X_{\mathrm{D}}] = \frac{\mathrm{d}\sigma'_{11}}{2G_0}[1 \pm k_2 X_{\mathrm{D}}] \tag{9.161}$$

where

$$X_{\mathrm{D}} = \sqrt{\frac{3}{2}}\frac{C_2}{fN_2}(C_2\sigma'_{11} - F_2 p_{11}) \tag{9.162}$$

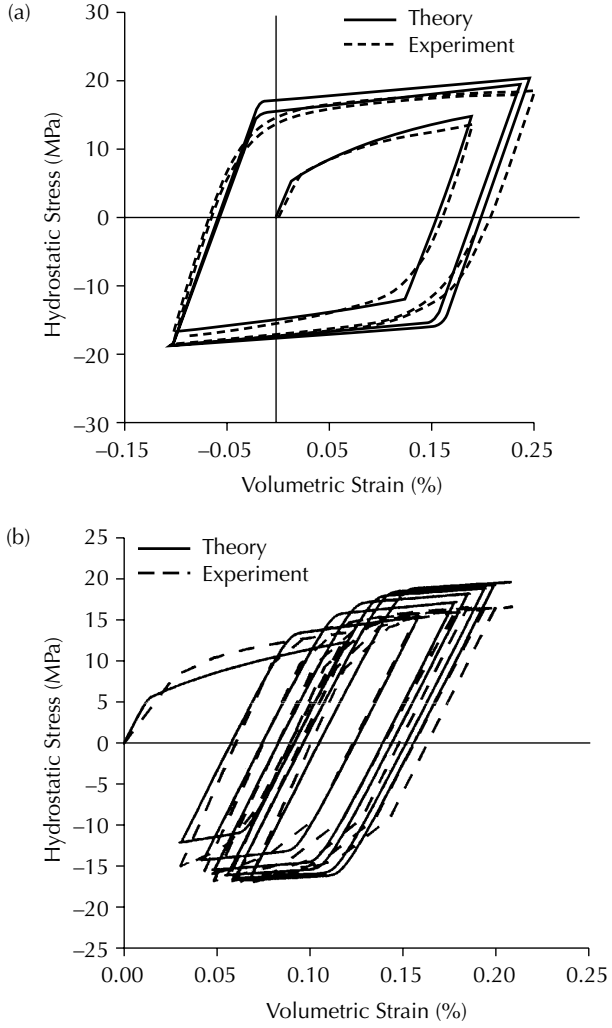

FIGURE 9.18
Cyclic volumetric stress–strain curve for porous aluminum: (a) test program 1, (b) test program 2 (From Wu, H.C. et al., *Int. J. Plasticity*, 6, 207, 1990. With permission from Elsevier).

The hardening function is

$$f(z_D) = C_D - (C_D - 1)\exp(-\mu z_D) \tag{9.163}$$

Equations (9.161) and (9.163) are used in a numerical procedure to compute the deviatoric stress–strain curves. Figures 9.19(a) and (b) are the deviatoric counterparts of Figures 9.18(a) and (b).

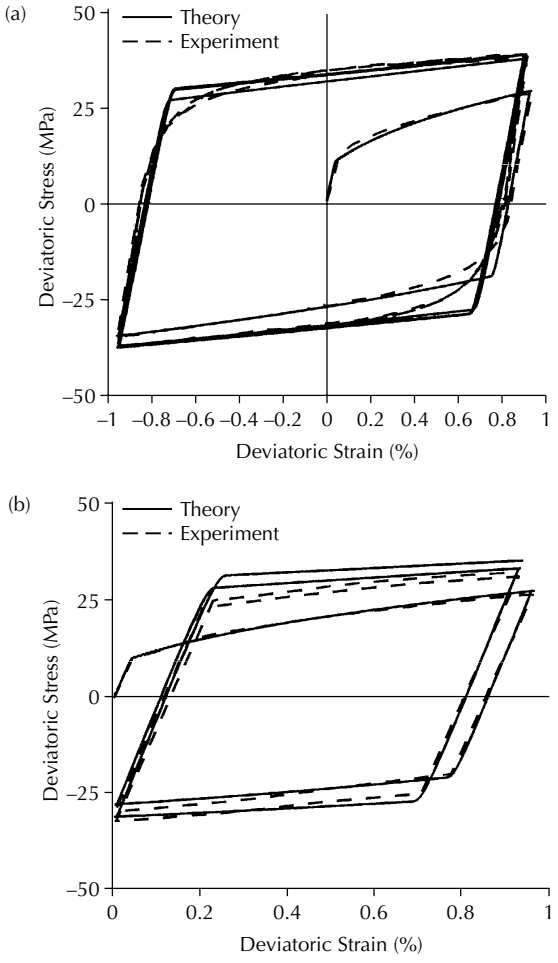

FIGURE 9.19
Deviatoric counterparts of Figure 9.18 (From Wu, H.C. et al., *Int. J. Plasticity*, 6, 207, 1990. With permission from Elsevier).

9.5 An Endochronic Formulation of a Plastically Deformed Damaged Continuum

9.5.1 Introduction

Typical work in continuum damage mechanics (CDM) often involves the damage-effect variables in the sense of Kachanov [47] and the effective stress/effective strain concepts. Consequently, damage mechanics theories are often derived from the usual constitutive theories by use of effective variables, which take into account the effects of damage, in place of

original variables. The thermodynamics framework of CDM often involves the concept of either the strain equivalence postulate [48] or the strain-energy equivalence postulate [49,50], or the hypothesis of stress working equivalence [51] along with the concepts of continuum mechanics and irreversible changes in the material internal structure. The microdefects are represented at the macroscopic level by a damage variable. A typical elastoplastic damage theory is based on the generalized damage theory initially proposed by Chaboche [52] and later by Lemaitre [53]. In [53], Lemaitre proposed that the damage energy release rate, that is, energy release by the system during the damaging process, is related to the elastic strain energy. The damage energy release rate is defined by the thermodynamic force conjugate to damage evolution. This treatment amounts to an uncoupled consideration between plasticity and damage processes.

These concepts of CDM have been proposed by different authors associated with different definitions and theories, and not all of them are needed in one theory. Some of the aforementioned concepts and definitions are not even compatible with each other. Following the work of Wu and Nanakorn [54], we discuss the existing concepts of CDM and propose a CDM constitutive framework using a set of concepts in a unified manner. The reproduction of [54] is with permission from Elsevier. Further constitutive modeling is required to arrive at explicit constitutive equations for CDM, which may be achieved by use of a concept such as damage potential within the proposed constitutive framework. Another approach is to formulate the constitutive equations based on an endochronic concept and still using the same constitutive framework. The endochronic formulation for CDM is discussed in this section.

9.5.2 The Anisotropic Damage Tensor

This work uses a second-order tensor as a parameter of damage. The tensor defines the loss of net area of material as in the original work of Kachanov [47]. The presentation of damage tensor D_{ij} in this section follows previous work by Murakami and Ohno [55] and Betten [56], in which the damage tensor is constructed using area vectors related to Cauchy's tetrahedron in a damaged state. In Murakami and Ohno's anisotropic damage theory of creep, the second-rank symmetric damage tensor D_{ij} is derived by representing the effects of microscopic grain-boundary cavities in terms of a dyadic product of the unit normal vector to the relevant boundary. On the other hand, in a macroscopic approach, Betten derived the damage tensor from a third-order, skew-symmetric, continuity tensor that represents the area vector. In [54], the derivation of D_{ij} is similar to Betten's derivation, but a second-order continuity tensor is used, which provides a simple and more meaningful physical interpretation.

Consider a differential tetrahedron of an undamaged material as shown in Figure 9.20(a). Note that the figure shows a special case where x_i axes coincide with the principal damage axes. In general, if $\mathrm{d}S_i^{(j)}$ denotes the i-component of

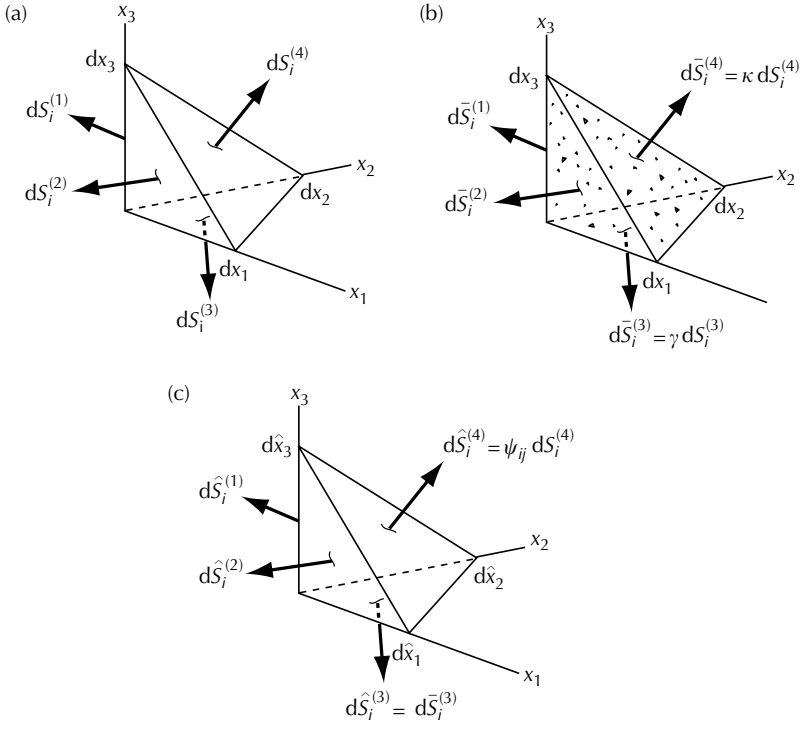

FIGURE 9.20
Definition of damage measure-load bearing area: (a) undamaged continuum, (b) actual damaged continuum, (c) fictitious undamaged continuum (From Wu, H.C. and Nanakorn, C.K., *Int. J. Solids Struct.*, 36, 5057, 1999. With permission from Elsevier).

a gross area element that has the normal $n_k^{(j)}$, then $dS_i^{(j)}$ can be characterized by

$$\begin{aligned} dS_i^{(1)} &= -\tfrac{1}{2} e_{ijk}\, dx_j^{(2)}\, dx_k^{(3)} \\ dS_i^{(2)} &= -\tfrac{1}{2} e_{ijk}\, dx_j^{(3)}\, dx_k^{(1)} \\ dS_i^{(3)} &= -\tfrac{1}{2} e_{ijk}\, dx_j^{(1)}\, dx_k^{(2)} \\ dS_i^{(4)} &= -\tfrac{1}{2} e_{ijk}\, (dx_j^{(1)} - dx_j^{(3)})(dx_k^{(2)} - dx_k^{(3)}) \end{aligned} \tag{9.164}$$

where e_{ijk} is the permutation tensor and the vectors $dx_i^{(j)}$ do not coincide with the principal damage axes in the general case. The sum of these vectors is zero due to closure of the surface area of tetrahedron, that is

$$dS_i^{(1)} + dS_i^{(2)} + dS_i^{(3)} + dS_i^{(4)} = 0_i \tag{9.165}$$

Consider now a tetrahedron of a material with internal damage as shown in Figure 9.20(b). The nominal dimensions of this tetrahedron are the same as those for Figure 9.20(a), but the areas are reduced by scalar factors α, β, γ, and κ from the previous tetrahedron with their corresponding normals unchanged. Then, the area vectors are

$$\begin{aligned}
\mathrm{d}\bar{S}_i^{(1)} &= -\tfrac{1}{2}\alpha_{ijk}\,\mathrm{d}x_j^{(2)}\,\mathrm{d}x_k^{(3)} = \alpha\,\mathrm{d}S_i^{(1)} \\
\mathrm{d}\bar{S}_i^{(2)} &= -\tfrac{1}{2}\beta_{ijk}\,\mathrm{d}x_j^{(3)}\,\mathrm{d}x_k^{(1)} = \beta\,\mathrm{d}S_i^{(2)} \\
\mathrm{d}\bar{S}_i^{(3)} &= -\tfrac{1}{2}\gamma_{ijk}\,\mathrm{d}x_j^{(1)}\,\mathrm{d}x_k^{(2)} = \gamma\,\mathrm{d}S_i^{(3)} \\
\mathrm{d}\bar{S}_i^{(4)} &= -\tfrac{1}{2}\kappa_{ijk}(\mathrm{d}x_j^{(1)} - \mathrm{d}x_j^{(3)})(\mathrm{d}x_k^{(2)} - \mathrm{d}x_k^{(3)}) = \kappa\,\mathrm{d}S_i^{(4)}
\end{aligned} \tag{9.166}$$

where $\alpha_{ijk} = \alpha e_{ijk}, \beta_{ijk} = \beta e_{ijk}, \gamma_{ijk} = \gamma e_{ijk}$, and $\kappa_{ijk} = \kappa e_{ijk}$. The areas in (9.166) represent net cross-sectional areas of the element. These are the areas that are effectively resisting loads and are perpendicular to the coordinate axes x_1, x_2, and x_3, respectively. Note that $\mathrm{d}\bar{S}_{\mathrm{i}}^{(4)}$ denotes the inclined side. The parameters α, β, and γ are discussed further later in this section. We note that the vectors $\mathrm{d}\bar{S}_i^{(1)}, \ldots, \mathrm{d}\bar{S}_i^{(4)}$, defined in (9.166), and the corresponding $\mathrm{d}S_i^{(1)}, \ldots, \mathrm{d}S_i^{(4)}$ defined in (9.164), differ in length, and the condition of closure cannot be satisfied, that is

$$\mathrm{d}\bar{S}_i^{(1)} + \mathrm{d}\bar{S}_i^{(2)} + \mathrm{d}\bar{S}_i^{(3)} + \mathrm{d}\bar{S}_i^{(4)} \neq 0_i \tag{9.167}$$

except for the case of isotropic damage where $\alpha = \beta = \gamma = \kappa$.

Because of the existence of microcavities in the material, the load-carrying net areas of the damaged continuum, Figure 9.20(b), are reduced. It is now postulated that there exists a fictitious undamaged continuum, as shown in Figure 9.20(c), which is mechanically equivalent to the damaged continuum. Thus, the damage state is represented by the fictitious undamaged continuum such that

$$\begin{aligned}
\mathrm{d}\hat{S}_i^{(1)} &= -\tfrac{1}{2}e_{ijk}\,\mathrm{d}\hat{x}_j^{(2)}\,\mathrm{d}\hat{x}_j^{(3)} = \mathrm{d}\bar{S}_i^{(1)} \\
\mathrm{d}\hat{S}_i^{(2)} &= -\tfrac{1}{2}e_{ijk}\,\mathrm{d}\hat{x}_j^{(3)}\,\mathrm{d}\hat{x}_j^{(1)} = \mathrm{d}\bar{S}_i^{(2)} \\
\mathrm{d}\hat{S}_i^{(3)} &= -\tfrac{1}{2}e_{ijk}\,\mathrm{d}\hat{x}_j^{(1)}\,\mathrm{d}\hat{x}_j^{(2)} = \mathrm{d}\bar{S}_i^{(3)} \\
\mathrm{d}\hat{S}_i^{(4)} &= -\tfrac{1}{2}e_{ijk}(\mathrm{d}\hat{x}_j^{(1)} - \mathrm{d}\hat{x}_j^{(3)})(\mathrm{d}\hat{x}_k^{(2)} - \mathrm{d}\hat{x}_k^{(3)})
\end{aligned} \tag{9.168}$$

where $d\hat{x}_i^{(j)}$ define the fictitious differential tetrahedron. Furthermore, the closure of the fictitious undamaged continuum is assumed to be satisfied. Thus,

$$d\hat{S}_i^{(1)} + d\hat{S}_i^{(2)} + d\hat{S}_i^{(3)} + d\hat{S}_i^{(4)} = 0_i \tag{9.169}$$

The three area vectors $d\hat{S}_i^{(j)}$ in (9.168) are identical to the vectors $d\bar{S}_i^{(j)}$ in (9.166) and are related to the vectors $dS_i^{(j)}$ in (9.164) by scalar factors α, β, and γ, respectively. The fourth vectors $d\hat{S}_i^{(4)}$ and $d\bar{S}_i^{(4)}$ are different in both magnitude and direction. Since (9.168) is used in the remaining part of this chapter, the parameter κ is not important and is not discussed further. It is reasonable to assume that $d\hat{S}_i^{(4)}$ and $dS_i^{(4)}$ are related by a linear relation

$$d\hat{S}_i^{(4)} = \psi_{ij}\, dS_j^{(4)} \tag{9.170}$$

where ψ_{ij} is a second-order tensor. In (9.170), $d\hat{S}_i^{(4)}$ represents the effective load-carrying area of the damaged material and $dS_j^{(4)}$ is the gross area on the inclined face of the material element. Therefore, tensor ψ_{ij} represents the fraction of $dS_j^{(4)}$ that can be used to carry load, accounting for the effect of damage. Tensor ψ_{ij} is known as the *continuity tensor*, since it describes the continuity state of the material.

The continuity tensor ψ_{ij} can be determined directly from (9.170). Substituting (9.164) and (9.165) into the right-hand side of (9.170), and (9.166), (9.168), and (9.169) into the left-hand side of (9.170), we obtain

$$\begin{aligned} &\alpha_{ijk}\, dx_j^{(2)}\, dx_k^{(3)} + \beta_{ijk}\, dx_j^{(3)}\, dx_k^{(1)} + \gamma_{ijk}\, dx_j^{(1)}\, dx_k^{(2)} \\ &\quad = \psi_{ir} e_{rjk} (dx_j^{(2)}\, dx_k^{(3)} + dx_j^{(3)}\, dx_k^{(1)} + dx_j^{(1)}\, dx_k^{(2)}) \end{aligned} \tag{9.171}$$

If the vectors $dx_i^{(j)}$ are aligned with the coordinate axes x_i, respectively, then $dx_i^{(j)} = \delta_{ij} |ds^j|$ (no sum on j), where $|ds^j|$ defines the magnitude of the vector $dx_i^{(j)}$. Then, for $i = 1$, (9.171) becomes

$$(\psi_{11} - \alpha) e_{123} |ds^2||ds^3| + \psi_{12} e_{231} |ds^3||ds^1| + \psi_{13} e_{321} |ds^1||ds^2| = 0 \tag{9.172}$$

Since $|ds^j|$, the magnitudes of $dx_i^{(j)}$, are independent of each other, they can be independently varied. But, due to the closure assumption, (9.172) cannot be violated. Therefore, (9.172) can be satisfied for all values of $|ds^j|$, if and only if

$$\psi_{11} = \alpha, \qquad \psi_{12} = 0, \qquad \psi_{13} = 0 \tag{9.173}$$

Similar discussions may be used for $i = 2$ and 3. Thus, the continuity tensor is found to be

$$[\psi] = \begin{bmatrix} \alpha & 0 & 0 \\ 0 & \beta & 0 \\ 0 & 0 & \gamma \end{bmatrix} \tag{9.174}$$

It is seen that when the x_i axes are principal damage axes, the continuity tensor ψ_{ij} is in a diagonal form.

In the case of uniaxial tension along the x_1 direction, let s be the total gross cross-sectional area and $\hat{s}$ be the effective area of resistance so that $\hat{s} < s$. In view of (9.170), vectors $\mathrm{d}\hat{S}_i^{(4)}$ and $\mathrm{d}S_i^{(4)}$ are represented by $[\hat{s},\ 0,\ 0]^{\mathrm{T}}$ and $[s,\ 0,\ 0]^{\mathrm{T}}$, respectively, with $n_i^{(4)} = [1,\ 0,\ 0]^{\mathrm{T}}$. Then, by use of (9.174), (9.170) reduces to

$$\hat{s} = \psi s \tag{9.175}$$

where $\psi = \psi_{11} = \alpha$. Therefore, $\psi = \hat{s}/s$ represents that fraction of the cross-sectional area which can be used to resist load. When $\psi = 1$, the material is in the virgin state without damage and $\hat{s}$ is identical to s. When $\psi = 0$, the material can no longer resist load, since its effective area of resistance is reduced to zero.

The *damage tensor* is defined as a complementary (dual) tensor of continuity [57]. In other words, the damage tensor represents the fraction of the cross-sectional area that was reduced by microdefects. In the uniaxial loading case, the damage variable can be expressed in terms of the continuity variable ψ as

$$D = \frac{s - \hat{s}}{s} = 1 - \psi \tag{9.176}$$

Thus, $D = 0$ corresponds to the undamaged state and $D = 1$ corresponds to the breaking state of the material. In the multiaxial case, a second-order damage tensor D_{ij} is defined as

$$D_{ij} = \delta_{ij} - \psi_{ij} \tag{9.177}$$

Note that D_{ij} is the damage tensor and is not to be confused with the rate of deformation tensor used in most chapters of this book. In the special case, when the x_i axes are also the principal axes of damage, tensor ψ_{ij} is given by (9.174), and the damage tensor is given by

$$[D] = \begin{bmatrix} D_1 & 0 & 0 \\ 0 & D_2 & 0 \\ 0 & 0 & D_3 \end{bmatrix} = \begin{bmatrix} 1-\alpha & 0 & 0 \\ 0 & 1-\beta & 0 \\ 0 & 0 & 1-\gamma \end{bmatrix} \tag{9.178}$$

It is seen that the principal values D_1, D_2, and D_3 are related to the principal continuity variables α, β, and γ, respectively. These principal values D_i can be measured on the test specimens cut along mutually perpendicular directions x_1, x_2, and x_3, respectively. Alternatively, the continuity tensor is given in terms of the principal values of the damage tensor as

$$[\psi] = \begin{bmatrix} \alpha & 0 & 0 \\ 0 & \beta & 0 \\ 0 & 0 & \gamma \end{bmatrix} = \begin{bmatrix} 1 - D_1 & 0 & 0 \\ 0 & 1 - D_2 & 0 \\ 0 & 0 & 1 - D_3 \end{bmatrix} \tag{9.179}$$

where $\alpha = 1 - D_1$, $\beta = 1 - D_2$, and $\gamma = 1 - D_3$.

9.5.3 Gross Stress, Net Stress, and Effective Stress

In the previous section, a definition of damage is derived by introducing a fictitious undamaged continuum that is mechanically equivalent to the actual damaged continuum. In this section, various definitions of stress, such as the gross stress, the net stress, and the effective stress, are discussed. The gross stress or the Cauchy stress, σ_{ij}, is the stress defined on the actual damaged continuum while the net stress, $\hat{\sigma}_{ij}$, and the effective stress, $\tilde{\sigma}_{ij}$, are the nonsymmetric and symmetric stress, respectively, defined on the fictitious undamaged continuum.

By considering the actual damaged continuum and the fictitious undamaged continuum under the same applied force, the corresponding stresses on the two continua are different, since the stresses are calculated over different cross-sectional areas of the continua. If the equilibrium of the actual damaged continuum is considered (Figure 9.21(a)), one can derive the relation between the stress vector t_i and the stress tensor σ_{ij}, that is,

$$t_i = \sigma_{ji} n_j \tag{9.180}$$

where n_i is the unit normal of an area element $\mathrm{d}S$. Similarly, the equilibrium of the fictitious undamaged continuum, with an area element $\mathrm{d}\hat{S}$ and unit normal $\hat{n}_i$ (Figure 9.21(b)) yields

$$\hat{t}_i = \hat{\sigma}_{ji} \hat{n}_j \tag{9.181}$$

where $\hat{\sigma}_{ij}$ is the *net stress* acting on the fictitious undamaged continuum and $\hat{t}_i$ is the corresponding stress vector. Since the area elements $\mathrm{d}S$ and $\mathrm{d}\hat{S}$ are subjected to the same force, that is, $\mathrm{d}\hat{P}_i = \mathrm{d}P_i$, we can conclude that

$$\mathrm{d}P_i = t_i \, \mathrm{d}S = \sigma_{ji} n_j \, \mathrm{d}S = \hat{\sigma}_{ki} \hat{n}_k \mathrm{d}\hat{S} = \hat{t}_i \, \mathrm{d}\hat{S} = \mathrm{d}\hat{P}_i \tag{9.182}$$

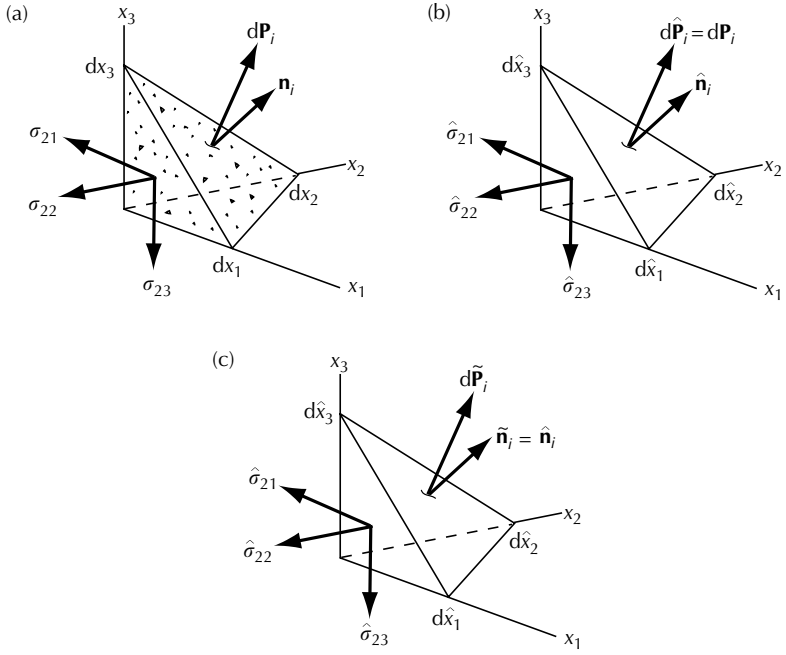

FIGURE 9.21
Definitions of stress tensor and pseudo-force: (a) Cauchy stress, (b) net stress, (c) effective stress (From Wu, H.C. and Nanakorn, C.K., *Int. J. Solids Struct.*, 36, 5057, 1999. With permission from Elsevier).

where dS and $d\hat{S}$ are scalar quantities and the corresponding vector expression is obtained from (9.170) as $\hat{n}_i\, d\hat{S} = \psi_{ij} n_j\, dS$. Thus, (9.182) becomes

$$(\sigma_{ji} - \hat{\sigma}_{ki}\psi_{kj}) n_j\, dS = 0 \tag{9.183}$$

and it follows that

$$\sigma_{ij} = \psi_{ki}\hat{\sigma}_{kj} \quad \text{and} \quad \hat{\sigma}_{ij} = \psi^{-1}_{ik}\sigma_{kj} \tag{9.184}$$

By use of (9.174), the net-stress $\hat{\sigma}_{ij}$ is found to be

$$[\hat{\sigma}] = \begin{bmatrix} \dfrac{\sigma_{11}}{\alpha} & \dfrac{\sigma_{12}}{\alpha} & \dfrac{\sigma_{13}}{\alpha} \\ \dfrac{\sigma_{21}}{\beta} & \dfrac{\sigma_{22}}{\beta} & \dfrac{\sigma_{23}}{\beta} \\ \dfrac{\sigma_{31}}{\gamma} & \dfrac{\sigma_{32}}{\gamma} & \dfrac{\sigma_{33}}{\gamma} \end{bmatrix} \tag{9.185}$$

which shows that the net-stress $\hat{\sigma}_{ij}$ is nonsymmetric, except for the case of isotropic damage. It is not convenient to use the nonsymmetric stress

tensor $\hat{\sigma}_{ij}$ together with a symmetric strain tensor and strain rate in the constitutive equations. Therefore, new symmetric stress measures, the *effective stress* $\tilde{\sigma}_{ij}$, have been defined on the fictitious undamaged continuum and used in the constitutive equations. Various definitions have been proposed to symmetrize $\hat{\sigma}_{ij}$. These definitions may be summarized based on various transformations operated on the net stress $\hat{\sigma}_{ij}$. They are

1. Betten [56] proposed a transformed net-stress tensor, which is an effective stress subjected to the following transformation

$$\tilde{\sigma}_{ij} = \tfrac{1}{2}(\hat{\sigma}_{ij}\psi_{kj}^{-1} + \psi_{ki}^{-1}\hat{\sigma}_{jk}) \tag{9.186}$$

Using (9.184), the expression becomes

$$\tilde{\sigma}_{ij} = \tfrac{1}{2}(\psi_{ik}^{-1}\psi_{ij}^{-1} + \psi_{jk}^{-1}\psi_{mi}^{-1})\sigma_{km} = M_{ijkm}\sigma_{km} \tag{9.187}$$

where

$$M_{ijkm} = \tfrac{1}{2}(\psi_{ik}^{-1}\psi_{ij}^{-1} + \psi_{jk}^{-1}\psi_{mi}^{-1}) \tag{9.188}$$

The fourth-order transformation tensor M_{ijkm} is referred to as the *damage-effect tensor*. For ψ_{ij} to have the diagonalized form of (9.174), (9.187) is expressed in the matrix form as

$$\begin{bmatrix} \tilde{\sigma}_{11} \\ \tilde{\sigma}_{22} \\ \tilde{\sigma}_{33} \\ \tilde{\sigma}_{12} \\ \tilde{\sigma}_{23} \\ \tilde{\sigma}_{31} \end{bmatrix} = \begin{bmatrix} \frac{1}{\alpha^2} & 0 & 0 & 0 & 0 & 0 \\ & \frac{1}{\beta^2} & 0 & 0 & 0 & 0 \\ & & \frac{1}{\gamma^2} & 0 & 0 & 0 \\ & & & \frac{1}{\alpha\beta} & 0 & 0 \\ & \text{sym} & & & \frac{1}{\beta\gamma} & 0 \\ & & & & & \frac{1}{\gamma\alpha} \end{bmatrix} \begin{bmatrix} \sigma_{11} \\ \sigma_{22} \\ \sigma_{33} \\ \sigma_{12} \\ \sigma_{23} \\ \sigma_{31} \end{bmatrix} \tag{9.189}$$

or

$$[\tilde{\sigma}] = \begin{bmatrix} \frac{\sigma_{11}}{\alpha^2} & \frac{\sigma_{12}}{\alpha\beta} & \frac{\sigma_{13}}{\alpha\gamma} \\ \frac{\sigma_{12}}{\alpha\beta} & \frac{\sigma_{22}}{\beta^2} & \frac{\sigma_{23}}{\beta\gamma} \\ \frac{\sigma_{13}}{\alpha\gamma} & \frac{\sigma_{23}}{\beta\gamma} & \frac{\sigma_{33}}{\gamma^2} \end{bmatrix} \tag{9.190}$$

which is a symmetric tensor.

2. The effective stress proposed by Cordebois and Sidoroff [58], also by Chow and Wang [59], is defined through its components given by

$$\tilde{\sigma}_{ij} = \sqrt{\hat{\sigma}_{ij}\hat{\sigma}_{ji}} \qquad \text{(no sum on } i \text{ or } j\text{)} \tag{9.191}$$

   Since the right-hand side of (9.191) is not a tensor operation, the effective stress $\tilde{\sigma}_{ij}$ as defined by (9.191) is not a tensor. However, in the matrix form, the above definition of effective stress can also give rise to a linear relationship between $\tilde{\sigma}_{ij}$ and σ_{ij}.
3. In a study of anisotropic damage in ductile solids, Stumvoll and Swobada [60] defined the effective stress as the symmetric part of the net-stress tensor, that is,

$$\tilde{\sigma}_{ij} = \tfrac{1}{2}(\tilde{\sigma}_{ij} + \tilde{\sigma}_{ji}) = \tfrac{1}{2}(\psi_{ik}^{-1}\delta_{jm} + \delta_{ik}\psi_{jm}^{-1})\sigma_{km} \tag{9.192}$$

   where the damage-effect tensor is

$$M_{ijkm} = \tfrac{1}{2}(\psi_{ik}^{-1}\delta_{jm} + \delta_{ik}\psi_{jm}^{-1}) \tag{9.193}$$

   By use of (9.179), M_{ijkm} may be written in terms of the principal damage D_1, D_2, and D_3 and it can be reduced to a form used by Rabotnov [61] and later by Chow and Lu [62].

In all cases, the effective stress $\tilde{\sigma}_{ij}$ is related to the Cauchy stress σ_{ij} by the equation

$$\tilde{\sigma}_{ij} = M_{ijkm}\sigma_{km} \tag{9.194}$$

where the exact expression for the damage-effect tensor M_{ijkm} depends on the method used in symmetrizing $\hat{\sigma}_{ij}$. With respect to the principal damage coordinate system, the damage-effect tensor M_{ijkm} is represented by a 6×6 diagonal matrix. In a special case, if the directions of principal stresses coincide with those of the principal damage, then these equations further reduce to

$$\begin{bmatrix} \tilde{\sigma}_{11} \\ \tilde{\sigma}_{22} \\ \tilde{\sigma}_{33} \end{bmatrix} = \begin{bmatrix} M_{1111} & 0 & 0 \\ 0 & M_{2222} & 0 \\ 0 & 0 & M_{3333} \end{bmatrix} \begin{bmatrix} \sigma_{11} \\ \sigma_{22} \\ \sigma_{33} \end{bmatrix} \tag{9.195}$$

where M_{1111}, M_{2222}, and M_{3333} are functions of principal damage variables D_1, D_2, and D_3.

The interpretation of the effective stress is now investigated. The net-stress tensor $\hat{\sigma}_{ij}$ is an actual nonsymmetric stress acting on the fictitious, undamaged continuum, which is subjected to the same applied force as the original, actual,

damaged continuum, that is, $\mathrm{d}\hat{P}_i = \mathrm{d}P_i$. On the other hand, the effective stress tensor $\tilde{\sigma}_{ij}$ is the fictitious symmetric stress acting on the fictitious undamaged continuum due to the application of the pseudo-force $\mathrm{d}\tilde{P}_i$, as shown in Figure 9.21(c). To validate this statement, the Cauchy formula, relating the pseudo-force $\mathrm{d}\tilde{P}_i$ to the effective stress $\tilde{\sigma}_{ij}$ is

$$\mathrm{d}\tilde{P}_i = \tilde{\sigma}_{ji}\hat{n}\,\mathrm{d}\hat{S} \tag{9.196}$$

where $\hat{n}_i$ and $\mathrm{d}\hat{S}$ were previously defined on the fictitious undamaged element. Using (9.170) and (9.194), the above relation can be rewritten in terms of the Cauchy stress and the area element $n_i\,\mathrm{d}S$ as

$$\mathrm{d}\tilde{P}_i = M_{jikm}\sigma_{km}\hat{n}_j\,\mathrm{d}\hat{S} = M_{jikm}\sigma_{km}\psi_{jr}n_r\,\mathrm{d}S \tag{9.197}$$

If Betten's definition of the damage-effect tensor (9.188) is used, (9.197) becomes

$$\mathrm{d}\tilde{P}_i = \psi_{ij}^{-1}\,\mathrm{d}P_j \tag{9.198}$$

This equation establishes that the pseudo-force $d\tilde{P}_i$ is related to the original applied force $\mathrm{d}P_i$ by the inverse-transpose of the continuity tensor ψ_{ij}. If, on the other hand, the damage-effect tensor is defined by (9.193), then the pseudo-force on the fictitious undamaged element is

$$\mathrm{d}\tilde{P}_i = \tfrac{1}{2}(\mathrm{d}P_i + \hat{\sigma}_{ij}\hat{n}_j\,\mathrm{d}\hat{S}) = \tfrac{1}{2}(\mathrm{d}P_i + \psi_{ik}^{-1}\sigma_{jk}\hat{n}_j\,\mathrm{d}\hat{S}) \tag{9.199}$$

We note that $\mathrm{d}P_i = \hat{\sigma}_{ji}\hat{n}_j\,\mathrm{d}\hat{S} \neq \hat{\sigma}_{ij}\hat{n}_j\,\mathrm{d}\hat{S}$, due to the nonsymmetric property of $\hat{\sigma}_{ij}$. The last term of (9.199) can be viewed as an additional abstract-force due to the actual stress σ_{ij} acting over the area of the fictitious undamaged continuum, that is, $\hat{n}_j\,\mathrm{d}\hat{S}$. Therefore, the pseudo-force corresponding to this definition of effective stress has no simple physical interpretation.

9.5.4 An Internal State Variables Theory

Based upon concepts of continuum mechanics and irreversible thermodynamics with internal variables, the Clausius–Duhem inequality (with thermal gradient) with respect to the actual, damaged continuum is given by (see [63])

$$\sigma_{ij}\dot{\varepsilon}_{ij} - \dot{\Psi}(\varepsilon_{ij}, q_{ij}^r, D_{ij}, \gamma_{ij}^s, \theta) - \eta\dot{\theta} - \frac{1}{\theta}h_j\theta_{,j} \geq 0 \tag{9.200}$$

In (9.200), the Helmholtz free energy Ψ is a function of total (elastoplastic) strain ε_{ij}, damage measure D_{ij}, temperature θ, and two sets of internal

state variables q_{ij}^r and γ_{ij}^s. There are n number of internal variables q_{ij}^r ($r = 1, 2, \ldots, n$), which describe the state of plastic deformation, and m number of internal variables γ_{ij}^s ($s = 1, 2, \ldots, m$), which specify the state of damage in the continuum. h_i is heat flux vector and η is entropy density.

In a typical damage mechanics model, the damage tensor D_{ij} is treated as an internal state variable (it is macroscopically not measurable by definition) that describes the irreversible process of internal structure due to microdefects. However, in the present work, the damage tensor D_{ij} is not an internal state variable and it represents a measurable quantity, that is, the fraction of reduction in load-resisting area. It is a measurable quantity in the description of damage, even though it may be difficult to measure. The role played by D_{ij} in the description of damage is similar to the role played by strain, which is also measurable, in the description of plastic deformation.

In [54], a set of internal state variables γ_{ij}^s has been introduced to describe the state of internal damage as a result of growth and/or nucleation of microcracks and/or microvoids. The set of m internal variables γ_{ij}^s, which evolves with loading histories, is introduced to distinguish one internal state of damage from the others, similar to the set of internal variables q_{ij}^r which describes the state of plastic deformation that cannot be uniquely described by the plastic strain alone. The damage variable D_{ij} describes the current fraction of area reduction but not the state of damage. To elaborate, two continua of the same initial damaged state, when undergoing different loading histories, may end up having the same load-resisting area momentarily, hence the same value of D_{ij}, but having two different states of damage.

The concept of using both damage tensor D_{ij} and damage internal state variables γ_{ij}^s in [54] is similar but not equal to the concept of Krajcinovic [64] proposed for the brittle CDM model. In Krajcinovic's model, the microcracks vector fields $\omega^{(i)}$, treated as internal variables, are used to describe the state of damage, and a scalar damage measure D is used to describe the overall damage of the material. However, D is the macroscopic counterpart of the microscopic $\omega^{(i)}$ (they are related by an integral) and D is, therefore, not measurable. In the present work, D_{ij} is defined by a definition not directly related to γ_{ij}^s and it is influenced by the current loading condition. Thus, at the same state of damage, a different incremental loading state will give rise to a different increment of D_{ij}. Hence, $\mathrm{d}D_{ij}$ is different when the material element is subjected to incremental tension, compression, or shear. As an illustration, consider uniaxial tension of a cylinder. The majority of the microcracks will develop in the plane perpendicular to the maximum tensile strain. If the specimen is then unloaded and subsequently subjected to a small compressive stress along its axial direction, the specimen will behave as though it were undamaged up to a certain compressive stress threshold, since all of the microcracks will be passive (crack closure). Consequently, the initial increment of D_{ij} depends on whether the stress increment is tensile or compressive, even though the state of damage is the same at that moment. Furthermore, with the second-order tensor representations of D_{ij} and γ_{ij}^s, the theory [54] is capable of describing both spherical (e.g., void volume fraction) and

planar (e.g., a system of planar microcracks) effects of microcracks, and their interactions.

In the fictitious undamaged configuration, the volume and surface area of the continuum are reduced by excluding the volume and area of the continuum that were previously occupied by microdefects. These are denoted by $\hat{V}$ and $\hat{S}$, respectively. Consequently, the fictitious undamaged matrix material becomes homogeneous and isotropic. For a given force field $\hat{P}_i = P_i$, the first law of thermodynamics written for this fictitious undamaged continuum is

$$\frac{\mathrm{d}}{\mathrm{d}t}\int_{\hat{V}}\left(\frac{1}{2}\hat{v}_i\hat{v}_i+\hat{\varepsilon}\right)\hat{\rho}\,\mathrm{d}\hat{V}=\int_{\hat{V}}\hat{\rho}\hat{b}_i\hat{v}_i\mathrm{d}\hat{V}+\int_{\hat{S}}(\hat{\sigma}_{ji}\hat{v}_i-\hat{h}_j)\hat{n}_j\,\mathrm{d}\hat{S}+\int_{\hat{V}}\hat{r}\,\mathrm{d}\hat{V} \tag{9.201}$$

where $(\wedge)$ is used to indicate that the quantity is associated with the fictitious undamaged continuum. In (9.201), $\hat{v}_i$ is the velocity; $\hat{\varepsilon}$ is the internal energy density; $\hat{\rho}$ is the mass density; $\hat{b}_i$ is the body force; and $\hat{r}$ is the heat source term. The first term in the surface integral represents the rate of work done by surface traction and is expressed in terms of the nonsymmetric net-stress tensor $\hat{\sigma}_{ij}$. When the pseudo-force field $\tilde{P}_i$ is introduced to the fictitious continuum so that the corresponding effective stress $\tilde{\sigma}_{ij}$ is symmetric, (9.201) is written as

$$\frac{\mathrm{d}}{\mathrm{d}t}\int_{\hat{V}}\left(\frac{1}{2}\tilde{v}_i\tilde{v}_i+\hat{\varepsilon}\right)\hat{\rho}\,\mathrm{d}\hat{V}=\int_{\hat{V}}\hat{\rho}\hat{b}_i\tilde{v}_i\,\mathrm{d}\hat{V}+\int_{\hat{S}}(\tilde{\sigma}_{ji}\tilde{v}_i-\hat{h}_j)\hat{n}_j\,\mathrm{d}\hat{S}+\int_{\hat{V}}\hat{r}\,\mathrm{d}\hat{V} \tag{9.202}$$

Due to the use of pseudo-force field $\tilde{P}_i$, the velocity vector in this configuration is $\tilde{v}_i$ instead of $\hat{v}_i$, as indicated in (9.202). Consequently, the deformation of the fictitious undamaged continuum subjected to pseudo-force field $\tilde{P}_i$ is different from that subjected to force field P_i. The rate of deformation for the fictitious undamaged configuration is then defined by

$$\dot{\tilde{\varepsilon}}_{ij}=\frac{1}{2}\left(\frac{\partial\tilde{v}_i}{\partial x_j}+\frac{\partial\tilde{v}_j}{\partial x_i}\right) \tag{9.203}$$

where $\tilde{\varepsilon}_{ij}$ defines the deformation of the fictitious undamaged continuum (with pseudo-force field $\tilde{P}_i$) and is referred to as the effective strain. According to (9.203), the relationship between the effective strain $\tilde{\varepsilon}_{ij}$ and the actual strain ε_{ij} depends on transformations between velocity vectors from v_i to $\hat{v}_i$ and from $\hat{v}_i$ to $\tilde{v}_i$. In general, the explicit forms of these transformations are difficult to define due to the complexity of the geometry and mathematics involved. In this work, the effective strain $\tilde{\varepsilon}_{ij}$ is expressed in terms of damage tensor D_{ij} and actual strain ε_{ij}, and this relationship is discussed later in this section. The postulate of free energy equivalence is applied in the subsequent discussion. According to this postulate, which was initially proposed

by Cordebois and Sidoroff [58] in the form of strain-energy equivalence, the free energy for an actual, damaged material has the same form as that for a fictitious, undamaged material, but the variables are replaced by the effective quantities. Thus,

$$\tilde{\Psi}\left(\tilde{\varepsilon}_{ij}, \tilde{q}^r_{ij}, \gamma^s_{ij}, \theta\right) \equiv \Psi\left(\varepsilon_{ij}, q^r_{ij}, D_{ij}, \gamma^s_{ij}, \theta\right) \tag{9.204}$$

where the $\tilde{q}^r_{ij}$'s are the effective q^r_{ij}'s. Note that D_{ij} does not explicitly appear as one of the state variables on the left-hand side of (9.204). In view of (9.204), the free energy available to do mechanical work and stored in the fictitious continuum is the same as that stored in the actual continuum, resulting in an equivalent mechanical behavior.

The second law of thermodynamics and the equation of motion at the fictitious configuration subjected to the pseudo-force field $\tilde{P}_i$ become

$$\frac{\mathrm{d}}{\mathrm{d}t}\int_{\hat{V}} \hat{\rho}\eta \,\mathrm{d}\hat{V} \geq \int_{\hat{V}} \frac{\hat{r}}{\theta}\,\mathrm{d}\hat{V} - \int_{\hat{S}} \frac{\hat{h}_i}{\theta}\hat{n}_j \,\mathrm{d}\hat{S} \tag{9.205}$$

$$\frac{\partial \tilde{\sigma}_{ji}}{\partial x_i} + \hat{\rho}\hat{b}_i = \hat{\rho}\tilde{f}_i \tag{9.206}$$

where $\hat{f}_i = \mathrm{d}\tilde{v}_i/\mathrm{d}t$. Using (9.202) to (9.206), the Clausius–Duhem inequality for the fictitious undamaged continuum in the isothermal condition is given by

$$\tilde{\sigma}_{ij}\dot{\tilde{\varepsilon}}_{ij} - \dot{\tilde{\Psi}}\left(\tilde{\varepsilon}_{ij}, \tilde{q}^r_{ij}, \gamma^s_{ij}\right) \geq 0 \tag{9.207}$$

so that

$$\left(\tilde{\sigma}_{ij} - \frac{\partial \tilde{\Psi}}{\partial \tilde{\varepsilon}_{ij}}\right)\dot{\tilde{\varepsilon}}_{ij} - \frac{\partial \tilde{\Psi}}{\partial \tilde{q}^r_{ij}}\dot{\tilde{q}}^r_{ij} - \frac{\partial \tilde{\Psi}}{\partial \gamma^s_{ij}}\dot{\gamma}^s_{ij} \geq 0 \tag{9.208}$$

In the fictitious continuum, $\tilde{\varepsilon}_{ij}, \tilde{q}^r_{ij}$, and γ^s_{ij} are the state variables so that they can be independently varied. Although, $\tilde{q}^r_{ij}$ may vary when $\tilde{\varepsilon}_{ij}$ changes, their relation is not one-to-one. Different $\tilde{\varepsilon}_{ij}$ histories may lead to the same $\tilde{q}^r_{ij}$, and a material with different $\tilde{q}^r_{ij}$ may correspond to the same $\tilde{\varepsilon}_{ij}$ momentarily. Thus, it is possible to vary $\tilde{\varepsilon}_{ij}$ so that $\tilde{q}^r_{ij}$ is left unchanged. Therefore, inequality (9.208) is always satisfied, if

$$\tilde{\sigma}_{ij} = \frac{\partial \tilde{\Psi}}{\partial \tilde{\varepsilon}_{ij}} \quad \text{and} \quad -\frac{\partial \tilde{\Psi}}{\partial \tilde{q}^r_{ij}}\dot{\tilde{q}}^r_{ij} - \frac{\partial \tilde{\Psi}}{\partial \gamma^s_{ij}}\dot{\gamma}^s_{ij} \geq 0 \tag{9.209}$$

According to the first equation of (9.209), the effective stress $\tilde{\sigma}_{ij}$ is derivable from the fictitious undamaged free-energy $\tilde{\Psi}$. The inequality (9.209) gives the thermodynamic constraints on the laws governing the evolution of the two sets of internal variables, $\tilde{q}^r_{ij}$ and γ^s_{ij}.

It is now possible to derive the explicit relationship for effective strain $\tilde{\varepsilon}_{ij}$. A relation similar to the first equation of (9.209) exists for the actual damaged continuum. When the postulate of free energy equivalence is assumed, this relation is

$$\sigma_{ij} = \frac{\partial \Psi}{\partial \varepsilon_{ij}} = \frac{\partial \tilde{\Psi}}{\partial \varepsilon_{ij}} = \frac{\partial \tilde{\Psi}}{\partial \tilde{\varepsilon}_{mn}} \frac{\partial \tilde{\varepsilon}_{mn}}{\partial \varepsilon_{ij}} + \frac{\partial \tilde{\Psi}}{\partial \tilde{q}^r_{mn}} \frac{\partial \tilde{q}^r_{mn}}{\partial \varepsilon_{ij}} \tag{9.210}$$

where the effective internal variable $\tilde{q}^r_{ij}$ is assumed to be a function of the actual internal variable q^r_{ij} and damage tensor D_{ij}. Note that, for the actual damaged continuum s independent variables are $\varepsilon_{ij}, q^r_{ij}$, and D_{ij}, so that the second term on the right-hand side of (9.210) drops out and the equation reduces to

$$\sigma_{ij} = \frac{\partial \tilde{\Psi}}{\partial \tilde{\varepsilon}_{mn}} \frac{\partial \tilde{\varepsilon}_{mn}}{\partial \varepsilon_{ij}} = \tilde{\sigma}_{mn} \frac{\partial \tilde{\varepsilon}_{mn}}{\partial \varepsilon_{ij}} \tag{9.211}$$

Using (9.194), (9.211) further reduces to

$$\frac{\partial \tilde{\varepsilon}_{mn}}{\partial \varepsilon_{ij}} = N_{ijmn} \tag{9.212}$$

where N_{ijmn} is the inverse of M_{ijmn} and is a function of D_{ij} only, or

$$M_{ijmn} N_{rsij} = I_{mnrs} \tag{9.213}$$

In (9.213), the fourth-order identity tensor is $I_{ijkm} = \delta_{ik}\delta_{jm}$ and δ_{ij} is Kronecker's delta. Thus, it follows from (9.212) that the effective strain $\tilde{\varepsilon}_{ij}$ is linearly related to ε_{ij} by

$$\tilde{\varepsilon}_{ij} = N_{kmij}\varepsilon_{km} \quad \text{or} \quad \varepsilon_{ij} = M_{kmij}\tilde{\varepsilon}_{km} \tag{9.214}$$

Then, it is assumed that the following relations are valid for the internal variable q^r_{ij}

$$\tilde{q}^r_{ij} = N_{kmij} q^r_{km} \quad \text{or} \quad q^r_{ij} = M_{kmij}\tilde{q}^r_{km} \tag{9.215}$$

Constitutive equations at the fictitious undamaged configuration must satisfy the inequality given by (9.207). By use of (9.214) this inequality can be written as

$$\sigma_{ij}\dot{\varepsilon}_{ij} - \dot{\tilde{\Psi}}(\tilde{\varepsilon}_{ij}, \tilde{q}^r_{ij}, \gamma^s_{ij}) + \tilde{\sigma}_{km} \frac{\partial \tilde{\varepsilon}_{km}}{\partial D_{ij}} \dot{D}_{ij} \geq 0 \tag{9.216}$$

where

$$\frac{\partial \tilde{\varepsilon}_{ij}}{\partial D_{mn}} = \frac{\partial N_{rsij}}{\partial D_{mn}} \varepsilon_{rs} \tag{9.217}$$

By observing (9.204), the first two terms of (9.216) are the same as the left-hand side of (9.200) in the isothermal case. During an incremental loading, the fictitious undamaged continuum undergoes a deformation in the matrix as well as an increase in damage. The first two terms of (9.216) are energy dissipated associated with this process. However, by definition, the state of the fictitious material remains undamaged at the end of each loading increment. The amount of energy dissipated in order to restore the fictitious continuum to the undamaged state is represented by the last term of inequality (9.216). For convenience, inequality (9.216) can be rewritten as

$$\sigma_{ij}\dot{\varepsilon}_{ij} - \dot{\tilde{\Psi}}\left(\tilde{\varepsilon}_{ij}, \tilde{q}^r_{ij}, \gamma^s_{ij}\right) - G_{ij}\dot{D}_{ij} \geq 0 \tag{9.218}$$

where

$$G_{ij} = -\tilde{\sigma}_{km}\frac{\partial \tilde{\varepsilon}_{km}}{\partial D_{ij}} \tag{9.219}$$

Tensor G_{ij} is the thermodynamic force associated with unit damage growth $\dot{D}_{ij}$, and, in this work, it is referred to as the "damage force" for simplicity. This quantity may also be considered as the energy release rate per unit damage advance. Physically, the negative of the damage force, $-G_{ij}$, can be interpreted as the "restoring force" that restores the fictitious continuum to its undamaged state after experiencing a unit damage growth $\dot{D}_{ij}$. It is seen from (9.219) that G_{ij} can be expressed in terms of $\tilde{\sigma}_{ij}$, $\tilde{\varepsilon}_{ij}$, and D_{ij}. A further discussion of the damage force can be found in the appendix of [54].

9.5.5 Plasticity and Damage

We now characterize the plastic deformation process, the damage process, and the coupling between the two processes. Starting with the actual damaged configuration, where the state variables are ε_{ij}, D_{ij}, q^r_{ij}, and γ^s_{ij}, the Clausius–Duhem inequality (9.200) can be rewritten for isothermal process as

$$\sigma_{ij}\dot{\varepsilon}_{ij} - \frac{\partial \Psi}{\partial \varepsilon_{ij}}\dot{\varepsilon}_{ij} - \frac{\partial \Psi}{\partial q^r_{ij}}\dot{q}^r_{ij} - \frac{\partial \Psi}{\partial D_{ij}}\dot{D}_{ij} - \frac{\partial \Psi}{\partial \gamma^s_{ij}}\dot{\gamma}^s_{ij} \geq 0 \tag{9.220}$$

Replacing Ψ by $\tilde{\Psi}$ and noting that D_{ij} and γ^s_{ij} are independent variables, (9.220) becomes

$$\sigma_{ij}\dot{\varepsilon}_{ij} - \frac{\partial \tilde{\Psi}}{\partial \tilde{\varepsilon}_{ij}}\frac{\partial \tilde{\varepsilon}_{ij}}{\partial \varepsilon_{km}}\dot{\varepsilon}_{km} - \frac{\partial \tilde{\Psi}}{\partial \tilde{q}^r_{ij}}\frac{\partial \tilde{q}^r_{ij}}{\partial q^r_{km}}\dot{q}^r_{km} - \left(\frac{\partial \tilde{\Psi}}{\partial \tilde{\varepsilon}_{ij}}\frac{\partial \tilde{\varepsilon}_{ij}}{\partial D_{km}} + \frac{\partial \tilde{\Psi}}{\partial \tilde{q}^r_{ij}}\frac{\partial \tilde{q}^r_{ij}}{\partial D_{km}}\right)\dot{D}_{km}$$
$$- \frac{\partial \tilde{\Psi}}{\partial \gamma^s_{ij}}\dot{\gamma}^s_{ij} \geq 0 \tag{9.221}$$

or, after regrouping of terms, it may be shown that

$$\sigma_{ij}\dot{\varepsilon}_{ij} - \dot{\tilde{\Psi}}\left(\tilde{\varepsilon}_{ij}, \tilde{q}^r_{ij}, \gamma^s_{ij}\right) \geq 0 \tag{9.222}$$

Constraint (9.222) represents the Clausius–Duhem inequality of the actual damaged configuration. However, unlike (9.200), inequality (9.222) involves the fictitious free energy $\tilde{\Psi}(\tilde{\varepsilon}_{ij}, \tilde{q}^r_{ij}, \gamma^s_{ij})$, which is defined in the fictitious undamaged configuration, where the fictitious material is isotropic. Therefore, $\tilde{\Psi}(\tilde{\varepsilon}_{ij}, \tilde{q}^r_{ij}, \gamma^s_{ij})$ involves only material constants that are isotropic tensors.

In an attempt to characterize the plastic deformation and the damage process, one recognizes that the damage process does not directly influence the mechanisms of plastic deformation; that is, there is no direct coupling between damage and plastic deformation. In general, plasticity is directly related to slips for metals and to other mechanisms for other materials. In all cases, damage influences plastic strains only because the net area of resistance decreases as the damage proceeds. In the present work, damage does not directly influence plastic deformation of the fictitious undamaged continuum, but it does influence the plastic deformation of the actual continuum. Based on this observation, the fictitious free energy $\tilde{\Psi}(\tilde{\varepsilon}_{ij}, \tilde{q}^r_{ij}, \gamma^s_{ij})$ is assumed to consist of two parts, the fictitious plastic potential $\tilde{\Psi}_1(\tilde{\varepsilon}_{ij}, \tilde{q}^r_{ij})$ and the damage potential $\tilde{\Psi}_2(D_{ij}, \gamma^s_{ij})$, that is,

$$\tilde{\Psi}\left(\tilde{\varepsilon}_{ij}, \tilde{q}^r_{ij}, \gamma^s_{ij}\right) = \tilde{\Psi}_1\left(\tilde{\varepsilon}_{ij}, \tilde{q}^r_{ij}\right) + \tilde{\Psi}_2\left(D_{ij}, \gamma^s_{ij}\right) \tag{9.223}$$

where potential $\tilde{\Psi}_1(\tilde{\varepsilon}_{ij}, \tilde{q}^r_{ij})$ characterizes the plastic process of the fictitious undamaged continuum while potential $\tilde{\Psi}_2(D_{ij}, \gamma^s_{ij})$ describes the damage process. During deformation, the microcracks and microvoids will extend, grow, and nucleate, resulting in progressive material deterioration. This damage deterioration is not arbitrary and it must obey thermodynamic constraints to be established. The damage potential $\tilde{\Psi}_2(D_{ij}, \gamma^s_{ij})$ is used to provide the equation of damage evolution and its necessary constraints. The state of microdefects is represented by the set of internal variables γ^s_{ij}. The change in microdefects together with the loading condition bring about a decrease in load-resisting area, which is represented at the macroscopic level by damage tensor D_{ij}. The effect is carried over to the deformation process, elastic or plastic, through the effective variables, $\tilde{\sigma}_{ij}$, $\tilde{\varepsilon}_{ij}$, and $\tilde{q}^r_{ij}$. Hence, an indirect coupling occurs between the plasticity and damage in the actual damaged continuum. Using (9.223), inequality (9.222) is written as

$$\sigma_{ij}\dot{\varepsilon}_{ij} - \dot{\tilde{\Psi}}_1\left(\tilde{\varepsilon}_{ij}, \tilde{q}^r_{ij}\right) - \dot{\tilde{\Psi}}_2\left(D_{ij}, \gamma^s_{ij}\right) \geq 0 \tag{9.224}$$

9.5.6 The Constitutive Equations and Constraints

Within an infinitesimal strain theory, the stress rate is usually represented by the material rate. In CDM, it is important, however, to consider the rotation of the principal directions of damage during the deformation process. The principal directions of damage do not generally coincide with the principal stress, when nonproportional loading takes place or when the material has suffered a prior damage. To satisfy the requirements of reference frame indifference, the rate of change of damage measure D_{ij} and the internal variables γ_{ij}^s are expressed by the corotational derivatives

$$D_{ij}^{\nabla} = \dot{D}_{ij} - \omega_{ik}D_{kj} + D_{ik}\omega_{kj}, \qquad \gamma_{ij}^{s\nabla} = \dot{\gamma}_{ij}^s - \omega_{ik}\gamma_{kj}^s + \gamma_{ik}^s\omega_{kj} \tag{9.225}$$

where ω_{ij} represents the spin of the principal damage coordinate frame with respect to the fixed reference coordinate frame. Thus, it follows from (9.224) that

$$\left(\sigma_{ij} - \frac{\partial\tilde{\Psi}_1}{\partial\tilde{\varepsilon}_{km}}\frac{\partial\tilde{\varepsilon}_{km}}{\partial\varepsilon_{ij}}\right)\dot{\varepsilon}_{ij} - \frac{\partial\tilde{\Psi}_1}{\partial\tilde{q}_{km}^r}\frac{\partial\tilde{q}_{km}^r}{\partial q_{ij}^r}\dot{q}_{ij}^r - \left(\frac{\partial\tilde{\Psi}_1}{\partial\tilde{\varepsilon}_{km}}\frac{\partial\tilde{\varepsilon}_{km}}{\partial D_{ij}} + \frac{\partial\tilde{\Psi}_1}{\partial\tilde{q}_{km}^r}\frac{\partial\tilde{q}_{km}^r}{\partial D_{ij}} + \frac{\partial\tilde{\Psi}_2}{\partial D_{ij}}\right)D_{ij}^{\nabla} - \frac{\partial\tilde{\Psi}}{\partial\gamma_{ij}^s}\gamma_{ij}^{s\nabla} \geq 0 \tag{9.226}$$

Since ε_{ij}, D_{ij}, q_{ij}^r, and γ_{ij}^s are independent state variables, fixing these values also fix the values of σ_{ij}, $\tilde{\Psi}_1$, and $\tilde{\Psi}_2$ because they are state functions. For inequality (9.226) not to be violated for any arbitrary choice of $\dot{\varepsilon}_{ij}$ while keeping D_{ij}, q_{ij}^r, and γ_{ij}^s unchanged, the following conditions must hold

$$\sigma_{ij} = \frac{\partial\tilde{\Psi}_1}{\partial\tilde{\varepsilon}_{km}}\frac{\partial\tilde{\varepsilon}_{km}}{\partial\varepsilon_{ij}}, \tag{9.227a}$$

$$-\frac{\partial\tilde{\Psi}_1}{\partial\tilde{q}_{km}^r}\frac{\partial\tilde{q}_{km}^r}{\partial q_{ij}^r}\dot{q}_{ij}^r - \left(\frac{\partial\tilde{\Psi}_1}{\partial\tilde{\varepsilon}_{km}}\frac{\partial\tilde{\varepsilon}_{km}}{\partial D_{ij}} + \frac{\partial\tilde{\Psi}_1}{\partial\tilde{q}_{km}^r}\frac{\partial\tilde{q}_{km}^r}{\partial D_{ij}} + \frac{\partial\tilde{\Psi}_2}{\partial D_{ij}}\right)D_{ij}^{\nabla} - \frac{\partial\tilde{\Psi}}{\partial\gamma_{ij}^s}\gamma_{ij}^{s\nabla} \geq 0 \tag{9.227b}$$

Using (9.212) and noting that N_{ijkm} is the inverse of M_{ijkm}, (9.227a) reduces to

$$\tilde{\sigma}_{ij} = \frac{\partial\tilde{\Psi}_1}{\partial\tilde{\varepsilon}_{ij}} \tag{9.228}$$

Thus, the effective stress is derivable from potential $\tilde{\Psi}_1(\tilde{\varepsilon}_{ij}, \tilde{q}_{ij}^r)$. Also, (9.227b) can be rearranged to yield

$$-\frac{\partial\tilde{\Psi}_1}{\partial\tilde{q}_{km}^r}\tilde{q}_{km}^{r\nabla} + \left(G_{ij} - \frac{\partial\tilde{\Psi}_2}{\partial D_{ij}}\right)D_{ij}^{\nabla} - \frac{\partial\tilde{\Psi}_2}{\partial\gamma_{ij}^s}\gamma_{ij}^{s\nabla} \geq 0 \tag{9.229}$$

where

$$G_{ij} = \frac{\partial \tilde{\Psi}_1}{\partial \tilde{\varepsilon}_{km}} \frac{\partial \tilde{\varepsilon}_{km}}{\partial D_{ij}} = -\tilde{\sigma}_{km} \frac{\partial \tilde{\varepsilon}_{km}}{\partial D_{ij}} \tag{9.230}$$

In the derivation, (9.228) and (9.219) were used. Note that the first term of (9.227b) and the second term in the bracket of the same inequality are combined to form the first term of (9.229).

From the assumption that damage does not directly influence the state of fictitious plasticity, that is, damage affects the deformation only through D_{ij}, the constraint (9.229) can be replaced by the following stronger conditions

$$-\frac{\partial \tilde{\Psi}_1}{\partial \tilde{q}^r_{ij}} \tilde{q}^{r\nabla}_{ij} \geq 0 \quad \text{and} \quad \left(G_{ij} - \frac{\partial \tilde{\Psi}_2}{\partial D_{ij}} \right) D^{\nabla}_{ij} - \frac{\partial \tilde{\Psi}_2}{\partial \gamma^s_{ij}} \gamma^{s\nabla}_{ij} \geq 0 \tag{9.231}$$

The conditions apply, respectively, to the fictitious plastic deformation process and the damage process. Furthermore, if the values of ε_{ij}, D_{ij}, q^r_{ij}, and γ^s_{ij} are fixed, then the values of G_{ij} and $\tilde{\Psi}_2$ are also fixed, since G_{ij} is a function of state variables as defined by (9.230), and $\tilde{\Psi}_2$ is a state function. For inequality (9.231b) not to be violated for an arbitrary choice of D^{∇}_{ij}, the following conditions must hold

$$G_{ij} = \frac{\partial \tilde{\Psi}_2}{\partial D_{ij}} \quad \text{and} \quad -\frac{\partial \tilde{\Psi}_2}{\partial \gamma^s_{ij}} \gamma^{s\nabla}_{ij} \geq 0 \tag{9.232}$$

For a more detailed investigation of a CDM model, the damage tensor D_{ij} can be divided into two parts, that is,

$$D_{ij} = D^r_{ij} + D^n_{ij} \tag{9.233}$$

The recoverable part D^r_{ij} is due to area reduction associated with the growth of microdefects that can be recovered during unloading. The nonrecoverable part D^n_{ij} involves the reduction of area due to the extension of existing microcracks and/or the nucleation of microdefects.

In summary, the constitutive equations for an isothermal damaged continuum are given by the following sets of equations and constraints

$$\tilde{\sigma}_{ij} = \frac{\partial \tilde{\Psi}_1}{\partial \tilde{\varepsilon}_{ij}} \qquad \text{with} \; -\frac{\partial \tilde{\Psi}_1}{\partial \tilde{q}^r_{ij}} \tilde{q}^{r\nabla}_{ij} \geq 0 \tag{9.234}$$

$$G_{ij} = \frac{\partial \tilde{\Psi}_2}{\partial D_{ij}} \qquad \text{with} \; -\frac{\partial \tilde{\Psi}_2}{\partial \gamma^s_{ij}} \gamma^{s\nabla}_{ij} \geq 0 \tag{9.235}$$

and

$$G_{ij} = -\frac{\partial \tilde{\Psi}_1}{\partial \tilde{\varepsilon}_{km}} \frac{\partial \tilde{\varepsilon}_{km}}{\partial D_{ij}} \tag{9.236}$$

Equation (9.234) characterizes the deformation of the fictitious undamaged continuum, and the inequality of (9.234) constrains the evolution of plastic internal variables. The set of equation and constraint (9.235) provides a relationship between the damage force G_{ij} and the damage measure D_{ij}. It also provides a constraint on the evolution of damage internal variables. Finally, the coupling between the deformation process and damage process is provided by (9.236). This is further explained in the subsequent paragraph.

Consider a fictitious, undamaged, element subjected to loading increment $\mathrm{d}\tilde{P}_i$. During loading, there are various forms of dissipation of energy associated with plasticity and damage processes. In particular, the rate of energy dissipation (caused by the damage force) due to a unit damage growth D_{ij}^{∇} with respect to the fictitious element is $(\partial \tilde{\Psi}_2/\partial D_{ij})D_{ij}^{\nabla}$. At the end of the loading period, it is required that the fictitious element returns to its undamaged state before the next loading can be applied. The restoring energy associated with this transformation is given by $-G_{ij}D_{ij}^{\nabla}$, where $-G_{ij}$ is the restoring force. Because the damage needed to be restored at the end of a loading period is equal to the negative of the damage growth during loading, the force associated with the two processes must be equal in magnitude. Therefore, (9.236) can be viewed as a constraint that must be satisfied for the fictitious deformation and damage process to occur simultaneously within the same continuum. In fact, this is a required constraint that arrives naturally from thermodynamic consideration.

Equations and constraints in (9.234) to (9.236) provide a framework for theories of CDM. Explicit constitutive equations may be obtained if functions for $\tilde{\Psi}_1$ and $\tilde{\Psi}_2$ are specified. Explicit evolution equations, which satisfy the inequalities of (9.234) and (9.235), for internal variables q_{ij}^r, and γ_{ij}^s should also be given. Different theories may be proposed based on this constitutive framework. One such theory has been formulated by Wu and Nanakorn [65] by use of the concept of endochronic plasticity. In that paper, the model has been applied to a one-dimensional case that describes uniaxial monotonic compression and tension of a concrete specimen. It successfully describes the strain-softening behavior after the peak load. In addition, the model has been applied to the description of deformation behavior for cyclically loaded concrete and mortar specimens. Satisfactory results have been obtained.

It is remarked that the internal variables are not observable. Using the evolution equations for these variables, these variables do not necessarily appear in the final form of the constitutive equations. Depending on the functional forms for $\tilde{\Psi}_1$ and $\tilde{\Psi}_2$ and the explicit forms for the evolution equations for q_{ij}^r, and γ_{ij}^s, a set of macroscopic parameters may be used for the model. These parameters may then be determined from experiments.

9.5.7 A Brief Summary of Wu and Nanakorn's Endochronic CDM

Several CDM models based on endochronic theory of plasticity have been proposed. The model of Valanis [66] is for brittle materials, while the models of Niu [67] and Chow and Chen [68] are for ductile materials. The model of Niu [67] is limited to isotropic damage due to the scalar representation of damage; the model of Chow and Chen [68] is an anisotropic damage model. Wu and Nanakorn's model [65] is applicable to ductile materials with anisotropic damage. The equations of the Wu–Nanakorn model are summarized in this section for later references with permission from ASCE. This model is different from that of Chow and Chen [68], which uses neither the damage internal variables γ_{ij}^s nor the concept of damage restoring force G_{ij}. Instead, Chow and Chen [68] uses D_{ij} as an internal variable and express the damage evolution equations in terms of the potential of damage dissipation and elastic strain energy release rate Y_{ij}.

In the Wu–Nanakorn model, the governing equations and constraints are given by (9.234) to (9.236). In this section, explicit forms of equations are derived by assuming the following quadratic forms for $\tilde{\Psi}_1(\tilde{\varepsilon}_{ij}, \tilde{q}_{ij}^r)$ and $\tilde{\Psi}_2(D_{ij}, \gamma_{ij}^s)$:

$$\tilde{\Psi}_1\left(\tilde{\varepsilon}_{ij}, \tilde{q}_{ij}^r\right) = \frac{1}{2}\sum_r A_{ijkm}\left(\tilde{\varepsilon}_{ij} - \tilde{q}_{ij}^r\right)\left(\tilde{\varepsilon}_{km} - \tilde{q}_{km}^r\right) \tag{9.237}$$

$$\tilde{\Psi}_2\left(D_{ij}, \gamma_{ij}^s\right) = \frac{1}{2}\sum_r H_{ijkm}\left(D_{ij} - \gamma_{ij}^s\right)\left(D_{km} - \gamma_{km}^s\right) \tag{9.238}$$

where A_{ijkm} and H_{ijkm} are positive semi-definite fourth-rank isotropic tensors. The free energies in (9.237) and (9.238) are defined on the fictitious undamaged material, which is isotropic. Represent now any fourth-order isotropic tensor W_{ijkm} by

$$W_{ijkm} = W_1\delta_{ij}\delta_{km} + W_2\delta_{ik}\delta_{jm}, \qquad \text{with } W_0 = 3\left(W_1 + \frac{W_2}{3}\right) \tag{9.239}$$

where W_1 and W_2 are constants, and symmetry of W_{ijkm} with respect to k and m is assumed. Also, the variables may be decomposed into the deviatoric and hydrostatic parts as

$$\tilde{\sigma}_{ij} = \tilde{\sigma}'_{ij} + \tfrac{1}{3}\delta_{ij}\tilde{\sigma}_{kk}, \qquad \tilde{\varepsilon}_{ij} = \tilde{e}_{ij} + \tfrac{1}{3}\delta_{ij}\tilde{\varepsilon}_{kk}, \qquad \tilde{q}_{ij}^r = \tilde{p}_{ij}^r + \tfrac{1}{3}\delta_{ij}\tilde{q}_{kk}^r \tag{9.240}$$

and

$$G_{ij} = g_{ij} + \tfrac{1}{3}\delta_{ij}G_{kk}, \qquad D_{ij} = d_{ij} + \tfrac{1}{3}\delta_{ij}D_{kk}, \qquad \gamma_{ij}^s = r_{ij}^s + \tfrac{1}{3}\delta_{ij}\gamma_{kk}^s \tag{9.241}$$

Using these notations, the explicit form of constitutive equations for damaged materials may be derived and are presented in the remaining part of this section.

9.5.7.1 Equations of plastic deformation

The deformation behavior is characterized by the effective stress-effective strain relationship given in (9.234). Using (9.237), this equation reduces to the following two equations by separating hydrostatic and deviatoric components:

$$\tilde{\sigma}_{kk} = \sum_r A_0^r (\tilde{\varepsilon}_{kk} - \tilde{q}_{kk}^r) \tag{9.242}$$

$$\tilde{\sigma}'_{ij} = \sum_r A_2^r (\tilde{e}_{ij} - \tilde{p}_{ij}^r) \tag{9.243}$$

where A_0^r and A_2^r are defined by (9.239) with W replaced by A.

Within a linear assumption, the evolution equations for the hydrostatic and deviatoric parts of $\tilde{q}_{ij}^r$ are given in the following form

$$L_0^r \left(\frac{\mathrm{d}\tilde{q}_{kk}^r}{\mathrm{d}\tilde{z}_\mathrm{H}} \right)^\nabla - \tilde{\sigma}_{kk} = 0 \quad \text{and} \quad L_2^r \left(\frac{\mathrm{d}\tilde{p}_{ij}^r}{\mathrm{d}\tilde{z}_\mathrm{D}} \right)^\nabla - \tilde{\sigma}'_{ij} = 0 \tag{9.244}$$

where $(\,)^\nabla$ indicates that the differentiation operator in bracket is corotational; L_0^r and L_2^r are constants; and $d\tilde{z}$ defines the intrinsic time with respect to the fictitious deformation. The intrinsic time is divided into the hydrostatic and deviatoric parts. An hydrostatic intrinsic time measure ζ_H is defined to register the hydrostatic deformation. It is scaled by the intrinsic time scale z_H so that it can properly describe strain hardening. They are related by

$$\mathrm{d}\zeta_\mathrm{H} = \left| \mathrm{d}\tilde{\varepsilon}_{kk} - k_1 \frac{\mathrm{d}\tilde{\sigma}_{kk}}{3K_0} \right| \qquad \text{with } \frac{\mathrm{d}\zeta_\mathrm{H}}{\mathrm{d}z_\mathrm{H}} = h\,(\zeta_\mathrm{H}) > 0 \tag{9.245}$$

where $0 \le k_1 \le 1$ and K_0 is the Bulk Modulus. The deviatoric intrinsic time ζ_D is defined based on an effective strain-like tensor $\tilde{Q}_{ij}$ which is given by

$$^\nabla\mathrm{d}\tilde{Q}_{ij} = {}^\nabla \mathrm{d}\tilde{e}_{ij} - k_2 \frac{^\nabla\mathrm{d}\tilde{\sigma}'_{ij}}{2\mu_0} \tag{9.246}$$

where $0 \le k_2 \le 1$ and μ_0 is the shear modulus. The operator $^\nabla\mathrm{d}$ denotes the corotational increment and is defined on a second-order tensor a_{ij} with respect to the intrinsic time z as

$$^\nabla\mathrm{d}a_{ij} = {}^t\mathrm{d}a_{ij} - W_{ik}a_{kj}\,\mathrm{d}z + a_{ik}W_{kj}\,\mathrm{d}z \tag{9.247}$$

where $^t\mathrm{d}$ denotes the increment based on material rate and W_{ij} is the spin tensor. The deviatoric intrinsic time is defined and scaled as follows:

$$\mathrm{d}\zeta_\mathrm{D}^2 = {}^\nabla\mathrm{d}\tilde{Q}_{ij}\,{}^\nabla\mathrm{d}\tilde{Q}_{ij} \quad \text{with } \frac{\mathrm{d}\zeta_\mathrm{D}}{\mathrm{d}z_\mathrm{D}} = f\,(\zeta_\mathrm{D}) > 0 \tag{9.248}$$

In (9.245) and (9.248), $h(\zeta_{\mathrm{H}})$ and $f(\zeta_{\mathrm{D}})$ are the strain-hardening functions corresponding to the hydrostatic and deviatoric deformation, respectively.

9.5.7.2 Equations of damage

Equations (9.235) and (9.238) lead to the following relations for the hydrostatic and deviatoric parts of damage force G_{ij}, respectively,

$$G_{kk} = \sum_s H_0^s \left(D_{kk} - \gamma_{kk}^s\right), \qquad g_{ij} = \sum_s H_2^s \left(\mathrm{d}_{ij} - \mathrm{r}_{ij}^s\right) \tag{9.249}$$

where H_0^s and H_2^s are constants. In the hydrostatic damage, microdefects expand and contract such that the overall symmetric properties of the material, that is, all planes of symmetry, are retained. In the deviatoric damage, the orientation of microcracks and microvoids changes, resulting in changes of overall symmetry properties and inducing the anisotropic behavior of the material.

Using the inequality of (9.235), the linear evolution equations of γ_{ij}^s can be further separated into hydrostatic and deviatoric parts as

$$J_0^s \left(\frac{\mathrm{d}\gamma_{kk}^s}{\mathrm{d}z_{\mathrm{H}}^{\mathrm{d}}}\right)^{\nabla} - G_{kk} = 0 \quad \text{and} \quad J_2^s \left(\frac{\mathrm{d}r_{ij}^s}{\mathrm{d}z_{\mathrm{D}}^{\mathrm{d}}}\right)^{\nabla} - g_{ij} = 0 \tag{9.250}$$

where J_0^s and J_2^s are constants; $dz_{\mathrm{H}}^{\mathrm{d}}$ and $dz_{\mathrm{D}}^{\mathrm{d}}$ are the damage intrinsic time increment corresponding to the hydrostatic and deviatoric damage, respectively. The hydrostatic damage intrinsic time and its timescale are defined, respectively, by

$$\mathrm{d}\zeta_{\mathrm{H}}^{\mathrm{d}} = \left|\mathrm{d}D_{kk} - k_3 \frac{\mathrm{d}G_{kk}}{3B_0}\right| \quad \text{with} \quad \frac{\mathrm{d}\zeta_{\mathrm{H}}^{\mathrm{d}}}{\mathrm{d}z_{\mathrm{H}}^{\mathrm{d}}} = h^{\mathrm{d}}\left(\zeta_{\mathrm{H}}^{\mathrm{d}}\right) > 0 \tag{9.251}$$

where $0 \le k_3 \le 1$ and B_0 is a material constant. Similarly, the deviatoric damage intrinsic time and its timescale are defined by

$$\left(\mathrm{d}\zeta_{\mathrm{D}}^{\mathrm{d}}\right)^2 = {}^{\nabla}\mathrm{d}R_{ij}\,{}^{\nabla}\mathrm{d}R_{ij} \qquad \text{with} \quad \frac{\mathrm{d}\zeta_{\mathrm{D}}^{\mathrm{d}}}{\mathrm{d}z_{\mathrm{D}}^{\mathrm{d}}} = f^{\mathrm{d}}\left(\zeta_{\mathrm{D}}^{\mathrm{d}}\right) > 0 \tag{9.252}$$

where the damage-like tensor ${}^{\nabla}\mathrm{d}R_{ij}$ is defined by

$${}^{\nabla}\mathrm{d}R_{ij} = {}^{\nabla}\mathrm{d}d_{ij} - k_4 \frac{{}^{\nabla}\mathrm{d}g_{ij}}{2M_0} \tag{9.253}$$

with $0 \le k_4 \le 1$ and M_0 is a material constant. The role played by material constants B_0 and M_0 in the G_{ij} versus D_{ij} relationship is similar to that played

by the bulk modulus K_0 and shear modulus μ_0 in the stress–strain relationship. The functions $h^{\mathrm{d}}(\zeta_{\mathrm{H}}^{\mathrm{d}})$ and $f^{\mathrm{d}}(\zeta_{\mathrm{D}}^{\mathrm{d}})$ describe the material damage resisting (hardening) behavior, which increases the damage threshold. These functions are similar to the hardening functions $h(\zeta_{\mathrm{H}})$ and $f(\zeta_{\mathrm{D}})$ of plastic deformation, but with a different physical meaning.

The role played by (9.251) and (9.252) in damage is analogous to that played by (9.245) and (9.248) in the stress–strain space for the limit case of $k_i \to 1$ $(i = 1, 2, 3, 4)$. The relations (9.251a) and (9.253) can be interpreted as the nonrecoverable hydrostatic and deviatoric parts of the damage tensor increment $\mathrm{d}D_{ij}$, respectively. Note that ζ^{d} is defined in terms of the nonrecoverable damage D_{ij}^{n} rather than the effective plastic strain $\tilde{\varepsilon}_{ij}^{\mathrm{p}}$, as in the theories of Niu [67] and Chow and Chen [68]. This new damage intrinsic time enables the present theory to describe the behavior of damage in brittle materials, where damage occurs within the elastic range, as well as in ductile materials.

9.5.7.3 Coupling between deformation and damage

The coupling between deformation and damage processes is achieved through the damage force G_{ij} given by (9.236). Using the quadratic form of $\tilde{\Psi}_1(\tilde{\varepsilon}_{ij}, \tilde{q}_{ij}^r)$ given in (9.237), (9.236) reduces to

$$\begin{aligned} G_{ij} &= -\sum_r A_{uvmn}^r (\tilde{\varepsilon}_{mn} - \tilde{q}_{mn}^r) \left(\frac{\partial \tilde{\varepsilon}_{uv}}{\partial D_{ij}}\right)^{\nabla} \\ &= -\sum_r A_{uvmn}^r \left(\tilde{\varepsilon}_{mn} - \tilde{q}_{mn}^r\right) \varepsilon_{pq} \left(\frac{\mathrm{d}N_{pquv}}{\mathrm{d}D_{ij}}\right)^{\nabla} \end{aligned} \tag{9.254}$$

This equation relates the damage force G_{ij} to the effective strain $\tilde{\varepsilon}_{ij}$ and effective internal variables $\tilde{q}_{ij}^r$, both of which are responsible for the deformation process of the fictitious continuum. On the other hand, the damage force is related to the damage potential $\tilde{\Psi}_2(D_{ij}, \gamma_{ij}^s)$ by (9.235), which, by use of (9.238), reduces to

$$G_{ij} = \frac{\partial \tilde{\Psi}_2}{\partial D_{ij}} = \sum_s H_{ijkm}^s \left(D_{km} - \gamma_{km}^s\right) \tag{9.255}$$

This equation relates damage force G_{ij} to the damage tensor D_{ij} and internal variables γ_{ij}^s. The interpretations of (9.254) and (9.255) are as follows: consider a fictitious, undamaged, material element subjected to a loading increment. During loading, different forms of energy associated with plasticity and damage process are dissipated. In particular, the rate of energy dissipation due to damage growth D_{ij}^{∇} in the fictitious element is $(\partial \Psi_2 / \partial D_{ij}) D_{ij}^{\nabla}$. At the end of the loading period, it is required that the fictitious element returns to its undamaged state before the next loading can be applied. The restoring energy

associated with this process is $-G_{ij}D_{ij}^{\nabla}$, where $-G_{ij}$ is the restoring force and the negative of the restoring force, G_{ij}, is given by (9.254). Because the damage to be restored at the end of the loading period is equal to the negative of the damage growth during loading, the force associated with the two processes must be equal in magnitude. Therefore, (9.255) with G_{ij} defined by (9.254), can be viewed as a constraint that must be satisfied for the deformation and damage processes to occur simultaneously within the fictitious continuum. In fact, this is a required constraint which arises naturally from the thermodynamic consideration.

9.5.8 Application

In this section, the model of the previous section is applied to investigate the problem of a cylindrical concrete specimen subjected to uniaxial compression in the x_3-direction. For such a problem, the state of stress and strain is given by

$$[\sigma] = \begin{bmatrix} 0 & 0 & 0 \\ 0 & 0 & 0 \\ 0 & 0 & \sigma_{33} \end{bmatrix} \qquad [\varepsilon] = \begin{bmatrix} \varepsilon_{11} & 0 & 0 \\ 0 & \varepsilon_{22} & 0 \\ 0 & 0 & \varepsilon_{33} \end{bmatrix} \tag{9.256}$$

where ε_{33} is prescribed for a strain control test. These are the principal stress and strain components and the directions of principal damage coincide with those of the principal stress and strain, if the specimen is initially isotropic and is subjected to proportional loading. In this case, the corotational rate reduces to the material rate. The increments of effective stress and effective strain are

$$[\mathrm{d}\tilde{\sigma}] = \begin{bmatrix} 0 & 0 & 0 \\ 0 & 0 & 0 \\ 0 & 0 & d\tilde{\sigma}_{33} \end{bmatrix} \qquad [\mathrm{d}\tilde{\varepsilon}] = \begin{bmatrix} \mathrm{d}\tilde{\varepsilon}_{11} & 0 & 0 \\ 0 & \mathrm{d}\tilde{\varepsilon}_{22} & 0 \\ 0 & 0 & \mathrm{d}\tilde{\varepsilon}_{33} \end{bmatrix} \tag{9.257}$$

Their deviatoric parts are

$$[\mathrm{d}\tilde{\sigma'}] = \frac{1}{3}\begin{bmatrix} -\mathrm{d}\tilde{\sigma}_{33} & 0 & 0 \\ 0 & -\mathrm{d}\tilde{\sigma}_{33} & 0 \\ 0 & 0 & 2\,\mathrm{d}\tilde{\sigma}_{33} \end{bmatrix}$$

$$[\mathrm{d}\tilde{e}] = \frac{1}{3}\begin{bmatrix} (2\,\mathrm{d}\tilde{\varepsilon}_{11} - \mathrm{d}\tilde{\varepsilon}_{22} - \mathrm{d}\tilde{\varepsilon}_{33}) & 0 & 0 \\ 0 & (-\mathrm{d}\tilde{\varepsilon}_{11} + 2\,\mathrm{d}\tilde{\varepsilon}_{22} - \mathrm{d}\tilde{\varepsilon}_{33}) & 0 \\ 0 & 0 & (-\mathrm{d}\tilde{\varepsilon}_{11} - \mathrm{d}\tilde{\varepsilon}_{22} + 2\,\mathrm{d}\tilde{\varepsilon}_{33}) \end{bmatrix} \tag{9.258}$$

The damage-effect tensor M_{ijkm} is selected according to Betten's definition of effective stress. Using (9.179) and (9.188), this tensor and its inverse are

expressed in the matrix form as

$$[M] = \begin{bmatrix} \dfrac{1}{(1-D_1)^2} & 0 & 0 \\ 0 & \dfrac{1}{(1-D_2)^2} & 0 \\ 0 & 0 & \dfrac{1}{(1-D_3)^2} \end{bmatrix} \tag{9.259}$$

$$[N] = \begin{bmatrix} (1-D_1)^2 & & \\ & (1-D_2)^2 & \\ & & (1-D_3)^2 \end{bmatrix}$$

where D_1, D_2, and D_3 are the principal damage in the x_1, x_2, and x_3 directions, respectively.

In this example, for the sake of simplicity, only one internal variable each for $\tilde{q}_{ij}$ and γ_{ij} is used. The use of only one internal variable was shown in previous applications of endochronic plasticity to be capable of capturing the main features of stress–strain responses in a plastically deformed continuum. The hydrostatic behavior of the fictitious deformation is now considered. Combining (9.242), (9.244a) and (9.245a), the following equation is obtained

$$\frac{\mathrm{d}\tilde{\sigma}_{kk}}{A_0} \pm k_1 X \frac{\mathrm{d}\tilde{\sigma}_{kk}}{3K_0} = (1 \pm X)\mathrm{d}\tilde{\varepsilon}_{kk} \qquad \text{with } X = \frac{\tilde{\sigma}_{kk}}{L_0 h(\zeta_{\mathrm{H}})} \tag{9.260}$$

where A_0 and L_0 are constants. The minus $(-)$ and plus $(+)$ signs, in (9.260), correspond to tension and compression, respectively. The material constant A_0 may be identified with the bulk modulus $3K_0$ by considering the fictitious undamaged material at its initial loading state, where $\tilde{\sigma}_{kk} = \tilde{q}_{kk} = 0$. Using the effective stress and effective strain of (9.257), (9.260) becomes

$$\mathrm{d}\tilde{\sigma}_{33} = 3K_0 F(k_1, X)(\mathrm{d}\tilde{\varepsilon}_{11} + \mathrm{d}\tilde{\varepsilon}_{22} + \mathrm{d}\tilde{\varepsilon}_{33}) \tag{9.261}$$

where

$$F(k_1, X) = \frac{1 \pm X}{1 \pm k_1 X} \quad \text{and} \quad X = \frac{\tilde{\sigma}_{33}}{L_0 h(\zeta_{\mathrm{H}})} \tag{9.262}$$

The deviatoric response of the fictitious undamaged material, from (9.243), (9.244b), and (9.258), is described by

$$-\mathrm{d}\tilde{\sigma}_{33} = A_2(2\,\mathrm{d}\tilde{\varepsilon}_{11} - \mathrm{d}\tilde{\varepsilon}_{22} - \mathrm{d}\tilde{\varepsilon}_{33}) + \frac{A_2\tilde{\sigma}_{33}}{L_2}\,\mathrm{d}z_{\mathrm{D}} \tag{9.263a}$$

$$-\mathrm{d}\tilde{\sigma}_{33} = A_2(-\mathrm{d}\tilde{\varepsilon}_{11} + 2\,\mathrm{d}\tilde{\varepsilon}_{22} - \mathrm{d}\tilde{\varepsilon}_{33}) + \frac{A_2\tilde{\sigma}_{33}}{L_2}\,\mathrm{d}z_{\mathrm{D}} \tag{9.263b}$$

$$2\,\mathrm{d}\tilde{\sigma}_{33} = A_2(-\mathrm{d}\tilde{\varepsilon}_{11} - \mathrm{d}\tilde{\varepsilon}_{22} + 2\,\mathrm{d}\tilde{\varepsilon}_{33}) - \frac{A_2\tilde{\sigma}_{33}}{L_2}\,\mathrm{d}z_{\mathrm{D}} \tag{9.263c}$$

Equation (9.261) and the two independent equations of (9.263) can be put in the matrix form as

$$\begin{bmatrix} 1 & -3K_0F(k_1,X) & -3K_0F(k_1,X) \\ 1 & 2A_2 & -A_2 \\ 1 & -A_2 & 2A_2 \end{bmatrix} \begin{bmatrix} \mathrm{d}\tilde{\sigma}_{33} \\ \mathrm{d}\tilde{\varepsilon}_{11} \\ \mathrm{d}\tilde{\varepsilon}_{22} \end{bmatrix} + \begin{bmatrix} 0 \\ 1 \\ 1 \end{bmatrix} \frac{A_2\tilde{\sigma}_{33}}{L_2}\,\mathrm{d}z_{\mathrm{D}} = \begin{bmatrix} 3K_0F(k_1,X) \\ A_2 \\ A_2 \end{bmatrix} \mathrm{d}\tilde{\varepsilon}_{33} \tag{9.264}$$

where $\mathrm{d}z_{\mathrm{D}}$ is related to the deviatoric components of the incremental effective strain $\mathrm{d}\tilde{\varepsilon}_{ij}$ and its relationship is now discussed. The following expression may be found from (9.246)

$$\mathrm{d}\tilde{Q}_{ij} = \varphi_{ij} + \psi_{ij}\,\mathrm{d}z_{\mathrm{D}} \tag{9.265}$$

where

$$\varphi_{ij} = (1-k_2)\mathrm{d}\tilde{e}_{ij} \quad \text{and} \quad \psi_{ij} = \frac{k_2\tilde{\sigma}'_{ij}}{L_2} \tag{9.266}$$

By use of (9.248) and (9.265), the relation for $\mathrm{d}z_{\mathrm{D}}$ is obtained as

$$\varphi_{ij}\varphi_{ij} + 2\varphi_{ij}\psi_{ij}\,\mathrm{d}z_{\mathrm{D}} + [\psi_{ij}\psi_{ij} - f(\zeta_{\mathrm{D}})^2]\mathrm{d}z_{\mathrm{D}}^2 = 0 \tag{9.267}$$

The equation of hydrostatic damage is found from (9.249a), (9.250a), and (9.251a) as

$$\frac{\mathrm{d}G_{kk}}{H_0} \pm k_3 Y \frac{\mathrm{d}G_{kk}}{3B_0} = (1 \pm Y)\,\mathrm{d}D_{kk} \qquad \text{with } Y = \frac{G_{kk}}{J_0 h^{\mathrm{d}}(\zeta_{\mathrm{H}}^{\mathrm{d}})} \tag{9.268}$$

where H_0, B_0, and J_0 are material constants. Considering the initial loading state, where $G_{kk} = \gamma_{kk} = 0$, it may be shown that H_0 is the initial slope of the G_{kk} versus D_{kk} curve and that $H_0 = 3B_0$. The minus ($-$) and plus ($+$) signs, in (9.268), correspond to tension and compression, respectively. Equation (9.268a) further reduces to

$$\mathrm{d}G_{kk} = H_0F(k_3,Y)\,\mathrm{d}D_{kk} \qquad \text{with } F(k_3,Y) = \frac{1 \pm Y}{1 \pm k_3Y} \tag{9.269}$$

The equation for deviatoric damage response may be obtained from (9.249b) and (9.250b) as

$$\mathrm{d}g_{ij} = H_2\left(\mathrm{d}d_{ij} + \frac{g_{ij}}{J_2}\,\mathrm{d}z_{\mathrm{D}}^{\mathrm{d}}\right) \tag{9.270}$$

where H_2 and J_2 are constants and H_2 may be identified with the initial slope of the deviatoric G_{ij} versus D_{ij} curve. Furthermore, $H_2 = 2M_0$. The damage intrinsic time increment $\mathrm{d}z_{\mathrm{D}}^{\mathrm{d}}$ is related to the deviatoric components of the damage force increment $\mathrm{d}g_{ij}$ and its relationship is now discussed. The following expression may be found from (9.253) and (9.270)

$$\mathrm{d}R_{ij} = \varphi_{ij}^{\mathrm{d}} + \psi_{ij}^{\mathrm{d}}\,\mathrm{d}z_{\mathrm{D}}^{\mathrm{d}} \tag{9.271}$$

where

$$\varphi_{ij}^{\mathrm{d}} = (1-k_4)\,\frac{\mathrm{d}g_{ij}}{H_2} \quad \text{and} \quad \psi_{ij}^{\mathrm{d}} = \frac{g_{ij}}{J_2} \tag{9.272}$$

By use of (9.252a) and (9.271), the relation for $\mathrm{d}z_D^{\mathrm{d}}$ is obtained as

$$\varphi_{ij}^{\mathrm{d}}\varphi_{ij}^{\mathrm{d}} + 2\varphi_{ij}^{\mathrm{d}}\psi_{ij}^{\mathrm{d}}\,\mathrm{d}z_{\mathrm{D}}^{\mathrm{d}} + \left[\psi_{ij}^{\mathrm{d}}\psi_{ij}^{\mathrm{d}} - f^{\mathrm{d}}(\zeta_{\mathrm{D}}^{\mathrm{d}})^2\right](\mathrm{d}z_{\mathrm{D}}^{\mathrm{d}})^2 = 0 \tag{9.273}$$

Using (9.236) and (9.257), the damage force G_{ij} reduces to

$$G_{ij} = -\tilde{\sigma}_{km}\frac{\partial\tilde{\varepsilon}_{km}}{\partial D_{ij}} = -\tilde{\sigma}_{33}\frac{\partial\tilde{\varepsilon}_{33}}{\partial D_{ij}} \tag{9.274}$$

Since $\tilde{\varepsilon}_{33} = (1-D_3)^2\varepsilon_{33}$, $\tilde{\varepsilon}_{33}$ does not depend on D_1 and D_2. Consequently, the only nonzero component of tensor G_{ij} is

$$G_{33} = \frac{2\tilde{\sigma}_{33}\tilde{\varepsilon}_{33}}{1-D_3} \tag{9.275}$$

and its increment is found to be

$$\mathrm{d}G_{33} = \frac{2\tilde{\sigma}_{33}}{1-D_3}\,\mathrm{d}\tilde{\varepsilon}_{33} + \frac{2\tilde{\varepsilon}_{33}}{1-D_3}\,\mathrm{d}\tilde{\sigma}_{33} + \frac{2\tilde{\sigma}_{33}\tilde{\varepsilon}_{33}}{(1-D_3)^2}\,\mathrm{d}D_3 \tag{9.276}$$

Thus, the deviatoric part of the increment of the damage force is

$$[\mathrm{d}g_{ij}] = \frac{1}{3}\begin{bmatrix} -\mathrm{d}G_{33} & 0 & 0 \\ 0 & -\mathrm{d}G_{33} & 0 \\ 0 & 0 & 2\mathrm{d}G_{33} \end{bmatrix} \tag{9.277}$$

Furthermore,

$$[\mathrm{d}d_{ij}] = \frac{1}{3}\begin{bmatrix} 2\,\mathrm{d}D_1 - \mathrm{d}D_2 - \mathrm{d}D_3 & 0 & 0 \\ 0 & -\mathrm{d}D_1 + 2\,\mathrm{d}D_2 - \mathrm{d}D_3 & 0 \\ 0 & 0 & -\mathrm{d}D_1 - \mathrm{d}D_2 + 2\,\mathrm{d}D_3 \end{bmatrix} \tag{9.278}$$

Equations (9.277) and (9.278) are substituted into (105) and the two independent equations of (9.269) to obtain the following matrix equation for the damage process:

$$\begin{bmatrix} H_0F(k_3,Y) & H_0F(k_3,Y) & H_0F(k_3,Y) \\ 2H_2 & -H_2 & -H_2 \\ -H_2 & 2H_2 & -H_2 \end{bmatrix} \begin{bmatrix} \mathrm{d}D_1 \\ \mathrm{d}D_2 \\ \mathrm{d}D_3 \end{bmatrix} = \begin{bmatrix} 1 \\ -1 \\ -1 \end{bmatrix} \mathrm{d}G_{33} - \begin{bmatrix} 0 \\ 1 \\ 1 \end{bmatrix} \frac{H_2G_{33}}{J_2}\,\mathrm{d}z_{\mathrm{D}}^{\mathrm{d}} \tag{9.279}$$

The equations derived in this section are now applied to the problem of uniaxial compression of cylindrical concrete specimen ($f_{\mathrm{c}}' = 73.8$ MPa and E=27.6 GPa). To determine the material parameters for the model, the analytical stress–strain curves obtained by Fonseka and Krajcinovic [69] is used. In this case, the directions of the principal damage coincide with those of the principal stress. The procedure of calculation is now described. An increment $\mathrm{d}\tilde{\varepsilon}_{33}$ is first specified. An initial value for $\mathrm{d}z_{\mathrm{D}}$ is assumed and (9.264) solved for $\mathrm{d}\tilde{\sigma}_{33}$, $\mathrm{d}\tilde{\varepsilon}_{11}$, and $\mathrm{d}\tilde{\varepsilon}_{22}$. These values are then used in (9.267) to solve for $\mathrm{d}z_{\mathrm{D}}$. An iteration procedure is applied to determine $\mathrm{d}G_{33}$. (9.273) is subsequently used to determine $\mathrm{d}z_{\mathrm{D}}^{\mathrm{d}}$. Thus, $\mathrm{d}D_1$, $\mathrm{d}D_2$, and $\mathrm{d}D_3$ are found from (9.279). An iteration procedure is also applied on $\mathrm{d}D_3$ to determine its value, which corresponds to the specified $\mathrm{d}\tilde{\varepsilon}_{33}$. Knowing $\mathrm{d}\tilde{\varepsilon}_{33}$ and $\mathrm{d}D_3$, $\mathrm{d}\varepsilon_{33}$ can be calculated from the incremental form of

$$\varepsilon_{33} = \frac{\tilde{\varepsilon}_{33}}{(1-D_3)^2} \tag{9.280}$$

This procedure continues for another specified $\mathrm{d}\tilde{\varepsilon}_{33}$.

Using a trial-and-error (curve-fitting) procedure, the following material parameters for the deformation equations have been determined: Poisson's ratio = 0.2, effective hydrostatic yield stress $L_0 = 4.55$ MPa, effective deviatoric yield stress $L_2 = 18.61$ MPa, strain-hardening parameters $\mu_{\mathrm{H}} = \mu_{\mathrm{d}} = 0$, and $k_1 = k_2 = 0.95$. The material parameters for the damage equations have been found to be: hydrostatic damage modulus $H_0 = 0.78$ MPa, deviatoric damage modulus $H_2 = 1.91$ MPa, hydrostatic damage threshold $J_0 = 0.61$ MPa, deviatoric damage threshold $J_2 = 1.93$ MPa, damage resisting (hardening) parameters $\mu_{\mathrm{H}}^{\mathrm{d}} = \mu_{\mathrm{D}}^{\mathrm{d}} = 0$, and $k_3 = k_4 = 0.95$.

The computed stress–strain curves are plotted in Figure 9.22. There are two curves in this figure. One curve is for the axial strain and the other for the lateral strain. The volumetric strain versus compressive stress is plotted in Figure 9.23. The curve shows a change of sign of the volumetric strain as the axial strain increases. The volumetric strain is initially negative and it changes to positive when the axial strain becomes large in magnitude. This phenomenon is typical in concrete and rocks, and it is due to the increase

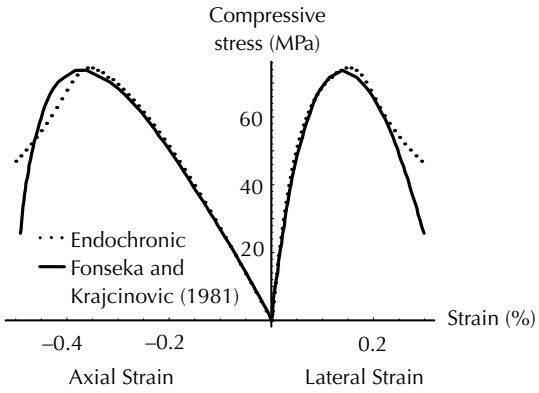

FIGURE 9.22
Stress versus axial and lateral strains in uniaxial compression of concrete (From Wu, H.C. and Nanakorn, C.K., *Int. J. Solids Struct.*, 36, 5057, 1999. With permission from Elsevier).

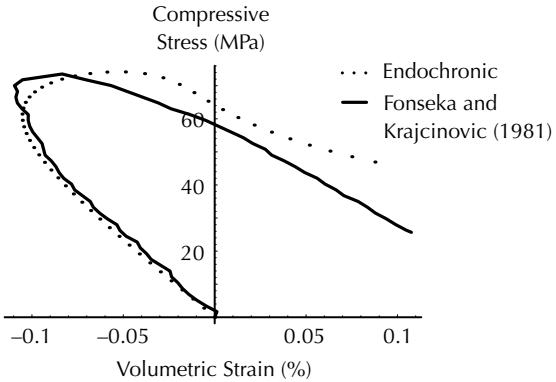

FIGURE 9.23
Stress versus volumetric strain in uniaxial compression of concrete (From Wu, H.C. and Nanakorn, C.K., *Int. J. Solids Struct.*, 36, 5057, 1999. With permission from Elsevier).

in the lateral-to-axial strain ratio $(-\varepsilon_{11}/\varepsilon_{33})$ as the axial strain increases. It is seen in Figure 9.24 that this ratio changes from 0.2 to approximately 0.6 as the axial compressive strain increases from 0 to 0.005. The results of this model presented in Figure 9.22 and Figure 9.23 show good agreement with the computed value obtained by Fonseka and Krajcinovic [69].

9.5.9 Concluding Remarks

The concepts of CDM have been discussed and a constitutive framework of CDM has been developed based on the internal variables approach. The framework involves transforming the actual damaged continuum into an equivalent fictitious undamaged continuum. The effects of damage are

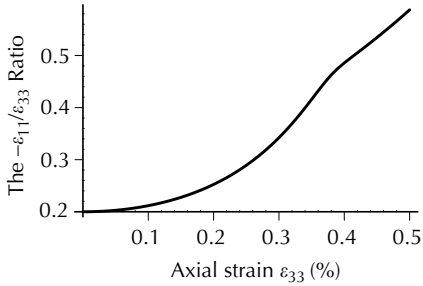

FIGURE 9.24
Lateral to axial strain ratio versus axial compressive strain (From Wu, H.C. and Nanakorn, C.K., *Int. J. Solids Struct.*, 36, 5057, 1999. With permission from Elsevier).

accounted for by replacing the actual stress σ_{ij} (gross stress) on the damaged continuum with the symmetric effective stress $\tilde{\sigma}_{ij}$. A distinction has been made between the state of damage and the damage measure D_{ij} and the concept of "damage force" has been introduced.

Within the proposed constitutive framework, the endochronic concept has been used to derive explicit constitutive equations. Two intrinsic times are used in the formulation. The first intrinsic time ζ is used to describe the plastic deformation history of the fictitious undamaged continuum and the second intrinsic time ζ^{d} is used to depict the damage history. The model is applicable to both brittle and ductile materials with damage. The following conclusions may be drawn from this study:

1. The damage tensor D_{ij} may be defined based on a second-order continuity tensor ψ_{ij}.
2. The damage-effect tensor M_{ijkm} defined by Betten [58] gives rise to an effective stress that has a simple physical interpretation, while other definitions of M_{ijkm} do not have the same significance.
3. The transformation equation for effective strain, (9.214), may be derived based on the free energy equivalence postulate.
4. In addition to damage tensor D_{ij}, which is a measurable quantity, a set of damage internal variables γ_{ij}^{s}, which are not measurable, is used in the formulation.
5. The constitutive equations for an isothermal damaged continuum include two sets of equations and constraints. The first set characterizes the deformation of the fictitious undamaged continuum and constrains the evolution of plastic internal variables q_{ij}^{r}. The second set provides a relationship between the damage force G_{ij} and the damage measure D_{ij}. It also provides a constraint on the evolution of damage internal variables γ_{ij}^{s}. In addition, (9.236) must be used to complete the constitutive equations. This equation is a constraint that

must be satisfied for the fictitious deformation and damage process to occur simultaneously within the same continuum.

6. The theory does not use the concepts of yield surface or damage surface as its prime requisite although both surfaces may be defined when necessary by setting all $k_i = 1$. Therefore, the constitutive equations of this theory are continuous without discontinuities, which is advantageous in the numerical calculation.
7. The proposed model has been shown to describe the three-dimensional state of deformation of a cylindrical concrete specimen subjected to uniaxial compression.

The focal point of the work of Wu and Nanakorn [54] is to formulate a constitutive framework that is self-consistent. Some well-known concepts have been discussed and it has been pointed out that some concepts are not compatible with others. Only concepts that are compatible to each other are used in the derivation. New concept such as the distinction between the state of damage and damage measure and the concept to restore the fictitious continuum to its undamaged state after each step of deformation and damage have been introduced. Finally, we mention that we use the corotational rate to account for rotation of principal damage directions during deformation.

References

1. Wu, H.C. and Yeh, W.C., Some considerations in the endochronic description of anisotropic hardening, *Acta Mech.*, 69, 59, 1987.
2. Ohashi, Y., Tokuda, M., Mitake, T., Kurita, Y., and Suzuki, T., Stress–strain relation of integral type for deformation of brass along strain trajectories consisting of three normal straight branches, *Arch. Mech.*, 32, 125, 1980.
3. Ohashi, Y., Tokuda, M., Suzuki, T., and Kurita, Y., Stress–strain relation of brass for the plastic deformation along bi-linear strain trajectories with various corner angles, *Bull. Japan. Soc. Mech. Eng.*, 24, 1909, 1981.
4. Wu, H.C., Hong, H.K., and Lu, J.K., An endochronic theory accounted for deformation induced anisotropy, *Int. J. Plasticity*, 11, 145, 1995.
5. Wu, H.C., Lu, J.K., and Pan, W.F., Endochronic equations for finite plastic deformation and application to metal tube under torsion, *Int. J. Solids Struct.*, 32, 1079, 1995.
6. Phillips, A. and Tang, J.L., The effect of loading path on the yield surface at elevated temperatures, *Int. J. Solids Struct.*, 8, 463, 1972.
7. Wu, H.C. and Yeh, W.C., On the experimental determination of yield surfaces and some results of annealed 304 stainless steel, *Int. J. Plasticity*, 7, 803, 1991.
8. Wu, H.C. and Lu, J.K., Further development and application of an endochronic theory accounted for deformation induced anisotropy, *Acta Mech.*, 109, 11, 1995.

9. Wu, H.C. and Hong, H.K., Endochronic description of plastic anisotropy in sheet metal, *Int. J. Solids Struct.*, 36, 2735, 1999.
10. Hill, R., A theory of yielding and plastic flow of anisotropic materials, *Proc. Roy. Soc.*, London, A, 193, 281, 1948.
11. Valanis, K.C., A theory of viscoplasticity without a yield surface, *Arch. Mech.* 23, 517, 1971.
12. Valanis, K.C., Proper tensorial formulation of the internal variable theory, The endochronic time spectrum, *Arch. Mech.*, 29, 173, 1977.
13. Valanis, K.C., Back stress and Jaumann rates in finite plasticity, *Int. J. Plasticity*, 6, 353, 1990.
14. Dafalias, Y.F., Plastic spin: necessity or redundancy?, *Int. J. Plasticity*, 14, 909, 1998.
15. Im, S. and Atluri, S.N., A study of two finite strain plasticity models: an internal time theory using Mandel's director concept, and a general isotropic/kinematic-hardening theory, *Int. J. Plasticity*, 3, 163, 1987.
16. Goddard, J.D. and Miller, C., An inverse for the Jaumann derivative and some applications to the rheology of viscoelastic fluids, *Rheol. Acta*, 5, 177, 1966.
17. Dafalias, Y.F., Corotational integral in constitutive formulations, *J. Eng. Mech.*, 113, 1967, 1987.
18. Swift, H.W., Length change in metal under torsional overstrain, *Engineering*, 163, 253, 1947.
19. Hart, E.W. and Chang, Y.W., Material rotation effects in tension–torsion test: experimental result, in *Plasticity Today*, Sawczuck, A. and Bianchi, G.E., Eds., Elsevier Appl. Sci., U.K., 1985, 235.
20. White, C.S., Bronkhorst, C.A., and Anand, L., An improved isotropic-kinematic hardening model for moderate deformation metal plasticity, *Mech. Mater.*, 10, 127, 1990.
21. Wu, H.C. and Xu, Z.Y., An extensometer investigation of the axial effect during torsion. *Proc. Int. Conf. on Constitutive Laws for Eng. Material*, Fan, J. and Murakami, S., Eds., Chongqing, China, 1989, 232.
22. Bailey, J.A., Haas, S.L., and Nawab, K.C., Anisotropy in Plastic Torsion, *J. Basic Eng.*, 94, 231, 1972.
23. Wu, H.C., Xu, Z., and Wang, P.T., Torsion test of aluminum in the large strain range, *Int. J. Plasticity*, 13, 873, 1998.
24. Canova, G.R., Kocks, U.F., and Jonas, J.J., Theory of torsion texture development, *Acta Metall.*, 32, 211, 1984.
25. Taylor, G.I. and Quinney, H., The plastic distortion of metal, *Phil. Trans. Roy. Soc.*, A, 230, 323, 1932.
26. Lowe, T.C. and Lipkin, J., Analysis of axial deformation response during reverse shear, Sand90-8417, Sandia National Lab., 1990.
27. Qian, Z. and Wu, H.C., A 2-D texture study based on a double-slip model of polycrystal plasticity with analysis of thin-walled tube under torsion, *Int. J. Solids Struct.*, 33, 4167, 1996.
28. Wu, H.C. and Aboutorabi, M.R., Endochronic modeling of coupled volumetric–deviatoric behavior of porous and granular materials, *Int. J. Plasticity*, 4, 163, 1988.
29. Wu, H.C., An endochronic theory for porous and granular materials, in *Modern Approaches to Plasticity*, Kolymbas, D., Ed., Elsevier, Amsterdam, 1993, 347.

30. Johnson, J.N. and Green, S.J., Mechanical response of porous media subject to static load, in *Effects of Voids on Material Deformation*, Cowin, S.C. and Carroll, M.M., Eds., AMD-16, ASME, New York, 1976, 93.
31. Scavuzzo, R., Stankowski, T., Gerstle, K.H., and Ko, H.Y., Stress–strain curves for concrete under multiaxial load histories, Report, Department of Civil, Environmental and Architectural Engineering, University of Colorado, Boulder, CO, 1983.
32. Wu, H.C., Wang, Z.K., and Aboutorabi, M.R., Endochronic modeling of sand in true triaxial test, *J. Eng. Mech., ASCE,* 111, 1257, 1985.
33. Bazant, Z.P. and Krizek, R.J., Endochronic constitutive law for liquefaction of sand, *J. Eng. Mech. Div., ASCE,* 102, 225, 1976.
34. Valanis, K.C. and Read, H.E., A new endochronic plasticity model for soils, in *Soil Mechanics-Transient and Cyclic Loads*, Pande, G.N. and Zienkiewicz, O.C., Eds., John Wiley, New York, 1982.
35. Valanis, K.C. and Peters, J.F., Configurational plasticity in granular media, in *Modern Approaches to Plasticity*, Kolymbas, D., Ed., Elsevier, Amsterdam, 1993, 1.
36. Wu, H.C., Wang, T.P., Endochronic description of sand response to static loading, *J. Eng. Mech., ASCE,* 109, 970, 1983.
37. Lade, P.V., Elasto-plastic stress–strain theory for cohesiveless soil with curved yield surfaces, *Int. J. Solids Struct.*, 13, 1019, 1977.
38. Cuellar, V., Bazant, Z.P., Krizek, R.J., and Silver, M.L., Densification and hysteresis of sand under cyclic shear, *J. Geotechn. Eng. Division, ASCE*, 103, 399, 1977.
39. Lee, K.L. and Seed, H.B., Drained strength characteristics of sands, *J. Soil Mech. Found. Div., ASCE*, 93, 117, 1967.
40. Wu, H.C. and Sheu, J.C., Endochronic modeling for shear hysteresis of sand, *J. Geotechn. Eng., ASCE*, 109, 1539, 1983.
41. Silver, M.L. and Seed, H.B., Deformation characteristic of sand under cyclic loading, *J. Soil Mech. Found. Div., ASCE*, 97, 1081, 1971.
42. Wu, H.C. and Aboutorabi, M.R., Endochronic model of sand with circular stress path, *J. Geotechn. Eng., ASCE*, 114, 93, 1988.
43. Aboutorabi, M.R., Wu, H.C., Wang, T.P., and Gao, Q.Y., Stress–strain behavior of porous aluminum, in *Proc. 2nd International Conf. on Constitutive Laws for Engineering Materials: Theory and Application*, Desai, C.S., Krempl, E., Kiousis, P.D., and Kundu, T., Eds., Elsevier, New York, 1987, 477.
44. Wang, P.T. and Wu, H.C., An endochronic model for compaction of porous metals, *Prog. Powder Metall.*, 41, 161, 1986.
45. Schock, R.N., Abey, A.E., and Duba A., Quasi-static deformation of porous beryllium and aluminum, *J. Appl. Phys.*, 47, 53, 1976.
46. Wu, H.C., Wang, P.T., Pan, W.F., and Xu, Z.Y., Cyclic stress–strain response of porous aluminum, *Int. J. Plasticity*, 6, 207, 1990.
47. Kachanov, L.M., On the time to failure during creep, *Izv. AN. SSSR.*, OTN.337,1958.
48. Lemaitre, J. and Chaboche, J.L., Aspects phénoménologique ge la rupture par endommagement, *J. Méc. Appl.*, 2, 167, 1978.
49. Sidoroff, F., Description of anisotropic damage application to elasticity, in *Physical Non-Linearities in Structure Analysis-IUTAM*, Hult, J. and Lemaitre, J., Eds., Springer-Verlag, New York, 1981, 237.

50. Lemaitre, J. and Chaboche, J.L., *Mécanique des Matériaux Solides*, Paris: Dunod; English Edition, Cambridge University Press, 1985.
51. Chow, C.L. and Lu, T.J., A comparative study of continuum damage models for crack propagation under gross yielding, *Int. J. Fract.*, 53, 43, 1992.
52. Chaboche, J.L., Sur l'utilisation des variables d'état interne pour la description du comportement viscoplastique et de la rupture par endommagement, *Symposium Franco-Polonais de Rhéologie et Mécanique*, Cracovie, 1977.
53. Lemaitre, J., A continuum damage mechanics model for ductile fracture, *J. Eng. Mater. Technol.*, 107, 83, 1985.
54. Wu, H.C. and Nanakorn, C.K., A constitutive framework of plastically deformed damaged continuum and a formulation using the endochronic concept, *Int. J. Solids Struct.*, 36, 5057, 1999.
55. Murakami, S. and Ohno, N., A continuum theory of creep and creep damage, in *Creep Structures*, Ponter A.R.S. and Hayhust, D.R., Eds., Springer, Berlin, 1981, 922.
56. Betten, J., Damage tensors in continuum mechanics, *J. Mecanique theorique et appliqué*, 2 , 13, 1983.
57. Rabotnov, Y.N., *Creep Problems in Structural Members*, North-Holland Series in Applied Math. and Mech., Vol. 7, Chap. 6, North-Holland, Amsterdam,1969.
58. Cordebois, J.P. and Sidoroff, F., Damage induced elastic anisotropy, *Comportement mecanique des solides anisotropes, EUROMECH*, 115, Proc. Coll., Int. du C.N.R.S., Boehler J.P. Ed., Villard-de-Lens, France, 1979, 761.
59. Chow, C.L. and Wang, J., An anisotropic theory of elasticity for continuum damage mechanics. *Int. J. Fract.*, 33, 3, 1987.
60. Stumvoll, M. and Swobada, G., Deformation behavior of ductile solids containing anisotropic damage, *J. Eng. Mech.*, 119, 1331, 1993.
61. Rabotnov, Y.N., Creep rupture, in *Proceedings, Applied Mechanics Conference*, Hetenyi, M. and Vincenti, H., Eds., Standford University, 1968, 342.
62. Chow, C.L. and Lu, T.J., On evolution laws of anisotropic damage, *Eng. Fract. Mech.*, 34, 679, 1989.
63. Valanis, K.C., *Irreversible Thermodynamics of Continuous Media*, Springer-Verlag, Udine, 1971.
64. Krajcinovic, D., Continuous damage mechanics revisited: basic concepts and definition, ASME, *J. Appl. Mech.*, 52, 829, 1985.
65. Wu, H.C. and Nanakorn, C.K., An endochronic theory of continuum damage mechanics, ASCE, *J. Eng. Mech.*, 124, 200, 1998.
66. Valanis, K.C., A theory of damage in brittle materials, *Eng. Fract. Mech.*, 36, 403, 1990.
67. Niu, X., Endochronic plastic constitutive equations coupled with isotropic damage and damage evolution models, *Eur. J. Mech., A/Solids*, 8, 293, 1989.
68. Chow, C.L. and Chen, X.F., An anisotropic model of damage mechanics based on endochronic theory of plasticity, *Int. J. Fract.*, 55, 115, 1992.
69. Fonseka, G.U. and Krajcinovic, D., The continuous damage theory of brittle materials, part 2: uniaxial and plane response modes. *J. Appl. Mech.*, 48, 816, 1981.

Problems

(1) Start from (9.10) and derive (9.11).

(2) Derive (9.13).

(3) Show that if the intrinsic time is defined by $\mathrm{d}\zeta^2 = \mathrm{d}\boldsymbol{\varepsilon}^{\mathrm{p}} \cdot \underline{\mathbf{K}} \cdot \mathrm{d}\varepsilon^{\mathrm{p}} + \mathrm{tr}(\mathbf{L} \cdot \mathrm{d}\boldsymbol{\varepsilon}^{\mathrm{p}})\,\mathrm{d}\zeta$, then the corresponding yield function is $(\boldsymbol{\sigma}' - \boldsymbol{\alpha}) \cdot \underline{\mathbf{K}} \cdot (\boldsymbol{\sigma}' - \boldsymbol{\alpha}) + \sigma_{\mathrm{y}}' f(z)\mathrm{tr}[\mathbf{L} \cdot (\boldsymbol{\sigma}' - \boldsymbol{\alpha})] = (\sigma_{\mathrm{y}}' f(z))^2$.

(4) In (9.37), the evolution equations of internal variables q_x^r and q_y^r are

$$\frac{\mathrm{d}q_x^r}{\mathrm{d}z} + P^r q_x^r + U^r q_y^r = P^r \varepsilon_x + U^r \varepsilon_y$$
$$\frac{\mathrm{d}q_y^r}{\mathrm{d}z} + Q^r q_y^r + V^r q_x^r = Q^r \varepsilon_y + V^r \varepsilon_x$$

where P^r, Q^r, U^r, and V^r are not functions of q_x^r and q_{y}^r. These two equations are coupled in q_x^r and q_{y}^r. Decouple the equations.

(5) Derive (9.45).

(6) For the PG materials discussed in Section 9.4.1, derive the governing equations given by (9.127) to (9.130).

(7) In the application to porous aluminum discussed in Section 9.4.4, derive (9.161) and (9.162) for the deviatoric stress–strain behavior.

10

Anisotropic Plasticity for Sheet Metals

10.1 Introduction

Sheet metal is a special product form of a material that is produced by the rolling process. The process of rolling is illustrated by considering a strip of metal passing between a pair of rolls with their axes parallel to each other. The sheet metal enters the rolls, and the marginal speed of the rolls on the entry side is higher than the entry speed of the sheet. The friction forces created between the rolls and the metal strip tend to pull the strip into the gap between the rolls, where plastic deformation takes place. On exiting the rolls, the friction forces change direction and the sheet acquires a reduced thickness, while the speed of the sheet is greater than the speed of the rolls. The thickness of a metal sheet can be reduced further by additional rolling, generating various degrees of anisotropy.

The anisotropy in the sheet metal is two-fold: the anisotropy in the yield stress and the anisotropy in the plastic flow. The anisotropy is usually specified with respect to the rolling direction (RD) of the sheet (Figure 10.1); TD denotes the transverse direction and ND, the normal direction, which is not shown in the figure. Tension specimens cut at various angles θ measured counterclockwise from the rolling direction can exhibit different yield stresses and different characteristics of plastic deformation. Generally, both the yield stress and the plastic deformation are functions of the orientation angle θ. However, it is possible that a material does not show noticeable anisotropy in the yield stress but shows significant anisotropy in the plastic deformation. The anisotropy of plastic flow is usually measured by the plastic strain-ratio R, which is defined by many recent researchers as

$$R = \frac{\mathrm{d}\varepsilon_{\mathrm{w}}^{\mathrm{p}}}{\mathrm{d}\varepsilon_{\mathrm{t}}^{\mathrm{p}}} \tag{10.1}$$

where $\mathrm{d}\varepsilon_{\mathrm{w}}^{\mathrm{p}}$ is the plastic strain increment in the width direction, and $\mathrm{d}\varepsilon_{\mathrm{t}}^{\mathrm{p}}$ that in the thickness direction of a tension specimen. The value of R can vary from one sheet material to the other. It can be greater than one or less than one, and $R = 1$ implies material isotropy. The R-ratio is an important parameter

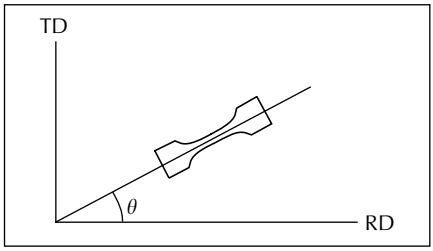

FIGURE 10.1
Tension specimen cut at angle θ.

of a sheet material. A large R means a small change in the thickness during longitudinal tension, while a small R corresponds to a large change in the thickness during longitudinal stretching. Therefore, a small R would lead to easy thinning and early failure of the sheet.

This definition of R-ratio is not universal, however. Recent researchers prefer the definition of (10.1) because of its apparent tie to the flow rule of plasticity. On the other hand, the ASTM Standards [1] define the R-ratio as

$$R = \frac{\varepsilon_w}{\varepsilon_t} \quad \text{where } \varepsilon_w = \ln\left(\frac{w_f}{w_0}\right) \quad \text{and} \quad \varepsilon_t = \ln\left(\frac{t_f}{t_0}\right) \tag{10.2}$$

The subscripts $()_0$ and $()_f$ denote the initial and final lengths, respectively; w stands for width and t, the thickness. Thus, the R-ratio is the ratio between the true width strain and the true thickness strain. Due to the thinness of sheets, the thickness strain is difficult to measure accurately. A practical method is to measure the longitudinal and width strains and make the assumption of volume constancy. Therefore, (10.2) reduces to

$$R = \frac{\ln(w_0/w_f)}{\ln(l_f w_f / l_0 w_0)} \tag{10.3}$$

where l is the longitudinal measurement.

Many researchers believe that the R-ratio does not vary appreciably with strain and make the assumption of constancy in their theoretical analyses. Detailed information concerning the strain level at which the measurements of R were taken is generally not reported in the literature. Some measurements were taken after the specimens had undergone large deformation. Some were taken midway between the first occurrence of nonuniform strain and the final fracture. Tracking of the R-ratio during experiments has indicated, however, that the R-ratio may vary greatly with the increasing plastic strain [2]. Mellor [2] and Lin and Ding [3] noted further that, due to the inaccuracy of the experimental data, the R-ratio could not be assessed closer to the initial yield region of the material. The variation of R-ratio with increasing plastic strain is discussed later in this chapter.

10.2 Standard Tests for Sheet Metal

10.2.1 The Uniaxial Tension Test

Tensile specimens are cut at predetermined angles θ (usually every 15°) to the rolling direction. Uniaxial tension tests are conducted on these specimens and yield stress σ_θ determined as a function of θ. The stress state is given by

$$\sigma_x = \sigma_\theta \cos^2\theta, \qquad \sigma_y = \sigma_\theta \sin^2\theta, \quad \text{and} \quad \sigma_{xy} = \sigma_\theta \sin\theta\cos\theta \tag{10.4}$$

After the test, strains in both the axial and width directions of the specimens are measured, and the thickness strain determined by the assumption of volume constancy.

10.2.2 Equibiaxial Tension Test

This experiment is performed to determine the *equibiaxial yield stress* σ_B. It can be accomplished by a self-designed loading frame attached to a universal test machine or a servo-hydraulic test system. When the sheet is thin and the static loading is of concern, the experiment could also be carried out by use of a self-designed dead-weight loading system. For a more versatile testing, two servo-controlled actuators may be placed 90° from each other to form the loading system.

10.2.3 Hydraulic Bulge Test

This test could also be used to determine the equibiaxial yield stress σ_B. In the bulge test, a thin disc of sheet metal is clamped around its periphery and then subjected to an increasing fluid pressure applied to one side. The region in the vicinity of the dome becomes nearly spherical in shape as the sheet bulges. The tensile stresses in the plane of the sheet are the same by symmetry. An advantage of the bulge test is that it can be carried out to strains far greater than the instability strain in tension and is not complicated by friction as is the compression test. However, the test results are not direct. A boundary value problem has to be solved in which a constitutive equation is needed.

10.2.4 Through-Thickness Compression Test

Cylindrical specimens are prepared from discs of the sheet material glued together with an epoxy adhesive. The specimens were tested in compression using Teflon sheet and graphite grease for lubrication between the specimen ends and platen of the test machine. Due to the usual assumption that hydrostatic stress does not affect yielding, the equibiaxial yield stress is also the compressive yield stress perpendicular to the sheet. Factors of uncertainty

arose from the epoxy adhesive, the Teflon sheet and graphite grease. Therefore, the equibiaxial tension test is preferred over the through-thickness compression test.

10.2.5 Plane-Strain Compression Test

In this test, a thin sheet is indented between long narrow dies. To ensure parallelism of the accurately ground, smooth die faces and to facilitate testing, the dies are mounted in a special leader pin die set. Incremental loading is used to make a 2 to 5% reduction in thickness each time, followed by measurement of the thickness and relubrication with a high-pressure lubricant. Stress is calculated by dividing the load by the area between the indenters, while a corresponding strain is computed from $\varepsilon = \ln(t/t_0)$, where t and t_0 are the current and initial thickness of the sheet. The stress–strain curve for plane strain can then be obtained. The accuracy of the results is workpiece geometry dependent. It is actually a boundary value problem and a slip-line field theory of the problem is available.

10.2.6 Simple Shear Test

Specimens having two regions to be sheared in-plane are fixed tightly to the shearing test jig with bolts in order to generate pure shear within the specified regions. The test can be carried out by the use of a universal test machine. The test attempts to produce a pure shear stress state. The stress state of this test is, however, never simple, and the test can at best be used as an approximation. We do not distinguish between pure shear and simple shear when the deformation is small.

10.3 Experimental Yield Surface for Sheet Metal

Extensive literature is available addressing the issue of experimental determination of yield surfaces in plasticity, as explained in Sections 6.2 and 7.2. Most of these works used tubular specimens and determined the yield surfaces in the shear stress versus axial stress subspace. From these investigations, it was clear that the definition of yield significantly influenced the characteristics of strain hardening. Yield defined by proportional limit leads to kinematic hardening and distortion of the yield surface, yield defined by a 0.2% proof strain leads to a combined isotropic–kinematic hardening, and yield defined by backward linear extrapolation or by a large proof strain leads to isotropic hardening.

The picture is not as clear in the case of sheet metals or metal plates. In this case, the experimental points on the yield surface are usually determined from the uniaxial tension test, the bulge test (balanced biaxial tension), the biaxial test using cruciform specimens, the plane-strain compression test, and

the through-thickness compression test. Test data using the uniaxial tension test, the bulge test, and the cruciform specimen test provide yield surface only in the tensile stress quadrant of the two-dimensional principal stress space. Test data of the plane-strain compression test and the through-thickness test can include information for the compression region, but these must be supplemented by the assumption that a superimposed hydrostatic stress does not influence yielding. Therefore, they are not direct experimental results.

In the discussion of sheet metals, usually a Cartesian coordinate system is used with the x-axis taken along the RD, the y-axis along the TD, and the z-axis along the ND. Szczepinski [4] investigated the effect of yield definition by use of uniaxial tension specimens cut out from metal sheets making various α angles with the rolling direction. The yield stress determined from each specimen is transformed into a set of stress components $(\sigma_x, \sigma_y, \sigma_{xy})$ by the use of Mohr's circle. These sets of stress components can then be plotted in a three-dimensional stress space, with σ_x and σ_y forming two perpendicular axes on the horizontal plane, and σ_{xy} the vertical axis normal to the horizontal plane. The initial yield surface for an isotropic material is an ellipsoid in this space. The subsequent yield surfaces are represented by the motion, distortion, and/or expansion of the ellipsoid and can be best viewed by two projections. The first projection is onto the (σ_x, σ_y) plane (the plane view) and the second projection (the elevation view) is onto a plane that passes through the σ_{xy} axis and the s-direction which bisects the right angle formed by the σ_x and $-\sigma_y$ axes and is perpendicular to the major axis of the ellipsoid. The kinematic hardening, which is difficult to identify based on data in the tension quadrant of the two-dimensional principal stress space, can be visualized in the aforementioned projections.

Experimental data of Lee and Backofen [5] show a strong kinematic hardening. Those of Lege et al. [6] show a difference in tensile and compressive yield stresses, hinting at the existence of kinematic hardening. Naruse et al. [7] determined the yield locus in the tension stress quadrant by use of a yield definition based on plastic work that corresponds to a tensile strain of 20%. The yield locus thus determined is significantly influenced by the deformation history. Tests by use of cruciform specimens were conducted by Kreissig and Schindler [8]. The experimental results show a significant kinematic-hardening effect on the yield surface of sheet metal materials. Lin and Ding [3] also determined the yield loci in the tension quadrant of the principal stress space by use of cruciform specimens.

In an attempt to provide test data in the compressive stress region, Tozawa [9] and Barlat et al. [10] used biaxial compression tests on cubic specimens made from laminated sheet samples. Tozawa [9] obtained yield loci, at various proof strains, which were concentric circles in the π-plane of the principal stress space for initially isotropic material. For the same material, when subjected to a predetermined amount of prestrain, the yield loci was enlarged and distorted, and this behavior repeated itself with increasing subsequent strain. Barlat et al. [10], using a procedure similar to that of Tozawa [9], determined the yield locus at a plastic strain of 10% and observed primarily the effect of isotropic hardening. A typical yield locus determined in [10] is

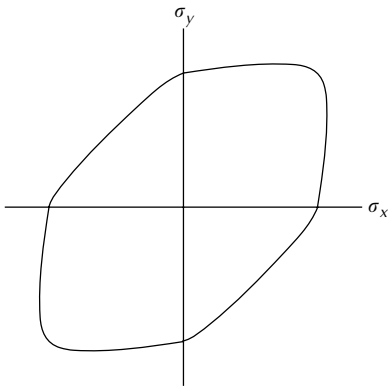

FIGURE 10.2
A typical yield locus for sheet metal assuming isotropic hardening (From Barlat, F. et al., *Int. J. Plasticity*, 13, 385, 1997. With permission from Elsevier).

shown in Figure 10.2. We see from the figure that the biaxial yield stress σ_B^Y is larger than the uniaxial tensile yield stress σ_u^Y and thus the yield locus cannot be described by the Mises ellipse (see Chapter 6). We mention here that a proof strain of 10% is a very large strain indeed to define a yield surface. A large amount of plastic deformation has already occurred within the yield surface. Each experimental point on the yield locus has its own deformation history and its own history of strain hardening. Therefore, if we use a small proof strain to define the yield point, then the data points on a yield locus of [10] do not belong to the same yield locus. Furthermore, we mention that the delamination of the test specimens can lead to inaccurate yield stress values.

It is seen from this summary of experimental findings that the sheet metals do show a significant amount of kinematic hardening. The conclusion is not as clear as that drawn from the axial–torsion test of tubes. The situation has been complicated by the different types of test setups and the limitation of most tests to obtaining yield loci in the tension quadrant of the two-dimensional principal stress space. However, it is our opinion that the results of Kreissig and Schindler [8] are the most convincing. Also, potentially significant results can be obtained from the type of test initially proposed by Szczepinski [4]. More experimental investigations are needed to confirm the kinematic-hardening effect on sheet metals.

10.4 Hill's Anisotropic Theory of Plasticity

10.4.1 The Quadratic Yield Criterion

The most well-known anisotropic yield criterion for sheet metals was due to Hill [11,12]. It is in a quadratic form and reduces to the Mises yield criterion

when the material is isotropic. Assuming that the hydrostatic pressure does not influence yielding, only the differences of the normal stress components can appear in the yield function. Thus, the yield function is written as

$$\begin{aligned} 2f(\sigma_{ij}) = {} & F(\sigma_{\mathrm{y}} - \sigma_z)^2 + G(\sigma_z - \sigma_x)^2 + H(\sigma_x - \sigma_{\mathrm{y}})^2 \\ & + 2L\sigma_{yz}^2 + 2M\sigma_{zx}^2 + 2N\sigma_{xy}^2 = 1 \end{aligned} \tag{10.5}$$

The material parameters F, G, H, L, M, and N represent the current state of anisotropy of the metal sheet, while σ_{ij} represents the components of the Cauchy stress. Hill's criterion assumes that there is no Bauschinger effect and considers the axes of anisotropy as the axes of reference, thus making x the rolling direction and y the transverse direction of the sheet metal. Equation (10.5) can be rearranged and written as

$$\begin{aligned} & \left[(G+H)\sigma_x^2 - 2H\sigma_x\sigma_{\mathrm{y}} + (F+H)\sigma_{\mathrm{y}}^2 + 2N\sigma_{xy}^2\right] \\ & \quad - 2(G\sigma_x + F\sigma_{\mathrm{y}})\sigma_z + 2(L\sigma_{yz}^2 + M\sigma_{zx}^2) + (F+G)\sigma_z^2 = 1 \end{aligned} \tag{10.6}$$

In the case of sheet metals, $\sigma_z = \sigma_{zx} = \sigma_{zy} = 0$, (10.7) reduces to

$$(G+H)\sigma_x^2 - 2H\sigma_x\sigma_{\mathrm{y}} + (F+H)\sigma_{\mathrm{y}}^2 + 2N\sigma_{xy}^2 = 1 \tag{10.7}$$

The anisotropic coefficients F, G, H, and N can be determined from experiments. In a tension test along the x-direction, the stresses are $\sigma_x \neq 0$, $\sigma_{\mathrm{y}} = \sigma_{xy} = 0$, and (10.7) reduces to

$$G + H = \left(\sigma_x^{\mathrm{Y}}\right)^{-2} \tag{10.8a}$$

where σ_x^{Y} is the yield stress in the x-direction. Similarly, a tension test along the y-direction leads to

$$H + F = \left(\sigma_{\mathrm{y}}^{\mathrm{Y}}\right)^{-2} \tag{10.8b}$$

where $\sigma_{\mathrm{y}}^{\mathrm{Y}}$ is the yield stress in the y-direction. Yielding under equibiaxial tension occurs when $\sigma_x = \sigma_{\mathrm{y}} = \sigma_{\mathrm{B}}^{\mathrm{Y}}$. In this case, (10.7) reduces to

$$G + F = \left(\sigma_{\mathrm{B}}^{\mathrm{Y}}\right)^{-2} \tag{10.8c}$$

Due to the usual assumption that hydrostatic stress does not affect yielding, this is also the compressive yield stress perpendicular to the sheet.

Equations (10.8a,b,c) can be solved for G, F, and H as

$$2G = \frac{1}{(\sigma_x^{\mathrm{Y}})^2} - \frac{1}{(\sigma_{\mathrm{y}}^{\mathrm{Y}})^2} + \frac{1}{(\sigma_{\mathrm{B}}^{\mathrm{Y}})^2} \tag{10.9a}$$

$$2F = \frac{1}{(\sigma_{\mathrm{y}}^{\mathrm{Y}})^2} - \frac{1}{(\sigma_x^{\mathrm{Y}})^2} + \frac{1}{(\sigma_{\mathrm{B}}^{\mathrm{Y}})^2} \tag{10.9b}$$

$$2H = \frac{1}{(\sigma_x^{\mathrm{Y}})^2} + \frac{1}{(\sigma_{\mathrm{y}}^{\mathrm{Y}})^2} - \frac{1}{(\sigma_{\mathrm{B}}^{\mathrm{Y}})^2} \tag{10.9c}$$

Finally, the coefficient N may be determined from the tension test of a specimen cut at 45° angle with the x-direction. The tensile yield stress for this specimen is denoted by σ_{45}, and $\sigma_x = \sigma_{\mathrm{y}} = \sigma_{xy} = (1/2)\sigma_{45}$. Using this condition, it may be found from (10.7) that

$$2N = \left(\frac{\sigma_{45}}{2}\right)^{-2} - \left(\sigma_{\mathrm{B}}^{\mathrm{Y}}\right)^{-2} \tag{10.9d}$$

Since σ_{45} is easily determined experimentally, N is thus determined from (10.9d). The shear yield stress σ_{xy}^{Y} is determined in pure shear with the material element parallel to the orthotropic axes. It may be shown from (10.7) that

$$\sigma_{xy}^{\mathrm{Y}} = \frac{1}{\sqrt{2N}} \tag{10.10}$$

In sheet metals, pure shear is difficult to realize experimentally. However, the simple shear test is sometimes used in the literature to determine N. We have thus shown that the coefficients of the yield function (10.7) can be determined by a set of tension tests. Well-controlled tension tests are simple to perform. The equibiaxial test can be carried out by use of cruciform specimens as in Makinde et al. [13] and Lin and Ding [3].

10.4.2 The Flow Rule and the *R*-Ratio

Assuming that the normality rule is valid, the increments of plastic strain components are

$$\begin{aligned} \mathrm{d}\varepsilon_x^{\mathrm{p}} &= \mathrm{d}\lambda\{(G+H)\sigma_x - H\sigma_{\mathrm{y}}\} \\ \mathrm{d}\varepsilon_y^{\mathrm{p}} &= \mathrm{d}\lambda\{(H+F)\sigma_{\mathrm{y}} - H\sigma_x\} \\ \mathrm{d}\varepsilon_{xy}^{\mathrm{p}} &= \mathrm{d}\lambda N\sigma_{xy} \end{aligned} \tag{10.11}$$

where $\mathrm{d}\lambda$ is a proportional factor, which varies with loading.

The R-ratio for a tensile specimen cut at an angle α from the rolling direction of the sheet is defined as in (10.1) by

$$R_\theta = \frac{\mathrm{d}\varepsilon^{\mathrm{p}}_{y'}}{\mathrm{d}\varepsilon^{\mathrm{p}}_{z'}} \tag{10.12}$$

where $\mathrm{d}\varepsilon^{\mathrm{p}}_{y'}$ is the plastic strain increment in the width direction, and $\mathrm{d}\varepsilon^{\mathrm{p}}_{z'}$ in the thickness direction. In this way, x' is oriented at an angle θ from the rolling direction, and it coincides with the longitudinal axis of the specimen. In addition, the normal axis of the sheet is $z = z'$. The R-values are usually assessed at a longitudinal strain >0.5. As a result, the elastic strain is negligible, and due to the incompressibility assumption, (10.12) may be written as

$$R_\theta = -\frac{\mathrm{d}\varepsilon^{\mathrm{p}}_{y'}}{\mathrm{d}\varepsilon^{\mathrm{p}}_{x'} + \mathrm{d}\varepsilon^{\mathrm{p}}_{y'}} = -\frac{g}{1+g} \qquad \text{where } g\left(\varepsilon^{\mathrm{p}}_{x'}\right) = \frac{\mathrm{d}\varepsilon^{\mathrm{p}}_{y'}}{\mathrm{d}\varepsilon^{\mathrm{p}}_{x'}} \tag{10.13}$$

The motivation for such transformation relies on the fact that during a tensile test, it is difficult to assess the strain along the thickness direction. This allows R-ratio to be evaluated in terms of the longitudinal and lateral strains only. These are experimental readings easy to obtain and also more reliable, and the function g can be easily determined.

By use of coordinate transformation between the (x, y, z) and (x', y', z') axes, (10.13) reduces to

$$R_\theta = -\left(\frac{\mathrm{d}\varepsilon^{\mathrm{p}}_x \sin^2\theta + \mathrm{d}\varepsilon^{\mathrm{p}}_y \cos^2\theta - 2\,\mathrm{d}\varepsilon^{\mathrm{p}}_{xy} \sin\theta\cos\theta}{\mathrm{d}\varepsilon^{\mathrm{p}}_x + \mathrm{d}\varepsilon^{\mathrm{p}}_y}\right) \tag{10.14}$$

where $\mathrm{d}\varepsilon^{\mathrm{p}}_x, \mathrm{d}\varepsilon^{\mathrm{p}}_y$, and $\mathrm{d}\varepsilon^{\mathrm{p}}_{xy}$ are the components of the plastic strain increment. Substituting (10.4) and (10.11) into (10.14), yields

$$R_\theta = \frac{H + (2N - F - G - 4H)\sin^2\theta\cos^2\theta}{F\sin^2\theta + G\cos^2\theta} \tag{10.15}$$

Then, for the case of a tensile test performed along the rolling direction ($\theta = 0$), (10.15) reduces to

$$R_0 = \frac{H}{G} \tag{10.16}$$

Similarly, it is possible to obtain the R-ratio along $\theta = 90°$ (TD), and $\theta = 45°$ orientations

$$R_{90} = \frac{H}{F} \quad \text{and} \quad R_{45} = \frac{1}{2}\left(\frac{2N}{G+F} - 1\right) \tag{10.17}$$

Most often the drawability of a metal sheet is assessed by evaluating the R-ratio. Researchers consider two parameters, $\bar{R}$, the average strain ratio, and ΔR, the variation in strain ratio in the plane of the sheet. The parameter $\bar{R}$ measures normal anisotropy, and is defined by

$$\bar{R} = \frac{R_0 + 2R_{45} + R_{90}}{4} \tag{10.18}$$

For instance, the material exhibiting $\bar{R} > 1$ usually possesses good drawability, while $\bar{R} = 1$ means equal flows of material occurring along the width and thickness direction and exhibiting moderate drawability.

The case of planar anisotropy, on the other hand, is assessed by ΔR. This parameter describes the variation of R-ratio in the plane of the sheet along different orientations, and provides a good indication of ear formation during the deep drawing process. In the case of an isotropic material, $\bar{R} = 1$ and $\Delta R = 0$. An ideal material for deep drawing purposes would exhibit $\bar{R} > 1$ and $\Delta R = 0$.

10.4.3 The Equivalent Stress and Equivalent Strain

Based on the yield criterion (10.7), Hill [12] suggested that the equivalent stress be represented by

$$\bar{\sigma} = K^{-1/2} = K^{-1/2}\left[(G+H)\sigma_x^2 - 2H\sigma_x\sigma_y + (F+H)\sigma_y^2 + 2N\sigma_{xy}^2\right]^{1/2} \tag{10.19}$$

where

$$K = \tfrac{2}{3}(F+G+H) \tag{10.20}$$

The increment of plastic work per unit volume is defined as

$$\mathrm{d}W^{\mathrm{p}} = \sigma_x\,\mathrm{d}\varepsilon_x^{\mathrm{p}} + \sigma_y\,\mathrm{d}\varepsilon_y^{\mathrm{p}} + 2\sigma_{xy}\,\mathrm{d}\varepsilon_{xy}^{\mathrm{p}} \tag{10.21}$$

After the substitution of (10.11) into (10.21) and using (10.7), we can show that

$$\mathrm{d}W^{\mathrm{p}} = \mathrm{d}\lambda \tag{10.22}$$

The equivalent plastic strain increment, $\mathrm{d}\bar{\varepsilon}^{\mathrm{p}}$, is defined so that the plastic work increment is given by

$$\mathrm{d}W^{\mathrm{p}} = \bar{\sigma}\,\mathrm{d}\bar{\varepsilon}^{\mathrm{p}} \tag{10.23}$$

Its expression may be obtained by observing that the flow rule (10.11) may be solved for stress as

$$\sigma_x \, \mathrm{d}\lambda = \frac{1}{M}[(F+H)\mathrm{d}\varepsilon_x + H \, \mathrm{d}\varepsilon_y], \qquad \sigma_y \mathrm{d}\lambda = \frac{1}{M}[(G+H)\mathrm{d}\varepsilon_y + H \, \mathrm{d}\varepsilon_x] \tag{10.24}$$

where

$$M = (F+H)(G+H) - H^2 \tag{10.25}$$

Upon the substitution of (10.24) into (10.7), we obtain

$$\begin{aligned}(G+H)&\left[\frac{(F+H)\mathrm{d}\varepsilon_x^{\mathrm{p}} + H \, \mathrm{d}\varepsilon_y^{\mathrm{p}}}{M}\right]^2 - 2H\left[\frac{(F+H)\mathrm{d}\varepsilon_x^{\mathrm{p}} + H \, \mathrm{d}\varepsilon_y^{\mathrm{p}}}{M}\right] \\ &\times \left[\frac{(G+H)\mathrm{d}\varepsilon_y^{\mathrm{p}} + H \, \mathrm{d}\varepsilon_x^{\mathrm{p}}}{M}\right] + (F+H)\left[\frac{(G+H)\mathrm{d}\varepsilon_y^{\mathrm{p}} + H \, \mathrm{d}\varepsilon_x^{\mathrm{p}}}{M}\right]^2 \\ &+ \frac{2N}{M_2}\left[\frac{M \, \mathrm{d}\varepsilon_{xy}^{\mathrm{p}}}{N}\right]^2 = (\mathrm{d}\lambda)^2\end{aligned} \tag{10.26}$$

From (10.19), (10.21), and (10.22), we found that

$$\mathrm{d}\bar{\varepsilon}^{\mathrm{p}} = K^{1/2} \, \mathrm{d}\lambda \tag{10.27}$$

Using (10.26), the equivalent $\mathrm{d}\bar{\varepsilon}^{\mathrm{p}}$ is given by

$$\begin{aligned}\mathrm{d}\bar{\varepsilon}^{\mathrm{p}} = K^{1/2} \Bigg\{ &(G+H)\left[\frac{(F+H)\mathrm{d}\varepsilon_x^{\mathrm{p}} + H \, \mathrm{d}\varepsilon_y^{\mathrm{p}}}{M}\right]^2 \\ &- 2H\left[\frac{(F+H)\mathrm{d}\varepsilon_x^{\mathrm{p}} + H \, \mathrm{d}\varepsilon_y^{\mathrm{p}}}{M}\right]\left[\frac{(G+H)\mathrm{d}\varepsilon_y^{\mathrm{p}} + H \, \mathrm{d}\varepsilon_x^{\mathrm{p}}}{M}\right] \\ &+ (F+H)\left[\frac{(G+H)\mathrm{d}\varepsilon_y^{\mathrm{p}} + H \, \mathrm{d}\varepsilon_x^{\mathrm{p}}}{M}\right]^2 + \frac{2N}{M^2}\left[\frac{M \, \mathrm{d}\varepsilon_{xy}^{\mathrm{p}}}{N}\right]^2 \Bigg\}^{1/2}\end{aligned} \tag{10.28}$$

It is noted that the intrinsic time defined by (9.54) is of the same form as (10.28).

10.4.4 The Anomalous Behavior

Hill [12] showed that for materials with rotational symmetry about the z-axis, $F = G$. Considering that the principal stress space with 1 denotes the RD

and 2 the TD, (10.7) reduces to

$$(G+H)\sigma_1^2 - 2H\sigma_1\sigma_2 + (G+H)\sigma_2^2 = 1 \tag{10.29}$$

in which σ_1 and σ_2 are principal stresses in the plane of the sheet. Using (10.8a), (10.29) is given as

$$\sigma_1^2 - \frac{2H}{G+H}\sigma_1\sigma_2 + \sigma_2^2 = \frac{1}{G+H} = \sigma_u^2 \tag{10.30}$$

where σ_u is the uniaxial yield stress along the RD. Using (10.16), (10.30) can be further reduced to

$$\sigma_1^2 + \sigma_2^2 - \frac{2R_0}{R_0+1}\sigma_1\sigma_2 = \sigma_u^2 \tag{10.31}$$

where R_0 is the plastic strain ratio along the RD. The yield stress for equibiaxial tension may then be determined by setting $\sigma_1 = \sigma_2 = \sigma_B$ in (10.31). We obtain

$$\sigma_B = \left(\frac{1+R_0}{2}\right)^{1/2}\sigma_u \tag{10.32}$$

Thus, (10.32) results in $\sigma_B > \sigma_u$ when $R_0 > 1$ and $\sigma_B < \sigma_u$ when $R_0 < 1$. This relationship is further illustrated by plotting (10.31) in Figure 10.3. Most sheet metals show a yield locus with $\sigma_B > \sigma_u$ in the tension quadrant of the two-dimensional principal stress space. It is seen from the figure that Hill's criterion (10.31) is satisfactory for the case of $R_0 > 1$, but it does not agree with observed results in the case of $R_0 < 1$. This "anomalous behavior"

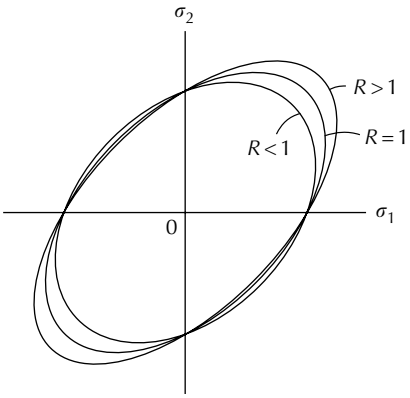

FIGURE 10.3
Quadratic yield loci with coefficients expressed in terms of R (From Wu, H.C., *Int. J. Plasticity*, 18, 1661, 2002. With permission from Elsevier).

was noted by Pearce [14] and Woodthorpe and Pearce [15] when they tested commercially pure aluminum sheets.

10.5 Nonquadratic Yield Functions

To accommodate the "anomalous behavior," Hill [16,17] proposed a number of possible generalizations of the quadratic yield function. These yield functions are generally more complex and are nonquadratic with additional anisotropic parameters.

Hill (1979):

$$F|\sigma_2-\sigma_3|^m + G|\sigma_3-\sigma_1|^m + H|\sigma_1-\sigma_2|^m + L|2\sigma_1-\sigma_2-\sigma_3|^m + M|2\sigma_2-\sigma_3-\sigma_1|^m + N|2\sigma_3-\sigma_1-\sigma_2|^m = 1 \tag{10.33}$$

Hill (1990):

$$|\sigma_1+\sigma_2|^m + \left(\frac{\sigma_B^m}{\tau^m}\right)|\sigma_1-\sigma_2|^m + |\sigma_1^2+\sigma_2^2|^{(m/2)-1} \times \left\{-2a\left(\sigma\left(\sigma_1^2-\sigma_2^2\right)\right) + b(\sigma_1-\sigma_2)^2\cos 2\alpha\right\}\cos 2\alpha = (2\sigma_B)^m \tag{10.34}$$

where m (with $m > 1$, integer or noninteger) is a material coefficient; σ_1, σ_2, and σ_3 are principal stresses and are expressed in the orthotropic symmetry axes x, y, and z; τ is the yield stress under pure shear parallel to the orthotropic axes. In addition,

$$a = \frac{(F-G)}{(F+G)} \quad \text{and} \quad b = \frac{(F+G+4H-2N)}{(F+G)} \tag{10.35}$$

Note that, in (10.33), the principal loads must coincide with the axes of orthotropy, whereas in (10.34) they can have any orientation. Furthermore, (10.34) is restricted to plane stress.

A yield function was proposed by Hosford [18] in the form of

$$F|\sigma_1-\sigma_2|^m + G|\sigma_2-\sigma_3|^m + H|\sigma_3-\sigma_1|^m = 1 \tag{10.36}$$

where m is 6 or 8 according to whether the crystal grains are body- or face-centered cubic, and the function does not include the anomaly.

Other nonquadratic forms have been proposed in the literature. Gotoh [19] proposed

$$\bar{\sigma}^4 = C_1\sigma_{xx}^4 + C_2\sigma_{xx}^3\sigma_{yy} + C_3\sigma_{xx}^2\sigma_{yy}^2 + C_4\sigma_{xx}\sigma_{yy}^3 + C_5\sigma_{yy}^4 + \sigma_{xy}^2(C_6\sigma_{xx}^2 + C_7\sigma_{xx}\sigma_{yy} + C_8\sigma_{yy}^2) + C_9\sigma_{xy}^4 \tag{10.37}$$

where $\bar{\sigma}$ is the effective stress; C_i are constants. Barlat and Lian [20] used the following criterion:

$$a|K_1 + K_2|^m + a|K_1 - K_2|^m + (2-a)|2K_2|^m = 2\bar{\sigma}^m$$

with

$$\begin{aligned} K_1 &= (\sigma_{xx} + h\sigma_{yy})/2 \\ K_2 &= \{[(\sigma_{xx} - h\sigma_{yy})/2]^2 + [p\sigma_{xy}]^2\}^{0.5} \end{aligned} \tag{10.38}$$

where a, h, p, and m are material constants.

Hill [21] pointed out that none of the above yield functions accounts for the behavior of the tensile yield to be the same along both the rolling and transverse directions, while the associated strain-ratios are markedly different. Hill then proposed the following nonquadratic yield function in the same paper to account for this effect:

$$\sigma_1^2 - \left(2 - \frac{\sigma_u^2}{\sigma_B^2}\right)\sigma_1\sigma_2 + \sigma_2^2 + \left\{(p+q) - \frac{(p\sigma_1 + q\sigma_2)}{\sigma_B}\right\}\sigma_1\sigma_2 = \sigma_u^2 \tag{10.39}$$

This function was proposed with applications to thin sheet in mind and is restricted to the tension quadrant of the (σ_1, σ_2) plane. An additional restriction of this form is that the tensile yield stress, denoted by σ_u, is the same in the rolling and transverse directions. The nondimensional parameters p and q are either positive or negative. The application of (10.39) is explained in [22], but that application was made in connection with the work contours which are not the same as the yield loci. Equation (10.39) accounts for the anomaly. A nonquadratic yield function was also presented in Hill [21] for the case when tensile yield stresses in rolling and transverse directions are distinct.

A nonquadratic yield criterion was proposed by Barlat et al. [23] as

$$\phi_1 = |S_1 - S_2|^m + |S_2 - S_3|^m + |S_3 - S_1|^m = 2\bar{\sigma}^m \tag{10.40}$$

where S_i is the principal value of an isotropic plasticity equivalent (IPE) stress tensor defined by

$$\mathbf{S} = \underline{\mathbf{L}} \cdot \boldsymbol{\sigma} \tag{10.41}$$

in which $\boldsymbol{\sigma}$ is the Cauchy stress and $\underline{\mathbf{L}}$ is a fully symmetric and traceless fourth-rank tensor. Tensor $\underline{\mathbf{L}}$ introduces the material anisotropy into the formulation. In the works of Barlat and coworkers, $\bar{\sigma}$ is sometimes referred to as the effective yield stress and sometimes as the uniaxial tensile yield stress in the rolling direction.

Karafillis and Boyce [24,25] constructed a yield criterion by mixing two yield functions, ϕ_1 and ϕ_2, which are defined by

$$\begin{aligned}\phi_1 &= |S_1 - S_2|^m + |S_2 - S_3|^m + |S_3 - S_1|^m \\ \phi_2 &= \frac{3^m}{2^{m-1}+1}\left(|S_1|^m + |S_2|^m + |S_3|^m\right)\end{aligned} \tag{10.42}$$

The Karafillis and Boyce yield criterion is then defined by the yield function:

$$\phi = (1-c)\phi_1 + c\phi_2 = 2\sigma_{\mathrm{u}}^m \tag{10.43}$$

where $c \in [0,1]$ and m is a constant. In the case of orthotropic symmetry, the components of tensor $\underline{\mathbf{L}}$ are

$$[L] = C\begin{bmatrix} 1 & \beta_1 & \beta_2 & 0 & 0 & 0 \\ \beta_1 & \alpha_1 & \beta_3 & 0 & 0 & 0 \\ \beta_2 & \beta_3 & \alpha_2 & 0 & 0 & 0 \\ 0 & 0 & 0 & \gamma_1 & 0 & 0 \\ 0 & 0 & 0 & 0 & \gamma_2 & 0 \\ 0 & 0 & 0 & 0 & 0 & \gamma_3 \end{bmatrix} \tag{10.44}$$

in which

$$\beta_1 = \tfrac{1}{2}(\alpha_2 - \alpha_1 - 1), \qquad \beta_2 = \tfrac{1}{2}(\alpha_1 - \alpha_2 - 1), \qquad \beta_3 = \tfrac{1}{2}(1 - \alpha_1 - \alpha_2) \tag{10.45}$$

Therefore, only $C, \alpha_1, \alpha_2, \gamma_1, \gamma_2$, and γ_3 are independent parameters.

Barlat et al. [10] further proposed the following yield criterion:

$$\phi = \alpha_1|S_1 - S_2|^m + \alpha_2|S_2 - S_3|^m + \alpha_3|S_3 - S_1|^m = 2\bar{\sigma}^m \tag{10.46}$$

where S_i are principal values of $S_{\alpha\beta}$ which is

$$[S] = \begin{bmatrix} \tfrac{1}{3}[C_3(\sigma_{xx} - \sigma_{yy}) - C_2(\sigma_{zz} - \sigma_{xx})] & C_6\sigma_{xy} & C_5\sigma_{zx} \\ C_6\sigma_{xy} & \tfrac{1}{3}[C_1(\sigma_{yy} - \sigma_{zz}) - C_3(\sigma_{xx} - \sigma_{yy})] & C_4\sigma_{zy} \\ C_5\sigma_{zx} & C_4\sigma_{zy} & \tfrac{1}{3}[C_2(\sigma_{zz} - \sigma_{xx}) - C_1(\sigma_{yy} - \sigma_{zz})] \end{bmatrix} \tag{10.47}$$

In (10.47), C_i are material constants and the coefficients α_i are further defined by

$$\alpha_i = \alpha_x p_{1i}^2 + \alpha_y p_{2i}^2 + \alpha_z p_{3i}^2 \tag{10.48}$$

where p_{ij} are the ith component of the jth principal direction of $\mathbf{S}$ (denoted as 1, 2, 3) with respect to the anisotropy axes of the material; α_x, α_y, and α_z are three additional functions. The expressions of these functions are given in [26].

Nonquadratic yield functions have also been proposed by Chakrabarty [27] with yield function given by

$$|\sigma_x + \sigma_y|^m + 2a\left(|\sigma_x|^m - |\sigma_y|^m\right) + b|2\sigma_{xy}|^m + c\left[(\sigma_x - \sigma_y)^2 + 4\sigma_{xy}^2\right]^{m/2} = (2\sigma_B)^m \tag{10.49}$$

where

$$\begin{aligned} 4a &= \left(\frac{2\sigma_B^Y}{\sigma_x^Y}\right)^m - \left(\frac{2\sigma_B^Y}{\sigma_y^Y}\right)^m, \qquad 2(1+c) = \left(\frac{2\sigma_B^Y}{\sigma_x^Y}\right)^m + \left(\frac{2\sigma_B^Y}{\sigma_y^Y}\right)^m, \\ 2b &= 2\left(\frac{2\sigma_B^Y}{\sigma_{45}}\right)^m - \left(\frac{2\sigma_B^Y}{\sigma_x^Y}\right)^m - \left(\frac{2\sigma_B^Y}{\sigma_y^Y}\right)^m \end{aligned} \tag{10.50}$$

and $m > 1$.

The aforementioned yield criteria are phenomenological criteria. A polycrystal model based on Taylor [28] and Bishop and Hill [29], the TBH model, can also be used to describe the deformation of sheet metals. Such study has been reported by Barlat and Richmond [30] and Lege et al. [6]. By use of the TBH model, the effects of rolling textures (Brass, Copper, S) and recrystallization textures (Cube, Goss) can be individually studied. The textures change with deformation, however, and the description of plastic deformation by the TBH model that accounts for the evolution of textures has not yet been demonstrated.

10.6 Anisotropic Plasticity Using Combined Isotropic–Kinematic Hardening

10.6.1 Introduction

From the summary of nonquadratic yield functions presented in the previous section, we see that these are generally very complicated expressions with additional material parameters. In a recent work, Lademo et al. [31] compared the models of Hill [11], Barlat and Lian [20], and Karafillis and Boyce [24] with their own experimental data of two aluminum materials and found that, for the first two models, calibrations based on yield stresses gave a good description of the yield stress anisotropy, but the same calibrations gave poor descriptions of the anisotropy in the R-ratio. Similarly, a calibration based on R-ratios gave a good description of the anisotropy in the R-ratio but a poor description of the yield stress anisotropy. The model of Karafillis

and Boyce [24] with zero back stress was unable to describe both kinds of anisotropy. It was then concluded that none of the models considered was capable of simultaneously describing both the anisotropy in the yield stress and the *R*-ratio for the alloys considered. The model of Karafillis and Boyce with nonzero back stress was not considered by Lademo et al. [31].

Due to these discrepancies, we feel that the theory of anisotropic plasticity needs to be fundamentally modified in order to obtain a realistic plasticity model. The existing anisotropic theory of plasticity for sheet metals proposes a yield function (quadratic or nonquadratic), assumes the normality condition for the plastic strain increments, and considers isotropic hardening. This theory is very different from the classical flow theory of plasticity in many aspects which are as follows: first, instead of a quadratic (initial) yield function for all metallic materials, this anisotropic theory for sheet metals uses a nonquadratic yield function with the exponent of the function depending on the material being considered. Furthermore, instead of the usual isotropic–kinematic hardening concept, this theory is entirely based on the concept of isotropic hardening. Another discrepancy is related to the experimental determination of the coefficients of the yield function. Traditionally, in the flow theory of plasticity, the yield function has been determined independent of the flow rule. In this theory, however, the flow rule has been extensively used in the determination of the coefficients of the yield function through the use of *R*. It should be pointed out that these different assumptions of the theory are not fully compatible. They have together created inconsistencies which have been demonstrated by the findings of Lademo et al. [31] that none of the models considered were capable of describing both aspects of anisotropy in the yield stress and the *R*-ratio for the alloys considered. The existing theory also leads to an undesirable situation that the sheet metal would require a different theory of plasticity from that used for the same material in other product forms.

In the existing theory of anisotropic plasticity, all experimental data, including yield loci and *R*-ratio, have been interpreted from the viewpoint of isotropic hardening. It is this viewpoint that has led to the concept of "anomalous behavior" and to the nonquadratic yield function. It has also led to the idea of expressing coefficients of the yield function in terms of the *R*-ratio. Since most experimentally determined yield loci for sheet metals have data only in the tension quadrant of the two-dimensional stress space, the isotropic hardening is but an assumption and, consequently, the yield locus is symmetrical with respect to the stress axes. Experimental results in compression, such as [10], support the idea of isotropic hardening. But, a closer look at [10] reveals that the plastic strain introduced during each probe of the yield surface was approximately 10%, which is a very large strain indeed. Due to this large strain definition of yield, the yield locus has been found to be symmetrical to both the σ_x and σ_y axes as shown in Figure 10.2. A large amount of plastic deformation has already taken place before a yield point is reached on the yield surface. If, on the other hand, a small proof strain is used to determine yield, then at each point on the yield locus of [10], the material

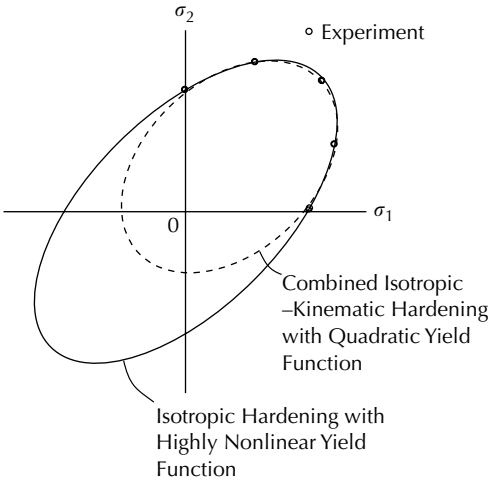

FIGURE 10.4
Two interpretations based on experimental data in tension quadrant.

has already experienced its own deformation history and its own history of strain hardening. In other words, these points do not belong to the same yield locus, if yield is defined by a small proof strain.

From the summary of experimental findings in Section 10.3, we are confident that the sheet metals do undergo isotropic as well as kinematic hardening, and we take this viewpoint in formulating an anisotropic theory of plasticity [32–34] and assume that the material undergoes a combined isotropic–kinematic hardening. Since most experimentally determined yield loci for sheet metals have data only in the tension quadrant of the two-dimensional stress space, the yield locus may either be viewed as having an isotropic hardening with a highly nonlinear yield function or as having a combined isotropic–kinematic hardening with the quadratic yield function. Both yield loci pass through the experimental points as shown in Figure 10.4.

10.6.2 The Anisotropic Theory Using Combined Isotropic–Kinematic Hardening

In this section, we present the theory propounded by Wu [34] with permission from Elsevier. In this development, the elastic deformation of the sheet material is assumed to be isotropic. In the case of plane stress, the equations are

$$\varepsilon_x^{\mathrm{e}} = \frac{1}{E}(\sigma_x - \nu\sigma_{\mathrm{y}}), \qquad \varepsilon_y^{\mathrm{e}} = \frac{1}{E}(\sigma_{\mathrm{y}} - \nu\sigma_x), \qquad \varepsilon_{xy}^{\mathrm{e}} = \frac{1}{2\mu}\sigma_{xy} \tag{10.51}$$

where the elastic strain components are

$$\varepsilon_x^{\mathrm{e}} = D_x^{\mathrm{e}}\,\mathrm{d}t, \qquad \varepsilon_y^{\mathrm{e}} = D_y^{\mathrm{e}}\,\mathrm{d}t, \qquad \varepsilon_{xy}^{\mathrm{e}} = D_{xy}^{\mathrm{e}}\,\mathrm{d}t \tag{10.52}$$

and D_x^e, D_y^e and D_{xy}^e are components of the elastic part of the rate of deformation D_x, D_y, and D_{xy}, respectively. In (10.51), E is the elastic modulus, μ is the shear modulus, and ν is Poisson's ratio.

The new yield function, like Hill's 1948 yield criterion [11], considers the axes of anisotropy as the axes of reference and is represented by (10.53). Hence, x denotes the rolling direction and y the transverse direction of the sheet metal. The yield function is

$$\begin{aligned} 2\phi = {} & (G+H)(\sigma_x - \alpha_x)^2 - 2H(\sigma_x - \alpha_x)(\sigma_y - \alpha_y) \\ & + (H+F)(\sigma_y - \alpha_y)^2 + 2N(\sigma_{xy} - \alpha_{xy})^2 = f^2 \end{aligned} \tag{10.53}$$

where the material parameters F, G, H, and N are determined by the initial state of anisotropy of the metal sheet. The components of the back stress, α_x, α_y, and α_{xy}, specify the center of the yield surface and are directly related to the kinematic hardening of the material. The function f specifies the size of the yield surface, and it is an expression of isotropic hardening. The function f increases with the accumulated plastic strain and will be further discussed. In the case of a material without isotropic hardening, $f = 1$; in the case of an annealed or an as-received material where the initial state of anisotropy is not apparent, $\alpha_x = \alpha_y = \alpha_{xy} = 0$, and the initial value of f is $f^0 = 1$. When there is a significant presence of anisotropy in the as-received material at initial yielding, the initial values for α_x, α_y, and α_{xy} are not zero. In this situation, it is then desirable to fit (10.53) to the experimental yield surface through an optimization procedure. In this way, it is possible to determine the values of coefficients (F, G, H, and N), and the initial back stress components.

Using (10.53) and the normality rule, the flow rule is

$$\begin{aligned} D_x^p &= \dot{\lambda}[(G+H)\xi_x - H\xi_y] \\ D_y^p &= \dot{\lambda}[-H\xi_x + (H+F)\xi_y] \\ D_{xy}^p &= \dot{\lambda}N\xi_{xy} \end{aligned} \tag{10.54}$$

where the components of the *effective stress vector* are

$$\xi_x = \sigma_x - \alpha_x, \qquad \xi_y = \sigma_y - \alpha_y, \qquad \xi_{xy} = \sigma_{xy} - \alpha_{xy} \tag{10.55}$$

The "effective stress vector" is defined by (10.55) and this definition has been used by other authors, such as Cho and Dafalias [35]. It should not be confused with the *equivalent stress* defined in (10.19), which is sometimes referred to as the "effective stress" in the plasticity literature. The flow rule (10.54) may be applied to calculate the rate of plastic deformation. Note that $\dot{\lambda}$ is the

plastic multiplier which is a positive scalar that may vary during the straining process, and D_x^{p}, D_y^{p}, and D_{xy}^{p} are the plastic parts of the rate of deformation, such that

$$D_x = D_x^{\mathrm{e}} + D_x^{\mathrm{p}}, \qquad D_y = D_y^{\mathrm{e}} + D_y^{\mathrm{p}}, \qquad D_{xy} = D_{xy}^{\mathrm{e}} + D_{xy}^{\mathrm{p}} \tag{10.56}$$

In the case of uniaxial tension test using a specimen cut out from a metal sheet at an orientation angle θ, measured counterclockwise from the rolling direction, the stress components are given by (10.4) and written as

$$\sigma_x = \sigma_\theta \cos^2\theta, \qquad \sigma_{\mathrm{y}} = \sigma_\theta \sin^2\theta, \qquad \sigma_{xy} = \sigma_\theta \sin\theta\cos\theta \tag{10.57}$$

where σ_θ is the stress along the axial direction x' of the specimen. Let y' be along the width direction of the specimen, the x'–y'–z' axes thus form a rectangular specimen coordinate system with x' and y' lying in the x–y plane and $z' = z$. In this case, the rate of deformation in the specimen coordinate system is

$$\begin{aligned} D_{x'} &= D_x \cos^2\theta + D_y \sin^2\theta + 2D_{xy}\sin\theta\cos\theta \\ D_{y'} &= D_x \sin^2\theta + D_y \cos^2\theta - 2D_{xy}\sin\theta\cos\theta \\ D_{xy'} &= -\tfrac{1}{2}(D_x - D_y)\sin(2\theta) + D_{xy}\cos(2\theta) \end{aligned} \tag{10.58}$$

and the corresponding plastic parts are related by

$$\begin{aligned} D_{x'}^{\mathrm{p}} &= D_x^{\mathrm{p}} \cos^2\theta + D_y^{\mathrm{p}} \sin^2\theta + 2D_{xy}^{\mathrm{p}}\sin\theta\cos\theta \\ D_{y'}^{\mathrm{p}} &= D_x^{\mathrm{p}} \sin^2\theta + D_y^{\mathrm{p}} \cos^2\theta - 2D_{xy}^{\mathrm{p}}\sin\theta\cos\theta \\ D_{xy'}^{\mathrm{p}} &= -\tfrac{1}{2}(D_x^{\mathrm{p}} - D_y^{\mathrm{p}})\sin(2\theta) + D_{xy}^{\mathrm{p}}\cos(2\theta) \end{aligned} \tag{10.59}$$

The equivalent stress, $\bar{\sigma}$, is similarly defined as in (10.19), but it includes the effect of kinematic hardening:

$$\bar{\sigma} = \left[\frac{(G+H)\xi_x^2 - 2H\xi_x\xi_y + (H+F)\xi_y^2 + 2N\xi_{xy}^2}{K}\right]^{1/2} \tag{10.60}$$

Combining (10.53) and (10.60), the equivalent stress can also be expressed by

$$\bar{\sigma} = \frac{f}{\sqrt{K}} \tag{10.61}$$

The equivalent plastic strain rate, $\bar{D}^{\mathrm{p}}$, is defined so that the rate of plastic work per unit volume is

$$\dot{W}^{\mathrm{p}} = \bar{\sigma}\bar{D}^{\mathrm{p}} \tag{10.62}$$

To obtain the expression for $\bar{D}^{\mathrm{p}}$, the rate of plastic work is first written as

$$\dot{W}^{\mathrm{p}} = (\sigma_{ij} - \alpha_{ij}) D_{ij}^{\mathrm{p}} = (\sigma_{ij} - \alpha_{ij}) \frac{\partial \phi}{\partial \sigma_{ij}} \dot{\lambda} \tag{10.63}$$

Upon the differentiation of the yield function, 2ϕ, with respect to the stress components and with the appropriate substitutions, (10.63) then reduces to

$$\dot{W}^{\mathrm{p}} = f^2 \dot{\lambda} = 2\phi \dot{\lambda} \tag{10.64}$$

Using (10.64) and (10.53), it can then be shown that (10.62) is satisfied if $\bar{D}^{\mathrm{p}}$ is given by the following expression:

$$\bar{D}^{\mathrm{p}} = \sqrt{\frac{K}{M}} \left\{ (F+H)\left(D_x^{\mathrm{p}}\right)^2 + 2HD_x^{\mathrm{p}} D_y^{\mathrm{p}} + (G+H)\left(D_y^{\mathrm{p}}\right)^2 + \frac{2M}{N}\left(D_{xy}^{\mathrm{p}}\right)^2 \right\}^{1/2} \tag{10.65}$$

where

$$M = (G+H)(H+F) - H^2 \tag{10.66}$$

It can also be found that

$$\dot{\lambda} = \frac{\bar{D}^{\mathrm{p}}}{f\sqrt{K}} \tag{10.67}$$

In this model, a combined isotropic–kinematic hardening is considered. The evolution of isotropic hardening is accomplished by the evolution of the isotropic function f and that of kinematic hardening through the evolution of the back stress $(\alpha_x, \alpha_y, \alpha_{xy})$. In the isotropic hardening, the effective plastic strain rate, $\bar{D}^{\mathrm{p}}$, is directly related to a monotonic increasing parameter (or it can be regarded as an intrinsic time as in the endochronic theory discussed in Chapter 8) ζ such that

$$\dot{\zeta} = \bar{D}^{\mathrm{p}} \tag{10.68}$$

where ζ represents the accumulated effective plastic strain. Following (6.62), the isotropic hardening is given by

$$f = f\left(\int \bar{D}^{\mathrm{p}}\,\mathrm{d}t\right) = f(\zeta) \tag{10.69}$$

which may be further expressed by a modified exponential function proposed by Wu and Yip [36] in (8.110) as

$$f(\zeta) = D_\theta - (D_\theta - 1)\mathrm{e}^{-\beta_\theta \zeta} \tag{10.70}$$

Note that D_θ and β_θ are material constants with values depending on the angle θ, that is, the isotropic hardening is direction dependent. The parameter D_θ, where $D_\theta \geq 1$, represents the asymptotic amount of isotropic hardening as $\zeta \to \infty$, while β_θ represents the rate of hardening. In addition, it is noted that $f(\zeta) = 1$ for a material without isotropic hardening. In the case of loading, (10.70) may be differentiated with D_θ and β_θ remaining constant for each specified direction, and, using (10.67) the following expression may be obtained:

$$\dot{f} = \sqrt{K}\beta_\theta(D_\theta - f)f\dot{\lambda} \tag{10.71}$$

Prager's linear kinematic-hardening rule [37] is used according to which the rate of translation of the center of the yield surface is in the direction of the plastic strain rate. Consequently, the deviatoric part of back stress rates are:

$$\begin{aligned}
\dot{\alpha}_x^{\mathrm{D}} &= CD_x^{\mathrm{p}} = C\dot{\lambda}[(G+H)\xi_x - H\xi_y] \\
\dot{\alpha}_y^{\mathrm{D}} &= CD_y^{\mathrm{p}} = C\dot{\lambda}[-H\xi_x + (H+F)\xi_y] \\
\dot{\alpha}_{xy}^{\mathrm{D}} &= CD_{xy}^{\mathrm{p}} = C\dot{\lambda}N\xi_{xy}
\end{aligned} \tag{10.72}$$

and

$$\dot{\alpha}_x^{\mathrm{D}} + \dot{\alpha}_y^{\mathrm{D}} + \dot{\alpha}_z^{\mathrm{D}} = 0 \tag{10.73}$$

Knowing that $\dot{\alpha}_z = 0$ for plane stress, it may be shown that

$$\dot{\alpha}_x = 2\dot{\alpha}_x^{\mathrm{D}} + \dot{\alpha}_y^{\mathrm{D}} \quad \text{and} \quad \dot{\alpha}_y = \dot{\alpha}_x^{\mathrm{D}} + 2\dot{\alpha}_y^{\mathrm{D}} \tag{10.74}$$

The scalar parameter C characterizes the material behavior. In this study, C is considered a constant, which leads to a linear-kinematic strain hardening.

The plastic strain ratio, R_θ, for a tension specimen cut at an angle θ from the rolling direction, is defined by

$$R_\theta = \frac{D^{\mathrm{p}}_{y'}}{D^{\mathrm{p}}_{z'}} = -\left(\frac{D^{\mathrm{p}}_{y'}}{D^{\mathrm{p}}_{x'} + D^{\mathrm{p}}_{y'}}\right) \tag{10.75}$$

where the plastic incompressibility of the material is assumed. Using of (10.59), (10.75) is reduced to

$$\begin{aligned} R_\theta = &-\frac{[(G+H)(\sigma_\theta \cos^2\theta - \alpha_x) - H(\sigma_\theta \sin^2\theta - \alpha_y)]\sin^2\theta}{[G(\sigma_\theta \cos^2\theta - \alpha_x) + F(\sigma_\theta \sin^2\theta - \alpha_y)]} \\ &+ \frac{[(H+F)(\sigma_\theta \sin^2\theta - \alpha_y) - H(\sigma_\theta \cos^2\theta - \alpha_x)]\cos^2\theta}{[G(\sigma_\theta \cos^2\theta - \alpha_x) + F(\sigma_\theta \sin^2\theta - \alpha_y)]} \\ &- \frac{2N(\sigma_\theta \sin\theta\cos\theta - \alpha_{xy})\sin\theta\cos\theta}{[G(\sigma_\theta \cos^2\theta - \alpha_x) + F(\sigma_\theta \sin^2\theta - \alpha_y)]} \end{aligned} \tag{10.76}$$

Note that the isotropic-hardening function, f, does not appear in (10.76), but the back stress components do. Therefore, the R-ratio is significantly influenced by kinematic hardening. From this equation, the following expressions can be found

$$\begin{aligned} R_0 &= \frac{\sigma_0 H - H\alpha_x + (H+F)\alpha_y}{\sigma_0 G - G\alpha_x - F\alpha_y} \\ R_{45} &= \frac{1}{2}\left[\frac{2N(\sigma_{45} - 2\alpha_{xy})}{\sigma_{45}(G+F) - 2G\alpha_x - 2F\alpha_y} - 1\right] \\ R_{90} &= \frac{\sigma_{90} H + (G+H)\alpha_x - H\alpha_y}{\sigma_{90} F - G\alpha_x - F\alpha_y} \end{aligned} \tag{10.77}$$

where σ_0, σ_{45}, σ_{90}, R_0, R_{45}, and R_{90} represent the yield stress and plastic strain ratio at orientations 0°, 45°, and 90° from the rolling direction, respectively. In the case of $\alpha_x = \alpha_y = \alpha_{xy} = 0$, (10.77) reduces to Hill's 1948 definition of plastic strain ratios given by (10.16) and (10.17).

For a given direction θ, the yield stress σ_θ may be found by the substitution of (10.57) into (10.53). The resulting equation is as follows:

$$\begin{aligned} &\sigma_\theta^2[(G+H)\cos^4\theta - 2H\cos^2\theta\sin^2\theta + (F+H)\sin^4\theta + 2N\sin^2\theta\cos^2\theta] \\ &\quad + \sigma_\theta\big[-2(G+H)\alpha_x\cos^2\theta + 2H(\alpha_x\sin^2\theta + \alpha_y\cos^2\theta) \\ &\quad - 2(H+F)\alpha_y\sin^2\theta - 4N\alpha_{xy}\sin\theta\cos\theta\big] \\ &\quad + (G+H)\alpha_x^2 - 2H\alpha_x\alpha_y + (H+F)\alpha_y^2 + 2N\alpha_{xy}^2 - f^2 = 0 \end{aligned} \tag{10.78}$$

10.6.3 Results and Discussion

It is shown in this section that the theory of the previous section is capable of predicting experimentally observed data for sheet metals. In particular, tension test of specimens cut at different θ angles measured from the rolling direction is of interest. The theoretical results are compared with two sets of experimental data for different aluminum materials. The return-mapping algorithm, of Simo and Hughes [38], is used in the computation to ensure that the updated stress point is on the current yield surface. The procedure is as follows:

1. Input time increment $\mathrm{d}t$ and angle θ to determine the initial yield stress σ_θ and the initial yield strain using (10.51), (10.57), and (10.78).
2. Use the return-mapping algorithm to determine the increment $\mathrm{d}\lambda$, so that the plastic part of rate of deformation and the plastic strain-ratio R may be found from (10.54), (10.58), and (10.75).
3. Update $\sigma_\theta, f, \alpha_x, \alpha_y$, and α_{xy} using (10.71)–(10.74) and the following equations of return-mapping algorithm:

$$\begin{aligned} &\text{Trial stress} = \sigma^{\mathrm{T}}_{\theta(n+1)} = \sigma_{\theta(n)} + E D_{x'(n)}\,\mathrm{d}t \\ &\sigma_{\theta(n+1)} = \sigma^{\mathrm{T}}_{\theta(n+1)} - E D^{\mathrm{p}}_{x'(n)}\,\mathrm{d}t \end{aligned} \tag{10.79}$$

The first example is related to the experimental data of Lademo et al. [31]. These authors tested two aluminum materials in uniaxial tension. Only AA7108-T1 is being considered here, and the other material can be similarly considered. The present writer agrees with Lademo et al. [31] that the uniaxial tension test is a desirable test to use for the calibration of a material model. At the present stage of knowledge, however, the tension test does not provide all the needed information. It does not, for example, provide information about the initial back stress, which is needed in the present model. Due to the thinness of the sheet material, a compression test is not practical. Therefore, more research needs to be conducted to determine the initial back stress components $(\alpha_x, \alpha_y, \alpha_{xy})$ which are present due to material processing.

The experimental data have been reproduced from table 2 of Lademo et al. [31]. Only specimen #1 for each θ angle is considered. The equation to reproduce the experimental stress–strain curve is

$$\bar{Y} = Y + \sum_k Q_k(1 - \exp(-C_k \bar{\varepsilon}^{\mathrm{p}})) \tag{10.80}$$

which was given in Lademo et al. [31]; $\bar{Y}$ is the flow stress; Y is the yield stress; $\bar{\varepsilon}^{\mathrm{p}}$ is the plastic strain; and Q_k and C_k are material parameters given in Table 2 of Lademo et al. [31]. It is to be noted that, in most cases, three exponential terms of (10.80) were used, and this equation reproduces the experimental data very well.

In the present computation by use of the proposed theory, only one exponential term with two parameters D_θ and β_θ for each loading direction is used in the isotropic-hardening function, (10.70), and one material parameter C is used in the kinematic-hardening rule, (10.72). The idea is to keep the number of parameters at its minimum so that the model can be used to predict material behavior under various loading conditions. Based on the experimental data, the variations of D_θ and β_θ as a function of θ have been determined. If more terms are used in equations (10.70) and (10.72), better agreement with the experimental results in discussion can be attained but, at the same time, the parameters need to be adjusted case by case as in Lademo et al. [31] and the model will lose its power of prediction.

From table 2 of Lademo et al. [31], we see that the elastic modulus E and Poisson's ratio vary slightly from one θ angle to the other. For simplicity, the average values of $E = 66,586$ MPa and $\nu = 0.345$ are used throughout the computation. The following constants have been used in this computation: $F = 4.919 \times 10^{-6}$ (MPa)$^{-2}$, $G = 8.862 \times 10^{-6}$ (MPa)$^{-2}$, $H = 5.309 \times 10^{-6}$ (MPa)$^{-2}$, $N = 0.000035$ (MPa)$^{-2}$, $D_\theta = 2.4$ for all θ's, $C = 300$ MPa, and β_θ varies as a function of θ as

$$\beta_\theta = -8.5046\,\theta^4 + 29.405\,\theta^3 - 32.789\,\theta^2 + 11.797\,\theta + 0.6 \tag{10.81}$$

This functional relation has been found by use of experimental data for the cases of $\theta = 0°$, $35°$, $45°$, $55°$, and $90°$. An improved relation would have been obtained if Lademo et al. [31] had reported data for $15°$ and $75°$. The author has tried to express (10.81) by simple mathematical expressions without success. The initial back stress has been determined to be $\alpha_x^\circ = 11$ MPa, $\alpha_y^\circ = -44$ MPa, and $\alpha_{xy}^\circ = 0$. Constants (F, G, H, N) and back stress ($\alpha_x^\circ, \alpha_y^\circ, \alpha_{xy}^\circ$) have been determined to fit the experimental data for all measured σ_θ, that is $\sigma_0, \sigma_{35}, \sigma_{45}, \sigma_{55}$, and σ_{90} and to satisfy the constraint imposed by (10.78).

The theoretical stress–strain curves (the solid curves) are compared with the experimental data of Lademo et al. [31] (the dotted curves) in Figure 10.5. Only the cases of $\theta = 0°$, $45°$, and $90°$ are shown. Curves for $\theta = 35°$ and $55°$ have also been obtained with a similar degree of agreement with the experimental data.

Figure 10.6 shows the flow stress plotted against θ at the initial yielding and at constant strain levels of 0.01, 0.02, 0.03, 0.1, and 0.14. Both theoretical curves and experimental data are shown. The theoretical curves show maxima occurring at about $15°$ and $75°$, but no experimental data in these regions have been reported by Lademo et al. [31]. Figure 10.7 shows the R-ratio plotted against θ. The experimental R-ratio was determined by applying linear regression to the plastic width strain versus thickness strain curve for each θ, which did not deviate much from a straight line. The R-ratio has only changed slightly as strain increases for this material. Two theoretical curves are shown: one for initial yielding and the other for strain at 0.14. Although there is a general

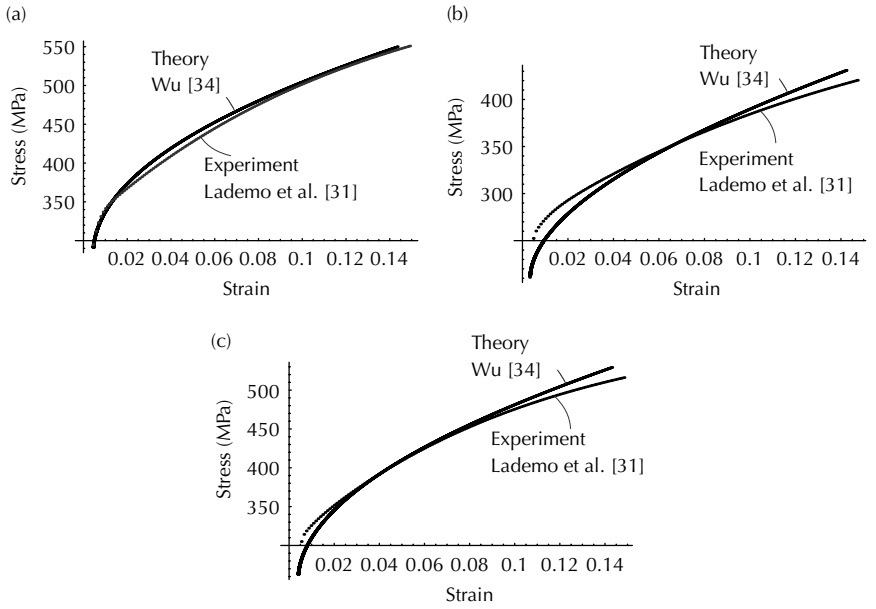

FIGURE 10.5
Tensile stress–strain curves for AA7108-T1 aluminum: (a) $\theta = 0°$, (b) $\theta = 45°$, and (c) $\theta = 90°$ (From Wu, H.C., *Int. J. Plasticity*, 18, 1661, 2002. With permission from Elsevier).

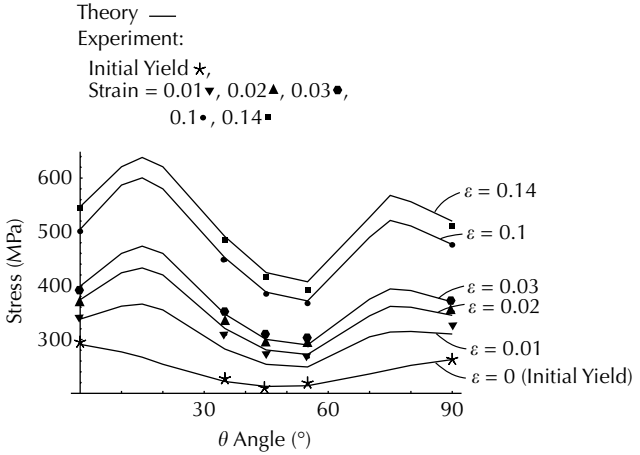

FIGURE 10.6
Flow stress versus θ for AA7108-T1 aluminum at constant strain levels of initial yielding, 1, 2, 3, 10, and 14% (From Wu, H.C., *Int. J. Plasticity*, 18, 1661, 2002. With permission from Elsevier).

agreement between theory and experiment, the poor agreement for $\theta = 90°$ cannot be explained.

Figure 10.8 shows the stress paths for tension tests for all θ angles as the longitudinal strain of the specimen increases. All are linear paths going from

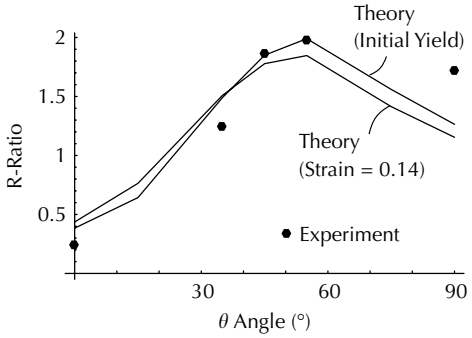

FIGURE 10.7
R-ratio versus θ for AA7108-T1 aluminum at initial yielding and 14% strain (From Wu, H.C., *Int. J. Plasticity*, 18, 1661, 2002. With permission from Elsevier).

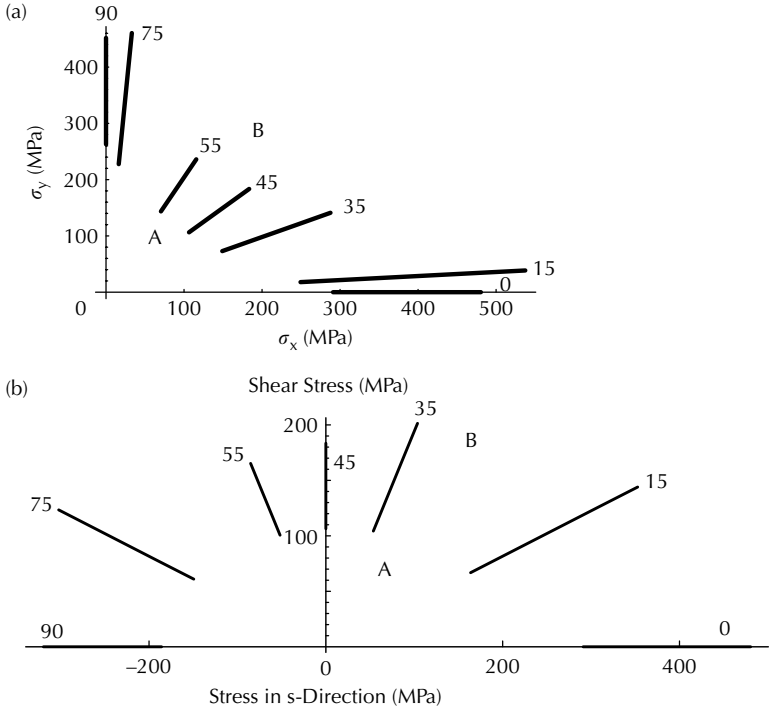

FIGURE 10.8
Stress paths for tension tests of AA7108-T1 aluminum with θ shown: (a) plane view, (b) elevation view (From Wu, H.C., *Int. J. Plasticity*, 18, 1661, 2002. With permission from Elsevier).

A to B, where B is the far end of each path. These paths do not stay in the (σ_x, σ_y) plane except for the cases of $\theta = 0°$ and 90°, but they are linear paths defined by (10.57). Both the plane view (Figure 10.8(a)) and the elevation view (Figure 10.8(b)) are shown. As it was mentioned earlier, the plane view

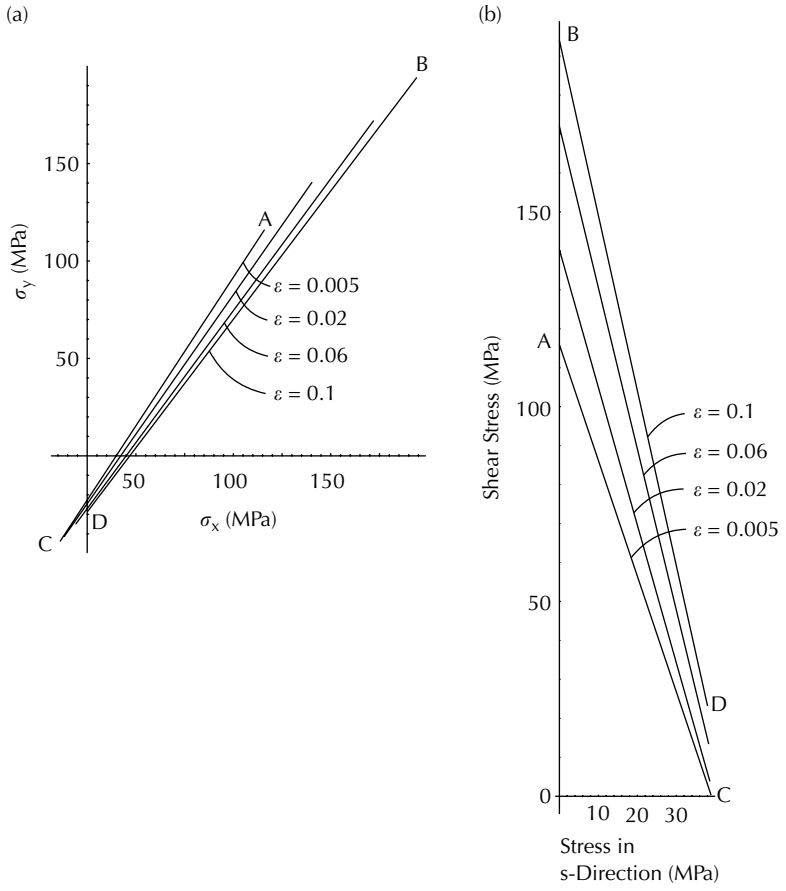

FIGURE 10.9
Direction of effective stress vector for tension test of AA7108-T1 aluminum at $\theta = 45°$: (a) plane view, (b) elevation view (From Wu, H.C., *Int. J. Plasticity*, 18, 1661, 2002. With permission from Elsevier).

is the projection of a three-dimensional figure onto the (σ_x, σ_y) plane; while the elevation view is the projection of the same figure onto a plane which passes through the σ_{xy} axis and the s-direction. The number marked at the far end of each path corresponds to the θ angle for that path. The corresponding back-stress-paths may be drawn and they are generally nonlinear paths. But, they are not shown due to the smallness of these paths.

Finally, Figure 10.9 shows the gradual change in direction of the "effective stress vector" for the case of $\theta = 45°$. Similar figures may be drawn for other θ angles. Figure 10.9(a) shows the plane view and Figure 10.9(b) the elevation view. The effective stress vector is the quantity (ξ_x, ξ_y, ξ_{xy}) defined by (10.55); it is represented by the vector from C to A when the axial strain is 0.005, and by the vector from D to B when the axial strain is 0.1. It is seen from the

figures that this vector changes direction as the axial strain increases. When this vector changes direction, the corresponding stress point moves along the yield surface, resulting in the change of direction of the corresponding plastic strain-rate vector.

In the conventional approach, the isotropic hardening fixes the shape of the yield surface and also the direction of the plastic strain increment (associated flow rule) as the load increases, leading to a poor description of the anisotropic flow properties. Lademo et al. [31] pointed out that the anisotropic flow properties may be better described by use of a nonassociated flow rule. In the theory of Wu [34], reasonable results are obtained by use of associated flow rule together with the concept of kinematic hardening. As shown in Figure 10.9, the direction of the plastic strain increment changes as the loading increases, and it is not necessary to use a nonassociated flow rule as suggested by Lademo et al. [31].

The second example is related to a set of uniaxial tension experiments conducted in the writer's laboratory by Y.P. Shiao and M. Loureiro. The experimental results are reported in Shiao [39]. The material was a 6061-O aluminum sheet tested at the as-received condition. Tension specimens were cut at 0°, 15°, 30°, 45°, 60°, 75°, and 90° from the rolling direction. Three samples were tested for each case. Postyield strain gauges, one along the axial direction and one along the width direction of the specimen, were used to measure strains for each specimen.

The theory of the previous section is used to model the tests. The same procedures as in the first example are followed in the determination of constants and in the computation. The following constants are used in the calculation: $E = 70$ GPa, $\nu = 0.33$, $F = 0.975 \times 10^{-4}$ (MPa)$^{-2}$, $G = 1.2546 \times 10^{-4}$ (MPa)$^{-2}$, $H = 1.0474 \times 10^{-4}$ (MPa)$^{-2}$, $N = 2.6611 \times 10^{-4}$ (MPa)$^{-2}$, $C = 0.2$ MPa, $\beta_\theta = 2.7$ for all θ's, and D_θ which is given by

$$D_\theta = D_0 \left(\frac{\sigma_0}{\sigma_\theta} \right)^m \tag{10.82}$$

where $D_0 = 2.9$ is the value of D_θ at $\theta = 0°$ and $m = 0.5$. Note that σ_θ are initial yield stresses and are known for each θ. In effect, (10.82) is expressing D_θ as a function of θ. The initial back stress has been determined to be $\alpha_x^0 = -20.8$ MPa, $\alpha_y^0 = -13$ MPa, and $\alpha_{xy}^0 = 0$.

The theoretical stress–strain curves (the solid curves) are now compared with the experimental data (the dotted curves). Only the case of $\theta = 0°$ is shown in Figure 10.10. The stress–strain diagrams indicate only a small influence of anisotropy for this material, eventhough a significant anisotropy is found in the initial yield stress and R-ratio, which will be further discussed. Figure 10.11 shows the calculated width strain plotted against the axial strain for the case of $\theta = 0°$. The dotted curve indicates the experimental data. The calculated R-ratios are plotted against the axial strains in Figure 10.12 for the cases of $\theta = 0°, 30°, 60°$, and $90°$, where the dots denote experimental data. Reasonable agreement between theory and experiment has been achieved.

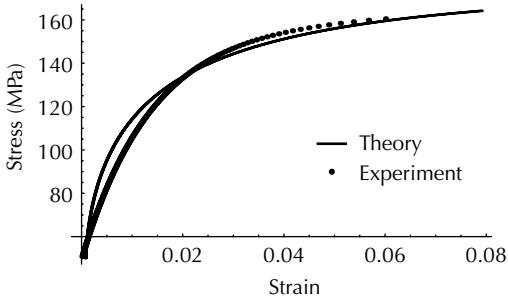

FIGURE 10.10
Tensile stress–strain curves for 6061-O aluminum, $\theta = 0°$ (From Wu, H.C., *Int. J. Plasticity*, 18, 1661, 2002. With permission from Elsevier).

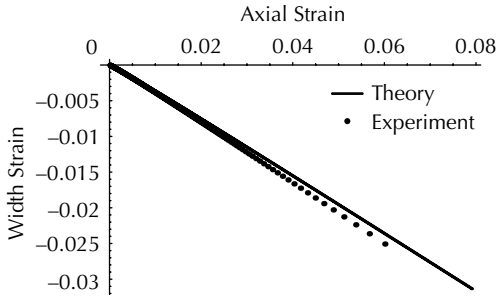

FIGURE 10.11
Width strain versus axial Strain for 6061-O aluminum, $\theta = 0°$ (From Wu, H.C., *Int. J. Plasticity*, 18, 1661, 2002. With permission from Elsevier).

Figure 10.13 shows the theoretical R-ratios plotted against θ at constant strain levels of 1, 2, 4, and 7%. No experimental data for larger strain levels have been obtained due to necking of the specimens. Figure 10.13 is constructed directly from Figure 10.12(a) to (d). No experimental data are shown in Figure 10.13 due to scatter, but a direct comparison between theory and experiment can be made in Figure 10.12. The initial yield stress is plotted against θ in Figure 10.14 with dots denoting again the experimental data.

10.6.4 Summary and Conclusion

A simple anisotropic theory of plasticity has been presented in this section. This theory uses Hill's 1948 quadratic yield criterion, the normality condition for the flow rule, and a combined isotropic–kinematic-hardening rule. This theory is, in fact, the same as that usually used in classical plasticity. The research presented in this section merely confirms that the flow theory of plasticity may be extended to the case of anisotropic sheet metals.

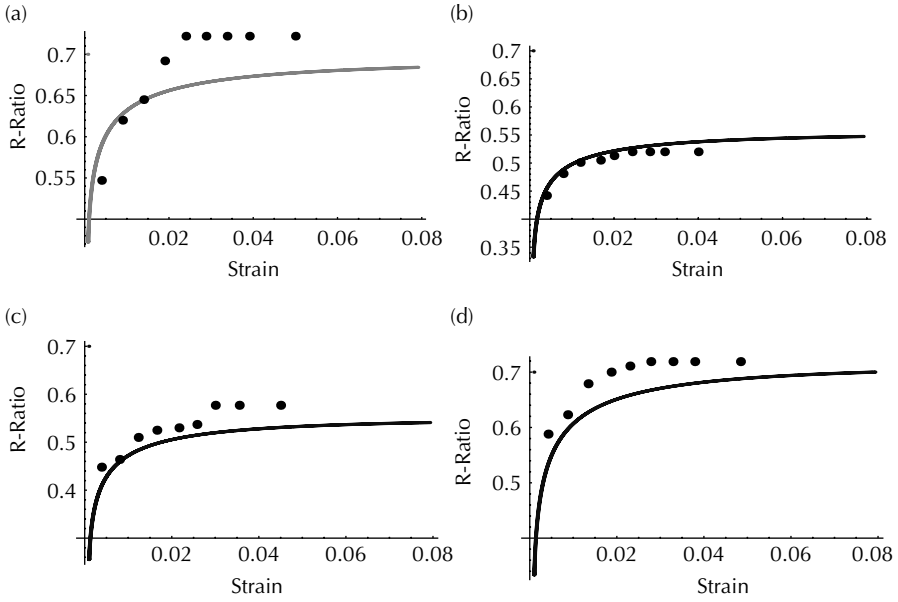

FIGURE 10.12
R-ratio for 6061-O aluminum: (a) $\theta = 0°$, (b) $\theta = 30°$, (c) $\theta = 60°$, and (d) $\theta = 90°$ (From Wu, H.C., *Int. J. Plasticity*, 18, 1661, 2002. With permission from Elsevier).

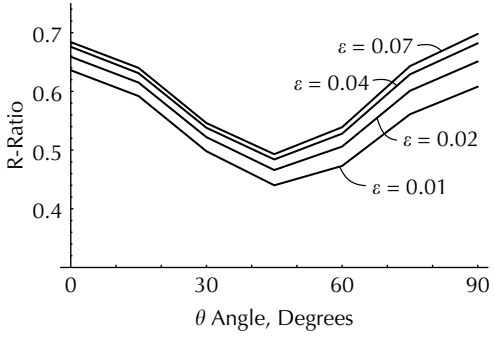

FIGURE 10.13
Theoretical *R*-ratio for 6061-O aluminum at constant strain levels of 1, 2, 4, and 7% (From Wu, H.C., *Int. J. Plasticity*, 18, 1661, 2002. With permission from Elsevier).

Although this is not surprising, the theory has not been previously verified against experimental data related to sheet metals. The results of this research indicate that the conventional nonquadratic yield functions are not necessary for sheet metals, and the proposed theory may be useful for analyses of sheet metal forming.

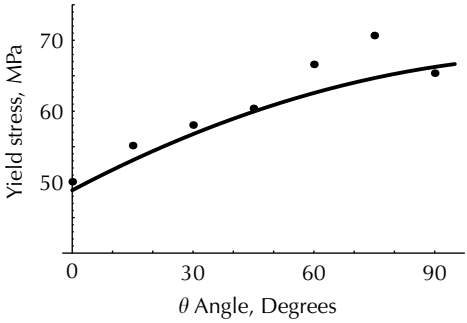

FIGURE 10.14
Initial yield stress versus θ or 6061-O Aluminum (From Wu, H.C., *Int. J. Plasticity*, 18, 1661, 2002. With permission from Elsevier).

In both examples considered, the present theory has achieved a general agreement with experimental results in both aspects of anisotropy (yield stress and R-ratio). The agreement is not perfect due to the simple expressions used to describe isotropic and kinematic hardening given by equations (10.70) and (10.72), and the fact that there are only two functions D_θ and β_θ and a parameter C in the equations. The agreement shown is very satisfactory, if one realizes that the experimental data of Lademo et al. [31] have been reproduced by (10.80) using three Q_k's and three C_k's for each θ to describe the axial stress–axial strain relation and an additional set of three Q_k's and three C_k's to describe the axial stress–width strain relation.

Anisotropy is two-fold in nature (yield stress and R-ratio) as previously mentioned. In the two examples considered, the materials are very different. They are different in the magnitude of yield stress and also in its variation with θ. They are also different in the magnitude of the R-ratio. In fact, the R-ratio for AA7108-T1varies from 0.3 at $\theta = 0°$ to 2.0 at $\theta = 55°$, while that for 6061-O aluminum remains less than 1.0 for all values of θs. In order to describe such a wide range of variations of material behavior, using the same constitutive equation, we find that the material functions are different for the two materials. For AA7108-T1, D_θ is taken as constant for all θs and β_θ varies with θ as in (10.81); for 6061-O aluminum, β_θ is taken as constant for all θs, but D_θ is made to vary with θ as in (10.82). The two variations are not the same due to different materials in the two examples.

The definitions of yield and their effect on the hardening rules of the sheet material have been discussed. It has been shown that strain hardening plays an important role in the determination of the R-ratios and yield stresses, which are obtained from uniaxial tension specimens, cut at θ angle measured from the rolling direction of the metal sheet. Furthermore, kinematic hardening makes it possible to have the directional change in the plastic strain rate without introducing the nonassociated flow rule into the formulation as suggested by Lademo et al. [31].

References

1. Annual Book of ASTM Standards, *Metal Test Methods and Analytical Procedures*, ASTM, West Conshohocken, PA, 3.01, 1996, 481.
2. Mellor, P.B., Experimental studies of plastic anisotropy in sheet metal, in *Mechanics of Solids*, Hopkins, H.G. and Sewell, M.J., Eds., Pergamon Press, Great Britain, 1982, 383.
3. Lin, S.B. and Ding, J.L., Experimental study of the plastic yielding of rolled sheet metals with the cruciform plate specimen, *Int. J. Plasticity*, 11, 583, 1995.
4. Szczepinski, W., On the effect of plastic deformation on yield condition, *Arch. Mech.*, 15, 275, 1963.
5. Lee, D. and Backofen, W.A., An experimental determination of the yield locus for titanium and titanium-alloy sheet, *Trans. Met. Soc., AIME*, 236, 1077, 1966.
6. Lege, D.J., Barlat, F., and Brem, J.C., Characterization and modeling of the mechanical behavior and formability of a 2008-T4 sheet sample, *Int. J. Mech. Sci.*, 31, 549, 1989.
7. Naruse, K., Dodd, B., and Motoki, Y., Evaluation of yield criteria for planar anisotropy in sheet metals using experimental results, in *Advances in Engineering Plasticity and Its Applications, Proceedings of the Asia-Pacific Symposium on Advances in Engineering Plasticity and Its Applications – AEPA92, Hong Kong*, Lee, W.B., Ed., 1993, 235.
8. Kreissig, R. and Schindler, J., Some experimental results on yield condition in plane stress state, *Acta Mech.*, 65, 169, 1986.
9. Tozawa, Y., Plastic deformation behavior under conditions of combined stress, in *Mechanics of Sheet Metal Forming*, Koistinem, D.P. and Wang, N.M., Eds., Plenum, New York, 1978, 81.
10. Barlat, F., Becker, R.C., Hayashida, Y., Maeda, Y., Yanagawa, M., Chung, K., Brem, J.C., Lege, D.J., Matsui, K., Murtha, S.J., and Hattori, S., Yielding description for solution strengthened aluminum alloys, *Int. J. Plasticity*, 13, 385, 1997.
11. Hill, R., A theory of yielding and plastic flow of anisotropic metals, *Proc. Roy. Soc. London*, A193, 281, 1948.
12. Hill, R., *The Mathematical Theory of Plasticity*, Clarendon Press, Oxford, 1950, 317.
13. Makinde, A., Thibodeau, L., and Neale, K.W., Development of an apparatus for biaxial testing using cruciform specimens, *Exp. Mech.*, 32, 138, 1992.
14. Pearce, R., Some aspects of anisotropic plasticity in sheet metals, *Int. J. Mech. Sci.*, 10, 995, 1968.
15. Woodthorpe, J. and Pearce, R., The anomalous behavior of aluminum sheet under balanced biaxial tension, *Int. J. Mech. Sci.*, 12, 341, 1970.
16. Hill, R., Theoretical plasticity of textured aggregates, *Proc. Camb. Phil. Soc.*, 85, 179, 1979.
17. Hill, R., Constitutive modeling of orthotropic plasticity in sheet metal, *J. Mech. Phys. Solids*, 38, 405, 1990.
18. Hosford, W.F., On yield loci of anisotropic cubic metals, *7th North Am. Metalworking Conf.*, SME, Dearborn, MI, 1979, 191.
19. Gotoh, M., A theory of plastic anisotropy based on a yield function of fourth order, *Int. J. Mech. Sci.*, 19, 505, 1977.

20. Barlat, F. and Lian, J., Plastic behavior and stretchability of sheet metals. Part I, A yield function for orthotropic sheet under plane stress conditions, *Int. J. Plasticity*, 5, 5, 1989.
21. Hill, R., A user-friendly theory of orthotropic plasticity in sheet metals, *Int. J. Mech. Sci.*, 35, 19, 1993.
22. Hill, R., Hecker, S.S., and Stout, M.G., An investigation of plastic flow and differential work hardening in orthotropic brass tubes under fluid pressure and axial load, *Int. J. Solids Struct.*, 31, 2999, 1994.
23. Barlat, F., Lege, D.J., and Brem, J.C., A six-component yield function for anisotropic materials, *Int. J. Plasticity*, 7, 693, 1991.
24. Karafillis, A.P. and Boyce, M.C., A general anisotropic yield criterion using bounds and a transformation weighting tensor, *J. Mech. Phys. Solids*, 41, 1859, 1993.
25. Cao, J., Yao, H., Karafillis, A.P., and Boyce, M.C., Prediction of localized thinning in sheet metal using a general anisotropic yield criterion, *Int. J. Plasticity*, 16, 1105, 2000.
26. Yoon, J.W., Barlat, F., Chung, K., Pourboghrat, F., and Yang, D.Y., Earing predictions based on asymmetric nonquadratic yield function, *Int. J. Plasticity*, 16, 1075, 2000.
27. Chakrabarty, J., A new yield function for planar anisotropy in sheet metal, *Ad. Mater. Process. Technol.*, City University, Dublin, 1993.
28. Taylor, G.I., Plastic strain in metals, *J. Inst. Metals*, 62, 307, 1938.
29. Bishop, J.W.F. and Hill, R., A theoretical derivation of the plastic properties of a polycrystalline face-centered metal, *Phil. Mag.* 42, 414, and 1298, 1951.
30. Barlat, F. and Richmond, O., Prediction of tricomponent plane stress yield surfaces, associated flow and failure behavior of strongly textured f.c.c. polycrystalline sheets, *Mat. Sci. Eng.*, 95, 15, 1987.
31. Lademo, O.-G., Hopperstad, O.S., and Langseth, M., An evaluation of yield criteria and flow rules for aluminum alloys, *Int. J. Plasticity*, 15, 191, 1999.
32. Wu, H.C., Hong, H.K., and Shiao, Y.P., Anisotropic plasticity with application to sheet metals, *Int. J. Mech. Sci.*, 41, 703, 1999 (Some of the discussions given in Sections 10.4 and 10.5 were from this paper. It is included with permission from Elsevier).
33. Wu, H.C. and Loureiro, M., An anisotropic plasticity for sheet metals, in *The Integration of Material, Process and Product Design*, Zabaras, N., Becker, R., Ghosh, S., and Lalli, L., Eds., A.A. Balkema, Rotterdam, 1999, 93.
34. Wu, H.C., Anisotropic plasticity for sheet metals using the concept of combined isotropic–kinematic hardening, *Int. J. Plasticity*, 18, 1661, 2002.
35. Cho, H.W. and Dafalias, Y.F., Distortional and orientational hardening at large viscoplastic deformations, *Int. J. Plasticity*, 12, 903, 1996.
36. Wu, H.C. and Yip, M.C., Endochronic description of cyclic hardening behavior for metallic materials, *J. Eng. Mat. Technol.*, 103, 212, 1981.
37. Prager, W., The theory of plasticity: a survey of recent achievements (James Clayton Lecture), *Proc. Inst. Mech. Eng.*, 169, 41, 1955.
38. Simo, J.C. and Hughes, T.J.R., *Computational Inelasticity*, Springer-Verlag, New York, 1998.
39. Shiao, Y.P., *A study on multiaxial cyclic loading and anisotropic plasticity of structural metals*, Ph.D. thesis, National Taiwan University, Taiwan, 2000.

Problems

(1) In the stamping operation of sheet metals, circles of 6.35 mm (0.25 in.) are printed on the sheet prior to the operation. After the stamping, the circles are changed into ellipses. Focusing on the deformation of one circle, if the major and minor axes of the ellipse are 8.26 and 6.99 mm, respectively, determine the equivalent strain $\bar{\varepsilon}$.

(2) For tension specimen cut at θ angle, if the longitudinal stress σ_{l} versus longitudinal strain ε_{l} and width strain ε_{w} curves are experimentally recorded, determine the expressions for $d\varepsilon_{\mathrm{l}}^{\mathrm{p}}$ and $d\varepsilon_{\mathrm{w}}^{\mathrm{p}}$. Determine also the $\varepsilon_{\mathrm{w}}^{\mathrm{p}}$ versus σ_{l} relation.

(3) Referring to Problem (2), determine the difference between R-ratio defined by $R = d\varepsilon_{\mathrm{w}}^{\mathrm{p}}/d\varepsilon_{\mathrm{t}}^{\mathrm{p}}$ and $R = \varepsilon_{\mathrm{w}}^{\mathrm{p}}/\varepsilon_{\mathrm{t}}^{\mathrm{p}}$, where $\varepsilon_{\mathrm{t}}^{\mathrm{p}}$ is the thickness strain.

(4) Referring to (10.5), show that in the case of rotational symmetry about the z-axis, we obtain $F = G$, $N = F + 2H$, and $L = M$.

(5) Referring to (10.5), show that in the case of material isotropy, we have $L = M = N = 3F = 3G = 3H$.

(6) Show that (10.28) and (10.65) are the same.

11

Description of Anisotropic Material Behavior Using Curvilinear Coordinates

11.1 Convected Coordinate System and Convected Material Element

The Cauchy stress, σ_{ij}, used in previous chapters is defined with respect to a square element fixed to a Cartesian coordinate system. Referring to Chapter 3, a material point P at the reference configuration in a continuous medium is deformed into p at the deformed configuration. At P, the square element is taken with reference to a Cartesian coordinate system defined at this configuration, and, at p, the square element is chosen with reference to a Cartesian coordinate system defined at the deformed configuration. The two square elements coincide if, for the sake of simplicity and without loss of generality, the two Cartesian coordinate systems coincide. Otherwise, they differ by a rigid-body rotation. The square element at the deformed configuration does not account for the change in size and distortion of the element, which occurs during deformation of the continuum. Therefore, by defining the Cauchy stress with respect to these squares, we do not follow the material element in our investigation of deformation and stress behavior of the material element.

A requirement supported by experimental findings is that constitutive equations describing plastic behavior of material depend on the deformation history of the material element. This dependence of the deformation history may be easily accounted for if a material element is being followed during the deformation process. Since the square element used to define the Cauchy stress is not the same as the deformed material element, the Cauchy stress is not an appropriate stress measure for nonprincipal stress states when the material is anisotropic.

In this chapter, we use *convected coordinates* to monitor the deformation history of a material element. The convected coordinates are also known as *imbedded coordinates*. If we draw an element with a marker on the surface of a continuum at the initial configuration, this element will assume a deformed shape at the deformed configuration as can be seen from the deformed marked element. Since the same material mass is contained

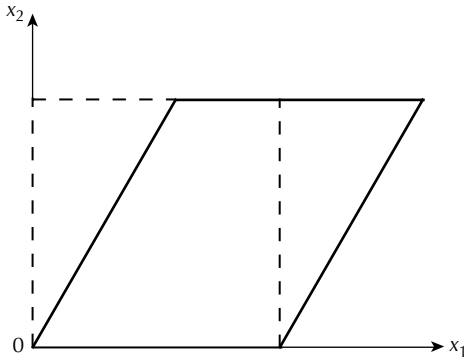

FIGURE 11.1
A convected material element due to simple shear.

within the marked element before and after deformation, the element will be referred to as a *convected material element*. In this way, a material element (with the same material mass) is being followed and the shape of the element changes during deformation. The convected coordinates are generally curvilinear coordinates.

Figure 11.1 shows a convected material element at the deformed configuration. When an initially rectangular material element is subjected to simple shear, for example, the element gets distorted and the deformed element is shown in this figure by the solid lines. The Cartesian square element is also shown by the dashed lines in the same figure. It is seen that the dashed element does not contain the original material mass.

We discuss the basic concepts related to curvilinear coordinate system and its tensor properties in Sections 11.2 to 11.6, and we discuss only topics of curvilinear coordinates that are needed to address the plastic deformation of an anisotropic continuum presented in the remaining part of this chapter. For further readings of the curvilinear coordinates, we refer to [1–5]. With this background information, we are then ready to discuss the plastic deformation behavior of a continuous medium using the convected coordinates. Readers who are familiar with the curvilinear coordinates may skip Sections 11.2 to 11.6 and start reading from Section 11.7.

11.2 Curvilinear Coordinates and Base Vectors

Referring to a right-handed Cartesian coordinate system, the position vector of a point P is $\mathbf{r}$, which can be expressed in terms of its components and base vectors as

$$\mathbf{r} = x_i \mathbf{e}_i \tag{11.1}$$

The base vectors for the Cartesian system are unit vectors denoted by $\mathbf{e}_i$. The increment of the position vector $\mathbf{r}$ is

$$\mathrm{d}\mathbf{r} = \frac{\partial \mathbf{r}}{\partial x_k}\mathrm{d}x_k = \mathrm{d}x_k \mathbf{e}_k \qquad \text{with } \mathbf{e}_k = \frac{\partial \mathbf{r}}{\partial x_k} \tag{11.2}$$

The length of the increment $\mathrm{d}\mathbf{r}$, denoted by $\mathrm{d}s$, is then given by

$$\mathrm{d}s^2 = \mathrm{d}\mathbf{r} \cdot \mathrm{d}\mathbf{r} = \mathrm{d}x_k \, \mathrm{d}x_k \tag{11.3}$$

The position vector of point P may also be expressed in terms of curvilinear coordinates. We now introduce general curvilinear coordinates θ^i by the transformation

$$\theta^i = \theta^i(x_j) \tag{11.4}$$

and assume that the transformation may be reversed so that

$$x_i = x_i(\theta^j) \tag{11.5}$$

with a nonzero Jacobian of the transformation, that is, $|\partial x_i / \partial \theta^j| \neq 0$. Thus, the coordinates of point P may either be expressed by (x_1, x_2, x_3) or $(\theta^1, \theta^2, \theta^3)$ in a three-dimensional Euclidean space. The coordinate curves are three curves as shown in Figure 11.2, and the coordinate surfaces are the surfaces passing through two of the coordinate curves with the third coordinate equal to zero.

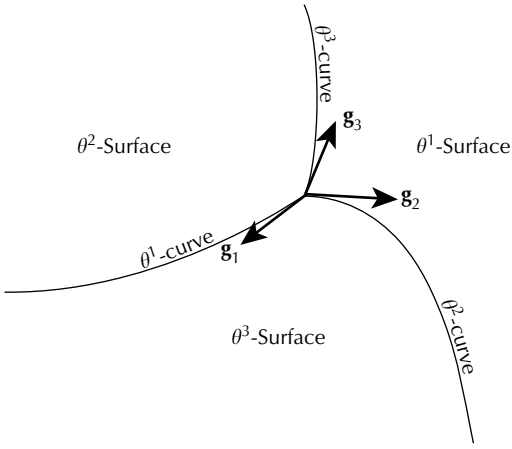

FIGURE 11.2
Coordinate curves and coordinate surfaces.

The increment of the position vector referred to the curvilinear coordinate system is now

$$\mathrm{d}\mathbf{r} = \frac{\partial \mathbf{r}}{\partial \theta^k}\mathbf{d}\theta^{\mathbf{k}} = \mathbf{d}\theta^{\mathbf{k}}\mathbf{g}_k \qquad (\text{but } \mathbf{r} \neq \theta^k \mathbf{g}_k) \tag{11.6}$$

where

$$\mathbf{g}_k = \frac{\partial \mathbf{r}}{\partial \theta^k} \tag{11.7}$$

are *covariant base vectors*. These are tangent to the coordinate curves as shown in Figure 11.2 and represent the rate of change of the position vector $\mathbf{r}$ with respect to the curvilinear coordinates θ^i. A relationship between the covariant base vectors and the Cartesian base vectors $\mathbf{e}_i$ may be found by writing

$$\mathrm{d}\mathbf{r} = \frac{\partial \mathbf{r}}{\partial x_i}\frac{\partial x_i}{\partial \theta^k}\mathrm{d}\theta^k = \mathrm{d}\theta^k \frac{\partial x_i}{\partial \theta^k}\mathbf{e}_i \tag{11.8}$$

Comparing (11.8) with (11.6), we see that

$$\mathbf{g}_k = \frac{\partial x_i}{\partial \theta^k}\mathbf{e}_i \quad \text{or} \quad \mathbf{e}_i = \frac{\partial \theta^k}{\partial x_i}\mathbf{g}_k \tag{11.9}$$

We note that (11.9) follows the *covariant rule of transformation*, and the vector $\mathbf{g}_k$ is a covariant vector. In the transformation between two coordinate systems θ^i and $\bar{\theta}^i$, where the variables are related by

$$\bar{\theta}^i = \bar{\theta}^i(\theta^1, \theta^2, \theta^3) \quad \text{and} \quad \theta^i = \theta^i(\bar{\theta}^1, \bar{\theta}^2, \bar{\theta}^3) \tag{11.10}$$

the components of a vector $\mathbf{u}$, denoted by $\tilde{u}_i$, obey the covariant transformation rule, if

$$\bar{\tilde{u}}_i = \frac{\partial \theta^j}{\partial \bar{\theta}^i}\tilde{u}_j \tag{11.11}$$

The components $\tilde{u}_i$ are called the *covariant components* of vector $\mathbf{u}$. The *contravariant components* $\tilde{u}^i$ of the same vector transform according to the *contravariant transformation rule* as

$$\bar{\tilde{u}}^i = \frac{\partial \bar{\theta}^i}{\partial \theta^j}\tilde{u}^j \tag{11.12}$$

The vector can then be represented by

$$\mathbf{u} = \tilde{u}^i \mathbf{g}_i = \tilde{u}_i \mathbf{g}^i \tag{11.13}$$

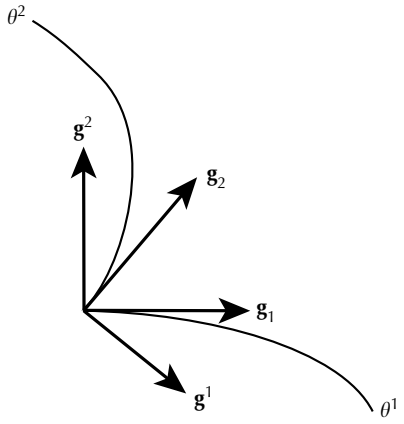

FIGURE 11.3
Covariant and contravariant base vectors.

where $\mathbf{g}^i$ are *contravariant base vectors*, which are the reciprocal base vectors defined by the following nine equations

$$\mathbf{g}_i \cdot \mathbf{g}^j = \delta_i^j \tag{11.14}$$

In the above equations, δ_i^j is the Kronecker delta. The base vector $\mathbf{g}^1$ is perpendicular to $\mathbf{g}_2$ and $\mathbf{g}_3$; $\mathbf{g}^2$ is perpendicular to $\mathbf{g}_1$ and $\mathbf{g}_3$; and $\mathbf{g}^3$ is perpendicular to $\mathbf{g}_2$ and $\mathbf{g}_1$. The covariant and contravariant base vectors are shown in Figure 11.3 for a two-dimensional drawing.

We now find the equations that relate $\mathbf{g}^i$ to $\mathbf{e}_i$. They can be easily found by substituting (11.9) into (11.14) and solving the resulting equations for $\mathbf{g}^i$. The equations are

$$\mathbf{g}^k = \frac{\partial \theta^k}{\partial x_i}\mathbf{e}_i \quad \text{or} \quad \mathbf{e}_i = \frac{\partial x_i}{\partial \theta^k}\mathbf{g}^k \tag{11.15}$$

Equations (11.15) obey the contravariant transformation rule for a vector as given in (11.12). The increment of the position vector given by (11.6) can be further written as

$$\mathrm{d}\mathbf{r} = \mathrm{d}\theta^k \mathbf{g}_k = \mathrm{d}\theta_k \mathbf{g}^k \tag{11.16}$$

where $\mathrm{d}\theta^k$ and $\mathrm{d}\theta_k$ are contravariant and covariant components, respectively, and are given by

$$\mathrm{d}\theta^i = \frac{\partial \theta^i}{\partial x_k}\mathrm{d}x_k \quad \text{and} \quad \mathrm{d}\theta_i = \frac{\partial x_k}{\partial \theta^i}\mathrm{d}x_k \tag{11.17}$$

We see that from the above equations, $d\theta^i$ can be identified with the usual differential of the variable θ^i, but $d\theta_i$ is not the differential of θ^i. Therefore, the differentials are contravariant components, and we will also use the upper index for variable θ^i for consistency, although it is not necessary to do so.

11.3 Tensors and Special Tensors

In Chapter 1, we defined a second-rank tensor as a linear combination of dyadic products. Using this definition of tensor and the base vectors $\mathbf{e}_i$, $\mathbf{g}^i$, and $\mathbf{g}_i$, tensor $\mathbf{T}$ may be expressed as

$$\mathbf{T} = T_{ij}\mathbf{e}_i \otimes \mathbf{e}_j = \tilde{T}^{ij}\mathbf{g}_i \otimes \mathbf{g}_j = \tilde{\mathbf{T}}_{ij}\mathbf{g}^i \otimes \mathbf{g}^j = \tilde{T}^i_j \mathbf{g}_i \otimes \mathbf{g}^j = \tilde{T}^j_i \mathbf{g}^i \otimes \mathbf{g}_j \tag{11.18}$$

where T_{ij} are the Cartesian components; $\tilde{T}^{ij}$ are the contravariant components; $\tilde{T}_{ij}$ are the covariant components; $\tilde{T}^i_j$ and $\tilde{T}^j_i$ are the mixed components of the same tensor. Note that $\tilde{T}^i_j = \tilde{T}^i_j = \tilde{T}^i_j$, if tensor $\mathbf{T}$ is symmetric. Throughout this chapter, we use the tilde (˜) to denote components referred to curvilinear base vectors. This is generally true for physical quantities discussed in this chapter, except for the true stress to be defined in Section 11.11 and some specifically defined tensors, such as $g_{ij}, \varepsilon_{ijk}$, etc. to be defined later in this section. The components in (11.18) refer to specific tensor bases shown and they are related. We can find the relationships by substituting (11.9) and (11.15) into (11.18). To find the relation (or transformation) between $\tilde{T}_{ij}$ and T^{ij}, we write

$$\mathbf{T} = T_{ij}\mathbf{e}_i \otimes \mathbf{e}_j = \tilde{T}^{ij}\mathbf{g}_i \otimes \mathbf{g}_j = \tilde{T}^{ij}\left(\frac{\partial x_r}{\partial \theta^i}\mathbf{e}_r\right) \otimes \left(\frac{\partial x_s}{\partial \theta^j}\mathbf{e}_s\right) = \tilde{T}^{ij}\frac{\partial x_r}{\partial \theta^i}\frac{\partial x_s}{\partial \theta^j}\mathbf{e}_r \otimes \mathbf{e}_s \tag{11.19}$$

Comparing the second and last identities of (11.19), we obtain

$$T_{ij} = \frac{\partial x_i}{\partial \theta^r}\frac{\partial x_j}{\partial \theta^s}\tilde{T}^{rs} \quad \text{or} \quad \tilde{T}^{ij} = \frac{\partial \theta^i}{\partial x_r}\frac{\partial \theta^j}{\partial x_s}T_{rs} \tag{11.20}$$

This is the rule of transformation between the Cartesian components and the contravariant components for a second-rank tensor. The same procedures can be used to obtain the transformation rule between the Cartesian components and the covariant components. The relations are

$$T_{ij} = \frac{\partial \theta^r}{\partial x_i}\frac{\partial \theta^s}{\partial x_j}\tilde{T}_{rs} \quad \text{and} \quad \tilde{T}_{ij} = \frac{\partial x_r}{\partial \theta^i}\frac{\partial x_s}{\partial \theta^j}T_{rs} \tag{11.21}$$

The same transformation rules apply to components of higher order tensors. For example, components of a third-rank tensor transform as

$$\tilde{T}_{ijk} = \frac{\partial x_r}{\partial \theta^i}\frac{\partial x_s}{\partial \theta^j}\frac{\partial x_t}{\partial \theta^k}T_{rst} \qquad \text{(covariant)} \tag{11.22}$$

$$\tilde{T}^{ijk} = \frac{\partial \theta^i}{\partial x_r}\frac{\partial \theta^j}{\partial x_s}\frac{\partial \theta^k}{\partial x_t}T_{rst} \qquad \text{(contravariant)} \tag{11.23}$$

We now discuss two special tensors. They are the Kronecker deltas and the permutation symbols. The Kronecker deltas (δ_{ij}, δ^{ij}, and δ^i_j) are the components of the unit tensor **1** referred to the Cartesian tensor bases formed by Cartesian base vectors $\mathbf{e}_i = \mathbf{e}^i$. The corresponding components referred to the curvilinear tensor bases are known as *metric tensors* and denoted by g_{ij}, g^{ij}, and g^i_j. Thus, the unit tensor may be written as

$$\begin{aligned}\mathbf{1} &= \delta^{ij}\mathbf{e}_i \otimes \mathbf{e}_j = \delta_{ij}\mathbf{e}^i \otimes \mathbf{e}^j = \delta^i_j \mathbf{e}_i \otimes \mathbf{e}^j = \delta^j_i \mathbf{e}^i \otimes \mathbf{e}_j \\ &= g^{ij}\mathbf{g}_i \otimes \mathbf{g}_j = g_{ij}\mathbf{g}^i \otimes \mathbf{g}^j = g^i_j \mathbf{g}_i \otimes \mathbf{g}^j = g^j_i \mathbf{g}^i \otimes \mathbf{g}_j\end{aligned} \tag{11.24}$$

The covariant metric tensor g_{ij}, the contravariant metric tensor g^{ij}, and the mixed metric tensor g^i_j are related to the Kronecker deltas by their respective tensor transformation laws given in (11.20) and (11.21) so that

$$g_{ij} = \frac{\partial x_r}{\partial \theta^i}\frac{\partial x_s}{\partial \theta^j}\delta_{rs} = \frac{\partial x_s}{\partial \theta^i}\frac{\partial x_s}{\partial \theta^j} \tag{11.25}$$

$$g^{ij} = \frac{\partial \theta^i}{\partial x_r}\frac{\partial \theta^j}{\partial x_s}\delta^{rs} = \frac{\partial \theta^i}{\partial x_s}\frac{\partial \theta^j}{\partial x_s} \tag{11.26}$$

$$g^i_j = \frac{\partial \theta^i}{\partial x_r}\frac{\partial x_s}{\partial \theta^j}\delta^r_s = \frac{\partial \theta^i}{\partial x_s}\frac{\partial x_s}{\partial \theta^j} = \delta^i_j \tag{11.27}$$

We note that $\delta_{ij} = \delta^{ij} = \delta^i_j = \delta^j_i = 0$ for $i \neq j$ and $= 1$ for $i = j$.
The determinants of the metric tensors are

$$g = |g_{ij}| = \left|\frac{\partial x_i}{\partial \theta^j}\right|^2 \quad \text{and} \quad \frac{1}{g} = |g^{ij}| = \left|\frac{\partial \theta^i}{\partial x_j}\right|^2 \tag{11.28}$$

and we note that

$$g_{is}g^{sj} = \frac{\partial x_k}{\partial \theta^i}\frac{\partial x_k}{\partial \theta^s}\frac{\partial \theta^s}{\partial x_r}\frac{\partial \theta^j}{\partial x_r} = \delta^j_i \tag{11.29}$$

Knowing g_{ij}, we solve (11.29) to yield

$$g^{ij} = \frac{\text{cofactor of } |g_{ij}|}{g} \tag{11.30}$$

Therefore, (11.30) can be used to determine g^{ij}. We further note that, using (11.9), (11.15), (11.25) and (11.26), we find that

$$\begin{aligned} &\mathbf{g}_i \cdot \mathbf{g}_j = \frac{\partial x_r}{\partial \theta^i}\mathbf{e}_r \cdot \frac{\partial x_s}{\partial \theta^j}\mathbf{e}_s = \frac{\partial x_s}{\partial \theta^i}\frac{\partial x_s}{\partial \theta^j} = g_{ij} \\ &\mathbf{g}^i \cdot \mathbf{g}^j = g^{ij}, \qquad \mathbf{g}^i \cdot \mathbf{g}_j = g^i_j = \delta^i_j \end{aligned} \tag{11.31}$$

Furthermore, g^{ij} and g_{ij} can be used to raise or lower the indices. For example,

$$\mathbf{g}^i = g^{ir}\mathbf{g}_r, \qquad \mathbf{g}_i = g_{ir}\mathbf{g}^r, \qquad v^i = g^{ir}v_r, \qquad T_{ij} = g_{ir}T^r_j \tag{11.32}$$

These relations may be easily proven. The first relation of (11.32), for instance, may be shown using (11.26), (11.9), and (11.15).

Similar to Chapter 1, the permutation symbols are defined in the Cartesian coordinate system as

$$\begin{aligned} e_{ijk} = e^{ijk} &= 1 \qquad \text{for even permutation of } ijk \\ &= -1 \qquad \text{for odd permutation of } ijk \\ &= 0 \qquad \text{for two or more equal indices} \end{aligned} \tag{11.33}$$

Thus, $e_{123} = 1$, $e_{132} = -1$, $e_{112} = 0$, $e_{231} = 1$, $e_{222} = 0$, etc. These are now transformed into the curvilinear coordinate system using the transformation rules of (11.22) and (11.23). The resulting equations are

$$\varepsilon_{ijk} = \frac{\partial x_r}{\partial \theta^i}\frac{\partial x_s}{\partial \theta^j}\frac{\partial x_t}{\partial \theta^k}e_{rst} \tag{11.34}$$

$$\varepsilon^{ijk} = \frac{\partial \theta^i}{\partial x_r}\frac{\partial \theta^j}{\partial x_s}\frac{\partial \theta^k}{\partial x_t}e^{rst} \tag{11.35}$$

The relation between (e_{ijk}, e^{ijk}) and $(\varepsilon_{ijk}, \varepsilon^{ijk})$ can be further established using a known identity in the matrix analysis. If the determinant of a matrix with elements T^i_j is denoted by $|T^i_j|$, then

$$e^{ijk}T^r_i T^s_j T^t_k = |T^i_j|e^{rst} \quad \text{and} \quad e_{ijk}T^i_r T^j_s T^k_t = |T^i_j|e_{rst} \tag{11.36}$$

Substituting (11.36) into the right-hand side of (11.34) and (11.35) and using (11.28), these equations reduce to

$$\varepsilon_{ijk} = \left|\frac{\partial x_r}{\partial \theta^s}\right| e_{ijk} = \sqrt{g}\, e_{ijk} \quad \text{and} \quad \varepsilon^{ijk} = \left|\frac{\partial \theta^r}{\partial x_s}\right| e^{ijk} = \frac{1}{\sqrt{g}} e^{ijk} \tag{11.37}$$

EXAMPLE 11.1 Determine the base vectors and metric tensors for the cylindrical coordinate system.

Solution

The transformation equations between the Cartesian coordinates (x_1, x_2, x_3) and the cylindrical coordinates $(\theta^1, \theta^2, \theta^3)$ are

$$x_1 = \theta^1 \cos\theta^2, \qquad x_2 = \theta^1 \sin\theta^2, \qquad x_3 = \theta^3 \tag{a}$$

and these equations may be inverted to obtain

$$\theta^1 = \sqrt{(x_1)^2 + (x_2)^2}, \qquad \theta^2 = \tan^{-1}\left(\frac{x_2}{x_1}\right), \qquad \theta^3 = x_3 \tag{b}$$

The covariant base vectors may be obtained using (11.9) and by differentiating (a). The resulting expressions are

$$\begin{aligned} \mathbf{g}_1 &= \cos\theta^2 \mathbf{e}_1 + \sin\theta^2 \mathbf{e}_2 \\ \mathbf{g}_2 &= -\theta^1 \sin\theta^2 \mathbf{e}_1 + \theta^1 \cos\theta^2 \mathbf{e}_2, \qquad \mathbf{g}_3 = \mathbf{e}_3 \end{aligned} \tag{c}$$

These vectors are shown in Figure 11.4. Note that the position vector for point P is given by

$$\begin{aligned} \mathbf{r} &= x_k \mathbf{e}_k = (\theta^1 \cos\theta^2)\mathbf{e}_1 + (\theta^1 \sin\theta^2)\mathbf{e}_2 + \theta^3 \mathbf{e}_3 \\ &= \theta^k \mathbf{g}_k = \theta^1 \mathbf{g}_1 + \theta^2 \mathbf{g}_2 + \theta^3 \mathbf{g}_3 \end{aligned} \tag{d}$$

The covariant metric tensor may be found from (11.31) by finding the inner products of the base vectors given by (c). The resulting matrix is

$$g_{ij} = \begin{bmatrix} 1 & 0 & 0 \\ 0 & (\theta^1)^2 & 0 \\ 0 & 0 & 1 \end{bmatrix} \qquad \text{with } g = \det g_{ij} = (\theta^1)^2 \tag{e}$$

The contravariant metric tensor may be found from (11.30) as

$$g^{ij} = \frac{\text{cofactor } g_{ij}}{g} = \frac{1}{(\theta^1)^2} \begin{bmatrix} (\theta^1)^2 & 0 & 0 \\ 0 & 1 & 0 \\ 0 & 0 & (\theta^1)^2 \end{bmatrix} = \begin{bmatrix} 1 & 0 & 0 \\ 0 & (\theta^1)^{-2} & 0 \\ 0 & 0 & 1 \end{bmatrix} \tag{f}$$

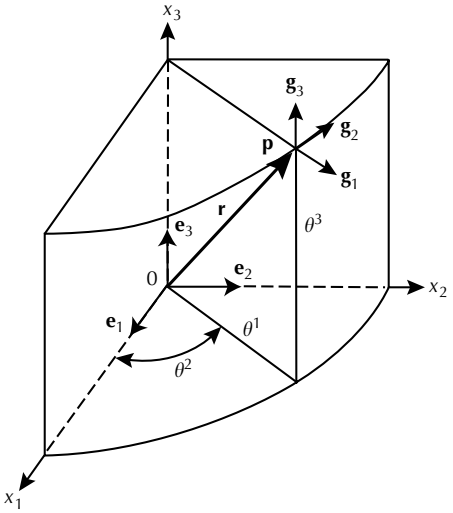

FIGURE 11.4
Coordinates and base vectors in the cylindrical coordinate system.

Since the cylindrical coordinate system is orthogonal, $g^{ij} = 1/g_{ij}$. The contravariant base vectors may be obtained from (11.15) by differentiating (b); and it may also be obtained by raising the index using the first equation of (11.32). Finally, we note that by using (11.31), the contravariant metric tensor can also be obtained.

EXAMPLE 11.2 Determine the base vectors and metric tensors for the spherical coordinate system.

Solution

The position vector of a point is denoted by

$$\mathbf{r} = x_k \mathbf{e}_k = R(\sin\alpha\cos\theta)\mathbf{e}_1 + R(\sin\alpha\sin\theta)\mathbf{e}_2 + R(\cos\alpha)\mathbf{e}_3 \tag{a}$$

where (R, α, θ) are the spherical coordinates. From (11.9) and (a), we find

$$\begin{aligned}
\mathbf{g}_1 &= \sin\alpha\cos\theta\mathbf{e}_1 + \sin\alpha\sin\theta\mathbf{e}_2 + \cos\alpha\mathbf{e}_3 \\
\mathbf{g}_2 &= R(\cos\alpha\cos\theta)\mathbf{e}_1 + R(\cos\alpha\sin\theta)\mathbf{e}_2 - R(\sin\alpha)\mathbf{e}_3 \\
\mathbf{g}_3 &= -R(\sin\alpha\sin\theta)\mathbf{e}_1 + R(\sin\alpha\cos\theta)\mathbf{e}_2
\end{aligned} \tag{b}$$

Using (11.31) we find that the covariant metric tensor is

$$g_{ij} = \begin{bmatrix} 1 & 0 & 0 \\ 0 & R^2 & 0 \\ 0 & 0 & R^2\sin^2\alpha \end{bmatrix} \tag{c}$$

and its inverse is

$$g^{ij} = \begin{bmatrix} 1 & 0 & 0 \\ 0 & R^{-2} & 0 \\ 0 & 0 & R^{-2}\sin^{-2}\alpha \end{bmatrix} \tag{d}$$

The base vector $\mathbf{g}^i$ can be determined by raising the index of $\mathbf{g}_i$. Thus, from the first of (11.32), we find

$$\mathbf{g}^1 = g^{11}\mathbf{g}_1 = \mathbf{g}_1, \qquad \mathbf{g}^2 = g^{22}\mathbf{g}_2 = R^{-2}\mathbf{g}_2, \qquad \mathbf{g}^3 = g^{33}\mathbf{g}_3 = R^{-2}\sin^{-2}\alpha\,\mathbf{g}_3 \tag{e}$$

EXAMPLE 11.3 In the two-dimensional space, a vector is $\mathbf{v} = 3\mathbf{e}_1 + 2\mathbf{e}_2$. Given that $\mathbf{g}_1 = \mathbf{e}_1$ and $\mathbf{g}_2 = K\mathbf{e}_1 + \mathbf{e}_2$ with $K = 0.5$, determine the metric tensors and covariant and contravariant components of $\mathbf{v}$.

Solution

The metric tensors are

$$g_{ij} = \begin{bmatrix} 1 & K & 0 \\ K & 1+K^2 & 0 \\ 0 & 0 & 1 \end{bmatrix} \quad \text{and} \quad g^{ij} = \begin{bmatrix} 1+K^2 & -K & 0 \\ -K & 1 & 0 \\ 0 & 0 & 1 \end{bmatrix} \tag{a}$$

and, using (11.32), we find that

$$\begin{aligned} \mathbf{g}^1 &= g^{11}\mathbf{g}_1 + g^{12}\mathbf{g}_2 = \mathbf{e}_1 - \mathrm{K}\mathbf{e}_2 = \mathbf{e}_1 - 0.5\mathbf{e}_2 \\ \mathbf{g}^2 &= g^{21}\mathbf{g}_1 + g^{22}\mathbf{g}_2 = \mathbf{e}_2 \end{aligned} \tag{b}$$

Thus,

$$\begin{aligned} &\tilde{v}_1 = \mathbf{v}\cdot\mathbf{g}_1 = (3\mathbf{e}_1 + 2\mathbf{e}_2)\cdot\mathbf{e}_1 = 3, \qquad \tilde{v}_2 = \mathbf{v}\cdot\mathbf{g}_2 = 3K + 2 = 3.5 \\ &\tilde{v}^1 = \mathbf{v}\cdot\mathbf{g}^1 = (3\mathbf{e}_1 + 2\mathbf{e}_2)\cdot(\mathbf{e}_1 - \mathrm{K}\mathbf{e}_2) = 3 - 2\mathrm{K} = 2, \qquad \tilde{v}^2 = \mathbf{v}\cdot\mathbf{g}^2 = 2 \end{aligned} \tag{c}$$

The vector may then be expressed as

$$\mathbf{v} = 3\mathbf{e}_1 + 2\mathbf{e}_2 = 3\mathbf{g}^1 + 3.5\mathbf{g}^2 = 2\mathbf{g}_1 + 2\mathbf{g}_2 \tag{d}$$

The base vectors and the components of vector $\mathbf{v}$ are shown drawn to scale in Figure 11.5.

EXAMPLE 11.4 Show that

$$\mathbf{g}_i \times \mathbf{g}_j = \varepsilon_{ijk}\mathbf{g}^k \quad \text{and} \quad \mathbf{g}^i \times \mathbf{g}^j = \varepsilon^{ijk}\mathbf{g}_k \tag{11.38}$$

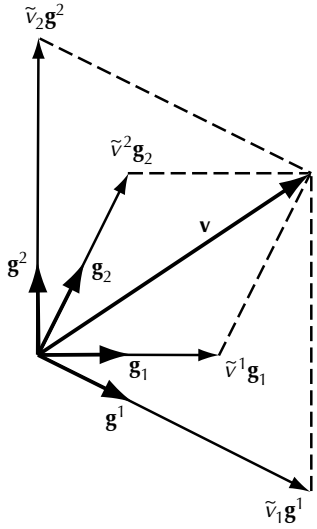

FIGURE 11.5
Base vectors and the components of vector **v**.

Solution

$$\begin{aligned}\text{LHS} &= \frac{\partial x_r}{\partial \theta^i}\mathbf{e}_r \times \frac{\partial x_s}{\partial \theta^j}\mathbf{e}_s = \frac{\partial x_r}{\partial \theta^i}\frac{\partial x_s}{\partial \theta^j}\mathbf{e}_r \times \mathbf{e}_s = \frac{\partial x_r}{\partial \theta^i}\frac{\partial x_s}{\partial \theta^j}e_{rst}\mathbf{e}_t \\ &= \frac{\partial x_r}{\partial \theta^i}\frac{\partial x_s}{\partial \theta^j}e_{rst}\left(\frac{\partial x_t}{\partial \theta^k}\mathbf{g}^k\right) = \varepsilon_{ijk}\mathbf{g}^k = \text{RHS} \end{aligned} \tag{a}$$

The second equality can be similarly proven.

11.4 Multiplication of Vectors

Two vectors **a** and **b** can be multiplied in two different ways. Their scalar product is

$$\begin{aligned}\mathbf{a}\cdot\mathbf{b} &= (\tilde{a}^i\mathbf{g}_i)\cdot(\tilde{b}^j\mathbf{g}_j) = \tilde{a}^i\tilde{b}^j g_{ij} = \tilde{a}^i\tilde{b}_i \\ &= (\tilde{a}_i\mathbf{g}^i)\cdot(\tilde{b}_j\mathbf{g}^j) = \tilde{a}_i\tilde{b}_j g^{ij} = \tilde{a}_i\tilde{b}^i \end{aligned} \tag{11.39}$$

and their vector product is

$$\begin{aligned}\mathbf{a}\times\mathbf{b} &= (\tilde{a}^i\mathbf{g}_i)\times(\tilde{b}^j\mathbf{g}_j) = \tilde{a}^i\tilde{b}^j\mathbf{g}_i\times\mathbf{g}_j = \varepsilon_{ijk}\tilde{a}^i\tilde{b}^j\mathbf{g}^k \\ &= (\tilde{a}_i\mathbf{g}^i)\times(\tilde{b}_j\mathbf{g}^j) = \tilde{a}_i\tilde{b}_j\mathbf{g}^i\times\mathbf{g}^j = \varepsilon^{ijk}\tilde{a}_i\tilde{b}_j\mathbf{g}_k \end{aligned} \tag{11.40}$$

11.5 Physical Components of a Vector

As previously mentioned in (11.13), a vector $\mathbf{u}$ may be written as

$$\mathbf{u} = \tilde{u}^i \mathbf{g}_i = \tilde{u}_i \mathbf{g}^i \tag{11.41}$$

in which the base vectors $\mathbf{g}^i$ and $\mathbf{g}_i$ are, in general, not of unit magnitude. We are now interested in knowing the dimensions of components $\tilde{u}^i$ and $\tilde{u}_i$. If $\mathbf{u}$ represents the displacement vector and has the dimension of length (L), then, in the case of cylindrical coordinates from (e) of Example 11.1, $|\mathbf{g}_1| = \sqrt{g_{11}} = 1$ (dimensionless), $|\mathbf{g}_2| = \sqrt{g_{22}} = \theta^1$ (dimension L), and $|\mathbf{g}_3| = \sqrt{g_{33}} = 1$ (dimensionless). Since all terms in (11.41) have the same dimensions, the dimensions of $\tilde{u}^i$ can be determined to be $\tilde{u}^1 \sim L$, $\tilde{u}^2 \sim 1$, and $\tilde{u}^3 \sim L$. We see that the components $\tilde{u}^i$ have different dimensions. Similarly, we find that components of $\tilde{u}_i$ do not have the same dimensions either.

In the engineering applications, physical quantities have known properties and dimensions and may be mathematically represented by tensors. We are interested in finding components of a tensor that have the same dimensions and these are known as *physical components*. We are interested in the physical components because they describe the characteristics of that physical quantity through its unit and dimension, and they are usually the experimentally determined quantities. The physical components of a vector are discussed in this section, while those of higher-order tensors are discussed later in this chapter.

The physical components of a vector may be defined by taking parallel projections of the vector on unit vectors lying along the coordinate curves. Therefore, (11.41) may be written as

$$\mathbf{u} = \tilde{u}^i \mathbf{g}_i = u^{\langle i \rangle} \mathbf{e}_i \tag{11.42}$$

where $\mathbf{e}_i$ are unit vectors defined by

$$\mathbf{e}_i = \frac{\mathbf{g}_i}{\sqrt{g_{\underline{i}\underline{i}}}} \qquad (i \text{ not summed}) \tag{11.43}$$

and are $u^{\langle i \rangle}$ the physical components. Unit vector $\mathbf{e}_i$ is in the same direction as base vector $\mathbf{g}_i$. Substituting (11.43) into (11.42), we find that

$$u^{\langle i \rangle} = \tilde{u}^i \sqrt{g_{\underline{i}\underline{i}}} \qquad (i \text{ not summed}) \tag{11.44}$$

Equation (11.44) gives the relationship between the physical and tensor components of a vector. To find the physical components for $\tilde{u}_i$, we use the metric tensor g_{ij} to lower the index. Thus, using (11.44),

$$\tilde{u}_i = g_{ij} \tilde{u}^j = \sum_j g_{ij} \frac{u^{\langle j \rangle}}{\sqrt{g_{jj}}} \tag{11.45}$$

The physical components of $\tilde{u}_i$ may also be defined by parallel projections of vector $\mathbf{u}$ on unit vectors lying along $\mathbf{g}^i$. Thus,

$$u_{\langle i \rangle} = \tilde{u}_i \sqrt{g^{ii}} \qquad (i \text{ not summed}) \tag{11.46}$$

This definition of the physical component is not consistent with the previous definition for $u^{\langle i \rangle}$ because the two sets of unit vectors defined based on $\mathbf{g}_i$ and $\mathbf{g}^i$ are not in the same directions. Therefore, for the sake of consistency, (11.46) should not be used.

11.6 Differentiation of a Tensor with Respect to the Space Coordinates

A tensor field differentiated with respect to the space variables leads to the *covariant differentiation* of a tensor. Both the components and the base vectors need to be differentiated. The differentiation of the components is partial differentiation of scalars with respect to θ^i and no special attention is needed. We will now discuss the differentiation of the base vectors. The quantity $\partial \mathbf{g}_i / \partial \theta^j$ indicates the rate of change in direction and length of the base vector $\mathbf{g}_i$ as it moves along coordinate θ^j. Differentiating (11.9) and noting that $\mathbf{e}_i$ does not vary, we have

$$\begin{aligned} \frac{\partial \mathbf{g}_i}{\partial \theta^j} &= \frac{\partial^2 x_k}{\partial \theta^i \partial \theta^j} \mathbf{e}_k = \frac{\partial^2 x_k}{\partial \theta^i \partial \theta^j} \frac{\partial \theta^m}{\partial x_k} \mathbf{g}_m = \Gamma_{ij}^m \mathbf{g}_m \\ &= \Gamma_{ij}^m \, g_{nm} \mathbf{g}^n = \Gamma_{ijk} \mathbf{g}^k \end{aligned} \tag{11.47}$$

Thus,

$$\frac{\partial \mathbf{g}_i}{\partial \theta^j} = \Gamma_{ij}^m \, \mathbf{g}_m = \Gamma_{ijk} \, \mathbf{g}^k \tag{11.48}$$

The derivative may either be expressed in terms of the covariant or the contravariant base vectors. The symbols Γ_{ijk} and Γ_{ij}^k are called the *Christoffel symbols of the first and second kind*, respectively, and they are given by the relations

$$\begin{aligned} \Gamma_{ijk} &= \Gamma_{ij}^m \, g_{km} = \frac{\partial^2 x_m}{\partial \theta^i \partial \theta^j} \frac{\partial x_m}{\partial \theta^k} \\ \Gamma_{ij}^k &= \frac{\partial^2 x_m}{\partial \theta^i \partial \theta^j} \frac{\partial \theta^k}{\partial x_m} = g^{km} \, \Gamma_{ijm} \end{aligned} \tag{11.49}$$

Note that (11.25) was used in the above equations. By the differentiation of (11.25) we can further show that

$$\Gamma_{ijk} = \frac{1}{2}\left(\frac{\partial g_{ik}}{\partial \theta^j} + \frac{\partial g_{jk}}{\partial \theta^i} - \frac{\partial g_{ij}}{\partial \theta^k}\right) \tag{11.50}$$

Both Christoffel symbols are symmetric in indices i and j.

Differentiating (11.14) and making use of (11.48), we obtain

$$\frac{\partial \mathbf{g}^i}{\partial \theta^k} \cdot \mathbf{g}_j = -\mathbf{g}^i \cdot \frac{\partial \mathbf{g}_j}{\partial \theta^k} = -\mathbf{g}^i \cdot \Gamma^m_{jk}\mathbf{g}_m = -\Gamma^i_{jk} \tag{11.51}$$

which leads to

$$\frac{\partial \mathbf{g}^i}{\partial \theta^j} = -\Gamma^i_{jk}\mathbf{g}^k \tag{11.52}$$

In the coordinate transformation from θ^i to $\bar{\theta}^i$, the transformation law for Γ^k_{ij} is

$$\bar{\Gamma}^k_{ij} = \Gamma^t_{rs}\frac{\partial \theta^r}{\partial \bar{\theta}^i}\frac{\partial \theta^s}{\partial \bar{\theta}^j}\frac{\partial \bar{\theta}^k}{\partial \theta^t} + \frac{\partial^2 \theta^s}{\partial \bar{\theta}^i \partial \bar{\theta}^j}\frac{\partial \bar{\theta}^k}{\partial \theta^s} \tag{11.53}$$

Due to the presence of the last term of (11.53), the Christoffel symbol Γ^k_{ij} are not components of a tensor. The same thing may be said of Γ_{ijk}.

11.6.1 Derivative of a Scalar

When the coordinates transform from θ^i to $\bar{\theta}^i$, the value of a scalar φ remains unchanged, that is, $\bar{\varphi} = \varphi$. But, its partial derivatives transform according to the covariant rule of transformation, such that

$$\frac{\partial \bar{\varphi}}{\partial \bar{\theta}^i} = \frac{\partial \bar{\varphi}}{\partial \theta^j}\frac{\partial \theta^j}{\partial \bar{\theta}^i} = \frac{\partial \theta^j}{\partial \bar{\theta}^i}\frac{\partial \varphi}{\partial \theta^j} \tag{11.54}$$

11.6.2 Derivatives of a Vector

The derivatives of a vector $\mathbf{u}$ with respect to θ^i-transform as

$$\frac{\partial \mathbf{u}}{\partial \bar{\theta}^i} = \frac{\partial \mathbf{u}}{\partial \theta^j}\frac{\partial \theta^j}{\partial \bar{\theta}^i} = \frac{\partial \theta^j}{\partial \bar{\theta}^i}\frac{\partial \mathbf{u}}{\partial \theta^j} \tag{11.55}$$

which is of the same form as (11.11) and obey the covariant transformation rule. Furthermore, by differentiating the first and second expressions

of (11.13), respectively, we obtain

$$\frac{\partial \mathbf{u}}{\partial \theta^i} = \frac{\partial \tilde{u}^j}{\partial \theta^i}\mathbf{g}_j + \tilde{u}^j \frac{\partial \mathbf{g}_j}{\partial \theta^i} = \frac{\partial \tilde{u}^j}{\partial \theta^i}\mathbf{g}_j + \tilde{u}^j \Gamma^k_{ji}\mathbf{g}_k = \left(\frac{\partial \tilde{u}^j}{\partial \theta^i} + \tilde{u}^k \Gamma^j_{ki}\right)\mathbf{g}_j = \tilde{u}^j|_i\, \mathbf{g}_j \quad (11.56)$$

and

$$\frac{\partial \mathbf{u}}{\partial \theta^i} = \frac{\partial \tilde{u}_j}{\partial \theta^i}\mathbf{g}^j + \tilde{u}_j \frac{\partial \mathbf{g}^j}{\partial \theta^i} = \frac{\partial \tilde{u}_j}{\partial \theta^i}\mathbf{g}^j - \tilde{u}_j \Gamma^j_{ik}\mathbf{g}^k = \left(\frac{\partial \tilde{u}_j}{\partial \theta^i} - \tilde{u}_k \Gamma^k_{ij}\right)\mathbf{g}^j = \tilde{u}_j|_i\, \mathbf{g}^j \quad (11.57)$$

We note that (11.52) was used in the derivation of (11.56), and (11.48) was used in the derivation of (11.57). The expressions $\tilde{u}^j|_i$ and $\tilde{u}_j|_i$ are called the *covariant derivatives* of the components $\tilde{u}^i$ and $\tilde{u}_i$ of vector $\mathbf{u}$, respectively. The expressions may be summarized as

$$\frac{\partial \mathbf{u}}{\partial \theta^i} = \tilde{u}^j|_i\, \mathbf{g}_j = \tilde{u}_j|_i\, \mathbf{g}^j \quad (11.58)$$

where

$$\tilde{u}^j|_i = \frac{\partial \tilde{u}^j}{\partial \theta^i} + \Gamma^j_{ki}\tilde{u}^k \quad (11.59)$$

$$\tilde{u}_j|_i = \frac{\partial \tilde{u}_j}{\partial \theta^i} - \Gamma^k_{ji}\tilde{u}_k \quad (11.60)$$

11.6.3 Derivatives of a Tensor

When a second-order tensor $\mathbf{T}$ is written in the form of (11.18), its derivatives are

$$\begin{aligned}\frac{\partial \mathbf{T}}{\partial \theta^r} &= \frac{\partial(\tilde{\mathbf{T}}_{ij}\mathbf{g}^i \otimes \mathbf{g}^j)}{\partial \theta^r} = \frac{\partial \tilde{\mathbf{T}}_{ij}}{\partial \theta^r}\mathbf{g}^i \otimes \mathbf{g}^j + \tilde{\mathbf{T}}_{ij}\frac{\partial \mathbf{g}^i}{\partial \theta^r} \otimes \mathbf{g}^j + \tilde{\mathbf{T}}_{ij}\mathbf{g}^i \otimes \frac{\partial \mathbf{g}^j}{\partial \theta^r} \\ &= \frac{\partial \tilde{\mathbf{T}}_{ij}}{\partial \theta^r}\mathbf{g}^i \otimes \mathbf{g}^j + \tilde{\mathbf{T}}_{ij}(-\Gamma^i_{rk}\mathbf{g}^k) \otimes \mathbf{g}^j + \tilde{\mathbf{T}}_{ij}\mathbf{g}^i \otimes (-\Gamma^j_{rk}\mathbf{g}^k) \\ &= \left(\frac{\partial \tilde{\mathbf{T}}_{ij}}{\partial \theta^r} - \Gamma^m_{ir}\tilde{T}_{mj} - \Gamma^m_{jr}\tilde{T}_{im}\right)\mathbf{g}^i \otimes \mathbf{g}^j = \tilde{\mathbf{T}}_{ij}|_r\, \mathbf{g}^i \otimes \mathbf{g}^j \end{aligned} \quad (11.61)$$

A similar procedure results in

$$\frac{\partial \mathbf{T}}{\partial \theta^r} = \frac{\partial(\tilde{\mathbf{T}}^i_j\, \mathbf{g}_i \otimes \mathbf{g}^j)}{\partial \theta^r} = \left(\frac{\partial \tilde{\mathbf{T}}^i_j}{\partial \theta^r} + \Gamma^i_{rm}\tilde{\mathbf{T}}^m_j - \Gamma^m_{jr}\tilde{\mathbf{T}}^i_m\right)\mathbf{g}_i \otimes \mathbf{g}^j = \tilde{\mathbf{T}}^i_j|_r\, \mathbf{g}_i \otimes \mathbf{g}^j \quad (11.62)$$

and

$$\frac{\partial \mathbf{T}}{\partial \theta^r} = \frac{\partial (\tilde{\mathbf{T}}^{ij} \mathbf{g}_i \otimes \mathbf{g}_j)}{\partial \theta^r} = \left(\frac{\partial \tilde{\mathbf{T}}^{ij}}{\partial \theta^r} + \Gamma^i_{rm} \tilde{\mathbf{T}}^{mj} + \Gamma^j_{rm} \tilde{\mathbf{T}}^{im} \right) \mathbf{g}_i \otimes \mathbf{g}_j = \tilde{\mathbf{T}}^{ij}|_r \, \mathbf{g}_i \otimes \mathbf{g}_j \tag{11.63}$$

Thus, the covariant derivatives of the components of second-rank tensor $\mathbf{T}$ are

$$\begin{aligned} \tilde{\mathbf{T}}^{ij}|_r &= \frac{\partial \tilde{\mathbf{T}}^{ij}}{\partial \theta^r} + \Gamma^i_{rm} \tilde{\mathbf{T}}^{mj} + \Gamma^j_{rm} \tilde{\mathbf{T}}^{im} \\ \tilde{\mathbf{T}}^i_j|_r &= \frac{\partial \tilde{\mathbf{T}}^i_j}{\partial \theta^r} + \Gamma^i_{rm} \tilde{\mathbf{T}}^m_j - \Gamma^m_{jr} \tilde{\mathbf{T}}^i_m \\ \tilde{\mathbf{T}}_{ij}|_r &= \frac{\partial \tilde{\mathbf{T}}_{ij}}{\partial \theta^r} - \Gamma^m_{ir} \tilde{T}_{mj} - \Gamma^m_{jr} \tilde{T}_{im} \end{aligned} \tag{11.64}$$

This procedure may be extended to the differentiation of a higher rank tensor. For example, the covariant derivatives of the mixed tensor component $\tilde{T}^i_{.jk}$ are found to be

$$\tilde{T}^i_{.jk}|_r = \frac{\partial \tilde{T}^i_{.jk}}{\partial \theta^r} + \Gamma^i_{mr} \tilde{T}^m_{.jk} - \Gamma^m_{jr} \tilde{T}^i_{.mk} - \Gamma^m_{kr} \tilde{T}^i_{.jm} \tag{11.65}$$

We now make the following remarks related to the covariant derivatives:

1. The metric tensor reduces to the Kronecker deltas in the Cartesian coordinate system. Since the derivatives of the Kronecker deltas are zero, the derivatives of the metric tensors vanish in all coordinate systems, that is,

$$g^{ij}|_r = g_{ij}|_r = g^i_j|_r = 0 \tag{11.66}$$

2. Since the derivatives of the permutation symbols e_{ijk} are zero in the Cartesian coordinate system, the derivatives of the permutation

symbols are zero in all coordinate systems, that is,

$$\varepsilon^{ijk}|_r = 0 \quad \text{and} \quad \varepsilon_{ijk}|_r = 0 \tag{11.67}$$

EXAMPLE 11.5 Determine the expressions of the Christoffel symbols in the cylindrical coordinate system.

Solution

In the cylindrical coordinate system, the metric tensors are given in (e) and (f) of Example 11.1. Using (11.50), the following components are obtained

$$\begin{aligned}
&\Gamma_{122} = \Gamma_{212} = \frac{1}{2}\left(\frac{\partial g_{12}}{\partial\theta^2} + \frac{\partial g_{22}}{\partial\theta^1} - \frac{\partial g_{12}}{\partial\theta^2}\right) = \frac{1}{2}(2\theta^1) = \theta^1 \\
&\Gamma_{221} = \frac{1}{2}\left(\frac{\partial g_{21}}{\partial\theta^2} + \frac{\partial g_{21}}{\partial\theta^2} - \frac{\partial g_{22}}{\partial\theta^1}\right) = -\frac{1}{2}(2\theta^1) = -\theta^1 \\
&\text{all other } \Gamma_{ijk} = 0
\end{aligned} \tag{a}$$

We use g^{ij} to raise the index so that $\Gamma^k_{ij} = g^{km}\Gamma_{ijm}$. Therefore,

$$\begin{aligned}
&\Gamma^2_{12} = \Gamma^2_{21} = g^{2m}\Gamma_{12m} = g^{21}\Gamma_{121} + g^{22}\Gamma_{122} + g^{23}\Gamma_{123} = \frac{1}{\theta^1} \\
&\Gamma^1_{22} = g^{1m}\Gamma_{22m} = g^{11}\Gamma_{221} + g^{12}\Gamma_{222} + g^{13}\Gamma_{223} = -\theta^1 \\
&\text{all other } \Gamma^k_{ij} = 0
\end{aligned} \tag{b}$$

For example, $\Gamma^1_{13} = g^{1m}\Gamma_{13m} = g^{11}\Gamma_{131} + g^{12}\Gamma_{132} + g^{13}\Gamma_{133} = 0$.

EXAMPLE 11.6 In the cylindrical coordinate system, determine the covariant derivatives $\tilde{u}^1|_1$ and $\tilde{u}^1|_2$ of vector $\mathbf{u}$.

Solution

We use (11.59) and the Christoffel symbols found in Example 11.5 to obtain

$$\tilde{u}^1|_1 = \frac{\partial\tilde{u}^1}{\partial\theta^1} + \Gamma^1_{1k}\tilde{u}^k = \frac{\partial\tilde{u}^1}{\partial\theta^1}$$

$$\tilde{u}^1|_2 = \frac{\partial\tilde{u}^1}{\partial\theta^2} + \Gamma^1_{2k}\tilde{u}^k = \frac{\partial\tilde{u}^1}{\partial\theta^2} + \Gamma^1_{22}\tilde{u}^2 = \frac{\partial\tilde{u}^1}{\partial\theta^2} - \theta^1\tilde{u}^2$$

EXAMPLE 11.7 Find the expressions for gradient, divergence, and curl in the curvilinear coordinates.

Solution

Define the del operator $\nabla = \mathbf{g}^k(\partial/\partial\theta^k)$, then gradient, divergence, and curl of a tensor field can be determined as

$$\text{gradient of scalar } \phi = \nabla\phi = \mathbf{g}^k \frac{\partial \phi}{\partial \theta^k} = g^{km}\mathbf{g}_m \frac{\partial \phi}{\partial \theta^k} = \mathbf{g}_k g^{km} \frac{\partial \phi}{\partial \theta^m} \tag{a}$$

$$\text{divergence of vector } \mathbf{a} = \nabla \cdot \mathbf{a} = \mathbf{g}^k \cdot \frac{\partial \mathbf{a}}{\partial \theta^k} = \mathbf{g}^k \cdot \mathbf{g}_m \tilde{a}^m|_k = \tilde{a}^k|_k \tag{b}$$

$$\begin{aligned}\text{curl of vector } \mathbf{a} &= \nabla \times \mathbf{a} \\ &= \mathbf{g}^k \frac{\partial}{\partial \theta^k} \times \mathbf{a} = \mathbf{g}^k \times \frac{\partial \mathbf{a}}{\partial \theta^k} = \mathbf{g}^k \times \tilde{a}_m|_k \, \mathbf{g}^m = \mathbf{g}^k \times \mathbf{g}^m \tilde{a}_m|_k \\ &= \varepsilon^{nkm}\mathbf{g}_n \tilde{a}_m|_k = \varepsilon^{kmn}\tilde{a}_n|_m \, \mathbf{g}_k = \frac{e^{kmn}}{\sqrt{g}}\tilde{a}_n|_m \, \mathbf{g}_k \end{aligned} \tag{c}$$

We used (11.56) in the derivation of $\nabla \times \mathbf{a}$ and (11.37), (11.38), and (11.57) in the derivation of $\nabla \times \mathbf{a}$.

EXAMPLE 11.8 Find the Laplacian ∇^2 in the cylindrical coordinates.

Solution

In the cylindrical coordinate system, the conventional variables are (r, θ, z). Therefore, $\theta^1 = r$, $\theta^2 = \theta$, and $\theta^3 = z$. The Laplacian of scalar field ϕ is the divergence of the gradient of ϕ, and we use the expression for the divergence given in Example 11.7 to derive

$$\begin{aligned}\nabla^2\phi = \text{div} \cdot (\text{grad}\,\phi) &= \nabla \cdot \left(\mathbf{g}_k g^{km} \frac{\partial \phi}{\partial \theta^m}\right) = \left(g^{km} \frac{\partial \phi}{\partial \theta^m}\right)\Big|_k = g^{km} \frac{\partial \phi}{\partial \theta^m}\Big|_k \\ &= g^{11} \frac{\partial \phi}{\partial \theta^1}\Big|_1 + g^{22} \frac{\partial \phi}{\partial \theta^2}\Big|_2 + g^{33} \frac{\partial \phi}{\partial \theta^3}\Big|_3 \\ &= \left(\frac{\partial^2 \phi}{\partial \theta^1 \partial \theta^1} - \Gamma^m_{11} \frac{\partial \phi}{\partial \theta^m}\right) + \frac{1}{r^2}\left(\frac{\partial^2 \phi}{\partial \theta^2 \partial \theta^2} - \Gamma^m_{22} \frac{\partial \phi}{\partial \theta^m}\right) + \left(\frac{\partial^2 \phi}{\partial \theta^3 \partial \theta^3} - \Gamma^m_{33} \frac{\partial \phi}{\partial \theta^m}\right) \\ &= \frac{\partial^2 \phi}{\partial r^2} + \frac{1}{r^2}\left(\frac{\partial^2 \phi}{\partial \theta^2} - \Gamma^1_{22} \frac{\partial \phi}{\partial r}\right) + \frac{\partial^2 \phi}{\partial z^2} \\ &= \frac{\partial^2 \phi}{\partial r^2} + \frac{1}{r}\frac{\partial \phi}{\partial r} + \frac{1}{r^2}\frac{\partial^2 \phi}{\partial \theta^2} + \frac{\partial^2 \phi}{\partial z^2} \end{aligned} \tag{a}$$

Note that (11.60) and the results of Example 11.5 for the Christoffel symbols were used in the above derivation.

EXAMPLE 11.9 Find the expression for curl **a** in terms of the physical components of **a** in the cylindrical coordinates.

Solution

Using the results of Example 11.7, curl **a** is

$$\begin{aligned}\nabla \times \mathbf{a} =& \frac{e^{kmn}}{\sqrt{g}}\tilde{a}_n|_m\,\mathbf{g}_k \\ =& \frac{e^{123}}{\sqrt{g}}\tilde{a}_3|_2\,\mathbf{g}_1 + \frac{e^{132}}{\sqrt{g}}\tilde{a}_2|_3\,\mathbf{g}_1 + \frac{e^{213}}{\sqrt{g}}\tilde{a}_3|_1\,\mathbf{g}_2 \\ &+ \frac{e^{231}}{\sqrt{g}}\tilde{a}_1|_3\,\mathbf{g}_2 + \frac{e^{312}}{\sqrt{g}}\tilde{a}_2|_1\,\mathbf{g}_3 + \frac{e^{321}}{\sqrt{g}}\tilde{a}_1|_2\,\mathbf{g}_3 \end{aligned} \tag{a}$$

Defining unit vectors $(\mathbf{e}_r, \mathbf{e}_\theta, \mathbf{e}_z)$, respectively, along the directions of the base vectors $(\mathbf{g}_1, \mathbf{g}_2, \mathbf{g}_3)$, we have

$$\mathbf{g}_1 = \sqrt{g_{11}}\mathbf{e}_r, \qquad \mathbf{g}_2 = \sqrt{g_{22}}\mathbf{e}_\theta, \qquad \mathbf{g}_3 = \sqrt{g_{33}}\mathbf{e}_z \tag{b}$$

By substituting the above equations and noting that $g = r^2$, we obtain

$$\nabla \times \mathbf{a} = \frac{1}{r}(\tilde{a}_3|_2 - \tilde{a}_2|_3)\mathbf{e}_r + (\tilde{a}_1|_3 - \tilde{a}_3|_1)\mathbf{e}_\theta + \frac{1}{r}(\tilde{a}_2|_1 - \tilde{a}_1|_2)\mathbf{e}_z \tag{c}$$

Using (11.60) and noting that $\Gamma^k_{ij} = \Gamma^k_{ji}$, it may be shown that

$$\tilde{a}_3|_2 - \tilde{a}_2|_3 = \left(\frac{\partial \tilde{a}_3}{\partial \theta^2} - \Gamma^k_{32}\tilde{a}_k\right) - \left(\frac{\partial \tilde{a}_2}{\partial \theta^3} - \Gamma^k_{23}\tilde{a}_k\right) = \frac{\partial \tilde{a}_3}{\partial \theta^2} - \frac{\partial \tilde{a}_2}{\partial \theta^3} \tag{d}$$

Similarly,

$$\tilde{a}_1|_3 - \tilde{a}_3|_1 = \frac{\partial \tilde{a}_1}{\partial \theta^3} - \frac{\partial \tilde{a}_3}{\partial \theta^1} \quad \text{and} \quad \tilde{a}_2|_1 - \tilde{a}_1|_2 = \frac{\partial \tilde{a}_2}{\partial \theta^1} - \frac{\partial \tilde{a}_1}{\partial \theta^2} \tag{e}$$

In the above expressions, $(\tilde{a}_1, \tilde{a}_2, \tilde{a}_3)$ are tensor components. We now express them in the physical components $(a^{\langle 1\rangle}, a^{\langle 2\rangle}, a^{\langle 3\rangle})$. In the conventional notations, we write $a^{\langle 1\rangle} = a_r$, $a^{\langle 2\rangle} = a_\theta$, and $a^{\langle 3\rangle} = a_z$ so that

$$\mathbf{a} = a_r\mathbf{e}_r + a_\theta\mathbf{e}_\theta + a_z\mathbf{e}_z \tag{f}$$

From (11.45) and Example 11.1, it may be found that

$$\tilde{a}_1 = a_r, \qquad \tilde{a}_2 = ra_\theta, \qquad \tilde{a}_3 = a_z \tag{g}$$

Hence,

$$\begin{aligned}\nabla \times \mathbf{a} =& \frac{1}{r}\left(\frac{\partial \tilde{a}_3}{\partial \theta^2} - \frac{\partial \tilde{a}_2}{\partial \theta^3}\right)\mathbf{e}_r + \left(\frac{\partial \tilde{a}_1}{\partial \theta^3} - \frac{\partial \tilde{a}_3}{\partial \theta^1}\right)\mathbf{e}_\theta + \frac{1}{r}\left(\frac{\partial \tilde{a}_2}{\partial \theta^1} - \frac{\partial \tilde{a}_1}{\partial \theta^2}\right)\mathbf{e}_z \\ =& \frac{1}{r}\left(\frac{\partial a_z}{\partial \theta} - \frac{\partial (r a_\theta)}{\partial z}\right)\mathbf{e}_r + \left(\frac{\partial a_r}{\partial z} - \frac{\partial a_z}{\partial r}\right)\mathbf{e}_\theta + \frac{1}{r}\left(\frac{\partial (r a_\theta)}{\partial r} - \frac{\partial a_r}{\partial \theta}\right)\mathbf{e}_z \\ =& \left(\frac{1}{r}\frac{\partial a_z}{\partial \theta} - \frac{\partial a_\theta}{\partial z}\right)\mathbf{e}_r + \left(\frac{\partial a_r}{\partial z} - \frac{\partial a_z}{\partial r}\right)\mathbf{e}_\theta + \left[\frac{1}{r}\frac{\partial (r a_\theta)}{\partial r} - \frac{1}{r}\frac{\partial a_r}{\partial \theta}\right]\mathbf{e}_z \end{aligned} \quad \text{(h)}$$

11.7 Strain Tensor

We now discuss the deformation of a continuum denoted by R_0 at its undeformed (or initial) configuration and by R_t at its deformed (or current) configuration. A fixed Cartesian coordinate system denoted by (x_1, x_2, x_3) is shown in Figure 11.6. A material point P at the undeformed configuration (time $t = 0$) has Cartesian coordinates (X_1, X_2, X_3) with position vector $\mathbf{R}$ so that

$$\mathbf{R} = X_i \mathbf{e}_i \tag{11.68}$$

As the continuum deforms from R_0 to R_t at time t, a generic point P in R_0 moves to point p in R_t. The position vector of p is

$$\mathbf{r} = x_i \mathbf{e}_i \tag{11.69}$$

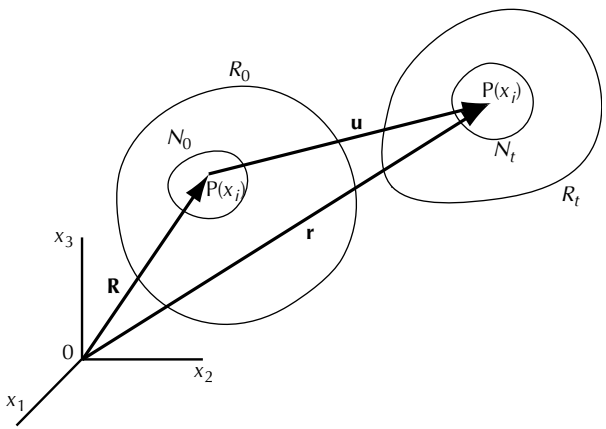

FIGURE 11.6
Position vectors of a point.

and the displacement is

$$\mathbf{u} = \mathbf{r} - \mathbf{R} \tag{11.70}$$

Throughout this chapter (and also the rest of the book) we shall use uppercase letters to denote quantities at the undeformed configuration and lowercase letters to denote quantities associated with the deformed configuration. The coordinates of P and p are related by the following transformation equations:

$$x_i = x_i(X_1, X_2, X_3, t) \tag{11.71}$$

These equations describe the motion of the continuum, and the functions in (11.71) are single-valued and continuous. These equations may be inverted to obtain

$$X_i = X_i(x_1, x_2, x_3, t) \tag{11.72}$$

The differentials of (11.71) and (11.72) are

$$\mathrm{d}x_i = \frac{\partial x_i}{\partial X_k}\mathrm{d}X_k \quad \text{and} \quad \mathrm{d}X_i = \frac{\partial X_i}{\partial x_k}\mathrm{d}x_k \tag{11.73}$$

We introduce a convected (or imbedded) curvilinear coordinate system to describe the deformation of the continuum. A brief introduction of the convected coordinates is previously given in Section 11.1. Here, we devote to the discussion of the deformation of a neighborhood N_0 around P, shown in Figure 11.6, which is deformed into neighborhood N_t around p. Figure 11.7 shows the details of N_0 and N_t. At the undeformed configuration, we use a marker to draw coordinate curves in N_0. The convected coordinates are θ^i and, in this two-dimensional illustration, we show only θ^1 and θ^2 in the figure. Coordinate curves of constant values for θ^1 and θ^2 are shown in the figure. If M denotes the origin of the convected coordinate system, then the M–M′ curve is the θ^1-coordinate axis and the M–M″ curve the θ^2-coordinate axis. Line

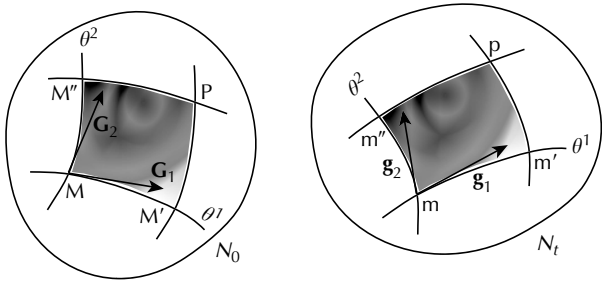

FIGURE 11.7
Neighborhood N_0 deforms into N_t.

segment MM′ is deformed into mm′ and line segment MM″ into mm″. If the length of MM′ is five units, say, then the length of mm′ remains at five units, except that the unit lengths for MM′ and mm′ are different. Similarly, if the length of MM″ is six units, then the length of mm″ is also six units. We note that the shaded material element in N_0 is deformed into the shaded material element in N_t, and we are dealing with the same material mass in both elements. The shaded pattern indicates that the material is anisotropic and the pattern gets deformed as the continuum undergoes deformation. Therefore, the element is a convected material element and we will follow the deformation history of this element in the study of plastic deformation of the continuum.

The position of P may now be described by the curvilinear coordinates, so that

$$X_i = X_i(\theta^1, \theta^2, \theta^3) \tag{11.74}$$

and the position of p described by

$$x_i = x_i(\theta^1, \theta^2, \theta^3) \tag{11.75}$$

The material line element at the undeformed and deformed configurations are, respectively,

$$\mathrm{d}\mathbf{R} = \frac{\partial \mathbf{R}}{\partial \theta^k}\mathrm{d}\theta^k = \mathrm{d}\theta^k \mathbf{G}_k \quad \text{and} \quad \mathrm{d}\mathbf{r} = \frac{\partial \mathbf{r}}{\partial \theta^k}\mathrm{d}\theta^k = \mathrm{d}\theta^k \mathbf{g}_k \tag{11.76}$$

where $\mathbf{G}_i$ and $\mathbf{g}_i$ are the base vectors at the undeformed and deformed configurations, respectively. $\mathbf{G}_i$ and $\mathbf{g}_i$ vary from point to point in the continuum, and are, as in (11.9), related to $\mathbf{e}_i$ by

$$\mathbf{G}_k = \frac{\partial X_i}{\partial \theta^k}\mathbf{e}_i \quad \text{and} \quad \mathbf{g}_k = \frac{\partial x_i}{\partial \theta^k}\mathbf{e}_i \tag{11.77}$$

If we denote the length of material line element in N_0 by $\mathrm{d}S$ and that in N_t by $\mathrm{d}s$, we write

$$(\mathrm{d}S)^2 = \mathrm{d}\mathbf{R} \cdot \mathrm{d}\mathbf{R} = \mathrm{d}\theta^i \mathbf{G}_i \cdot \mathrm{d}\theta^k \mathbf{G}_k = G_{ik}\,\mathrm{d}\theta^i\,\mathrm{d}\theta^k \tag{11.78}$$

and

$$(\mathrm{d}s)^2 = \mathrm{d}\mathbf{r} \cdot \mathrm{d}\mathbf{r} = \mathrm{d}\theta^i \mathbf{g}_i \cdot \mathrm{d}\theta^k \mathbf{g}_k = g_{ik}\,\mathrm{d}\theta^i\,\mathrm{d}\theta^k \tag{11.79}$$

where G_{ik} and g_{ik} are the covariant metric tensors referred to the undeformed and deformed configurations, respectively.

A strain tensor $\tilde{\gamma}_{ij}$ may be defined related to the change in length of the line element. Thus, subtracting (11.79) from (11.78), we obtain

$$\mathrm{d}s^2 - \mathrm{d}S^2 = (g_{ij} - G_{ij})\,\mathrm{d}\theta^i\,\mathrm{d}\theta^j = 2\tilde{\gamma}_{ij}\,\mathrm{d}\theta^i\,\mathrm{d}\theta^j \tag{11.80}$$

where

$$\tilde{\gamma}_{ij} = \tfrac{1}{2}(g_{ij} - G_{ij}) \tag{11.81}$$

is the strain tensor. The strain tensor thus defined may be viewed as a measure of the change of the metric tensor during deformation. When the body remains rigid, both the length of the line element and the metric tensor are unchanged, $\mathrm{d}s = \mathrm{d}S$ and $g_{ij} = G_{ij}$, the strain is then zero. The strain defined in (11.81) are covariant components. They together with the contravariant base vectors form two strain tensors as

$$\boldsymbol{\Gamma} = \tilde{\gamma}_{ij}\mathbf{G}^i \otimes \mathbf{G}^j \quad \text{and} \quad \boldsymbol{\gamma} = \tilde{\gamma}_{ij}\mathbf{g}^i \otimes \mathbf{g}^j \tag{11.82}$$

The tensor $\boldsymbol{\Gamma}$ is defined in the space of the undeformed state, and $\boldsymbol{\gamma}$ in the deformed space. These are two different tensors with the same covariant components. It is possible to define mixed and contravariant strain components by raising the indices of $\tilde{\gamma}_{ij}$ using g^{ij} and G^{ij} and using covariant base vectors $\mathbf{G}_i$ and $\mathbf{g}_i$. However, no clear physical meaning can be found relating these strain components to the convected material element and, therefore, they will not be further discussed.

We now investigate the physical meaning of the covariant strain $\tilde{\gamma}_{ij}$. We will show that the diagonal terms $\tilde{\gamma}_{11}$, $\tilde{\gamma}_{22}$, and $\tilde{\gamma}_{33}$ determine the extensions of the line elements along the coordinate curves, and the off-diagonal terms $\tilde{\gamma}_{12}$, $\tilde{\gamma}_{23}$, and $\tilde{\gamma}_{31}$ are related to the angle changes between line elements along two different coordinate curves. These properties of $\tilde{\gamma}_{ij}$ indicate that $\tilde{\gamma}_{ij}$ is a reasonable definition of strain.

The relative elongation along curvilinear coordinate curves is defined by

$$\varepsilon_{(\mathrm{i})} = \frac{\mathrm{d}s_i - \mathrm{d}S_i}{\mathrm{d}S_i} \qquad (i \text{ not summed}) \tag{11.83}$$

A line element lying along coordinate axis θ^1 may be written as

$$\mathrm{d}\mathbf{r}_{(1)} = \frac{\partial \mathbf{r}}{\partial \theta^k}\mathrm{d}\theta^k = \mathrm{d}\theta^1\mathbf{g}_1 \quad \text{with } \mathrm{d}s_{(1)} = \sqrt{g_{11}}\,\mathrm{d}\theta^1 \tag{11.84}$$

Similarly, along the other two coordinate axes, we have

$$\mathrm{d}s_{(2)} = \sqrt{g_{22}}\,\mathrm{d}\theta^2 \quad \text{and} \quad \mathrm{d}s_{(3)} = \sqrt{g_{33}}\,\mathrm{d}\theta^3 \tag{11.85}$$

Substituting (11.84) and (11.85) into (11.83), we obtain

$$\varepsilon_{(i)} = \frac{\sqrt{\mathbf{g}_{ii}} - \sqrt{G_{ii}}}{\sqrt{\mathbf{G}_{ii}}} = \sqrt{\frac{\mathbf{g}_{ii}}{\mathbf{G}_{ii}}} - 1 = \sqrt{1 + \frac{2\tilde{\gamma}_{ii}}{\mathbf{G}_{ii}}} - 1 \qquad (i \text{ not summed}) \quad (11.86)$$

It is seen from (11.86) that $\tilde{\gamma}_{11}$ is related to relative elongation $\varepsilon_{(1)}$, $\tilde{\gamma}_{22}$ is related to relative elongation $\varepsilon_{(2)}$, and $\tilde{\gamma}_{33}$ is related to relative elongation $\varepsilon_{(3)}$.

If ϕ_{ij} is the angle between line elements $\mathrm{d}\mathbf{r}_{(i)}$ and $\mathrm{d}\mathbf{r}_{(j)}$ in N_t, then the scalar product between these vectors is

$$\cos\phi_{ij} = \frac{\mathrm{d}\mathbf{r}_{(i)} \cdot \mathrm{d}\mathbf{r}_{(j)}}{\mathrm{d}\mathbf{s}_{(i)}\mathrm{d}\mathbf{s}_{(j)}} = \frac{\mathbf{g}_{ij}}{\sqrt{\mathbf{g}_{ii}\mathbf{g}_{jj}}} = \frac{\mathbf{G}_{ij} + 2\tilde{\gamma}_{ij}}{\sqrt{(\mathbf{G}_{ii} + 2\tilde{\gamma}_{ii})(\mathbf{G}_{jj} + 2\tilde{\gamma}_{jj})}}$$
$$(i,\ j \text{ not summed},\ i \neq j) \quad (11.87)$$

Note that (11.81), (1.84), and (11.85) were used in the derivation of (11.87). Equation (11.87) shows that $\tilde{\gamma}_{13}$, $\tilde{\gamma}_{23}$, and $\tilde{\gamma}_{12}$ are related to angle changes ϕ_{13}, ϕ_{23}, and ϕ_{12}, respectively.

11.8 Strain–Displacement Relations

The position vectors of points P and p and the displacement vector from P to p denoted by $\mathbf{u}$ are related by (11.70). Rewrite the equation as

$$\mathbf{r} = \mathbf{R} + \mathbf{u} \quad (11.88)$$

we can then differentiate it with respect to the curvilinear coordinates θ^i to obtain

$$\mathbf{g}_i = \frac{\partial \mathbf{r}}{\partial \theta^i} = \frac{\partial \mathbf{R}}{\partial \theta^i} + \frac{\partial \mathbf{u}}{\partial \theta^i} = \mathbf{G}_i + \frac{\partial \mathbf{u}}{\partial \theta^i} \quad (11.89)$$

The metric tensor may then be found as

$$g_{ij} = \mathbf{g}_i \cdot \mathbf{g}_j = \left(\mathbf{G}_i + \frac{\partial \mathbf{u}}{\partial \theta^i}\right) \cdot \left(\mathbf{G}_j + \frac{\partial \mathbf{u}}{\partial \theta^j}\right)$$
$$= G_{ij} + \mathbf{G}_i \cdot \frac{\partial \mathbf{u}}{\partial \theta^j} + \mathbf{G}_j \cdot \frac{\partial \mathbf{u}}{\partial \theta^i} + \frac{\partial \mathbf{u}}{\partial \theta^i} \cdot \frac{\partial \mathbf{u}}{\partial \theta^j} \quad (11.90)$$

Substituting (11.90) into (11.81), the covariant strain components can be found to be

$$\tilde{\gamma}_{ij} = \frac{1}{2}\left(\mathbf{G}_i \cdot \frac{\partial \mathbf{u}}{\partial \theta^j} + \mathbf{G}_j \cdot \frac{\partial \mathbf{u}}{\partial \theta^i} + \frac{\partial \mathbf{u}}{\partial \theta^i} \cdot \frac{\partial \mathbf{u}}{\partial \theta^j}\right) \quad (11.91)$$

The derivative of a vector with respect to θ^i was discussed in Section 11.6.2. Applying (11.58), (11.91) becomes

$$\begin{aligned}\tilde{\gamma}_{ij} &= \tfrac{1}{2}(\mathbf{G}_i \cdot \tilde{U}_m|_j^0\, \mathbf{G}^m + \mathbf{G}_j \cdot \tilde{U}_m|_i^0\, \mathbf{G}^m + \tilde{U}_m|_i^0\, \mathbf{G}^m \cdot \tilde{U}_n|_j^0\, \mathbf{G}^n) \\ &= \tfrac{1}{2}(\tilde{U}_i|_j^0 + \tilde{U}_j|_i^0 + \tilde{U}_m|_i^0\, \tilde{U}_n|_j^0\, g^{mn}) \end{aligned} \tag{11.92}$$

Therefore,

$$\tilde{\gamma}_{ij} = \tfrac{1}{2}(\tilde{U}_i|_j^0 + \tilde{U}_j|_i^0 + \tilde{U}^m|_i^0\, \tilde{U}_m|_j^0) \tag{11.93}$$

In this strain–displacement relation, the strain is expressed in terms of displacement components referred to $\mathbf{G}_i$ and $\mathbf{G}^i$ in the undeformed configuration, that is, $\mathbf{u} = \tilde{U}^i \mathbf{G}_i = \tilde{U}_i \mathbf{G}^i$. The covariant derivatives are from (11.59) and (11.60) given by

$$\tilde{U}^j|_i^0 = \frac{\partial \tilde{U}^j}{\partial \theta^i} + {}_0\,\Gamma_{ki}^j \tilde{U}^k \quad \text{and} \quad \tilde{U}_j|_i^0 = \frac{\partial \tilde{U}_j}{\partial \theta^i} - {}_0\,\Gamma_{ji}^k \tilde{U}_k \tag{11.94}$$

in which ${}_0\Gamma_{ji}^k$ is calculated in the undeformed configuration, such that

$${}_0\Gamma_{ij}^k = G^{km}\, {}_0\Gamma_{ijm} \quad \text{and} \quad {}_0\Gamma_{ijk} = \frac{1}{2}\left(\frac{\partial G_{ik}}{\partial \theta^j} + \frac{\partial G_{jk}}{\partial \theta^i} - \frac{\partial G_{ij}}{\partial \theta^k}\right) \tag{11.95}$$

Similarly, we may also express the strain–displacement relation in the deformed configuration and referring the displacement vector to $\mathbf{g}_i$ and $\mathbf{g}^i$, so that $\mathbf{u} = \tilde{u}^i \mathbf{g}_i = \tilde{u}_i \mathbf{g}^i$. In this case, we rewrite (11.70) as

$$\mathbf{R} = \mathbf{r} - \mathbf{u} \tag{11.96}$$

Differentiating this equation with respect to θ^i, we then find

$$G_{ij} = \mathbf{G}_i \cdot \mathbf{G}_j = g_{ij} - \mathbf{g}_i \cdot \frac{\partial \mathbf{u}}{\partial \theta^j} - \mathbf{g}_j \cdot \frac{\partial \mathbf{u}}{\partial \theta^i} + \frac{\partial \mathbf{u}}{\partial \theta^i} \cdot \frac{\partial \mathbf{u}}{\partial \theta^j} \tag{11.97}$$

Combining (11.97) with (11.81), we find

$$\tilde{\gamma}_{ij} = \frac{1}{2}\left(\mathbf{g}_i \cdot \frac{\partial \mathbf{u}}{\partial \theta^j} + \mathbf{g}_j \cdot \frac{\partial \mathbf{u}}{\partial \theta^i} - \frac{\partial \mathbf{u}}{\partial \theta^i} \cdot \frac{\partial \mathbf{u}}{\partial \theta^j}\right) \tag{11.98}$$

Using the equations for covariant derivatives, (11.59) and (11.60), equation (11.98) reduces to

$$\tilde{\gamma}_{ij} = \tfrac{1}{2}(\tilde{u}_i|_j + \tilde{u}_j|_i - \tilde{u}^m|_i\, \tilde{u}_m|_j) \tag{11.99}$$

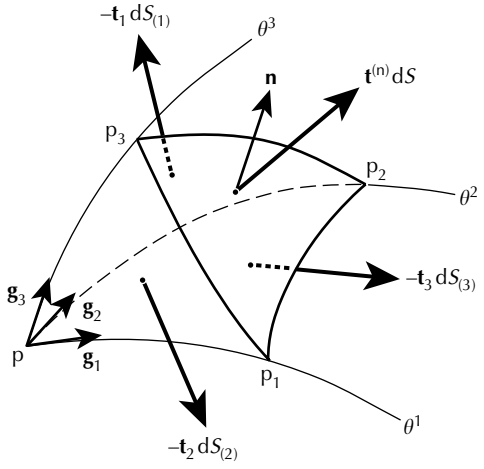

FIGURE 11.8
Convected material element cut by a plane with normal **n**.

The covariant derivatives $\tilde{u}_i|_j$ and $\tilde{u}^m|_i$ are given by (11.59) and (11.60) and the Christoffel symbols by (11.49) and (11.50) in the deformed configuration. Note that $\tilde{\gamma}_{ij}$ is the same strain as in (11.93), but the displacement components are now referred to the deformed configuration.

If the convected coordinates are Cartesian at the undeformed state, that is, $\theta^i = X_i$, then (11.81) and (11.93) reduce to

$$E_{ij} = \frac{1}{2}(g_{ij} - \delta_{ij}) = \frac{1}{2}\left(\frac{\partial U_i}{\partial X_j} + \frac{\partial U_j}{\partial X_i} + \frac{\partial U_m}{\partial X_i}\frac{\partial U_m}{\partial X_j}\right) \tag{11.100}$$

where $U_i = \tilde{U}_i$ are the Cartesian components of $\mathbf{u}$. The Lagrangian strain E_{ij} was previously discussed in Chapter 3. On the other hand, if, in the deformed configuration, the convected coordinates are Cartesian, then $\theta^i = x_i$, and the covariant strain, referred to (11.99), becomes

$$e_{ij} = \frac{1}{2}(\delta_{ij} - G_{ij}) = \frac{1}{2}\left(\frac{\partial u_i}{\partial x_j} + \frac{\partial u_j}{\partial x_i} - \frac{\partial u_m}{\partial x_i}\frac{\partial u_m}{\partial x_j}\right) \tag{11.101}$$

where $u_i = \tilde{u}_i$ refer to Cartesian coordinates at the deformed configuration. The strain e_{ij} is known as the Eulerian strain and was also discussed in Chapter 3. Note that the two strains in (11.100) and (11.101) are not equal. In (11.100), a square element is deformed into a parallelogram and, in (11.101), a parallelogram is deformed into a square element. The two expressions of strain do not refer to the same material element.

11.9 Stress Vector and Stress Tensor

We now define the stress vector and the stress tensor for the convected material element in the deformed configuration. Figure 11.8 shows the convected material element cut by a plane with a unit normal $\mathbf{n}$. This plane and the curvilinear coordinate planes form an infinitesimal tetrahedron whose edges are the coordinate curves. We denote the area of triangle $\Delta p_1p_2p_3$ by dS with an outward unit normal $\mathbf{n}$; denote the area of Δpp_2p_3 by $dS_{(1)}$ with unit outward normal $\mathbf{n}_{(1)}$; denote the area of Δpp_3p_1 by $dS_{(2)}$ with unit outward normal $\mathbf{n}_{(2)}$; and denote the area of Δpp_1p_2 by $dS_{(3)}$ with unit outward normal $\mathbf{n}_{(3)}$. Due to the closure of the surface of the tetrahedron, the vectorial sum of all faces expressed by vectors is zero. Therefore, we may write

$$\mathbf{n}\,dS + \mathbf{n}_{(1)}\,dS_{(1)} + \mathbf{n}_{(2)}\,dS_{(2)} + \mathbf{n}_{(3)}\,dS_{(3)} = 0 \tag{11.102}$$

Let us consider the unit normals $\mathbf{n}_{(1)}$, $\mathbf{n}_{(2)}$, and $\mathbf{n}_{(3)}$. Take $\mathbf{n}_{(3)}$, for example. This is the outward normal of Δpp_1p_2, and this triangle is represented by $\frac{1}{2}d\mathbf{r}_{(2)} \times d\mathbf{r}_{(1)}$. The line elements of this triangle are

$$\overrightarrow{pp_1} = d\mathbf{r}_{(1)} = d\theta^1\mathbf{g}_1 \quad \text{and} \quad \overrightarrow{pp_2} = d\mathbf{r}_{(2)} = d\theta^2\mathbf{g}_2 \tag{11.103}$$

Thus,

$$\begin{aligned}\Delta pp_1p_2 &= \frac{1}{2}d\mathbf{r}_{(2)} \times d\mathbf{r}_{(1)} = \frac{1}{2}\mathbf{g}_2 \times \mathbf{g}_1\,d\theta^1\,d\theta^2 = -\frac{1}{2}\varepsilon_{123}\mathbf{g}^3\,d\theta^1\,d\theta^2 \\ &= -\frac{1}{2}\varepsilon_{123}\sqrt{g^{33}}\frac{\mathbf{g}^3}{\sqrt{g^{33}}}d\theta^1\,d\theta^2\end{aligned} \tag{11.104}$$

It is seen from (11.104) that

$$\mathbf{n}_{(3)} = -\frac{\mathbf{g}^3}{\sqrt{g^{33}}} \quad \text{and} \quad d\mathbf{S}_{(3)} = \frac{1}{2}\varepsilon_{123}\sqrt{g^{33}}\,d\theta^1\,d\theta^2 \tag{11.105}$$

Similarly, we can obtain

$$\mathbf{n}_{(1)} = -\frac{\mathbf{g}^1}{\sqrt{g^{11}}} \quad \text{and} \quad \mathbf{n}_{(2)} = -\frac{\mathbf{g}^2}{\sqrt{g^{22}}} \tag{11.106}$$

Substituting (11.105) and (11.106) into (11.102), we then find

$$\tilde{n}_i\mathbf{g}^i\,dS = \sum_{i=1}^{3}\frac{dS_{(i)}}{\sqrt{g^{ii}}}\mathbf{g}^i \tag{11.107}$$

By equating the coefficients of $\mathbf{g}^i$ on both sides of (11.107), we obtain the following equation relating the areas of different faces of the tetrahedron

$$\tilde{n}_i \sqrt{g^{ii}} \mathrm{d}S = \mathrm{d}S_{(i)} \qquad (i \text{ not summed}) \tag{11.108}$$

We now consider forces acting on the surfaces of the infinitesimal tetrahedron. The stress vector (force per unit area) acting on $\Delta \mathrm{p}_1\mathrm{p}_2\mathrm{p}_3$ is $\mathbf{t}^{(n)}$, the stress vector acting on $\Delta \mathrm{pp}_3\mathrm{p}_2$ is $-\mathbf{t}_{(1)}$, that acting on $\Delta \mathrm{pp}_1\mathrm{p}_3$ is $-\mathbf{t}_{(2)}$, and that on $\Delta \mathrm{pp}_2\mathrm{p}_1$ is $-\mathbf{t}_{(3)}$. The negative signs are related to the normals of the surfaces pointing to the negative directions, as seen from (11.105) and (11.106). Considering the equations of motion of the tetrahedron and realizing that the body forces and inertia forces are of a higher order of smallness compared to the surface traction, we obtain

$$\mathbf{t}^{(n)} \, \mathrm{d}S = \mathbf{t}_{(i)} \, \mathrm{d}S_{(i)} \tag{11.109}$$

Substituting (11.108) into (11.109), we have

$$\mathbf{t}^{(n)} = \sum_{i=1}^{3} \tilde{n}_i \mathbf{t}_{(i)} \sqrt{g^{ii}} \tag{11.110}$$

This equation relates the stress vectors acting on the surfaces of the tetrahedron.

We now define a stress tensor denoted by $\boldsymbol{\tau}$, which is known as the *true stress*. In (2.8), we defined a stress tensor based on the stress vector and the unit normal of the inclined surface of the tetrahedron. We now rewrite this relationship using stress tensor $\boldsymbol{\tau}$ as

$$\mathbf{t}^{(n)} = \mathbf{n} \cdot \boldsymbol{\tau} \tag{11.111}$$

Comparing (11.110) with (11.111), we see that if we define stress tensors based on $\mathbf{t}_{(i)} \sqrt{g^{ii}}$, then we would be able to put (11.110) in the form of (11.111). The quantity $\mathbf{t}_{(i)} \sqrt{g^{ii}}$ represents the stress vector multiplied by a factor $\sqrt{g^{ii}}$ and it has a contravariant type of property because, when multiplied by the area, it is a force acting on a surface defined by covariant bases $\mathbf{g}_i$. On the other hand, a force acting on a surface defined by contravariant bases $\mathbf{g}^i$ has a covariant property. In addition, we note that this quantity forms an invariant with the covariant $\tilde{n}_i$ in (11.110), and, therefore, it has a contravariant type of property.

Decomposing $\mathbf{t}_{(i)} \sqrt{g^{ii}}$ into the directions of the base vectors, we can write

$$\mathbf{t}_{(i)} \sqrt{g^{ii}} = \tau^{ij} \mathbf{g}_j = \tau^i_j \mathbf{g}^j \tag{11.112}$$

in which τ^{ij} and τ^i_j are contravariant and mixed components of the stress tensor $\boldsymbol{\tau}$, respectively. These are true stresses defined on the convected

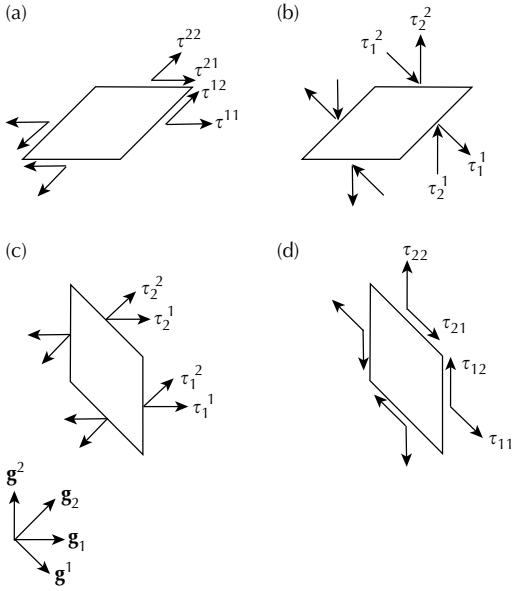

FIGURE 11.9
Stress components: (a) τ^{ij}, (b) τ^i_j, (c) τ^i_j, and (d) τ_{ij}.

material element at the deformed configuration. The stress components τ^{ij} and τ^i_j are shown in Figure 11.9(a) and (b), respectively. On the other hand, mixed and covariant stress components τ^i_j and τ_{ij} may be defined based on an element formed by the contravariant bases. They are shown in Figure 11.9(c) and (d). These stress components are not useful in the study of plasticity because they do not refer to the convected material element.

We now write the true stress in the following form:

$$\boldsymbol{\tau} = \tau^{ij}\mathbf{g}_i \otimes \mathbf{g}_j = \tau^i_j \mathbf{g}_i \otimes \mathbf{g}^j \tag{11.113}$$

Substituting the first equality of (11.113) into (11.111), we have

$$\tilde{t}^{(n)j}\mathbf{g}_j = \tilde{n}_j \mathbf{g}^j \cdot \tau^{rs}\mathbf{g}_r \otimes \mathbf{g}_s = \tilde{n}_j \tau^{rs}\mathbf{g}^j \cdot \mathbf{g}_r \otimes \mathbf{g}_s = \tilde{n}_j \tau^{rs}\delta^j_r \mathbf{g}_s = \tilde{n}_i \tau^{ij}\mathbf{g}_j \tag{11.114}$$

Thus, we obtain

$$\tilde{t}^{(n)j} = \tilde{n}_i \tau^{ij} \tag{11.115}$$

If we substitute the second equality of (11.113) into (11.111), then we can obtain

$$\tilde{t}^{(n)}_j \mathbf{g}^j = \tilde{n}_j \mathbf{g}^j \cdot \tau^r_s \mathbf{g}_r \otimes \mathbf{g}^s = \tilde{n}_j \tau^r_s \delta^j_r \mathbf{g}^s = \tilde{n}_i \tau^i_j \mathbf{g}^j \tag{11.116}$$

Therefore,

$$\tilde{t}_j^{(n)} = \tilde{n}_i \tau_j^i \tag{11.117}$$

Equations (11.115) and (11.117) relate the stress tensor components to the components of the stress vector.

11.10 Physical Components of the Stress Tensor

We discussed the physical components of a vector in Section 11.5 and we now discuss the physical components of the stress tensor $\boldsymbol{\tau}$, which is represented in (11.113) by its components and base vectors. In the curvilinear coordinate system, the base vectors are generally not unit vectors and they are not dimensionless, and not all the tensor components τ^{ij} and τ_j^i have the dimension of stress. We now replace the base vectors of the first equality of (11.113) by their corresponding unit vectors as

$$\boldsymbol{\tau} = \sum_{i,j} \tau^{ij} \sqrt{g_{ii}} \sqrt{g_{jj}} \frac{\mathbf{g}_i}{\sqrt{g_{ii}}} \otimes \frac{\mathbf{g}_j}{\sqrt{g_{jj}}} = \tau^{\langle ij \rangle} \mathbf{e}_i \otimes \mathbf{e}_j \tag{11.118}$$

Thus, the physical components of τ^{ij} may be defined as

$$\tau^{\langle ij \rangle} = \tau^{ij} \sqrt{g_{ii}} \sqrt{g_{jj}} \tag{11.119}$$

All physical components $\tau^{\langle ij \rangle}$ have the dimension of stress. On the other hand, the physical components of τ^{ij} may also be defined using (11.112). We note that $\mathbf{t}_{(i)} \sqrt{g^{ii}}$ is not the stress vector, but $\mathbf{t}_{(i)}$ is, and $\mathbf{t}_{(i)}$ instead of $\mathbf{t}_{(i)} \sqrt{g^{ii}}$ has the unit of force per unit area. Thus, we can rewrite (11.112) as

$$\mathbf{t}_{(\mathrm{i})} = \sum_{j=1}^{3} \frac{\tau^{ij} \mathbf{g}_j}{\sqrt{g^{ii}}} = \sum_{j=1}^{3} \sqrt{\frac{g_{jj}}{g^{ii}}} \tau^{ij} \frac{\mathbf{g}_j}{\sqrt{g_{jj}}} = \sum_{j=1}^{3} \tau^{\langle ij \rangle} \mathbf{e}_j \qquad (i \text{ not summed}) \tag{11.120}$$

Therefore, we may define the physical components of τ^{ij} as

$$\tau^{\langle ij \rangle} = \sqrt{\frac{g_{jj}}{g^{ii}}} \tau^{ij} \tag{11.121}$$

which has the unit of force per unit area. Equations (11.121) and (11.119) are the same for orthogonal coordinates, because, in this case, $\sqrt{g_{ii}} = 1/\sqrt{g^{ii}}$. But, they are not the same in general and the definition of (11.121) conforms to the expectation that $\mathbf{t}_{(i)}$ is a stress vector whereas the definition of (11.119) does

not say anything about $\mathbf{t}_{(i)}$. In a similar way, the second equality of (11.112) leads to

$$\tau^{\langle i\rangle}_{\langle m\rangle} = \sqrt{\frac{g_{mm}}{g^{ii}}}\, g^{jm}\tau^{i}_{j} = \sqrt{\frac{g_{mm}}{g^{ii}}}\,\tau^{im} \tag{11.122}$$

If orthogonal,

$$\tau^{\langle i\rangle}_{\langle m\rangle} = \sqrt{g_{mm}g_{ii}}\,\tau^{im} \tag{11.123}$$

Finally, we note that the physical components are not components of a tensor and they do not follow the tensor transformation rules.

11.11 Other Stress Tensors and the Cartesian Stress Components

Some commonly used stress tensors are the true stress $\boldsymbol{\tau}$, the Kirchhoff stress $\mathbf{S}$, and the second Piola–Kirchhoff stress (or simply the 2nd P–K stress) Π. The true stress was discussed in Section 11.9 and is expressed in the tensor form in (11.113). The Kirchhoff stress is defined by

$$\mathbf{S} = J\boldsymbol{\tau} = J\tau^{ij}\mathbf{g}_i \otimes \mathbf{g}_j = \tilde{S}^{ij}\mathbf{g}_i \otimes \mathbf{g}_j \tag{11.124}$$

with

$$\tilde{S}^{ij} = J\tau^{ij} \quad \text{and} \quad J = \rho_0/\rho \tag{11.125}$$

where J is the Jacobian of transformation representing deformation, ρ_0 is the density of the undeformed continuum, and ρ is the density of the deformed continuum. The 2nd P–K stress is defined by

$$\boldsymbol{\Pi} = \mathbf{F}^{-1}\cdot\mathbf{S}\cdot\mathbf{F}^{-\mathrm{T}} = \tilde{S}^{ij}\mathbf{G}_i \otimes \mathbf{G}_j = \tilde{\Pi}^{ij}\mathbf{G}_i \otimes \mathbf{G}_j \tag{11.126}$$

where $\mathbf{F}$ is the deformation gradient and its expression in the convected coordinate system is now discussed. The deformation gradient $\mathbf{F}$ transforms the undeformed line element $\mathrm{d}\mathbf{R}$ into the deformed line element $\mathrm{d}\mathbf{r}$ and they are related by

$$\mathrm{d}\mathbf{r} = \mathbf{F}\cdot\mathrm{d}\mathbf{R} \tag{11.127}$$

Using (11.76), $\mathbf{F}$ transforms $\mathbf{G}_i$ into $\mathbf{g}_i$, that is,

$$\mathbf{g}_i = \mathbf{F}\cdot\mathbf{G}_i \tag{11.128}$$

Using (11.68), (11.69), and (11.76), (11.127) may be further written as

$$\mathrm{d}\mathbf{r} = \mathrm{d}x_i\mathbf{e}_i = \frac{\partial x_i}{\partial \theta^j}\mathrm{d}\theta^j\mathbf{e}_i = \mathrm{d}\theta^j\mathbf{g}_j = (\mathrm{d}\mathbf{R}\cdot\mathbf{G}^j)\mathbf{g}_j = \mathbf{g}_j(\mathbf{G}^j\cdot\mathrm{d}\mathbf{R}) = (\mathbf{g}_j\otimes\mathbf{G}^j)\cdot\mathrm{d}\mathbf{R} \tag{11.129}$$

Comparing (11.129) with (11.127), we see that

$$\mathbf{F} = \mathbf{g}_j\otimes\mathbf{G}^j \tag{11.130}$$

The expressions for the inverse and transpose of $\mathbf{F}$ may be found using (11.128) and (11.130). We use the notations $\mathbf{F}^{-\mathrm{T}} = (\mathbf{F}^{\mathrm{T}})^{-1} = (\mathbf{F}^{-1})^{\mathrm{T}}$ for simplicity. They are

$$\begin{aligned}
&\mathbf{G}_i = \mathbf{F}^{-1}\cdot\mathbf{g}_i \qquad &&\text{with } \mathbf{F}^{-1} = \mathbf{G}_i\otimes\mathbf{g}^i\\
&\mathbf{G}^i = \mathbf{F}^{\mathrm{T}}\cdot\mathbf{g}^i \qquad &&\text{with } \mathbf{F}^{\mathrm{T}} = \mathbf{G}^i\otimes\mathbf{g}_i\\
&\mathbf{g}^i = \mathbf{F}^{-\mathrm{T}}\cdot\mathbf{G}^i \qquad &&\text{with } \mathbf{F}^{-\mathrm{T}} = \mathbf{g}^i\otimes\mathbf{G}_i
\end{aligned} \tag{11.131}$$

From (11.130) and (11.131), we see that the matrices of $\mathbf{F}$, $\mathbf{F}^{-1}$, $\mathbf{F}^{\mathrm{T}}$, and $\mathbf{F}^{-\mathrm{T}}$ are all unit matrices when referred to the covariant and contravariant base vectors of the convected coordinate system in the undeformed and deformed configurations.

We now substitute (11.131) into (11.126),

$$\begin{aligned}
\boldsymbol{\Pi} &= \mathbf{F}^{-1}\cdot\mathbf{S}\cdot\mathbf{F}^{-\mathrm{T}} = (\mathbf{G}_i\otimes\mathbf{g}^i)\cdot(\tilde{S}^{mn}\mathbf{g}_m\otimes\mathbf{g}_n)\cdot(\mathbf{g}^j\otimes\mathbf{G}_j)\\
&= \tilde{S}^{mn}(\mathbf{g}^i\cdot\mathbf{g}_m)(\mathbf{G}_i\otimes\mathbf{g}_n)\cdot(\mathbf{g}^j\otimes\mathbf{G}_j) = \tilde{S}^{mn}\delta^i_m(\mathbf{g}_n\cdot\mathbf{g}^j)(\mathbf{G}_i\otimes\mathbf{G}_j)\\
&= \tilde{S}^{mn}\delta^i_m\delta^j_n(\mathbf{G}_i\otimes\mathbf{G}_j) = \tilde{S}^{ij}(\mathbf{G}_i\otimes\mathbf{G}_j)
\end{aligned} \tag{11.132}$$

We see that (11.132) is the same as (11.126). By comparing (11.124) with (11.126), we conclude that the Kirchhoff stress and the 2nd P–K stress have the same components $\tilde{S}^{ij}$ but with different bases. The Kirchhoff stress refers to the bases of the deformed configuration, while the 2nd P–K stress refers to the undeformed configuration.

We now determine the components of the true stress σ^{ij}, the Kirchhoff stress S^{ij}, and the 2nd P–K stress Π^{ij} with respect to the Cartesian coordinate system. In the case of true stress, we write

$$\boldsymbol{\tau} = \tau^{ij}\mathbf{g}_i\otimes\mathbf{g}_j = \sigma^{ij}\mathbf{e}_i\otimes\mathbf{e}_j \tag{11.133}$$

Note that $\sigma^{ij} = \sigma_{ij}$ is the Cauchy stress. Applying (11.9), we can find from (11.133) that

$$\tau^{ij} = \frac{\partial\theta^i}{\partial x_p}\frac{\partial\theta^j}{\partial x_q}\sigma^{pq} \quad\text{and}\quad \sigma^{ij} = \frac{\partial x_i}{\partial\theta^p}\frac{\partial x_j}{\partial\theta^q}\tau^{pq} \tag{11.134}$$

The components τ^{ij} refer to the convected material element in the deformed configuration as shown in Figure 11.9(a). These components are transformed into σ^{ij} using (11.134). The components σ^{ij} are defined on an imaginary square element based on the Cartesian coordinate system. The Cartesian components of the Kirchhoff stress are related to σ^{ij} by

$$S^{ij} = J\sigma^{ij} \tag{11.135}$$

This relationship may be shown as

$$\mathbf{S} = J\boldsymbol{\tau} = J\tau^{ij}\mathbf{g}_i \otimes \mathbf{g}_j = J\tau^{ij}\frac{\partial x_r}{\partial \theta^i}\frac{\partial x_s}{\partial \theta^j}\mathbf{e}_r \otimes \mathbf{e}_s = J\sigma^{rs}\mathbf{e}_r \otimes \mathbf{e}_s = S^{rs}\mathbf{e}_r \otimes \mathbf{e}_s \tag{11.136}$$

which leads to (11.135). In addition, we find

$$\tilde{S}^{ij} = \frac{\partial \theta^i}{\partial x_r}\frac{\partial \theta^j}{\partial x_s}S^{rs} \quad \text{and} \quad S^{ij} = \frac{\partial x_i}{\partial \theta^r}\frac{\partial x_j}{\partial \theta^s}\tilde{S}^{rs} \tag{11.137}$$

Using (11.77), (11.132) may be written as

$$\begin{aligned}\boldsymbol{\Pi} &= \tilde{S}^{ij}(\mathbf{G}_i \otimes \mathbf{G}_j) = \tilde{S}^{ij}\frac{\partial X_r}{\partial \theta^i}\mathbf{e}_r \otimes \frac{\partial X_s}{\partial \theta^j}\mathbf{e}_s = \tilde{S}^{ij}\frac{\partial X_r}{\partial \theta^i}\frac{\partial X_s}{\partial \theta^j}\mathbf{e}_r \otimes \mathbf{e}_s \\ &= \frac{\partial \theta^i}{\partial x_m}\frac{\partial \theta^j}{\partial x_n}S^{mn}\frac{\partial X_r}{\partial \theta^i}\frac{\partial X_s}{\partial \theta^j}\mathbf{e}_r \otimes \mathbf{e}_s = \frac{\partial X_r}{\partial x_m}\frac{\partial X_s}{\partial x_n}S^{mn}\mathbf{e}_r \otimes \mathbf{e}_s \\ &= \Pi^{rs}\mathbf{e}_r \otimes \mathbf{e}_s\end{aligned} \tag{11.138}$$

We found from the last two expressions of (11.138) that

$$\Pi^{ij} = \frac{\partial X_i}{\partial x_m}\frac{\partial X_j}{\partial x_n}S^{mn} = J\frac{\partial X_i}{\partial x_m}\frac{\partial X_j}{\partial x_n}\sigma^{mn} \tag{11.139}$$

Note that in (11.139), σ^{ij}, S^{ij}, and Π^{ij} are all Cartesian components.

11.12 Stress Rate and Strain Rate

The contravariant true stresses τ^{ij} are defined with respect to a convected material element. Since $\mathbf{g}_i$ are marked on the convected material element and τ^{ij} refers to $\mathbf{g}_i$, the components of τ^{ij} are invariant with respect to the orientation of an observer. The material rate of change $\mathrm{D}\tau^{ij}/\mathrm{D}t$, denoted by $\dot{\tau}^{ij}$ for simplicity, also remains invariant with respect to the orientation of an observer. Equation (11.134) transforms τ^{ij} into the Cauchy stress σ^{ij} referred to

the Cartesian coordinate system. We would like to find a stress-rate tensor $\dot{\boldsymbol{\tau}}^{(1)}$ with components $\dot{\tau}^{ij}$ that transform according to the same rule of transformation as in (11.134) into a convected stress rate σ^{*ij} in the Cartesian coordinate system. We write

$$\dot{\boldsymbol{\tau}}^{(1)} = \dot{\tau}^{ij}\mathbf{g}_i \otimes \mathbf{g}_j = \sigma^{*ij}\mathbf{e}_i \otimes \mathbf{e}_j \tag{11.140}$$

We note that tensor $\dot{\boldsymbol{\tau}}^{(1)}$ is only a part of tensor $\dot{\boldsymbol{\tau}}$ and this point will be further discussed in Section 11.13. To find the relationship that transforms $\dot{\tau}^{ij}$ into σ^{*ij}, let us differentiate the second equation of (11.134) and obtain

$$\begin{aligned}
\dot{\sigma}^{ij} &= \frac{\partial x_i}{\partial \theta^p}\frac{\partial x_j}{\partial \theta^q}\dot{\tau}^{pq} + \frac{\partial v_i}{\partial \theta^p}\frac{\partial x_j}{\partial \theta^q}\tau^{pq} + \frac{\partial x_i}{\partial \theta^p}\frac{\partial v_j}{\partial \theta^q}\tau^{pq} \\
&= \frac{\partial x_i}{\partial \theta^p}\frac{\partial x_j}{\partial \theta^q}\dot{\tau}^{pq} + \frac{\partial v_i}{\partial x_k}\frac{\partial x_k}{\partial \theta^p}\frac{\partial x_j}{\partial \theta^q}\tau^{pq} + \frac{\partial x_i}{\partial \theta^p}\frac{\partial v_j}{\partial x_k}\frac{\partial x_k}{\partial \theta^q}\tau^{pq} \\
&= \frac{\partial x_i}{\partial \theta^p}\frac{\partial x_j}{\partial \theta^q}\dot{\tau}^{pq} + \frac{\partial v_i}{\partial x_k}\sigma^{kj} + \frac{\partial v_j}{\partial x_k}\sigma^{ik}
\end{aligned} \tag{11.141}$$

where v_i are Cartesian components of the particle velocity and are given by

$$v_i = \frac{\mathrm{D}u_i}{\mathrm{D}t} = \frac{\mathrm{D}(x_i - X_i)}{\mathrm{D}t} = \frac{\mathrm{D}x_i}{\mathrm{D}t} \tag{11.142}$$

Therefore, we write

$$\sigma^{*ij} = \dot{\sigma}^{ij} - \frac{\partial v_i}{\partial x_k}\sigma^{kj} - \frac{\partial v_j}{\partial x_k}\sigma^{ik} = \frac{\partial x_i}{\partial \theta^p}\frac{\partial x_j}{\partial \theta^q}\dot{\tau}^{pq} \tag{11.143}$$

It is seen from (11.143) that

$$\sigma^{*ij} = \frac{\partial x_i}{\partial \theta^p}\frac{\partial x_j}{\partial \theta^q}\dot{\tau}^{pq} \quad \text{and} \quad \dot{\tau}^{ij} = \frac{\partial \theta^i}{\partial x_p}\frac{\partial \theta^j}{\partial x_q}\sigma^{*pq} \tag{11.144}$$

The quantity σ^{*ij} is the rate of change of the contravariant true stress, $\dot{\tau}^{ij}$, projected onto the Cartesian spatial frame x_i, and it is known as the convected stress rate of τ^{ij}. The convected rates have been discussed in [6–8].

The covariant stress τ_{ij} are defined based on an element formed by contravariant bases as mentioned in Section 11.9 and they are shown in Figure 11.9(d). Even though they are not useful in the study of plasticity, the rate of change of τ_{ij} is considered for making an important point related to the Jaumann rate. In terms of the covariant stress components, the stress tensor may be written as

$$\boldsymbol{\tau} = \tau_{ij}\,\mathbf{g}^i \otimes \mathbf{g}^j = \sigma_{ij}\mathbf{e}_i \otimes \mathbf{e}_j \tag{11.145}$$

Applying (11.15), we can find from (11.145) that

$$\sigma_{ij} = \frac{\partial \theta^p}{\partial x_i}\frac{\partial \theta^q}{\partial x_j}\tau_{pq} \quad \text{or} \quad \tau_{ij} = \frac{\partial x_p}{\partial \theta^i}\frac{\partial x_q}{\partial \theta^j}\sigma_{pq} \tag{11.146}$$

Following (11.140), we write the stress rate as

$$\dot{\boldsymbol{\tau}}_{(1)} = \dot{\tau}_{ij}\,\mathbf{g}^i \otimes \mathbf{g}^j = \sigma^{\circ}_{ij}\mathbf{e}_i \otimes \mathbf{e}_j \tag{11.147}$$

Differentiating the second equation of (11.146), we obtain

$$\begin{aligned}\dot{\tau}_{ij} &= \frac{\partial x_p}{\partial \theta^i}\frac{\partial x_q}{\partial \theta^j}\dot{\sigma}_{pq} + \frac{\partial v_p}{\partial \theta^i}\frac{\partial x_q}{\partial \theta^j}\sigma_{pq} + \frac{\partial x_p}{\partial \theta^i}\frac{\partial v_q}{\partial \theta^j}\sigma_{pq} \\ &= \frac{\partial x_p}{\partial \theta^i}\frac{\partial x_q}{\partial \theta^j}\dot{\sigma}_{pq} + \frac{\partial v_p}{\partial x_k}\frac{\partial x_k}{\partial \theta^i}\frac{\partial x_q}{\partial \theta^j}\sigma_{pq} + \frac{\partial x_p}{\partial \theta^i}\frac{\partial v_q}{\partial x_k}\frac{\partial x_k}{\partial \theta^j}\sigma_{pq}\end{aligned} \tag{11.148}$$

Multiplying both sides of (11.148) by $(\partial\theta^i/\partial x_r)(\partial\theta^j/\partial x_s)$, we then obtain

$$\sigma^{\circ}_{ij} = \dot{\sigma}_{ij} + \frac{\partial v_p}{\partial x_i}\sigma_{pj} + \frac{\partial v_p}{\partial x_j}\sigma_{ip} = \frac{\partial \theta^p}{\partial x_i}\frac{\partial \theta^q}{\partial x_j}\dot{\tau}_{pq} \tag{11.149}$$

The quantity σ°_{ij} is the rate of change of the covariant true stress, τ_{ij}, projected onto the Cartesian spatial frame x_i, and it is known as the convected stress rate of τ_{ij}.

An interesting point to observe is that the Jaumann rate σ^{∇}_{ij} is the average of the two convected rates σ^{*ij} and σ°_{ij}, that is,

$$\begin{aligned}\sigma^{\nabla}_{ij} &= \frac{1}{2}(\sigma^{*}_{ij} + \sigma^{\circ}_{ij}) = \frac{1}{2}\left[\left(\dot{\sigma}_{ij} - \frac{\partial v_i}{\partial x_k}\sigma_{kj} - \frac{\partial v_j}{\partial x_k}\sigma_{ik}\right) + \left(\dot{\sigma}_{ij} + \frac{\partial v_p}{\partial x_i}\sigma_{pj} + \frac{\partial v_p}{\partial x_j}\sigma_{ip}\right)\right] \\ &= \dot{\sigma}_{ij} + \frac{1}{2}\left(\frac{\partial v_k}{\partial x_i} - \frac{\partial v_i}{\partial x_k}\right)\sigma_{kj} + \frac{1}{2}\left(\frac{\partial v_k}{\partial x_j} - \frac{\partial v_j}{\partial x_k}\right)\sigma_{ik} \\ &= \dot{\sigma}_{ij} + W_{ki}\sigma_{kj} + W_{kj}\sigma_{ik}\end{aligned} \tag{11.150}$$

where W_{ij} is the spin tensor. Both σ^{*ij} and σ°_{ij} have clear physical meanings: σ^{*ij} is defined based on the convected material element and σ°_{ij} is defined based on an element defined by the contravariant base vectors at the deformed state.

Since σ_{ij}^{∇} is the average of σ^{*ij} and σ_{ij}°, the physical meaning of σ_{ij}^{∇} is not clear. This observation was made in [7–9].

The strain rate may be found by differentiating (11.81) and we obtain

$$\frac{\mathrm{D}\tilde{\gamma}_{ij}}{\mathrm{D}t} = \frac{1}{2}\frac{\mathrm{D}g_{ij}}{\mathrm{D}t} \tag{11.151}$$

We then differentiate (11.25) to find

$$\begin{aligned}\frac{\mathrm{D}g_{ij}}{\mathrm{D}t} &= \frac{\partial x_m}{\partial \theta^i}\frac{\partial v_m}{\partial \theta^j} + \frac{\partial v_m}{\partial \theta^i}\frac{\partial x_m}{\partial \theta^j} \\ &= \frac{\partial x_m}{\partial \theta^i}\frac{\partial v_m}{\partial x_n}\frac{\partial x_n}{\partial \theta^j} + \frac{\partial v_m}{\partial x_n}\frac{\partial x_n}{\partial \theta^i}\frac{\partial x_m}{\partial \theta^j} = \frac{\partial x_m}{\partial \theta^i}\frac{\partial x_n}{\partial \theta^j}\left(\frac{\partial v_m}{\partial x_n} + \frac{\partial v_n}{\partial x_m}\right)\end{aligned} \tag{11.152}$$

From (11.151) and (11.152) we find that

$$\frac{\mathrm{D}\tilde{\gamma}_{ij}}{\mathrm{D}t} = \frac{1}{2}\frac{\mathrm{D}g_{ij}}{\mathrm{D}t} = \frac{\partial x_m}{\partial \theta^i}\frac{\partial x_n}{\partial \theta^j}D_{mn} \tag{11.153}$$

Equation (11.153) shows that the strain rate $\dot{\tilde{\gamma}}_{ij}$ is transformed into the rate of deformation D_{ij} in the Cartesian coordinate system. The transformation in (11.153) follows the covariant rule of transformation.

EXAMPLE 11.10 Show that the convected stress rate σ^{*ij} is objective.

Solution

In an observer transformation, let the second observer observe quantities denoted by an overhead bar, and the two observers are differed by their orientation, which is denoted by $\mathbf{Q}$. Note that $\mathbf{Q}$ is an arbitrary orthogonal tensor. The Cauchy stress transforms as

$$\bar{\boldsymbol{\sigma}} = \mathbf{Q}^{\mathrm{T}} \cdot \boldsymbol{\sigma} \cdot \mathbf{Q} \tag{a}$$

and its material differentiation gives

$$\dot{\bar{\boldsymbol{\sigma}}} = \mathbf{Q}^{\mathrm{T}} \cdot \dot{\boldsymbol{\sigma}} \cdot \mathbf{Q} + \dot{\mathbf{Q}}^{\mathrm{T}} \cdot \boldsymbol{\sigma} \cdot \mathbf{Q} + \mathbf{Q}^{\mathrm{T}} \cdot \boldsymbol{\sigma} \cdot \dot{\mathbf{Q}} \tag{b}$$

We now make use of the following equations, which were established in (4.96)

$$\bar{\mathbf{L}} = \mathbf{Q}^{\mathrm{T}} \cdot \mathbf{L} \cdot \mathbf{Q} + \dot{\mathbf{Q}}^{\mathrm{T}} \cdot \mathbf{Q} \quad \text{and} \quad \bar{\mathbf{L}}^{\mathrm{T}} = \mathbf{Q}^{\mathrm{T}} \cdot \mathbf{L}^{\mathrm{T}} \cdot \mathbf{Q} + \mathbf{Q}^{\mathrm{T}} \cdot \dot{\mathbf{Q}} \tag{c}$$

Using these equations, the convected stress rate σ^{*ij} can be calculated as

$$\begin{aligned}\bar{\sigma}^* &= \dot{\bar{\sigma}} - \bar{\mathbf{L}}\cdot\bar{\sigma} - \bar{\sigma}\cdot\bar{\mathbf{L}}^{\mathrm{T}} = \mathbf{Q}^{\mathrm{T}}\cdot\dot{\boldsymbol{\sigma}}\cdot\mathbf{Q} + \dot{\mathbf{Q}}^{\mathrm{T}}\cdot\boldsymbol{\sigma}\cdot\mathbf{Q} + \mathbf{Q}^{\mathrm{T}}\cdot\boldsymbol{\sigma}\cdot\dot{\mathbf{Q}} \\ &\quad - [\mathbf{Q}^{\mathrm{T}}\cdot\mathbf{L}\cdot\mathbf{Q} + \dot{\mathbf{Q}}^{\mathrm{T}}\cdot\mathbf{Q}]\cdot\mathbf{Q}^{\mathrm{T}}\cdot\boldsymbol{\sigma}\cdot\mathbf{Q} - \mathbf{Q}^{\mathrm{T}}\cdot\boldsymbol{\sigma}\cdot\mathbf{Q}\cdot[\mathbf{Q}^{\mathrm{T}}\cdot\mathbf{L}^{\mathrm{T}}\cdot\mathbf{Q} + \mathbf{Q}^{\mathrm{T}}\cdot\dot{\mathbf{Q}}] \\ &= \mathbf{Q}^{\mathrm{T}}\cdot[\dot{\boldsymbol{\sigma}} - \mathbf{L}\cdot\boldsymbol{\sigma} - \boldsymbol{\sigma}\cdot\mathbf{L}^{\mathrm{T}}]\cdot\mathbf{Q} = \mathbf{Q}^{\mathrm{T}}\cdot\boldsymbol{\sigma}^*\cdot\mathbf{Q} \end{aligned} \tag{d}$$

Therefore, the convected stress rate σ^{*ij} is objective.

EXAMPLE 11.11 Show that the contravariant stress τ^{ij} and the covariant strain $\tilde{\gamma}_{ij}$ are work conjugates.

Solution

In the curvilinear coordinate system, the rate of work per unit mass is

$$\dot{W} = \frac{1}{\rho}\tau^{ij}\dot{\tilde{\gamma}}_{ij} = \frac{1}{2\rho}\tau^{ij}\frac{\mathrm{D}g_{ij}}{\mathrm{D}t} \tag{a}$$

Using (11.134) and (11.153), the above expression may be written as

$$\dot{\mathbf{W}} = \frac{1}{\rho}\frac{\partial\theta^i}{\partial\mathbf{x}_p}\frac{\partial\theta^j}{\partial\mathbf{x}_q}\sigma^{pq}\frac{\partial\mathbf{x}_m}{\partial\theta^i}\frac{\partial\mathbf{x}_n}{\partial\theta^j}\mathbf{D}_{mn} = \frac{1}{\rho}\delta_p^m\delta_q^n\sigma^{pq}\mathbf{D}_{mn} = \frac{1}{\rho}\sigma^{ij}\mathbf{D}_{ij} \tag{b}$$

The last expression is the expression for rate of work referred to the Cartesian coordinate system. Therefore, τ^{ij} and $\tilde{\gamma}_{ij}$ are work conjugates.

EXAMPLE 11.12 Show that the co-rotational rate of σ_{ij} is expressed as

$$\dot{\boldsymbol{\sigma}} = \sigma_{ij}^{\nabla}\mathbf{e}_i\otimes\mathbf{e}_j \tag{11.154}$$

Solution

If a Cartesian system co-rotates with the continuum, the rate of change $\dot{\boldsymbol{\sigma}}$ is referred to the co-rotational system and then referred back to a pre-assigned x_i system. Expressing in terms of components and tensor basis, we have

$$\begin{aligned}\dot{\boldsymbol{\sigma}} &= \dot{\sigma}_{ij}\mathbf{e}_i\otimes e_j + \sigma_{ij}\dot{e}_i\otimes e_j + \sigma_{ij}\mathbf{e}_i\otimes\dot{e}_j \\ &= \dot{\sigma}_{ij}\mathbf{e}_i\otimes e_j + \sigma_{ij}W_{ik}e_k\otimes e_j + \sigma_{ij}\mathbf{e}_i\otimes W_{jk}e_k \\ &= (\dot{\sigma}_{ij} - W_{ik}\sigma_{kj} + \sigma_{ik}W_{kj})\mathbf{e}_i\otimes e_j \\ &= \sigma_{ij}^{\nabla}\mathbf{e}_i\otimes e_j \end{aligned} \tag{a}$$

In the derivation, we used

$$\dot{e}_i = W_{ik}e_k \tag{b}$$

11.13 Further Discussion of Stress Rate

A line element initially at $d\mathbf{R}$ moves to $d\mathbf{r}$ and they are expressed as in (11.76) by

$$d\mathbf{r} = dx^i \mathbf{e}_i = d\theta^i \mathbf{g}_i, \qquad d\mathbf{R} = d\theta^i \mathbf{G}_i \tag{11.155}$$

The particle velocity in the Cartesian reference system is

$$\mathbf{v} = \frac{d\mathbf{r}}{dt} = \frac{\partial x^i}{\partial t}\mathbf{e}_i = v^i \mathbf{e}_i \tag{11.156}$$

but it is zero in the convected system. Some properties of the base vectors are

$$\begin{aligned} &\dot{\mathbf{G}}_i = 0, \qquad \dot{\mathbf{G}}^i = 0, \qquad \mathbf{g}_i = \frac{\partial \mathbf{r}}{\partial \theta^i} = \frac{\partial x^j}{\partial \theta^i}\mathbf{e}_j \\ &\dot{\mathbf{g}}_i = \frac{\partial \mathbf{v}}{\partial \theta^i} = \tilde{v}^j|_i \, \mathbf{g}_j = \frac{\partial^2 x^j}{\partial \theta^i \partial t}\mathbf{e}_j, \qquad \dot{\mathbf{g}}^i = -\tilde{v}^i|_j \, \mathbf{g}^i \end{aligned} \tag{11.157}$$

where $\tilde{v}^j|_i$ are covariant derivatives of the components $\tilde{v}^j$.

Referring to the current configuration, the true stress tensor is

$$\boldsymbol{\tau} = \tau^{ij}\mathbf{g}_i \otimes \mathbf{g}_j = \sigma_{ij}\mathbf{e}_i \otimes \mathbf{e}_j \tag{11.158}$$

We note that the components τ^{ij} are defined with respect to $\mathbf{g}_i$, which moves with the continuum undergoing a motion. In the case of a rigid-body motion of the continuum, we propose that the components τ^{ij} remain constant, that is, $\dot{\tau}^{ij} = 0$. Define now a tensor

$$\mathbf{P} = \tau^{ij}\mathbf{G}_i \otimes \mathbf{G}_j \tag{11.159}$$

The components in (11.159) are the same as in (11.158), but the base vectors are different. At the reference configuration t_0, $\boldsymbol{\tau} = \mathbf{P}$, but at $t > t_0$, $\boldsymbol{\tau} \neq \mathbf{P}$. We can say that $\mathbf{P}$ is a different tensor from $\boldsymbol{\tau}$. The material differentiation of (11.158) gives

$$\begin{aligned} \dot{\boldsymbol{\tau}} &= \dot{\tau}^{ij}\mathbf{g}_i \otimes \mathbf{g}_j + \tau^{ij}\dot{\mathbf{g}}_i \otimes \mathbf{g}_j + \tau^{ij}\mathbf{g}_i \otimes \dot{\mathbf{g}}_j \\ &= [(\dot{\tau}^{ij})_{\theta^i = \text{ const}} + \tau^{mj}\tilde{v}^i|_m + \tau^{im}\tilde{v}^j|_m]\mathbf{g}_i \otimes \mathbf{g}_j \\ &= (\dot{\sigma}_{ij})_{\theta^i = \text{ const}}\mathbf{e}_i \otimes \mathbf{e}_j \end{aligned} \tag{11.160}$$

We see from (11.160) that, for components τ^{ij} to remain constant, $\dot{\boldsymbol{\tau}}$ is generally nonzero. Differentiating (11.159), we have

$$\dot{\mathbf{P}} = (\dot{\tau}^{ij})_{\theta^i = \text{ const}}\mathbf{G}_i \otimes \mathbf{G}_j \tag{11.161}$$

Based on (11.161), we further define another tensor $\dot{\boldsymbol{\tau}}^{(1)}$. Tensors $\dot{\mathbf{P}}$ and $\dot{\boldsymbol{\tau}}^{(1)}$ have the same components but different bases. The new tensor is

$$\dot{\boldsymbol{\tau}}^{(1)} = (\dot{\tau}^{ij})_{\theta^i = \text{const}} \mathbf{g}_i \otimes \mathbf{g}_j \tag{11.162}$$

The two tensors $\dot{\mathbf{P}}$ and $\dot{\boldsymbol{\tau}}^{(1)}$ are generally not equal for $t > t_0$, but at t_0, $\mathbf{G}_i = \mathbf{g}_i$ and $\dot{\mathbf{P}} = \dot{\boldsymbol{\tau}}^{(1)}$. Substituting (11.162) into (11.160), we obtain

$$\dot{\boldsymbol{\tau}} = \dot{\boldsymbol{\tau}}^{(1)} + [\tau^{mj}\tilde{v}^i|_m + \tau^{im}\tilde{v}^j|_m]\mathbf{g}_i \otimes \mathbf{g}_j \tag{11.163}$$

Thus, $\dot{\boldsymbol{\tau}}^{(1)}$ is a part of $\dot{\boldsymbol{\tau}}$ and it does not contain the parts of $\dot{\boldsymbol{\tau}}$ that are related to the spin of the base vectors.

Using (11.157), the first equality of (11.160) is

$$\begin{aligned} &\dot{\tau}^{ij}\frac{\partial x^m}{\partial \theta^i}\mathbf{e}_m \otimes \frac{\partial x^n}{\partial \theta^j}\mathbf{e}_n + \tau^{ij}\frac{\partial v^m}{\partial \theta^i}\mathbf{e}_m \otimes \frac{\partial x^n}{\partial \theta^j}\mathbf{e}_n + \tau^{ij}\frac{\partial x^m}{\partial \theta^i}\mathbf{e}_m \otimes \frac{\partial v^n}{\partial \theta^j}\mathbf{e}_n \\ &\quad = (\dot{\sigma}_{mn})|_{\theta^i = \text{const}}\mathbf{e}_m \otimes \mathbf{e}_n \end{aligned} \tag{11.164}$$

The coefficients on both sides of (11.164) are related by

$$\dot{\tau}^{ij}\frac{\partial x^m}{\partial \theta^i}\frac{\partial x^n}{\partial \theta^j} + \tau^{ij}\frac{\partial v^m}{\partial \theta^i}\frac{\partial x^n}{\partial \theta^j} + \tau^{ij}\frac{\partial x^m}{\partial \theta^i}\frac{\partial v^n}{\partial \theta^j} = (\dot{\sigma}_{mn})|_{\theta^i = \text{const}} \tag{11.165}$$

Substituting (11.134) into (11.165), we find

$$\dot{\sigma}_{mn} - \sigma_{kn}\frac{\partial v^m}{\partial x^k} - \sigma_{mk}\frac{\partial v^n}{\partial x^k} = \frac{\partial x^m}{\partial \theta^i}\frac{\partial x^n}{\partial \theta^j}\dot{\tau}^{ij} \tag{11.166}$$

Therefore, a stress rate may be defined as

$$\sigma^*_{mn} = \dot{\sigma}_{mn} - \frac{\partial v^m}{\partial x^k}\sigma_{kn} - \frac{\partial v^n}{\partial x^k}\sigma_{mk} \tag{11.167}$$

so that (11.166) becomes

$$\sigma^*_{mn} = \frac{\partial x^m}{\partial \theta^i}\frac{\partial x^n}{\partial \theta^j}\dot{\tau}^{ij} \tag{11.168}$$

Finally, we substitute (11.168) into (11.162) and using (11.157) to obtain

$$\dot{\boldsymbol{\tau}}^{(1)} = \dot{\tau}^{ij}\mathbf{g}_i \otimes \mathbf{g}_j = \sigma^*_{ij}\mathbf{e}_i \otimes \mathbf{e}_j \tag{11.169}$$

We note that the base vectors $\mathbf{g}_i$ spin with the continuum during a rigid-body motion, but the contravariant stress components τ^{ij} remain stationary.

Therefore, $\dot{\tau}^{ij} = 0$. From (11.168) we see that the convected rate $\sigma^{*}_{ij} = 0$ during a rigid-body motion. We will call $\dot{\boldsymbol{\tau}}^{(1)}$ the stress-rate tensor which is zero during rigid-body motions. In addition, we note that when the yield function is expressed as a function of the components τ^{ij}, it is independent of the rigid-body motion of the continuum. We conclude that, for use in the constitutive equation of plasticity, the convected stress rate is a preferred stress rate.

11.14 A Theory of Plasticity for Anisotropic Metals

We are now ready to write a theory of plasticity for anisotropic metals. The material may be initially anisotropic due to the manufacturing process. In this case, an anisotropic initial yield function will be used. We will also consider the deformation induced anisotropy. The yield surface will undergo, in addition to isotropic and kinematic hardening, distortion and rotation. The latter two effects have been experimentally observed and are presented in Chapter 12 and these effects are discussed using the present theory. In the case that initial anisotropy of material is not apparent, we assume the material to be initially isotropic and use von Mises yield criterion for the initial yielding. This kind of material will be subjected to deformation induced anisotropy as well and the material will experience isotropic–kinematic hardening, distortion and rotation of the yield surface.

In Chapter 10, we discussed works of anisotropic plasticity addressing the deformation of sheet metals. The validity of these works is usually verified against metal sheets subjected to a principal stress state with symmetric axes of orthotropy coinciding with the principal stress directions. Very few experimental verifications have been published, however, which address the case of nonprincipal state of stress. In the nonprincipal stress state, an initially rectangular material element becomes distorted after deformation. This fact is significant, particularly in the case of finite strain of anisotropic materials, and most metal-forming operations do encounter nonprincipal states of stress in the large strain range. It is this distortion of material element that mandates the consideration of a convected material element described in Sections 11.1 and 11.9 and it requires the use of convected curvilinear coordinates.

The present theory of anisotropic plasticity was first presented by the author in [9] and it was extended in two recent papers [10,11] to discuss torsion of a thin-walled tube and the evolution of the subsequent yield surface. The theory is presented in this section, with permission from Elsevier, and its applications are given in Chapter 12. The following concepts have been incorporated into the constitutive framework: (1) the convected coordinates and the contravariant true stress, (2) an observer independent yield function, (3) the convected rate for general kinematics of deformation, and (4) the rotation of material texture expressed by a constitutive spin. In the formulation, we use the contravariant true stress τ^{ij} and its rate; the latter, discussed in Sections 11.12 and 11.13, transforms by (11.145) into the convected stress rate

σ^{*ij} referred to a Cartesian system. We use the covariant strain $\tilde{\gamma}_{ij}$ and its rate, which transforms by (11.154) into the rate of deformation D_{ij} referred to the Cartesian system.

The deformation-induced textures represent an overview of shape and orientation changes of the crystallites. Since the back stress is related to the shape and orientation of grains, we see a relation between the back stress and the texture and postulate that the evolution of back stress be related to the rotation of texture in a macroscopic relation. We use the corotational rate to account for the spin of material texture. One way of observing the texture experimentally and theoretically (polycrystal plasticity) is to plot the pole figures. In the case of torsion of thin-walled tubes or solid bars, the preferred texture orientation can rotate (or tilt) with increasing shear strain. This phenomenon was observed experimentally by Montheillet et al. [12], Stout and O'Rourke [13], Toth et al. [14], and Wang et al. [15]; and the observed tilting was in the range of ± 2 to 5°. Computer simulations of torsion by use of polycrystal plasticity have also led to tilting of the ideal orientation, Canova et al. [16,17], Harren et al. [18] and Toth et al. [19–21]. In [22], we obtained an analytical solution, which predicted the tilting of texture in torsion by use of a double-slip model of polycrystal plasticity. Since these studies refer to a Cartesian coordinate system, we will refer to the same system for the characterization of the material texture spin, and, therefore, the use of corotational rate involving the constitutive spin is justified. As discussed in Chapter 7, Dafalias [23] coined the term "constitutive spin" to denote the difference of the material spin and plastic spin, and used the constitutive spin to form the corotational rate. He argued against expressing the plastic spin in terms of the kinematics of finite deformation and used the continuum approach to propose an expression for the plastic spin. Dafalias' [23] argument is supported by the experimental finding that the tilting of texture in torsion is first opposite to the direction of the increasing shear strain and then reverses its direction as the shear strain further increases. This observation shows that the rotation of texture is not directly related to the kinematics of shear deformation. In Chapter 12, we present a study of the free-end torsion problem and assume that the rule of constitutive spin follows the tilting effect observed in the torsion problem. The constitutive spin, denoted by ϖ, is assumed to influence the evolution of the back stress through its corotational rate. The constitutive spin for problems with other specimen geometry and loading condition is not yet clear and needs to be further investigated.

The theory as presented here uses the simplest equations of the flow theory of plasticity discussed in Chapter 6. Refinements by use of sophisticated expressions are possible. A classical flow theory is formulated based on a yield criterion, a flow rule, strain-hardening rules, and a loading–unloading condition. These are augmented in the present theory by considering the distortion and rotation of the subsequent yield surface. We discuss the yield function, the flow rule, and the strain-hardening rules in the remaining part of this chapter, and, in Chapter 12, we discuss in detail an application of the theory in the study of combined axial–torsion of thin-walled tubes.

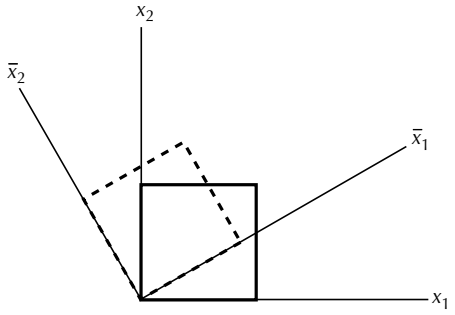

FIGURE 11.10
The two elements do not contain the same material mass.

11.14.1 The Yield Function

Since the Cauchy stress components are not invariant with respect to rotation of a Cartesian spatial frame, a yield function is observer independent when it is defined in terms of the Cauchy stress invariants. This definition of yield function is useful for isotropic materials, but it is questionable when the material is anisotropic. The reason is that the spatial rectangular element used to define the Cauchy stress varies with the choice of Cartesian spatial frame, and the element will not contain the same material mass when a different Cartesian spatial frame is used (see elements described by solid and dashed lines in Figure 11.10). This fact is not important in the case of isotropic materials, as long as the value of the yield function, which is defined by stress invariants, remains unchanged. However, the element not containing the same material mass is an important issue in the case of anisotropic materials, when the deformation history of a material element is being followed. Therefore, defining the yield function using the Cauchy stress invariants is not appropriate in the case of anisotropic plasticity.

In this investigation, an observer-independent yield function will be expressed in terms of the contravariant true stress τ^{ij}. In this way, the stress components are defined with respect to the convected coordinates and do not vary with the observer. For metals, since the hydrostatic pressure does not influence yielding, the deviatoric stress is used to define the yield function. Following (11.134), (11.25), and (11.26), the deviatoric stress $\tilde{p}^{ij}$ transforms according to the equation

$$\tilde{p}^{ij} = \tau^{ij} - pg^{ij} = \frac{\partial \theta^i}{\partial x_p}\frac{\partial \theta^j}{\partial x_q}\left(\sigma^{pq} - \frac{1}{3}\sigma^{kk}\delta^{pq}\right), \qquad \text{where } p = \frac{1}{3}g_{pq}\tau^{pq} = \frac{1}{3}\sigma^{kk} \tag{11.170}$$

It is convenient to define a yield function in terms of the physical components due to their equi-dimensional properties. Generally, the yield criterion is experimentally determined in the stress space and it has the dimension

of stress. Therefore, it is desirable to formulate the yield function in terms of the physical components. The physical components of the stress deviator $\tilde{p}^{ij}$ may be defined in the same way as we defined stress based on (11.120). From (11.120), we write

$$\sum_{j=1}^{3} \frac{(\tau^{ij} - pg^{ij})\mathbf{g}_j}{\sqrt{g^{ii}}} = \sum_{j=1}^{3} \sqrt{\frac{g_{jj}}{g^{ii}}}(\tau^{ij} - pg^{ij})\frac{\mathbf{g}_j}{\sqrt{g_{jj}}} = \sum_{j=1}^{3} \tilde{p}^{\langle ij\rangle}\mathbf{e}_j \tag{11.171}$$

Therefore,

$$\tilde{p}^{\langle ij\rangle} = \tau^{\langle ij\rangle} - pg^{ij}\frac{\sqrt{g_{jj}}}{\sqrt{g^{ii}}} \qquad (i,\ j \text{ not summed}) \tag{11.172}$$

Using a polynomial expressed by the physical components of the stress deviator, the yield function for plane stress problems may be written as

$$\begin{aligned} 2\phi = {} & h_{11}(\tilde{p}^{\langle 11\rangle})^2 + h_{22}(\tilde{p}^{\langle 22\rangle})^2 + h_{33}(\tilde{p}^{\langle 33\rangle})^2 + h_{55}(\tilde{p}^{\langle 23\rangle})^2 \\ & + 2h_{12}\tilde{p}^{\langle 11\rangle}\tilde{p}^{\langle 22\rangle} + 2h_{13}\tilde{p}^{\langle 11\rangle}\tilde{p}^{\langle 33\rangle} + 2h_{23}\tilde{p}^{\langle 22\rangle}\tilde{p}^{\langle 33\rangle} \\ & + 2h_{15}\tilde{p}^{\langle 11\rangle}\tilde{p}^{\langle 23\rangle} + 2h_{25}\tilde{p}^{\langle 22\rangle}\tilde{p}^{\langle 23\rangle} + 2h_{35}\tilde{p}^{\langle 33\rangle}\tilde{p}^{\langle 23\rangle} \\ & + b_{11}\tilde{p}^{\langle 11\rangle} + b_{22}\tilde{p}^{\langle 22\rangle} + b_{33}\tilde{p}^{\langle 33\rangle} + b_{55}\tilde{p}^{\langle 23\rangle} + b_{00} \\ = {} & f^2 \end{aligned} \tag{11.173}$$

where h_{ij} and b_{ij} are coefficients of anisotropy and f specifies the size of the yield surface. Simplified yield functions can be deduced from (11.173) depending on the material considered. We now consider some special cases in the following subsections. The more general case of combined axial–torsion will be discussed in Chapter 12.

11.14.1.1 Yield function in uniform extensions

We use fixed Cartesian coordinates to define the undeformed configuration R_0 of a block (unit cube) and identify convected coordinates θ^i with X_i so that

$$\theta^1 = X_1, \quad \theta^2 = X_2 \quad \text{and} \quad \theta^3 = X_3 \tag{11.174}$$

We now deform the unit cube in a way that the sides which are initially parallel to the axes (X_1, X_2, X_3) remain parallel to the axes, respectively, but with changed length of the sides. The deformed block may be referred to the fixed Cartesian axes with coordinates x_i, so that

$$x_1 = \lambda_1 X_1, \qquad x_2 = \lambda_2 X_2, \qquad x_3 = \lambda_3 X_3 \tag{11.175}$$

in which λ_i are the stretch ratios and can be functions of time. We consider a simple case here that λ_i are constants. The base vectors $\mathbf{G}_i, \mathbf{G}^i, \mathbf{g}_i, \mathbf{g}^i$ remain in the directions of X_i axes, and the metric tensors for the undeformed and deformed configurations can be found from (11.174) and (11.175), using (11.25) and (11.26), as

$$G_{ij} = G^{ij} = \delta_{ij}, \quad G = 1$$
$$g_{ij} = \begin{bmatrix} \lambda_1^2 & 0 & 0 \\ 0 & \lambda_2^2 & 0 \\ 0 & 0 & \lambda_3^2 \end{bmatrix}, \qquad g^{ij} = \begin{bmatrix} \lambda_1^{-2} & 0 & 0 \\ 0 & \lambda_2^{-2} & 0 \\ 0 & 0 & \lambda_3^{-2} \end{bmatrix}, \qquad g = \lambda_1^2\lambda_2^2\lambda_3^2 \tag{11.176}$$

From (11.121), the physical components of contravariant stress are

$$\tau^{\langle 11\rangle} = \lambda_1^2\tau^{11}, \qquad \tau^{\langle 22\rangle} = \lambda_2^2\tau^{22}, \qquad \tau^{\langle 33\rangle} = \lambda_3^2\tau^{33}, \qquad \text{other } \tau^{\langle ij\rangle} = 0 \tag{11.177}$$

Using (11.172), we obtain

$$\begin{aligned} \tilde{p}^{\langle 11\rangle} &= \lambda_1^2\tau^{11} - p = \tfrac{1}{3}(2\lambda_1^2\tau^{11} - \lambda_2^2\tau^{22} - \lambda_3^2\tau^{33}) \\ \tilde{p}^{\langle 22\rangle} &= \lambda_2^2\tau^{22} - p = \tfrac{1}{3}(2\lambda_2^2\tau^{22} - \lambda_3^2\tau^{33} - \lambda_1^2\tau^{11}) \\ \tilde{p}^{\langle 33\rangle} &= \lambda_3^2\tau^{11} - p = \tfrac{1}{3}(2\lambda_3^2\tau^{33} - \lambda_1^2\tau^{11} - \lambda_2^2\tau^{22}) \\ &\text{Other } \tilde{p}^{\langle ij\rangle} = 0 \end{aligned} \tag{11.178}$$

with the hydrostatic pressure given by

$$p = \tfrac{1}{3}g_{pq}\tau^{pq} = \tfrac{1}{3}(\lambda_1^2\tau^{11} + \lambda_2^2\tau^{22} + \lambda_3^2\tau^{33}) \tag{11.179}$$

We now assume that the material is initially isotropic and use a simplified form of (11.173) as the yield criterion. We consider an expression similar to the von Mises yield criterion and write

$$\tfrac{1}{2}\tilde{p}^{\langle ij\rangle}\tilde{p}^{\langle ij\rangle} = \tfrac{1}{3}Y^2 \qquad \text{where } Y = \text{yield stress in tension} \tag{11.180}$$

which reduces to

$$(\tilde{p}^{\langle 11\rangle})^2 + (\tilde{p}^{\langle 22\rangle})^2 + (\tilde{p}^{\langle 33\rangle})^2 = \tfrac{2}{3}Y^2 \tag{11.181}$$

The true stress and the Cauchy stress are related by (11.134). Using (11.175), (11.134) reduces to

$$\sigma^{11} = \lambda_1^2 \tau^{11}, \qquad \sigma^{22} = \lambda_2^2 \tau^{22}, \qquad \sigma^{33} = \lambda_3^2 \tau^{33}, \qquad \sigma^{12} = \sigma^{23} = \sigma^{31} = 0 \tag{11.182}$$

Comparing (11.177) and (11.182), we see that the Cauchy stress and the physical components are equal in this case. This is a case that a rectangular element remains rectangular without distortion. Substituting (11.182) and (11.178) into (11.181), the yield criterion is now expressed by

$$(\sigma^{11} - \sigma^{22})^2 + (\sigma^{22} - \sigma^{33})^2 + (\sigma^{33} - \sigma^{11})^2 = 2Y^2 \tag{11.183}$$

This is the von Mises yield criterion discussed in Chapter 6.

On the other hand, we may solve this same problem by identifying the convected coordinates with x_i at the deformed configuration. In this case,

$$\theta^1 = x_1 = \lambda_1 X_1, \qquad \theta^2 = x_2 = \lambda_2 X_2, \qquad \theta^3 = x_3 = \lambda_3 X_3 \tag{11.184}$$

The metric tensors are

$$g_{ij} = g^{ij} = \delta_{ij}, \qquad g = 1$$
$$G_{ij} = \begin{bmatrix} \lambda_1^{-2} & 0 & 0 \\ 0 & \lambda_2^{-2} & 0 \\ 0 & 0 & \lambda_3^{-2} \end{bmatrix}, \qquad G^{ij} = \begin{bmatrix} \lambda_1^2 & 0 & 0 \\ 0 & \lambda_2^2 & 0 \\ 0 & 0 & \lambda_3^2 \end{bmatrix}, \qquad G = \lambda_1^{-2}\lambda_2^{-2}\lambda_3^{-2} \tag{11.185}$$

Using (11.121) and (11.184), we found

$$\tau^{\langle 11\rangle} = \tau^{11}, \qquad \tau^{\langle 22\rangle} = \tau^{22}, \qquad \tau^{\langle 33\rangle} = \tau^{33} \tag{11.186}$$

and, from (11.134), the Cauchy stress is

$$\sigma^{ij} = \frac{\partial x_i}{\partial \theta^p}\frac{\partial x_j}{\partial \theta^q}\tau^{pq} = \frac{\partial x_i}{\partial x^p}\frac{\partial x_j}{\partial x^q}\tau^{pq} = \delta_p^i \delta_q^j \tau^{pq} = \tau^{ij} \tag{11.187}$$

Therefore, the Cauchy stress components are equal to the true stress and are also equal to the physical components in this case. From (11.172) and (11.185), we obtain

$$\begin{aligned} \tilde{p}^{\langle 11\rangle} &= \tfrac{1}{3}(2\tau^{11} - \tau^{22} - \tau^{33}) \\ \tilde{p}^{\langle 22\rangle} &= \tfrac{1}{3}(2\tau^{22} - \tau^{33} - \tau^{11}) \\ \tilde{p}^{\langle 33\rangle} &= \tfrac{1}{3}(2\tau^{33} - \tau^{11} - \tau^{22}) \qquad \text{with } p = \tfrac{1}{3}(\tau^{11} + \tau^{22} + \tau^{33}) \end{aligned} \tag{11.188}$$

The yield criterion (11.180), with (11.187) and (11.188) substituted, reduces to the same expression as in (11.183).

We note that both approaches, by setting $\theta^i = X_i$ and by setting $\theta^i = x_i$, have led to the same yield function (11.183) expressed in terms of the physical components and in terms of the Cauchy stress. This yield function is independent of the amount of deformation, because it is defined with respect to unit area of the element, either deformed or undeformed. Due to (11.182), we see that $\tau^{ij}$is not defined per unit area when we set $\theta^i = X_i$. But, from (11.186), τ^{ij} is defined per unit area when we set $\theta^i = x_i$. We also note that no distortion due to prestrain can occur in the yield surface as defined by (11.183).

11.14.1.2 Yield function in simple shear

Simple shear is described in Figure 11.11. A square block at the undeformed configuration has base vectors $\mathbf{G}_i$ shown in Figure 11.11(a). This block is deformed into the parallelogram shown in Figure 11.11(b) with base vectors $\mathbf{g}_i$ and $\mathbf{g}^i$. Each material point in the block moves parallel to the X_1 axis by an amount proportional to its X_2 coordinate. A material point with initial coordinates X_i moves to a point with coordinates x_i, so that

$$x_1 = X_1 + KX_2, \qquad x_2 = X_2, \qquad x_3 = X_3 \tag{11.189}$$

where K is a constant denoting the amount of shearing. We identify $\theta^i = X_i$, and, from (11.9) and (11.15), the base vectors are

$$\begin{aligned} &\mathbf{G}_1 = \mathbf{G}^1 = \mathbf{e}_1, \qquad \mathbf{G}_2 = \mathbf{G}^2 = \mathbf{e}_2, \qquad \mathbf{G}_3 = \mathbf{G}^3 = \mathbf{e}_3 \\ &\mathbf{g}_1 = \mathbf{e}_1, \qquad \mathbf{g}_2 = K\mathbf{e}_1 + \mathbf{e}_2, \qquad \mathbf{g}_3 = \mathbf{e}_3 \\ &\mathbf{g}^1 = \mathbf{e}_1 - K\mathbf{e}_2, \qquad \mathbf{g}^2 = \mathbf{e}_2, \qquad \mathbf{g}^3 = \mathbf{e}_3 \end{aligned} \tag{11.190}$$

and the metric tensors are

$$\begin{aligned} &G_{ij} = G^{ij} = \delta_{ij}, \quad G = 1 \\ &g_{ij} = \begin{bmatrix} 1 & K & 0 \\ K & 1+K^2 & 0 \\ 0 & 0 & 1 \end{bmatrix}, \qquad g^{ij} = \begin{bmatrix} 1+K^2 & -K & 0 \\ -K & 1 & 0 \\ 0 & 0 & 1 \end{bmatrix}, \qquad g = 1 \end{aligned} \tag{11.191}$$

In the J_2'-theory discussed in (6.6), the yield function for plane stress is

$$\sigma_x^2 - \sigma_x\sigma_y + \sigma_y^2 + 3\tau_{xy}^2 = Y^2 \tag{11.192}$$

Using this yield function, but in terms of the physical components $\tau^{\langle ij\rangle}$, we may write

$$(\tau^{\langle 11\rangle})^2 - \tau^{\langle 11\rangle}\tau^{\langle 22\rangle} + (\tau^{\langle 22\rangle})^2 + 3(\tau^{\langle 12\rangle})^2 = Y^2 \tag{11.193}$$

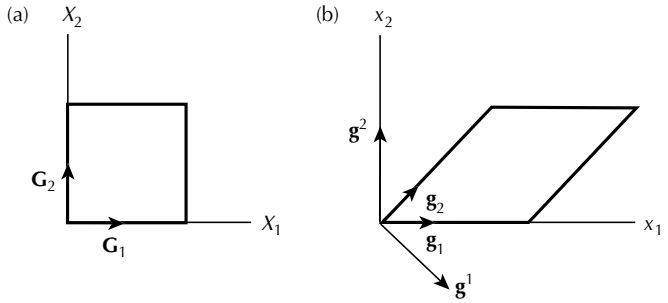

FIGURE 11.11
Base vectors during simple shear.

where, using (11.121), we have

$$\tau^{\langle 11\rangle} = \frac{\tau^{11}}{\sqrt{1+K^2}}, \qquad \tau^{\langle 22\rangle} = \sqrt{1+K^2}\tau^{22}, \qquad \tau^{\langle 12\rangle} = \tau^{12} \tag{11.194}$$

Substituting (11.194) into (11.193), the yield criterion is obtained as

$$(\tau^{11})^2 - (1+K^2)\tau^{11}\tau^{22} + (1+K^2)^2(\tau^{22})^2 + 3(1+K^2)(\tau^{12})^2 = Y^2(1+K^2) \tag{11.195}$$

This is the yield function expressed in terms of the true stress τ^{ij}, and we may express it in terms of Cauchy stress σ^{ij} if we use (11.134) to find

$$\tau^{11} = \sigma^{11} + K^2\sigma^{22} - 2K\sigma^{12}, \qquad \tau^{22} = \sigma^{22}, \qquad \tau^{12} = \sigma^{12} - K\sigma^{22} \tag{11.196}$$

Combining (11.195) and (11.196), we obtain the yield function as

$$\begin{aligned}(\sigma^{11})^2 + (2K^2+1)^2(\sigma^{22})^2 + (7K^2+3)(\sigma^{12})^2 + (K^2-1)\sigma^{11}\sigma^{22} \\ - 4K(2K^2+1)\sigma^{12}\sigma^{22} - 4K\sigma^{11}\sigma^{12} = Y^2(K^2+1)\end{aligned} \tag{11.197}$$

This equation describes a family of ellipsoids in the three-dimensional stress space with varying K-values. The cross-sections of the ellipsoids cut by the plane $\sigma^{12} = 0$ are shown in Figure 11.12(a) for various K-values. The initial yield surface at $K = 0$ is the same as the von Mises yield criterion, but the yield curves for other Ks show distortion and rotation of the yield surface. Figure 11.12(b) shows the yield surfaces cut by the $\sigma^{11} = 0$ plane. The

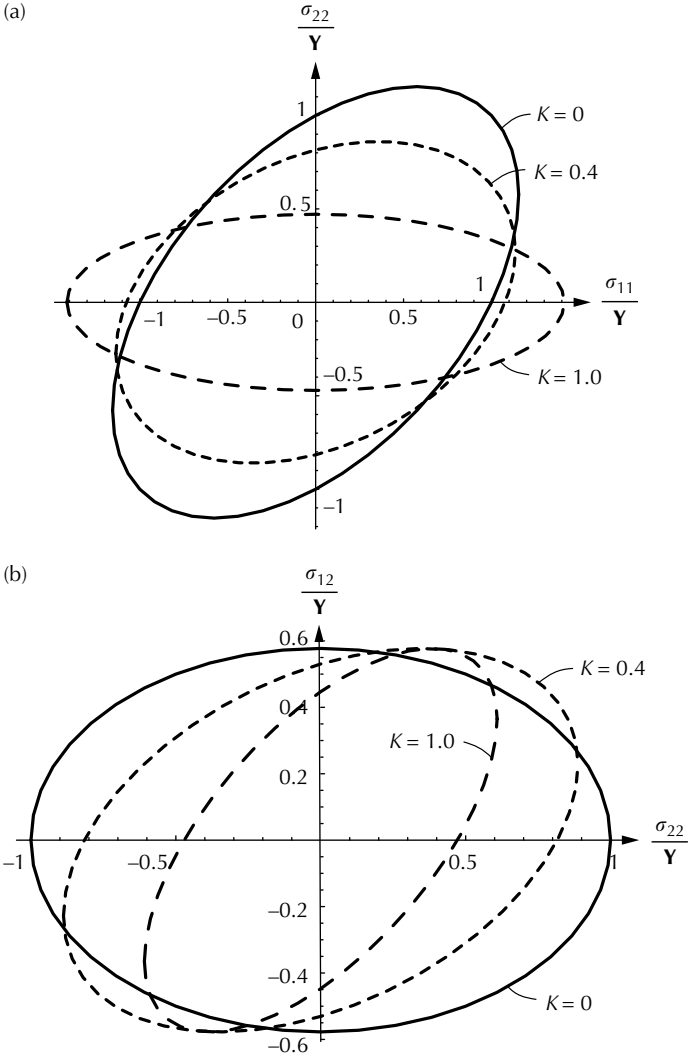

FIGURE 11.12
Yield surfaces for simple shear at various K-values: (a) cut by $\sigma^{12} = 0$ plane, (b) cut by $\sigma^{11} = 0$ plane.

equations are

$$(\sigma^{11})^2 + (2K^2+1)^2(\sigma^{22})^2 + (K^2-1)\sigma^{11}\sigma^{22} = Y^2(K^2+1) \qquad \text{for } \sigma^{12} = 0$$
$$(2K^2+1)^2(\sigma^{22})^2 + (7K^2+3)(\sigma^{12})^2 - 4K(2K^2+1)\sigma^{12}\sigma^{22} = Y^2(K^2+1)$$
$$\text{for } \sigma^{11} = 0 \tag{11.198}$$

We note that the yield surfaces in Figure 11.12(a) and (b) have been obtained based on the yield criterion given by (11.193). Since no experimental results are available for comparison, the results presented in Figure 11.12 cannot be verified.

11.14.2 The Flow Rule

Referring to (11.153), the rate of deformation may be decomposed into the elastic and the plastic parts as

$$D_{ij} = D^e_{ij} + D^p_{ij}, \qquad D^{\mathrm{e}}_{ij} = \frac{1}{2}\frac{\partial \theta^{\mathrm{r}}}{\partial x_i}\frac{\partial \theta^s}{\partial x_j}\frac{\mathrm{D}g^e_{rs}}{\mathrm{D}t} \quad \text{and} \quad D^p_{ij} = \frac{1}{2}\frac{\partial \theta^r}{\partial x_i}\frac{\partial \theta^s}{\partial x_j}\frac{\mathrm{D}g^{\mathrm{p}}_{rs}}{\mathrm{D}t} \tag{11.199}$$

in which D^e_{ij} and g^e_{ij} are the elastic part and D^p_{ij} and g^p_{ij} are the plastic part, respectively. The flow rule is

$$\frac{\mathrm{D}^p_{ij}}{\mathrm{D}t} = \dot{\Lambda}\frac{\partial \phi}{\partial \tau^{ij}} \tag{11.200}$$

where $\dot{\Lambda}$ is the plastic multiplier.

11.14.3 The Strain Hardening

We discuss isotropic and kinematic hardening in this subsection. We use an equivalent plastic strain-rate $\dot{g}^p$ to define isotropic hardening first. The equivalent plastic strain-rate may be defined using the concept of rate of plastic work, which is

$$\dot{W}^p = \tfrac{1}{2}\bar{\tau}\dot{g}^p \tag{11.201}$$

where $\bar{\tau}$ is the equivalent stress. The expressions for $\bar{\tau}$ and $\dot{g}^p$ are dependent on the explicit form of the yield function and are further discussed, when we consider the problem of combined axial–torsion of thin-walled tubes in Chapter 12. Following (8.110) [24], the isotropic-hardening function is given by

$$f(\zeta) = D - (D-1)e^{-\beta\zeta} \tag{11.202}$$

where D and β are material parameters; and ζ is a positive, monotonically increasing parameter that accounts for the history of plastic deformation. It is assumed that the rate of change is

$$\dot{\zeta} = |\dot{g}^p| \tag{11.203}$$

It has been discussed in the introductory paragraph of Section 11.14 that the kinematic hardening is described by the evolution of the back stress, which, in turn, is governed by a corotational rate involving the constitutive spin ϖ. Using the linear kinematic-hardening rule of Prager [25] discussed in (6.74), the evolution equation for the back stress is

$$\overset{\nabla}{\alpha}{}^{\mathrm{D}}_{ij} = \bar{c} D^{\mathrm{p}}_{ij} \qquad \text{with } \overset{\nabla}{\alpha}{}^{\mathrm{D}}_{11} + \overset{\nabla}{\alpha}{}^{\mathrm{D}}_{22} + \overset{\nabla}{\alpha}{}^{\mathrm{D}}_{33} = 0 \tag{11.204}$$

where α^{D}_{ij} is the deviatoric part of α_{ij}, such that

$$\overset{\nabla}{\alpha}_{ij} = \overset{\nabla}{\alpha}{}^{\mathrm{D}}_{ij} + \tfrac{1}{3}\delta_{ij}\overset{\nabla}{\alpha}_{kk} \tag{11.205}$$

We denote the back stress in the τ^{ij}- stress space by $\tilde{\alpha}^{ij}$, which may be projected onto a fixed Cartesian spatial frame x_i with components α_{ij} and the transformation equations given by

$$\alpha_{ij} = \frac{\partial x_i}{\partial \theta^p}\frac{\partial x_j}{\partial \theta^q}\tilde{\alpha}^{pq} \tag{11.206}$$

The material parameter $\bar{c}$ in (11.204) can take different values for different components of back stress. This extended feature of the linear kinematic-hardening rule would allow for the consideration of a material with anisotropic rate of kinematic hardening. The corotational rate of the back stress is

$$\boldsymbol{\alpha}^{\nabla} = \frac{\mathrm{D}\alpha}{\mathrm{D}t} - \varpi \cdot \boldsymbol{\alpha} + \boldsymbol{\alpha} \cdot \varpi \tag{11.207}$$

11.14.4 Elastic Constitutive Equations

Assuming that the elastic behavior is isotropic, the elastic constitutive equation is given by the following tensor relation in the rate form

$$2\mu\dot{\boldsymbol{\gamma}}^{e} = \dot{\boldsymbol{\tau}} - \dot{\boldsymbol{\alpha}} \tag{11.208}$$

To refer the components of (11.207) to the x_i system, we use the convected rate for the first two terms and the co-rotational rate for the last term. By use of (11.198), (11.168), and (11.154), the component equation of (11.208), referred to the tensor bases $e_i \otimes e_j$ is

$$2\mu D^{e}_{ij} = \sigma^{*}_{ij} - \overset{\nabla}{\alpha}_{ij} \tag{11.209}$$

where D^{e}_{ij} is the elastic part of rate of deformation given by (11.199).

References

1. Synge, J.L. and Schild, A., *Tensor Calculus*, University of Toronto Press, Toronto, 1949.
2. Green, A.E. and Zerna, W., *Theoretical Elasticity*, Clarendon Press, Oxford, 1954.
3. Flügge, W., *Tensor Analysis and Continuum Mechanics*, Springer-Verlag, Berlin, 1972.
4. Sedov, L.I., *A Course in Continuum Mechanics*, Vol. 1, Wolters-Noordhoff Publishing, Groningen, The Netherlands, 1971.
5. Fung, Y.C., *Foundations of Solid Mechanics*, Prentice-Hall, Englewood Cliffs, NJ, 1965.
6. Oldroyd, J.G., On the formulation of rheological equations of state, *Proc. Roy. Soc.*, A, 200, 523, 1950.
7. Green, A.E. and Adkins, T.E., *Large Elastic Deformations*, Oxford University Press, Oxford, 1960.
8. Valanis, K.C., Back stress and Jaumann rates in finite plasticity, *Int. J. Plasticity*, 6, 353, 1990.
9. Wu, H.C., On finite plastic deformation of anisotropic metallic materials, *Int. J. Plasticity*, 19, 91, 2003.
10. Wu, H.C., On the finite plastic deformation of anisotropic metallic materials, in *Proceedings of the 2001 Mechanics and Materials Summer Conference*, San Diego, 2001, 240.
11. Wu, H.C., Effect of loading-path on the evolution of yield surface for anisotropic metals subjected to large pre-strain, *Int. J. Plasticity*, 19, 1773, 2003.
12. Montheillet, F., Cohen, M., and Jonas, J.J., Axial stresses and texture development during the torsion testing on Al, Cu and a-Fe, *Acta Metall.*, 32, 2077, 1984.
13. Stout, M.G. and O'Rourke, J.A., Experimental deformation textures of OFE copper and 70 : 30 brass from wire drawing, compression and torsion, *Metall. Trans.*, 20A, 125, 1989.
14. Toth, L.S., Jonas, J.J., Daniel, D., and Bailey, A., Texture development and length changes in copper bars subjected to free end torsion, *Textures Microstruct*, 19, 245, 1992.
15. Wang, P.T., Panchanandeeswaran, S., and Wu, H.C., Comparison of flow stress and texture for P0818 cast aluminum deformed in compression and in torsion. Alcoa Technical Center Research Report, 1995.
16. Canova, G.R., Kocks, U.F., and Jonas, J.J., Theory of torsion texture development, *Acta Metall.*, 32, 211, 1984.
17. Canova, G.R., Kocks, U.F., Tome, C.N., and Jonas, J.J., The yield surface of textured polycrystals, *J. Mech. Phys. Solids*, 33, 371, 1985.
18. Harren, S., Lowe, T.C., Asaro, R.J., and Needleman, A., Analysis of large-strain shear in rate-dependent face-centered cubic polycrystals: correction of micro- and macromechanics, *Phyil. Trans. R. Soc. Lond.*, A, 328, 443, 1989.
19. Toth, L.S., Gilormini, P., and Jonas, J.J., Effect of rate sensitivity on the stability of torsion textures, *Acta Metall.*, 36, 3077, 1988.
20. Toth, L.S., Neale, K.W., and Jonas, J.J., Stress response and persistence characteristics of the ideal orientations of shear textures, *Acta Metall.*, 37, 2197, 1989.

21. Toth, L.S., Jonas, J.J., Gilormini, P., and Barcroix, B., Length changes during free-end torsion: a rate sensitive analysis, *Int. J. Plasticity*, 6, 83, 1990.
22. Qian, Z. and Wu, H.C., A 2-D texture study based on a double-slip model of polycrystal plasticity with analysis of thin-walled tubes under torsion, *Int. J. Solids Struct.*, 33, 4167, 1996.
23. Dafalias, Y.F., Plastic spin: necessity or redundancy?, *Int. J. Plasticity*, 14, 909, 1998.
24. Wu, H.C. and Yip, M.C., Endochronic description of cyclic hardening behavior for metallic materials, *J. Eng. Mater. Technol.*, 103, 212, 1981.
25. Prager, W., The theory of plasticity: a survey of recent achievements (James Clayton Lecture), *Proc. Inst. Mech. Eng.*, 169, 41, 1955.

Problems

(1) Prove (11.15).

(2) Starting from $\mathbf{F} = \mathbf{g}_j \otimes \mathbf{G}^j$, express $\mathbf{F}$ in terms of Cartesian components and Cartesian base vectors $\mathbf{e}_i \otimes \mathbf{E}_k$, where $\mathbf{e}_i$ and $\mathbf{E}_k$refer to current and initial configurations, respectively.

(3) Show that $\mathbf{F}^{-1} = \mathbf{G}_i \otimes \mathbf{g}^i$ and $\mathbf{F}^{-\mathrm{T}} = \mathbf{g}^i \otimes \mathbf{G}_i$.

(4) Show that the coordinate transformation law for Γ^k_{ij} is

$$\bar{\Gamma}^k_{ij} = \Gamma^t_{rs} \frac{\partial \theta^r}{\partial \bar{\theta}^i} \frac{\partial \theta^s}{\partial \bar{\theta}^j} \frac{\partial \bar{\theta}^k}{\partial \theta^t} + \frac{\partial^2 \theta^s}{\partial \bar{\theta}^i \partial \bar{\theta}^j} \frac{\partial \bar{\theta}^k}{\partial \theta^s}$$

(5) Show that the covariant derivative of the contravariant component of the second-rank tensor

$$\mathbf{H} = \tilde{H}^{ij} \mathbf{g}_i \otimes \mathbf{g}_j \text{ is } \tilde{H}^{ij}|_k = \frac{\partial \tilde{H}^{ij}}{\partial \theta^k} + \tilde{H}^{mj} \Gamma^i_{mk} + \tilde{H}^{im} \Gamma^j_{mk}$$

(6) Show that $(v^k + w^k)|_i = v^k|_i + w^k|_i$.

(7) Show that $(v^j w^k)|_i = v^j|_i \, w^k + v^j \, w^k|_i$.

(8) In the case of simple shear, use the Kirchhoff stress to define the Mises yield criterion and compare the result with the Mises yield criterion defined by the Cauchy stress.

(9) In the case of simple shear, use the 2nd P–K stress to define the Mises yield criterion and compare the result with the Mises yield criterion defined by the Cauchy stress.

(10) The yield criterion defined by

$$(\sigma_x - \sigma_y)^2 + (\sigma_y - \sigma_z)^2 + (\sigma_z - \sigma_x)^2 + 2\sigma_{xy}^2 + 2\sigma_{yz}^2 + 2\sigma_{zx}^2 = f^2$$

is independent of hydrostatic pressure. Express this yield criterion in terms of the physical components $\tau^{\langle ij \rangle}$.

(11) In the case of simple shear, express the result of Problem (10) in terms of the Cauchy stress components.

(12) Express the yield criterion of Problem (10) in terms of the 2nd P–K stress components and then, in the case of simple shear, reduce it to a criterion in terms of the Cauchy stress.

(13) The yield function in the case of simple shear is assumed to be

$$\begin{aligned} 2\phi &= (\tilde{\xi}^{11})^2 - (1+K^2)\tilde{\xi}^{11}\tilde{\xi}^{22} + (1+K^2)^2(\tilde{\xi}^{22})^2 + 3(1+K^2)(\tilde{\xi}^{12})^2 \\ &= Y^2(1+K^2) \end{aligned}$$

where $\tilde{\xi}^{ij} = \tau^{ij} - \tilde{\alpha}^{ij}$; $\tilde{\alpha}^{ij}$ is the back stress in the convected system and it may be projected onto a fixed Cartesian spatial frame x_i with components α_{ij}. The transformation equations are $\alpha_{ij} = (\partial x_i/\partial\theta^p)(\partial x_j/\partial\theta^q)\tilde{\alpha}^{pq}$. If the flow rule is given by (11.200), find explicit expressions for the flow rule expressed in terms of the Cartesian components D^p_{ij} and $\xi_{ij} = \sigma_{ij} - \alpha_{ij}$.

12

Combined Axial–Torsion of Thin-Walled Tubes

12.1 Introduction

We focus on in the combined axial–torsion of thin-walled tubes, because this geometry of testing provides results that are most needed for the verification of multidimensional plasticity models. This test can determine the evolution of the yield function in the two-dimensional, shear stress versus axial stress, stress space, which is one of the simplest multiaxial stress spaces and one in which the test conditions can be well controlled. The other two-dimensional state of stress is achieved by the biaxial test subjected to tensile loads, which is not easily conducted, however. We further state that the combined axial–torsion test can provide the nonprincipal state of stress, while the biaxial test provides the principal state of stress. The combined axial–torsion test has been discussed in Chapters 5 and 7 and the biaxial test in Chapter 10. Details of experimental considerations have also been discussed.

A second reason for focusing on the testing of thin-walled tubes is in the determination of material behavior subjected to torsion, which includes the free-end torsion and the fixed-end torsion. In the free-end torsion, we apply torque to the tube freeing the two ends to elongate, and we detect length change during the experiment, which is the axial effect also known as the Swift effect [1]. In the fixed-end torsion, the torque is applied with the two ends of the specimen being fixed so that length change is not possible. Because of this restriction in the length change, axial compressive stress develops with increasing torque. The free-end torsion is frequently used by constitutive modelers to test their models. The shear stress–strain curve and the Swift effect are of interest. It is often possible to calibrate the parameters of different models to fit the experimental data. Therefore, the torsion test itself is not a sensitive test for model verification.

In this chapter, we apply the theory of anisotropic plasticity discussed in Chapter 11 to describe the evolution of the yield surface subjected to different loading paths. One of the loading paths addresses the torsion problem. Different types of nonlinear kinematic-hardening rules are used

and compared. We also consider a loading history involving axial loading and unloading followed by torsion. This test is one of the tests that can identify a good model for nonproportional loading.

12.2 Convected Coordinates in the Combined Axial–Torsion of a Thin-Walled Tube

In the combined axial–torsion of a thin-walled tube, we assume that the wall is so thin that the thickness is not a factor in the analysis. Cylindrical coordinates are used, and, at the undeformed state, a point P has coordinates (R, Θ, Z) with $\theta^1 = R$, $\theta^2 = \Theta$, and $\theta^3 = Z$. The coordinate transformation equations are

$$X_1 = R\cos\Theta, \qquad X_2 = R\sin\Theta, \qquad X_3 = Z \tag{12.1}$$

and the base vectors are,

$$\mathbf{G}_1 = \cos\Theta\mathbf{e}_1 + \sin\Theta\mathbf{e}_2, \quad \mathbf{G}_2 = -R\sin\Theta\mathbf{e}_1 + R\cos\Theta\mathbf{e}_2, \quad \mathbf{G}_3 = \mathbf{e}_3 \tag{12.2}$$

$$\mathbf{G}^1 = \mathbf{G}_1, \qquad \mathbf{G}^2 = \frac{1}{R^2}\mathbf{G}_2, \qquad \mathbf{G}^3 = \mathbf{G}_3 \tag{12.3}$$

We then determine the metric tensors as

$$G_{ij} = \begin{bmatrix} 1 & 0 & 0 \\ 0 & R^2 & 0 \\ 0 & 0 & 1 \end{bmatrix}, \qquad G^{ij} = \begin{bmatrix} 1 & 0 & 0 \\ 0 & \dfrac{1}{R^2} & 0 \\ 0 & 0 & 1 \end{bmatrix}, \qquad G = |G_{ij}| = R^2 \tag{12.4}$$

Point P in the undeformed state transforms into p in the deformed state. Point p has coordinates (r, θ, z) and the coordinate transformation equations are

$$x_1 = r\cos\theta, \qquad x_2 = r\sin\theta, \qquad x_3 = z \tag{12.5}$$

The two sets of cylindrical coordinates are related by

$$r = r(R), \qquad \theta = \Theta + \psi Z, \qquad z = \lambda Z \tag{12.6}$$

where ψ is the angle of twist per unit undeformed length and λ is the extension ratio. The base vectors for the deformed state are

$$\begin{aligned} &\mathbf{g}_1 = r_R(\cos\theta\mathbf{e}_1 + \sin\theta\mathbf{e}_2), \qquad \mathbf{g}_2 = r(-\sin\theta\mathbf{e}_1 + \cos\theta\mathbf{e}_2), \\ &\mathbf{g}_3 = \psi\mathbf{g}_2 + \lambda\mathbf{e}_3 \qquad \text{with } r_R = \frac{\mathrm{d}r(R)}{\mathrm{d}R} \end{aligned} \tag{12.7}$$

$$\mathbf{g}^1 = \frac{1}{r_R^2}\mathbf{g}_1, \qquad \mathbf{g}^2 = \left(\frac{\psi^2}{\lambda^2} + \frac{1}{r^2}\right)\mathbf{g}_2 - \frac{\psi}{\lambda^2}\mathbf{g}_3, \quad \mathbf{g}^3 = \frac{1}{\lambda}\mathbf{e}_3 \tag{12.8}$$

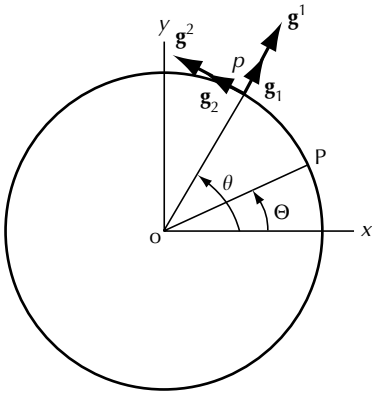

FIGURE 12.1
Base vectors at the deformed configuration for a thin-walled tube (From Wu, H.C., *Int. J. Plasticity*, 19, 91, 2003. With permission from Elsevier).

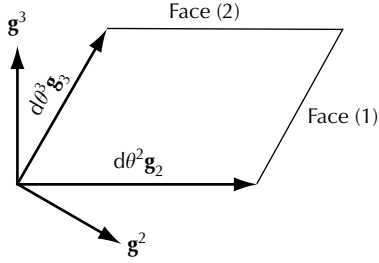

FIGURE 12.2
Convected material element in combined axial–torsion (From Wu, H.C., *Int. J. Plasticity*, 19, 91, 2003. With permission from Elsevier).

Figure 12.1 shows the covariant and contravariant base vectors at the deformed configuration and a fixed Cartesian coordinate system (x, y, z) with origin o located at the center of the circular cross-section of the tube. In this discussion, the Cartesian coordinate systems (X_i, O) and (x_i, o) are taken to coincide with (x, y, z, o). These base vectors together with the convected material element are also shown in Figure 12.2. Note that $d\theta^2\mathbf{g}_2$ and $d\theta^3\mathbf{g}_3$ define the sides of the convected material element. The metric tensors in the deformed configuration are

$$g_{ij} = \begin{bmatrix} \dfrac{1}{\lambda} & 0 & 0 \\ 0 & r^2 & \psi r^2 \\ 0 & \psi r^2 & \psi^2 r^2 + \lambda^2 \end{bmatrix}, \qquad g^{ij} = \begin{bmatrix} \lambda & 0 & 0 \\ 0 & \dfrac{\psi^2}{\lambda^2} + \dfrac{1}{r^2} & -\dfrac{\psi}{\lambda^2} \\ 0 & -\dfrac{\psi}{\lambda^2} & \dfrac{1}{\lambda^2} \end{bmatrix},$$

$$g = |g_{ij}| = r^2\lambda \tag{12.9}$$

where g_{ij} and g^{ij} are seen from (12.9) to be independent of θ. In the subsequent discussion, θ is taken to be zero, that is, $\mathbf{g}_1$ is lying along the x-direction and $\mathbf{g}_2$ is lying along the y-direction, referring to Figure 12.1. In arriving at (12.9), an assumption has been made related to no volume change, which is approximately true when the plastic deformation is large; thus, $g = G$. From (12.4) and (12.9), this assumption leads to

$$r_R^2 r^2 \lambda^2 = R^2 \quad \text{or} \quad r\frac{\partial r}{\partial R}\lambda = R \tag{12.10}$$

The last equation may be integrated. Since the stress state is uniform throughout the gauge section of the specimen, the radius r should be independent of Θ and Z. Therefore, we find

$$\lambda r^2 = R^2 \quad \text{and} \quad r_R = \frac{1}{\sqrt{\lambda}} \tag{12.11}$$

From (11.122) and (12.9), we determine the physical components $\tau^{\langle ij\rangle}$ as

$$\begin{aligned} &\tau^{\langle 11\rangle} = \frac{\tau^{11}}{\lambda}, \qquad \tau^{\langle 22\rangle} = \frac{r^2}{\sqrt{1+(\gamma/\lambda)^2}}\tau^{22}, \qquad \tau^{\langle 23\rangle} = \lambda r \tau^{23}, \\ &\tau^{\langle 33\rangle} = \lambda^2\sqrt{1+\left(\frac{\gamma}{\lambda}\right)^2}\,\tau^{33} \end{aligned} \tag{12.12}$$

where

$$\gamma = \psi r = \text{shear strain} \tag{12.13}$$

The shear strain γ is defined as per unit undeformed length along the longitudinal direction of the tube. The stress of the deformed element τ^{ij} may be projected onto a fixed Cartesian spatial frame x_i and the transformation equations are given by (11.135). Using (12.5) with $\theta = 0$, (11.135) is reduced to

$$\begin{aligned} &\sigma_{11} = \frac{1}{\lambda}\tau^{11}, \qquad \sigma_{22} = r^2\tau^{22} + 2r\gamma\tau^{23} + \gamma^2\tau^{33}, \qquad \sigma_{23} = \sigma_{32} = \lambda(r\tau^{23} + \gamma\tau^{33}), \\ &\sigma_{33} = \lambda^2\tau^{33}, \qquad \sigma_{12} = \sigma_{21} = \sigma_{13} = \sigma_{31} = 0 \end{aligned} \tag{12.14}$$

Since the hoop stress is $\sigma_{22} = 0$, from (12.14), it is found that

$$\tau^{22} = -\frac{\gamma}{r^2}(2r\tau^{23} + \gamma\tau^{33}) \tag{12.15}$$

12.3 The Yield Function

12.3.1 The Mises Yield Criterion

We first consider the von Mises yield function due to its simplicity. If defined in the $p^{\langle ij\rangle}$ space, the yield function is

$$\frac{1}{2}\{(\tilde{p}^{\langle 11\rangle})^2 + (\tilde{p}^{\langle 22\rangle})^2 + (\tilde{p}^{\langle 33\rangle})^2 + 2(\tilde{p}^{\langle 23\rangle})^2\} = \frac{Y^2}{3} \tag{12.16}$$

We note that (12.16) is a special case of (11.173). Using (11.172) and (12.9), we find

$$\begin{aligned}
\tilde{p}^{\langle 11\rangle} &= \tau^{\langle 11\rangle} - p = \frac{\tau^{11}}{\lambda} - p \\
\tilde{p}^{\langle 22\rangle} &= \tau^{\langle 22\rangle} - p\sqrt{1+\left(\frac{\gamma}{\lambda}\right)^2} = \frac{r^2\tau^{22}}{\sqrt{1+(\gamma/\lambda)^2}} - p\sqrt{1+\left(\frac{\gamma}{\lambda}\right)^2} \\
\tilde{p}^{\langle 33\rangle} &= \tau^{\langle 33\rangle} - p\sqrt{1+\left(\frac{\gamma}{\lambda}\right)^2} = \lambda^2\sqrt{1+\left(\frac{\gamma}{\lambda}\right)^2}\tau^{33} - p\sqrt{1+\left(\frac{\gamma}{\lambda}\right)^2} \\
\tilde{p}^{\langle 23\rangle} &= \tilde{p}^{\langle 32\rangle} = \tau^{\langle 23\rangle} + p\left(\frac{\gamma}{\lambda}\right) = \lambda r\tau^{23} + p\left(\frac{\gamma}{\lambda}\right) \\
\tilde{p}^{\langle 13\rangle} &= \tilde{p}^{\langle 12\rangle} = 0
\end{aligned} \tag{12.17}$$

where

$$p = \frac{1}{3}\left\{\frac{\tau^{11}}{\lambda} + r^2\tau^{22} + 2r\gamma\tau^{23} + (\lambda^2+\gamma^2)\tau^{33}\right\} \tag{12.18}$$

From (12.14), the true stress and the Cauchy stress are related by

$$\tau^{11} = 0, \qquad \tau^{33} = \frac{\sigma^{33}}{\lambda^2}, \qquad \tau^{23} = \frac{\sigma^{23}}{\lambda r} - \frac{\psi}{\lambda^2}\sigma^{33}, \qquad \tau^{22} = -\psi(2\tau^{23} + \psi\tau^{33}) \tag{12.19}$$

In the combined axial–torsion of thin-walled tubes, both the radial stress σ^{11} and the hoop stress σ^{22} are 0. We now substitute (12.17) to (12.19) into (12.16) to obtain

$$\begin{aligned}
&(\sigma^{23})^2\left(\frac{1}{r^2\lambda^2} + \frac{2\gamma^2}{r^4\lambda^2}\right) + \sigma^{23}\sigma^{33}\left(-\frac{4\gamma}{3r^2\lambda^3} + \frac{2\gamma}{3r^4\lambda} - \frac{4\gamma^3}{3r^4\lambda^3}\right) \\
&\quad + (\sigma^{33})^2\left(\frac{1}{18r^4} + \frac{2}{9\lambda^4} + \frac{\lambda^2}{18} + \frac{4\gamma^2}{9r^2\lambda^4} - \frac{2\gamma^2}{9r^4\lambda^2} + \frac{2\gamma^4}{9r^4\lambda^4}\right) = \frac{Y^2}{3}
\end{aligned} \tag{12.20}$$

This is the von Mises yield criterion expressed in the σ^{ij} space. If plotted in the σ^{23} versus σ^{33} space, (12.20) describes a family of ellipses, when λ or γ is varied. In the determination of yield surface with shear prestrain, the extension ratio λ is approximately 1. In this case, (12.20) reduces to

$$(\sigma^{23})^2\left(\frac{1}{r^2}+\frac{2\gamma^2}{r^4}\right)+\sigma^{23}\sigma^{33}\left(-\frac{4\gamma}{3r^2}+\frac{2\gamma}{3r^4}-\frac{4\gamma^3}{3r^4}\right)$$
$$+(\sigma^{33})^2\left(\frac{1}{18r^4}+\frac{5}{18}+\frac{4\gamma^2}{9r^2}-\frac{2\gamma^2}{9r^4}+\frac{2\gamma^4}{9r^4}\right)=\frac{\Upsilon^2}{3} \tag{12.21}$$

The size and the semi-axes of the ellipse will change with the value of γ according to (12.21). In addition, the ellipse will rotate in the σ^{23} versus σ^{33} space due to the presence of the $\sigma^{23}\sigma^{33}$ term. This term will vanish only when $\gamma = 0$, that is, at the initial yielding. This is a result that is not supported by experimental observations. Experimental results reported in Wu [2] show that the subsequent yield surface does not rotate in the case of prestrain in torsion. Therefore, the yield criterion defined by (12.16) is not realistic, and a realistic yield criterion is defined in the next section.

12.3.2 A Yield Criterion Proposed by Wu

We show in this section that, following Wu [2,3] with permission from Elsevier, we may derive a yield criterion that is suitable for use in describing the observed experimental findings of combined axial–torsion. The material under consideration can be either initially isotropic or anisotropic, but deformation induced anisotropy can occur in either case. Therefore, a yield criterion, which accounts for the evolution of yield surface, should be derived based on anisotropic considerations. For this purpose, we refer to the yield function given in (11.173), in which h_{ij} are constants and the expressions for b_{ij} may be so chosen that, after the substitution of (12.17), (11.173) reduces to

$$\begin{aligned}2\phi = {} & h_{11}(\tau^{\langle 11\rangle})^2+h_{22}(\tau^{\langle 22\rangle})^2+h_{33}(\tau^{\langle 33\rangle})^2+h_{55}(\tau^{\langle 23\rangle})^2\\ & +2h_{12}\tau^{\langle 11\rangle}\tau^{\langle 22\rangle}+2h_{13}\tau^{\langle 11\rangle}\tau^{\langle 33\rangle}+2h_{23}\tau^{\langle 22\rangle}\tau^{\langle 33\rangle}\\ & +2h_{15}\tau^{\langle 11\rangle}\tau^{\langle 23\rangle}+2h_{25}\tau^{\langle 22\rangle}\tau^{\langle 23\rangle}+2h_{35}\tau^{\langle 33\rangle}\tau^{\langle 23\rangle}\end{aligned} \tag{12.22}$$

As mentioned in Section 11.14, a preferred texture orientation develops in the tangential plane of the cylindrical surface of the tube during torsion and the direction of the preferred orientation is generally not parallel to the z-direction. It is also anticipated that a preferred texture orientation develops in the case of combined axial–torsion, but no experimental results to this effect have been reported in the literature. As a result of preferred orientation, the material is not orthotropic.

Applying the conditions of combined axial–torsion of a thin-walled tube, that is, the radial stress $\sigma_1 = \sigma_x = \tau^{\langle 11\rangle} = 0$, $\sigma_y = \sigma_2 =$ hoop stress, $\sigma_z = \sigma_3 =$ axial stress, and $\tau_{xy} = \tau_{zx} = 0$, (12.22) becomes

$$2\phi = h_{22}(\tau^{\langle 22\rangle})^2 + h_{33}(\tau^{\langle 33\rangle})^2 + h_{55}(\tau^{\langle 23\rangle})^2 + 2h_{23}\tau^{\langle 22\rangle}\tau^{\langle 33\rangle} + 2h_{25}\tau^{\langle 22\rangle}\tau^{\langle 23\rangle} + 2h_{35}\tau^{\langle 33\rangle}\tau^{\langle 23\rangle} \tag{12.23}$$

Using the anisotropy coefficients similar to those used by Hill [4] and discussed in Chapter 10, (12.23) may be written as

$$(G+H)(\tau^{\langle 22\rangle})^2 - 2G\tau^{\langle 22\rangle}\tau^{\langle 33\rangle} + 2G(\tau^{\langle 33\rangle})^2 + 2B\tau^{\langle 23\rangle}(\delta\tau^{\langle 22\rangle} + \tau^{\langle 33\rangle}) + 2M(\tau^{\langle 23\rangle})^2 = f^2 \tag{12.24}$$

where G, H, and M are material constants. In (12.24), index 2 indicates the hoop direction; 3 indicates the axial direction; δ is a parameter; and f specifies the size of the yield surface. The term containing B is a mixed normal-shear stress term and is present because the material is not orthotropic. The expression for B will be subsequently determined based on the experimental observation that the yield surface does not rotate as the shear prestrain increases. Note that Hill's (1948) quadratic yield function reduces to

$$(G+H)\sigma_y^2 - 2G\sigma_y\sigma_z + 2G\sigma_z^2 + 2M\tau_{yz}^2 = 1 \tag{12.25}$$

for a thin-walled tubular specimen with the assumption of material orthotropy. Equation (12.24) is different from (12.25) in the term that contains B and in the use of $\tau^{\langle ij\rangle}$. The yield function (12.24) was shown by Wu [2] to describe the distortion of yield surface for specimens subjected to torsion prestrain, but it has been found in a subsequent investigation [3] that it does not describe the distortion of yield surface for specimens subjected to axial prestrain. In fact, for the case of material element subjected to normal stress only, as in the case of uniform extensions reported in Section 11.14.1.1, the yield criterion defined by the physical components of the true stress τ^{ij} cannot account for the distortion of the yield surface.

In order to account for the distortion associated with axial prestrain, an axial distortion function h is introduced into the yield function, through the component $h\tau^{\langle 33\rangle}$, so that the yield function reads

$$(G+H)(\tau^{\langle 22\rangle})^2 - 2G\tau^{\langle 22\rangle}(h\tau^{\langle 33\rangle}) + 2G(h\tau^{\langle 33\rangle})^2 + 2B\tau^{\langle 23\rangle}(\delta\tau^{\langle 22\rangle} + h\tau^{\langle 33\rangle}) + 2M(\tau^{\langle 23\rangle})^2 = f^2 \tag{12.26}$$

Using (12.12), (12.26) may be expressed in terms of τ^{ij} as

$$2\phi = A_1(\tau^{22})^2 - 2A_2\tau^{22}\tau^{33} + A_3(\tau^{33})^2 + 2A_4\tau^{23}\tau^{22} + 2A_5\tau^{23}\tau^{33} + 2A_6(\tau^{23})^2 = f^2 \tag{12.27}$$

where

$$A_1 = (G+H)\frac{R^4}{1+(\gamma/\lambda)^2}, \qquad A_2 = Gh\lambda^2R^2, \qquad A_3 = 2Gh^2\lambda^4\left(1+\left(\frac{\gamma}{\lambda}\right)^2\right),$$
$$A_4 = \frac{B\delta\lambda R^3}{\sqrt{1+(\gamma/\lambda)^2}}, \qquad A_5 = BRh\lambda^3\sqrt{1+\left(\frac{\gamma}{\lambda}\right)^2}, \qquad A_6 = M\lambda^2R^2 \tag{12.28}$$

Since the experimental yield surfaces are determined in the σ_{23} versus σ_{33} space, (12.27) is transformed into this space by use of (12.19), and the result is

$$\sigma_{23}^2\left[2M - \frac{4B\delta\gamma}{\lambda\sqrt{1+\gamma^2/\lambda^2}} + \frac{4G\gamma^2}{(1+\gamma^2/\lambda^2)\lambda^2} + \frac{4H\gamma^2}{(1+\gamma^2/\lambda^2)\lambda^2}\right]$$
$$+ \sigma_{23}\sigma_{33}\left[2Bh\sqrt{1+\frac{\gamma^2}{\lambda^2}} + \frac{4(Gh-M)\gamma}{\lambda} + \frac{6B\delta\gamma^2}{\lambda^2\sqrt{1+\gamma^2/\lambda^2}}\right.$$
$$\left. - \frac{4(G+H)\gamma^3}{(1+\gamma^2/\lambda^2)\lambda^3}\right] + \sigma_{33}^2\left[2Gh^2\left(1+\frac{\gamma^2}{\lambda^2}\right) - \frac{2Bh\gamma\sqrt{1+\gamma^2/\lambda^2}}{\lambda}\right.$$
$$\left. - \frac{2(Gh-M)\gamma^2}{\lambda^2} - \frac{4B\delta\gamma^3}{\lambda^3\sqrt{1+\gamma^2/\lambda^2}} + \frac{G\gamma^4}{(1+\gamma^2/\lambda^2)\lambda^4} + \frac{H\gamma^4}{(1+\gamma^2/\lambda^2)\lambda^4}\right]$$
$$= f^2 \tag{12.29}$$

From the experimental observations discussed in Chapter 7, the yield surface will undergo change in size, translation, and distortion as prestrain increases. For proportional loading shown by paths (1), (2), and (3) of Figure 7.2, the initial yield surface, which is a circle, will gradually become distorted as the prestrain increases with the flattened ellipse facing the origin of the stress space. This phenomenon can be described when the coefficient of $\sigma_{23}\sigma_{33}$ in (12.29) is given by the following expression

$$2Bh\sqrt{1+\frac{\gamma^2}{\lambda^2}} + \frac{4(Gh-M)\gamma}{\lambda} + \frac{6B\delta\gamma^2}{\lambda^2\sqrt{1+\gamma^2/\lambda^2}} - \frac{4(G+H)\gamma^3}{(1+\gamma^2/\lambda^2)\lambda^3} = \xi\sin 2\varphi \tag{12.30}$$

where ξ is a material parameter to be determined; φ is the angle determined by the plastic strain path as suggested by Helling et al. [5] and the relation is

$$\varphi = \tan^{-1}\left(\frac{2D_{23}^{\mathrm{p}}}{D_{33}^{\mathrm{p}}}\right) \tag{12.31}$$

where D_{23}^{p} and D_{33}^{p} are the plastic parts of the rate of deformation for the shear and axial components, respectively. From (12.30), B can be derived as

$$B = \frac{(4(G+H)\gamma^3)/(1+\gamma^2/\lambda^2)\lambda^3 - (4(Gh-M)\gamma)/\lambda + \xi\sin 2\varphi}{2h\sqrt{1+\gamma^2/\lambda^2} + [6\delta\gamma^2/\lambda^2\sqrt{1+\gamma^2/\lambda^2}]} \tag{12.32}$$

Upon the substitution of (12.32) into (12.29), the yield surface is now written as

$$A_{23}\sigma_{23}^2 + A_{2333}\sigma_{23}\sigma_{33} + A_{33}\sigma_{33}^2 = f^2 \tag{12.33}$$

with

$$\begin{aligned}
A_{23} &= \frac{2\{(2hH+hM+2H\delta-M\delta)\gamma^4 + (2hH+2hM-M\delta)\gamma^2\lambda^2 + hM\lambda^4\}}{(\gamma^2+\lambda^2)[3\gamma^2\delta + h(\gamma^2+\lambda^2)]} \\
&\quad + \frac{2\{2G\gamma^2[\gamma^2\delta + h(1+2\delta)(\gamma^2+\lambda^2)] - \gamma\delta\lambda(\gamma^2+\lambda^2)\xi\sin 2\varphi\}}{(\gamma^2+\lambda^2)[3\gamma^2\delta + h(\gamma^2+\lambda^2)]} \\
A_{2333} &= \xi\sin 2\varphi \\
A_{33} &= \frac{G[-\gamma^6\delta - h\gamma^4(3+2\delta)(\gamma^2+\lambda^2) + 2h^2\gamma^2(1+3\delta)(\gamma^2+\lambda^2)^2 + 2h^3(\gamma^2+\lambda^2)^3]}{\lambda^2(\gamma^2+\lambda^2)[3\gamma^2\delta + h(\gamma^2+\lambda^2)]} \\
&\quad - \frac{\gamma^2\{\gamma^2\delta[H\gamma^2 - 2M(\gamma^2+\lambda^2)] + h(\gamma^2+\lambda^2)[3H\gamma^2 + 2M(\gamma^2+\lambda^2)]\}}{\lambda^2(\gamma^2+\lambda^2)[3\gamma^2\delta + h(\gamma^2+\lambda^2)]} \\
&\quad - \frac{\gamma\lambda(\gamma^2+\lambda^2)[\gamma^2\delta + h(\gamma^2+\lambda^2)]\xi\sin 2\varphi}{\lambda^2(\gamma^2+\lambda^2)[3\gamma^2\delta + h(\gamma^2+\lambda^2)]}
\end{aligned} \tag{12.34}$$

Equation (12.33) describes an ellipse and it can account for the distortion of the yield surface through the change in the aspect ratio of the ellipse as the plastic strain increases. It is interesting to see that the coefficients of (12.33) are functions of extension ratio λ and shear strain γ, which is a consequence of defining the yield function in terms of $\tau^{\langle ij\rangle}$. This is a natural way to account for changes in the shape and size of the yield surface. If we set $\varphi = 0$ and $\gamma = 0$, which is the case of axial loading corresponding to path (1) of Figure 7.2,

the yield criterion (12.33) is reduced to

$$2M\sigma_{23}^2 + 2Gh^2\sigma_{33}^2 = f^2 \tag{12.35}$$

We see that without the function h, (12.35) is not capable of describing the distortion of the yield surface during axial loading. The form of h will be proposed later, but it will be a function of the axial prestrain $\varepsilon = \ln \lambda$, with the constraint that h reduces to 1 when $\varepsilon = 0$.

A combined isotropic–kinematic-hardening rule is applied in this investigation, and the yield function from (12.27) is written as

$$\begin{aligned} 2\phi = {} & A_1(\tilde{\xi}^{22})^2 - 2A_2\tilde{\xi}^{22}\tilde{\xi}^{33} + A_3(\tilde{\xi}^{33})^2 + 2A_4\tilde{\xi}^{23}\tilde{\xi}^{22} + 2A_5\tilde{\xi}^{23}\tilde{\xi}^{33} \\ & + 2A_6(\tilde{\xi}^{23})^2 = f^2 \qquad \text{with } \tilde{\xi}^{ij} = \tau^{ij} - \tilde{\alpha}^{ij} \end{aligned} \tag{12.36}$$

where $\tilde{\alpha}^{ij}$ is the back stress in the τ^{ij} — stress space. The evolution of the back stress is discussed later; but the back stress $\tilde{\alpha}^{ij}$ may be projected onto a fixed Cartesian spatial frame x_i with components α_{ij} and the transformation equations are

$$\alpha_{ij} = \frac{\partial x_i}{\partial \theta^{\mathrm{P}}} \frac{\partial x_j}{\partial \theta^q} \tilde{\alpha}^{pq} \tag{12.37}$$

In the case of combined axial–torsion, the nonzero components of α_{ij} are α_{22}, α_{23}, and α_{33}. Thus, (12.37) reduces to

$$\tilde{\alpha}^{22} = \frac{\alpha_{33}\gamma^2 - 2\alpha_{23}\gamma\lambda + \alpha_{22}\lambda^2}{r^2\lambda^2}, \qquad \tilde{\alpha}^{23} = \frac{-\alpha_{33}\gamma + \alpha_{23}\lambda}{r\lambda^2}, \qquad \tilde{\alpha}^{33} = \frac{\alpha_{33}}{\lambda^2} \tag{12.38}$$

12.4 Flow Rule and Strain Hardening

The rate of change of the strain tensor may be projected onto the fixed Cartesian spatial frame x_i and the transformation equations are, from (11.154),

$$D_{ij} = \frac{1}{2} \frac{\partial \theta^{\mathrm{P}}}{\partial x_i} \frac{\partial \theta^q}{\partial x_j} \frac{\mathrm{D} g_{pq}}{\mathrm{D}t} \tag{12.39}$$

where D_{ij} is the rate of deformation tensor and it may be decomposed into the elastic and the plastic parts as

$$D_{ij} = D^e_{ij} + D^{\mathrm{p}}_{ij}, \qquad D^e_{ij} = \frac{1}{2}\frac{\partial \theta^{\mathrm{p}}}{\partial x_i}\frac{\partial \theta^{q}}{\partial x_j}\frac{\mathrm{D}g^e_{ij}}{\mathrm{D}t}, \quad \text{and} \quad D^{\mathrm{p}}_{ij} = \frac{1}{2}\frac{\partial \theta^{\mathrm{p}}}{\partial x_i}\frac{\partial \theta^{q}}{\partial x_j}\frac{\mathrm{D}g^{\mathrm{p}}_{ij}}{\mathrm{D}t} \tag{12.40}$$

in which D^e_{ij} and g^e_{ij} are the elastic part and D^{p}_{ij} and g^{p}_{ij} are the plastic part, respectively. The flow rule from (11.200) is

$$\frac{\mathrm{D}g^{\mathrm{p}}_{ij}}{\mathrm{D}t} = \dot{\Lambda}\frac{\partial \phi}{\partial \tau^{ij}} \tag{12.41}$$

where $\dot{\Lambda}$ is the plastic multiplier. Using (12.36), the flow rule becomes

$$\begin{aligned}
\frac{\mathrm{D}g^{\mathrm{p}}_{22}}{\mathrm{D}t} &= \dot{\Lambda}(A_1\tilde{\xi}^{22} - A_2\tilde{\xi}^{33} + A_4\tilde{\xi}^{23}) \\
\frac{\mathrm{D}g^{\mathrm{p}}_{33}}{\mathrm{D}t} &= \dot{\Lambda}(-A_2\tilde{\xi}^{22} + A_3\tilde{\xi}^{33} + A_5\tilde{\xi}^{23}) \\
\frac{\mathrm{D}g^{\mathrm{p}}_{23}}{\mathrm{D}t} &= \dot{\Lambda}\left(\frac{1}{2}A_4\tilde{\xi}^{22} + \frac{1}{2}A_5\tilde{\xi}^{33} + A_6\tilde{\xi}^{23}\right)
\end{aligned} \tag{12.42}$$

On the other hand, the third equation of (12.40), using (12.5) with $\theta = 0$ and (12.42), reduces to

$$\begin{aligned}
\frac{\mathrm{D}g^{\mathrm{p}}_{22}}{\mathrm{D}t} &= 2r^2 D^{\mathrm{p}}_{22} = \dot{\Lambda}(A_1\xi^{22} - A_2\xi^{33} + A_4\xi^{23}) \\
\frac{\mathrm{D}g^{\mathrm{p}}_{33}}{\mathrm{D}t} &= 2\gamma^2 D^{\mathrm{p}}_{22} + 4\gamma\lambda D^{\mathrm{p}}_{23} + 2\lambda^2 D^{\mathrm{p}}_{33} = \dot{\Lambda}(-A_2\xi^{22} + A_3\xi^{33} + A_5\xi^{23}) \\
\frac{\mathrm{D}g^{\mathrm{p}}_{23}}{\mathrm{D}t} &= 2r\gamma D^{\mathrm{p}}_{22} + 2r\lambda D^{\mathrm{p}}_{23} = \dot{\Lambda}\left(\frac{1}{2}A_4\xi^{22} + \frac{1}{2}A_5\xi^{33} + A_6\xi^{23}\right)
\end{aligned} \tag{12.43}$$

where

$$\xi^{ij} = \sigma^{ij} - \alpha^{ij} \tag{12.44}$$

This set of equations may be solved to obtain

$$\begin{aligned}
D^{\mathrm{p}}_{33} &= \dot{\Lambda}(\eta_1\xi_{23} + \eta_2\xi_{33} - \eta_6\alpha_{22}) \\
D^{\mathrm{p}}_{23} &= \dot{\Lambda}(\eta_3\xi_{23} + 0.5\eta_1\xi_{33} - 0.5\eta_5\alpha_{22}) \\
D^{\mathrm{p}}_{22} &= \dot{\Lambda}(\eta_5\xi_{23} + \eta_6\xi_{33} + \eta_9\alpha_{22})
\end{aligned} \tag{12.45}$$

where

$$\begin{aligned}
\eta_1 &= \frac{A_5}{2r\lambda^3} + \frac{(A_2 - A_6)\gamma}{r^2\lambda^3} + \frac{3A_4\gamma^2}{2r^3\lambda^3} - \frac{A_1\gamma^3}{r^4\lambda^3} \\
\eta_2 &= \frac{A_3}{2\lambda^4} - \frac{A_5\gamma}{r\lambda^4} - \frac{(A_2 - A_6)\gamma^2}{r^2\lambda^4} - \frac{A_4\gamma^3}{r^3\lambda^4} + \frac{A_1\gamma^4}{2r^4\lambda^4} \\
\eta_3 &= \frac{A_6}{2r^2\lambda^2} - \frac{A_4\gamma}{r^3\lambda^2} + \frac{A_1\gamma^2}{r^4\lambda^2}, \qquad \eta_5 = \frac{A_4}{2r^3\lambda} - \frac{A_1\gamma}{r^4\lambda} \\
\eta_6 &= -\frac{A_2}{2r^2\lambda^2} - \frac{A_4\gamma}{2r^3\lambda^2} + \frac{A_1\gamma^2}{2r^4\lambda^2}, \qquad \eta_9 = -\frac{A_1}{2r^4}
\end{aligned} \tag{12.46}$$

and the axial strain is $\varepsilon = \ln\lambda$ and $\lambda = \mathrm{e}^{\varepsilon}$.

The rate of plastic work is

$$\dot{W}^{\mathrm{p}} = \frac{1}{2}\tilde{\xi}^{ij}\frac{\mathrm{D}g^{\mathrm{p}}_{ij}}{\mathrm{D}t} = \xi_{ij}D^{\mathrm{p}}_{ij} \tag{12.47}$$

and it is possible to define an equivalent stress $\bar{\tau}$ and an equivalent plastic strain rate $\dot{g}^{\mathrm{p}}$ such that

$$\dot{W}^{\mathrm{p}} = \tfrac{1}{2}\bar{\tau}\dot{g}^{\mathrm{p}} \tag{12.48}$$

The expressions are

$$\begin{aligned}
\bar{\tau} &= K^{-1/2}\{A_1(\tilde{\xi}^{22})^2 - 2A_2\tilde{\xi}^{22}\tilde{\xi}^{33} + A_3(\tilde{\xi}^{33})^2 + 2A_4\tilde{\xi}^{23}\tilde{\xi}^{22} \\
&\quad + 2A_5\tilde{\xi}^{23}\tilde{\xi}^{33} + 2A_6(\tilde{\xi}^{23})^2\}^{1/2} \\
&= \frac{f}{\sqrt{K}}
\end{aligned} \tag{12.49}$$

and

$$\dot{g}^{\mathrm{p}} = \sqrt{K}f\dot{\Lambda} = \sqrt{K}\sqrt{\frac{MM}{NN}} \tag{12.50}$$

where

$$\begin{aligned}
MM &= (A_5^2 - 2A_3A_6)(\dot{g}^{\mathrm{p}}_{22})^2 + 4(A_3A_4 + A_2A_5)\dot{g}^{\mathrm{p}}_{22}\dot{g}^{\mathrm{p}}_{23} \\
&\quad + (4A_2^2 - 4A_1A_3)(\dot{g}^{\mathrm{p}}_{23})^2 - 2(A_4A_5 + 2A_2A_6)\dot{g}^{\mathrm{p}}_{22}\dot{g}^{\mathrm{p}}_{33} \\
&\quad + 4(A_2A_4 + A_1A_5)\dot{g}^{\mathrm{p}}_{23}\dot{g}^{\mathrm{p}}_{33} + (A_4^2 - 2A_1A_6)(\dot{g}^{\mathrm{p}}_{33})^2
\end{aligned} \tag{12.51}$$

$$NN = 2A_2A_4A_5 + A_1A_5^2 + 2A_2^2A_6 + A_3(A_4^2 - 2A_1A_6) \tag{12.52}$$

Note that $K = M$ and the dot "." is an abbreviated notation of $\mathrm{D}/\mathrm{D}t$. There are several definitions of K in the literature. Hill [6] and Hosford and Caddell [7] defined K based on the tension test so that $\bar{\tau} = \sigma_{11}$ in the case of simple tension. In the present work, K is defined based on free-end torsion. The different expressions for K differ only by a constant factor and they do not affect the analysis of this investigation. In the case of free-end torsion, $\sigma_{33} = \tau^{33} = 0$, and, (12.38) reduces to

$$\tilde{\alpha}^{33} = \alpha_{33} = 0, \qquad \tilde{\alpha}^{23} = \frac{\alpha_{23}}{\lambda r}, \qquad \tilde{\alpha}^{22} = \frac{\alpha_{22}}{r^2} - \frac{2\psi}{\lambda r}\alpha_{23} \tag{12.53}$$

By use of (12.19), the following expressions can then be obtained

$$\begin{aligned} \tilde{\xi}^{22} &= \tau^{22} - \tilde{\alpha}^{22} = -\left(\frac{2\psi}{\lambda r}\xi_{23} + \frac{\alpha_{22}}{r^2}\right) \\ \tilde{\xi}^{33} &= \tau^{33} - \tilde{\alpha}^{33} = 0 \\ \tilde{\xi}^{23} &= \tau^{23} - \tilde{\alpha}^{23} = \frac{\xi_{23}}{\lambda r} \end{aligned} \tag{12.54}$$

Substituting (12.54) into (12.49) and letting $\gamma = \alpha_{23} = \alpha_{22} = 0$, the resulting expression is

$$\bar{\tau} = \sqrt{2\frac{M}{K}}\sigma_{23} = \sqrt{2}\sigma_{23} \tag{12.55}$$

The last equality was obtained by setting $K = M$. It is seen that in the case of free-end torsion at small strain, $\bar{\tau}$ reduces to the shear stress.

Following Wu and Yip [8], the isotropic-hardening function is given by

$$f(\zeta) = D - (D-1)\mathrm{e}^{-\beta\zeta} \tag{12.56}$$

where D and β are material parameters, and ζ is a positive, monotonically increasing parameter that accounts for the history of plastic deformation. It is assumed that

$$\dot{\zeta} = \left|\dot{g}^{\mathrm{P}}\right| \tag{12.57}$$

During the loading process, the following equation governs the evolution of the isotropic-hardening function f

$$\dot{f} = \beta\sqrt{K}(D-f)f\dot{\Lambda} \tag{12.58}$$

The equation was derived by differentiating (12.56), and using (12.57) and the first equality of (12.50).

In the case of kinematic hardening, the corotational rate is given by

$$\boldsymbol{\alpha}^{\triangledown} = \frac{\mathrm{D}\boldsymbol{\alpha}}{\mathrm{D}t} - \boldsymbol{\varpi}\cdot\boldsymbol{\alpha} + \boldsymbol{\alpha}\cdot\boldsymbol{\varpi} \tag{12.59}$$

It has been assumed that for the combined axial–torsion problem under consideration, the spin of the ideal texture orientation may be taken as the constitutive spin $\boldsymbol{\varpi}$. Thus,

$$\boldsymbol{\varpi} = \begin{pmatrix} 0 & \omega \\ -\omega & 0 \end{pmatrix} \tag{12.60}$$

The spin $\omega(\gamma)$ is found from Qian and Wu [9] where the function $\vartheta(\gamma)$ is given, which describes the change in the orientation of the ideal texture as a function of shear strain. Thus,

$$\omega = \dot{\vartheta} = \frac{\mathrm{D}\vartheta}{\mathrm{D}\gamma}\dot{\gamma} = \frac{\mathrm{D}\vartheta}{\mathrm{D}\gamma}(2D_{23}) \tag{12.61}$$

Using the linear kinematic-hardening rule of Prager [10], the evolution equation for the back stress, from (11.204), is

$$\begin{aligned}
\overset{\triangledown}{\alpha}_{22} &= \frac{\mathrm{D}\alpha_{22}}{\mathrm{D}t} - 2\omega\alpha_{23} = 2\overset{\triangledown}{\alpha}^{\mathrm{D}}_{22} + \overset{\triangledown}{\alpha}^{\mathrm{D}}_{33} = c\bar{\kappa}(2D^{\mathrm{p}}_{22} + D^{\mathrm{p}}_{33}) \\
\overset{\triangledown}{\alpha}_{23} &= \frac{\mathrm{D}\alpha_{23}}{\mathrm{D}t} + \omega(\alpha_{22} - \alpha_{33}) = \overset{\triangledown}{\alpha}^{\mathrm{D}}_{23} = cD^{\mathrm{p}}_{23} \\
\overset{\triangledown}{\alpha}_{33} &= \frac{\mathrm{D}\alpha_{33}}{\mathrm{D}t} + 2\omega\alpha_{23} = \overset{\triangledown}{\alpha}^{\mathrm{D}}_{22} + 2\overset{\triangledown}{\alpha}^{\mathrm{D}}_{33} = c\bar{\kappa}(D^{\mathrm{p}}_{22} + 2D^{\mathrm{p}}_{33})
\end{aligned} \tag{12.62}$$

where c is a constant and $\bar{\kappa}$ is a parameter that specifies the anisotropic rate of kinematic hardening. The proposed form for $\bar{\kappa}$ is

$$\bar{\kappa} = \bar{\kappa}_{\mathrm{T}} + (\bar{\kappa}_{\mathrm{A}} - \bar{\kappa}_{\mathrm{T}})\cos\,\varphi \tag{12.63}$$

where $\bar{\kappa}_{\mathrm{A}}$ is the value of $\bar{\kappa}$ for the case of axial prestrain, and $\bar{\kappa}_{\mathrm{T}}$ is the value of $\bar{\kappa}$ for the case of torsion.

12.5 Elastic Constitutive Equations

In the combined axial–torsion problem, the rate of deformation and the spin tensors are

$$\mathbf{D} = \begin{pmatrix} D_{22} & D_{23} \\ D_{23} & D_{33} \end{pmatrix} \quad \text{and} \quad \mathbf{W} = \begin{pmatrix} 0 & D_{23} \\ -D_{23} & 0 \end{pmatrix} \tag{12.64}$$

respectively. The convected stress rate can be found from (11.143) and (12.64), referring to the x_i frame, as

$$\sigma_{ij}^{*} = \frac{\mathrm{D}\sigma_{ij}}{\mathrm{D}t} - \begin{pmatrix} 2\sigma_{23}D_{23} & \sigma_{23}(D_{22}+D_{33}) + \sigma_{33}D_{23} \\ \sigma_{23}(D_{22}+D_{33}) + \sigma_{33}D_{23} & 2(\sigma_{23}D_{23} + \sigma_{33}D_{33}) \end{pmatrix} \tag{12.65}$$

In the formulation to be presented, we assume for simplicity that the elastic behavior is isotropic. This assumption has minimal effect on the anisotropic, large plastic deformation. The elastic constitutive equation is

$$2\mu D_{ij}^{\mathrm{e}} = 2\mu(D_{ij} - D_{ij}^{\mathrm{p}}) = \sigma_{ij}^{*} - \overset{\nabla}{\alpha}_{ij} \tag{12.66}$$

Using (12.62) and (12.65), the three component equations of (12.66) are

$$\begin{aligned} 2\mu D_{22} &= -2\sigma_{23}D_{23} + 2(\mu - c\bar{\kappa})D_{22}^{\mathrm{p}} - c\bar{\kappa}D_{33}^{\mathrm{p}} \\ 2(\sigma_{33}+\mu)D_{33} &= \frac{\mathrm{D}\sigma_{33}}{\mathrm{D}t} - 2\sigma_{23}D_{23} - c\bar{\kappa}D_{22}^{\mathrm{p}} + 2(\mu - c\bar{\kappa})D_{33}^{\mathrm{p}} \\ (2\mu+\sigma_{33})D_{23} &= \frac{\mathrm{D}\sigma_{23}}{\mathrm{D}t} - \sigma_{23}(D_{22}+D_{33}) + 2(\mu - c\bar{\kappa})D_{23}^{\mathrm{p}} \end{aligned} \tag{12.67}$$

These are the equations for determination of the rate of deformation.

12.6 Algorithm for Computation

The return-mapping algorithm [11] is used for computation. By use of (12.65) and (12.66), the elastic trials are

$$\begin{aligned} (\sigma_{23})_{n+1}^{\mathrm{T}} &= (\sigma_{23})_n + \Delta\sigma_{23} = (\sigma_{23})_n + \Delta^{*}\sigma_{23} + \sigma_{23}(D_{22}+D_{33})\Delta t + \sigma_{33}D_{23}\Delta t \\ (\sigma_{33})_{n+1}^{\mathrm{T}} &= (\sigma_{33})_n + \Delta\sigma_{33} = (\sigma_{33})_n + \Delta^{*}\sigma_{33} + 2(\sigma_{23}D_{23} + \sigma_{33}D_{33})\Delta t \end{aligned} \tag{12.68}$$

where $\Delta^{*}\sigma_{23}$ and $\Delta^{*}\sigma_{33}$ are the stress increments using the convected rate and Δt is the time increment. The stresses are

$$\begin{aligned} (\sigma_{23})_{n+1} &= (\sigma_{23})_{n+1}^{\mathrm{T}} - 2\mu D_{23}^{\mathrm{p}}\Delta t = (\sigma_{23})_n + \sigma_{23}(D_{22}+D_{33})\Delta t \\ &\qquad + \sigma_{33}D_{23}\Delta t + 2\mu D_{23}\Delta t - (2\mu - c)D_{23}^{\mathrm{p}}\Delta t \\ (\sigma_{33})_{n+1} &= (\sigma_{33})_{n+1}^{\mathrm{T}} - 2\mu D_{33}^{\mathrm{p}}\Delta t = (\sigma_{33})_n + 2\mu D_{33}\Delta t + 2(\sigma_{23}D_{23} + \sigma_{33}D_{33})\Delta t \\ &\qquad + [c\bar{\kappa}D_{22}^{\mathrm{p}} + 2(c\bar{\kappa} - \mu)D_{33}^{\mathrm{p}}]\Delta t \end{aligned} \tag{12.69}$$

The increment of the back stress may be determined from (12.62) as

$$\begin{aligned}(\alpha_{22})_{n+1} &= (\alpha_{22})_n + 2(\omega\Delta t)(\alpha_{23})_n + c\bar{\kappa}(2D^{\mathrm{p}}_{22} + D^{\mathrm{p}}_{33})\Delta t \\ (\alpha_{33})_{n+1} &= (\alpha_{33})_n - 2(\omega\Delta t)(\alpha_{23})_n + c\bar{\kappa}(D^{\mathrm{p}}_{22} + 2D^{\mathrm{p}}_{33})\Delta t \\ (\alpha_{23})_{n+1} &= (\alpha_{23})_n - (\omega\Delta t)(\alpha_{22} - \alpha_{33})_n + cD^{\mathrm{p}}_{23}\Delta t\end{aligned} \tag{12.70}$$

and that of the isotropic-hardening function f, from (12.58), as

$$f_{n+1} = f_n + \beta\sqrt{K}(D - f_n)f_n\Delta\Lambda \tag{12.71}$$

In addition,

$$\begin{aligned}(\xi_{23})_{n+1} &= (\sigma_{23})_{n+1} - (\alpha_{23})_{n+1} \\ &= (\xi_{23})_n + (\omega\Delta t)(\alpha_{22} - \alpha_{33})_n + (2\mu + \sigma_{33})D_{23}\Delta t \\ &\quad + \sigma_{23}(D_{22} + D_{33})\Delta t - 2\mu D^{\mathrm{p}}_{23}\Delta t \\ (\xi_{33})_{n+1} &= (\sigma_{33})_{n+1} - (\alpha_{33})_{n+1} \\ &= (\xi_{33})_n + (2\omega\Delta t)(\alpha_{23})_n + 2(\mu + \sigma_{33})D_{33}\Delta t \\ &\quad + 2\sigma_{23}D_{23}\Delta t - 2\mu D^{\mathrm{p}}_{33}\Delta t\end{aligned} \tag{12.72}$$

where

$$\Delta\Lambda = \dot{\Lambda}\Delta t \tag{12.73}$$

and

$$\begin{aligned}D^{\mathrm{p}}_{33}\Delta t &= \Delta\Lambda(\eta_1\xi_{23} + \eta_2\xi_{33} - \eta_6\alpha_{22}) \\ D^{\mathrm{p}}_{23}\Delta t &= \Delta\Lambda(\eta_3\xi_{23} + 0.5\eta_1\xi_{33} - 0.5\eta_5\alpha_{22}) \\ D^{\mathrm{p}}_{22}\Delta t &= \Delta\Lambda(\eta_5\xi_{23} + \eta_6\xi_{33} + \eta_9\alpha_{22})\end{aligned} \tag{12.74}$$

By use of (12.14) and (12.38), the yield function (12.36) reduces to

$$\Phi = 2\phi = A_{23}\xi^2_{23} + A_{2333}\xi_{23}\xi_{33} + A_{33}\xi^2_{33} = f^2 \tag{12.75}$$

and the consistency condition of the yield function may be found by setting up the function

$$g = \Phi_{n+1} - f^2_{n+1} \tag{12.76}$$

with the conditions that if $g < 0$, then $\Delta\Lambda = 0$; and if $g \geq 0$, then $\Delta\Lambda$ is determined by iteration so that $g = 0$. Knowing $\Delta\Lambda$, $\dot{\Lambda}$ can be determined from (12.73) and the result substituted into (12.74) to determine the plastic strain components. Finally, the axial strain ε and the shear strain γ

are updated by use of

$$\begin{aligned}(\varepsilon)_{n+1} &= (\varepsilon)_n + D_{33}\Delta t \\ (\gamma)_{n+1} &= (\gamma)_n + 2D_{23}\Delta t\end{aligned} \tag{12.77}$$

12.7 Nonlinear Kinematic Hardening

We use the nonlinear-hardening rule of endochronic theory for kinematic hardening and, by use of the corotational rate, write

$$\overset{\triangledown}{\alpha}{}^{\mathrm{D}}_{ij} = \frac{2}{3}cD^{\mathrm{p}}_{ij} - \kappa\alpha^{\mathrm{D}}_{ij}\dot{\zeta} \qquad \text{with } \overset{\triangledown}{\alpha}{}^{\mathrm{D}}_{11} + \overset{\triangledown}{\alpha}{}^{\mathrm{D}}_{22} + \overset{\triangledown}{\alpha}{}^{\mathrm{D}}_{33} = 0 \tag{12.78}$$

where α^{D}_{ij} is the deviatoric part of back stress α_{ij}; c and κ are parameters. Wu and Yang [12] and Wu et al. [13] had applied this rule to investigate loading of nonproportional axial–torsion strain paths. Equation (12.78) is similar to (6.87) and is also known as the Armstrong and Frederick [14] kinematic-hardening rule. By use of (12.78), (12.62) should be replaced by, see Wu [15],

$$\begin{aligned}\overset{\triangledown}{\alpha}_{22} &= \frac{\mathrm{D}\alpha_{22}}{\mathrm{D}t} - 2\omega\alpha_{23} = 2\overset{\triangledown}{\alpha}{}^{\mathrm{D}}_{22} + \overset{\triangledown}{\alpha}{}^{\mathrm{D}}_{33} = \frac{2}{3}c(2D^{\mathrm{p}}_{22} + D^{\mathrm{p}}_{33}) - \kappa\alpha_{22}\dot{\zeta} \\ \overset{\triangledown}{\alpha}_{23} &= \frac{\mathrm{D}\alpha_{23}}{\mathrm{D}t} + \omega(\alpha_{22} - \alpha_{33}) = \overset{\triangledown}{\alpha}{}^{\mathrm{D}}_{23} = \frac{2}{3}cD^{\mathrm{p}}_{23} - \kappa\alpha_{23}\dot{\zeta} \\ \overset{\triangledown}{\alpha}_{33} &= \frac{\mathrm{D}\alpha_{33}}{\mathrm{D}t} + 2\omega\alpha_{23} = \overset{\triangledown}{\alpha}{}^{\mathrm{D}}_{22} + 2\overset{\triangledown}{\alpha}{}^{\mathrm{D}}_{33} = \frac{2}{3}c(D^{\mathrm{p}}_{22} + 2D^{\mathrm{p}}_{33}) - \kappa\alpha_{33}\dot{\zeta}\end{aligned} \tag{12.79}$$

Similarly, (12.67) should be replaced by the following set of equations

$$\begin{aligned}2\mu D_{22} &= -2\sigma_{23}D_{23} + 2\left(\mu - \frac{2}{3}c\right)D^{\mathrm{p}}_{22} - \frac{2}{3}cD^{\mathrm{p}}_{33} + \kappa\alpha_{22}\dot{\zeta} \\ 2(\sigma_{33} + \mu)D_{33} &= \frac{\mathrm{D}\sigma_{33}}{\mathrm{D}t} - 2\sigma_{23}D_{23} - \frac{2}{3}cD^{\mathrm{p}}_{22} + 2\left(\mu - \frac{2}{3}c\right)D^{\mathrm{p}}_{33} + \kappa\alpha_{33}\dot{\zeta} \\ (2\mu + \sigma_{33})D_{23} &= \frac{\mathrm{D}\sigma_{23}}{\mathrm{D}t} - \sigma_{23}(D_{22} + D_{33}) + 2\left(\mu - \frac{2}{3}c\right)D^{\mathrm{p}}_{23} + \kappa\alpha_{23}\dot{\zeta}\end{aligned} \tag{12.80}$$

12.8 Description of Yield Surface with Various Preloading Paths

In the testing of thin-walled tubes under combined axial–torsion condition, the axial load F and torque T are measurable quantities and they need to

be transformed into normal and shear stresses applied to the end-sections of a tubular specimen. An initially rectangular element on the wall of the tube will become distorted, and the convected material element is shown in Figure 12.2, where 3 is along the axial direction of the tube. Face (2) of the deformed element is parallel to the end-sections of the tubular specimen and the normal and tangential forces acting on this face are now considered. The unit normal to Face (2) is

$$\mathbf{n} = \frac{\mathbf{g}^3}{\sqrt{g^{33}}} = \lambda \mathbf{g}^3 \tag{12.81}$$

with $\tilde{n}_3 = \lambda$, $\tilde{n}_1 = \tilde{n}_2 = 0$. From (11.114), the stress vector is

$$\mathbf{t}^{(n)} = \tilde{n}_i \tau^{ij} \mathbf{g}_j = \lambda \tau^{3j} \mathbf{g}_j \tag{12.82}$$

and the tangential and normal components of the stress vector are

$$t^{(n)t} = \mathbf{t}^{(n)} \cdot \frac{\mathbf{g}_2}{\sqrt{G_{22}}} = \sigma_{23} \quad \text{and} \quad t^{(n)n} = \mathbf{t}^{(n)} \cdot \frac{\mathbf{g}^3}{\sqrt{g^{33}}} = \sigma_{33} \tag{12.83}$$

respectively. Thus, the torque and the force are expressed as

$$T = 2\pi \int_{\rho_\mathrm{i}}^{\rho_\mathrm{o}} \rho^2 \sigma_{23} \, \mathrm{d}\rho \quad \text{and} \quad F = 2\pi \int_{\rho_\mathrm{i}}^{\rho_\mathrm{o}} \rho \sigma_{33} \, \mathrm{d}\rho \tag{12.84}$$

where ρ is the radial coordinate of the tube and ρ_i and ρ_o are the inner and outer radii of the tube, respectively. In the case of a thin-walled tube, the approximated expressions are

$$T = 2\pi r^2 t \sigma_{23} \quad \text{and} \quad F = 2\pi r t \sigma_{33} \tag{12.85}$$

where r is the outer radius and t the wall-thickness of the tube. Therefore, σ_{23} and σ_{33} may be calculated and plotted to determine yield surfaces in the Cauchy stress space, when T and F have been experimentally measured. The experimental results obtained in our laboratory are used in the remaining part of this section.

The theory presented in Sections 12.3 to 12.5 and 12.7 is now applied to describe the evolution of yield surface subjected to various preloading paths. The algorithm for computation presented in Section 12.6 is used, supplemented by specific conditions imposed in each case. The problem considered is related to the combined axial–torsion of a thin-walled tube with prestrains into the large strain range.

As mentioned in Chapter 7, only experiments reported in [3,5,16] have determined subsequent yield surfaces with prestrain in the large strain range. The paper by Helling et al. [5] is very informative and it presented yield

surfaces with several different preloading paths. It does not, however, contain the axial preloading path, which is shown as path (1) in Figure 7.2. This is an important path because it determines parameters and material functions associated with yield surface distortion subjected to axial prestrain and it, therefore, also influences the surface distortion for combined axial–torsion paths. On the other hand, the experiments conducted in our laboratory and reported in [3,16] have determined yield surfaces with both preloading paths (1) and (2), and this set of data provide more complete information for the determination of material constants. In this regard, we report an investigation by Wu [3] for the case of "linear" kinematic hardening and by Wu [15] for the case of nonlinear kinematic hardening. In both investigations path (1) has been used to determine material parameters associated with axial loading and path (2) to determine material parameters associated with torsion. These parameters are then used in the calculation of other paths. The material used in the experiment was high-purity cast aluminum, and its behavior in torsion was reported in Wu et al. [17] and Wu [2]. The elastic moduli for this material are $E = 70.3$ GPa and $\mu = 26.2$ GPa.

Assuming that $G = pH$ and $M = qH$, where p and q are parameters, (12.33) reduces to the following expression for the case of $\gamma = 0$, $\varepsilon = 0$, and $h = 1$, that is, the initial yield surface,

$$q\sigma_{23}^2 + p\sigma_{33}^2 = \frac{f^2}{2H} \tag{12.86}$$

It can be easily seen that, when $q = 3p$, (12.86) reduces to the von Mises yield criterion. The material tested was an annealed high-purity cast aluminum with its initial yield surface closely resembling a Mises ellipse (see Figure 12.6(a)). The choice of $q = 3p$ leads to a reasonable description of the experimental data for this material and will be used in the remaining part of this chapter. Other relations between p and q may be used, if the experimental data deviates from the Mises ellipse. For a tube with anisotropy, the yield stress is higher in the 3-direction than in the 2-direction, which means $G + H > 2G$, as may be seen from (12.26) with $h = 1$. Thus, $H > G$ and $p < 1$. In this discussion, $p = 0.8$ is used for calculation. With this value of p and the relation of $q = 3p$, (12.86) reduces to the following expression for the initial yield surface

$$3\sigma_{23}^2 + \sigma_{33}^2 = \frac{1}{p}\left(\frac{f^2}{2H}\right) = (11.0 \text{ MPa})^2 \tag{12.87}$$

The last expression of (12.87) is the size of the experimental initial yield surface. Since $f = 1$ at initial yielding, the value of H may be determined as

$$H = \frac{1}{2p(11.0)^2} = 5.165 \times 10^{-3} \text{ MPa}^{-2} \tag{12.88}$$

There are two parameters c and $\bar{\kappa}$ in the linear kinematic-hardening rule (12.64). We found that if c is a constant, then the back stress would vary linearly with strain ε in the case of tensile prestrain and vary linearly with shear strain γ in the case of torsion prestrain. As it will be seen in the ensuing d iscussion that the corresponding experimental relationships are nonlinear, we will therefore use nonlinear kinematic-hardening rules. Several different nonlinear rules are possible; but, we consider two cases, compare their results, and show that different kinematic-hardening rules do lead to different results in the case of a nonproportional path. Therefore, kinematic-hardening rules should be investigated further experimentally, particularly for combined loading. In the first case, we use the linear kinematic hardening rule (12.64). In order to make the relation nonlinear, we propose that c varies as a linear function of ζ so that

$$c = c_0(1 - 1.15\zeta) \qquad \text{with } c_0 = 180 \text{ MPa} \tag{12.89}$$

In addition, we assume that $\bar{\kappa}$ depends on angle φ through (12.63), and we use $\bar{\kappa}_{\mathrm{A}} = 0.7$ and $\bar{\kappa}_{\mathrm{T}} = 0.0005$ in the calculation. This is a case of mild nonlinearity and we refer to it as the "linear" case henceforth. In the second case, we use the equations of Section 12.8, and it is a fully nonlinear case, and we refer to it as the nonlinear case henceforth. Again, there are two parameters c and κ in (12.78). But, we make these two parameters vary according to the following relations

$$\begin{aligned} c &= c_0(1 + q\zeta), \qquad \text{with } c_0 = c_{0\mathrm{T}} + (c_{0\mathrm{A}} - c_{0\mathrm{T}})\cos\varphi \\ &\text{and } q = q_{\mathrm{T}} + (q_{\mathrm{A}} - q_{\mathrm{T}})\cos\varphi \end{aligned} \tag{12.90}$$

where $c_{0A} = 425$ MPa, $c_{0\mathrm{T}} = 360$ MPa, $q_{\mathrm{A}} = 0$, $q_{\mathrm{T}} = 0.18$, and

$$\kappa = \kappa_{\mathrm{T}} + (\kappa_{\mathrm{A}} - \kappa_{\mathrm{T}})\cos\,\varphi \tag{12.91}$$

in which c_0 is the value of c when the history parameter $\zeta = 0$; $\kappa_{\mathrm{A}} = 7$; and $\kappa_{\mathrm{T}} = 3$; the subscripts A and T in (12.90) and (12.91) denote the values corresponding to axial prestrain and torsion prestrain, respectively. In addition, we use $\delta = -0.45$.

12.8.1 Path (1) — Axial Tension

This is a special case of proportional loading with $\varphi = 0$. Axial prestrain was performed with a constant axial strain rate of $D_{33} = 0.001\ \mathrm{s}^{-1}$ and the shear stress $\sigma_{23} = 0$. The isotropic-hardening function f can be determined from the experimental data reported in [3]. The size of the yield surface is determined by measuring the maximum length of the ellipse $\sigma_{23\mathrm{yield}}$ along a direction parallel to the σ_{23} axis in the σ_{23} versus σ_{33} space, and its values are

TABLE 12.1

Experimental f Values for Path (1)

Axial strain ε	History parameter ζ	Isotropic-hardening f
0	0	1.0
0.02	0.0557	2.698
0.116	0.3082	3.687
0.231	0.6079	4.075
0.45	1.175	4.417

Source: From Wu, H.C., *Int. J. Plasticity*, 19, 1773, 2003. With permission from Elsevier.

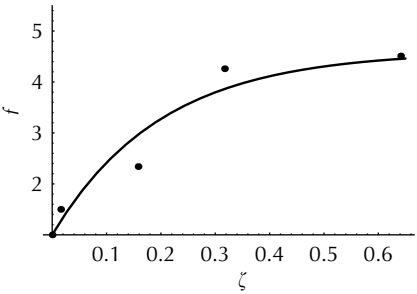

FIGURE 12.3
Isotropic-hardening function f; • Exp., — theory.

listed in Table 12.1. The values for f are then determined by setting $\sigma_{33} = 0$ in (12.33). Thus,

$$f = \sigma_{23\,\text{yield}}\sqrt{A_{23}} \tag{12.92}$$

The plastic deformation history parameter ζ is determined by integrating (12.57) with respect to time using (12.50), and its values with the corresponding axial strain ε are also listed in Table 12.1. The values of f, when plotted versus ζ, can be fitted by (12.56) with $D = 4.6$ and $\beta = 5$. The experimental data and the fitted curve are shown in Figure 12.3.

The aspect ratio of the yield surface is determined from (12.35) as

$$\frac{\sigma_{23\,\text{yield}}}{\sigma_{33\,\text{yield}}} = \sqrt{\frac{Gh^2}{M}} \tag{12.93}$$

and it has been found that the following function h can be used to describe the aspect ratio satisfactorily

$$h = [\mathrm{e}^{\varepsilon}(2.7 - 1.7\mathrm{e}^{-m\varepsilon})]^{1/2} \qquad \text{with } m = 50 \tag{12.94}$$

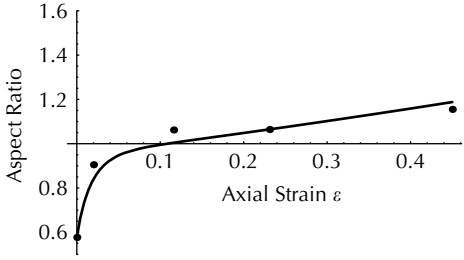

FIGURE 12.4
Aspect ratio for path (1): axial loading; • Exp., — theory (From Wu, H.C., *Int. J. Plasticity*, 19, 1773, 2003. With permission from Elsevier).

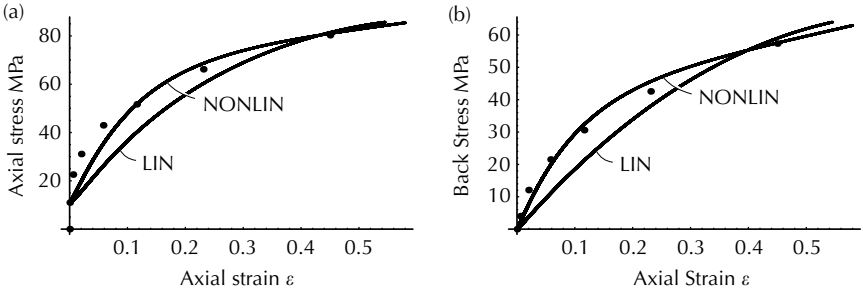

FIGURE 12.5
Path (1): (a) axial stress–strain curve, (b) back stress: • Exp., — theory (From Wu, H.C., *Int. J. Plasticity*, 19, 1773, 2003. With permission from Elsevier).

The aspect ratio for this path is plotted versus ε in Figure 12.4. The motion of the yield surface is described by the kinematic-hardening rules as previously explained. Due to $D_{23} = 0$, the constitutive spin given by (12.60) is not a factor in this case.

The numerical results are now compared with the experiments reported in [3]. Figure 12.5(a) shows the axial stress–strain curves and Figure 12.5(b) shows the back stress α_{33} plotted against ε. The theoretical curves of case 1 (the "linear" case), case 2 (the nonlinear case), and experimental data are shown. The experimental data for back stress α_{33} were determined from the experimental yield surfaces and they were the centers of the yield surfaces. The theoretical yield surfaces using nonlinear kinematic hardening at prestrains of 0, 0.58, 5.8, 11.6, 23.1, and 45% were calculated from the yield function given by (12.36) and they are shown in Figure 12.6(a) to (f) together with experimental data reported in [3]. For each value of prestrain, the isotropic-hardening function f was calculated from (12.56) and the back stress α_{33} from data of Figure 12.5(b). Figure 12.6(g) shows all theoretical yield surfaces of Figure 12.6(a) to (f) plotted in one graph. The yield surface has a significant increase in size and the aspect ratio also increases with the increasing prestrain. The yield surfaces calculated from the "linear" case are not shown, but they are in reasonable agreement with the experimental data.

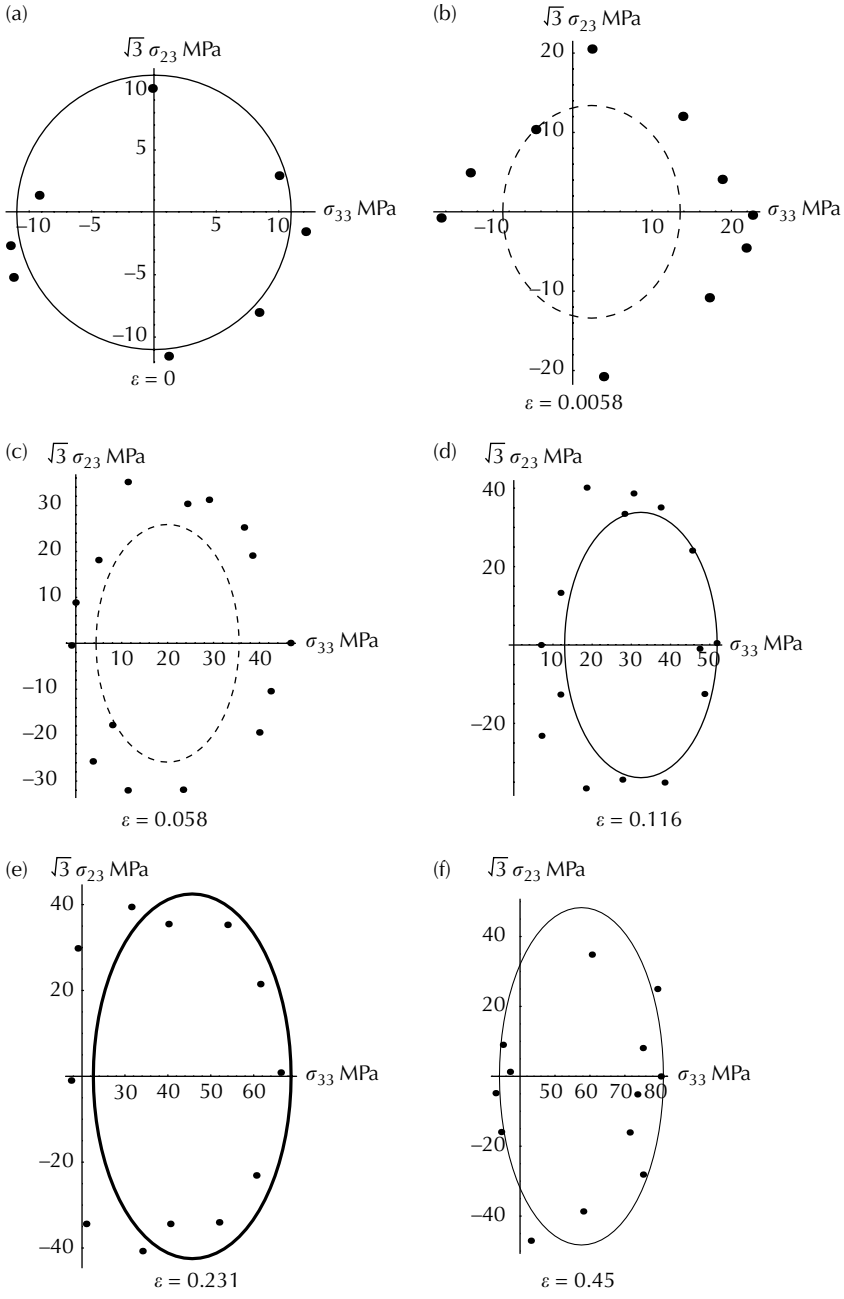

FIGURE 12.6
Yield surfaces for path (1): (a) $\varepsilon = 0$, (b) $\varepsilon = 0.58\%$, (c) $\varepsilon = 5.8\%$, (d) $\varepsilon = 11.6\%$, (e) $\varepsilon = 23.1\%$, (f) $\varepsilon = 45\%$; • Exp., — or - - - theory, (g) theoretical yield surfaces (From Wu, H.C., *Int. J. Plasticity*, 19, 1773, 2003. With permission from Elsevier).

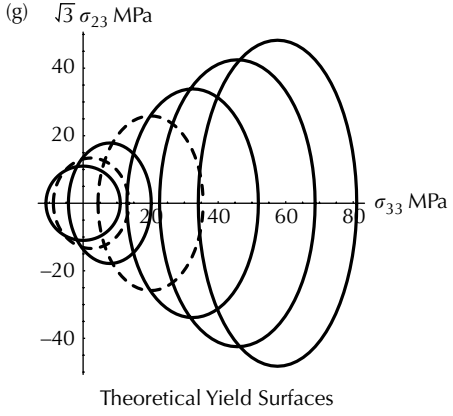

FIGURE 12.6
(Continued).

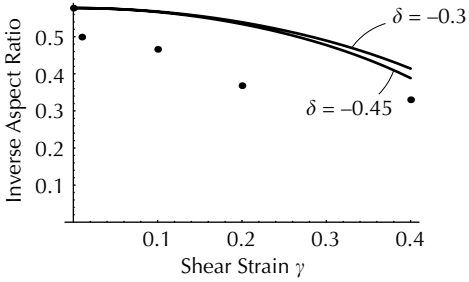

FIGURE 12.7
Inverse aspect ratio for path (2): torsion; • Exp., — theory (From Wu, H.C., *Int. J. Plasticity*, 19, 1773, 2003. With permission from Elsevier).

12.8.2 Path (2) — Torsion

We now use the same procedures as in path (1) to determine parameters of path (2). This path is also a special case of proportional loading with $\varphi = \pi/2$. The torsion prestrain was performed with a constant shear strain rate of $D_{23} = 0.001732\ \text{s}^{-1}$ and the axial stress $\sigma_{33} = 0$ in a free-end torsion condition. The inverse aspect ratio for the ellipse is

$$\frac{\sigma_{23\,\text{yield}}}{\sigma_{33\,\text{yield}}} = \sqrt{\frac{A_{33}}{A_{23}}} \tag{12.95}$$

which has the value of 0.577 (Mises) when $\gamma = 0$ and 0.388 when $\gamma = 0.4$ for the case of $\delta = -0.45$. Thus, the ellipse flattens as the plastic strain increases. The amount of flattening is influenced by the value of δ. The inverse aspect ratio for this path is plotted versus γ in Figure 12.7 for the cases of $\delta = -0.3$ and -0.45.

TABLE 12.2

Experimental f Values for Path (2)

Shear strain γ	History parameter ζ	Isotropic-hardening f
0	0	1.0
0.01	0.0156	1.50
0.1	0.158	2.34
0.2	0.317	4.26
0.4	0.641	4.51

Source: From Wu, H.C., *Int. J. Plasticity*, 19, 1773, 2003. With permission from Elsevier.

The isotropic-hardening function f has been determined earlier by use of the data of path (1). The parameters of (12.56) were found to be $D = 4.6$ and $\beta = 5$. We found that these parameters and the function also describe the data of path (2). The size of the experimental yield surface is determined by measuring the maximum length of the ellipse along a direction parallel to the σ_{33} axis; its values are listed in Table 12.2. The values for f are determined by setting $\sigma_{23} = 0$ in (12.33). Thus,

$$f = \sigma_{33\,\text{yield}}\sqrt{A_{33}} \tag{12.96}$$

The plastic deformation history parameter ζ is determined by integrating (12.57) with respect to time and its values with corresponding shear strains γ are listed in Table 12.2 together with the experimental f values for path (2). These values of f, when plotted versus ζ, can be well described by (12.56).

The spin of the ideal texture orientation is significant for path (2) and may be taken as the constitutive spin. The constitutive spin was determined from (12.61), where the function $\mathrm{D}\vartheta/\mathrm{D}\gamma$ was found from Qian and Wu [9] by a polynomial approximation. The expression used in the calculation was

$$\begin{aligned}\omega = 2\{&-0.431(b+\gamma)^4 + 5.1472(b+\gamma)^3 - 23.1651(b+\gamma)^2 \\ &+ 46.894(b+\gamma) - 35.97\}D_{23}\end{aligned} \tag{12.97}$$

The parameter b was used so that (12.97) became suitable for use for the material under consideration. The function ϑ found by Qian and Wu [9] was a prediction of the double-slip model of polycrystal plasticity, and it should be adjusted. We found that $b = 3$ gave us reasonable results for this calculation.

The numerical results are now compared with the experiments reported in [3]. Figure 12.8(a) shows the shear stress–strain curve; Figure 12.8(b) shows the "Swift effect"; and Figure 12.8(c) shows the back stress α_{23} plotted against γ. Theoretical curves of the "linear" case are almost identical to those of the nonlinear case. The theoretical curves and experimental data are shown. The experimental data for back stress α_{23} were determined from the experimental yield surfaces and they were the centers of the yield surfaces. The theoretical yield surfaces at prestrains of 0, 1, 10, 20, and 40%

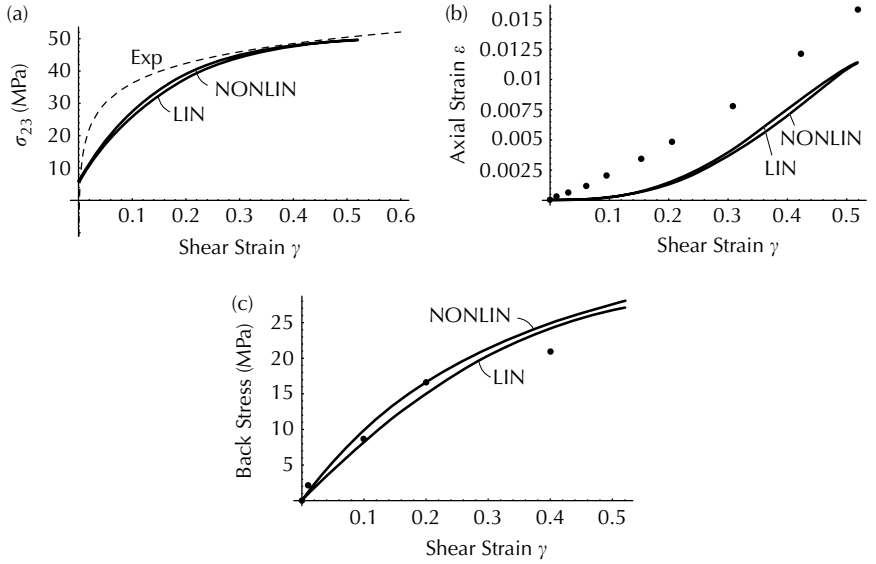

FIGURE 12.8
Path (2): (a) shear stress–strain curve, (b) the Swift effect, (c) back stress; • or - - - Exp., — theory (From Wu, H.C., *Int. J. Plasticity*, 19, 1773, 2003. With permission from Elsevier).

were calculated from the yield function given by (12.36) and they are shown in Figure 12.9(a) to (e) together with the experimental data reported in [3]. For each value of prestrain, the isotropic-hardening function f was calculated from (12.56) and the back stress α_{23} from data of Figure 12.8(b). Figure 12.9(f) shows all theoretical yield surfaces of Figure 12.9(a) to (e) plotted in one graph. The yield surface increases in size and the reverse aspect ratio reduces with the increasing prestrain.

The parameters of the theory have been determined from the tension and the free-end torsion tests, which are two special cases of proportional loading. The two rules of kinematic hardening employed in the calculation do not lead to noticeable differences in the solutions. We show in the subsequent subsections, however, that they give rise to significantly different results in the general case of proportional and nonproportional paths.

The agreement of the theory with experiment is acceptable judging from Figures 12.3 to 12.9. We mention that in these figures the theory has been tested against the following sets of experimental data: (1) axial stress–strain curve, (2) axial back stress versus axial strain, (3) subsequent yield surfaces up to a prestrain of $\varepsilon = 0.45$, (4) shear stress–strain curve, (5) the "Swift effect," (6) shear back stress versus shear strain, and (7) subsequent yield surfaces up to a shear prestrain of $\gamma = 0.40$. In the literatures, we have seen theories compared with only two sets of test data, for example, data sets (4) and (5) for the torsion test. Since only two sets of data are described by those models, it was possible to choose model parameters so that the models closely describe the two data sets. A greater challenge is whether any model can successfully describe the aforementioned seven sets of data.

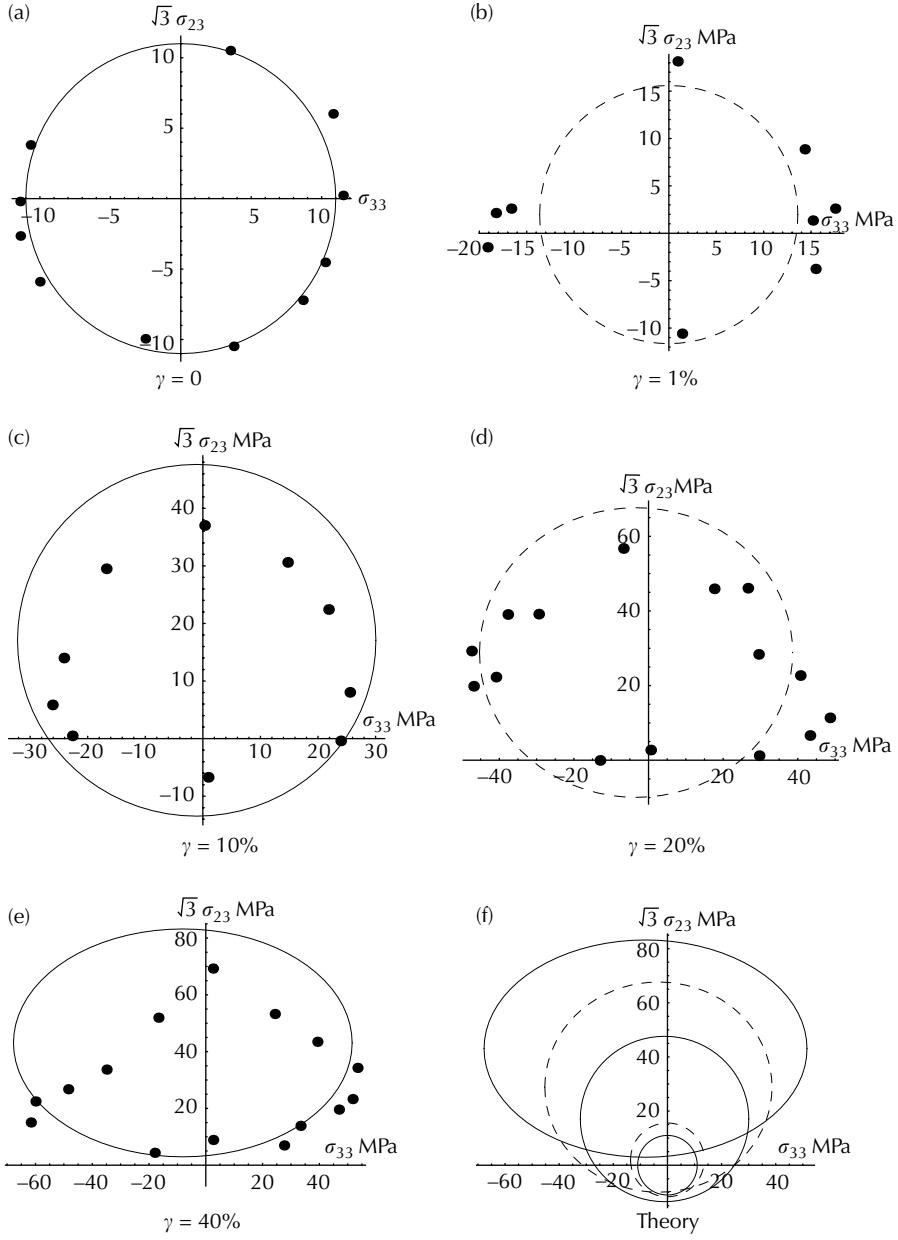

FIGURE 12.9
Yield surfaces for path (2): (a) $\gamma = 0$, (b) $\gamma = 1\%$, (c) $\gamma = 10\%$, (d) $\gamma = 20\%$, (e) $\gamma = 40\%$, (f) theory; • Exp., — or - - - theory (From Wu, H.C., *Int. J. Plasticity*, 19, 1773, 2003. With permission from Elsevier).

12.8.3 Path (3) — Proportional Loading

We use material parameters and functions determined from paths (1) and (2) to describe proportional and nonlinear paths discussed in the remaining subsections of Section 12.8. Parameter ξ has been introduced in (12.30) to describe the combined axial–torsion loading. This parameter is further expressed by

$$\xi = 0.02\varepsilon h^2 \tag{12.98}$$

A proportional strain-controlled path with constant strain-rate is defined by the angle

$$\Omega = \tan^{-1}\left(\frac{2D_{23}}{D_{33}}\right) \tag{12.99}$$

where Ω is an angle to be specified for each proportional path. The axial distortion function h of (12.94) is now modified to read

$$h = [\mathrm{e}^{\varepsilon\,\cos^2\varphi}(2.7 - 1.7\mathrm{e}^{-m\varepsilon\cos^2\varphi})]^{1/2} \qquad \text{with } m = 50 \tag{12.100}$$

which reduces to (12.94) when $\varphi = 0$. By use of nonlinear kinematic hardening, the predicted subsequent yield surfaces are shown in Figure 12.10(a) for the case of $\Omega = \pi/6$. The surfaces shown are for proportional prestrains of $\varepsilon = 0$, 0.1, 0.2, 0.3, and 0.35, respectively. Figure 12.10(b) shows the evolution of the yield surface for the case of $\Omega = \pi/3$. Yield surfaces are plotted for proportional prestrains of $\gamma = 0$, 0.1, 0.2, 0.3, 0.4, and 0.5, respectively. The dots in the figures denote the loading points for the yield surfaces, and together they form the stress paths of these tests. It is seen that a proportional strain path does not necessarily lead to a proportional stress path. Paths with other slopes can also be calculated. Figure 12.10(c) and (d) shows the corresponding yield surfaces predicted by the use of the "linear" kinematic-hardening rule. It is seen that the stress paths are different for different kinematic-hardening rules, and these different stress paths are summarized in Figure 12.11.

12.8.4 Tor–Ten Path (4)

This is the first of three nonlinear tor–ten paths to be considered. The example presented is calculated by use of "linear" kinematic hardening. It describes a case of pretorsion from 0 to a shear strain of $\gamma = 0.1$ (with a corresponding shear stress of $\sigma_{23} = 22.87$ MPa) followed by an elastic unloading to $\sigma_{23} = 5.21$ MPa, which is an approximated center of the current yield surface. Axial loading is then applied while keeping the shear stress constant at 5.21 MPa. This is a stress-controlled test with a prescribed stress increment $\Delta\sigma_{33}$ for each increment of time Δt. This section of the loading path is similar to an axial test with angle $\varphi = 0$ and $\kappa = \kappa_{\mathrm{A}} = 0.7$. The initial conditions

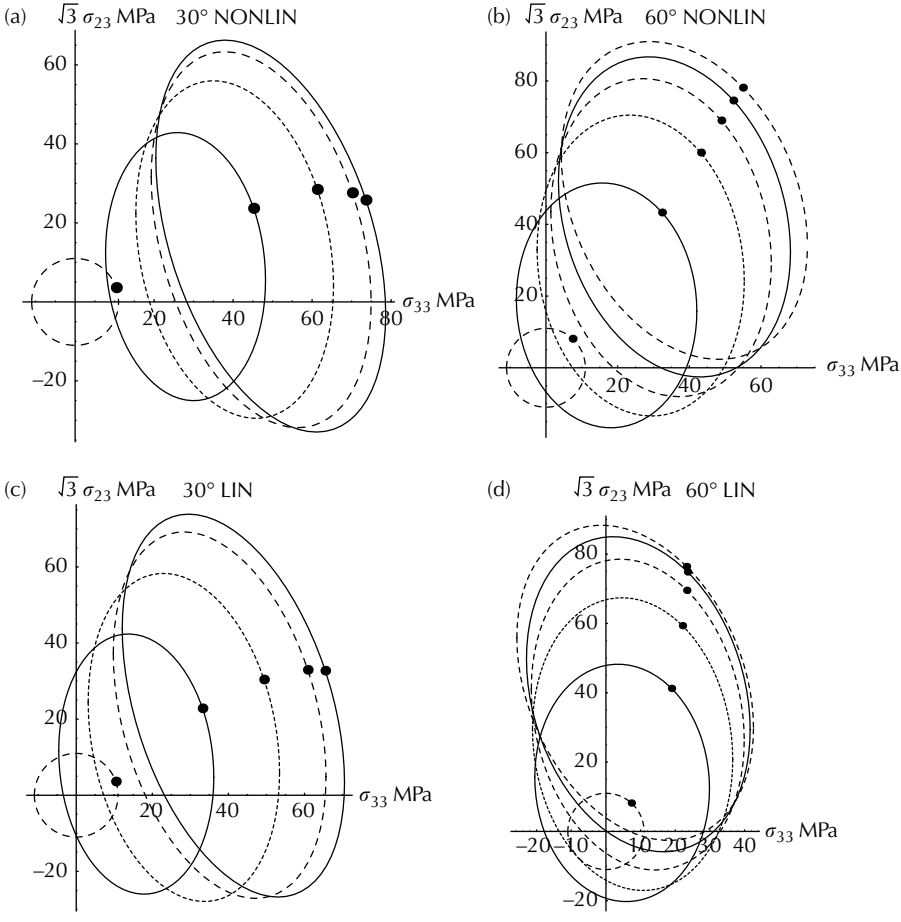

FIGURE 12.10
Theoretical yield surfaces for path (3): (a) $\Omega = \pi/6$ (nonlinear kinematic hardening), (b) $\Omega = \pi/3$ (nonlinear kinematic hardening), (c) $\Omega = \pi/6$ ("linear" kinematic hardening), (d) $\Omega = \pi/3$ ("linear" kinematic hardening); • loading point on each yield surface (From Wu, H.C., *Int. J. Plasticity*, 19, 1773, 2003. With permission from Elsevier).

are: $\sigma_{33} = 30.93$ MPa (determined from the elastic loading), $f = 2.8118$, $\alpha_{23} = 5.21$ MPa, $\alpha_{22} = 0.16$ MPa, and $\alpha_{33} = -0.16$ MPa. These data are obtained from path (2) when $\gamma = 0.1$.

The incremental expressions for the computation of this path are

$$
\begin{aligned}
(\sigma_{23})_{n+1} &= (\sigma_{23})_n \\
(\sigma_{33})_{n+1} &= (\sigma_{33})_n + \Delta\sigma_{33}\Delta t \\
(\xi_{23})_{n+1} &= (\xi_{23})_n + (\omega\Delta t)(\alpha_{22} - \alpha_{33})_n - cD^{\mathrm{p}}_{23}\Delta t \\
(\xi_{33})_{n+1} &= (\xi_{33})_n + (2\omega\Delta t)(\alpha_{23})_n + \Delta\sigma_{33}\Delta t - c\kappa(D^{\mathrm{p}}_{22} + 2D^{\mathrm{p}}_{33})\Delta t
\end{aligned}
\tag{12.101}
$$

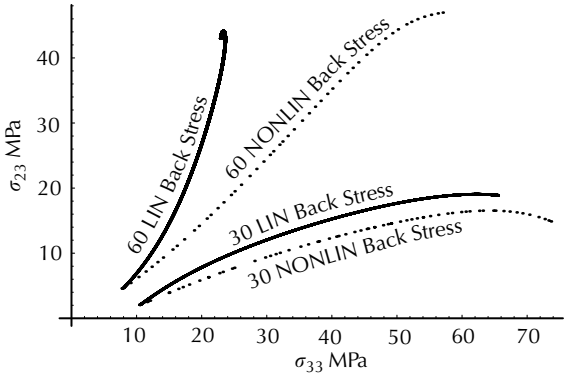

FIGURE 12.11
Stress paths in proportional straining.

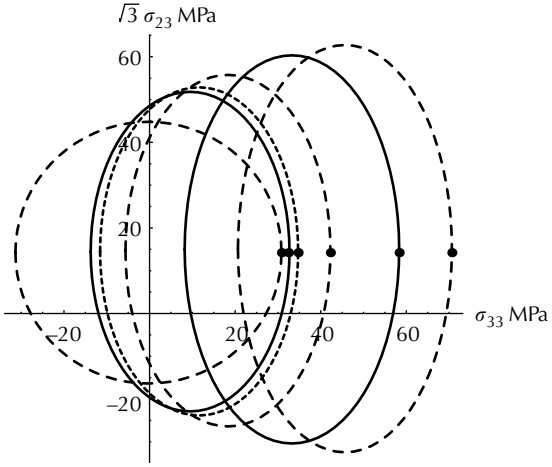

FIGURE 12.12
Evolution of yield surface for path (4) (From Wu, H.C., *Int. J. Plasticity*, 19, 1773, 2003. With permission from Elsevier).

Figure 12.12 shows the evolution of yield surface for this path. The dots represent stress points on each yield surface. By connecting these dots, one can envisage the stress path. This figure shows that no rotation of the yield surface has taken place during this loading.

12.8.5 Tor–Ten Path (5)

We consider now the case of free-end torsion to a prestrain of $\gamma = 0.1$ followed by an axial stressing. This is a path previously discussed by Helling et al. [5], but with strain in the small strain range of $\varepsilon < 0.05$. In the present case, the shear stress is kept at a constant value of $\sigma_{23} = 27.49$ MPa

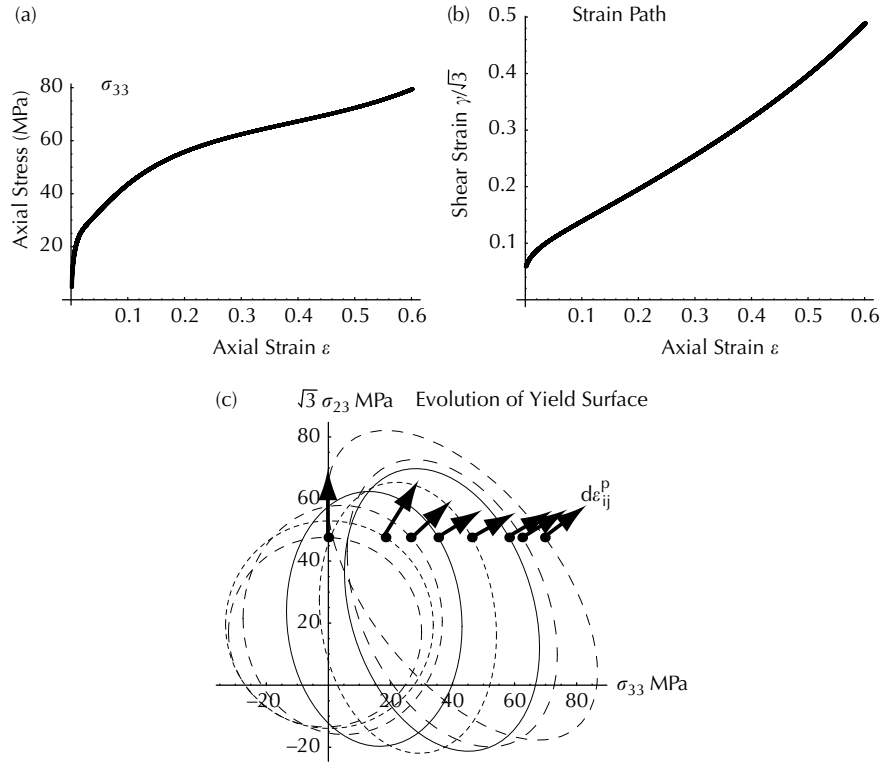

FIGURE 12.13
Path (5): (a) axial stress–strain relation, (b) strain path during the axial stressing stage, (c) evolution of yield surface with plastic strain increment vector (From Wu, H.C., *Int. J. Plasticity*, 19, 1773, 2003. With permission from Elsevier).

while the axial load is increased. In the calculation, $\sigma_{22} = 0$ and σ_{33}, α_{33}, α_{22}, α_{23}, D_{33}, D_{22}, and D_{23} need to be updated. Nonlinear kinematic hardening is used in the calculation. Figure 12.13(a) shows the axial stress plotted against the axial strain; Figure 12.13(b) shows the strain path during the axial stressing stage; and Figure 12.13(c) shows the evolution of yield surface for this path. The yield surfaces plotted are those with axial prestrains of 0, 0.0058, 0.02, 0.058, 0.116, 0.231, 0.30, and 0.45. The dots in this figure, when connected, represent the stress path and the plastic strain increment vector is plotted at each intersection point of the stress path with the corresponding yield surface. The plastic strain increment vector is normal to the yield surface at these points. Both the magnitude and the direction of the vector vary as the stress path is traversed. The angle that the plastic strain increment vector makes with the σ_{33} axis changes from 90°, at the point when the stress path abruptly changes its direction, to about 30° as the tensile stressing proceeds. But, the angle does not remain constant. This theoretical prediction is comparable to that experimentally observed by Phillips and Kaechele [18] from their testing of aluminum specimens.

12.8.6 Tor–Ten Path with Constant Shear Strain

This is a path previously investigated by Ohashi et al. [19] and Wu et al. [20] for the multiaxial stress–strain behavior of metals in the small strain range. But, the evolution of yield surface was not investigated by them. The example presented is a pretorsion from 0 to a shear strain of $\gamma = 0.1$ (with a corresponding shear stress of $\sigma_{23} = 22.87$ MPa) followed by an axial loading while keeping the shear strain constant at $\gamma = 0.1$. The calculation is carried out by use of the "linear" kinematic-hardening rule and keeping $D_{33} = 0.001\ \text{s}^{-1}$ during axial loading, while allowing σ_{23} and σ_{33} to vary. Figure 12.14(a) shows that the shear stress drops quickly as the axial loading is applied. The shear stress drops to a value of 5.65 MPa at an axial strain of $\varepsilon = 0.002$, to a value

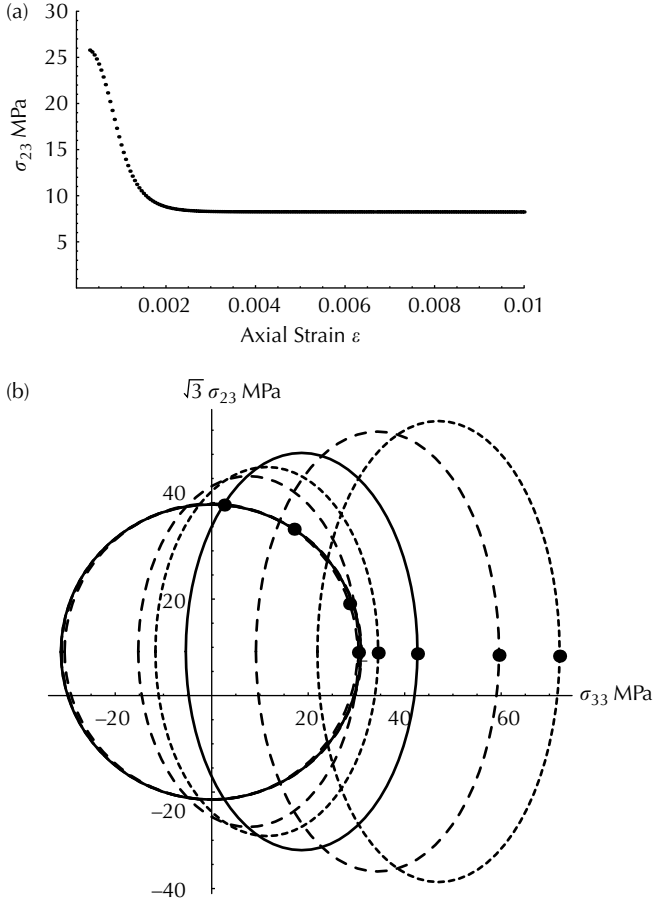

FIGURE 12.14
Tor–ten path with constant shear strain: (a) shear stress, (b) evolution of yield surfaces; • loading point on each yield surface (From Wu, H.C., *Int. J. Plasticity*, 19, 1773, 2003. With permission from Elsevier).

of 5.06 MPa at $\varepsilon = 0.08$, and it stays almost constant thereafter, although still slowly decreasing as the axial strain increased. The shear stress is 4.68 MPa at $\varepsilon = 0.3$. Figure 12.14(b) shows the evolution of yield surface for this path and the stress point for each yield surface is denoted by a dot. It is seen that the stress path follows the yield locus during the initial portion of the axial loading. The yield surfaces show apparent isotropic–kinematic hardening with distortion. But, no rotation is predicted by the model because the shear strain was kept constant during axial loading.

12.9 A Stress Path of Tension-Unloading Followed by Torsion

This is a stress path investigated by Khan and Wang [21]. These authors conducted combined axial–torsion tests on OHFC copper, following two nonproportional stress paths. In one of the stress paths, the specimen was stressed in tension from O to a into the plastic region (see Figure 12.15). Partial unloading and reverse loading then took place from a to b while keeping the shear stress 0. Finally, torsion was increased from b to D while keeping the axial stress constant. In the other path, the specimen was subjected to shear stress followed by an unloading. Axial stress was then applied while keeping the shear stress constant. The two paths are similar in nature, and we discuss here only the first path mentioned above. The experimental data reported in [21] are not complete in that no yield surfaces were determined. Nevertheless,

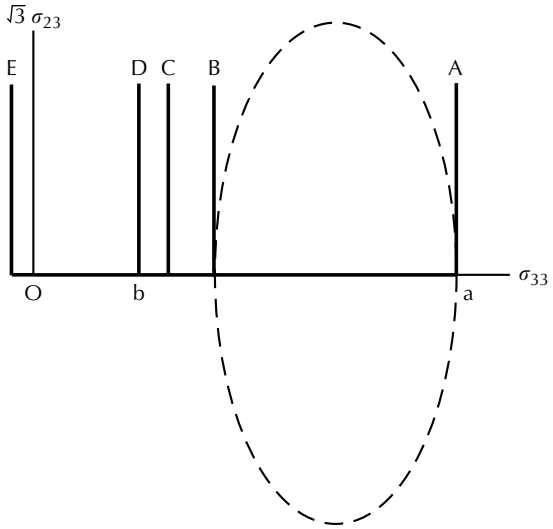

FIGURE 12.15
Schematic stress paths of axial stressing followed by unloading and reverse loading, and then torsion while keeping the axial stress constant.

this set of data is useful in that it may be used to test a model subjected to a nonproportional path.

Referring to Figure 12.15, Wu [15], using the nonlinear kinematic-hardening model of the previous section, investigated the strain path during the final torsion stage, which begins at various stages of unloading. The yield surface shown in dashed curve is obtained from an axial stressing to $\sigma_{33} = 81.03$ MPa with a prestrain of $\varepsilon = 0.45$. Several torsion stress paths denoted by A, B, C, D, and E were investigated, each starting at a different stage of unloading identified by the value of ε. Path A has no unloading in the axial stress, and torsion is applied while keeping $\sigma_{33} = 81.03$ MPa; in path B, torsion is applied immediately after an elastic axial unloading, keeping $\sigma_{33} = 34.11$ MPa; path C has a reverse loading down to $\varepsilon = 0.4413$, keeping $\sigma_{33} = 26.39$ MPa while torsion is applied; path D has a reverse loading down to $\varepsilon = 0.4343$, keeping $\sigma_{33} = 20.10$ MPa while torsion is applied; and path E has a reverse loading down to $\varepsilon = 0.3943$, keeping $\sigma_{33} = -9.42$ MPa while torsion is applied. The corresponding strain paths are shown in Figure 12.16. The specimen elongates as torsion is applied in path A. Immediately after an elastic unloading in path B, the initial plastic yielding would produce a negative plastic strain increment, which would quickly turn positive as torsion increases. Since σ_{33} is kept constant during this process, all axial strain increments are plastic strain increments. The specimen shortens initially and quickly turns into elongation as torsion increases. Paths C, D, and E show the similar behavior of plastic strain increment changing sign while the corresponding axial stress remains constant. This behavior is similar to the experimental results reported in Khan and Wang [21]. However, the sign change of the plastic strain increment is delayed by the amount of reverse loading before torsion is applied. The further the reverse loading goes, the larger the torsion that must be applied to cause the plastic strain increment to change sign. If the reverse loading is large enough, then no sign change in the plastic strain increment is predicted, and, in this

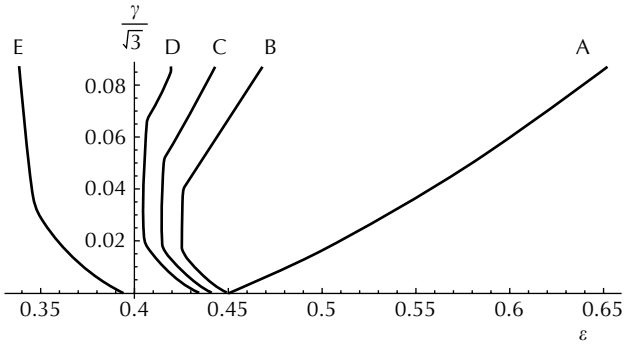

FIGURE 12.16
Strain paths corresponding to stress paths of Figure 12.15 using nonlinear kinematic-hardening rule.

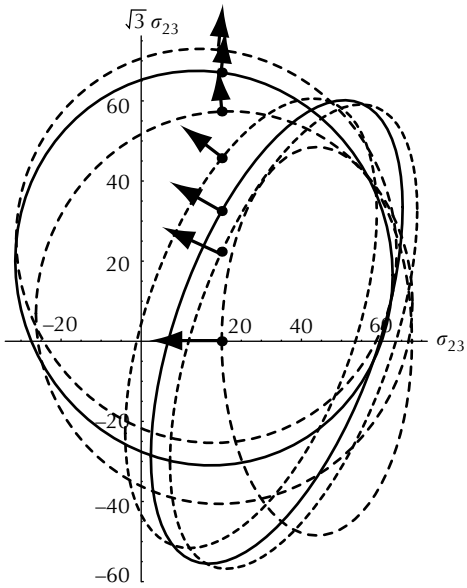

FIGURE 12.17
Evolutions of yield surface and plastic strain increment vector during the torsion stage of stress path D shown in Figure 12.15.

case, the specimen will shorten when torsion is applied. Further experimental investigation is needed to determine the characteristics of the strain path.

The evolution of the yield surface for path D is shown in Figure 12.17. Referring to Figure 12.15, path D follows path O–a–b–D. The first yield surface shown at the right-hand side of Figure 12.17 corresponds to the stress state at b, after an unloading and reverse loading from point a. At this point, $\sigma_{33} = 20.10$ MPa and $\sigma_{23} = 0$. The plastic strain increment is shown by the arrow and it is pointing to the negative direction of the σ_{33}-axis. As torsion is increased, the yield surface deforms, translates, and rotates, and the plastic strain increment, shown by the arrow, changes its direction from negative to positive.

A similar investigation was conducted by Wu [15] using the "linear" kinematic-hardening rule. The strain paths of this calculation are shown in Figure 12.18. Path A has no unloading in the axial stress before torsion is applied. The axial strain at this point is $\varepsilon = 0.45$. In path B, torsion is applied immediately after an elastic axial unloading. The axial strain at this point is $\varepsilon = 0.4493$. Curve C represents two cases: torsion applied at $\varepsilon = 0.4413$ and 0.4343. But the two curves are indistinguishable in the figure. Curve D represents the case when torsion is applied at $\varepsilon = 0.4293$. We see that the plastic strain increment does not change sign in curves B, C, and D in contradiction to the experimental results obtained by Khan and Wang [21]. In particular, we mention that curve A predicts an elongation of the specimen

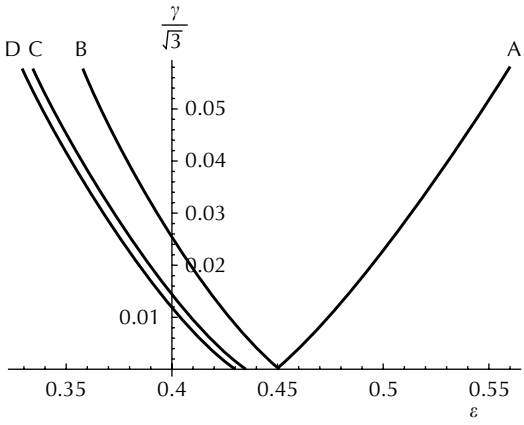

FIGURE 12.18
Strain paths corresponding to stress paths of Figure 12.15 using "linear" kinematic-hardening rule.

when torsion is applied, whereas curve B predicts a shortening of the specimen. This is physically impossible because the two cases differ only by an elastic unloading. Therefore, we must conclude that the "linear" kinematic hardening leads to unreasonable behavior.

12.10 Summary and Discussion

This section discusses the evolution of the yield surface due to different (proportional and nonproportional) loading paths with prestrains in the large strain range. It has been concluded that the evolution of yield surface depends significantly on the preloading path. The evolution includes the change in size (isotropic-hardening), distortion, translation (kinematic hardening), and rotation of the yield surface. No rotation of yield surface has been observed for the specimen subjected to a proportional preloading path. Rotation of yield surface may or may not occur, depending on the nonproportional path followed. The following conclusions may be drawn about the anisotropic plasticity model of Wu [3,15]:

1. Both "linear" and nonlinear kinematic-hardening rules give reasonable results in one-dimensional cases such as the axial tension test or the free-end torsion test.
2. In addition to describing the aforementioned seven sets of experimental data, this model has been shown to describe the change in the direction of the plastic strain increment in the case of torsion followed by axial stressing. The results agree with the findings of Phillips and Kaechele [18].

3. The nonlinear kinematic-hardening model predicted the change of sign in the plastic strain increment as observed by Khan and Wang [21]. This phenomenon is not predicted by the "linear" kinematic-hardening model. Therefore, we can conclude that the nonlinear kinematic-hardening rule gives reasonable results in the combined axial–torsion stress states.

References

1. Swift, H.W., Length changes in metals under torsional overstrain, *Engineering*, 163, 253, 1947.
2. Wu, H.C., On finite plastic deformation of anisotropic metallic materials, *Int. J. Plasticity*, 19, 91, 2003.
3. Wu, H.C., Effect of loading-path on the evolution of yield surface for anisotropic metals subjected to large pre-strain, *Int. J. Plasticity*, 19, 1773, 2003.
4. Hill, R., A theory of yielding and plastic flow of anisotropic metals, *Proc. Roy. Soc. London*, A193, 281, 1948.
5. Helling, D.E., Miller, A.K., and Stout, M.G., An experimental investigation of the yield loci of 1100-0 aluminum, 70:30 brass, and an oberaged 2024 aluminum alloy after various prestrains, *J. Eng. Mater. Technol.*, 108, 313, 1986.
6. Hill, R., *The Mathematical Theory of Plasticity*, Clarendon Press, Oxford, 1950, 332.
7. Hosford, W.F. and Caddell, R.M., *Metal Forming-Mechanics and Metallurgy*, 2nd Edn., PTR Prentice Hall, Englewood Cliffs, NJ, 1993, 276.
8. Wu, H.C. and Yip, M.C., Endochronic description of cyclic hardening behavior for metallic materials, *J. Eng. Mater. Technol.*, 103, 212, 1981.
9. Qian, Z. and Wu, H.C., A 2-D texture study based on a double-slip model of polycrystal plasticity with analysis of thin-walled tubes under torsion, *Int. J. Solids Struct.*, 33, 4167, 1996.
10. Prager, W., The theory of plasticity: a survey of recent achievements (James Clayton Lecture), *Proc. Inst. Mech. Eng.*, 169, 41, 1955.
11. Simo, J.C. and Hughes, T.J.R., *Computational Inelasticity*, Springer-Verlag, New York, 1998.
12. Wu, H.C. and Yang, R.J., Application of the improved endochronic theory of plasticity to loading with multi-axial strain-path, *Int. J. Non-Linear Mech.*, 18, 1983, 395.
13. Wu, H.C., Yang, C.C., and Chu, S.C., Further application of endochronic constitutive equation to loading with non-proportional axial-torsional strain-path, *Int. J. Non-Linear Mech.*, 20, 1985, 41.
14. Armstrong, P.J. and Frederick, C.O., A mathematical representation of the multiaxial Bauschinger effect, G.E.G.B. Report RD/B/N 731, Berceley Nuclear Laboratories, 1966.
15. Wu, H.C., The evolution of yield surface in the finite strain range, presented at *16th ASCE Engineering Mechanics Conference*, University of Washington, Seattle, July 16–18, 2003 (paper submitted to *International Journal for Plasticity* for publication).

16. Wu, H.C., Lu, J.K., and Pan, W.F., Some observations on yield surfaces for 304 stainless steel at large strain, *J. Appl. Mech.*, 62, 626, 1995.
17. Wu, H.C., Xu, Z., and Wang, P.T., Torsion test of aluminum in the large strain range, *Int. J. Plasticity*, 13, 873, 1998.
18. Phillips, A. and Kaechele, L., Combined stress tests in plasticity, *J. Appl. Mech.*, 23, 43, 1955.
19. Ohashi, Y., Tokuda, M., and Tanaka, Y., Precise experimental results on plastic behavior of brass under complex loading, *Bull. De L'Acad. Polon. Des Sci.*, Ser. Sciences Tech., 26, 261, 1978.
20. Wu, H.C., Yang, C.C., and Chu, S.C., Further application of endochronic constitutive equation to loading with non-proportional axial–torsional strain-path, *Int. J. Non-Linear Mech.*, 20, 1985, 41.
21. Khan, A.S. and Wang, X., On non-proportional infinitesimal plastic deformation after finite plastic prestressing and partial unloading, *J. Mech. Phys. Solids*, 36, 519, 1988.

Problems

(1) Show that Hill's quadratic yield function reduces to (12.25).

(2) Derive (12.50).

(3) Use (12.86) to plot the initial yield surface using $q = \bar{m}\, p$, where $\bar{m}$ is a parameter.

(4) In the combined axial–torsion of a thin-walled tube, consider the material element depicted by Figure 12.2. On Face (2), the stress vector is $\mathbf{t}^{(n)} = \tilde{t}^{(n)i}\mathbf{g}_j = \tilde{n}_j \tau^{ji}\mathbf{g}_j$. Show that its tangential component is σ_{23} and its normal component along the axial direction of the tube is σ_{33}. Show the tangential and normal components in a sketch.

(5) Find the physical components of the stress vector $\mathbf{t}^{(n)}$ of Problem (4). Draw a sketch to show these components.

(6) Plot curves to show the yield surface evolution, if a ten–tor path depicted by path OaA of Figure 12.15 is followed.

Answers and Hints to Selected Problems

Chapter 1

(2) $\delta_{ij}\delta_{ij} = \delta_{ii} = 3.$

(4a) 2.

(4d) 12.

(9) No.

(10) $$\begin{bmatrix} \left(\dfrac{11}{4} + \dfrac{3\sqrt{3}}{2}\right) & \left(\dfrac{3}{2} - \dfrac{5\sqrt{3}}{4}\right) & 0 \\ \left(\dfrac{3}{2} - \dfrac{5\sqrt{3}}{4}\right) & \left(\dfrac{1}{4} - \dfrac{3\sqrt{3}}{2}\right) & 0 \\ 0 & 0 & 1 \end{bmatrix}.$$

(15) $$\begin{bmatrix} T'_{11} & T'_{12} & T'_{13} \\ T'_{21} & T'_{22} & T'_{23} \\ T'_{31} & T'_{32} & T'_{33} \end{bmatrix} = \begin{bmatrix} T_{11} & -T_{12} & -T_{13} \\ -T_{21} & T_{22} & T_{23} \\ -T_{31} & T_{32} & T_{33} \end{bmatrix}.$$

(16) $(\mathbf{e}_p \otimes \mathbf{e}_p) \cdot \mathbf{a} = (\mathbf{a} \cdot \mathbf{e}_p)\mathbf{e}_p = a_p \mathbf{e}_p = \mathbf{a} = \mathbf{I} \cdot \mathbf{a}.$

(20) $$[Q_1] = \begin{bmatrix} 0 & 0 & 1 \\ 0 & 1 & 0 \\ -1 & 0 & 0 \end{bmatrix}.$$

(21) $$[Q_2] = \begin{bmatrix} 1 & 0 & 0 \\ 0 & 0 & -1 \\ 0 & 1 & 0 \end{bmatrix}, \quad [\bar{a}] = \begin{bmatrix} 1 \\ 0 \\ 1 \end{bmatrix}.$$

(22) $$[\bar{a}]^* = \begin{bmatrix} 1 \\ -1 \\ 0 \end{bmatrix}.$$

(23) $$\begin{bmatrix} 0.6404 \\ 0.9822 \\ -0.7924 \end{bmatrix}.$$

Chapter 2

(2) $p \begin{bmatrix} -\sin\theta \\ \cos\theta \\ 1 \end{bmatrix}$.

(4) $\frac{2}{3}\begin{bmatrix} -10 \\ 77 \\ 80 \end{bmatrix}$ MPa.

(6) $[t^{(n)}] = \begin{bmatrix} 0.35 \\ -0.39 \\ -0.06 \end{bmatrix}$, normal $= -0.103$, shear $= 0.517$.

(10) $\sigma_1 = 0$, $n^{(1)} = [0, 0, 1]$, $\sigma_2 = \alpha(\nu_1' + 1)$, $n^{(2)} = \left[\sqrt{\frac{1+\nu_1'}{2}}, \frac{\nu_2'}{\sqrt{2(1+\nu_1')}}, 0\right]$,

$\sigma_3 = \alpha(\nu_1' - 1)$, $n^{(3)} = \left[-\sqrt{\frac{1-\nu_1'}{2}}, \frac{\nu_2'}{\sqrt{2(1-\nu_1')}}, 0\right]$.

(13) (b) $A_1F_3 = F_2A_2$, (c) $[\sigma] = \begin{bmatrix} \frac{F_1}{A_1} & \frac{F_2}{A_1} \\ \frac{F_3}{A_2} & \frac{F_4}{A_2} \end{bmatrix}$.

(14) $J_1' = 0$, $J_2' = -\frac{100}{3} - 3400$, $J_3' = \frac{308000}{27}$.

(15) $\frac{40}{\sqrt{3}}[1, 0, 4]$.

Chapter 3

(1) $[F] = \begin{bmatrix} \lambda_1 & 0 & 0 \\ 0 & \lambda_2 & 0 \\ 0 & 0 & \lambda_3 \end{bmatrix}$, $[R] = \begin{bmatrix} 1 & 0 & 0 \\ 0 & 1 & 0 \\ 0 & 0 & 1 \end{bmatrix}$.

(2) Length $= 1.755$.

(4) $\lambda_1 = 1$, $n^{(1)} = \begin{bmatrix} 0 & 0 & 1 \end{bmatrix}$, $\lambda_2 = \frac{1}{2}(k^2 + 2 + k\sqrt{k^2+4})$,

$n^{(2)} = \left[\sqrt{\frac{2}{k^2 + k\sqrt{k^2+4} + 4}}, \sqrt{\frac{k^2 + k\sqrt{k^2+4} + 2}{k^2 + k\sqrt{k^2+4} + 4}}, 0\right]$,

$$\lambda_3 = \tfrac{1}{2}(k^2 + 2 - k\sqrt{k^2+4}),$$

$$n^{(3)} = \left[\sqrt{\frac{2}{k^2 - k\sqrt{k^2+4}+4}}, \sqrt{\frac{k^2 - k\sqrt{k^2+4}+2}{k^2 - k\sqrt{k^2+4}+4}}, 0 \right].$$

(5) $[\mathrm{d}x] = [1+k, 1, 0]$.

(7) $[F] = \begin{bmatrix} 0.8 & 0.5 \\ 0.2 & 0.9 \end{bmatrix}$, $[C] = \begin{bmatrix} 0.68 & 0.58 \\ 0.58 & 1.06 \end{bmatrix}$.

(11) (a) $\left\{ \left(\frac{\alpha}{2}\right)^2 + \beta^2 + \gamma^2 \right\}^{1/2}$, (b) $\cos^{-1}\left(\frac{-\alpha}{\sqrt{\alpha^2 + 4\beta^2}} \right)$, (c) $\alpha\beta\gamma = 1$.

(12) $[C] = \begin{bmatrix} 1.44 & -0.72 & 0 \\ -0.72 & 1.17 & 0 \\ 0 & 0 & 0.81 \end{bmatrix}$, $[\mathrm{e}] = \begin{bmatrix} -0.16 & -0.23 & 0 \\ -0.23 & -0.27 & 0 \\ 0 & 0 & -0.11 \end{bmatrix}$.

(15) (b) $\mathrm{d}\mathbf{x}^{(1)} \cdot \mathrm{d}\mathbf{x}^{(2)} = 0$, $\phi = 90°$, (c) $\mathrm{d}\mathbf{x}^{(1)} \cdot \mathrm{d}\mathbf{x}^{(2)} = \mathrm{d}X^{(1)}\,\mathrm{d}X^{(2)}$, $\phi = 45°$.

(16) $\alpha^2\beta = 1$; $\mathrm{d}s = \sqrt{\alpha^2\tau^2R^2 + \beta^2}$, $\mathrm{d}S = 1$; $\mathrm{d}s = 1$, $\mathrm{d}S = \dfrac{1}{\beta}(1 + R^2\tau^2)^{1/2}$.

(17) $[F] = (1 + \alpha\Delta T)[\delta_{ij}]$, $l = (1 + \alpha\Delta T)L$.

(18) $\kappa = 2$, $[E] = \begin{bmatrix} \frac{2}{3} & 10\frac{\sqrt{3}}{9} & 0 \\ 10\frac{\sqrt{3}}{9} & \frac{26}{9} & 0 \\ 0 & 0 & 0 \end{bmatrix}$, $\kappa = -2$, $[E] = \begin{bmatrix} -\frac{26}{9} & 10\sqrt{\frac{3}{9}} & 0 \\ 10\sqrt{\frac{3}{9}} & -\frac{2}{3} & 0 \\ 0 & 0 & 0 \end{bmatrix}$.

(24) $[v] = \left[\tfrac{1}{2}X_2^2, 0, 0\right] = \left[\tfrac{1}{2}x_2^2, 0, 0\right]$, $[f] = [0, 0, 0]$.

(29) (c) $[D] = \begin{bmatrix} 0 & \frac{2ktx_2}{(1+kt)^2} & 0 \\ \frac{2ktx_2}{(1+kt)^2} & \frac{k}{1+kt} & 0 \\ 0 & 0 & 0 \end{bmatrix}$, $[W] = \begin{bmatrix} 0 & \frac{2ktx_2}{(1+kt)^2} & 0 \\ -\frac{2ktx_2}{(1+kt)^2} & 0 & 0 \\ 0 & 0 & 0 \end{bmatrix}$,

(d) $\dfrac{\mathrm{d}V}{\mathrm{d}V_0} = \det[F] = 1 + kt$.

(33) $n_1^2 + n_2^2 + n_3^2 = 1$ and $n_1 + n_2 + n_3 = \pm 1$.

Chapter 4

(2) $B_{ij}n_j = \lambda n_i$, material model is $\boldsymbol{\sigma} = \alpha\mathbf{B} + \beta\mathbf{B}\cdot\mathbf{B} + \gamma\mathbf{I}$. Show that $\sigma_{ij}n_j = (\alpha\lambda + \beta\lambda^2 + \gamma)n_i = m\,n_i$.

(4) $[\sigma] = \hat{\chi}_0(k^2)\begin{bmatrix}1&0&0\\0&1&0\\0&0&1\end{bmatrix} + \hat{\chi}_1(k^2)\begin{bmatrix}1+k^2&k&0\\k&1&0\\0&0&1\end{bmatrix} + \hat{\chi}_{-1}(k^2)\begin{bmatrix}1&-k&0\\-k&1+k^2&0\\0&0&1\end{bmatrix}$, $\sigma_{12} = \sigma_{21} = \mu k$, show that normal stresses are not zero.

Chapter 5

(4) For small strain, ε^{p} does not affect the Nadai equation.

(6) 0.248.

(10) $\sqrt{3}\times 10^{-4}\ \mathrm{s}^{-1}$.

Chapter 6

(1) (a) 125 MPa, (b) 20 MPa, (c) -30 MPa.

(4) 18.75 mm.

(6) 287.35 MPa.

(10) $\bar{\sigma} = \sigma$.

(11) $\mathrm{d}\bar{\varepsilon}^{\mathrm{p}} = \mathrm{d}\varepsilon^{\mathrm{p}}$.

(14) Mises yield criterion, $\dfrac{\partial f}{\partial \sigma_{km}} = \sigma'_{km} - c(\kappa_1)\varepsilon^{\mathrm{p}}_{km}$, $\dfrac{\partial f}{\partial \varepsilon^{\mathrm{p}}_{km}} = -c\dfrac{\partial f}{\partial \sigma_{km}}$, $\dfrac{\partial f}{\partial \kappa_1} = -\dfrac{\partial c}{\partial \kappa_1}\dfrac{\partial f}{\partial \sigma_{km}}\varepsilon^{\mathrm{p}}_{km}$, and $\dfrac{\partial f}{\partial \sigma_{km}}\dfrac{\partial f}{\partial \sigma_{km}} = 2f = 2\kappa_0$.

(15) $E_t = \dfrac{3}{4}\left(2c + \sqrt{6}\dfrac{\partial c}{\partial \kappa_1}\varepsilon^{\mathrm{p}}\right)$.

Chapter 7

(6) $\dfrac{\mathrm{d}\sigma_{22}}{\mathrm{d}t} = 0$, $\dfrac{\mathrm{d}\sigma_{12}}{\mathrm{d}t} = 2\omega(\sigma_{22} + \mu)$, $\dfrac{\mathrm{d}\sigma_{11}}{dt} = 4\omega\sigma_{12}$.

(8) Unloading starts at t^*, where $\sigma^*_{12} = \dfrac{Y}{\sqrt{3}} + \dfrac{h}{3}\sin\gamma^*$, $\gamma = 2\omega t^* - 2\omega(t - t^*)$, $\sigma_{12} = \sigma'_{12} = -\dfrac{Y}{\sqrt{3}} + \alpha^{\mathrm{D}}_{12}$, $\sigma_{11} = \sigma'_{11} = \alpha^{\mathrm{D}}_{11}$, $\sigma_{22} = \sigma'_{22} = \alpha^{\mathrm{D}}_{22}$, $\dfrac{\mathrm{d}^2\alpha^{\mathrm{D}}_{12}}{\mathrm{d}t^2} = -4\omega^2\alpha^{\mathrm{D}}_{12}$ same as loading.

(9) Use the flow rule.

(12) $r = \left(x_1^2 + x_2^2 + x_3^2\right)^{1/2},\ \theta = \tan^{-1}\left\{\dfrac{(x_1^2 + x_2^2)^{1/2}}{x_3}\right\},\ \phi = \tan^{-1}\left(\dfrac{x_2}{x_1}\right).$

$$[F] = \begin{bmatrix} \dfrac{\partial r}{\partial R} & \dfrac{1}{R}\dfrac{\partial r}{\partial \Theta} & \dfrac{1}{R\sin\Theta}\dfrac{\partial r}{\partial \Phi} \\ r\dfrac{\partial \theta}{\partial R} & \dfrac{r}{R}\dfrac{\partial \theta}{\partial \Theta} & \dfrac{r}{R\sin\Theta}\dfrac{\partial \theta}{\partial \Phi} \\ r\sin\theta\dfrac{\partial \phi}{\partial R} & \dfrac{r}{R}\sin\theta\dfrac{\partial \phi}{\partial \Theta} & \dfrac{r\sin\theta}{R\sin\Theta}\dfrac{\partial \phi}{\partial \Phi} \end{bmatrix}.$$

(13) $\bar{\sigma} = \sigma,\ \bar{T}^{(0)} = \mathrm{e}^{-\varepsilon}\bar{\sigma},\ \bar{\Pi} = \mathrm{e}^{-2\varepsilon}\bar{\sigma},\ \bar{\varepsilon} = \varepsilon.$

(14) $\bar{\sigma} = \sqrt{3}\tau, \bar{T}^{(0)} = \bar{\sigma}\sqrt{\dfrac{4}{3}\eta^2 + 1}, \bar{\Pi} = \bar{\sigma}\sqrt{\dfrac{16}{3}\eta^2 + 1}, \bar{\varepsilon} = \dfrac{2\eta}{\sqrt{3}}.$

Chapter 8

(1) Use (8.65) in (8.64) and write the resulting equations in component form. Add equations for σ_{11}, σ_{22}, σ_{33} to obtain (8.66a). Get (8.66b) by using $\sigma'_{ij} = \sigma_{ij} - \frac{1}{3}\delta_{ij}\sigma_{kk}$. Use a similar procedure to obtain (8.67).

(4) $k_1 = \sqrt{\frac{3}{2}},\ k_2 = \sqrt{2}.$

(9) $\tau = \tau^*,\ \mathrm{d}\tau = 0,\ \mathrm{d}\eta = \mathrm{d}\eta^{\mathrm{p}}$, let $z - z^* = t$ and $z' - z^* = t'$, (8.131) becomes $\tau^* = \sigma'_{\mathrm{y}}\dfrac{\mathrm{d}\eta}{\mathrm{d}t} + 2\mu_2\,\mathrm{e}^{-\alpha(t+z^*)}X - 2\mu_2\int_0^t \mathrm{e}^{-\alpha(t-t')}\dfrac{\mathrm{d}\eta}{\mathrm{d}t'}\mathrm{d}t' + 2\mu_1\eta.$
Use L-transform to find $\bar{\eta}$, then reverse transform to find $\eta(z)$.

(10) The stress will jump higher and gradually merge with the higher constant strain-rate curve.

Chapter 10

(1) $\varepsilon_1 = 0.263,\ \varepsilon_2 = 0.096,\ \varepsilon_3 = -(\varepsilon_1 + \varepsilon_2) = -0.359,\ \bar{\varepsilon} = 0.372.$

(2) $\mathrm{d}\varepsilon_1^{\mathrm{p}} = \mathrm{d}\varepsilon_1 - \dfrac{\mathrm{d}\sigma_1}{E},\quad \mathrm{d}\varepsilon_{\mathrm{w}}^{\mathrm{p}} = \mathrm{d}\varepsilon_{\mathrm{w}} + \nu\dfrac{\mathrm{d}\sigma_1}{E}.$

(3) $R = R_s + \varepsilon_{\mathrm{t}}^{\mathrm{p}}\dfrac{\mathrm{d}R_s}{\mathrm{d}\varepsilon_{\mathrm{t}}^{\mathrm{p}}},\quad R_s = \dfrac{\varepsilon_{\mathrm{w}}^{\mathrm{p}}}{\varepsilon_{\mathrm{t}}^{\mathrm{p}}},\quad R = \dfrac{\mathrm{d}\varepsilon_{\mathrm{w}}^{\mathrm{p}}}{\mathrm{d}\varepsilon_{\mathrm{t}}^{\mathrm{p}}}.$

(4) Substitute stress transformation equations into (10.6). Expand and regroup the resulting equation in a form similar to (10.6) and the stresses are now expressed in the primed system. Require the coefficient of each term to be the same as

that of the corresponding term in (10.6), we obtain $N+F+2H$ and $L=M$. For $\sigma_z=\sigma_{z'}$, the requirement of $(G\sigma_x+F\sigma_y)\sigma_z=(G\sigma_{x'}+F\sigma_{y'})\sigma_{z'}$ leads to $G=F$.

(5) Due to symmetry for isotropic material, (10.5) leads to $F=G=H$ and $L=M=N$. But $N=F+2H$ due to rotational symmetry, therefore, $N=3F$.

Chapter 11

(2) $\mathbf{F}=\dfrac{\partial x_i}{\partial X_k}\mathbf{e}_i\otimes\mathbf{E}_k$.

(4) Consider $\dfrac{\partial\bar{\mathbf{g}}_i}{\partial\bar{\theta}^j}=\Gamma^m_{ij}\bar{\mathbf{g}}_m$, where $\bar{\mathbf{g}}_i=\dfrac{\partial\theta^m}{\partial\bar{\theta}^i}\mathbf{g}_m$.

$$\frac{\partial\bar{\mathbf{g}}_i}{\partial\bar{\theta}^j}=\frac{\partial}{\partial\bar{\theta}^j}\left(\frac{\partial\theta^m}{\partial\bar{\theta}^i}\mathbf{g}_m\right)=\frac{\partial^2\theta^m}{\partial\bar{\theta}^i\partial\bar{\theta}^j}\mathbf{g}_m+\frac{\partial\theta^m}{\partial\bar{\theta}^i}\frac{\partial\mathbf{g}_m}{\partial\bar{\theta}^j}$$
$$=\frac{\partial^2\theta^s}{\partial\bar{\theta}^i\partial\bar{\theta}^j}\frac{\partial\bar{\theta}^m}{\partial\theta^s}\bar{\mathbf{g}}_m+\Gamma^t_{rs}\frac{\partial\theta^r}{\partial\bar{\theta}^i}\frac{\partial\theta^s}{\partial\bar{\theta}^j}\frac{\partial\bar{\theta}^m}{\partial\theta^t}\bar{\mathbf{g}}_m.$$

(5) $$\frac{\partial\mathbf{H}}{\partial\theta^r}=\frac{\partial(\tilde{\mathbf{H}}^{ij}\mathbf{g}_i\otimes\mathbf{g}_j)}{\partial\theta^r}=\frac{\partial\tilde{\mathbf{H}}^{ij}}{\partial\theta^r}\mathbf{g}_i\otimes\mathbf{g}_j+\tilde{\mathbf{H}}^{ij}\frac{\partial\mathbf{g}_i}{\partial\theta^r}\otimes\mathbf{g}_j+\tilde{\mathbf{H}}^{ij}\mathbf{g}_i\otimes\frac{\partial\mathbf{g}_j}{\partial\theta^r}$$
$$=\left(\frac{\partial\tilde{\mathbf{H}}^{ij}}{\partial\theta^r}+\Gamma^i_{rm}\tilde{\mathbf{H}}^{mj}+\Gamma^j_{rm}\tilde{\mathbf{H}}^{im}\right)\mathbf{g}_i\otimes\mathbf{g}_j=\tilde{\mathbf{H}}^{ij}|_r\mathbf{g}_i\otimes\mathbf{g}_j.$$

(6) $$(v^k+w^k)|_i=\frac{\partial(v^k+w^k)}{\partial\theta^i}+(v^j+w^j)\Gamma^k_{ji}=v^k|_i+w^k|_i.$$

(7) View v^jw^k as contravariant components of a second-rank tensor, then $(v^jw^k)|_i=\dfrac{\partial(v^jw^k)}{\partial\theta^i}+\Gamma^j_{im}(v^mw^k)+\Gamma^k_{im}(v^jw^m)=v^j|_iw^k+v^jw^k|_i$.

(9) $\sigma_{11}=\Pi^{11}+2K\,\Pi^{12}+K^2\Pi^{22}$, $\sigma_{12}=\Pi^{12}+K\,\Pi^{22}$, $\sigma_{22}=\Pi^{22}$

$$2\phi=\sigma_{11}^2+(1+K^2)^2\sigma_{22}^2+(2K^2-1)\sigma_{11}\sigma_{22}+(3+4K^2)\sigma_{12}^2$$
$$-4K\sigma_{12}[\sigma_{11}+(1+K^2)\sigma_{22}]=Y^2$$

(13) $$D^{\mathrm{p}}_{11}=-\frac{\dot{\Lambda}}{4}[-2\xi_{11}+4K\xi_{12}+(1-K^2)\xi_{22}],$$
$$D^{\mathrm{p}}_{22}=-\frac{\dot{\Lambda}}{4}[(1-K^2)\xi_{11}+2K(5+7K^2)\xi_{12}-2(1+6K^2+6K^4)\xi_{22}],$$
$$D^{\mathrm{p}}_{12}=-\frac{\dot{\Lambda}}{4}[2K\xi_{11}-2(3+5K^2)\xi_{12}+K(5+7K^2)\xi_{22}].$$